Proceedings of the

3rd International Fire Safety Symposium

IFireSS 2019

Ottawa, Ontario, June 5-7, 2019

Organizers:
Department of Civil and Environmental Engineering,
Carleton University, Ottawa, Ontario

National Research Council of Canada

CIB – International Council for Research and Innovation in Building Construction

Editors:
George Hadjisophocleous
Rheanna Johnson

Proceedings of the

3rd International Fire Safety Symposium

IFireSS 2019

Ottawa, Ontario, June 5-7, 2019

Organizers:
Department of Civil and Environmental Engineering,
Carleton University, Ottawa, Ontario

National Research Council of Canada

CIB – International Council for Research and Innovation in Building Construction

Editors:
George Hadjisophocleous
Rheanna Johnson

IFireSS 2019 – 3ⁿᵈ International Fire Safety Symposium

Ottawa, Ontario, Canada, June 5-7, 2019

Proceedings of the 3ʳᵈ International Fire Safety Symposium, IFireSS 2019
Held in the Department of Civil and Environmental Engineering, Carleton University
Ottawa, Ontario, Canada
June 5-7, 2019

Organizers:
Department of Civil and Environmental Engineering,
Carleton University, Ottawa, Ontario

National Research Council of Canada

CIB – International Council for Research and Innovation in Building Construction

Editors:
George Hadjisophocleous
Rheanna Johnson

SPONSORS

Platinum sponsors

Gold sponsor

Silver sponsors

Organising Committee

George Hadjisophocleous, Carleton University, Chair
Dr. Ahmed Kashef, National Research Council, Co-Chair
Jim Mehaffey, Adjunct Professor, Carleton University
Dr. Noureddine Benichou, National Research Council
Prof. Mario Santana, Carleton University
Aba Owusu, Carleton University
Rheanna Johnson, Carleton University

Scientific Committee
Ahmed Kashef, National Research Council Canada, Chair
Ali Faris, University of Ulster, UK
Andrews Gordon, University of Leeds, UK
Beth Weckman, University of Waterloo, Canada
Bilotta Antonio, Università di Napoli Federico II, Italy
Bisby Luke, University of Edinburgh, UK
Bjegovic Dubravka, University of Zagreb, Croatia
Block, Florian, BuroHappold Engineering, UK
Bontempi Franco, Università di Roma La Sapienza, Italy
Boustras George, European University of Cyprus, Cyprus
Cajot Louis-Guy, ArcelorMittal, Luxembourg
Chow Wan-Ki, Hong Kong Polytechnic University, Hong Kong
Christian Dagenais, FPInnovations, Canada
Cruz Hernandez Ricardo, Universidad Santander, Colombia
Del Prete, Iolanda, BuroHappold Engineering, UK
Dhima Dhionis, CSTB, France
Ehab Zalok, Carleton University, Canada
Fahy Rita, National Fire Protection Association, USA
Franssen Jean Marc, Liège University, Belgium
Gambarova Pietro, Politecnico di Milano, Italy
Green Mark, Queen's University, Canada
Hadjisophocleous George, Carleton University, Canada
John Gales, York University, Canada
Kazu Harada, Kyoto University, Japan
Klippel, Andrea, University of Magdeburg, Germany
Kodur Venkatesh, Michigan State University, USA
Landolfo Raffaele, Università di Napoli Federico II, Italy
Lindsay Ranger, FPInnovations, Canada
Maluk Cristian, University of Queensland, Australia
Meacham Brian, WPI, USA
Mistakidis Euripidis, University of Volos, Greece
Nadjai Ali, University of Ulster, UK
Nigro Emidio, University of Naples Federico II, Italy
Osama Salem, Lakehead University, Canada
Pignatta e Silva Valdir, São Paulo University, Brazil
Rein Guillermo, Imperial College, UK
Rodrigues Correia João Paulo, Coimbra University, Portugal
Romero Manuel, Universidad Politecnica de Valencia, Spain
Simo Hostikka, Aalto University, Finland
Steven Gwynne, National Research Council, Canada
Tan Kang Hai, Nanyang Technological University, Singapore
Torero Jose, University of Maryland, USA
Ulf Wickstrom, Luleå University of Technology, Sweden
Vila Real Paulo, Aveiro University, Portugal
Wang Yong, University of Manchester, UK
Zhao Bin, CTICM, France

TABLE OF CONTENTS

KEYNOTE PAPERS

TUNNEL SAFETY- PUBLIC AND RESPONDERS

Deputy Chief Gary English (ret)
Seattle Fire Department, Seattle, USA
Underground Command and Safety

ABSTRACT

Millions of people move safely through thousands of tunnels daily and the public generally presumes they are safe. However, some of the public still asks 'Are we really safe in tunnels?' And, tunnel owners/ operators ask what liability they might have if a big incident occurs. Tunnels safety has evolved over decades of improvements, yet we continue to have tunnel incidents with fatalities and lengthy closures with major economic impact. Responder risks their lives and sometime die. Why are these incidents still happening?

This brief paper explores the evolution of tunnels safety, history, regulations, and possible lethal consequences where the public and responder safety has failed. This paper is not 'research' rather points out dangerous tunnel practices which need to be resolved. These are identified in italics and listed in conclusion as potential areas for more research and changes in safety regulations.

1   PUBLIC PERCEPTION

Although the public and tunnel engineers seemed surprised when the 1999 Mt Blanc fire occurred with 39 fatalities, fire responders could predict some of the consequences. The surprise centered around the higher than expected energy released by ordinary commodities, i.e. margarine and flour, and how cars not directly involved with the incident burning due to extreme heat. This incident was quickly followed by the Tauern and Gotthard tunnel fires with 23 additional fatalities. Again ordinary commodities (paint) and vehicle fuel were the fire sources. European public and political perception of tunnel safety was diminished, and they recognized there are greater risk in tunnels. As a direct result, considerable European investments in research and scientific tests provided proof the tunnel fires could grow faster and release more energy than a similar fire above ground reaching peak temperatures of 1350 degrees C compared to building fire growth curve which reaches 600 degrees C in the same 10 minutes. (1) This surprised even the responders.

Europe's considerable tunnel fire research resulted in their mandatory retroactive safety measures at considerable expense, i.e. Directive 2004/54/EC "Minimum safety requirements for tunnels in the Trans-European Road Network". (2) However, *there are no retroactive safety requirements in US tunnels.* And, unlike Europe where many countries such as France have established tunnel safety centers to ensure safety is a priority, e.g. 'le Centre d'études des tunnels' (Center for Tunnel Studies,) (3), *the US has not established a research center for tunnel safety.* The visible impacts of physical changes to Europe's road tunnels and considerable press on the safety improvements have rightly improved their public perception of tunnel safety. These safety improvements have also positively impacted US newest road tunnels by establishing a more realistic approach to the tunnel fire size and growth rate in US road safety standards. However, the US standards modifications did not fully match the potential fire size identified in research, thus leaving a probable gap in safety. Also, unlike Europe, the US has failed to address the thousands of older legacy road and rail tunnels with inadequate or missing safety systems by modern standards. More importantly the *US has not*

yet experienced the plethora of major tunnel fires with multiple fatalities as occurred in Europe. Lacking catastrophic tunnel loss of life there appears to be no immediate need for significant safety changes to standards or retrofits in tunnels. This assumption is dangerous.

2   EVOLUTION OF TUNNEL SAFETY

2.1 Safety regulations

Tunnels have been constructed and used by humans since before recorded history. The simple geometry of a tunnel: narrow spaces, long distances to limited exits with resultant limited egress (and responder access), limited air supplies, and bigger, faster fires than many thought possible, magnifies the consequences of incidents. These physical constraints make emergency safety difficult. For example, for a passenger in a burning car or train on the surface, simply moving a short distance away almost always assures safety. However in a tunnel, moving a short distance away, leaves the passenger in the same environment of the incident, i.e. the limited tunnel space does not allow heat, and smoke to readily move away from occupants.

One of the biggest challenges is acknowledging Underground Passenger Rail (UPR), and road tunnels we use today were built over many decades resulting in significant differences in tunnel design, systems, and safety. *Safety regulations were non-existent in the earliest tunnels.* For example the Burlington Northern Rail Tunnel (Seattle) was finished in 1904 and since then passenger rail use has increased exponentially. The lack of safety requirements when constructed meant there was no emergency lighting, ventilation, fire standpipes, walkable surfaces, and the nearest exit could be nearly a mile away. *We are behind when compared to Europe tunnel safety.*

The 'Evolution of Safety' regulations in buildings vs tunnels is dramatic. Building safety is embedded in building and fire safety codes and is accepted as a baseline. The phrase the 'code was written in blood' is in part true. Incidents of consequence, (loss of lives) resulted in new language being inserted into safety codes to prevent a recurrence. For example, we take for granted the fire exit stairs have doors to prevent fire and smoke from entering the stairs. This was not always true. The 1958 Lady of Angles fire (4) had 95 casualties (92 children) in a stairway for lack of a single door i.e. there was no separation between the exit path and the fire. This incident and many others are examples of 'hard learned lessons' which resulted in safety improvements.

For comparison, modern buildings have prescriptive code language based on deadly lessons and safety analysis. As a baseline this specifies rooms have at least two exits of minimum width, with fire rated exit paths, fire doors, etc. Rooms with high volumes of people, e.g. over 1000 (roughly a train load) require at least four exits. These minimums ensure speedy exiting is of paramount importance.

Comparing this with UPR tunnels demonstrates a distinct difference in safety evolution. UPR exit pathway minimum width has remained at 24" (61 cm) for years compared to building 44" (112 cm). The narrower path requires single file evacuation (i.e. everyone moves at speed of slowest person) and a longer time to evacuate.

Closest exit distance can be 800 feet (244 m) vs buildings at 1/3 the distance.   However, in UPR no exits are required in tunnels up to *2500 ft (762 m) tunnels which is beyond reach of responder rescue teams* as their air supply is limited. (5, 6.3)   Buildings now require fire rated exits paths, close to the public to the exterior. Why not the same minimum safety in tunnels?

Since the distance to the surface in tunnels can be extreme, (sometimes measured in miles/kms), rapidly exiting to the outside to safety in many locations is impossible. Given these restraints road and UPR tunnels use an approved alternate safety approach by moving people to a 'Point of Safety' (POS). This is a well-defined term in building safety codes which use a combination of the three paraphrased options; A POS is (a) short distance to outside (not possible in tunnels), (b) fire sprinklers (required in nearly all buildings) yet not required in tunnels or underground stations, (c) another area of building with smoke barriers and means of escape or exit can provide safety Combining these UPR distances with narrow walkways and high volumes of people makes evacuation to safety take considerably longer than buildings. Also the POS is not always safe. Their use in the Mt Blanc road tunnel led to several deaths as the POS lacked adequate ventilation and doors were not designed for the higher temperatures.

US regulations for UPR stations does not require fire/smoke doors in exits but allows the use of mechanical ventilation to protect evacuees as part of their point of safety definition. This works well if the mechanical ventilation does not fail, and the mechanical ventilation is designed to meet the possible fire size. Unfortunately, the European tests showed the *older ventilation systems (which were designed for a smaller fire) could not protect evacuees by ventilation alone.* (In some jurisdictions the building codes are applied to UPR stations in which case the reliance on mechanical ventilation to maintain a point of safety is not permitted and fire sprinklers are required).

2.2 Tenability during evacuation

Tenable spaces are defined as "environment that permits evacuation or rescue, or both, of occupants for a specific period of time." (6, 3.38). This is measured by heat exposure, (skin/respiratory), visibility impacts (smoke), and toxicity (toxic gasses, reduced oxygen). Smoke is "The airborne solid and liquid particulates and gases evolved when a material undergoes pyrolysis or combustion, together with the quantity of air that is entrained or otherwise mixed into the mass.". (6, 3.3.46) Ventilation which does not remove smoke as fast as it develops results in reduced visibility i.e. ability to see a path to move away from a fire, find an exit, or locate an emergency phone to call for help. Since smoke cannot rapidly move away inside a tunnel, smoke rapidly becomes denser to the point of zero visibility, thus reducing occupant movement to 'walking or crawling blind' which is remarkable slow. At this point, self-rescue is seriously limited. (Fig. 1 below diagrams inadequate air flow allowing smoke to back layer towards people)
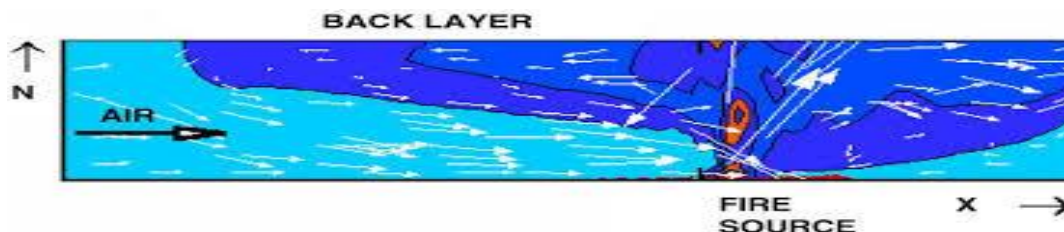
Responders are less impacted by heat and gasses as their safety gear protects them from moderate heat and provides fresh air. But loss of visibility for responders due to undersized ventilation greatly slows the process to find and save people in smoke. This can reduce the ability to reach all those needing assistance and move them to safety.

3   TUNNEL HAZARDS

3.1 History and efforts to improve safety

Some of the earliest tunnels were not for public transportation rather were built for freight hauling. Those tunnels moved freight and later passengers by horse drawn teams. Although horses had their own emissions, these were not considered lethal. Horses were replaced by coal fired steam locomotives pulling passenger cars on rails. Coal fire engines create large volumes of smoke which obscures visibility and is high in toxic Carbon Monoxide (CO) gas. These engines consumed oxygen to the point they became ineffective. Tunnel engineers tackled these problems by creating some of the first large scale mechanical ventilation systems to control CO. However, these *older mechanical ventilation was not designed to address smoke from fires*, rather internal combustion engine exhaust, notably Carbon Monoxide.

New York Holland road tunnel (1927) was one of the first to seriously design and build to address the public safety issue of vehicle emissions (carbon monoxide) in a road tunnel. The 'new-fangled' mechanical ventilation supplied fresh air under the length of the road deck to strategically placed vents along the entire tunnel length. The ceiling also contained a full length exhaust plenum with vents designed to pull CO out of the road tunnel i.e. a 'Full Transverse' ventilation system. CO was managed and public safety was enhanced. (Also, a hazardous material fire in this tunnel in 1949 tunnel resulted in the first use of mechanical ventilation to control smoke from a hazardous material fire.)

This ground breaking mechanical ventilation to protect public became a new benchmark for road tunnel safety. Many tunnels were built with this type of system, however this ventilation system is not designed to manage smoke from fires which is greater than CO. In 2003, the same test which demonstrated faster fire growth rate also demonstrated a much higher than expected heat release rate for ordinary combustibles in a road tunnel at over 200 MW(1) with greater smoke.

NFPA 502 Road Tunnel, Bridges and Limited Access Highways (6), increased the minimum recommended design fire size and recognized fire sprinklers might be an effective way of suppressing road tunnel fires. These actions improved public and responder safety. Road tunnels which recognized the actual potential of large, fast fires and have installed fire sprinklers are likely the safest road tunnels by suppressing a fire, and stopping or reducing fire growth rate thus reducing heat and smoke and minimizing tunnel closure time from days to hours.

Meanwhile, UPR had growing passenger ridership. UPR agencies started using mechanical ventilation systems to provide fresh air, and later, to provide limited heating, ventilation and cooling, i.e. HVAC. For example the January 2015 WA D.C. fatality subway smoke incident was originally thought to be a fire system ventilation failure, but this ventilation system was not designed to manage fire smoke, rather was only an HVAC system.

Fires like this increased the awareness of the risk of tunnel fires in US and affirmed the European understanding of higher probabilities of significant US UPR fires. This was validated as the Chunnel was expected to have a working fire every 50 years, yet three occurred in 12 years.

3.2 Stratification and Ventilation Flaws

One large challenge for public safety is the mistaken assumption that smoke in a tunnel will neatly stratify at the ceiling, therefore allowing occupants to move to safety under the hot smoke layer. The belief in stratification comes from the common practice of burning diesel in test fires which produces a hot smoke layer at the ceiling.

Actual fires in vehicles and contents combust and pyrolyze at different temperatures releasing smoke with different buoyancies which spreads from top to bottom of a tunnel.

Sometimes stratification can occur if enough heat is produced to entrain all the smoke into the thermal column. Even if stratification occurs, smoke rapidly cools, or mechanical ventilation which supplies air quickly mixes smoke with cooler air and destratifies smoke layer. *Smoke does not always stratify*.

Longitudinal ventilation (LV), i.e. moving air in a tunnel downstream of a fire is considered more effective than transverse ventilations. However, there are 'fatal flaws' of LV in three scenarios. 1) for road tunnels with traffic backed up within the tunnel, a vehicle fire in stopped traffic will result in smoke being pushed over the downstream vehicles. 2) For rail tunnels with LV, a stopped train with a fire near the middle, smoke is pushed towards the fewest people, i.e. either the front or rear of a train. With a trainload of roughly 1000 people, approximately one half (500 people) will be downstream and caught in the smoke as they attempt to escape. 3) Of greatest concern is allowing multiple rail vehicles in the same ventilation zone, e.g. where distance between exits is long, as occurs in some older tunnels under rivers. With multiple trains stopped, a fire anywhere in one of middle trains, could put trainloads (thousands) of people in the smoke and heat if LV is used. But, not using LV would allow smoke to spread over all trains as stratification might only be effective for a short distance. *Longitudinal ventilation can expose people downstream to dangerous smoke/ heat*.

3.3 Traction Power

Most UPR now utilize electric traction power which does not have emission problems but presents a new hazard i.e. electrocution. Placing an energized rail on the ground at track rail level, means evacuees cannot safely move from the very narrow walkway to the track area, until power is deenergized. Since deenergizing traction power can be delayed and *there are no local indicators to identify when traction power been deenergized,* the passenger are loath to walk near the third rails if they need to evacuate. This further increases the time needed to evacuate as evacuees stay on the narrow emergency walkway instead of dispersing beyond the train end. Also, responders in many jurisdictions simply refuse to enter the tunnel to fight fire, perform rescue, etc., while traction power might be energized requiring coordination with tunnel operators and delays.

3.4 Tunnel Collapse

Earliest tunnels lacked the modern engineering understanding of the soils in which tunnels were constructed. This resulted in partial and full tunnel collapses in earlier tunnels. Even today, tunnels under construction have had partial or full collapses. Fortunately full collapses of operating UPR and road tunnels are very rare. More likely are partial structural and systems collapse, e.g. 2012 Sasago (Japan) road tunnel ceiling collapse where 1.2 ton panels fell along a 110 meter long section, resulting in 5 deaths and a fire. In 2006 Central Artery Project (USA) a ceiling panel collapse killed one woman. These incidents were found to be the result of ceiling hanger failures. The 2006 incident sparked a US federal level regulation change in road tunnels with the establishment of new mandatory US road tunnel inventory and a tunnel operations maintenance and inspection evaluation manual (TOMIE) and program which identifies and requires repairs. *TOMIE is a remarkable advance in tunnels safety but does not match minimum fire system inspection requirements.* The legislation also created a road tunnel inventory, but fell short of establishing a US Center for Tunnel Safety.

3.5 Hazardous Materials (Dangerous Goods)

Road tunnels routinely have hazardous materials transportation through tunnels either as cargo or simply as vehicle fuel. An accidental release can be in different forms; solid, liquids and gases and can be immediately hazardous to life safety even in small quantities. US states have the authority to regulate state highways, but limited capacity to limit interstate commerce on interstate highways, yet federal government does not regulate cargo in these tunnels. Removing motorists to safety is time consuming and dependent on product type based on the motorist risks.

Gaseous releases could be mitigated by fire ventilation systems moving gases out of the tunnel, but this could endanger people outside the tunnel. Fire service recommendation is for hazardous gaseous release to initially be confined to area of origin, i.e. *by a 'net zero' air movement in the tunnel*. This would require modifying ventilation systems or designed them for this effect.

3.5 Terrorism
Terrorism takes many forms and tunnels provide opportunities not available on the surface, notably narrow enclosed spaces with high volume of people with slow egress. This allows relatively small devices to impact hundreds of people. There have been multiple terrorist attacks in tunnels, most commonly UPR given the possible immediate impacts and disruption of regional transportation. Gasoline fires, bombs, sarin gas, etc. have been used with mixed results. Road tunnels are not immune and possibly makes terrorist incidents simpler by providing large quantities of regulated substances such as bulk fuels.

3.6 Medical Emergencies
Tunnels do not in themselves create medical emergencies. The key tunnel difference is time, i.e. time to identify, report and locate an accident, time for responders to arrive at a tunnel and move to the incident site, and time to transport patients out of the tunnel. E.g. a surface accident might take 20-60 minutes to process, in a road tunnel this same accident might take 45- 120 minutes, i.e. possibly beyond the time when medical assistance is effective.

In UPR tunnels, the lack of road access for emergency vehicles can add significantly to the delay as responders might need to either walk long distances, use 'carts', or establish a rescue train. For example, a derailed train over a mile from a station or portal with multiple injuries might necessitate the *use of rescue trains to allow responders to arrive at incident with necessary equipment and move large numbers of injured our of the tunnel.* Rescue trains can be used to relocate injured from the tunnel and to a location proximate to a hospital. This can be more expeditious than transferring patients to ambulances at a portal and driving through street traffic. Logistical coordination of multiple rescue trains, high numbers of patients and responders is very difficult and time consuming and must be practiced.

With train crush loads often exceeding 1000 passengers, many/most of them could be injured in a serious derailment. Typical derailments present a wide array of trauma injuries and potentially fire/smoke. Critically injured needs immediate care therefore rapid patient access, stabilization and movement to hospitals is essential. Since these patients require high numbers of responders to stabilize and transport, limited responder resources may result in triaging all patients and supporting only those most likely to survive.

Simply moving adequate medical equipment such as backboards to in the incident scene is difficult. Some jurisdictions now cache responder medical equipment in tunnel stations to ensure reasonable equipment is readily available, however, the *lack of cached responder transport equipment near tunnels can seriously delay emergency medical treatment.*

Road tunnel incidents typically have fewer patients than UPR systems incidents, as they are usually the result of vehicle accidents or medical emergencies which involve fewer people. Accessing patients by driving into a tunnels seems simple, however, often the route is blocked by other vehicles stopped in the tunnel. This required driving against traffic in in parallel tunnels both of which are challenging. *Tunnel response plans should include optimizing responder access and patient transport to hospitals.*

3.7 Multi Hazards

Combining hazards can greatly magnify problems. Either a hazardous material spill, or a fire create severe difficulties for responders and safety of occupants. Combining a hazardous material spill/ gas release with a fire can dramatically increase the safety problems. For example, some burning hazardous materials result in much faster growing and hotter fire which can negate mechanical ventilation. *Establishing and enforcing hazardous materials restrictions is important*.

4 RESPONDER SAFETY

Emergency Responders include four major groups; fire, medical, law enforcement (LE) and tunnel staff. They face extraordinary challenges to perform rescues in tunnels. Tunnels present a different and unfamiliar geometry, (long, narrow) for most responders with very limited surface access, few, if any fire and life safety systems, communications problems, high numbers of moving people (i.e. in trains and motor vehicles), sometimes with moving hazardous materials. Tunnels often have large capacity ventilation systems which are not familiar to responders. These differences contribute to making responder activities in tunnels difficult and more dangerous.

This lack of familiarity necessitates significant effort to train responders via orientations for new tunnels, and frequent refresher training on emergency plans, drills and tabletop exercises to understand systems, practice unified command, and annual full scale exercises for all shifts. Most importantly the hazards which could impact responders of all types should be identified.

Responders are typically multi-function specialists. Firefighters not only fight fires, but perform rescues, treat patients, use tunnel fire and life safety systems, identify mitigage hazardous material, etc. Many firefighters are trained to deal with medical emergencies, but separate medical specialists are also common in some areas.

In all situations, use of live/remote cameras in tunnels, on trains, on responder vehicles can provide critical information to responders. Personal cameras could be linked to displays allowing responders better intelligence, as could the use of drones designed for use in tunnels.

Fire commanders can be faced with difficult decisions based on survivability profiles of tunnel occupants. Should commanders send responders into space where tenability is not possible. E.g. UPR passengers who have evacuated into untenable spaces may have perished. Full scale tunnel test fires have demonstrated the available oxygen downstream of these fires can be as low as 10% which is too low to sustain life. What is the survivability profile in that space?

5 CONCLUSION

Millions safely use tunnels every day. However, there is the very real potential a catastrophic tunnel incident could occur today, or tomorrow. Fortunately the odds of this happening are slim. But when catastrophic fires occurs in North America as occurred in Europe, we will move through a similar process

of research, safety requirement upgrades and retrofits to existing tunnels. Rather than waiting for catastrophe, we could concentrate on the needed additional research to have a basis for revising safety requirements and provide tunnel designers, operators and responders a clear understanding of the risks. This is more urgent as we understand hundreds of tunnels ventilation systems we 'thought' would provide safety, are undersized which is an unrecognized risk. Upgrading ventilation systems to match the modern understanding of fire sizes is extraordinarily expensive. However, installing fire sprinklers could reduce the fire growth rate and size to a level where the existing ventilation systems could be effective, and could dramatically reduce fire resistance in tunnels.

Italicised safety/ research issues identified in the text and listed below.

- *1. There are no retroactive safety requirements in US tunnels and the US has not established research center(s) to address tunnel safety*
- *2.1 Emergency evacuation in rail tunnels is severely limited by exit widths and exit distances resulting in excessive exiting times to safety.*
- *2.1 Safety regulations were non-existent in the earliest tunnels*
- *2.1 US is behind compared to European Tunnel Safety*
- *2.1 2500 ft (762 m) tunnels are beyond reach of responder rescue teams* as their air supply is limited.
- *2.1 older ventilation systems (which were designed for a smaller fire) could not protect evacuees by ventilation alone.*
- *2.1* fire sprinklers (required in nearly all buildings) are not required in tunnels or underground stations
- *3.2 tunnel fires can grow faster and release more energy than previously acknowledged.*
- *3.2 Most ventilation systems in road and rail tunnels were not designed to handle all smoke*
- *3.2 Longitudinal ventilation can expose all people downstream to dangerous smoke/ heat, especially as we know, Smoke does not always stratify*
- *3.4 Control hazardous gas releases by a 'net zero' air movement in the tunnel.*
- *3.4 TOMIE is a remarkable advance in tunnels safety but does not match minimum fire system inspection requirements.*
- *3.6 Tunnel distances compound the time for responders to perform rescues especially when distances from responder access to the incident is beyond the limits of their air supply.*
- *3.6 Lack of cached responder transport equipment near tunnels can seriously delay emergency medical treatment.*
- *3.6 Tunnel response plans should include optimizing responder access and patient transport to hospitals..*
- *3.6 Use of rescue trains to save people in tunnels is difficult but necessary and is logistically very challenging and time consuming, guidelines for rescue trains is needed.*
- *3.7 Establishing and enforcing hazardous materials restrictions is important*
- *4. Understanding survivability profile vs responder capability should be researched*

REFERENCES

[1] Large Scale Fire Tests in the Runehamar Tunnel, 2003
https://www.sp.se/en/index/research/runehamar/sidor/default.aspx

[2] Directive 2004/54/EC "Minimum safety requirements for tunnels in the Trans-European Road Network" http://data.europa.eu/eli/dir/2004/54/oj

[3] Center for Tunnel Studies http://www.cetu.developpement-durable.gouv.fr/

[4] Groves, Adam, https://www.fireengineering.com/articles/print/volume-161/issue-1 2/features/our-lady-of-the-angels-school-fire-50-years-later.html

[5] NFPA 130, 2017 Standard for Fixed Guideway Transit and Passenger Rail Systems, National Fire Protection Association , 1 Batterymarch Park, Quincy, MA

[6] NFPA 502, 2017 Standard for Road Tunnels, Bridges and Limited access Highways. National Fire Protection Association , 1 Batterymarch Park, Quincy, MA

MODELLING AND MAPPING WILDFIRE EVACUATION

Gwynne, S.M.V.[1], Ronchi, E.[2], Bénichou, N.[3], Kinateder, M.[3], Kuligowski, E.D. [4], Gomaa, I.[3], Adelzadeh, M.[3]

[1]Movement Strategies, [2]Lund University, [3]National Research Council Canada, [4]National Institute of Standards and Technology

ABSTRACT

Wildland-Urban Interface (WUI) incidents are likely to become more severe and affect more people. incidents require a multi-domain approach to assess their impact and the effectiveness of response. Several of the authors recently produced a specification for a simulation framework that quantifies evacuation performance during WUI incidents [1]. This included inputs from three core domains: fire development, pedestrian performance, and vehicular traffic. The intention was for this framework to produce new insights by simulating evolving conditions of WUI incidents based on developments and interactions between the core components. The proposed framework would also advance geo-spatial mapping of WUI incidents, as it would natively produce results in this format. The concept of dynamic vulnerability is enabled by the integrated simulation framework and the emergent conditions predicted. The generation of dynamic vulnerability allows users to construct richer incident narratives from the perspective of specific locations or sub-populations establishing localized capacity to cope with wildfires and to make fewer simplifying assumptions regarding interactions between the three core domains.

Keywords: Wildland-Urban Interface; simulation; dynamic vulnerability; evacuation

1   INTRODUCTION

Large WUI (wildfire urban interface) fires are associated with severe negative consequences. These include community evacuation, property losses, disruption, damage to infrastructure, as well as evacuee and responder fatalities/injuries [2-9]. The challenge posed by wildfires is likely to become more complex in future events given social, physical and climatic factors. The social and physical geography associated with WUI communities presents a special challenge that needs to be addressed to ensure life safety; i.e., understanding the fire development alone is an insufficient predictor of the impact of the incident on nearby populated areas [10,11]. Therefore, WUI incidents require a multi-domain approach to assess their impact and the effectiveness of any mitigation efforts implemented.

The emergency response to WUI fires includes the ability of the affected community to prepare for the hazards, adapt their response to the evolving conditions of the incident and eventually recovery actions in the aftermath of the incident. To ensure that this preparation and response is adequate, the effectiveness of pre-incident decisions and responder/manager decisions taken during the incident needs to be understood - to assess these decisions before they are put into practice.

A mechanism is required that can translate empirical and theoretical understanding into evidence-based projections for use by key stakeholders. A simulation framework is suggested that can evaluate evacuation performance ahead of time and with relatively little cost – complementing current planning and educational approaches. Such a framework might be used to predict how an evacuation develops based on current and possible future fire conditions, given different affected populations and evacuation decisions and the access / availability of different resources.

What follows is a speculative discussion building on previous work [1], outlining how the simulation of multiple domains enables the *time-based vulnerability mapping* of affected populations given their capacity to cope with the conditions faced.

2   GENERAL

Various computer simulation tools are available today that evaluate different aspects concerning WUI fires. These models provide evidence in support of the design and execution of community measures. At a minimum, three different elements of WUI fires are apparent: fire models (addressing wildfire propagation such as models for fire spread, smoke transport, spotting fires due to firebrands, etc.) [5, 12-14], pedestrian models (models representing the pedestrian evacuation movement and behaviours) [15,16], and traffic models (evacuation model for traffic movement) [17-19]. To date, the development and use of modelling tools from different areas of disaster response have been performed mostly independently with only limited coupling between embedded models. This significantly reduces their potential to enhance response in case of wildfires threatening urban areas and to inform decisions on the need to evacuate an area; i.e., the incompleteness of the coupling loses the representation of key interactions and possibly key influences. These limitations become all the more apparent when mapped onto a geographic information system (GIS) platform, where the absence of the situational context (i.e., the fire conditions without human response, or vice versa) deprives the user of key benchmarks by which the severity of the situation is assessed. Finally, numerous efforts have been made to produce results that can be spatially represented on GIS [11,20, 21-27]. A variety of different approaches are adopted in these efforts. The mapping capabilities employed are largely constrained by the modelling approaches used to inform them.

Previous work developed specifications for an integrated simulation framework capable of estimating future wildfire evacuation conditions [for a detailed description, see 1]. The output describes evacuee responses given WUI fire conditions in the form of pedestrian and vehicle performance. The specified design includes sub-models from different subject domains known to influence the outcome of a WUI evacuation. These sub-models would be coupled by exchanging information with one another enabling agent decision-making and represented conditions to be sensitive to relevant external factors.

A simplified schematic of the proposed software system design is shown in Figure 1. Information can be provided to the system by external information sources (databases, sensors, field reports) or directly from a user via a graphical user interface (GUI). This allows the generation of a scenario description based on input on the topography, environment, incident, demographic attributes, procedure / behavior, infrastructure, resources, etc. The nature of this scenario (scale, complexity, time constraints, required accuracy, etc.) informs the degree of model granularity that is possible. For instance, in real-time applications, time will be a key constraint as results need to be available

in sufficient time to examine them and affect the decision-making process. In planning applications, this time constraint may not be so pressing.

In other applications, the results of one sub-model might be specified by a user to perform consequence analysis, instead of reflecting current real-world conditions. Here, the user would be establishing the planning impact of possible scenarios and the effectiveness of responses, rather than current conditions. For instance, the existence / severity of the fire might be set (reflecting a historical occurrence) to determine the effectiveness of a particular procedure. This might be done to explore specific questions or compensate for model limitations.
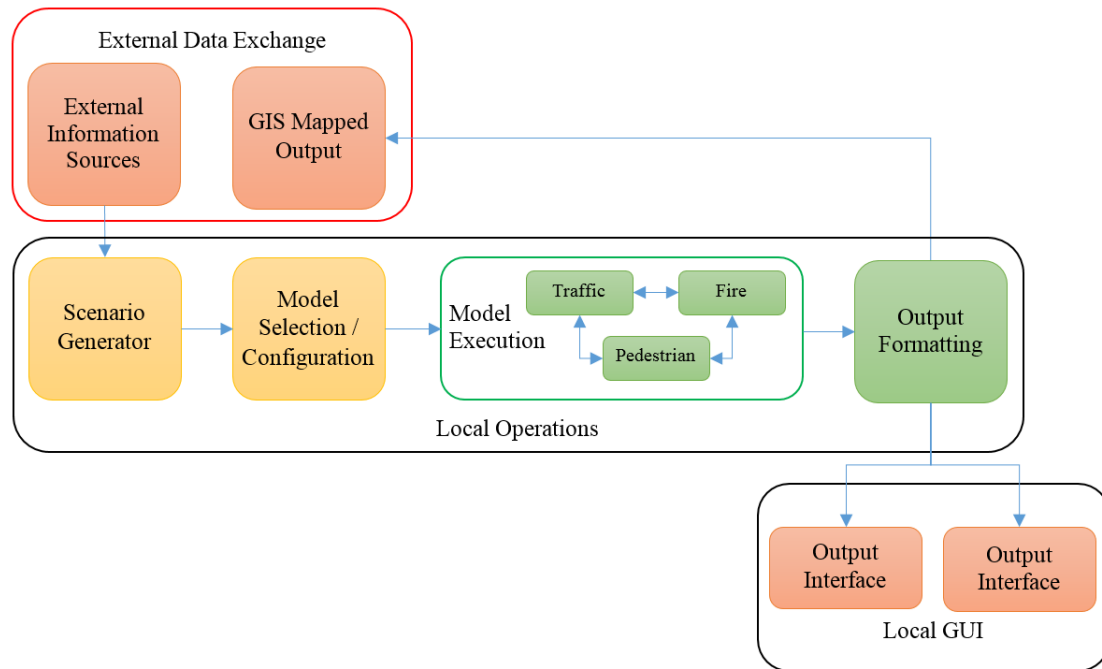
Figure 1. Schematic of simulation framework, derived from [1].

The simulation framework would be able to produce simulated insights into the evolving conditions as an incident progresses and into the eventual outcomes produced.

3 SUGGESTED MAPPING APPROACH

Here, we describe the benefits of mapping *dynamic vulnerability* enabled by the implementation of the simulation framework outlined above. The term dynamic vulnerability is defined as *the projected capacity of social agents to cope with evolving environmental conditions faced given the resources available [46]*. It assumes that

(1) the conditions mapped will emerge from simulated results rather than being compiled from high-level factors.
(2) the conditions will be integrated within a *single simulated environment* and will therefore not require artificial assumptions to determine interactions.
(3) the mapped results will *evolve over time* in line with the simulated output. Dynamic vulnerability will vary across a population at any point in time and may vary for any agent over time as the conditions faced and decisions made change.

The dynamic vulnerability index is a function of three modelling layers (F = fire, P = pedestrian, T = traffic, t = time) weighted in relation to the dynamic conditions within each layer. The index

13

changes over time to reflect evolving fire conditions. Note that the actual weights and variables will need to be carefully identified and calibrated.

The simulation framework would be able to receive external information on the current situation and then simulate future conditions. It would do this both for the fire development and for the human response to it (e.g., the pedestrian and traffic conditions). This would assess both the risk posed by the fire development and the capacity of those affected to respond to the incident. The results from this simulated framework would co-locate current incidents, projected fire fronts, current traffic and pedestrian conditions, and equivalent projected conditions. The results are presented within the same mapping platform; however, they would already exist within the same simulation framework and have been generated in a coupled manner. The susceptibility of certain populations or infrastructure will become evident as the simulated conditions (from different domains) interact and evolve.

Such simulated output could be compiled to produce a dynamic vulnerability map – reflecting the severity of the situation and a community's capacity to absorb / mitigate the conditions faced as time progresses (see Figure 2). The contours generated in such maps indicate areas of equivalent vulnerability to the conditions faced, given the impact of simulated preparation, simulated fire conditions, and the simulated responses (e.g., capacity to get to a place of safety), in conjunction with the actions of the emergency responders. These contours would expand / contract to describe the current population and fire conditions, reflecting the dynamic simulated projections and derived susceptibilities. The vulnerability contours then evolve to reflect the developing simulated updates being provided.
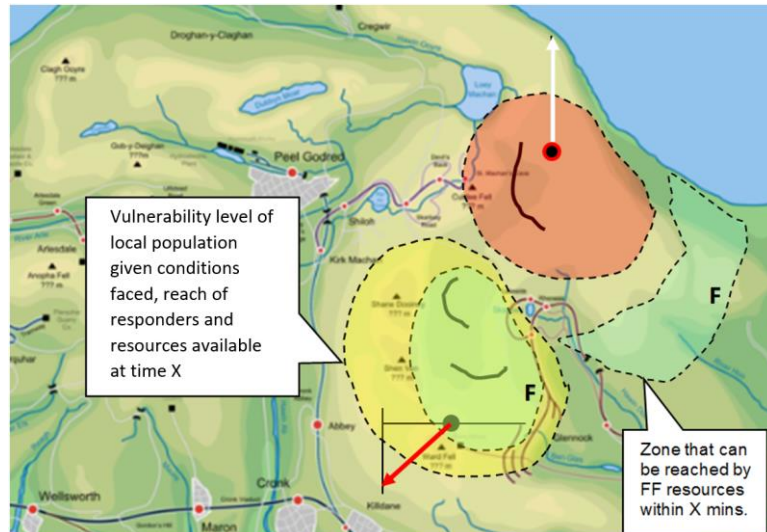
Figure 2. Contours representing areas of vulnerability formed from reported / calculated threat and the resilience of the infrastructure, fire fighter resources and capacity to evacuate. Red contours reflect 'high' levels of vulnerability (e.g., given proximity to fire), yellow contours indicate 'moderate' levels and green contours indicate 'low' levels of vulnerability.

Depending on the user and intended use, the output generated would provide different insights. For an emergency responder, the refinement and scope of the data may be key to ensure the most comprehensive picture of the incident affecting resource allocation; for a member of the public, the information may have to inform and convince them to prepare (through demonstrating the nature and severity of the incident assuming that the results are presented to them by a credible source in

support of emergency guidance); for local government agencies it may affect land management and urban planning decisions.

4 CONCLUSIONS

The present work has reported previously developed specifications for an integrated simulation framework to examine WUI evacuations. The framework involves sub-models representing the development of the fire and the evacuee response – whether as pedestrians or as vehicle users. These sub-models exchange information to ensure that the conditions affect each other to produce more representative outcomes.

The proposed framework enables the representation of an incident as a function of factors from three different core domains (fire, pedestrian movement, and traffic movement) and builds on the tools and insights employed in the built environment (e.g., in performance-based design). Using an integrated simulation framework, the concept of vulnerability mapping may evolve in several ways: becoming dynamic and being based on emergent predictions. This enhancement was labelled the *dynamic vulnerability* of the population of interest. Such an approach should allow vulnerability levels to emerge during the predicted response phase. This allows for a richer incident narrative to be constructed from the perspective of specific locations and sub-populations and makes fewer simplifying assumptions regarding the output needed. The framework outlined would allow such an *dynamic vulnerability* index to be visualized and overlaid on a mapping platform to locate the coping capacity both temporally and spatially – enabling a richer understanding of an incident's impact for interest parties.

REFERENCES

[1] Ronchi, E., et al., e-Sanctuary: Open Multi-Physics Framework for Modelling Wildfire Urban Evacuation. 2017.

[2] Caton, S.E., et al., Review of pathways for building fire spread in the wildland urban interface part I: exposure conditions. Fire technology, 2017. 53(2): p. 429-473.

[3] Maranghides, A. and W. Mell, A case study of a community affected by the Witch and Guejito wildland fires. Fire technology, 2011. 47(2): p. 379-420.

[4] Maranghides, A., et al., Initial Reconnaissance of the 2011 Wildland-Urban Interface Fires in Amarillo, Texas. Fire Technology, 2014. 50(1): p. 93-104.

[5] Mell, W.E., et al., The wildland–urban interface fire problem–current approaches and research needs. International Journal of Wildland Fire, 2010. 19(2): p. 238-251.

[6] Jolly, W.M., et al., Climate-induced variations in global wildfire danger from 1979 to 2013. Nat Commun, 2015. 6: p. 7537.

[7] Wolshon, B. and E. Marchive III, Emergency planning in the urban-wildland interface: Subdivision-level analysis of wildfire evacuations. Journal of Urban Planning and Development, 2007. 133(1): p. 73-81.

[8] Manzello, S.L., et al., Summary of workshop for fire structure interaction and urban and wildland-urban interface (WUI) Fires–operation Tomodachi–fire research. Fire Safety Journal, 2013. 59: p. 122-131.

[9] McLennan, J., et al., Should We Leave Now? Behavioral Factors in Evacuation Under Wildfire Threat. Fire Technology, 2018: p. 1-30.

[10] Cutter, S.L., Vulnerability to environmental hazards. Progress in human geography, 1996. 20(4): p. 529-539.

[11] Cutter, S.L., J.T. Mitchell, and M.S. Scott, Revealing the vulnerability of people and places: a case study of Georgetown County, South Carolina. Annals of the association of American Geographers, 2000. 90(4): p. 713-737.

[12] Sullivan, A.L., Wildland surface fire spread modelling, 1990–2007. 3: Simulation and mathematical analogue models. International Journal of Wildland Fire, 2009. 18(4): p. 387-403.

[13] Sullivan, A.L., Wildland surface fire spread modelling, 1990–2007. 2: Empirical and quasi-empirical models. International Journal of Wildland Fire, 2009. 18(4): p. 369-386.

[14] El Houssami, M., et al., Framework for submodel improvement in wildfire modeling. Combustion and flame, 2018. 190: p. 12-24.

[15] Gwynne, S.M.V., et al., A review of the methodologies used in the computer simulation of evacuation from the built environment. Building and environment, 1999. 34(6): p. 741-749.

[16] Kuligowski, E.D., R.D. Peacock, and B.L. Hoskins, A review of building evacuation models, 2nd edition, NIST Technical Note 1680. 2010: US Department of Commerce, National Institute of Standards and Technology Gaithersburg, MD.

[17] Pel, A.J., M.C. Bliemer, and S.P. Hoogendoorn, A review on travel behaviour modelling in dynamic traffic simulation models for evacuations. Transportation, 2012. 39(1): p. 97-123.

[18] Chiu, Y.-C. and P.B. Mirchandani, Online behavior-robust feedback information routing strategy for mass evacuation. IEEE Transactions on Intelligent Transportation Systems, 2008. 9(2): p. 264-274.

[19] Riad, J.K., F.H. Norris, and R.B. Ruback, Predicting evacuation in two major disasters: Risk perception, social influence, and access to resources 1. Journal of Applied Social Psychology, 1999. 29(5): p. 918-934.

[20] Shirley, W.L., B.J. Boruff, and S.L. Cutter, Social vulnerability to environmental hazards. 2003: Social Science Quarterly.

[21] Solangaarachchi, D., A.L. Griffin, and M.D. Doherty, Social vulnerability in the context of bushfire risk at the urban-bush interface in Sydney: a case study of the Blue Mountains and Ku-ring-gai local council areas. Natural hazards, 2012. 64(2): p. 1873-1898.

[22] Nguyen, C.V., et al., Assessment of social vulnerability to climate change at the local scale: development and application of a Social Vulnerability Index. Climatic Change, 2017. 143(3-4): p. 355-370.

[23] Edwards, J., M. Gustafsson, and B. Näslund-Landenmark, Handbook for vulnerability mapping: EU Asia Pro Eco Project disaster reduction through awareness, preparedness and prevention mechanisms in coastal settlements in Asia. Demonstration in tourism destinations. Stockholm, Sweden: Swedish Rescue Services Agency & EU and International Affairs Department, 2007.

[24] Cutter, S.L. and C. Finch, Temporal and spatial changes in social vulnerability to natural hazards. Proc Natl Acad Sci U S A, 2008. 105(7): p. 2301-6.

[25] Arce, R.S.C., et al., Risk awareness and intended tsunami evacuation behaviour of international tourists in Kamakura City, Japan. International journal of disaster risk reduction, 2017. 23: p. 178-192.

[26] Yorke, C., et al., Incorporating evacuation potential into place vulnerability analysis. Geomatics, Natural Hazards and Risk, 2015. 6(3): p. 195-211.

[27] Chang, S., et al. A community resilience approach to assessing transportation risk in disasters. in 16th World Conference on Earthquake Engineering. Santiago. 2017.

[28] Stephen, L. and T.E. Downing, Getting the Scale Right: A Comparison of Analytical Methods for Vulnerability Assessment and Household-level Targeting. Disasters, 2001. 25(2): p. 113-135.

FIRE SAFETY OF EXPOSED MASS TIMBER IN HIGH-RISE BUILDINGS -RESEARCH APPLICATION, CHALLENGES AND SOLUTIONS

David Barber
Arup, Washington DC, USA

ABSTRACT

Mass timber buildings are sustainable, efficient in their build and becoming a popular form of construction as they are a differentiator. National model building codes are being updated globally to allow for high-rise mass timber construction. To assist with building code changes, a number of compartment fire tests with mass timber have been completed, typically using cross laminated timber (CLT). The mass timber compartment fire tests have shown large areas of exposed timber impacts fire size and duration, as the exposed timber provides an additional volume of combustible fuel. Understanding the compartment fire is key to determining an accurate mass timber char rate and depth, for structural capacity to be assessed. This becomes difficult, when the compartment fire is impacted by the unpredictable behaviour of CLT char fall off. This paper provides a summary of the compartment fire testing undertaken, summarises trends and introduces methods for design solutions. The paper also provides a number of areas for further mass timber research in fire.

1 INTRODUCTION

Mass timber buildings are becoming a popular form of medium and high-rise construction, due their sustainability benefits, building efficiency and because owners and tenants like the difference of a timber building. Over the last seven years there has been an acceleration in national construction code development for high-rise mass timber buildings, with codes changing relatively rapidly. Significant code changes to permit mass timber construction have occurred in Australia [1], Canada [2] and the US [3], with continued evolution of codes that already permit mass timber in countries such as Germany, France, Norway and Sweden [4]. The code changes are very positive and are changing the way buildings are designed and built, also resulting in a series of growing pains.

As codes start to change, researchers, designers and constructors are finding difficulties in determining efficient and cost-effective building solutions. When compared to traditional construction of steel and concrete, the engineering of mass timber buildings is more unique, driven by architectural design, limited by availability of compliant building solutions and a limited construction back-catalogue. This individuality makes timber construction less competitive, which is often compounded by CLT and glulam market supply issues, specifically in North America. Cost is a major factor in determining construction materials and many projects start with the right intentions of using mass timber for a sustainable solution, but inefficiencies through design and pre-construction can result in other materials being chosen. For mass timber to be truly sustainable, buildings need to be built with efficient design solutions that do not over-use timber.

This paper provides an overview of the current fire research that has directly impacted code changes and where there needs to be new applied research and mass timber product development so that high-rise mass timber buildings can move forward as a competitive construction material.

2   BUILDING STABILITY DURING FIRE - EXPECTED BUILDING PERFORMANCE OF MASS TIMBER WHEN EXPOSED TO FIRE

2.1 Primary Structure Fire Resistance

Building primary structural elements are required to perform to an acceptable standard during a fire to enable safe occupant evacuation, prevent fire spread to neighbouring buildings and for firefighters to conduct their search, rescue and extinguishment operations [5]. Model building codes, such as the International Code Council's International Building Code (IBC) [6] provide guidance on the fire protection to the building and structure, based on use, number of occupants, area and height. Low rise buildings of up to three stories have minimal fire protection for the structure. Medium rise buildings are required to have a 60 minute fire resistance rating (FRR), with sprinkler protection and limited in area and use. High-rise buildings that are 22.9m (75ft) or more to the highest occupied floor, require a FRR of 120 minutes to the primary structure, sprinkler protection and many additional fire protection features. For high-rise buildings, the level of protection to the structure is increases such that collapse should be prevented in the event of a fire [7]. The higher fire ratings support the longer occupant evacuation time and fire department intervention. The intent of the fire resistance requirements is for the structure to survive the burnout of a severe, realistic fully developed fire, where the sprinkler protection fails with no water applied, firefighting intervention is not able to occur internally or externally to the building, and the building structure must remain structurally intact for the duration of the fully developed fire [8].

The IBC currently requires high-rise buildings to have non-combustible construction used for the primary structural elements. A high-rise building utilizing mass timber can only be approved by the Authority Having Jurisdiction (AHJ) through an "*alternative materials, design and methods of construction and equipment*" approach to a building permit. From 2021 the IBC will introduce two new categories for mass timber high-rise buildings, a significant change [3].

2.2 Mass Timber Compliance Fire Testing

Where a building element is part of the primary structure and requires a FRR, "standard" fire testing is used to show a proven load-carrying capacity under fire exposure. Standard fire testing is carried out to methods such as ASTM E119 [9] or CAN/ULC-S101 [10]. By passing a standard fire test a manufacturer is providing AHJ's, architects, engineers and contractors with products that are certified for use and meet the requirements of the applicable code.

Engineered timber members such as glulam and laminated veneer lumber (LVL) have calculation methods to determine a FRR provided within codes or guides, such as the NDS [11]. Collective historical standard fire test data has been used to determine conservative correlations for standard fire exposure, using the reduced cross-section method. For CLT, standard fire testing was initially carried out in Europe [12, 13, 14], with additional testing in Canada [15, 16, 17]. By carrying out standard fire tests on panels, data has been gathered and utilised to better understand how panels respond to fire, which can be compared to the results of other engineered timbers, such as glulam. Correlations have been developed to predict the char rate and hence a FRR, for CLT panels, such as those in the CLT Handbook [18]. The CLT Handbook allows designers to assess the fire resistance of panel lay-ups that differ from those fire tested without needing to undertake additional fire testing, based on the pyrolysis fundamentals, but are still yet to be widely accepted by AHJ's. Authorities typically still requiring a manufacturer provided fire test. The correlations for assessing fire resistance are appropriately conservative. The method for assessing fire resistance of CLT panels in North America differs from the European method [19, 20].

2.3 The Reaction to Fire of CLT Panels

When a CLT panel is exposed to the radiative heat flux of a standard fire or a fully developed compartment fire for a duration exceeding 60 minutes, the initial charring behaviour in the first ply is identical to that of sawn timber or glulam of the same density and initial moisture content. As the charring reaches the adhesive line, there are two possible events. Either the charring continues consistently through the adhesive line; or the protective char will dislodge due to lack of adhesive strength under heating, exposing the unburnt wood below, an effect called char fall off. The behaviour of char fall off at the adhesive line when a CLT panel is exposed to fire has been referred to as delamination or char de-bonding [12, 13, 14, 16, 21] (see Fig. 1). When char fall off occurs, the heat insulating function of the char is lost. The unburnt timber below the char then becomes exposed to the heat of the fire and there is a rapid localized increase in the pyrolysis, and hence charring rate. This increased burning occurs until a new char layer is formed, which then insulates the timber and the normal char rate returns. CLT panels located horizontally (underside of floors) are more susceptible to char fall off than panels located vertically (walls).
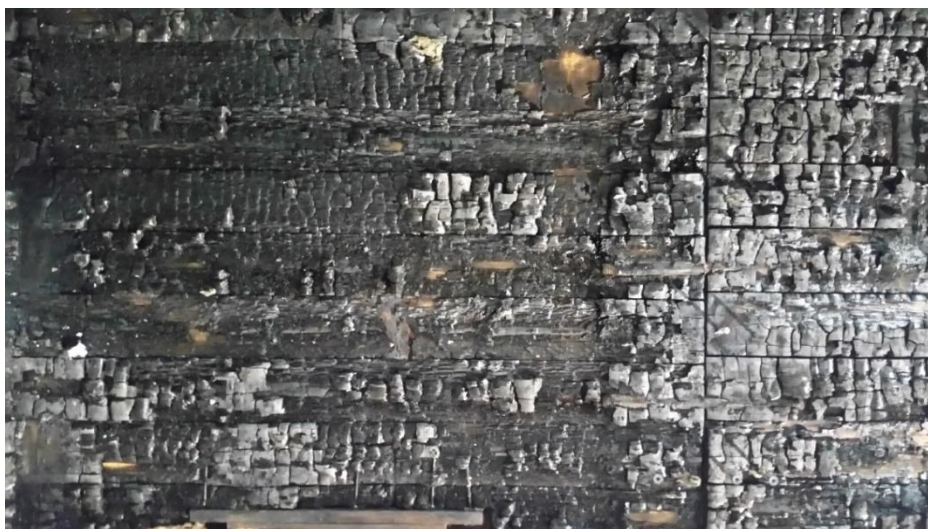
Fig 3: CLT panel that has been fire tested and is showing char fall off

The process of char fall off in CLT has been shown to be adhesive dependent [16, 18, 22, 23]. The impact of adhesives on CLT stability in fire was first investigated by Frangi [22], with testing on a range of polyurethane (PUR) and melamine urea formaldehyde (MUF) adhesives showing that char fall off only occurred in the PUR bonded CLT. Frangi concluded that CLT panel performance in fire is dependent on adhesive type used. Further evidence of adhesive performance impacting char fall off has been shown in the fire testing by Friquin [24], which showed no evidence of char fall off with CLT panels bonded with MUF adhesive. A comprehensive and detailed review of CLT fire testing and the influence of adhesives was completed by Klippel [12]. The instability at the ply interface discussed by Klippel and Frangi is consistent with the findings from Medina [25] and Aguanno [26]. The influence of adhesive type and the relatively consistent result of specific PUR adhesives used for CLT manufacture failing to adhere at temperatures above 200°C (390°F) is the major factor in char fall off.

2.4 Mass Timber Compartment Fire Testing

Standard fire testing of building elements provides limited information on fire performance of a building element. Interactions with the changing fuel and ventilation conditions are not able to be assessed and the standard fire curve does not represent an expected fully developed fire, with a

growth and decay phase. With the motivation to change building codes and provide a path for high-rise mass timber buildings, a number of compartment fire tests, or natural fires, have been completed with mass timber, including exposed CLT. These include tests by ETH [27], VTT [28], Carleton University [25, 29], Delft University of Technology [30], University of Edinburgh [31], SP Norway [32], University of Queensland [33], FPRF [34], ICC [35], Tallinn University of Technology [36] and NRCC [37] (see Fig 2).

Fig 4: CLT compartment fire from the Fire Protection Research Foundation series of tests (undertaken by National Research Council, Canada with RISE, Sweden, at the National Institute of Standards and Technology)

These natural fire tests have shown that a combination of exposed surface area, configuration (orientation of exposed surfaces), reliability of the CLT protection and CLT susceptibility to char fall off can influence fire behaviour and if the compartment fire decays or not. The tests have shown the additional fuel introduced by the exposed mass timber will increase the compartment heat release rate and duration of the fire in the highly unlikely scenario of a fully developed fire.

2.5 Impact of Exposed CLT Surfaces and Fire Decay

In reviewing the compartment tests completed, there are a number that have included partially protected CLT – those by Carleton University, University of Edinburgh, Delft University, FPRF, ICC, Tallinn University of Technology and NRCC. The testing has shown that the area and location of the exposed CLT surfaces will impact the compartment heat release rate (HRR) and HRR decay may be delayed or not occur if there is char fall off in the CLT.

The key consideration for compartment fire decay is that once the all the moveable fuel (fixtures and fittings) within the compartment are consumed by the fire, the heat release rate starts to decay and there is insufficient radiation from the fire to keep the exposed CLT ignited. This decay in the fire occurs even if there is available ventilation, as the fuel and subsequent radiative flux that causes the CLT panels to pyrolyze, has been removed. The decay in HRR will be adversely impacted by CLT char fall off or failure of the mass timber protection (such as fire rated gypsum board).

If char fall off occurs in exposed CLT, unburnt timber is exposed to the fire with a resulting increase in burning rate at the freshly exposed timber, until a new layer of char has formed. Where

the extent of the char fall off is significant, the increase in burning rate can lead to more char fall off and result in another significant growth in HRR, termed a "second flashover" (see Fig. 3). The process of char fall off and fire re-growth is unpredictable and is linked directly to the compartment ventilation and the area of exposed CLT and has been observed in fire tests by Carleton University, SP Norway, University of Edinburgh, FPRF and Tallinn University of Technology.

Fig 5: Regrowth of exposed CLT wall, 1 hr and 57mins through to 2hrs and 14mins into a compartment fire; from FPRF compartment fire test 1-5

Where self-extinguishment occurred, there is typically a single surface exposed or limited areas of mass timber exposed. With a single surface exposed, radiation from the protected surfaces and decaying compartmenting fire is insufficient to maintain pyrolysis of the exposed surface. Char fall off also had a lesser impact and reliability of CLT protection is imperative. Ventilation conditions are also a factor in fire decay but have not been well quantified.

There are cases where self-extinguishment occurred with two opposing or adjacent surfaces exposed. One test carried out by the University of Edinburgh did not show repeatability with fire re-growth occurring the second time the test was carried out. A single test by the University of Queensland was set up with ventilation, fire load and a CLT panel with a thick outer ply to show that under certain specific conditions, self-extinguishment can be shown to occur, provided fire decay occurred before CLT delamination. These test outcomes should be used with caution, rather than a predictor for normal behaviour. Decay also occurred in ICC tests 2 and 3, due to the limited areas of exposed CLT and the relatively high ventilation.

Fire re-growth can also occur when the mass timber protection from board products such as fire rated gypsum starts to fail. Board products are used to protect the mass timber from contributing to the compartment fire. If the board product used fails before the fire has decayed, then the unburnt timber will be ignited, and the compartment fire will re-grow. The specification of the board products to protect the mass timber is important as the timber needs to be kept below the temperature for charring, or it will char behind the board surface and can speed up the time to failure of the board product. There has been little research into the failure of gypsum board products used to protect CLT. Fire test data used for cavity walls with timber studs cannot be used as the basis for gypsum board failure [38].

2.6 Is Fire Decay Possible with Exposed CLT?

If HRR decay does not occur then the building structure is at risk, given that high-rise buildings are required to survive burn-out of a fully developed fire. The conditions for fire decay with exposed CLT have been the focus of recent research [19, 30, 31], which has been aimed at quantifying the conditions for the transition from flaming combustion, to smouldering combustion to extinguishment. Crielaard's work showed that the transition from smouldering to self-extinguishment occurred when received heat flux was below $10kW/m^2$, which correlates well with the piloted ignition of timber, at $12.5kW/m^2$.

Self-extinguishment of the CLT will occur if the conditions for piloted ignition are not present. Thus, if the received radiation at the CLT (or other elements of mass timber) is below $10kW/m^2$, then self-extinguishment can occur. If the CLT experiences char fall off during the transition from flaming combustion through to smouldering combustion, then the exposed unburnt wood can result in fire re-growth. If CLT char fall off is eliminated or mass timber protection is appropriately specified and installed, then fire regrowth can be prevented, and the fire will continue to decay.

3   MASS TIMBER COMPARTMENT FIRE TESTING – GLOBAL INFLUENCE

The compartment testing that has occurred over the last six years has been fundamental in influencing code changes that allow for high-rise mass timber construction. Standard fire testing has shown the impact of PUR adhesives used in the manufacture of CLT, but the full impact of char fall off was not apparent until compartment fire tests provided conclusive evidence of the fire regrowth issue. The importance of these collective fire tests and the applied research completed and published cannot be understated in its importance, particularly with regard to demonstrating the impact of fire regrowth. Increased char rates due to char fall off can be accounted for in design correlations, but fire regrowth from char fall off cannot be predicted. The compartment tests are directly applicable to building construction where mass timber and exposed CLT is used. The tests have shown that CLT with char fall off will significantly impact the fire dynamics. The influence of adhesive on char fall off has resulted in the North American CLT manufacturing standard ANSI / APA PRG-320 [39] being revised to exclude adhesives that can lead to char fall off, from 2021.

By identifying the issues with CLT that is susceptible to char fall off, the fire tests have also shown there is a potential significant benefit to be gained by carrying out large scale CLT compartment tests with CLT that is not susceptible to char fall off. The only tests to date with exposed CLT that does not exhibit char fall off have been the medium scale tests at NRCC [37]. These tests had very encouraging results in showing predictable fire decay. With the market demanding more mass timber is exposed in multi-story and high-rise buildings, the missing link are large scale CLT compartment tests, with CLT exposed that is not susceptible to char fall off.

4   FIRE SAFE DESIGN OF HIGH-RISE MASS TIMBER BUILDINGS

Mass timber compartment fire tests have shown large areas of exposed timber impacts fire size and duration, as the exposed timber provides an additional volume of combustible fuel [40]. If the total combustible fuel within the space (furniture, fixtures and exposed timber) can result in a fire that releases more energy than the primary structure can resist, this may result in localized failure. Understanding the compartment fire is key to determining accurate char rate and char depth for the mass timber, so structural capacity can be assessed. This becomes difficult, or impossible, when the compartment fire is impacted by the unpredictable behaviour of CLT char fall off. A combination

of exposed surface area, configuration, reliability of CLT protection, compartment ventilation and CLT susceptibility for char fall off, are critical parameters that influence the predictability of the compartment HRR, so that structural capacity can be determined. These factors also determine whether a compartment fire decays, or not.

4.1 Hazard and Consequence Based Approach to Fire Safety of High-Rise Mass Timber

To determine appropriate fire safety for a mass timber building an approach based on height, fire protection and area of exposed timber can be used. First proposed by Buchanan, Frangi and Östman [41], and further developed by Buchanan [42], the methodology is based on examining the fundamentals of building height, use and area of exposed mass timber, and providing appropriate fire safety measures (see Fig 4). This includes combinations of active measures, fire resistance ratings and additional measures to improve the reliability of sprinkler protection.

The decision-making process will be informed by the extent of mass timber that can be exposed and whether the CLT being used has char fall off or not. Where the CLT has char fall off, then decisions on protection of the CLT become very important.

Height	Low-rise	Mid-rise	Tall	Very tall	High-rise
Storeys	1-2	3-5	6-8	9-15	>15
Likely escape	Quick escape	Slow escape	Assisted escape	Assisted escape	Difficult escape
No sprinklers	Local areas exposed	No exposed wood	Not allowed	Not allowed	Not allowed
Normal sprinklers	Large areas exposed	Local areas exposed	No exposed wood	Full encapsulation	Full encapsulation
Special sprinklers	Large areas exposed	Large areas exposed	Local areas exposed	No exposed wood	Full encapsulation

Fig 6: Table replicated from Buchanan showing fire protection based on building height and area of mass timber exposed (for full description, see Buchanan)

4.2 Compartment Model Development

Another step in the progression of efficient engineering for the fire safety of mass timber buildings will be the development of correlations for compartment fire dynamics, where mass timber is exposed. These correlations will most likely be based on adapting current correlations or proving that existing models are appropriate. Determining the fire performance of exposed mass timber is not a new issue, but with the greater use of CLT and the desire for walls, underside of floors, or both to be exposed, existing models are being re-evaluated. There is a limited area of exposed timber that is always going to be acceptable within a compartment, as it won't significantly impact the compartment fire. But there is also a limit to how much timber can be exposed before the mass timber significantly increases the HRR and duration of the fire.

For an exposed mass timber structure, the fundamental basis of proving an FRR is by members being increased in area to resist the expected heat release rate and the fire duration (reduced area method [11]). But increasing the sectional area also introduces combustible fuel to the compartment. As designers are asked to consider large areas of mass timber, the FRR to be provided by the exposed load-bearing timber structure needs to be determined to include the combustible fuel introduced by the structure itself. Hence, an approach based on fundamental compartment fire dynamics needs to be used to determine the maximum amount of energy released

by the fully developed fire. In doing so, the energy released by the fully developed fire can be assessed against the capacity of the constructed building elements. A constant char rate cannot be used given the complexities of the compartment fire with a combustible structure.

The predictive analysis of the compartment fire cannot be accurately and conservatively determined when char fall off occurs and therefore, char rate and depth cannot be determined for structural capacity. Until a predictive model of CLT char fall off and resultant impact on the compartment fire is developed, modelling compartment fire behaviour should be undertaken with an abundance of caution, if at all. The most appropriate solution is to utilize CLT that does not result in char fall off.

5   WHERE TO NEXT FOR MASS TIMBER SUPPLY? AREAS FOR FURTHER RESEARCH AND PRODUCT TESTING

With codes changing, high-rise mass timber buildings will be easier to construct, typically based on a load bearing structure with an FRR of 120 minutes. Unfortunately, when architects, engineers and contractors want to design and specify 120 minute rated construction, there are inefficiencies. Product supply gaps can be engineered around and do not prevent a building from being designed, approved and constructed. But the solutions are not efficient and will be over-designed, leading to increased construction costs, making mass timber less competitive and slowing down efficient construction. There are several areas where further research is warranted and needed.

Compartment ventilation and fire re-growth: Compartments with higher ventilation may not result in fire re-growth, as seen in FPRF tests [34]. Further work is needed to provide conclusive results on the link between ventilation factor, area of exposed CLT and regrowth.

Glulam char rate with PUR adhesives: Many glulam manufacturers are changing from MF adhesives to PUR adhesives. Fire testing for glulam has not been based on the new PUR adhesives. The change in adhesives may have no significant change to the assumed glulam char rate, but there is no data to prove or disprove a change to the historical char rate.

Beam to Column connectors: Glulam and LVL beam to column and column to column connection FRR's are not well proven. Tests with connectors that contractors want to construct with and testing elements under actual building load conditions is needed.

Exterior walls with load-bearing CLT: If CLT is protected behind fire rated gypsum boards, it can be used as an exterior wall element. Mass timber should not be exposed on a building exterior, given the vertical fire spread issues. There are few tests to show that CLT can be used as a load-bearing exterior wall if detailed correctly to protect the timber and prevent vertical fire spread.

Vertical fire spread via windows where CLT is exposed within a compartment: Fire spread via unprotected windows up the exterior of a building wall is a complex fire safety issue. The impact of exposed CLT within a compartment on flame extension and heat flux above the window has very limited research to date. Full-scale fire testing is required to determine flame dimensions and temperature for a compartment with large areas of exposed interior CLT, to understand if there are any differences in radiative heat flux, compared with a compartment of non-combustible structure.

Penetration and joint fire rated seals: Globally there is a shortage of solutions for mass timber construction where there are edge joints that need a fire seal or penetrations through mass timber as part of a fire separation. This impacts buildings with FRR's of 60, 90 and 120 minutes.

Mass timber protection solutions: Reliable protection solutions are needed that prevent mass timber from forming part of the combustible load in a compartment by preventing charring for the full duration of a fire. Boards and sprays are possible solutions. Specifications are needed for designers and AHJ's so when mass timber is required to be protected, it stays protected and does not char.

Compartment fire tests with non-residential fire loads: Compartment fire tests have been completed with fire loads representative of residential uses. The fire loads have often been very conservatively assessed and many tests have loads in the order 550MJ/m^2. The influence of typical office fire loads will be an important area of further research, to confirm current modelling for fire duration periods.

Practical definition of fire self-extinguishment: The term is regularly used in research and fire testing and is defined through a rate of mass loss or a critical heat flux. For building engineering, fires are normally defined by HRR and more work is required to link current research on CLT panel self-extinguishment and compartment fire size.

6   CONCLUSIONS

Mass timber construction is becoming more prevalent globally, as sustainable construction is seen as being an imperative for current and future cities. There has been a significant investment in research and testing to allow mass timber to be a main stream construction material and the changes to date have been very positive. The change in building codes that permit high-rise mass timber buildings has been relatively fast and solutions in research, engineering, building supply and construction are still being developed for efficient construction, in response to demands from building developers, building owners and design architects.

Fire safety of mass timber buildings continues to grow and develop as the market demands more of the mass timber is exposed within high-rise buildings. The work to date to understand the impact of CLT char fall off has been substantial, and the work is not complete. In North America, the change to the CLT manufacturing standard to eliminate CLT that is susceptible to char fall off is a positive change that allows for greater predictability in engineering modelling and potentially towards future code amendments permitting more mass timber to be exposed for some high-rise buildings.

REFERENCES

[1] WoodSolutions, 2016 "Fire Safety Design of Mid-rise Timber Buildings - Basis for the 2016 changes to the National Construction Code" Technical Design Guide issued by Forest and Wood Products Australia

[2] https://www.nrc-cnrc.gc.ca/eng/solutions/advisory/codes_centre/public_review/2017.html

[3] https://www.awc.org/news/2018/12/19/awc-tall-mass-timber-code-changes-get-final-approval

[4] Östman, B., Schmid, J., Klippel, M., Just, A., Werther, N., Brandon, D., 2018, "Fire Design of CLT in Europe", Wood and Fiber Science, Vol 50 Special issue (https://wfs.swst.org/index.php/wfs/article/view/2650)

[5] Custer R., and Meacham B., 1997, "Introduction to Performance-Based Fire Safety" Society of Fire Protection Engineers

[6] International Code Council, 2018, "International Building Code"

[7] American Society of Civil Engineers, 2016, "ASCE/SEI 7-16, Minimum Design Loads for Buildings and Other Structures"

[8] Department of Commerce, 1942, "Building Materials and Structures, Report BMS92, Fire Resistance Classification of Structures", National Bureau of Standards, Report of Sub-committee on Fire Resistance Classifications of Central Housing Committee on Research, Design and Construction

[9] American Society for Testing and Materials, 2016, "ASTM E119: Standard Test Methods for Fire Tests of Building Construction and Materials"

[10] Standards Council of Canada, 2007, "CAN/ULC-S101-07 Standard Methods of Fire Endurance Tests of Building Construction and Materials"

[11] American Wood Council, 2015, "National Design Specification for Wood Construction", Leesburg, Virginia

[12] Klippel, M., 2014, "Fire safety of bonded structural timber elements", ETH Zurich, Institute of Structural Engineering, Thesis Number 359

[13] Frangi, A., Fontana, M., Knobloch, M., Bochicchio, G., 2008, "Fire Behaviour of Cross-Laminated Solid Timber Panels". Zurich, Switzerland: Institute of Structural Engineering, ETH Zurich.

[14] Klippel, M., Fahmi, R., 2017, "COST Action FP 1404: Expert Meeting CLT, The way to standardization – definition of gaps, (joint meeting WG1/TG4 and WG2/TG1)", ETH Zurich

[15] Osborne, L., Dagenais, C., Benichou, N., 2012, "Preliminary CLT Fire Resistance Testing Report", FPInnovations and NRC-CNRC, Project No. 301006155

[16] Craft, S.T., Desjardins, R., Mehaffey, J., 2011, "Investigation of the Behaviour of CLT Panels Exposed to Fire", Proceedings of the Twelfth International Conference Fire and Materials.

[17] Embury-Williams, L., Karacabeyli, E., 2009, "Application of Analysis Tools from NEWBuildS Research Network in Design of a High-Rise Wood Building", NSERC Strategic Research Network on Innovative Wood Products and Building Systems (NEWBuildS) in Partnership with FPInnovations

[18] Karacabeyli E., Douglas B., 2013, "CLT Handbook, US Edition" FPInnovations SP529-E

[19] Klippel, M., Schmid, J., Frangi, A., 2016, "Fire Design of CLT", paper submitted for joint event of COST Actions FP1402 and FP1404, KTH Stockholm

[20] Klippel, M., Schmid, J., 2017, "Design of Cross-Laminated Timber in Fire", Structural Engineering International Nr. 2/2017

[21] Aguanno, M., 2013, "Fire Resistance Tests on Cross-Laminated Timber Floor Panels: An Experimental and Numerical Analysis". Dept of Civil and Environmental Engineering, Carleton University, Ottawa, Canada

[22] Frangi, A., Fontana, M., Hugi, E., Jobstl, R., 2009 "Experimental analysis of cross-laminated timber panels in fire", Fire Safety Journal 44 pp 1078-1087

[23] Hasburgh, L., Bourne, K., Peralta, P., Mitchell, P., Schiff, S., Pang, W., 2016 "Effect of Adhesives and Ply Configuration on The Fire Performance of Southern Pine Cross-Laminated Timber", Proceedings from the World Conference of Timber Engineering, August 22-25, Vienna

[24] Friquin, K., Grimsbu, M., Hovde, P., 2010 "Charring Rates for Cross Laminated Timber Panels Exposed to Standard and Parametric Fires", Proceedings World Conference on Timber Engineering,

[25] Medina-Hevia, A., "Fire Resistance of Partially Protected CLT Rooms', Thesis, Carleton University, 2014

[26] Aguanno, M., "Fire Resistance Tests on Cross-Laminated Timber Floor Panels: An Experimental and Numerical Analysis", Thesis, Carleton University, 2013

[27] Frangi, A., Bochicchio, G., Ceccotti, A., 2008 "Natural Full-Scale Fire Test on a 3-Storey XLam Timber Building", Fire Safety Science–Proceedings of The Ninth International Symposium, pp. 1279-1290

[28] Hakkarainen, T., 2002, "Post-Flashover Fires in Light and Heavy Timber Construction Compartments" Journal of Fire Sciences pp 133-175

[29] McGregor, C., 2013, "Contribution of Cross Laminated Timber Panels to Room Fires", Thesis, Carleton University

[30]   Crielaard, R., 2015, "Self-Extinguishment of Cross-Laminated Timber", Thesis, Delft University of Technology, Netherlands

[31]   Hadden, R., Bartlett, A., Hidalgo, J., Santamaria, S., Wiesner, F., Bisby, L., Deeny S., Lane, B., 2017, "Effects of Exposed Engineered Timber on Compartment Fire Dynamics", Proceedings of the 12th International Association of Fire Safety Science Symposium, Lund, June 10 to 16

[32]   Hox, K., et al, 2015, "Branntest av massivtre" SP Fire Research, Report A15301 (in Norwegian, translated by Arup)

[33]   Emberley, R., Gorska C., Bolanosa, A., Lucherinia, A., Solartea, A., Soriguera, D., Gutierrez, M., Humphreys, K., Hidalgoa, J., Maluka, C., Law, A., Torero, J., 2017, "Description of Small and Large-scale Cross Laminated Timber Fire Tests", Fire Safety Journal 91, pp 327–335

[34]   Su, J., LaFrance, P., Hoehler, M., Bundy, M., 2018, "Fire Safety Challenges of Tall Wood Buildings – Phase 2: Task 2 & 3 Cross Laminated Timber Compartment Fire Tests" Fire Protection Research Foundation, Report No. FPRF-2018-01

[35]   Zelinka, S., Hasburgh, L., Bourne, K., Tucholski, D., Ouellette, J., 2018, "Compartment Fire Testing of a Two-Story Mass Timber Building" General Technical Report FPL–GTR–247, May 2018

[36]   Just, A., Brandon, D., Nele Mäger, K., Pukk, R., Sjöström, J., Kahl, F., 2018 "CLT Compartment Fire Test", Proceedings of World Conference on Timber Engineering, August 20-22, 2018, Seoul.

[37]   Su, J., Leroux, P., Lafrance, P., Berzins, R., Gratton, K., Gibbs, E., Weinfurter, M., 2018, "Fire Testing of Rooms with Exposed Wood Surfaces in Encapsulated Mass Timber Construction", National Research Council, Canada Report No. A1-012710.1

[38]   Just, A., Mäger, K., Kraudok, K., 2018, "CLT protected by gypsum boards. Design models", COST FP1404 WG2 TG1 meeting, 4-5 July 2018 Vienna.

[39]   ANSI / APA, 2015 "PRG-320 Standard for Performance-Rated Cross-Laminated Timber"

[40]   Barber, D., Crielaard, R., Li, X., 2016, "Towards Fire Safe Design of Exposed Timber in Tall Timber Buildings", Proceedings of the World Conference of Timber Engineering, Vienna, 22nd – 25th August 2016

[41]   Buchanan, A., Östman, B., Frangi, A., "White Paper - Fire Resistance of Timber Structures, A Report for the National Institute of Standards and Technology", Draft report 31 March 2014

[42]   Buchanan, A., 2015, "Fire resistance of multi-storey timber buildings", Invited keynote lecture, The 10th Asia-Oceania

FIRE DESIGN OF STRUCTURES ACCORDING TO EUROCODES

João Paulo Correia Rodrigues
Coimbra University, Portugal

ABSTRACT

The fire design of structures with Eurocodes can be achieved not only by experimental tests but also by tabulated data, simplified calculation methods and advanced calculation methods. Whilst the experimental tests and the simplified calculation methods are more dedicated to single elements, the advanced calculation methods can be used for single elements, parts of structure or the whole structure. The advanced calculation methods are in this case more accurate because they can take into account with the interaction between the elements subjected to fire and the surrounding structure. This paper aims to give an overview of the parts of Eurocodes related to fire design, the actual situation and the future developments for the new generation. It will be presented the different methods with a critical analysis about their accuracy, state of development and ways of improvement. The aspects foresee for the new generation of the parts of Eurocodes related to fire design are also presented and discussed in this paper. The limitations that will continue to exist in the fire parts are also discussed for a possible evolution of the Eurocodes.

Keywords: fire, structure, design, Eurocodes, modelling

1 INTRODUCTION

The parts of Eurocodes related to fire design have started to be developed in the 90 's. At that time were set up committees of experts in Europe which had the responsibility to produce these parts for Eurocodes. These parts were a compilation of existing fire design methods and had the objective to harmonize the structural design in Europe.

The documents have been developed and passed to final versions that were published as Euronorms over the last decades. At the moment, all parts of fire design of Eurocodes and documents with them related are already published: EN 1990 (2002); EN 1991-1.2 (2002); EN 1992-1.2 (2004); EN 1993-1.2 (2005); EN 1994-1.2 (2005); EN 1995-1.2 (2004); EN 1996-1.2 (2005); EN 1999-1.2 (2007). In parallel with this action, the various Member States of the European Union (EU) began to translate these documents for their own languages and issuing them as National Standards. The National Annexes were also drawn up and published along with the Eurocodes. The National Annexes are documents, where are defined the parameters and coefficients set out in the Eurocodes that were left open for choice by each Member State, as well as the applicability of the Informative Annexes or Explanatory Parts of these documents.

The fire design parts of the Structural Eurocodes allow different ways of verification of the fire resistance of structures. So the verification can be carried out for single elements, parts of structure or the entire structure. The verification is performed by experimental tests, usually following ISO 834 standard fire curve, but can be performed by tabulated values, simplified or advanced calculation methods. While the experimental tests, tabulated data and simplified calculation methods are mainly for single elements, the advanced calculation methods can be used for single elements, parts of structures or, and here is the great advantage of these in relation to the others, to the entire structure (*Fig. 1*).

Most of the structural elements of different materials are nowadays tested as parts of structure, starting a trend in Europe to test new situations. This new way of testing allows taking into account the interaction between the elements and the surrounding cold structure. Some European groups have tried to equip their Labs with experimental means for studying parts of structure. In this we can refer the existing test system at the *Bundesanstalt für Materialforschung -und prüfung* (BAM), in Berlin, Germany and more recently the system built at the *Centre Scientifique et Technique du Bâtiment* (CSTB), in Marne-la-Vallée, France.

At the moment the fire design parts of Eurocodes are in reformulation for incorporating new methods resulting from the research carried out in Europe in the recent years. These parts are belonging to the second generation of the Eurocodes which is currently in preparation. This new generation, in addition to the improvement of existing Eurocodes, will create two new Eurocodes, one on Structural Glass and another on the Assessment and Strengthening of Existing Structures.
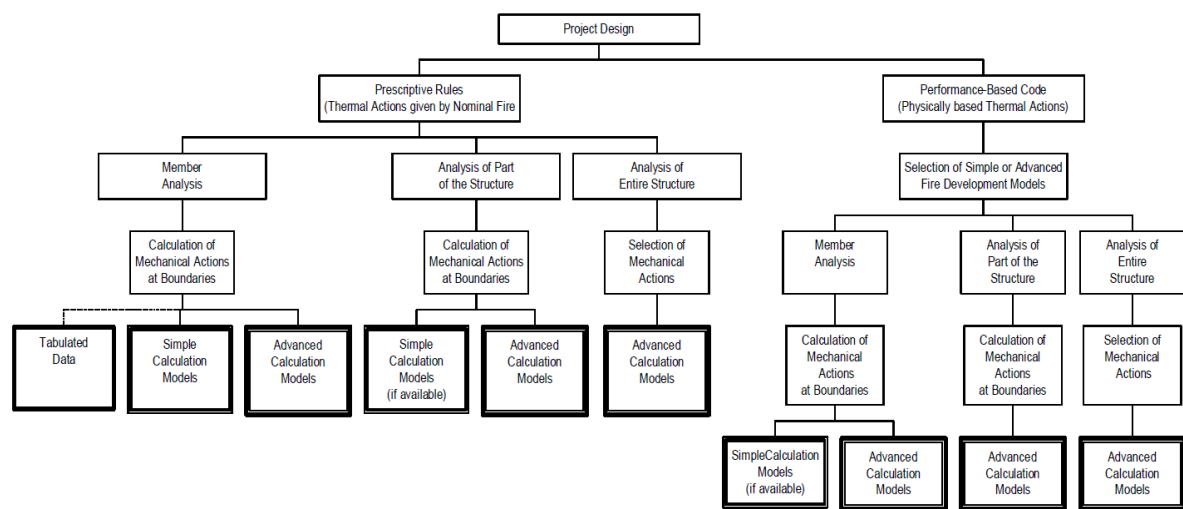
Fig. 1 – Design Procedure according to Eurocodes

In this paper it will be discussed the different parts of Eurocodes for fire design of structures. It will be presented the different verification ways and the fire design methods of structures. It will be also made a critical analysis to the current methods and a discussion of the future perspectives of development.

2 CURRENT FIRE PARTS OF EUROCODES

2.1 Eurocode 0 (EN 1990:2002)

The EN 1990:2002, known by many as Eurocode 0, is a standard where is presented and established the bases of calculation used in the different parts of the Structural Eurocodes (EN 1991-1.1:2002, EN 1992-1.1:2004, EN 1993-1.1:2005, EN 1994-1.1:2004, EN 1995-1.1:2004, EN 1996-1.1:2005, EN 1999-1.1:2007). This standard is applied across to all Eurocodes including their parts of fire design of structures.

In this standard, it is indicated that the structural analysis must be based on calculating fire scenarios (EN 1991-1.2:2004) and should consider models of evolution of temperature in the structure, as well as models of mechanical behavior at high temperatures. The performance criteria, required for a structure subject to fire, can be verified by an analysis of the whole structure, parts of

structures or single elements using the calculation methods or by tabulated data or test results. The fire behavior of a structure should be assessed taking into account the exposure to a nominal fire or the parametric fire curve including respective accompanying actions.

The structural behavior at high temperatures should be evaluated according to parts 1.2 of EN 1992 to EN 1996 and EN 1999 using thermal and structural models. The thermal models are based on the assumption of a uniform or non-uniform temperature along the transversal section and longitudinal direction of the elements. These models can be used for an analysis of single elements or considering their interaction with the surrounding structure during fire exposure.

2.2 Eurocode 1 part 1.2 (EN 1991-1.2:2002)

The Eurocode 1 part 1.2 (EN 1991:1.2:2002) presents methods for assessing the actions in case of fire. In this document they are provided two types of actions. The thermal actions for an analysis in terms of temperature and the mechanical actions for a structural analysis. With regard to the mechanical actions they are represented by the combination of accidental actions. With regard to the thermal actions they are defined in terms of a heat flux density incident on the surface of the element and is composed by two terms, one due to radiation and another due to convection.

For the characterization of the thermal actions it shall be determined the temperature of the gas in the vicinity of the element exposed to fire. This temperature can be calculated by the nominal fire curves or by natural fire models. The **nominal fire curves** foreseen in EN 1991-1.2 are: the standard fire curve (ISO 834); the external fire curve and the hydrocarbon fire curve.

With regard to the **natural fire models**, they are divided in simplified fire models (parametric fire curves and localized fire models) and advanced fire models (models of one zone; models of two zones and computational fluid dynamics models (CFD)).

2.3 Eurocode 2 part 1.2 (EN 1992-1.2:2004)

The EN 1992-1.2:2004 indicates that the fire safety of concrete structures can be made by tabulated data, simplified calculation methods or advanced calculation methods.

The application of the **tabulated data method** is the easiest and most intuitive way of verifying the fire safety of a structural member, however it is a quite conservative method. In EN 1992-1.2:2004, they are presented tabulated data for columns (methods A and B), simply supported and continuous beams, simply supported and continuous massive slabs, flat and ribbed slabs and walls with or without loadbearing function.

The EN 1992-1-2:2004 presents also two **simplified calculation methods** for verification of the fire safety of concrete structures. These are the 500°C isotherm method and zone method that are based on reducing the concrete area to a residual that effectively contributes to the loadbearing capacity of the element. Both simplified calculation methods are applicable to reinforced and pre-stressed concrete elements subjected to axial stresses, bending moments or any combination of those.

2.4 Eurocode 3 part 1.2 (EN 1993-1.2:2005)

The EN 1993-1.2:2005 is intended for verifying the fire safety of steel structures. This check is made by simplified or advanced calculation methods and does not exist tabulated data. The analyses can be made for single elements, parts of structure or the entire structure.

The EN 1993-1.2:2005 provides a set of simplified calculation methods for verifying the strength of the sections. These methods are similar to those used for ambient temperature but in this case the yield strength of the steel is affected by a reduction coefficient dependent of the steel temperature. The steel temperature can be determined by a simplified method existing in EN 1993-1.2:2005 and

further mentioned or by an advanced calculation method. So there are methods for members in tension; in compression with cross sections of class 1, 2 or 3; in bending with cross sections of class 1 and 2 or 3 in which the lateral buckling is not a relevant buckling mode; in bending with cross sections of class 1 and 2 or 3 in which the lateral buckling is a relevant buckling mode; in shear with cross sections of class 1 and 2 or 3; subjected to bending and compression with cross sections of class 1 and 2 or 3.

In EN 1993-1.2:2005, it is also indicated a simplified calculation method for verifying the safety of a steel member by limiting its temperature. This is known as critical temperature method and is an extremely simple way of verification of fire safety of steel structures. The structure will be safe, in case of fire, if the temperature of its elements do not exceed a certain limit value calculated according to the type of element.

In this Eurocode they are still presented two important methods for determining the evolution of temperature in protected and unprotected steel members. These methods of simple use give values very close to the reality, as already demonstrated in experimental tests and numerical simulations. The thermal properties of the fire protection materials, such as the thermal conductivity and specific heat, have influence on the evolution of temperatures in the section. The degree of moisture of these materials that obviously cause a delay in the heating of the steel section can be determined by the provisions of ENV 13381-4:2002.

Finally, in what concerns to the joints, these are in general the strongest part of a structure and normally does not enter in collapse before the beam or the column. However, the Annex D of EN 1993-1.2:2005, presents a methodology for calculating the fire resistance of bolted and welded steel joints. The methods presented are based in the ones of EN1993-1.8:2005 but taking into account the effect of the temperature by a reducing coefficient for the strength of the bolts in tension, shear or bending and for the welding. The strength of the various parts of the joint depends on their temperature and are calculated in a simplified way.

2.5 Eurocode 4 part 1.2 (EN1994-1.2:2005)

The EN 1994-1.2:2005 is dedicated to the verification of fire resistance of composite steel-concrete elements. This verification can be made by tabulated data, simplified calculation or advanced calculation methods.

In what concerns to the **tabulated data** they are presented tables for **composite beams comprising a steel beam with partial concrete encasement, composite columns made of totally encased steel sections, composite columns made of partially encased steel sections** or **composite columns made of concrete filled hollow sections**;

With regard to the **simplified calculation methods** they are presented **fire design rules for composite slabs and beams**. It is presented in Annex E a **simplified method for calculating moments on a steel beam connected to a concrete slab**.

As regards to the **shear strength of connectors** it is presented a fire design method for the stud shear connectors. None is presented for other type of connectors.

In Annex F it is presented a **model for calculating the sagging and hogging moment resistances of a partially encased steel beam connected to a concrete slab and exposed to fire beneath the concrete slab according to the standard temperature-time curve**. This is a very good model that has been showing good results on the design of this type of beams.

In Annex G it is presented a **model for calculating the fire resistance of composite columns made with partially encased steel sections, for bending around the weak axis, exposed to fire all around the column according to the standard temperature-time curve**.

Finally, in Annex H it is presented a **simple calculation model for concrete filled hollow sections exposed to fire all around the column according to the standard temperature-time curve**. This model is considered unsafe all over Europe specially for slender columns.

2.6 Eurocode 5 part 1.2 (EN 1995-1.2:2004)

The timber structures are in general known as having enhanced fire resistance when compared to other types of structures. This happens because timber has a low heat conductivity, a large amount of moisture that will slow down the heating and burning will produced a charred layer that still has a lower thermal conductivity and with this protecting the residual cross-section of the timber element. The joints will be even the most critical part of timber structures in a fire, due to the type of connectors, the lower fire protection in the screw joints or the vitrifying of the adhesive in glued joints.

The verification of fire safety in this Eurocode is made using simplified calculation or advanced calculation methods in the absence of tabulated data. The **simplified calculation methods** are based on the change of mechanical properties with temperature or on the reduction of the section by charring of the timber. The **advanced calculation methods** are based on the direct application of the concept of temperature profile and the similar concept of moisture content profile. Tracing these profiles in the cross section and knowing the relationship between the mechanical properties with the temperature and/or moisture, it is possible to determine the distribution of stiffness and strength in the section.

Unlike other materials the consideration of the variation of properties with temperature is done in a different way. In this case they are used calculation values for the strength and stiffness properties of the timber in function of the temperature that depend of the quantile of 20% of the respective property of strength or stiffness at ambient temperature, affected by a modification coefficient for the fire situation.

The timber when burning will form an outer charred layer. The thickness of this charred layer must be taken into account for all surfaces of timber and timber-based panels that are directly exposed to fire and, when appropriate, for initially fire protected surfaces where the charring of the timber occurs during a relevant fire exposure time. The charring depth will depend on a charring rate that depends on the timber spicy and density.

This Eurocode presents two **simplified calculation methods** for assessing the strength. The **method of the reduced cross-section** and the **method of reduced mechanical properties**. The **method of the reduced cross-section** is of very simple resolution and perhaps this is why it is the recommended by EN1995-1.2:2004. As regards the **method of reduced properties**, as its name implies, they are reduced the strength properties of the timber. According to EN 1995-1.2:2004, this method should only be used for elements of resinous timber, with three or four sides exposed to fire for rectangular cross-sections, or with all the perimeter exposed to fire for circular cross-sections.

The **joints** are important parts of timber structures in case of fire. In this part of Eurocode 5, they are defined the joints between elements subjected to the standard fire exposure, for fire resistances of not more than 60 minutes. The rules presented are valid for joints made with nails, screws, bolts, nail plates, fasteners and toothed plates.

The Eurocode presents methods for protected and unprotected joints. For unprotected joints there are a set of tabulated data of fire resistance, according to the type of connector, but not exceeding 30 minutes. This resistance can be increased if the height and width of the side elements are increased, thus increasing the distance from the connector to the sides.

In relation to the protected joints, by timber panels, timber-based panels or gypsum-based boards, there are expressions for determining the time of onset of charring.

There are also expressions for calculating the fire resistance of joints with internal and external steel plates referring EN 1995-1.2:2004 for the case of joints with external steel plates, when not protected, they should be adopted the fire design methods of EN1993-1.2:2005, which does not seem a good solution.

2.7 Eurocode 6 part 1.2 (EN1996-1.2:2005)

The masonry structures are known to have an enhanced fire behavior when compared with those of other materials. The weak part is the seating joints that can be damaged in case of fire. The verification of the fire resistance can be made by tabulated data, mostly, a simplified calculation or advanced calculation methods.

This part of the Eurocode begins by presenting the different types of walls: internal walls without loadbearing function; external walls without loadbearing function; internal walls with loadbearing and with or without partitioning functions; external walls with loadbearing and with or without partitioning functions.

The tabulated data indicated in EN 1996-1.2:2005 refers to the minimum thicknesses of the different types of walls so that comply with certain fire resistance class. These are indicated according to the type of masonry and mechanical characteristics of their seating joint in cement mortar, mainly on the loadbearing capacity walls.

The simplified calculation method indicated in EN 1996-1.2:2005 is very similar to the method of the reduced cross-section used for timber in EN 1995-1.2:2004. After considering a damaged zone, the residual internal core is considered for the calculation of the loadbearing capacity of the element as at ambient temperature according to the precepts of EN 1996-1.1:2005.

2.8 Eurocode 9 part 1.2 (EN1999-1.2:2007)

The EN 1999-1.2:2007 describes the principles and rules for the fire design of aluminium and its alloys structures.

As defined in part 1-2 of the other structural Eurocodes, the fire design of aluminum and its alloys structures, can be performed by simplified calculation methods (single elements and parts of structure) or advanced calculation methods (single elements, parts of structure or the whole structure) or by experimental tests.

In relation to the **simplified calculation methods** there are methods of resistance and methods for determining the evolution of temperatures in protected and non-protected elements. These methods are very similar to those considered in EN 1993-1.2:2005 for steel structures but obviously there are differences in the variation of the mechanical and thermal properties of the aluminum and its alloys with temperature. As methods of this type it exists the ones for elements in tension, bending, compression and compression and bending.

3 IMPROVEMENTS AND LIMITATIONS OF THE FIRE PARTS OF EUROCODES

The European Commission issued in 2015 a Mandate for amending the existing Eurocodes and extending the scope of the Structural Eurocodes (M/515). This Mandate have a duration of 5 years until 2020 by which time they should be submitted the final documents of the new generation of the Structural Eurocodes. The essential aspects that were set in response to the Mandate M/515 were:

Reduction of the number of Determined Parameters at National Level;

Improve the use of the Eurocodes by clarification, when necessary; simplification of calculation rules; limitation, when possible, to the inclusion of alternative calculation rules and; non-inclusion or removal of rules of reduced practical use in project.

Creation of two **new Eurocodes**, one on **Structural Glass** and another on **Assessment and Strengthening of Existing Structures.**

3.1 Eurocode 1 part 1.2 (EN 1991-1.2)

The new version of this Eurocode will have improvements in Heskestad method for calculating, in a localized fire, the temperatures in more points than the ones along the vertical axis of the flame. In the method for determining the fire load density there will be also changes in the various partial parameters ranging from the type of occupancy to the active measures of fire safety that are part of the formula.

However, it is considered that these changes will not be enough and it should be introduced more values for the fire load density (Table E.4) and fire growth rates (Table E.5) for more occupancies, such as for industrial buildings. This would have to be achieved by a rigorous survey of the fire loads by use-type throughout Europe. Apart from this fact, the introduction of combustion factors for other materials that not only for the cellulose ones it is also very important for the determination of the thermal action on structures.

3.2 Eurocode 2 part 1.2 (EN 1992-1.2)

The concrete structures are known as having an enhanced fire behavior and this is certainly a reason why research in this area is still not too much. In the next generation of Eurocodes they are foreseen a few changes. These include new formulations for verifying the fire resistance of **columns belonging to unbraced concrete structures**. Another aspect is related to the robustness considering the **global behavior** of the structure. It will be also considered properties for the **concrete on the cooling phase**, mainly for using with the advanced calculation methods.

Another aspect that has generated a lot of discussion at European level is the curve for the thermal conductivity to consider in each case. So there is a need for harmonization in Europe about this topic and also as regards to the thermal properties in general between Eurocodes 2 and 4.

Nothing is foreseen about changes in the tabulated data or simplified calculation methods, however it is believed that in relation to the tabulated data method there should be a differentiation between the application to square and circular columns, namely there should be separate tables for each of these columns because the shape of the cross-section certainly has influence on the covering thickness of steel reinforcement.

A possible abolition of the 500ºC isothermal method should be also considered since it is less rigorous when compared with the zone method.

Another aspect still unclear, despite several research works that have already existed, is the spalling effect in concrete structures. This effect is not yet taken into account in the simplified calculation methods and is deficiently taken into account in the advanced calculation methods.

The stiffness of the surrounding structure is also not yet considered in the simplified calculation methods and this is a parameter which influences the fire resistance. The effect of this stiffness may have in cases of slender structures a negative influence on the fire resistance.

There are some studies that criticize the way of calculating the buckling length of columns in case of fire saying that the procedure is not on the safe side for some structures and that would be better to calculate this as for ambient temperature.

The shear failure is an extremely critical factor in reinforced concrete flat slabs. This phenomenon will certainly be aggravated in a fire situation and surely requires more research for mitigating it and needs the development of new fire design methods and construction solutions.

3.3 Eurocode 3 part 1.2 (EN 1993-1.2)

Most of the research is on steel structures because these when not well design have a poor fire behavior. So this is a type of structure still need many studies and development of new fire design methods. The next generation of Eurocode 3 will have a lot of changes including is parte 1.2.

As the first time they will be provided new **properties for the cooling phase**.

Another aspect is related to the **buckling length of columns** belonging to unbraced frames. This buckling length should be determined as for ambient temperature.

It will still be introduced detailed information about **geometric imperfections** on the buckling modes and **residual stresses** at the materials level for being used with the advanced calculation methods. For the residual stresses it will be made a distinction between the hot-rolled and welded sections.

Another change is the improvement of the **lateral buckling curves** in order to take into account the influence of the loading type.

The introduction of calculation rules for **stainless steel** distinct of the **carbon steel** will be one of the novelties of the next generation of part 1.2 of Eurocode 3.

New rules will be also introduced on verifying the fire resistance of **slender cross sections (class 4).**

The introduction of calculation rules for **profiles of variable inertia** will be also one of the novelties.

The **cellular beams** will have the introduction of new fire design rules resulting from the research carried out in the last years mainly in UK.

It should also be added in the new generation of Eurocodes, the fire behavior of **high-strength steels**. Currently the rules for verifying the fire safety set out in part 1.2 of Eurocode 3 are valid only for S460 steels or of inferior grade.

The verification of the **shear resistance** of steel beams will be also introduced in the new generation of Eurocodes.

The **cold-formed steel elements** will have also new fire design methods because the currently were based on the hot-rolled ones, using the mechanical and thermal properties of these but limiting the temperature to 350°C (EN1993-1.3: 2006).

However, it is considered that there is still a trek to cross in the development of this part of Eurocode and changes can still be higher in the future. One of the points is with the introduction of the influence of the stiffness of the surrounding structure on the simplified calculation methods for beams and columns. The studies conducted in recent years will enable the development of new methods taking into account this parameter.

The consideration of the differential heating in the fire design of steel beams and columns embedded on walls or slabs should be also a concern in the future. The introduction of new section factors for these situations is a need in part 1.2 of Eurocode 3.

Although nowadays they are used very little welding steel profiles there still exist many cases of welded seams and other connections that need simplified calculation methods for their fire design. The development of fire design methods for welding connections is of outmost importance.

Another parameter that can results in savings is the consideration of the catenary effect on the fire design of steel beams. The research that already exists allows the development of new formulations for taking into account with this parameter.

With regard to joints they have been developed in the recent past fire design methods for screwed and bolted joints in hot-rolled steel structures but very little still exists for welded joints and nothing exists for cold-formed steel joints. In this area there are a lot to do for developing new fire design methods.

3.4 Eurocode 4 part 1.2 (EN1994-1.2)

The composite steel and concrete structures are perhaps one of the best ways to take advantage of the materials to an enhanced fire behavior of this type of structures. The concrete works not only as a strength material but also as fire protection material. Due to the fact that this type of structures is being more and more used then research, including for fire situation, has increased.

The new generation of this Eurocode 4 will introduce new **fire design methods for composite beams with large openings in the web**.

Another evolution will be the consideration of the **catenary effect** developed in composite steel deck slabs that could lead to a **reduction in the design and fire protection** (no use) on about 60 to 45% of the beams.

The **slim floor beams or the partially embedded beams in a slab** will have also new fire design methods. These new methods will take into account not only the temperature distribution in the profile but also in the steel reinforcement being the calculation of strength dependent on this distribution.

Finally, **Annex H (simplified calculation model for concrete filled hollow columns exposed to standard fire)** of EN 1994-1-2 will have new formulations and calculation rules for this type of structural elements. It should be noted that this method came to be criticized by different EU Member States considering it unsafe.

However, it is considered that these amendments are not sufficient and Eurocode 4 in its new part 1.2 could go further. As proposal for improving the fire design of this type of structures it can be mentioned the reduction of the requirements on the tabulated data methods that in some cases are too much on the safe and uneconomical side.

The method for assessing the resistant moment in composite steel deck slabs should be also improved. Aspects that have to do with the conditions of support and effect of continuity in intermediate supports should be taken into account in future evolutions of the simplified calculation method for this type of slabs.

Another aspect is related with the consideration of the restraining to the thermal elongation in the simplified calculation methods. This aspect existing in real structures can condition the fire performance of this type of structures.

The phenomenon of the lateral buckling should be less likely in composite than in steel beams as the concrete protects the web of the beams, however the phenomenon also exists and should be investigated with a view to be considered in the simplified calculation methods.

The Annex H of this part of Eurocode 4 will be revised as a result of the research carried out in the recent years on fire design methods of composite columns made with concrete filled hollow sections. It is believed that would be also important the introduction of fire design methods for elliptical hollow sections.

The development of a new simplified calculation method for fire design of composite columns made with double-tube or double-skin steel tubular sections or hollow columns with internal steel cores (e.g. H or other shape steel sections) is also very important as a consequence of the increasing use of this type of columns.

The study of the buckling length in this type of columns is also important because the values now proposed are unsafe at high temperatures.

This part of Eurocode 4 is still weak in simplified calculation methods for other types of shear connectors beyond the studs. So they are necessary fire design methods for crestbonds, perfobonds, among others.

3.5 Eurocode 5 part 1.2 (EN 1995-1.2)

The part 1.2 of Eurocode 5 is perhaps the one that most developments have had in recent years. Apart this, due to the complex behavior of timber in fire, due to the large amount of species that exist, this part of Eurocode 5 still requires more evolutions on the simplified calculation methods.

The EN 1995-1-2 provides two simplified calculation methods (the reduced cross-section method and the method of the reduced properties) for fire design of timber elements. The field of application of the **method of the reduced cross-section** should be extended (for example for I beams, composite timber-concrete elements, etc.) while the **method of the reduction of properties** will be abandoned.

In Annex C of EN 1995-1-2, dedicated to **lightweight walls and floors whose cavities are completely filled with thermal insulation**, the existing fire design model based on the method of the reduced properties should be abandoned and replaced by the method of the reduced cross-section.

The calculation model in Annex E, for **partitioning walls and floors**, is based on data taken from a limited number of fire resistance tests. A more general calculation model will be implemented in the new generation of this Eurocode.

However, it would be necessary to do more with this Eurocode and carrying out a complete study of the stiffness and strength mechanical properties and thermal properties of the different timbers at high temperatures for being used with the simplified calculation and advanced calculation methods.

The timber industry in the last years is very evolutionary with the development of new joints. The joints are a weak part of a timber structure in case of fire. Thus the development of new fire design methods is of utmost importance in particular with those that have outer steel plates.

3.6 Eurocode 6 part 1.2 (EN1996-1.2)

The part 1.2 of Eurocode 6 is maybe the less developed of all fire parts of Eurocodes. The next version of this part of Eurocode 6 will have developments in the **simplified calculation method existing at Annex C**. The use of recent researches should lead to improvements in the fire design methods for masonry structures.

However, it would still need more such as a complete study of the mechanical and thermal properties of the masonries at high temperatures for being used with the simplified and advanced calculation methods.

The simplified calculation method currently existing requires improvements because it is based in principles that are not similar for all types of masonry.

The introduction of construction solutions for an enhanced fire behavior of masonry walls is also very important.

Finally, it is important the consideration in the future of the impact strength on the fire design of masonry walls.

3.7 Eurocode 9 part 1.2 (EN1999-1.2)

The part 1.2 of Eurocode 9 is the latest of all those developed in the current generation of Eurocodes. This fact can be explained by the lower use of aluminum and their alloys in construction. The developments in the new version of this part of Eurocode will not be too many and are limited to the identification of active fire protection systems that can improve the overall behavior of these structures. The aim is to present an updated standard that does not penalize the aluminum in competition with other materials.

However, it is necessary more research in this area with a complete study of the mechanical and thermal properties of the aluminum and its alloys at high temperatures. These properties are very important for the simplified and advanced calculation methods.

The simplified calculation methods need a lot of research for their development because they are at the moment very similar to those of part 1.2 of Eurocode 3.

The calculation of the buckling length for various situations of stiffness of aluminum structures needs also a study because if the calculation for steel structures is considered unsafe the same is true for the aluminium structures.

It is also considered essential the development of simplified calculation methods for fire design of joints in aluminium structures.

4 CONCLUSIONS

In this paper it was made a presentation of the current parts of Eurocodes regarding to fire design of structures: concrete, steel, composite steel and concrete, timber, masonry, aluminium and its alloys. This verification can be made by tabulated data, except in EN 1993-1.2:2010, EN 1995-1.2:2004 and EN 1999-1.2:2007, simplified calculation or advanced calculation methods.

The verification by tabulated data is the most appealing to the common designer, due to its simplicity, but is also the most conservative and uneconomic. The simplified calculation methods, as the name indicate, are of simple use, or intend to be, but nowadays to take into account the different types of fire phenomena on the structures, begin to be a bit complex. They are finally the advanced calculation methods that are more accurate, because it allows the modeling of the structure as a whole, but also the most complex and not available to all designers. These methods are associated with software capable to model structures in fire situation.

The parts 1.2 of the Eurocodes offer nowadays a great number of tools for verifying the fire safety of structures, as the requirements of the fire safety regulations of buildings of the different countries, some of more prescriptive nature and thus more suited to the use of tabulated data or simplified calculation methods and others more performance-based and thus more suited to the use of advanced calculation methods.

In Eurocodes, nothing is foreseen with regard to fire design of structures after earthquake. The history has shown that after an earthquake there quite always fires and the behavior of the structural elements to the fire will not be the same as originally. So it is necessary in the future the development of a new Part 1.2 for Eurocode 8 for fire design of structures after earthquake.

REFERENCES

[1] EN 1990 – *Eurocode - Basis of structural design*, European Committee for Standardization (CEN), 2002.

[2] EN 1991-1.1 – *Eurocode 1 - Actions on structures - Part 1-1: General actions - Densities, self-weight, imposed loads for buildings*, European Committee for Standardization (CEN), 2002.

[3] EN 1991-1.2 - *Eurocode 1 - Actions on structures - Part 1-2: General actions - Actions on structures exposed to fire*, European Committee for Standardization (CEN), 2002.

[4] EN 1992-1-1 – *Eurocode 2: Design of concrete structures - Part 1-1: General rules and rules for buildings*, European Committee for Standardization (CEN), 2004.

[5] EN 1992-1-2 – *Eurocode 2: Design of concrete structures - Part 1-2: General rules - Structural fire design*, European Committee for Standardization (CEN), 2004.

[6] EN 1993-1-1 - *Eurocode 3: Design of steel structures - Part 1-1: General rules and rules for buildings*, European Committee for Standardization (CEN), 2005.

[7] EN 1993-1-2 - *Eurocode 3: Design of steel structures - Part 1-2: General rules - Structural fire design*, European Committee for Standardization (CEN), 2005.

[8] EN 1993-1-3 - *Eurocode 3: Design of steel structures - Part 1-3: General rules - Supplementary rules for cold-formed members and sheeting*, European Committee for Standardization (CEN), 2006.

[9] EN 1993-1-8 - *Eurocode 3: Design of steel structures - Part 1-8: Design of joints*, European Committee for Standardization (CEN), 2005.

[10] EN 1994-1-1 - *Eurocode 4: Design of composite steel and concrete structures – Part 1-1: General rules and rules for buildings*, European Committee for Standardization (CEN), 2004.

[11] EN 1994-1-2 – *Eurocode 4: Design of composite steel and concrete structures – Part 1-2: General rules - Structural fire design*, European Committee for Standardization (CEN), 2005.

[12] EN 1995-1-1 - *Eurocode 5: Design of timber structures - Part 1-1: General - Common rules and rules for buildings,* European Committee for Standardization (CEN), 2004.

[13] EN 1995-1-2 - *Eurocode 5: Design of timber structures - Part 1-2: General - Structural fire design*, European Committee for Standardization (CEN), 2004.

[14] EN 1996-1-1 - *Eurocode 6: Design of masonry structures - Part 1-1: General rules for reinforced and unreinforced masonry structures*, European Committee for Standardization (CEN), 2005.

[15] EN 1996-1-2 - *Eurocode 6: Design of masonry structures - Part 1-2: General rules - Structural fire design*, European Committee for Standardization (CEN), 2005.

[16] EN 1999-1-1 - *Eurocode 9: Design of aluminium structures - Part 1-1: General structural rules*, European Committee for Standardization (CEN), 2007.

[17] EN 1999-1-2 - *Eurocode 9: Design of aluminium structures - Part 1-2: Structural fire design*, European Committee for Standardization (CEN), 2007.

[18] ENV 13381-4 - Test methods for determining the contribution to the fire resistance of structural members. Applied protection to steel members, European Committee for Standardization (CEN), 2002.

FIRE SAFETY ENGINEERING

SFPE CORE COMPETENCIES FOR THE FIRE PROTECTION ENGINEERING PROFESSION

[1]Jimmy Jönsson, [2]Anthony Militello,[3] Brian Meacham
[1]JVVA Fire and Risk, Madrid, Spain
[2]Department of the Navy, Washington, DC, USA
[3]Meacham Associates, Shrewsbury, MA, USA

ABSTRACT

The practice of fire protection engineering (FPE), or fire engineering (FE) or fire safety engineering (FSE) as it is otherwise known in different parts of the world, varies widely among countries. The lack of universal agreement on professional qualifications can create uncertainty within a market, result in wide variations in engineering analysis and design, and contribute to increased risk to public safety. To provide a global foundation for professional qualifications, the Society of Fire Protection Engineers (SFPE) embarked on a project to develop a set of *Recommended Minimum Technical Competencies for Fire Protection Engineering* (Core Competencies) [1]. Practitioners from several countries crafted a draft document that was improved by the public comment process. The resulting publication details the knowledge base, education, and experience needed to obtain a set of 'core competencies' that underpin the practice of fire protection engineering.

1   INTRODUCTION

The Society of Fire Protection Engineers (SFPE), whose mission is "to define, develop, and advance the use of engineering best practices; expand the scientific and technical knowledge base; and educate the global fire safety community, to reduce fire risk," is the largest worldwide professional body of fire protection engineering and fire safety engineering practitioners. Of the more than 4000 members, over 1600 hold qualifications as licensed / registered Professional Engineers or equivalent. Such a professional credential reflects the pinnacle of recognition: an indication an engineer has demonstrated minimum technical competence and can be entrusted with the responsibility of integrating fire science into the practice of fire protection engineering. This requires engineers working in fire safety engineering to understand foundational skills, knowledge areas, and practical behaviours of the profession, while simultaneously upholding a high degree of professional ethics that holds paramount public safety and health. To advance the SFPE's mission, and to increase the global awareness of the minimum technical competencies required to practice in the profession, it was deemed appropriate to develop guidance in this area.

When embarking on this effort, the SFPE recognized that requirements governing the use of the term 'engineer' or the ability to practice 'engineering' varies widely around the world. In some countries, one can call themselves an engineer upon graduation with a university degree in engineering. Other countries have very specific governing regulations that specify in great detail the knowledge and experience required prior to legally using the term "engineer" or with respect to fire, the term "fire protection engineer". In stark contrast, many parts of the world have no prescriptive or performance requirements governing the use of the term engineer or the knowledge and experience required to practice engineering, or fire protection engineering in particular.

The SFPE's Core Competencies document is not intended to circumvent any jurisdiction's authority or requirements around the practice of engineering, in general, or fire protection engineering, in particular. However, the SFPE believes that a minimum technical competency framework that represents the values of the Society's membership and the profession, and that advocates for the profession in a way that has global applicability, has significant benefit and societal value.

2   DEFINING COMPETENCY

2.1. Terminology

Competency can be defined and interpreted in many ways. An objective of this effort was to clearly define technical competency within the context of an engineering profession, while balancing universal agreement on terminology with sufficient flexibility to enable local interpretation and applicability. As such, the following terms are defined for the purpose of providing clarification of in the context of the Core Competencies document [1]. These definitions should not be considered as 'official definitions', but rather, descriptions created to enhance contextual understanding.

Minimum competency: A minimum competency is the accumulation of the academic knowledge base and the applied experience necessary to successfully perform a certain task.

Knowledge area: A knowledge area is an important subject area that forms part of the overall knowledge base needed for a certain competency.

Adequate knowledge base: An adequate knowledge base is the summary of the information about a particular subject known by an individual; that information must be sufficient for an individual to be able to perform related tasks.

Minimum knowledge: Minimum knowledge is considered the knowledge base needed to gain a comprehensive understanding of a specific subject; to be able to understand how to appropriately apply the knowledge of that specific subject.

Minimum qualifying experience: This is practical experience that is indicative of growth in engineering competency and achievement of not less than four years, three of which shall have been in responsible charge of fire protection engineering work. A post graduate degree may serve in lieu of one year of practical experience.

2.2. Competency Model

In the USA, competency for an engineering professional is defined as "a cluster of related knowledge, skills, and abilities that affects a major part of one's job (a role or responsibility), that correlates with performance on the job, that can be measured against well accepted standards, and that can be improved through training, development, and experience." [2] While different definitions exist in other countries, they largely embody the same principles. The competency model in the USA is quite detailed and comprehensive, starting with broad personal effectiveness competencies and core science, technology, engineering and mathematics requirements, and culminating with management and occupation-specific competencies [2]. Since each engineering discipline is different, the model has many common tiers of competency requirements, as well as an undefined level, Tier 5, which builds on Tiers 1-4 and is intended to be defined by specific industry sectors. The information presented in the SFPE Core Competencies document establishes a set of industry-specific criteria for the fire protection engineering profession and represents competency requirements for Tier 5 as specific to fire protection engineering. *Fig. 1* provides a diagram that

illustrates the different tiers, starting with a broad learning skill set and academic preparation, and culminating in the fire protection engineering knowledge base that is profession specific.
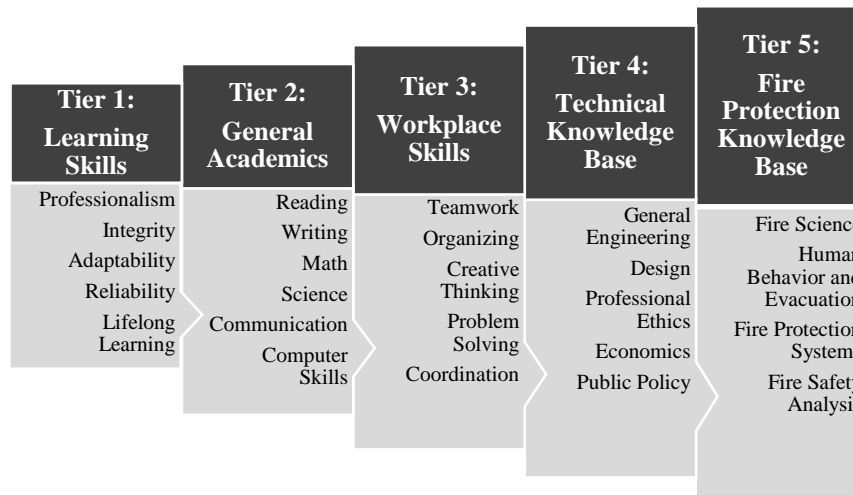

Fig. 1. Tiers of Knowledge in Engineering Competency Model for USA - adapted for FPE [1]

As observed in *Fig.1*, the basis is academic preparation, but academic knowledge alone is insufficient to reach the competency referenced here. Professional experience that is diverse and progressive in complexity is an essential element in the development of the breadth of knowledge necessary to transform a student of the profession into a competent practitioner. Credit-worthy experience is measured by duration of time and effective depth of understanding, which is obtained through interactive feedback from peers, who provide new knowledge and reinforce sound judgement and decisions.

3   USES OF THE CORE COMPETENCY MODEL

It is the hope of the authors that the SFPE's Core Competencies document can serve as an essential reference for organizations evaluating or relying upon the knowledge and skills of fire protection engineers. Organizations such as the National Council of Examiners for Engineering and Surveying (NCEES), which develops, administers, and scores examinations used for engineering and surveying licensure in the United States, provide support for, and consistency of, engineering competency for many recognized practices. Similar to the specifications used for NCEES testing in fire protection engineering [3], the recommended minimum technical competencies exemplify the information areas individual need to practice fire protection engineering. The minimum technical competencies are independent of geographic location and may serve as a basis for jurisdictions that lack fire protection engineering credentialing programs or prescribed minimum competencies.

Educational institutions considering new programs related to fire protection engineering or reviewing current programs can align their curriculum to the SFPE Core Competencies document, in order to provide their students with the opportunity to gain the academic knowledge needed to enter the workplace and, with practice, become competent. For additional guidance on recommended curricula, the SFPE has model curricula for a Bachelor's degree and Master's degree in fire protection engineering and Bachelor's degree in fire protection engineering technology [4][5][6]. These documents are focused on the development of a university program, whereas the

information herein is dedicated to achieving professional competency, which will need experience in the industry and may need supplemental education to reach the desired breadth of knowledge.

The SFPE Core Competencies document can also be used by engineering degree program accreditation bodies to evaluate curriculum and instruction while ensuring institutions provide service to the fire protection engineering profession. The Accreditation Board for Engineering and Technology (ABET) is an example of an organization that evaluates university programs. Accreditation compliments this effort by ensuring those striving to become fire protection engineers have received the appropriate education upon completion of a fire protection engineering program.

Practitioners are responsible to maintain their knowledge and skills up-to-date, and can reference these core competencies to identify technical areas where they lack knowledge and need further development. Employers or other organizations can use the SFPE Core Competencies document when evaluating employees, soliciting for professional services, or otherwise establishing requirements for desired competencies of fire protection engineers. As reflected in the tiered model [2], corporate entities and others will likely impose additional competency requirements in terms of management skills, capability and experience, as well as industry / occupation specific knowledge, for an individual to reach the level of overall professional competency.

4 DEFINING FIRE PROTECTION ENGINEERING

It is understood that in some countries, definitions of the practice vary, with 'fire engineer' or 'fire safety engineer' focusing on design strategy and analysis, 'fire protection engineer' focusing on active fire protection system design, and 'fire prevention engineer' focusing on passive system design. However, the SFPE does not make this distinction. When referring to a "fire protection engineer" in the document, the core competencies apply to anyone performing the defined functions, regardless of their professional title. To assist in clarifying the individuals who should meet the minimum competencies laid out in the SFPE Core Competencies document, the term fire protection engineer has been defined, along with expected knowledge and skill sets [1].

Fire Protection Engineer: A fire protection engineer is an individual, who, by formal training and professional experience, carries the necessary competency and skills to provide guidance and direction to protect life, property and environment from threats posed by fire and its effects.

The definition above refers to a practitioner that has a university education in fire protection engineering (e.g. a graduate of an engineering curriculum of accepted standing) and relevant experience in the industry. Individuals engaged in the fire protection engineering profession, but are lacking this level of education and experience, should strive to reach the same knowledge base held by a fire protection engineer referred to in the document. To help facilitate a common understanding of the role of a fire protection engineer, the following roles are described.

Fire protection engineers identify hazards, characterize risks, and design safeguards that aid in preventing, controlling, and mitigating the effects of fires. They have the ability to use and develop engineering methods and techniques related to fire safety design of buildings, industrial constructions, infrastructures, equipment and environment interfaces.

It is understood that the competence carried by the fire protection engineer is used within any sector of the fire safety industry, such as the building industry, the oil and gas industry, the nuclear industry, the forestry industry, etc. A fire protection engineer is expected to identify and manage

44

complex issues independently and collaboratively. Through technical analysis the fire protection engineer is able to analyse, evaluate and develop various technical solutions to fire safety problems. Fire protection engineers have an interdisciplinary role assisting project/design teams (which may include but are not limited to architects, building owners and developers) in reaching life safety, property protection and environmental protection goals.

In addition to understanding general engineering principles, the fire protection engineer is expected to understand: fire science, active fire protection, passive protection, human behaviour & evacuation, performance-based design, fire protection analysis, computational modelling, fire hazard and risk assessment, general building design, and codes and regulations.

5   TECHNICAL KNOWLEDGE BASE AND EXPERIENTIAL COMPETENCIES

A practitioner must understand fire protection principles and the application of these principles in the engineering analysis and design of fire safety measures. Only by understanding these core subjects will the professional achieve the minimum knowledge base considered necessary for the professional practice of fire protection engineering. It is considered extremely important that when practicing fire protection engineering one must work within the scope of one's professional and technical competency, as is true in any engineering discipline. Understanding one's technical and professional limitations is an integral part of professional ethics related to the practice of engineering. Such ethical standards are in place to help assure that professionals undertake and complete only the tasks which they are competent to perform.

5.1   Core Technical Competencies

As a fire protection engineer, one is often required to include and rely on the expertise and competency of other professionals (such as engineers in other disciplines, architects, scientists, etc.) as part of delivering a competent analysis / competent design (i.e., building design, infrastructure design, or other). The other members of a team have a similar expectation for the fire protection engineer. This shared expectation, that each team member is qualified and competent in their respective discipline, is fundamental to engineering a fire safe world.

While the minimum technical competencies are foundationally essential, they will not generally translate to *expertise* in all those areas. Expertise in all of the areas of minimum technical competency is not practical, and probably not possible for an individual over the course of a professional life. The individual fire protection engineer will develop expertise in particular areas of practice and may maintain only basic understanding in other areas.

It is understood that any individual, depending on his/her current competence and his/her specific area of expertise, might concentrate on only some of these core technical competencies when developing their expertise. However, competence in the following four (4) areas are considered to be core to the profession of fire protection engineering [1]:

Fire Science: A comprehensive understanding of the underlying physical principles of fire and its related mechanisms, including ignition, combustion, heat transfer, fire chemistry, and fire dynamics.

Human Behaviour and Evacuation: A comprehensive understanding of human behaviour and the principles of means of egress design. This would include the behaviour of persons during an emergency, tools and methods to perform egress, evacuation, and escape assessments.

Fire Protection Systems: A comprehensive understanding of fire mitigation, including water and non-water-based suppression; fire detection and alarm systems; smoke management systems; passive systems; fire testing and code and standard concerns.

Fire Protection Analysis: A comprehensive understanding of the principles of technical analysis related to fire protection design. This would include means of identifying and quantifying fire related risks and hazards, design approaches, design evaluation, application of numerical methods and computer fire models, establishing boundary conditions, and limits of analysis and design.

5.2 Core Technical Knowledge Areas

For each of the core technical competencies, a number of core technical knowledge areas have been identified. The expectation is that the practitioner is proficient in these knowledge areas, i.e., in the application of science and engineering to protect the health, safety and welfare of the public along with protecting property from the impacts of fire. The knowledge areas can be viewed as descriptions of the objectives of courses needed to be taken to achieve proficiency in each specific topic. *Table 1* reflects the core technical knowledge areas. Descriptions of the technical knowledge areas can be found in the SFPE Core Competencies document. [1]

Table 1. Core Technical Knowledge Areas for Fire Protection Engineering [1]

	Fire Science	Human Behaviour and Evacuation	Fire Protection Systems	Fire Protection Analysis
Core Knowledge Areas	- Heat transfer - Fire Chemistry - Fire Dynamics	- Human Behavior and Physiological Response to Fire - Egress and Life Safety Design Concepts	- Passive systems - Active systems - Fire Detection and Alarm - Fire Suppression	- Performance Based Design - Smoke Management - Evacuation Analysis - Structural Fire Protection - Risk Management - Numerical Methods and Computer Fire Modeling - Building and Fire Regulations & Standards

6 RECOMMENDED TIME TO ATTAIN COMPETENCY

6.1. Learning Time

The Core Competencies document is not designed to give specify length of study needed for these topics if part of a formalized education program. However, it was considered to be of utmost importance to show a recommended range of hours considered necessary to gain a minimum knowledge level for each topic. The ranges of recommended hours presented have been estimated based on input from the academic communities in the USA and Europe, and on the European Credit Transfer and Accumulation System (ECTS) [7][8][9], where credits are a standard means for comparing the "volume of learning based on the defined learning outcomes and their associated workload," and where "workload indicates the time students typically need to complete learning activities (e.g. lectures, projects, practical work, self-study and examinations) required to achieve expected learning outcomes." *Table 2.* shows a range of recommended minimum learning hours, which could be transformed to ECTS credits by estimating one (1) ECTS credit as 25 – 30 hours.

Table 2. Recommended Minimum Learning Hours for Fire Protection Engineering [1]

Minimum Competency	Fire Science	Recommended Hours	Human Behavior and Evacuation	Recommended Hours
Knowledge Areas	Heat transfer	120 - 160	Human Behavior and Physiological Response to Fire	80 - 120
	Fire Chemistry	7 - 120	Egress and Life Safety Design	80 - 120
	Fire Dynamics	160 - 200		
Minimum Competency	Fire Protection Systems	Recommended Hours	Fire Protection Analysis	Recommended Hours
Knowledge Areas	Passive systems	60 - 90	Performance Based Design	160 - 200
	Active systems	60 - 90	Smoke Management	120 - 160
	Fire Detection and Alarm	120 - 160	Evacuation Analysis	120 - 160
	Fire Suppression	120 - 160	Structural Fire Protection	120 - 160
			Risk Management	140 – 180
			Numerical Methods and Computer Fire Modeling	160 – 200
			Building and Fire Regulations & Standards	60 – 90

6.2. Experience

The hours shown in *Table 2.* must be seen as a proposed range of recommended hours needed to gain a comprehensive understanding of the knowledge area, not to reach the minimum competence level. To reach the minimum competence level it is necessary to add project experience. Also, taking a course on a specific knowledge area does not mean that an individual will be considered an expert or can be considered to have achieved a minimum competence level on the subject. It is the view of the SFPE that the development of minimum fire protection engineering competence should begin with completion of a curriculum at a university or educational institution of accepted standing.[1] Following the educational foundation, a fire protection engineering practitioner should have practical experience that is indicative of growth in engineering competency and achievement of not less than four years, three of which shall have been in responsible charge of fire protection engineering work. A post graduate degree may serve in lieu of one year of practical experience.

8   ETHICS

Ethical conduct of engineers is of the utmost importance. Moral values are an imperative foundation for honest and open transactions, and it is only when professionals demonstrate their values in this way that they are able to work without partiality. Engineering ethics holds paramount interests of public safety, client and employer relations, and sets professional standards against which practitioners are held to account for their actions. The integrity of the profession depends on ethics;

---

[1] Per the SFPE Qualifications Board Table, "Accepted Standing" related to engineering curriculum is defined as an engineering curriculum which is ABET (Accreditation Board for Engineering and Technology) accredited (USA), CEAB (Canadian Engineering Accreditation Board) accredited (Canada), FEANI listed (European Federation of National Engineering Associations), or equivalent. This also includes programs outside North America that have been reviewed and accepted by ECEI (Engineering Credentials Evaluation International) or WES (World Education Services) and found to be comparable to those accredited in the USA.

therefore, it is considered critical to include a brief section highlighting ethical considerations. All fire protection engineers are expected to read, accept, and abide by the SFPE Canons of Ethics. [10]

9   CONCLUSIONS

A set of minimum core technical competencies for the practice of fire protection engineering have been described. Knowledge areas and learning time have been overviewed. It is understood that the most efficient route to gain the knowledge for a foundation in fire protection engineering is through university study specifically in fire protection engineering. These recommended minimum technical competencies for fire protection engineering are not intended to replace an in-depth university education in fire protection engineering. University courses traditionally offer a more in-depth look at a particular subject due to the length of instruction and activities, such as homework and projects, associated with the course. In addition to classroom education, becoming competent also involves practicing and applying the knowledge to real world projects and receiving constructive feedback.

However, the SFPE acknowledges that, as one of the younger engineering disciplines, fire protection engineers may follow different paths to reach a competent level of practice. Although it is important to understand that the path to minimum technical competency may vary from one individual to another, university programs are essential to provide a fundamental grounding in engineering knowledge, which every fire protection engineer should possess.

The SFPE Core Competencies document does not prescribe the precise means and methods by which the identified minimum standards are obtained. University-level programs with specialized fire protection coursework are deliberately designed to deliver a comprehensive set of learning outcomes that build foundational knowledge in the recommended core competencies. Alternative methods for obtaining knowledge in core competencies should be carefully evaluated using the standards identified in this document. Regardless of how foundational knowledge is obtained, minimum competency can only be achieved through observed and verified professional practice.

Aside from university education, Continuing Professional Development (CPD) is critical. CPD is the main method for practitioners to ensure they maintain the minimum level of competency needed throughout their career. CPD essentially adapts the base knowledge and skills for new needs evolving over time. Engineers within the fire protection industry must take the necessary steps to develop and maintain knowledge, skills, and expertise necessary to perform their roles successfully throughout their career. By participating in relevant training, professional development programs, and mentoring and independent research, they can remain competent through education on new technologies, new methodologies and improved ways of implementing fire protection engineering.

REFERENCES

[1] SFPE, Recommended Minimum Technical Competencies for Fire Protection Engineering, Link: https://cdn.ymaws.com/www.sfpe.org/resource/resmgr/docs/core_competencies/minimum_fpe_competencies_fin.pdf

[2] Competency model for engineering, Link: AAES or USDLETA websites (e.g., https://www.careeronestop.org/CompetencyModel/competency-models/engineering.aspx).

[3] NCEES Principles and Practice of Engineering Examination Fire Protection Exam Specifications, Link: https://ncees.org/wp-content/uploads/PE-Fire-Oct-2018.pdf

[4] SFPE, Model Curriculum for a Bachelor's of Science (BS) Degree in Fire Protection Engineering (FPE), Link: https://c.ymcdn.com/sites/sfpe.site-ym.com/resource/collection/24609C80-7253-49A5-83AF-D0499353EAEA/SFPE_BS_Model_Curriculum.pdf

[5] SFPE, Bachelors of Science in Engineering For Fire Protection Engineering Technology Model Curriculum, Link: https://cdn.ymaws.com/www.sfpe.org/resource/resmgr/docs/model_curriculum_/BS_FPET_Model_Curriculum-201.pdf

[6] SFPE, Recommended Curriculum Content for an MS/ME in Fire Protection Engineering, Link: https://c.ymcdn.com/sites/sfpe.site-ym.com/resource/collection/24609C80-7253-49A5-83AF-D0499353EAEA/131027_MS_Program_in_FPE_-_Final.pdf

[7] ECTS Users' Guide, 2015, Link: https://ec.europa.eu/education/sites/education/files/ects-users-guide_en.pdf

[8] European Commission Education and training ECTS Users guide, Link: http://ec.europa.eu/education/ects/users-guide/key-features_en.htm

[9] ECTS and U.S. College Credit System, Link: https://www.mastersportal.com/articles/1110/what-you-need-to-know-about-academic-credit-systems-in-the-us.html

[10] SFPE Canons of Ethics, Link: http://www.sfpe.org/page/CodeofEthics

THE STATE OF FIRE SAFETY ENGINEERING IN SEVEN COUNTRIES: SURVEY OUTCOMES AND PRELIMINARY ANALYSIS

[1]Joakim Astrom, [1]Elin Axelsson, [1]Sofia Lindahl, [2]Brian Meacham
[1]Lund University, Lund, Sweden
[2]Meacham Associates, Shrewsbury, MA, USA

ABSTRACT

An online survey regarding the global situation with fire safety engineering was conducted in late 2016 and early 2017. The survey was distributed via social media (e.g., LinkedIn) and direct email distribution. The survey was published in English and Spanish languages. Overall there were more than 400 respondents from 41 countries, although not all respondents completed the full survey. The questions were wide-ranging, with an aim to obtain a sense of how fire safety engineering was working (or not), what types of analyses are being undertaken, whether there are sufficient numbers of qualified practitioners, authorities, etc., and what types of strategies might be appropriate to advance fire safety engineering in the future. Analysis focuses largely on countries with the highest number of responses. Commonalities and differences between the countries are explored. Findings suggest broad agreement on the need for more engineers, greater competence and more education.

1   INTRODUCTION

Countries around the world began transitioning from prescriptive-based to performance-based building regulatory systems in the 1980s [1-4]. Concurrently, the practice of fire safety engineering began to become more widely recognized, and frameworks for fire safety engineering and performance-based design for fire emerged [1,4-7]. Over the past thirty years, various research has been conducted around frameworks and approaches for fire safety engineering [e.g.,5-8], yet little research seems to have been published with respect to how practitioners and others in the market view the situation with fire safety engineering and performance-based design approaches in use.

In 2016 and 2017, with support from the Australian Building Codes Board (ABCB), the technical research organization of the Netherlands (TNO), the New Zealand Ministry of Business, Innovation and Employment (MBIE), the Scottish Government, Building Standards Division (BSD), a Fulbright Global Scholar Award (https://www.cies.org/program/fulbright-global-scholar-award) that supported visits to Japan, Spain and Sweden, and Worcester Polytechnic Institute (WPI), research was conducted on the situation with performance-based building regulations and the situation regarding fire safety engineering and performance-based design for fire seven countries. As part of this research, interviews were conducted with government officials, fire safety engineering practitioners, and other stakeholders. Brief summaries of in-country research findings are available elsewhere [9-10].

To supplement the in-country research, an on-line survey was developed. The aim of the on-line survey was to collect data regarding the situation with fire safety engineering and performance-based design for fire from practitioners, authorities and other stakeholders in various countries. The survey was distributed via social media (e.g., LinkedIn) and direct email distribution. The aim of the survey was to obtain perspectives on how fire safety engineering is working (or not), what types of analyses are being undertaken, whether there are sufficient numbers of qualified practitioners, and what types of strategies or directions might be appropriate going forward.

2   THE SURVEY AND RESPONDENTS

The survey consisted of 46 questions. Formats included selection from pre-determined options, pre-determined ranges, rank ordering, percentages, and free response. The survey was made available in

English and Spanish languages. A copy of the survey can be provided upon request. Responses were received from people in 41 countries. There were 404 respondents to the English survey and 44 to the Spanish survey. The completion rate was just under 50%, with about 200 complete surveys. A majority of respondents identified as fire safety engineers (n = 267, 66%) and the largest sectors represented were consulting (n = 207, 51%) and building engineering / engineering analysis and design (n = 152, 38%). The range of professional experience of the respondents (n = 398) was rather equally distributed: less than 10 years, 35% (n = 141); 11 – 20 years, 30% (n = 120), and 21 years or more, 35% (n = 139). About half of the respondents answered questions associated with performance-based design (PBD) for fire (n = 228). The significant majority of respondents (85%) had 20 year or less of experience with PBD for fire, with 66% having 15 years or less.

3 EVALUATION OF THE DATA

Evaluation of the data is ongoing. Until now, the evaluation has considered the following: responses from all participants, responses by persons within a select group of countries (for which the largest number of data points are available), and comparison of responses between countries. From these data, trends can be inferred. No detailed statistical analysis has been undertaken to this point. However, this is planned in the coming months. In addition, if sufficient data are available, factors such as differences between actor perspectives (e.g., fire safety engineer and enforcement official) will be explored, overall and by country. As with any data set, some responses are not considered due to anomalies in the responses, incomplete responses, or other. For the outcomes presented here, the analysis is limited to the data from complete surveys only, for a set of seven countries (n = 188 respondents). In the future, more detailed analysis of specific questions is planned, for which only internal consistency is required (i.e., based on all responses to this question, the data suggest X).

The countries selected for initial analysis and comparison and associated number of respondents are: Australia (n = 50), England (n = 22), New Zealand (n = 24), Scotland (n = 28), Spain (n = 19), Sweden (n = 10) and the United States (n = 29). It should be noted that the authors recognize that the data set from Sweden is small, and the data may not be statistically significant. However, it is a country of particular interest for the authors, so is included in the trend analysis. It should also be noted that some assumptions where made in categorizing the responses from England. A number of responses indicated 'UK' as the country. Since specific outreach was made to practitioners in Scotland, as separate from England, responses from the UK have been merged with the responses from England. It is understood that this introduces error into the dataset labelled England. For trend analysis, however, this was deemed to be acceptable.

4 SELECTED SURVEY RESULTS

As noted above, the survey consisted of 46 questions. It is not possible to provide detailed discussion around every question in this analysis. As such, the focus here is around perspectives on the general state of fire safety engineering for PBD, the value of existing fire safety engineering guidance, the competency in the market, and what is suggested to improve the situation in the future. Note that for each countries of focus, there is a performance-based building regulatory system in place, with the exception of the USA. Issues on the regulatory system can be found in [9].

4.1 Situation with PBD for Fire

At a general level, respondents from the countries of focus think that the situation is largely 'good' with respect to how the system is working (defined as "in terms of qualifications, competency, regulatory acceptance of designs, etc."). However, it is interesting to note that in Spain, the response is that the situation is largely 'bad' (defined as "in a practical sense, there is little or no PBD").

Table 1. General Sense of How Well PBD for Fire is Working

	Very Good	Good	Bad	Very Bad	n
Australia	**10%**	**58%**	32%	0%	50
England	**9%**	**55%**	36%	0%	22
New Zealand	4%	**54%**	**33%**	8%	24
Scotland	0%	**44%**	**56%**	0%	25
Spain	0%	16%	**53%**	**32%**	19
Sweden	0%	**90%**	10%	0%	10
USA	3%	**59%**	28%	10%	

4.2 Reasons for Applying a PBD Approach

In Australia, New Zealand and Sweden, the highest reported reason for applying a PBD approach is **"the 'deemed-to-satisfy' requirements are too restrictive / do not fit all parts of the building** (i.e., do not address or do not permit a desired building feature / system / material)." In the USA, highest reported reason is "**to develop solutions for difficult problems**." England, Scotland and Spain were split 50/50 amongst these choices. Other choices included: the building code is performance-based, so therefore the solution must also be, to facilitate innovative materials or methods of construction, the 'deemed-to-satisfy' requirements are too costly and unnecessary to apply to all parts of the building (ranked 2nd in several countries), to increase fire safety of an existing building, but not to the level of current 'deemed-to-satisfy' provisions, to optimize solutions, to address occupant vulnerabilities, and to address unique hazards.

4.3 Percentage 'Deemed-to-Satisfy' to Fully PBD

The highest reported use of PBD for fire, as compared with full compliance with 'deemed-to-satisfy' (DTS), occurs in Australia, New Zealand and England. Compliance with DTS, and minor deviations from DTS, are prevalent in Scotland, Spain, Sweden and the USA.

Table 2. Percentage DTS, Full PBD, and In-Between

	In complete compliance with 'DTS' provisions	Minor deviations from 'DTS' provisions	Major deviations from 'DTS' provisions	Completely / significantly PBD
Australia	16.5	37.8	**33.4**	**12.3**
England	25.3	31.8	**30.3**	**12.7**
New Zealand	47.2	18.8	**14.6**	**19.4**
Scotland	**51.3**	**29.7**	15.0	4.3
Sweden	42.0	35.4	16.1	7.2
USA	44.4	31.0	17.3	7.5
Spain	**56.6**	**25.4**	12.9	**4.4**

4.4 Primary Scope and Evaluation Framework of PBD

Across all countries, the primary use of PBD was for life safety analysis and design, with all but the USA being over 50%. In the USA, just under 50% of PBD is for life safety, with 23% for property protection. The outcomes are similar with respect to the approach most often applied, with ASET < RSET analysis being 50% or higher in all countries. Structural fire engineering was 2nd in most.

4.5 Use of Risk-Informed or Risk-Based PBD Approaches

The use of risk-informed or risk-based PBD approaches varies widely. Such approaches are rarely used in New Zealand, Sweden and the USA. They are most used in Australia, England and Spain. Existing standards and guidance on risk-informed / risk-based are largely viewed as inadequate.

Table 3. Percentage which are Risk-Informed PBD

	More than 75%	Between 50% and 75%	Between 25% and 50%	Between 5% and 25%	Less than 5%
Australia	14%	22%	18%	**24%**	**20%**
England	**21%**	16%	32%	21%	11%
New Zealand	4%	8%	8%	**21%**	**58%**
Scotland	**29%**	**29%**	13%	4%	25%
Sweden	0%	10%	**30%**	**30%**	**30%**
USA	11%	14%	11%	**39%**	**25%**
Spain	**27%**	13%	13%	13%	**33%**

4.6 Primary Standards / Guidelines Used for PBD

To understand which standards and guidelines are most often used, a select set of commonly used documents was presented, and respondents were asked to rank their usage. Table 4 reflects the top two documents by country. All countries find the existing guidance to be mostly adequate.

Table 4. Top Two Most Used Standards or Guidelines by Country

	BS7974	BS9999	CIBSE Guidelines	IFEG	ISO FSE Standards	NFPA Standards	NZ C/VM2	SFPE PBD Guide
Australia				1				2
England	2	1						
New Zealand				2			1	
Scotland	1	2						
Spain						1		2
Sweden					2			1
USA						2		

4.7 Top Needs for Additional Standards / Guidelines for PBD

Consistent with previous responses, risk-based guidance tops the list of needed standards / guides.

Table 5. Top Areas for Additional Standards / Guidelines
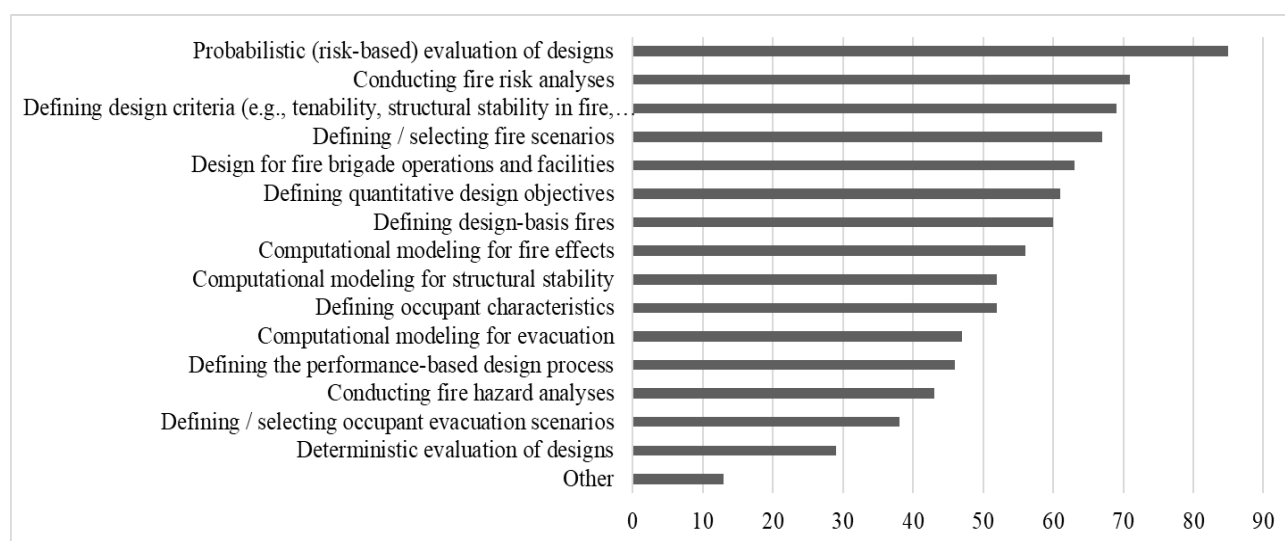
4.8 Are Only Qualified FSE Undertaking Fire Safety Engineering Designs

Looking at the broader FSE environment, including and beyond PBD, there is a large concern that fire safety engineering designs are being undertaken by people not qualified to do so.

Table 6. Are Only Qualified FSE Undertaking Fire Safety Engineering Designs

	Australia	England	New Zealand	Scotland	Spain	Sweden	USA
Yes	22.4%	31.8%	25.0%	39.3%	52.6%	20.0%	28.6%
No	**77.6%**	**68.2%**	**75.0%**	**60.7%**	47.4%	**80.0%**	**71.4%**

4.9 View of Review and Approvals Process for PBD

With respect to the review and approvals process, the choices were structured around how well the PBD process is understood by all, the consistency of reviews from one authority to the next, consistency with resulting level of safety being delivered, and competency and ability of authorities to review designs. On the whole, there is about a 50-50 split. New Zealand views the situation as particularly good (74%) and Spain as particularly bad (83% bad or very bad).

4.10 Percent of PBD Reviewed by Qualified FSE

Consistent with concerns that FSE designs are not being undertaken by qualified FSEs, there is a concern in that significant numbers of reviews / approvals are not being made by qualified persons.

Table 7. Percent of PBD Reviewed by Qualified FSE

	More than 75%	Between 50% and 75%	Between 25% and 50%	Between 5% and 25%
Australia	**26.1%**	**26.1%**	21.7%	26.1%
England	15.8%	10.5%	**47.4%**	**26.3%**
New Zealand	**34.8%**	**43.5%**	8.7%	13.0%
Scotland	15.4%	**34.6%**	11.5%	**38.5%**
Sweden	11.1%	33.3%	22.2%	33.3%
USA	0.0%	39.1%	**30.4%**	**30.4%**

4.11 Sufficient Number of Qualified / Competent FSEs in the Market

Aligning closely with perceptions that designs and approvals are being undertaken by persons without FSE qualifications, all countries report a significantly lack of qualified FSE in the market.

Table 8. Are There Enough Qualified FSE in Your Country

	Australia	England	New Zealand	Scotland	Spain	Sweden	USA
Yes	32.0%	9.1%	25.0%	14.3%	0.0%	40.0%	17.9%
No	**68.0%**	**90.9%**	**75.0%**	**85.7%**	**100.0%**	**60.0%**	**82.1%**

4.12 University Degree Programs

Tied to the above perspectives and the table below, a majority of countries do not think there are enough university programs in FSE, with only New Zealand and Sweden reflecting that the market largely thinks there are enough programs.

Table 9. Sufficient Number of Appropriate University Programs to Educate FSE in Your Country?

	Australia	England	New Zealand	Scotland	Spain	Sweden	USA
Yes	29%	15%	**88%**	**52%**	0%	**90%**	25%
No	**71%**	**85%**	13%	48%	**100%**	10%	**75%**

To improve the situation, respondents from Sweden and USA believes that asking professional organizations for more educational programs is the best alternative, while those from Australia recommend that the government should invest in more fire safety engineering programs. Respondents from England, New Zealand, Scotland and Spain do not see a singular focus. Instead, they would like to see a more diversity in options, including

legislating requirements around certification for FSE and protecting the title of 'fire safety engineer' to those who are suitably qualified.

4.13 Professional Licensing

There is wide variation on perspectives regarding the need for professional licencing / registration, and on what countries view as appropriate options in these regards. All of the countries, except USA, agree on that the mechanism for professional qualification or certification are inadequate in their respective country. As can be seen in the table below, most countries think that a legally required license or a professional qualification would be sufficient. There were also some free response answers that addressed this topic, including mandating similar requirements in all states (Australia) and requiring demonstration of competency gained through practice (England), specifically: "The requirement is correct, but the application leans heavily towards academic qualification. There should be additional requirement to demonstrate practical knowledge and experience as well as academic qualification."

Table 10. What would be your recommendation for qualification/certification/recognition of fire safety engineers?

	Australia	England	New Zealand	Scotland	Spain	Sweden	USA
Legally required / mandated	**37%**	**32%**	**67%**	36%	50%	46%	14%
Professional society qual.	13%	32%	19%	52%	46%	36%	18%
N/A	19%	8%	9%	4%	0%	9%	50%
Other	**31%**	**28%**	5%	8%	4%	9%	18%

4.14 Specialty Certification

One option to assist in raising competency could be through specialist certification, for example in such areas as CFD modeling, evacuation modeling, and risk assessment. All countries except New Zealand and Sweden agree that this might help. New Zealand and Sweden are both divided 50/50, which offers an indication that even here this might be well accepted.

Table 11. Would specialist Certification be helpful?

	Australia	England	New Zealand	Scotland	Spain	Sweden	USA
Yes	**61%**	**82%**	46%	**79%**	**95%**	50%	**64%**
No	39%	18%	54%	21%	5%	50%	36%

5 LIMITATIONS

As noted, the dataset for analysis is rather limited, with just under 200 complete surveys, with a range of 10 to 50 respondents from the countries considered. Assumptions were made regarding responses from the U.K. as being largely from England (based on respondents from Scotland identifying separately). No assessment of statistical significance was undertaken. However, one of the authors has spent between time in all of the countries for which data are provided, including conducting face-to-face interviews with stakeholders and working with regulatory, academic and research institutions in each on related topics (outcomes from some of which have been published [12-14], as well as practicing as a fire safety engineer. As such, there is confidence that the survey results largely reflect the perceptions of a large number of practicing engineers in the respective countries in terms of the quality of the regulatory system, the qualifications of actors, and the overall sense of how the system is working and where beneficial change would be welcome.

6 DISCUSSION AND CONCLUSIONS

Fire safety engineering, in particular performance-based design for fire, has become widely used. This is the case in countries with performance-based building regulations as well as in countries with prescriptive-based regulations. While there is a general sense that performance-based approaches are generally being applied in an appropriate manner, the scope of application is somewhat limited, and there are concerns over some aspects of design and review. There is also widespread concern over the lack of appropriate qualifications mechanisms and measures of competency.

The primary use is life safety analysis and design, applying the ASET versus RSET concept, for major deviations from 'deemed-to-satisfy' (DTS) alternatives and where the DTS simply do not apply. The *SFPE Engineering Guide to Performance-Based Fire Protection*, the *International Fire Engineering Guidelines*, BSI7476, BSI9999, and the New Zealand CV/M2 are most widely used. Except for respondents from Spain, the market largely thinks the performance-based regulatory and design environment is working generally well, and that existing standards and guidelines are adequate, but more standards / guidelines are desired around risk-informed / risk-based fire engineering analysis and design, as well as on design criteria, designing for fire brigade needs, and defining and selecting fire scenarios are needed

Even though respondents perceive the system as working generally well, practitioners, authorities and others have significant concerns about the lack of qualified practitioners for development and approval of such designs. In all countries, it is reported that there are not enough qualified and competent fire safety engineers, and there is significant concern that unqualified persons are undertaking and approving engineered designs.

With respect to why there may be a lack of qualified practitioners, most countries report an insufficient number of university programs in FSE, the lack of specialist certification in specific topics such as CFD modelling, evacuation modelling, and risk assessment competency, and inadequate controls around limiting the practice of FSE to appropriately qualified persons.

While the lack of legal requirements around the practice of FSE is concerning to many, there is wide variation on perspectives regarding the need for professional licencing / registration, and on what countries view as appropriate options in these regards. However, clearer means of formal recognition is desired. Largely, however, a legally mandated approach is desired.

Looking to the future, finding ways to address the issues of education and knowledge of practitioners in all sectors of the market, increasing the level of competency for all practitioners, and implementing clear and robust qualification / certification systems, are seen as critical to facilitating proper application and review of performance-based fire safety design, and expansion of fire safety engineering as a 'recognized' discipline [11]. Some steps have been taken, such as the publication of the *SFPE Recommended Minimum Technical Competencies for Fire Protection Engineering* [15], but there is much more work to be done.

REFERENCES

[1] Meacham, B.J. (1998). The evolution of performance-based codes and fire safety design methods, NIST GCR 98–761, NIST, Gaithersburg, MD, USA.

[2] Hadjisophocleous G.V., Benichou, N., Tamin, A.S. (1998). Literature review of performance-based codes and design environment. J Fire Protect Eng, Vol. 9(1): 12–40.

[3] Meacham, B.J., Moore, A., Bowen, R. and Traw, J. (2005). Performance-based building regulation: current situation and future needs, BR&I, Vol.33, No.1, 91-106.

[4] Meacham B.J. (2000). International experience in the development and use of performance-based fire safety design methods: Evolution, current situation and thoughts for the future, Proceedings, 6th International Symposium for Fire Safety Science, IAFSS, pp.59–76.

[5] Loa, S.M, Gaob, L.J., Yuena, K.K. (2007). The development of performance-based fire safety engineering in Hong Kong and Japan, International Journal on Engineering Performance-Based Fire Codes, Volume 9, Number 3, p.133-139.

[6] Lloydd, D. (2008). Evaluation of the conceptual framework for performance-based fire engineering design in New Zealand, M.Sc. Thesis, University of Canterbury, Christchurch.

[7] Alvarez, A., Meacham, B.J., Dembsey, N.A., Thomas, J.R. (2013). 20 years of performance-based fire protection design: challenges faced and a look ahead, J Fire Prot Eng 23:249–276.

[8] Alvarez, A., Meacham, B.J., Dembsey, N.A., Thomas, J.R. (2014). A framework for risk-informed performance-based fire protection design for the built environment, Fire Technology, 50:161-181, DOI 10.1007/s10694-013-0366-1

[9] Meacham, B.J. (2018). Situation with performance-based codes and fire safety design in seven countries, Proceedings, 12th International Conference on Performance-Based Codes and Fire Safety Design Methods, SFPE, Gaithersburg, MD.

[10] Meacham, B.J. (2018). An international perspective on the state of performance-based design for fire, Fire Protection Engineering, Q3, Issue 79, SFPE, pp18-26.

[11] Astrom, J., Axelsson, E., Lindahl, S., Meacham, B.J. (2019). What is needed to increase the use and acceptance of fire safety engineering: analysis of survey data from seven countries, 2019 SFPE Europe Conference, Malaga, Spain, 21-22 May 2019, SFPE, Bethesda, MD.

[12] Meacham, B.J. (2017) Research to Support the Improvement of the Design Verification of Fire Engineered Solutions as Part of the Scottish Building Regulatory System, prepared for Scottish Government, Building Standards Division, Livingston, Scotland, July 2016 (available for download https://www.webarchive.org.uk/wayback/archive/20171001135836/http://www.gov.scot/Topics/Built-Environment/Building/Building-standards/publications/pubresearch/researchfire/resfirdvfes, last accessed 20 April 2019).

[13] Meacham, B.J. (2017). Observations on the Situation with Performance-Based Building Regulation and Fire Safety Engineering Design in Sweden and the Potential for Incorporation of More Risk-Based Concepts, Report from Fulbright Global Scholar research, Sweden, March 2017 (https://www.boverket.se/sv/byggande/sakerhet/brandskydd/riskbaserade-byggregler/, last accessed 20 April 2019)

[14] Meacham, B.J. (2018). Feasibility of a Centralised Hub for Verification of Complex Fire Engineered Solutions in Scotland, research report prepared for Scottish Government, Building Standards Division, Livingston, Scotland, May 2018 (https://www.gov.scot/publications/feasibility-centralized-hub-verification-complex-fire-engineered-solutions-scotland/, last accessed 20 April 2019).

[15] SFPE (2018). Recommended Minimum Technical Competencies for Fire Protection Engineering, Society of Fire Protection Engineers, Gaithersburg, MD, USA (Available for download from SFPE at https://cdn.ymaws.com/www.sfpe.org/resource/resmgr/docs/core_competencies/minimum_fpe_competencies_fin.pdf, last accessed April 20, 2019).

EMERGENCY PLANNING BASED ON FIRE SCENARIOS

[1]António Braz Leiras, [1]João Paulo Rodrigues, [2]Brian Meacham
[1]Coimbra University, Portugal
[2]Meacham Associates, U.S.A.

ABSTRACT

The effectiveness of occupant response during a fire event, in particular emergency response functions, depends significantly on adequate emergency planning in advance of an event. In order to develop effective emergency response plans, it is crucial that the fire safety management personnel undertake an appropriate emergency planning process. Such a process can be quite complex, in order to simplify planning and make the process more efficient, an emergency planning methodology based on potential fire scenarios is proposed. This methodology allows fire safety management personnel to execute the planning and to evaluate its results using carefully selected fire scenarios, taking into account the fire risk factors arising from the building itself and the nature of its occupation.

Keywords: scenario, fire, planning, response, emergencies.

1 INTRODUCTION

Reality has proven that the efficiency with which a particular organization or community deals with an emergency situation depends on how well-prepared emergency responders are in advance of an event, especially given the unknowns associated with any event [1]. The best way to prepare is through development and exercising of an emergency plan. For this reason, emergency planning should be formally documented, approved by the authority with jurisdiction in the building, adequately publicized to all the building occupants, and sufficiently exercised by all interveners. In some countries, such plans may be legally required, since it is recognized that the development of effective plans, emergency actions and appropriate training can result in less serious injuries and less damage to facilities [2].

To assist fire safety managers in the development of effective emergency response plans, a new methodology is proposed: Emergency Planning Based on Fire Scenarios (EPBFS). In the development of the EPBFS methodology, the existence of two types of emergency planning is considered: (i) internal emergency planning and (ii) external emergency planning. Internal emergency planning is the responsibility of emergency response organizations made up of building occupants, who must have basic education and training [3] to carry out first response activities. External emergency planning refers to public organizations that are made up of specifically educated and trained emergency response professionals (for example, firefighters) [4]. In addition, the development of the EPBFS methodology considers that an emergency is generally an unplanned, sudden event, which may result from several causes, have a variety of potential impacts, and have differing outcomes based on the response time and preparedness of the responders. Although this article examines the use of the EPBFS methodology only for emergency situations caused by fire, the same methodology can be used in planning the response to emergency situations of another nature involving other types of emergency organizations.

2   EMERGENCY PLANNING OVERVIEW

Emergency response planning considers internal and external intervention. The primary purpose of internal fire response planning for buildings is to create an effective strategy for immediate fire extinguishment, and if this is not possible, to reduce as far as possible the fire impact on the occupants, the building and its contents. External emergency response planning is focused on response of emergency public services (e.g., local fire service). The complexity of emergency planning that is required will depend on factors such as the type of facility, the nature of the occupation and the risks involved [5], as well as the operational capacity of the emergency public services and their maximum response times.

Irrespective of the complexity, it is essential to consider a set of basic questions, as reflected in Figure 1.

Fig. 1- Questions to be answered by any planning process (source: authors).

Specifically, the questions to be answered include: who is responsible for what actions? At what point in the fire (when) and from what location (where) does response action occur? Why is the action needed (purpose)? How should the actions/operations be undertaken, and what resources (personnel, equipment) are needed (who)?

Emergency plans should be characterized by a modular organization, integrated communications, unified command structure, consolidated action plans, feasible control limits, pre-defined incident features and understandable resource management [1]. Plans should clearly define, for each responder, issues such as mission, roles and responsibilities, principles of action and hierarchical dependence in the context of emergency response. It is also important that plan clearly and effectively define the delegation of authority in emergency management and the authority to carry out the emergency actions required to control the situation and to quickly restore normal activity for business continuity.

Some of the basic aspects of emergency planning for fire are to understand the fire risk, reduce those risks and prepare the organization for a potential fire [6]. An important factor in achieving efficient fire response by organizations occupying buildings is the quality of the management process of these organizations in the three possible modes of operation: routine mode, training mode and emergency mode. As for the management of any other activity, for emergency management it is important that the functional levels established in the planning phase continuously run through all phases of the management circle.

It is suggested that, in order to sustain an adequate emergency management process, three functional levels are needed: institutional (strategic), intermediate (tactical), and operational (technician).

There are three temporal phases which can be considered for the emergency management process. First, there is the "pre-emergency" phase (planning process), in which the representatives of all entities or services that are part of the response to emergencies work together to develop and effective approach, including defining emergency management policies, organizational structure, resource allocation, and operational firefighting systems needed to support operations. Second is the "emergency" phase, which covers the duration of the emergency response – the stage at which the emergency plan is activated and in which the plan is executed. Third is the "post-emergency" phase, which involves recovery, safeguarding of assets, and business continuity operations. At this stage, joint meetings are also held to assess the performance of all organizations involved in emergency response and the planning process itself, in order to propose and validate improvement proposals.

3   FIRE SCENARIO OVERVIEW

In general terms, a fire scenario represents a technical description of the social expectation related to fire safety, which should include all potential fire elements in relation to building behavior and human response [7]. A fire scenario should describe the critical factors for the occurrence of fire, such as ignition source, nature and fuel configuration, ventilation, characteristics and location of the occupants and the structural conditions of the building. The National Fire Protection Association [5] defines *fire scenario* as the set of conditions relating to the development of a fire, its propagation, the products released, the reaction of the people and the effects of the products of combustion. The same source defines *Design Fire Scenarios* (DFS) as being a set of fire scenarios that can be selected for the purpose of fire safety performance evaluation of solutions in the design phase. DFS specify the fire conditions against which a particular proposal or technical solution is expected to meet the fire safety targets. In NFPA documents, eight design fire scenarios are specified [5].

The process of developing and using fire scenarios for analysis and decisions concerning fire safety assessment, the following points are critical [8]: i) the importance of collecting information about the conditions that are intended to be analyzed, ii) the definition of the goals of that evaluation, iii) selection of criteria to be applied, iv) development and selection of fire scenarios and v) study, selection and development of appropriate solutions. In addition, it is important to quantify design fire scenarios into engineering terms for use in analysis. There are many ways to accomplish this. According to the main standards organization of Norway [12], the design fire scenarios should represent typical severe fires that may occur in the specific building category. A worst credible case scenario is typically represented by a rapid growth rate and a high heat release rate (HRR). It is possible to analyze the most important events that intervene in the fire due to the HRR and the time.

One of the most used approaches to define HRR is the αt^2 equation. It is assumed that the energy release rate of a fire increases proportionally with the square of time. Based on this equation, the following fire growth rates are used, depending on the type of building occupation: slow, medium, fast and ultra-fast. In this way, it is possible to analyze the main events that compete for the fire function to the HRR and the time.

Using the DFS model above the concept of Emergency Responder Fire Scenario (ERFS) is proposed defined as "a fire scenario that specifies the fire conditions from which emergency planning can be carried out or whether a given technical-operational solution fire response (organization, structure, resources, etc.) meets fire safety goals. It is suggested that the use of ERFS for the purpose of planning and evaluating the response to emergencies caused by fire is as valid as the use of DFS for fire safety systems planning and evaluation. As with development of DFS for fire safety systems performance assessment, time is an important component in the development of ERFS for evaluating emergency intervention. Here, description of the ERFS starts from established burning and includes the time required for any internal response to the emergency, through the arrival of the public fire services within the building at the attack point [9].

Development of the ERFS requires considerations of, i) space-time dimension that is intended to be assumed for that scenario, ii) type of building occupancy and activity risk factors, iii) most probable sources of fire, iv) location and size of the fire under the most unfavorable conditions reasonably foreseeable, v) velocity of fire spreading according to the physical and chemical characteristics of fuels, vi) fire load, vii) conditions relating to the production and control of combustion products, viii) subdivision conditions, ix) immediate and remote exposures to fire, x) evacuation and rescue conditions and xi) installed capacity of active means of fire safety. The ERFS is a main component of the EPBFS approach.

4 EMERGENCY PLANNING BASED ON FIRE SCENARIO

There may be more than one EFRS for a building or facility. Each ERFS should present a set of conditions that represents a fire with an effective risk of occurrence, qualitatively or quantitatively determined. It is fundamental that it be developed from a justifiable cause or event and that the consequences represented by it correspond to the expected development of the fire in the space. For this reason, it is important that the EPBFS process starts with a fire risk assessment, which identifies the range of possible emergency fire scenarios that could occur, from which a sufficient number of emergency planning scenarios are selected. Selection should consider both likelihood of occurrence and the expected magnitude of their consequences. For example, a scenario may be technically possible but highly unlikely and, in this case need not be considered for emergency planning purposes. It is also important to note that the project fire scenarios used are reality based and developed in accordance with the type of occupation and in the worst conditions that are reasonably foreseeable [10].

As part of the EFRS development process, the time from ignition or established burning to intervention must be estimated. This can be expressed as the Established Scenario Time (EST). The EST must be equal to or greater than the response time guaranteed by the public fire services (TGFS) to the area of the building (arrival on scene and first water application). The EST can be represented in a timeline, as illustrated in Figure 2. In a way, this allows for comparison of the time

for fire development compared with emergency response in a manner similar to available safe egress time (ASET) versus required safe egress time (RSET) analysis for occupant evacuation.
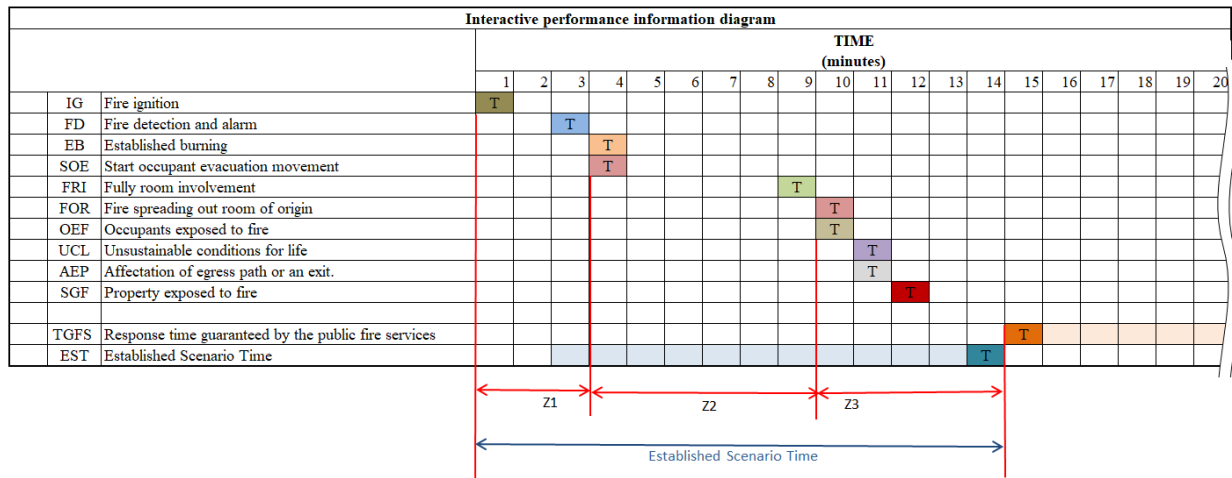
Interactive performance information diagram																						
		: TIME (minutes)																				
		1	2	3	4	5	6	7	8	9	10	11	12	13	14	15	16	17	18	19	20	
IG	Fire ignition	T																				
FD	Fire detection and alarm		T																			
EB	Established burning				T																	
SOE	Start occupant evacuation movement				T																	
FRI	Fully room involvement									T												
FOR	Fire spreading out room of origin										T											
OEF	Occupants exposed to fire										T											
UCL	Unsustainable conditions for life											T										
AEP	Affectation of egress path or an exit.											T										
SGF	Property exposed to fire												T									
TGFS	Response time guaranteed by the public fire services															T						
EST	Established Scenario Time														T							

Z1   Z2   Z3

Established Scenario Time

Fig. 2- Interactive performance information diagram

Figure 2 shows an example of a dynamic analysis ERFS where the analysis zones (Z1, Z2 and Z3) and the Established Scenario Time (EST) can be verified. The Z1 allows to analyze aspects such as resources for immediate intervention (by any building occupants) or features for immediate fire extinguishing (fire extinguishers, low flow water lines, etc.) or features for evacuation. The Z2 allows to analyze features for protection against exposures, for rescue or for first aid to victims. The Z3 allows to analyze aspects such as the internal organization of fire response (first and / or second intervention), operational structures, training needs, as well as material and human resources to be made available for the response to the fire scenario under analysis.

Once all aspects of emergency planning have been effectively implemented, their performance can and should be assessed by an assessment process based on emergency fire scenarios. Figure 3 presents the methodology of emergency planning based on fire scenarios.

In the last phase of the EPBFS process, the structure shown in Figure 4 is used to determine the four factors of capacity and compatibility.

Based on the process of identifying fire risk factors (1), the nature and magnitude of the ERFS are identified, as a function of the critical factors that integrate them (2). The TGFS and the operational capacity of the public fire services (3) are determined using joint training and mutual aid protocols. The TGFS must be determined by a sufficient number of response time test exercises to be performed by the public fire services of the community where the building is located. These test exercises shall be carried out under the most unfavorable conditions reasonably foreseeable. Taking into account the previous phases and using the process of dynamic analysis of selected ERFS (Figure 2), the nature of the missions and the levels of intervention [11] to be assigned to the internal emergency organization (4) are determined.
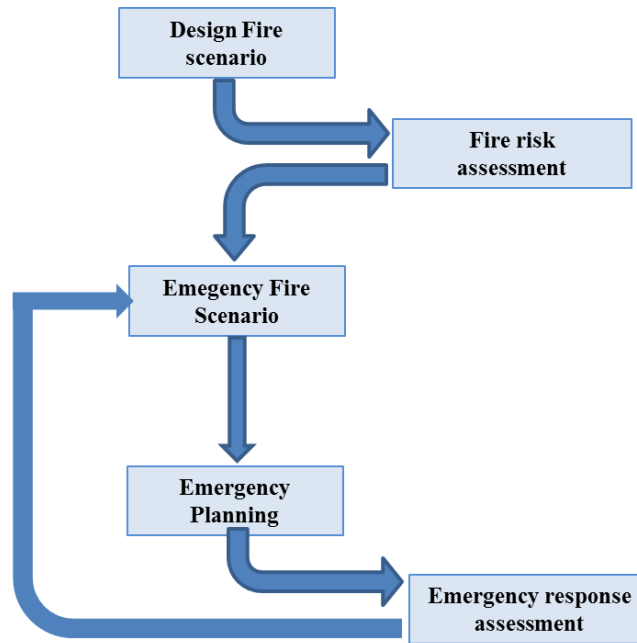
Fig. 3- Methodology for the use of fire scenario (source: authors)

Capacity and compatibility factors for emergency response
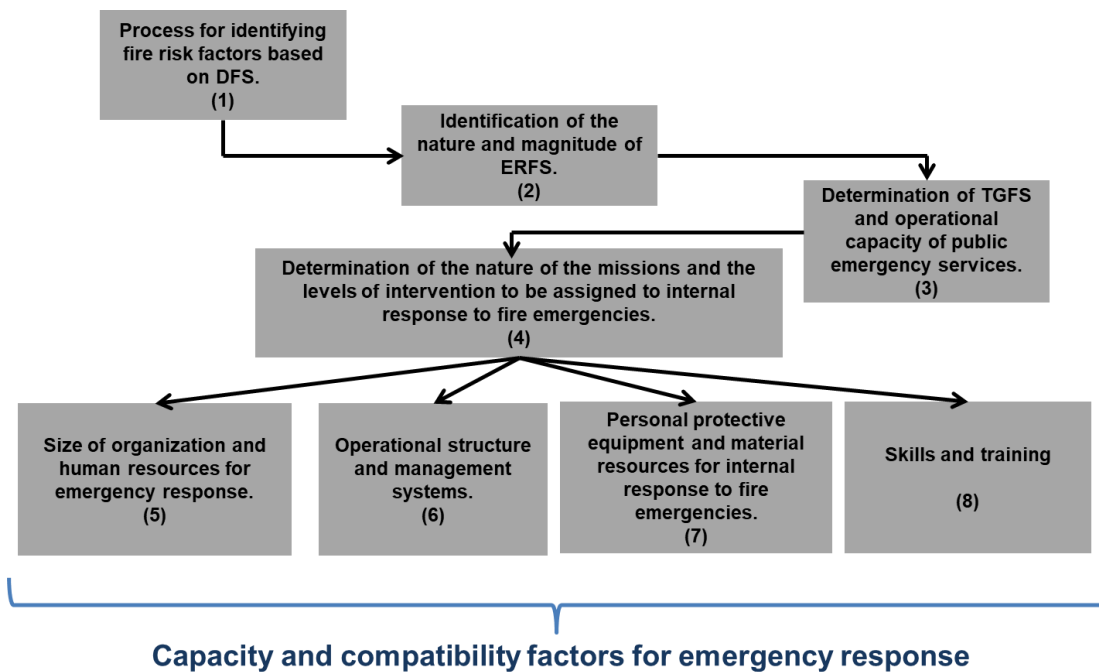
Fig. 4- Analysis methodology to determine resource needs for emergency response.

Based on the results of the previous phases, obtained in the dynamic analysis of all selected ERFS, the operational organization and the human resources are dimensioned so that the internal fire response organization can fulfill the missions assigned to it and perform the levels of response that the magnitude of ERFS requires (5). In view of the results of the previous phase, the operational structure and management systems necessary to ensure safe, efficient and expeditious operation (6) are determined. Depending on the tasks required to perform the missions and the response levels, the needs of individual protection equipment are analyzed in view of the risks to which personnel can be exposed and of resources to respond to the selected ERFS (7). Lastly, the competences

necessary to fulfill the missions and the assigned levels of intervention and the operation of the assigned equipment are identified. According to these competences, a diagnosis of education and training needs is made and a training and performance evaluation program is defined (8).

For the purpose of demonstrating the EPBF methodology, an example of ERFS is presented, which can be represented by fire as a function of HRR with time and the interactive performance information diagrams (IPID) as in Figure 2.

Assume there is a 10-storey hotel. The ERFS is a fire on the 3rd floor. Ignition is caused by a short circuit in a bedside table lamp near the bed. The room is not occupied. There are smoke detectors in each room. There are no sprinklers. The doors have no fire rating. As reflected in Figure 2, the response time guaranteed by the public fire services (TGFS) to the area of initial firefighting within the building is considered 14 minutes. Also as seen in Figure 2, it is estimated that occupants outside of the room of fire origin will begin to be exposed to smoke and hot gases after 9 minutes (flashover in room of origin and failure of door), and the conditions in the horizontal evacuation route on the 3rd floor will be dangerous to occupants within 10 minutes. By the time the fire service arrives (TGFS), the fire will involve the room of origin, the corridor, and potentially more rooms on the 3rd floor (EST).

Using the IPID, one can see that both the TGFS and the EST are 14 minutes, the fire service will have no hope to safeguard people on the 3rd floor, since it is expected that the fire will have spread outside the room of fire origin, the 3rd floor horizontal exit pathway will be untenable, and there is some chance that other compartments may be involved in the fire. This means that in order to safeguard people, the fire must be controlled earlier (reduce the EST), there needs to be efficient response planning in place by trained teams within the building to assist people and fight the fire, or the TGFS needs to be significantly reduced (from 14 minutes to perhaps 5 minutes).

By using the EPBF methodology, it can therefore be shown how the interrelationship between the emergency response teams and the building fire safety systems must perform to safeguard occupants and property.

5   CONCLUSIONS

The effectiveness of internal (occupant-based) and external (public fire service) emergency response operations in case of fire in buildings depends significantly on adequate emergency planning. In order to increase the reliability and effectiveness of emergency response planning, a methodology based on use of emergency response fire scenarios is presented. The cluster of reasonably foreseeable emergency fire response scenarios is formally assumed for emergency planning purposes. Based on this cluster of scenarios, a resource needs analysis is carried out, using four capacity and compatibility factors for emergency response. It can be concluded that the EPBFS methodology has been shown to be simple and effective to quantitative and qualitative emergency response planning based on fire scenarios.

REFERENCES

[1] OSHA (2015). 1910 Subpart E App - Exit Routes, Emergency Action Plans, and Fire Prevention Plans. Available in internet: https://www.osha.gov/law-regs.html.

[2] National Fire Protection Association (2015). *NFPA 101: Life Safety Code.* (pp. 31) Massachusetts, Codes and standards NFPA.

[3] National Fire Protection Association (2018). NFPA 1081 - Standard for Industrial Fire Brigade Member Professional Qualification. EUA, 53 p.

[4] National Fire Protection Association (2012), NFPA 1001 - Standard for Fire Fighter Professional Qualifications, EUA, 20 p.

[5] National Fire Protection Association (2015). *NFPA 101: Life Safety Code.* (pp. 31) Massachusetts, Codes and standards NFPA.

[6] Brunacini A.V. (2002) – Fire Command. EUA, 416 p.

[7] Feasey, R. (2005). *Guidelines for Managing Fire Risks in Historic Buildings and Heritage Collections.* (pp. 5). Hamilton: Opus International Consultants.

[8] Brannigan, V. (2000). *Fire Scenarios or scenario fire? Can fire safety science provide the critical inputs for performance based fire safety analyses.* (pp. 214). Boston. Curtat, M., Editor.

[9] Meacham, B.J. (1998). Assessment of the technological requirements for the realization of performance-based fire safety design in the United States. (pp. 12). Washington, DC. Robert A. Peck, Commissioner.

[10]   Fitzgerald R. B. and Meacham B. J. (2017). *Building fire performance analysis*, 670 p. Massachusetts, John Wiley e Sons.

[11]   Alexander D. (2012). Principles of emergency planning and management, 319 p.

[12]   Standards Norway (2013) - prINSTA TS 950 - Fire Safety Engineering - Verification of fire safety design in buildings, 43 p.

DEFINING A BURNOUT RESISTANCE RATING TO COMPARE STRUCTURAL COMPONENTS UNDER REAL FIRES

Thomas Gernay

Department of Civil Engineering, Johns Hopkins University, Baltimore, U.S.A. tgernay@jhu.edu

ABSTRACT

Standard metrics are useful for comparing design solutions. Structural fire engineering largely relies on the fire resistance rating, but the latter quantifies the performance under rising temperatures only, and does not contemplate the capability to survive until full burnout. Here, a new metrics is introduced to quantify the resistance to burnout under fires with heating and cooling phases. This burnout resistance rating is evaluated for different structural components in concrete, steel and timber. For RC columns, an analysis on 74 specimens allows deriving a linear relationship between the burnout resistance and the fire resistance. Preliminary results for protected steel columns and RC beams indicate a similar trend, while timber beams seem to have a relatively lower burnout resistance at given fire resistance. Adoption of the burnout resistance alongside the fire resistance provides a more accurate picture of comparative performance for elements under real fires.

1 INTRODUCTION

The fire resistance rating has proven very useful for standardized, prescriptive methods in fire safety engineering. Yet, the absence of consideration for the decay phases of fires and their effects on structural behaviour is an important shortcoming. Structural components can fail during or after the time of maximum gas temperature, due to a number of factors that include: delayed temperature increase in the component sections, stress and load redistributions due to the incompatibility of strains and/or the interactions between components, and additional material degradation (e.g. loss of compressive strength in concrete, continued charring in timber). Importantly, these factors are in part material- and component-dependent. This means that, possibly, different structural components with a same fire resistance may exhibit a significantly distinct behaviour under a real fire, where one of them might survive until full burnout while the other one fails. This is a considerable difference as, in the end, two designs deemed equivalent based on the current fire resistance rating might lead to completely distinct outcomes at the end of a fire event. It results that the fire resistance alone is ill-defined to fully depict the performance of even simple (isolated) structural components under fire, and hence to inform on the best design solution.

It has recently been proposed by the author to define a new metrics, the burnout resistance [1]-[2]. This metrics quantifies the ability of a structural component to survive throughout the entire duration of a fire. Therefore, the burnout resistance arguably provides a more representative and fair rating than the fire resistance for comparing different components, since any real fire comprises a decay phase. In this paper, a brief description of the new metrics is given, after which the burnout resistance is assessed for a variety of structural components in concrete, steel and timber.

2 BURNOUT RESISTANCE RATING

2.1 Definition

For any structural component under given loads and boundary conditions, one can define the shortest natural fire for which the component will eventually fail, see Fig. 1, provided a definition of a set of 'standardized natural fires' is adopted where the fires can be ranked in severity. A convenient choice for standardized natural fires are the Eurocode parametric fires in which the

parameter Γ is set equal to 1. By setting Γ = 1, the heating phase of the parametric fire approximates the ISO 834 standard temperature-time curve, and the fire is unequivocally defined in heating and cooling as a function of a single variable, the duration of the heating phase (DHP, in minutes) [1]. By this definition, a component's burnout resistance is the DHP of the shortest 'standardized natural fire' that the component cannot survive (Fig. 1).

It is important to notice that the burnout resistance DHP of a member does not coincide with the time at which it fails. Indeed, the DHP is always smaller than the fire resistance R, due to the factors acting during cooling as listed in the previous section. Generally, structural collapse can occur several minutes or hours after the time corresponding to the DHP, and it may even occur after the end of the fire, when the temperature in the compartment is back to ambient.

The burnout resistance is a standardized rating, as is the fire resistance. Therefore, it should not be considered as an exact time quantity but as a qualitative index for comparing the performance of different structural components under real fires. The burnout resistance rating is correlated with the ability to survive a fire until full burnout; it conceptually divides the time domain between fires that are short enough to be survived until burnout and fires that bring so much heat/damage that they will result in eventual collapse.
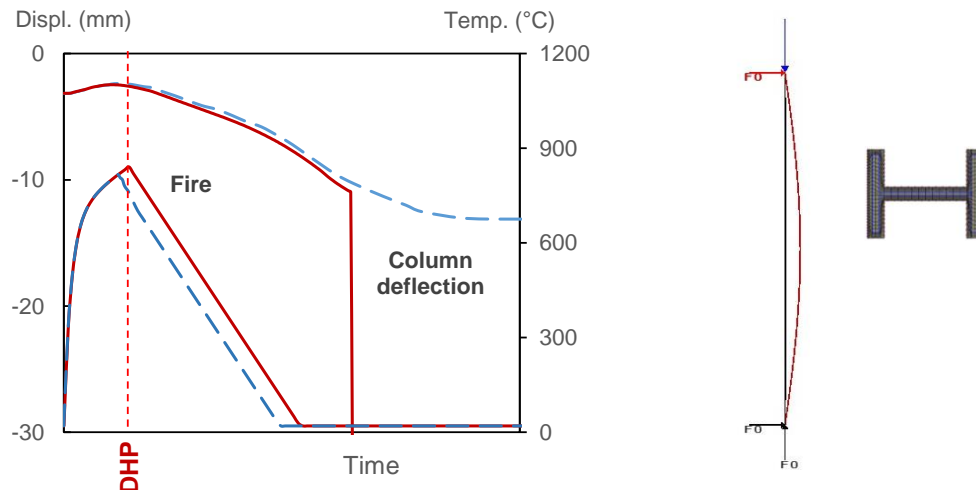
Fig. 1. The burnout resistance (DHP) is defined as the shortest fire that a member cannot survive, as illustrated here by the continuous red line. To make it a standard metrics, an agreed set of natural fires must be adopted. The proposed set of natural fires uses the Eurocode parametric fire model where the heating phase is set similar to the ISO 834 fire.

2.2 Method to derive the burnout resistance

Except for the simplest elements, the analysis of a structural component under natural fire necessarily requires a verification in the entire time domain by a step-by-step iterative method, since verification in the load domain at the time of maximum gas temperature does not guarantee against failure at a later stage. Therefore, numerical analyses by the finite element method are used to assess the thermo-structural response of the components under natural fires.

Finding the DHP of a component requires an iterative procedure, where temperature-time curves of increasing duration of heating phase are applied to the component until failure is observed. Each calculation must be run for long enough to ensure that the temperatures have returned back to ambient inside the sections and that no failure is going to occur. The iterative procedure with multiple thermo-mechanical simulation for a given component can be automatized using a simple script [2]. In this paper, the software SAFIR [3] developed at Liege University and Johns Hopkins University is used for running the simulations.

As the burnout resistance entails analyzing the behavior during the cooling phase, emphasis is put on accurate modeling of the materials properties during cooling. In particular, it must be ensured that properties are not recovered when they should not (e.g. concrete strength; timber properties in the charred layer; etc.). In the analyses, irreversible thermal and mechanical properties are employed where appropriate based on literature data. In addition, transient creep strain is incorporated explicitly in the concrete material law based on the ETC model by the author [4].

3 APPLICATION OF THE RATING TO STRUCTURAL COMPONENTS

3.1 Reinforced concrete columns

Experimental data on standard fire resistance tests of RC columns have been gathered from 74 tests coming from three countries. These include 39 tests conducted at the Technical University of Braunschweig in Germany [5], 16 tests conducted at the University of Ghent and University of Liege in Belgium [6], and 19 tests conducted at the National Research Council in Canada [7]. In each of the 74 tests, a loaded reinforced concrete column was exposed to a standard temperature-time curve (either ISO 834 or ASTM E119) on its four sides. Parameters vary between the tests including the end conditions, length of the column, cross-section geometry, reinforcement ratio, material strengths, and magnitude and eccentricity of the load. Square and rectangular cross-sections were tested. The experimentally obtained fire resistance is noted 'R Test'.

First, the 74 tests have been simulated using SAFIR. Fiber-based beam finite elements have been used. The material properties of Eurocode were adopted. For concrete, the explicit transient creep formulation [4] was used to guarantee non-recovery of the transient creep strain. Fig. 2a plots the computed and test data for the 74 columns. The average value of the ratio R Model / R Test is 0.95 with a standard deviation of 0.29. The dispersion is noticeable yet in line with other computational studies on RC columns; it is explained mainly by inherent variability in the tests and lack of information about some test parameters (e.g. temperature-dependent concrete behavior).

Secondly, the same 74 columns have been analyzed under the 'standardized natural fire' with cooling phase. The iterative computational procedure for deriving the burnout resistance was applied to each column considering increasing durations of the standardized natural fire until finding the shortest fire that could not be survived until burnout. This shortest fire has a duration of heating phase noted as 'DHP'.

Fig. 2b plots the relationship between DHP and R as computed numerically with SAFIR for the 74 columns. By definition, the DHP is always shorter than R for a given column. The difference between the DHP and R increases with R. The increase in the difference (R – DHP) indicates a higher propensity to fail during or after the cooling phase for columns with longer fire resistance times.

Interestingly, it is found that the DHP is approximately linearly proportional to R for the investigated RC columns [2]. A linear regression on the data of Fig. 2b yields the very simple formulation of Eq. 1, where the DHP can be obtained directly as a function of R:

$$DHP = 0.72 \times R - 3.0 \quad \text{(in min)} \qquad \text{Eq. 1}$$

Considered jointly, the couple (DHP, R) informs on the propensity of a structure to exhibit delayed failure. A member which metrics DHP and R are close, is unlikely to fail during or after the cooling phase of a fire. If such member is still standing when the fire fighters start extinguishing the fire, the most likely outcome is that it will survive full burnout. In contrast, structural members with a DHP much shorter than their fire resistance are at risk of delayed failure. Indeed, there are a potentially large number of fires that, while not leading to immediate collapse (i.e. the heating is less severe

than a duration R of the ISO fire), affect the member to such an extent that it will eventually fail (i.e. the heating is more severe than a duration DHP of the standardized natural fire).
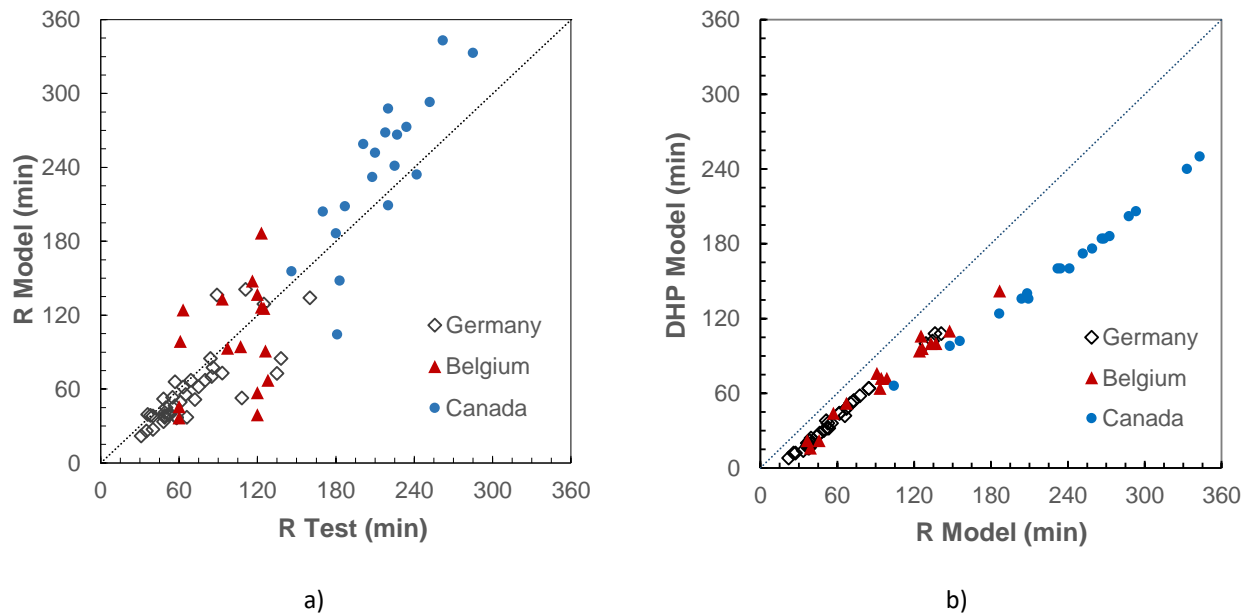

a)   b)

Fig. 2. a) Numerical modelling of 74 fire resistance tests on the RC columns; b) Relationship between the ratings of "fire resistance R" and "burnout resistance DHP" for the RC columns.

3.2 Steel columns

The studied steel columns are thermally insulated HEB 400 profiles in S355 exposed to fire on their four sides. The columns are 4 m long with a sinusoidal imperfection of amplitude L/300. They are simply supported at both ends and axially loaded at the top. Weak axis flexural buckling was prevented. Two thicknesses of insulation are used: P1 and P2 are designed to provide respectively a 60 min and 120 min fire resistance under 50% applied load ratio. The two columns are analysed under four load ratios varying from 30% to 60%; in each case both the fire resistance (R) and burnout resistance (DHP) are evaluated. Failure occurs by buckling of the columns.

The results are plotted in Fig. 3. It is found that the data points for the protected steel columns match quite well the relationship obtained for the RC columns (Eq. 1) (although a closer look reveals that the ratio DHP/R for P1 and P2 differs slightly from the one for the RC column). This result was not necessarily expected as different phenomena occur in the two types of structural components during cooling. At the material level, concrete exhibits a 10% additional loss of strength during the cooling phase, while steel recovers (most of) its strength. The thermal inertia of the sections are also different. Yet, it appears that the overall effect of the natural fire is similar for the RC and steel columns. This finding should be confirmed in further studies.

3.3 Reinforced concrete beams

The reinforced concrete beams, simply supported with a 6 m span, are exposed to fire on three sides. Two rectangular cross-section sizes are considered: 50 cm height by 22 cm width, and 41 cm height by 18 cm width. Both are reinforced by 3 lower bars of 20 mm diameter and 3 upper bars of 10 mm diameter, with a concrete cover of 40 mm. The applied load is uniformly distributed on the beam and maintained constant during the fire. The mechanical strength of concrete and steel reinforcement are 30 MPa and 500 MPa, respectively. The beams were analysed under four different applied load values.

The results, plotted in Fig. 3, again suggest a relationship between burnout resistance and fire resistance that reasonably agrees with Eq. 1. For these RC beams exposed on three sides, it is expected that the main effect governing the possible failure during cooling is the delayed heat transfer towards the lower rebars. Further studies will seek to confirm the observed results.
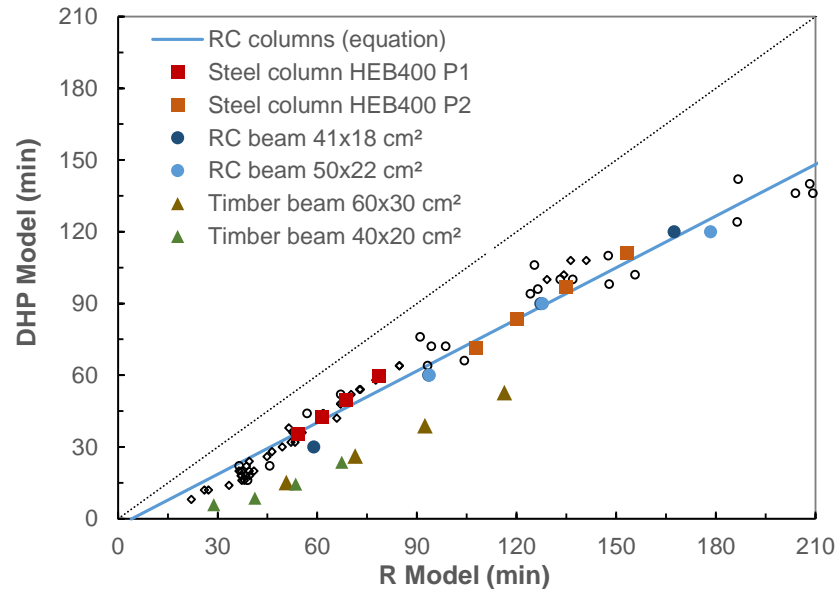

Fig. 3. Relationship between burnout resistance DHP and fire resistance R for different structural components. The steel and RC components fall approximately on a same line, while the timber beams have a lower DHP (at same R).

3.4 Timber beams

The timber beams are softwood timber beams, simply supported with a 4 m span, exposed to fire on three sides. Two rectangular cross-section sizes are considered: 40 cm height by 20 cm width, and 60 cm height by 30 cm width. The uniformly distributed applied load is maintained constant during the fire. The Young's modulus and characteristic bending strength at ambient temperature are 11 GPa and 24 MPa, respectively. Four different applied load values were considered.

Modelling the response of a timber component during the cooling phase is complex. Questions arise regarding charring and auto-extinction, thermal penetration depth, residual properties, etc. Research is ongoing to improve understanding of the behaviour of timber elements under real fires. Recent full-scale experimental research on exposed cross-laminated timber walls has indicated that the thermal penetration depth continued to increase for more than an hour after auto-extinction and halt of the charring front, which resulted in continued reduction of the structural capacity in the decay phase [9].

Here, the method of Annex B in Eurocode 5 is adopted. This method relies on numerical simulations based on the theory of heat transfer and evolution of the properties with temperature. It computes the temperature evolution in the entire cross-section; then, it applies temperature dependent reduction factors for the material mechanical properties. However, the evolution of properties with temperature is only given for standard fire exposure (as these "effective" properties were calibrated on standard fire resistance tests). It is assumed here that these properties are not recovered during cooling; they keep the value corresponding to the maximum reached temperature. Yet, additional data is needed on residual properties of heated, uncharred timber. Another limitation is the fact that these properties do not capture the additional energy possibly generated through member combustion during cooling (depending on time of auto-extinction). These limitations must be kept in mind while interpreting the results. Meanwhile, as the characterization of the burnout

resistance of timber members is of crucial importance, reliable models for analysing timber structures under natural fires are needed.

In Fig. 3, the results for the timber beams show a trend differing from Eq. 1. A linear relationship between DHP and R seems again to emerge, but with a factor considerably smaller than 0.72. This suggests a higher propensity to delayed failure for the timber beams, compared to the other studied members. This is probably due to the fact that the mechanical properties of timber are affected even at relatively low temperature, so that the delayed heat transfer affects the strength of the section core. Besides, these properties have been assumed as irrecoverable.

4   SENSITIVITY OF THE RATING TO MATERIAL PROPERTIES ASSUMPTIONS

Since the burnout resistance (DHP) entails analysing the structural response under cooling as well, assumptions must be made about the reversibility of the material properties. Notably regarding the material strengths, it is not enough to know the retention factors at elevated temperature; the residual values after cooling are also required.

The sensitivity of the DHP to the assumption for strength loss during cooling is considered here. In Section 3, the assumption for concrete strength was that a 10% additional loss occurs during cooling with respect to the retention factor at the maximum reached temperature [2]. For steel, a residual loss of yield strength of 0.3MPa/°C was assumed once it has been heated beyond 600°C (compared to the ambient strength); while the steel strength was considered as reversible where its temperature had not exceeded 600°C [10].

The sensitivity for steel was considered by re-running the simulations adopting, first, a larger residual loss of 1.0MPa/°C beyond 550°C, and second, no residual loss of strength. The first case means that steel heated to 750°C and cooled down would have a residual strength reduced by 200 MPa, compared to the initial value. The second case means full strength recovery. Yet, analyses showed no influence at all of the steel strength recovery assumption on the DHP.

For instance, the column P2 under 50% load ratio (R120) has a DHP of 84 min, irrespective of the steel strength recovery assumption. In all cases, this column fails after 148 min when exposed to the natural fire with 84 min heating phase, while it survives under the fire with 82 min heating phase. Looking at the heat transfer results in this protected section (Fig. 4) reveals that the time of failure coincides with the average time of peak steel temperature. Accordingly, the phenomenon governing the delayed failure here is the delayed temperature increase in the section, due to the thermal protection and thermal inertia, while the material behaviour in cooling plays no role.
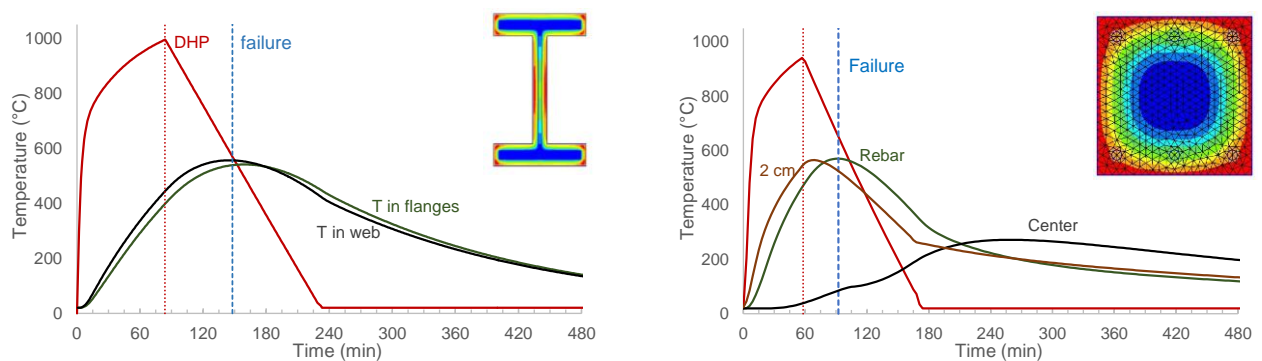

Fig. 4. (left) Temperature increase in the protected steel column section P2 under the shortest natural fire leading to failure (DHP 84 min). Failure occurs at time of peak steel temperature. *(right)* Temperature increase in a concrete column section under DHP fire of 58 min. At time of failure, most of the section is still heating up.

For the concrete members, the sensitivity to the value of the additional loss during cooling was checked by considering additional losses of 0%, 10% or 20% when cooling down from maximum temperature back to ambient. Selected simulations on columns were re-run under these three assumptions. For concrete, the temperature distribution in the section is not uniform and, at the time of failure, part of the section is in cooling (Fig. 4). The relative area of the section in cooling depends on the case, but generally, most of the section is still heating up when failure occurs under DHP fire. Therefore, for most cases no significant effect of the residual strength assumption on the DHP was observed.

If we were interested in residual capacity of the columns, then the assumption on strength recovery would be important. But this assumption appears insignificant when we are interested in failure of an element during cooling (i.e. burnout resistance), for the considered cases at least. It should be noted that configurations different from those simulated here might lead to a different conclusion, for instance when considering unsymmetrical fire exposure or structural assemblies. Additional studies are needed to explore other typologies and boundary conditions.

5   BURNOUT RESISTANCE OF A STRUCTURAL ASSEMBLY

It is the author's opinion that the prescriptive classification of structural members could rely on a pair of metrics (DHP, R) rather than on the fire resistance only, the two metrics providing a more complete picture of the structural fire response until complete burnout and, in combination, informing on the vulnerability to delayed structural failure. Among the factors affecting delayed failures, thermally-induced forces may be significant, such as tensile forces that build up in members and connections during cooling. For instance, load redistributions among columns subjected to distinct heating-cooling histories may threaten the stability of steel frames during the cooling phase [8]. As these effects emerge at the structural system level, the question arises whether the burnout resistance metrics can be used to characterize structural assemblies. It seems reasonable to apply the metrics to relatively simple structural systems where a post-flashover (uniform) fire is likely to occur, to comparatively assess systems vulnerability to cooling. Yet as the fire exposures and structure under consideration become more sophisticated, multiple potential failure modes can be observed for different fire scenarios (including non-uniform fires) [11], making it difficult to rely on a 'standardized set of natural fires'. It is useful to remember here that the objective behind the burnout resistance is to provide a standard metrics that allows easy comparison and classification, and certainly not to replace performance-based assessment supported by first principles of structural fire engineering and advanced computational analysis.

6   CONCLUSIONS

- While fires' cooling phases may affect structural stability for a number of reasons (material- and component-dependent), the fire resistance rating provides no insight into these effects.

- A 'burnout resistance' rating has been introduced to quantify the ability of components to survive throughout burnout. It is defined as the shortest fire that a member cannot survive.

- Analysis of a dataset of reinforced concrete columns heated on four sides revealed a linear relationship between burnout resistance and R. Preliminary results for other RC and steel members suggest that approximately the same relationship holds.

- Analysis of eight data points for timber beams showed a considerably lower burnout resistance than for RC and steel members at given fire resistance. This result needs to be confirmed through additional analyses; also, more reliable data and methods for timber behaviour in cooling are needed.

REFERENCES

[1] Gernay, T., Franssen, J.M. (2015). *A performance indicator for structures under natural fire*. Engineering Structures 100 (2015). https://doi.org/10.1016/j.engstruct.2015.06.005, 94-103 pp.

[2] Gernay, T. (2019). *Fire Resistance and Burnout Resistance of Reinforced Concrete Columns*. Fire Safety Journal 104 (2019). https://doi.org/10.1016/j.firesaf.2019.01.007, 67-78 pp.

[3] Franssen, J.M., Gernay, T. (2017). *Modeling structures in fire with SAFIR®: Theoretical background and capabilities*. Journal of Structural Fire Engineering 8 (2017), 300-323 pp.

[4] Gernay, T., Franssen, J. M. (2012). *A formulation of the Eurocode 2 concrete model at elevated temperature that includes an explicit term for transient creep*. Fire Safety Journal 51 (2012), 1-9 pp.

[5] Haß, R. (1986). "*Zur praxisgerechten brandschutztechnischen Beurteilung von Stützen aus Stahl und Beton*". Inst. für Baustoffe, Massivbau und Brandschutz der Technishen Univ. Braunschweig, Heft 69.

[6] Dotreppe, J.C., Franssen, J.M., Bruls, A., Baus, R., Vandevelde, P., Minne, R., Van Nieuwenburg, D., Lambotte, H. (1997). *Experimental research on the determination of the main parameters affecting the behaviour of reinforced concrete columns under fire conditions*. Magazine of Concrete Research 49 (179), 117-127 pp.

[7] Lie, T. T., Woollerton, J. L. (1988). *Fire resistance of reinforced concrete columns: test results*. Ottawa, Canada: National Research Council of Canada, Institute for Research in Construction.

[8] Gernay, T., Gamba, A. (2018). *Progressive collapse triggered by fire induced column loss: Detrimental effect of thermal forces*. Engineering Structures 172. DOI:10.1016/j.engstruct.2018.06.060, 483-496 pp.

[9] Wiesner, Felix, et al. (2019). *Structural capacity in fire of laminated timber elements in compartments with exposed timber surfaces*. Engineering Structures 179 (2019), 284-295 pp.

[10] Kirby BR, Lapwood D.G., Thomson G. (1986). *The reinstatement of fire damaged steel and iron framed structures*. London, UK: B.S.C., Swinden Laboratories. 0 900206 46 2.

[11] Rackauskaite, E., Kotsovinos, P., Jeffers, A., Rein, G. (2019). *Computational analysis of thermal and structural failure criteria of a multi-storey steel frame exposed to fire*. Engineering Structures 180 (2019), 524-543 pp.

POTENTIAL INSIGHTS FROM PERFORMANCE-BASED DESIGN OF FIRE PROTECTION IN TALL BUILDINGS

[1]Pierre Ghisbain, [1]Jenny Sideri, [1]Reyhaneh Abbasi, [1]Luciana Balsamo,[2] Reza Imani, [1]Ali Ashrafi,
Thornton Tomasetti, 40 Wall St., New York, USA
Thornton Tomasetti, 650 California St., San Francisco, USA

ABSTRACT

Performance-Based Fire Engineering (PBFE) is particularly applicable to tall buildings since a traditional prescriptive approach does not account for specific features and characteristics of tall structures. In this study, a PBFE approach is applied to a tall building and its potential impacts on the design are investigated. An example mixed-use tower is considered to investigate the PBFE approach through simulation of various fire scenarios and assessment of the building's structural response. Parametric temperature-time curves from Eurocode 1 are used to generate compartment fires representing fire scenarios. Subsequent thermal and mechanical response analyses are performed with a finite element model of the building. The study focuses on assessing the fire performance at critical locations of the building such as steel trusses of a transfer level, where large fire scenarios may lead to global effects as a result of a local fire.

1   INTRODUCTION

Traditional prescriptive fire protection of structural members in a building relies on unrealistic fire tests at component level. For a tall building, such an approach might miss important features of the response of the structural system to realistic fires, including the response of special structural features of such buildings that could have a global impact on the response to fire. This study is an attempt to examine some of such features. By employing a Performance-Based Fire Engineering (PBFE) approach, the engineer can explore the challenges and possible benefits of assessing the structural performance of a specific structure under realistic fire conditions, in order to develop more resilient and potentially cost-effective designs. In this study, a PBFE approach is employed on a mixed-used tall building structure, while various fire rating assignments are explored in order to gain a quantitative insight of the structural performance under realistic fire conditions, as opposed to code-prescribed fire exposures and fire ratings.

2   BUILDING AND FIRE SCENARIOS

2.1 Building Description

The process of PBFE is demonstrated through the example of a generic 50-story mixed-used tall building, which is representative of a common type of modern tall building design in the United States (Figure 1). The bottom 30 floors are office floors, with a concrete core and perimeter steel columns. The top 20 floors are residential floors, with a concrete core and concrete columns. The inner concrete columns are supported by transfer trusses at level 30. Transfer levels are commonly used in mixed-use tall buildings to create a transition from upper floors with large number of columns to lower levels which are designed to have an open plan with fewer columns.

2.2 Fire Scenario

The PBFE process starts with the identification of the worst-case yet realistic fire scenarios that can occur at the most vulnerable locations within a structure. The fire scenario considered in this study involves a fire event under the steel transfer trusses of the building. The occupancy of transfer levels is typically storage or mechanical, which have the potential to cause a fire with a large

amount of fuel. Such fire incidents might be deemed critical for the performance of the overall structure since they can potentially affect the upper parts of the structure supported by the transfer trusses.

In this particular building, the transfer level comprises of several interconnected transfer trusses that are 4 m deep, and occupy a space of 340 m^2 with a ceiling at 7 m height. It is assumed that combustible material such as stored items or mechanical equipment is spread over the majority of the space, producing a characteristic fire load density of 511 MJ/m^2 and a design fire load density of 620 MJ/m^2. These values are consistent with Annex E of Eurocode 1 (EC-1) [1] for the 80% fractile of office occupancy (in absence of a specific occupancy related to storage spaces).
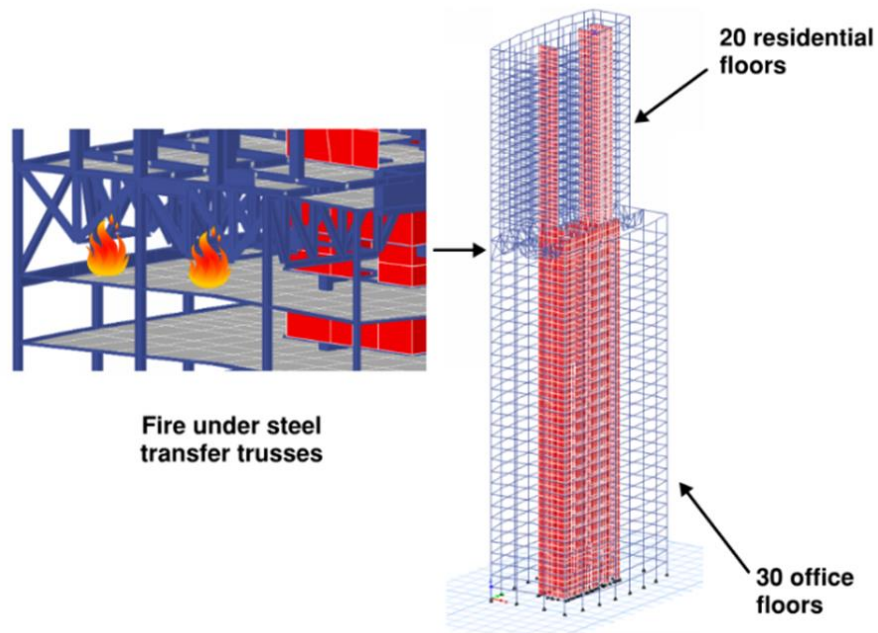
Fig. 1. Building configuration and fire scenario

3   ANALYSIS METHOD

3.1 Fire Simulation

Fire simulation is the next step in the PBFE process. Among the research and design community, several methods are used to simulate fires, whose complexity and accuracy varies significantly; from the non-realistic and highly conservative prescriptive standard fire curves such as the ISO 834 and the ASTM E-119 [8] fire curves which form the basis of fire rating tests, to fires generated from sophisticated computational fluid dynamic models such as NIST's Fire Dynamics Simulator (FDS) [2]. This study relies on the Eurocode-1 Annex A [1] parametric fire curve method, which although prescriptive, takes into account specific characteristics of the compartment under examination (area of the compartment, area and height of ventilation openings, thermal properties of compartment boundaries). One of the key assumptions of this method is that during post-flashover conditions, the compartment temperature is fairly uniform due to the upper hot gas layer having overfilled the compartment almost entirely.

Depending on the amount of ventilation available, highest compartment temperatures typically happen in a ventilation-controlled as opposed to fuel-controlled regime. Furthermore, between two fires with the same maximum compartment temperature, the ventilation-controlled fire will have the longer duration ([3], [4]). In this study, two EC-1 ventilation-controlled parametric fire scenarios with different opening factors are constructed (Figure 2). Fire Scenario 1 is defined with an opening factor of 0.08 which leads to a maximum average compartment temperature of approximately 1100°C and a total fire duration of approximately one hour. This scenario can be considered as a very high temperature but short duration scenario. At the other end of the spectrum, Fire Scenario 2 is defined with a lower opening factor of 0.025 that leads to a lower average compartment temperature of approximately 940°C but to a much longer fire duration of four hours. Alternative scenarios with opening factors higher than 0.1 are fuel-controlled fires with temperatures less than 1100°C and durations less than one hour and thus are deemed not critical. For the compartment boundary properties of both fire scenarios examined, lightweight concrete properties are utilized as a conservative assumption given the low conductivity of lightweight concrete, leading to higher compartment temperatures. Another conservative assumption is the application of the EC-1 parametric fire method for a compartment height exceeding the 4 m limit of EC-1, because taller compartments are less likely to accumulate heat as intensely as described in EC-1.
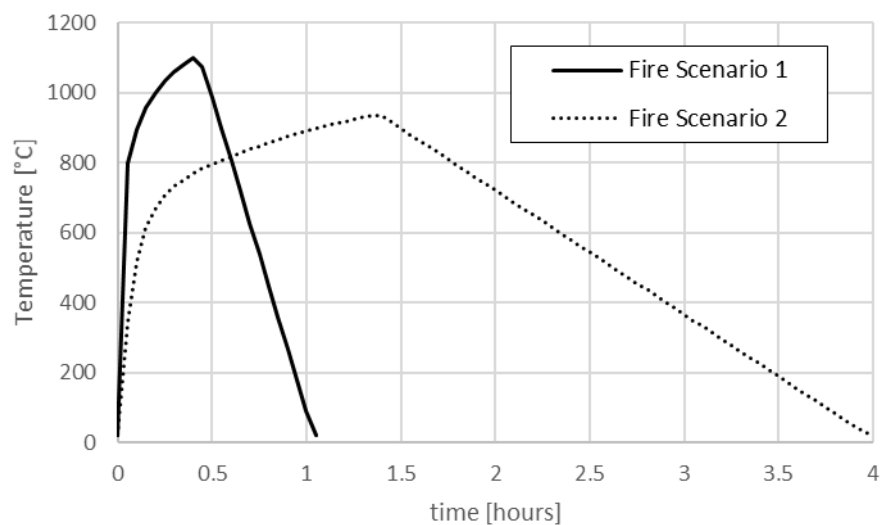
Fig. 2. Parametric temperature-time curves from Annex A of Eurocode 1 for Fire Scenario 1 & 2.

3.2 Heat Transfer FE Analysis

The fire simulation of the EC-1 parametric fire methodology is followed by sequentially coupled thermo-mechanical analyses in the general purpose FE analysis software Abaqus [5]. The time histories obtained from EC-1 are uniformly applied as convection and radiation interactions on the member surfaces, except at the upper chords of the trusses which are embedded in concrete. Steel thermal properties are modelled as temperature-dependent per Eurocode 3 [6]. The wide-flange sections and gusset plates at the connections are modelled with 4-node composite layered shell elements, which present the advantage of allowing for local failure modes (for example web buckling) and give flexibility to quickly change the fireproofing layer properties to achieve different fire ratings.

Code-compliant fire protection design for this particular structure would require a 3-hour fire rating on the steel members. However in this study, three different cases of fire protection scheme are examined: 1-hour, 2-hour and 3-hour fire rating. The fireproofing shell thicknesses for each case are calculated per the applicable UL design [7]. The goal of investigating these fire protection cases is to gain quantitative insight into the performance of the structure under more realistic fire conditions than the widely-used highly conservative ASTM E-119 fire tests.

Figure 3 illustrates the temperature time-history of an example shell element at the flange of a bottom truss chord for the 1-hour fire rated case, for the two EC-1 fire scenarios. It is evident that the fireproofing reduces the steel temperatures dramatically. In addition, Fire Scenario 2 is more detrimental for the structure since the steel temperatures are higher than the temperatures in Fire Scenario 1; even if Fire Scenario 2 displays lower peak compartment temperatures, its much longer duration allows for more intense heating of the steel members than Fire Scenario 1. This can be further explained by observing that for Fire Scenario 2 the trusses are exposed to temperatures above 800°C for more than 1.5 hours, while for Fire Scenario 1 the compartment temperature exceeds 800°C for approximately 0.5 hour. Therefore, further analysis results are only shown for Fire Scenario 2. The analysis duration for Fire Scenario 2 continues for an additional 8 hours beyond the end of the fire in order to allow for cooling of the structure.

Figure 4a-c depicts temperature contours of the underlying steel for the 1-hour, 2-hour and 3-hour fire rated cases for Fire Scenario 2, at a thermal analysis time where maximum steel temperatures are reached for each case; the maximum temperature of the structural elements are 525°C, 394°C and 314°C, respectively.
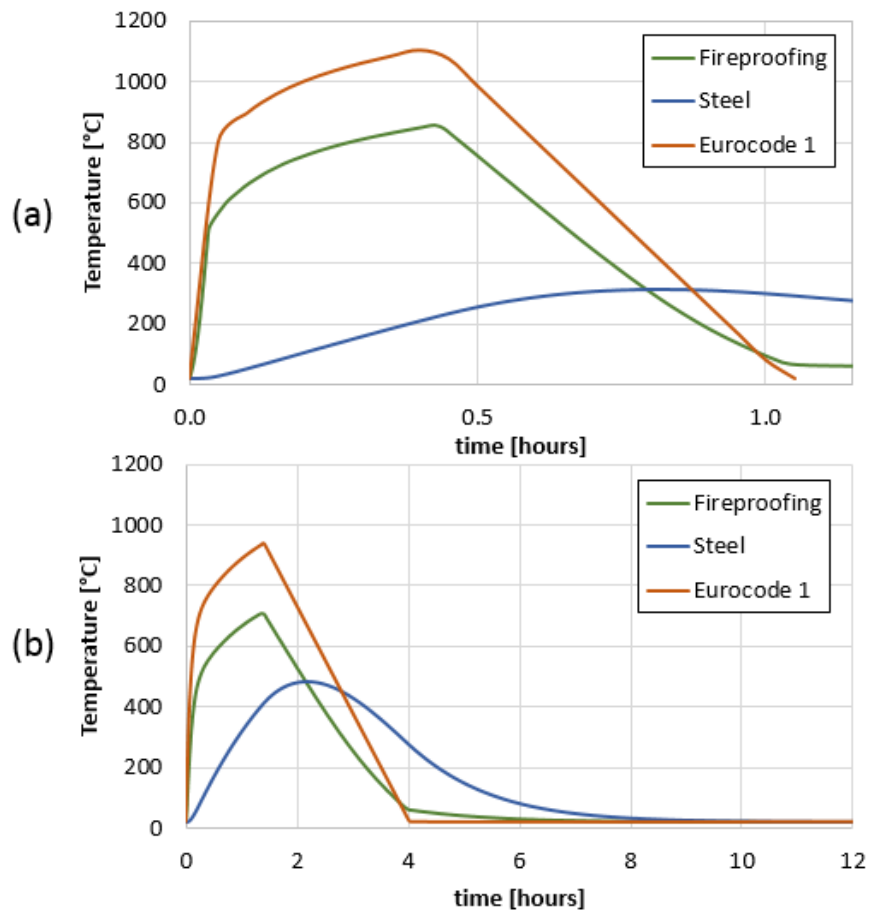
Fig. 3. Temperature time history 1-hour of fire rated case at the bottom flange of a bottom truss chord, for a) Fire Scenario 1 and b) Fire Scenario 2 including the cooling phase
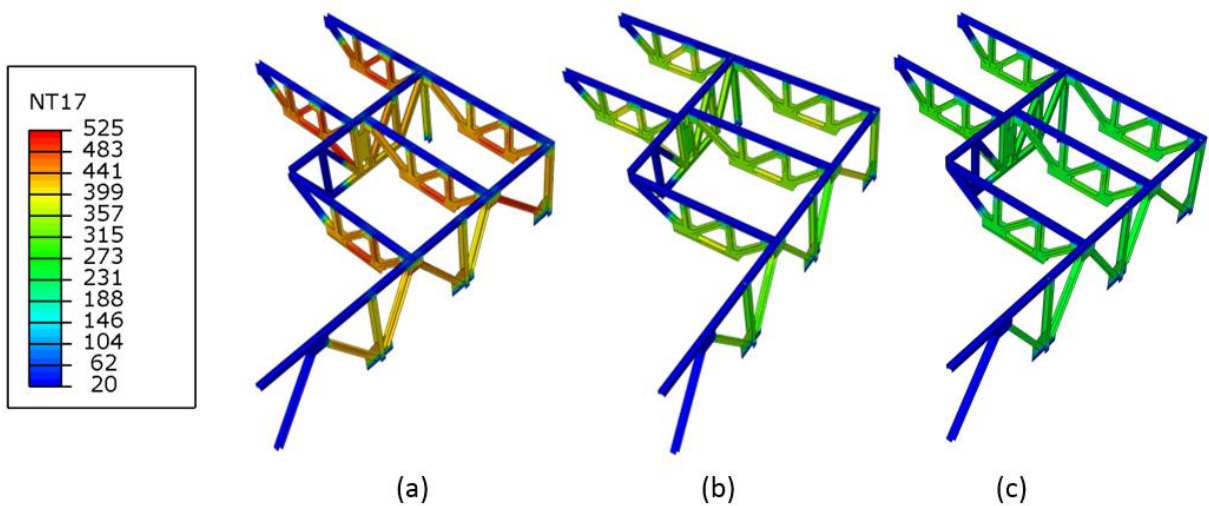

Fig. 4. Temperature contours in Celsius for Fire Scenario 2 of underlying steel members for a) 1-hr fire rating, b) 2-hr fire rating, d) 3-hr fire rating.

3.3 Structural FE Analysis

Subsequent structural analysis is conducted since elevated temperatures are expected to decrease the strength and stiffness of the steel members, as well as cause thermal stresses due to thermal expansion. Since the fire scenario occurs under the transfer trusses which support the upper 20 concrete stories of the structure, it is essential to include a larger portion of the building in order to sufficiently evaluate the global structural response. The transfer trusses subjected to fire are modelled with layered shell elements, since they are expected to exhibit significant plastic behavior. However, the rest of the trusses as well as the upper floors of the building need less modelling detail and are thus modelled with beam elements. Fixed translational and rotational boundary conditions are utilized to simulate the rigidity of the interior concrete core. Fixity is also applied at the bottom of all columns. The material for the steel members is A992 with yield stress of 345 MPa and ultimate stress of 450 MPa at ambient temperature conditions, while temperature-dependent mechanical properties are defined per Eurocode 3 [6]. The model is initially subjected to gravity loads per the extreme event load combination of ASCE 7 [9] and subsequently subjected to the temperature time-histories mapped from the previous heat transfer analysis.

The upper 20 concrete stories are modeled with columns and beams representing slab strips, with an elastic concrete material. In order to allow for potential slab plasticity, plastic hinges are assigned at both ends of each slab strip in the form of connectors which include isotropic hardening with yield and ultimate moment capacity calculated for each concrete slab section. To simplify the structural model, since the upper 20 concrete stories are identical, a 1-story frame with equivalent properties is used to model the effect of the upper stories. The plastic hinges assigned to those strips are also calculated to match the plastic behavior of the condensed concrete sections. The global model of the building is depicted in Figure 5.
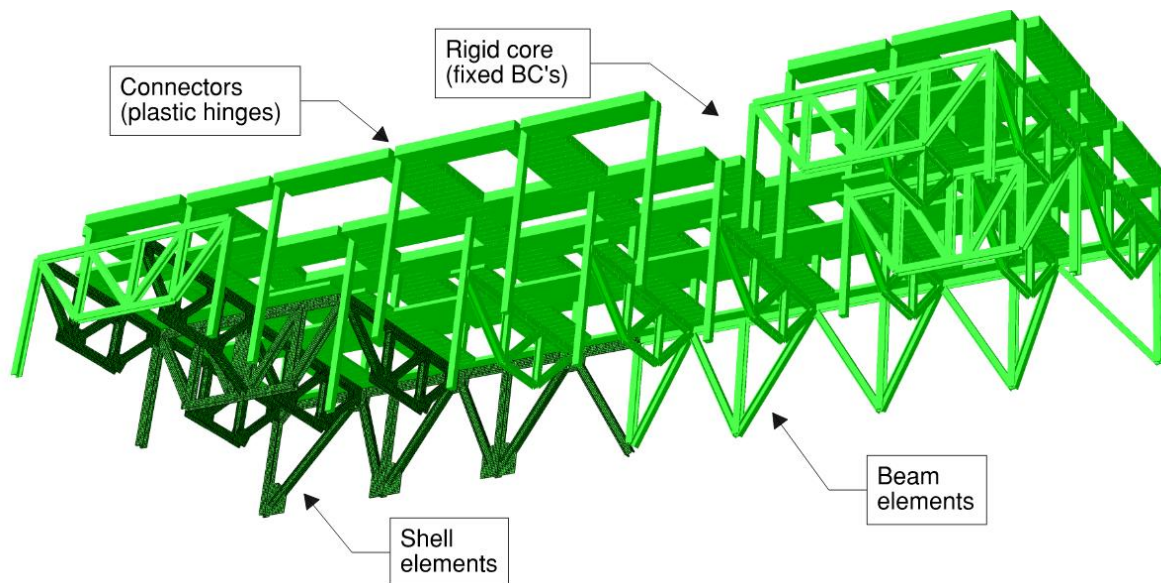
Fig. 5. Global structural analysis model

Figure 6 illustrates the deformed shape along with vertical deformation contours, both for the 1-hour fire rated steel case. Since the temperatures of the truss members have reached up to 525°C, steel material has lost about 30% of its strength and 50% of its stiffness. Therefore, the loss of stiffness of members at the interior bays in combination with thermal expansion of perimeter exterior columns causes a maximum differential displacement of 0.11 m. This deflection includes the initial downward deflection of the trusses due to gravity loads, which is approximately equal to 0.015 m. The differential displacement of 0.11 m causes the plastic hinges of a significant number of slab strips to activate, and thus many of them reach their yield moment capacity, meaning that the slabs of all the floors above have undergone significant structural

damage. Moreover, two truss members exhibit large out-of-plane displacements reaching a maximum of 0.10 m. The deflections of the transfer trusses cause large deflections and overstress of the slabs at all the upper floors.
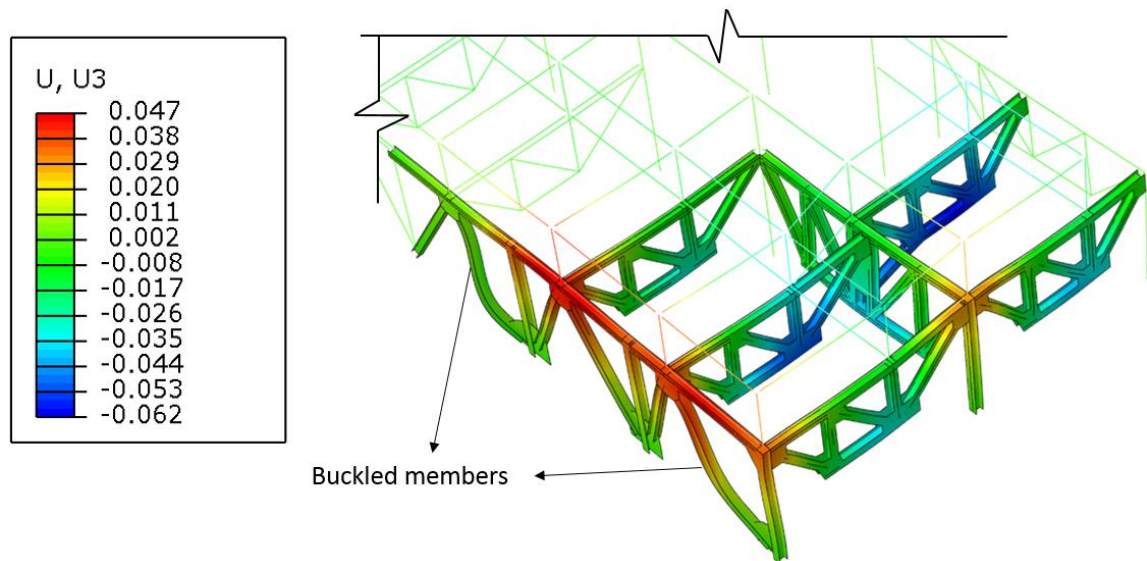

Fig. 6. 1-hour fire rated steel case for Fire Scenario 2; deformed shape during heating along with vertical deformation of entire structure in meters

For the 2-hour and 3-hour fire rated cases; steel temperatures are lower and therefore induce less loss of stiffness and less thermal expansion. The portion of the differential displacement due to fire between perimeter columns and interior bays for these cases is approximately 0.07 m and 0.05 m, respectively. In terms of structural damage to the slabs, a significant number of plastic hinges are also activated for the 2-hour and 3-hour fire rated cases. Therefore, in this case study, a fire under the transfer trusses does lead to damage at the upper floors.

4   CONCLUSIONS

In the present study, fires affecting transfer trusses for a 50-story mixed-used building are modeled and their impact on the performance of the structure is studied.

The analysis results indicate the following:

For 1-hour rated fireproofing on the transfer trusses, significant differential displacement between perimeter columns and interior bays is observed, as well as yielding of all of the slabs above the fire. This behavior indicates that the local fire scenario has a global impact on the structure.

For 2-hour and 3-hour (code-compliant) rated fireproofing on the transfer trusses, smaller differential displacement is observed, however slab plasticity is still present. This highlights the fact that, even for code compliant designs and for fire scenarios that result in temperatures for which loss of steel strength has not initiated, global damage to the structure in terms of widespread deformation is still possible.

Analysis results for different fireproofing schemes underline the significance of fire protection for both structural stability and global serviceability considerations.

These results are limited to the geometry and member design for the specific structure and fire scenario considered. Additional studies including different building configurations and fire scenarios are required in order to generalize the observations made herein. Nonetheless, this study

shows the usefulness of PBFE to understand realistic response of structures to fires, including the effects of their unique feature on structural responses.

5   REFERENCES

[1]   EN 1991-1-2, 2002. Eurocode 1: Actions on Structures–Part 1–2: General actions–Actions on structures exposed to fire. British Standards Institute.

[2]   McGrattan K., et al. Fire Dynamics Simulator (Version 6.6.0), User's guide. NIST Special Publication 1019-6, Gaithersburg, MD, USA. 2017 Nov; 1019(6):1-309.

[3]   Thomas, P.H. and Heselden, A.J.M., 1972. Fully-developed fires in single compartments. Fire Research Station. A cooperative research programme of the Conseil Internationale du Bâtiment. Conseil Internationale du Bâtiment Report No. 20, Fire Research Note No. 923.

[4]   Drysdale, D., 2011. An introduction to fire dynamics. John Wiley & Sons.

[5]   Abaqus/CAE 2019. Dassaults Systemes Simulia Corp.

[6]   EN 1993-1-2, 2005. Eurocode 3: Design of steel structures–Part 1-2: General rules–Structural fire design. British Standards Institute.

[7]   UL, Fire Resistance Ratings. ANSI/UL 263, Design No. N790, Underwriters Laboratories Inc., Northbrook, IL, USA. 2004.

[8]   ASTM E119-16, 2016. Standard Test Methods for Fire Tests of Building Construction and Materials, American Society for Testing and Materials, Philadelphia, PA.

[9]   American Society of Civil Engineers, 2016. Minimum Design Loads and Associated Criteria for Buildings and Other Structures. ASCE 7-16.

REVIEW OF OXYGEN REDUCTION SYSTEMS IN WAREHOUSE STORAGE APPLICATIONS

[1]Brian Meacham, [2]Martin Nilsson, [3]Patrick van Hees, [3]John Barton

[1]Meacham Associates, Shrewsbury, MA, USA

[2]Zurich Insurance plc, Stockholm, Sweden

[3]Lund University, Lund, Sweden

ABSTRACT

The primary purpose of oxygen reduction systems (ORS) for fire prevention applications is to create an environment of sufficiently low oxygen concentration to prevent, or significantly inhibit, fire initiation, development and spread. Two standards are currently available that provide guidance on design, installation and maintenance of ORS for fire. However, the Fire Protection Research Foundation (FPRF) identified issues with each of these standards that warranted further study. A research project was commissioned to conduct a literature review, from which gaps could be highlighted and research needs going forward could be identified. As summarized here, the review addresses factors that a test method needs to address in order to obtain ignition threshold values (reduced oxygen levels) for the system to be effective as a fire prevention system, and the suggests potential performance requirements for possible alternative test method to those currently available. Furthermore, the review addresses reliability issues with ORS.

1   INTRODUCTION

The fundamental operating principle of ORS is to reduce the oxygen concentration in a compartment to a sufficiently low level so as to minimize the potential for ignition of a fire [1-4]. As described by Chiti [3], in a compartment protected by an ORS, a normobaric hypoxic atmosphere is continuously retained, wherein hypoxic means that the partial pressure of the oxygen is lower than at the sea level, and normobaric means that the barometric pressure is equal to the barometric pressure at the sea level. In general, ORS work by replacing a certain amount of oxygen molecules by the same amount nitrogen molecules to obtain this normobaric hypoxic atmosphere. In unoccupied spaces, ORS can function as a fire prevention system, maintaining an oxygen concentration that is sufficiently low to prevent ignition or established burning, or as a fire suppression, like other inert gas systems, such as CO2 systems provided the correct level is chosen. At present, there are only two standards, VdS 3527en:2007, *Oxygen Reduction Systems Planning and Installation* [5] and EN 16750:2017 E, *Fixed firefighting systems - Oxygen reduction systems - Design, installation, planning and maintenance* [6], which provide guidance on design, installation and maintenance of ORS for fire safety.

It is important to note that EN 16750:2017 recently replaced British Standards Institution PAS 95, *Hypoxic Air Fire Prevention Systems* [7]. Much like BSI PAS 95 and VdS 3527en:2007, EN 16750:2017 E provides exemplar data on minimum oxygen concentration levels for ignition of select materials. Furthermore, the test methods to determine ignition thresholds (oxygen levels) in EN 16750:2017, BSI PAS 95 and VdS 3527 are very similar and will therefore result in similar ignition thresholds. While EN 16750:2017 has not been investigated in detail, concerns have been raised with both BSI PAS 95 and VdS 3527en:2007 [8]. One concern is that the testing procedures specified by the standards for assessing the ignition thresholds for materials within reduced oxygen environments may be insufficient to cover real-scale scenarios and may as such result in oxygen

concentrations too high to prevent ignition in real-scale scenarios. Another concern is that both standards have limited guidance on the inspection, testing, and maintenance (ITM) of ORS for fire.

Given these concerns, the Fire Protection Research Foundation (FPRF) commissioned a literature review with the objective to produce a report that investigates the factors that a test method needs to address in order to obtain ignition threshold values (reduced oxygen levels) for the system to be effective, suggests potential performance requirements for possible alternative test method to those currently available, and identifies research that is needed to fill gaps and needs [8]. The project was bounded by a focus on fire prevention as compared with fire protection (i.e., controlling a fire once it starts), with a specific aim to identify issues faced in 'real-world' applications of ORS for fire, such as reliability issues relating to inspection, testing and maintenance, component reliability and operational issues. The review applies to all ORS for fire, but does not address the efficacy of ORS in cases where ignition occurs and a fire develops in a reduced oxygen atmosphere. In addition, factors such as preventing further ignition or controlling / extinguishing fire in reduced oxygen environments was not studied and warrants further investigation. Furthermore, safety of people in reduced oxygen atmospheres, without protection, has also not been addressed. The project report [9] is available of the FPRF website. The discussion below is excerpted from the project report, with modifications, with permission from the FPRF. Significantly more discussion is available in the full report [9].

2   WAREHOUSE STORAGE APPLICATIONS AND ORS CONCERNS

Real world applications have often much more complexity compared to standardized and theoretical set-ups of the ORS. As such there might be an impact on the efficacy of the ORS. The most important property of an ORS is the choice of the oxygen level and the quality of the oxygen level in the real-world application. The test method defines the required level of oxygen, according to the standards, for the content of the real-world application. However, the determined oxygen level is only applicable for the test conditions [13] and it might not cover the real-world application with deviations in fuel composition, fuel configuration etc. It is important to compare the type of materials/product/configuration used in the test method with the actual conditions in the building itself. Deviations from the fuel content and configuration in the test with the real-world application might result in the fact that the oxygen level is too high and still allows ignition. In that case the efficacy of the ORS may not be reliable enough.

Another important aspect is the determination of the oxygen level in test method compared to the one necessary to prevent ignition by real life ignition sources and thermal impacts. The existing test method(s) have a simple low heat release pre-mixed flame with high momentum. This type of ignition source is only one of the possible real-life ignition sources, and international standardization documents such as ISO 11925 Part 3 [10], list a number of other flame ignitions sources. Apart from those there exist also ignitions sources resulting from short circuit arcs which might contain a lot more energy and create higher temperatures.

Within the facility in which the ORS is installed it is important to guarantee that the chosen level of oxygen is obtained in the whole facility. This puts requirements on the measurements system and the number and place of the measurements. While existing standards give guidance, it has not been clear from the study how the choices have been made with connection to real life applications [9].

When the oxygen level is chosen, it has to be kept constant as a function of time. Leakage as function of time is therefore of importance to monitor. Movement of commodity between compartments requires openings, which can result in leakages when open. While it might be possible to estimate such opening time and associated leakage during any given time period (e.g., total opening time and leakage volume per day) to estimate required concentration, such estimation

would require margins of safety to account for unintended opening, barrier failures and so forth. It would also require adherence to operational plans as well as maintenance of opening protectives (i.e., doors, dampers, shutters, etc.). Special designs might be necessary.

There is also impact of other failure of the building envelope on the system performance (e.g., external fire, vehicle damage, etc.). The latter is a weakness of the system as the oxygen level will not be able to maintain in case some parts of the containment fails due to an intense local fire or explosion, that was not foreseen in the design phase, e.g. due to breaking of a window. It is also important that access to the facility will influence the level of oxygen due to entrance of fresh air. Finally, the oxygen concentration can be influenced as a function of time due the impact of general system degradation and/or building aging over time.

It is critical to be able to verify a fire prevention or protection system's operational condition and associated effectiveness. To be able to do this one would like to make sure that the system is maintained properly so that it continues to work during the conditions when the system is needed. Furthermore, inspections are critical to verify that the system is in operating condition (e.g. is the system turned on) and free of physical damage. In addition, testing is needed in order to verify the operational status of the system or a component thereof through physical checks.

Impairments to fire protection/prevention systems in general is a common reason for the systems not being able to perform as intended. Impairments could be planned or emergency impairments due to some failure. Impairments in general needs to be limited in time and frequency which requires good system and component reliability as well as early discovery of an emergency impairment. Currently there is no industry practice for ITM of ORS and there is a need for such a standard to be developed including weekly, monthly, quarterly and annual inspections and tests as well as required maintenance on the system.

A typical attribute for warehouses as compared to the general issues that affect the oxygen concentration is the fact that we often do not know the content of all possible products/storage in a warehouse and their content as a function of time. Oxygen level determination might be different. The products might also contain a lot of different materials and be mounted into a specific system which can influence the overall behavior and oxygen level due to trapped oxygen. Another important aspect is that the products might be in packaging which contain oxygen and this will in its turn affect the conditions if the packaging sealing is destroyed by the local fire and give an additional access of air to the fire locally which might lead to fire spread. It is also possible that the first ignition item might be different from one warehouse facility to another and its should be investigated how this influences the required oxygen level. There should be a link to a risk analysis of the facility.

The type of geometry used in warehouses can be a significant concern, especially those with large volumes, many openings, and rack storage. A particular concern is the 'tightness' of the volume, how it can be assessed, and how reliable this tightness is. There can be issues with movement of goods between spaces, ventilation systems between spaces, and permeability of the exterior surfaces. Although it is not particular only for warehouses, tightness is of great importance for ORS application and lifecycle reliability.

The occupancy classification of warehouses can differ considerably depending on the commodity(ies) being stored. Some commodities are more difficult to protect than others. For ORS, this is indicated by the ignition threshold values. For sprinkler systems, it is indicated by the commodity classification and the associated sprinkler design requirement. The nature of ORS makes it difficult to determine different commodity classifications since different materials have different ignition thresholds and the driving factor for the threshold is not fully understood. It may

be the case that a commodity classification similar to the sprinkler system commodity classification may not be possible, but no research has been done apart from a comparison by Zhou et al. [11].

3   IGNITION THRESHOLDS AND PERFORMANCE REQUIREMENTS

Given the various issues associated with warehouse storage applications and potential impacts on ORS for fire efficacy, some of the most critical factors are explored in more detail.

3.1 Test Environments and Real-World Challenges

For most fuels, ignition and subsequent burning can be prevented when the oxygen concentration is less than 10% [12]. For unoccupied spaces, this is technically possible, assuming the compartment tightness can be maintained, and the ORS continuously operates in a reliable manner. In practice, however, particularly in warehouse storage applications, spaces may be occupied some of the time, and there will be openings in compartment boundaries for movement of goods. Design, operation and maintenance of the ORS should take into account openings in the compartment barriers, permeability of compartment barrier materials, and length of time the space may be occupied to assure target concentrations are maintained. Since design oxygen concentration levels of around 14-15% is typically used for occupied spaces (see e.g. [3]), ORS efficacy as a fire prevention system may be reduced and ignition of ordinary combustibles may still occur at that oxygen level depending on the ignition source [12].

3.2 Test Criteria

The performance of an ORS is dependent on the oxygen concentrations, energy and duration of the ignition source, and fuel characteristics. According to PAS 95:2011 [7], VdS 3527en [5] and EN 16750:2017 E [6], different oxygen concentrations should be used depending on the material subject to burning [13]. In Table 1 below, different values of oxygen concentrations, below which burning cannot take place in the test application, are shown.

Table 1. Oxygen concentrations below which burning cannot occur in the test [9]

Substance	VdS Ignition threshold (Vol.%) (Design concentration Vol%) (VdS 2007)	Limiting Oxygen Concentration (LOC) (Vol%) (Xin and Khan, 2007)
Methanol	11.0 (10.0)	11.64
Ethanol	12.8 (11.8)	12.40
PMMA	15.9 (14.9)	10.48
Polyethylene	HD: 16.0 (15.0) LD: 15.9 (14.9)	LD: 11.39
Corrugated Board	15.0 (14.0)	12.86
PVC	16.9 (15.9)	-

It can be seen that the values differ quite widely; this is dependent upon the test procedure. The limiting oxygen concentration (LOC) was obtained by Xin and Khan [14] in the Fire Propagation Apparatus (FPA) with an external heat flux of 30 kW/m^2 for solid fuels and with no external heat flux for the liquids. In Table 1, it can be seen that according to the VdS standard, a 15 % oxygen concentration may be applicable for several fuel types. However, the values provided by Xin and Khan [14] shows significantly lower concentrations are needed due to the applied external heat flux, which is not present in the test method in VdS 3527en. An external heat flux could be obtained, for

example, if an arson fire occurs where flammable liquids are used as an ignition source, or if materials are reradiating towards each other, as in the parallel panel test or between pallet loads in a rack storage arrangement [9].

3.3 Test Methods

With respect to testing procedure for assessing ignition thresholds, Nilsson and van Hees [13] identified the following in VdS 3527 and in British Standards Institution PAS 95, *Hypoxic Air Fire Prevention Systems* [7], a forerunner to EN 16750:2017 E [6].

The oxygen acetylene torch has a high burning velocity and results in a very local heat transfer causing burn through of the material and blowout of any diffusion flames on the sample

The flame presents virtually no radiation

The fuel configuration and reradiation between fuel packages is not taken into account

Test criteria, procedure and ignition source are imprecise and poorly defined

Nilsson and van Hees [13] concluded that the ignition thresholds obtained using the tests described in VdS 3527 and BSI PAS 95 are only valid for the tested conditions and may not represent real-world conditions. Their conclusion is supported by Xin and Khan [14], where laboratory scale testing suggested that lower oxygen concentrations than those found using the VdS 3527 or BSI PAS 95 methods are necessary for adequate fire prevention. These conclusions have been reconfirmed through recent larger scale testing [11, 12, 15].

4   SUMMARY OF RESEARCH/DEVELOPMENT NEEDS FOR ORS FOR FIRE

4.1 Test Methods

The research suggests that the test methods in EN 16750:2017 and VdS 3527e:2017 may not be sufficient to cover real-scale scenarios and may result in oxygen concentrations too high to prevent ignition in the real-scale scenarios. Therefore, the following research is suggested:

The actual test methods used in existing standards are rather limited as described. No full- or real-scale validation has been done. Therefore, the test methods might not be sufficient for all types of contents in case of warehouses. Other alternatives should be studied.

The test method in the EN and VdS standards have only one type of ignition source. This is not representative of reality. This type of ignition source is only one of the possible real-life ignition sources and international standardization documents such as ISO 11925 part 3 [10] lists a number of other flame ignitions sources. The goal of a test method should be to establish a challenging ignition source with a high enough probability of occurrence that one can consider the risk of ignition from unconsidered sources as very remote. To address this, other ignition sources / strengths should be studied and incorporated into the text method.

As the test methods are mainly based on a small flame application, there is need for development of alternative test method(s) or procedure with existing test method to investigate radiative and electrical high energy arc ignition sources. The methods need to have much clearer and detailed test methodologies and criteria than currently exist.

More data on ignition potential based on material type and storage arrangement, in different O_2 concentrations, would be helpful. In particular, fuels where oxygen is also present in the packaging, for example, is critically needed.

Data on real life scenarios with the systems are very limited. Research by Zhou et al. [11] identify some concerns, as does this work [9]. Both also suggests that existing standards do not address reliability and maintenance issues to the required extent

Tied to (d) and (e) above, further research on required oxygen concentration is needed, i.e., what level should be used, for what fuels, in which applications, under what conditions. This is needed to support fire safety design and guidance for warehouse occupancies.

4.2 ORS for Fire Operational and Environmental Considerations

There is inadequate knowledge, data and guidance around 'real-world' environmental impacts and on reliability, maintainability and operability of ORS for fire operations.

a. Research into failure rates / reliability of ORS components is needed. Based on current research, data are lacking on critical components, such as compressors and sensors. This research may use existing reliability data for components.

b. Failure mode analysis of ORS to determine appropriate industry standard Inspection, Test and Maintenance (ITM) programs as well as a failure analysis of the components in order to determine relevant requirements for listing of systems and components (required indications, alarms etc.) is needed.

   a. This should include identification of critical components that need to be in operating conditions and establish a requirement that the operating condition is visually indicated and easy to inspect.

   b. Guidance is needed on what is required to verify for the ORS on a regular basis, e.g., available production rate of nitrogen (compare to flow test of fire pump), testing of alarm signals (low oxygen, loss of power, high temperature on air compressors, etc.), and tightness of room. Maintaining the oxygen concentration over time when the building is starting to leak, the frequency of opening doors, and related factors need to be explored. Guidance on ITM intervals is also needed.

   c. Guidance on back-up / emergency power requirement is also needed as well as securing electrical power in terms of cable routing, breaker sizing etc. The standard UL 67377 [16] provides a starting point for the work.

c. Failure mode analysis of ORS to determine potential reasons for impairments and associated needs to early detect such impairments is needed. An operation safety management plan should be part of the guidance coming out of such research.

d. Development of acceptance (compliance / commissioning) testing procedures is needed.

e. An industry-standard calculation method for ORSs and required documentation for plan review is needed.

f. Information on operational costs for ORSs to aid in benefit-cost decisions is needed.

g. Research into how leakages in warehouse storage buildings, particularly those targeted for ORS application, increase over time, is needed.

h. Research is needed to gain an understanding of how tightness tests can be done for large volume spaces.

i. Research on back-up system needs for ORS reliability and availability is required.

j. Interaction of ORS and active fire protection, including smoke and heating venting systems, and sprinkler systems, would be beneficial.

k. The effect of moving a commodity into an ORS-protected space, that has previously been stored at ambient oxygen conditions, should be investigated. This is particularly true for porous materials which can absorb oxygen into void spaces, which will be released in the reduced oxygen environments.

4.3 Fire Service Intervention and Other

While the focus of this work was related to the ORS as fire prevention system, it is clear from the literature study that the following areas, which were deemed outside of the scope of this study, would benefit from further research as well.

a. Research is needed to better understand and assess / model manual firefighting interventions, such as smoke and heat venting, opening doors for firefighter access, etc., on ORS effectiveness and reliability.

b. Level of oxygen acceptable with respect to medical conditions of people inside an ORS environment

   a. Lack of medical data is an open issue – more definitive testing / assessment by medical professionals would seem to be warranted to answer heath effect questions.

   b. Research appears to be needed not only on medical health, but also ability to make the correction decisions in oxygen-reduced environment.

c. Knowledge and data (e.g. experimental data) on the fire protection abilities of ORS, i.e., how much is fire spread reduced when an ignition occurs, despite the reduced oxygen level.

   a. More data on burning rates and HRR based on material and storage arrangement, in different O_2 concentrations, would be helpful to further quantify the system benefit if the ignition threshold level is not met due to malfunction or impairment of the system

   b. Damage criteria to be studied and defined.

5 SUMMARY AND CONCLUSIONS

This study consisted of a literature study and a research gap analysis for ORS for warehouse storage applications. One of the major focus areas of the studies has been, but not limited to, ignition prevention and associated test methods. Furthermore, reliability issues have been studied. That is, the contents of the report apply to all ORS for fire, but the report does not address the efficacy of ORS in cases where ignition is not prevented and a fire develops in a reduced oxygen atmosphere. Factors such as preventing further ignition or controlling / extinguishing fire in reduced oxygen environments warrants further study. Furthermore, safety of people in reduced oxygen atmospheres, without protection, has also not been addressed. Potential health and safety impacts on people working in low oxygen environments warrants further study.

This research revealed clearly that the test methods in EN 16750:2017 and VdS 3527 may not be sufficient to cover real-scale scenarios and that considerable research is needed to further develop the test methods through full-scale fire tests. Other ignition scenarios should also be investigated in real-scale and linked to small scale tests. In addition, actual products and systems should be investigated, and it should be determined how the oxygen level should be determined and if a similar approach such as commodities for sprinkler can be applied.

The need for investigation into reliability of ORS for fire is highlighted, as is the need for research on how to design robust systems that are easy to inspect and maintain. Non or malfunction of the ORS can lead to serious fire spread and damage. Procedures need to be established to check the reliability and/or real-life data is needed.

A large number of recommendations for further research were identified with respect to ORS test methods, the ORS operation and its specific application, to planned and emergency interventions in ORS-protected spaces.

Finally, during the study it became clear that more research is needed by health specialists to determine the acceptable health levels at different oxygen concentrations and work-effort conditions. There is also no or little data available on potential benefits or downsides should a fire occur despite the reduced oxygen atmosphere.

ACKNOWLEDGMENT

REFERENCES

[1] Berg, P. and Lindgren, A. (2004). *Fire Prevention and Health Assessment in Hypoxic Environment,* Report 5144, Department of Fire Safety Engineering, Lund University, Lund, Sweden.

[2] Jensen G, Holmberg JG, Gussiås A. (2006). *Hypoxic air venting for protection of heritage, report within COST Action C17 project*, ISBN 82-7574-037-1, Riksantikvaren, Directorate for Cultural Heritage and Crown.

[3] Chiti, S. (2010). T*est methods for hypoxic air fire prevention systems and overall environmental impact of applications,* Masters Thesis, Università degli Studi di Modena e Reggio Emilia (2009), Reprint COWI Fire Research Report 01/2010.

[4] Clauss, P. (2014). *Fixed Firefighting Systems - Oxygen Reduction Systems: Active fire prevention vs. passive fire protection*, Proceedings, SUPDET Conference, Orlando, USA, March 4-7 2004.

[5] VdS 3527en:2007, *Guidelines for Inerting and Oxygen Reduction Systems*, VdS Schadenverhütung GmbH, Köln, Germany.

[6] EN 16750:2017 E, *Fixed firefighting systems - Oxygen reduction systems - Design, installation, planning and maintenance*, CEN, Brussels

[7] British Standards Institution PAS 95, *Hypoxic Air Fire Prevention Systems*, BSI, London

[8] FPRF (2018), *Review of Oxygen Reduction Systems for Warehouse Storage Applications*, Request for Proposals, FPRF, 2018.

[9] Van Hees, P., Barton, J., Nilsson, M. and Meacham, B.J. (2018). *Review of Oxygen Reduction Systems for Warehouse Storage Applications*, Report number FPRF-2018-13, FPRF, Quincy, MA, USA.

[10] ISO 11925 - Part 3 (1997), *Reaction to fire tests -- Ignitability of building products subjected to direct impingement of flame -- Part 3: Multi-source test*, Geneva, ISO.

[11] Zhou X, Xin, Y., Dorofeev S. (2018). *Evaluation of Oxygen Reduction System (ORS) in Large-scale Fire Tests*. 3rd ESFSS Symposium*,* Nancy, France, 2018

[12] FM Global (2018). *Evaluation of oxygen reduction systems (ORS) in large scale fire tests*, Project ID 0003058222, FM, January 2018.

[13] Nilsson, M. and van Hees, P. (2014). *Advantages and challenges with using hypoxic air venting as fire protection*, Fire and Materials, 38, p. 559-575.

[14] Xin, Y. and Khan, M. (2007). *Flammability of combustible materials in reduced oxygen environment*, Fire Safety Journal, 42(8), p. 536-547.

[15] FM Global (2018b). *Fire prevention: concentrating on oxygen*, https://www.fmglobal-touchpoints.co.uk/fire-prevention-concentrating-on-oxygen.htm/

[16] UL (2016), UL 67377, *Outline of Investigation for Oxygen Reduction Fire Protection System Units*, Underwriters Laboratories, Northbrook, IL, USA.

FIRE SAFETY OF STEEL STRUCTURES

DEVELOPMENT OF HYBRID FIRE TESTING BY NUMERICAL AND EXPERIMENTAL SUBDIVISION

Nicolas PINOTEAU[1], Duc Toan PHAM[1], Romain MEGE[1], Hong Hai NGUYEN[1]

[1] Université Paris-Est, Centre Scientifique et Technique du Bâtiment (CSTB), 84 avenue Jean Jaurès, Champs-sur-Marne, 77447 Marne-la-Vallée Cedex 2, FRANCE

ABSTRACT

The Hybrid Fire Testing (HFT) method relies on the subdivision of a studied structure into a numerical substructure (NS) which is modeled and a physical substructure (PS) which is tested. The element is tested under a thermo-mechanical loading while the effect of the surrounding structure is calculated using a finite element software. This paper presents the theoretical analysis, technical developments and experimental results carried out to install the hybrid method. The theoretical analysis is performed on the iterative communication sequence (of loads and displacements) between both substructures to ensure mechanical equilibrium at the interface. The technical choices to establish a communication interface between the finite element software and the test rig are presented. Three hybrid tests performed on a steel structure are presented to compare the measured behavior with the theoretical expectations.

1   INTRODUCTION

A great number of tests have been carried out over the last thirty years to study the fire resistance of structures, mainly as regards to the fire behavior of independent structural elements. These classic tests are often carried out with a constant load and do not assess an element within its real structural configuration. Hybrid Fire Tests (HFT) allow to reproduce the actions of a building on a tested structure by simulating the building in real time during the fire test. To do this, the building is divided into a Numerical Substructure (NS) (which is modeled) and a Physical Substructure (PS) (which is tested).

Initially used in Japan in the 1960s, the hybrid testing method was developed in the seismic field fueled by technical progress of both numeric calculators and hydraulic jack regulation systems. In the 1990s, some of the researchers working in the seismic field pioneered the introduction of the hybrid method in the field of fire testing (Korzen *et al.*, 1999 [1] followed later by Mostafaei, 2013 [2]). Since 2016, several institutes contribute in developing HFT such as Tondini *et al.*, 2016 [3], Sauca *et al.*, 2016 [4], Schulthess *et al.*, 2016 [5]. One of the main difficulties of the method is that a gap always exists between the determined equilibrium position and the "real" position during the test caused by the time lag (in updating the data for the simulation). This may induce convergence problems towards a mechanical equilibrium between both substructures. The equilibrium is defined by load and displacement boundary conditions at the interface between the substructures. Recent publications have put into light the influence of stiffness ratios between the two substructures in converging towards equilibrium Sauca *et al.*, 2016 [4]. The success of HFT relies on modeling (calculation), testing (jack control) and interfacing (algorithms) capabilities.

This paper presents an example of three HFT performed on a steel structure. The goal was to check the interface development and identify possible paths of improvements (that might have been

missed through preliminary theoretical analysis). This paper does not present the study of a realistic fire behavior of an element though HFT. First, the substructures and testing conditions are presented. Secondly, results from three HFT are exposed (where the PS and NS interact together). These results are compared to theoretical equilibrium positions during the fire (calculated from the PS and NS <u>considered separately</u>). This comparison allows to identify the phenomena that are linked to test methodology.

2 TEST AND METHOD

2.1 Studied Structure

The studied structure and method are described extensively in the paper under submission (Pinoteau *et al.*, 2018 [6]) which presents tests carried out at ambient temperature (by only simulating the fire in the NS). It was shown (in support to Sauca *et al.*, 2016 [4]) that convergence towards an equilibrium is ensured if the stiffness ratio (k_P/k_N) remains lower than 1 during the test. The present study adds the effect of fire on the PS by performing furnace tests.

The structure was a steel frame made of HAE120 beams and columns. The PS is a steel column heated on one side and loaded as a cantilever. The NS is the rest of the frame with HEA120 heated on all four sides (to avoid substantial thermal curvature). Mechanical equilibrium was studied at the interface point (top left of Fig. 1(*a*)) only along the horizontal direction. The two substructures could be considered as springs (Fig. 1(*b*)). The equilibrium was changing during the fire as the result of the variations of thermal displacements and stiffness of each spring.
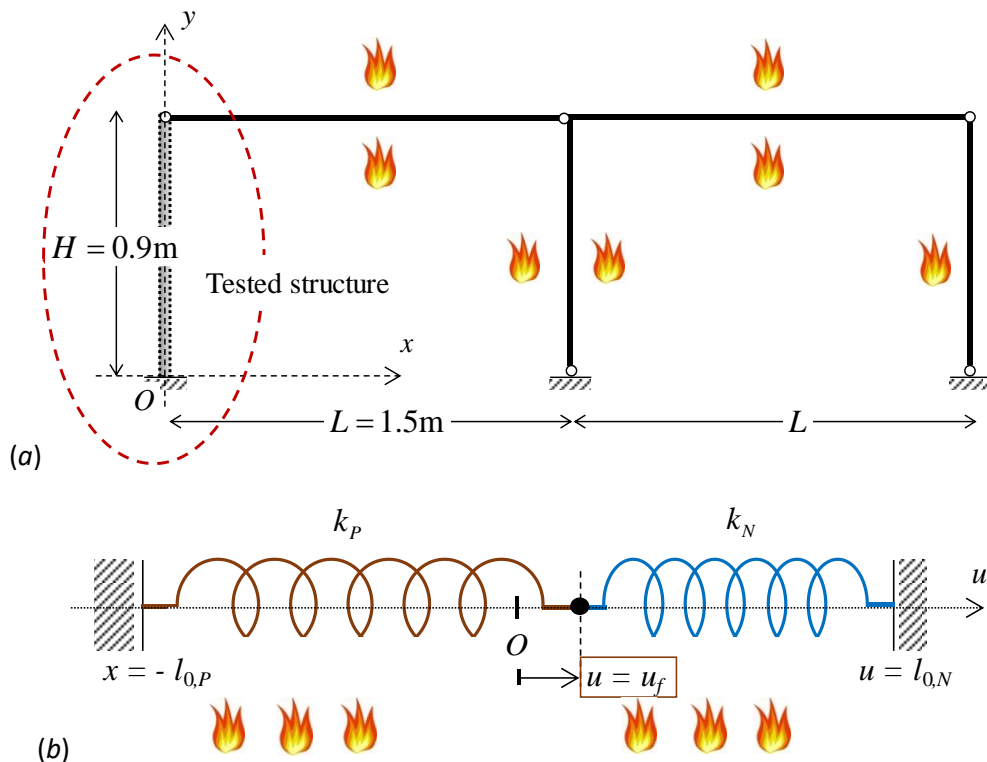
Fig. 1. (a) Sketch of the frame structure and (b) the spring model

The NS was modelled in real time using the finite element software SAFIR (Franssen, 2005 [7]). Each modelling step was composed of a thermal calculation between time t and $t+\Delta t$ followed by a mechanical calculation (using the thermal field obtained at $t+\Delta t$). The thermal calculation was

performed from the measured temperature inside the furnace (and not the theoretical ISO834-1 curve (EN1991-1-2, 2002 [8])). This allowed to start the hybrid communication loop before launching the burners.

Values of load and temperature were measured on the test sample and inputted in the simulation while updated displacement values are outputted from the simulation and applied on the tested sample. The communication loop between t and $t+\Delta t$ was composed of the following steps (described in more details in Pinoteau *et al.*, 2018 [6]).

- Measure the furnace temperature θ_{ISO} and load F.
- Inject θ_{ISO} and F in SAFIR, run a calculation and output a target displacement u.
- Apply u with the hydraulic jack.

2.2 Test program

Five fire tests were carried out (presented in Tab. 1). The two first tests were static 'traditional' tests with a constant load to identify the behaviour (thermal displacement u_P^{th} and stiffness k_P) of the PS. The three other tests were HFT using the communication loop. The first two HFT were performed in identical conditions (using a time step of Δt=30s) to assess repeatability. The last HFT used a step of Δt=10s to assess the influence of the time step. All tests were performed using different steel HEA120 beams (from the same steel batch) and used the same NS

Table 1. Test Program

Test name	Description	Goal
Static test 1	Constant load F=0 kN	
Static test 2	Constant load F=-2.4 kN	Determine the behaviour of the PS (u_P^{th} , k_P)
Hybrid test "a"	Time step Δt=30s	Assess repeatability of the hybrid method
Hybrid test "b"	Time step Δt=30s	Assess repeatability of the hybrid method
Hybrid test "c"	Time step Δt=10s	Assess the influence of the time step

2.3 Test setup

The tests were carried out on a small gas furnace presenting an exposed surface of 1.0×0.6m² to apply a conventional ISO834-1 heating curve (EN1991-1-2, 2002 [8]). For technical reasons, the PS (column) was tested horizontally, thus neglecting the effect of self-weight. The furnace was controlled using conventional plate thermometers positioned 10cm from the exposed surface of the PS. Only the lower surface of the HEA120 was exposed. The upper surface and middle section of the HEA120 were exposed to ambient air. This was achieved using insolation material (Fig. 2).
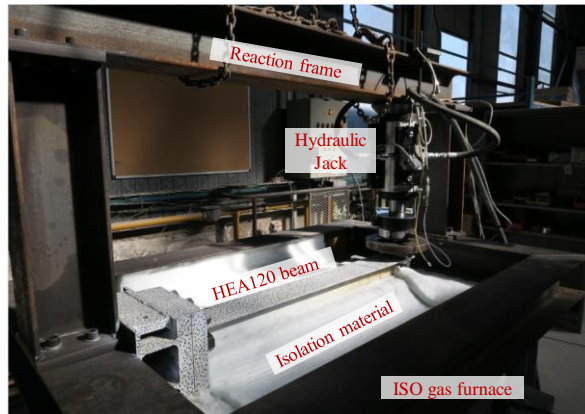
Fig. 2. Photography of the test device

A hydraulic jack was used to apply a vertical load representing the action of the rest of the frame (NS substructure). The vertical displacement and load were measured at the position of the hydraulic jack (corresponding to the interface between the PS and NS). The connection of the jack with the PS allowed movements in both ways in the vertical direction and allowed horizontal sliding of the HEA120 (that could be induced by longitudinal thermal expansion to avoid any transversal force). The hydraulic jack was controlled in displacement using a PID regulation system connected with the computer on which ran the SAFIR simulation.

3   RESULTS AND DISCUSSION

3.1   Behaviour of the Physical Substructure (PS)

During the two static tests on the PS, the evolution of displacement was measured (Fig. 3). The positive displacement corresponds to the PS bending towards the furnace (when the load of -2.4 kN is applied). The negative displacement corresponds to the PS bending outside the furnace (due to thermal curvature when heated on one side).
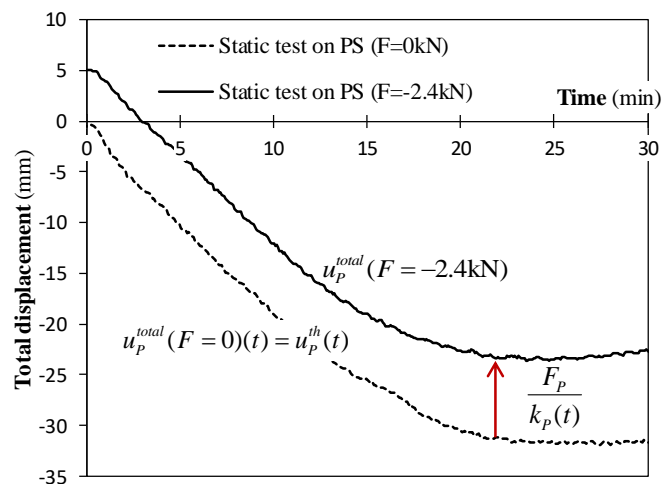
Fig. 3. Measured behaviour of the Physical Substructure (u_P^{th}, k_P)

From these measurements, the evolutions of the thermal displacement u_P^{th} and stiffness k_P were determined (Fig. 4). The thermal displacement u_P^{th} is equal to the displacement the PS which is not loaded ($F=0$). The stiffness was determined from the difference between the two curves.

3.2 Behaviour of the Numerical Substructure (NS)

For the NS, the evolutions of thermal displacement u_N^{th} and stiffness k_N were determined using SAFIR. Several simulations were performed on the NS frame alone by applying different constant loads as boundary conditions on the interface point. Outputted displacements allowed to determine thermal displacements and the stiffness with the same method as for the PS.

Figure 4 presents the evolutions of thermal displacements and stiffness for the PS and the NS. The thermal displacements are negative corresponding to a shifting of the interface point towards the left on Fig. 1. For the PS, this is due to thermal bending of the column heated on only one side. For the NS this is due to the longitudinal thermal expansion of the horizontal beams on the frame. Since all HEA120 are heated on all sides in the NS, there is no substantial thermal bending.

It can be noted that the convergence criteria on the stiffness ($k_P/k_N < 1$) is no more respected after about 15 minutes. This leads to a none equilibrium between both substructures beyond this time.
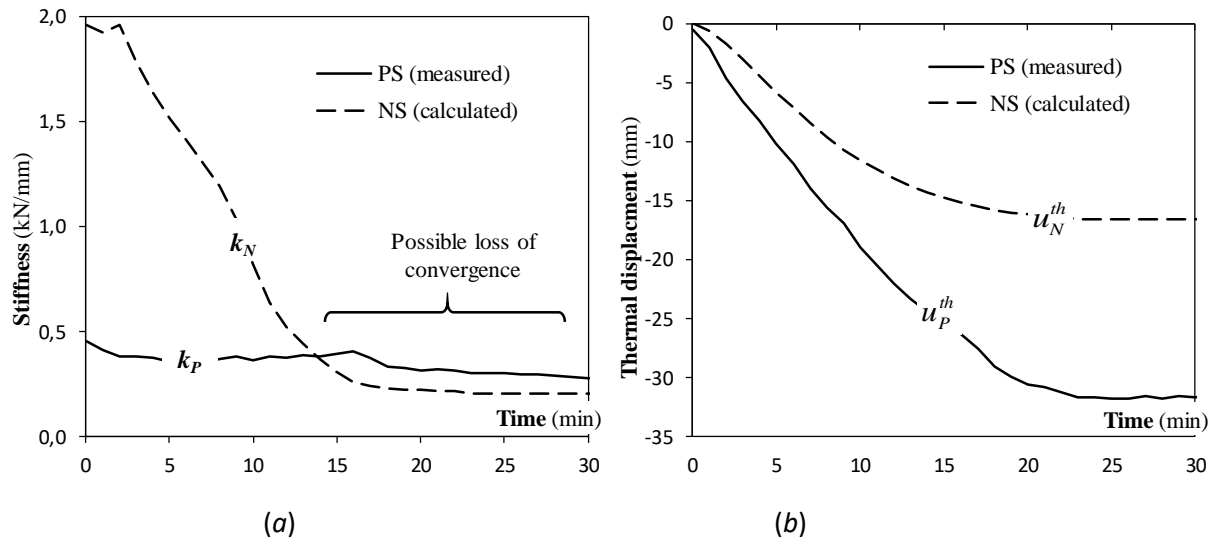
Fig. 4. (*a*) Stiffness and (*b*) thermal displacements on the PS and NS

Knowing the values of stiffness (k_P, k_N) and thermal displacements (u_P^{th}, u_N^{th}), it is possible to analytically calculate the equilibrium position of the interface point using equations (1) and (2). The demonstration of these equations is presented in Pinoteau *et al*., 2018 [6] and is based on the spring model presented in Fig. 1. At equilibrium, the loads of each spring are opposite, and the displacements are equal. The linear behaviour law of each spring is expressed through stiffness and the fact that the total displacement is the sum of mechanical displacement and thermal displacement

$$u_{eq} = \frac{k_P u_P^{th} + k_N u_N^{th}}{k_P + k_N} \tag{1}$$

$$F_{eq} = \frac{k_P k_N}{k_P + k_N}(u_N^{th} - u_P^{th}) \tag{2}$$

3.3 Hybrid Test results

Figure 5 presents the evolutions of load, displacement and furnace temperature measured during each HFT. The theoretical equilibrium values u_{eq} and F_{eq} calculated with equations (1) and (2) are compared with the measured displacements and loads.

Furnace temperatures

The temperatures measured by standardized thermo-plates present high repeatability among the three HFT. The maximal temperature differences (<50°C) between the tests are obtained during the first seconds of heating.

Displacements

The displacements are negative and decreases signifying that the equilibrium point shifts towards the left (Fig. 1). This is in good accordance with the negative thermal displacements of both substructures considered separately (presented in Fig. 4). It can be noted that between 4 and 15 minutes, the theoretical u_{eq} is close to the HFT experimental displacement curves. Before 4 and after 15 minutes, u_{eq} is higher.

Loads

Negative values of load represent the 'pulling back' force (towards the right on Fig. 1) from the NS frame on the PS. The decrease of F_{eq} at the beginning of the test is caused by the blocking of the thermal displacement of the PS by the NS (which 'holds it back'). The stabilization of F_{eq} after about 10 minutes is caused by the decrease of stiffness. The slight undulations around 16 minutes can be explained by the variations of k_P determined experimentally (Fig. 4).

$$F_{eq} = \frac{k_P k_N}{k_P + k_N}(u_N^{th} - u_P^{th})$$
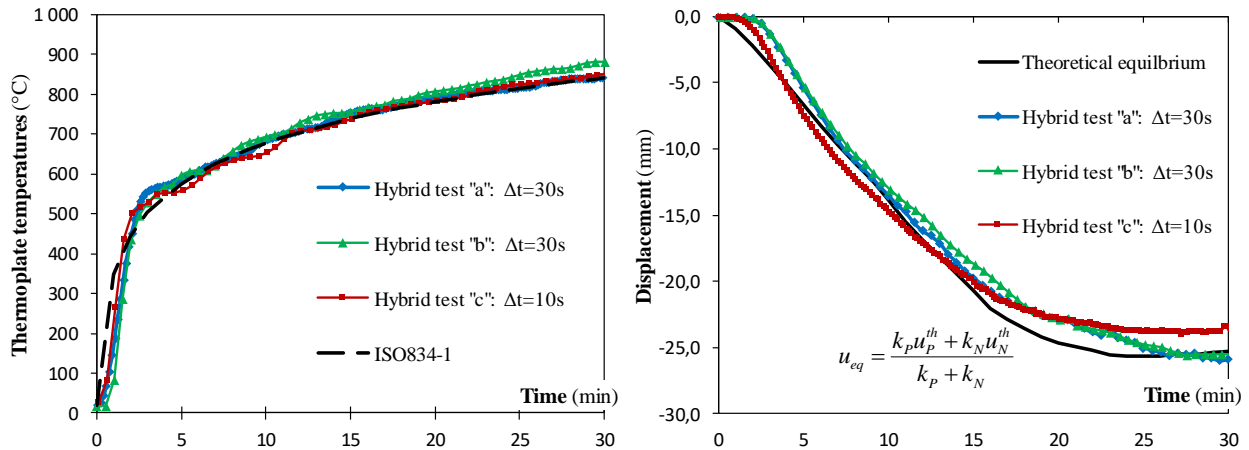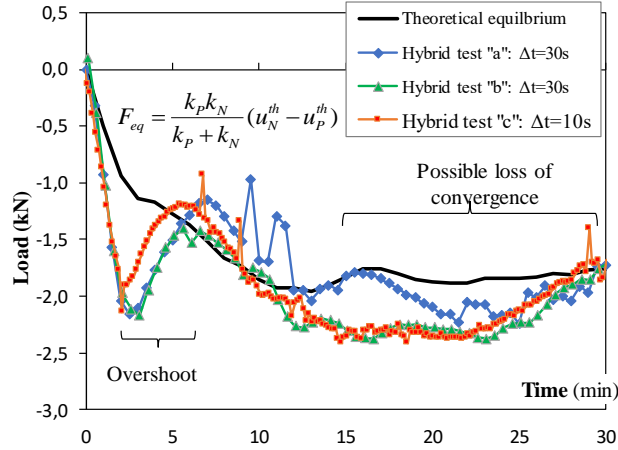
Fig. 5. Evolutions of furnace temperature, displacement and load during HFT

It can be noted that after about 12-15 minutes the theoretical F_{eq} is higher than the HFT experimental curves. This can be caused by the value (>1) of the convergence criterion (k_P/k_N) after 15 minutes presented previously (Fig. 4).

More interestingly, a sudden decrease of load occurs during the first 2 minutes. The load then re-establishes trajectory to join the theoretical F_{eq} after about 5 minutes. This observation is referred to as the 'overshoot' phenomenon hereafter and is analysed through Fig. 6.

It can be noted that the behaviour of the NS was determined using SAFIR with an ISO834-1 heating. Figure 5 shows that the ISO834-1 curve was above the experimental temperatures before 2 minutes and under the experimental temperatures between 2 and 6 minutes. Thus, the calculated u_N^{th} and k_N (Fig. 4) were overestimated (from 0 to 2 minutes) and underestimated (from 2 to 6 minutes).

Assuming that the system behaviour was controlled mainly by thermal displacement (and not stiffness decay) during the first 6 minutes, this leads to the following remarks on equilibrium. From equation (1), u_{eq} was overestimated (from 0 to 2 minutes) and underestimated (from 2 to 6 minutes). From equation (2), F_{eq} was underestimated (from 0 to 2 minutes) and overestimated (from 2 to 6 minutes). Consequently, u_{eq} and F_{eq} would be closer to the experimental curves during the overshoot phenomena.

3.4 Analysis

Figure 6 presents the displacement-load diagram with the behaviour laws of both substructures. The reading of this diagram (presented in Pinoteau *et al*., 2018 [6]) presents a visual alternative for identifying equilibrium points and the system convergence.

The linear behaviour laws of the PS ($F_P(u_P)$ in red) and the NS ($-F_N(u_N)$ in blue) are represented every minute to clarify reading. Initially, both lines pass by the origin (0; 0). As the fire develops, the lines are shifted towards the left (negative thermal displacements) and their slope decreases (decrease of stiffness). At each time, the intersection of the lines represents the equilibrium point. This point is never reached perfectly since it moves with time while the communication loop lags behind. As an example, the path of the substructure interaction is represented in a black line with 2 iterations per minute (Δt=30s) and assumes that the behavior law shifts every minute. This path is established from the communication loop presented in part 2.

(i) The load F_P is measured on the PS and applied on the NS at 1 minute

98

(ii) The NS calculates a displacement u_N and applies it to the PS

(iii) The load F_P is measured on the PS and applied on the NS

(iv) The NS calculates a displacement u_N and applies it to the PS associated to 2 minutes (which has shifted due to thermal expansion and stiffness loss).
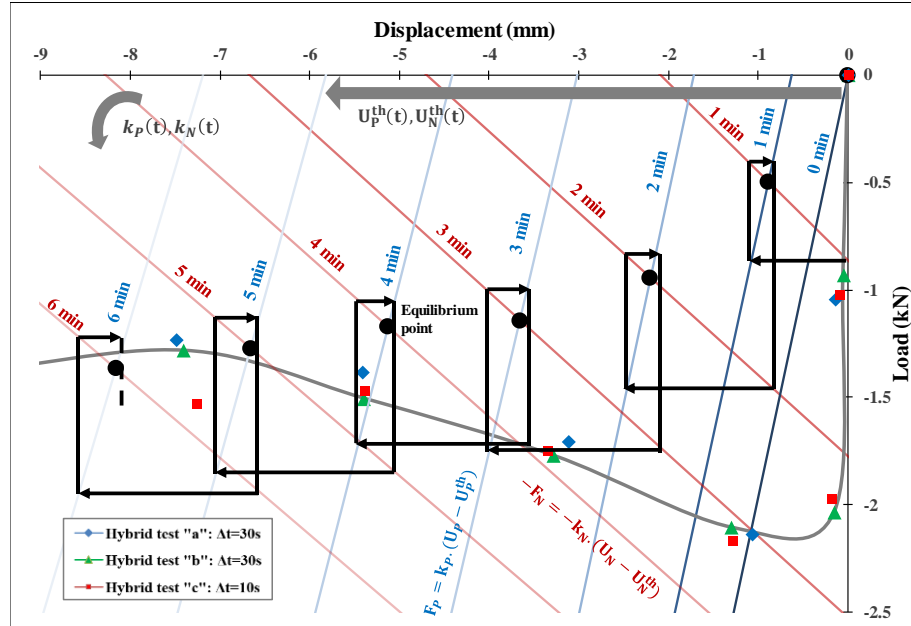
Fig. 6. HFT path towards equilibrium on the displacement-load diagram

The path presents an ideal situation in which the behaviour laws of both substructures are synchronized. In reality, the information (temperature and load) transferred to the NS is late in comparison to the constantly evolving PS. While the calculation is carried out on SAFIR, the PS has heated, and the equilibrium conditions have changed. Furthermore, in this study, the temporary text files used to transfer the information from the test analog signals were stored in the iteration loop for another time step. This creates a lag of the NS which outputs out of date data. At the beginning of the test SAFIR does not receive initial thermal perturbations (which present a high rate). Thus, the jack remains at a zero displacement. Since the PS is blocked while heating, the reaction load shoots up. After about 2 minutes, the displacements start (figure 5) which progressively allows the load to reach the theoretical equilibrium value. The HFT "c" performed with a shorter time step Δt=10s, allows the displacement to start earlier and the load to regain equilibrium faster causing an overshoot of lower amplitude.

4   CONCLUSIONS

In the long term, HFT present a promising alternative in evaluating the fire behavior of structural elements in an environment closer to reality than traditional testing methods, without carrying out delicate, expensive or even impossible full-scale tests.

The study presented aimed at evaluating the feasibility of a HFT on simplified structures as a milestone in the development of the method. The following conclusions have been drawn:

- The convergence criterion based on the stiffness ratio (established in previous publications Sauca *et al.*, 2016 [4], Pinoteau *et al.*, 2018[6]) has been confirmed.

- An overshoot phenomenon may occur due to the non-synchronized action of both substructures. This leads to substantial loads when the thermal expansion rate is high.
- The communication loop allows the system to re-establish equilibrium after the overshoot.
- Smaller time steps (Δt) limit the amplitude and shorten the overshoot phenomenon.
- Apart the overshoot and convergence loss, the HFT follows accurately the expected equilibrium point.

From the identification of the overshoot, two paths of development spring to mind to reduce the delay of the NS. First, the number and duration of time steps required to bring the information can be reduced. Secondly, forward extrapolation may be performed to predict the entry data of the NS in advance. This allows to input up-to-date information in the NS (before the PS has reached the state) to ensure synchronicity. Even if the extrapolated data is misestimated, it has been shown that the system can regain equilibrium after an overshoot. Some forward prediction methods have been developed in the field of seismic hybrid tests and may be adapted for HFT.

ACKNOWLEDGMENT

REFERENCES

[1]   Korzen M., Magonette M., Buchet Ph. (1999). *Mechanical Loading of Columns in Fire Tests by Means of the Substructuring Method*. Zeitschrift für Angewandte Mathematik und Mechanik, 79: S617-S618.

[2]   Mostafaei H. (2013). *Hybrid fire testing for assessing performance of structures in fire – Methodology*. Fire Safety Journal, 58:170-179.

[3]   Tondini N., Abbiati G., Possidente L., Stojadinovic B. (2016). *A Static Partitioned Solver for hybrid Fire Testing*. Structures in Fire 2016 proceedings, 827-835.

[4]   Sauca A., Gernay T., Robert F., Tondini N., Franssen J. M. (2016). *Stability in Hybrid Fire Testing*. Structures in Fire 2016 proceedings, 836-843

[5]   Schulthess P., Neuenschwander M., Knobloch M., Fontana M. (2016). *Consolidated Fire Analysis—Coupled Thermo-mechanical Modelling for Global Structural Fire Analysis*. Structures in Fire 2016 proceedings, 819-826.

[6]   Pinoteau N., Pham D. T., Nguyen H. H., Degiovanni P. G., Mège R. (2018). *Hybrid Fire Testing by total subdivision of physical and numerical substructures: from theory to application* (under review).

[7]   Franssen JM. (2005). SAFIR: *A thermal/structural program for modeling structures under fire.* A.I.S.C. Engineering Journal 42 (3): 143-158.

[8]   EN1991-1-2. (2002). *Eurocode 1, Part 1-2: Actions on structures: general actions – actions on the structures exposed to fire.*

AN EXPERIMENTAL AND NUMERICAL STUDY ON THE BEHAVIOUR OF SPLICE CONNECTIONS AT ELEVATED TEMPERATURES

Paul Akagwu, Faris Ali, Ali Nadjai.
Ulster University, Belfast, United Kingdom

ABSTRACT

This paper investigates the behaviour of bolted web-flange splice connections in fire. The results from two full-scale furnace tests which are part of a series of tests being conducted on spliced connections to understand their structural response in fire are reported herein. Preliminary results show that bolt shear failure is the dominant failure mode for these connections. Using FE analysis, the relative ultimate capacities of the splices and the connected beam were varied from 0.5 to 1.1 to cover a realistic range of partial strength and full-strength connections with a goal to understanding the implications for fire resistance. The results did not reveal any significant change in the fire resistance times. The wider implication of this is that full advantage can be taken of the benefits of partial strength connections without compromising the fire resistance of steel moment frames.

1   INTRODUCTION

The behaviour of steel connections in fire continues to attract attention due to their crucial role in the resistance of structural steel frames to failure. Previous research has focused mainly on beam to column connections and only very scarce data [1] – [4] on the behaviour of beam to beam connections at elevated temperatures exist in the literature. Bolted web-flange spliced connections have wide applications in construction with their use often dictated by factors such as material limitations, transportation constraints, the need to alter a section size due to strength variation along a beam span etc. They are a common feature in column-tree steel frames, bridges and industrial constructions.

Whereas, this class of connections has been traditionally designed in buildings to be at least of equal capacity to the connected beams, semi-rigid partial-strength splices have been shown to offer many advantages over full-strength splices, like preventing the development of large moments in steel frames by acting as buffers, enhancing damping and vibration periods in frames etc. [5]. However, there is a lack of information on the degree to which bolted connection strength affects the resistance of steel I-beams in fire. Experimental testing and numerical analysis have been conducted on spliced connections to provide some reasonable insight on this as well as their general behaviour in fire. Results from two of the specimens tested as part of an ongoing study are presented. Details of the testing methodologies and numerical simulations are provided in the subsequent sections.

2   EXPERIMENTAL TESTING

2.1 Test set-up & methodology

Two S355 UB203X102x23kg I-beams with central splices were tested. Although connections are not placed at locations of high moment forces in practice, it was convenient in this instance to do this because of the failure modes being investigated. Both specimens had similar geometries. Each specimen had a total length of 2m with a clear span of 1.75m. The web and flange splices had thicknesses of 6mm and 10mm respectively and were fastened to the beams with grade 8.8 M16 structural bolts installed in 18mm holes. Further details are provided in *Fig. 1*. Type K Cromel-Almel

thermocouples were installed at 13 locations to capture the temperature distributions within each specimen during the test as shown in *Fig.2* with readings taken at 3 seconds intervals.
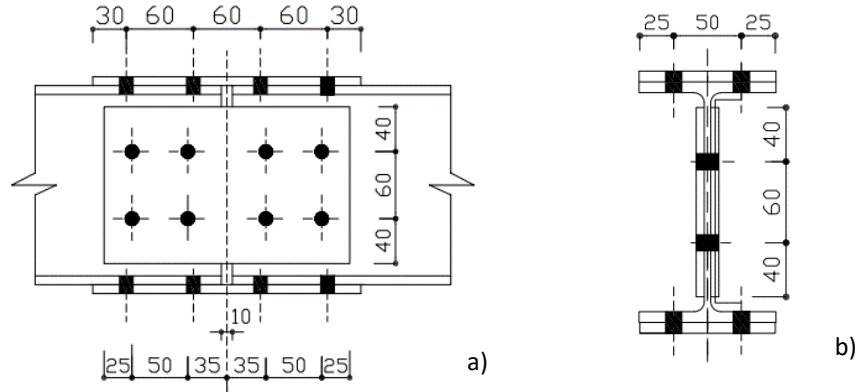

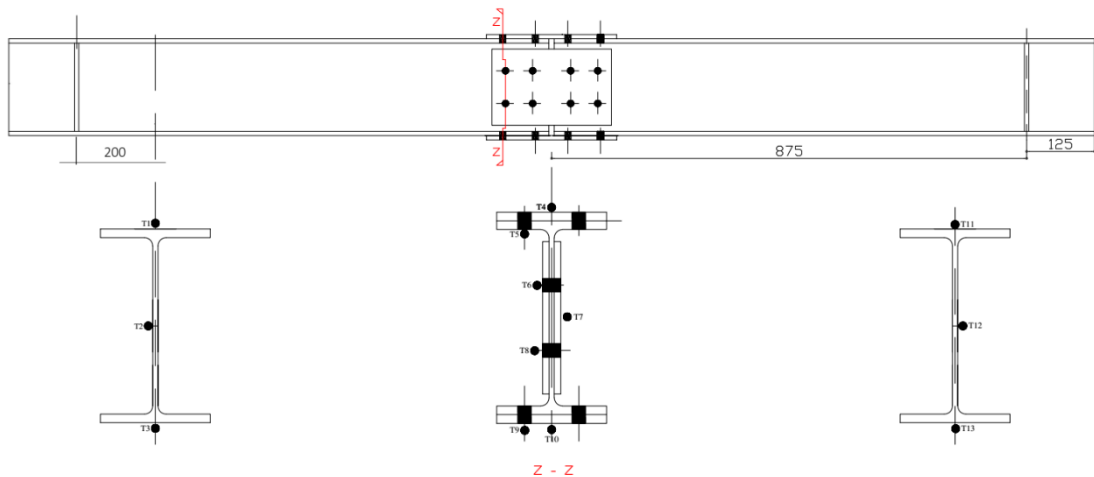*Fig. 1. a)* Elevation. b) Sectional view

Fig. 2. Thermocouple locations.

The load was applied with a single cylinder Enerpac hand-operated hydraulic pump. A 100 kN load cell positioned between the ram and the beam measured the applied loading while a custom-made loading pad was placed between the load cell and the specimen to transfer the load to the later.

Load ratios of 0.4 and 0.6 which are representative of realistic loadings on structures in practice [6], were applied via a 3-point loading arrangement as shown in *Fig.3*. The load ratio describes the percentage of the load applied during the test in relation to the beam's ultimate plastic capacity under ambient conditions. A transient testing approach in which the required load is applied incrementally, followed by heating to failure was implemented. This method closely mimics the actual loading sequence of a real structure subjected to an accidental fire. Failure is governed by the conventional criteria of deflection and deflection rate limits of span/20 and $L^2/9000d$ respectively with the latter applicable as from L/30 deflection [7]. For each case, the mechanical loading was applied in 10% increments up to the full test load followed by a 10 minutes stabilisation period prior to applying the thermal load. Two linear variable differential transformers (LVDTs) were installed adjacent to the loading ram to measure the deflection of each specimen as per *Fig.3*. The LVDTs were placed at

about 120mm distance from the loading ram and their readings were averaged to obtain the deflection at midspan over the test duration. The specimens were heated on three sides from the bottom flanges and the web with five burners in a furnace with an internal compartment of 1500mm x 1500mm x 1500mm and two custom-made demountable concrete roof covers. The concrete covers provided lateral restraint to the beam top flange and were positioned with sufficient clearance to prevent interference with the deflection of the beam during the test. The top flanges were covered with ceramic fibre blanket to prevent any damage to the instrumentation from escaping hot gases. The furnace was programmed to follow the standard ISO 834 curve. The specimens were simply supported, and the final set up in the furnace is presented in *Fig. 4.*
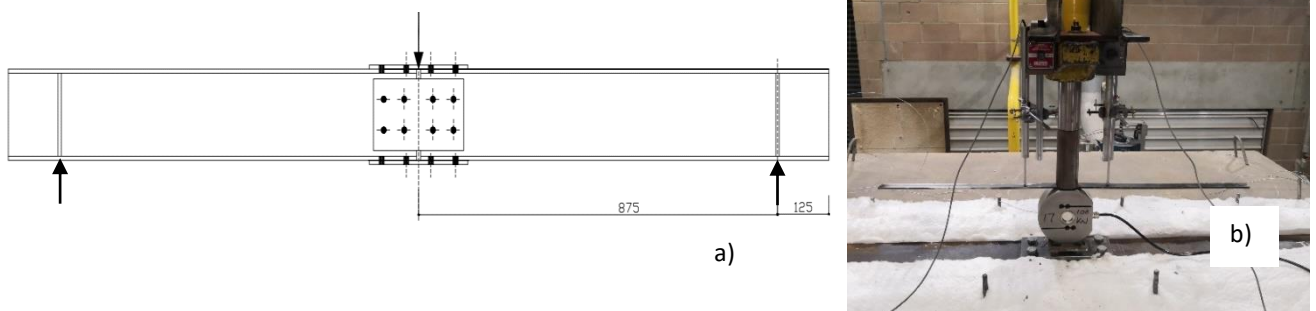
Fig.3 a) Loading details, b) Instrumentation

Fig.4 Specimen setup

3 NUMERICAL SIMULATIONS

3.1 Methodology

Three-dimensional models were created to simulate the behaviour of the beam as observed in the experiments. While solid elements are computationally expensive, they provide the closest approximation to real life structural behaviour. All the simulations were run in Abaqus standard which implements an implicit integration scheme in solving for the displacement fields. While Abaqus explicit has been used in the past for similar problems [2], it is more difficult to ascertain the accuracy of results obtained in this way. Temperature fields were defined for the 13 temperature domains shown in *Fig. 2*. The complex geometries in the model were meshed with the reduced integration eight-node brick elements C3D8R with hourglass control activated to prevent loss of stiffness in the elements, while the sections with more simple profiles were meshed with the incompatible mode eight-node brick element C3D8I which is generally recommended for bending dominated problems,

[8]. The C3D8I elements can produce results in bending problems that are comparable to quadratic elements at significantly lower computational cost and it has been shown that a mesh with a single C3D8I element through a beam in bending can produce results that are within reasonably close range of the theoretical value if significant mesh distortions are absent in the model. [9]. A very refined mesh was used for the bolt and holes.
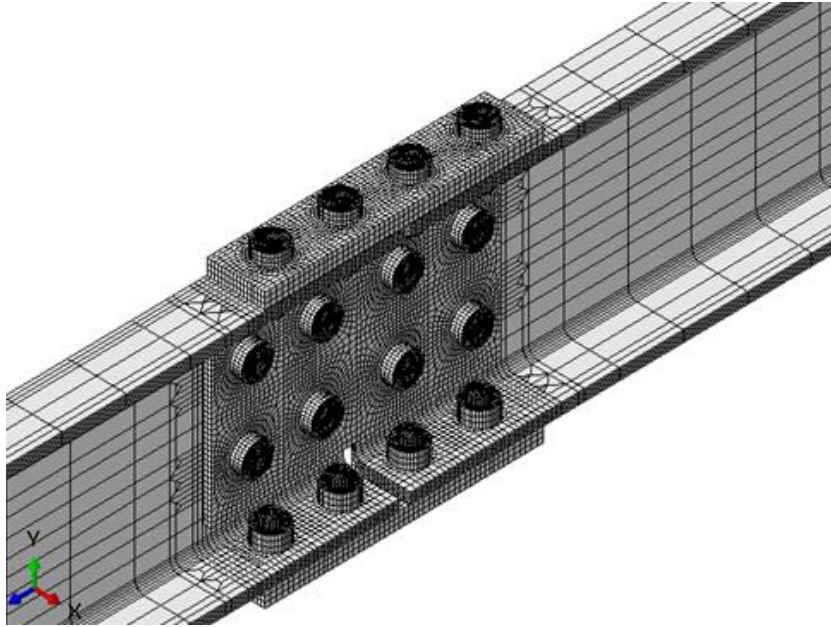
Fig. 5 a) FE Model

To reduce the computational resources required, half of the model was created along the longitudinal axis as shown in *Fig. 5.* An obvious implication of this simplification is the assumption of similarity between the bolt nuts and the bolt heads, enabling the former to be discarded in the model. This assumption is of no consequence to the integrity of the results because the bolts at those locations are in a pure shear working mechanism, hence, replacing the nuts with the bolt heads in the numerical model will have no significant influence on the structural behaviour of the system. Such an assumption would be inadmissible if the bolts were under pure tensile stresses where the additional length of the bolt on the nut side provides an added flexibility to the system since thread stripping could contribute to the ductility of the system before failure [8]. It is worth mentioning that although the model is geometrically symmetrical in both axes, a quarter model was not used because of the non-symmetry in temperature distribution along the longitudinal axis as observed from the thermocouple readings.

Contact interactions were defined for all the relevant surfaces. For the normal directions, a hard contact algorithm was implemented via the non-linear penalty enforcement method, an approach which allows a little penetration between surfaces in contact without compromising the accuracy of the results. It avoids the numerical difficulties often associated with the large contact forces arising from the default 'no penetration' enforcement method. For the tangential interactions, a penalty method with a friction coefficient of 0.1 was defined. Damping was applied to the contact pairs involving the bolts and plates to prevent numerical difficulties arising from rigid body movement due to the initial gaps between the bolt shanks and the bolt holes in the webs and flanges. A damping scaling factor of 0.01 chosen via trial and error, provided sufficient stability to the model without changing the physics of the problem. This was easily verified by checking that the ratio of the

damping dissipation energies to the internal energies of the specimen was below 5% for all the simulations as recommended by Abaqus [9].

3.2 Materials properties

The material properties for the beams and plates obtained from coupon tests conducted on four samples cut from the beam flange and web are given as follows, young's modulus – 196 GPa, yield strength – 408 MPa and ultimate strength – 516 MPa. Nominal yield and ultimate strength values of 640 MPa and 800 MPa were adopted [10] for the bolts with a young's modulus value of 210 GPa.

The elevated temperature stress-strain curve and material degradation factors for the beams and bolts are as per the Eurocode [11]. A constant coefficient of thermal expansion of 1.2 E-5 $^\circ$ C^{-1} was applied.

4 RESULTS AND DISCUSSIONS

4.1 Observations

The temperature histories of both specimens are shown in *Fig.* 6. A common trend can be observed for both cases where the highest and lowest temperatures occurred in the bottom flanges and the top bolts respectively. The temperature distribution is largely non-uniform due to the thermal protection applied to the top flange of both specimens.

Temperature and displacement curves from the test and FE simulations are presented in *Fig.7 and Fig.8.* The plots show a good agreement between the experimental and numerical results. The deflection profile in both curves follow a gradually increasing slope in the initial phase of the heating and as the materials degraded further, there was an appreciable increase in the rate of deflection until failure occurred.

A momentary loss of stiffness associated with a sudden increase in deflection was observed in specimen 1 at about 500 $^\circ$C due to premature shearing of some of the bottom flange bolts caused by unequal load distribution while the beam was deforming. It is often the case that the transition from frictional resistance to bearing resistance is non-uniform for these connections because of the difficulty in achieving a perfect alignment of the bolts in the holes at the start of the experiment. Once the load was redistributed, it stabilised at a deflection of about 40mm and continued to resist the applied loading until runaway deflection was observed.

The critical temperature and failure time from the graph are 640 $^\circ$C and 23 minutes respectively. The corresponding values for the FE analyses of 660 $^\circ$C and 24.5 minutes as observed from the plots are reasonably close to the test results. Loading was stopped at 26 minutes at a deflection of 91mm, following a rapid loss of strength to prevent damage to the furnace.

A closer agreement between the experimental and numerical results can be seen in specimen 2 where as expected, failure occurred at a higher critical temperature of about 725 $^\circ$ $^\circ$C and a failure time of 32.5 minutes, due to the smaller load ratio. A slightly lower critical temperature and failure time of 720 $^\circ$C and 32 minutes can be observed for the FE model in *Fig.8.*

Bolt shear failure was observed in both specimens at the end of the tests. *Fig.9* shows a picture of specimen 2 at the end of the test and the corresponding FE contour plot from the simulations.
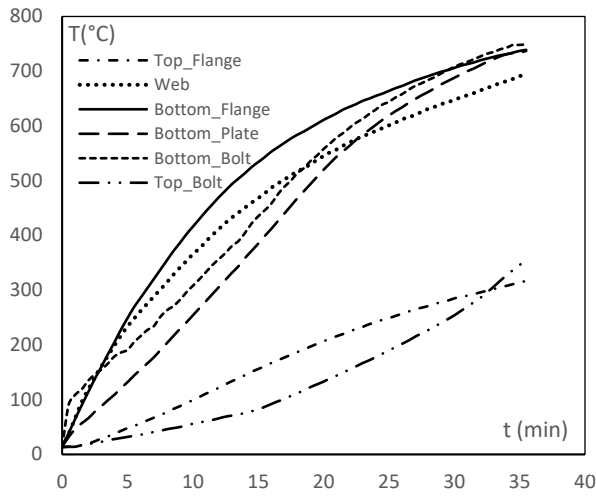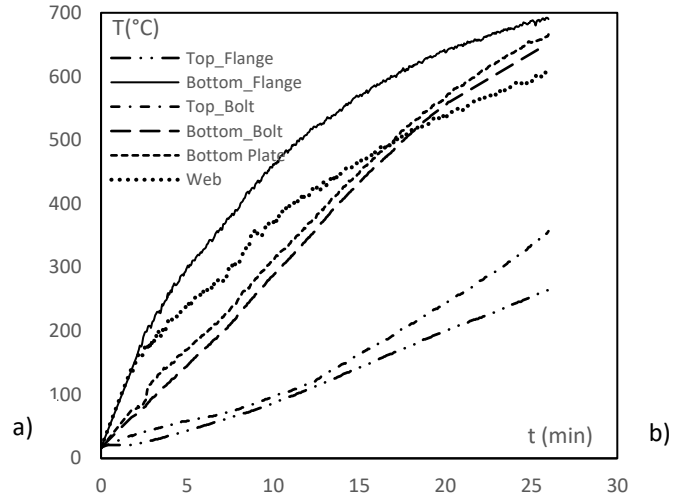
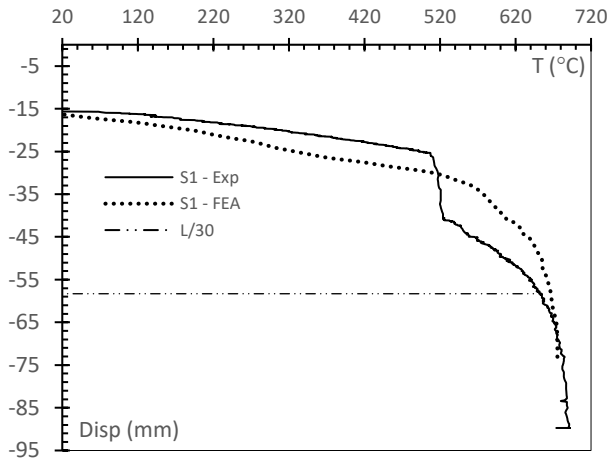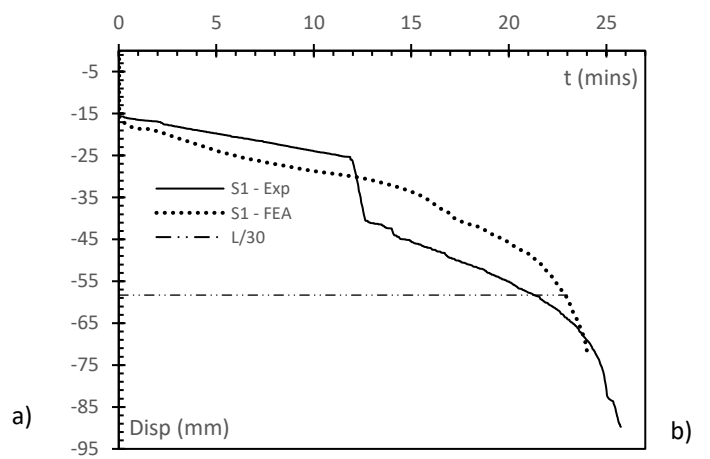*Fig.6* a) Specimen 1 temperature history plot.   b) *S*pecimen 2 temperature history plot

Fig.7 a) *S1* Bottom flange temperature vs midspan deflection plot. b) S1 midspan deflection plot
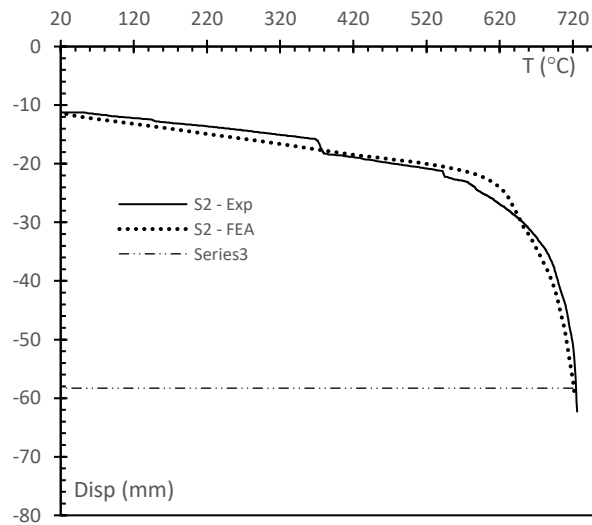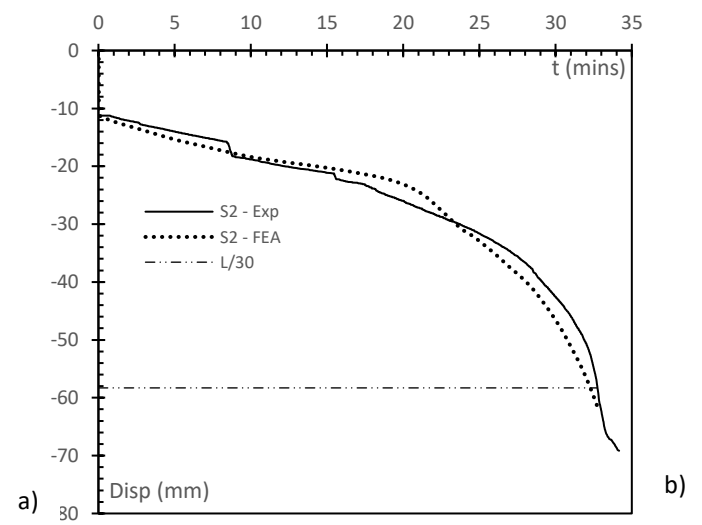

Fig.8 a) S2 Bottom flange temperature vs midspan deflection plot. b) S2 midspan deflection plot

106

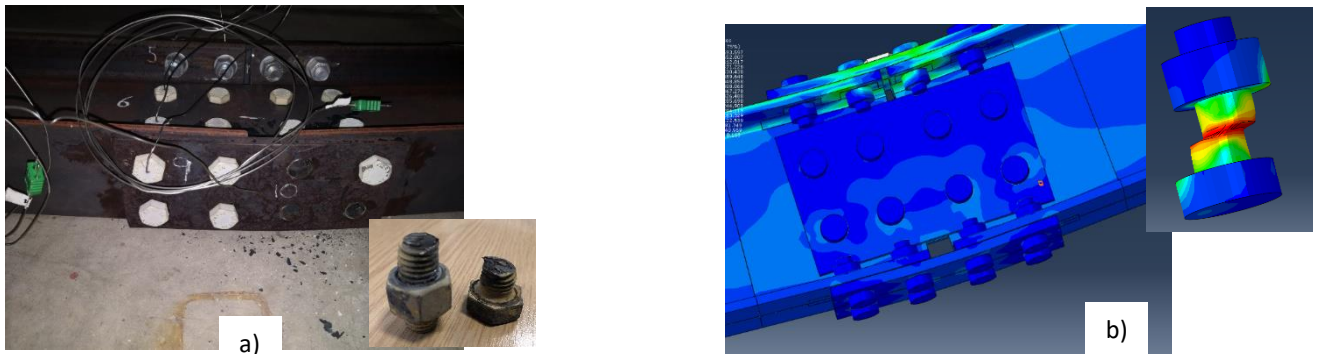The FE model reasonably replicated the failure profile of the specimens as shown in *Fig. 9 below*.

Fig.9 a) Failed specimen 2. b) Specimen 2 von mises stress plot.

4.2 Effect of Splice strength on beam behaviour.

The validated FE model was used to investigate the influence of splice connection strength on the behaviour of the beam in fire. The geometry and span of the tested beam were not altered in the numerical model however, the load was applied at an offset from the centre to ensure a uniform shear in the connection. A load ratio of 0.6 was used for all the cases and the main variable investigated was the flange thickness which governs the splice moment capacity. Splice strength ratios (SR), of 0.5, 0.7 and 1.1 corresponding to flange thicknesses of 6mm, 8.5mm and 13mm were investigated and the results are presented in *Fig. 10*.
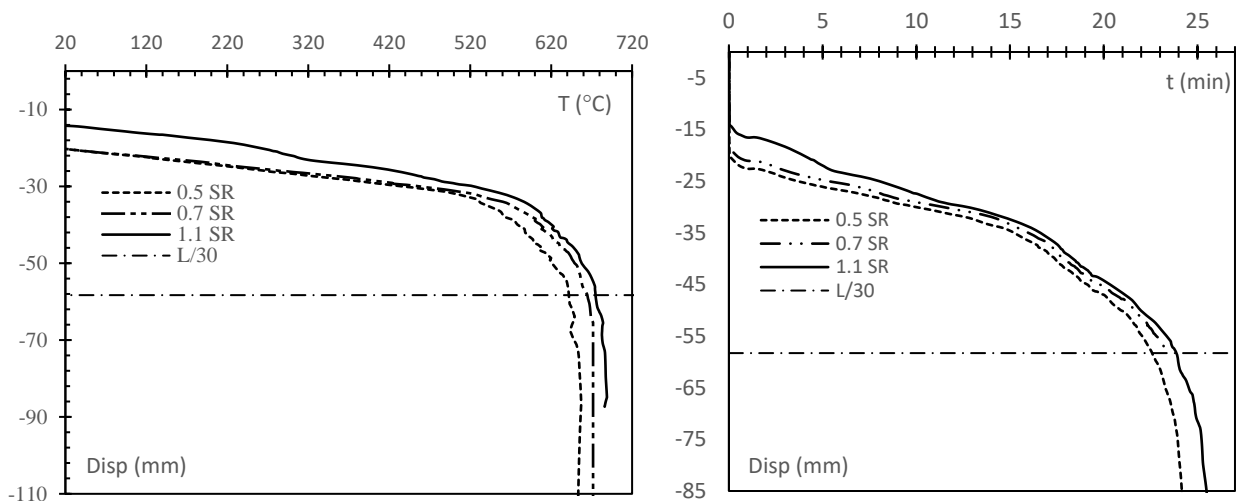
Fig.10 a) Temperature vs displacement plot. b) Midspan deflection plot

The plot shows that reducing the moment capacity of the splice does not necessarily result in a proportionate reduction in fire resistance. The critical temperatures for the 0.5 SR and 1.1 SR cases observed from the plots are 640 °C and 680 °C respectively with corresponding fire resistance times of about 22.5 mins and 24 mins. Significant plate bearing deformation was observed in the 0.5 SR model. However, the bolts were only slightly deformed. For the 1.1 SR model the reverse was the case as the bottom flange bolts underwent significant shear deformation while the splice plates were largely intact. This can be explained by the disparity in the splice plates thicknesses. Bolt shear failure

107

governs in connections with thick splice plates like 0.7 SR and 1.1 SR as evident from the results in the FEA. This is an undesirable failure mode because of its abrupt nature as compared to the more ductile failure mode observed in the 0.5 SR case. It appears from the above that, adopting a strong-bolt weak-plate approach in connections such as this will guarantee the formation of plastic hinges in the connection which would in turn prevent large forces and moments from developing at the column faces in column-tree frame construction for instance where splice connections are located on stub beams welded to the columns.

5   CONCLUSIONS

Fire tests have been conducted on two I-beams with web-flange splice connections to understand their behaviour when exposed to elevated temperatures. The results from the experimental tests were used to validate finite element models for the purposes of investigating the effect of connection strength on the overall response of the beam assembly in fire. The following conclusions can be drawn from this study.

- The use of semi-rigid partial strength connections does not necessarily reduce the fire resistance of the connected beams in moment frames.
- The observed dominant failure mode for both connections in the experiment was bolt shear. The plate splices were generally intact and very little bearing deformation was observed. The same trend was observed with the numerical models except for the 0.5 SR case where bearing failure occurred in the bottom flange splice.
- The use of a weak-bolt strong plate combination for splice connections could prevent a ductile failure from happening since bolt shear failure is bound to occur.
- The effect of other parameters like end restraints, bolt size etc, on fire resistance, will be subsequently investigated numerically.

REFERENCES

[1]   Yahyai, M., & Rezaeian, A. (2016). *Behavior of beams in bolted column-tree frames at elevated temperature.* Fire and Materials, 40(3), pp 482–497.

[2]   Hirashima, T., Taib M., Wong B., Burgess I. (2012). *The behaviour of steel beams with moment-resisting beam-splice connections in fire*, 7th International Conference on Structures in Fire, Zurich Switzerland, 12-15 June 2012, pp 125–134.

[3]   Taib M., Hirashima, B. Wong, and I. Burgess, Burgess I. (2012). *A component-based model for moment-resisting beam splice connections with high-strength bolts at elevated temperature*, 7th International Conference on Structures in Fire, Zurich Switzerland, 12-15 June 2012, pp 135-144.

[4]   Eslami M., Kodur V., Rezaeian A. (2018). *Behavior of Steel Column-Trees under Fire Conditions.* Journal of Structural Engineering. 144 (9) pp 04018135-1-15.

[5]   Astaneh A. (1998). *Seismic design of steel column-tree moment-resisting frames*. Structural Steel Education Council, Steel TIPS Report. p 8.

[6]   Buchanan, A. H. (2002). *Structural design for fire safety*.

[7]   European Committee for Standardization. (1987). BS 476-20. *Fire Tests on Building Materials and Structure, Part 20: Method for Determination of the Fire Resistance of Elements of Construction,* Brussels, Belgium.

[8]   Bursi, O. S., & Jaspart, J. P. (1997). *Benchmarks for finite element modelling of bolted steel connections*. Journal of Constructional Steel Research, *43*(1–3), pp 17–42

[9]   ABAQUS (2017). *Abaqus analysis user's guide, Dassault Systems.*

[10] CEN. (2013). *BS EN ISO 898-1 Mechanical properties of fasteners made of carbon steel and alloy steel Part 1 : Bolts , screws and studs with specified property classes - Coarse thread and fine pitch thread.* London, UK.

[11] CEN. (2005). *BS EN 1993-1-2:2005 Eurocode 3. Design of steel structures. General rules. Structural fire design.* London, UK

BUCKLING ANALYSIS OF STEEL COLUMNS STRENGTHENED BY PRESTRESSED CFRP AT ROOM TEMPERATURE AND EXPOSED TO FIRE

[1]Lili Hu, [1]Peng Feng, [2]Elyas Ghafoori, [3]Mario Fontana

[1]Key Laboratory of Civil Engineering Safety and Durability of China Education Ministry, Beijing, China
[2]Empa, Swiss Federal Laboratories for Materials Science and Technology, Duebendorf, Switzerland
[3]Institue of Structural Engineering, ETH Zurich, Zurich, Switzerland

ABSTRACT

Carbon fiber reinforced polymer (CFRP) has been proven to be effective for strengthening of steel structures. Due to the rapid degradation of the steel and polymer materials with an increasing temperature, the fire safety is of significant concern. In this paper, the efficiency of strengthening steel column by prestressed (PS) CFRP is studied at room temperature and exposed to fire. At room temperature, the test and the finite element method (FEM) results show that the weak axis buckling load can be increased to the strong axis buckling load. This study also presents a coupled thermo-mechanical FE analysis for the specimens exposed to fire. The results show that to reach an adequate fire resistance time, the CFRP and the steel need to be protected. With a preload of 50% design load (P_d), the fire exposure time of the strengthened specimen can be extended to more than 80 minutes. Thus, the strengthening method is effective at room temperature and under fire exposure with protection.

1   INTRODUCTION

Many accidents have occurred due to the buckling of columns in structures. Avoiding the overall buckling of steel columns is an important concern in the design of steel structures. FRPs have been widely employed for strengthening steel structures, especially CFRPs, due to their excellent properties of high strength and light weight. In 1963, prestressed stayed columns were proposed by Chu and Berge [1]. Subsequently, they were shown to be very efficient, with the buckling loads increasing to several times those of pure steel columns [2, 3]. It is noted that applying CFRPs rather than steel wires in this system offers some benefits [4]. In addition, it has been shown that prestressed CFRP strips can enhance the buckling behavior of the steel beams substantially [5, 6]. However, there are only very limited studies on their application on steel columns. Therefore, in this paper, the performance of the steel columns strengthened with prestressed CFRP strips is studied. As civil structures can be subjected to fire exposures, the effect of elevated temperatures on the retrofitted columns will be numerically investigated in this paper. The finite element modelling (FEM) has been conducted on thermal transfer analysis and mechanical analysis. The pure steel columns and strengthened steel columns are preloaded and then exposed to fire. The relationships of the time and the lateral displacement at room temperature and exposed to fire are obtained. Based on it, the buckling behaviors are obtained.

2   CONCEPT OF STEEL COLUMN STRENGTHENED BY PS CFRP

As shown in Fig. 1, a steel column strengthened by PS CFRP strips is mainly composed of three parts: (1) an I-section steel column; (2) two CFRP strips, which will be prestressed; (3) a PS system, which includes two anchorages and two PS chairs or saddles. The implementation method is as follows: CFRP strips are placed along the length of a steel column, with the two ends anchored by anchorages. Then, the CFRPs are stretched at the mid-span of the steel column by the PS chairs [4].
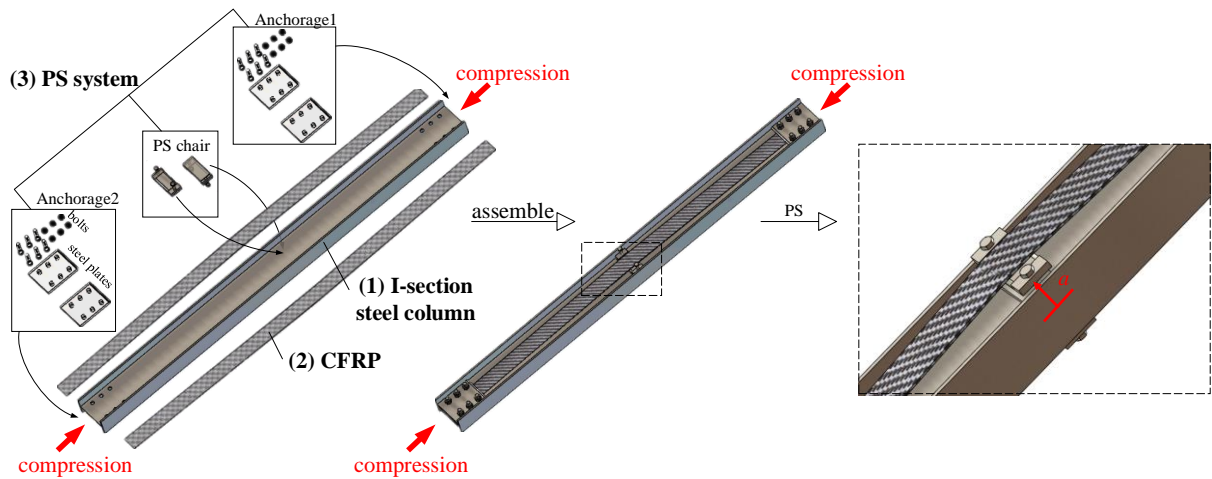
110

Fig. 1. Schematic diagram of the steel columns strengthened by PS CFRP strips [4]
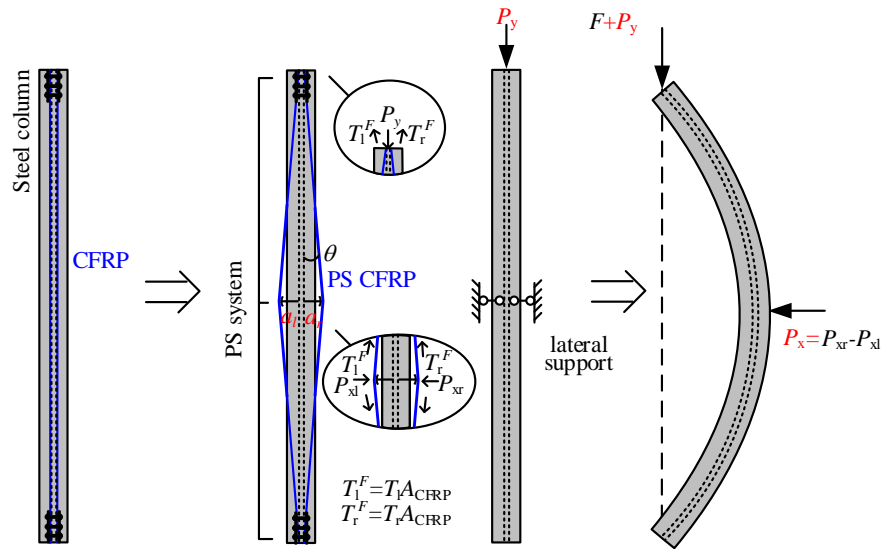

Fig. 2. Mechanical system

As shown in Fig. 2, the steel columns strengthened by PS CFRPs form a self-balanced system. When a_l and a_r are increased by the PS chairs, the CFRPs are stretched with the prestress value T_l and T_r (the corresponding force are T_l^F and T_r^F) from the left and the right side, respectively. At the same time, the steel column is subjected to a compressive force of P_y. If the column has lateral deformation towards right under compression, T_l^F decreases and T_r^F increases, and the difference of them form a transverse force P_x at the mid-span. In summary, the PS CFRPs introduce two forces (i.e., P_x and P_y) to the steel column, where P_x equals to $(T_r^F - T_l^F)\sin\theta$ and P_y equals to $(T_r^F + T_l^F)\cos\theta$. It is seen that P_x provides an effective lateral support to resist buckling although P_y can be disadvantageous. Thus, when a suitable prestress value is applied, the combination of P_x and P_y will give the self-balanced system greater stiffness compared to the pure steel column; thus, the buckling behavior can be improved [4].

3   BEHAVIOR AT ROOM TEMPERATURE

3.1 Experimental results

Table 1. Details of specimens

Specimen		λ	strengthening method	L_b (mm)	T (MPa)	a (mm)
I140 series	I140-U	140	-	2218	-	-
	I140-S	140	by anchoring CFRP	2220	0	0
	I140-PS	140	by anchoring PS CFRP	2224	302	70

Table 2. Sizes of the steel and CFRP sections

width of the steel section b_s	height of steel section h_s	thickness of steel flange t_{sf}	thickness of steel web t_{sw}	CFRP width b_f	CFRP thickness t_f
70 mm	114 mm	5 mm	5 mm	50 mm	3 mm
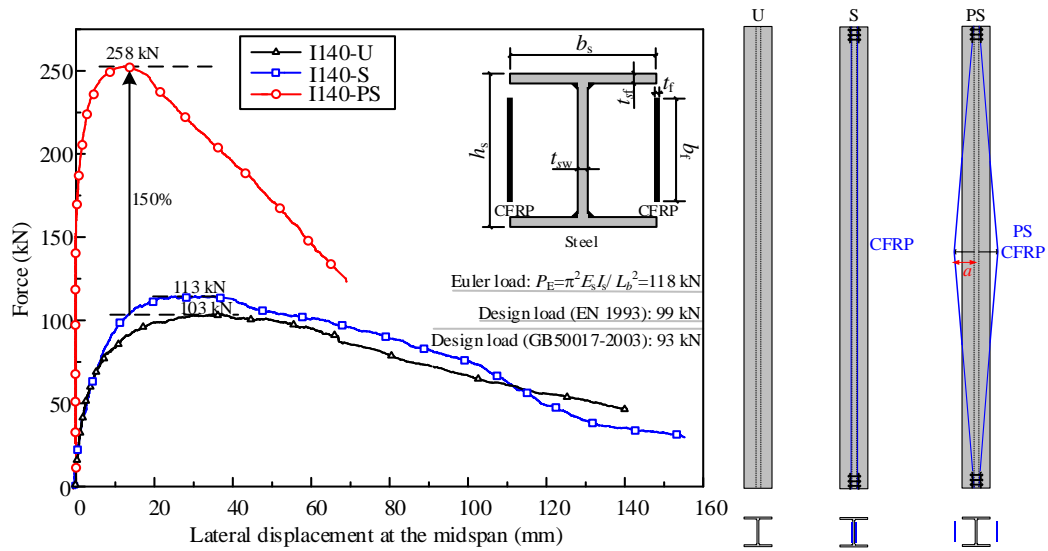
Fig. 3. Typical force and lateral displacement curves

At room temperature, axial compression tests were conducted, and the details of the specimens are shown in Table 1. In total, there are three types (i.e., U, S, PS). λ is the design slenderness and the real slenderness is 145; L_b is the buckling length; a is the distance between the CFRP and the web of the steel column at the mid-span. For the steel material, the average values of the yield point (f_y), the ultimate strength (f_u), the elastic modulus (E_s) are 682 MPa, 765 MPa and 206 GPa, respectively. For the CFRP strips, the average values of the elastic modulus (E_{CFRP}) and the ultimate strength ($f_{u,CFRP}$) are 171 GPa and 2450 MPa, respectively. In addition, the sizes of the steel and CFRP sections are shown in Table 2 and Fig. 3.The experimental results are shown in Fig. 3, and based on it the buckling load refers to the maximum point of the force and lateral displacement curve. For I140-PS, the buckling load is 258 kN, which has been improved 150% compared to the control specimen I140-U (i.e., 103 kN) [4], and is larger than the design load (i.e., 163 kN) and the Euler load of the strong axis (i.e., 193 kN) of I140-U according to Eurocode 3 [7].

3.2 FEM results
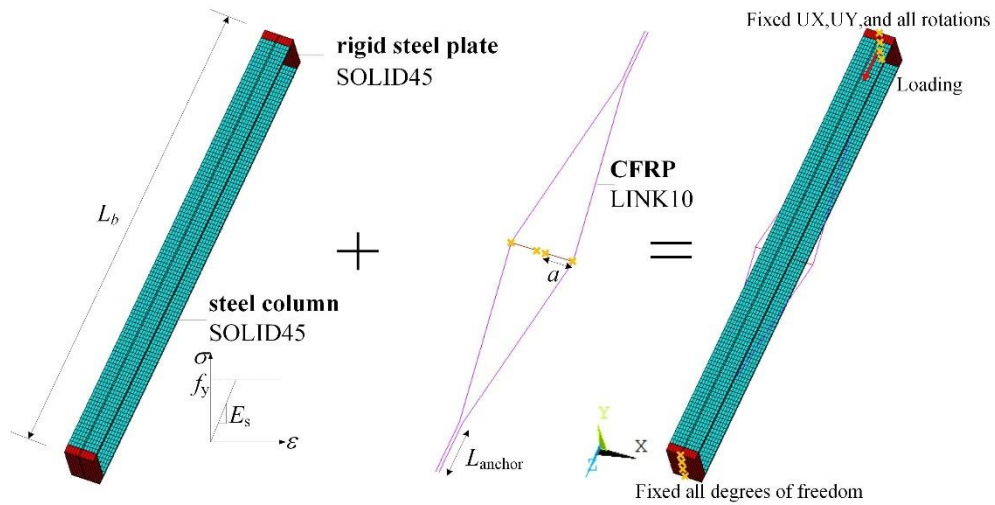
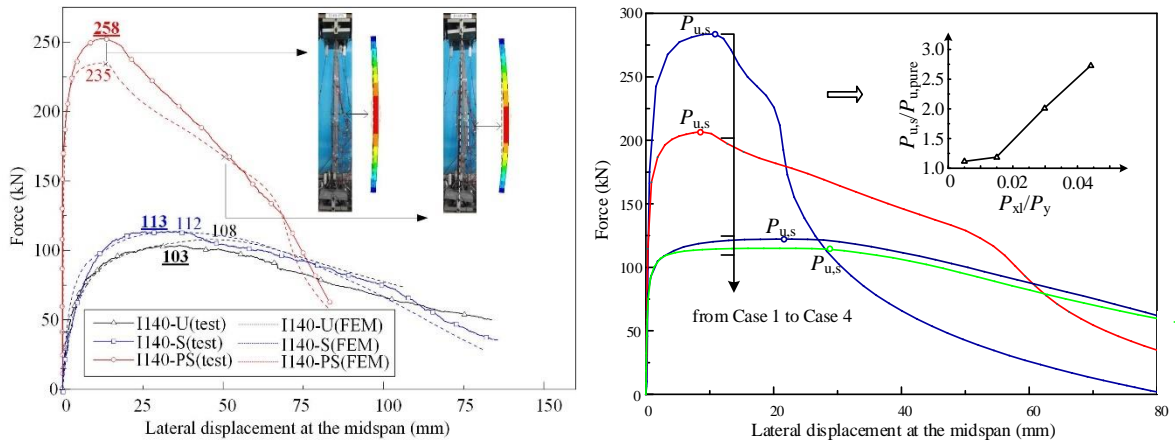*Fig. 4.* Geometric model and boundary conditions

Fig. 5. a) Comparison of FEM and experimental results; b) Force and lateral displacement curves with different prestress values *T* in Table 3

Compression buckling analysis was performed using the ANSYS software package [8]. The geometric model, related parameters and boundary conditions are shown in Fig. 4, and they are based on the real experiment as stated in Part 3.1. The steel column was meshed using solid element SOLID45 and the CFRP was modelled using element LINK10. The PS chair is simplified as a rigid component. First, an eigenvalue buckling analysis was conducted to obtain the first-order buckling mode; then, the initial imperfection was added to the original specimen to update the finite element model. Finally, a nonlinear buckling analysis was conducted using the arc length method. The element refining has been checked in Ref. [4]. The accuracy is verified, as shown in Fig. 5 (a).

Table 3. Ultimate buckling loads with different prestress values

case No.	a (mm)	T (MPa)	T^F (kN)	$P_{xl}=P_{xr}$ (kN)	P_y (kN)	P_{xl}/P_y	$P_{u,s}$ (kN)	$P_{u,s}/P_{u,pure}$
1	90	504	76	6.71	150.60	4.46%	283.6	2.75
2	60	223	33	1.98	66.78	2.97%	206.8	2.00
3	30	52	8	0.23	15.59	1.49%	122.2	1.19
4	10	1	0.2	0.00	0.30	0.50%	114.9	1.12

To analyse the relationship of the prestress value T and the ultimate buckling load $P_{u,s}$ for the strengthened specimens, the following analysis was performed based I140-PS with only changing a and T. In Table 3, T is the prestress value; T^F is the prestress force; P_{xl}, P_{xr}, P_y correspond to Fig. 2; $P_{u,pure}$ is the ultimate buckling loading of I140-U. As shown in Fig. 5 (b) and Table 3. Without considering the fire, the optimal prestress value of CFRP is the maximum prestress value achieved by the PS chair. Especially, $P_{u,s}$ is influenced by the value of P_{xl}/P_y. When P_{xl}/P_y ($=P_{xr}/P_y$) is above 0.50%, the strengthening system works safely; and when P_{xl}/P_y is above 2.97%, the value of $P_{u,s}/P_{u,pure}$ is above 2.00, and the strengthening efficiency is considered to be pronounced.

4   BEHAVIOR UNDER FIRE

As civil structures may have degradations at the elevated temperature due to a possible fire exposure, the high temperature behavior of the critical load-carrying elements is of great importance. Therefore, in this section, the elevated temperature behavior of the steel columns strengthened with PS CFRP will be investigated.

Firstly, the thermal transfer analysis is conducted to obtain the time-dependent temperature distribution. Then, the mechanical analysis is to apply a preload and then the thermal boundary conditions to the specimen. Specifically, the steel column is applied the preload of 50%P_d (51.5 kN) at room temperature. Then the temperature of the gas around the steel columns is increased according to time-temperature-curve ISO 843. This situation appears when the pure steel column is under a service load of 50%P_d, and the service load needs improving, so the PS CFRP is applied. After the reinforcement, if the fire starts, the preload is still 50%P_d.
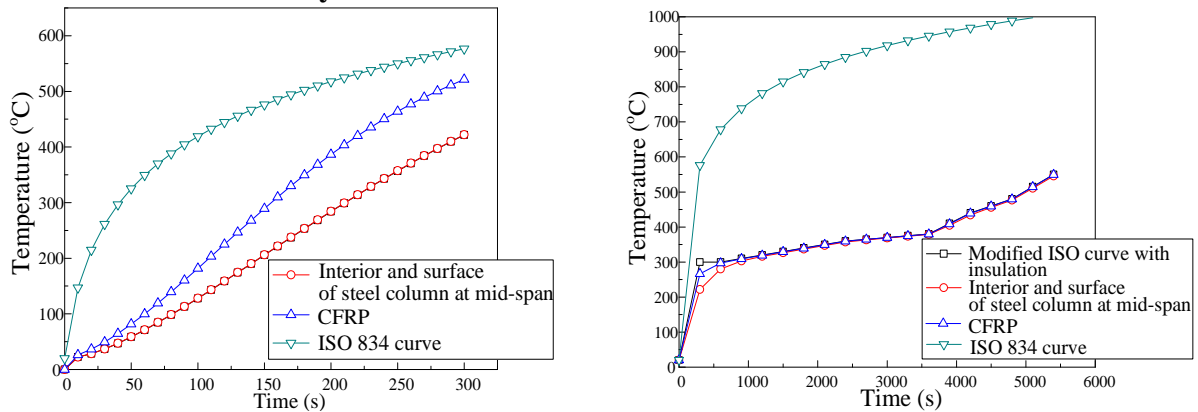
4.1 Thermal transfer analysis

Fig. 6. Relationship of time and temperature: a) without protection; b) with protection

Thermal properties of the steel and the CFRP were described by the thermal conductivity $\square_a$, the specific heat C_a, the unit mass (i.e. the density) ρ_a and the coefficient of thermal expansion (CTE). For steel, λ_a is set as a constant of the value at 20°C (53.335 W/m·K); For temperatures $\square_a$ from 20°C to 600 °C, C_a is calculated by Eq. (1); ρ_a is set as 7850 kg/m^3 and CTE is set as 1.4×10^{-5}/K [9]. For the CFRP, λ_a in the longitudinal direction is set as 50 W/m·K and ρ_a is set as 1600kg/m^3 [10]; C_a is set as 1300J/kg·K [11] and CTE is set as -0.09×10^{-6}/K [12].

$$C_a = 425 + 0.773 \times \theta_a - 1.69 \times 10^{-3} \times \theta_a{}^2 + 2.22 \times 10^{-6} \times \theta_a{}^3 \ (\text{J/kg·K}) \tag{1}$$

The geometric model is the same as that in Fig. 4. For the steel column, 3-D thermal element SOLID69 was adopted, which is a corresponding element in thermal analysis to SOLID45 in structural analysis. For the CFRP, the temperature distribution is obtained by element SHELL 57 in thermal analysis and then it will be imposed to element LINK10 modelling the CFRP in the mechanical analysis [8]. For the boundary conditions, the thermal convection and thermal radiation are applied to all the nodes of the exposed surfaces of the steel column and the CFRP [12]. The standard temperature-time curve (ISO 834) is given by: $\theta_g = 20 + 345\lg(8t+1)$, where θ_g is the gas temperature in the fire compartment and t is the time. The coefficient of heat transfer by convection α_c is 25 [W/m^2·K] for all structures. The Stephan Boltzmann constant is 5.67×10^{-8} W/m^{2}K^4. The emissivity related to the steel surface is equal to 0.7 for carbon steel [9], which is assumed to be the same for the CFRP. The results are shown in Fig. 6. Without protection, the temperature increases relatively fast and almost linear because the section factor for the unprotected steel member is large. With protection (i.e. insulation of a 2mm-thickness intumescent coating [13-15]) of the CFRP and the steel, the speed of the temperature significantly slows down. In addition, the temperature of the CFRP increases faster than the steel because it has a smaller section factor compared to that of the steel. In addition, as the thickness of the anchorage is highest, the temperature of the anchorage system will be lower than that of CFRP, so the anchorage is not expected to fail before the failure of the CFRP and the steel column.

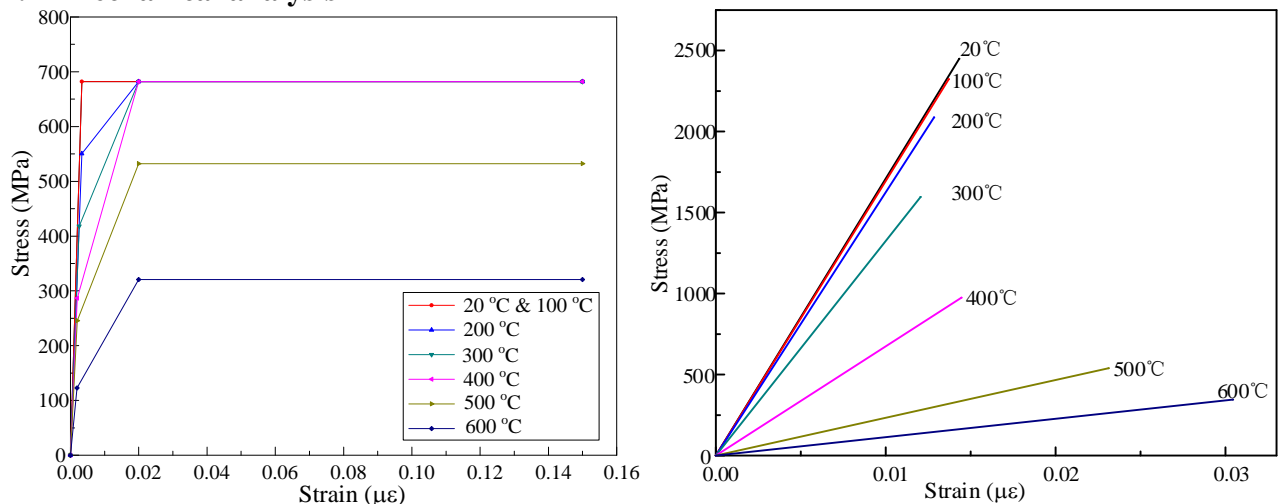## 4.2 Mechanical analysis

Fig. 7. a) Stress-strain curves of steel; b) Stress-strain curves of CFRP at different temperatures

A simplified model based on Eurocode 3 [9] is used for the material properties of the steel under high temperature; and the material properties of the CFRP under high temperature are based on Ref. [10], as shown in Fig. 7. The geometric model and the boundary conditions are the same as that in

Fig. 4. For the loading, firstly 50%P_d of the I140-U is applied. Then, the thermal boundary conditions are imposed as the time increases until the buckling happens.

Firstly, four specimens without protection are analyzed. Among them, I140-PS-0, I140-PS-60, I140-PS-270 have the same value of *a* but different values of *T* as 0 MPa, 60 MPa, 270 MPa. The result without protection is shown in Fig. 8. I140-PS series (i.e., I140-PS-0, I140-PS-60, I140-PS-270) have a 32% to 34% longer fire resistance time than that of I140-U. Fig. 9 shows the reason behind, that is, because the CFRP has a negative CTE, , the prestress value of CFRP increases with the increasing temperature at the beginning. After around 150s, due to the decrase of the CFRP stiffness under the high temperature and the large lateral defection of the steel column, the stresses of CFRP decrease, but they are both above zero when the buckling happens. It means CFRPs are tight and effective during the whole process, supporting the steel column and delaying the buckling. Comparing I140-PS-0, I140-PS-60 and I140-PS-270, which have almost the same fire resistance time, it is found that it is not necessary to apply a very large prestress value.

However, if the specimen is expected to resist under fire for a much longer time, it is necessary to protect the steel and the CFRP. The result with protection is shown in Fig. 10. It is seen that with a good protection I140-PS-0 has a fire resistance time as 86.25 minutes, which extends the time 25 minutes of I140-U 3.45 times.
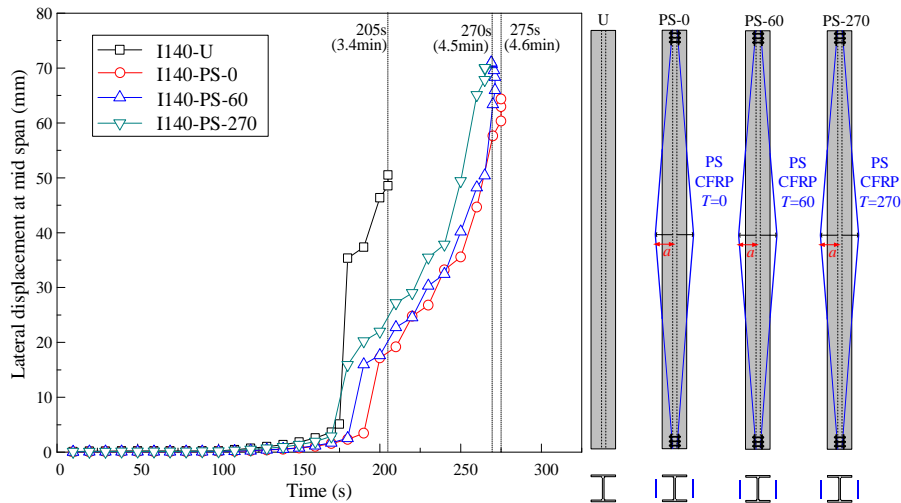
Fig. 8. Time and lateral displacement of the steel column at mid-span without protection
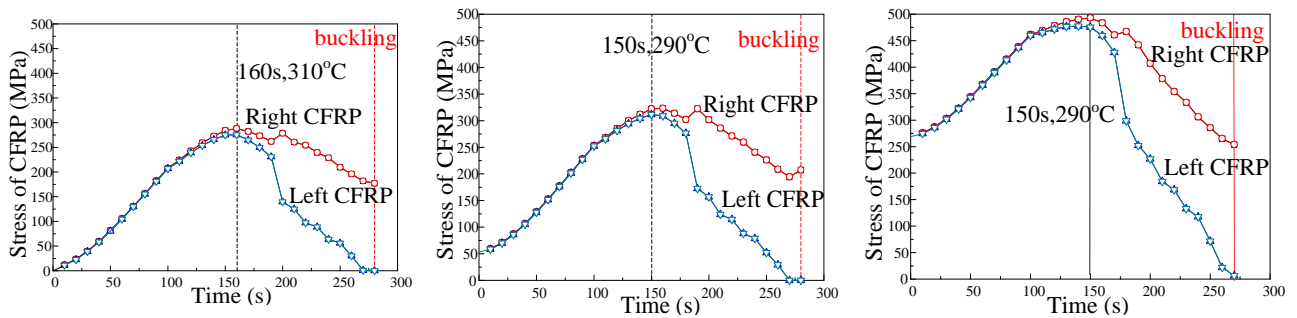
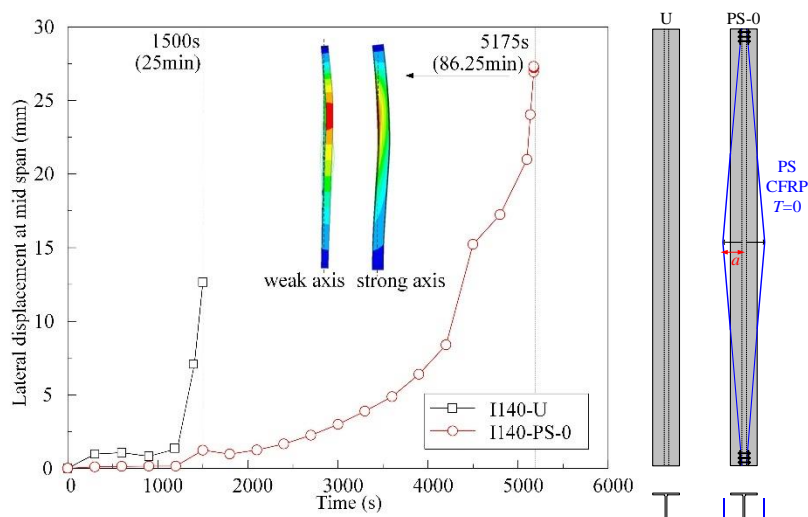*Fig. 9.* Relationship of CFRP stress and time without protection: a) I140-PS-0; b) I140-PS-60; c) I140-PS-270

Fig. 10. Time and lateral displacement of the steel column at mid-span with protection

5 CONCLUSIONS AND OUTLOOKS

The following conclusions can be drawn:

(1) At room temperature, test results show that the strong axis buckling resistance is about the weak axis, achieved by the PS CFRP strengthening. FEM results show that the strengthening system works safely when P_{xl}/P_y is above 0.50% and works efficiently when P_{xl}/P_y is above 2.97%.

(2) For design of the strengthend specimen with unprotected CFRP, a CFRP prestress value a little bit lower than the target value is recommned if the $P_{u,s}$ will not be decreased too much. This is because the stress of the unprotected CFRP increases fast in the beginning of the fire due to its negative CTE. While for the specimens with protected CFRP, it is recommned to choose the target CFRP prestress value becaue the insulation makes the CFRP prestress increasing not siginificant.

(3) If the specimen is expected to resist under fire for more than 30 minutes, the protection of the steel column and the CFRP is important. The protection not only helps to slow down the degradation of the steel and the CFRP, and the increasing of the CFRP prestress, but also helps to guarantee the effciency of the anchorage and to aviod the smoke problem of CFRP.

(4) The strengthening method is effective at room temperature and exposed to fire with a good protection of the steel and the CFRP.

In the future, instead of the CFRP, iron-based shape memory alloy (Fe-SMA), which has a good elevated temperature behavior, could be used for prestressed-strengthening of steel structures under fire. In addtion, the application of the coating on the thin PS CFRP needs further studies.

ACKNOWLEDGMENT

REFERENCES

[1]   Chu K., Berge S. (1963). *Analysis and design of struts with tension ties*. J Struct Div 89(1), pp 127-164.

[2]   Wadee M., Gardner L., Hunt T. (2013). *Buckling mode interaction in prestressed stayed columns*. Proc Inst Civil Eng-Struct Build 166(8), pp 403-412.

[3]   Saito D., Wadee M. (2008). *Post-buckling behaviour of prestressed steel stayed columns*. Eng Struct 30(5), pp 1224-1239.

[4] Peng F, Lili H. *Steel columns strengthened/reinforced by prestressed CFRP strips: concepts and behaviors under axial compressive loads*. Composite structures (to be published).

[5] Ghafoori E., Motavalli M. (2015). *Innovative CFRP-Prestressing System for Strengthening Metallic Structures*. Journal of Composites for Construction 19(6), pp 04015006.

[6]   Ghafoori E., Motavalli M. (2015). *Lateral-torsional buckling of steel I-beams retrofitted by bonded and un-bonded CFRP laminates with different prestress levels: experimental and numerical study*. Construction and Building Materials 76, pp 194–206.

[7] EN 1993-1-2 (2005): Eurocode 3: Design of steel structures-Part 1-1:General rules and rules for buildings.

[8]   ANSYS Inc., 2017b. ANSYS Mechanical Documentation - Release 18.2.

[9] EN 1993-1-2 (2005): Eurocode 3: Design of steel structures-Part 1-2:General rules-Structural fire design.

[10] Bisby L. (2003). *Fire behaviour of fibre-reinforced polymer (FRP) reinforced or confined concrete*. Queen's university. Doctor thesis.

[11] Kalogiannakis G., Hemelrijck D. (2003). *Numerical study on the nonlinear effects of heat diffusion in composites and its potential in nondestructive testing*. Review of Scientific Instruments 74(1), pp 462-464.

[12] Mallick P.(1988). *Fibre-Reinforced Composites: Materials, Manufacturing, and Design*. Marcel Dekker Inc., New York, NY.

[13] Yew, M. C., Sulong, N. R. (2012). *Fire-resistive performance of intumescent flame-retardant coatings for steel*. Materials & Design 34, pp 719-724.

[14] Jimenez, M., Duquesne, S., Bourbigot, S. (2006). *Characterization of the performance of an intumescent fire protective coating*. Surface and coatings Technology 201(3-4), pp 979-987.

[15] Raveglia, E. (2006). *Fire resistance of structural member protected by intumescent surface system*. 6th International PhD Symposium in Civil Engineering, 120, pp 120-121.

EFFECT OF PROBABILISTIC STRENGTH RETENTION FACTORS FOR STEEL AND CONCRETE ON STRUCTURAL RELIABILITY OF COLUMNS IN FIRE

Ramla Qureshi[1], Shuna Ni[2], Negar Elhami Khorasani[1], Ruben Van Coile[3], Danny Hopkin[4], Thomas Gernay[2]

[1] University at Buffalo, NY USA.
[2] Johns Hopkins University, Baltimore, MD USA.
[3] Ghent University, Belgium.
[4] The University of Sheffield, UK.

ABSTRACT

With the advent of performance based design within the domain of structural fire safety, there is a need for an increased level of confidence in properties of construction materials. As test data depict a significant scatter in temperature dependent material strengths of steel and concrete, systematic quantification of this variability is important for application within performance based fire engineering. The objective of this research is to examine different stochastic models to quantify uncertainty in steel and concrete strengths at elevated temperature. Based upon a collection of experimental data from literature, different probabilistic models are proposed for the retention factors of steel yield strength and concrete compressive strength, which are then compared based on application to the structural fire performance of columns under fire. This research improves understanding of effects of model choice for material uncertainties on the structural fire response.

1   INTRODUCTION

When designing structures to resist high temperature loads, it is important for structural engineers to capture the inherent uncertainty in properties exhibited by construction materials when exposed to heat. Both steel and concrete have been experimentally observed to show a dispersal in the value of their respective structural strengths, both at room temperature (commonly taken to be at 20ºC), but most significantly at elevated temperatures. This scatter in temperature dependent strength values can induce unexpected values of critical temperature, time to failure, or maximum capacities, affecting structural reliability under fire hazards. The structural fire engineering community is now increasingly adopting the concepts of risk and reliability to support performance based design approaches. These concepts are central to the realization of complex buildings, where reliance on precedent is insufficient, and an adequate level of safety must be explicitly demonstrated. However, probabilistic evaluation of structures in fire requires the availability of well-established sets of material models to capture the above-mentioned uncertainty in inputs over a range of temperatures. These models are currently missing from design practices.

In this study, different probabilistic material models are presented for the yield strength of steel and compressive strength of concrete in a manner that: a) captures the effect of data scatter at different values of temperature, and b) is efficiently applicable within finite element computations. A step-wise approach is taken where first the sources of data variability are characterized into probabilistic functions, and then the structural response is analyzed in a stochastic manner, including uncertainty in strength retention factors to calculate distributions of failure time or temperature. For this purpose, data collection included experimentally obtained values from numerous different elevated temperature material tests reported by researchers over the past few decades. This is further explained in the subsequent section. These datasets cover a temperature range of 20°C to 1030°C for steel and 17°C to 864°C for concrete. The datasets are grouped at different temperature intervals in order to conduct various statistical analyses to investigate 'goodness of fit' for different distribution functions, such as the lognormal distribution, etc. Alternatively, continuous probabilistic functions using a Bayesian-based formulation are fit to these datasets as well. Then, using the developed probabilistic models, different case studies are conducted

where the fire performance of columns are analyzed using Monte Carlo simulations. For the steel case study, failure temperature is evaluated using the provisions in Eurocode 3 (or EC3) for column buckling at high temperature [1]. For the concrete case study, structural fire performance of a reinforced concrete (RC) column is investigated through finite element modeling of the thermal-mechanical response. The continuity in reliability appraisals during transition from normal to elevated temperature design is also discussed.

2   HIGH TEMPERATURE TEST DATA FOR STEEL AND CONCRETE

Within civil engineering literature, the yield strength of steel is commonly reported as that defined by the 0.2% strain offset method, denoted as F_y. To facilitate modeling of material strength functions, the retained strength at any particular temperature, T is normalized with respect to the value measured at ambient conditions and presented as a dimensionless retention factor, $k_{y,T}$ However, for the purpose of structural design under fire, the EC3 high temperature steel material model reports retention factors for yield strength calculated for 2% strain, represented within this paper as $k_{y,\,2\%,T}$. Test data pertaining to both these definitions has been included in this research. A total of 764 experimental data points for $k_{y,T}$ and 387 data points for $k_{y,\,2\%,T}$ were obtained from a 2011 study on various different types of standardized steel elements conducted by the National Institute of Standards and Technology (NIST) [2]. This test data is plotted in *Fig. 1a* and *1b*, along with the EC3 steel material model for elevated temperatures. It is noteworthy that the retained yield strength at strain equal to 2% has been normalized by the room-temperature value of 0.2% offset yield strength, which reflects the effect of strain hardening that would prevail at lower temperatures.

Concrete, on the other hand, is a highly versatile construction material that can be classified based on aggregate type and characteristic strength in compression. For the purposes of this study, variability in concrete compressive strength under high temperatures is assessed from test data limited to normal strength concrete, with siliceous aggregate. Note that here normal strength concrete is categorized as that having value of characteristic compressive strength less than 50 MPa. A total of 242 data points have been included in this study from 24 different tests [3-11]. The compressive strength retention factor at elevated temperature for concrete, $k_{c,T}$ was defined as the measured compressive strength of concrete at elevated temperature, $f_{c,T}$ divided by the mean value of measured strength at ambient, $f_{cm,20}$. High strength concrete, and concretes made with calcareous aggregate are also widely used in the construction industry, but variations in their temperature dependent mechanical properties are a subject of later research.

2.1 Variability at room temperature vs. elevated temperatures

Spread in test data for the 0.2% offset steel F_y can be observed as fairly even around unity for $k_{y,T}$ at 20°C. The variability at ambient temperature for structural reliability has been previously established and is retained as such within this research, assuming a lognormal distribution with the mean as the characteristic value plus two standard deviations ($F_{ym,20}=F_{yk,20}+2\sigma$) and coefficient of variation of 0.07 [12]. For $k_{y,\,2\%,T}$, there is a significant scatter in the dataset even at 20°C accounting for strain hardening at lower temperature. The variability at ambient temperature is therefore explicitly reflected within the dataset. It can be seen from *Fig. 1* and *Fig. 3* that strength retention factors for both 0.2% and 2% offset models, $k_{y,T}$ and $k_{y,\,2\%,T}$ show similar trends at elevated temperatures, as the effect of strain hardening starts to disappear at temperatures above 500°C.

For siliceous concrete, there is a wide variation in data depicting the measured room temperature compressive strengths ($f_{c,20}$ ranging from 25 MPa to 55 MPa), and also for different concrete mixes, curing methods, etc. The variability at ambient temperature can be defined as a lognormal distribution with mean as the characteristic value at ambient plus two standard

deviations ($f_{cm,20}=f_{ck,20}+2\sigma$) and coefficient of variation in a range from 0.05 to 0.18, depending on the production procedure [12].

2.2 Data Grouping

In order to efficiently post-process raw test data into stochastic material models, it is necessary to capture variations at different values of temperature. Therefore, available data was discretized into subgroups at temperature intervals of 50°C, and data points within the range of ±10°C from specified temperature value were included in each group. Any particular dataset thus grouped was discarded if the total number of points in the dataset were less than or equal to 5. In this manner, 20 temperature groups for retention factors for $k_{y,T}$ (ranging from 20°C to 1030°C), and 16 groups for $k_{y,2\%,T}$ (from 20°C to 800°C) were respectively defined. Similarly, 10 data temperature groups were created from test data available for siliceous concrete between the range of 20°C to 800°C.

3 PROBABILISTIC MODELING USING GROUPED DATA

Thirteen probability density functions were fit to the materials test data within the above-mentioned temperature groups. These included continuous functions such as the Beta44 (Beta function bounded by 3 × standard deviation), Gamma, Normal, Lognormal, Logistic, Loglogistic, Inverse Gaussian, t Location-scale and the Extreme Value functions. Other distributions included the Nakagami, Rician, Bimbaum-Saunders, and the two-parameter Weibull probability distribution function. These distributions were compared temperature by temperature with quantitative methods and the final selection was made based on best model fit and the ease of application in analyses.

3.1 Selection of optimal distribution functions

The corrected Akaike information criterion (AICc) was used to get an unbiased estimate of 'goodness of fit' for the considered candidate distributions. This method compares the above-mentioned thirteen distributions and provides an estimate of each function's quality relative to the others. The distribution function with the lowest mean AICc value represented the greatest model quality [13]. For the datasets considered in this research, the Beta distribution for $k_{c,T}$, Gamma for $k_{y,T}$, and the Rician distribution for $k_{y,2\%,T}$ gave the lowest mean value across the different temperature groups of the AICc. However, a lack of closed form formulation for the cumulative distribution function of each of these leads to complex computational processes. Keeping in mind optimal utility and application during stochastic evaluation of structural response, the lognormal function was selected for both steel models representing $k_{y,T}$ and $k_{y,2\%,T}$, and the Weibull function was selected to represent the concrete dataset, respectively. The mean AICc values for these selected distributions are within 1% of the lowest mean value of the AICcs.

3.2 Statistical models

The parameters for the lognormal distribution were estimated for each temperature group individually, and subsequently generalized by fitting a regression curve. The final fitted equations for input parameters of the lognormal distribution for $k_{y,T}$ are:

$$\mu_{ln}(T) = -1.45 \times 10^{-9} \times T^3 - 1.78 \times 10^{-6} \times T^2 - 2.5 \times 10^{-5} \times T + 1.19 \times 10^{-2} \qquad (1)$$

$$\sigma_{ln}(T) = 1.895 \times 10^{-7} \times T^2 + 1.15 \times 10^{-4} \times T + 5.62 \times 10^{-2} \qquad (2)$$

And for $k_{y,2\%,T}$, the lognormal fit gives the following equations:

$$\mu_{ln}(T) = -6.89 \times 10^{-9} \times T^3 + 1.84 \times 10^{-6} \times T^2 - 8.39 \times 10^{-5} \times T + 1.48 \times 10^{-1} \qquad (3)$$

$$\sigma_{ln}(T) = 2.41 \times 10^{-7} \times T^2 + 1.07 \times 10^{-4} \times T + 9.77 \times 10^{-2} \qquad (4)$$

where μ, σ are temperature dependent parameters of the lognormal distribution.

It should be noted here that for $k_{y,T}$ data, a mean value of 1.0 and coefficient of variation equal to 0.07 were manually imposed on the model for $T = 20°C$. *Fig. 1* shows the lognormal models in comparison with EC3 models and measured data. The EC3 model in *Fig. 1a* is based on 0.2% offset

strain when constructing the full stress-strain curve using EC3 guidelines, while the EC3 model in *Fig. 1b* shows retention factors prescribed by the code for yield strength at 2% strain.

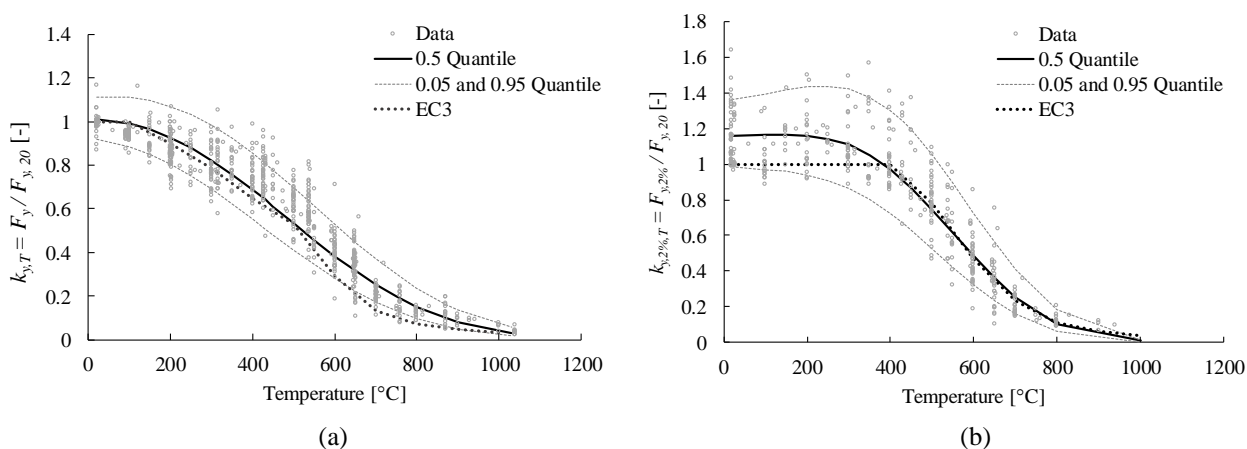(a)   (b)

Fig. 1 Strength retention factors vs. temperature, based on lognormal fit for a) $k_{y,T}$, and b) $k_{y,2\%,T}$

For siliceous concrete, in order to maintain consistency within the probabilistic model at ambient and elevated temperatures, a Weibull distribution is fitted to approximately match the average lognormal distribution with mean of 1.0 and coefficient of variation ranging from 0.05 to 0.18. This Weibull distribution data point is included in the regression as an evaluation at room temperature, i.e. $k_{c,20}$. Final fitted equations for the Weibull distribution parameters are as follows:

$$\lambda(T) = -8.434 \times 10^{-7} \times T^2 - 4.089 \times 10^{-4} \times T + 1.059 \tag{5}$$

$$k(T) = \frac{9.735}{0.923 + 1.978 \times 10^{-3} \times T} \tag{6}$$

where λ, k are the scale and shape parameters for the Weibull distribution.

Fig. 2 shows the 0.5 quantile and one standard deviation envelope for $k_{c,T}$ calculated per the Weibull distribution and compared to the values provided by the Eurocode 2 (EC2) [14].
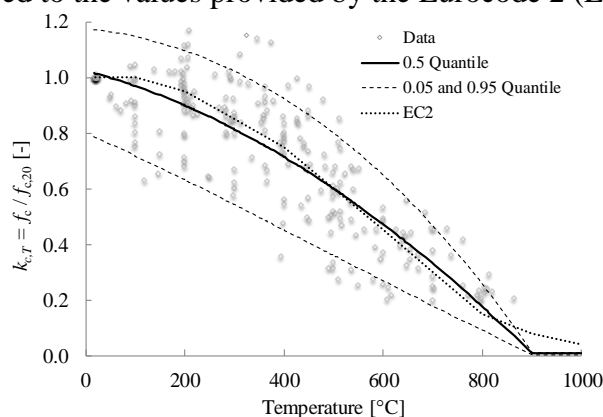
Fig. 2 Strength retention factors vs. temperature for $k_{c,T}$ based on the Weibull distribution

4   PROBABILISTIC MODELING USING CONTINUOUS LOGISTIC FUNCTION

Further to the above-mentioned probabilistic approaches, continuous logistic functions are also considered for the stochastic models for steel and concrete retention strength. For steel data, a Bayesian approach with the EC3 steel model as a deterministic basis is applied to the $k_{y,2\%,T}$ data to arrive at a logistic distribution, first presented in [15]. The 0.5 quantile value of $k_{y,2\%,T}$ is presented in *Fig. 3a* and is compared with the EC3 retention factors. The formulation is given in *Eq. (7)*:

$$k_{y,2\%,T} = 1.7 \times \frac{\exp\left[logit(\hat{k}^*_{y,2\%,T})+0.412-0.81\times10^{-3}\times T+0.58\times10^{-6}\times T^{1.9}+0.43\times\varepsilon\right]}{\exp\left[logit(\hat{k}^*_{y,2\%,T})+0.412-0.81\times10^{-3}\times T+0.58\times10^{-6}\times T^{1.9}+0.43\times\varepsilon\right]+1} \tag{7}$$

where $logit(\hat{k}^*_{y,2\%,T})$ is equal to $\ln\left(\frac{\hat{k}^*_{y,2\%,T}}{1-\hat{k}^*_{y,2\%,T}}\right)$,

$\hat{k}^*_{y,2\%,T}$ is equal to $\frac{\hat{k}_{y,2\%,T}+10^{-6}}{1.7}$,

$\hat{k}_{y,2\%,T}$ is the temperature-specific retention factor as provided by the EC3, and

ε is the standard normal distribution.

Taking a similar approach, a continuous logistic function (with no deterministic base) was fitted to the siliceous concrete data set for $k_{c,T}$. *Eq. (8)* presents the probabilistic model where the modeling error is calibrated as $0.45 \times \varepsilon$, and ε represents the standard normal distribution.

$$k_{c,T} = 1.4 \times \frac{exp\left[0.8892-0.6319\times10^{-3}\times T-3.295\times10^{-6}\times T^2+0.45\times\varepsilon\right]}{exp\left[0.8892-0.6319\times10^{-3}\times T-3.295\times10^{-6}\times T^2+0.45\times\varepsilon\right]+1} \tag{8}$$

Strength retention factors calculated using the above approach for siliceous concrete are presented in *Fig. 3b* below.

(a)   (b)
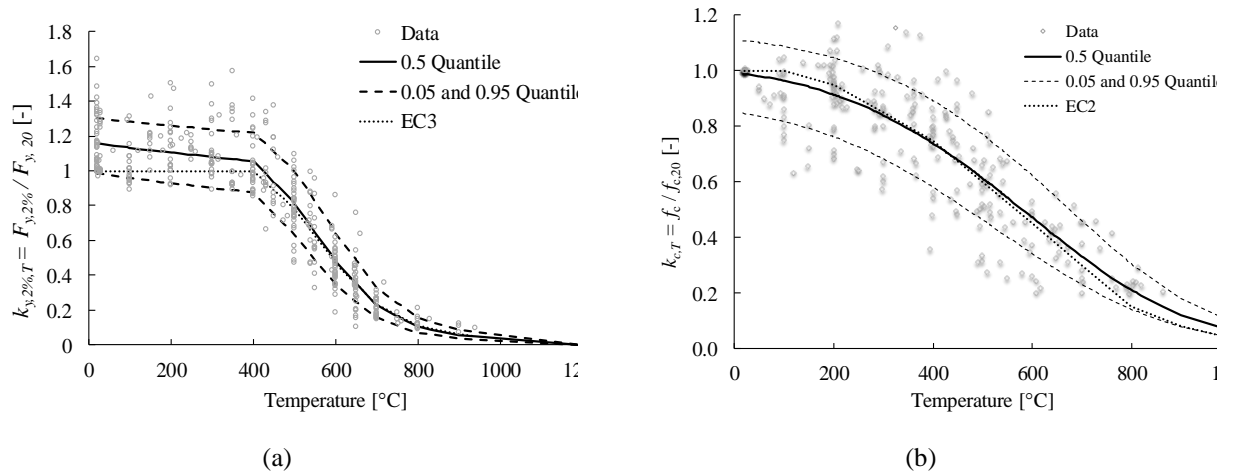
Fig. 3 Strength retention factors vs. temperature based on a continuous logistic fit for a) steel $k_{y,2\%,T}$, and b) siliceous concrete $k_{c,T}$

5 CASE STUDIES

Next, the probabilistic thermo-structural response of fire-exposed columns was evaluated using the established stochastic models for steel and concrete retention factors. A failure limit state was pre-defined for each of the steel and concrete columns considered. Then, Monte Carlo simulations were run to evaluate the reliability of these columns under elevated temperatures, and a probability of failure, p_f was determined for 2000 simulations for the steel column and 5000 simulations for the reinforced concrete column.

5.1 Steel column from One Meridian Plaza

For steel, the failure limit state function is considered as buckling of the column at high temperature. The temperature at failure is obtained as that where the value of applied thermal loads and service compression loads becomes equal to the column capacity i.e., the utility ratio equals to unity. An unprotected steel perimeter column from the One Meridian Plaza with a wide flange column cross section W14×311 is considered [16]. A pin connection is considered at column ends, and the total effective length of the column is 3.56 m. An applied load of 0.25 $F_{yk,20}A_s$ (A_s is the cross-sectional area of steel column) is assumed. Here, the characteristic yield strength of steel, $F_{yk,20}$ is taken as 250 MPa, making the mean $F_{ym,20}$ equal to 290.7 MPa. The EC3 formulation is used to calculate the temperature-specific column capacity. A total of 2000 Monte Carlo simulations are run for each of the lognormal functions for $k_{y,T}$ and $k_{y,2\%,T}$ respectively, and also for the EC3-based continuous logistic function for $k_{y,2\%,T}$. Fragility curves for the steel column failure temperature are developed for each of the candidate models, as presented in *Fig. 4*.

5.2 Reinforced concrete column from a five-story office building

For evaluating a probability of failure for a siliceous concrete RC member, a column section with cross-sectional dimensions 450 mm×450 mm was considered. This column is extracted from a 5-story office building, and has a total considered length equal to 3.87 m. The column cross-section is reinforced with 12 longitudinal rebars of 25.2 mm diameter (M25). The compressive load value applied to the column is taken equal to 50% $f_{ck,20}A_c$ (A_c is the area of the column section), and thermal load is provided by applying the ASTM E119 fire exposure [17] on all four sides of the column. The above-mentioned Weibull and logistic distributions are used to capture the uncertainty within the concrete strength retention factor as is required to assess column fragility. The finite element software SAFIR [18] is used to perform thermo-mechanical analysis of the column and quantify the failure time of the column when it loses its load-bearing capacity under fire. This is the load-bearing (mechanical) fire resistance, and is considered as the failure limit state function for the RC column in this study. In total, 5000 Monte Carlo simulations are run for each of the probabilistic models. The percentage failure obtained is depicted in *Fig. 5*.
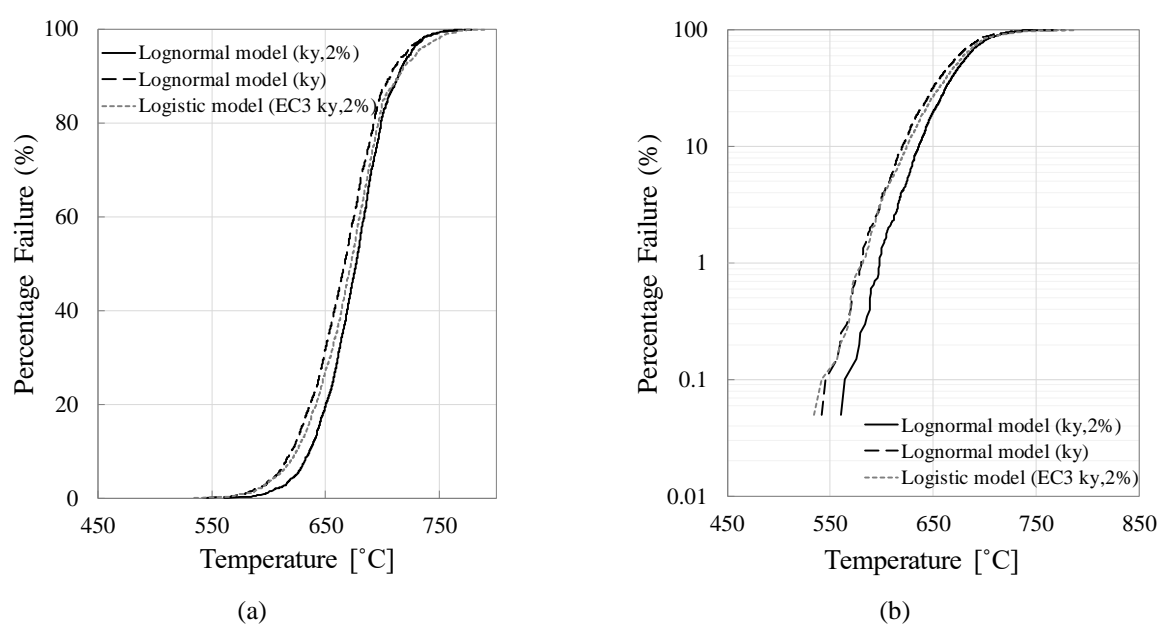

(a)   (b)

Fig. 4 Fragility curves for steel column with a) different considered models for retention factor b) logarithmic axis percentage failure
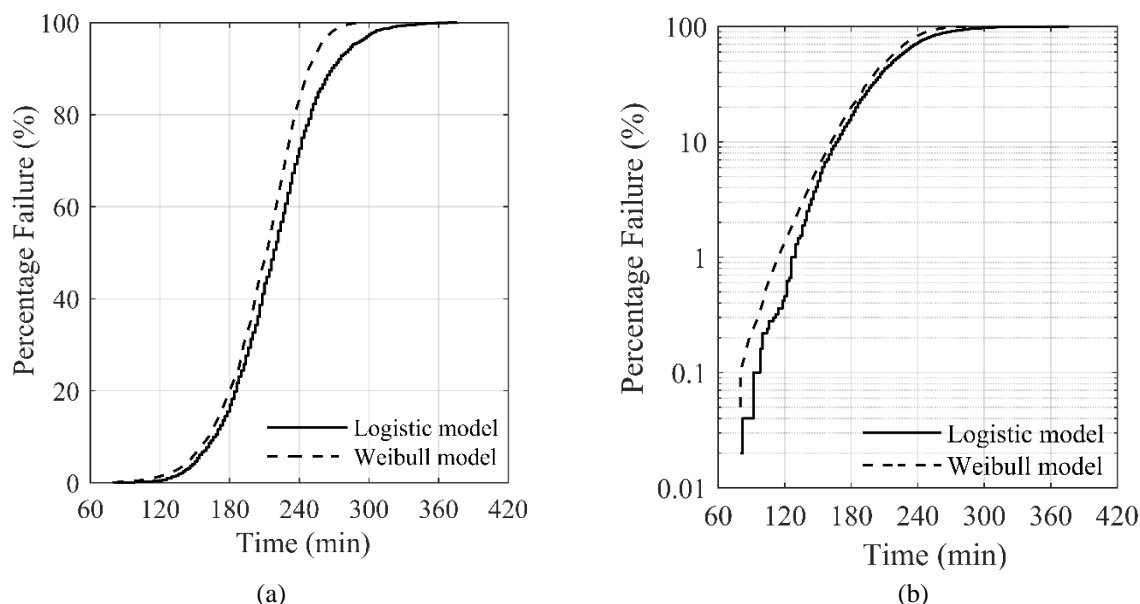

(a)　　　　　　　　　　　　　　　　(b)

Fig. 5 Fragility curves for RC column with a) different considered models for retention factor b) logarithmic axis percentage failure

6 DISCUSSION AND CONCLUSIONS

The results of case studies in *Fig. 4* and *Fig. 5* show minor differences in fragilities obtained for the failure temperature and time of steel and RC columns when uncertainty in strength retention factors are captured using different modeling approaches. If the target probability of failure is considered within 1% to 10%, the maximum difference in failure temperature of steel is 17 °C and the maximum difference in the time to failure of concrete column is approximately 16 minutes. In case of steel, it should be noted that the failure temperature for the column under study is above 550°C, for which the effect of strain hardening (2% versus 0.2% offset models) is not significant.

It can be argued that, for the case studies considered in this study, the effect of model choice on the results at elevated temperatures is negligible. In order to quantify uncertainty in strength retention factors of steel and concrete at elevated temperatures, two approaches were considered. First, probabilistic models based on distribution fits to groups of data at different temperature were investigated. This approach led to selection of lognormal and Weibull distributions for steel and concrete, respectively. The second approach applied a continuous fit to the data using a logistic function that included the model error. In both approaches, efficiency and ease of application of models in finite element computation process were considered. This study will be expanded in future to investigate the effect of model choice on a number of case studies, including models for calcareous concrete, to generalize the results.

REFERENCES

[1]　　CEN: European Committee for Standardization (2005). "Eurocode 3: Design of steel structures. General rules. Structural fire design. Standard EN 1993-1-2."

[2]　　Luecke W. E., Banovic S. W., and McColskey J. D., "High-temperature tensile constitutive data and models for structural steels in fire," 2011.

[3]　　Malhotra H. (1956). "The effect of temperature on the compressive strength of concrete," *Magazine of concrete research,* vol. 8, pp. 85-94.

[4]   Abrams M. S. (1971). "Compressive strength of concrete at temperatures to 1600F," *Special Publication,* vol. 25, pp. 33-58.

[5]   Marechal J. (1972). "Variations in the modulus of elasticity and Poisson's ratio with temperature," *Special Publication,* vol. 34, pp. 495-504.

[6]   Anderberg Y. and Thelandersson S. (1976). "Stress and deformation characteristics of concrete at high temperatures. 2. Experimental investigation and material behaviour model," *Bulletin of Division of Structural Mechanics and Concrete Construction, Bulletin 54*.

[7]   Furumura F., Abe T., and Shinohara Y. (1995). "Mechanical properties of high strength concrete at high temperatures," in *Proceedings of the Fourth Weimar Workshop on High Performance Concrete: Material Properties and Design*, 1995.

[8]   Khoury G. (1996). "Performance of Heated Concrete—Mechanical Properties," *Contract NUC/56/3604A with Nuclear Installations Inspectorate, Imperial College, London*.

[9]   Bali A., Boutemeur R., and Purkiss J. (2005). "Strength of Concrete at Elevated Temperatures," in *Application of Codes, Design and Regulations: Proceedings of the International Conference held at the University of Dundee, Scotland, UK on 5–7 July 2005*, 2005, pp. 427-434.

[10]   Fu Y., Wong Y., Poon C., and Tang C. (2005). "Stress–strain behaviour of high-strength concrete at elevated temperatures," *Magazine of Concrete Research,* vol. 57, pp. 535-544.

[11]   Kakae N., Miyamoto K., Momma T., Sawada S., Kumagai H., Ohga Y.*, et al.* (2017). "Physical and thermal properties of concrete subjected to high temperature," *Journal of advanced concrete technology,* vol. 15, pp. 190-212.

[12]   Holický M. and Sýkora M. (2010). "Stochastic models in analysis of structural reliability," in *Proceedings of the international symposium on stochastic models in reliability engineering, life sciences and operation management, Beer Sheva, Israel*, 2010.

[13]   Hurvich C. M. and Tsai C. L. (1993). "A corrected Akaike information criterion for vector autoregressive model selection," *Journal of time series analysis,* vol. 14, pp. 271-279.

[14]   European Committee for Standardization (2004). "Eurocode 2: Design of concrete structures—Part 1-1: General rules and rules for buildings," *Brussels, Belgium*.

[15]   Elhami Khorasani N., Gardoni P., and Garlock M. (2015). "Probabilistic fire analysis: material models and evaluation of steel structural members," *Journal of Structural Engineering,* vol. 141, p. 04015050.

[16]   Routley J. G., Jennings C., and Chubb M. (1991). "Highrise Office Building Fire, One Meridian Plaza, Philadelphia, Pennsylvania," *United States Fire Administration, Washington, DC, Technical Report No. USFA-TR-049*.

[17]   ASTM (2012). "Standard test methods for fire tests of building construction and materials," 2012.

[18]   Franssen J.-M. and Gernay T. (2017). "Modeling structures in fire with SAFIR®: Theoretical background and capabilities," *Journal of Structural Fire Engineering,* vol. 8, pp. 300-323.

A SIMPLIFIED MODEL TO EVALUATE THE THERMAL-INDUCED STRESSES IN STEEL STATICALLY INDETERMINATE STRUCTURES SUBJECTED TO FIRE

Francesco Corradino[1], Donatella de Silva[2], Emidio Nigro[2]

[1] Italian Air Force, Rome, Italy

[2] University of Naples Federico II, Naples, Italy*

ABSTRACT

Using modern software, there is the possibility of evaluating the structural response in fire conditions, conducting advanced thermo-mechanical analyses and taking into account the thermal-induced indirect actions that may arise in the event of fire. These effects may affect the internal stresses of the structural members compared to the normal temperature conditions. Sometimes these advanced analyses are complicated arising significant computational burden, so a simplified method aimed to simulate or interpret the interaction between the adjacent members of the structure and to evaluate such thermal-induced stresses in case of fire, would be useful. In order to perform simplified but realistic analyses on steel members, in this paper, a non-linear procedure, based on analytical expressions, is proposed.

1   INTRODUCTION

The evaluation of the mechanical response of structures under fire requires to consider the complex mechanical and geometric non-linear behaviour in the presence of high temperatures.

One of the main aspects to analyse is the mechanical non-linearity of the materials; indeed, as temperatures increase, the strength and stiffness of the structural materials tend to degrade. In order to take into account this degradation for steel, Eurocode 3 [1] provides the values of the reduction factors of stiffness $k_{E,\vartheta}$ and yield strength $k_{y,\vartheta}$ as a function of temperature. At the same time, the increase of temperatures generates thermal expansion and curvature in the structural members, that, if prevented by the restraints, can cause additional stresses and internal forces. However, these stresses are directly related to the mechanical properties of the materials, as they can't exceed the structure capacity. In addition, there is a direct link between the mechanical and geometric non-linearities, due to the second-order effects, which for example arise in beams due to the axial force induced by thermal expansion and the large displacements under fire. Based on experimental results on axially restrained steel beams under fire, a "new" collapse mechanism appeared and it was confirmed by mechanical simulations [2]: the catenary action. The structural large deflection behaviour, combined with high temperatures, can modify the structural scheme. Indeed, if the flexural stiffness of the beam tends to zero, the load is no longer absorbed by bending and the tensile stress balances the load. In this case, the structural collapse can occur if the tensile capacity is reached. Several researchers proposed simplified analysis method in order to take into account the catenary action in steel beams at elevated temperatures.

In the current scientific literature there are some simplified methods to evaluate the mechanical or geometric non-linearities of simple structures subject to fire; only few methods take into account both non-linearities. Wang et al. ([3],[4]) describe the results of a numerical investigation of the large deflection behaviour of steel beam, providing a discussion on practical implications of using catenary action in steel beams as a means of eliminating fire protection [2]. Usmani et al. ([7],[2]) present theoretical descriptions of the key phenomena that govern the behaviour of composite framed structures in fire.

Since the structural fire analyses can be very complex, the Eurocodes ([1],[8]) allow to decompose each structure into simpler substructures, making possible to carry out accurate structural analyses on remarkable static schemes, but in a quick use way.

In this paper the structural response of steel beams under fire is investigated and a simplified method is proposed, which allows to analyse the structural response of steel beam under fire, varying the load level and the restraint conditions. Although the proposed method is simple to apply, being based on some analytical expressions, it allows to take into account geometric and mechanical non-linearities and the real collapse mechanism such as the catenary action.

2 PROPOSED SIMPLYFIED METHOD

Applying a thermal action, the structure is deformed according to the temperatures in the cross-sections. Considering the beam of *Fig. 1*, restrained by translational and rotational end springs with stiffness k_t and k_r, which replace the stiffness of the members adjacent to the beam, these restraints counteract the imposed thermal action, generating additional stresses which can be evaluated using compatibility equations.
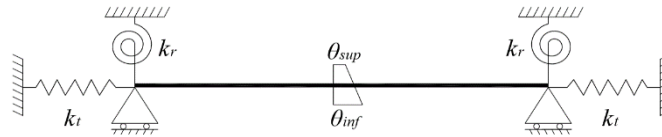
Fig. 1. Steel beam under non-uniform temperature distribution

The uniform component of the thermal path generates an axial compressive force on the beam, given by the following formula within the elastic behaviour:

$$N = \frac{E_\vartheta A\, \alpha\, \Delta\vartheta}{1 + 2\dfrac{E_\vartheta A}{k_t l}}$$

(1)

where:

E_ϑ is the average Young's modulus of the steel, degrading with temperature;

A   is the cross section's area;

α   is the coefficient of linear thermal expansion of the steel;

$\Delta\vartheta = \vartheta_m - 20°$, is the difference between the average temperature in the cross- section and the ambient temperature.

It results:

$k_t = \infty$ rigid restraint to translation: $N = E_\vartheta A\, \alpha\, \Delta\vartheta$

$k_t = 0$ absence of restraint to translation: $N = 0.$

Similarly the rotation end restraints oppose to the thermal curvature, generating an hogging bending moment on the beam, provided by the following formula within the elastic behaviour:

$$M = \frac{E_\vartheta I \chi_\vartheta}{1 + 2\dfrac{E_\vartheta I}{k_r l}} \qquad (2)$$

where:

- $\chi_\vartheta = \alpha \dfrac{\vartheta_{inf} - \vartheta_{sup}}{h}$ is the thermal curvature;

I is the second moment of area of the cross section.

It results:

$k_r = \infty$ rigid restraint to rotation: $M = E_\vartheta I \chi_\vartheta$;

$k_r = 0$ absence of restraint to rotation: $M = 0$.

However, these thermal-induced internal forces on the beam have to consider the non-linear mechanical properties of the materials, not exceeding their capacity. In the proposed method, a simplified elastic–plastic stress-strain relationship for steel at elevated temperatures is considered as shown in *Fig. 2*.
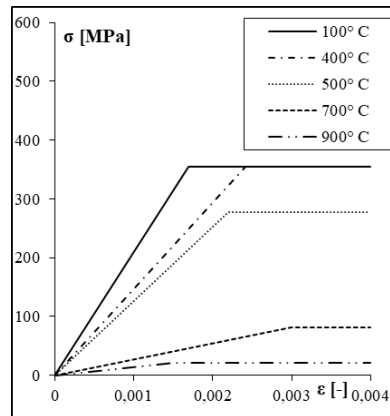
Fig. 2. Simplified elastic–plastic stress-strain relationship for steel at elevated temperatures.

2.1 Thermal analysis

In the proposed method, a generic fire curve may be considered and the steel beam is subjected to the adopted fire curve for an observation period T. Assuming $n = \dfrac{T}{\Delta t}$, the generic instant of time is:

$$t_i = i \cdot \Delta t \quad \text{with } i = 0, \ldots, n \qquad (3)$$

The beam cross-section is divided in "m" fibres and the j-th fiber is characterized by the following properties:

y_j : distance of the j-th fiber from the centroid of the cross-section [mm];

s_j : thickness of the j-th fiber [mm];

b_j : width of the j-th fiber [mm];

A_j : area of the j-th fiber [mm^2].

The thermal analysis provides the evaluation of the temperature $\vartheta_{i,j}$ of each fiber and, therefore, the Young's modulus and yield strength reduction factors $k_{E,\vartheta}$ and $k_{y,\vartheta}$ can be calculated, using the expressions proposed in EN1993-1-2 [1].

2.2 Simply supported beam (axially fixed at both ends)

It is considered first of all a simply supported steel beam (horizontal displacements prevented), subjected to a uniformly distributed load "q" and with. For each time step, the stress distribution in the midspan section can be calculated using the Navier's elastic formulation:

$$\sigma_{eli,j} = \frac{N_{i-1}}{A} + \frac{M_{i-1}}{I} y_j + \alpha\, E\left[\left(\vartheta_{m,i} - 20°\right) k_{E,\vartheta,i} - \left(\vartheta_{m,i-1} - 20°\right) k_{E,\vartheta,i-1}\right] \tag{4}$$

The stresses are limited to the yield strength $f_{y,\vartheta_{i,j}}$:

$$\begin{cases} \sigma_{i,j} = \min\left\{\sigma_{eli,j}; f_{y,\vartheta i,j}\right\} & \sigma_{eli,j} > 0 \\ \sigma_{i,j} = \max\left\{\sigma_{eli,j}; -f_{y,\vartheta i,j}\right\} & \sigma_{eli,j} < 0 \end{cases} \tag{5}$$

If the yield strength is exceeded in the j-th fiber, an imbalance between the applied stress state, which is elastic, and the reactive one, which is plastic, arises:

$$\Delta\sigma_{i,j} = \sigma_{eli,j} - f_{y,\vartheta i,j} \tag{6}$$

This unbalanced stress, integrated on all the yielded fibers, generates a plastic axial force and a bending moment, which are redistributed in the still elastic part of the section, characterized by area $A_{el,i}$, center of gravity $y_{Gel,i}$ and inertia $I_{el,i}$ variables with t_i:

$$\Delta N_{pl,i} = \sum_j \Delta\sigma_{Pi,j}\, A_{Pj} \tag{7}$$

$$\Delta M_{pl,i} = \sum_j \Delta\sigma_{Pi,j}\, A_{Pj}\, y_{Pj} \tag{8}$$

$$A_{el,i} = \sum_j A_{eli,j} \tag{9}$$

$$y_{Gel,i} = \frac{\sum_j A_{elj,i}\, y_{jel,i}}{\sum_j A_{elj,i}} \tag{10}$$

$$I_{el,i} = \sum_j \frac{b_{jel,i} h_{jel,i}^3}{12} + A_{jel,i} \left(y_{jel,i} - y_{Gel,i} \right)^2 \tag{11}$$

So, the actual stresses are:

$$\begin{cases} \sigma_{i,j} = f_{y,\vartheta i,j} & \text{if} & \sigma_{eli,j} > 0 & \text{and} & \sigma_{eli,j} > f_{y,\vartheta i,j} \\ \sigma_{i,j} = \sigma_{eli,j} + \Delta\sigma_{eli,j} & \text{if} & \sigma_{eli,j} > 0 & \text{and} & \sigma_{eli,j} < f_{y,\vartheta i,j} \end{cases} \tag{12}$$

$$\begin{cases} \sigma_{i,j} = -f_{y,\vartheta i,j} & \text{if} & \sigma_{eli,j} < 0 & \text{and} & \sigma_{eli,j} > -f_{y,\vartheta i,j} \\ \sigma_{i,j} = \sigma_{eli,j} + \Delta\sigma_{eli,j} & \text{if} & \sigma_{eli,j} < 0 & \text{and} & \sigma_{eli,j} < -f_{y,\vartheta i,j} \end{cases} \tag{13}$$

in which:

$$\Delta\sigma_{eli,j} = \frac{\Delta N_{pl,i}}{A_{el,i}} + \frac{\Delta M_{pl,i}}{I_{el,i}} \left(y_{jel,i} - y_{Gel,i} \right) \tag{14}$$

After evaluating the agent stress state, the axial force can be evaluated as follows:

$$N_i = \sum_j A_j \, \sigma_{i,j} \tag{15}$$

In order to take into account, the second-order effect, that can modify the bending moment, the midspan deflection at time t_i may be evaluated with the following expression

$$v_i = (v_{m,i} + v_{\vartheta,i} + v_{N,i}) \tag{16}$$

In eq. (16) the term $v_{m,i}$ is the deflection induced by the bending moment

$$v_{m,i} = \frac{5}{48} \chi_{mech,i} l^2 \tag{17}$$

and

- $$\chi_{mech,\,i} = \frac{\varepsilon_{i,sup} - \varepsilon_{i,inf}}{h} \qquad \text{is the mechanical curvature;} \tag{18}$$

- $$\varepsilon_{i,sup(inf)} = \frac{\sigma_{i,el,sup(inf)}}{E_{\vartheta,i,sup(inf)}} \qquad \text{is the mechanical strain.} \tag{19}$$

The term $v_{\vartheta,i}$ in (16) is the thermal deflection:

$$v_{\vartheta,i} = \frac{\chi_{\vartheta,i} \, l^2}{8} \tag{20}$$

being $\chi_{\square,i}$ the thermal curvature.

The term $v_{N,i}$ in (16) is the deflection induced by the second-order effects:

131

$$v_{N,i} = \frac{(N_i v_{i-1}) l^2}{8 E_{\vartheta,i} I} \tag{21}$$

The large deflections, combined with the high temperatures in the cross-sections, which leads to a significant decrease of the flexural stiffness, may involve the activation of the "catenary action". The structural scheme changes, passing from a beam to a cable configuration. In this case the failure is due to tension and not to bending. In order to evaluate the development of this effect, which arise in the presence of large displacements, a midspan deflection control is necessary. In the proposed method it is assumed that the catenary action happens when the following condition is verified:

$$n_i = \frac{v_i}{l} > \frac{1}{20} \tag{22}$$

The expressions (15) and (16) can be modified to take into account the catenary action:

$$N_i = \sum_j A_j \, \sigma_{i,j} - T_i \tag{23}$$

Considering the load ratio $\mu_0 = \frac{E_{fi,d}}{R_{fi,d,0}}$ in fire condition, we can write:

$$T_i = \frac{q l^2}{8 \, v_{i-1}} \sqrt{1 + 16 \, n_{i-1}^2} \tag{24}$$

$$v_i = \frac{q l^2}{8 \, T_i} \sqrt{1 + 16 \, n_{i-1}^2} \left(1 + \frac{1}{10} \frac{k_{E,\vartheta,i}}{2 - \mu_0} \right) \tag{25}$$

where:

  - T_i is the tension force in the catenary;
  - v_i is the midspan deflection.

The midspan bending moment can be evaluated, as the sum of the first- and the second-order bending moments, induced by the increase of both the axial force and the midspan deflection:

$$M_i = M^I + M^{II}_i = \frac{q l^2}{8} + N_i \, v_i \tag{26}$$

2.3 Double-fixed beam (axially and rotational fixed at both ends)

In this case the steel beam is axially and rotationally restrained at both ends. As in the previous case, the stress state is evaluated at the midspan section. However, also the effects of the rotational restraints to the thermal curvature have to be taken into account in this case. Therefore, the eq. (4) will be modified in the following expression, in which the last term takes into account the constraints effect:

$$\sigma_{eli,j} = \frac{N_{i-1}}{A} + \frac{M_{i-1}}{I} y_j + \alpha \, E \left[\left(\vartheta_{m,i} - 20° \right) k_{E,\vartheta,i} - \left(\vartheta_{m,i-1} - 20° \right) k_{E,\vartheta,i-1} \right] + \chi_\vartheta E_{\vartheta,i} \, y_j \tag{27}$$

The stress distribution and the axial force are evaluated following the steps from (5) to (15) of the previous paragraph.

The midspan deflection is evaluated with the following expression:

$$v_i = (v_{m,i} + v_{N,i})$$ (28)

In the Eq. (28) the term $v_{m,i}$ is the deflection induced by the bending moment, where the term $\chi_{mech,i}$ is evaluable with Eq. (18):

$$v_{m,i} = \frac{3}{48} \chi_{mech,i} l^2$$ (29)

$$v_{N,i} = \frac{N_i v_{i-1} l^2}{4 E_{\vartheta,i} I}$$ (30)

Therefore, the midspan bending moment is evaluated as follows:

$$M_i \left(\frac{1}{2}\right) = M^I + M^{II}_i + M_{\vartheta,i} = \frac{ql^2}{24} + N_i v_i - \chi_\vartheta E_\vartheta I$$ (31)

Because of the statically indeterminate structural scheme, if the midspan bending moment is equal to the resistant one, the structure does not collapse. It determines a midspan plastic hinge which leads to a bending moment redistribution on the ends of the beam.

The structural scheme can be analysed as a couple of cantilever connected to each other by a plastic hinge. Definite $t_i = t_{i*}$ the time when the midspan bending moment equals the resistant one, the midspan deflection is evaluated with the following equation:

$$v_i = v_{i*} + \Delta v_i$$ (32)

in which Δv_i is the deflection's increase due to the structural scheme's modification:

$$\Delta v_i = \frac{ql^4}{64 E I}\left(\frac{1}{k_{E,\vartheta,i}} - \frac{1}{k_{E,\vartheta,i*}}\right)$$ (33)

The end section's stress state is estimated with the following equation, where the already calculated value of N_i (Eq. (15)) is used:

$$\sigma_{eli,j} = \frac{N_i}{A} + \frac{M_0}{I} y_j + \chi_\vartheta E_{\vartheta,i} y_j$$ (34)

We then proceed to the stress redistribution phase, following the steps from (5) to (14).

The end section bending moment is then evaluated as the sum of each fiber's contribution:

$$M_i = \sum_j A_j \sigma_{i,j} y_j$$ (35)

2.4 Validation against FEM numerical simulation

With the aim of validate the simplified proposed method, the comparison between the results obtained applying the simplified method and the results provided by a FEM model carried out using SAFIR 2016 [9] is reported in the following, with reference to a 6m long IPE300 steel beam with

different boundary conditions and subjected to standard fire ISO834 curve. *Fig. 3* and *Fig. 4* show the curves of axial force, bending moments and midspan deflection vs fire exposure time, reported varying the load ratio μ_0: the results obtained applying the proposed method are generally in a good agreement with the FEM ones, both in terms of failure time and type of attained collapse. In particular, in the simply supported beam, the collapse occurs due to tensile force. The compressive axial force (see *Fig. 3*a)) increases up to a maximum value, according to the applied load; at the same time, the midspan bending moment (see *Fig. 3*b)) increases, due to the second-order effects. However, the bending moment remains lower than the bending capacity and tends to zero as a result of development of the catenary action, which occurs in large displacements. The trend of the midspan deflection (see Fig. 3c)) follows three distinct phases. In the first phase, the displacements are elastic because the steel has not yielded yet; after that the beam plasticization occurs, with a considerable increase in deformability; the last phase represents the midspan deflection trend due to the catenary action.
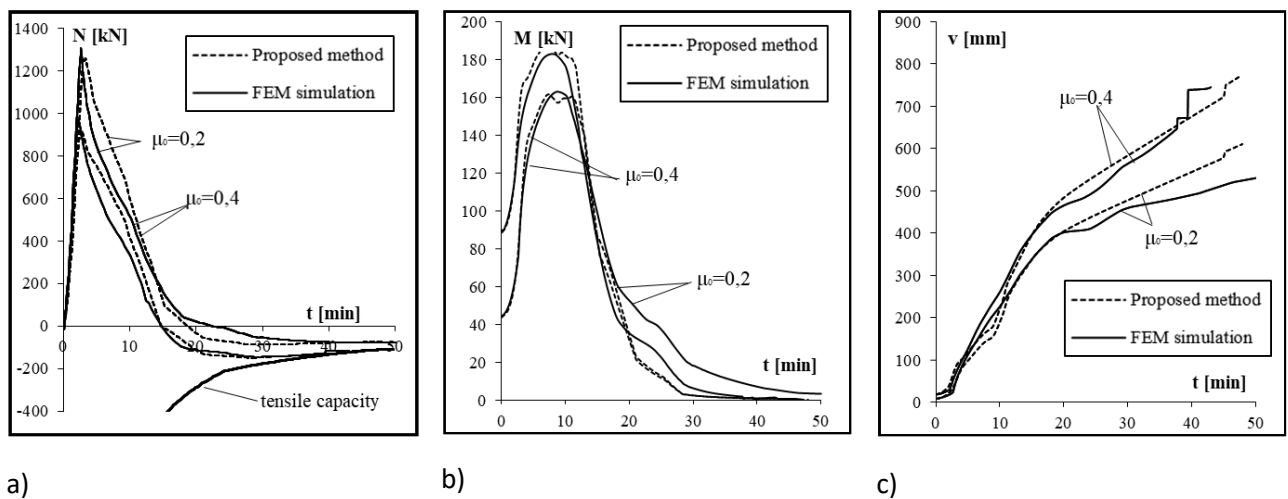
Fig. 3. Comparison between results of FEM model (SAFIR 2016) and simplified method for a simply supported beam
a) Midspan axial force; b) Midspan bending moment; c) Midspan deflection

In the fully axially and rotationally restrained beam, the failure does not happen due to tension, but because the bending capacity is reached. In the midspan section, after a first phase in which the bending moment (*Fig. 4*b)) tends to decrease due to thermal effect, the second-order effects develop, which increase the bending moment until the formation of the midspan plastic hinge. At the end beam section (*Fig. 4*c)), after the first phase in which the bending moment tends to increase due to the thermal curvature, the second-order effects develop. When the midspan plastic hinge is formed, the bending moment redistributes and the effect of the thermal curvature becomes predominant again.

The collapse of the beam occurs when two plastic hinges at the ends of the beam are formed too and no equilibrium configuration is reached.
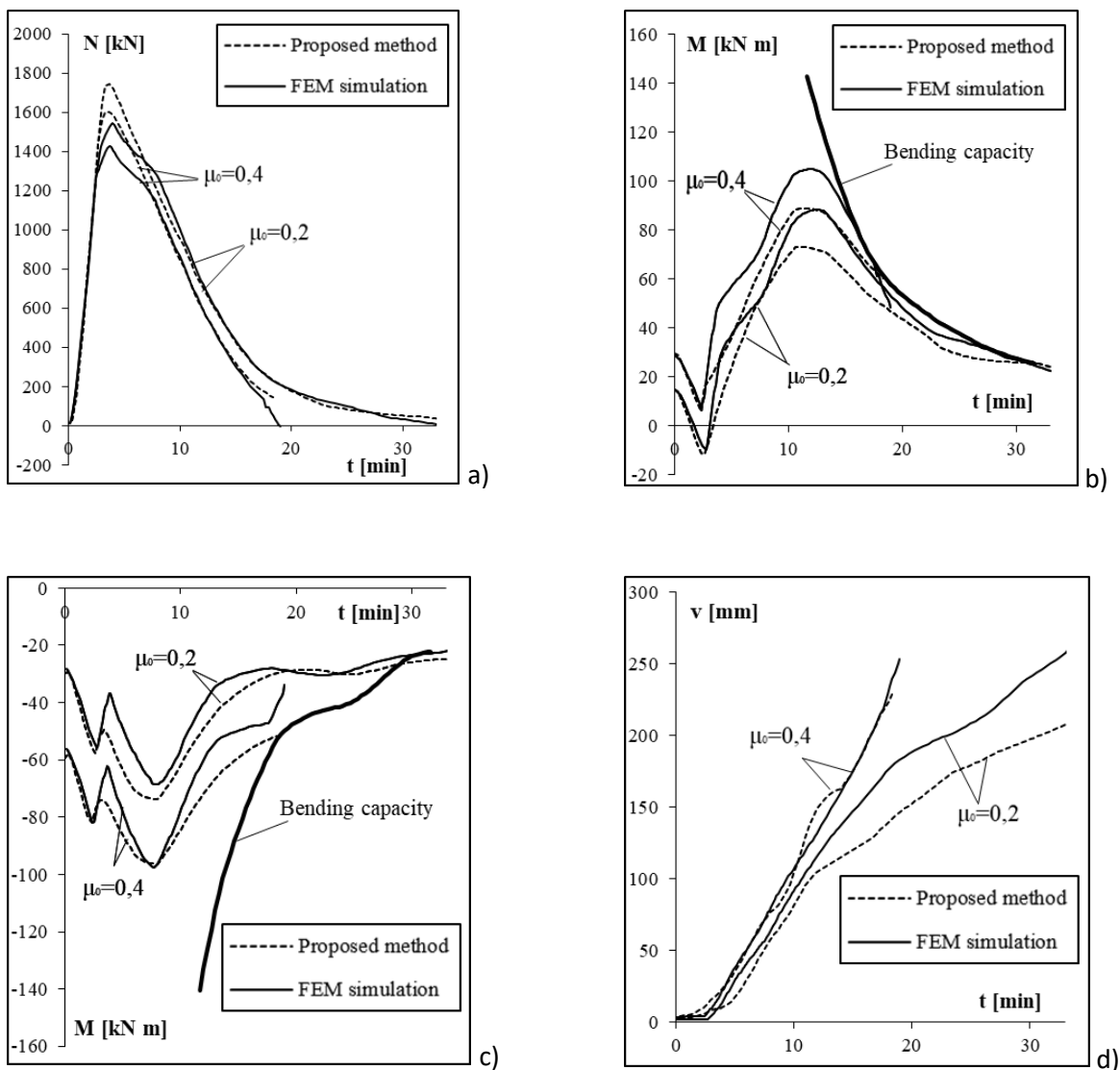
Fig. 4. Comparison between results of FEM model (SAFIR 2016) and simplified method. for a beam fixed at both ends. a) Midspan axial force; b) Midspan bending moment; c) End bending moment; d) Midspan deflection.

3   CONCLUSIONS

In this paper a simplified method to evaluate and interpret the effects of fire on steel structural members is proposed.

The validation of this method is carried out for different restraint conditions and different load level, through the comparison with a FEM model. The results provided by the simplified method with reference to some relevant examples are in a good agreement with the FEM model, in terms of failure time, forces and displacements values vs exposure time and type of attained collapse, allowing to use the proposed method and reducing the computational burden.

The application of the simplified method to some examples allows also some interesting remarks:

The material mechanical properties influence the value of thermal-induced internal forces and limit their development. Indeed, the stress level check verifying the fibers' yielding and the evaluation of the stress and internal force redistribution are necessary.

Fixing the fire curve and the geometric and mechanical properties, the indirect actions due to prevented thermal expansion and curvature depend on the restraints and load level.

The large deflections and the thermal-induced axial forces generates second-order effects that have to be considered in the structural analysis.

The restraint conditions influence the collapse mechanism of the structure: for the simply supported beam the collapse occurs due to tension, developing the "catenary action", while for the double-fixed beam the flexural collapse occurs. This aspect involves a different structural capacity as a different collapse time. Indeed, for the same load level, if the catenary effect has the possibility to develop completely, the collapse time is greater.

The proposed method can be also applied to steel members extracted from framed or truss structures in order to estimate the possible fire collapse modes of complex structures or interpret and check in a simple way the results of fire analyses performed through advanced thermo-mechanical analyses on wide structures. The restraint conditions may be simulated by introducing translational and rotational springs having appropriate stiffness variable with temperature.

REFERENCES

[1] EN1993-1-2 (2005), Eurocode 3, Design of steel structures – Part 1-2: General Rules - Structural Fire Design.

[2] Yu, H. X. and Liew, J. Y. R. (2002), Catenary action of axially restrained steel beams at elevated temperature, Proc. of the Fifteenth KKCNN Symp. on Civil Engineering, Singapore.

[3] Yin, Y. Z. and Wang, Y. C. (2005), Analysis of catenary action in steel beams using a simplified hand calculation method, Part 1: theory and validation for uniform temperature distribution, Journal of Constructional Steel Research, Volume 61, Issue 2, February 2005, Pages 183-211

[4] Yin, Y. Z. and Wang, Y. C. (2005), Analysis of catenary action in steel beams using a simplified hand calculation method, Part 2: theory and validation for non-uniform temperature distribution, Journal of Constructional Steel Research, Volume 61, Issue 2, February 2005, Pages 183-211

[5] Y. C. Wang and Y. Z. Yin (2007). A simplified analysis of catenary action in steel beams in fire and implications on fire resistant design.

[6] J.M. Rotter, A.S. Usmani, (2000). Fundamental principles of structural behaviour under thermal effects. Proceedings of the First International Workshop on Structures in Fire, Copenhagen, Denmark.

[7] A.S. Usmani, J.M. Rotter, S.Lamont, A.M. Sanad, M.Gillie (2001). Fundamental principles of structural behaviour under thermal effects, School of Civil and Environmental Engineering, University of Edinburgh.

[8] Yin, Y. Z. (2004), Advanced behaviour of steel beams under fire conditions, PhD Thesis, The University of Manchester, UK.

[9] SAFIR User's manual Version 2016, University of Liege

[10] EN1994-1-2 (2005), Eurocode 4, Design of Composite Steel and Concrete Structures – Part 1-2: General Rules - Structural Fire Design.

[11] Pidatella, Ferrari, Aggradi, (2012), Corso di meccanica, macchine ed energia (in Italian), Zanichelli

[12] Chi Kin Iu, Siu Lai (2004), A simulation-based large deflection and inelastic analysis of steel frames under fire, Chan Department of Civil and Structural Engineering , The Hong Kong Polytechnic University, Kowloon, Hong Kong

BEHAVIOUR OF LSF WALLS EXPOSED TO FIRE ON BOTH SIDES

Anthony D Ariyanayagam and Mahen Mahendran
Queensland University of Technology (QUT), Brisbane, Australia

ABSTRACT

Light gauge steel frame (LSF) walls made of steel studs and lined with gypsum plasterboards are commonly used as load bearing walls in buildings. Previous studies conducted on LSF walls were based on walls exposed to fire on one side, and design rules were developed assuming a non-uniform temperature distribution across the stud cross-section. However, fire on both sides of the walls is a possible event in buildings, where fires are not contained within a single compartment. In this event, LSF walls are exposed to fire on both sides with a time lag. Numerical studies were conducted in this research on LSF walls exposed to fire on one side only and both sides. The plasterboard and stud temperatures were obtained from thermal finite element models, which were then used in structural finite element models to determine the load ratio versus failure time curves. This papers presents the results and evaluates the effects of fire on both sides.

1   INTRODUCTION

Light gauge steel frame wall (LSF) systems made of cold-formed steel studs and lined with gypsum plasterboards are used as load bearing walls in low- and mid-rise buildings. Generally, lipped channel studs are used as studs and unlipped channel sections as tracks. Under fire conditions, cold-formed thin-walled steel stud sections heat up quickly resulting in fast reduction to their strength and stiffness. Therefore they are commonly used in structural wall systems with plasterboard and insulation materials as fire protecting wall lining materials on both sides of steel studs (*Fig. 1*).
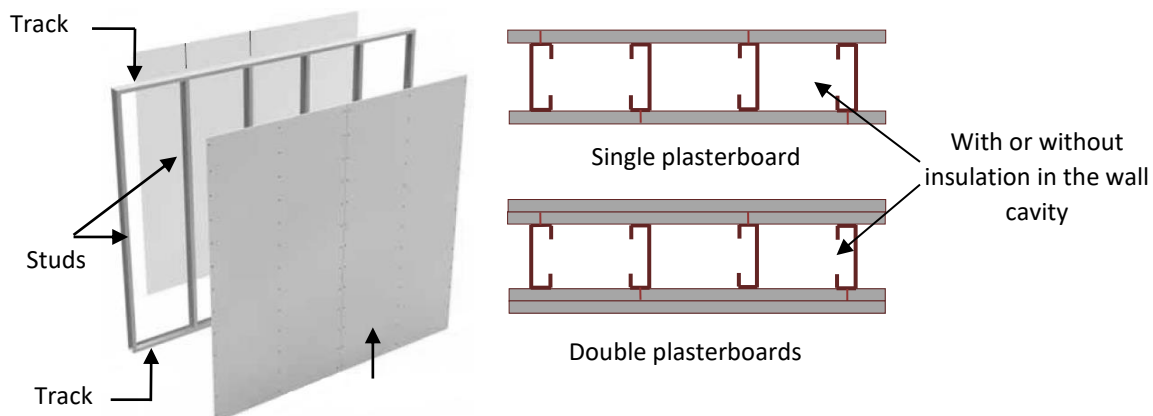
Fig. 1. LSF wall

In general, LSF walls are exposed to fire on one side. The fire resistance rating of load bearing LSF wall is determined based on the standard time-temperature curve given in ISO 834 [1] on one side. The studs heated from one side will develop a temperature gradient across the stud cross-section (i.e. hot and cold flanges in channel studs) and tend to bow towards the fire source due to differential thermal expansion of steel studs. Further this temperature distribution will induce non-uniform distribution of strength and stiffness within the steel stud cross-section. Therefore the studs

subject to axial compression loads at ambient temperature will become beam-columns due to the additional bending action when exposed to fire on one side. Many experimental and numerical studies have been undertaken to investigate the fire performance of LSF walls exposed to fire on one side and suitable design rules have been developed [2-7]. However, in modern mid-rise apartments, where room sizes are less than 3 m by 3 m, fires in one compartment can move to another through openings (door, vent, false ceiling, etc.) and ignite the combustibles present in other compartments. These fires will burn for a longer period of time than the fires contained within a compartment. The fire duration is mostly governed by the presence of fuel loads and ventilation when active fire protections are not in place. This is called the travelling fires and discussed by many researchers [8-10], similar to that used in bridge design where the live load combinations are considered to represent the vehicular movement along the bridge. Travelling fires have been observed in large compartment fires where they burn locally and consume the fuel loads available, move across the floor plates and burn for longer durations [8-13]. In a compartment, if the fire spreads through an opening and the adjoining compartment starts to burn, then the wall that separates these compartments is subjected to fires on both sides. However, there could be a time lag between these fires. In one compartment the fire could be in the growth/decay phase, while it is in the flashover/growth phase in another. In these situations the particular wall experiences fires on both sides, i.e. higher temperatures on both sides, causing both flanges of the studs to rise with time. In LSF walls exposed to fire on one side, only one flange of the stud heats up quickly and conducts heat to the other flange through conduction heat transfer mode. Thus LSF walls exposed to fires on both sides will have a different non-uniform temperature distribution across the stud than what was observed in LSF walls exposed to fire on one side.

A study of four-story steel moment resisting frame exposed to travelling fires revealed that structural collapse occurred under 25% of fire size (based on exposed frame and fire intensity and duration) travelling along the frame, while no collapse occurred during 12.5%, 50% and 100% fire [14]. It also highlighted that the steel frame temperatures were higher for the 25% fire size than for 100% of fire. This contradicts with the traditional belief that 100% fire on one side is more severe than all other fire scenarios [14]. Fire size is mainly dependent on the fire spread rate, heat release rate and the structural element location along the fire path, and studies are in progress in determining the fire model/size for various compartments incorporating different parameters that influence the size of travelling fires. The current building regulations and standard codes of practice do not address the travelling fire concept, and fires burning in multiple compartments with or without a time lag. The current practice is suitable only for small enclosed fires. However, fires are expected to travel along the floor in a compartment and move quickly. More studies are to be conducted in mid-rise cold-formed steel buildings, where fires could spread easily from one compartment to another due to the presence of higher fuel loads and reduced thermal mass in walls compared to conventional masonry walls.

Past studies on LSF walls exposed to fires have shown that stud failures are mostly governed by their hot flange temperatures. Gunalan and Mahendran [6] proposed simplified design equations for stud hot flange temperatures as a function of load ratio (applied load in fire to ambient temperature stud capacity) for a range of wall configurations. Different wall configurations will have dissimilar temperature distributions across the stud cross-section and a sole equation for load ratio versus stud hot flange temperature was not possible, as the cold-flange stud temperatures also slightly influence the stud failures [6]. When LSF walls are exposed to fire on both sides, the temperature distribution across the studs will be different to that of LSF walls exposed to fire on one side. Further depending on the time lag and fire duration, the non-uniform temperature distribution across the studs will shift towards a uniform temperature distribution. This means reduced thermal bowing and neutral axis shift and thus the axial compression capacity of the stud will not be the same due to reduced bending action. This study focuses on LSF walls exposed to fire on both sides and investigates the

fire resistance of two wall configurations, single and double 16 mm thick gypsum plasterboards lined LSF walls exposed to fire on both sides. Time lags of 15 and 30 min were assumed in this numerical study, where the initially unexposed side was exposed to fire with a time lag of 15 and 30 min following a standard fire exposure on one side. Standard fire curve was used as the fire curve for ease of comparison. Numerical study included both thermal and structural finite element analyses. Thermal finite element analyses were conducted to obtain the plasterboard and stud time-temperature curves while structural analyses were conducted to determine the load bearing capacity of 3 m LSF wall panels in fire. The stud failure times and temperatures were obtained and compared. This paper presents the details of this numerical study on LSF walls exposed to fire on both sides and the results.

2   THERMAL FINITE ELEMENT ANALYSIS

Abaqus CAE was used for the thermal Finite Element (FE) analysis of stud walls lined with gypsum plasterboards. Heat transfer analyses assume that the thermal response is not influenced by the mechanical behaviour of wall panel. Thus plasterboard and stud temperatures across and along the LSF wall were obtained by only conducting thermal FE analyses. Thermal FE models were developed with two studs and gypsum plasterboard linings as shown in *Fig. 2* [15]. LSF walls were modelled using 8-node linear heat transfer brick elements DC3D8: diffusion (D) continuum (C) three-dimensional (3D) eight node (8) heat transfer. The heat transfer modes of conduction, convection and radiation were considered in the form of appropriate boundary conditions and material property values.

A mesh density of 20 mm along the surface and 4 mm through thickness were selected for gypsum plasterboard. A mesh density of 10 mm was selected for the 90x35x8x1.15 mm lipped channel studs. Mesh densities of LSF wall components were selected based on the mesh sensitivity analyses conducted by Rusthi et al. [15] for similar LSF wall configurations. Tie constraints were used to ensure heat transfer in both directions; plasterboard to stud hot flange (fire side) and stud cold flange to plasterboard (ambient side) and between the plasterboards in two layers of plasterboard lined LSF walls. This will simply constrain the temperatures at corresponding points of an interface to have the same value with gap conductance equals to 1, where heat is exchanged between the surfaces. Elevated temperature material properties of LSF wall components such as specific heat, thermal conductivity and relative density were obtained from [15]. The convective heat transfer coefficients of 25 and 10 $W/m^2.ºC$ were assigned to fire exposed and ambient surfaces of gypsum plasterboards based on literature and standards [15]. The radiation heat transfer coefficient (emissivity) of 0.9 was assigned to the fire exposed and ambient plasterboard surfaces. Further, closed cavity radiation was used for the heat transfer through cavity and an emissivity coefficient of 0.9 was assigned to the cavity facing surfaces. Stefan Blotzmann constant of 5.67 x 10-8 $W/m^2.ºC$ was assigned to the thermal FE model to obtain the radiation heat transfer. Transient heat transfer analysis was performed with standard fire curve as amplitude. This was assigned to the fire exposed surface of the plasterboard as boundary condition for all the models, while it was assigned to the ambient surface with a time lag of 15 and 30 min for both side fire exposed FE models. *Figs. 3 and 4* show the plasterboard and stud time-temperature curves obtained for both single and double plasterboard lined LSF walls exposed to standard fire curve on one side, and both sides with time lags of 15 and 30 min.
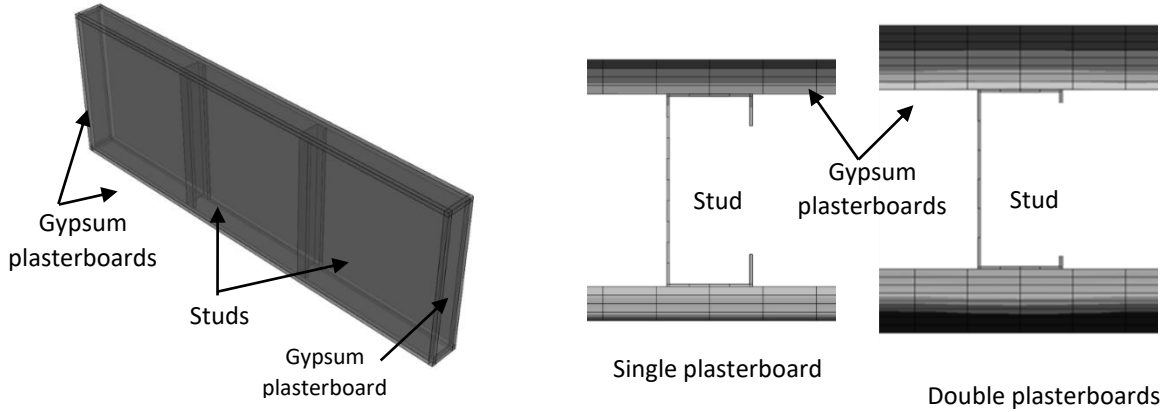
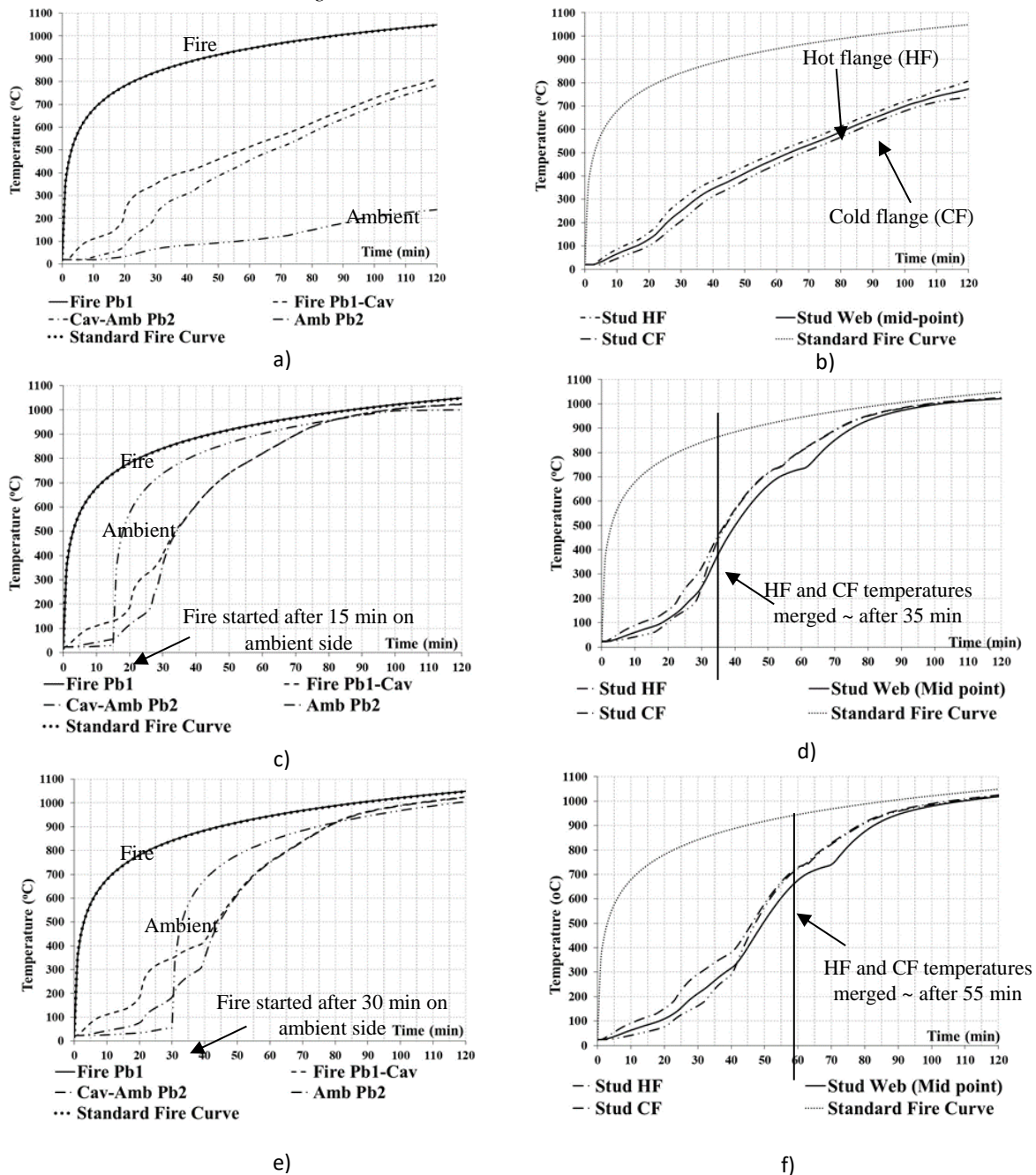*Fig. 2.* Thermal finite element model of LSF wall

Fig.3 Plasterboard and stud time-temperature curves for single plasterboard lined LSF wall a) and b) exposed on one side, c) and d) exposed on both sides with t=15 min lag and e) and f) exposed on both sides with t=30 min lag
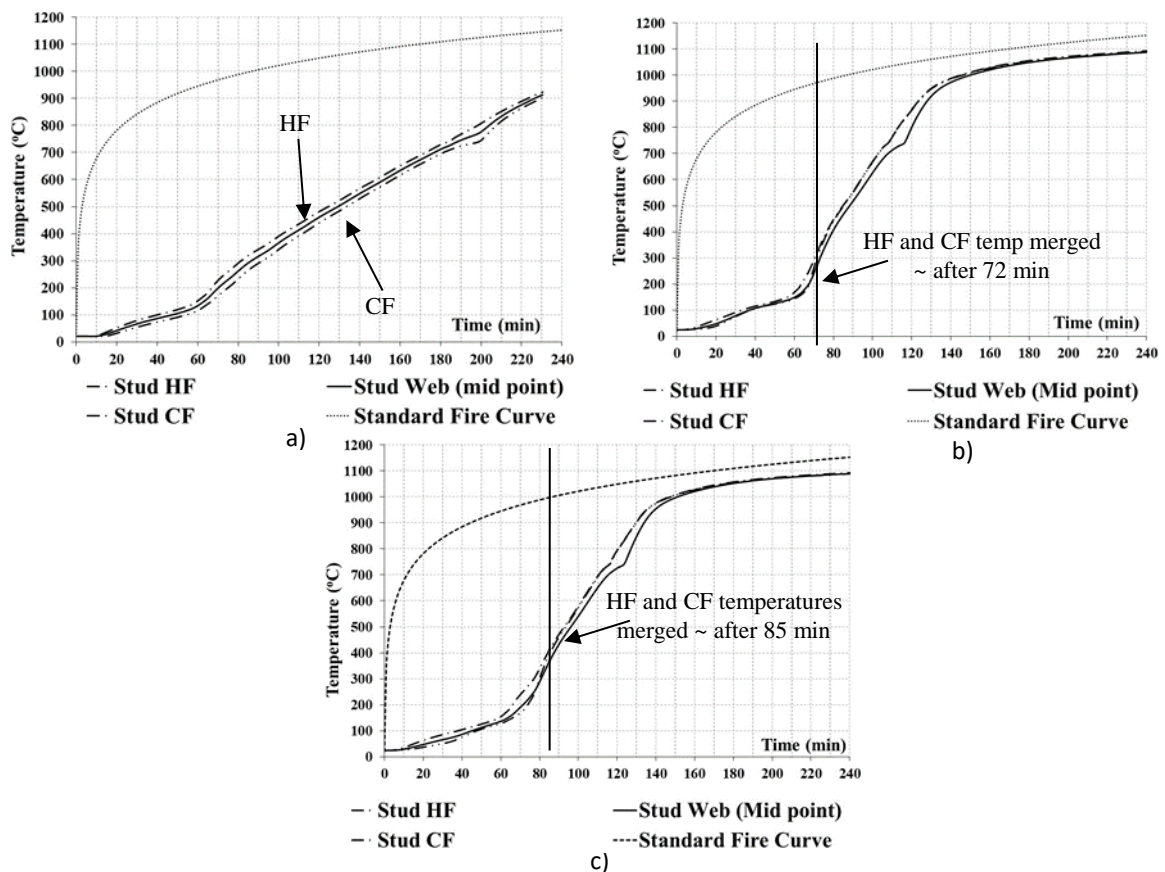
140

Fig. 4. Stud time-temperature curves for double plasterboards lined LSF wall a) exposed on one side, b) exposed on both sides with t=15 min lag c) exposed on both sides with t=30 min lag

As seen in *Fig. 3*, in the initial stages of the fire the wall lining delays the temperature rise in all LSF walls and both plasterboard and stud temperatures across the wall are nearly the same during this time period. *Figs. 3 (a) and (b)* show the time-temperature curves of LSF walls exposed to fire on one side, where a unique pattern of temperature profile can be seen. The fire side surfaces are hotter than the ambient side plasterboard and stud surfaces. Stud hot flange (HF) temperature is always higher than the web and cold flange (CF) temperatures. For LSF walls exposed to fire on both sides, the ambient plasterboard surface temperatures rapidly increased after 15 and 30 min, due to the standard fire exposure on the ambient side surface as well. Thus both cavity facing surface temperatures (Fire Pb1-Cav and Cav-Amb Pb2) merged together after ~ 35 and 55 min of fire exposure. This can be seen in stud HF and CF temperatures as well (*Figs. 3 (d) and (f)*). Thus the non-uniform temperature distribution seen in stud HF and CF temperatures in LSF walls exposed to fire on one side does not exist for fire on both sides after 35 and 55 min, and the stud HF and CF temperatures are nearly the same after this time period. However, web (mid-point) temperatures are 10-40°C less than the stud HF and CF temperatures for the entire duration. Similar pattern also exists in double plasterboards lined LSF walls, where after ~ 72 and 85 min, the stud HF and CF temperatures are the same while the web (mid-point) temperatures are lower than the stud HF and CF temperatures. This creates two temperature gradients across the stud section, one being from HF to web (mid-point) and another from web (mid-point) to CF. This is different to that of LSF walls exposed to fire on one side with a single temperature gradient from HF to CF across the stud used in finite element analyses and design of LSF walls.

141

3   STRUCTURAL FINITE ELEMENT ANALYSIS

A structural finite element analysis based study was undertaken for 3 m long studs in LSF wall panels with appropriate loading and boundary conditions. Lipped channel section of 90x35x8x1.15mm thick G550 steel was used in Abaqus FE analyses. The shell element type S4R with 4 mm x 4 mm mesh size and boundary conditions were used to model the stud based on previous FE studies used for similar conditions [16]. The stud temperatures obtained from thermal finite element analyses were used in this study, and the mechanical properties at elevated temperatures were based on [17]. Transient state FE analyses were conducted where the stud was subjected to a predetermined axial compression load and then the stud temperatures were increased until failure. The applied axial compression load was based on the load ratios from 0.2 to 0.7. *Fig. 5* shows the load ratio versus stud failure times (FRL) of LSF walls exposed to fire on one side and both sides obtained from structural FE analyses and *Fig. 6* shows the stud failure temperatures.
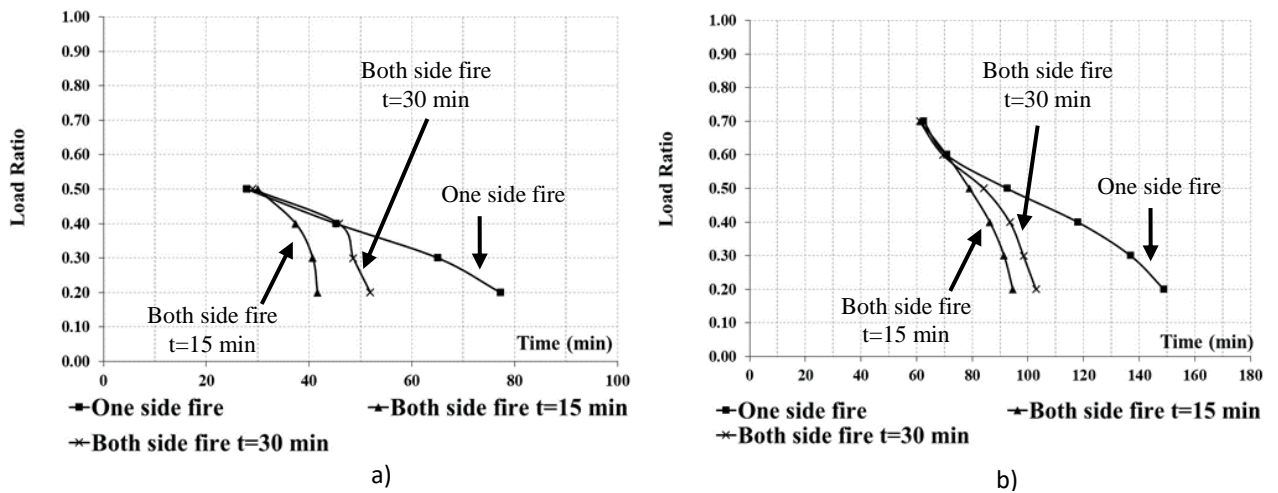
Fig. 5. Load ratio versus time curves a) single plasterboard b) double plasterboards lined walls
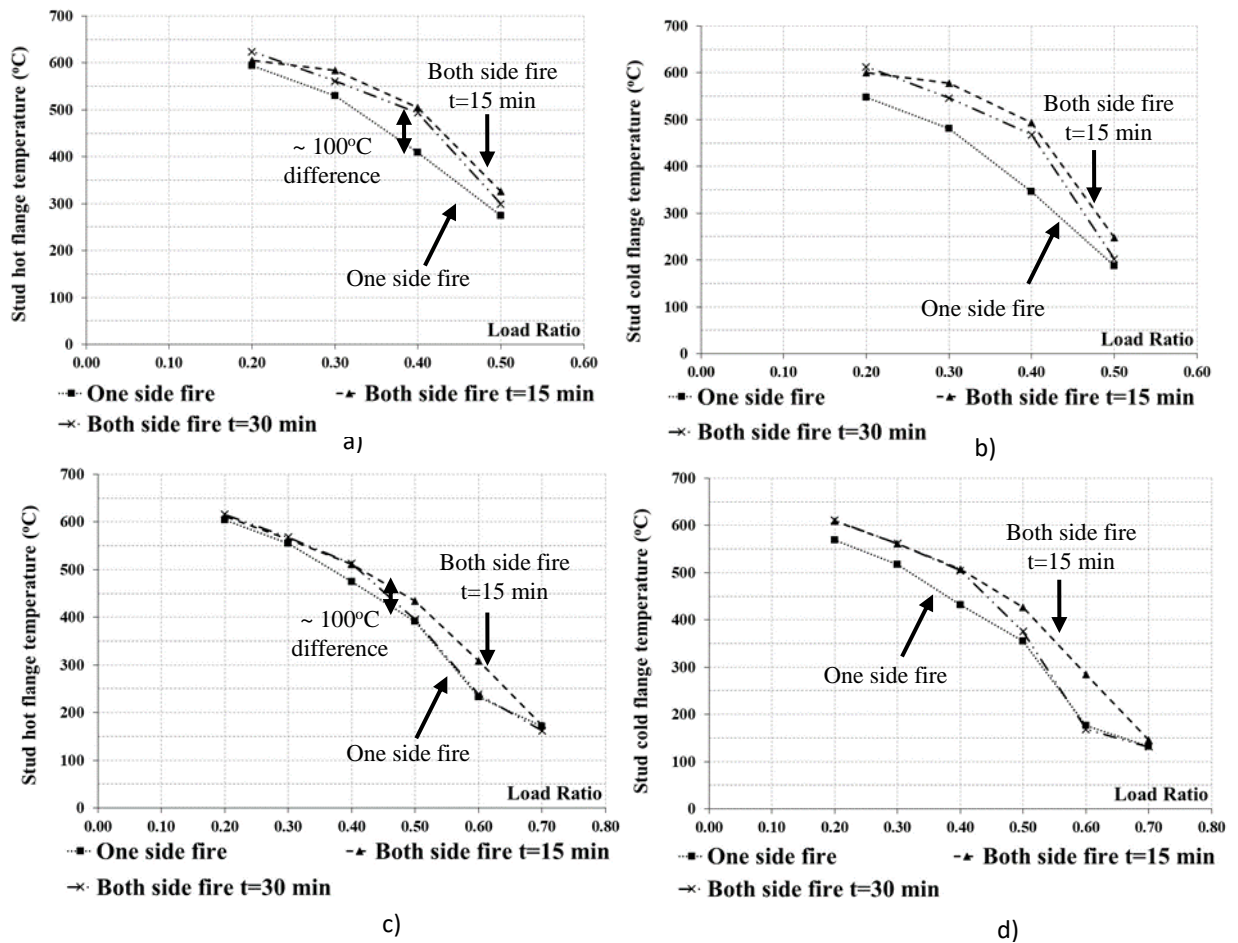
Fig. 6. Stud hot flange temperature versus load ratio curves a) stud hot flange and b) cold flange temperature of single plasterboard lined walls and c) stud hot flange and d) cold flange temperature of double plasterboard lined walls

As seen in *Fig. 5*, LSF walls exposed to fire on both sides structurally failed much earlier than the LSF walls exposed to fire on one side only. For instance, for a load ratio of 0.2, single plasterboard lined wall exposed to fire on both sides with 15 and 30 min time lags failed at 42 and 52 min respectively, whereas it was 77 min for LSF wall exposed to fire on one side only (*Figs 5(a))*. Similarly they were 95 and 103 min versus 149 min for double plasterboards lined walls (*Figs 5(b))*. This is because, the lower the load ratio, the fire duration is longer and studs will be exposed to higher temperatures. Thus LSF walls exposed to fire on both sides will heat up quickly and stud temperatures increase rapidly than in LSF walls exposed to fire on one side. This shows the importance of incorporating fire exposure on both sides in the design. However, for load ratios of 0.5 and above, the stud failure times are nearly the same or only a small difference was observed. As the studs subjected to higher axial compression loads fail at much lower temperatures, the presence of gypsum plasterboard on both sides of the studs delays the stud temperature rise until it dehydrates and calcination occurs in fire. Thus LSF walls subjected to higher load ratios and exposed to fires from one side or both sides have nearly the same stud failure times.

Fig. 6 shows the stud hot and cold flange temperatures at failure. It shows that studs exposed to fire on one side always have lower stud hot flange (HF) and cold flange (CF) temperatures than studs exposed to fire on both sides, and the difference in HF and CF temperatures is also high. This is because as the walls are exposed to fire on one side, it generates higher thermal gradient across the studs resulting in thermal bowing, neutral axis shift, eccentric loading and higher second order deflections due to bending. Thus studs in LSF walls exposed to fire on one side failed at lower stud

143

HF temperatures than those exposed to fire on both sides. Studs in LSF walls exposed to fire on both sides will have a near uniform temperature across the stud cross-section with time, and it results in less contribution from bending action. As a result the stud HF temperatures in single plasterboard lined walls exposed to fire on both sides are significantly high for the load ratios in the range of 0.3 to 0.5, where a difference of about 100ºC was noticed (*Fig. 6(a)*). The difference is only about 50ºC in double plasterboard lined walls (*Fig. 6(b)*). This is due to the presence of an additional layer of gypsum plasterboard that delayed the stud temperature rise. This temperature difference is not noticed in load ratios less than 0.2 and above 0.6, since with lower loads and associated longer fire duration, the stud temperature distribution across the cross-section will become nearly uniform even in walls exposed to fire on one side. At higher load ratios, gypsum plasterboard delays the stud temperature rise and thus the stud HF temperatures are the same for walls exposed to fire on one side and both sides.

4   CONCLUSIONS

This paper has presented the details of finite element studies conducted on LSF walls exposed to fire on both sides. Thermal finite element analysis showed that with fire duration the cavity facing plasterboard surface temperatures merged together in walls exposed to fire on both sides, and heat the studs from both sides. This resulted in nearly the same stud hot and cold flange temperatures. Therefore the stud temperature distribution does not exhibit a linear reduction from hot flange to cold flange as observed in walls exposed to fire on one side. In walls exposed to fire on both sides two temperature gradients were observed, from hot flange to web (mid-point) and web (mid-point) to cold flange. Thus studs will not experience the thermal bowing, neutral axis shift and second order effects and bending action observed in walls exposed to fire on one side. Hence studs are able to sustain higher hot flange temperatures as shown by structural finite element analyses and simplified design equations developed for one side fire exposure are not suitable for both side fire exposure. However, the failure of LSF wall studs occurs much earlier when exposed to fire on both sides for load ratios less than about 0.5. This study has highlighted the importance of considering LSF walls exposed to fire on both sides in the building regulations and design standards. Research is in progress in verifying the applicability of existing fire design rules for LSF walls exposed to fire on both sides.

ACKNOWLEDGMENTS

REFERENCES

[1]   ISO 834-1, Fire Resistance Tests – Elements of Buildings Construction – Part-1 General requirement, International Organization for Standardization, Switzerland, 1999.

[2]   Alfawakhiri F. (1999). Fire resistance of load bearing steel-stud walls protected with gypsum board: A Review, Fire Technology 35(4): 308-335.

[3]   Feng M., Wang Y.C. (2005). An analysis of the structural behaviour of axially loaded full-scale cold-formed thin-walled steel structural panels under fire conditions, Thin-Walled Structures 43, 291-332.

[5]   Kodur. V.K.R., Sultan M.A. (2006). Factors influencing fire resistance of load bearing steel stud walls, Fire Technology 42: 5-26.

[6]   Gunalan S., Mahendran M. (2014). Fire peformance of cold-fromed steel wall panels and prediction of their fire resistance rating, Fire Safety Journal 64: 61-80.

[7]   Ariyanayagam A.D., Mahendran M. (2012). Fire Tests of Load Bearing Steel Stud Walls Exposed to Real Building Fires, 7th Int. Conference on Structures in Fire, 6-8 June, Switzerland, pp. 105-114.

[8]   Law A., Stern-Gottfried J., Gillie M, Rein G. (2011). The Influence of travelling fires on a concrete frame, Engineering Structures 33(5): 1635-1642

[9]   Rackauskaite E., Hamel C., Law A., Rein, G. (2015). Improved formulation of travelling fires and application to concrete and steel structures, Structures 3: 250-260

[10]   Dai x., Welch S., Usmani, A. (2017). A critical review of travelling fire scenarios for performance-based structural engineering, Fire Safety Journal 91: 568-578.

[11]   Torero J.L., Mjadlani A.H., Empis A., Cowlard A. (2014). Revisting the compartement fire, In the 11th International Symposium on Fire Safety Science, pp. 28-45

[12]   Hidalgo J.P., Cowlard A., Empis A., Maluk C., Majdalani A.H., Kahrann S., Hilditch R., Krajcovic M., Torero J.L. (2017). An experimental study of full-scale open floor plan enclosure fires, Fire Safety Journal 89: 22-40.

[13]   Rush D., Lange D., Maclean J., Rackauskaite E. (2016). Modelling ther thermal and structural performance of a concrete column exposed to a travelling fire – Tisova fire test, In Proceedings of the 9th International conference on structures in fire, pp. 110-118.

[14] Rezvani F.H., Behnam B., Ronagh H., Jeffers, A.E. (2015). Effect of travelling fire on structural response of a generic steel fire protected moment resisting frame, International Conference on Performance-based and Life-cycle Structural Engineering, Brisbane, Australia.

[15] Rusthi M.I., Keerthan P., Mahendran M., Ariyanayagam A.D. (2010). Investigating the fire performance of LSF wall systems using 3-D finite element analyses, J. Struct. Fire Engineering. 8 (4): 354–376

[16]   Ariyanayagam A.D., Mahendran, M. (2018). Fire performance of load bearing LSF wall systems made of low strength steel studs, Thin-Walled Structures 130: 487-504.

[17] Dolamune Kankanamge N., Mahendran M. (2010) Mechanical properties of cold-formed steels at Elevated temperatures, Thin-Walled Structures 49: 26–44.

FIRE RESISTANCE OF SLIM FLOOR BEAMS, FROM EXPERIMENTAL WORK TO SIMPLE FIRE DESIGN METHODS

Naveed Alam[1], Ali Nadjai[1], Faris Ali[1], Francois Hanus[2], Olivier Vassart[2]
[1] Fire Safety Engineering and Technology (FireSERT), Ulster University, Belfast, UK
[2] ArcelorMittal Global R&D, Esch-sur-Alzette, Luxembourg

ABSTRACT

Response of the slim floor beams at elevated temperatures has fascinated various researchers and several investigations have been conducted to understand and analyse their behaviour in fire. The results obtained from the previous investigations have shown that these beams offer a higher fire resistance in comparison with the traditional steel-concrete composite beams. Although several investigations have been conducted to analyse the response of slim floors in fire, limited attempts have been made to devise simple fire design methods. This study is initiated to devise simple fire design methods for slim floor beams. An experimental investigation is initially conducted to analyse the response of slim floor beams in fire while the response exhibited during the test is replicated through numerical modelling. The validated numerical modelling method is later used to conduct a parametric study to investigate the response of slim floor beams under different degrees of utilizations. Using the results from the parametric study, simple fire design methods are devised by establishing a relationship between the degree of utilization and their fire resistance. The proposed fire design method is the state-of-the-art and will serve as a design tool for future use. The proposed fire design method will contribute to the current database of knowledge and will reduce the current fire protection requirements and associated finances in addition to providing a better understanding on the behaviour of slim floor beams exposed to elevated temperatures.

1   INTRODUCTION

During the last quarter of the 20th century, the use of slim floor systems gained popularity in the Nordic countries as they offer numerous advantages over the traditional steel-concrete composite beams [1]. Although the slim floor technology has recently gained admiration, the art of shallow floor construction is being used since the 1790s as the filler joist type of shallow floor systems were frequently used [2]. The slim floor technology was introduced in the United Kingdom (UK) during the 1990s [3]. Since their introduction, various designs of these floors are now used by the construction industry. Amongst these various design types, slim floor beams (SFBs) are very common as they offer longer spans and are easy to fabricate using the existing steel sections and plates [3]. Like the other forms of slim floor systems, SFBs offer various benefits including a flat soffit, ease of installation of the hydraulic and electric services and a reduced floor depth. During the floor construction, most part of the steel section is encased within the concrete with only the welded steel plate being exposed. The encased concrete between the flanges contributes towards the second moment of area of SFBs and induces a partial encasement keeping the steel section protected from direct exposure to fire. As a result, low temperatures are maintained in most parts of the steel section. Hence, SFBs have an inherent fire resistance of around 60 minutes [4] [5]. The combination of SFBs with the metal decking reduces the construction time and eliminates any requirements of the formwork [5]. Several investigations have been previously conducted to analyse the response of slim floor systems in fire. These previous studies include the experimental investigations [6], [7], the numerical investigations [8], [9], [10], as well as the simple equations to estimate temperature distributions across their sections [11]. Although simple equations, to estimate the temperature distributions across the slim floors, have been previously established, any empirical

146

solutions to estimate their fire resistance have not yet been proposed. The simple design solutions to estimate the fire resistance of SFBs can either be in terms of a relationship between their degree of utilization and their fire resistance time or in terms of a relationship between their degree of utilization and critical temperatures as proposed in the Eurocodes, BS EN-1993-1-2 [12]

1.1 Aims and objectives

The aim of this investigation is to study the response of SFBs in fire and to devise simple fire design methods for future use. To achieve this aim, an experimental investigation has been conducted to understand and analyse the response of SFBs in fire while the numerical modelling has been conducted to examine the influence of different degrees of utilization on their response. Results from the numerical modelling are used to establish a relationship between the degree of utilization of SFBs and their fire resistance. This relationship will be used by engineers as a design tool to estimate the fire resistance of SFBs in future.

2 EXPERIMENTAL INVESTIGATION

During the experimental investigation, a fire test was conducted on a SFB assembly consisting of a fabricated steel section and a steel-concrete composite floor. The total width of the test assembly was 1000 mm while its length was 5000 mm as shown in *Fig. 1 (a)*. The beam was fabricated using a HEA-180 steel section and by welding a steel plate, 350 mm wide and 15 mm thick, along its bottom flange. Both steel beam and the welded plate were manufactured using grade S355 structural steel. The depth of the steel section was 195 mm while the total depth of the SFB assembly including the composite slab was 245 mm. The composite floor of the test assembly was constructed using MD-50 steel decking and normal weight concrete with a target strength of 30 N/mm^2 at 28 days. Concrete cubes were prepared to measure the moisture content as well as to perform the compression strength tests. The concrete slab above the top flange was reinforced using A-142 steel mesh. The outer edges of the SFB assembly consisted of plain steel sheets as shown in *Fig. 1 (b)*. These steel sheets served as a permanent formwork and remained a part of the SFB assembly during the casting of concrete and during the fire tests. The test assembly was positioned on the furnace frame in such a way that the distance between the end supports was 4500 mm as shown in *Fig. 1 (a)*.

Detailed instrumentation was conducted to record the temperatures and deflections of the SFB assembly. The thermal data was recorded using five thermocouples provided in the steel plate, the bottom flange, the steel web and the top flange of the steel beam section as shown in *Fig. 1 (c)*. The structural response of the SFB assembly was monitored using Linear Variable Differential Transformer (LVDTs) provided along its span, including LVDT-1, which was positioned in the middle of the test assembly, at span/2.

The external loads on the test assembly were applied at two positions, 1750 mm from the edges as shown in *Fig. 1 (a)*. These loads were applied using hydraulic rams resting on the spreader beams positioned on top of the finished concrete surface of the composite slab. During the test, the SFB assembly was first loaded by applying the external loads. The maximum load applied on the test assembly represented a degree of utilization of 0.55 of the steel beam section. The maximum applied load was maintained for 30 minutes before exposing the SFB assembly to elevated temperatures. The heating conditions during the test were in accordance with the standard temperature-time curve, ISO-834.

The recorded temperatures across the steel section, and the average temperatures in the furnace, recorded during the test, are shown in *Fig. 1 (d)*. The average temperatures of the furnace were in accordance with the standard time-temperature curve while a significant thermal gradient was observed across the section of the SFB assembly. The maximum temperatures were recorded on the

welded steel plate while the minimum temperatures were recorded on the top flange. A substantial temperature difference was observed between the welded steel plate at thermocouple position 1 and on the bottom flange at thermocouple position 2 as seen in Fig. 1 (d). A similar observation has been made in a previous investigation conducted by the authors [13]. It was also observed that with increase in distance from the bottom flange, the magnitude of the recorded temperatures on the steel web decreases. This is evident from the temperatures recorded at thermocouple positions 3 and 4 shown in Fig. 1 (d).
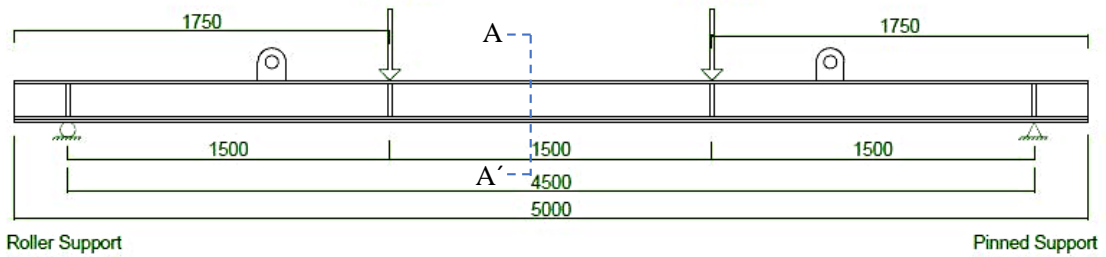
(a)

(b)
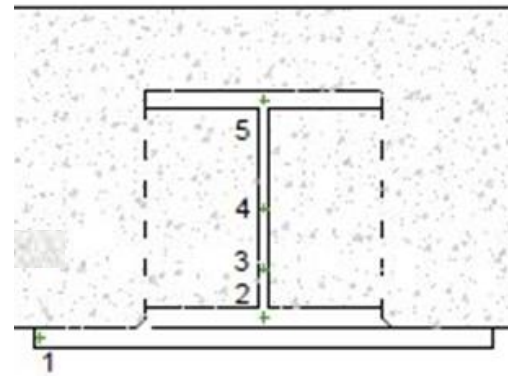
(c)
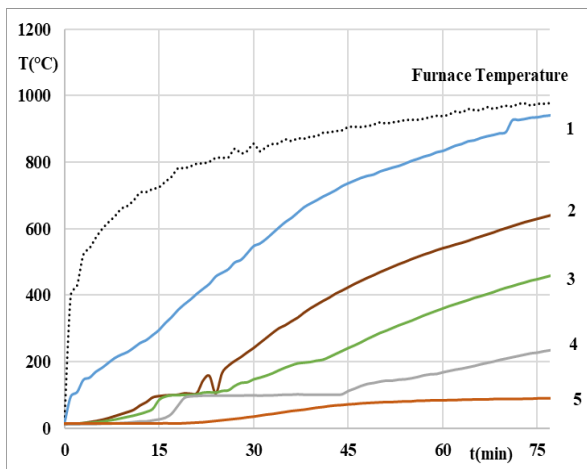
(d)
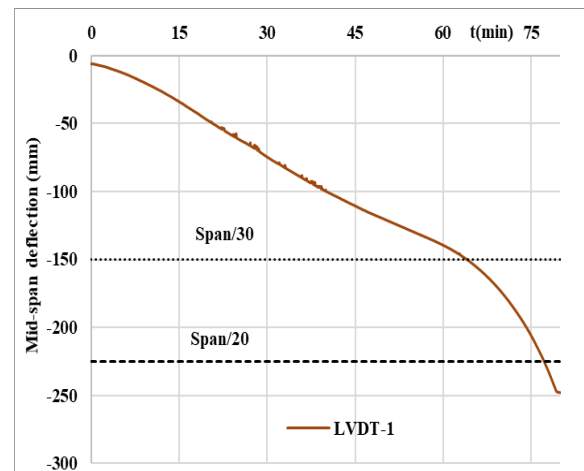
(e)

Fig. 1. a) Test arrangement; b) preparation of test assembly; (c) instrumentation detail at section AA´; (d) Thermal test data; (f) recorded mid-span deflection

148

The structural response of SFB assembly was analysed in terms of the maximum recorded mid-span deflection and the maximum rate of the mid-span deflection as proposed in the British Standards, BS 476-20 [14]. The test assembly offered a fire resistance of 77 minutes before reaching the recommended limits related to the maximum rate of deflection [14]. The recorded rate of deflection at failure was 9.20 mm/min which was higher than the maximum permissible value of 9.18 mm/min for the tested SFB assembly. Hence the SFB assembly offered a fire resistance of 77 minutes under a degree of utilization of 0.55.

The Eurocodes, EN-19931-2 [12], propose the fire resistance of the structural members in terms of critical temperatures corresponding to their degree of utilization. Considering the recommendations of the Eurocodes [12], the critical temperature at failure for a 0.55 degree of utilization is 570.5°C. During the test, the maximum temperatures recorded on the exposed welded steel plate were 570.5°C after 33 minutes of fire exposure. According to Eurocodes [12], the SFB assembly offered a fire resistance of 33 minutes. The recorded mid-span deflection for the SFB assembly after 33 minutes of fire exposure was only 82 mm. The SFB assembly continued to support the external loads for a much longer duration of fire until the rate of mid-span deflection increased after 77 minutes. These results show that the recommendations given in the Eurocodes [12] provide highly conservative results when adopted for SFBs. Although these recommendations may give conservative results for SFBs, they may provide more accurate results for other forms of structural steel work.

3   NUMERICAL MODELLING

Numerical modelling for the SFB assembly was conducted using ABAQUS [15]. Most of the previous numerical investigations conducted on the response of slim floor systems in fire [16] address the asymmetric slim floor beams (ASBs). The numerical modelling method adopted during this study is similar to the method proposed in the earlier publications by the authors [13] [17]. During the numerical modelling, full scale model for the span between the supports of the SFB assembly was developed. The numerical model was 4500 mm long and 245 mm deep while its width was 1000 mm. The thermal properties of concrete and structural steel were taken from the Eurocodes [18] [19], while the mechanical properties of the materials during the numerical modelling were taken from the results obtained during the laboratory tests conducted at Ulster University. The two-phase method proposed earlier by the authors [13] [17] was used to analyse the response of the SFB assembly in fire. During the first phase of the numerical modelling, the SFB assembly was exposed to the recorded furnace temperatures and thermal contours were obtained. The heat transfer across the air-gap between the bottom flange and the steel plate was modelled via cavity radiation. The second phase of the numerical modelling consisted of two steps. During the first step, the external loads were applied while in the later step, the SFB assembly was heated using the thermal contours obtained during the first phase. Further details related the numerical modelling can be found in the publications listed in the references [13] [17].

The results from the numerical modelling for the SFB assembly are presented in *Fig 2*. The results from the thermal part of the modelling are in very good agreement with the recorded test data for all thermocouple positions as shown in *Fig 2 (b)*. Similar to the test, a significant thermal gradient is seen across the section and the temperature differences between the welded steel plate and the bottom flange are also high. The results from the thermo-mechanical part of the analysis are presented in terms of the mid-span deflection in *Fig 2 (c)*. The mid-span deflection, predicted using the numerical modelling, is in close agreement with the test data. In addition, the deflected shape of the SFB assembly at failure is also shown in *Fig 2 (a)*.

The results from the numerical modelling and their resemblance with the test data shows that the response of SFBs can be predicted using the proposed numerical modelling method. In the

following sections, the validated method is used to conduct a parametric study to investigate the response of SFBs under various degrees of utilizations.
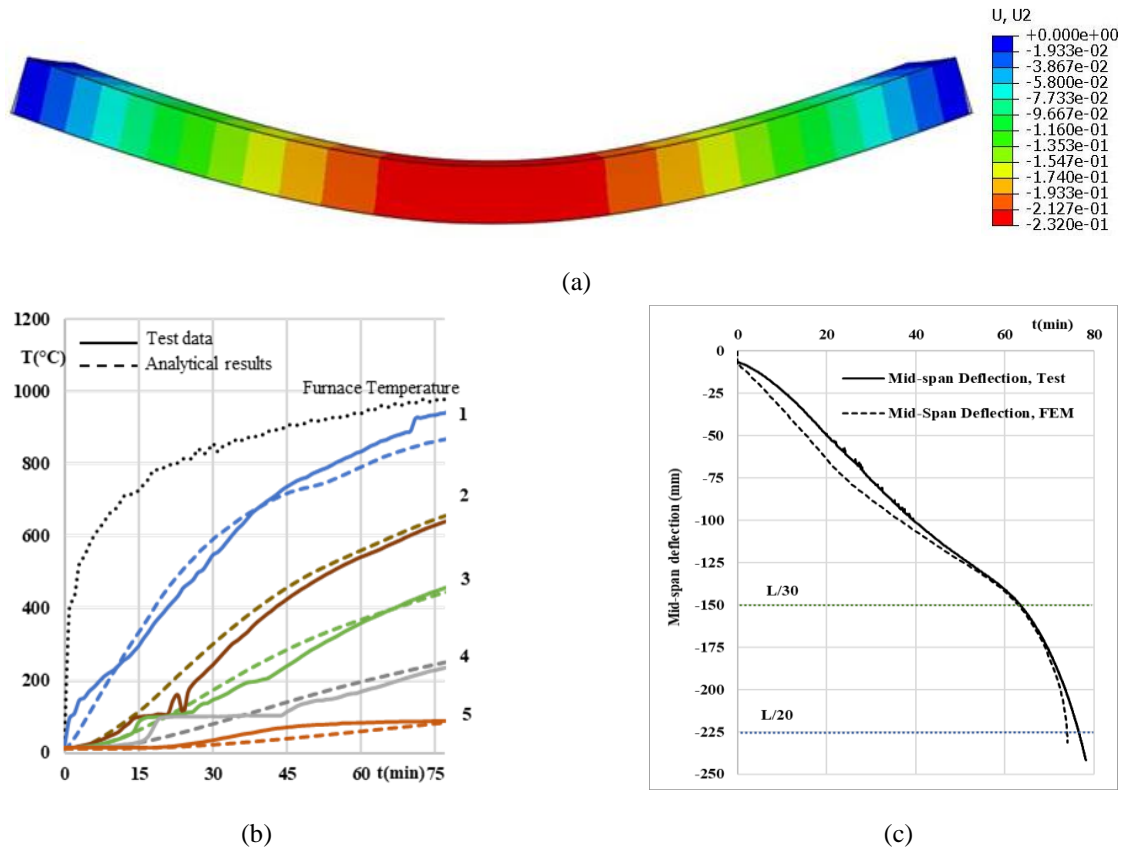

(a)

(b)

(c)

Fig. 2. a) Deflected shape of SFB assembly from numerical modelling; b) test data vs numerical results, the thermal response; b) test data vs numerical modelling, the mid-span deflection

4   PARAMETRIC STUDIES

To study the influence of the degree of utilization on the response of SFBs in fire, a parametric study was conducted using the numerical modelling method described above. During the parametric study, seven analyses were conducted. The heating conditions during the sensitivity studies were in accordance with the standard time-temperature curve while the degree of utilization of the SFB assembly was kept different in each case. For the first case, a lower value of the degree of utilization, 0.2, was used while for the final case, a higher value of 0.8 was used as given in *Table 1*. The fire resistance offered by the SFB assembly was analysed using the deflection-based limits from the British Standards [14].

Table 1. Results from the sensitivity study

S#	Degree of utilization	Fire resistance (minutes)	Maximum steel temperature at failure (°C)
1	0.20	233	1103
2	0.30	143	1012
3	0.40	96	922
4	0.50	76	867
5	0.60	63	813
6	0.70	56	771
7	0.80	49	734

The SFB assembly offered a fire resistance of 233 minutes under 0.20 degree of utilization while the same under 0.8 degree of utilization was 49 minutes. The fire resistance offered by the SFB assembly under various degrees of utilizations is given in *Table 1*. In addition to the fire resistance, the maximum temperatures predicted on the welded steel plate of the beam section at failure are also provided in *Table 1*.

5   SIMPLE DESIGN METHODS

The results obtained from the parametric studies show that for lower degrees of utilizations, the fire resistance offered by the SFBs is higher as compared to that obtained for higher degrees of utilizations. As mentioned in section 2, the recommendations related to critical temperatures provided in Eurocodes [12] produce highly conservative results when applied to SFBs. Hence, using the results given in *Table 1*, a relationship is established between the degree of utilization (μ_0) and the fire resistance (t) of the SFBs and is presented in *Fig 3*. The quantity along the horizontal axis in *Fig 3* is the degree of utilization (μ_0) while that along the vertical axis is the fire resistance in terms of time (t). The relationship between μ_0 and t can be expressed in terms of a polynomial with order four as given in *Eq. (1)*. This relationship provides a more accurate fire design approach for SFBs. It should be realised that the relationship presented in *Eq. (1)* is only applicable when the fire exposure conditions are in accordance with the standard time-temperature curve.
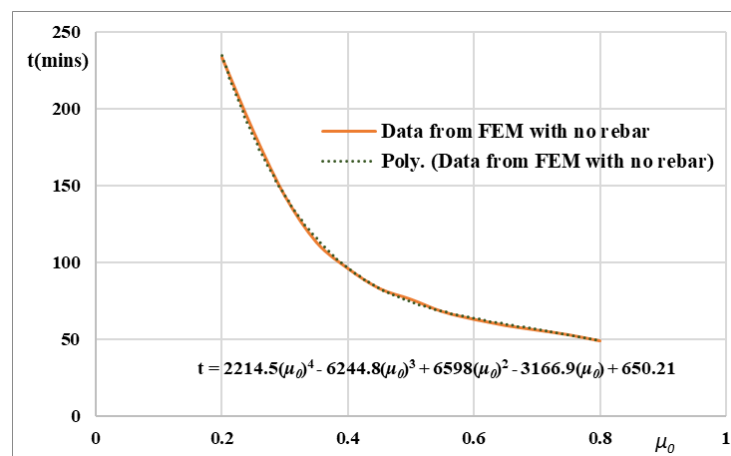
Fig. 3. Relationship between the degree of utilization and fire resistance of the SFB assembly

$$t = 2214.5\,(\mu_0)^4 - 6244.8\,(\mu_0)^3 + 6598(\mu_0)^2 - 3166.9\,(\mu_0) + 650.21 \qquad (1)$$

Where;

t = time (mins)

μ_0 = degree of utilization

The estimated fire resistance offered by the SFB assembly in terms of time in minutes corresponding to the respective degrees of utilizations using Eq. (1) is given in Table 2. The minimum value of the degree of utilization is set at 0.22 while the maximum value is set at 0.8. The fire resistance is given for 0.02 intervals of the degree of utilization which is similar to the approach used to produce Table 4.1 of the Eurocodes [12]. Further, the range of μ_0 between 0.22 and 0.8 is also kept similar to that given in the Eurocodes [12].

Table 2. Fire resistance of SFB assembly under various degrees of utilizations

μ_0	t (min)	μ_0	t (min)	μ_0	t (min)
0.22	211	0.42	90	0.62	62
0.24	191	0.44	85	0.64	60
0.26	173	0.46	80	0.66	59
0.28	157	0.48	77	0.68	57
0.30	143	0.50	74	0.70	56
0.32	131	0.52	71	0.72	54
0.34	120	0.54	69	0.74	53
0.36	111	0.56	67	0.76	51
0.38	103	0.58	65	0.78	50
0.40	96	0.60	63	0.80	49

The results provided in *Table 2* can be used to estimate the response of the SFBs in fire under various degrees of utilizations. The results presented in *Table 2* are more accurate as compared to the ones proposed in the Eurocodes [12]. These results show that the SFBs offer a higher fire resistance as compared to traditional steel-concrete composite beams. Such a response of SFBs can be attributed to the partial concrete encasement which imparts a significant thermal gradient across the section. The encased parts of the SFBs remain at low temperatures and retain their strength and stiffness, as a result, they continue to support the external loads even in longer durations of fire exposure.

6   CONCLUSIONS AND RECOMMENDED FUTURE WORK

This research presents the results of an experimental and numerical investigation conducted to study the response of SFBs in fire. The data obtained from the experimental investigation has shown that the SFBs offer a higher fire resistance due the partial concrete encasement of the steel section. The concrete encasement protects the steel section from direct exposure to heat, as a result, a higher thermal gradient is observed across the steel section. The tested SFB assembly offered a fire resistance of 77 minutes before reaching the deflection-based failure limits. The deflection-based fire resistance offered by the SFB assembly is significantly higher than the critical temperature-

based fire resistance recommended in the Eurocodes. The numerical modelling used to predict the response of SFB was able to replicate their response in fire. The method was later used to analyse the response of SFBs under different degrees of utilization. It was found that the fire resistance offered by the SFBs decreases with the increase in their degree of utilization. Results from the parametric study were used to develop a relationship between the degree of utilization of SFBs and their fire resistance. The proposed relationship was used to estimate the fire resistance of SFBs under degrees of utilization in the range of 0.22 to 0.8. The results presented in this research can be used to conduct the fire design of SFBs exposed to standard fires.

The authors of this research are currently working on developing simple relationships between the degree of utilization of various slim floor systems and the critical temperatures as proposed in the Eurocodes.

REFERENCES

[1]   Lu, X. & Mäkeläinen, P. (1996). *Slim Floor Developments in Sweden and Finland.* Structural Engineering International, 6(2), pp. 127–129.

 [2]   Maraveas, C., Wang, Y.C. & Swailes, T., (2013). *Thermal and mechanical properties of 19th century fireproof flooring systems at elevated temperatures.* Construction and Building Materials, 48, pp.248–264.

[3]   Mullet, D.L., (1998). Composite Floor Systems. 1st edition. London. The Steel Construction Institute.

[4]   Bailey, C.G., (1999). *The behaviour of asymmetric slim floor steel beams in fire*. Journal of Constructional Steel Research, 50(3), pp.235–257.

[5]   Newman, G.M., (1995). *Fire resistance of slim floor beams*. Journal of Constructional Steel Research, 33(1-2), pp.87–100.

[6]   Latham, D. J., Thomson, G., Kay, T. R., Preston, R. R. (1986). *BS 476 Part-8:1986. (1986). Fire tests on two slim floor assemblies*. British Standards Institution

[7]   The steel construction institute. (2008). *Report to corus CSD, slimflor comendium, Document RT1147, Version 01*. The steel construction institute, Berkshire.

[8]   Alam, N., Nadjai, A., Ali, F., & Nadjai, W. (2018). *Structural response of unprotected and protected slim floors in fire*. Journal of Constructional Steel Research, 142, pp.44–54. Available at: http://dx.doi.org/10.1016/j.jcsr.2017.12.009

[9]   Maraveas, C., Swailes, T. & Wang, Y., (2012). *A detailed methodology for the finite element analysis of asymmetric slim floor beams in fire*. Steel Construction, 5(3), pp.191–198.

[10]   Alam, N., Nadjai, A., Ali, F., Vassart, O., Hanus, F. (2019). *A detailed investigation on thermal behaviour of slim floor beams with web openings at elevated temperatures*. Journal of Structural Fire Engineering.

[11]   Zaharia, R. & Franssen, J.M., (2012). Simple equations for the calculation of the temperature within the cross-section of slim floor beams under ISO Fire. Steel & Composite structures, 13(2), pp.171–185.

[12]   European Committee for Standardization (2009), *BS EN 1993-1-2 Eurocode 3: Design of steel structures, Part 1-2, General rules – Structural fire design*. European Committee for Standardization.

[13]   Alam, N., Nadjai, A., Maraveas, C., Tsarvdaridis, K., & Kahanji, C. (2018). *Effect of air-gap on response of fabricated slim floor beams in fire*. Journal of Structural Fire Engineering. Available at: http://dx.doi.org/10.1108/jsfe-04-2018-0011

[14]   British Standards Institution. (1987). BS 476 Part-20:1987. (2012). *Fire tests on building materials and structures. Method for determination of the fire resistance of elements of construction (general principles)*.

[15]   ABAQUS (2018), *Finite Element Modelling Programme and Standard User's Manual*. Version 6.14. SIMULIA.

[16]   Alam, N., Nadjai, A., Maraveas, C., Tsavdaridis, K. D., & Ali, F. (2018). *Response of Asymmetric Slim Floor Beams in Parametric-Fires*. Journal of Physics: Conference Series, 11-07, p. 032009

[17]   Alam, N., Nadjai, A., Ali, F., Vassart, O., Hanus, F. (2018). Experimental and analytical investigations on thermal performance of slim floor beams with web openings in fire. SiF 2018– The 10th International Conference on Structures in Fire, FireSERT, Ulster University, Belfast, UK, June 6-8, 2018.

[18]   Eurocode 4: EN 1994-1–2: (2014). *Design of composite steel and concrete structures - General rules — Structural fire design*. European Committee for Standardization, Vol. 3.

[19]   European Committee for Standardization (2009), BS EN 1991-1-2, *Eurocode 1 – Actions on structures – Part 1–2: General Rules –Structural Fire Design,* European Committee for Standardization.

CONSOLIDATED FIRE ANALYSIS - A COUPLED EXPERIMENTAL AND NUMERICAL FRAMEWORK FOR THE ANALYSIS OF STEEL STRUCTURES SUBJECTED TO FIRE

Reto Grolimund, Mario Fontana

Institute of Structural Engineering, ETH Zurich, Zurich,Switzerland

ABSTRACT

The global behaviour of a small-scale steel structure subjected to a compartment fire scenario is assessed in a consolidated fire analysis (CFA). CFA allows for integration of physically tested components into a thermo-mechanical finite element model in such a way that the physically tested components constitute a part of finite element model. With full-scale specimen, the method promises to produce results equivalent to full-scale fire tests at significantly lower costs. A CFA framework is introduced that enables the first analysis of the non-linear dynamic load redistribution process of a structure in response to fire by means of interchanging static and pseudo-dynamic solution procedures. A comparison of successful CFA results and a finite element analysis of the test is presented. The comparison indicates that thermal creep influences CFA markedly and that a real-time framework is needed to capture thermal creep in dynamic analysis.

1   INTRODUCTION

To assess the global behaviour of structures in fire, recent research efforts aim to develop coupled experimental-numerical testing methods. In hybrid fire tests or consolidated fire analyses (CFA), the investigated structure is partitioned into a simulated numerical substructure (NS) and an experimentally tested physical substructure (PS). A computational-experimental framework consolidates the NS and PS to one interacting structural model that can be subjected to thermal and mechanical loads. CFA promises to give insights into the global response of structures to fire that are equivalent to large-scale fire experiments.

Advanced dynamic hybrid simulation frameworks can simulate the mechanical response of structures to earthquakes by means of implicit and explicit dynamic solution procedures in real-time, faster than real-time or slower than real-time (pseudo-dynamic). The NS and the load scenario are modelled in a finite element (FE) software. In course of an analysis, the FE solver accesses the PS similar to a finite element. In the experimental setup, loads or displacements are imposed automatically to the PS and the corresponding deformations or reactions are fed back to the solver. CFA is an adoption of the hybrid simulation method. In addition to the mechanical degrees of freedom (DOF), a CFA framework allows to control the temperature of the PS. To date, only few CFA frameworks have been proposed (e.g. [1-5]). In these reported CFA, structures that deform slowly in response to fire were analysed, which facilitated new developments. Also, except for [4], who used a dynamic solution procedure, only static solution procedures were selected in the frameworks. However, thermally induced stability problems or single bolt failures in connections can lead to temporary dynamic behaviour, without leading to global failure of the structure. To improve the understanding of the global behaviour in fire, it is therefore desirable to simulate the dynamic load redistribution that follows the failure of a single structural component.

For that reason, a framework that was developed for CFA of tensile steel elements at ETH [5], has been extended to analyse the dynamic response of a steel structure to fire [6]. The extended CFA framework incorporates Abaqus/Standard 6.11 as FE software and unifies the advantages of static and dynamic solution procedures. The paper introduces the framework and presents results of a

CFA of the dynamic load redistribution of a steel structure due to thermal buckling. The results agree well with the results of an FE-analysis. A reasonable explanation for the remaining deviations is presented. The comparison of numerical and experimental results allows concluding that CFA enables to capture the structural behaviour well. The presented extensions of the CFA framework represent a valid approach and the repeatability of CFA promises to enable cost efficient parameter studies.

2   CONSOLIDATED FIRE ANALYSIS FRAMEWORK

In a CFA, to capture dynamic effects correctly, incremental dynamic solution procedures must be applied. However, to profit from the robustness of static solution procedures for analysis of the usually slow thermal deformations, a multi-solver approach is proposed. The multi-solver approach in the presented framework enables CFA with an incremental static solution procedure and with an implicit dynamic solution procedure that both use Newton's method for iteration in the increments. According to the requirements from the structural response, the developed framework automatically selects the solution procedure, based on predefined thresholds.

2.1   Control Architecture
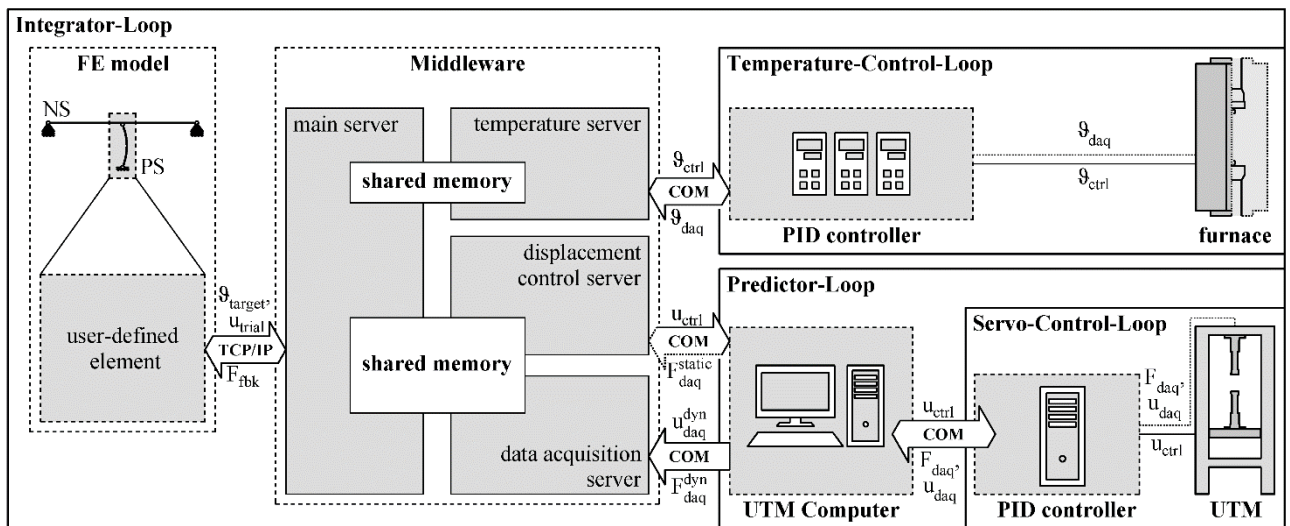
Fig. 1. Schematic overview of the CFA framework control architecture, the middleware and the communication interfaces.

Fig. 1 displays a schematic overview of the control architecture, the communication channels and the hardware components in the framework. The *servo-control-loop* is the innermost loop for control of the mechanical DOF. It consists of the PID controller that adjusts the crosshead position of a Zwick Roell 1484 AllroundLine universal testing machine (UTM). The controller is connected via a serial interface (COM) to the *predictor-loop* that consists of a customised control software provided by the UTM manufacturer and that runs on a separate computer. The software facilitates the coupling of the UTM and the middleware. The *predictor-loop* is connected via COM to the *integrator-loop*. This outermost control loop consists of a computer that runs the FE-software Abaqus/Standard 6.11 and the newly developed middleware that manages the CFA. The FE software and middleware communicate with each other over a TCP port. The three aforementioned control loops form a three-loop control architecture, as established in dynamic hybrid simulation. In addition to this traditional three-loop architecture, a *temperature-control-loop* is connected to the *integrator-loop*, also via COM. It consists of three PID controllers that control the heating coils of a Könn STE-12 HR/350 electrical split-tube furnace.

The developed CFA framework enables simultaneous control of thermal and kinematical DOF in the PS by means of the furnace and UTM, respectively. However, whereas the software that runs the predictor-loop enables to use the UTM inherent PID control system, it also represents the bottleneck in the presented control framework as it limits the control signal frequency to about 10 Hz. Consequently, in the presented application, only the static procedure can be performed in real-time, whereas the dynamic procedure is run pseudo-dynamically, 500 times slower than real-time.

2.2 Solution Process and Middleware

The middleware developed by [5] was extended to handle static and dynamic solution procedures in a CFA. In the middleware, the control of the CFA is distributed to four independent processes (*Fig. 1*) that are best introduced by means of a numerical solution procedure. First, note that a direct FE solver starts each static or dynamic solution increment by enforcing the prescribed boundary conditions (e.g. temperature) to all elements, including the PS. Subsequently, the solver iteratively finds the solution of the incremental equilibrium equation, given the imposed incremental boundary conditions.

During the solution process, a user-defined element (UEL) represents the PS in the Abaqus model and communicates with the main server process of the middleware. Each time, the UEL (and thus the PS) is called, target temperatures ϑ_{target} and trial displacements u_{trial} are sent from the UEL to the main server. The main server returns force feedback F_{fbk} of the PS corresponding to the current ϑ_{target} and u_{trial}. The main server stores the temperature commands in a shared-memory with the temperature server. The temperature server generates continuous temperature control signals ϑ_{ctrl} for the furnace controller and provides current specimen temperatures ϑ_{daq} to the main server through shared memory. In each new increment, the main server only allows to start the mechanical iteration procedure, when the incremental target temperature (i.e. an incremental boundary condition) is reached in the specimen.
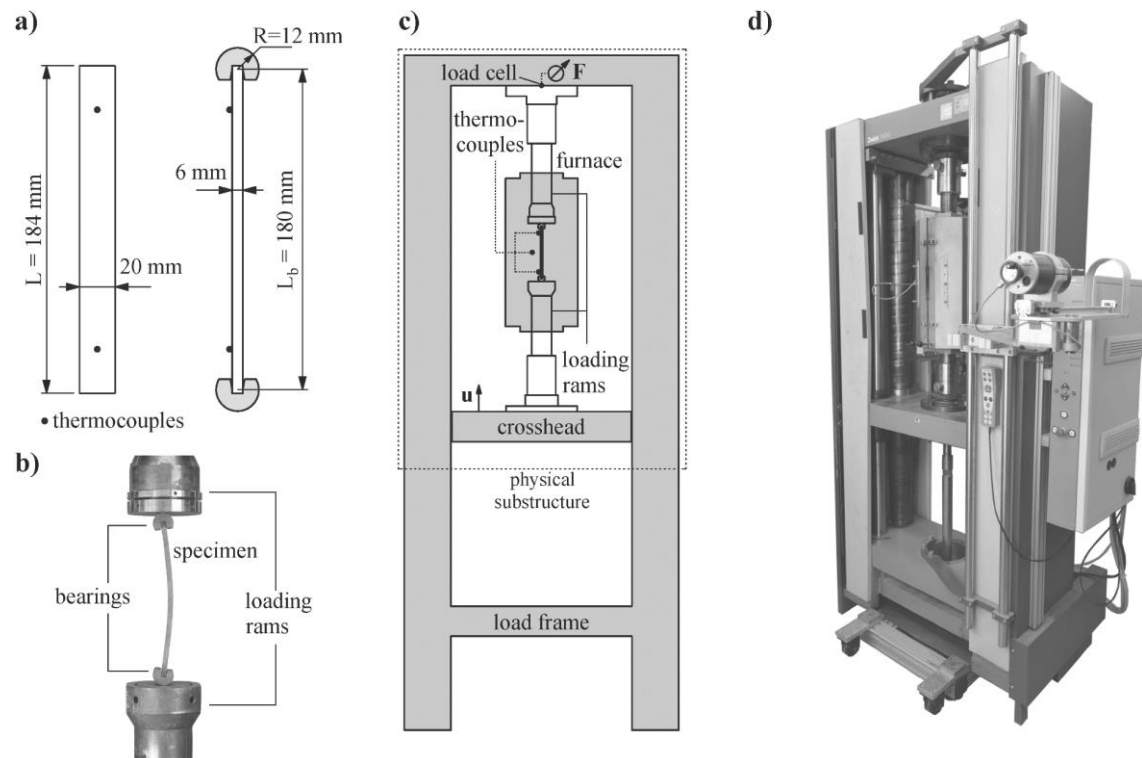
Fig. 2. a) Dimensions of steel specimen and roller bearings; b) close-up of installed steel specimen; c) schematic overview of universal testing machine (UTM) and furnace; d) UTM with furnace

In a static solution procedure, each iterative trial displacement that is larger than a threshold of 1.5 μm is imposed to the PS by adjustment of the crosshead position. The displacement control server forwards the trial displacement as control signal u_{ctrl} to the UTM computer and waits for the static force feedback $F_{daq,static}$. $F_{daq,static}$ is returned to the main server, where it is used to extrapolate the force in the PS according to the procedure proposed in [5]. If the mentioned threshold is not reached, the crosshead remains still and the force response is extrapolated from the previous displacement. For all extrapolations of forces, the initial stiffness of the PS is used.

In an implicit dynamic solution procedure, the main server stores all u_{trial} to the shared memory with the displacement control server as well. However, in the dynamic procedure, the displacement control server numerically interpolates a second order polynomial that describes the crosshead position based on the four latest converged displacements and corresponding times. The polynomial coefficients and a time reference are sent to the UTM control computer for signal generation. Simultaneously, the data acquisition server numerically fits two second order polynomials through the 10 latest displacement $u_{daq,dyn}$ and force $F_{daq,dyn}$ readings and corresponding acquisition times. Utilising these two polynomials, the force feedback F_{fbk} that corresponds to u_{trial} is obtained without physical iterations on the PS, employing the iteration strategy presented by [7]. More information about the implementation of the developed middleware and the control sequences is given in [6].

2.3 Experimental Setup and Physical Substructure

Fig. 2 gives an overview over the experimental setup used to apply and measure loads on the PS. *Fig. 2a* displays the dimensions of the used steel specimen and the heat resistant circular bearings. The buckling length of the specimen equals $L_b = 180$ mm and is given by the distance between the centres of the two bearings. Two loading rams allow imposing axial loads on the steel specimen

inside the heating chamber of the furnace (see *Fig. 2c*). When buckling occurs, the specimen rolls sideways (*Fig. 2b*), while the circular bearings ensure vertical load imposition on the two pinned ends. Because the trial displacements are imposed by adjusting the crosshead position, the PS consists not only of the steel specimen, but also of the temperature resistant loading rams and bearings, which is indicated in *Fig. 2c*. A load cell at the upper end of the load frame measures the specimen force. The photography in *Fig. 2d* shows how the electrical furnace and UTM are arranged in the laboratory.

Two K-type thermocouples fixated by steel clamps at the upper and lower parts of the specimen (*Fig. 2a*) are used to measure the specimen temperature. An N-type thermocouple introduced through the furnace mantle measures the air temperature in the centre of the heating chamber.

3   CASE STUDY
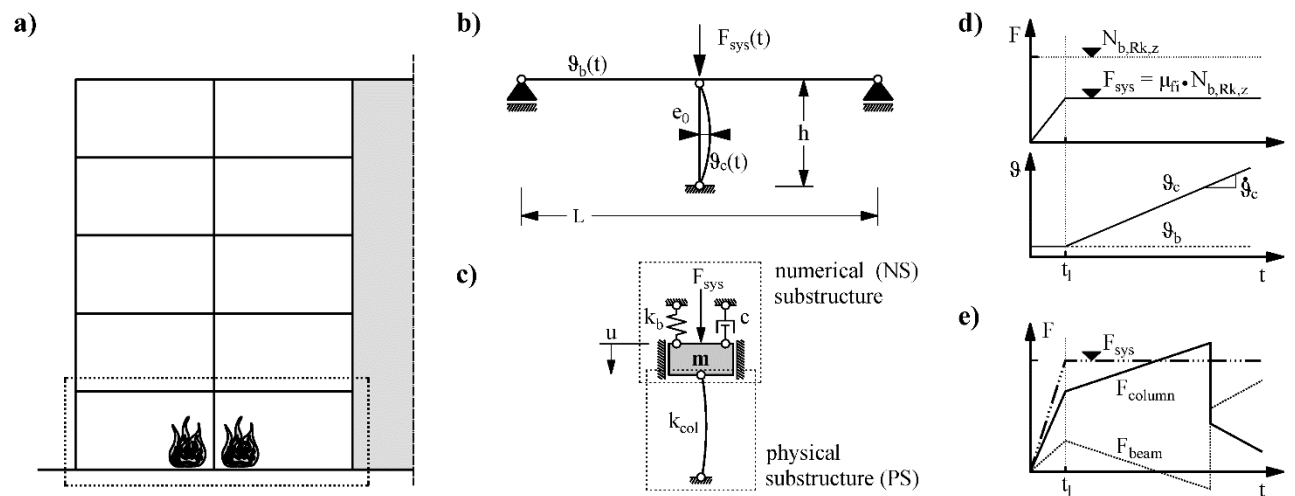
Fig. 3. a) Steel building with compartment fire; b) investigated substructure; c) simplified model of investigated substructure; d) mechanical and thermal load protocols, respectively; e) expected force distribution over time of column and beam

3.1 Problem Statement

By means of the developed CFA framework, the behaviour of the exposed part of a steel structure in a compartment fire scenario is analysed (*Fig. 3a*) in small-scale. The dimensions of the simplified structure illustrated in *Fig. 3b,* are selected according to the limitations provided by the UTM (*Fig. 2a*). The upper storey loads are imposed as a concentrated force above the analysed column. The column with nominal buckling resistance of $N_{b,fi,t,Rd} = 11,546$ N at the beginning of fire, is loaded to a factor of utilisation in the case of fire of $\mu_{fi} = 0.51$ ($F_{sys} = 5,890$ N). In dynamic analysis, a lumped mass of $m = 600$ kg provides inertia at the load imposition point. It corresponds to F_{sys} divided by the gravitational constant. A dashpot ($c = 16,720$ N s m^{-1}) provides $\xi = 5\%$ of critical viscous damping at ambient temperature to simulate structural damping. The beam is simplified as linear elastic spring (*Fig 3c*) providing a beam to column stiffness ratio of 5%. The thermal and mechanical load protocols displayed in *Fig. 3d* simplify a realistic scenario: In a construction phase up to t_1, the structure is gradually loaded to F_{sys} at ambient temperature. Subsequently, the column temperature is linearly increased at a rate of 15°C min^{-1}, whereas the beam remains at ambient temperature.

Fig. 3e shows the expected distribution of F_{sys} to beam and column in course of the analysis. In the construction phase, the load is shared according to the stiffness distribution. During the temperature increase, the column expands thermally but is restrained by the beam. Because of material

159

degradation and the increased load due to axial restraint, the column eventually buckles. Consequently, the load redistributes according to the remaining bearing capacity of the buckled column and the deflected beam. The redistribution process is expected to be dynamic.

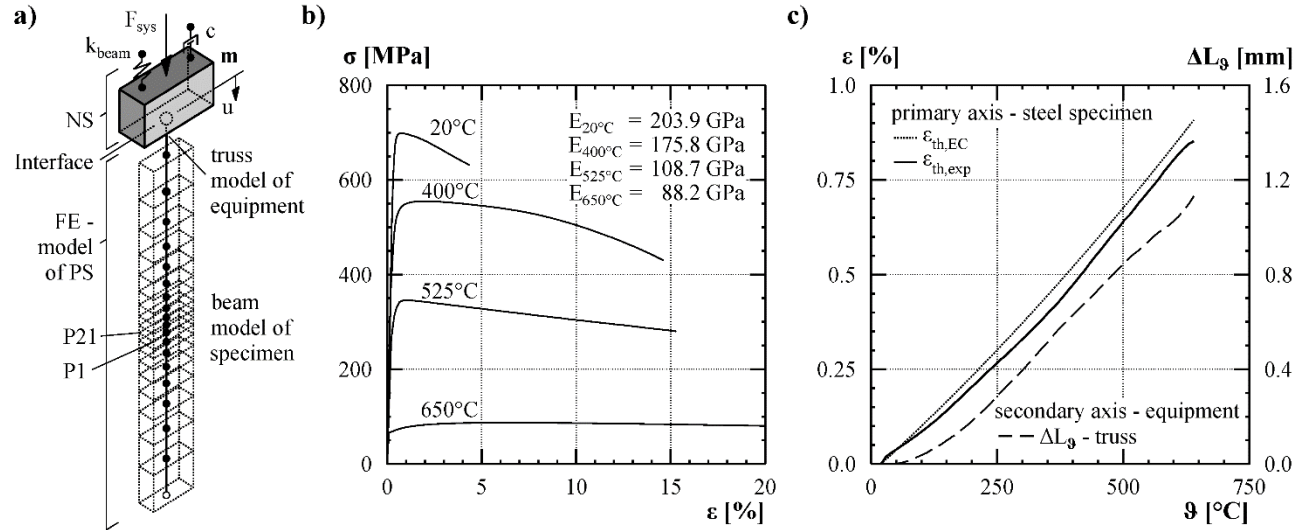## 3.2 Physical Substructure and FE-Model of Physical Substructure

Fig. 4. a) FE-Model of the investigated structure; b) experimentally derived stress-strain relationships of the specimen material at different temperatures; c) experimentally derived thermal expansion strains

In the CFA, the PS consists of the loading rams and the steel specimen as denoted in *Fig. 2c*. Before the start of the CFA, the stiffness of the PS representing the column was experimentally determined as $k_{col} = 44.21$ kN mm^{-1} and the imperfection of the steel specimen was measured as $e_0 = 0.01$ mm.

For verification of the CFA results, the CFA is replicated by the FE model illustrated in *Fig. 4a.* Euler-Bernoulli beam elements and a truss element represent the steel specimen and loading rams, respectively.

The beam elements have different lengths of 4 mm (column center) to 20 mm (upper and lower ends) to reduce longitudinal oscillation-modes in the simulation, while still accurately capturing the plastic hinge. The measured geometric imperfection is enforced to the numerical specimen, in the shape of the lowest elastic buckling mode. The material properties of the utilised steel were derived by three tensile material tests at 20°C and two tests each at 400°C (creep becomes relevant [8]), 525°C and 650°C (maximum temperature for loading rams) using the setup and procedure of [9]. All material tests were performed with a constant strain-rate of 0.5%/min. *Fig. 4b* shows the resulting mean data that were used as tabular input for the temperature dependent elasto-plastic material model in Abaqus. The thermal expansion law was derived during the heating phase of the tensile tests and is plotted against the primary axis in *Fig. 4c*. It correlates well with the thermal expansion model proposed in Eurocode. The loading rams and the crosshead are modelled by a 2-node truss element with a constant axial stiffness of $k_{machine} = 84.53$ kN/mm that was determined at ambient temperature in [6]. Preliminary measurements of the thermal expansion of the loading rams are used to generate an expansion law for the truss element, which is plotted against the secondary axis in *Fig. 4c*.

4   RESULTS AND DISCUSSION

Fig. 5 presents the summarised results of the FE-analysis and the CFA. The envelope in the upper left corner of *Fig. 5a* is derived from isothermal buckling tests of the FE-model of the PS (see

Fig. 4a) as follows: First, the model of the PS (specimen and loading rams) is heated and left to expand freely. Next, at the test temperatures, a displacement controlled buckling test of the specimen is performed. In *Fig. 5a,* the numerical buckling tests at 525°C and 650°C are shown with thin dotted lines and their respective free thermal elongations are indicated. The said envelope connects the maxima of these curves. A load state above the envelope is not possible and any load state on the envelop leads to global buckling of the PS.

According to the load protocol, the structure is loaded with F_{sys} at ambient temperature in $t_1 = 100$ s, as can be seen in the force time-histories in *Fig. 5b*. Points A in *Fig. 5* mark the end of this analysis step. The load is distributed to the beam and column according to the initial stiffness distributions. Next, the temperature ramp is started. Consequently, the column expands and the axial load increases due to the restraint provided by the beam. Because the beam and column remain in equilibrium with the imposed load, the load path of the column (*Fig. 5a*) is bound to a straight line with gradient $-k_{beam}$ during the expansion and $F_{beam} + F_{col} = F_{sys}$. In the FE-model, global buckling occurs at 588°C, exactly when the load path of the column reaches the envelope (points B in *Fig. 5*). In the CFA, the PS buckles at 534.5°C.

Once the buckling load is reached, the column resistance decreases with increasing deflection u (softening behaviour with negative tangent stiffness) and the combined resistance of beam and column is temporarily lower than the imposed load $F_{beam} + F_{col} < F_{sys.}$. The system becomes a statically instable mechanism: the mass accelerates, damping and inertia forces develop and the column deforms plastically. In the FE-model, the load path of the PS follows exactly the pushdown curve of the PS at 561°C during buckling, until the restoring forces stop the plastic deformation and the mass diminishingly oscillates about a new equilibrium point (point C). The CFA shows a lower buckling resistance, but a significantly higher resistance during the buckling process. Thus, less kinetic energy develops and the amplitudes of the oscillations after buckling remain smaller. In the FE analysis, after the load transition, the mass oscillates on a nearly linear curve in *Fig. 5a*, which represents the reduced post buckling stiffness of the column. In the CFA, a continuing degradation of the column resistance during the oscillations is observed. Once the oscillations stop, the column gradually softens due to the increasing temperature and the load redistributes to the beam in a slow process.

In the CFA, to explain the higher resistance of the PS during buckling (i.e. between points B and C) compared to the FE analysis, the way of the derivation of the material properties gives an indication. The tensile tests were performed at a constant strain rate of 0.5% min^{-1}. However, according to the FE-analysis, the buckling process takes place in less than a second. The maximum strain rates of two section points marked in *Fig. 4a* are visualised in *Fig. 5d* that shows the history of total strains. Strain rates of up to 38% s^{-1} develop in the plastic hinge. In the CFA, because the dynamic step was performed 500 times slower than real-time, strain rates of up to 4.56% min^{-1} were to be measured during buckling, which is about 9 times faster than the material input data. [8] showed that mild steel at temperatures above 400°C provides a significantly higher resistance in the plastic state at higher strain rates, presumably due to creep and relaxation. Also, in accordance with the conclusions drawn by [10] about the behaviour of restraint steel beams subjected to fire, creep buckling would explain the lower buckling load of the specimen.
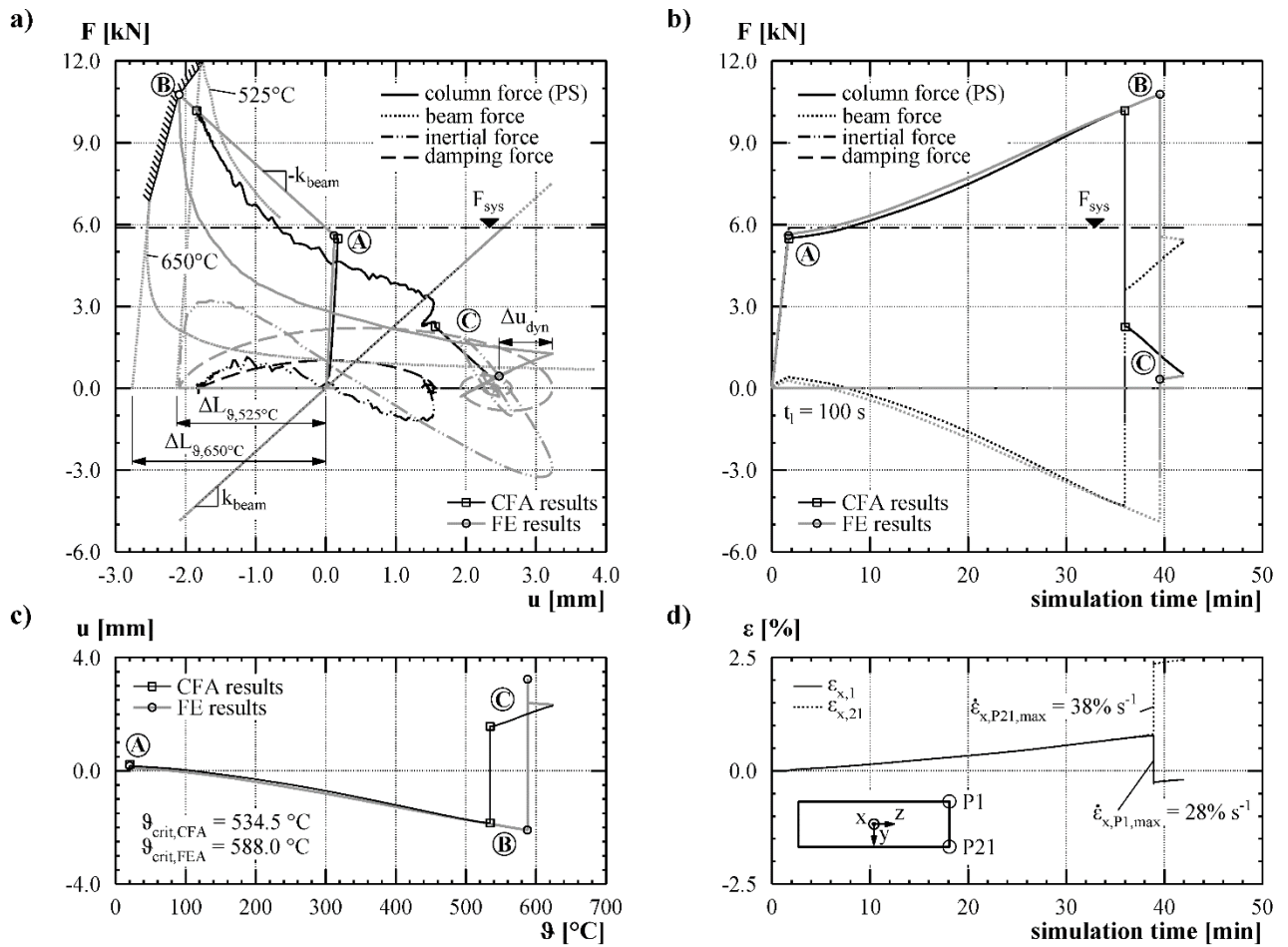
Fig. 5. Analysis results of FE-analysis and of CFA: a) force time-histories; b) force-displacement diagram; c) time-history of axial strains in denoted section points; d) temperature-deflection curves

Fig. 5c displays the deflections against the temperatures. The predicted and measured behaviour is similar up to the buckling temperatures that differ by 26.5°C. After buckling, i.e. after point C, in the CFA, the deformations of the PS instantly increase with increasing temperatures, whereas in the FE analysis, they remain constant. This follows from the mass overshooting the static equilibrium position by $\varDelta u_{dyn}$ in the FE-simulation (*Fig. 5a*). Consequently, after the oscillations, the simulated column remains in an elastically unloaded state and provides a positive stiffness. Because the temperature continuously increases, the column material degrades further. However, simultaneously thermal expansion increases the column length, which results in a nearly constant beam deflection until the column once more reaches a plastic state. This behaviour is not observed in the CFA, because the dynamic overshoot is practically zero due to the higher column resistance during buckling.

The comparison of results indicates that the developed CFA framework is suitable for analysis of the highly non-linear load redistribution process of a restraint steel column that buckles due to a compartment fire. The results of both methods show a similar characteristic structural behaviour of the investigated system. High temperature creep is a possible explanation for the small deviations between the FE analysis and CFA results. However, to capture thermal creep correctly in fast processes, a real-time dynamic CFA framework must be developed. For that purpose, the mechanical control of the CFA framework should be built, according to state of the art dynamic hybrid simulation frameworks.

5   SUMMARY, CONCLUSIONS AND OUTLOOK

In recent years, several consolidated fire analyses (CFA) revealed the potential of the hybrid simulation method in fire safety engineering to gain better understanding of the global structural response to fire. A CFA framework with an extended three-loop architecture that allows to perform static and pseudo-dynamic CFA with Abaqus/Standard 6.11 is introduced. The temperature transient, non-linear dynamic load redistribution process of a small-scale steel structure in a compartment fire scenario is assessed successfully with the developed CFA framework and the following conclusions are drawn:

- A finite element (FE) model with experimentally derived material properties of the physical substructure (PS) of the small-scale steel structure delivers results that are similar to the CFA results.
- The comparison of results of the CFA and the FE-model indicates that the CFA captures thermal creep effects that are not covered by the material input data of the FE-model. High temperature creep effects are a probable reason for the deviations of the obtained results.
- To capture the effect of thermal creep on the dynamic global response of a steel building to fire, a CFA framework that is capable to control a furnace and actuators in real-time during the fast deformations of an experimental substructure in the moment of buckling or local failure is needed.

The development of a real-time CFA framework will be covered in a future research project.

REFERENCES

[1]   Kiel M. (1989). *Entwicklung einer intelligenten Prüfmaschine für brandbeanspruchte Gesamttragwerke.* Braunschweiger Brandschutz-Tage 1989, Braunschweig, Germany, 6-7 September 1989, pp 51–62.

[2]   Korzen M., Magonette G., Buchet Ph. (1999). *Mechanical Loading of Columns in Fire Tests by Means of the Substructuring Method.* Journal of Applied Mathematics and Mechanics 79 (1999). 617–618 pp.

[3]   Mostafaei H. (2013). *Hybrid fire testing for assessing performance of structures in fire—Application.* Fire Safety Journal 56 (2013). doi:10.1016/j.firesaf.2012.12.003, 30–38 pp.

[4]   Whyte C., Mackie K., Stojadinovic B. (2016). *Hybrid Simulation of Thermomechanical Structural Response.* Journal of Structural Engineering (2016). doi:10.1061/(ASCE)ST.1943-541X.0001346.

[5]   Schulthess P., Neuenschwander M., Knobloch M., Fontana M. (2015). *Consolidated Fire Testing - A Framework for Thermo-Mechanical Modelling.* Coupled Problems, Venice, Italy, 18-20 Mai 2015, 8 pp.

[6]   Grolimund R. (tbp 2019). *A Consolidated Fire Analysis Framework for Steel Columns in Fire.* Doctoral Thesis, NR…,ETH Zurich, Switzerland. – *to be published 2019*

[7]   Mosqueda G., Ahmadizadeh M. (2009). *Implicit Numerical Integration in Hybrid Simulation with Iteration Strategy for Experimental Substructures.* American Control Conference, St. Louis, USA, 10-12 June 2009, 6 pp.

[8]   Knobloch M., Pauli J., Fontana M. (2013). *Influence of the strain-rate on the mechanical properties of mild carbon steel at elevated temperatures.* Materials & Design 49 (2013). doi: 10.1016/j.matdes.2013.01.021, 553–565 pp.

[9]   Neuenschwander M., Knobloch M., Fontana M. (2017). *Elevated temperature mechanical properties of solid section structural steel.* Construction and Building Materials 149 (2017). doi:10.1016/j.conbuildmat.2017.05.124, 186–201 pp.

[10]   Kodur V., Dwaikat M. (2010). *Effect of high temperature creep on the fire response of restrained steel beams.* Materials and Structures 43 (2010). doi:10.1617/s11527-010-9583-y, 1327–1341 pp.

FIRE PERFORMANCE OF LIGHT GAUGE STEEL FRAMED WALLS LINED WITH DIFFERENT WALLBOARDS

Sayilacksha Gnanachelvam, Anthony Ariyanayagam and Mahen Mahendran*

Queensland University of Technology (QUT), Brisbane, Australia

ABSTRACT

The use of light gauge steel framed (LSF) walls has increased recently, especially in low and mid-rise building constructions. Their fire performance has gained significant attention due to many recent fire hazards. Wallboards used in these LSF walls shield the internal steel frame from adverse effects caused by fires. Although different types of wallboards are used for this purpose, their performance in fire remains largely unknown. This paper investigates the fire performance of magnesium sulphate, gypsum plasterboard, magnesium oxide and calcium silicate boards in LSF walls. A series of standard fire tests was conducted on non-load bearing LSF walls lined with these four types of wallboards. Experimental results are presented in the form of time-temperature profiles and fire resistance ratings. Overall, significant variations in fire performance were observed for these LSF walls.

1   INTRODUCTION

Light gauge steel framed (LSF) wall systems are widely used as load bearing or non-load bearing elements in the construction industry. They are made of cold-formed steel (CFS) studs and lined with different types of wallboards. Fire safety has become one of the most important parameters in building design due to recent fire incidents such as Dubai 75-storey apartment block fire in 2016, London Grenfell tower fire in 2017, Bur Dubai building fire in 2018 and Melbourne apartment complex fire in 2019. In Australia, building elements should have specific fire resistance as required by the National Construction Code (NCC). Fire resistance of load bearing elements is measured under three failure criteria, structural adequacy, integrity and insulation, whereas it is measured under two criteria, integrity and insulation, for non-load bearing elements [1]. Structural adequacy is the ability of an element to withstand the required load whereas integrity is the ability to resist flames and hot gases from fire side to ambient side in a fire. Insulation failure is the ability of the ambient side to maintain the temperature below a specified limit, which is 140 °C on average or 180 °C at any point (maximum temperature of the ambient side) above the room temperature.

Failures of steel studs are caused in load bearing LSF walls exposed to fire, due to the reduction in mechanical properties of CFS studs at elevated temperatures [2]. These structural failures are delayed by wallboards as they act as fire protective layers and delay the temperature rise in studs. Fire rated gypsum plasterboards are commonly used as wallboards in LSF wall systems. Pure Gypsum, known as Calcium sulphate di-hydrate ($CaSO_4 \cdot 2H_2O$), consists of Calcium sulphate with 4–5% of free water and 15–18% of chemically bound water by weight [3, 4]. Many researchers have studied the fire performance of different LSF wall systems lined with gypsum plasterboards [5-7]. However, different types of wallboards are introduced and used in building construction due to their improved physical and thermal properties for impact resistance, acoustic and sound insulation, moisture resistance, lightweight and cost-effectiveness. Wallboards such as calcium silicate board, magnesium oxide board, phase change material added plasterboards, fibre cement board and magnesium sulphate board are some of them. Fire performance of LSF walls lined with

calcium silicate board, magnesium oxide board and phase change material added plasterboards incorporated LSF wall systems has been investigated and the results are presented in [8-10].

Magnesium oxide boards are currently replaced by magnesium sulphate boards, because of their observed lower fire performance and severe cracking caused by a higher mass loss at elevated temperatures [10]. Recently, calcium silicate board lining is increasingly used in LSF wall systems because of its improved physical and thermal properties [8, 11]. Also, the fire performance of many wallboards available in the market is unknown even though they are being used in LSF wall systems. In this study, the commonly used gypsum plasterboard, magnesium sulphate board, magnesium oxide board and calcium silicate board were selected as wallboards for LSF wall systems. Standard fire tests of non-load bearing walls lined with gypsum plasterboard and magnesium sulphate board were conducted and the results were compared with those available for calcium silicate board and magnesium sulphate board. The time-temperature profiles and insulation/integrity based failure times of all the LSF wall systems were measured and compared to identify the best performing LSF wall system. This paper presents the details of the above-mentioned fire test series and the results.

2 EXPERIMENTAL STUDIES

2.1 Test description

Standard fire tests were conducted for two non-load bearing LSF wall systems made of gypsum plasterboards and magnesium sulphate boards of 1.4 m width and 1.2 m height to study their fire performance according to AS 1530.4 [1]. LSF wall systems lined with these two types of boards were used in the tests with single layer of wallboard lining on both sides (see *Fig. 7*). Standard fire test results of magnesium oxide board and calcium silicate board lined LSF wall systems were obtained from Rusthi et al. [10] and Ariyanayagam and Mahendran [8], respectively. Details of the wallboards considered in this study are listed in *Table 1*.

Fig. 7. LSF wall system lined with single layer of board

Table 1. Test specimen details

Test no	Wallboard type	Wallboard thickness (mm)	Test details
1	Gypsum plasterboard	16	This study
2	Magnesium sulphate board	10	This study
3	Magnesium oxide board	10	Rusthi et al. [10]
4	Calcium silicate board	20	Ariyanayagam and Mahendran [8]

Thermocouple wires were attached to the test panels on fire side, fire side cavity, stud hot flange, stud cold flange, ambient side cavity and ambient side at three heights. They were then connected to a data logger to record the time-temperature profiles during the tests. Standard fire tests of 1.4 m x 1.2 m LSF wall panels were conducted in a gas furnace (*Fig.* 2). The external gas supply to the furnace was terminated when the ambient side temperature reached the limiting average or maximum insulation failure temperature or when an integrity failure was observed.

2.2 Experimental observations

Various observations were made during the standard fire test of each LSF wall system, such as water drops, discolouration and cracks on the ambient side, etc. Initial smoke was seen in the plasterboard fire test, which was due to the burning of the paper. Water drops were also seen due to dehydration. Discolouration was seen on the ambient side of the plasterboard without any cracks (see *Fig. 8*(a)). Discolouration and severe cracks were seen on the ambient side of the LSF wall panel lined with magnesium sulphate board. Cracks were mostly observed at screw locations as shown in *Fig. 8*(b). This might have occurred due to the restraint provided by screws after considerable shrinkage and mass loss of magnesium sulphate board.

Fig. 8. a) Discolouration on the ambient side gypsum plasterboard; b) Discolouration and cracks on the ambient side magnesium sulphate board, after the fire tests
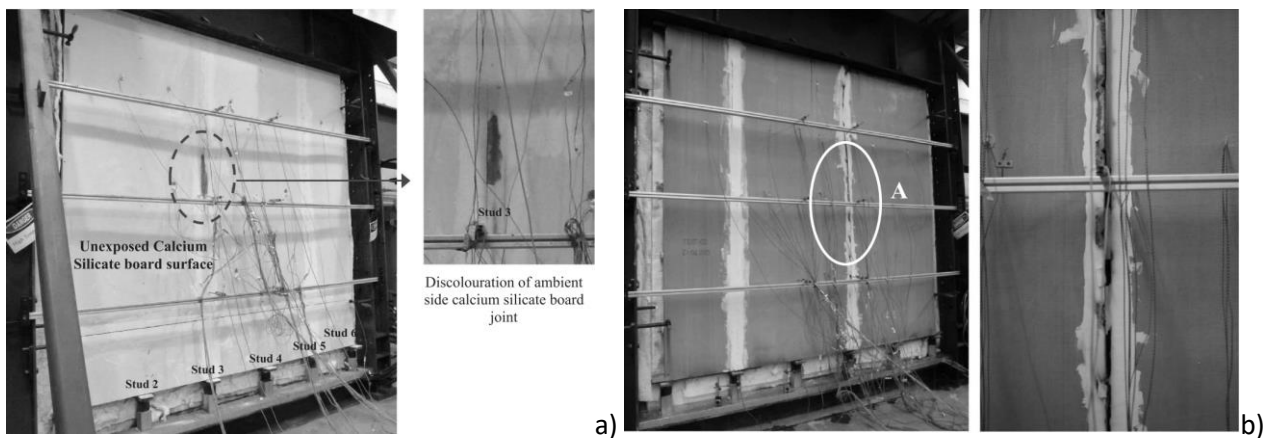
Fig. 9. a) Discolouration of the ambient side calcium silicate board; b) Vertical joint crack on the ambient side of magnesium oxide board, after the fire tests

No cracks were seen on the ambient side of the LSF wall lined with calcium silicate boards. There was no significant discolouration on the ambient side wallboard other than at the board joint as shown in *Fig. 9*(a). Water vapour was seen in the initial stages of the fire test of magnesium oxide board lined LSF wall. Water dripping from the test panel was also seen and this was due to the condensation of evaporated water from the test panel. Discolouration was seen on the ambient side along the vertical stud joints, which developed vertical joint cracks as shown in *Fig. 9*(b).

2.3 Experimental results

2.3.1 Test-1 – Gypsum plasterboard lined LSF wall

Fig. 10 (a) shows the average time-temperature profiles for Test panel-1 with single layer of gypsum plasterboard on both sides. Fire side temperature agreed well with the standard fire curve

with a maximum deviation of 20 °C, which is well below the acceptable limit specified in AS 1530.4 [1]. Initially, the temperatures of all plasterboard surfaces were maintained at a constant value, which is less than 100 °C for a certain period of time, due to the dehydration process. Time taken to reach 100 °C was 10, 22 and 65 min for Fire side cavity, Ambient side cavity, and Ambient side, respectively. This observation is similar to that in Ariyanayagam and Mahendran [8]. Sudden increments were observed in the plasterboard temperatures after the dehydration process. However, the gradient of the temperature of the cavity surfaces reduced after 60 min and the difference between the two cavity surface temperatures was constant until the end of the test. The maximum fire side temperature of 1050 °C was achieved at 143 min. Insulation failure was observed at 82 min when the average ambient side temperature exceeded the limit of 168 °C, where the initial temperature was 28 °C. However, the test was continued until 140 min. *Fig. 10*(b) shows the average time-temperature profiles of hot and cold flanges (HF, CF) of studs. The maximum HF temperature was of 650 °C at 143 min while the maximum difference between HF and CF temperatures was 160 °C at 40 min.
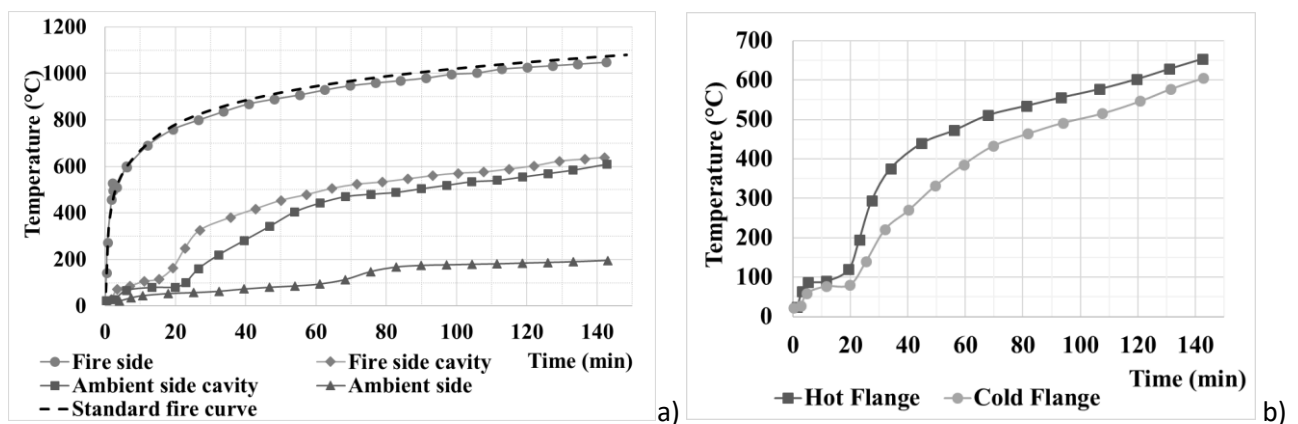
Fig. 10. a) Average gypsum plasterboard temperatures; b) Average stud (HF & CF) temperatures of Test-1

2.3.2   Test-2 – Magnesium sulphate board lined LSF wall

Fig. 11(a) shows the average time-temperature profiles for Test panel-2 lined with single layer of magnesium sulphate board on both sides. Fire side temperature of the test agreed with the standard fire curve within the limit specified in AS 1530.4 [1]. Temperatures of all the board surfaces showed continuous increments from the beginning to the end of the test and no temperature plateaus were observed in this test. The maximum fire side temperature of 850 °C was achieved at 44 min. Insulation failure was observed at 42 min when the average ambient side temperature exceeded the limit of 160 °C, where the initial temperature was 20 °C. The test was terminated at 44 min. *Fig. 11*(b) shows the average HF and CF time-temperature profiles of studs in Test panel-2. The maximum HF temperature of 550 °C was reached at 44 min while the maximum difference between HF and CF temperatures was 160 °C at 31 min.
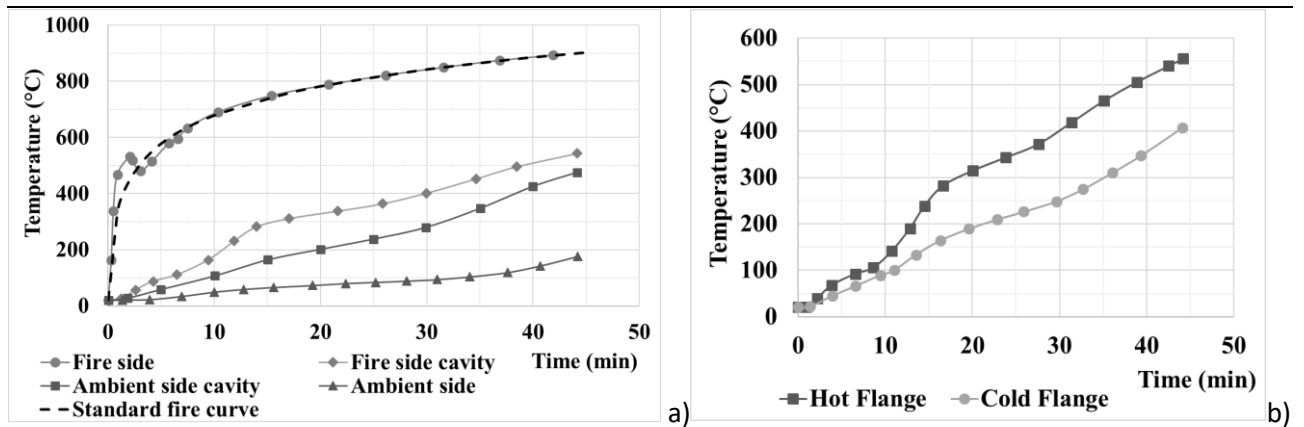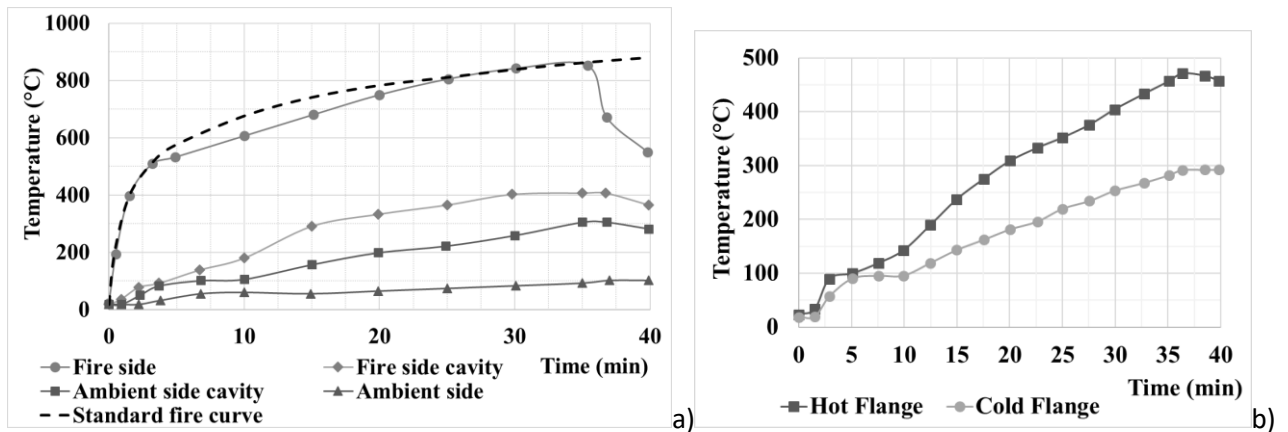
Fig. 11. a) Average magnesium sulphate board temperatures; b) Average stud (HF & CF) temperatures of Test-2

2.3.3   Test-3 – Magnesium oxide board lined LSF wall [10]

Fig. 12(a) shows the average time-temperature profiles for Test panel-3 lined with single layer of magnesium oxide board on both sides. Fire side temperature of the test agreed well with the standard fire curve within the limit specified in AS 1530.4 [1]. Initially, the temperatures on both sides of the ambient side magnesium oxide board layer were maintained at a constant value, which is less than 100 °C for a certain period of time. The maximum fire side temperature of 870 °C was reached at 35 min. The test was terminated at 35 min due to integrity failure. This was due to the widening of vertical cracks on the ambient side magnesium oxide board due to shrinkage and bowing. *Fig. 12(b)* shows the average HF and CF time-temperature profiles of studs in Test panel-3. The maximum HF temperature of 470 °C was achieved at 37 min while the maximum difference between HF and CF temperatures was 135 °C at 22 min.

Fig. 12. a) Average magnesium oxide board temperatures; b) Average stud (HF & CF) temperatures of Test-3

2.3.4   Test-4 – calcium Silicate board lined LSF wall [8]

Fig. 13(a) shows the average time-temperature profiles for Test panel-4 lined with single layer of calcium silicate board on both sides. Fire side temperature of the test had a maximum deviation of 50 °C from the standard fire curve, which is within the acceptable limit specified in AS 1530.4 [1]. Initially, the temperatures across the calcium silicate wall system were maintained at a constant value, which is below 100 °C for a 30 min period due to the dehydration process. This is supported by the water drops seen along the board edges. Sudden increments were observed in board temperatures (Fire side cavity and Ambient side cavity) after the dehydration process. However, the gradient of the cavity surface temperatures reduced after 80 min and continued to have constant difference until the end of the test. The maximum fireside temperature of 1000 °C was achieved at

140 min. Insulation failure was observed at 113 min when one of the thermocouples on the ambient side recorded the maximum temperature of 204 °C, where the initial temperature was 24 °C. However, the test was continued until 160 min. *Fig. 13(b)* shows the average HF and CF time-temperature profiles of studs. The maximum HF temperature was 600 °C at 160 min while the maximum difference was 150 °C at 60 min.
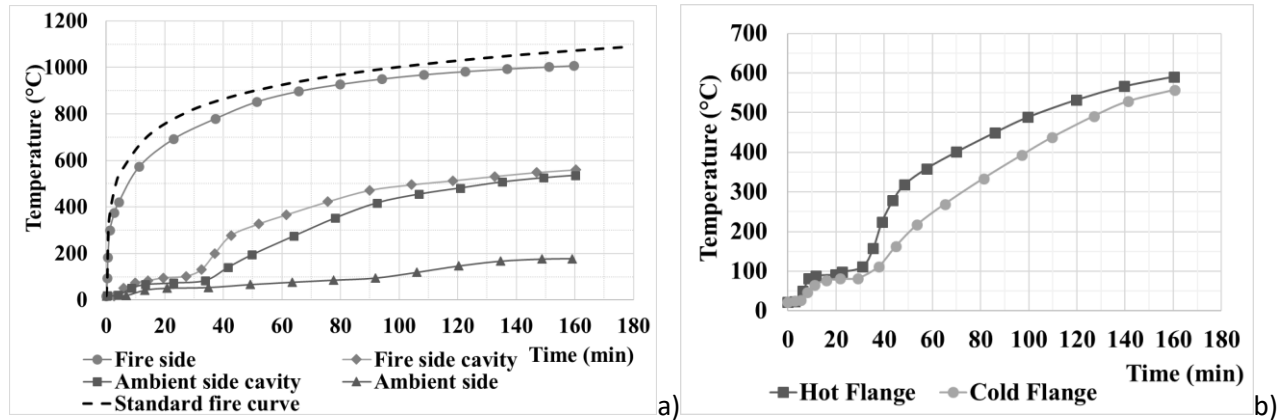
Fig. 13. a) Average calcium silicate board temperatures; b) Average stud (HF & CF) temperatures of Test-4

3   DISCUSSION

Table 2 provides a summary of fire test results in terms of failure times (fire resistance ratings based on insulation or integrity criterion) and hot flange temperatures after 30 min and at failure. Standard fire test results revealed that LSF wall lined with 20 mm calcium silicate board and 16 mm gypsum plasterboard exhibited some similar behavioural characteristics in fire, but the former provided higher fire resistance, partly due to higher thickness. The dehydration process in both calcium silicate board and gypsum plasterboard helps to maintain lower temperatures across the wall for a significant time period, which increases the wall's fire resistance. Further, no cracks were seen/visible on the ambient side of these wallboards attached to LSF walls. This might be due to their thickness and fibrous materials added. However, gypsum plasterboards exhibited discolouration on the ambient side plasterboards, whereas it was not visible in calcium silicate boards.

In contrast, LSF walls lined with 10 mm magnesium sulphate and magnesium oxide boards exhibited severe cracking with discolouration on the ambient side. Cracks were mostly observed at screw locations for magnesium sulphate board, whereas it was seen at the vertical board joints for magnesium oxide board. These cracks occurred due to the restraints provided by screws after shrinkage and heavy mass loss. As seen in *Table.2*, these two boards performed poorly despite higher expectations of their fire resistance ratings using such thinner boards, considered to be equivalent to the other thicker boards. The fire resistance ratings of non-load bearing LSF walls lined with magnesium sulphate and magnesium oxide boards can only be 30 min whereas those lined with gypsum plasterboard and calcium silicate board can be 60 and 90 min, respectively.

Table 2. Summary of fire test results

Test no	Wallboard type	Failure times (min)	Hot flange temperatures at Failure (°C)	Hot flange temperatures at 30 min (°C)	Failure time in min (Stud HF at 500 °C)
1	Gypsum plasterboard	82	530	330	62

2	Magnesium sulphate board	42	535	400	38
3	Magnesium oxide board	35	450	400	<40
4	Calcium silicate board	113	520	105	102

Although load bearing tests were not conducted in this study, past research has shown that the critical parameter for the fire resistance of LSF walls is the hot flange temperature of studs. From the measured hot flange temperatures in *Figs. 4(b) to 7(b)* and assuming a hot flange failure temperature of 500 °C for a load ratio of 0.4, structural integrity based fire resistance ratings of tested walls can be approximately predicted [12] and the results are given in Table 2. These predictions also show that load bearing magnesium sulphate and magnesium oxide board lined walls will have reduced fire resistance ratings compared to walls lined with other two boards. It is to be noted that two of the tests in this study were based on small scale panels and thus their results could have been slightly overestimated due to higher thermal bowing deformations.

4 CONCLUSIONS

This paper has presented the details and results of standard fire tests of non-load bearing LSF wall systems lined with four types of wallboards, gypsum plasterboard, magnesium sulphate board, magnesium oxide board and calcium silicate board. Fire resistance was determined based on insulation or integrity failure criterion. Findings from these standard fire tests are as follows.

- LSF wall lined with 20 mm thick calcium silicate board gave the highest fire resistance of 113 min under standard fire conditions based on insulation failure criterion.
- Fire resistance of 16 mm thick gypsum plasterboard lined LSF wall (82 min) was higher than that of walls lined with magnesium sulphate board and magnesium oxide board.
- Fire resistance of 10 mm magnesium sulphate board lined LSF wall was higher than that of LSF wall lined with magnesium oxide board of the same thickness. Unlike other boards, magnesium oxide board lined wall failed under integrity criterion.
- Severe cracks were seen on the ambient sides of LSF walls lined with magnesium sulphate boards and magnesium oxide boards, whereas no cracks were seen on the ambient sides of calcium silicate board and gypsum plasterboard lined LSF walls.

Structural adequacy based failure times were predicted based on the limiting hot flange temperatures, which showed that they are the lowest for magnesium sulphate board and magnesium oxide board lined LSF walls. The highest failure time is for calcium silicate board lined LSF wall.

REFERENCES

[1] Standards Australia (AS) AS 1530.4:2014, (2014) Method for fire test on building materials, components and structures, Part-4: Fire-resistance test of elements of construction, Sydney, Australia.

[2] Kankanamge N.D., Mahendran M. (2011) *Mechanical properties of cold-formed steels at elevated temperatures.* Thin-Walled Structures 49 (1) (2011). pp 26-44.

[3] Thomas G. (2002) *Thermal properties of gypsum plasterboard at high temperatures.* Fire and Materials 26 (1) (2002). pp 37-45.

[4] Wakili K.G., Hugi E., Wullschleger L., Frank T.H. (2007) *Gypsum Board in Fire-Modeling and Experimental Validation.* Journal of Fire Sciences 25 (2007). pp 267-282.

[5]   Feng M., Wang Y.C. (2005) *An experimental study of loaded full-scale cold-formed thin-walled steel structural panels under fire conditions.* Fire Safety Journal 40 (1) (2005). pp 43-63.

[6]   Kodur V.K.R., Sultan M.A. (2006) *Factors Influencing Fire Resistance of Load-bearing Steel Stud Walls.* Fire Technology 42 (1) (2006). pp 5-26.

[7]   Nassif A.Y., Yoshitake I., Allam A. (2014) *Full-scale fire testing and numerical modelling of the transient thermo-mechanical behaviour of steel-stud gypsum board partition walls.* Construction and Building Materials 59 (2014). pp 51-61.

[8]   Ariyanayagam A.D., Mahendran M. (2017) *Fire tests of non-load bearing light gauge steel frame walls lined with calcium silicate boards and gypsum plasterboards.* Thin-Walled Structures 115 (2017). pp 86-99.

[9]   Gnanachelvam S., Mahendran M., Ariyanayagam A., Keerthan P. (2018) *Thermal characterisation and fire performance of phase change material incorporated plasterboards*. 10th International Conference on Structures in Fire, Belfast, Northern Ireland, 6-8 June 2018.

[10] Rusthi M., Ariyanayagam A., Mahendran M., Keerthan P. (2017) *Fire tests of Magnesium Oxide board lined light gauge steel frame wall systems.* Fire Safety Journal 90 (2017). pp 15-27.

[11] Wang Y., Chuang Y.-J., Lin C.-Y. (2015) *The Performance of Calcium Silicate Board Partition Fireproof Drywall Assembly with Junction Box under Fire.* Advances in Materials Science and Engineering 2015 (2015). pp 12.

[12] Gunalan S., Mahendran M. (2014) *Fire performance of cold-formed steel wall panels and prediction of their fire resistance rating.* Fire Safety Journal 64 (2014). pp 61-80.

EXPERIMENTAL INVESTIGATIONS ON THE SHEAR CAPACITY OF COMPOSITE DOWELS AT ELEVATED TEMPERATURES

[1]Peter Schaumann, [1]Patrick Meyer, [2]Martin Mensinger, [2]Suet Kwan Koh

[1]Institute for Steel Construction, Leibniz Universität Hannover. GERMANY

[2]Technical University Munich. GERMANY

ABSTRACT

Composite dowels are commonly used to ensure longitudinal shear in composite steel-concrete girders. While the shear capacity of composite dowels has been thoroughly investigated at room temperature, the influence of elevated temperatures on the shear capacity of composite dowel has not been quantified. To close this gap of knowledge, within a German research project a series of push-out tests have been performed to determine the shear capacity of composite dowels at elevated temperatures.

This paper presents experimental investigations on the shear capacity of composite dowels in clothoidal shape at room and elevated temperatures. The objective is to evaluate the influence of elevated temperatures on the shear capacity of composite dowels. The test results and the analysis of the local bearing mechanisms allow to justify the shear force-slip relation of the composite dowels.

1 INTRODUCTION

In a German research project, a composite slab system has been developed considering sustainability and economic efficiency. This integrated and sustainable composite slab system, called *InaDeck*, consists of a prestressed concrete slab, an unprotected, bisected hot rolled I-profile with composite dowels either in puzzle or clothoidal shape, and removable floor panels on the top of the I-profile (see Fig. 1). Within several research projects in Germany [1-3], the load-bearing behaviour of the slab system was investigated in fire conditions using the ISO standard fire curve and a natural fire scenario.

Composite dowels are special shear connectors and guarantee the bond (shear force) between an I-section and a concrete slab. In comparison to other shear connectors, the composite dowels are more economical due to the manufacturing process and have a higher shear capacity. To describe the load-bearing behaviour of the slab system in case of fire within numerical simulations, knowledge about the temperature-dependent shear capacity as well as the failure mechanism of the composite dowels is required [1]. Therefore, a number of push-out tests according to EN 1994-1-1 Annex B [4] have been performed to determine the temperature-dependent shear capacity of the composite dowels.

This paper presents the experimental investigations on the shear capacity of composite dowels in clothoidal shape. The specimens were heated homogenously to three temperature levels (200 °C, 350 °C and 500 °C) and the shear capacity of the composite dowels was determined. Besides the effect of elevated temperatures on the shear force-slip relation of the composite dowels, the influence of different arrangements of the reinforcement on the shear capacity of the composite dowels was investigated.
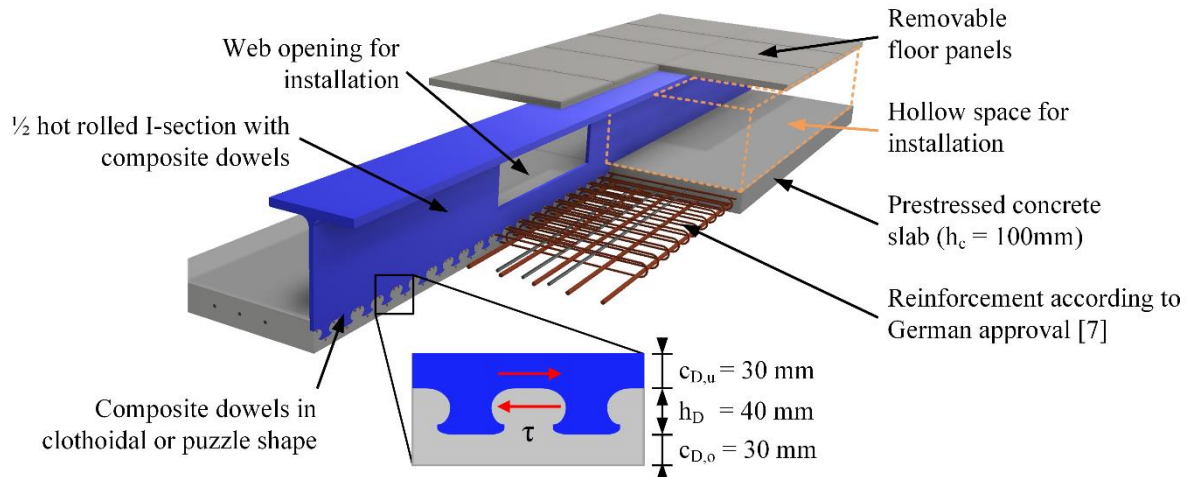
Fig. 1. Overview of the innovative composite slab system *InaDeck* with composite dowels in clothoidal shape

2 PAST AND PRESENT RESEARCH ACTIVITIES

As aforementioned, the bond between the I-section and concrete slab of the slab system *InaDeck* is ensured by composite dowels either in clothoidal or puzzle shape. Composite dowels are a type of shear connectors, which are not comprised by the regulation of EN 1994-1-1 [4]. Hence, a number of studies of e.g. Heinemeyer (2011) [5] and Claßen (2016) [6] have been performed to identify the shear force-slip behaviour and the shear capacity of composite dowels. The dimensions and different shapes of the dowels are regulated by the German approval for composite dowels [7]. Within this approval, the arrangement of the reinforcement of the composite dowel is defined (see Fig. 2) as well as the determination of the decisive shear capacity of the composite dowel at room temperature. The composite dowel is reinforced with 1. bottom reinforcement (reinforcement of composite dowel), and 2. upper reinforcement. The upper reinforcement is arranged above in the centre line of each steel dowel. In each recess of the composite dowel are two rebars named as reinforcement of the concrete dowel (see Fig. 2).
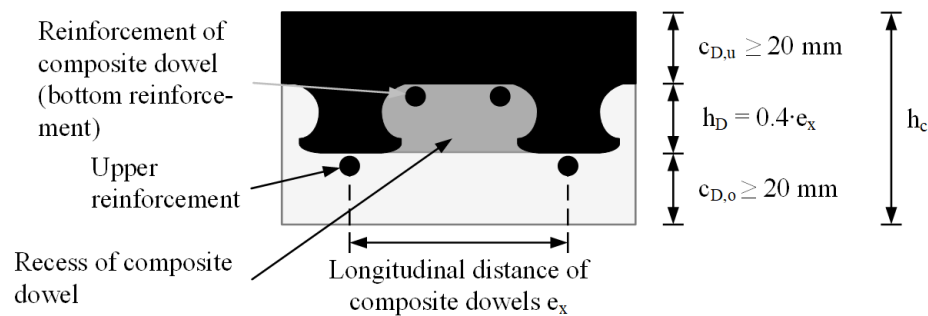
Fig. 2. Composite dowel in clothoidal shape with the arrangement of the reinforcement and characteristic dimensions

The investigations on the shear capacity of composite dowels of e.g. Heinemeyer (2011) [5] and Claßen (2016) [6] have been performed at room temperature. These experimental investigations analysed the shear force-slip behaviour of the dowels as well as the failure mechanisms. Additionally, the failure mechanism of the composite dowel can be derived by the shear force-slip relation. However, the experimental investigations of [5] and [6] observed primary and secondary failure mechanisms of the composite dowels. The secondary failure mechanism is characterised by a local failure respectively crushing of concrete in front of the dowel caused by high contact strains between the surface of the composite dowel and the concrete in the recess of the composite dowel. This secondary failure mechanism is not critical for the shear capacity of the composite dowel and the shear force increases until a primary failure mechanism occurs. The primary failure mechanisms

are a steel failure (see Fig. 3a)), a concrete pry-out failure (see Fig. 3b)), and a shear failure of the concrete. Mainly steel or concrete pry-out failure occurs because the reinforcement of the composite dowel avoids a shear failure of the concrete. Characteristic for the steel failure is a ductile behaviour of the shear force-slip relation in comparison to the concrete pry-out failure. The ductile behaviour results from the plastic behaviour of the steel dowel. Whereas the concrete pry-out failure occurs with a concrete failure cone and is a brittle failure (see Fig. 3b)).
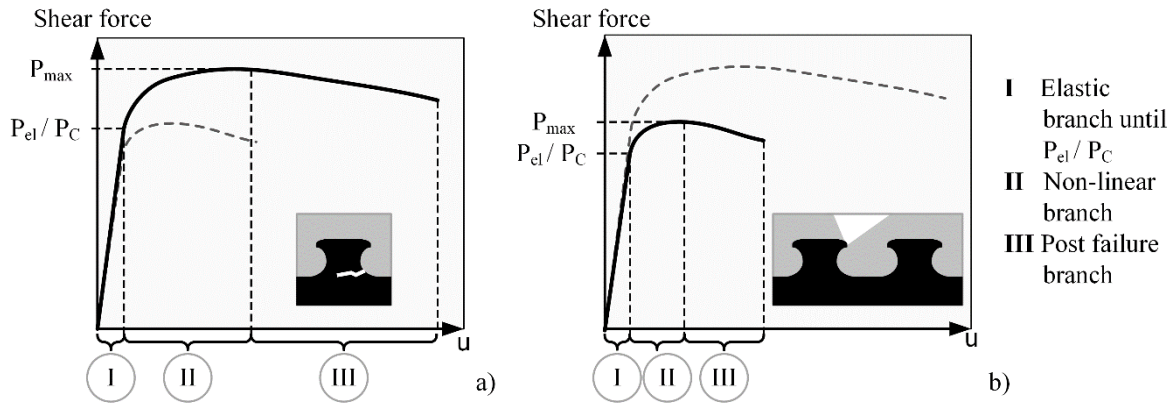
Fig. 3. Qualitative characteristic curves of the composite dowels with: a) Steel failure; b) Concrete pry-out failure; according to [5]

3 EXPERIMENTAL PROGRAM

3.1 Test set-up

A series of push-out tests have been performed to determine the temperature-dependent shear capacity of the composite dowels in clothoidal shape. To perform the push-out tests, a test set-up was designed and manufactured to ascertain the shear capacity of the composite dowels at room and elevated temperature with the same test set-up (Fig. 4a)). Basically, the test set-up consists of the supporting structure, the specimen, the electric furnace, and the hydraulic cylinder. The specimens were heated in an electric furnace until the appropriate homogeneous temperature field was reached. The contours of the electric furnace are shown in Fig. 4a). The load was applied on the top end of the specimen's I-section outside of the electric furnace.

3.2 Test procedure

The test procedure to determine the shear capacity of the composite dowels at room and elevated temperature is according to Annex B of EN 1994-1-1 [4]. The procedure of the experimental investigations is divided into three parts: 1. pre-loading, 2. heating (only at elevated temperatures), and 3. loading until failure of the specimen (see Fig. 4b)). As failure criteria, a reduction of 20 % of the maximum shear capacity was used for the specimen according to EN 1994-1-1 [4]. At room temperature, first the specimens are dynamically loaded with 25 cycles and afterwards loaded until failure occurs respectively the failure criteria of EN 1994-1-1 [4] was reached. By analogy to the specimens at room temperature, the specimens at elevated temperature are dynamically loaded with 25 cycles. The heating phase of the specimen subsequently initiates after the pre-loading of the specimen. The unstressed specimens (push-out tests) at elevated temperature are heated in the furnace until the reference temperature was reached. After reaching the reference temperature, the shear capacity was determined while the specimens remained in the furnace to ensure the temperature of the specimen during the loading until failure. The test procedure to determine the shear capacity is shown in Fig. 4b).

174
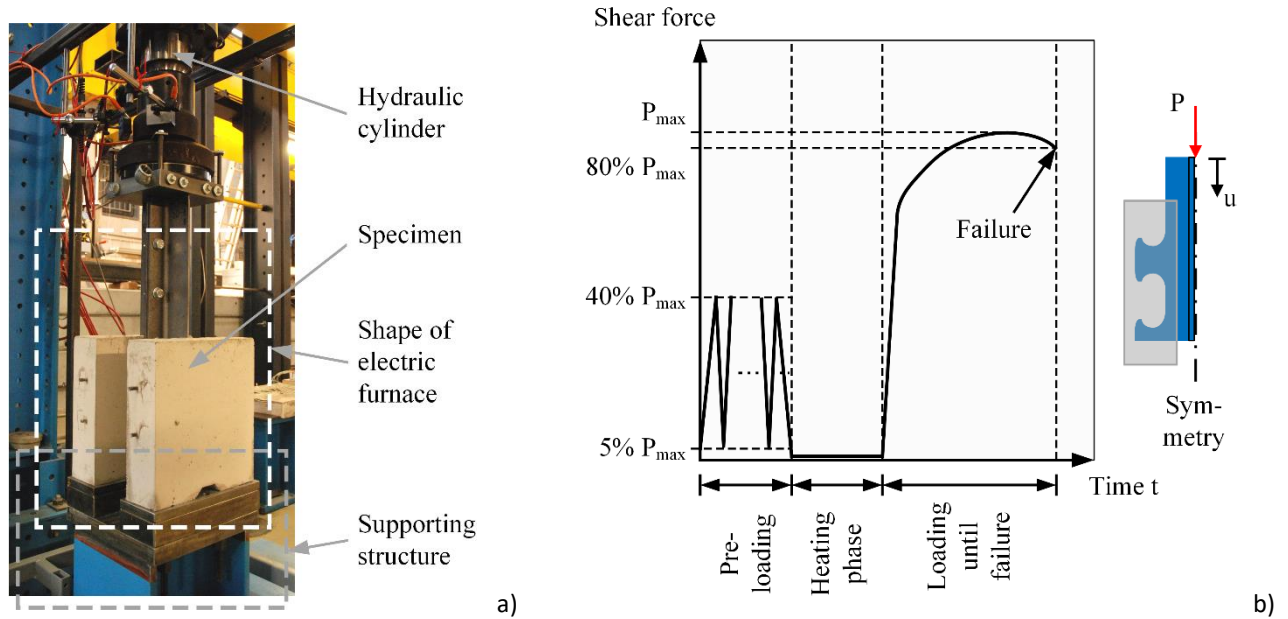
Fig. 4. a) Test set-up of the push-out tests; b) Procedure of the push-out tests according to EN 1994-1-1 Annex B [4]

3.3 Test specimens

Detailed investigation on the shear capacity of composite dowels in clothoidal shape have been performed with a series of push-out tests. The dimensions of the specimens are in correlation with the dimensions of the slab system *InaDeck* (see Fig. 1 and Fig. 5). The push-out specimens have a scale factor of 1:1. The structure of the push-out specimens is symmetric and the specimens consisted of a hot rolled I-section IPE220 and a reinforced concrete slab with a thickness of 100 mm. The composite dowels were in clothoidal shape with a longitudinal distance e_x of 100 mm (see Fig. 5).
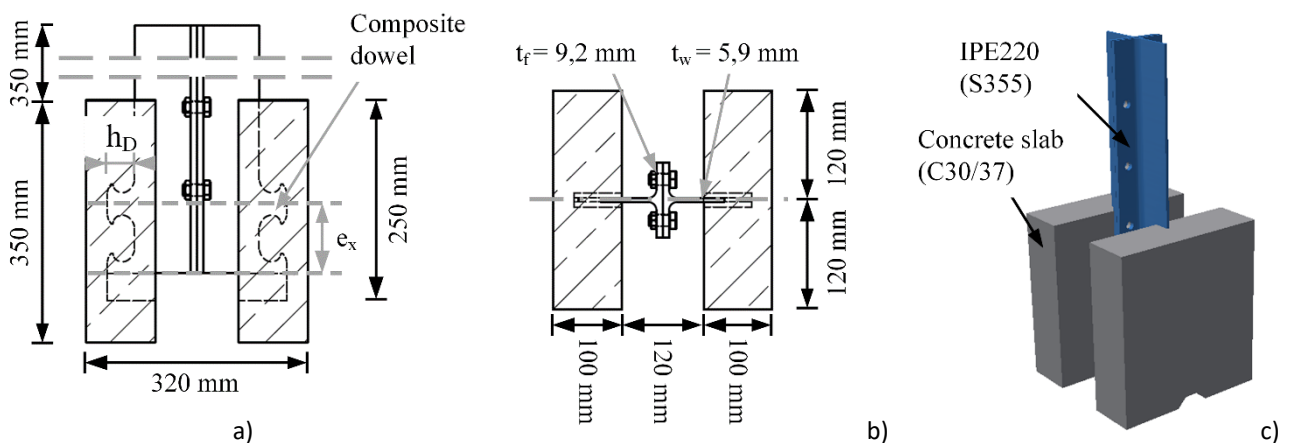
Fig. 5. Different views of the specimen: a) Side view; b) Top view; c) Isometry

During the heating phase, the temperatures inside the specimens were measured with thermocouples of type K. The specimens were heated until a homogeneous temperature field of 200 °C, 350 °C, or 500 °C was reached. The shear capacity of the composite dowels were determined at room temperature (RT) and high temperatures (HT) of 200 °C, 350 °C, or 500 °C. The push-out tests at room temperature serve as reference to assess the influence of temperature on the shear capacity of

the composite dowels (see Table 3). Besides the influence of the temperature, the main parameters of the experimental investigations on the shear capacity are the influence of the upper reinforcement and the number of rebars within the recess of the composite dowel (see Table 3). The series PO-V1 represent the reinforcement layout of the slab system *InaDeck.* With the series PO-V2 the influence of the reinforcement on the multiaxial stress state is investigated, in series PO-V3 the influence of the rebars within the recess of the composite dowel is analysed. The specimen's parameters of the push-out tests are presented in Table 3. A comprehensive description of the test set-up, the setup of the specimens, the material properties, and the arrangement of the thermocouples is given in [3].

Table 3. Specimen's parameters of the push-out tests at room temperature (RT) and elevated temperatures (HT)

Series	Longitudinal distance ex [mm]	θ_{Ref} [°C]	No. of tests [-]	Reinforcement			h_c/ h_d/ c_D [mm]
				Reinforcement of composite dowel [mm]	Upper reinforce-ment [mm]	Longitudinal reinforcement [mm]	
PO-V1 (reference)	100	RT	2	2 x Ø8	Ø8	Ø10	
		HT	6				
PO-V2	100	RT	1	2 x Ø8	-	Ø10	100/ 40/ 30
		HT	5				
PO-V3	100	RT	2	1 x Ø8	Ø8	Ø10	
		HT	6				

4 RESULTS OF THE EXPERIMENTAL INVESTIGATIONS

4.1 Room temperature

The behaviour of composite dowels in shear is characterised by the shear-force slip relation. As a result of the shear-force slip relation the load-bearing behaviour of the composite dowels can be analysed and the failure mechanism can be derived.

At first, the push-out tests at room temperature were performed to determine the shear capacity and the shear force-slip relation of the composite dowel as reference value for the push-out tests at elevated temperature. The shear force-slip relation represents the relative displacement of the steel dowel to the concrete slab of the specimen.

The shear force-slip relation of the three push-out series at room temperature is shown in Fig. 6a). The main emphasis of the experimental investigations was to determine the influence of the upper reinforcement and the number of rebars within the recess of the composite dowel. Due to the ductile behaviour and large displacements of the shear force-slip relation of each push-out series steel failure of the composite dowel can be concluded. In addition, the three aforementioned characteristics of the shear force-slip relation are identifiable. After the pre-loading of the specimens the shear force-slip relation has a linear branch followed by a non-linear branch until the maximum shear force is reached (see Fig. 6a)). The shear force-slip relation after the maximum shear capacity of the composite dowel is characterised by the post failure branch until failure of the composite dowel occurs. The upper reinforcement has no significant influence on the shear capacity or the shear force-slip relation of the composite dowel (see Fig. 6a)). Whereas the number of rebars

176

within the recess of the composite dowel has a significant influence on the shear capacity of the composite dowel. The maximum shear capacity of the composite dowel with one rebar within the recess of the composite dowels is reduced by 25 kN to 175 kN compared to 200 kN with two rebars in the recess.

To verify the failure mechanism and to analyse the local bearing behaviour of the composite dowel, the specimens were separated along the composite dowels. Within these investigations centre cuts along the composite dowels were conducted (see Fig. 6b) and c)) to assess the local bearing mechanisms of the composite dowel. The detailed investigations confirmed a steel failure of the composite dowel as failure mechanism (see Fig. 6b)). However, besides the primary failure mechanism the secondary failure mechanism of crushed concrete in the recess of the composite dowel occurred (see Fig. 6c)). With increasing the load, the contact pressure between the front surface of the dowel and the concrete increases until the maximum strain of the concrete is reached. At this particular point of exceeding the compressive strains of the concrete, the concrete in front of the dowel crushes (see Fig. 6c)). This failure mechanism is evoked by the high steel strength in combination with the thin web of the I-section, which is resulting in a high contact pressure. The contact pressure exceeds the ultimate concrete strength and therefore the concrete fails. Nevertheless, the load increases on a non-linear branch until the maximum shear capacity. Due to this process, the composite dowel respectively the steel dowel deforms plastically because the base point of the dowel (see Fig. 6b)) gets in contact with the reinforcement of the composite dowel. With increasing load and deformation, a bending of the dowel occurs (see Fig. 6b)). Due to the bending of the dowel a concrete failure cone appears. Subsequently, the multiaxial stress state fails and the load decreases (displacement increases) until the failure criteria is fulfilled.
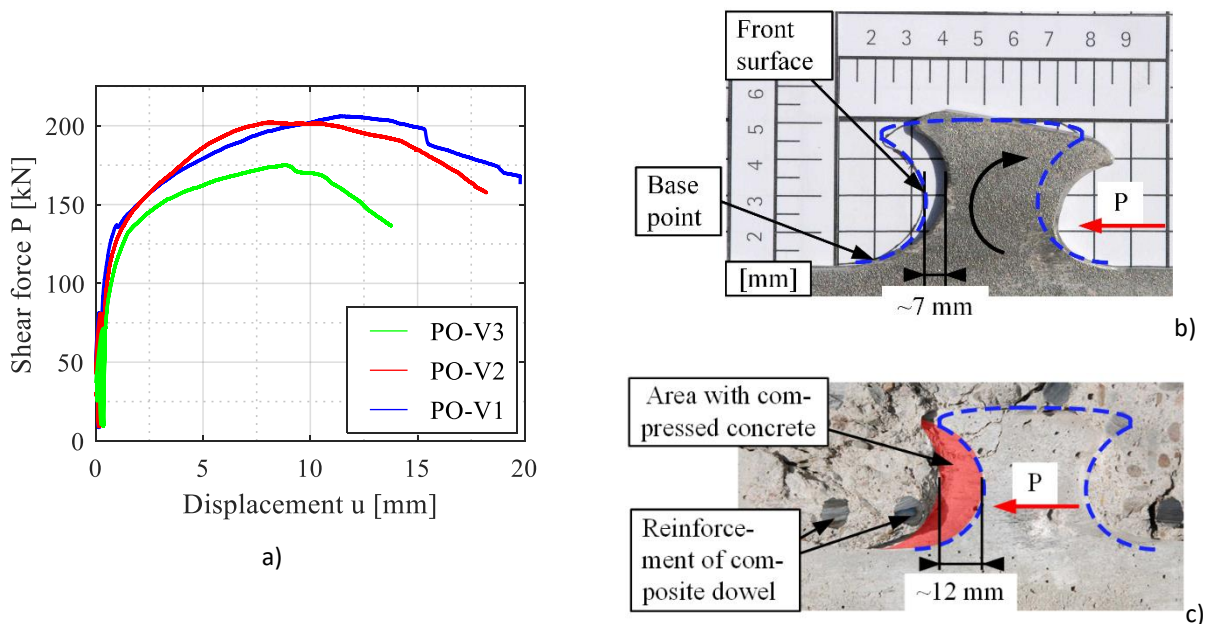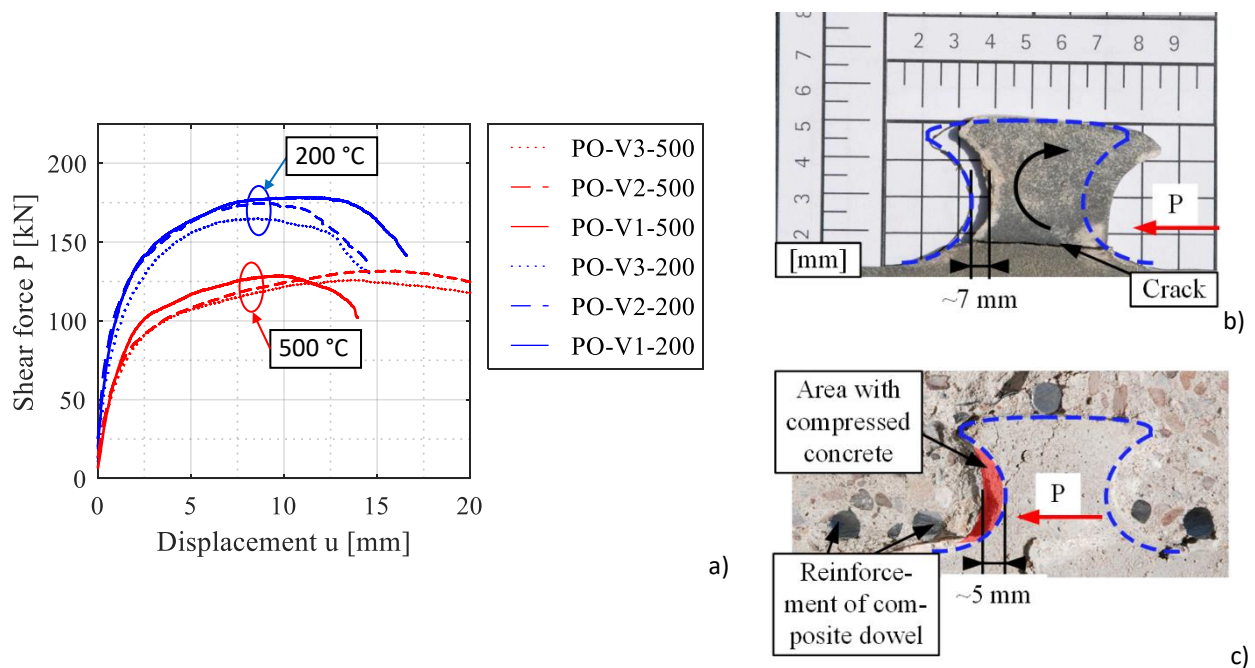

Fig. 6. a) Comparison of the shear force-slip relation of the specimen at room temperature; b) Local analyses of the bearing behaviour of the steel dowel at 20 °C (series PO-V1); c) Local analyses of the bearing behaviour of the concrete at 20 °C (series PO-V1)

4.2 Elevated temperatures

Besides the experimental investigations at room temperature, push-out tests at elevated temperature have been performed to determine the shear capacity of the composite dowels. Based on the shear force-slip relations of the specimens at each reference temperature a steel failure of the composite dowel can be deduced (see Fig. 7a)). Consequently, a change of primary failure mechanism of the

177

composite dowels with increasing temperature did not occur. As well as at room temperature, the influence of the upper reinforcement on the shear capacity of the composite dowel is neglectable (see Fig. 7a)). Moreover, the number of rebars within the recess of the composite dowel has an influence on the shear capacity. The difference in the maximum shear capacity of 25 kN and the shear force-slip behaviour between the reference series and the specimen with one rebar in the recess is identical at room temperature and until a specimen temperature of 350 °C (see Fig. 12). With increasing temperature, the influence of the number of rebars on the shear capacity in the recess decreases. At a temperature of 500 °C the shear capacity is almost identical (see Fig. 7a)). For the specimens at elevated temperature, centre cuts along the composite dowel of the specimens were performed. The specimens of each reference temperature show the secondary and primary failure mechanisms compared to the specimens at room temperature. Nevertheless, the local bearing mechanism of the composite dowel differs slightly from the behaviour at room temperature. The differences are that the steel dowel completely shears off (primary failure, see Fig. 7b)) and the area of crushed concrete is significantly smaller (secondary failure, see Fig. 7c)).

Fig. 7. a) Comparison of the shear force-slip relation of the specimens at elevated temperatures; b) Local analyses of the bearing behaviour of the steel dowel at 500 °C (series PO-V1); c) Local analyses of the bearing behaviour of the concrete at 500 °C (series PO-V1)

4.3 Influence of temperature

Finally, the shear capacity of the push-out series at each reference temperature is compared (see Fig. 12). The shear capacity at temperatures of 200 °C and 350 °C of the specimen without the upper reinforcement is smaller compared to the reference series with the upper reinforcement. This difference is attributable to the multiaxial stress state, which is not caused by the upper reinforcement. With an increasing temperature of the specimen (temperature of 500 °C) the influence of the upper reinforcement on the shear capacity decreases and the shear capacity is almost identical. In comparison, the number of rebars influences the shear capacity of the composite dowel. The difference in the shear capacity between the reference series and the push-out series with one rebar in the recess of the composite dowel amounts approximately 25 kN at room temperature. This difference in the shear capacity remains unchanged until a temperature of 350 °C. With increasing temperature of the composite dowel the difference of the shear capacity decreases. The shear capacity of the composite dowel with two (reference series) or one (push-out series 3) rebar in the recess of the composite dowel is almost the same (see Fig. 12).
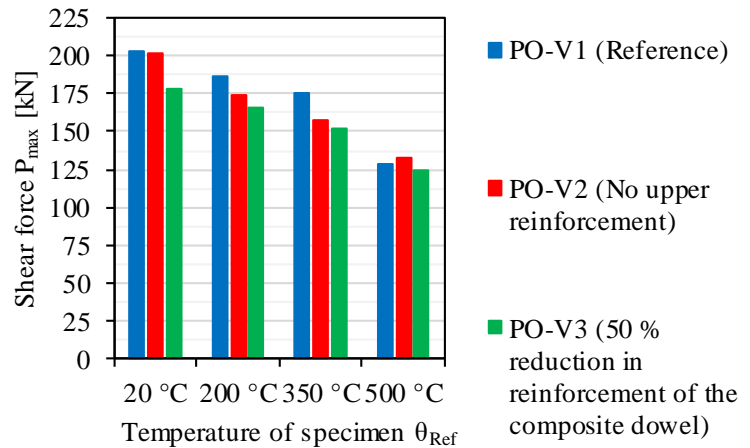
At a temperature of 350 °C the reduction in the shear capacity is mere 10 to 15 %, while a sizeable reduction occurs at higher temperature (500 °C). The shear capacity at a temperature of 500 °C of the composite dowel is reduced by 30 to 35 %. With an increase of the temperature of 150 °C (from 350 °C to 500 °C) the reduction of the shear capacity is doubled.

5 CONCLUSIONS

The longitudinal shear resistance is crucial for composite beams at room temperature as well as in fire conditions. The influence of elevated temperature on the shear capacity and behaviour of shear connectors the composite dowels in clothoidal shape is not investigated yet. Within this paper, experimental investigations (push-out tests) on the shear capacity of composite dowels at room and elevated temperatures are presented. The shear capacity of the composite dowels were determined besides room temperature at a homogenously temperature field of 200 °C, 350 °C, and 500 °C. Besides the influence of the temperature on the shear capacity, the influence of the upper reinforcement and numbers of rebars in recess of the composite dowel was investigated.

With the performed push-out tests, the shear capacity of the composite dowel at each reference temperature was determined. At room temperature steel failure of the composite dowel occurred. However, with increasing temperature of the composite dowel a change of the primary failure mechanism did not occur. The shear capacity is reduced up to a temperature of 350 °C of approximately 10 to 15 %. With increasing temperature, the shear capacity decreases and the shear capacity is reduced by approximately 30 to 35 % at a temperature of 500 °C. The influence of the numbers of rebars within the recess of the composite dowels is decreasing with increasing temperature and the shear capacity at 500 °C is almost identical.

REFERENCES

[1] Schaumann P., Meyer P., Mensinger M., Koh S.K. (2018). Experimental and Numerical Investigations on the Load-Bearing Behaviour of an Innovative Prestressed Composite Slab System under a Natural Fire Scenario. 10th International Conference on Structures in Fire (SiF '18), Belfast, United Kingdom, 6-8 June 2018, pp. 553-560.

[2] Schaumann P., Meyer P., Mensinger M., Koh S.K. (2018). Experimental investigations on the load-bearing behaviour of an innovative prestressed composite floor system in fire. 12th International Conference on Advances in Steel-Concrete Composite Structures (ASCCS 2018), Valencia, Spain, 27-29 June 2018, pp. 811-818.

[3] Mensinger M., Koh S.K., Schaumann P., Meyer P. (2019). Temperaturentwicklung in Hohlräumen abgehängter Decken sowie in Hohl- und Doppelböden und deren Auswirkungen auf das Tragverhalten innenliegender Stahlkonstruktionen. (unpublished research report).

[4] DIN EN 1994-1-1 (2004). Design of composite steel and concrete structures – Part 1-1: General rules and rules for buildings. European Committee for Standardization, Brussels.

[5] Heinemeyer S. (2011). Zum Trag und Verformungsverhalten von Verbundträgern aus ultrahochfesten Beton mit Verbundleisten. RWTH Aachen.

[6] Claßen M. (2016). Zum Trag- und Verformungsverhalten von Verbundträgern mit Verbunddübelleisten und großen Stegöffnungen. RWTH Aachen.

[7] Allgemeine Bauartengenehmigung (2018). Z-26.4-56: Stahlverbundträger mit Verbunddübelleisten in Klothoiden- und Puzzleform. Deutsches Institut für Bautechnik

FIRE TEST RESEARCH ON NEW COLD-FORMED STEEL STRUCTURES

ChenWenwen[1], Ye Jihong[2]
[1]Southeast University, Nanjing , China;
[2]China university of Mining and Technology, Xuzhou, China

ABSTRACT

A new cold-formed steel (CFS) structures system which adopted new composite wall, floor system and so on instead of conventional ones was proposed to make the development of CFS structures from low-rise to mid-rise building. In order to investigate the fire performance of the new CFS structure, a new full-scale CFS structure with plan size of 7.2m×7.2m and height of 3m was constructed for fire experiment. It was divided into 4 compartments, one of which was evenly distributed timber as fired-compartment and the other three were non-fired compartments. The detail process of fire development was recorded in this paper. And the experimental phenomenon, failure mode of the structure and varieties of gas and structure temperature were detail analyzed.

1 INTRODUCTION

The cold-formed steel (CFS) structures consist of walls, floor systems and other connective components. With rapid construction, light weight, high strength and excellent seismic performance, CFS structures have been widely built in North America, Europe, Australia and other regions.

In order to investigate the fire resistance of CFS structures, many components such as composite walls and floors were tested in fire furnace. Sultan and Lougheed[1]presented the results of 22 full-scale and 49 small-scale fire resistance tests conducted at the National Fire Laboratory on insulated and non-insulated full-scale gypsum board protected wall assemblies. Feng[1]presented the results of 6 tests on loaded full-scale cold-formed thin-walled steel walls exposed to the standard fire condition on one side. A detailed experimental study of 14 full-scale steel stud wall assemblies was conducted in Kodur's[2] research. Both single row and double rows steel stud configurations with installation of gypsum board on each of the exposed and unexposed sides, and with and without insulation in the cavity, were considered in the experimental program. Sultan[3] presented and discussed the results of 40 full-scale wall fire resistance tests conducted at the National Research Council of Canada in accordance with ULC-S101/ASTM E119 standard fire exposure. A new CFS wall system based on a composite panel in which the insulation was sandwiched between two panels instead of cavity insulation was proposed in Kolarkar's[4] research. In Gunalan's[7]research, 11 full scale tests were conducted on conventional load bearing steel stud walls with and without cavity insulation, and the new composite panel system to study their thermal and structural performance under standard fire conditions. A few studies have been performed on the thermal and mechanical performance of CFS floor systems under fire conditions. For instance, Sultan[14][15] summarized the results of fire resistance tests on 16 full-scale CFS floor assemblies that consisted of plywood or steel decks with concrete to players as the subfloors and one or two layers of fire-resistant gypsum plasterboard as the ceiling finishes. Sakumoto[16] reported the results of fire tests of CFS walls and floor ceiling systems.

Overall structural fire tests were necessary to carry out because the interaction between components of structural system could not be shown in the component furnace tests. From 1996 to 2003, BRE (Building Research Establishment)[9-11] conducted seven actual fire tests on the Cardington test building (Fig. 1). Fire performance of the restrained beam, plane frame and composite slab were studied. Meanwhile, the indoor fire test (under closed doors and windows), the test in a large fire zone and the actual fire test in the normal office were also studied. French CTICM et al.[12]

conducted three actual fire tests on a steel frame-combined floor open-air parking lot in Vernon. L. Pyl et al.[13] reported a three-dimensional cold-formed steel portal frame fire test (Fig. 2).
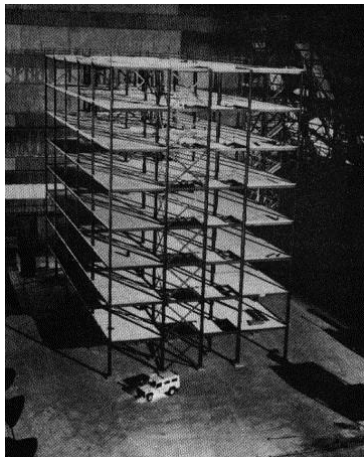

Fig. 1 Cardington fire model

Fig. 2 Cold-formed thin-walled steel portal frame

To extend the use of CFS structures from low-rise to mid-rise buildings, a new type of cold-formed steel structure system-cold-formed steel framed composite shear wall systems-with good seismic performance was proposed in Ye's[17] research. The cold-formed steel framed composite shear wall systems adopted new composite walls and floor assemblies whose fire resistance had been investigated in literature [6][7] and [18] respectively. In order to explore the fire resistance of this new structural system, a full-scale single-story building was conducted. The detail process of fire development was recorded in this paper. And the experimental phenomenon, failure mode of the structure and varieties of gas and structure temperature were detail analyzed.

2   INTRODUCTION TO FULL SCALE FIRE TEST BUILDING

2.1   Dimension of the frame

A 7.2m×7.2m single-storey cold-formed steel structure of the height of 3.0m was constructed, asshown in Fig. 3. A fired-compartment of 3.6 m×3.6 m was chosen to stack wood cribs equably (Fig. 3). Non-fired compartment R_2,R_3,R_4 and fired-compartment R_1 were connected with each other by door(Fig. 4). Vertical loads were applied to the structure according to a design load of 2.0 kN/m^2.
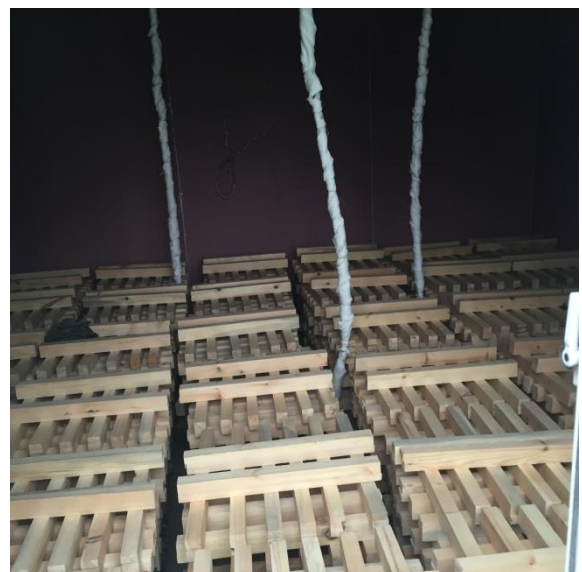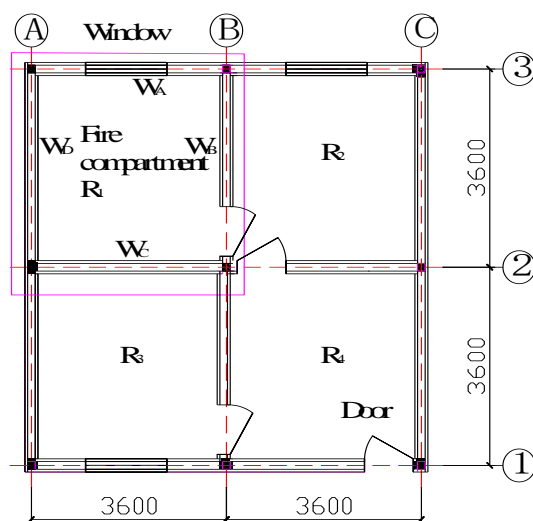
Fig. 4 Wood cribs with a weight of 55 kg/m^2 for a fire load density of935MJ/m^2 and fire ignition using gasoline

New composite walls developed by the authors' research group with composite panels in which the insulation is sandwiched between two panels are applied for interior walls W_B,W_C (Fig. 5) and e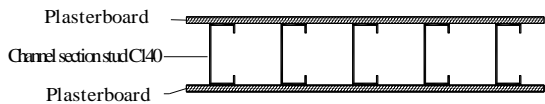xterior walls W_A,W_D (Fig. 6). Non-fire compartments $R_2$-$R_4$ adopt conventional CFS walls lined with single-layer plasterboard (Fig.7). The sizes of the wall stud channel section are shown in (Fig. 9(a)). Construction of new floor assemblies which adopted plasterboards as ceiling finishes and autoclaved lightweight concrete (ALC) boards covered with concrete as slab floor is shown in Fig. 8.The joist section sizes are shown in (Fig. 9(b)).

Plasterboard
Aluminumsilicate wool
Plasterboard
Channel section stud C140
Plasterboard
Aluminumsilicate wool
Plasterboard
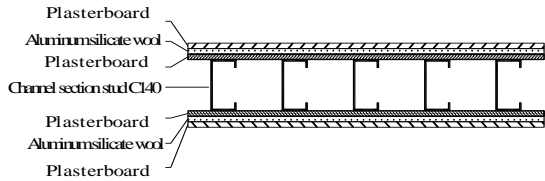
Fig. 5New composite interior walls

Plasterboard
Aluminumsilicate wool
Plasterboard
Channel section stud C140
Plasterboard
ALCboard
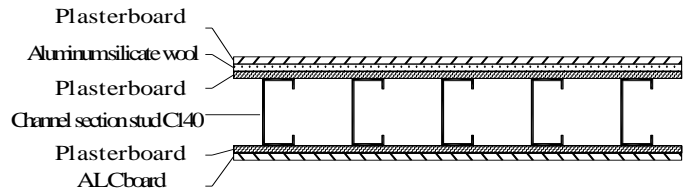
Fig. 6New composite exterior wall

Plasterboard
Channel section stud C140
Plasterboard

Fig. 7 Conventional CFS walls lined with single-plasterboard

Lightweight concrete
ALCboard
Channel section stud C240
Plasterboard
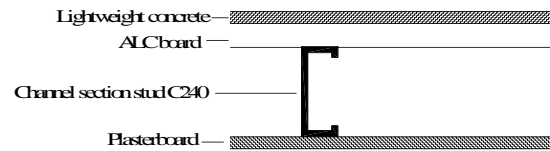
Fig. 8 Construction of floor assemblies
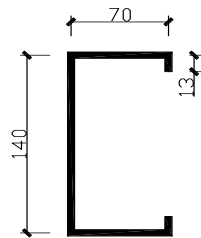
（a）C140 Channel section stud (mm)
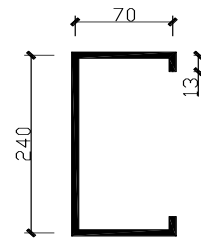
（b）C240 Channel section joist (mm)

Fig. 9 Channel section sizes

2.2 Measurement Setup

Type K thermocouples for the higher temperature range were used to record the structure and gas temperatures. Circles in Fig. 10 showed the position of the thermocouple trees. At each location, three thermocouples were placed to measure the gas temperatures along the height of the compartment. Take thermocouple tree 1RT1 (Fig.11) as an example, 1RT1-0.5 measured the gas temperature at 50cm height from the ground, 1RT1-1.38 represented the gas temperature at height of 1.38m and 1RT1-2.26 was arranged 50cm away from the ceiling. The 3RT1-3RT5 thermocouples trees were inside the fired-compartment, while 3RT6-3RT7thermocouples trees measured the gas temperature in R2 non-fired compartment and 3RT8-3RT9 recorded the gas temperature of R3 non-fired compartment.
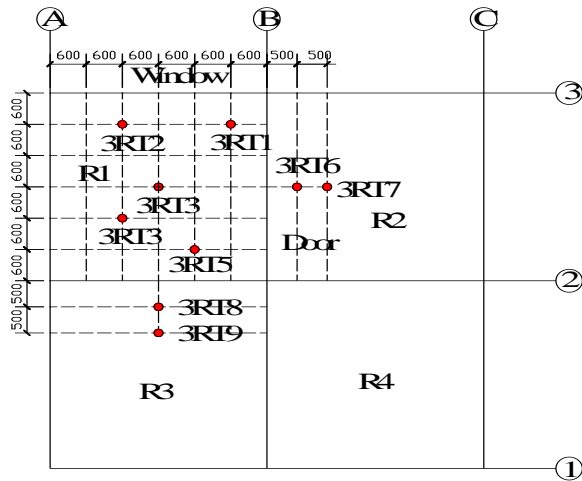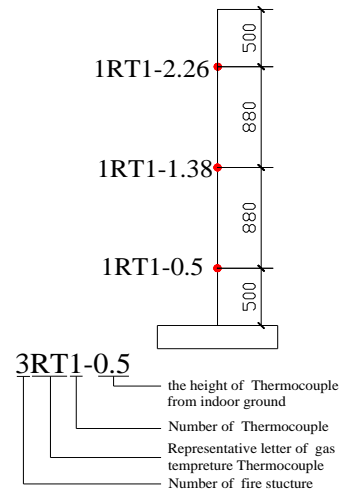
Fig. 10 Position of the thermocouple trees

Fig. 11 Thermocouple trees

The layout of thermocouples in the structural members is shown in Fig. 12. A plurality of thermocouple groups were arranged in the four walls of the fired-compartment (Fig. 12). Each thermocouple group was generally composed of two thermocouple clusters which recorded the heat transfer of the same position, such as 3W1 and 3W2 (Fig. 12).3W1 recorded the temperature transfer of section which was consisted of keel steel stud and panels, whereas 3W2 recorded the temperature transfer of section with cavity and panels. Except for 3W9 and 3W10,measuring points of the thermocouple clusters were all located at 1.38m elevation. 3W9 thermocouple cluster was at 2.26m height and the 3W10 thermocouple cluster was at 0.5m height. Both 3W9 and 3W10 thermocouple clusters were located at the same stud with the 3W7. The purpose was to measure the temperature difference at different heights of the same stud.
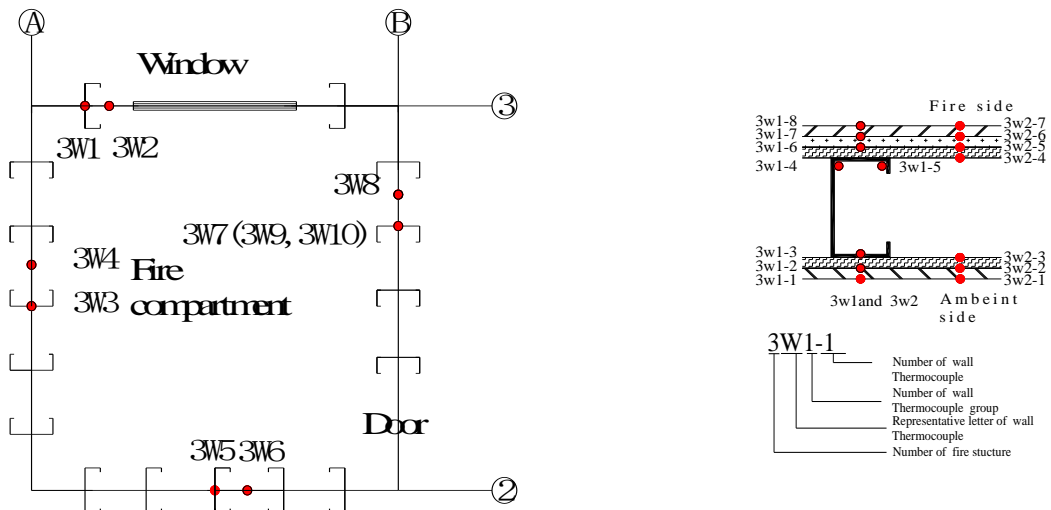
Fig. 12 Layout of thermocouples in the cross section of walls

3   TEST PROCESS

Gasoline in oil box was ignited at 11:28 on April 4, 2018. Due to poor ventilation, no flame was observed after about 7 minutes. At 11:46, the fire loads were re-ignited (Fig. 13). After a few minutes, fired-compartment R1 space was filled with smoke without obvious flames meaning entered the

smoldering stage (Fig. 14). At 67 minutes, obvious cracks at window glass (Fig. 15) indicated fresh air entered the fire room resulting in continued developed fire. At 78 minutes, part of the floor ceiling plasterboards fell off. Part of the flames escaped outside the window(Fig. 16) after 86 minutes, predicting fire spreading to the adjacent storeys and buildings. The glass fell off 89 minutes past ignition and the gypsum boards on the floor all fell off after 95 minutes. The window completely burned out with fire complete development (Fig. 17) after 112 minutes. The fire was difficult to control in 119 minutes, and then the fire was extinguished (Fig. 18).

Fig. 13 Ignition

Fig. 14 Smoldering stage

Fig. 15 Obvious cracking of window glass

Fig.16 Flame escaped out of the compartment

Fig.17 Complete development of the fire

Fig.18 Extinguishment of the fire

4   FAILURE MODE ANALYSIS

4.1   Overall behavior of the structure

The overall damage undergone by the structure is shown in Figure 19. The window was completely destroyed during the fire. The black carbonized solid residue around the window hole on the outer ALC boards indicated that the flame had been out of the compartment which means fire spreading

to the adjacent buildings. A long crack on concrete surface of floor system appeared between fired compartment and the non-fire compartment(Fig. 20). The reason for the above phenomenon is that the joists of fired-compartment directly subjected to fire on account of the fallen off of the ceiling plasterboards occurred expansion deformation resulted in different vertical displacements between fired-compartment and the non-fire compartment.

Fig. 19 Overalldamage of the structure

Fig.20 Crack on the concrete roof surface

4.2 Detailed behavior of composite walls

Without completely fallen off, the outside plasterboards on fire side had completely lost its insulation in fired-compartment (Fig. 21). The inside plasterboards and the aluminum wool between the two plasterboards maintained integrity and heat insulation. Due to the entire enclosed of fire compartment during the fire test, the smoke could not spread to other non-fired compartments. Hence, there was no damage to the plasterboard in non-fired compartments(Fig. 22).

Fig. 21 Breakdown of panels in fire-compartment

Fig. 22 Panels in fire-compartment

5   TEST RESULTS OF TEMPERATURE RISE

In general, the measured gas time-temperature curve(Fig. 23) was different from ISO 834 standard fire. The fire experienced a long growth period of about 67 minutes with temperatures below 300℃, compared to 500℃of ISO fire at 3 minutes. After67 minutes, the fire entered a period of rapid development due to the entry of fresh air resulted from the breakage of the window glass. And the temperature rose to 500℃. After that, time-temperature curve presented a platform that maintained at 500℃ and continued to 112 minutes when the window was completely destroyed. And then, the fire entered its development period with a rapid temperature rise. The gas temperature reached its maximum value of about 800℃ (Fig. 23). The gas time-temperature curves of the fired-compartment were approximate along the height.

The temperature in the compartments devoid of fire load (R2 and R3) were lower than fired-compartment (Fig. 23-Fig.24). The maximum temperature in R2 compartment was about 80 ℃, whereas the maximum temperature in R3 compartment was lower than 40℃. The highest temperature for room R1, R2 and R3 were all recorded by the thermocouples at 2.26m height. The value of thermocouple 3RT2-0.5 was similar with 3RT2-1.38 which was different from 3RT2-2.26

showed that there was an obvious temperature layer in R2 compartment. In contrast with R2 compartment, R3 compartment appeared temperature diversity of the three thermocouples 3RT3-0.5, 3RT3-1.38 and 3RT3-2.26.

Fig. 26 showed the distribution of temperature on the outer wall section of the fired-compartment. 3WA-1-3WA-7 was in turn arranged from the ambient side to fire side of the outer wall(Fig. 12). Suddenly increment in temperature of 3WA-6 at 117 minutes indicated that the plasterboards on fire side lost theirs heat insulation. The temperature difference between 3WA-5 and 3WA-4 showed that the inner filling of aluminum wool had not fallen.
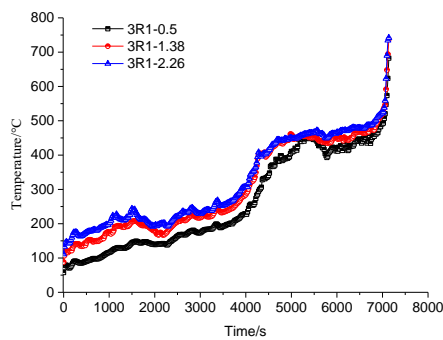
Fig. 23 Temperature rise curve along the height of fire compartment R1
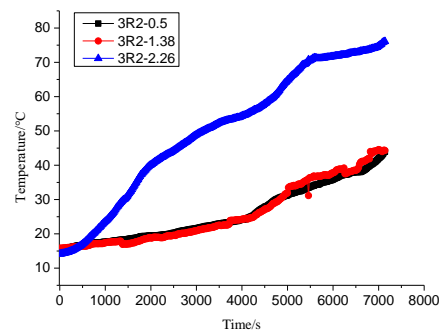
Fig. 24 Temperature rise curve along the height of non-fire compartment R2
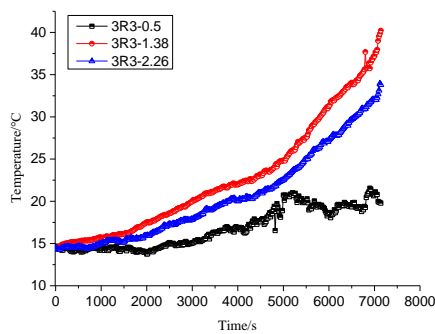
Fig. 25 Temperature rise curve along the height of non-fire compartment R3
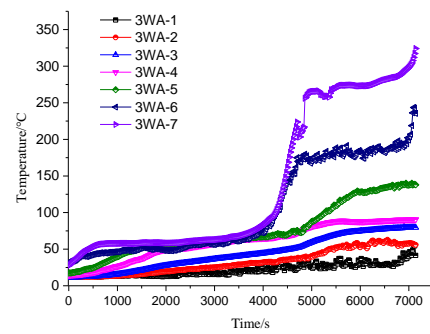
Fig. 26 Temperature rise curve along the cross section of composite wall

6   CONCLUSION

This paper analyze the performance of a new full scale 7.2 m×7.2m cold-formed structure under natural fire conditions. A fired-compartment of 3.6 m×3.6 m is chosen to evenly stack wood cribs. The fire performance of an innovative cold-formed structure is presented and discussed. The following conclusions can be drawn:

(1)The steel joists on the floor assemblies were directly exposed to fire resulting in uneven vertical displacement between fired-compartment and non-fired compartment duo to the falling off of ceiling plasterboard. That uneven vertical displacement produced large cracks in the floor caused the collapse of the structure

(2)In the compartment provided with fire load, the plasterboards on fire side lost their insulation. However, the sandwiched filling aluminum wool had not lost the heat insulation without falling off indicating the superior fire resistance of the composite walls.

(3)The measured gas time-temperature curve was different from ISO 834 standard fire. After accumulated process of heat in the space field, the fire was fully developed with the maximum temperature 800℃. The maximum temperature in real fire were higher than 800℃ because the test fire was extinguished in advance in consideration of safety.

REFERENCE

[1]   Sultan M A, Lougheed G D. Results of fire resistance tests on full-scale gypsum board wall assemblies[J]. Institute for Research in Construction, National Research Council Canada, August 2002, 2002.

[2]   Feng M, Wang Y C. An experimental study of loaded full-scale cold-formed thin-walled steel structural panels under fire conditions[J]. Fire safety journal, 2005, 40(1): 43-63.

[3]   V K R, Sultan M A. Factors influencing fire resistance of load-bearing steel stud walls[J]. Fire technology, 2006, 42(1): 5-26.

[4]   Sultan M A. Comparison of gypsum board fall-off in wall and floor assemblies exposed to furnace heat[C]//12th Int. Conf. on Fire Science and Engineering. 2010: 1-6.

[5]   Kolarkar P N. Structural and thermal performance of cold-formed steel stud wall systems under fire conditions[D]. Queensland University of Technology, 2011.

[6]   Chen W, Ye J, Bai Y, et al. Full-scale fire experiments on load-bearing cold-formed steel walls lined with different panels[J]. Journal of Constructional Steel Research, 2012, 79: 242-254.

[7]   Chen W, Ye J, Bai Y, et al. Improved fire resistant performance of load bearing cold-formed steel interior and exterior wall systems[J]. Thin-Walled Structures, 2013, 73: 145-157.

[8]   Gunalan S, Kolarkar P, Mahendran M. Experimental study of load bearing cold-formed steel wall systems under fire conditions[J]. Thin-Walled Structures, 2013, 65: 72-92.

[9]   Wang Y C. An analysis of the global structural behaviour of the Cardington steel-framed building during the two BRE fire tests[J]. Engineering Structures, 2000, 22(5):401-412.

[10] Gillie M, Usmani A S, Rotter J M. A structural analysis of the Cardington British Steel Corner Test[J]. Journal of Constructional Steel Research, 2002, 58(4):427-442.

[11] F. Wald, L. Simões da Silva, D.B. Moore, et al. Experimental behaviour of a steel structure under natural fire[J]. Fire Safety Journal, 2006, 41(7):509-522.

[12] Zhao B, Kruppa J. Structural behaviour of an open car park under real fire scenarios[J]. Fire & Materials, 2004, 28(2-4):269–280.

[13] Pyl L, Schueremans L, Dierckx W, et al. Fire safety analysis of a 3D frame structure based on a full-scale fire test[J]. Thin-Walled Structures, 2012, 61(6):204-212.

[14] Sultan, M. A.Comparison of gypsum board fall-off in wall andfloor assemblies.12th Int. Conf. on Fire Science and EngineeringConf., Interscience Communications, London, 1–6.

[15] Sultan M A . Fire Resistance of Steel C-Joist Floor Assemblies[J]. Fire Technology, 2010, 46(2):375-405.

[16] Sakumoto, Y., Hirakawa, T., Masuda, H., and Nakamura, K. "Fireresistance of walls and floors using light-gauge steel shapes." J. Struct.Eng., 10.1061/(ASCE)0733-9445(2003)129:11(1522), 1522–1530.

[17] Ye Jihong. An introduction of mid-rise thin-walled steel structures: Research progress on cold-formed steel-framed compositeshear wall systems[J]. Journal of Harbin Institute of Technology, 2016, 48(6): 1-9. (in Chinese)

[18] Ye J H, Chen W, Wang Z. Fire-resistance behavior of a newly developed cold-formed steel composite floor. Journal ofStructural Engineering, 2017, 143(6): 04017018.

DETERMINATION OF THE STRUCTURAL BEHAVIOUR OF SINGLE STOREY STEEL BUILDINGS IN CASE OF FIRE BY A SIMPLIFIED FORCE-BASED METHOD

Tom Molkens, Barbara Rossi
KULeuven TC Construction, Belgium

ABSTRACT

The actual Eurocode design procedures to assess the structural reliability in case of fire permit a whole scope of methodologies. On the one hand, the code allows to simply combine design rules with member analysis through tabulated data or via simple calculation models. On the other hand, complex performance-based design approaches are proposed, which's results are unique and highly dependent on the boundary conditions. There are then all the other methodologies laying in between those two extreme options offering many advantages. For instance, the effects of thermal expansion can be incorporated, the applicability of the methods is more general, and the final verifications can still be considered as simple. For single storey steel portal frames, the verifications can be simplified to the consideration of some critical sections instead of the whole structure. The present paper proposes a methodology to verify the integrity of single storey steel portal frames after real fire exposures, based on the force-based method.

1   INTRODUCTION

Since finite element model (FEM-) based tools are widely available, and rather easy to use, they became the favourite tools for practical applications. The displacement-based method also has the big advantage to be straightforward and does not generally require any engineering judgement. In the frame of manual calculations however, the displacement-based method is inapplicable as the generated output rapidly becomes difficult to manage, and therefore to analyse. For simple statically indeterminate structures, as presented in *Figure 14*, there exist however the force-based method (FBM) or sometimes also called flexibility method. Recent literature is mostly dedicated to machinery development and seismic applications [1], structural application are rare to find [2].
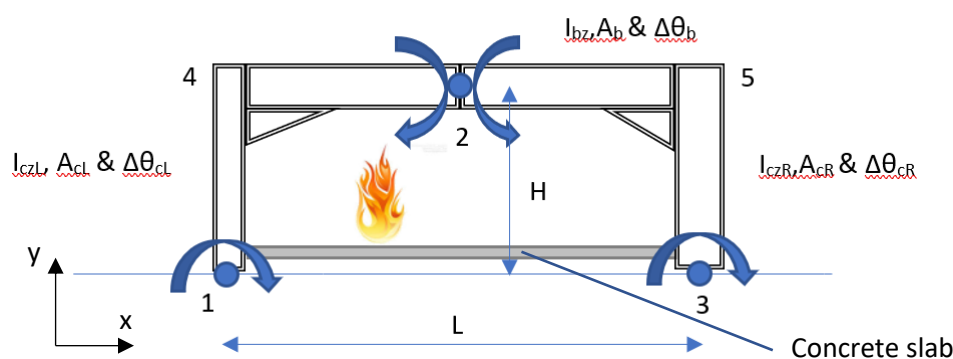

Figure 14. Typical portal frame of an industrial steel building (different column types in this example)

Depending on the degree of indeterminacy, it is possible to directly calculate the set of internal forces and moments at a limited number of locations. Of course, some engineering expertise is needed beforehand to select the critical forces which will cause the failure mode. It should be noted that, in case of fire, the degree of indeterminacy can be higher than at ambient temperature, this is due to the possible presence of concrete floor slabs that blocks the horizontal movements and rotations at the bottom level. And, this is of course only valid if the considered column passes through this concrete slab down to a lower level. For rather simple structures, as the one presented in *Figure 14*, the critical sections can easily be based on the engineer's expertise, but could also be deduced from a FEM analysis until failure (subjected to a standard fire). For example, two failure modes of such a portal frame are shown in *Figure 15*, they were obtained using the thermal-structural programme SAFIR® [3]. Failure is clearly initiated by plastic hinges occurring at the foundation level and at midspan, which become the critical sections.
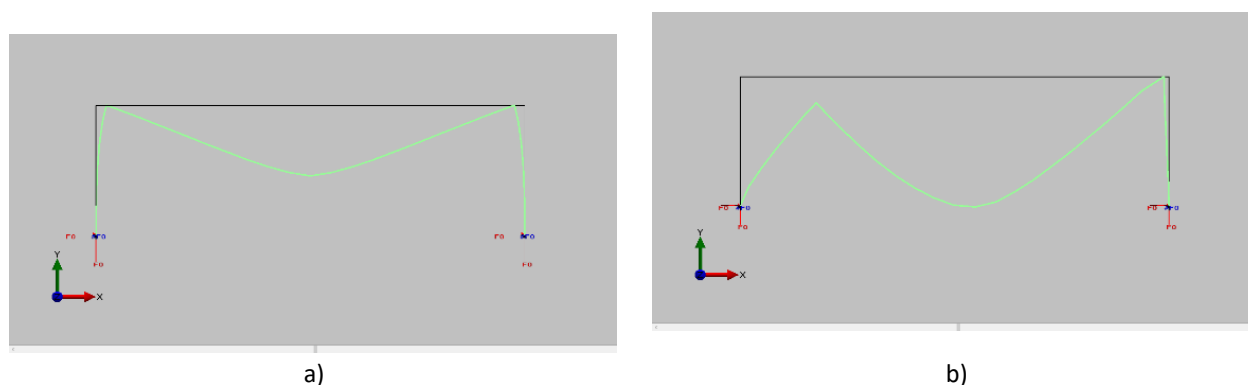

| a) | b) |

Figure 15. Failure modes due to a) uniform heating; b) heating of the left column and the beam

This paper focusses on real fires under low temperatures so that the structural response of the frame remains in the linear-elastic domain and with a failure mode in the plane of the frame. The presented method is therefore suitable for the evaluation of steel structures which are only subjected to local fires or for the assessment of structures which survived a real fire. The portal frame displacements stay in its plane which is only possible if the columns and beam are sufficiently supported by girders or steeldeck. The scope of this paper is limited to bending and instability phenomena are disregarded. It is our intention to propose a method allowing a quick but accurate structural assessment based on a limited amount of information, of structures that survived a local fire.

To illustrate the possibilities and limitations of the proposed calculation model based on the FBM, a case-study is developed in section 4. A portal frame is chosen which respects, under ambient conditions, the usual code requirements. A fixed uniformly distributed load p (including the own structure weight) of 2.3 kN/m was applied on the roofbeam. It is assumed that the horizontal wind load (which may be reduced by a factor Ψ_{fi}) can be neglected. European IPE330 profiles made of S235 are considered. They are heated on four sides; no shadow factor is considered and the reductions of the yield strength as well as Young's modulus due to the temperature are based on [4].

2   REAL FIRE VERSUS NOMINAL FIRE

2.1 Nominal fire limitations

Nominal fires, such as the ISO834 standard fire, are widely used because they have the advantage that the outcome of the analysis can be compared in a quantitative way. In many countries, regulations are prescribing (and sometimes even by law) the use of this type of fires (see *Figure 16,*

solid lines). By using nominal fires, the designed structures perform similarly i.e. up to the same safety level as they withstand the same duration of a nominal fire. A great number of experiments on elements resulted in relatively simple design equations and even tabulated database simplifying the design. However, in case of statically indeterminate structures, the effect of the thermal expansion is generally not included, which may result in unconservative design situation. It is nowadays a common practice to assess structures in case of fire, with a time dependent uniform heating over its length. Only the latest versions of for example SAFIR® also allows the use of local fires or temperature development curves resulting from computational fluid dynamic simulations [5].

2.2 Design procedures

When real fires are considered, their effects are often only local ones. With a limited number of users in the building and a rather limited amount of fire load, it is often useless to design for a complete flash-over, which is the case for the nominal fire prescribed by ISO834. But if badly located as next to a column, the influence of a local fire can generate important displacement and/or forces in the whole structure, which must then be carefully checked if not collapsed. In this case, we are outside the application of the codified methods and a third-party verification is needed. If this could be based on safe and simple models, precious time would be saved resulting in economic benefits for all parties. By way of simplification, a real fire can be modelled as a combination of an ISO834 fire applied on a column (local fire), a beam (in a hot smoke layer for a two-zone model) or the combination of both (to increase accuracy in temperature distribution following [6]), see the dashed line in *Figure 16*.
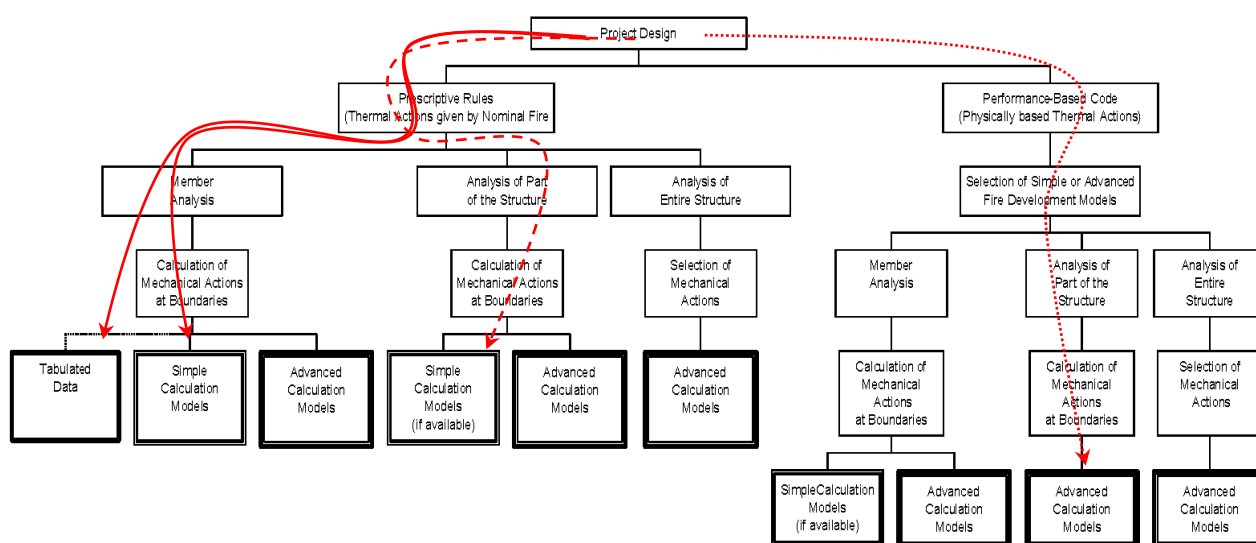

Figure 16. Design procedures following [6]

In practice, for a great deal of applications, the use of an uniform temperature over the length of the member will result in accurate results and the effect of elongations can be captured. In the next paragraphs, a uniform temperature over the member will also be presumed therefore no bending moments due to a difference in temperature along the height of a member will be generated. For unprotected steel profiles, this assumption is reasonable. The proposed method can be seen as a "Simple calculation model" as in *Figure 16*.

2.3 Procedures for the assessment of existing structures

Sometimes we're dealing with an existing structure which survived a fire, but, despite all regulations, it is still quite hard to investigate its influence on the reliability of the structure. In this case, there is a number of uncertainties and a quick assessment would be helpful to investigate several scenarios. Most of the time, only a range of smoke temperatures can be assumed through observations of cable insulation, roof lights, zinc layers, lead or aluminium elements, or any other damaged or melted materials. Presently, plastic design is not of interest since the structure still has to fulfil his function after the fire. Validation up to a limited smoke temperature of about 600°C is needed, otherwise we would be dealing with (partial) failure.

3 SIMPLIFIED FORCE-BASED METHOD FOR A PORTAL FRAME

3.1 Force-based method

With the force base method, the distribution of the internal forces X_j of a statically indeterminate structure can be assessed taking into account the effects of external forces, temperature, settlements, prestressing, etc. In this paper, we will limit ourselves to the effect of the temperature only, an elastic response and Euler-Bernoulli beams. The unknown forces X_j are obtained based on the compatibility equations, and the deformations and flexibility matrix are needed.

3.2 Deformations

Based on the principles of virtual work, the deformations D_j of a system submitted to a uniformly distributed load p are provided by *Eq. (1)* for internal moments and normal forces (neglecting shear) part and by *Eq. (2)* for the temperature part without considering the curvature due to non-uniform heating of the cross-section. If, in *Eq. (2)*, the elongation is written as $\Delta L/L$ instead of using the thermal expansion coefficient α and a temperature difference $\Delta\theta$, we have:

$$D_{j,0} = \int_0^L \frac{M_p \cdot \overline{M_J}}{E \cdot I_z} dx + \int_0^L \frac{N_p \cdot \overline{N_J}}{E \cdot A} dx \tag{1}$$

$$D_t = \int_0^L \overline{N_J} \cdot \alpha \cdot \Delta\theta \cdot dx = \int_0^L \overline{N_J} \cdot \frac{\Delta L}{L} \cdot dx = D_{t,fi} \tag{2}$$

where $D_{j,0}$ is the displacement at the location j for an isostatic system (rotation in rad.),

       L is the integration domain, it includes the whole length of all elements (m),

       M_p/N_p Moment/Normal force due to a uniformly distributed load p in N/m (Nm),

       M_j/N_j Moment/Normal force due to a unit displacement at the location j (Nm),

       E Young's modulus depending on the temperature of the element θ (N/m²),

       I_z Second moment of area of the cross-section, the subscripts cL (column Left), b (beam) and cR (column right) are used, see Figure 14 (m⁴),

       A Area of the cross-section, with the same subscripts (m²),

       DL/L   Thermal elongation depending on the temperature of the element θ (-).

For a portal frame as depicted in *Figure 14*, the sum of *Eqs (1)* and *(2)* is provided in *Eqs (3) to (5)* for the rotations at the nodes (1), (3) and the relative rotation at node (2).

$$D_{1,0} + D_{1,t} = \frac{pL^2H}{24}\left(\frac{-1}{E_{cL}\cdot I_{czL}} + \frac{1}{2\cdot E_{CR}\cdot I_{czR}}\right) - \frac{pH}{2}\left(\frac{1}{E_{cL}\cdot A_{cL}} - \frac{L^3}{8\cdot E_b\cdot A_b\cdot H^3} - \frac{1}{E_{CR}\cdot A_{cR}}\right) + \left(\left(\frac{\Delta L}{L}\right)_{cL}\frac{H}{L} - \left(\frac{\Delta L}{L}\right)_b\frac{L}{2H} - \left(\frac{\Delta L}{L}\right)_{cR}\frac{H}{L}\right) \tag{3}$$

$$D_{2,rel,0} + D_{2,t} = \frac{pL^2H}{24}\left(\frac{1}{E_{cL}\cdot I_{czL}} + \frac{L}{H\cdot E_b\cdot I_{bz}} + \frac{1}{E_{CR}\cdot I_{czR}}\right) + \frac{pH}{2}\left(\frac{L^3}{4\cdot E_b\cdot A_b\cdot H^3}\right) - \left((\frac{\Delta L}{L})_b \frac{L}{H}\right) \tag{4}$$

$$D_{3,0} + D_{3,t} = \frac{pL^2H}{24}\left(\frac{-1}{2\cdot E_{cL}\cdot I_{czL}} + \frac{1}{E_{CR}\cdot I_{czR}}\right) - \frac{pH}{2}\left(\frac{1}{E_{cL}\cdot A_{cL}} + \frac{L^3}{8\cdot E_b\cdot A_b\cdot H^3} - \frac{1}{E_{CR}\cdot A_{cR}}\right) + \left((\frac{\Delta L}{L})_{cL}\frac{H}{L} + (\frac{\Delta L}{L})_b\frac{L}{2H} - \alpha_{cR}(\frac{\Delta L}{L})_{cR}\frac{H}{L}\right) \tag{5}$$

3.3 Flexibility matrix

Without the numerical derivation of all flexibility components, *Eqs (6)* to *(11)* provide the different elements to compose the flexibility matrix, with the meaning of the symbols given in *Figure 14* and *Eq (1)*.

$$f_{11} = \frac{H}{12}\left(\frac{7}{E_{cL}\cdot I_{czL}} + \frac{L}{E_b\cdot I_{bz}\cdot H} + \frac{1}{E_{CR}\cdot I_{czR}}\right) + \frac{H}{L^2}\left(\frac{1}{E_{cL}\cdot A_{cL}} + \frac{L^3}{4\cdot E_b\cdot A_b\cdot H^3} + \frac{1}{E_{CR}\cdot A_{cR}}\right) \tag{6}$$

$$f_{12} = f_{21} = \frac{H}{6}\left(\frac{-2}{E_{cL}\cdot I_{czL}} + \frac{1}{E_{CR}\cdot I_{czR}}\right) + \frac{H}{L^2}\left(\frac{L^3}{2\cdot E_b\cdot A_b\cdot H^3}\right) \tag{7}$$

$$f_{13} = f_{31} = \frac{H}{6}\left(\frac{1}{E_{cL}\cdot I_{czL}} + \frac{L}{2\cdot E_b\cdot I_{bz}\cdot H} + \frac{1}{E_{CR}\cdot I_{czR}}\right) + \frac{H}{L^2}\left(\frac{1}{E_{cL}\cdot A_{cL}} - \frac{L^3}{4\cdot E_b\cdot A_b\cdot H^3} + \frac{1}{E_{CR}\cdot A_{cR}}\right) \tag{8}$$

$$f_{22} = \frac{H}{6}\left(\frac{2}{E_{cL}\cdot I_{czL}} + \frac{6\cdot L}{E_b\cdot I_{bz}\cdot H} + \frac{2}{E_{CR}\cdot I_{czR}}\right) + \frac{H}{L^2}\left(\frac{L^3}{4\cdot E_b\cdot A_b\cdot H^3}\right) \tag{9}$$

$$f_{23} = f_{32} = \frac{H}{6}\left(\frac{-1}{E_{cL}\cdot I_{czL}} + \frac{2}{E_{CR}\cdot I_{czR}}\right) + \frac{H}{L^2}\left(\frac{1}{E_{cL}\cdot A_{cL}} + \frac{L^3}{4\cdot E_b\cdot A_b\cdot H^3} + \frac{1}{E_{CR}\cdot A_{cR}}\right) \tag{10}$$

$$f_{33} = \frac{H}{6}\left(\frac{1}{2\cdot E_{cL}\cdot I_{czL}} + \frac{L}{2\cdot E_b\cdot I_{bz}\cdot H} + \frac{7}{2\cdot E_{CR}\cdot I_{czR}}\right) + \frac{H}{L^2}\left(\frac{1}{E_{cL}\cdot A_{cL}} - \frac{L^3}{4\cdot E_b\cdot A_b\cdot H^3} + \frac{1}{E_{CR}\cdot A_{cR}}\right) \tag{11}$$

3.4 Methodology

In the case of this portal frame, the 3 moments M_1, M_2 and M_3 at the node locations or critical sections can be obtained by the use of the matrix equation *Eq. (12)*. It can be solved at any time for a known steel temperature calculated for example according to [4] section 4.2.5.1, for unprotected internal steelwork.

$$\begin{Bmatrix} M_1 \\ M_2 \\ M_3 \end{Bmatrix} = \begin{bmatrix} f_{11} & f_{12} & f_{13} \\ f_{21} & f_{22} & f_{23} \\ f_{31} & f_{32} & f_{33} \end{bmatrix}^{-1} \cdot \begin{Bmatrix} -D_{10} - D_{1,t} \\ -D_{20} - D_{2,t} \\ -D_{30} - D_{3,t} \end{Bmatrix} \tag{12}$$

After finding the moments, the result should be compared to the bending moment capacity of the section at the given temperature $M_{Rd,\theta,fi}$ out of [4], see *Eq. (13)*. Plastic redistribution of the forces can be assumed, as it is allowed in *Annex E* of [7].

$$M_{Rd,\theta,fi} = k_{y,\theta}\frac{W_{net}f_y}{\gamma_{M,fi}} \tag{13}$$

where $M_{Rd,\theta,fi}$ is the moment resistance of the gross cross-section in case of fire (Nm),

$k_{y,\theta}$ is the reduction factor for the yield strength at a temperature θ (-),

W_{net} Section modulus, W_{pl} for class 1 and 2, W_{el} for class 3 and W_{eff} for class 4 sections (m³),

f_y Yield or 0.2% proof strength at 20°C (N/m²),

$\gamma_{M,fi}$ Material safety factor in case of fire (-).

To obtain an estimation of the failure moment, a unity check formulation, provided in *Eq. 14*, can be used. It uses the favourable effects of a possible moment redistribution.

$$Unity\ check = MAX\left\{\left(\frac{|M_1|}{M_{Rd,\theta,fi,1}} + \frac{|M_3|}{M_{Rd,\theta,fi,3}}\right)\frac{1}{2} \middle| \left(\frac{|(M_4+M_5)/2|}{M_{Rd,\theta,fi,4}} + \frac{|M_2|}{M_{Rd,\theta,fi,2}}\right)\frac{1}{2}\right\} \quad (14)$$

4 VERIFICATION

Several scenarios of fire load based on the temperature development provided in ISO834 will be presented in the following sections, the obtained FBM results after 5, 10, 7.6, 10, 15, 20 minutes and at failure time (solid lines) will be compared with the results of the same cases using SAFIR® (dashed lines). To 7.6 minutes corresponds a steel temperature of 400°C at which the yield strength starts to decrease. In all figures, the grey dotted line with its index "EB limit" indicates until when the Euler-Bernoulli hypotheses is valid (i.e. when the deflection is lower than h/2).

Once the flexibility components (*Eqs. (6) to (11)*) are included in a calculation sheet, *Eq. (12)* can be solved for several times or temperatures.

4.1 Complete structure subjected to an ISO834 fire

In this simulation all profiles are heated according to the ISO834 curve, or a fully developed fire. In *Figure 17 a)*, the temperature development is provided but this will be not be repeated in the other graphs. It can been seen that the mid-span moments M_2, FEM and $M_{2,FBM}$ (see Figure 14, node numbers in between brackets can be found in Figure 14) are very similar which is also the case for the averaged value of the beam-to-column nodes (M_4 and M_5), calculated as $pL^2/8$, see section 1 for symbols. For the moment at the foundation level of the column, denoted M_1 and M_3, a deviation occurs around 7 minutes and reaches the maximum moment capacity after 10 minutes or about 500°C steel temperature T_a. This has no influence on the beam moments but after 17.5 minutes or $T_a = 690$°C, the deflection D_y becomes bigger than h/2 which is seen as the limit of the simplified method.
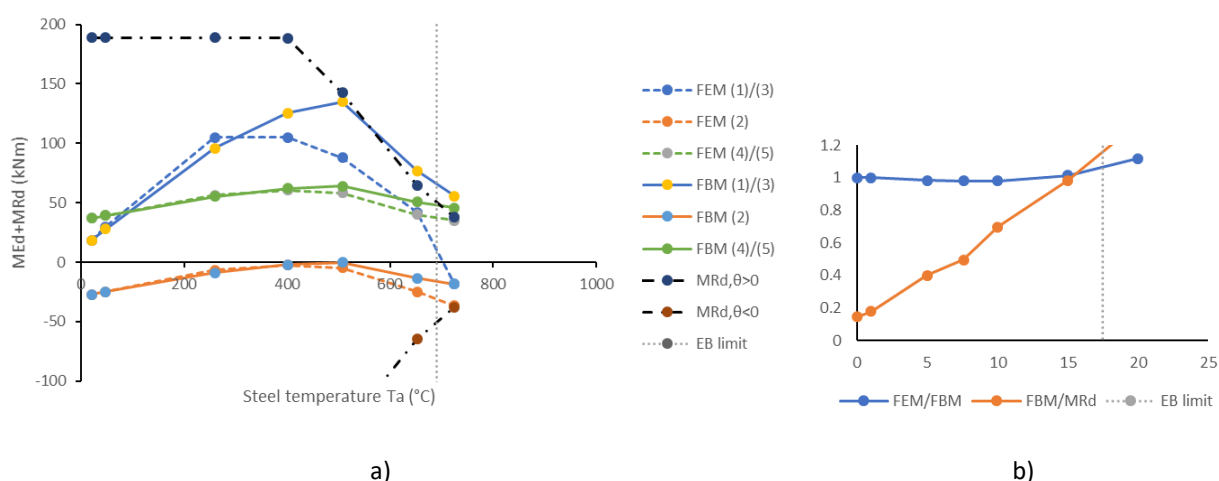

a)

b)

Figure 17. Comparison of results a) M_{Ed} and $M_{Rd,fi}$ in function of T_a, b) FEM-to-FBM ratio in beam + UC

A comparison between the beam moment sum $(|M_4| + |M_5|)/2 + |M_3|$ (FEM-to-FBM ratio) with redistribution is presented in *Figure 17 b)*. The unity check (UC) following *Eq. (14)* is also provided. A reasonable estimation of the failure time is given when the UC becomes higher than 1.0. These results will be further discussed in section 5.5.

4.2 Single column subjected to an ISO834 fire

This is a typical load case that occurs when a column is subjected to a local fire, therefore only the column is heated following the standard fire ISO834. *Figure 18* shows that very good agreement is obtained at all locations and at any time. Deformations stays limited till the end of the simulations, so the Euler-Bernoulli hypotheses stays valid in this case. Geometrical imperfections are not included in both models reason why buckling doesn't occur in the column.
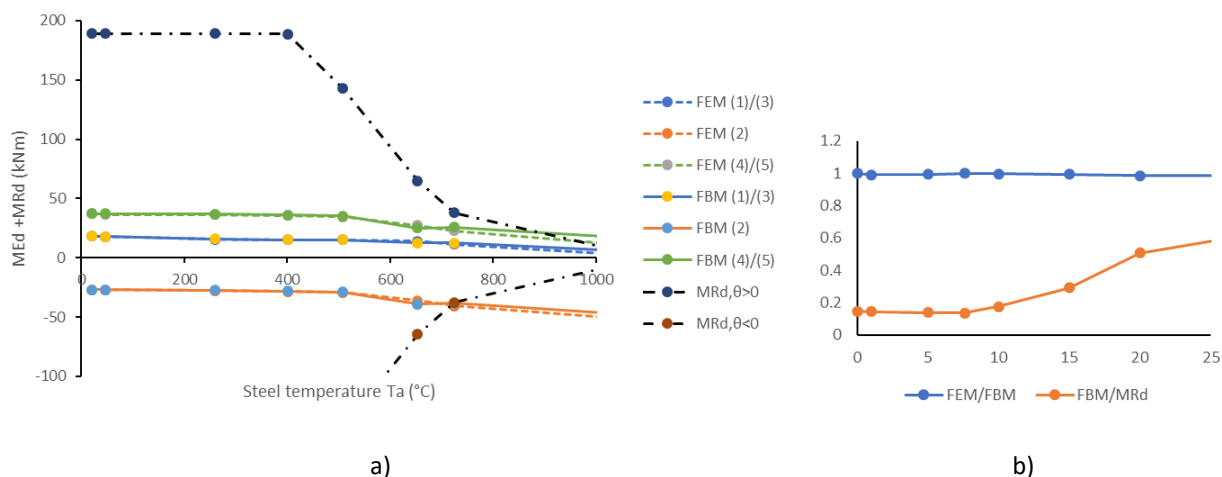

a)   b)

Figure 18. Comparison of results a) M_{Ed} and $M_{Rd,fi}$; b) FEM-to-FBM ratio in beam + UC

4.3 Beam subjected to an ISO834 fire

This situation occurs when the beam is subjected to the influence of a hot smoke layer. *Figure 19* provides the comparison showing that, till 10 minutes or 508°C steel temperature, and at all locations very good agreement is obtained and even further as can be seen on *Figure 19 b)* showing the FEM-to-FBM ratio. After 16 minutes or $T_a = 670°C$, the deflection Dy is higher than h/2.
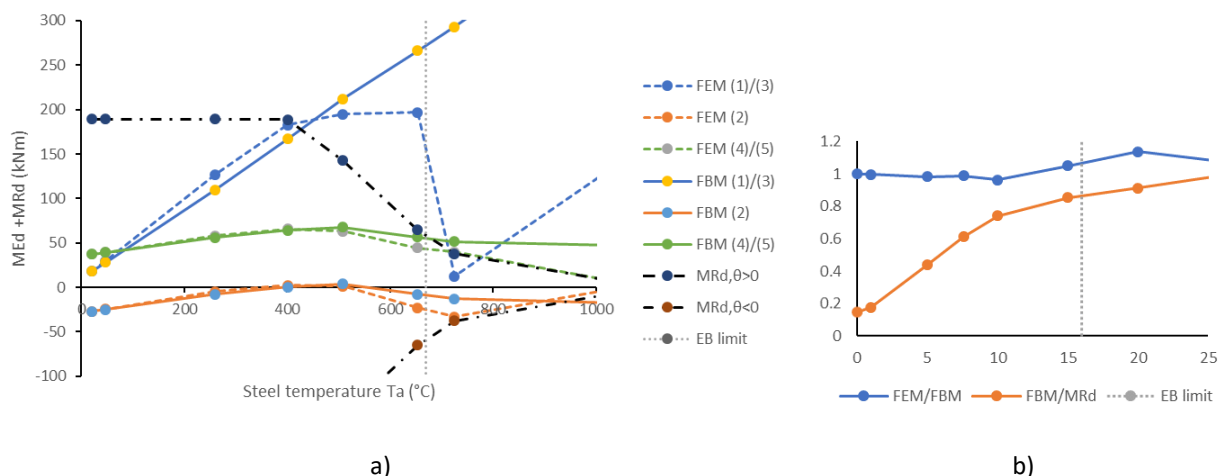

a)   b)

Figure 19. Comparison of results a) M_{Ed} and $M_{Rd,fi}$; b) FEM-to-FBM ratio in beam + UC

4.4 Single column and beam subjected to an ISO834 fire

In the final stage of a fire, the structure can be influenced by a local fire next to the column and a beam engulfed in a smoke layer, the corresponding results are given in *Figure 20*.
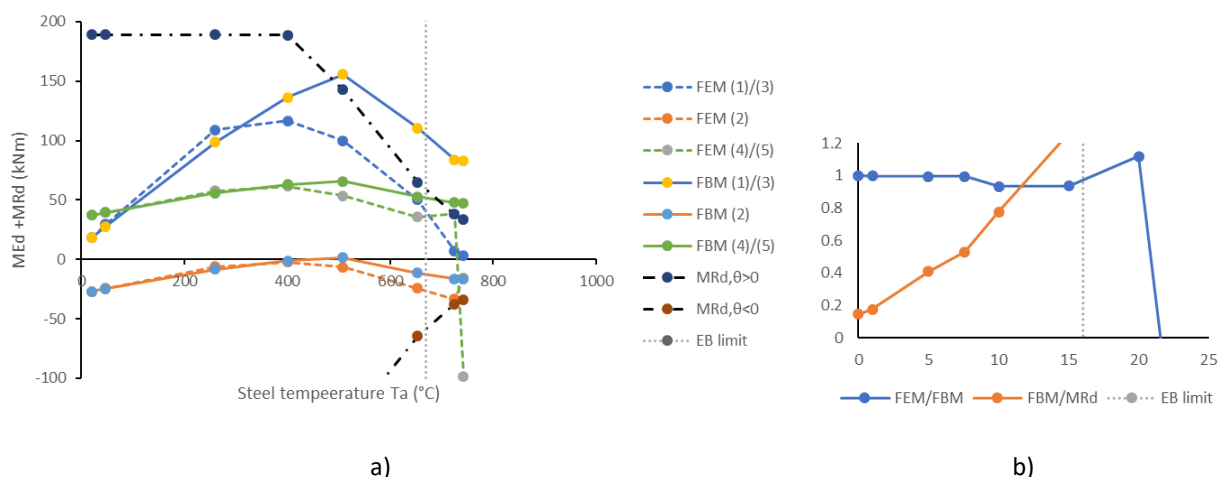
a)   b)

Figure 20. Comparison of results a) M_{Ed} and $M_{Rd,fi}$; b) FEM-to-FBM ratio in beam + UC

Quite good similarity is achieved although, at the foundation level, only till 5 minutes (where the
steel and smoke temperature T_a equal 260°C and 576°C respectively). Based on the FEM-to-FBM
ratio in the beam, very good agreement is obtained up to 20 minutes ($T_a = 725$°C). After 16 minutes
or $T_a = 670$°C, the Euler-Bernoulli approximation for the deflection is strictly no longer valid, the
failure mode is shown in *Figure 15 b)*.

4.5 Discussion

As explained in section 189, the simplified method is proposed for real fire applications during
which relatively low temperatures are observed i.e. structures which survived a fire. The most
important advantages are the CPU-time which is lower than 1 second, which makes the verification
of multiple scenario's and sensibility analysis possible, an accurate simulation for the beam forces
and a conservative prediction of the failure time. All those elements, are summarized in

Table 4. Our concern is given to the beam since the column ends, at foundation level, are most of
the time not heated (excepted for the single column heating scenario) so in order of occurrence it is
for practical reasons unlikely to occur at this location.

Table 4 Summary of results

Fire load case	CPU-time (min)	Accurate simulation time (min) & steel temperature (°C)	Failure time FEM (min)	Failure time FBM (min)
All profiles §5.1	4	15 & θ_a = 653°C	20.5	15.2
Single column §5.2	1	>25 & θ_a = 756°C	>120	53.2
Roof beam §5.3	2	15 & θ_a = 653 °C	>120	26.9
Column + beam §5.4	5	>20 & θ_a = 725°C	23.4	12.3

5   CONCLUSIONS

The present paper describes a simplified method based on the force-based method (FBM) for
structures which survived a fire. The proposed method is promising and could fill up the gap of
simple calculation models.

The best agreement could be achieved for local fires with a limited influence on a single column. Here, the method performs well till steel temperatures up to 750°C. Furthermore, it is shown that the FBM is a valuable simplified calculation model which can be used in cases where the steel temperature stays limited till about 650 °C and localized fire as it is mostly the case for the assessment of structures which survived a fire. Only for a fully developed fire the method reaches his limits at 400°C. However, in combination with moment redistribution, a good agreement could be obtained even up to quite high deflections and the highest temperatures (≥ 650°C) in all kind of applications.

The method will be checked in the near future for several influencing factors as the section's height-to-span ratio, the second moment of area of each element included in the frame, natural fires, …

REFERENCES

[1] S. Shahrokh, G. Majid and A. K. Mohammad, „Simplified force-based seismic design procedure for linked column frame system," *Soil Dynamics and Earthquake Engineering*, pp. 87-101, 2019.

[2] A. Bigtari, P. Harrison en N. Bicanic, „Quasi-hinge beam element implemented within the hybrid force-based method," *Computers and Structures,* vol. 137, pp. 31-45, 2014.

[3] J. Franssen and T. Gernay, „Modelling structures in fire with SAFIR," *Journal of Structural Fire Engineering, vol. 8, nr. (3),* pp. 300-323, 2017.

[4] EN 1993-1-2, Design of steel structures - Part 1-2: General rules - Structural fire design, Brussels: CEN, 2004.

[5] K. McGrattan, S. Hostikka, R. Mc Dermott, J. Floyd en M. Vanella, Fire Dynamics Simulator - User's Guide, Maryland: NIST, 2018.

[6] EN 1991-1-2, Actions on structures - Part 1-2: General actions - Actions on structures exposed to fire, Brussels: CEN, 2002.

[7] EN 1992-1-2, Design of concrete structures - Part 1-2: General rules - Structural fire design, Brussels: CEN, 2004.

[8] J. Sheng, G. Dan, C. Hongyu, C. Rui and Z. Xuhong, „A force-based method for identifying the deformation modes of thin-walles members," *Thin-Walles Structures*, pp. 473-497, 2018.

[9] M. Fox, T. Sullivan en K. Beyer, „Comparison of Force-based and displacement-based design approaches for RC coupled walls in New Zealand," *Bulletin of the NZSEE,* pp. 190-205, 2014.

FIRE SAFETY OF CONCRETE STRUCTURES

EFFECT OF THE STATIC SCHEME ON THE BEHAVIOUR OF FRP REINFORCED CONCRETE SLABS IN FIRE

Antonio Bilotta, Alberto Compagnone, Laura Esposito, Emidio Nigro

University of Naples Federico II, Naples, Italy

ABSTRACT

Composite materials play a central role in the evolution of construction materials (e.g. Fiber Reinforced Polymer - FRP) and structural typologies. Although these materials have excellent mechanical behaviour at room temperature, they can take affect the structural response at high temperature. When the temperature exceeds the glass transition temperature, the polymeric matrix that surrounds the fibres is unable to transfer stresses. The authors investigated the behaviour of the Glass FRP reinforced concrete (GFRP-RC) members exposed to fire, through a 3D FEM model validated on experimental tests performed on statically determined GFRP-RC slabs exposed to Standard fire curve. This paper shows the effect of redundant boundaries condition, as well as number and length of the spans. The results showed that in redundant static scheme fire scenarios significantly affect the stresses in the structural members analysed with the numerical model.

1   INTRODUCTION

In recent decades the civil engineering industry has focused its attention to the development and use of innovative materials, with the aim to overcome some problems concerning the "traditional" building materials and in order to extend the actual service life of the structures. Use of fibres reinforced polymer (FRP) bars or grids instead of traditional steel reinforcements is an interesting application. The choice of FRP bars is primarily favoured by the high corrosion resistance but also by high strength-to-weight ratio, as well as possible high stiffness-to-weight ratio, degree of chemical inertia and fatigue tolerance. Nevertheless, there are also disadvantages such as the vulnerability at high temperatures due to the degradation of the resin. Indeed, the bar is unable to transfer shear stress between the individual fibres and to the surrounding concrete, once it achieves the glass transition temperature.

The authors have investigated the behaviour of Glass FRP RC slabs exposed to Standard fire (ISO834 curve) with a FEM model validated on experimental results (*Bilotta et al. (2019)* [1]). In this paper, we show the results obtained with different static schemes, studied to analyse the redundant restraint effect in fire condition. Indeed, it is known that there is a variation of the stresses and the structural response changes, if thermal expansion is prevented.

The modelled slabs were designed according to CNR DT 203/2006 [2]. The design of RC members reinforced with FRP rebars is governed by service condition, due to the low value of the Glass FRP's young modulus. Generally, the design of RC members strengthened with FRP rebars starts from SLS (Serviceability Limit State), because if service condition checks (i.e. deformability and stress level) are satisfied probably also ULS (Ultimate Limit State) checks are satisfied.

2   THERMO-MECHANICAL MODELS FOR THE MATERIALS

The concrete thermal properties have been simulated with the relationships provided by EN1992-1-2 [3]. In particular, a correction of the specific heat between 100 °C and 200 °C has been assumed to take in account the latent heat of the water evaporation. As concern the FRP, the specific heat and thermal conductivity relationships provided by Bai et al. (2007) [4] for GFRP bars were assumed.

The coefficient of linear thermal expansion of the GFRP has been set equal to $6.0 \cdot 10^{-06}$ [C$^{\circ-1}$], according to fib 2007 [5].

Compressive behaviour of concrete C25/30 has been assumed according to the stress-strain relationship provided by EN1992-1-2 for calcareous aggregate, while the tensile behaviour has been defined according to the model provided in Belarbi & Hsu (1994) [6] with the factors provided by EN1992-1-2 [3] for strength and stiffness reduction at high temperature.

The mechanical behaviour of GFRP bar in tension has been assumed linear-elastic up to the failure. To take into account the reduction of stiffness and strength as temperature increases, a reduction coefficient has been defined, according to E. McIntyre et al. (2014, [7]). It is worth noting that the experimental results in E. McIntyre et al. (2014) [7] were obtained by tests carried out on GFRP bars with 12mm diameter. The strength reduction law obtained by interpolating those experimental results has been also used to model the behaviour in fire of rebars with different diameters. About that, composites materials consisting of fibre and polymeric matrix are characterised by *shear lag effect*, which implies a reduction of strength with the increase of bar diameter. This shear lag effect should be less significant at high temperature, because the resin is no more effective. For this reason, the use of the coefficients proposed in [7] for bars with diameter greater than 12mm is probably conservative, if the resistance at ambient is reduced to take into account the shear lag effect.

Fig. 1 shows the stress–strain law for concrete in compression and tension (Fig.1 a,b) and GFRP (Fig1 c) varying the temperature. As concerns the GFRP rebars in compression, the strength at ambient temperature is low and it is usually neglected in the design of GFRP-RC members (according to CNR DT 203/2006 [2]). At high temperatures the compressive strength vanishes, due to transition from solid to rubbery state of the polymeric matrix when glass transition temperature is achieved. To take in account this and to overcome numerical convergence problem in the model, the compressive behaviour of GFRP is assumed the same of surrounding concrete.
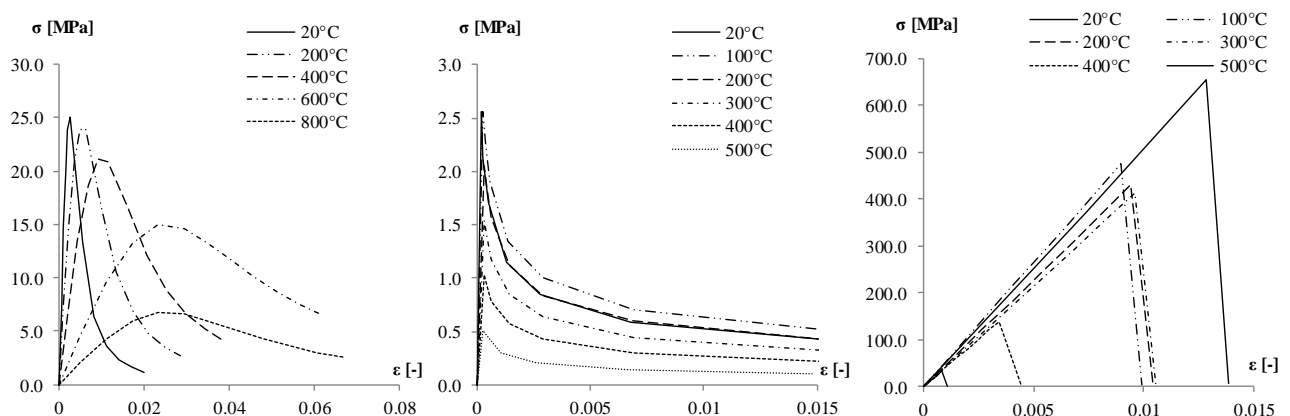

Fig. 1. Strain – stress constitutive laws for concrete (a,b) and GFRP (c)

3 GEOMETRY, STATIC SCHEME AND LOAD

A slab exposed to fire from below exhibits a thermal gradient along the cross section and high compression stresses arises in the structural member, supposed of homogeneous material, if there are longitudinal translation restraints. Moreover, rotational restraints generate hogging bending moments. To investigate the structural behaviour of these members in flexure, the authors have built some FEM models in *Abaqus/Standard* [8] based on the thermo-mechanical model validated in *Bilotta et al. (2019)* [1], which takes into account the above mentioned non-linear thermo-mechanical behaviour of the materials and the large displacements. *Fig. 2* shows the static schemes

and the fire scenarios analysed through the FEM model. For each geometrical configuration (i.e. S1, S2, S3 and S4) two different boundary conditions have been analysed: free and prevented longitudinal expansion, named "free" and "fixed" in the label, respectively. In particular S1 is a simply supported slab with a 4000mm long span and exposed to fire from below. The scheme S2 is equal to S1, but it has a longer span (5000mm). The scheme S3 is a continuous slab with two spans, each of which has the same length of scheme S1 (i.e. 4000mm); in this scheme both spans are exposed to fire from below ("FF" in the label). The scheme S4 is equal to S3 but only one span is exposed to fire ("F" in the label). The names of the analyses are summarised in *Table 1*.
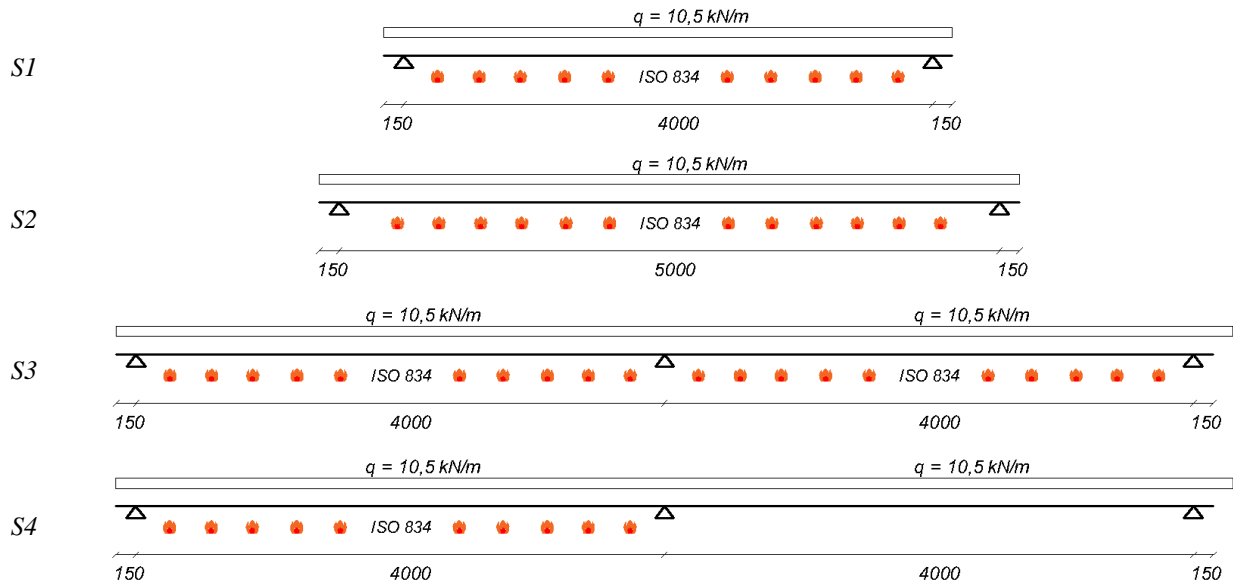
Fig. 2. Static schemes and fire scenario
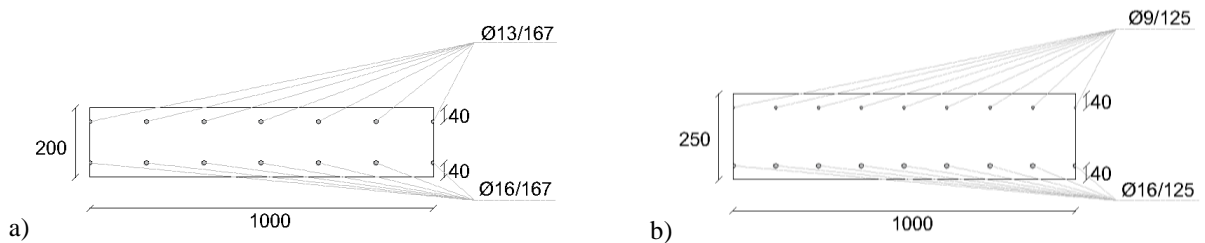
Fig. 3. Cross sections of the slabs

The cross section of S1, S3 and S4 is 200 mm height and reinforced with 6Φ16 and 6Φ13 per meter, on the bottom and top side, respectively (see *Fig. 3a*). The slab S2 is 250mm high, so that the ratio $L/h =20$ is the same of S1 slab, and it is reinforced with 8Φ9 and 8Φ16 per meter on top and bottom side respectively (see *Fig. 3b*). Note that the higher bar area at the bottom is due to the serviceability limit state checks. The slabs have been designed for the same load level , i.e. fire load level $\eta_{fi} = \dfrac{E_{d,fi}}{E_d} = \dfrac{G_k + \psi_{fi}Q_{k1}}{\gamma_G G_k + \gamma_{Q,1}Q_{k,1}} \cong 0.65$ and degree of utilization $\mu_{fi} = M_{Ed,fi}/M_{Rd} \cong 0.4$.

The constant and uniformly distributed load is calculated with semi-permanent load combination, according to NTC 2018 [9] In particular, in addition to structural weight G_{k1}, the permanent non-structural load G_{k2} and the accidental load Q_k were imposed respectively equal to 4kN/m² and 2.5 kN/m², according to code for buildings destined for traffic areas and parking of lightweight vehicles. The concrete cover is 40mm. The slabs S1 and S2 were designed according to CNR DT

203/2006 [2], by neglecting the compressive contribution of GFRP rebar. As expected, the design was governed by the verifications against the SLS. For direct comparisons the slabs S3 and S4 have the same cross section and length of the slab S1: the check on deflection is certainly fulfilled and negative bending resistance on central support was verified with the top reinforcement (i.e. 6Φ13 per meter).

To consider that the ends of the slabs are not directly exposed to fire because they are embedded in the beams supporting them, an adiabatic zone was defined at the constrained zone. This unexposed zone allows to ensure a cold anchoring length of rebars [10].

The numerical simulation consisted of two stages: Stage 1, uniformly distributed load and Stage 2, exposure to the ISO 834 standard curve from below up to 120 minutes, with constant load.

Table 1. Analyses labels

Scheme	Free longitudinal expansion	Prevented longitudinal expansion
S1	4m_free	4m_fix
S2	5m_free	5m_fix
S3	4m+4m_free_FF	4m+4m_fix_FF
S4	4m+4m_free_F	4m+4m_fix_F

4 RESULTS OF THE NUMERICAL ANALYSES

Table 2 summarizes the results obtained by numerical analyses: exposure time at failure, maximum displacement and the ratio $\sigma_\theta / \sigma_{\theta max}$ between the tensile stress and tensile strength in bottom rebar at failure or at 120min if failure did not occur. $\sigma_{\theta max}$ considers the strength reduction due to the temperature. No coefficient is listed if the bar is in compression. The statically-determinate slabs designed with the same load level (i.e. 4m_free and 5m_free) have the same time and kind of failure: after about 90 minutes of exposure to standard fire curve the GFRP strength, dependent on temperature, is achieved in bottom rebars. When longitudinal expansion was prevented (i.e. fixed), compression stresses arise in each cross section due to redundant restraints. *Fig. 4* shows the comparison between the stresses map in 4m_free and 4_fix scheme: the black zone indicates the part of the compressed slab. The resultant force of these stresses produces a negative bending moment due to its eccentricity with respect to the centroid of the cross section, but this effect seems localized. The slabs 4m_fix and 5m_fix have shown the failure at 90 and 116 minutes respectively, but the failure mode should still be investigated. The continuous slabs (i.e. S3 and S4) didn't show the failure within 120 minutes of exposure to ISO834 fire curve.

Table 2. Analyses result

Analysis label	Time of failure	v_{max} [mm]	$\sigma_\theta / \sigma_{\theta,max}$
4m_fix	90	51	0.3
4m_free	92	84	1.0
5m_fix	116	61	0.7
5m_free	95	97	1.0
4m+4m_fix_FF	>120	11	-
4m+4m_free_FF	>120	46	0.37

4m+4m_fix_F	>120	11	-
4m+4m_free_F	>120	50	0.39

Fig. 5 shows the curves time-displacement for each slab obtained by numerical analyses respectively for slab with one (i.e. S1 and S2) and two (i.e. S3 and S4) spans. *Fig. 5a* shows that the slab with a 5m long span (continuous line) is more deformable than the 4m slab (dashed line), having the same L/h ratio but different equivalent inertia and length. On the other hand, the slabs 4m_fix and 5m_fix show quite similar displacements up to failure of the first one, because the normal forces reduce the cracking of the slab, and the un-cracked cross section of the 5m slab is stiffer than the 4m slab. It is evident that preventing longitudinal thermal expansion reduce vertical displacements. As concerns the continuous slabs (i.e. S3 and S4 in *Fig. 5b*), the continuous static scheme strongly reduces the displacements and there is no failure until 120 minutes. The effect of normal force is confirmed significant in reducing the displacement. *Fig. 6* shows the deformed shape of continuous slabs at 0 minutes (i.e. semi–permanent load applied), 30 and 60 minutes of exposure to fire.

0 minutes

30 minutes
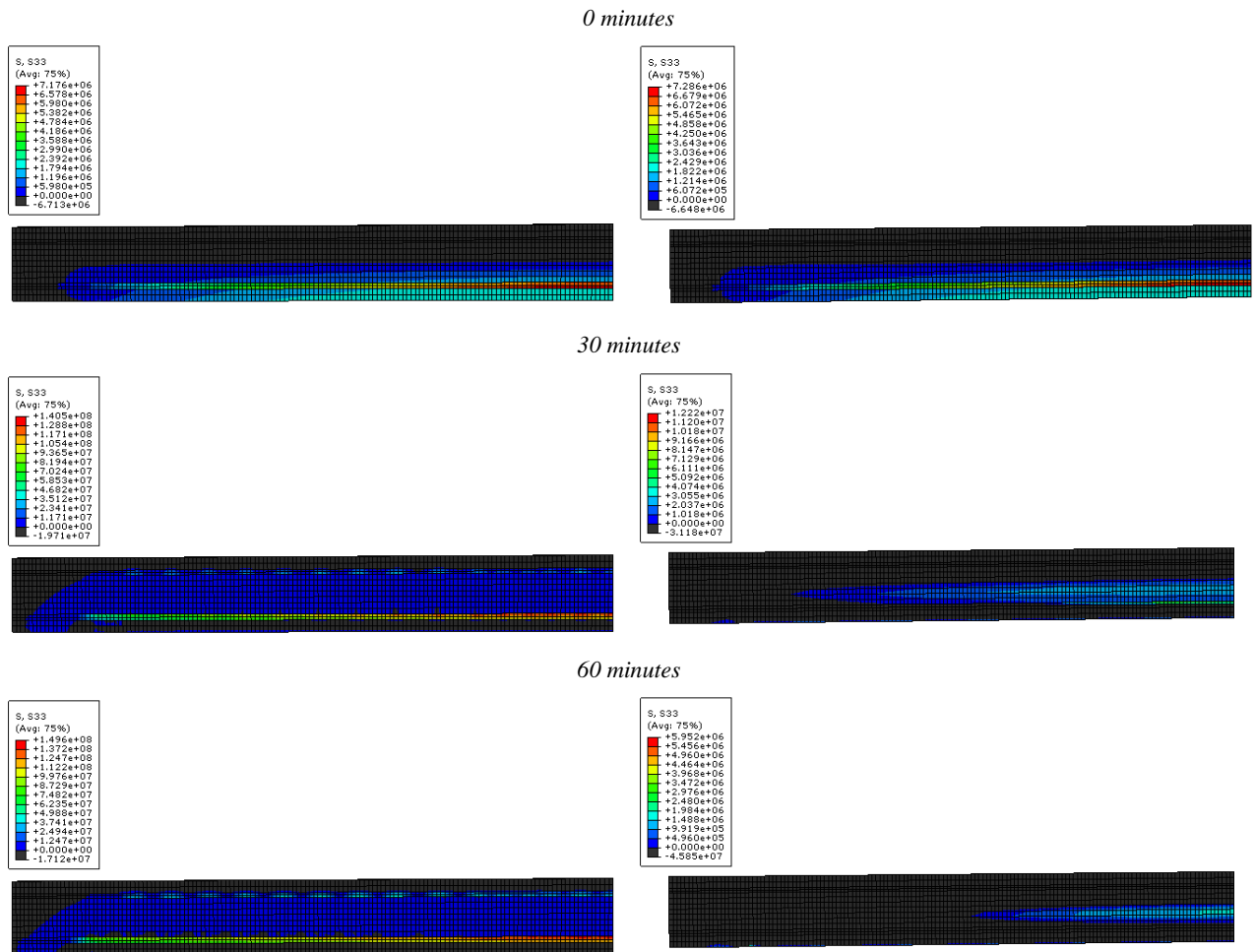
60 minutes

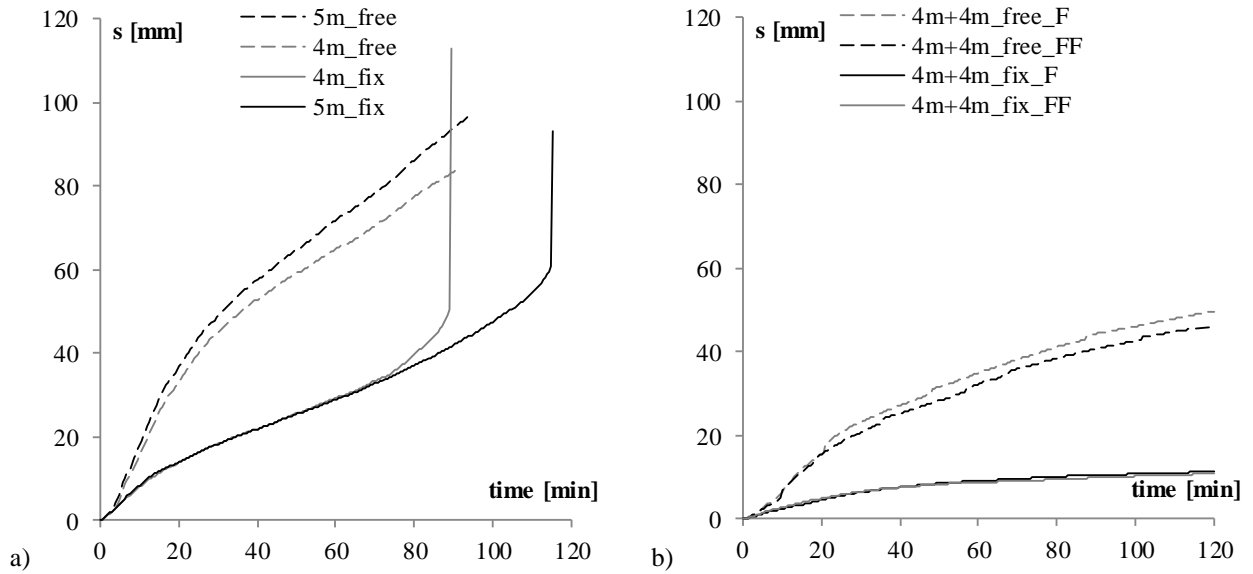Fig. 4. Stresses comparison between 4m_free and 4m_fix
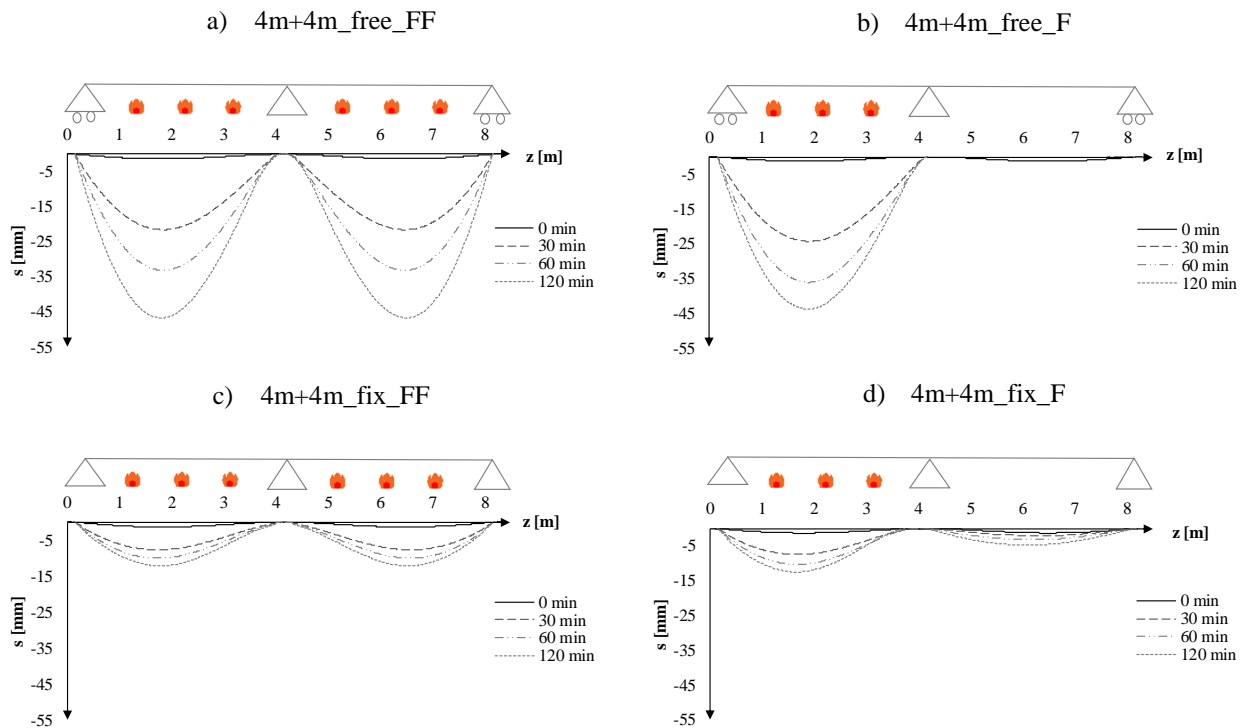
Fig. 5. Time – displacement curve

Fig. 6. Deformed shape of the slabs (S3 and S4)

Fig. 7 and *Fig. 8* show the bending moment diagrams for each slab at 0, 30 and 60 minutes of exposure to fire. *Fig. 7a,b* show that the bending moments are constant in the isostatic slabs , while *Fig. 7c,d* show the increasing positive bending moment as the exposure time increases when longitudinal expansion is prevented, although there are not redundant rotation restraints. This is due to the second order effects: the compression normal force that arises as a result of prevented thermal expansion induces a secondary moment. This secondary bending moment can be calculated, in a geometrical non-linear analysis, by multiplying the normal force value by vertical displacement. The increment of bending moment due to second order effects is very high. For example, for the 4m_fix scheme the bending moment arises from about 20kNm at ambient temperature to about

56kNm after 60 minutes of exposure to the ISO834 fire curve. Note that the increment of bending moment is accompanied by an increase of resistance according to moment-axial force domain that ensure the material compatibility.

Fig. 8 shows that with redundant rotation restraints there is an additive hogging bending moment due to the thermal curvature induced by the temperature gradient along the height of the slab. This hogging bending moment, increasing along the temperature, is maximum on central support; if redistribution due to cracking is possible the bending moment can increase, but less quickly. Since it is in the field of great displacements, there may be effects of the second order: also in this case, when longitudinal thermal expansion is prevented, there is an additive positive bending moment due to normal force in the cross section. It is important to highlight that when only one span was exposed to fire there is a strong increment of negative bending moment also on the not-exposed span (see *Fig. 8d*), balanced in the exposed span by the second-order effects, which can lead to different failure modes with respect to the case of fire on both spans. Therefore, the stresses in the structural members are strongly influenced by the specific fire scenario.
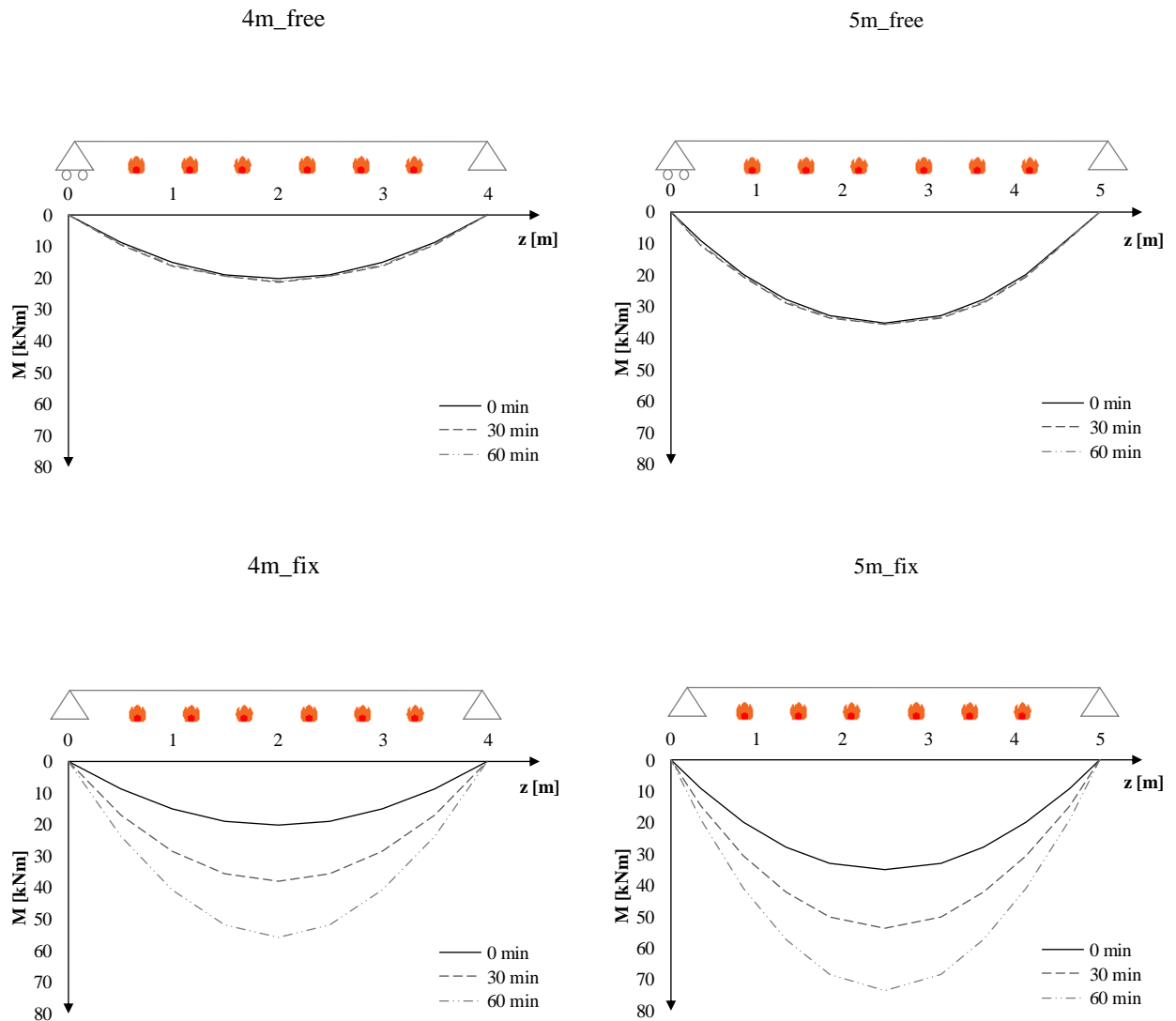

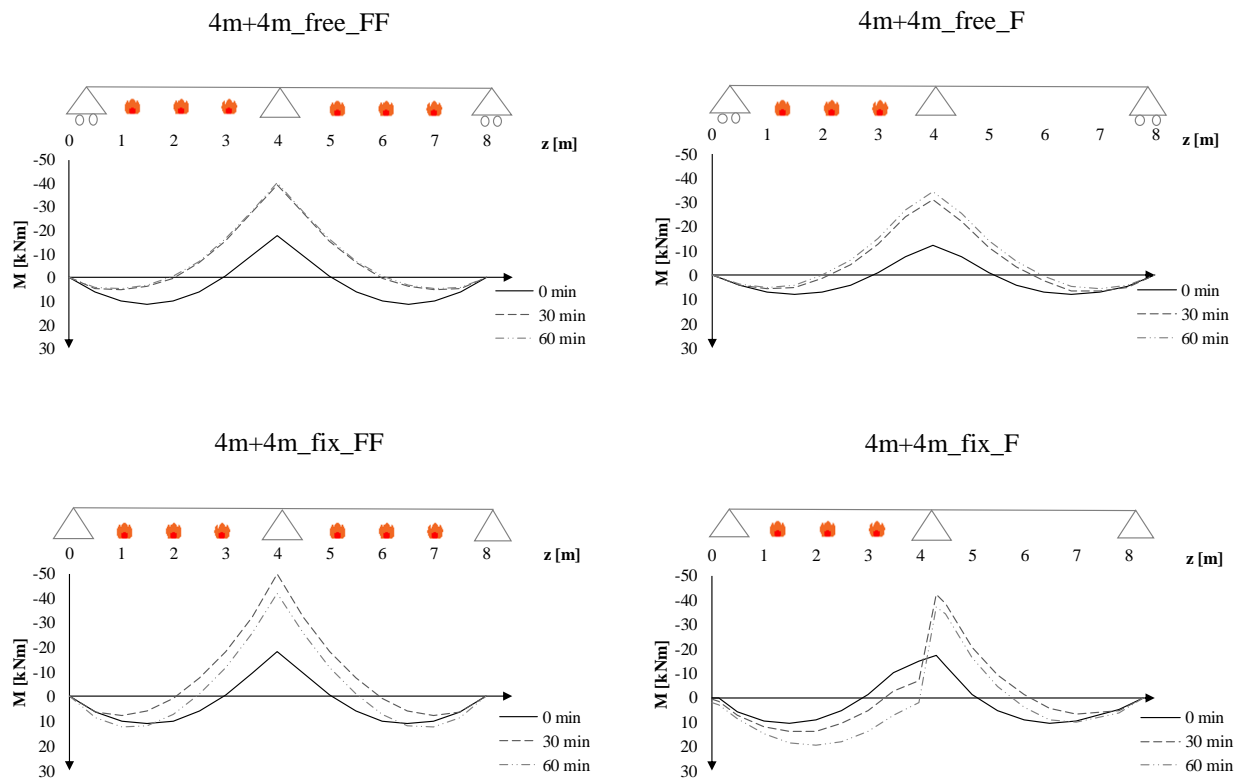Fig. 7. Bending moment versus exposure time – simply supported beams

Fig. 8. Bending moment diagrams versus exposure time – continuous beams

5   CONCLUSIONS

Numerical analyses on simply supported and continuous GFRP-RC slabs, in the conditions of free or prevented thermal expansions, showed how much boundary conditions affect the structural members response in fire. The slabs designed with the same value of load level and different span length collapse at similar time of exposure to standard ISO834 fire curve, due to failure of GFRP rebars when thermal expansion is not constrained. For longitudinal expansion constrained, high compression stresses arise in the slab and the failure mode of the slab changes. Therefore, the isostatic scheme generally used in the design step (i.e. free thermal expansion) could be very conservative for estimating slab displacements and bearing capacity of GFRP-RC slabs. Moreover, the continuous scheme is undoubtedly advantageous for reducing the slab displacements, which are significantly lower than those of the isostatic scheme also in the case of fire exposure. Nevertheless, it is necessary to pay attention to the additional forces and stresses that arise due to thermal curvature, which depend on the specific fire scenario.

REFERENCES

[1]   Bilotta A., Compagnone A., Esposito L., Nigro E. (2019). *Numerical analyses of the structural behaviour of steel and FRP reinforced slabs in fire.* Applications of Structural. Fire Eng. (ASFE), Singapore, 13-14 June.

[2]   CNR - DT 203/2006 (2007). Guide for the design and construction of concrete structure reinforced with fiber - reinforced polymer bars. National research council. Italy, Rome, June 2007.

[3]   European committee for standardization (2004). EN 1992-1-2. Eurocode 2. Design of concrete structures – Part 1-2: General Rules – Structural Fire Design. March 2004.

[4]   Bai Y, Vallée T, Keller T. (2007). *Modeling of thermo-physical properties for FRP composites under elevated and high temperature*. Composites Science and Technology, Vol. 67, doi:10.1016/j.compscitech.2007.04.019, pp. 3098–3109.

[5]   Fib 2007, Technical report prepared by a working party of Task Group 9.3, FRP (Fibre Reinforced Polymer) reinforcement for concrete structures (September 2007)

[6]   Belarbi H., Hsu T.C.C., 1994. *Constitutive laws of concrete in tension and reinforcing bars stiffened by concrete*. ACI Structural Journal. 91(4), pp. 465-474.

[7]   McIntyre E., Bilotta A., Bisby L. A., Nigro E. (2014). *Mechanical properties of fibre reinforced polymer reinforcement for concrete at high temperature*. 8th Int.Conf. on Structures in Fire, 11-13 June, Shanghai, China, p. 1227 - 1234.

[8]   Abaqus Standard/Exlpicit User's Manual. (2006). Hibbitt, Karlsson and Sorensen, Inc. Vol. 1, 2 and 3, Version 6.5, USA.

[9]   NTC 2018. Italian technical standard for construction. Rome.

[10] Nigro E., Cefarelli G., Bilotta A., Manfredi G., Cosenza E. (2012). *Performance under fire situations of concrete members reinforced with FRP rods: bond models and design nomograms.* Journal of composites for construction. vol. 16, p. 395-406, ISSN: 1090-0268, doi: 10.1061/(ASCE)CC.1943-5614.0000279

Influence of Pull-Out Fire Test Conditions on the Thermal Distribution and the Prediction of Load-Bearing Capacity of Bonded Anchors

THE EFFECTS OF EMBEDMENT LENGTH ON THE BOND PERFORMANCE OF GFRP REINFORCING BARS AT HIGH TEMPERATURES

Arshia Mousavi[1], Hamzeh Hajiloo[2], Mark F. Green[3]

[1] PhD Student, Dept. of Civil Engineering, Queen's University, Kingston, ON, Canada
[2] Postdoctoral Fellow, Dept. of Civil Engineering, Queen's University, Kingston, ON, Canada
[3] Professor, Dept. of Civil Engineering, Queen's University, Kingston, ON, Canada

ABSTRACT

Glass Fibre reinforced polymer (GFRP) reinforcing bars have demonstrated outstanding characteristics to assure a desirable long-term performance of reinforced concrete structures. However, the fire performance of GFRP reinforced concrete is still a concern. Recent research contributions have provided substantial information regarding the properties of GFRP bars at high temperatures. This study adopted a modified pullout test method at which 350 mm long cylindrical GFRP reinforced concrete specimens are tested after reaching a desired temperature in the GFRP to the concrete interface. The #4 (13 mm in diameter) sand-coated GFRP bars are used in the specimens. The high capacity heating tapes are wrapped around the concrete cylinders to heat them. Although the standard pullout tests (i.e., 150 to 200 mm cubes) with a short embedment length have shown a significant reduction in the bond strength of GFRP bars, they do not fully demonstrate the effects of embedment length on the remaining bond strength. This study investigates the remaining bond strength of the specimens at high temperatures up to 300 °C. Early research by the co-authors has shown that the GFRP bars have lost 83% of their original bond strength at 200 °C. These long pullout specimens will determine if an additional embedment length provides cumulative bond strength over the embedded length of the GFRP bars and as such provides enhanced fire resistance for GFRP reinforced concrete elements. Five specimens were already tested which showed a little contribution of longer embedment in providing additional bond strength at high temperatures.

1   INTRODUCTION

The outstanding characteristics of FRP materials such as corrosion resistance, high strength-to-weight ratio, and low thermal conductivity have made them a competitive alternative to steel bars as internal reinforcement in many structures. Different investigations indicated the important characteristics and differences of FRP reinforcing bars and steel reinforcement [1-3]. One of the important concerns in the application of FRP is the bond interaction between FRP and concrete at high temperatures. There have been some investigations into the bond deterioration of FRP reinforcing bars and concrete.

Katz et al. [1] performed several pullout tests on the four types of GFRP bars of 12.7 mm diameter with various types of surface treatment as well as steel bars of 12 mm. The embedment length of steel or GFRP bars in concrete was 5d (60 mm), where d is the bar diameter, and the specimens were heated up to 250°C. While the bond strength of GFRP bars at room temperature is 6 to 37% higher than steel reinforcement, steel bars showed better performance at high temperature. The reduction of bond strength in steel bars was 38% at 200°C, while it was very significant (around 80%) in GFRP bars below 200°C especially close to the glass transition temperature (T_g). At 200 °C, the bond strength reduction of GFRP bars was approximately 90%, but it was 34% for steel bars. The results showed the reduction of bond stiffness in GFRP and steel reinforcing bars are almost similar. Therefore, it is concluded that the surface properties of the reinforcing bars play an important role in bond strength and stiffness performance of reinforcement.

Rosa et al. [2] studied the bond strength of sand-coated GFRP bars at temperatures up to 140°C. The diameter of the GFRP bars was 10 mm and two different scenarios were considered for the embedment length. The standard embedment length equal to 50 mm (5d) and a long 90 mm embedment length (9d) in order to analyze the impact of embedment length on the bond strength of GFRP bars and concrete. The results showed that the failure of specimens happened due to the pullout of the GFRP bars in both cases. It was observed that the adhesion between the surface treatment of GFRP bars (e.g., sand coating or ribs) and bar's core play an important role in the bond strength of GFRP bars and concrete at room and elevated temperatures. It was reported that the bond strength reduced by 29% at 60°C and 80% to 90% at 100°C and 140°C, respectively. Also, the results presented the same bond strength reductions for two different embedment lengths at different temperatures. Therefore, it is concluded that the bond strength between GFRP bars and concrete is significantly affected by increasing the temperature, especially close to the glass transition temperature of GFRP bars.

Hajiloo et al. [3] tested 104 pullout specimens at high temperatures to analyze the bond performance of GFRP bars. For covering a wide variety of products in the market, three different types of GFRP bars with different surfaces such as sand-coated (GA), two helically wound braids of fibres (GB) and ribbed surface (GC) with 16-mm nominal diameter have been used. The tests have been performed under steady-state and transient temperatures. It is concluded that the bond strength of GFRP bars and concrete is impacted at high temperature; for example, the reduction of bond strength of GA bars at 75°C was 31%. Bond strength reduction is more significant when the temperature was close and above the T_g, which was 74% at 135°C and 89% at 200°C.

In recent years, there has been increased interest in the bond strength of GFRP bars and concrete at high temperature due to the susceptibility of GFRP bars in a severe fire, especially after the T_g. Because after T_g, the high temperature degrades the properties of the GFRP bars, and it reduces the bond capacity of GFRP reinforcing bars. However, the number of investigations on the impact of embedment length on the bond behavior of GFRP bars and concrete at elevated temperatures are very limited. Consequently, after studying different cases [1-2] and as *Hajiloo et al.* [3] recommended, there is a need for further investigation on the effect of long embedment length of GFRP bars at high temperature using methods other than standard pullout tests. Therefore, the innovative approach with the embedment length of 350 mm has been designed for this investigation.

2 EXPERIMENTAL PROGRAM

2.1 Materials

In this section, the details of the materials such as the mechanical properties of GA reinforcement and concrete mix have been discussed.

2.1.1 *GFRP Reinforcing Bars*

In this study, one type of GFRP bar is used and denoted as GA. It has a coarse sand coating surface and the mechanical properties are represented in Table 5. The nominal diameter of the GFRP bar was 13 mm (#4) and the measured actual diameter was measured by a digital caliper (15.5 mm). The T_g value of GA bar is 118.3 °C that was reported by the manufacturer.

Table 5. Manufactural mechanical properties of GA bar

Property	Unit	GA
Nominal diameter	(mm)	13
Measured sand-coated actual diameter	(mm)	15.5
Nominal cross-sectional area	(mm^2)	126.7
Actual cross-sectional area	(mm^2)	197
Average tested tensile strength	(MPa)	1,760
Nominal modulus of elasticity	(MPa)	69,600
Ultimate elongation	(%)	2.5
Fibre content (by weight)	(%)	84.1
Glass transition temperature	(°C)	118.3 (DSC)

2.1.2 Concrete

Normal strength concrete has been used for this experiment. The compressive strength of concrete just before the pullout test began was around 31 MPa after 4 months and one concrete mix was used for this investigation, as shown in Table 6.

Table 6. Concrete Mix

Material	Weight (kg/m^3)
Cement	350
Water	195
Coarse aggregate	1,060
Sand	735
Total	2,340

The specimens were stored in a lab environment with an average temperature of 20°C and the first pullout test was performed after 4 months of fabrication.

2.2 Specimen Preparation

CSA S806 [4] recommends an embedment length of 4d where (d is the nominal diameter of the bar). However, since the aim of this research is to analyze the effect of long embedment length of GFRP bars, concrete cylinders of 100 mm diameter and 350 mm embedment length were prepared. GA reinforcing bars were placed in the middle of the concrete cylinders. A small dummy steel rod was used in each specimen to accommodate the internal thermocouples perpendicular to the bar's surface. The dummy rod was placed 25 mm from the bar's surface to minimize any disturbance to the concrete-bar interface (Fig. 9-a). Therefore, 3 thermocouples attached in the middle of 3 different segments for measuring the temperature in different zones along the concrete cylinders, as highlighted in Fig. 9 (c). For the fabrication of the cylinders, the concrete was placed in 3 layers of almost equal thickness, and each layer was vibrated and tapped 25 times with a 16-mm-diameter rod. After 24 hours, the specimens were removed from the forms and stored indoors for 4 months.

The future goal of this experimental investigation is to study the effect of gradient temperature on the bonding of GFRP bars and concrete. For this purpose, there have been considered 3 various segments with the internal thermocouples along the concrete cylinders of each specimen.
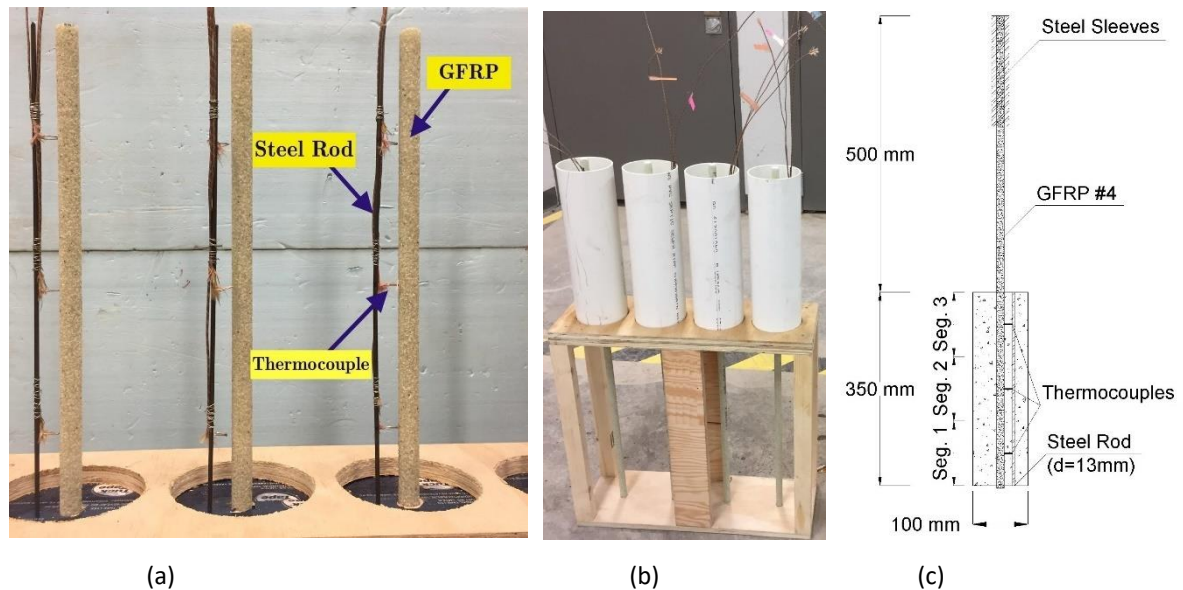

Fig. 9. Specimens preparation. a) details of each specimen, b) the stand for casting the specimens, c) specimen's sketch

2.3 Test Setup and Test Plan

To perform the modified pullout tests, an Instron SATEC (Norwood, Massachusetts) testing machine along with 3 heating tapes and controllers for heating the specimens have been used. The high-capacity heating wires were wrapped around the concrete cylinder of each specimen in three equal lengths. They were controlled by three different heating controllers as shown in Fig. 10, and they were insulated within a heating jacket. The application of three various heating tapes has two main reasons. One of which was that the available furnace interior allowed 150-mm specimens and smaller. Also, analyzing the bond behaviour of GFRP bars and concrete at the gradient temperature. Therefore, there is a need to use different heating tapes in order to have various temperature along the specimen. The designed heating jacket consists of steel wire net, aluminum foil, and fiberglass insulation has been used for thermal insulation.

Fig. 10 shows the details of the test setup and the Instron SATEC testing machine. There have been 2 steel plates (fixtures) with a thickness of 50-mm and grooved cuts through the centre line to accommodate the specimens for the pullout tests. The free end of the GFRP bar placed in a steel pipe as a sleeve, as shown in Fig. 9 (c), which distributes the load over the designed length of the bar and prevents failure in the anchor. The gap between GFRP bar and steel sleeve was filled with the expansive grout. *CSA S806* [4] recommends the displacement rate of the load applied to the steel sleeve for pullout test should not be greater than 1.27 mm/min. Therefore, the displacement rate of 1.0 mm/min has been used for these experiments. A 25-mm linear variable differential transformer (LVDT) sensor has been used and placed beneath the GFRP bar in order to measure the slip, as shown in Fig. 10.
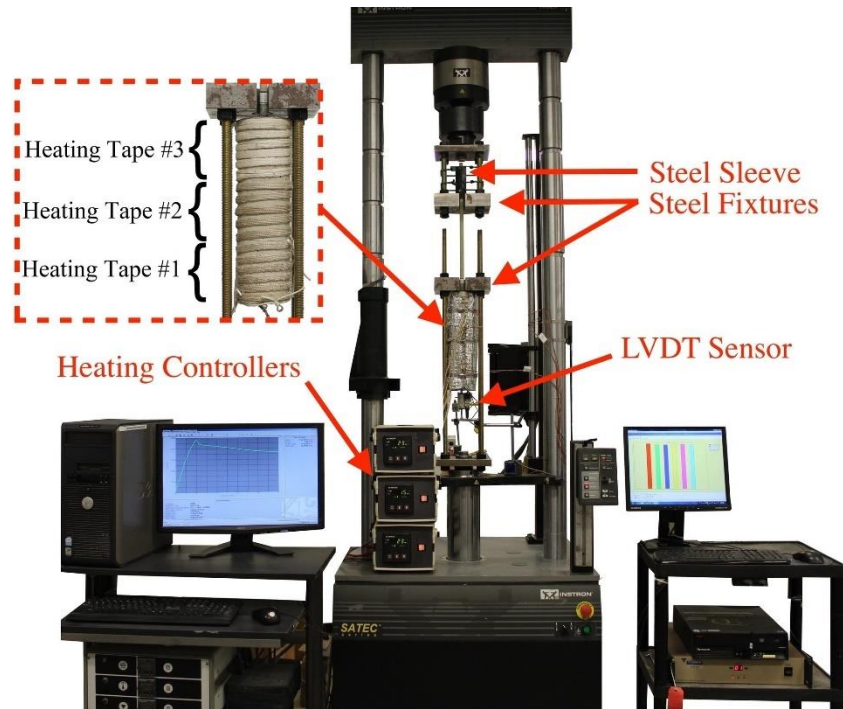
Fig. 10. Test setup (Instron SATEC testing machine)

2.4 Heat distribution in concrete specimens

Considering the novelty and different variables of this approach, various trial tests have been performed in order to find the heating regimes and performance of the heating tapes for the real tests. For heat distribution purpose in concrete specimens, 3 heating tapes have been wrapped around the specimens. 3 thermocouples placed in three different zones measured the concrete-to-bar interface temperature during the tests.

Fig. 11 shows the results of one trial test with the target temperature of 160 °C. The continuous blue line marked as Seg. 1, represented the surface temperature of GFRP bar inside of the concrete in segment 1. The other 2 curves show the surface temperature of GFRP bar in the other 2 segments of the concrete cylinder. According to the results, the 3 heating tapes increased the temperature along the specimen uniformly and the concrete-to-bar interface temperature reached the desired temperature in 120 min and remained almost constant after that time. Based on the results, different temperatures such as 160, 180, 200, 250, 300 °C have been chosen for the current experimental tests.
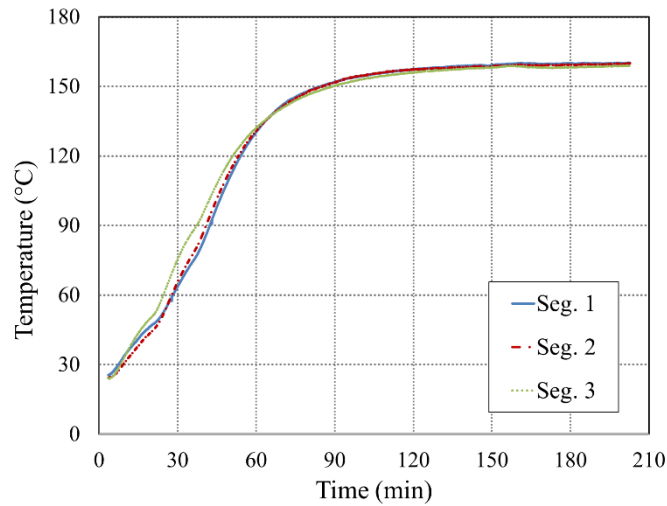
Fig. 11. Heating regime

3   EXPERIMENTAL RESULTS

Based on literature review [1-3], it became clear that there is a need to study the bond behavior of GFRP reinforcing bars and concrete in case of gradient temperature. Table 7 shows the test matrix of the underway experimental tests. The total number of 49 specimens were cast and it has been tried to allocate at least two samples for each temperature set. The experimental tests study the effects of various levels of heat intensity on the bond strength when the temperatures rise uniformly over the entire embedment length. The second and very critical part of this study is to quantify the effects of gradient temperatures over the embedment length. The tests are conducted under steady-state and transient temperature protocols.

Table 7. Test matrix of ongoing experiments

Segments	#1 (°C)	#2 (°C)	#3 (°C)
	20	20	20
	60	60	60
	80	80	80
	100	100	100
Constant Temperature	140	140	140
	160	160	160
	180	180	180
	200	200	200
	250	250	250
	300	300	300
	300	300	250
Gradient Temperature	300	300	200
	300	250	200

The early results of 5 specimens are presented in this paper. Fig. 12 shows the results of 5 specimens and test is undergoing for lower temperature such as 60, 80, 100, 140 °C. Early results of 5 specimens at high temperatures showed a significant reduction in the pullout capacity of the specimens at high temperature. For instance, the pullout capacity was significantly reduced from 46.6 kN to 12.2 kN by increasing temperature from 160 to 300 °C.
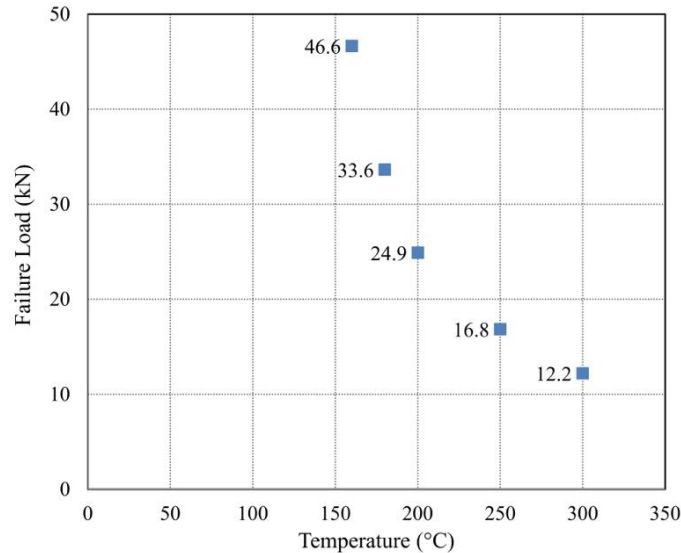

Fig. 12. Steady-state test results

4   CONCLUSIONS

This paper presents an ongoing experimental study on the effects of embedment length on the bond strength of GFRP reinforcing bars at a high temperature. The preliminary results showed a significant reduction in bond strength with increasing temperature and little contributions by increased embedment length. More importantly, the effects of gradient temperature over the embedment length will be tested subsequently. The research is continuing, and the results will be used in developing design guidelines for the overall behaviour of GFRP reinforced concrete elements in a fire.

REFERENCES

[1] Katz, A., N. Berman, and L.C. Bank, *Effect of high temperature on bond strength of FRP rebars.* Journal of Composites for Construction, 1999. **3**(2): p. 73-81.

[2] Rosa, I., et al., *Bond behaviour of sand coated GFRP bars to concrete at elevated temperature–Definition of bond vs. slip relations.* Composites Part B: Engineering, 2019. **160**: p. 329-340.

[3] Hajiloo, H. and M. Green. *Bond strength of glass fibre reinforced polymer bars in concrete at high temperature.* in *Proc Annual Conf–Canadian Society for Civil Engineering.* 2015.

[4] Association, C.S., *Design and construction of building components with fibre-reinforced polymers.* 2012, Mississauga, ON: CSA: Canadian Standards Association

.

BOND STRENGTH OF BONDED ANCHORS IN THERMALLY-DAMAGED CONCRETE

Viktor Hlavička[(a)], Éva Lublóy[(b)]
(a) PhD candidate, Budapest, Hungary
(b) Associate professor, Budapest, Hungary

ABSTRACT

In our work we analysed the bond strength of bonded anchors placed in thermally-damaged reinforced concrete. Our primary goal was to assist the strengthening work of reinforced concrete structural elements damaged in fire events. For the tests, 8 mm diameter threaded rods fastened with epoxy and vinyl-ester hybrid adhesive were used, with an embedment depth of 50 mm. Thermal loading of concrete specimens occurred in three stages (200, 300, 400 °C), with respect to the embedment depth.

1 INTRODUCTION

1.1 Concrete at elevated temperature

Hardened concrete is a composite material that consists mainly of two components: aggregate and cement stone. During increase of temperature both materials undergo some physical and chemical changes.

At higher temperatures strength properties deteriorate. Properties of concrete cannot be gained back after cooling down, because high temperatures cause irreversible changes in the structure of concrete that can cause deterioration and finally failure.

Failure of concrete at high temperatures (fire loads) has two main origins [1]: chemical changes in the components of concrete and spalling of concrete cover.

Strength of concrete at high temperatures mainly depends on the following [2]: type of cement, type of aggregate, water-cement ratio, aggregate-cement ratio, initial moisture content, way of temperature loading.

In the following we shortly summarize the most important physical and chemical changes in concrete subjected to high temperatures:

Around 100 °C decrease of mass is caused by evaporation of water from the macro pores. Decomposition of ettringite ($3CaOAl_2O_3 \cdot 3CaSO_4 \cdot 32H_2O$) takes place between 50 °C and 110 °C [3]. Around 200 °C further dehydration occurs that causes decrease of mass. Water content (water-cement ratio), type of cement and age of concrete affect the amount of evaporated pore water and chemically bonded water. Initial moisture content can have significant effect on the loss of mass especially in case of light-weight concretes. Above 250-300 °C further decrease of mass cannot be detected.

Between 450 °C and 550 °C decomposition of not carbonated portlandite occurs ($Ca(OH)_2 \rightarrow CaO + H_2O\uparrow$). This process leads to an endothermic peak and consequently to further loss of mass [4]. Dehydration of portlandite causes the most significant loss of strength in concrete [5].

In case of conventional concretes α to β quartz inversion takes place at 573 °C with a smaller endothermic peak. This quartz inversion causes 5-7% volume increase [6], that leads to

significant deterioration of concrete. Above this temperature concrete has no significant load bearing capacity.

At 700 °C CSH (calcium-silicate-hydrate) compound decompose with water output that courses further volume increase and loss of strength [7].

Due to the physical and chemical changes in concrete strength properties also change.

Other source of concrete failure in case of fire is spalling, that has two main reasons:

1.   increased pore pressure causes spalling of the surface layer of concrete.
2.   the exposed zone cannot bear further stresses caused by heat expansion therefore it cracks an crushes [8].

1.2   Anchorage in concrete

Several post-installed anchors are available with different methods of load-transfer. The commercially available fastenings can transfer the load to the host material via the following mechanisms: mechanical interlock, friction or bond. Furthermore, the most recent techniques use combined bond and friction (e.g. bonded expansion anchors). In case of expansion anchors, the load is transferred by friction. Generally, an expansion sleeve is expanded by an exact displacement or torque applied on the anchor head during the installation process. Chemical fastenings are anchored by bond. Bonded anchors can be divided into two subgroups: capsule or injection systems. The bond material can be either organic, inorganic or a mixture of them. In this case the loads are transferred from the steel (normally a threaded rod, rebar) into the bonding material and are anchored by bond between the bonding material and the sides of the drilled holes. The load bearing capacity of bonded anchors with the same embedment depth depends on the type of the resin. [9].

Load bearing of fastenings can be determined by taking the minimum of ultimate loads corresponding to different failure modes. In case of tensioned anchors steel failure, concrete cone failure, pull-out failure and splitting can occur (*Fig. 1*) [9].
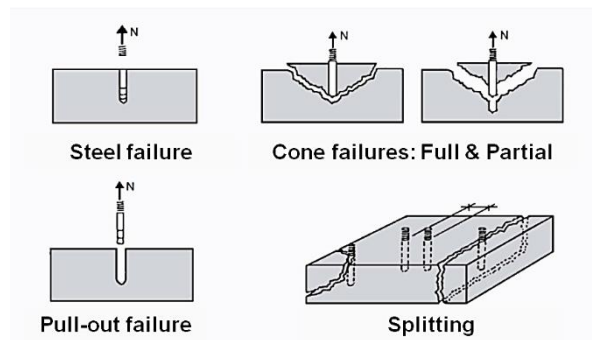

Fig. 1. Failure modes of anchors

Steel failure depends on the tensile strength of the steel rod. Steel capacity can be calculated from the ultimate steel strength and the cross-sectional area.

Splitting failure is caused by reaching the critical edge-spacing distances. Load bearing capacity can be influenced by distances from edges and by spacing distances; these effects can be taken into account by reduction factors.

Pull-out failure has to be discussed separately for bonded and expansion anchors. Pull-out failure of mortar bonded anchors means bond failure between mortar and concrete, while pull-out failure excluding mortar means bond failure between the steel fastening and the bonding material. The bond strength depends on the certain product, but its value is included in the corresponding approvals.

Ultimate load that corresponds to pull-out failure can be calculated as:

$$N_u = \pi \cdot d \cdot h_{ef} \cdot \tau_u$$

(1)

where: d   is the anchor bolt diameter [mm]

hef   is the embedment depth [mm]

τu   is the bond strength [MPa]

Concrete cone failure can be calculated by the C-C Method (Concrete Capacity Method) [10]. The method is based on laboratory tests and numerical calculation:

$$N_u = k \cdot \sqrt{f_c} \cdot h_{ef}^2 \cdot \frac{1}{h_{ef}^{0.5}} = k \cdot \sqrt{f_c} \cdot h_{ef}^{1.5}$$

(2)

where: k   is the factor that depends on the type of the anchor

h_{ef} is the embedment depth [mm]

f_c is the concrete compressive strength [N/mm^2]

f_{ct} is the concrete tensile strength [N/mm^2]

In *Eq.* (2), h_{ef}^2 corresponds to the failure surface and *$1/h_{ef}^{0.5}$* takes into account the size effect [11]. New result of this method is that it assumes a cone angle of 35° compared to former methods that used 45° [12]. Nowadays several design guides and standards suggest this method [13-15].

Based on already published papers and test results, behaviour of anchors installed in concretes subjected to high temperatures can be examined by different methods. In the most general case the whole connection is subjected to heat load, which means that the steel anchor, the concrete base material (together with the glue if applied) are subjected to high temperatures at the same time. In this case temperature of steel anchors increase faster, therefore they conduct heat to their proximate environment, which leads to faster degradation of the concrete or of the glue [16]. During testing of bonded anchors at high temperatures heating is applied together with a certain tensile force [17], because in this case sensitivity of the glue to high temperatures typically causes failure of the glue and pull out failure of the connection [18].

Other method is to install the anchors into thermally damaged concrete that is previously subjected to heat loading. This method is typical in case of strengthening of buildings after fire damage. In this case:

- the anchor does not conduct extra heat to the concrete structure,
- the connection is not subjected to high temperatures therefore strength of the steel anchor and of the glue is not decreased by increased temperature.

In the literature concerning this second test method, tests of undercut anchors as post-installed anchors used in thermally damaged concretes are documented only. Based on the results resistance of these anchors highly depended on the embedment depth, as much higher resistance could be measured if the head of the anchors was installed in slightly damaged or undamaged concrete layers. Calculations showed that the C-C method did not give correct results neither if residual

strength at the embedment depth was applied nor if mean value of the strength at the surface and at the embedment depth was used [19].

Out main aim was to examine the behaviour of anchors installed in thermally damaged concretes, and to extend this field of research to the examination of bonded anchors.

2 EXPERIMENTAL STUDY

In our experiments, we analysed the bond strength of anchors placed in thermally damaged reinforced concrete as a function of thermal load. In the tests carried out earlier, undercut fasteners were used. These studies did not address the behaviour of other types of fasteners, and that is why we used bonded anchors in our investigations to test the load bearing capacity of the bonded connection and its damage.

During the experiment, the specimens were exposed to fire load on one side until they reached the desired temperature, then they were allowed to cool down at laboratory temperature (20 °C). The day after the fire load, typically after 24 hours, when the specimens had been cooled down, the fasteners were installed in the thermally damaged specimens. In order to allow the cross-linking of the adhesive, loading of the fasteners took place after further 24 hours.

2.1 Tested anchors

During our tests two different types of bonded anchors were used, one type with epoxy resin, and on type with vinyl-ester hybrid bonding material.

Proper mixing of high performance epoxy resin glues is ensured by special mixing rods. The bond is stress-free; therefore it can be applied in case of small edge distances and spacing. Consistency of the epoxy resin is higher than that of other glues therefore it can enter to the pores and can reach an adequate depth before hardening, resulting in higher amount of load transmission by adhesion. Average bond strength of the glue (τ_u) is 27 MPa (determined on the basis of confined tension test results in non-cracked normal concrete).

Vinyl-ester hybrid is a combined glue, that includes organic (vinyl-ester) and inorganic (cement) compounds. The glue is universal, it can be used for all kinds of building materials and loading types. The bond is stress-free; therefore it can be applied in case of small edge distances and spacing. The consistency of it is more granular than that of the epoxy resin and this property also remains after hardening. Its characteristic bond strength (τ_u) is 21 MPa (determined on the basis of confined tension test results in non-cracked normal concrete).

During our tests with bonded anchors, size M8 and grade 10.9 threaded rods were applied. The high tensile strength of the rod prevented steel failure therefore cone failure of concrete could be examined. Applied embedment depth was 50 mm in each case.

2.2 Concrete mixture

Composition of the examined concrete mixture is given in the *Table 1*.

Table 1. The concrete mixture

Materials	Type	Density [kg/m^3]	Volume [l/m^3]
Aggregate	0/4 mm	833	315
	4/8 mm	463	175
	8/16 mm	556	210
	SUM	1852	700
Cement	CEM I 42,5 N	290	93.5
Water		196	196
Superplasticiser		0.58	0.58
Air		-	10
SUM		2338	1000

The specimens were held under water for 7 days and then kept at laboratory temperature (20 °C) for additional 21 days. The dimensions of concrete specimens for pull-out tests were 300x300x150 mm. This geometry corresponds to the prescribed parameters of the *ETAG 001* [15]. In case of this geometry the probability of splitting is very low.

Compressive strength properties were tested on additional 3 cubes of 150x150x150 mm. Uniaxial compressive strength tests were carried out on concrete cubes 28 days after casting. Regarding concrete, the results were evaluated in accordance with *EN 12390 -3:2009* [20]. The mean value of the compressive strength for the mixture was $f_c = 49.77$ N/mm^2.

2.3 Thermal loading

In laboratory tests, the concrete specimens were exposed to thermal load on one side. An electric furnace was used for thermal loading, with a heat-up curve shown on *Fig. 2*. Based on the measured data, the curve of the furnace is different from the standard fire curve according to *ISO 834-1* [21], therefore the experiment cannot be called a standard test. However, the heating curve of the furnace remained unchanged even after several checks, so it was well suited for the comparison of the specimens with varying degrees of thermal load, as well as for the preparation of a possible future standard test.

Thermal loading of the specimens was carried out in three different thermal steps measured at the embedment depth: 200, 300, 400 °C (*Table 2*).

Table 2. Test matrix.

Test	Time [min]	Temperature at the embedment depth [°C]	Specimens [piece]
Test 0	0	20	3
Test 1	120	200	3
Test 2	190	300	3
Test 3	370	400	3

The arrangement for the thermal loading test is shown on *Fig. 3.* Temperature was measured in the embedment depth by a thermocouple, which had been placed from the "cold" side of the specimen through an inspection hole (Ø 6 mm). *Fig. 3.* shows that the specimen is gradually warmed, with a significantly slower tendency than the furnace. In the specimen, after reaching 100 °C, the temperature increases for a short time, then water in the concrete vaporizes and starts flowing out from the concrete. The temperature does not rise because the heat energy is entirely devoted to the change of state of the water. After evaporation pore water, temperature of the specimen continues to increase.
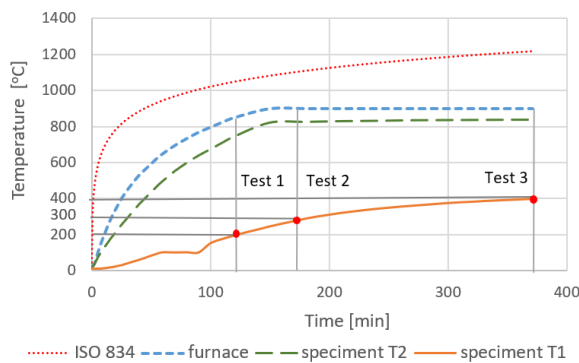
Fig. 2. Temperature increase as a function of time
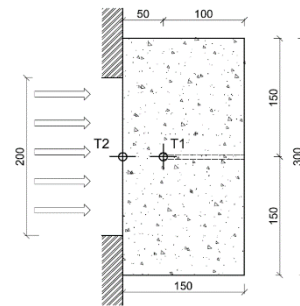
Fig. 3. Arrangement of heating for the specimen

We did not observe spalling of the concrete in any of the specimens during the test. This may be due to the fact that water vapour generated in the concrete was not accumulated in the specimen due to the dimension of the specimen and the arrangement of the measurement, as no moisture barrier was created. The vapour was able to flow out freely though the test hole made for temperature measurement and the sides of the specimen. Therefore, the results of the test can be used only in cases where spalling does not occur in the reinforced concrete structure during the fire.

2.4 Pull-out test

Our confined test setup is shown in *Fig. 4.* The loading device was a displacement-controlled test apparatus, which allowed the recording of residual stress after the failure. This setup enabled only the pull-out failure mode. The measurement setup was capable to measure, record and show the applied load and related displacement of the anchor in real-time. The perpendicular pin-joints ensured the centrality of the acting force. Two electronic transducers measured the displacement, while three additional independent displacement transducers were used to record the deformation of the surface. The load was measured by a calibrated load cell. The tests were carried out in accordance with the instructions given in *ETAG 001 Annex A* [15].
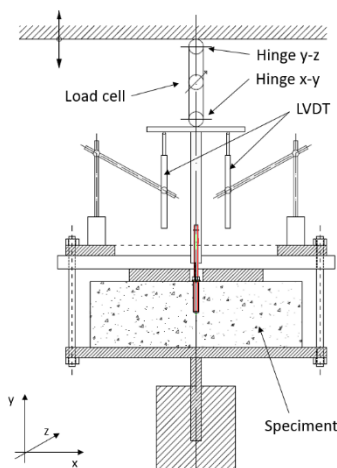
Fig. 4. Arrangement of pull-out test

3   RESULTS OF EXPERIMENTS

Fig.5 shows the resistance values measured during the pull-out tests as a function of the maximum temperature load. In case of the reference tests (Test 0) with epoxy resin steel failure occurred in all the three cases, therefore the results shown in *Fig. 5.* are values calculated by Eq (1) using the preciously measured $\tau_u = 27$ MPa bond strength. In case of vinyl-ester hybrid glue the reference test specimens failed by pull-out failure caused by failure of the glue. In other cases pull-out failure occurred by combined failure of the bond material and of the concrete.
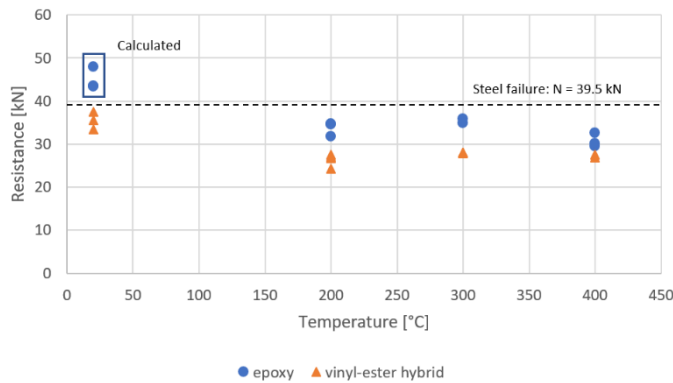
Fig. 5. Relationship between the tensile resistance and the temperature at the embedment depth (some points cover each other)

Fig. 6. Typical combined pull-out failure

In case of combined pull-out failure, in the upper zone of the embedment, the concrete is deteriorated significantly and therefore it is not capable to transfer the loads and consequently it is pulled out together with the bonded threaded rod. In the deeper zones the glue fails, as bond between the glue and the concrete is quasi-perfect. A typical combined pull-out failure can be seen in *Fig. 6.*

Fig. 7 shows the relative resistance values (reference values correspond to the tests without temperature load (at 20 °C) as a function of the temperature load in case of the two tested glues.

The results show that the resistance values decrease as the maximum temperature increases, bonded anchors in thermally-damaged concretes cannot bear the same load as in case of normal concretes.
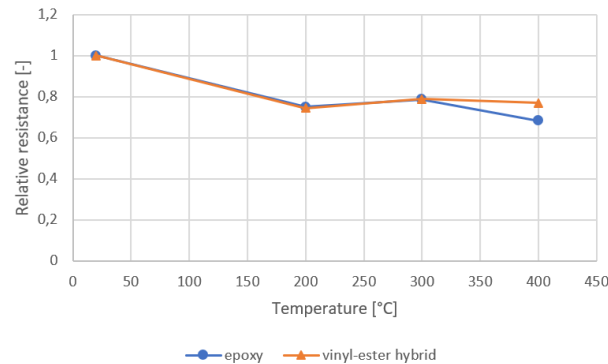

Fig. 7. Relationship between the relative residual resistance and the temperature in the embedment depth (each point is the mean value of 3 results)

The tendency of decreasing is similar in case of the two glues at lower temperatures, difference is only visible above 300°C (Test 3), when the epoxy resin shows more intense decrease in relative strength than the vinyl-ester.

Decrease of the resistance of bonded anchors can be explained by the combined pull-out failure, that is the combined failure of the glue and of the concrete. The upper zone of the concrete that has suffered more severe damages due to the temperature load cannot transfer the loads. Therefore tension is not transferred along the total embedment depth, only along a part of it. This phenomenon shows that in case of thermally-damaged concretes not the total embedment depth can be taken into account during the calculation of the resistance.

4 CONCLUSIONS

In our work we analyzed the bond strength capacity of bonded anchors placed in thermally-damaged reinforced concrete. Our primary goal was to assist the reinforcement work of reinforced concrete structural members damaged in fire events.

During the investigation we found no delamination (spalling) of the concrete in any of the specimens, so the results of the test can be used only in cases where spalling does not occur in the reinforced concrete structure during fire.

In case of the reference tests (Test 0) with epoxy resin steel failure occurred in all the three cases. In case of vinyl-ester hybrid glue the reference test specimens failed by pull-out failure caused by failure of the glue. In other cases pull-out failure occurred by combined failure of the bond material and of the concrete. In case of combined pull-out failure, in the upper zone of the embedment, the concrete is deteriorated significantly and therefore it is not capable to transfer the loads and consequently it is pulled out together with the bonded threaded rod. In the deeper zones the glue fails, as bond between the glue and the concrete is quasi-perfect.

The results show that the resistance values decrease as the maximum temperature increases, bonded anchors in thermally-damaged concretes cannot bear the same load as in case of normal concretes. The tendency of decreasing is similar in case of the two glues at lower temperatures, difference is only visible above 300°C (Test 3), when the epoxy resin shows more intense decrease in relative strength than the vinyl-ester.

ACKNOWLEDGMENT

REFERENCES

[1] Kordina, K. (1997). *Über das Brandverhalten punktgestützter Stahbetonbalkaen*, Deutscher Ausschuss für Stahlbeton, Heft 479, ISSN 0171-7197, Beuth Verlag GmbH, Berlin

[2] Thielen, K. Ch. (1994*). Strength and Deformation of Concrete Subjected to high Temperature and Biaxial Stress-Test and Modeling*, (Festigkeit und Verformung von Beton bei hoher Temperatur und biaxialer Beanspruchung - Versuche und Modellbildung), Deutscher Ausschuss für Stahlbeton, Heft 437, ISSN 0171-7197, Beuth Verlag GmbH, Berlin

[3] Khoury, G. A., et al. (2001) *Fire Design of Concrete Materials structures and modelling*, Proceeding of 1st fib Congress, Osaka, Japan, Oct.

[4] Schneider, U., Weiß, R. (1977) *Kinetische Betrachtungen über den thermischen Abbau zementgebundener Betone und dessen mechanische Auswirkungen*, Cement and Concrete Research, Vol 11, pp. 22-29

[5] Lublóy, É., Balázs, Gy. L. (2007) *Concrete properties in fire depending on type of cement, aggregate and fibre*, CCC2007 Visegrád Proceedings (Eds: Balázs, L. Gy., Nehme, S. G.), ISBN 978-963-420-923-2, pp.: 327-332

[6] Waubke, N. V. (1973) *Über einen physikalischen Gesichtspunkt der Festigkeitsverluste von Portlandzementbetonen bei Temperaturen bis 1000°C-Brandverhalten von Bauteilen*, Dissertation, TU Braunschweig

[7] Hinrichsmeyer, K. (1987) *Strukturorientierte Analyse und Modellbeschreibung der thermischen Schädigung von Beton*, Heft 74 IBMB, Braunschweig

[8] Winterberg, R., Dietze, R. (2004) *Efficient passive fire protection systems for high performance shotcrete*, Proceeding for the Second International Conference on Engineering Developments in Shotcrete, Cairnis, Australia, October, 2004 ISBN: 0404358981

[9] Eligehausen R., Mallée R., Silva J. F. (2006) *Anchorage in Concrete Construction*, Ernst&Sohn 2006, ISBN: 978-3-433-01143-0

[10] Fuchs, W., Eligehausen, R., Breen, E. J. (1995) *Concrete Capacity Design (CCD) Approach for Fastening to Concrete*, ACI Structural Journal, January-February, pp. 73-94.

[11] Bažant, Z. P. (1984) *Size Effect in Blunt Fracture: Concrete, Rock, Metal*, Journal of Engineering Mechanics, ASCE, 110, No. 4, April 1984, pp. 518-535

[12] ACI Committee 349*: Code Requirements for Nuclear Safety Related Concrete Structures (ACI 349-85)*, Anerican Concrete Institute, Detroid, 1985

[13] *fib* MODEL CODE 2010 (2013) ISBN: 978-3-433-03061-5

[14] *prEN 1992-4 Eurocode 2 Design of concrete structures - Part 4 Design of fastenings for use in concrete*, European committee for standardization, CEN/TC 250, Brussels, FprPREN 1992-4:2015

[15] *ETAG 001: Guideline for european technical approval of metal anchors for use in concrete*, EOTA, Avenue des Arts 40 Kunslaan, B – 1040 Brussels, 2013

[16] Ožbolt, J., Kožar, I., Eligehausen, R., Periskic, G. (2004) *Transient Thermal 3D FE Analysis of Headed Stud Anchors Exposed to Fire*, Fire Design of Concrete Structures: What now? What next?, (Edited by: Gambarova G. P., Felicetti R., Meda A., Riva P.), Milan, Italy, December 2-3, pp. 185-198.

[17] *EAD 330087-00-0601: Systems for post-installed rebar connections with mortar*, EOTA, Draft 2015

[18] Reichert, M., Thiele, C. (2017) *Qualification of Bonded Anchors in Case of Fire*, 3rd International Symposium on Connections between Steel and Concrete (Editors: Sharman, A., Hofmann, J.), Stuttgart, Germany, 27-29 September 2017, pp. 1091-1099. ISBN 978-3-945773-06-2

[19] Bamonte P. F., Bruni M., Gambarova P.G. (2012) *On the application of fracture mechanics to undercut fasteners installed in thermally-damaged concrete*, Befestigunstechnik Bewerungstechnik und … II (Rolf Eligehausen zum 70. Geburstag) (Edited by: Fuchs W, Hofmann J.), Stuttgart 2012, pp. 79-93. ISBN-13:978-3-8382-0397-3

[20] *EN 12390-3:2009 Testing hardened concrete – Part 3: Compressive strength of test specimens*

[21] *ISO 834-1: Fire-resistance Tests – Elements of building construction, Part 1: General requirements*, 1999.

Influence of Pull-Out Fire Test Conditions on the Thermal Distribution and the Prediction of Load-Bearing Capacity of Bonded Anchors

226

EXPERIMENTAL ASSESSMENT OF THE FIRE BEHAVIOR OF CONCRETE FILLED TUBULAR COMPOSITE COLUMNS

[1]João Paulo Rodrigues, [2]António M. Correia, [3]Venkatesh Kodur

[1]Coimbra University, Portugal
[2]Coimbra Polytechnic - ISEC, Coimbra, Portugal
[3]Michigan State University, U.S.A.

ABSTRACT

In this paper, a great number of experimental results of the fire resistance of concrete filled steel tubular columns (CFST) is to be presented, for four different cross-sections, and for different values of the main parameters involved in the fire resistance: The slenderness, and the rotational and axial stiffness are variables that have been taken, with different values, in order to evaluate their influence in the fire resistance of the columns.

Results to be presented in this study are the evolution of the restraint forces during the event of fire, the evolution of the axial and lateral displacements and also the stiffness of the columns during the fire. The stiffness of the surrounding structure is the main parameter to be analysed in the present study. This experimental programme was conceived and developed to provide data for new simplified design methods for this type of columns.

Keywords: fire, hollow column, experimental, thermal restraining

1 INTRODUCTION

Concrete filled steel tubular (CFST) columns are increasingly assuming a greater role in civil construction. Concrete filling offers an attractive practical solution for providing fire protection to steel hollow columns without any external protection. The fire resistance of concrete-filled steel hollow columns may be between 50 and 100 minutes, depending on the type of concrete filling (plain concrete, bar-reinforced concrete or steel fibre-reinforced concrete) [1]. This type of columns has the particularity of the steel tube first expands more than the concrete core, due to the higher temperature and thermal expansion coefficient of the steel, which sustains the serviceability load applied to the column. In the latter stages the steel tube starts to buckle locally, due to the degradation of the mechanical properties at high temperatures and consequent loss of loadbearing capacity, transferring this way the load to the concrete core. Finally, when the concrete core loses its strength, the column as a whole buckle [2].

2 EXPERIMENTAL TESTS

2.1 Test Set-up

The experimental set-up is viewed in *Figure 1*. A three-dimensional (3D) frame was built, that allowed positioning the testing columns in the centre and thus simulating the surrounding structure to the column. With this experimental set-up different axial restraint, k_a could be imposed by the surrounding structure on the CFST columns, by positioning the peripheral columns at different distances of the centre. Two values of this stiffness are considered, a higher value of 110 kN/mm (*hka*) and a lower one corresponding to 30 kN/mm (*lka*) are considered in this work. The system is also composed by a two-dimensional (2D) frame, in which a hydraulic jack was positioned, to apply the serviceability loads to the columns.

Influence of Pull-Out Fire Test Conditions on the Thermal Distribution and the Prediction of Load-Bearing Capacity of Bonded Anchors

227

Fig. 1. General views of the test set-up

The columns were placed in the centre of the 3D restraining frame and tested with semi-rigid support conditions. The columns had at each end a steel plate S355 that fitted directly to the 3D restraining frame (semi-rigid support conditions) or to the pinned support (pin-ended support condition). The connection of the column to the supports have been done in both cases by four M24 steel grade 8.8 bolts.

Additionally, above the specimen a 3MN compression load cell was placed to monitor the axial restraining forces generated in the CFST columns during the test. The thermal action was applied by a vertical modular electric furnace programmed to reproduce the ISO 834 standard fire curve (ISO 834-1 1999).

2.2 Tested columns

A great number of experiments on the behaviour of concrete filled circular (CC), square (SC), rectangular (RC) and elliptical (EC) hollow columns at high temperatures, was carried out under this experimental program. The specimens were full-scale columns made of hollow steel profiles completely filled with reinforced concrete (Fig. 2), with the mentioned steel cross-sections. All reinforcing bars used in the test specimens were of S500 structural steel and all specimens presented a similar concrete of C25/30 class with calcareous aggregates, according to EN 1992-1-1:2004. In addition, all steel profiles were 3.15 m tall of S355 grade (with a nominal yield strength of 355 MPa and a tensile strength of 510 MPa), according to EN 1993-1-1:2004. Another important point to note is that about five days after concrete casting, the moisture content of the concrete was about 4.5%, according to the procedure described in EN 1097-5:2009. This parameter was measured as soon as possible because the water loss from the concrete inside the steel tubes was too limited.
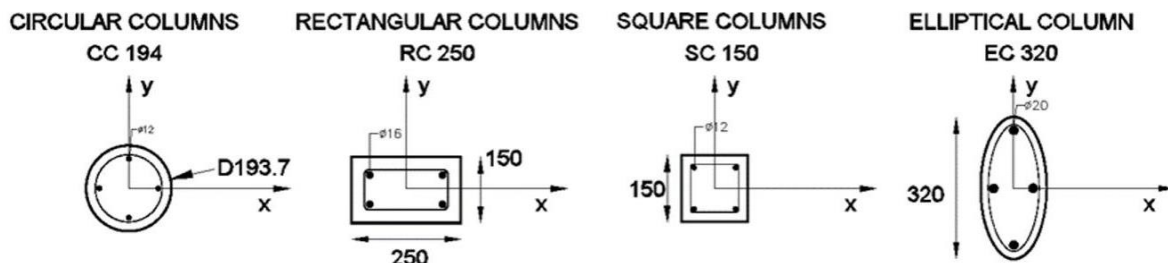

Fig. 2. Scheme of the cross-sections of the tested columns

The following table (Table 1) presents the characteristics of the columns and the calculation of the serviceability loads for the tests carried out. In the last columns of the table, the axial and rotational

Influence of Pull-Out Fire Test Conditions on the Thermal Distribution and the Prediction of Load-Bearing Capacity of Bonded Anchors

228

adimensional stiffness, are also presented. In this paper the columns were tested with axial stiffness of 110 kN/mm and 30 kN/mm. This stiffness is referenced in the figures by hka and lka. As the main objective of the paper is to analyse the effect of the surrounding stiffness on the behaviour of the columns at high temperatures, only results for the case of semi-rigid support conditions (SR) are shown. However, these tests are part of a bigger experimental programme.

Table 1. Tested columns [mm]

Test reference	A (mm^2)	A$_m$ / V (m^{-1})	$\bar{\lambda}$	N$_{pl,Rd}$ (kN)	N$_{cr}$ (kN)	N$_{b,Rd}$ (kN)	P$_0$ (kN)	k$_a$/k$_{a,c}$	k$_r$/ (k$_r$+k$_{r,c}$)
CC194-hka-sr	29468	20.7	0.58	2178	7097	1956	587	0.19	0.95
RC250-hka-sr	37500	21.3	0.63	3436	9258	3016	905	0.13	0.94
SC150-hka-sr	22500	26.7	0.65	2043	5158	1776	533	0.22	0.96
EC320-hka-sr	40212	19.8	0.69	4118	9216	3248	974	0.11	0.94
CC194-lka-sr	29468	20.7	0.58	2178	7097	1956	587	0.05	0.93
RC250-lka-sr	37500	21.3	0.63	3436	9258	3016	905	0.04	0.92
SC150-lka-sr	22500	26.7	0.65	2043	5158	1776	533	0.06	0.95
EC320-lka-sr	40212	19.8	0.69	4118	9216	3248	974	0.03	0.92

Table 2. Geometric characteristics of the specimens

Test reference	d (mm)	b (mm)	t (mm)	f$_y$ (MPa)	f$_c$ (MPa)	rebars	ρ_s (%)	d / t	d / b
CC194	193.7	- - -	8.0	365	33	4ϕ12	1.9	24.2	- - -
SC150	150.0	150.0	8.0	410	33	4ϕ12	2.6	18.8	1.0
RC250	250.0	150.0	10.0	420	33	4ϕ16	2.7	25.0	1.7
EC320	320.0	160.0	12.5	375	33	4ϕ20	4.2	25.6	2.0

The largest circular and square columns had eight longitudinal rebars, four of which were 16 mm in diameter (4ϕ16) and the other four were 10 mm (4ϕ10). The narrowest column had four longitudinal rebars of 12 mm in diameter (4ϕ12). On the other hand, the largest rectangular column had six longitudinal rebars, four of which of 16 mm in diameter (4ϕ16) and the others of 10 mm (2ϕ10), whereas the narrowest rectangular column had four longitudinal rebars of 16 mm in diameter (4ϕ16). For the elliptical columns were used 4 rebars of 10 mm in diameter (4ϕ10).

Note that these longitudinal rebars were chosen for this study in order to have similar longitudinal reinforcement ratios between columns with the same geometric shape. As well as that the widest rebars were placed at the corners of the cross-sections and the others in the middle, as shown in *Figure 2* and *Table 2*.

Influence of Pull-Out Fire Test Conditions on the Thermal Distribution and the Prediction of Load-Bearing Capacity of Bonded Anchors

229

For each test column, 8-mm diameter stirrups (spaced 150 mm apart until about 800 mm from end-supports and 200 mm in central part) were used. The distance between longitudinal rebars axes and the inner surface of steel tube walls was approximately 30 mm in all cases

3   RESULTS

3.1 Axial restraint forces and axial displacements

In *Figure 3*, the results for the circular column CC-194 show no major differences in terms of fire resistance between the two values of stiffness, neither for the relative axial forces nor for the vertical displacements.
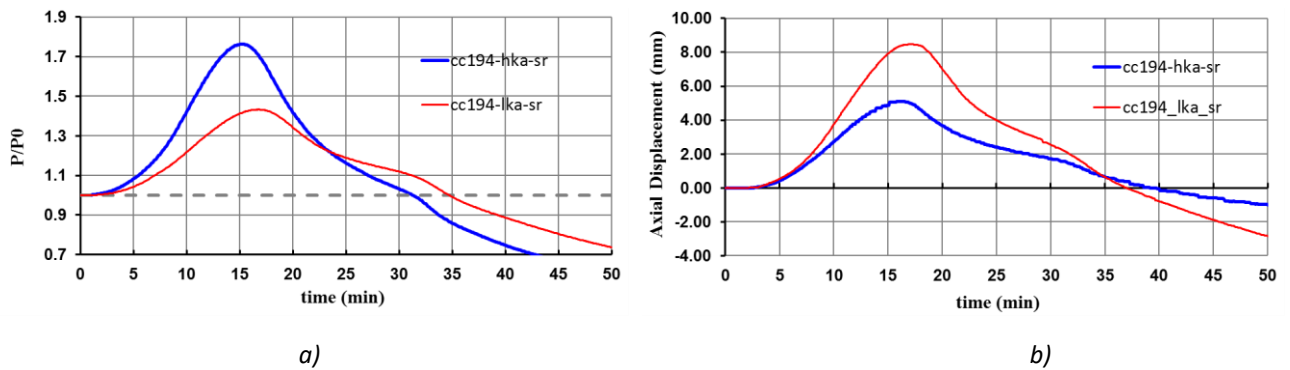
Fig. 3. Column CC194-sr a) Relative Axial Restraint Force   b) Axial Displacements

In *Figure 4*, the results for the elliptical column EC-320 show important differences between the two values of stiffness, but only in terms of the maximum axial restraining forces observed. For the high value of stiffness, the restraining forces achieved 200% the initial axial force. In both situations, the columns experienced a soft decay of the relative restraint forces. This post-buckling behavior is important in terms of the analysis of the global behavior of the whole structure. It is very different the behavior of a structure with columns suffering an instantaneous loss of resistance than with columns suffering smooth a decay of the load bearing capacity.
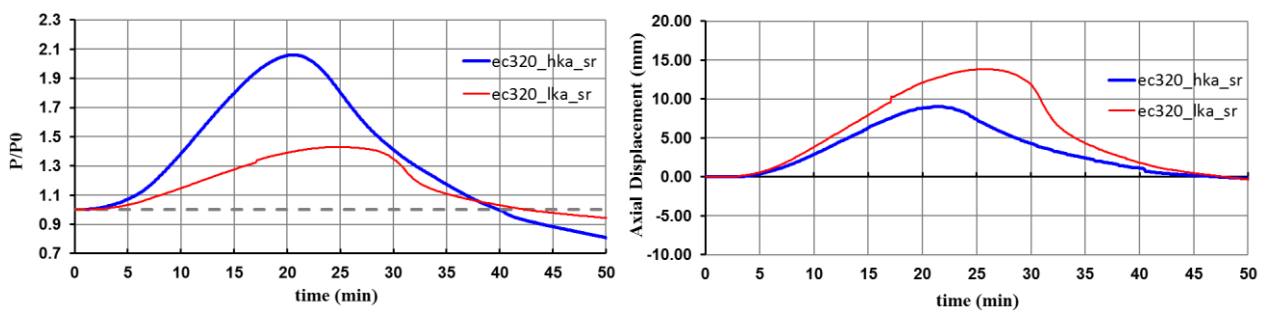
In *Figure 5*, the results for the rectangular column RC-250 are presented. Despite of the small difference in the critical times, with higher resistance presented by the low stiffness, the column in a stiffener frame experiences much greater restraint forces and more abrupt decay of axial resistance.

Influence of Pull-Out Fire Test Conditions on the Thermal Distribution and the Prediction of Load-Bearing Capacity of Bonded Anchors

230

a)

b)
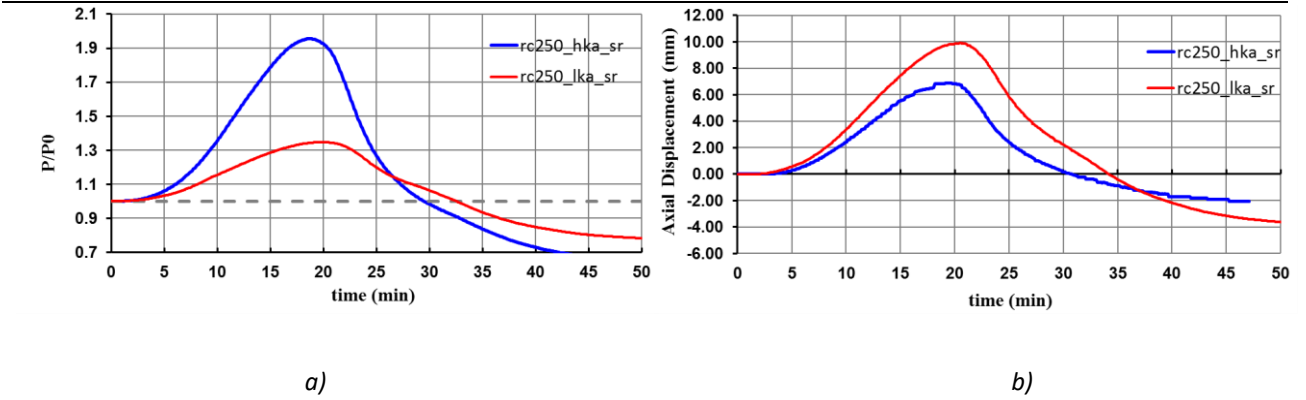
Fig. 5. Column RC250-sr a) Relative Axial Restraint Force   b) Axial Displacements

In *Figure 6*, the results for the square columns SC150, show negligible differences on the critical times for both situations.

In general, it can be said that in columns with regular cross-sections, with two similar buckling axes, it is not observed any major influence of the stiffness of the surrounding structure. On the other hand, columns with two distinct buckling axes, the ones with higher stiffness of the surrounding structure, showed abrupt buckling that occurs around the weak buckling axis.

a)

b)
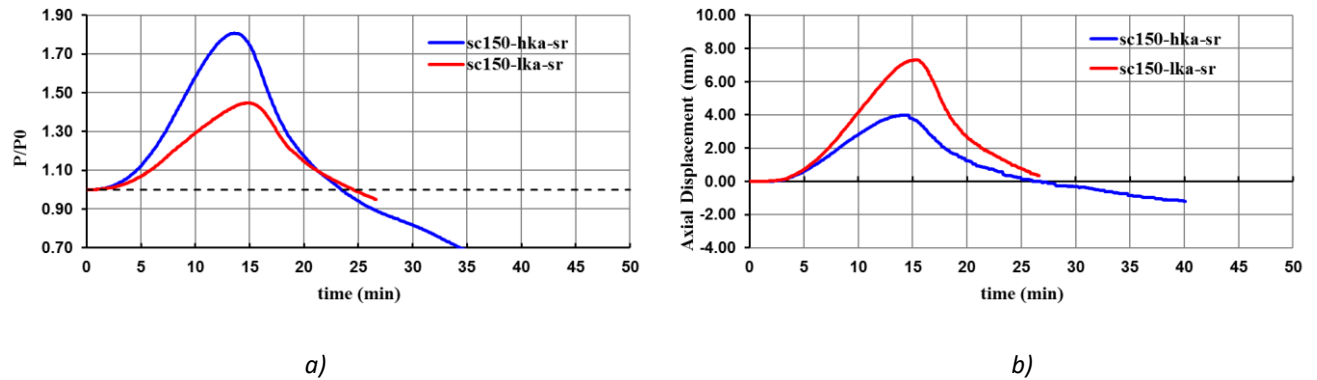
Fig. 6. Column SC150-sr a) Relative Axial Restraint Force   b) Axial Displacements

3.2 Stiffness of the system

Figures 7 to 10, depict the stiffness of the set, composed by the column and the surrounding frame, for the different types of columns.

In *Figure 7*, for the circular column CC194, the stiffness for the case of the high stiffness was 111.4 kN/mm, and for the case of the low stiffness was 31.5 kN/mm.

Influence of Pull-Out Fire Test Conditions on the Thermal Distribution and the Prediction of Load-Bearing Capacity of Bonded Anchors

231
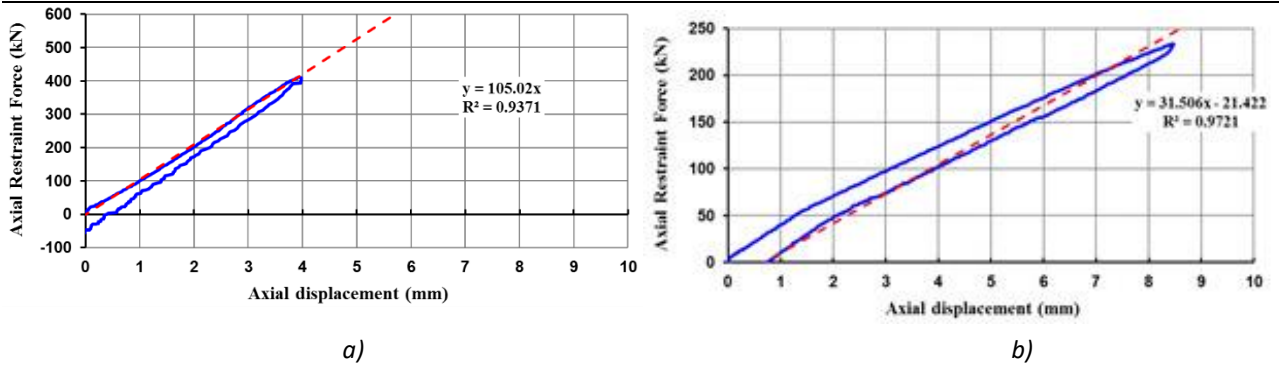
Fig. 7. Stiffness of column CC194-sr for a) hka and b) lka

In *Figure 8*, for the elliptical column EC320, the stiffness for the case of the high stiffness was 112.7 kN/mm, and for the case of the low stiffness 29.5 kN/mm.
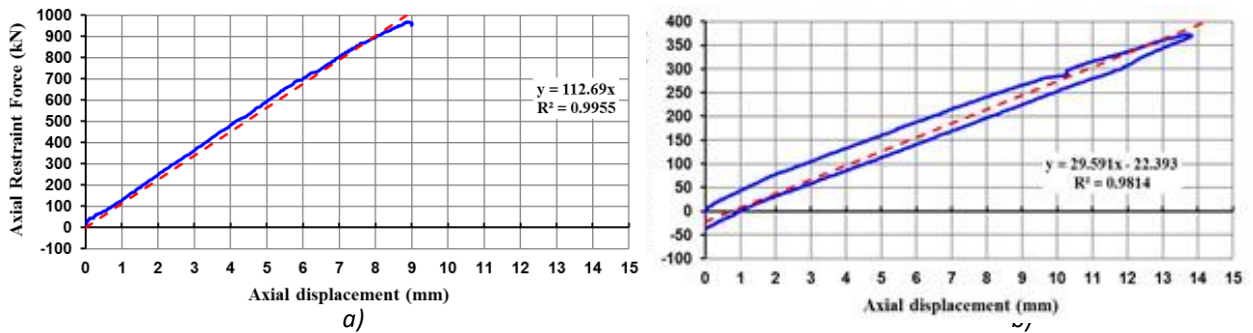
Fig. 8. Stiffness of column EC320-sr for a) hka and b) lka
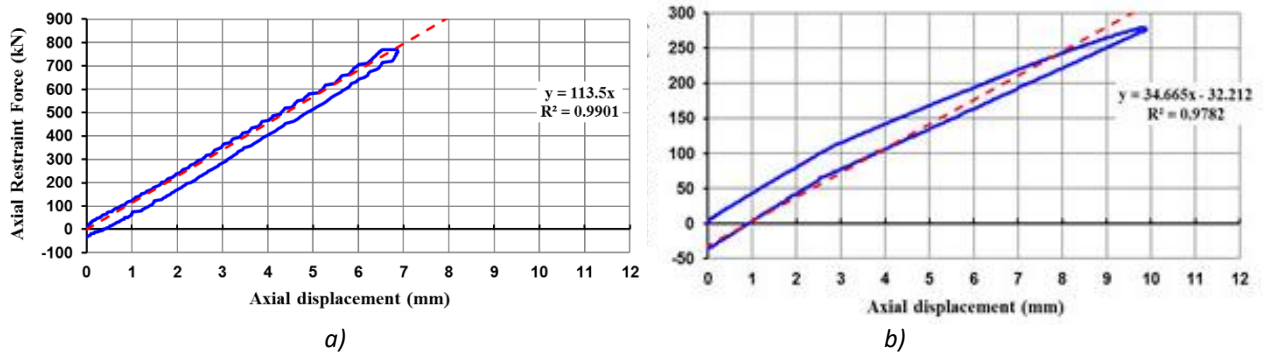
Fig. 9. Stiffness of column RC250-sr for a) hka and b) lka

In Figure 9, for the rectangular column RC250, the values of the stiffness were: 113.5 kN/mm for higher stiffness, and 34.7 kN/mm for the lower stiffness.

In Figure 10, the lowest values observed were for the square columns: 105.0 kN/mm for the higher stiffness, and 31.1 kN/mm for the lower stiffness.

As expected, in all cases the global stiffness was always higher for the case of the high stiffness frame condition.

Influence of Pull-Out Fire Test Conditions on the Thermal Distribution and the Prediction of Load-Bearing Capacity of Bonded Anchors

232
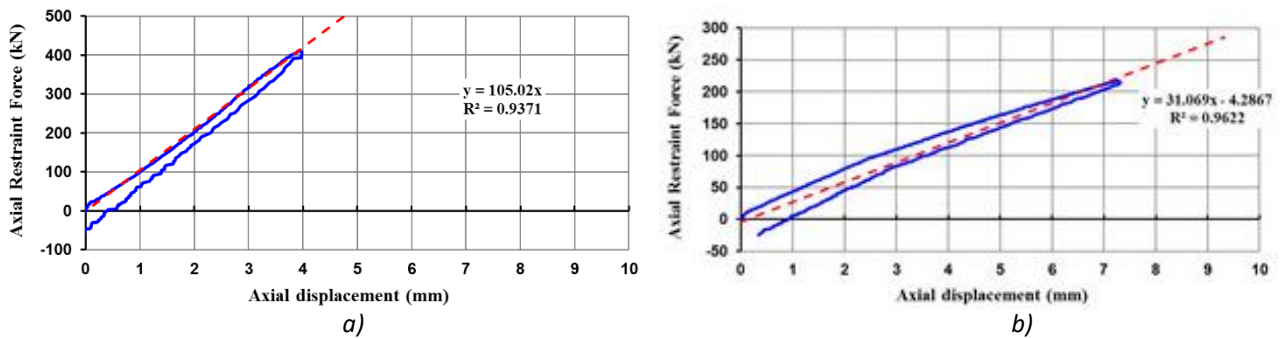
Fig. 10. Stiffness of column SC150-sr for a) hka and b) lka

3.3 Deformed shapes of the columns and pictures

Figures 11 to 14 depict the photographs and the deformed shapes of the columns, in the end of the tests, meaning, in the moment considered the collapse of the element. The deformed shapes are drawn around minor and major axis, for each column, elliptical, circular, rectangular and square, for the case of low stiffness. In general, as expected, greater deflections were observed for deflections around minor axis, and for double-symmetric cross-sections no important differences were noticed.

Figure 11 depicts the deformed shapes on the circular columns CC194. Both graphs were plotted for the critical times of 35 minutes, equal for both end conditions.

Figure 12 depicts the deformed shapes on the elliptical columns EC320. It must be stated that these deformed shapes were plotted for critical time of 42 minutes.

Figure 13 depicts the deformed shapes on the rectangular columns RC250. In this case a strange result was obtained. The column presented a greater deflection around major axis. This result was not expectable at all, and may be explained by the strong local buckling observed in this case, or initial imperfections.

In *Figure 14*, the deformed shapes on the square columns SC150 are depicted. In this case, as observed in the circular column, no major differences were observed in the deflections around minor and major axis.

a)   b)   c)
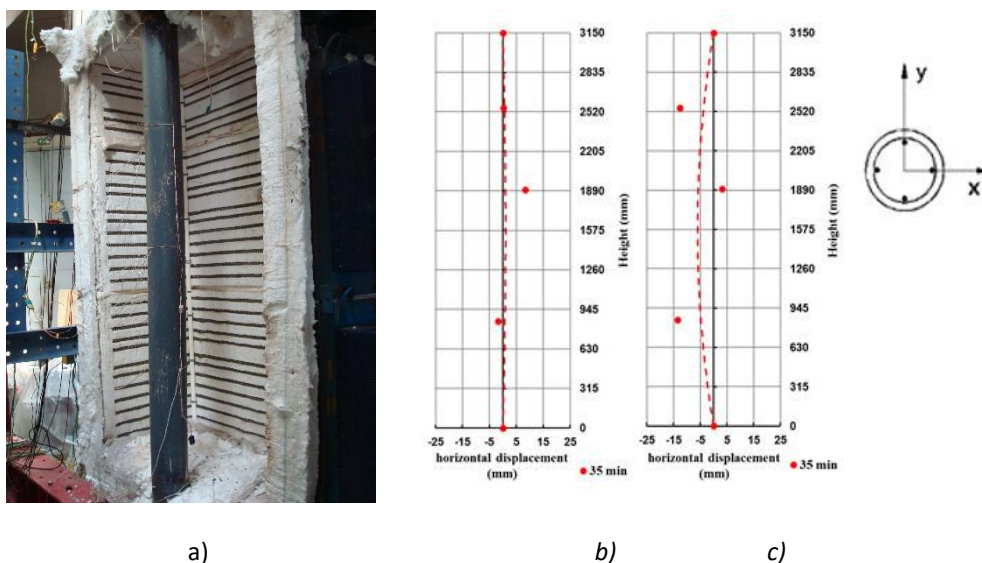
Fig. 11. Lateral deflections for column CC194-lka: a) photograph; b) sr-y axis; c) sr-x axis

Influence of Pull-Out Fire Test Conditions on the Thermal Distribution and the Prediction of Load-Bearing Capacity of Bonded Anchors

233

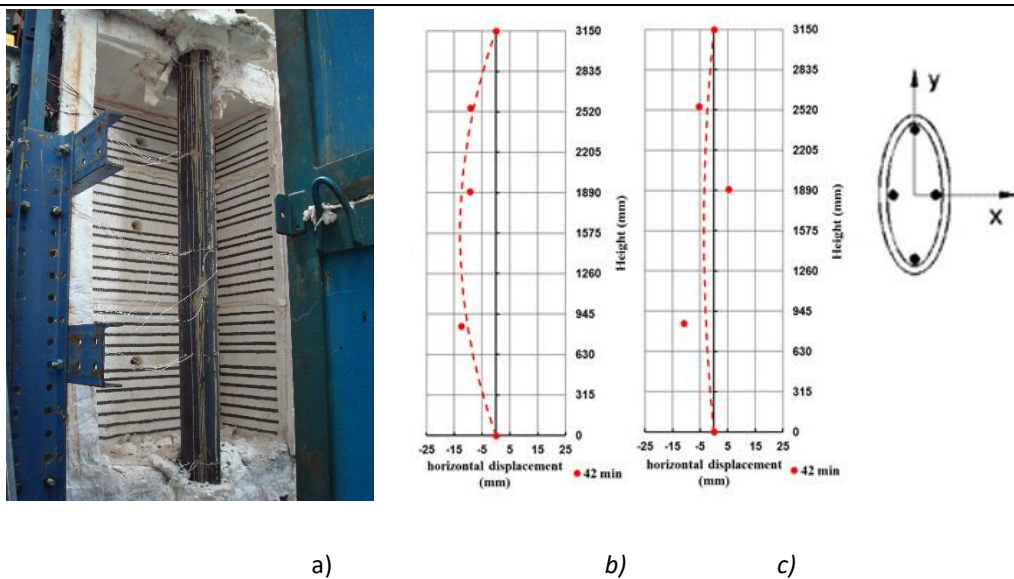a)   b)   c)

Fig. 12. Lateral deflections for column EC320-lka: a) photograph; b) sr-y axis; c) sr-x axis
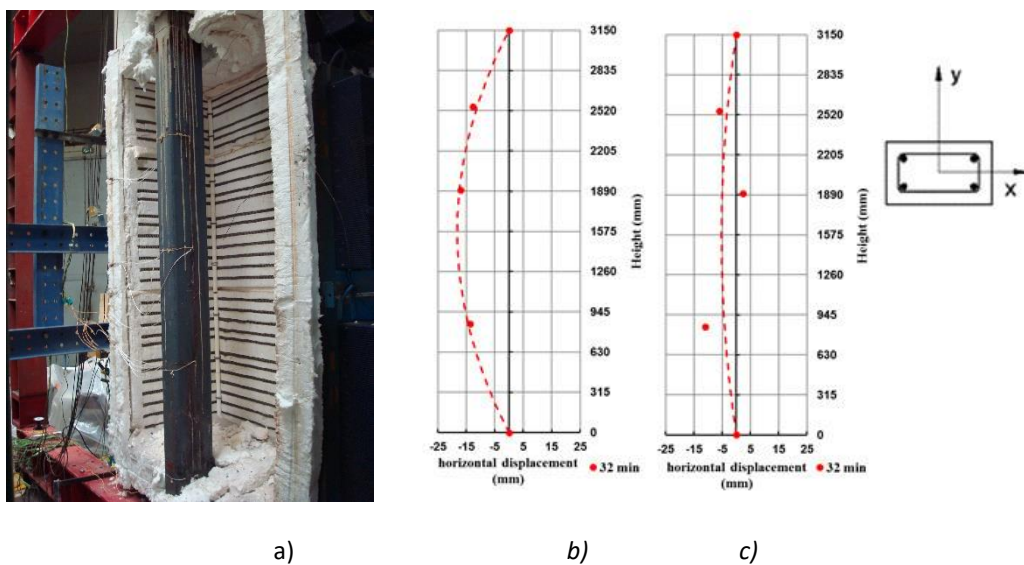

a)   b)   c)

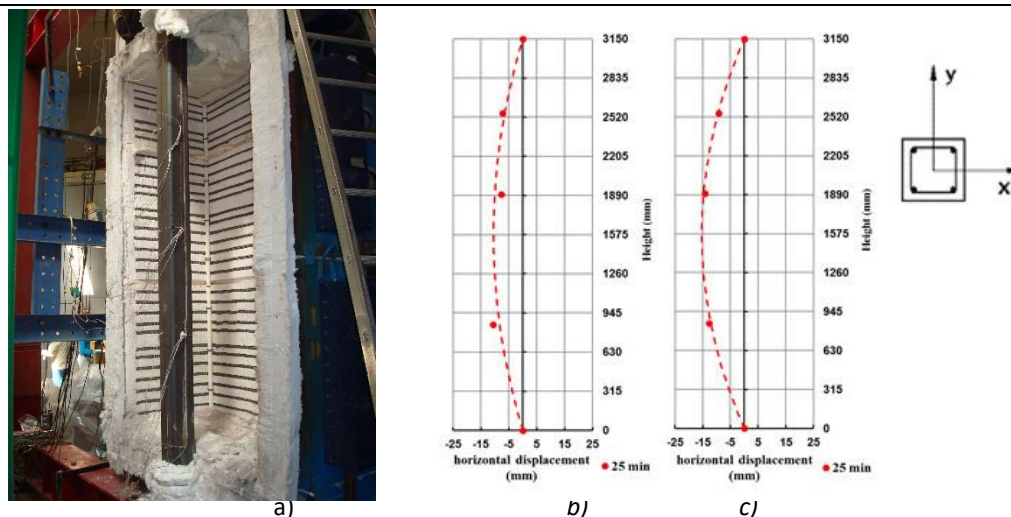*Fig. 13.* Lateral deflections for column RC250-lka: a) photograph; b) sr-y axis; c) sr-x axis

Influence of Pull-Out Fire Test Conditions on the Thermal Distribution and the Prediction of Load-Bearing Capacity of Bonded Anchors

234

Fig. 14. Lateral deflections for column SC250-lka: a) photograph; b) sr-y axis; c) sr-x axis

4   CONCLUSIONS

The main purpose of this research was to provide data for assessing the fire resistance of the concrete filled hollow columns. The adoption of elliptical columns, as the ones used in the present study is very interesting from the aesthetic point of view. However, as they have two well-defined buckling axes sudden collapse around the weak axis, is a possibility to be assessed, as observed in the present study.

Comparing the rectangular with the square columns, the first ones presented a greater fire resistance, despite the fact that they were tested with a bigger cross-section.

Comparing the elliptical with the circular columns, the elliptical presented greater fire resistance because semi-rigid boundary conditions were considered.

The quantitative results of this research project are valuable to provide data for future numerical studies with focus on parametric analysis of the behaviour of these solutions under fire conditions.

REFERENCES

[1]   Kodur V. (1999). Performance-based fire resistance design of concrete-filled steel columns. Journal of Constructional Steel Research 51. pp 21-36.

[2]   Espinos A., Romero M. L., Lam D. (2016). *Fire performance of innovative steel-concrete composite* columns using high strength steels. Thin-Walled Structures 106. pp 113–128.

[3]   Espinos A., Romero M. L., Serra E., Hospitaler A. (2015). *Experimental investigation on the fire behaviour of rectangular and elliptical slender concrete-filled tubular columns*. Thin-Walled Structures 93. pp 137-148.

[4] Rodrigues J. P. C., Laim L. (2017a). *Fire response of restrained composite columns made with concrete filled hollow sections under different end-support conditions*. Eng. Structures 141. pp 83-96.

[5] Rodrigues J. P. C., Laim L. (2017b). *Fire resistance of restrained composite columns made of concrete filled hollow sections*. Journal of Constructional Steel Research 133. pp 65-76.

[6] Rodrigues J. P. C., Correia A. J. M., Kodur V., (2018). *Boundary Conditions and Fire Behavior of Concrete Filled Tubular Composite Columns*. International Journal of High-Rise Buildings, Vol 7, No 4, 313-325, https://doi.org/10.21022/IJRB.2018.7.4.313

Influence of Pull-Out Fire Test Conditions on the Thermal Distribution and the Prediction of Load-Bearing Capacity of Bonded Anchors

235

INFLUENCE OF PULL-OUT FIRE TEST CONDITIONS ON THE THERMAL DISTRIBUTION AND THE PREDICTION OF LOAD-BEARING CAPACITY OF BONDED ANCHORS

Omar Al-Mansouri[1,2*], Romain Mege[1], Nicolas Pinoteau[1], Amine Lahouar[1], Sébastien Rémond[2]

[1] Université Paris-Est, Centre Scientifique et Technique du Bâtiment (CSTB), 84 avenue Jean Jaurès, Champs-sur-Marne, 77447 Marne-la-Vallée Cedex 2, France.
[2] IMT Lille-Douai, Univ. Lille, EA 4515 – LGCgE, Département Génie Civil & Environnemental, F-59000 Lille, France

ABSTRACT

Until this day, the applied method for the evaluation of bonded anchors directly exposed to fire subjected to tensile loads is inspired from the existing method for mechanical anchors (without resin). This method only covers steel failure mode, whereas the literature has shown that pull-out failure is more frequent in fire situations. Thus, there is a need to extend the current qualification methods.

This experimental study deals with the influence of different test parameters to establish a pull-out characterization procedure for bonded anchor systems under fire. Pull-out fire tests were conducted following the current guidelines under a standard ISO 834 fire followed by unloaded fire investigation tests with different configurations for anchors in a building. This paper quantifies the accuracy of the load prediction using a resistance integration method based on temperature profiles associated to this type of anchors, which are directly exposed to fire.

1 INTRODUCTION

Adhesive resins are commonly used in the field of building for bonding anchors in concrete. This bonding technique insures better performances at ambient temperature compared to other anchor systems such as mechanical anchors or cast-in anchors. The bond presents a capacity at ambient temperature, which is equal or superior to concrete cone or steel failure allowing them to be used for many structural purposes, retrofitting, and renovation works. This type of anchors can be bonded using polyester, vinylester and epoxy resins [1]. Studies at service temperature by means of pull-out tests have shown that bonded anchors present higher failure bond strength than mechanical anchors [2].

Research has shown that mortars have a high sensitivity to the increase of temperature which affects their material properties such as elastic modulus, flexural strength and decreases their strength [2]. Studies on polymer adhesive joints for a temperature range from -60 °C to 200 °C have shown that the deformability of these adhesives is high whereas their load bearing capacity is low at high temperatures [3]. The properties of the resin are strongly product dependent and depend on its quantity in the structural bearing element [4]. Many researchers consider the glass transition as an indicator of durability of polymers [5]. Epoxy mortars are more temperature sensitive than other polymeric mortars [6].

In order to establish the bond strength vs. fire exposure time relationship, the guidelines of design and assessment of the structural integrity of anchors defined in EOTA TR 048 [7] have to be followed. This technical report covers the evaluation of mechanical anchors for different failure modes. Many failure modes are possible for bonded anchors under tensile loads (concrete failure, steel failure, combined failure…). The pull-out assessment of bonded anchors under fire is not

Influence of Pull-Out Fire Test Conditions on the Thermal Distribution and the Prediction of Load-Bearing Capacity of Bonded Anchors

236

covered by this technical report. Only steel failure mode is mentioned for bonded anchors. It has been shown that steel resistance could be greater than bond resistance at high temperatures. Furthermore, there exists a good simplified method for the design of post-installed rebars at high temperatures whereas no guideline exists for bonded anchors under fire.

The resistance integration method presented promising results in the work of Pinoteau et al. on the pull-out of PIRs (post-installed rebars) at high temperatures [8-10]. The resistance integration method has shown good accordance between experimental and numerical determination of pull-out capacity of bonded anchors exposed to fire [11]. This method establishes a relationship between bond strength and temperature based on temperature profiles along the anchor depth of the anchor. The anchor is then divided into segments which are given a certain resistance in function of temperature using tests on PIRs at high temperatures described in EAD 330087-00-0601 [12].

A combination of different types of fire tests and numerical simulations was conducted on bonded anchor systems under fire by the university of Kaiserslautern [13]. This project demonstrated that the technical report EOTA TR 020 [14] which was integrated in [7] contains no regulations for the experimental evaluation of chemical anchor systems. Furthermore, the existing guidelines for fire tests on bonded anchors are unclear till this day.

Many parameters may influence the accuracy of bond strength prediction of bonded anchors under fire. Indeed, an anchor may exist in different conditions and configurations inside a building. In order to precisely calculate bond strength vs. fire exposure time relationship by the resistance integration, a good knowledge of temperature profiles along the anchor depth of the anchor must be insured.

In this paper, pull-out fire tests were conducted using the existing evaluation method of bonded anchors under tensile loads under ISO 834 fire [7]. The influence of the following parameters on the precision of the estimated bond strength was highlighted:

- Anchor diameter.

- Concrete bearing element thickness.

- Existence of a fixture on the anchor.

- Insulation around the fixture.

2   EXPERIMENTAL STUDY

The fire tests were conducted at the fire resistance laboratory, CSTB. The results for anchor configurations with different conditions under one sided fire exposure are presented.

2.1 Experimental furnace and used loading system

Fig. 21 shows the loading system and furnace used for fire tests. Bonded anchors were installed on the exposed surface. Concrete elements consist of concrete beams of 230 mm of width and 1500 mm of length. Some bonded anchors were equipped with thermocouples to measure temperature profiles along the embedment depth. The temperature inside the furnace was controlled to follow the ISO 834 fire curve. The dimensions of the furnace were: 1.4 m of length, 1 m of width and 1.05 of height. Three bonded anchors were loaded using a loading system. The loading system applied a downward mechanical constant load on a system of metallic tubes surrounding the concrete beam. Tube dimensions were: 40 mm x 40 mm. Anchors were facing the inside of the furnace and. Fixtures were connected to the anchors transferring the applied load from the tubes. Fixture dimensions in EOTA TR 048 [7] were adopted for fixtures. Loads were applied since the beginning of tests.
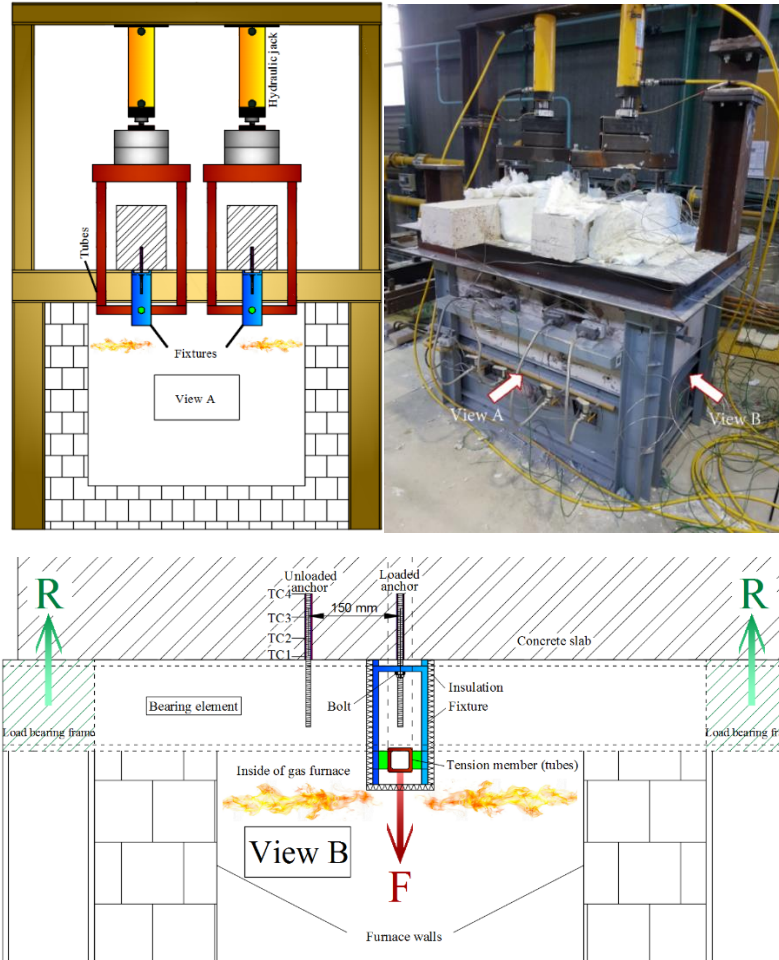
Influence of Pull-Out Fire Test Conditions on the Thermal Distribution and the Prediction of Load-Bearing Capacity of Bonded Anchors

237

Fig. 21. View A, B, and photo showing the gas furnace and the loading system.

In order to insure a one dimensional heat transfer inside concrete beams and along bonded anchors, beams were insulated using glass wool (50 mm thickness) on lateral faces. Bonded anchors were fastened using a polymer based resin. In order to avoid influencing bond surface between the resin and the steel of the rod, no thermocouples were placed on loaded anchors. This would result in a decrease of adherence between resin and steel leading to a false estimation of bond strength. In order to measure temperature profiles along loaded anchors without influencing their strength, another identical unloaded bonded anchor was installed in the same beam. At least 4 thermocouples were placed on unloaded bonded anchors. Unloaded anchors were installed in a position where they would be exposed to the same homogenous fire inside the furnace without interacting mechanically with loaded anchors. Thus, a choice of 150 mm distance was taken between loaded (centered above the furnace) and unloaded anchors.

As recommended in the technical report TR 048 [7], fixtures and tension members were insulated. Insulating material was put in place to protect steel from reaching failure before the pull-out of the anchor.

2.2 Experimental results

Three loaded pull-out tests were conducted following the configuration in EOTA TR 048 [7] with insulated fixtures attached to anchors, whereas unloaded anchors were directly exposed to the same homogenous fire inside the furnace. Loaded and unloaded anchors were subjected to the same homogeneous fire inside the furnace. Therefore, unloaded anchors are supposed to emulate the

Influence of Pull-Out Fire Test Conditions on the Thermal Distribution and the Prediction of Load-Bearing Capacity of Bonded Anchors

238

same temperature profiles along the loaded anchors. The three anchors were installed in beams of 180 mm thickness. Table 2 shows the details of these tests.

Table 8. Details of loaded pull-out fire tests

Fire type	Test n°	Bond geometry			Beam dimensions (m)	Load	Experimental failure time	Predicted failure time
		ϕ (mm)	h_{eff} (mm)	N° of TC	Length × width × thickness	(kN)	(min)	(min)
ISO 834	1	12	110	8	1.5 × 0.23 × 0.18	9	29	28
	2	12	110	4	1.5 × 0.23 × 0.18	1.8	60	48
	3	8	70	4	1.5 × 0.23 × 0.18	0.75	75	96

Where : ϕ is anchor diameter, h_{eff} is embedment depth of anchors.

Table 8 shows that for high load levels, predicted failure time is more accurate than for low load levels. This could be linked to the fact that, for low load levels, failure is reached for temperatures at which the adhesive resin has minimal resistance due to the degradation of its mechanical properties. It is also supposed that the difference obtained for low level loads is large due to the poor knowledge of temperature profiles. The hypothesis that loaded and unloaded anchors have similar temperature profiles leads to uncertain results for the prediction of failure time. Therefore, further investigation was conducted on unloaded anchors to determine the influence of the loading system on thermal distribution and the precision on the prediction method.

The adhesive resin presents a bond stress up to 25 MPa at ambient temperature for threaded rods with diameters below 16 mm. Resin properties at high temperatures according to EAD 330087-00-0601 [10] are presented in Fig. 22.
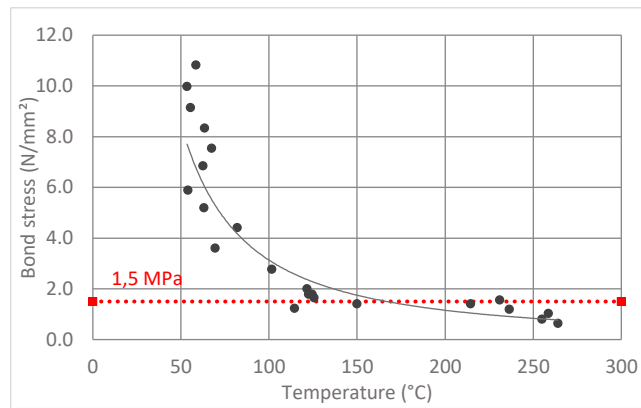
Fig. 22. Bond stress vs. Temperature relationship of the used polymer resin

Conducted thermal investigation tests are summarized in Table 9. Some tests were conducted several times for repeatability purposes. Details are presented in the following sections.

Table 9. Details of thermal investigation fire tests

Fire type	Test n°	Test configuration	Bond geometry		Concrete element dimensions (m)
			Ø (mm)	h_{eff} (mm)	Length × width × thickness
ISO 834	4	1	8	60	1.2 × 0.45 × 0.10
	5	1	12	60	1.2 × 0.45 × 0.10
	6	1	16	60	1.2 × 0.45 × 0.10
	7	2	8	70	1.5 × 0.23 × 0.15
	8	2	8	70	1.5 × 0.23 × 0.18

Influence of Pull-Out Fire Test Conditions on the Thermal Distribution and the Prediction of Load-Bearing Capacity of Bonded Anchors

239

9	2	8	70	$1.5 \times 0.23 \times 0.30$
10	2	12	110	$1.5 \times 0.23 \times 0.18$
11	2	12	110	$1.5 \times 0.23 \times 0.18$
12	3	12	110	$1.5 \times 0.23 \times 0.30$

The first studied parameter was anchor diameter. Three anchors with different diameters were tested (8 mm, 12 mm and 16 mm) with an embedment depth of 60 mm in a slab with the following dimensions: 1,2 m × 0,45 m × 100 mm. Cast-in thermocouples were installed along the thickness of the slab. Anchors were directly exposed to fire with no fixture or insulation.

Fig. 23 shows temperature profiles for different fire exposure durations (15, 30, 60 and 90 min). This comparison shows that a bigger diameter gives a slightly higher temperature at the same point of observation. The difference of temperature profiles between different diameters increases with fire exposure duration. It also decreases towards the bottom (less hot part) of the embedment depth.
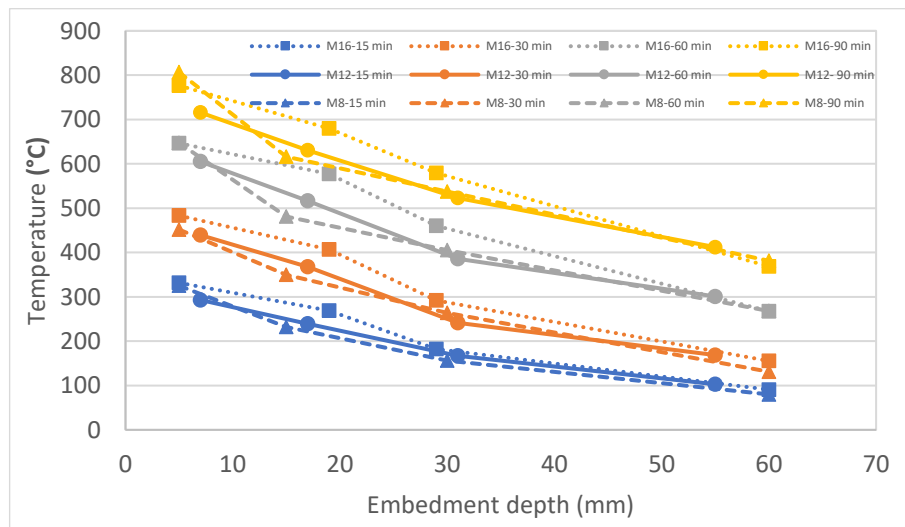
Fig. 23. Comparison between temperature profiles of three different anchor diameters

In order to quantify the influence of this slight difference, the resistance integration method was applied on the three diameters. For an applied load of 0.75 kN (same as loaded anchor n°3), the predicted failure times for anchors were: 51 min for the M8 rod, 64 min for the M12 rod and 43 min for the M16 rod. The fact that a higher diameter does not necessarily lead to faster failure due to higher thermal profile could mean that for a given stress applied on the anchor, there is an optimal diameter/anchor depth ratio that corresponds to the best load bearing capacity vs. fire exposure time curve.

The second studied parameter was the thickness of the concrete beam. Indeed, the change of boundary conditions of the thermal diffusion may influence temperature profiles of anchors. In order to assess the influence of this parameter, two different beam thicknesses were tested (180 mm and 300 mm) with M8 bonded rods installed with a 70 mm anchor depth. Fig. 24 shows a comparison between temperature profiles of the two cases. A thinner beam leads to higher temperatures at the same point of observation. This difference decreases towards the bottom of the anchor. The difference near the exposed surface is slightly larger than at the bottom of the anchor due to heat transfer conditions. The exposed part of anchors is subjected to convection and radiation of hot gases inside the furnace (which are hard to control during repeated fire tests). The difference between both cases is not significant and supposed to be in the dispersion margin of fire tests. Numerical simulation of this case could give almost identical temperature profiles. Further investigation is needed.

Influence of Pull-Out Fire Test Conditions on the Thermal Distribution and the Prediction of Load-Bearing Capacity of Bonded Anchors

240

The resistance integration method was used to assess the influence of this parameter on the predicted failure time. For an applied load of 0.75 kN on the anchor (same as loaded anchor n°3), the following failure times were predicted: 75 min for the 180 mm beam and 71 min for the 300 mm beam. This small difference is most likely negligible for higher load levels as well.

The third studied parameter was the influence of the existence of a fixture on anchors. The current guidelines in EOTA TR 048 [7] represent only fixtures with details. Due to the absence of requirements, an anchor inside a building may be exposed to fire without metal plates attached to it. This causes thermal transfer via the rod directly. In order to assess the influence of this parameter, 3 beams with 2 bonded anchors without fixtures in each and 6 beams with two bonded anchors with fixtures in each were tested.
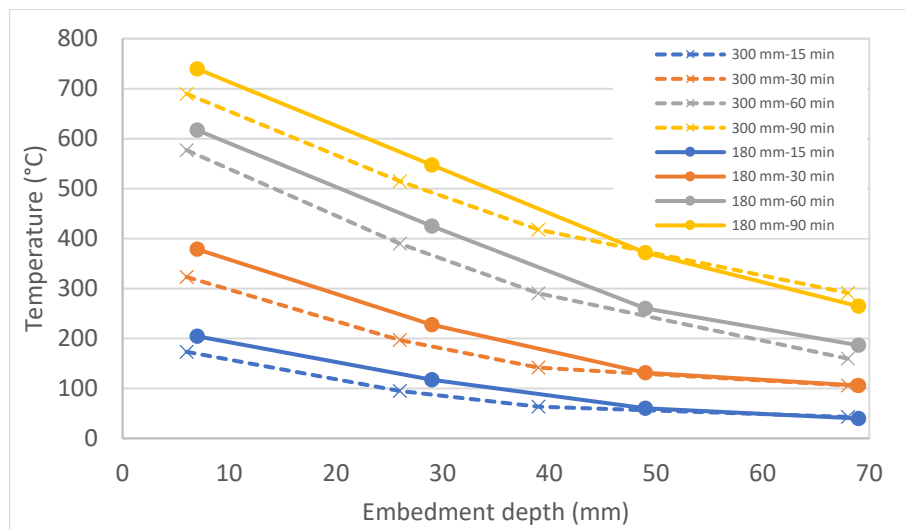
Fig. 24. Comparison between temperature profiles vs. Embedment depth for two anchors in different beam thicknesses.

Fig. 25 shows temperature profiles for different fire exposure durations for M12 bonded anchors with and without fixtures. A slight difference is observed between the two cases. This difference decreases after 90 min of fire exposure. This is caused by the homogenization of fixture temperature with furnace temperature. The fixture interferes with the thermal transfer mode and limits it to conduction. Without the fixture, thermal transfer is mostly done by radiation.
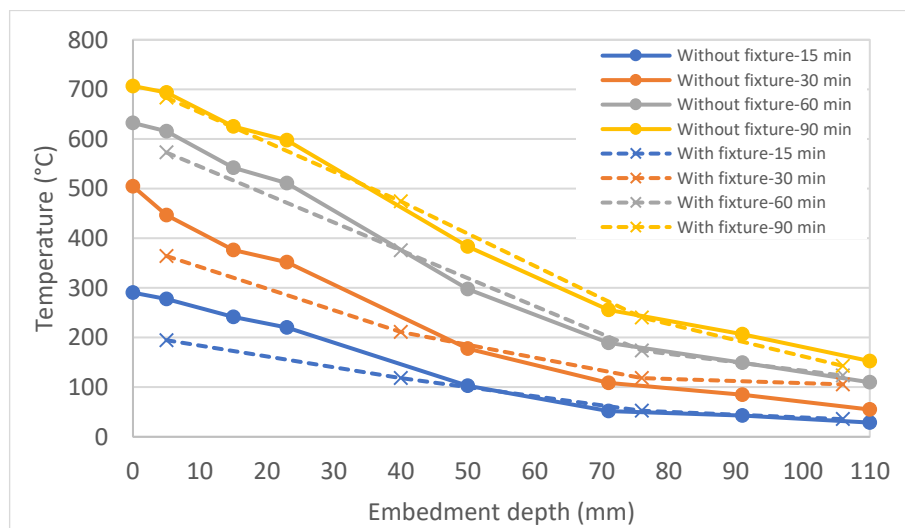
Fig. 25. Comparison between temperature profiles vs. Embedment depth for anchors with/without the fixture.

Influence of Pull-Out Fire Test Conditions on the Thermal Distribution and the Prediction of Load-Bearing Capacity of Bonded Anchors

241

In order to assess the influence of this parameter on the predicted load bearing capacity, the resistance integration method was applied. For an applied load of 1.8 kN (same as loaded anchor n°2), the predicted failure times for anchors were: 74 min for the rod without the fixture and 80 min for the rod with the fixture. However, for a load of 9 kN (same as loaded anchor n°1) the predicted failure times were: 27 min for the rod without the fixture and 28 min for the rod with the fixture.

The influence of this parameter on the prediction of failure time is negligible. However, the small difference could be attributed to several factors. Thermally, the metallic fixture acts as a thermal sink at the beginning of fire exposure, then steel temperature homogenizes with furnace temperature. In addition, in terms of failure load prediction, resin properties according to EAD 330087-00-0601 [10] in Fig. 22 present a slight variation of failure temperature for relatively high load levels. However, for low load levels (failure temperatures above 150°C), the slightest load variation could lead to a much higher or much lower failure temperature for this fitting curve. Hence, it is important to apply a constant mechanical loading with very minimal load variation during testing.

The forth studied parameter was thermal insulation around the fixture as required in the technical report EOTA TR 048 [7]. In order to study the influence of this parameter, four beams with 300 mm thickness with 2 bonded M12 anchors per beam were tested. Fig. 26 shows the insulation of beams for fire tests.
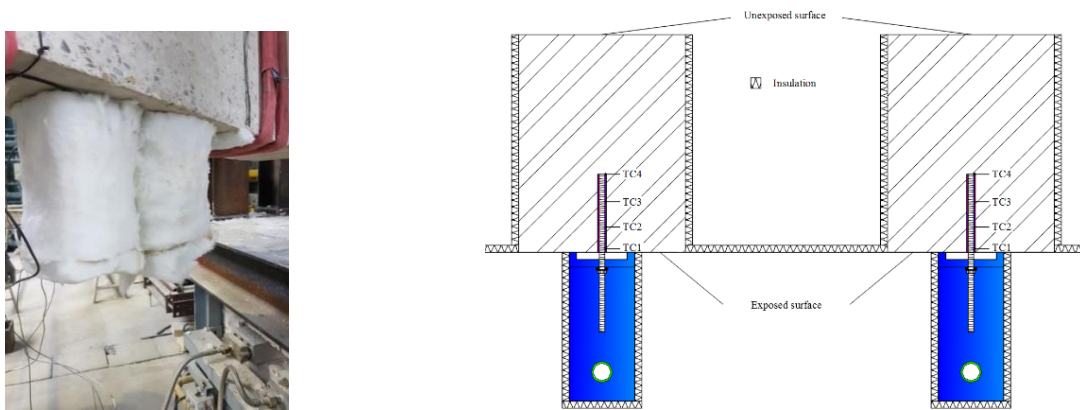
Fig. 26. Insulation of the fixtures and the lateral sides of beams (view B).

The results presented in Fig. 27 show a significant reduction in temperature profiles for insulated fixtures, compared to non-insulated fixtures.
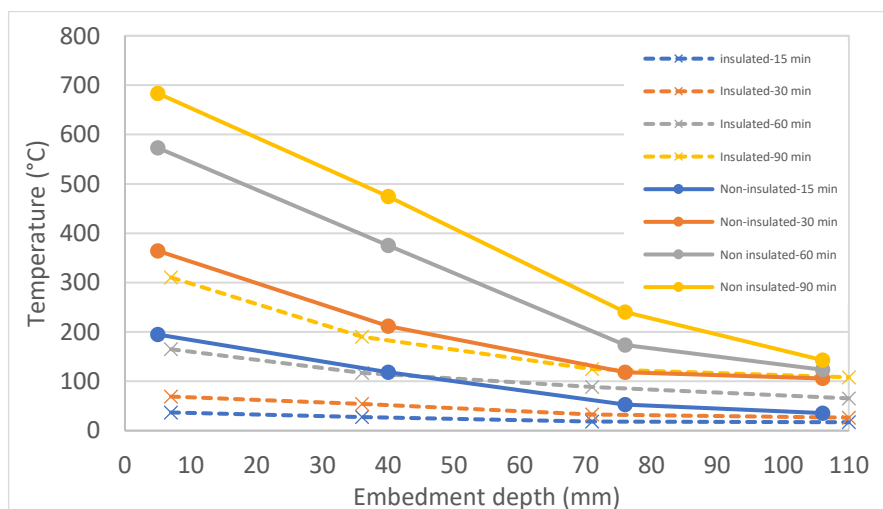
Fig. 27. Comparison between temperature profiles for insulated and non-insulated fixtures

Influence of Pull-Out Fire Test Conditions on the Thermal Distribution and the Prediction of Load-Bearing Capacity of Bonded Anchors

242

In order to assess the influence of this difference in temperature profiles, the resistance integration method was used to predict failure time. For an applied load of 9 kN (same as loaded anchor n°1), the predicted failure times were: 28 min for non-insulated fixtures, and 69 min for insulated fixtures. For an applied load of 1.8 kN (same as loaded anchor n°2), the predicted failure times were: 80 min for non-insulated fixtures, and 160 min for insulated fixtures. This means that insulation delays failure significantly for high and low load levels.

3   CONCLUSION

This paper aimed to highlight the influence of testing conditions described in the existing guidelines for evaluating the pull-out strength of bonded anchors in concrete under fire. A series of tests were conducted to investigate the following parameters: anchor diameter, concrete element thickness, existence of fixtures on anchors and insulation around fixtures. Testing derived the following conclusions:

- A larger anchor diameter results in higher temperature profiles but not necessarily faster failure because of the increase of bond surface around the rod.

- Concrete element thickness and fixtures attached to anchors have very minimal influence on the predicted bond resistance and failure time.

- Insulation around fixtures significantly decreases temperature profiles along the embedment depth of the anchor. Insulation prevents thermal exchange between the anchor and the fixture on one side and fire on the other side. This limits the thermal diffusion to the concrete element and delays the degradation of the bond.

This paper recommends to take into account the intended configuration for the anchor in the design procedure. The boundary conditions must consider whether the metallic fixture transferring loads to the anchor is directly exposed to fire or insulated. Further numerical investigations are advised to confirm the thermal results presented in this paper.

REFERENCES

[1] Cook R. Behavior of chemically bonded anchors (2015). J Struct Eng 1993;119(9):2744–62.

[2] Reis J. Effect of temperature on the mechanical properties of polymer mortars. Mater Res 2012;15(4):645–9.

[3] Adams R, Coppendale J, Mallick V, Al-hamdan H. The effect of temperature on the strength of adhesive joints. Int J Adhes Adhes 1992;12(3):185–90.

[4] Reis J. M. L. Effect of temperature on the mechanical properties of polymer mortars. Material Research. 2012; 15(4): p. 645-9.

[5] Frigione, M., Aiello, M. & Naddeo, C. Water effects on the bond strength of concrete/concrete adhesive joints. Construction and building materials. 2006; 20; p. 957-70.

[6] M.C.S. Ribeiro, P.J.R.O. Nóvoa, A.J.M. Ferreira, A.T. Marques. Flexural performance of polyester and epoxy polymer mortars under severe thermal conditions. Cem Compos; 2004; (26): p. 803-9.

[7] EOTA TR 048. Details of tests for post-installed fasteners in concrete. European Organization for Technical Approvals Technical report no. 48; August 2016.

[8] Pinoteau N, Heck J. V, Rivillon Ph, Avenel R, Pimienta P, Guillet T, Rémond S. Prediction of failure of a cantilever-wall connection using post-installed rebars under thermal loading. Eng Struct J 2013; 56: p. 1607-19.

[9] Lahouar M A, Pinoteau N, Caron J-F, Forêt G, Mège R. A nonlinear shear-lag model applied to chemical anchors subjected to a temperature distribution. Int J Adhe Adhes 2018; 84: 438-50.

[10] Lahouar M A, Pinoteau N, Caron J-F, Forêt G, Guillet T, Mège R. Chemically-bonded post-installed steel rebars in a full scale slab-wall connection subjected to the standard fire (ISO 834-1). In: Proceedings of

Influence of Pull-Out Fire Test Conditions on the Thermal Distribution and the Prediction of Load-Bearing Capacity of Bonded Anchors

243

the 3rd international symposium on Connections between Steel and Concrete. Stuttgart, Germany, September 2017; p. 1119-30.

[11] Lakhani H, Hofmann J. A numerical method to evaluate the pull-out strength of bonded anchors under fire. In: Proceedings of the 3rd international symposium on Connections between Steel and Concrete. Stuttgart, Germany, September 2017; p. 1179-90.

[12] EOTA, EAD 330087-00-0601, Systems for post-installed rebar connections with mortar. no. EOTA14-33-0087-06.01; July 2015.

[13] Reichert M, Thiele C. Qualification of bonded anchors in case of fire. In: Proceedings of the 3rd international symposium on Connections between Steel and Concrete. Stuttgart, Germany, September 2017; p. 1191-9.

[14] EOTA TR 020. Evaluation of Anchorages in Concrete concerning Resistance to Fire. European Organization for Technical Approvals Technical report no. 20; May 2005.

PREDICTION OF FAILURE TIME OF POST-INSTALLED REBARS AT HIGH TEMPERATURES USING A NON-LINEAR SHEAR-LAG MODEL

Mohamed Amine LAHOUAR[1], Omar AL-MANSOURI[1,2], Nicolas PINOTEAU[1], Romain MEGE[1], Thierry GUILLET[1]

[1]Université Paris-Est, Centre Scientifique et Technique du Bâtiment, France.
[2]Département Géne Civil & Environnemental, France

ABSTRACT

Thanks to the improvement in mechanical and adhesion properties of polymer resins, Post-Installed Rebars (PIRs) are increasingly used in bridges and building constructions. However, some incidents occurred in the last 20 years have shown the vulnerability of PIRs in a fire situation.

Recent studies carried out between 2011 and 2017 have shown that a stress redistribution occurs along PIRs in a fire situation. These studies have also highlighted that a stress concentration could lead in some cases to the pull-out and failure of PIRs.

This paper presents a non-linear shear-lag model allowing the prediction of the evolution of stress profiles and load bearing capacity of PIRs during a fire situation. The model predictions are compared to experimental results in order to evaluate their accuracy.

1   INTRODUCTION

Post-Installed Rebars (PIRs) are a construction technique consisting of anchoring a steel rebar in a precast concrete using a polymer resin. This technique is used to ensure the load transfer between two neighbouring structural elements. Indeed, PIRs offer advantageous solutions for concrete construction by proposing a viable and economical method for adding new concrete sections or attaching steel members to existing structures [1]. PIRs are also used today in new constructions to meet the high architectural requirements by providing more flexibility in the planning and design of concrete structures [2].

Several studies have been focused during the last seven decades on the analysis of axial, shear and peel stress distribution along the anchors [3]. Volkersen [4], was the first to suggest a shear-lag model in 1938, basically developed to predict the stress distribution along mechanical joints using several fasteners. Very quickly, the model has been improved to be adapted to chemical anchors and to take into account new parameters, such as the deformation of the adherents [5].

In the 1970's, with the advent of computer tools, several numerical models were developed based on the shear-lag theory. These models allowed to include new points of interest and widen the scope of study concerning the mechanical analysis of PIRs.

However, in the light of the focus on the analysis of the mechanical behaviour of PIRs under the influence of several parameters, the temperature effect on the stress distribution and on the modification of the mechanical properties of polymer resins was neglected.

This paper presents a non-linear shear-lag model allowing the determination of the stress distribution along PIRs as a function of the temperature distribution and predicting the moment when failure can occur.

The shear-lag model is validated in this paper as a comparison with a fire test carried out on a cantilever beam, connected to a reinforced concrete wall using PIRs. The comparison showed good agreement between model prediction and experimental results.

2   SHEAR-LAG MODEL APPLIED TO PIRs IN A FIRE SITUATION

This section presents the shear-lag equations applied to PIRs subjected to thermal stress. The studied configuration is composed of a concrete cylinder drilled axially in its centre, and a steel rebar of radius R, introduced into the drilled hole along an embedment length L. The spacing between the steel rebar and concrete represents the thickness of the adhesive joint, denoted e (*Fig. 1*). An axial tensile force F is applied at the beginning of the rebar. The axial stress is assumed equal to zero at the bottom of the PIR. The PIR is studied using a cylindrical coordinate system, where the axis of the rebar corresponds to the X-axis and the abscissa zero corresponds to the bottom of the PIR.
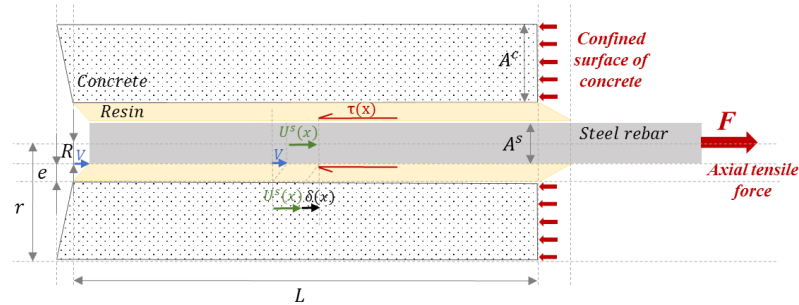
Fig. 28. Geometrical and mechanical configuration of the studied PIR

2.1 Model assumptions and notions

Five assumptions are made in order to simplify the shear-lag resolution.

i.   Adherents (rebar and concrete) are homogeneous and linear elastic.
ii.   The adhesive transfers the axial load from the rebar to concrete only by shear stress.
iii. Bending effects are neglected.
iv.   Normal stresses are uniformly distributed over the cross sections of the rebar and concrete.
v.   The thickness and width of the adhesive and the adherents are constant throughout the bond line.

Mechanical and geometrical quantities used in this paper are presented below.

σ^s : Axial stress in the steel rebar section [MPa]

σ^c : Axial stress in the concrete section [MPa]

ε^s : Steel rebar axial strain

ε^c : Concrete axial strain

E^s : Steel rebar elastic modulus (*independent of temperature*) [MPa]

E^c : Concrete elastic modulus (*temperature dependent*) [MPa]

A^s : Steel rebar section [mm²]

A^c : Concrete section [mm²]

R : Steel rebar radius [mm]

L : Embedment length [mm]

τ : Adhesive bond stress [MPa]

$U^s(x)$: Elastic axial displacement of the steel rebar [mm]

$U^c(x)$: Elastic axial displacement of the concrete induced by concrete crushing [mm]

V: Axial displacement induced by the shearing of the adhesive at the bottom of the PIR [mm]

δ : Rebar slip [mm]

θ : Temperature of the element of PIR [°C]

2.2 Shear-lag model constitution

The development of the shear-lag model relies on the forces equilibrium in an elementary section of a PIR, as presented in *Fig. 2,* and described in *Eq. (1)*.
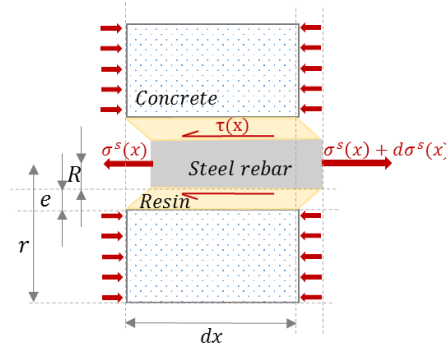
Fig. 29. Forces equilibrium in an elementary section of PIR

$$\sigma^s(x) A^s + \sigma^c(x) A^c = 0 \tag{1}$$

Axial stress is assumed to be independent of the radial coordinate of the PIR element (*assumptions iv and vi*), which is generally accepted and used for steel, but should be checked in the concrete section A^c.

The load equilibrium on the elementary section of length dx allows to obtain the relationship between the axial stress and adhesive bond stress (*Eq. (2)*).

$$\tau(x) = \frac{R}{2} \frac{d\sigma^s(x)}{dx}$$
(2)

The PIR slip $\delta(x)$ is defined as the difference between the rebar and the concrete displacement at the position x (*Eq. (3)*). The rebar displacement is divided into a displacement denoted $U^s(x)$ induced by the elastic elongation of the steel (which depends on x), and a displacement V corresponding to the rebar displacement at the bottom of the PIR, induced by the shearing of the bond joint (independent of x). The concrete displacement denoted $U^c(x)$, is induced by the concrete compression and depends on the position x of the PIR element.

$$\delta(x) = U^s(x) + V - U^c(x) \tag{3}$$

As steel and concrete are considered as elastic materials, *(assumption i)*, the Hooke's law can be applied to express the axial strain as a function of axial stress and Young's moduli in steel and concrete (*Eq. (4)*). Since the studied temperatures do not exceed 200°C, it is assumed that the steel elastic modulus is independent of temperature *(according to Eurocode 2 part 1-2)*, while the concrete elastic modulus varies with temperature.

$$\frac{d\delta(x)}{dx} = \frac{dU^s(x)}{dx} - \frac{dU^c(x)}{dx} = \varepsilon^s(x) - \varepsilon^c(x) = \frac{\sigma^s(x)}{E^s} - \frac{\sigma^c(x)}{E^c(\theta(x))} \tag{4}$$

Therefore, by substituting *Eq. (1)* into *Eq. (4)*, we obtain a relationship between the PIR displacement and axial stress, as described by *Eq. (5)*.

$$\frac{d\delta(x)}{dx} = \sigma^s(x)\left(\frac{1}{E^s} + \frac{A^s}{A^c}\cdot\frac{1}{E^c(\theta(x))}\right) \tag{5}$$

Thus, the constitutive equation of the shear-lag model applied to PIRs in a fire situation (*Eq. (6)*) is obtained by combining *Eq. (2)* and *Eq. (5)*.

$$\frac{d^2\delta(x)}{dx^2} = \frac{2}{R}\left(\frac{1}{E^s} + \frac{A^s}{A^c}\cdot\frac{1}{E^c(\theta(x))}\right)\tau(x) \tag{6}$$

To solve the shear-lag equation, it is therefore essential to transform the *Eq. (6)* into a second-order differential equation. Consequently, it is necessary to establish a relationship between the shear stress and the rebar displacement as function of temperature, as described in *Eq. (7)*.

$$\tau(x) = f(\delta(x), \theta(x)) \tag{7}$$

In our case study, this relationship is established experimentally by a pull-out test campaign carried out at different temperatures, as detailed in section 4.

3   NUMERICAL RESOLUTION OF THE SHEAR-LAG CONSTITUTIVE EQUATION USING FINITE DIFFERENCE METHOD

The complexity of the constitutive equation of the shear-lag model makes its analytical resolution extremely difficult for unusual forms of $\tau(\delta(x), \theta(x))$ relationship (*Eq. (7)*). However, numerical resolution helps to overcome this problem and offers the opportunity to use more realistic forms of $\tau(\delta(x), \theta(x))$ relationship while obtaining more accurate results.

Thus, the PIR is discretized into n elements of length Δx, numbered from 1 to n, chosen sufficiently small to assume a uniform bond stress distribution over the element. Each element has two borders, shared with the neighbouring elements. The border between two successive elements of the PIR is denoted by an index i varying from 0 to N. The index 0 corresponds to the beginning of the PIR and the index N corresponds to the bottom of the PIR. Three mechanical quantities are associated to each element: δ_i, τ_i and σ_i^S. These quantities are characteristic for each element and vary according to its temperature and position in the PIR. δ_i and σ_i^S are expressed at the border indexed i, however τ_i is expressed over the element comprised between the borders indexed i and i+1 (*Fig. 3*).
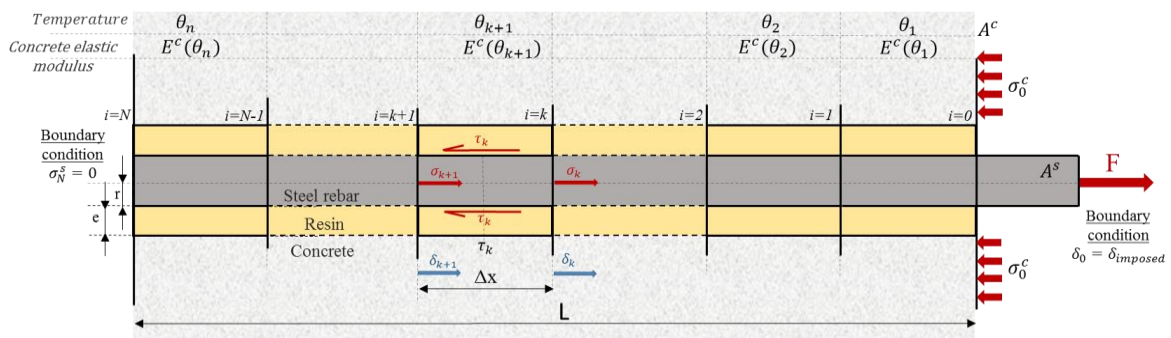
Fig. 3. PIR discretization into n elements

The finite difference numerical model presented in this paper is designed to impose a displacement value at the beginning of the PIR. Therefore, the resolution of the shear-lag differential equation is based on three boundary conditions.

- The amount of displacement at the beginning of the PIR is equal to the imposed displacement.

$$\overline{\delta_0} = \overline{\delta_{imposed}} \tag{8}$$

- The amount of bond stress in the first element of the anchor is deduced from the amount of the imposed displacement using *Eq. 7*.

$$\overline{\tau_0} = f(\overline{\delta_0}) \tag{9}$$

- The axial stress at the bottom of the anchor is equal to zero.

$$\sigma_N^S = 0 \tag{10}$$

Therefore, the discretization of the anchor into n elements requires the rewriting of the shear-lag equations according to the finite difference form as follows.

- The axial stress at the border i+1 is equal to the axial stress value at the border i, decreased by the bond stress generated in the element i.

$$\overline{\sigma_{i+1,J}} = \overline{\sigma_{i,J}} - \left(\frac{2}{R}\overline{\tau_{i,J}}\,\Delta x\right) \tag{11}$$

- The value of the slip at the border i+1 is equal to the slip at the border i decreased by the slip induced by the axial stress applied over the element i+1 (equal to the average axial stress between the borders i and i+1).

$$\overline{\delta_{i+1,J}} = \overline{\delta_{i,J}} - \Delta x \left(\frac{1}{E^S} + \frac{A^S}{A^C E^C(\overline{\theta})}\right)\left(\frac{\overline{\sigma_{i+1,J}} + \overline{\sigma_{i,J}}}{2}\right) \tag{12}$$

- The bond stress over the element i+1 is deduced from the slip at the border i+1 using *Eq. (7)*.

$$\tau_{i+1,j} = f(\delta_{i+1,j}) \tag{13}$$

The resolution of the shear-lag differential equation using the Finite Difference Method (FDM) with imposed displacement is done by iteration and is based on a convergence calculation ensuring the uniqueness of the solution. Therefore, an index j is introduced in the equations indicating the number of the convergence loop. The convergence criterion suggested in this study is the False Position Method (called also Regula Falsi Method) [6].

4   BOND STRESS – DISPLACEMENT & TEMPERATURE RELATIONSHIP

This section presents the relationship between the adhesive bond stress and the PIR displacement for different temperatures. This relationship is obtained experimentally through pull-out tests performed between 20°C and 130°C. Indeed, previous Differential Scanning Calorimetric tests (DSC) have shown that the glass transition temperature of the resin is between 60°C and 80°C, and that at temperatures above 110°C, the resin is softened. The pull-out test at 130°C allowed to check the low mechanical strength of the resin at this temperature range. *Fig. 4* shows some curves obtained experimentally by performing pull-out tests at stabilized temperature on steel rebars chemically bonded into concrete cylinders.

θ [°C]	τmax [MPa]	δ₁ [mm]	δ₂ [mm]	δ₃ [mm]	α
20	27,1	0,1	0,7	6,1	0,3
25	29,9	0,2	0,8	6,7	0,7
38	27,2	0,2	1,1	6,8	0,6
45	27,2	0,5	0,9	6,3	0,4
66	14,4	0,6	1,0	2,1	0,8
73	12,6	0,7	1,1	2,1	0,7
80	9,1	0,7	0,9	2,6	0,6
91	6,4	0,9	1,6	3,3	0,7
101	6,0	0,8	0,9	2,2	0,9
113	4,9	0,9	1,2	1,9	0,9
130	1,2	0,7	1,1	3,2	0,7
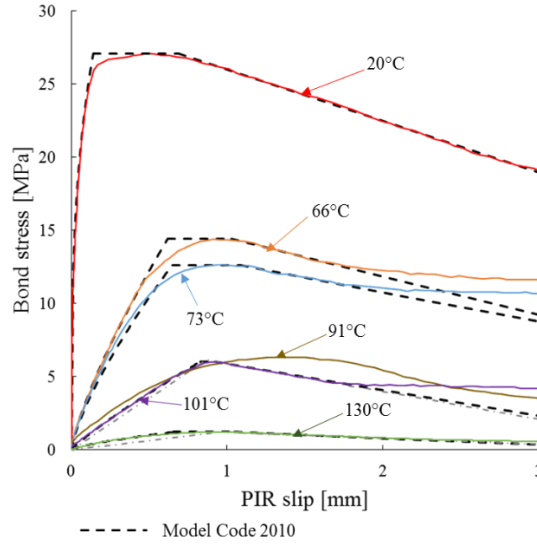
Fig. 4. Bond stress – anchor slip curves obtained by pull-out tests at different temperatures

In order to use data shown in *Fig. 4* in solving the shear-lag constitutive equation with Finite Difference Method (FDM), the curves have been fitted using the Model Code 2010 law (MC2010) [7] described by *Eq. (14)*. Fitting curves are represented with dark dashed lines in *Fig. 4*. *Table 1* shows the different parameters used to fit the curves on *Fig. 4*.

$$\tau(\delta(x), \theta(x)) = \begin{cases} \tau_{max}(\theta) \left(\frac{\delta(x,\theta)}{\delta_1(\theta)} \right)^{\alpha(\theta)} & when \ 0 \leq \delta(x,\theta) \leq \delta_1(\theta) \\ \tau_{max}(\theta) & when \ \delta_1(\theta) < \delta(x,\theta) \leq \delta_2(\theta) \\ \frac{\tau_{max}(\theta)}{\delta_2(\theta)-\delta_3(\theta)} \left(\delta(x,\theta) - \delta_2(\theta) \right) + \tau_{max}(\theta) & when \ \delta_2(\theta) < \delta(x,\theta) \leq \delta_3(\theta) \\ 0 & when \ \delta(x,\theta) > \delta_3(\theta) \end{cases}$$

(14)

5   MODEL VALIDATION

5.1   Shear-lag model applied to a cantilever beam exposed to fire

In this section, the shear-lag model is applied to a reinforced concrete structure, exposed to ISO 834 fire. The studied structure is composed of a 450 mm x 450 mm x 320 mm concrete wall, supporting a cantilever beam, measuring 1000 mm x 300 mm x 120 mm, positioned at a height of 100 mm from the underside of the wall. The connection between the wall and the cantilever slab is realised via two steel rebars of 16 mm diameter, anchored at 135 mm inside the wall using the same polymer resin studied by pull-out tests (*Fig. 4*). Rebars are positioned at 20 mm underside of the cantilever beam exposed to fire. *Fig. 5* describes the studied fire test configuration.

The cantilever beam is mechanically loaded by a constant load of 5 kN applied at 800 mm from the lateral surface of the wall. Only the inferior surface of the beam and the lateral surface of the wall under the beam are exposed to ISO 834 fire.
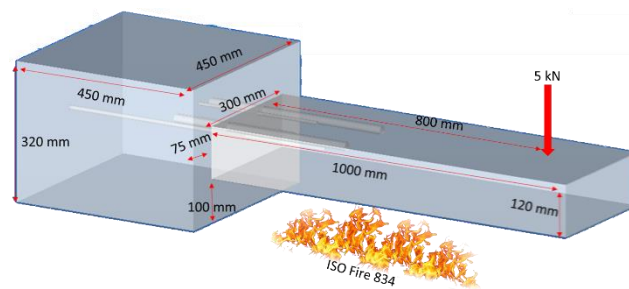
Fig. 5. Description of the selected fire test configuration

Mechanical calculations at cold state performed on the selected configuration have shown that the tensile force supported by each rebar is equal to 53.3 kN. Finite element thermal calculations carried out on SAFIR 2016 software allowed to determine the temperature evolution at the PIR position at different times of fire exposure (*Fig. 6a*). This data was injected into the shear-lag model in order to determine the evolution of the shear stress along the PIR (*Fig. 6b*) as well as to determine the evolution of its load bearing capacity as function of the fire exposure duration (*Fig. 7*). The amount of displacement imposed at the beginning of PIR is determined as the quantity of displacement allowing the generation of a tensile force in the rebar equal to that determined by calculations.

Fig. 6a) and *6b)* show that when the thermal gradient along the PIR is low, the shear stress is concentrated at the beginning of the PIR, and is almost zero at the bottom. *Fig. 6a)* shows that the thermal gradient becomes important starting from 60 minutes of fire exposure. From this moment, *Fig. 6b)* highlights a new distribution of shear stress in the PIR, with a higher concentration in the coldest areas (bottom of the PIR). With temperature increase, the bond resistance at the beginning of the PIR becomes extremely weak, and the PIR continues to resist thanks only to its cold part.

Over time, the temperature continues to increase in the PIR and the shear stress becomes more and more concentrated towards the bottom, until the PIR becomes no longer resistant to the applied tensile load.
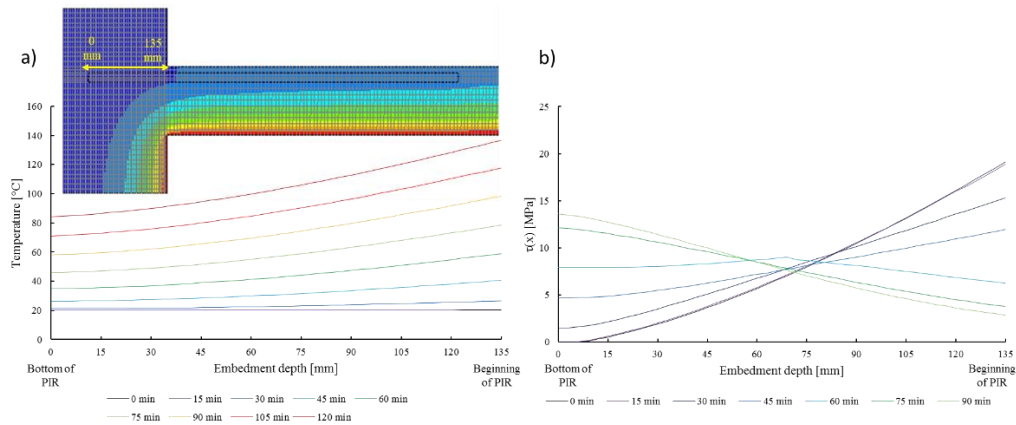
Fig. 6. a) Temperature evolution in the PIR; b) Shear stress distribution during fire exposure

Fig. 7 presents the evolution of the load bearing capacity of the PIR as function of time of fire exposure. *Fig. 7* shows that for low temperatures along the PIR, the load bearing capacity is constant, and equal to 184.3 kN (provided that the steel does not yield in tension). From 60 minutes, a remarkable decrease in the bearing capacity generated by the temperature increase in the PIR is observed. The shear-lag model predicts a ruin of PIRs at 96 minutes under ISO 834 fire exposure.
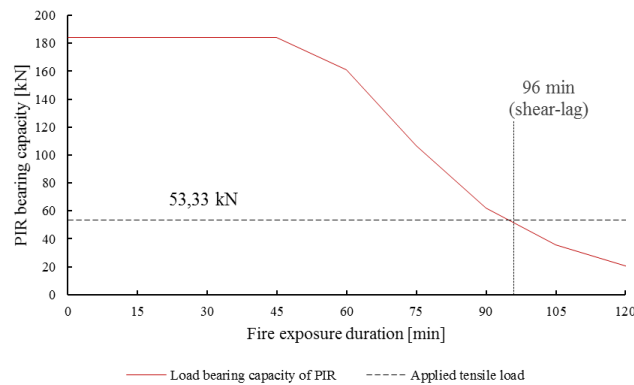
Fig. 7. Evolution of the load bearing capacity of the PIR during fire exposure

5.2 Fire test on a cantilever beam

In order to verify the results provided by the shear-lag model, a fire test was carried out on the studied configuration at CSTB. The mechanical loading was applied via a hydraulic jack. The applied load was continuously measured using a load cell. The temperature at the PIRs was measured using thermocouples positioned at the same height as the rebars. The displacement at the free end of the cantilever beam was measured using an LVDT sensor. The displacement of the beam was also measured using a stereo image correlation system (DIC).

Fig. 8a) and *Fig. 8b)* show respectively the test specimen set up on the furnace of the CSTB, and the results obtained by the DIC system.
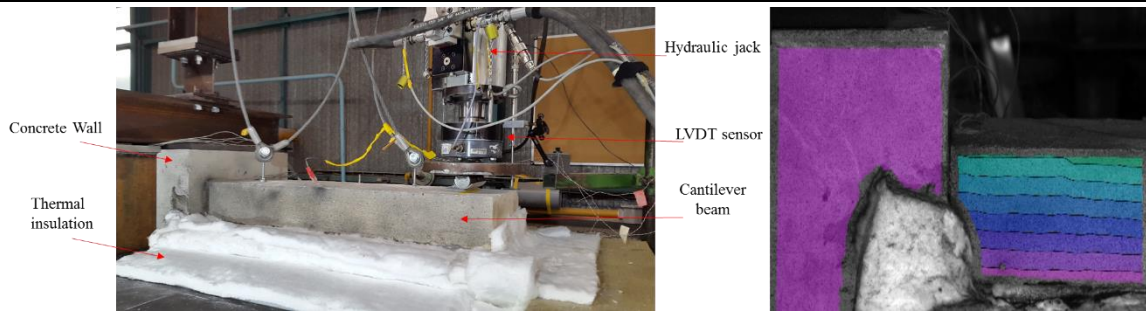
Fig. 8. a) Test specimen set up; b) Cantilever beam deformation measured by the DIC system
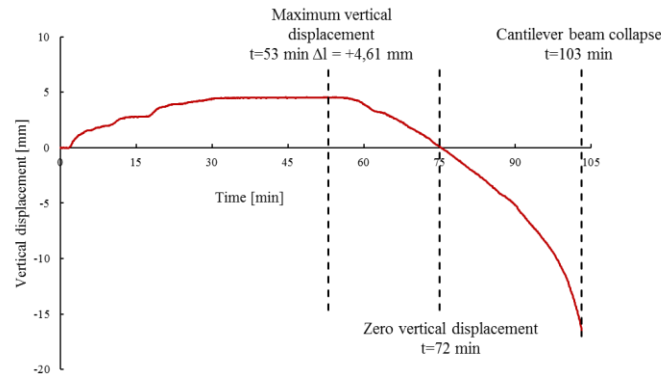
Fig. 9. Displacement of the free end of the cantilever beam during the fire test

Fig. 9 presents the evolution of the displacement at the free part of the beam during the fire test. The zero position was set after the application of the load and at the beginning of the fire. The results highlight a vertical outward the furnace since the beginning of the test. This displacement is generated by the differential deformation in the thickness of the beam, due to the thermal gradient. This gradient induces thermal curvature causing the beam to bend away from the fire. The maximum vertical displacement was recorded at 53 minutes and was equal to +4.61 mm. The initial vertical position was reached again after 72 minutes of fire exposure due to the temperature uniformity in the thickness of the beam. Finally, results show a collapse of the beam after exactly 103 minutes of exposure to fire, at a moment very close to that predicted by the shear-lag model.

6 CONCLUSIONS

This paper presented a non-linear shear-lag model applied to PIRs at a fire situation. The model allowed to describe the shear stress profile and to study its evolution under thermal stress. In a fire situation, the model highlighted a redistribution of the shear stress in the coldest area of the PIR, which allows it to resist to the applied tensile force, despite the degradation of bond resistance on the hotter areas of the rebar. The shear-lag model presented in this paper also allowed to predict the fire resistance of PIRs by quantifying their bearing capacity as a function of the fire exposure duration. The shear-lag model predictions were compared to a fire test. Obtained results showed good agreement between model and experimental results. For this case, the theoretical predictions of failure were on the safe side.

REFERENCES

[1] Cook. R. (1993). *Behavior of Chemically Bonded Anchors.* Journal of Structural Engineering, vol. 119(9), 1993, pp. 2744-2762.

[2] Bickel T., Shaikh A. (2002). *Shear Strength of Adhesive Anchors*. Precast Concrete Institute Journal, 2002, pp. 92-100.

[3] Goland M., Reissner E. (1944). *The Stresses in Cement Joints*. Journal of Applied Mechanics, vol. 11, 1944; pp. 17–27.

[4] Volkersen O. (1938). *Die Niektraftverteilung in Zugbeanspruchten mit Konstanten Laschenquerschritten*. Luftfahrtforschung, vol (15), 1938, pp. 41–47.

[5] Oplinger D. (1991). *A layered beam theory for single lap joints*. Army Mater Technology Laboratory Report, 1991, pp. 91-123.

[6] Press WH, Teukolsky SA., Vetterling WT., Flannery BP (1992). *Numerical Recipes in C: the art of scientific computing*. Cambridge: Cambridge University Press, ISBN 0-521-43108-5; 1988-1992. NASA-CR-112236.

[7] CEB-FIB. (2011), Model Code 2010, final draft, September 2011.

EFFECT OF WATER QUENCHING AND POST-FIRE CURING ON STRENGTH OF FIRE-DAMAGED ULTRA-HIGH PERFORMANCE CONCRETE

Ye LI, Kang Hai TAN
Nanyang Technological University, , Singapore

ABSTRACT

This research investigates change of compressive strength of UHPC and mortar samples after heat exposure, water quenching, and re-curing. The specimens were heated in an electric furnace to 300, 600, and 900°C with a low heating rate of 1 °C/min and then cooled either in furnace or in water immediately. For re-cuing, the specimens were re-cured in water for 0, 7, and 28 days. Changes of compressive strength were measured. Microstructure changes of UPHC was investigated by means of field emission scanning electron microscope (FESEM). The results show that the compressive strength of UHPC increases significantly after heated to 300°C, but a sharp loss was observed after 600 and 900°C exposure. Water quenching reduced the compressive strength of the UHPC mixes significantly. Strength of UHPC cannot be recovered by either water or air re-curing. But water re-curing can help to recover strength of mortar without silica fume.

1   INTRODUCTION

Fire is one of the most detrimental scenarios for reinforced concrete (RC) structures. Although concrete is inflammable, severe damages at elevated temperature will cause degradation of mechanical properties. Ultra-high performance concrete (UHPC) has become common in construction industry due to its high strength, improved ductility, and good durability [1-6]. The excellent mechanical properties of UHPC allow significant reduction of size and weight of RC members [7]. The enhanced durability leads to longer service life and lower costs for maintenance. Therefore, UHPC has been utilized in the construction industry around the world across [6, 8-12]. However, UHPC structures with slender dimensions are more vulnerable to fire attack. Information on mechanical properties of UHPC after heat exposure is still limited.

Investigation of residual mechanical properties of concrete after fire exposure are important for proper evaluation of post-fire capacity of RC structures. Most accidental fires are extinguished by water spraying. Rapid cooling can potentially introduce thermal shock to the heated concrete and the interaction with water may change chemical composition of concrete matrix. It is therefore necessary to study effects of water quenching on residual performance of concrete. Comparison between furnace cooling and water quenching on residual performance of high-performance concrete (HPC) [13], normal strength concrete (NSC) [13], and concrete containing high volume of palm oil fuel ash (POFA) [14] has been made. Difference between natural cooling and water quenching was also investigated for concrete with fine aggregates partially replaced by waste rubber fibers [15], with expanded perlite aggregates (EPA), and with pumice aggregates (PA) [16] subjected to elevated temperature. However, to the best of the authors' knowledge, effects of water quenching on residual performance of UHPC has yet been investigated.

Autogenic self-healing methods such as post-fire curing has been shown to recover the mechanical properties of concrete [17-21]. Poon et al. [19] indicated that the post-fire curing resulted in substantial strength recovery. Lin et al. [17] investigated the microstructures of fire-damaged concrete and found that rehydration of calcium oxide and unhydrated cement

grains can refill the void spaces. Akca and Özyurt [21] study was conducted to understand the effects of mineral admixtures, fiber reinforcement, air entrainment and different re-curing regimes on residual properties of concrete. However, these studies cannot be generalized for UHPC due to its different composition and properties.

The above concerns prompted to investigate effects of elevated temperature, water quenching, and re-curing on strength of UHPC. UHPC mix with PP fiber and normal concrete mortar were prepared. For effects of water quenching, UHPC samples were exposed up to 900°C and then experienced either furnace cooling or water quenching. Compressive strengths of UHPC samples at residual state were measured. Changes in micro structures of UHPC were investigated by means of the field emission scanning electron microscope (FESEM). For effects of re-curing, after 900°C heat exposure, UHPC samples and mortar samples were stored in water for 0, 7, and 28 days. After re-curing, their compressive strengths were measured.

2   EXPERIMENTAL PROGRAM

2.1   Materials and mix proportions

Table 10 shows the mix proportions in this study. The UHPC matrix consisted of cement (C), aggregates (AG), silica sand (SS), silica fume (SF), superplasticizers (SP), and water (W). Portland cement ASIA$^@$ CEM I 52.5 N, natural river sand sieved to 2 mm as fine aggregate, silica sand with a median particle size of 130 μm and Grade 940 silica fume from Elkem Microsilica$^@$ were used. Water-to-binder ratio was 0.2 to achieve dense packing and ultra-high strength. A polycarboxylate-based superplasticizer (Sika$^@$ ViscoCrete$^@$-2044) was used to adjust workability in the fresh state. Monofilament cylindrical PP fibers (P) with 12 mm in length and 30 μm in diameter supplied by DFL were added in the mix to prevent explosive spalling. The mortar mix consists cement, fine aggregates, and water. Water-to-binder ratio was 0.5.

Table 10. Mix proportions of UHPCs [kg/m^3]

Mix Design	Mass of ingredients						PP fiber
	C	AG	SS	SF	SP	W	
UHPC	833.3	916.7	208.3	208.3	25.0	208.3	3
Mortar	600.0	1500.0	0.0	0	0	300.0	0

C: cement, AG: aggregates, SS: silica sand, SF: silica fume, SP: superplasticizer, W: water

The UHPC was prepared in a Hobart@ planetary mixer. Cement, fine aggregate, micro silica sand, and silica fume were dry-mixed for 2 min. Thereafter, pre-mixed water and superplasticizer were added into the dry ingredients and mixed for another 3 to 5 min until the fresh UHPC was homogenous and consistent. PP fibers were then gradually added and mixed for another 3-5 min to ensure uniform dispersion. The mortar was mixed with water for 3 to 5 min. The fresh mixtures were cast into 50 mm cube molds with vibration to remove entrapped air. After casting, the specimens were sealed and kept in ambient air (28±2°C, 80%RH) for 24 h before they were demolded and stored in lime-saturated water (26°C) for another 27 days prior to testing.

2.2   Experimental procedures

At the age of 28 days, UHPC samples were exposed to elevated temperature (i.e., 300°C, 600°C, or 900°C) in an electrical furnace with a heating rate of 1°C/min. After reaching the pre-determined temperature, specimens were then held for 3 h to ensure uniform temperature

distribution inside the sample. The UHPC samples were either cooled down to ambient temperature inside the furnace or immediately quenched by water in a water tank. UHPC samples heated to 900°C were used to investigate re-curing effects. The mortar samples were only heated to 900°C and cooled down inside the furnace for further re-curing.

The compressive strength tests were conducted following ASTM C109/C109M-11 [22]. The hydraulic compression machine had a capacity of 3,000 kN. A constant loading rate of 100 kN/min was adopted and the maximum force was recorded automatically. At least three samples were tested for each mix design.

The microstructure of UHPC samples was observed. The samples were cut from the 50 mm cube specimens by a diamond saw to about $8\times8\times3$ mm^3. Samples were oven-dried at 105°C for 24 hours to remove evaporable water. Finally, all samples were coated with platinum for 45 s under vacuum. The SEM examinations were performed using a field emission scanning electron microscope (FESEM, JSM-7600F, JEOL) to detect micro-structural changes.

3 RESULTS AND DISCUSSIONS

3.1 Temperature history during cooling

Temperature history at the center and on the surface of the UHPC sample is shown in Fig. 30. As can be seen in Fig. 30a, for furnace cooling (F), the cooling rate is very slow and temperature difference between the surface and the center of the specimen was very small (less than 5°C). Water quenching (W), however, significantly increases cooling rate of the specimen and significant temperature difference between the surface and the center of the specimen can be observed. As can be seen in Fig. 30b, the largest temperature differences between the surface and the center of the specimens were 191.4°C, 481.1°C and 693.8°C for specimens heated to 300°C, 600°C, and 900°C, respectively.
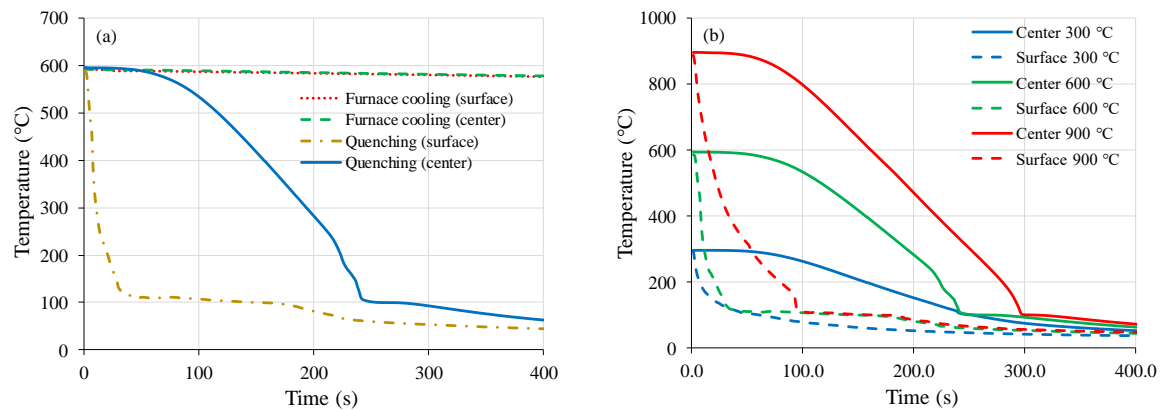
Fig. 30. Temperature history at the center and on the surface of UHPC specimen by means of (a) water quenching and slow cooling in furnace (specimens heated to 600°C) (b) water quenching (specimens heated to different exposure temperatures).

3.2 Compressive strength

Fig. 31 shows the residual compressive strengths of UHPC mix with different exposure temperatures subjected to furnace cooling (F) or water quenching (W). At ambient temperature, the compressive strength was 138.3 MPa. Residual strength of UHPC exposed to 300°C after furnace cooling increased significantly to 185.7 MPa. The increased mechanical properties are probably due to the combined effects of an enhanced cement hydration and to a contribution from the reactions of the pozzolanic materials [23]. Khoury

[24] assumes that removing of water in concrete at high temperature causes loss of bond water in silanols groups, which induces shorter and stronger siloxane elements (Si–O–Si) with probably larger surface energies. In the presence of silica fume at temperatures above 100°C, a pozzolanic reaction takes place, the formation of both tobermorite and xonolite is associated with a favorable development of strength [25, 26]. For specimens exposed to 300°C and water quenching, compressive strength of all UHPCs reduced significantly to 137.1 MPa.

After exposed to 600°C, the compressive strength decreased to 127.6 MPa, which are lower than the strength before high temperature exposure. Water quenching made the strength even lower to 91.5 MPa. After exposure to 900°C and furnace cooling, compressive strength further decreased to 51.1 MPa, which is only 36.9% of their strength before heating. After water quenching, the strong thermal shock decreased the strength to only 43.6 MPa. As can be seen, water quenching (legend with "W") significantly lowers the residual compressive strength of UHPC. This reduction of strength can be attributed to the formation of microcracks as a result of large thermal gradients within the UHPC samples as shown in *Fig. 1*.
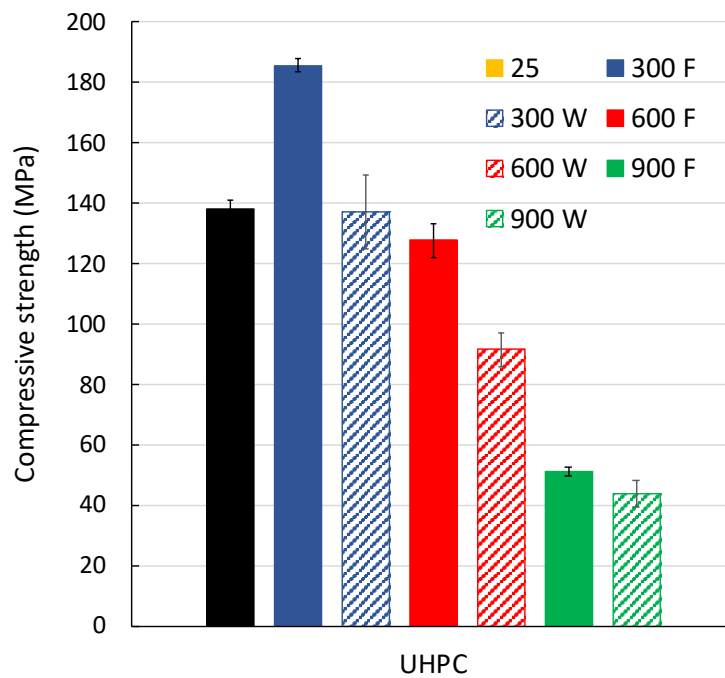
Fig. 31. Compressive strengths of UHPC mixtures after heat exposure and water quenching.

3.3 Change of microstructure

The FESEM images of UHPC samples before high temperature exposure are shown in *Fig. 32*. As can be see, before exposure to elevated temperatures, the UHPC sample showed dense and compact microstructure. Fine microcracks due to expansion of unhydrated clinker and shrinkage of cement paste during drying at 105°C can be observed [27].
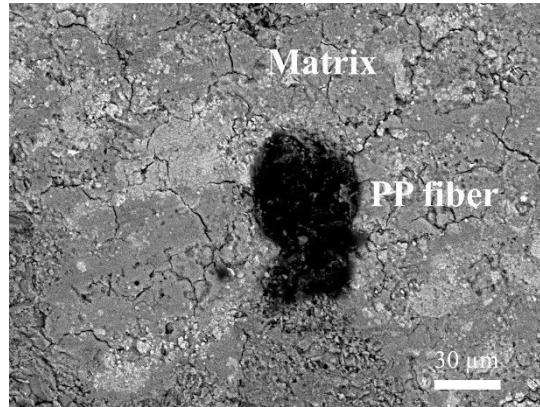
Fig. 32. The SEM images of UHPC before high temperature exposure.

Fig. 33 presents the UHPC after 300, 600, and 900°C heating with different cooling methods. As can be seen from Fig. 33a, at 300°C the matrix of UHPC samples maintained a dense microstructure. But the PP fibers melted and left empty fiber channels. Expansion of PP fibers at high temperature induced thin microcracks in the radial direction of fiber channels [28]. There is a large amount of unhydrated cement in the UHPC matrix due to the very low water-to-cement ratio [1, 4, 29]. Thus, the increased compressive strength is likely attributed to the enhanced UHPC matrix by further hydration of unhydrated cement clinkers as a result of increased pozzolanic reaction of silica fume.

From Fig. 33b, the microcracks after water quenching seemed to be wider. This was caused by the thermal shock from water quenching and it accounted for the significantly lower strength of water quenched samples. From Fig. 30, temperature difference between the surface and the center of the sample was 191.4°C during water quenching.
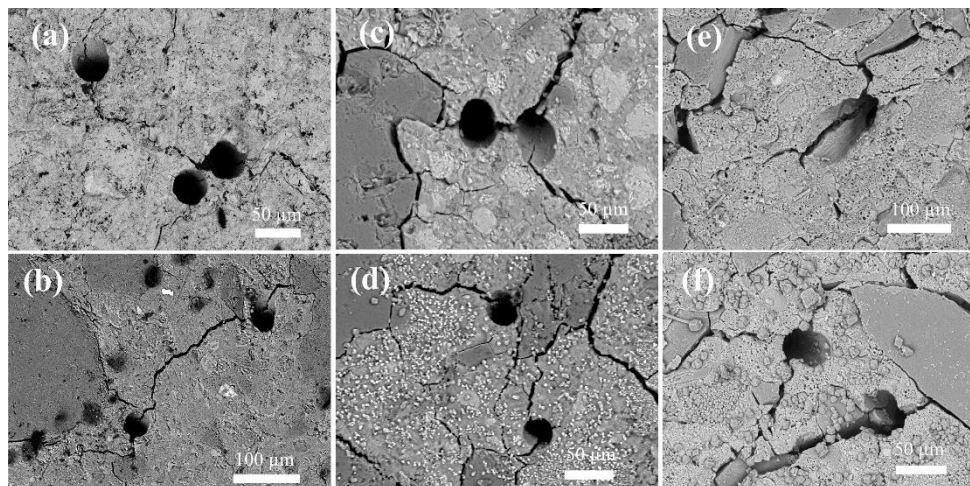
Fig. 33. The SEM images of UHPC samples after furnace cooling and water quenching at elevated temperature. (a/b) 300°C furnace cooling/water quenching (c/d) 600°C furnace cooling/water quenching (e/f) 900°C furnace cooling/water quenching

Fig. 33c shows the microstructure of UHPC samples after 600°C exposure. As can be seen, further increase of temperature up to 600°C resulted in formation of wider microcracks. It is believed that dehydration and recrystallization of C-S-H start from 450-500°C [27, 30], resulting in shrinkage of hydration products. Coarsening of pore structure may be another reason for significantly loss of strength at 600°C [31]. As shown in Fig. 30, the temperature difference reached 481.1°C between the surface and the center of UHPC specimen during

water quenching, which explains the decrease of strength after water quenching at 600°C *Fig. 33d.* After heated to 900°C, residual compressive strength of UHPC dropped to about 40 MPa. *Fig. 33e* and *f* illustrate the microstructure of UHPCs at this temperature level. As can be seen, all the main hydrated phase appeared loose and porous. The coarsening of pore structure is the main reason for the reduction of mechanical properties [32]. The C-S-H transformed to β-C_2S in the form of particles and then merged into large β-C_2S particles accompanied by larger volume change [30]. It seems that the deterioration of UHPC matrix dominated the decrease of compressive strength of the UHPC mixtures even after water quenching.

3.4 Effect of re-curing

Fig. 34 shows the effect of re-curing on compressive strength of UHPC and mortar samples. The legend shows information of re-curing duration and method. The first letter U stands for UHPC and M stands for Mortar. The follow number shows the number of days of re-curing. The last letter W means water re-curing and A means re-curing in air. It can be observed that for UHPC, neither air nor water re-curing increased compressive strength of UHPC after 28 days significantly. Water re-curing only recovered the strength of UHPC from 41.4 to 47.2 MPa. On the other hand, water re-curing increased strength of mortar significantly after 28 days. The strength of mortar increased from 13.8 to 46.0 MPa, which is near the strength of UHPC, even the strength of mortar was much lower than that of UHPC before and just after heat exposure. It is worth noting that, air re-curing did not help to recover strength of mortar significantly.

A possible explanation is that after 900°C heating, β-C_2S is one of the decomposition products of C-S-H at elevated temperatures[30]. Wollastonite can be formed when silica-bearing fluids are introduced into calcareous sediments during metamorphism, which is the environment inside UHPC with silica fume. However, the wollastonite is insoluble in water and the intrinsic reaction rate of β-C_2S with water is slow. It only has positive influence on strength of concrete at 5 to 10 years [33]. For mortar samples, dehydrated C–S–H, CaO, β-C_2S and noncrystal dehydrated phases might be the main compositions [34]. When contact with water, CaO and CH gradually form CH solution that can create the formation surrounding of other rehydration products. The new C–S–H gel reappears as a result of rehydration of dehydrated C–S–H. Rehydration of C–S–H can fill micro pores and help to heal and recover strength [17].
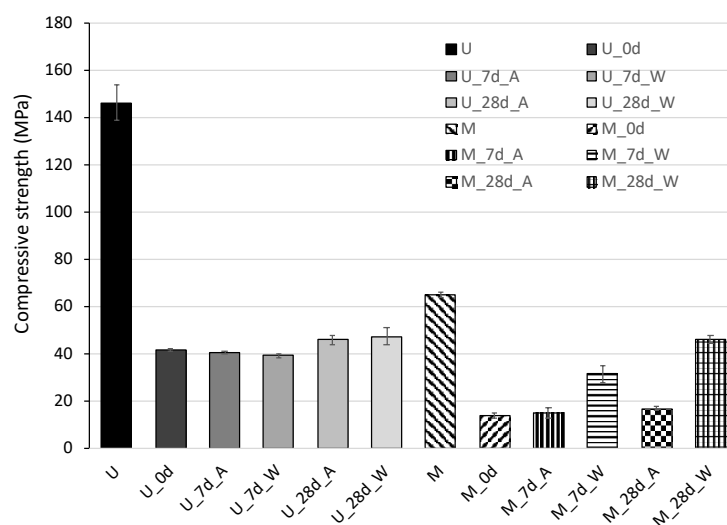
Fig. 34. Compressive strengths of UHPC and mortar after re-curing.

4   CONCLUSIONS

- At 300°C, the residual strength of UHPC mixtures increased significantly, which was attributed to hydration of unhydrated cement clinkers and accelerated pozzolanic reaction.
- Due to decomposition of cementitious compound and widened microcracks, a sharp loss of compressive strength was observed after 600°C exposure.
- At 900°C, the UHPC paste appeared as very loose and porous formations and the residual compressive strength was only about 37% of that at the ambient temperature.
- Water quenching reduced the compressive strength of the UHPC significantly.
- Strength of UHPC cannot be recovered by either water or air re-curing. But water re-curing can help to recover strength of mortar.

This study is a preliminary work for evaluation of concrete structural resistance after fire. More information is still needed from the concrete in real situations experienced different sizes and temperature distributions.

ACKNOWLEDGMENT

REFERENCES

[1] R. Yu, P. Spiesz, H.J.H. Brouwers, Mix design and properties assessment of Ultra-High Performance Fibre Reinforced Concrete (UHPFRC), Cement and Concrete Research 56 (2014) 29-39.
[2] D.-Y. Yoo, S. Kim, G.-J. Park, J.-J. Park, S.-W. Kim, Effects of fiber shape, aspect ratio, and volume fraction on flexural behavior of ultra-high-performance fiber-reinforced cement composites, Composite Structures (2017).
[3] D. Wang, C. Shi, Z. Wu, J. Xiao, Z. Huang, Z. Fang, A review on ultra high performance concrete: Part II. Hydration, microstructure and properties, Construction and Building Materials 96 (2015) 368-377.
[4] C. Shi, Z. Wu, J. Xiao, D. Wang, Z. Huang, Z. Fang, A review on ultra high performance concrete: Part I. Raw materials and mixture design, Construction and Building Materials 101 (2015) 741-751.
[5] D.J. Kim, S.H. Park, G.S. Ryu, K.T. Koh, Comparative flexural behavior of Hybrid Ultra High Performance Fiber Reinforced Concrete with different macro fibers, Construction and Building Materials 25(11) (2011) 4144-4045.
[6] S. Yang, S. Millard, M. Soutsos, S. Barnett, T. Le, Influence of aggregate and curing regime on the mechanical properties of ultra-high performance fibre reinforced concrete (UHPFRC), Construction and Building Materials 23(6) (2009) 2291-2298.
[7] C.M. Tam, V.W.Y. Tam, K.M. Ng, Assessing drying shrinkage and water permeability of reactive powder concrete produced in Hong Kong, Construction and Building Materials 26(1) (2012) 79-89.
[8] L. Wan, R. Wendner, B. Liang, G. Cusatis, Analysis of the behavior of ultra high performance concrete at early age, Cement and Concrete Composites (2016).
[9] M. Schmidt, E. Fehling, Ultra-high-performance concrete: research, development and application in Europe, ACI Special publication 228 (2005) 51-78.
[10] J. Resplendino, First recommendations for ultra-high-performance concretes and examples of application, International Symposium on Ultra High Performance Concrete, 2004, pp. 79-90.
[11] P. Buitelaar, Heavy reinforced ultra high performance concrete, Proceedings of the Int. Symp. on UHPC, Kassel, Germany, 2004, pp. 25-35.
[12] E. Denarié, E. Brühwiler, Structural rehabilitations with ultra high performance fibre reinforced concretes, international journal for restoration of buildings and monuments 12(MCS-ARTICLE-2007-011) (2006) 453-465.

[13] X. Luo, W. Sun, S.Y.N. Chan, Effect of heating and cooling regimes on residual strength and microstructure of normal strength and high-performance concrete, Cement and Concrete Research 30(3) (2000) 379-383.

[14] A.A. Awal, I. Shehu, M. Ismail, Effect of cooling regime on the residual performance of high-volume palm oil fuel ash concrete exposed to high temperatures, Construction and Building Materials 98 (2015) 875-883.

[15] T. Gupta, S. Siddique, R.K. Sharma, S. Chaudhary, Effect of elevated temperature and cooling regimes on mechanical and durability properties of concrete containing waste rubber fiber, Construction and Building Materials 137 (2017) 35-45.

[16] M.B. Karakoç, Effect of cooling regimes on compressive strength of concrete with lightweight aggregate exposed to high temperature, Construction and Building Materials 41 (2013) 21-25.

[17] W.-M. Lin, T. Lin, L. Powers-Couche, Microstructures of fire-damaged concrete, ACI Materials Journal 93(3) (1996).

[18] Y. Lin, C. Hsiao, H. Yang, Y.-F. Lin, The effect of post-fire-curing on strength–velocity relationship for nondestructive assessment of fire-damaged concrete strength, Fire Safety Journal 46(4) (2011) 178-185.

[19] C.-S. Poon, S. Azhar, M. Anson, Y.-L. Wong, Strength and durability recovery of fire-damaged concrete after post-fire-curing, Cement and concrete research 31(9) (2001) 1307-1318.

[20] S.-J. Park, H.J. Yim, H.-G. Kwak, Effects of post-fire curing conditions on the restoration of material properties of fire-damaged concrete, Construction and Building Materials 99 (2015) 90-98.

[21] A.H. Akca, N. Özyurt, Effects of re-curing on residual mechanical properties of concrete after high temperature exposure, Construction and Building Materials 159 (2018) 540-552.

[22] A.S.T. Mater., ASTM C 109/C 109 M-11, Standard Test Method for Compressive Strength of Hydraulic Cement Mortars (Using 2-in. or 50-mm Cube Specimens), 2011.

[23] H. Yazıcı, E. Deniz, B. Baradan, The effect of autoclave pressure, temperature and duration time on mechanical properties of reactive powder concrete, Construction and Building Materials 42 (2013) 53-63.

[24] G. Khoury, Compressive strength of concrete at high temperatures: a reassessment, Magazine of concrete Research 44(161) (1992) 291-309.

[25] H. Yazıcı, M.Y. Yardımcı, S. Aydın, A.Ş. Karabulut, Mechanical properties of reactive powder concrete containing mineral admixtures under different curing regimes, Construction and Building Materials 23(3) (2009) 1223-1231.

[26] I. Odler, Hydration, setting and hardening of Portland cement, Lea's chemistry of cement and concrete (1998).

[27] J. Piasta, Heat deformations of cement paste phases and the microstructure of cement paste, Materials and Structures 17(6) (1984) 404-420.

[28] G.A. Khoury, B. Willoughby, Polypropylene fibres in heated concrete. Part 1: Molecular structure and materials behaviour, Magazine of Concrete Research 60(2) (2008) 125-136.

[29] C. Wang, C. Yang, F. Liu, C. Wan, X. Pu, Preparation of Ultra-High Performance Concrete with common technology and materials, Cement and Concrete Composites 34(4) (2012) 538-544.

[30] Q. Zhang, G. Ye, E. Koenders, Investigation of the structure of heated Portland cement paste by using various techniques, Construction and Building Materials 38 (2013) 1040-1050.

[31] C.-S. Poon, S. Azhar, M. Anson, Y.-L. Wong, Comparison of the strength and durability performance of normal-and high-strength pozzolanic concretes at elevated temperatures, Cement and Concrete Research 31(9) (2001) 1291-1300.

[32] Q. Ma, R. Guo, Z. Zhao, Z. Lin, K. He, Mechanical properties of concrete at high temperature—A review, Construction and Building Materials 93 (2015) 371-383.

[33] A.M. Neville, Properties of concrete, Longman London1995.

[34] Z. Shui, D. Xuan, H. Wan, B. Cao, Rehydration reactivity of recycled mortar from concrete waste experienced to thermal treatment, Construction and Building Materials 22(8) (2008) 1723-1729.

NUMERICAL MODEL FOR CFRP-STRENGTHENED RC BEAMS SUBJECTED TO FIRE

[1]Thiago B. Carlos, [1]João Paulo Rodrigues, [2]Dhionis Dhima, [3]Rogério A. de Lima
[1]Coimbra University, Portugal
[2]CSTB, France
[3]Federal University of Santa Maria, Brazil

ABSTRACT

The aim of this paper is to present an accurate 3D Finite Element (FE) model capable of simulating the CFRP-strengthened concrete beam's flexural behaviour at ambient temperature and under fire conditions, especially its interaction with the different surrounding elements. In order to achieve the goals, several amounts of thermal and mechanical numerical simulations have been performed to validate the already developed FE models. Experimental results reported in two parallel studies by Carlos et al. and by Carlos and Rodrigues [1,2] were used to FE model's validation. The numerical model has been satisfactorily validated and the results had a good predictability with the experimental results in terms of thermal and mechanical behaviour.

Keywords: fire, concrete, beams, CFRP strengthened, numerical simulation

1   INTRODUCTION

The temperature variation significantly affects the mechanical performance of the Carbon Fibre Reinforced Polymer (CFRP) strengthening system on concrete structures. Thus, the knowledge of the temperature effects is a key factor in the fire design of this type of construction, especially as it develops at the CFRP-concrete bond which is a critical zone very sensitive to thermal exposure. This better understanding makes possible a reliable and safe design in case of fire. In order to contribute to this end, few numerical investigations concerning the fire behaviour of CFRP-strengthened reinforced concrete (RC) members have been carried out over the last years [3–7]. However, most of them did not measure the thermal influence due to the interactions with the surrounding building elements or simply did not have a good agreement with the existing experiments. Furthermore, only a few authors have considered the CFRP-concrete interface's thermal degradation and have used 3D models that are theoretically more realistic. The literature shows that the numerical efforts to simulate the fire behaviour of CFRP-strengthened concrete beams are still very limited. Moreover, numerical results have shown that accurate predictions of the fire response of CFRP-strengthened beams require the inclusion of explicit temperature-dependent bond-slip models for the CFRP-concrete interface, which has been neglected in most of these studies. The reason for that is the lack of experimental data available in this respect (that are sometimes contradictory), making it difficult to validate more accurate models to better simulate the behaviour of CFRP-strengthened RC beams subjected to fire. In this regard, the present research intends to be an important contribution for the validation of an accurate model capable to simulate the fire behaviour of CFRP-strengthened concrete beams, as well as evaluate different parameters not experimentally tested yet. Therefore, this research becomes essential to bring a deep/better understanding and fill the gaps on the fire behaviour of this type of composite structures, also contributing to further researches.

2   NUMERICAL INVESTIGATION

2.1 Model geometry

The FE models' geometry consisted of a replication of the ones that composes the beams tested in the experimental investigation by Carlos et al. [1], as well as for the other elements and materials involved. Three-dimensional FE models of simply supported RC beams flexurally strengthened with EBR-CFRP laminates (*Fig. 1a*) were modelled using the commercial software package Abaqus to simulate the mechanical response at ambient and elevated temperatures. In addition, 3D models of unstrengthened beams were also developed for the mechanical analysis (*Fig. 1b*).

MODEL ELEMENTS:
- concrete beam
- steel reinforcement
- CFRP laminate
- steel supports and loading points

a)

MODEL ELEMENTS:
- concrete beam
- steel reinforcement
- steel supports and loading points

b)
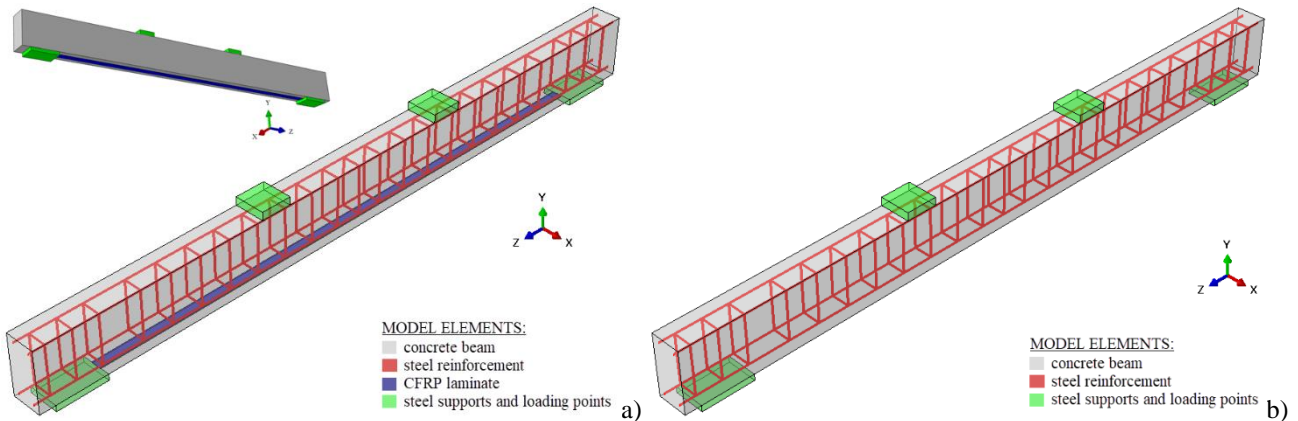
Fig. 1. 3D numerical models of the a) CFRP-strengthened and b) unstrengthened beams for mechanical analysis

Two-dimensional (2D) FE models for both type of beams were also developed exclusively for the heat transfer analysis since this is a type of uncoupled analysis. The 2D models were developed based on the tested cross-sections of the beams, including the modelling of the concrete slab cross-section in order to simulate the thermal interactions between the elements, as intended in the experimental study [1]. The use of three different fire protection materials, the ones previously fire tested in the CFRP-strengthened beams by Carlos et al. [1], were also numerically investigated in terms of thermal response. Four representative heat transfer models (*Figs. 2a-d*) were numerically simulated under fire conditions. The nomenclature adopted for the 2D FE models of the beams is analogous to the ones experimentally tested specimens [1]. The unstrengthened and unprotected RC beam is referred by RC. The three CFRP-strengthened RC beams fire protected with expanded clay, ordinary Portland and vermiculite-perlite mortar are referred by EC-35, OP-35 and VP-35, respectively. The thickness (*t*) of the fire protection systems was 35mm.
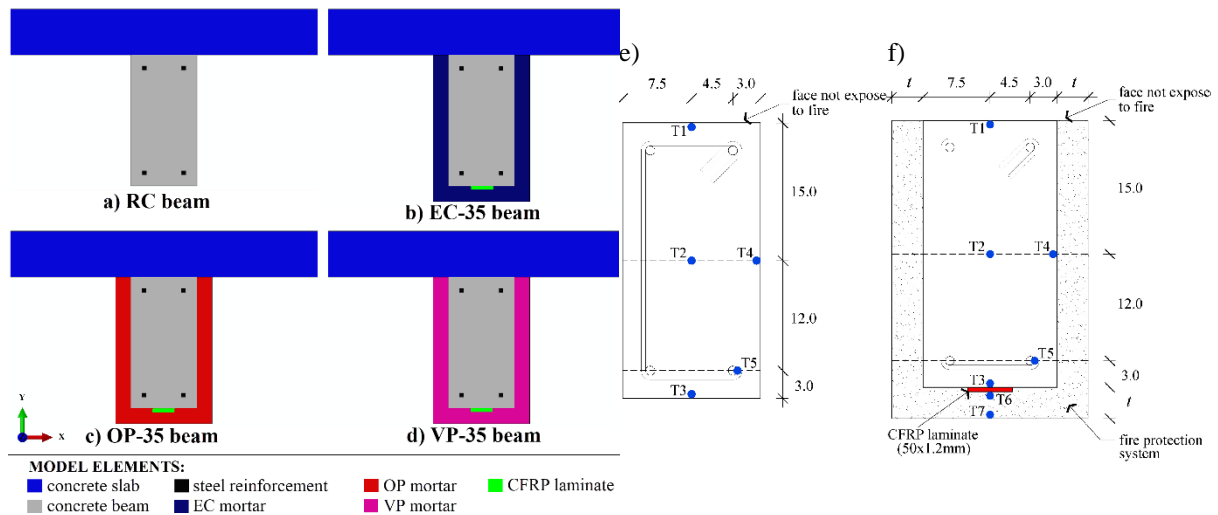
Fig. 2. Numerical models for heat transfer analysis: a) RC, b) EC-35, c) OP-35 and d) VP-35 beam; Location and nomenclature of thermocouples at mid-span cross-section of e) unstrengthened and f) CFRP-strengthened [1]

The predicted results of these simulations were compared with the experimental data obtained by Carlos et al. [1] in terms of temperatures vs. time of fire exposure at different locations of the mid-span cross-section. To allow comparison between results, the same thermocouples arrangement used in the previous experimental study [1] was defined in the current heat transfer analysis, as shown in *Fig. 2e* and *2f* for the unstrengthened and CFRP-strengthened beams, respectively.

2.2 Material modelling and analysis criteria

The specimens were modelled using the material non-linearity according the isotropic hardening method and, especially for the concrete material, based on the fracture energy cracking criteria. The thermophysical temperature-dependent properties of the materials used in the FE models, such as specific heat, thermal conductivity, density, emissivity and convection, were modelled based on the literature [8–11] and standardization [12–14]. The variation of the mechanical properties of the concrete and steel reinforcement at elevated temperatures were defined based on the reduction factors suggested in EN-1992-1-2 [12] and EN 1994-1-2 [15]. The temperature-dependent mechanical properties of the CFRP was based on the relations proposed by Wang et al. [16] and Bisby [17] for the tensile strength and modulus of elasticity, respectively. The variation of the CFRP-concrete bond mechanical properties at elevated temperatures was based on the temperature-dependent results obtained from the Single-lap Shear Tests (SST) carried out by Carlos and Rodrigues [2].

2.3 Boundary, loading and contact conditions

In order to reproduce the real test set-up as reported by Carlos et al. [1], the supports of the beam and the loading were also modelled in the numerical models on rigid plates attached to the beams so as to distribute possible concentrated forces on them, as shown in *Fig 3a*. The models were subjected to a fixed mechanical load applied to the direction -Y in a four-point bending configuration (see *Fig 3a*) as used in the experimental tests [1]. The preload applied in the simulations (24 kN) correspond to 70% of the design value of the loadbearing capacity of the RC beam at ambient temperature, as defined in the experimental test procedure [1]. Regarding the support system, all degrees of freedom of the nodes located on the bottom surface and at the middle of the respective rigid plate were constrained to simulate the pinned support, whereas for the roller support only the translations in the directions X and Y were constrained. In addition, all nodes located at each end of both supports were constrained to

translations in the direction X in order to prevent their lateral deformation (*Fig 3a*). The surface-to-surface contact method was used to simulate the contact between the concrete beam and the other materials (*Fig 3b*). Small-sliding formulation was used in the contact tracking algorithm between the beams and the CFRP laminates. In this case, the geometric nonlinearity is included in the model. A penalty method (damage) was defined as the cohesive contact property between the concrete and CFRP surfaces. Thus, two bond damage criteria were adopted: maximum nominal stress and fracture energy. These values (temperature-dependent) were inputted in the FE model based on the experimental data obtained from the SST tests performed by Carlos and Rodrigues [2].
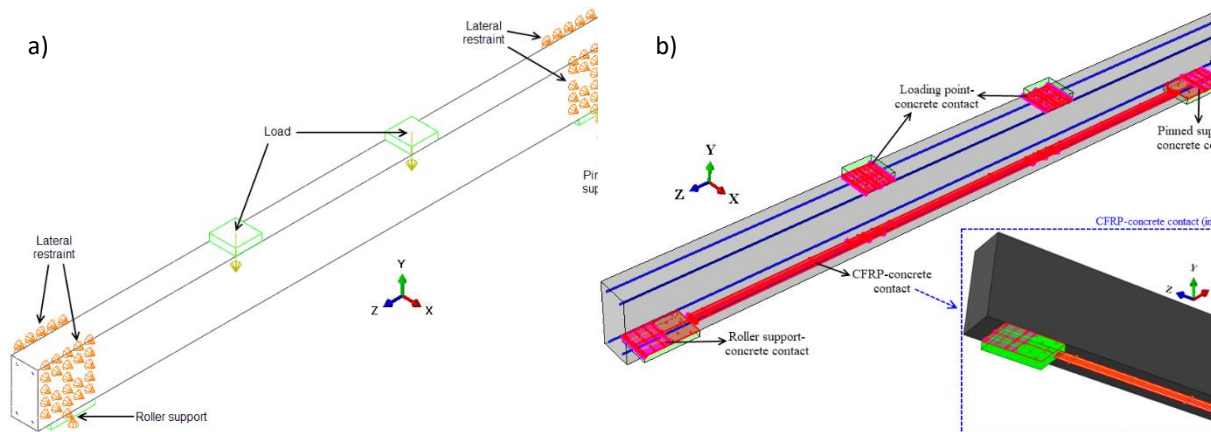
Fig 3. a) boundary and loading conditions and b) contact conditions of 3D numerical models used in the FE analysis

Finally, the fire action was applied in the 3D model. The heat transfer step was applied after the preloading of the model and performed according to the furnace temperatures registered in the experimental tests in order to validate the FE model. In these simulations, a 4-node linear heat transfer quadrilateral element (DC2D4) was chosen and a 2D numerical model (see *Fig. 2a-d*) was developed to estimate the temperature distribution in the cross-sections of the beams. In order to accurately simulate the experimental test conditions [1], the bottom and lateral surface of the models of the beams were directly exposed to the heating. The upper face of the beam in the model was superposed by a surrounding concrete slab which in turn was submitted to a constant ambient temperature, as adopted in the experimental tests [1]. The initial temperatures of the models were defined based on the measurements recorded in the experimental tests [1]. Radiation and convection heat transfer modes were considered on exposed surfaces. The resultant emissivity was taken as 0.49, considering the emissivity coefficients of the electric resistance of the furnace and the beams both equal to 0.7. A convection coefficient of 15 W/m^2 °C (constant with temperature) was adopted, as suggested in EN-1992-1-2 [12].

3 VALIDATION OF THE FINITE ELEMENT MODEL

3.1 Mechanical response at ambient temperature

Numerical simulations on an unstrengthened and EBR-CFRP-strengthened beam (referred as RC_AT and CFRP_AT, respectively) were performed to assess the ability and accuracy of the 3D FE models described above in predicting the mechanical response of these beams. The results of experimental tests reported in a relevant parallel study by Carlos et al. [1] were used to FE model's validation. *Fig. 4* shows a comparison of the load vs. vertical mid-span displacement curves for the unstrengthened and CFRP-strengthened RC beams obtained from the experimental tests (Exp.) [1] and FEA (Num.).
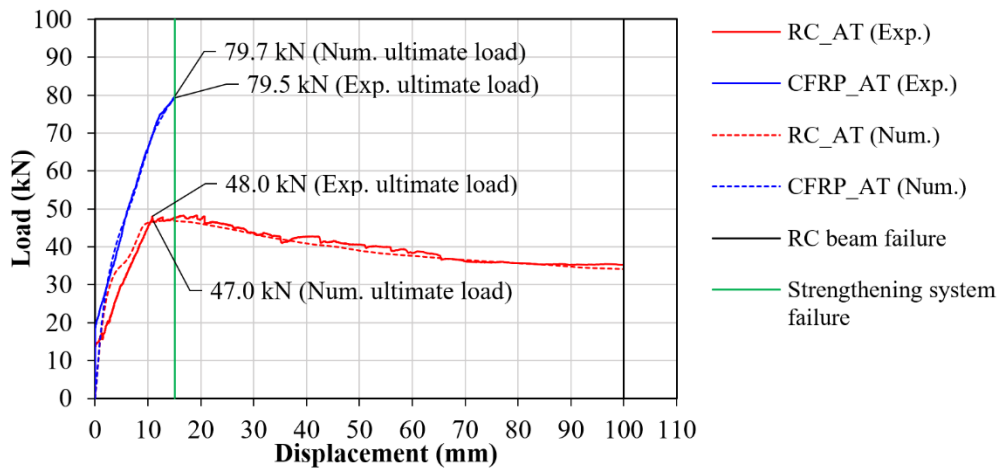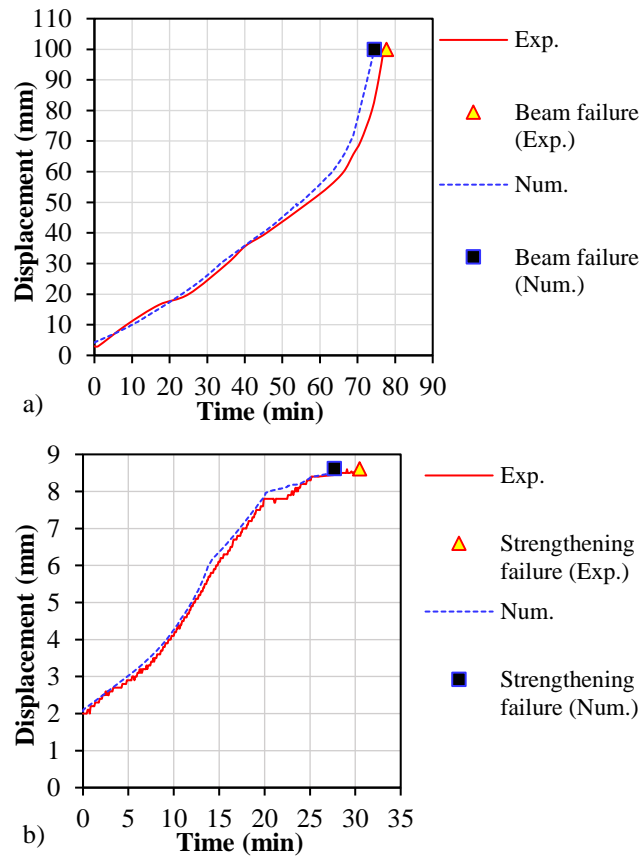
Fig. 4. Experimental (Exp.) [1] and predicted (Num.) load vs. mid-span displacement curves for the unstrengthened and CFRP-strengthened RC beams at ambient temperature

Fig. 4 reveals that all predicted results generally fit closely with the experimental curves for both specimens, especially for obtained peak loads (ultimate load). The ultimate predicted load of the RC_AT and CFRP_AT beams was 47.0 kN and 79.7 kN, respectively. The ultimate load experimentally obtained for the unstrengthened and CFRP-strengthened beams was 48.0 and 79.5, respectively. These results were very similar to those obtained numerically for both specimens. Therefore, the values of the predicted-to-experimental loading capacity ratios (P_{NUM} / P_{EXP}) for the RC_AT and CFRP_AT beams corresponds to 0.98 and 1.00, respectively. Finally, an excellent agreement and accuracy between the experimental and numerical results was noticed, ensuring a strong validity of the developed FE model in predicting the mechanical response of both RC beam strengthened with EBR-CFRP laminate and unstrengthened RC beam at ambient temperature.

3.2 Mechanical response under fire conditions

The experimental results from fire resistance tests carried out by Carlos et al. [1] on the CFRP-strengthened beam EC-35 were used to validate the mechanical response of the 3D numerical model under fire conditions (see *Fig. 5b*). Furthermore, for the mechanical validation of the FE model that represents the RC beam subjected to fire (see *Fig. 5a*), the experimental data from the unstrengthened specimen (RC) [1] were assigned for comparative purposes. The comparison of the displacement-temperature curves of the simply supported RC beam and CFRP-strengthened beams from the experimental tests and FEA are presented in *Figs. 5a* and *Fig. 5b*, respectively. The results are presented in terms of ultimate failure for the RC beam and strengthening debonding for CFRP-strengthened beam. The mechanical results developed after the strengthening system debonding (ultimate failure of the strengthened beam) is not presented, since it is not relevant to bond analysis.

Fig. 5. Experimental (Exp.) [1] and predicted (Num.) displacement-temperature curves for the a) unstrengthened and b) CFRP-strengthened RC beams, in terms of ultimate beam failure and strengthening system debonding, respectively

Similar tendencies with an equivalent slope were obtained from the FEA in comparison with the experimental results [1] for both RC beam and CFRP-strengthening system (specimens RC and EC-35, respectively). The experimental curves presented a slightly higher stiffness than the numerical ones, indicating that the respective predicted data is on the safe side. A good agreement between the FEA and experimental [1] analysis in terms of critical fire resistance time for the RC beam (FR_{time}) was obtained, as shown in *Table 1*. The failure instant of this beam was experimentally achieved at 78.2 min of fire exposure, while for the numerical model a fit close and slight conservative time of 74.5 min was noticed. In the case of strengthened beam, a satisfactory convergence of results between the models was also obtained. The fire resistance time at the CFRP debonding instant ($FR_{time,CFRP}$) for the strengthened beam was quite similar for both experimental and numerical models, corresponding to 30.5 and 27.7 min, respectively, as showed in *Table 1*. Therefore, the results showed that the differences between experimental and numerical fire resistance times were less than 5% and 10%, respectively for unstrengthened RC beam and CFRP-strengthening system (*Table 1*). In addition, a relationship between the FR_{time} or $FR_{time,CFRP}$ at different displacements obtained by the numerical and experimental analysis for both type of beams was also presented in *Table 1*.

Table 1. Experimental (Exp.) [1] and numerical (Num.) fire resistance time at different displacements of unstrengthened beam and CFRP-strengthening system

	FR_{time} at 50 mm displacement (min)		FR_{time} at 75 mm displacement (min)		FR_{time} at beam failure instant (min)		FR_{time} ratio at failure instant of the beam
unstrengthened RC beam	Exp. [1]	Num.	Exp. [1]	Num.	Exp. [1]	Num.	
	57.0	54.9	72.3	69.5	78.2	74.5	0.95

	$FR_{time,CFRP}$ at 5 mm displacement (min)		$FR_{time,CFRP}$ at 8 mm displacement (min)		$FR_{time,CFRP}$ at CFRP failure instant (min)		$FR_{time,CFRP}$ ratio at failure instant of the CFRP system
CFRP-strengthening system	Exp. [1]	Num.	Exp. [1]	Num.	Exp. [1]	Num.	
	12.2	11.8	23.0	20.1	30.5	27.7	0.91

Notwithstanding the slight differences abovementioned, the models presented general good agreement and accuracy between the experimental and numerical results of the RC beam and CFRP-strengthening system. All these results indicate that the estimated data is generally on the safe side but not too conservative, though. The satisfactory agreement and accuracy between the experimental and numerical results confirm the validity of the developed FE models and attest to their ability to simulate the mechanical response of simply supported RC and CFRP-strengthened beams under fire conditions.

3.3 Heat transfer analysis

The suitability of 2D thermal models developed using the heat transfer option available in Abaqus was assessed in this section. The purpose of this numerical approach was to determine the appropriate modelling parameters, in particular, especially the input thermal boundary conditions and material thermal properties, so that standard fire resistances tests of unstrengthened and CFRP-strengthened RC beams can be simulated. It should be also noted that an uniform temperature along the entire longitudinal length of the beam was intended for the validation study, in contrast to the recorded at the mid-spam cross-section of beams tested in Laboratory [1]. Moreover, in order to calibrate the FE model for fire simulation of CFRP-strengthened RC beams, the furnace fire curve data registered from the fire resistance tests [1] were used. Note that the emissivity, the heat transfers and the thermal contact conductance coefficients were constant with temperature evolution. The radiative heat flux was calculated as 0.49 using an emissivity of 0.7 for fire and 0.7 for the concrete surface. The Stefan-Boltzmann constant was defined as 5.67×10^{-8} W/m^{2}K^4.

Figs. 6b, 6c and 6d shows respectively the comparison between experimental (Exp.) [1] and predicted (Num.) temperatures as a function of fire exposure time for the different thermocouples at mid-span (cf. *Fig. 2f*) of the CFRP-strengthened beams fire-protected by 35 mm thick of VP, OP and EC mortar (referred as EC-35, OP-35 and VP-35, respectively). The temperature vs. fire exposure time evolution for the different thermocouples (cf. *Fig. 2e*) of the unstrengthened and unprotected RC beam (referred as RC) is shown in *Fig. 6a*. It is worthwhile mentioning that the temperature evolution in the CFRP-strengthened RC beams was presented in *Figs. 6b-d* only until the collapse instant of the respective fire protection material reported in the experimental data [1], since the results after that time are negligible for the purpose of this numerical study. Regarding the RC beam, the results were plotted in *Fig. 6a* until the collapse of the beam.
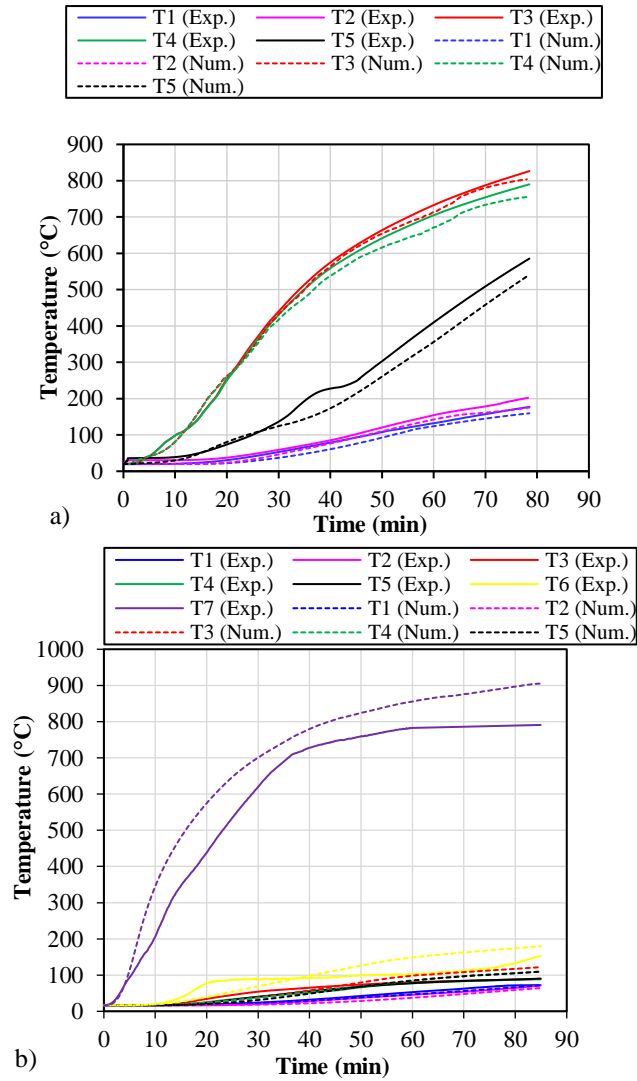
Fig. 6. Experimental (Exp.) [1] and predicted (Num.) temperatures vs. fire exposure time curves at different points of the mid-span cross-section for the beams: a) RC, b) VP-35, c) OP-35 and d) EC-35
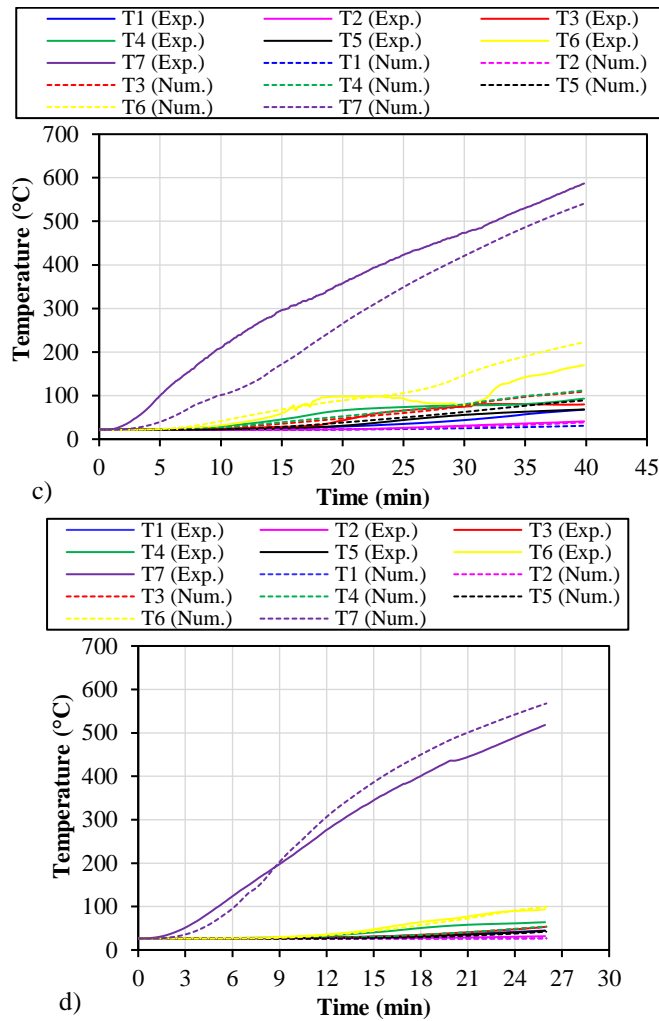
Fig. 6. Experimental (Exp.) [1] and predicted (Num.) temperatures vs. fire exposure time curves at different points of the mid-span cross-section for the beams: a) RC, b) VP-35, c) OP-35 and d) EC-35 (continuation)

Overall, all FE models provided a good agreement with the experimental results in terms of temperatures evolution, as noticed in the *Figs. 6a-d*. With exception of thermocouples T6 and T7 (positioned on the bottom surfaces of the laminate and the fire protection material, respectively) for the strengthened beams protected by OP and VP mortar, all other temperature distribution at different points of the cross-section were accurately predicted by the models. Small deviations between Exp. and Num. temperatures in T6 and T7 of the VP-35 and OP-35 beams were observed, as depicted in *Figs. 6b and 6c*, respectively. In spite of that, the FE models were still able to simulate the thermal behaviour tendency with a relative consistency in the above-mentioned thermocouples. Concerning the strengthened EC-35 and RC beams (*Figs. 6a* and *6d*, respectively), the numerical results by the heat transfer analysis presented an excellent convergence with the experimental measurements for all thermocouples. To sum up, the tools of Abaqus program for the application of thermal actions allowed simulating the phenomenon of heat transfer between hot air and composite structural elements with satisfactory results. Despite the above-mentioned deviations, all models overall provided a good estimate between the experimental and numerical results, confirming the ability of the FE models to accurately simulate the thermal response of unstrengthened and EBR-CFRP-strengthened RC beams subjected to fire, even when using complex and different fire protection materials.

4   CONCLUSIONS

Based on results obtained from the numerical study, the following conclusions may be drawn:

−   The thermal response of the fire-protected CFRP-strengthened RC beams subjected to fire was accurately predicted by the FE models, similarly to the heat transfer analysis of the unprotected and unstrengthened RC beam. Moreover, the modelling of the surrounding building slab allowed to represent the thermal interactions and influence between the elements as faithful as possible, providing a better predicting of the experimental results and, consequently, more realist.

−   Concerning the prediction of the mechanical response at ambient temperature, the 3D models presented a satisfactory accuracy for both unstrengthened and CFRP-strengthened RC beams, especially for estimating the ultimate load capacity.

−   The developed FE models also estimate with precision the mechanical response of unstrengthened and CFRP-strengthened RC beams simultaneously subjected to a flexural load and high temperatures. An accuracy of about 91% and 95% was respectively achieved by the numerical models that represents the RC and CFRP-strengthened RC beams in terms of failure instant.

−   The FE models confirmed that the materials used as fire protection system contributing to the fire performance of the CFRP-strengthened RC beams, either by preservation of CFRP-concrete bond for longer exposure time or by keeping lower temperatures in the interior of the beams and steel reinforcement zones. As a result, it increased the mechanical effectiveness of the EBR-CFRP strengthening system, as proved in the simulations at high temperatures. Moreover, the fire behaviour of the fire protection materials was predicted with good accuracy by the 2D FE models.

−   Finally, the presented results confirmed the validity of the developed FE models and strongly guarantee an accurate prediction of the mechanical response of both strengthened and unstrengthened RC beams at ambient and high temperatures. They also confirmed the capacity of the models to estimate the thermal performance of these structures along with the use of different fire protection materials. Furthermore, it is still possible to stated that this developed FE models can be used as an auxiliary tool for the design of fire protection systems for CFRP-strengthened RC structural members or in parametric studies outside the bounds of experimental field, as well as to provide safe and economical structural solutions for these type of structures in fire situation.

ACKNOWLEDGMENTS

REFERENCES

[1]   Carlos TB, Rodrigues JPC, de Lima RCA, Dhima D. *Experimental analysis on flexural behaviour of RC beams strengthened with CFRP laminates and under fire conditions.* Compos Struct 2018;189:516–28. doi:10.1016/j.compstruct.2018.01.094.

[2]   Carlos TB, Rodrigues JPC. *Experimental bond behaviour of a CFRP strengthening system for concrete elements at elevated temperatures.* Constr Build Mater 2018;193:395–404. doi:10.1016/j.conbuildmat.2018.10.184.

[3]   Hawileh RA, Naser M, Zaidan W, Rasheed HA. *Modeling of insulated CFRP-strengthened reinforced concrete T-beam exposed to fire.* Eng Struct 2009;31:3072–9.

doi:10.1016/j.engstruct.2009.08.008.

[4] Ahmed A, Kodur VKR. *Effect of bond degradation on fire resistance of FRP-strengthened reinforced concrete beams.* Compos Part B Eng 2011;42:226–37. doi:10.1016/j.compositesb.2010.11.004.

[5] Dai JG, Gao WY, Teng JG. *Finite Element Modeling of Insulated FRP-strengthened RC Beams Exposed to Fire.* Civ Eng 2010. doi:10.1061/(ASCE)CC.1943-5614.0000509.

[6] Firmo JP, Arruda MRT, Correia JR. *Numerical simulation of the fire behaviour of thermally insulated reinforced concrete beams strengthened with EBR-CFRP strips.* Compos Struct 2015;126:360–70. doi:10.1016/j.compstruct.2015.02.084.

[7] Firmo JP, Arruda MRT, Correia JR, Rosa IC. *Three-dimensional finite element modelling of the fire behaviour of insulated RC beams strengthened with EBR and NSM CFRP strips.* Compos Struct 2018;183:124–36. doi:10.1016/j.compstruct.2017.01.082.

[8] Griffis CA, Masumura RA, Chang CI. T*hermal response of graphite epoxy composite subjected to rapid heating.* J Compos Mater 1981;15:427–42. doi:10.1177/002199838101500503.

[9] Firmo JP, Correia JR, França P. *Fire behaviour of reinforced concrete beams strengthened with CFRP laminates: Protection systems with insulation of the anchorage zones.* Compos Part B Eng 2012;43:1545–56. doi:10.1016/j.compositesb.2011.09.002.

[10] Bai Y, Keller T, Correia JR, Branco FA, Ferreira JG. *Fire protection systems for building floors made of pultruded GFRP profiles - Part 2: Modeling of thermomechanical responses.* Compos Part B Eng 2010;41:630–6. doi:10.1016/j.compositesb.2010.09.019.

[11] MAXIT International. *Thermal properties at high temperatures of clay concrete,* Internal Report. Denmark: 2005.

[12] EN 1992-1-2. *Eurocode 2: Design of concrete structures - Part 1-2: General rules - structural fire design.* vol. 2. Brussels, Belgium: European Committee for Standardization (CEN); 2004.

[13] Annexe Nationale à la NF EN 1992-1-2. *Eurocode 2: Calcul des structures en béton - Partie 1-2: Règles générales - Calcul du comportement au feu.* vol. 2. Saint-Denis, France: AFNOR; 2007.

[14] EN 1993-1-2. *Eurocode 3: Design of steel structures - Part 1-2: General rules - structural fire design.* vol. 2. Brussels, Belgium: European Committee for Standardization (CEN); 2010.

[15] EN 1994-1-2. *Eurocode 4: Design of composite steel and concrete structures - Part 1-2: General rules - structural fire design.* Brussels, Belgium: European Committee for Standardization (CEN); 2005.

[16] Wang K, Young B, Smith ST. *Mechanical properties of pultruded carbon fibre-reinforced polymer (CFRP) plates at elevated temperatures.* Eng Struct 2011;33:2154–61. doi:10.1016/j.engstruct.2011.03.006.

[17] Bisby LA. *Fire behaviour of FRP reinforced or confined concrete.* PhD thesis. Queen's University, 2003.

DEFINITION OF DAMAGE STATES FOR CONCRETE TUNNEL LININGS SUBJECTED TO FIRE ACTION

Donatella de Silva[1], Marco Andreini[2], Antonio Bilotta[1], Saverio La Mendola[2], Emidio Nigro[1]

[1] Department of Structures for Engineering and Architecture. University of Naples Federico II

[2] European Organization for Nuclear Research (CERN), Switzerland

ABSTRACT

The paper proposes the definition of the damage states for concrete tunnel linings, based on the analysis of the consequences of in 66 fire events really occurred. The most recurrent damage factors are considered, such as the presence of cracks, their extension and depth, the concrete spalling and the local or global collapse. Considerations on the definition of the related limit state functions are then given. A proposal to link such damage states to either the post-fire rehabilitation interventions and the performance levels is presented. Such performance levels can be adopted in the design and assessment of concrete linings toward the fire action in underground infrastructures such as railway and road tunnels or complex research infrastructures.

1 INTRODUCTION

In the last decade, the interest in tunnel fire safety has enhanced mainly for the relevance of the consequences tied to the unviability and the associated costs for the rehabilitation interventions.

To date, several contributions are available in the literature on the fluid-dynamic aspects, ignition phenomena, fire and smoke propagation, fuel and ventilation influence, human behaviour in case of fire evacuation, etc. [1].

Fire in tunnels may cause structural damage of concrete lining that may lead to loss of bearing capacity, causing long interruptions of service. The behavior of tunnel linings subjected to fire depends on several factors, such as the reduction of strength and stiffness of the structural material, load patterns, boundary conditions given by the interaction with the surrounding soil [2].

As the temperature increases, the thermal expansions of the lining produce an alteration to the stress field on the encasing soil, which determines variations of the internal forces in the lining. Hence, due to this mutual phenomenon, the lining may suffer significant variations of stress due to thermal expansion, reaching progressive damage levels, including the lining collapse wherever the fire is of a significant severity (*Fig. 1*).

Lai et al. [3] analysed the fire occurred in the New Qidaoliang Highway Tunnel, reporting the seriousness of the structural damages; starting from the colour of the concrete lining, they traced back to the maximum temperatures reached inside the tunnel. Furthermore, other researchers focused on the spalling phenomenon on concrete linings in the analysis of the tunnel damages following fire events [4]. During the past years, the interest of the scientific community has been oriented also in performing numerous full-scale tests to better understand the fire dynamics in tunnels [5][6].

However, in the international regulation and standard frameworks about fire safety of tunnels, most of the structural requirements are given without specifying the different damage levels of the tunnel lining in case of fire.

This paper proposes the definition of damage states that can be reached by the concrete lining during fires, starting from an analysis of the consequences of real fire events. In the following sections, some considerations on the limit state functions are also given and a proposal to link such damage states to either the post-fire rehabilitation interventions and the performance levels is shown.

Fig. 1. a) Sectionally collapsed ceiling in the Gotthard Tunnel after the fire of October 24, 2001; b) Burnt out lorry transporter in the Channel Tunnel between the UK and France (fire incident on Nov. 18, 1996).

2 FROM A DATABASE OF REAL FIRES IN TUNNEL TO THE DEFINITION OF DAMAGE STATES

Sixty-six fire events in railway or road tunnels [7][8][9] were collected in a database (*Table 1*). Each fire event has been analyzed focusing on the structural damages of the tunnel lining [9] [10] [11]. The subsequent rehabilitation interventions were proportional to the damages and limited in those few cases where passive or active fire protection systems were present [12][13][14]. Indeed, if fires are controlled in their early stages, the consequences can be generally reduced; the detrimental effects of fires become significantly greater and the ability to control them become significantly more difficult when fires become fully developed. Hence, the lining damage was negligible or significantly limited when the intervention of the fire fighters was immediate or in presence of active fire protection systems.

Considering the most common consequences on concrete elements exposed to fire and basing on the description of these fire events, we define the following five different damage states ds_i for the tunnel linings (*Fig. 2*):

- $ds0$ **(None):** No structural damage;
- $ds1$ **(Minor):** Localised and shallow cracks;
- $ds2$ **(Moderate):** Several cracks and localised spalling;
- $ds3$ **(Serious):** Wide and deep cracks, extensive spalling and local collapses;
- $ds4$ **(Collapse):** Lining collapse.

These damage states account for the many phenomena that fire may cause on the tunnel lining, such as the reduction of strength and stiffness of the structural material, cracks in the concrete lining, spalling of the concrete cover and, in some cases, the lining collapse. *Fig. 3*

illustrates the histogram of the frequencies of the different damage states shown in the database.

ds0   ds1   ds2   ds3   ds4

None   Minor   Moderate   Serious   Collapse
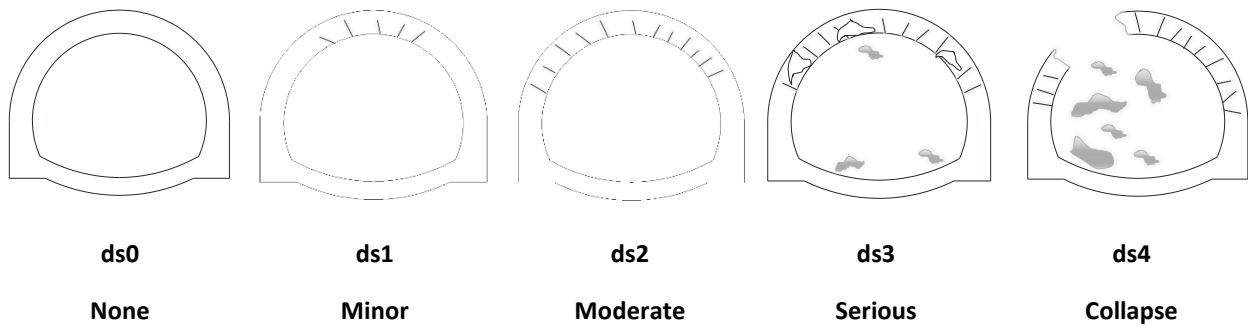
Fig. 2. Proposed Damage States.

Table 1. Analysed fire events in tunnels with observed damages.

Tunnel	Country	Year	Structural Damages
Gudvanga tunnel	Norway	2013	Minor
Oslofjord tunnel	Norway	2011	Moderate
Melburne	Australia	2007	None
Runehamar	Norway	2003	None
Floyfjell-Bergen	Norway	2003	Moderate
Mornay	France	2003	Minor
Daegu metro	South Korea	2003	Serious
Homer-Milford	New Zeland	2002	Minor
Williams tunnel	USA	2002	None
Motorway tunnel	France	2001	Moderate
Gleinalm	Austria	2001	Serious
Kaprun	Austria	2001	Minor
St Gotthard	Switzerland	2001	Collapse
Howard	USA	2001	Moderate
Shipol airport	Netherlands	2001	None
Honk Hong	Cina	2000	None

Definition of Damage States for Concrete Tunnel Linings Subjected to Fire Action

Oslofjord	Norway	2000	None
Toulon	France	2000	Minor
Saukopftunel	Germany	2000	Minor
Laerdal	Norway	2000	None
Seljestad	Norway	2000	Serious
Colli Berici	Italy	1999	None
Tauern	Austria	1999	Serious
Salerno	Italy	1999	Serious
Mont Blanc	France / Italy	1999	Collapse
Gueizhou tunnel	China	1998	Collapse
A32 Torino-Bardonecchia	Italy	1997	Serious
Exilles rail-Susa	Italy	1997	Serious
Channel Tunnel	UK / France	1996	Serious
Isola delle Femmine	Italy	1996	Moderate
Pfänder	Austria	1995	Serious
Baku underground	Azerbaijan	1995	Minor
Great Belt	Denmark	1994	Serious
Kingsway	UK	1994	Minor
Hunguenot	South Africa	1994	Moderate
Serra Ripoli	Italy	1993	Minor
Memorial	USA	1993	Minor
Hovden	Norway	1993	Moderate
Moscow	Russia	1991	Minor
Roldal	Norway	1990	Minor
Rapperfijord	Norway	1990	Moderate
Gueizhou	China	1988	Collapse
Gumefens	Switzerland	1987	Minor
Tanzenberg	Austria	1987	Serious

Definition of Damage States for Concrete Tunnel Linings Subjected to Fire Action

Grand central station	USA	1985	Serious
Felbertauern	Austria	1984	Moderate
Summit	UK	1984	Serious
Landungs	Germany	1984	Serious
San Benedetto	Italy	1894	Serious
Pecorile galleria	Italy	1983	Minor
Frejus	France	1983	Serious
Hauptbahnhof	Germany	1983	Serious
Caldecott	USA	1982	Serious
Mazar-e-Sharif	Afganistan	1982	Serious
Ramersdorf	Germany	1981	Moderate
London Underground	UK	1981	Serious
Moscow underground	Russia	1981	Serious
Kajiwara	Japan	1980	Serious
Nihonzaka	Japan	1979	Serious
Velsen	Netherland	1978	Serious
Hansaring	Germany	1978	Moderate
Metro Montreal	Canada	1976	Serious
Porte d'Italie B6	France	1976	Serious
Spain	Guadarrama	1975	Serious
Moorfleet	Germany	1968	Serious
Holland tunnel	USA	1949	Serious
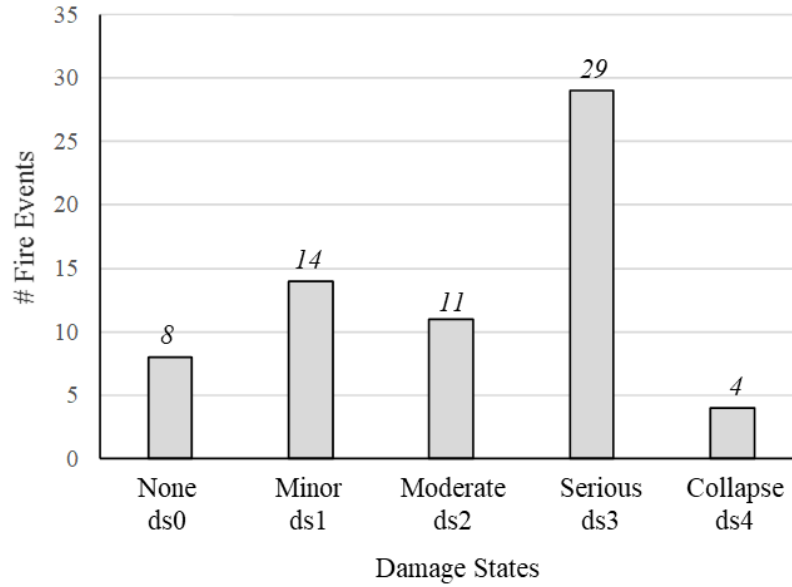
Fig. 3 Frequencies of the damage states defined for the fire events of Table 1.

3   SOME CONSIDERATIONS ON THE LIMIT STATES

To design or assess a concrete tunnel lining toward the fire action, for a specific damage state *dsi*, the related limit state function $g_i(\mathbf{X})$ should be defined, accounting for the most influential parameters X_i that rule the generic damage state, e.g.:

$$g_i(\mathbf{X}) = g_i\left(\varepsilon_t(\theta),\ t_{exp},\ \theta_{texp}, R_{d,t,fi},\ E_{d,t,fi}\right), \tag{1}$$

where $\mathbf{X}$ is the vector gathering the various X_i, $\varepsilon_{t,}(\theta)$ is the total deformation of the structural element section subjected to fire, t_{exp} is the time of fire exposure, θ_{texp} is the temperature inside the structural section, $R_{d,t,fi}$ and $E_{d,t,fi}$ are respectively the resistance of the lining and the effect of the mechanical actions in case of fire. These parameters are not independent and may vary for different tunnel boundary conditions (surrounding soil), lining constructive technology (e.g. precast or not) and fire severity (e.g. fire load and heat release rate [5]). Indeed, these aspects can considerably affect the reduction of strength and stiffness of the structural material and the variation of stress inside the tunnel lining.

To account for the several uncertainties related to these parameters, $\mathbf{X}$ can be treated as a random vector and, consequently, the probability that a state of damage (DS) reaches or exceed a certain *dsi*, $P(\mathrm{DS} \geq \mathrm{ds}i)$, is given by the well-known formula:

$$P(\mathrm{DS} \geq \mathrm{ds}i) = \int\limits_{g_i(\mathbf{X}) \leq 0} f(\mathbf{X}) d\mathbf{X}, \tag{2}$$

where $f(\mathbf{X})$ is the joint probability density function of $\mathbf{X}$. The Equation (2) can be treated with the classical methodologies of the reliability analysis.

4   POST-FIRE REHABILITATING INTERVENTIONS, PERFORMANCE LEVELS AND PERFORMANCE BASED DESIGN APPROACH

From the analysis of the database described in previous sections, it emerges that some tunnel linings did not collapse or had serious structural lining damages, but presented slightly

damaged, even if significant quantities of toxic gases were generated and propagated, causing fatalities. Rehabilitation interventions might be needed depending on the significance of the damage and the period required to re-establish the tunnel's viability and exploitation; a link between the damage states of the lining and the related rehabilitation intervention is proposed in *Table 2*.

Table 2. Rehabilitation according with each damage level.

Damage States	Rehabilitation of lining
ds0 and ds1	No structural intervention
ds2	Light interventions
ds3	Significant interventions
ds4	Complete reconstruction

As the *Table 2* shows, a wide and remarkable rehabilitation may be needed for the levels of damage ds3 and ds4, causing significant costs and possible long period of tunnel operation interruption.

This way, it is also easy to see that the proposed levels of damage can be tied-up to the different level of performance that may be required to a tunnel in case of fire.

As stated in [15], even if the European codes [16] define five safety performance levels for the building fire resistance design, there is no regulation which contains the possibility of application of performance based approach for fire resistance tunnel lining design. We propose the four performance levels (PLs) indicated in *Table 3*, each of those is guaranteed if the related damage state is not reached or exceed.

Table 3. Proposed performance levels of tunnels subjected to fire and link to the defined damage states.

Performance level	Description	Corresponding damage state to be not reached
I	Fire resistance for a period of time consistent with safe evacuation of occupants.	ds4 (Collapse)
II	Fire resistance for fire natural duration or for defined period of time in case of standard fire curves.	ds3 (Serious)
III	Fire resistance sufficient to guarantee, after the end of the fire, limited damages to the tunnel lining with light rehabilitation interventions.	ds2 (Moderate)
IV	Fire resistance sufficient to guarantee, after the end of the fire, the total operativity of the tunnel.	ds0 (None) and ds1 (Minor)

The definition of such PLs is needed in the performance-based design (PBD) of tunnels subjected to fire.

Although the fire safety goals and objectives that define the various PLs are not treated in this paper, it is worth mentioning that different use categories of tunnels (i.e. railway, road, mineral, complex research infrastructures, etc.) might require different performance levels.

Indeed, in some cases the evacuation is the most important aspect to guarantee, in other cases, such as industrial complex galleries with limited or null access for the personnel, to preserve all the equipment present in the tunnels is essential, given their considerable economic value.

Hence, in PBD approach of a tunnel lining subjected to fire, the following steps should be followed:

1. definition of the fire safety goals and objectives
2. definition of the performance level according with the tunnel use;
3. definition of the lining structural features;
4. selection of the relevant fire scenarios;
5. determination of the corresponding design fires
6. determination of the (i) heat flux on the exposed surfaces, (ii) temperature within the structural members (iii) mechanical behaviour of the lining exposed to fire;
7. check if the performance level criteria are met.

Note that in the step 6 the points (i), (ii) and (iii) are not necessarily coexistent. It depends on the specific definition of the limit state function $g_i(\mathbf{X})$ expressed in (1).

In case the performance level criteria are met, the design or the assessment of the lining is finished; otherwise, a new definition of the lining structural features or the adoption of some fire protective measures are necessary.

5 CONCLUSIONS AND FUTURE DEVELOPMENTS

Starting from a collection of about sixty-six real fires in tunnel, this paper shows the definition of five damage states for concrete linings, which account for the most relevant thermo-mechanical phenomena that occur during the fire exposure.

Four performance levels are then presented and linked to the related damage states, considering the possibility of accepting different structural damages for the tunnel lining. The steps for a performance-based design approach of underground structures are finally given.

The presented damage states and performance levels may be used in the common tunnel design practice for the following reasons:

- they cover a regulation lack about fire resistance of tunnel;
- they can be applied to several kinds of tunnel (road, railway, complex research infrastructures, etc.);
- they can used for both design and assessment of tunnel linings in case of fire;
- they accomplish a performance based approach design of tunnels in fire situation.

Among the future developments, the main one is the definition of the limit state functions and the related parameters (section 3), to better mark the boundaries between the various damage states.

REFERENCES

[1] State of the Art of Tunnel Fire Research, Haukur Ingason, Fire Technology SP Technical Research Institute of Sweden Box 857 SE-50115 Borås, Sweden

[2] de Silva D., Di Marino E., Viglione A., Nigro E., Pedicini M. (2017) *Fire safety assessment of concrete lining of a railway tunnel.* "IFireSS – International Fire Safety Symposium, Naples, Italy, 7th-9th June 2017"

[3] Lai H., Wang S. and Xie Y. (2016) *Study on the Fire Damage Characteristics of the New Qidaoliang Highway Tunnel: Field Investigation with Computational Fluid Dynamics (CFD) Back Analysis.* International Journal of Environmental Research and Public Health.

[4] Khoury, G.A. (2000). *Effect of fire on concrete and concrete structures.* Progress in Structural Engineering and Materials 2(4) : 429-447.

[5] Ingason, H., Lönnermark, A., (2003), *Large-scale Fire Tests in the Runehamar tunnel – Heat Release Rate (HRR).* Proc. Int. Symp. Catatstrophic Tunnel Fires (CTF) / Borås / 20-21 November 2003, Ingason (ed.), Borås: SP Swedish National Testing and Research Institute

[6] Keski-Rahkonen, O., Holmlund, C., Loikkanen, P., Ludvigsen, H., Mikkola, E. (1986) *Two full scale pilot fire experiments in a tunnel.* Espoo: Technical Research Centre of Finland (VTT). Research Report 453.

[7] H. Ingason, Y.Z. Li , A. L.(2011) *Runehamar tunnel fire tests.* Fire Technology SP Report 2011: 55 SP Technical Research Institute of Sweden

[8] Promat tunnel fire protection. Report. www.promat-tunnel.com

[9] Larsson K. *Fires in tunnels and their effect on rock- a review.* Research report. Luleå University of Technology.

[10] E.Cafaro, V. Bertola (2009) - *Fires in Tunnels: Learning from Disasters* XXVII International Conference on Transportation Engineering, Hengdu, China, July 25-27, 2009.

[11] Beard, A. N., & Carvel, R. (2005). *The Handbook of Tunnel Fire Safety.* Thomas Telford.

[12] Eberl, G., (2001), *The Tauern Tunnel incident – what happened and what has to be learned.* Proc. 4th Int. Conf. Safety in Road and Rail Tunnels / Madrid / 2-6 April 2001, Vardy (ed.), Dundee: University of Dundee, pp 17-28

[13] Egger, M., (2005), Chapter 16 in *Handbook of Tunnel Fire Safety.* Beard and Carvel (eds.), London: Thomas Telford Publ. ISBN:0-7277-3168-8 Firetun, 1995, Fires in transport tunnels: Report on full-scale tests. EUREKA-Project EU499; Firetun, Studiengesellscha ft Stahlanwendung elV. D-40213 Dusseldorf 54

[14] Ingason, H., (2005), Chapter 11 in *Handbook of Tunnel Fire Safety.* Beard and Carvel (eds.), London: Thomas Telford Publ. ISBN:0-7277-3168-8 Ingason, H., 2003, Fire Development in Catastrophic Tunnel Fires (CTF). Proc. Int. Symp. Catatstrophic Tunnel Fires (CTF) / Borås / 20-21 November 2003, Ingason (ed.), Borås: SP Swedish National Testing and Research Institute

[15] Del Prete I., Cefarelli G., Nigro E. *Application of criteria for selecting fire scenarios for structures within fire safety engineering approach* Journal of Building Engineering Volume 8, December 2016, Pages 208-217

[16] Interpretative Document n° 2 "Safety in case of fire" relates to Council Directive 89/106/EEC of 21 December 1988

NUMERICAL ANALYSIS OF THE HORIZONTAL FORCES ACTING ON COLUMNS IN REINFORCED CONCRETE FRAMES IN FIRE

Jorge S. Suaznábar, Valdir P. Silva
University of Sao Paulo, Sao Paulo, Brazil

ABSTRACT

This paper presents the results of thermo-structural analyses of reinforced concrete frames in fire situation. They were performed using the DIANA Displacement Analyzer software. The analysis considers the variation of the mechanical and thermal properties of the concrete and steel. The effects of axial and rotational restraints are analyzed, evaluating their consequences on the behavior of the columns in fire. Several frames are analyzed considering fires located in their compartments. As a result of the fire, the materials lose resistance, reducing the stiffness of the structure. Moreover, thermal elongation occurs in the beams and columns of the frames. Both phenomena occur at the same time and generate horizontal forces that act on the columns. From the results obtained in the analysis, the values of the horizontal forces are calculated.

1   INTRODUCTION

In order to carry out analyses of reinforced concrete structures in fire, a tendency of the last years has been to change prescriptive approaches by performance approaches. In this context, some thermo-structural analyses were performed using the DIANA Displacement Analyzer software, in order to calculate the horizontal forces acting on columns.

Structural elements belonging to a compartment in fire lose strength and stiffness and suffer thermal elongation, however, the rest of the structure retains its stiffness, constraining the deformations of the compartment structure.

As a consequence of the fire, thermal elongation occurs with the beams and columns of the frame (Fig. 1.a-b). In addition, the materials lose strength and the structure loses stiffness (Fig. 1.c-d).
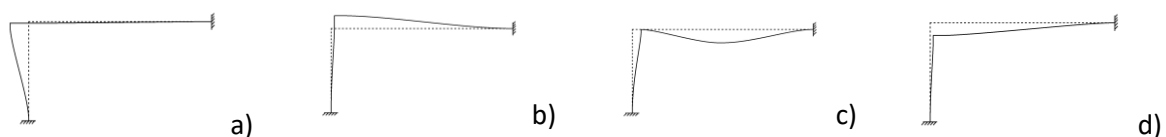
Fig. 1. a) Beam elongation; b) Column elongation; c) Stiffness loss of the beam; d) Stiffness loss of the column

Depending on the stiffness of the structural elements and the time of exposure to fire, these forces may be relatively large and should be considered for the column design.

In this article, the effects of axial and rotational constraints are analyzed, evaluating their consequences on the behavior of the columns. Several frames belonging to different structural arrangements are analyzed (Suaznábar, 2018).

The analyses were performed in the DIANA software, in two stages. At the beginning, the thermal analysis with finite elements for transient heat transfer was carried out according to the standard temperature-time curve ISO 834-1:1999 (International Organization for

Standardization ISO 834-1, 1999). Subsequently, based on the temperature fields calculated in the thermal analysis, the structural analysis was performed with finite elements for structural analysis considering the variation of the physical properties of the materials with the temperature.

2 OBJECTIVE

The objective of this article is to analyze and show the importance of the studied phenomenon, quantifying the values of the horizontal forces acting on the columns. The results of this article are part of more extensive research on the same subject and intends to send them for evaluation and inclusion in the Brazilian standard of concrete structures in a fire situation ABNT NBR 15200: 2012 (Brazilian Association of Technical Standards, 2012). The approach of this article does not aim to discuss the development of new numerical methods.

3 MATERIALS

In the analyses, the recommendations of EN 1992-1-2:2004 (European Committee for Standardization, 2004) and ABNT NBR 15200:2012 (Brazilian Association of Technical Standards, 2012) were used for the properties of the materials in fire situation.

Following, the stress-strain diagrams for concrete and reinforcing steel will be presented.

3.1 Concrete

For the compressed concrete in fire situation, the European Standard EN 1992-1-2:2004 and the Brazilian Standard ABNT NBR 15200:2012 consider the stress-strain relation of Figure 2, shown in Equation 1.
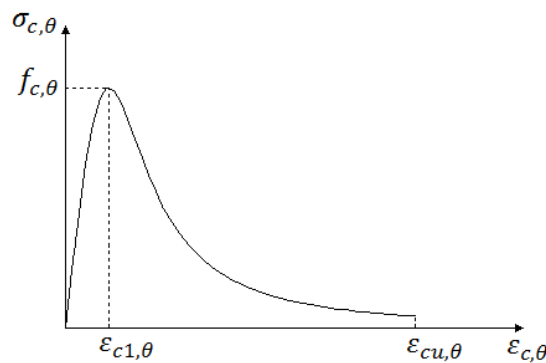
Fig. 2. Stress-strain diagram of concrete in fire situation

$$\frac{\sigma_{c,\theta}}{f_{c,\theta}} = \frac{3\left(\frac{\varepsilon_{c,\theta}}{\varepsilon_{c1,\theta}}\right)}{2+\left(\frac{\varepsilon_{c,\theta}}{\varepsilon_{c1,\theta}}\right)^3} \tag{1}$$

where $\sigma_{c,\theta}$ is the stress of the compressed concrete at temperature θ

$f_{c,\theta}$ is the compressive strength of the concrete at temperature θ

$\varepsilon_{c,\theta}$ is the strain of the concrete at temperature θ

$\varepsilon_{c1,\theta}$ is the strain corresponding to $f_{c,\theta}$

$\varepsilon_{cu,\theta}$ is the ultimate strain of the compressed concrete at temperature θ

Tensile strength of concrete in fire situation was ignored.

3.2 Steel

For the steel in fire situation, the European Standard EN 1992-1-2:2004 and the Brazilian Standard ABNT NBR 15200:2012 consider the stress-strain relation of Figure 3, shown in Equations 2.
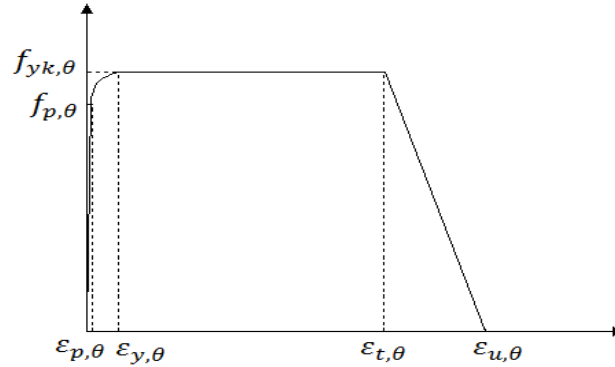
Fig. 3. Stress-strain diagram of steel in fire situation

$$\sigma_{s,\theta} = f_{p,\theta} - c + \frac{b}{a} \cdot \sqrt{a^2 - \left(\varepsilon_{y,\theta} - \varepsilon_{p,\theta} + \frac{c}{E_{s,\theta}}\right)} \qquad \varepsilon_{p,\theta} \leq \varepsilon_{s,\theta} \leq \varepsilon_{y,\theta}$$

$$\sigma_{s,\theta} = f_{yk,\theta} \qquad\qquad\qquad \varepsilon_{y,\theta} \leq \varepsilon_{s,\theta} \leq \varepsilon_{t,\theta}$$

(2)

$$\sigma_{s,\theta} = f_{yk,\theta} \cdot \left[1 - \frac{(\varepsilon_{s,\theta} - \varepsilon_{t,\theta})}{(\varepsilon_{u,\theta} - \varepsilon_{t,\theta})}\right] \qquad \varepsilon_{t,\theta} \leq \varepsilon_{s,\theta} < \varepsilon_{u,\theta}$$

where $\sigma_{s,\theta}$ is the stress of the steel at temperature θ

$\varepsilon_{s,\theta}$ is the strain of the steel at temperature θ

$E_{s,\theta}$ is the elastic modulus of the steel at temperature θ

$f_{p,\theta}$ is the proportional limit of the steel at temperature θ

$f_{yk,\theta}$ is the yield strength of the steel at temperature θ

$\varepsilon_{p,\theta}$ is the strain corresponding to the proportional limit of the steel at temperature θ

$\varepsilon_{y,\theta}$ is the strain corresponding to the beginning of the yield plateau of the steel

$\varepsilon_{t,\theta}$ is the strain corresponding to the end of the yield plateau of the steel

$\varepsilon_{u,\theta}$ is the ultimate strain of the steel

4 NUMERICAL MODELS USED IN DIANA

The processing of the thermo-structural analysis is done in two stages. The first stage, consists of thermal analysis, which considers heat transfer by conduction, convection and radiation. The second stage, is the structural analysis and is based on the results of the first

stage, considering the materials at high temperatures. The software allows to model its behavior considering the variation of the thermal and mechanical properties with the increase of temperature.

The procedures used for de thermo-structural analysis in the DIANA software have been validated in Suaznábar (2018).

4.1 Thermal analysis

Thermal analysis is a transient heat-flow analysis. It is made with finite elements for transient heat transfer, according to the standard temperature-time curve ISO 834-1:1999.

In this step, four-node rectangular isoparametric finite elements of type BQ4HT (Figure 4) were used, with linear interpolation and Gaussian integration (TNO DIANA, 2016).

This element is specific for boundary surfaces of heat-flow in solids and integration is linear and Gaussian.
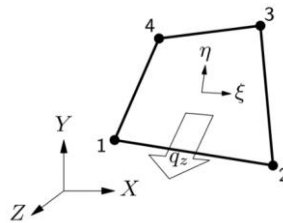
Fig. 4. Four-node isoparametric quadrilateral element (TNO DIANA, 2016)

The polynomial for the heat-flow potential (TNO DIANA, 2016) is expressed by Equation 3.

$$\varphi(\xi, \eta) = a_0 + a_1\xi + a_2\eta + a_3\xi\eta$$

$$(3)$$

4.2 Structural analysis

In structures in a fire situation not only lose of resistant capacity but other phenomena occurs such as dilation, variation of the stress-strain diagram, modulus of elasticity decrease and cracking, among others. As a consequence, the displacements and internal stresses in the structure change.

The structural analysis is done with hexahedral isoparametric finite elements of twenty nodes, type CHX60 (Figure 5), with quadratic interpolation and Gaussian integration (TNO DIANA 2016).
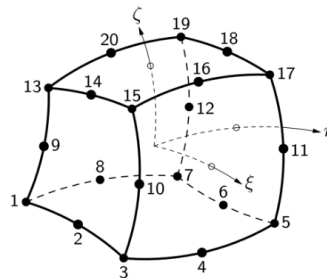
Fig. 5. Twenty-node isoparametric solid brick element (TNO DIANA, 2016)

The polynomial for the displacements is shown in Equation 4.

$$u_i(\xi, \eta, \zeta) = a_0 + a_1\xi + a_2\eta + a_3\zeta + a_4\xi\eta + a_5\eta\zeta + a_6\xi\zeta + a_7\xi^2 + a_8\eta^2 + a_9\zeta^2 + a_{10}\xi\eta\zeta + a_{11}\xi^2\eta + a_{12}\xi^2\zeta + a_{13}\xi\eta^2 + a_{14}\xi\zeta^2 + a_{15}\eta^2\zeta + a_{16}\eta\zeta^2 + a_{17}\xi^2\eta\zeta + a_{18}\xi\eta^2\zeta + a_{19}\xi\eta\zeta^2 \quad (4)$$

According to TNO DIANA (2016), with this element, the strains and stresses are approximated according to the following indications: The strain ε_{xx} and the stress σ_{xx} vary linearly in x direction and vary quadratically in y and z direction. The strain ε_{yy} and the stress σ_{yy} vary linearly in y direction and vary quadratically in x and z direction. The strain ε_{zz} and the stress σ_{zz} vary linearly in z direction and vary quadratically in x and y direction.

5   STRUCTURES ANALYZED

Three structures have been analyzed, two two-dimensional frames and one three-dimensional frame, they were named 2DF1 (Figure 6), 2DF2 (Figure 7) and 3DF1 (Figure 8).
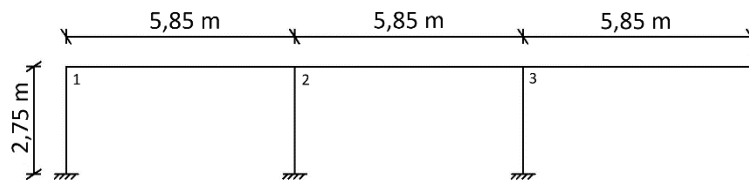
Fig. 6. Two-dimensional frame 1 (2DF1)
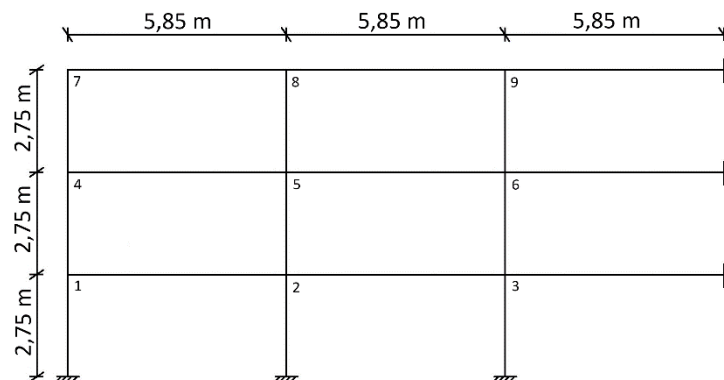
Fig. 7. Two-dimensional frame 2 (2DF2)
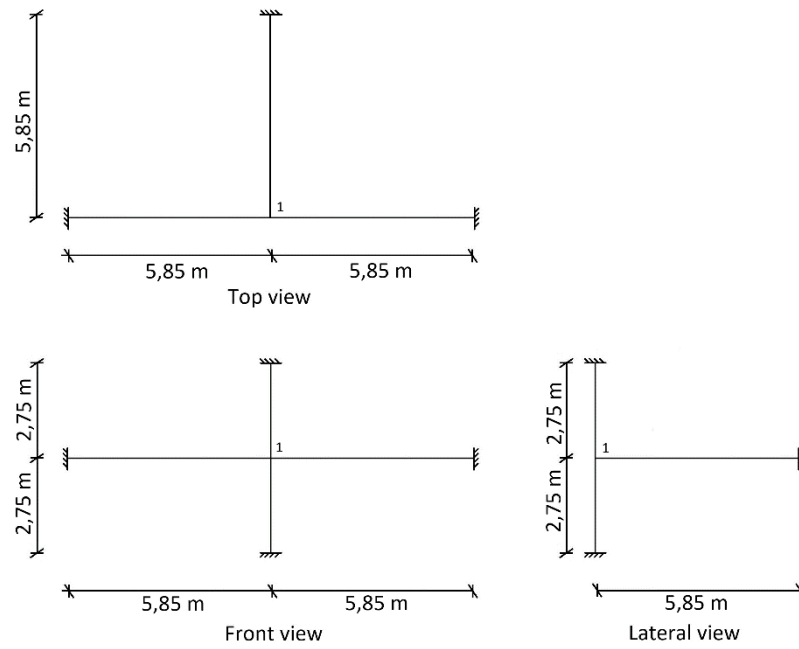
Fig. 8. Three-dimensional frame 1 (3DF1)

All columns and beams of the frames have the cross-sections shown in Figure 9. All dimensions in Figure 9 are expressed in mm.

Concrete with f_{ck} = 35 MPa and steel with f_y = 500 MPa was used.
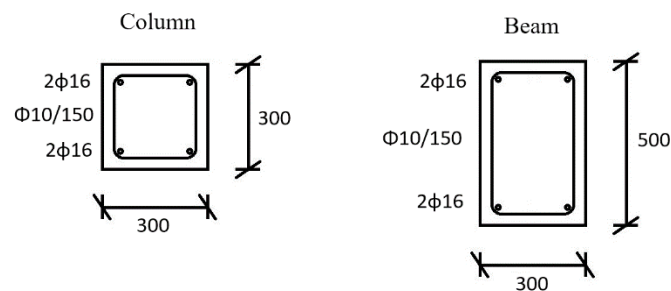
Fig. 9. Cross-sections of columns and beams of the frame

A 38 kN/m uniformly distributed load was considered acting on beams and fire according to the ISO 834:1999 curve acting on the faces indicated.
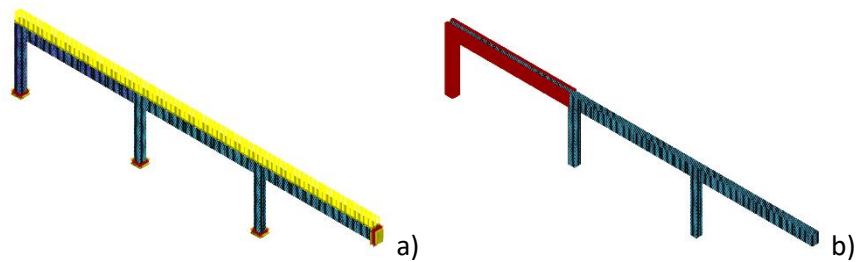
Fig. 10. a) Uniformly distributed load on 2DF1; b) Action of fire on 2DF1
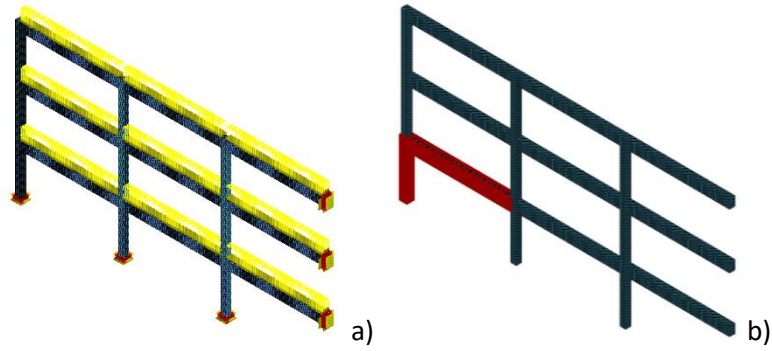
Fig. 11. a) Uniformly distributed load on 2DF2; b) Action of fire on 2DF2
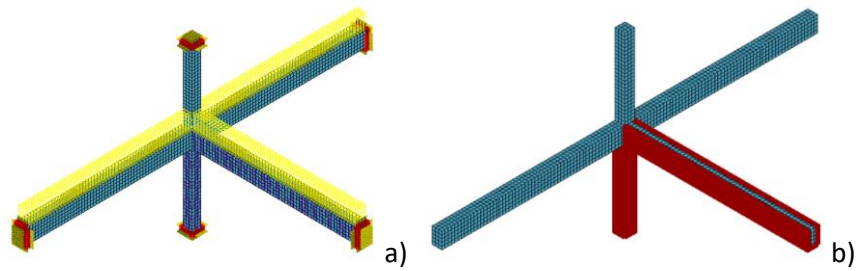
Fig. 12. a) Uniformly distributed load on 3DF1; b) Action of fire on 3DF1

5.1 Results of the 2DF1 analysis

The temperature fields of the 2DF1 thermal analysis for 30 min, 60 min, 90 min and 120 min is shown in Figure 13.
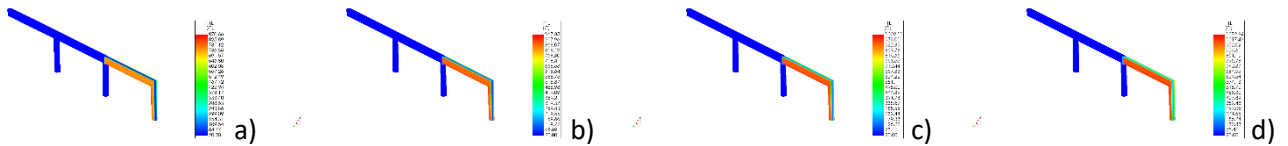
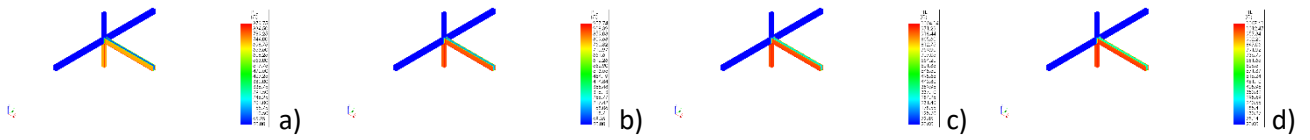*Fig. 13.* Temperature fields of the 2DF1 thermal analysis a) 30 min; b) 60 min; c) 90 min; d) 120 min

The horizontal displacement fields of the 2DF1 thermo-structural analysis for 30 min, 60 min, 90 min and 120 min is shown in Figure 14.
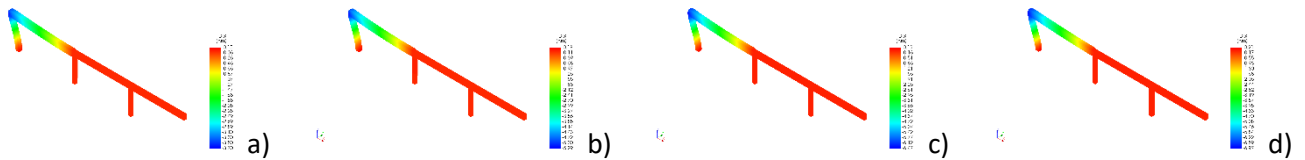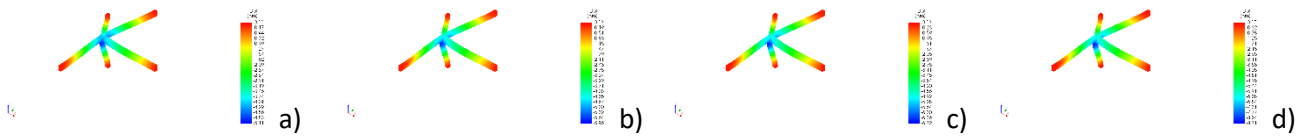

Fig. 14. Horizontal displacement fields of the 2DF1 thermo-structural analysis a) 30 min; b) 60 min; c) 90 min; d) 120 min

The vertical displacement fields of the 2DF1 thermo-structural analysis for 30 min, 60 min, 90 min and 120 min is shown in Figure 15.
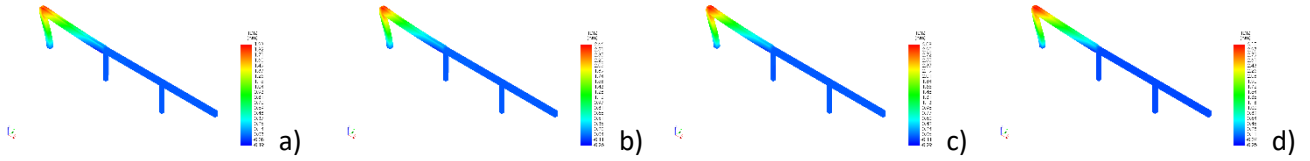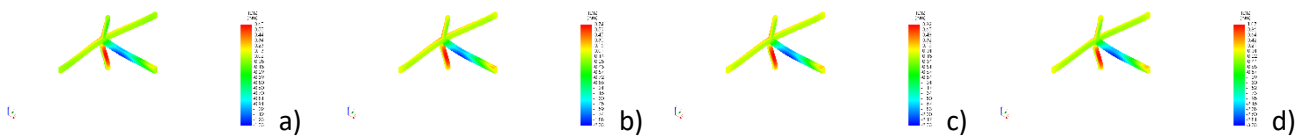
Fig. 15. Vertical displacement fields of the 2DF1 thermo-structural analysis a) 30 min; b) 60 min; c) 90 min; d) 120 min

5.2 Results of the 2DF2 analysis

The temperature fields of the 2DF2 thermal analysis for 30 min, 60 min, 90 min and 120 min is shown in Figure 16.
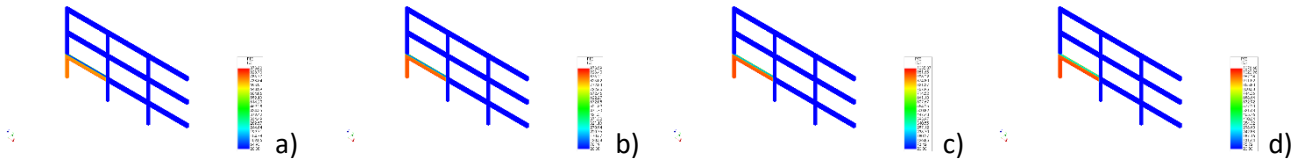
Fig. 16. Temperature fields of the 2DF2 thermal analysis a) 30 min; b) 60 min; c) 90 min; d) 120 min

The horizontal displacement fields of the 2DF2 thermo-structural analysis for 30 min, 60 min, 90 min and 120 min is shown in Figure 17.
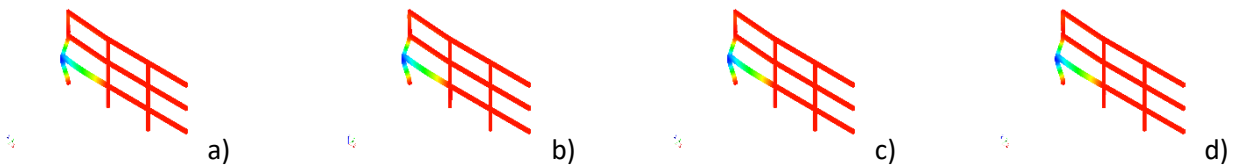
Fig. 17. Horizontal displacement fields of the 2DF2 thermo-structural analysis a) 30 min; b) 60 min; c) 90 min; d) 120 min

The vertical displacement fields of the 2DF2 thermo-structural analysis for 30 min, 60 min, 90 min and 120 min is shown in Figure 18.
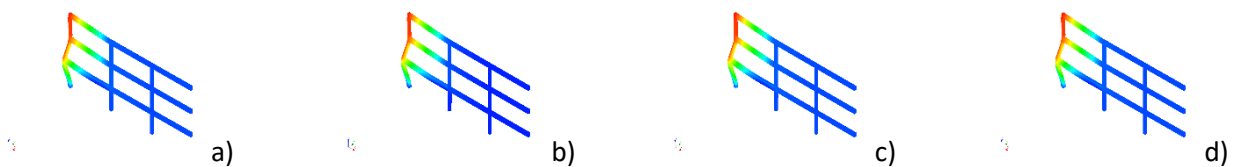
Fig. 18. Vertical displacement fields of the 2DF2 thermo-structural analysis a) 30 min; b) 60 min; c) 90 min; d) 120 min

5.3 Results of the 3DF1 analysis

The temperature fields of the 3DF1 thermal analysis for 30 min, 60 min, 90 min and 120 min is shown in Figure 19.

Fig. 19. Temperature fields of the 3DF1 thermal analysis a) 30 min; b) 60 min; c) 90 min; d) 120 min

The horizontal displacement fields of the 3DF1 thermo-structural analysis for 30 min, 60 min, 90 min and 120 min is shown in Figure 20.

Fig. 20. Horizontal displacement fields of the 3DF1 thermo-structural analysis a) 30 min; b) 60 min; c) 90 min; d) 120 min

The vertical displacement fields of the 3DF1 thermo-structural analysis for 30 min, 60 min, 90 min and 120 min is shown in Figure 21.

Fig. 21. Vertical displacement fields of the 3DF1 thermo-structural analysis a) 30 min; b) 60 min; c) 90 min; d) 120 min

5.4 Comparison of the horizontal forces

The horizontal force in the node 1 marked in Figures 6, 7 and 8 was calculated. The curves Horizontal Force – Time of 2DF1, 2DF2 and 3DF1 are shown in Figure 22.
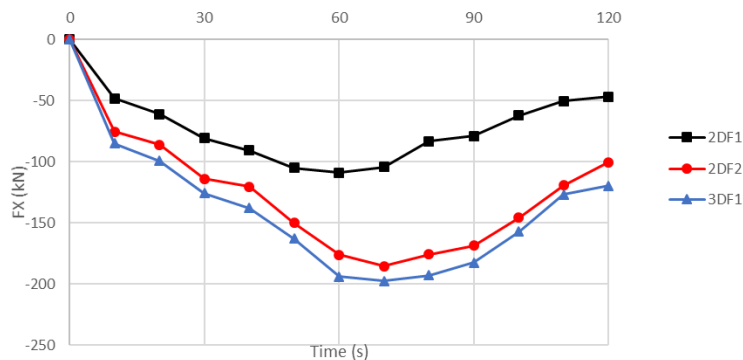
Fig. 22. Horizontal force – Time curves of all frames

6   CONCLUSIONS

The horizontal force, which derives mainly from the thermal elongation of the beam, may be very high. If this is not considered in the design, the column may be compromised. The horizontal force increases greatly at the beginning of the fire due to the combination of the thermal elongation of the beam with a structure that has not yet lost much stiffness. Subsequently, due to the increase in temperature, the modulus of elasticity of the materials decreases, which causes the stiffness of the structure to decrease as well. Other words, the structure "softens" and, consequently, the horizontal force falls. It has also been observed that columns with higher levels of loading or higher axial restraint, present larger horizontal forces due to the restriction of displacements in vertical direction. Other words, the restraint causes lower values of the vertical component of the displacement vector and the most important component of the displacement vector is the one in horizontal direction.

ACKNOWLEDGMENT

REFERENCES

[1]   Suaznábar (2018), *Analysis of the effects of the interactions between columns and beams of concrete structures in fire.*, Ph.D. Thesis, University of São Paulo, São Paulo, Brazil.

[2]   International Organization for Standardization (1999), ISO 834–1:1999 Fire–resistance Tests – Elements Of Building Construction - Part 1: General Requirements, ISO, Geneva, Switzerland.

[3]   European Committee for Standardization (2004b), EN 1992-1-2, Eurocode 2: Design Of Concrete Structures – Part 1-2: General Rules - Structural Fire Design, CEN, Brussels, Belgium.

[4]   Technical Standards Brazilian Association (2012), NBR 15200 Concrete Structures In Fire Project, ABNT, Rio de Janeiro, Brazil.

[5]   TNO DIANA 10.0 User's Manual: Element Library. Delft: TNO DIANA BV, 2016. 588 p.

SHEAR TRANSFER STRENGTH OF CONCRETE MADE WITH RECYCLED CONCRETE AGGREGATE AFTER EXPOSURE TO HIGH TEMPERATURES

Md. Yusuf, Patrick St-Onge, Salah Sarhat, and Mark Green,
Queen's University, Kingston, Canada

ABSTRACT

The performance of recycled concrete aggregate (RCA) concrete during and after exposure to elevated temperatures is critical to estimate its fire resistance and strength after exposure to fire. This paper presents the results of 24 initially un-cracked push-off specimens made with natural and recycled concrete coarse aggregates at four RCA replacement levels, 0%, 30%, 70%, and 100%. The push-off specimens were tested under direct shear after being subjected to 500ºC with one hour of soaking. Measurements were taken for residual shear transfer, shear transfer-crack slip response, residual shear modulus. The results indicate that concrete with aggregate both fully and partially replaced with RCA can be considered comparable to natural aggregate concrete in terms of shear transfer strength under loading at ambient temperature. Whereas, after getting the exposure to elevated temperature, it showed a slightly higher reduction rate for RCA concrete. Greater load versus crack width and slip responses were recorded for heated specimens compared to their unheated counterpart specimens.

1 INTRODUCTION

The use of recycled concrete aggregate (RCA) to replace natural aggregate is important to reduce the pressure on natural quarries, minimize the demolition of wastages and creat resource recovery. Because of the presence of residual mortar, RCA may have different physical and thermal properties compared to natural virgin aggregate. The behavior of RCA concrete under different loading types is a well-studied topic at both material and structural levels. However, only little attention has been paid to study the shear transfer in RCA concrete, especially when subjected to elevated temperatures. The shear transfer strength of concrete depends largely on the aggregate interlock resistance that usually happens across planes of existing or potential cracks in the concrete structures, such as the interface between slab and precast beam, cold joint between shear wall and foundations, and the vertical interface of corbel with adjacent column [1]. The shear transfer strength is composed of frictional resistance, aggregate interlock resistance and the dowel force developed in the transverse reinforcement [2]. Shear strength transfer of concrete is measured by testing small scale specimens under shear stress as shown in *Fig. 1*. The tested data from these specimens are used to develop shear-transfer models used by different design codes (such as the CPI [3] and the ACI [4]). It is necessary to accurately estimate the shear transfer strength of concrete to provide enough shear resistance along these planes. Previous studies [1, 5, 6] have shown that the use of RCA may affect the shear transfer strength at ambient. The shear transfer strength of RCA concrete during or after exposure to high temperatures yet to be understood.
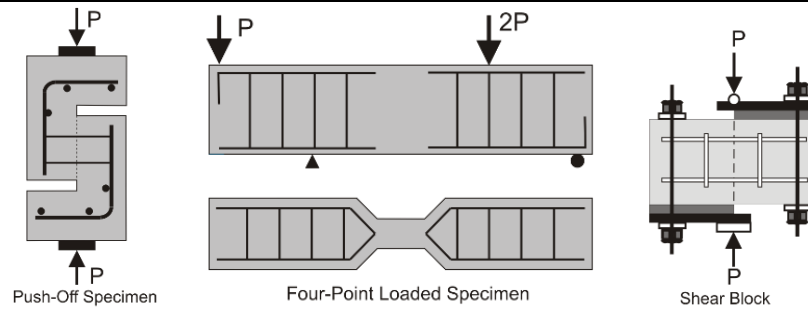
Fig. 1: Types of testing specimen to determine shear transfer strength. [7]

2   LITERATURE REVIEW

The presence of RCA in concrete has the potential to affect the aggregate interlock force due to residual mortar attached to surfaces of recycled aggregate particles. The mortar is weaker than the original coarse aggregate, and therefore, recycled aggregates cannot support the same magnitude of applied shear force as can natural aggregates [2]. Fonteboa et al. [6] tested the shear transfer behaviour of RCA concrete with 50% aggregate replacement level and compared it to natural aggregate concrete (NAC). The results of this study showed that shear failure in RCA specimens occurred at applied loads that were approximately 20% lower than in NAC. The effect of elevated temperatures on shear transfer of natural aggregate concrete was examined by Smith et al. [2] who tested reinforced concrete blocks in direct shear and heated to temperatures of 17˚C (ambient), 112˚C, 188˚C, 390˚C, 475˚C, and 622˚C. The results of this study showed that the peak exposure temperature had a negative effect on shear transfer strength of concrete, with the concrete samples heated to the highest temperatures demonstrating ultimate strengths that were approximately 50% smaller than the unheated samples. As the current body of literature has established a definite relationship between increased exposure temperature and a decrease in shear strength of reinforced concrete elements [8-11], the presence of RCA can further exacerbate shear strength during or after exposure to elevated temperatures [12].

Xiao and Lange [12] tested the effect of the joint interface conditions of RCA beams on the shear strength and found that the aggregate interlock force was inversely correlated to the percent of RCA replacement. The literature on this subject has established a negative correlation between aggregate replacement and concrete shear strength, although limited percentages of replacement have been tested. Yang et al. [13] studied concrete samples with RCA replacement levels of 0%, 50%, and 100% that were exposed to temperatures of 20˚C, 200˚C, 300˚C, and 400˚C. The results indicated that RCA replacement level did not have a significant impact on the mechanical properties of concrete at low temperatures, but that there was a significant negative impact at higher temperatures. This drop in shear strength was generally larger for samples that had higher RCA percentages. Although Yang et al. [13] established a general relationship between exposure temperature, aggregate replacement, and shear strength, only certain replacement percentages were tested, and the exposure temperature was limited to 400°C. The purpose of this paper is to present the results of a series of tests on initially un-cracked push-off specimens made of concrete with aggregate both fully and partially replaced with RCA to investigate the effect of elevated temperature on shear transfer strength.

3   EXPERIMENTAL PROGRAM

3.1 Test matrix

The main focus of this experimental work is to assess the residual shear transfer capacity for RCA concrete using push-off specimens. Four different mixes were employed in this project and they are distinguished by different types and combinations of coarse aggregate. One mix was made with 100% natural crushed limestone coarse aggregate and serves as the reference mix. The natural aggregate in the other three mixes was replaced by recycled concrete coarse aggregates at three RCA replacement levels, 30%, 70%, and 100% (see *Table 1*). A total of 24 initially un-cracked push-off specimens were cast and tested under direct shear, with 6 specimens for each concrete mix. Of these six, three specimens were employed for measuring the shear transfer strength at ambient (unheated) and three specimens for finding residual shear transfer after exposure to 500ºC. The heated specimens were let to cool down gradually and kept in the lab for one week until being tested at room temperature. In addition to push off specimens, a total of 40 (100mmx200mm) cylinders were cast from the same concrete mixes to measure the compressive and splitting tensile strengths, with ten specimens for each concrete mix. Of these ten, six cylinders were employed in the unheated compressive and the splitting tensile strengths tests, three cylinders for each test. The other four cylinders were used to measure residual compressive and splitting tensile strengths after exposure to 500ºC, two for each test. A summary of test matrix is presented in *Table 1*.

Table 1. Summary of the test matrix

Temperature (ºC)	20ºC			500ºC		
Type of Specimen	Cylinders		Push-off Specimen	Cylinders		Push-off Specimen
Concrete type/Test	Compressive Strength	Splitting Tensile Strength	Shear Transfer strength	Compressive Strength	Splitting Tensile Strength	Shear Transfer strength
100%CL-0%RCA	3	3	3	2	2	3
70%CL-30%RCA	3	3	3	2	2	3
30%CL-70%RCA	3	3	3	2	2	3
0%CL-100%RCA	3	3	3	2	2	3

The un-cracked push-off specimens (260x140x100 mm) were used to measure the shear transfer strength. Fig. 2 shows the details dimensions and reinforcement layout of the specimen. The average shear plane was 9000mm2 (length 90mm and width 100mm) and the resulted strengths ware calculated with respect to as-built dimensions. Two 10M L shaped reinforcement were placed parallel to the shear plane to avoid the flexural failure of the specimens.
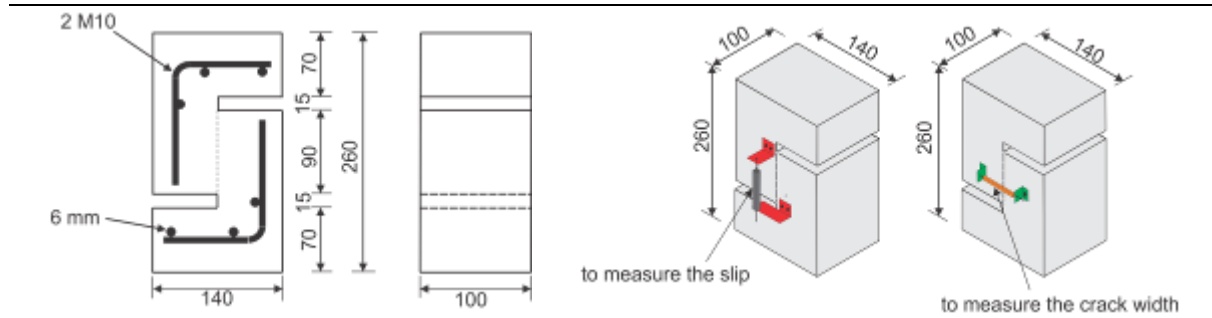
Fig. 2. Details of the push-off specimen.

3.2 Materials

Portland limestone cement produced in Canada was used in all mixes. Natural river sand with
a fineness modulus of 2.66 was used as fine aggregate. Crushed limestone was used as
natural aggregate and RCA was originated from the demolition of the large concrete roadside
curbs (as shown in *Fig. 3a*). As the common practice in road construction is to add a layer of
natural coarse aggregate under roadside cubes as a base, the RCA used in this project
contained about 12% of natural aggregate. The data (12%) is an average of five random
samples and was measured with quartering sampling techniques through visual screening and
by weight. For consistency, each aggregate was separated into two different size fractions
using a sieve shaker and recombined to a predetermined gradation (50% passed 12.5 mm and
retained on 9.5 mm sieve and 50% passed 9.5 mm and retained on 4.75 mm sieve).
Aggregates were cleaned from impurities and washed before conducting any test or using
them for casting. The physical properties of the coarse and fine aggregates were determined
and are summarized in *Table 2*.

Table 2. The physical properties of the coarse and fine aggregates.

Aggregate type	Maximum size, mm	Unit weight, kg/m^3	Relative density (OD)*	Relative density (SSD)**	Water absorption (%)	Aggregate crushing value (%)
Crushed Limestone (CL)	12.50	1760	2.60	2.64	1.03	21.45
Recycled Concrete Aggregate (RCA)	12.50	1440	2.34	2.45	4.53	24.53
Fine aggregate (FA)	4.75	1750	2.61	2.66	0.98	-

*OD- oven dry, **SSD- saturated surface dry

3.3 Concrete mixes

Concrete mix proportions were determined according to the absolute volume method as
described in *Table 3*. Concrete made with only natural crushed limestone was prepared as
Control Concrete and termed as 100%CL0%RCA. Three RCA concrete mixes were made
with different RCA replacement ratio (RRR) of 30%, 70%, and 100%. To rationally evaluate
the effects of each type of coarse aggregate on the shear transfer strength of concrete after
exposure to elevated temperatures, the coarse aggregate volume was kept constant in all
mixes. Water-cement ratio was kept constant for all the mixture. All aggregates were
introduced into the mixing process in a saturated-surface dry condition. They were weighted
and stored in plastic containers, 24 hours before mixing, together with the exact amount of
water needed to achieve their saturated surface-dry condition. The plastic containers were
agitated intensively, after placing the aggregates with their amount of absorption water into
them and prior to mixing, in order to guarantee a uniform distribution of the absorption water

within the aggregates. Small amounts of superplasticizer (SP) were used to maintain a slump value of 90-100 mm with the increase of RCA replacement ratio. Proper compaction was achieved by vibrating the sides of the wooden mould using a needle vibrator (Fig. 3b). Casted specimens were kept wrapped with polythene sheets for one week. The specimens were then demolded and stored in a room maintained at a temperature of 22°C and relative humidity of 65% for 28 days.

Table 3. Mixing proportion (kg/m^3)

Concrete type	RRR (%)	CL	RCA	FA	Cement	Water	SP
100%CL0%RCA	0	912		804	416	216	0
0%CL100%RCA	100	0	804	804	416	216	0.75
30%CL70%RCA	70	273.6	562.74	804	416	216	0. 5
70%CL30%RCA	30	638.4	241.17	804	416	216	0.25

3.4 Heating of the specimens

The push-off specimens and cylinders chosen for the residual tests were preheated at 80ºC in a closed chamber for about 24 hours to evaporate their inner moisture to eliminate the possibility of concrete spalling during heating to 500ºC. A furnace of volume (200 x 200 x 280mm) made by Hotpack corporation was used to heat the samples (*Fig. 4a*). The rate of heating was 5ºC/minute and the target temperature (500 ºC) was maintained for 1 hour, after which the furnace was turned off and its door was kept closed for next three hours to avoid any thermal shock due to sudden temperature change. The specimens were then allowed to cool naturally to room temperature. Both the furnace air temperature and the temperature at the shear surface were recorded. The temperature inside the push-off specimens was recorded by K-type thermocouple placed at the layer of the shear plane during casting depicted in *Fig 3c*.
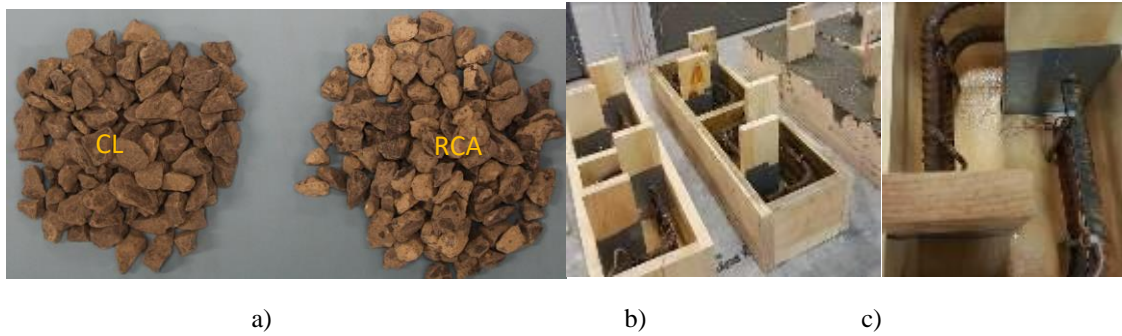
Fig. 3. a) Crushed limestone (CL) and Recycled concrete aggregate (RCA), b) Mould with steel casing, c) thermocouple placement at the level of shear plane.

3.5 Testing setup

All tests for unheated and heated push off specimens and cinders, were carried out in the materials laboratory of Queen's University at age of six weeks (42 days). For the residual strength, push-off specimens and cylinder that heated to 500°C were kept outside the oven for air cooling for one week and tested at room temperature. Instron 1350 was used to test the shear transfer strength as indicated in *Fig. 4b* and the compression load was applied to push-off specimens at a constant rate of 0.3mm/minute. Two steel plates of 20mm thickness were used on the top and bottom of the sample to get the uniform distribution of compression loading and a roller was introduced under the bottom plate to eliminate any flexural effect. In one side of the push-off specimen LP (Linear Potentiometers) used to measure the crack width and two LPs were placed vertically on the other side of the specimen measuring the vertical displacement (slip).

Fig. 4. a) Sample inside the furnace Hotpack for heating, b) Test setup for testing push-off specimen with LP for measuring vertical displacement.

4   RESULT AND DISCUSSION

All twenty four push-off specimens witnessed brittle pure shear failures along the shear transfer plane, causing each one to split into two pieces. *Table 4* shows that the mode of failures of the specimens are independent of the replacement level of RCA, being tested unheated at ambient or after exposure to elevated temperatures. *Table 5* presents the summary of the experimental results obtained. The shear transfer strength are taken as the average of three test results. At room temperature, the compressive strength varies from 42.88 to 48.35 MPa and the splitting tensile strength is about one-tenth of the compressive strength of the concrete. Exposure to 500°C cause different concrete types to lose about half of their compressive and tensile strengths. *Fig. 5* illustrates the furnace air temperature and

inside temperatures of the push-off specimens during heating. Most of the specimens experienced about 450°C temperature at the plane where the shear transfer was measured. The shear transfer stress was calculated from the peak load divided by the area of the shear plane and the average of three test results at ambient and residual for each type of concrete mix are reported in *Fig. 6*. It can be seen in *Fig. 6* that there is no significant difference in shear transfer strength between the natural aggregate and RCA concrete specimens. After exposure to temperatures of 500°C, the push-off specimens showed decreases in shear transfer strength ranging from 63% to 69%, with the RCA concrete specimens exhibited slightly greater reductions, compared to shear transfer strengths at ambient. This observation indicates that the effect of elevated temperature is more pronounced on the shear transfer strength than other mechanical properties such compressive strength and tensile strength. The reduction in shear transfer strength after exposure to elevated temperatures can be attributed to the mismatch of thermal expansion properties between the aggregate and cement paste. This mismatch results in weaker interface transition zone between the aggregate and cement leading to bond deterioration between aggregate particles and surrounding cement. Visual inspection of the shear plane textures for tested specimens after failure showed that less coarse aggregate particles were cut along shear plane in heated specimens than those in unheated ones. It can be concluded that exposure to elevated temperatures is conducive to reducing aggregate interlock capacity and this effect is exacerbated when concrete is made with recycled concrete aggregates.

Table 4. The mode of failures of push-off specimens

Type of Concrete	100%CL0%RCA	70%CL30%RCA	30%CL70%RCA	0%CL100%RCA
20 °C				
500 °C				

Table 5. Summary of the test results of cylinders and push-off specimens.

Temperature (°C)	20°C						500°C					
Concrete Type	f_c' MPa	f_t MPa	P_{peak} kN	τ_s MPa	Slip mm	Crack width mm	f_c' MPa	f_t MPa	P_{peak} kN	τ_s MPa	Slip mm	Crack width mm
100%CL0%RCA	45.25	4.31	58.63	6.73	1.33	0.22	19.70	2.05	20.52	2.44	0.36	0.10
70%CL30%RCA	42.88	4.42	59.23	6.49	1.37	0.18	19.32	2.10	19.57	2.07	0.48	0.20
30%CL70%RCA	47.35	4.87	61.94	7.02	1.58	0.18	23.33	2.07	20.49	2.34	0.59	0.12
0%CL100%RCA	48.35	4.41	56.32	6.44	1.62	0.33	20.42	2.31	17.56	2.01	0.34	0.18

Fig. 7 and Fig. 8 represents the shear transfer strength versus slip along the shear plane and crack width, respectively. With the application of the same amount of load, higher deformations (slip and crack width) were recorded for the push-off specimens exposed to high temperature. For example, a slip of 0.3 mm occurred due to the application of 2.5 kN and 3.2kN loads for natural aggregate concrete and 70% RCA concrete respectively at ambient. While, regardless of the aggregate type, it was required to apply only 1.7kN load to cause the 0.3 mm slip in the corresponding heated specimens. Similarly, to get a crack width of 0.01mm, the required load at ambient was three times higher than the load applied for heated specimens. These results show that exposure to elevated temperature induces the formation of wider cracks in concrete and reduce the aggregate interlock capacity leading to smaller shear transfer strengths.
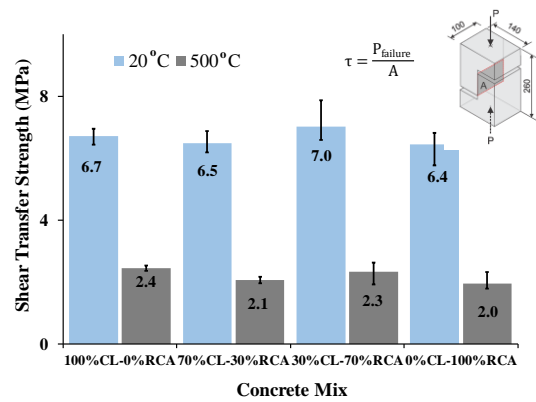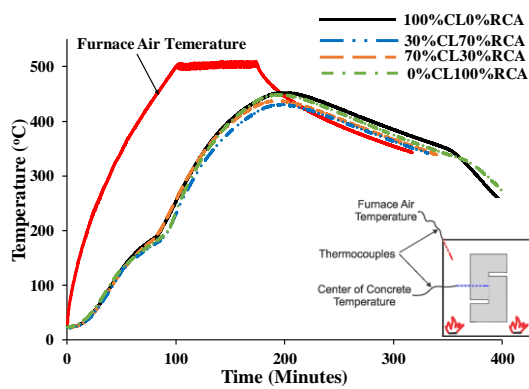

Fig. 5. Development of temperature inside concrete.

Fig. 6. Shear transfer strength both at ambient and residual for concrete made with different RCA replacement ratio.
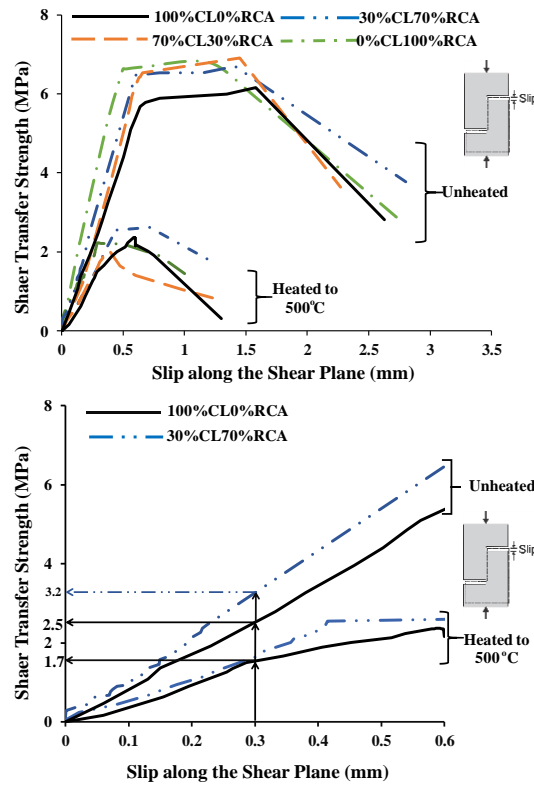
Fig. 7. Shear transfer strength versus measured slip for concrete at ambient and residual conditions.
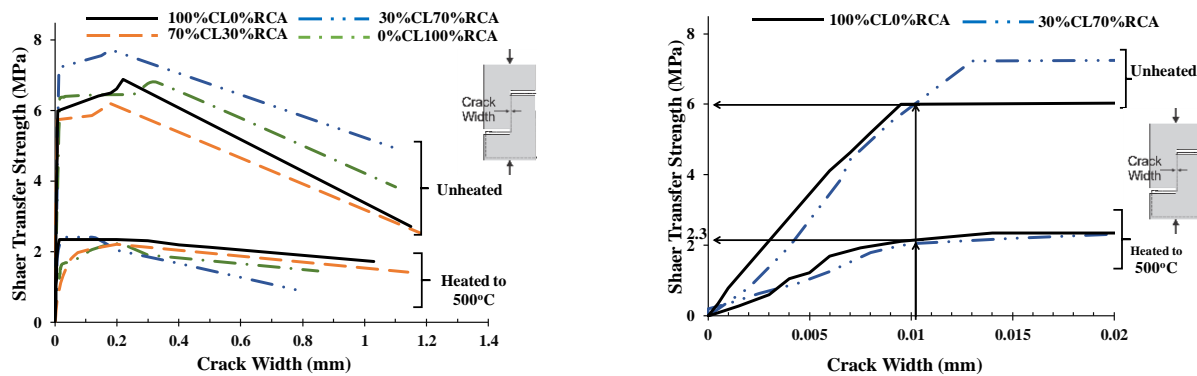

Fig. 8. Shear transfer strength versus crack width for concrete at ambient and residual conditions.

5 CONCLUSIONS

The following conclusions could be made from this study:

- Pure and brittle shear failures were observed in the tested push-off specimens regardless of aggregate type.
- The reduction in shear transfer strength after exposure to 500°C temperature was more pronounced than the reductions in compressive and tensile strengths.
- At ambient temperatures, there was no significant difference in shear strength between the natural and RCA concrete samples. After exposure to temperatures of 500°C, concrete specimens showed decreases in the shear transfer strength of approximately 70%. RCA concrete exhibited slightly greater reductions than those for natural aggregate concrete.

- The exposure to elevated temperature not only reduce the shear transfer strength but it affected shear deformations as well. Larger crack widths and slips were recorded for the push-off specimens exposed to high temperature.
- The test results indicated that exposure to elevated temperatures was conducive to the formation of cracks in concrete, reducing aggregate interlock capacity. This effect was exacerbated when concrete was made with recycled concrete aggregates.

REFERENCES

[1] Rahal K., Khaleefi A., Al-Sanee A. (2016). An experimental investigation of shear transfer strength of normal and high strength self-compacting concrete, Engineering Structures, 109 (2016). pp.16–25.

[2] Smith H., Reid E., Beatty A., Stratford T., Bisby L. (2011). Shear strength of concrete at elevated temperature. Application of structural fire engineering, April, 2011, Czech Republic.

[3] Prestressed Concrete Institute (PCI) (2010), PCI Design Handbook, 4th ed., PCI, Chicago.

[4] ACI Committee 318, American Concrete Institute, Farmington Hills, Michigan, 2014.

[5] Shejwadkar, N., Singh, B., and Waseem, S. (2017). Shear Friction in Recycled Aggregate Concrete. Journal of Sustainable Cement-Based Materials. 6:1 (2017). pp.17-36.

[6] Fonteboa, B., Martinez, F., Carro, D., and Eiras, J. (2010). Shear friction capacity of recycled concretes. Materiales de Construccion, 60:299 (2010). pp.53–67.

[7] Sarhat, S., and Green, M. (2017). Effect of elevated temperatures on the shear transfer strength of concrete: A review. 2nd International Fire Safety Symposium- IFireSS 2017, Naples, Italy. pp.581-588.

[8] Diab, M. (2014). Shear capacity of reinforced concrete beams at elevated temperatures. Master's thesis, Western University. Electronic Thesis and Dissertation Repository-1884.

[9] El-Hawary M., Ragab A., El-Azim A., Elibiari S. (1997). Analysis of reinforced concrete frames exposed to fire based on advanced calculation methods. Computer and Structures, 65:2 (1997). pp.281-287.

[10] Saqier, A. (2008). Effect of fire flame exposure on flexural behavior and shear strength of reinforced NSC and HPC beams. M.Sc. thesis, Babylon University College of Engineering.

[11] Annerel, E., and Taerwe, L. (2015). Design considerations for shear failure of flat concrete slabs exposed to fire. Concrete - Innovation and Design, fib Symposium, Copenhagen May 18-20, 2015

[12] Xiao J., Li Z., Li J (2014). Shear transfer across a crack in high-strength concrete after elevated temperatures. Constrution and Building Materials, 71 (2014). pp.472–48.

[13] Yang H., Qin Y., Liao Y., Chen W. (2016). Shear behavior of recycled aggregate concrete after exposure to high temperatures. Construction and Building Materials, 106 (2016). pp.374–381.

EXPERIMENTAL STUDY ON SHEAR PERFORMANCE OF SIMPLE SUPPORTED REINFORCED CONCRETE BEAMS WITHOUT WEB BAR UNDER FIRE

Yamin Song[1*], Chuanguo Fu [2], Shuting Liang [1], Xinyao Chen [2]

1.School of Civil Engineering, Southeast University, Nanjing, China

2. School of Civil Engineering, Shandong Jianzhu University, Jinan, China

ABSTRACT

The experiments were performed for assessing the influence of loading ratio on the fire resistance of reinforced concrete (RC) beam specimens without web bar under fire. Four full-scale RC beams without web bar were fabricated either under room temperature or at high temperature. The fire tests were conducted in horizontal furnace chamber of Shandong Jianzhu University. The experimental results show that the failure mode of the specimen at ambient temperature is typical shear failure, but the failure mode may be either shear failure or shear-bend failure at high temperature. Under the thermodynamic coupling, the larger the load ratio, the smaller the measured failure time of non-web reinforced concrete beams.

Keywords: fire resistance; reinforced concrete; simply supported beams; shear capacity; load ratio

1   INTRODUCTION

When the fire occurs in building, the high temperature will seriously degrade the bearing capacity of the reinforced concrete members. The internal force and stress redistribution as a result of the high temperature will have a complex impact on the shear bearing mechanism of RC members. The bearing safety of the diagonal section of RC members under high temperature should be highly concerned, and the steel bars affected by the high temperature should be strengthened. It is very urgent to strengthen the research on shear bearing capacity of RC beams exposed to fire. At present, there are few relevant data for the experimental study on the bearing capacity of RC beams considering the effect of fire. Xiao et al. [1] analyzed the effects of high temperature on the strength and deflection of concrete, and focused on the differences of the fire resistance between ordinary concrete and high strength concrete, and systematically studied the phenomenon and mechanism of concrete bursting after fire. Zhang et al. [2] collected the performance of RC structures under high temperature, and put forward effective suggestions on how to carry out effective structural repair and reinforcement. Ren et al. [3] summarized the existing fire resistance research and design methods, and proposed the fire resistance methods of concrete structures. Zhang [4] conducted fire test on 16 full-scale reinforced concrete beams. The tests summarized the deflection and performance of the simply supported beams under high temperature fire. Lu et al. [5] conducted fire resistance tests with one, two and three sides heating of 12 reinforced concrete simply supported beams, considering the parameters of loads, heating curves and thickness of steel protective layer. Fu et al. [6,7] analyzed the temperature field distribution of RC frame joints and RC beams under the ISO834 standard heating curve. Liu et al. [8] studied the failure mode of reinforced concrete beams with carbon fiber cloth under fire. Lie.T.T, Irwin. R.J etal.[9,10] conducted experimental study on the properties of reinforced concrete compression-bending members under high temperature. El-Hawary. M. M, Ragab. A. M et al. [11,12] conducted fire resistance tests of eight reduced-scale beams, and analyzed the effects of fire time and concrete protective thickness on the ultimate bearing capacity of beams. Studies on the failure mechanism of RC members under fire are still very limited. Fire simulation test research examples are still insufficient, lack of effective test verification data.

This study investigated the shear behavior and failure mechanism of RC beams without web bar in fire. Four full-scale RC beams without web bar were designed, considering the effects of loading ratio. The RC beams adopt three-side fire condition with ISO834 international standard curve [13]. The main objective of these tests was to study the effect of load ratio on fire resistance of RC beams without web reinforcement.

2 EXPERIMENTAL TESTS

2.1 Specimens geometry and material data

To study the effect of load ratio on fire resistance of simple supported RC beam without web bar under thermodynamic coupling, four full-scale RC specimens without web bar (as shown in Fig. 1 and Table 1) were fabricated: one was unfired and employed as a reference, the other was fired in a furnace chamber of Shandong Jianzhu University. The design length of RC beam specimens is 4000 mm, and the cross-sectional size is 250 mm×400 mm. The shear span ratio λ, and longitudinal reinforcement ratio of all the beams was 2.1 and 1.96%, respectively. The thickness of the concrete cover was 25 mm. Stirrups are placed in the beam-ends. Table 1 shows that the standard reinforcement used for longitudinal reinforcement has a cross-sectional diameter φ=25 mm and a tested yield stress f_y of approximately 450 MPa. The tested average compressive strength of three concrete cubes (150 mm×150 mm ×150 mm) was 31.6 MPa.

Table 1. Design parameters of specimens

Specimen	Section size/mm	ρ/%	λ	Load ratio
CWZJL1-W	250×400	1.96	2.1	/
ZJL1-W	250×400	1.96	2.1	$0.4P_u$
ZJL2-W	250×400	1.96	2.1	$0.6P_u$
ZJL3-W	250×400	1.96	2.1	$0.5P_u$

Note: contrastive specimen number: CWZJL-W; specimen number under fire: ZJL-W; P_u: ultimate load bearing capacity at ambient temperature
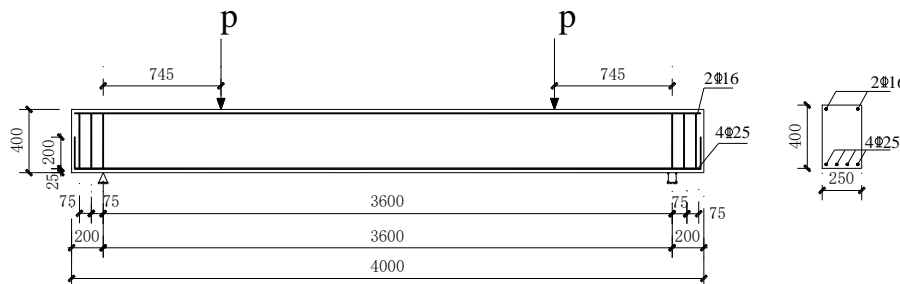

Fig.1. Dimensions and reinforcement details of specimens (dimensions in mm).

2.2 Test setup

The fire tests of specimens were carried out in the large-scale horizontal furnace chamber in the fire laboratory of Shandong Jianzhu University. The furnace had 9000×4500×1500 mm of internal dimensions and was capable to heat up following ISO 834 fire curves, as shown in Fig. 2(a). The beams were placed in the furnace as illustrated in Fig. 2(b). Before heating up, the beam was firstly added to the applied load. After the load was stabilized, the ignition

heated up. The load was kept constant during the fire test and the general arrangement of the test set-up was shown in Fig. 3. All measurements of thermocouples, displacement transducers were recorded by a computer data logger.

The temperature in the furnace was measured through thermocouple previously set in the furnace chamber. The internal temperature distribution of specimens was obtained by thermocouple pre-buried in the cross-section (as shown in Fig. 4), in which the 1-1 section is the middle of beam, and the 2-2 section is the middle of the support and loading point of the specimen.

Through four linear variable differential transducers (LVDTS) and the data acquisition instrument, the deflection deformation of the simply supported beam specimen was monitored in real time, as shown in Fig. 5. The displacement gauges were respectively arranged at the one end support, the two loading points and the mid-span of specimen to measure the vertical deformations along the loading direction, the displacement gauge had a range of 200 mm.
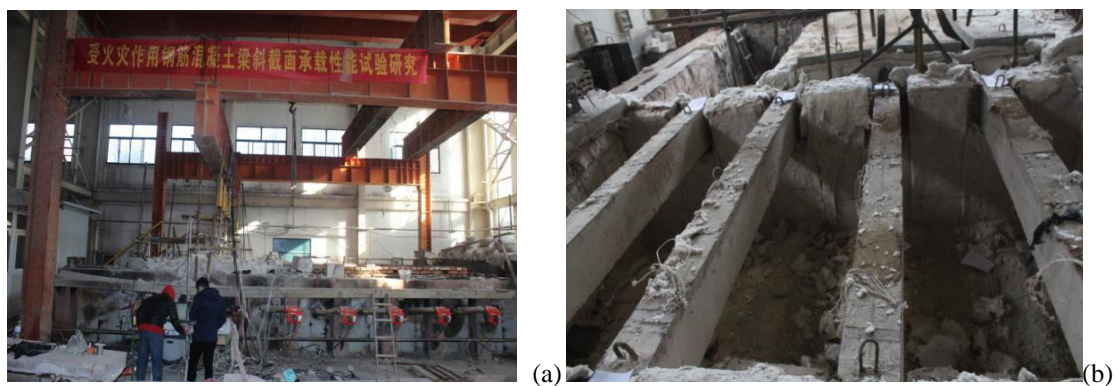

(a)   (b)

Fig. 2. Layout of the fire test: a) The furnace chamber; b) Specimens arrangement in fire furnace.
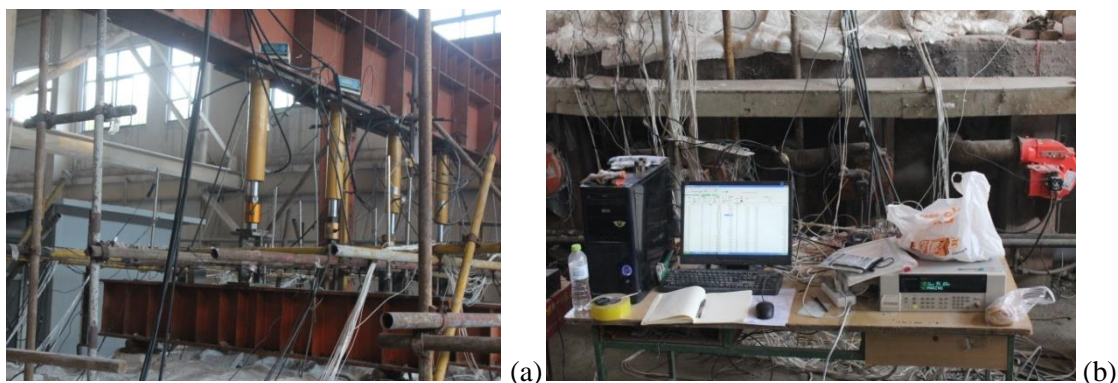

(a)   (b)

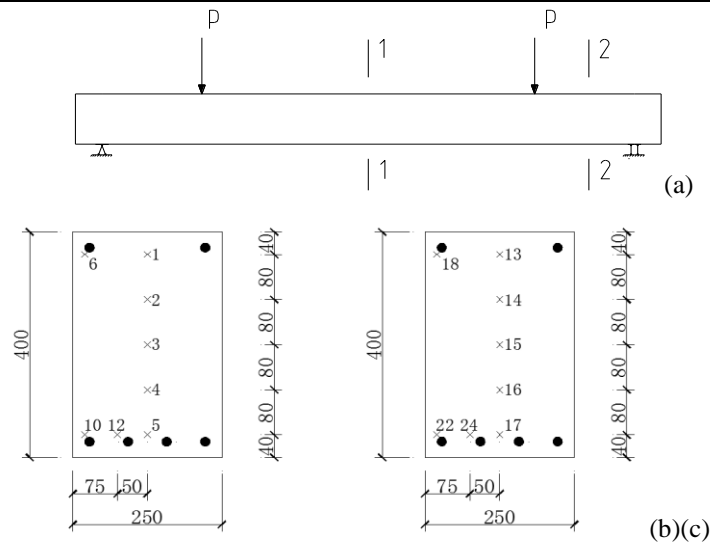*Fig. 3.* Fire test set-up: a) Vertical load; b) Date collection.

Fig. 4. Location of thermocouples (dimensions in mm): a) Thermocouple; b) 1-1 section; c) 2-2 section
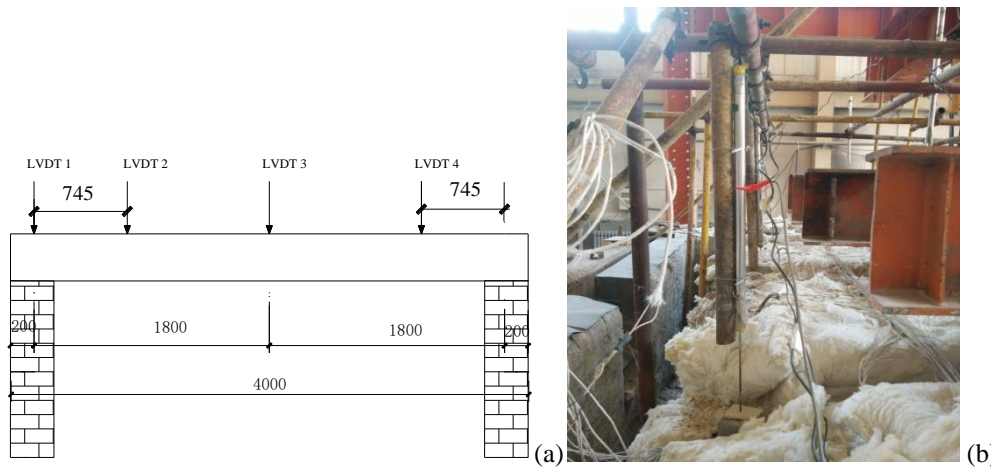

Fig.5. Displacement meters layout of specimens (dimensions in mm):a)LVDTS layout; b)LVDTS layout in site

2.3 Failure criterion

Considering that the failure mode of the specimens without web bar was difficult to predict under the thermodynamic coupling effect, the failure criterion of the specimens was referred to the fire endurance regulations for flexural members of Chinese Standard [14] :

Deformation: $D = \dfrac{L^2}{400d}$ mm   (1)

Deformation rate: $\dfrac{dD}{dt} = \dfrac{L^2}{9000d}$ mm/min   (2)

Where L is the net span of specimen (mm) and d is the height between the compression point and the tensile point on the cross section of specimen (mm). When either of the indices exceeds the deformation (Eq. 1) and deformation rate (Eq. 2), It was considered that the beam had reached the fire resistance limit.

At the same time, considering that the shear brittle failure may occur on the oblique section of the beam, when the reinforced concrete beams without web bar is brittle failure at high temperature and momentary loses its bearing capacity, the specimens is also considered to reach the fire endurance limit.

3   RESULTS AND DISCUSSION

3.1   Thermal response

Through the data acquisition results of temperature sensor data acquisition and displacement transducers during the fire test, the temperature rise in the fire test furnace and the measured vertical displacement of the specimens were monitored in real time.

During the thermodynamic coupling test, the test phenomena in furnace chamber were inconvenient to observe due to the sealing of the top cover of the specimen. Only the exposed part of specimens could be observed. After about 20 minutes after the start of the heating test, the measured temperature inside the furnace increased sharply, and some water vapor gradually emerged from the joint portion of the test furnace cover plate. After about 60 minutes of the heating test, some water stains were deposited at both ends of the specimens and the vertical deflection of the measured test beam span changed significantly. As the fire time increased, a clearer cracking burst sound gradually appeared in the furnace, which could be caused by the bursting of the surface layer concrete of specimens under high temperature conditions. When the fire endurance was approached, the vertical deformation of the test beam was obviously accelerated and did not converge, the fire endurance reached quickly and the specimen was suddenly destroyed. After the specimens reached the fire endurance limit, they stopped the fire and unload it. After cooling to normal temperature by natural cooling method, the furnace covers were open and the specimens were hoisted out for detailed appearance observation, recording and photographing.

The fire tests were carried out simultaneously with other specimens. According to the overall arrangements of the test plan, three specimens were subjected to thermodynamic coupling tests in two batches, ZJL1-W was the first batch and ZJL2-W and ZJL3-W were the second batch. The comparison between the measured heating curves in the furnace and the ISO834 heating curve is shown in Fig. 6(a). As can be seen from Fig. 6(a), the temperature rise curve of the measured furnace in the two batches is basically consistent with the heating trend of the ISO834 international standard heating curve, but the first test of the measured furnace temperature is always slightly lower than the ISO834 international standard heating curve about 40 °C. The temperature curve at the partial measuring points of the specimens with the fire time is shown in Fig. 6.
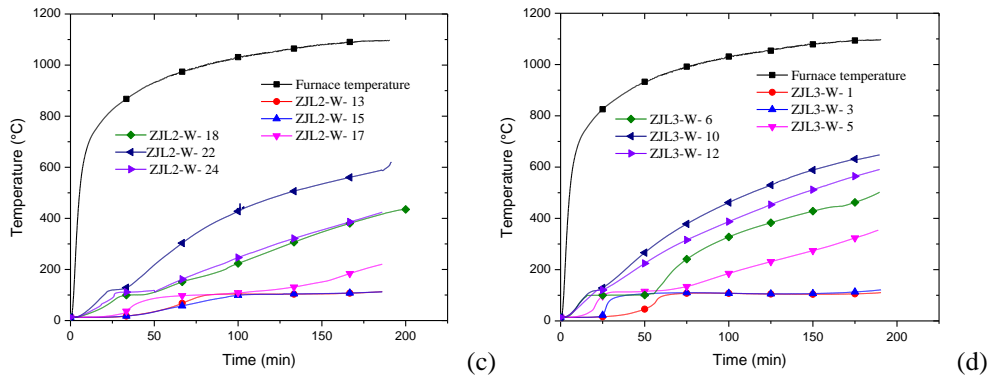

(a)   (b)
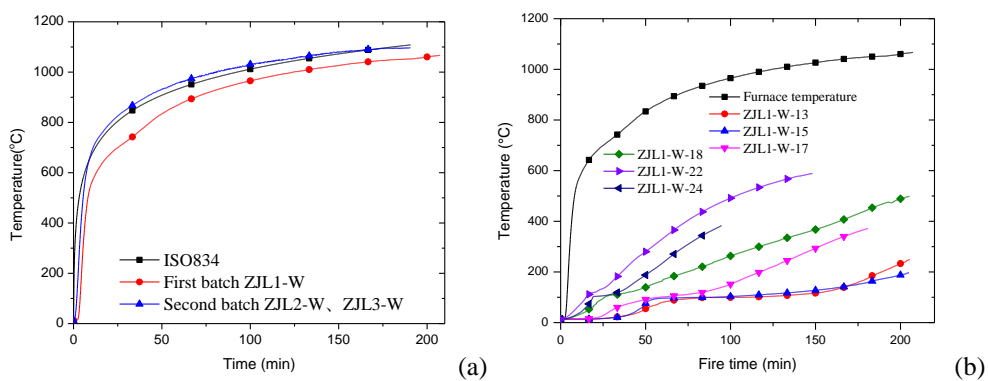
Fig. 6. Measured temperature-time curves: a) Furnace temperature curves; b) ZJL1-W; c) ZJL2-W; d) ZJL3-W

3.2 Vertical displacement

Table 3. Measured fire resistance limit and vertical displacement

Specimen	λ	Load ratio	Failure time/min	Vertical displacement/mm
ZJL1-W	2.1	$0.4P_u$	198	102
ZJL2-W	2.1	$0.6P_u$	184	91
ZJL3-W	2.1	$0.5P_u$	191	76

FIG. 7 shows the relation curves of measured vertical displacement with temperature rise time of specimens. Table 3 shows the measured fire resistance limit and the displacement of each specimen. It can be seen that under the thermodynamic coupling of different load ratios, the vertical displacement changes of the specimens ZJL1-W and ZJL3-W relatively gentle before the temperature rise to 130 minutes, and the vertical deformation is basically similar with about 180 minutes. Compared with the specimens ZJL1-W and ZJL3-W, the specimen ZJL2-W with the largest load ratio has a relatively smooth vertical deformation before180 minutes. When approaching the fire resistance limit, the vertical deformation increases sharply and enters the rapid destruction. The specimen ZJL1-W reaches the fire endurance as early as 184 minutes. The load ratio of the specimen ZJL3-W during heating is $0.5P_u$, the vertical displacement increases rapidly at 191 minutes, and the second one reaches the fire endurance limit. The load ratio of the specimen ZJL1-W is $0.4 P_u$, and the last one reached the fire endurance when the temperature rises to 198 minutes. As can be seen, the greater the load ratio under thermal coupling is, the smaller the measured fire resistance limit of reinforced concrete beams without web bar is.
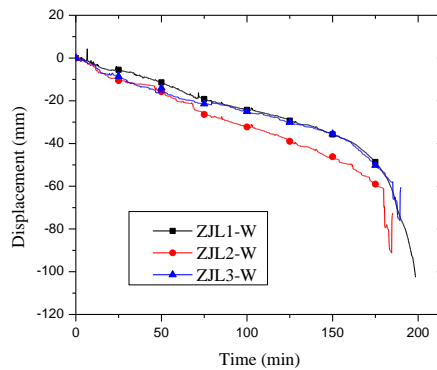

Fig. 7. Vertical displacement-time curve

3.3 Failure modes

The purpose of static load test for reference specimens at ambient temperature is as follows: firstly, to obtain the ultimate load bearing capacity and failure mode of specimen at ambient temperature; secondly, to determine the load size at the fire test; thirdly, to compare and analyze the results of the thermal coupling fire resistance limit test and failure modes with the normal temperature comparison specimens. The reference specimen CWZJL1-W had the expected diagonal cross-section tensile failure mode in the normal temperature static load test. The measured ultimate load Pu of specimen CWZJL1-W is 155kN, and the failure mode is shown in Fig. 8(a).

After reaching the fire resistance, the specimens were cooled naturally to normal temperature, and then the specimens were lifted out by the furnace covers for detailed appearance observation, recording and photographing.

As can be seen from Fig. 8(b), the bottom of the specimen ZJL1-W has a peeling effect of the concrete protective layer with a length of nearly 3m and the longitudinal steel bar is exposed. A large length of concrete cracking appears at the top of the beam along the longitudinal direction of the beam, exposing the upper edge of the steel bar. This longitudinal splitting crack should be caused by the thermal expansion of the concrete without the restraint of the stirrup. The vertical cracks of the specimen are mostly distributed in the pure bending section of the beam, the maximum crack width is about 6mm. while there are many through cracks along the loading point to the support in the shear-bending section, the maximum crack width is about 3mm.The failure mode of specimen CWZJL1-W is typical shear failure, while the shear failure of specimen ZJL1-W is not obvious. When the specimen ZJL1-W reaches the fire resistance limit, it exhibits the characteristics of bending failure. Therefore, the failure mode of the non-abdominal beam at ambient temperature may also present the form of bending failure under the thermodynamic coupling effect.

The specimen ZJL2-W has many vertical cracks in the pure bending section, while there is a through-slope crack with a maximum width of 20mm along the direction of the support and the loading point in the shear-bending section, as shown in Fig. 8(c). One of the main diagonal cracks extends from the support at a lateral direction of about 250mm toward the loading point, and the crack width is up to 4mm.Therefore, specimen ZJL2-W has the characteristics of obvious shear failure mode.

The specimen ZJL3-W has several vertical cracks with the width of mostly 1-3mm in the bending section, as illustrated in Fig. 8(c). However, there are many diagonal cracks in the shear-bending section, and most of the cracks extend along the support to the loading point. There are at least 5 obvious diagonal cracks in the shearing section on the east side of the specimen. The maximum width of the through diagonal crack is 21 mm. Therefore, the specimen ZJL3-W has characteristics of the shear failure, which is similar to the specimen ZJL2-W.
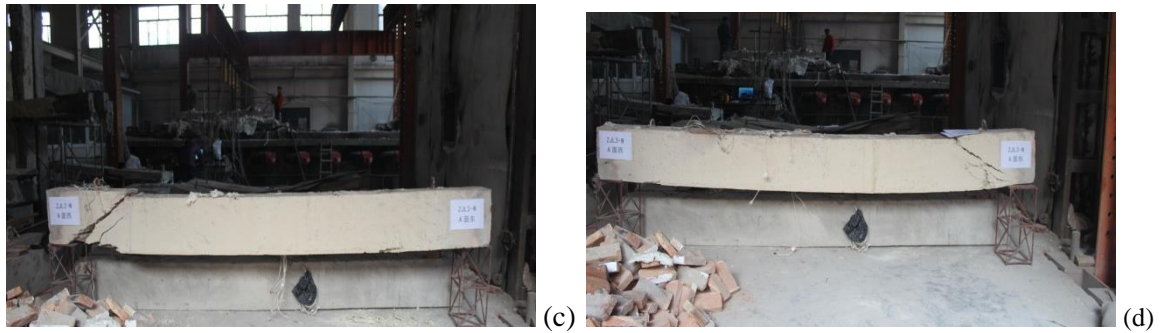

(a)

(b)

Fig. 8. Failure modes of specimens: a) CWZJLI-W; b) ZJL1-W; c) ZJL2-W; d) ZJL3-W

4   CONCLUSIONS

According to the experimental results, the conclusions can be drawn:

(1) The failure mode of the non-web reinforced concrete beam is the typical shear failure at ambient temperature. When the fire resistance reaches under thermodynamic coupling, the two specimens appear the shear failure mode, while one specimen shows the bending failure mode.

(2) Under the thermodynamic coupling, the larger the load ratio, the smaller the measured fire resistance limit of the non-web reinforced concrete beam.

(3) The vertical deformation rate of the no-web specimens near failure time increases rapidly. The damage is sudden near the fire resistance limit, and the larger the load ratio, the more pronounced this suddenness.

ACKNOWLEDGMENTS

REFERENCES

[1] Xiao J. Z., Li J., Sun Z. P. (2001). *Review of studies on the fire-resistance behavior of HPC structures* [J]. Industrial Construction, 2001, 31(6):53-56.

[2] Zhang Z. M., Ye Z. M., Liu T. (2007). *Research progress in fire resistance of reinforced concrete structures*. Journal of Natural Disasters, 2007, 16(1):127-135.

[3] Ren H. M., Xiao J. Z. (2004). *Investigation on state-of-the-art of fire-resistance design for concrete structures in China*. Concrete, 2004(11):15-17.

[4] Zhang W. Z. (2007). E*xperimental investigation on the mechanical performance of full-scale simple reinforced concrete beams under and afire elevated temperature*. Industrial Construction, 2007, 37(4):37-41.

[5] Lu Z.D., Zhu B. L., Zhou Y. H. (1993). *Experimental study on fire response of simple supported reinforced concrete beams*. China Civil Engineering Journal, 1993(3):47-54.

[6] Fu C. G, Wang G. Y., Wang Y. Z. (2009). *The Temperature field analysis of reinforced concrete frame joints under fire*. Journal of Shandong Jianzhu University,2009,24(01):1-8+17.

[7] Fu C. G., Song Y. M., Yin A. K., Liang S. T., Yam K. (2018). *Experimental study on shear bearing capacity of reinforced concrete beams under thermodynamic coupling*. Journal of Shandong Jianzhu University,2018, 33(05):1-10+23.

[8] Liu Fentao,Wo Bo,Wei Demin.(2009). *Failure Models of Reinforced Concrete Beams Strengthened with Carbon Fiber Sheet in Fire*. Fire Safety Journal, 2009, 44(7): 941-950

[9] NgAHB, MirzaM S, LieTT. (1990). *Response of Direct Models of Reinforced Concrete Columns*

Subjected to Fire. ACI Structural Journal, 1990, 87(3): 313-323

[10] Lie. T. T, Irwin. R. J.(1993). *Method to Calculate the Fire Resistance of Reinforced Concrete Columns with Rectangular Cross Section*. ACI Structural Journal, 90(1), 1993:52-60.

[11] Moetaz M. El-Hawary,Ahmed M. Ragab,Ahmed Abd El-Azim,Shadia Elibiari. (1996). *Effect of fire on flexural behaviour of RC beams*. Construction and Building Materials,1996,10(2).

[12] Moetaz M. El-Hawary,Ahmed M. Ragab,Ahmed Abd El-Azim,Shadia Elibiari.(1997). *Effect of fire on shear behaviour of RC beams*. Construction and Building Materials,1997,65(2).

[13] ISO 834: Fire-resistance tests: elements of building construction, part 1.1: general requirements for fire resistance testing. ISO- International Organization for Standardization, Geneva, Switzerland; 1999.

[14] General Administration of Quality Supervision, Inspection and Quarantine of People's Republic of China, Standardization Administration of the People's Republic of China . Fire-resistance tests-Elements of building construction [M]. GB/T 9978.8-2008. Beijing : Standards Press of China. 2008.14 .

EVALUATING COMPRESSIVE STRENGTH OF CEMENT PASTE AT ELEVATED TEMPERATURES USING METAKAOLIN

Nabil Abdelmelek[1], Eva Lubloy[2]

Budapest University of Technology and Economics, Budapest, Hungary

abdelmelek.nabil@epito.bme.hu[1] and lubloy.eva@epito.bme.hu[2]

ABSTRACT

This study investigated the effect of elevated temperatures on the mechanical and physical properties of cement paste. The main parameters of the test are the cement type, water to binder ratio and supplementary cementitious materials (SCMs). In which specimens were subjected to different maximum temperatures i.e. 50, 150, 300, 400, 500, 800 and 900°C, respectively. Using metakaolin as a supplementary material in cement paste showed significant effect on surface cracking appearance and residual compressive strength of high strength paste. Different dosages of metakaolin were used in this study 0, 3, 6, 9, 12 and 15 % mass as a replacement of cement. In addition to that, two w/b ratios were used 0.3 and 0.35. In total, 288 cubes have been tested to investigate the effect of previous parameters on the residual compressive strength of the paste.

1 INTRODUCTION

World cement demand and production are increasing dramatically especially in the developing countries [1]. One of the efforts to produce more environmental friendly concrete is to replace large amount of portland cement in concrete with supplementary materials in large volume such as ground-granulated blast-furnace slag and fly ash [2].Thus, decreasing environmental impact and enhancing economic benefits [3]. It is found that the incorporation of these materials in concrete enhances the strength and durability and plays an important role in the performance at fire [4].

Metakaolin (MK) showed excellent properties for producing high performance and high strength concrete (HSC) [5]. It is gaining popularity due to its consistent composition and production, light colour; appear to satisfy a number of economical, performantial and environmental requirements [6]. From other hand the use of MK enhances the strength and durability of concrete through three primary actions which are the filler effect, the acceleration of ordinary Portland cement (OPC) hydration and the rapid pozzolanic reaction with calcium hydroxide (CH) [7-9]. The compressive strength development, porosity and pore size distribution of MK concrete were found to be very close or superior to the silica fume concrete [8, 10]. It is essential that the fundamental behaviour of HSC at elevated temperatures to be understood to ensure that structural fire design involving HSC will be safe [11]. High strength paste during fire underwent to physical and chemical changes. They are summarized as follow in the *Table 1*:

Table 1. General behaviour of hardened cement paste at temperatures

Hydration Products	At 110–150 °C, alumina, ferric oxide, tri-sulfate and alumina, ferric oxide, mono-sulfate phases dehydrates [12]. portlandite or Calcium hydroxide – $Ca(OH)_2$ (CH) either disintegrates into lime (CaO) and water at 350 °C, or transforms into additional CSH gel [13]. Calcium silicate hydrate gel decomposes in the range of 400–600 °C, as concrete loses its main binding agent [14, 15].

Cracking and deterioration of microstructure	Above 100 °C, micro-cracks start to appear in the paste matrix [16]. Up to 93 °C, the cement paste tends to expand and then contracts till 491 °C [17]. This differential shrinkage is due to the expulsion of water vapours [18]. However, a proportional rise in porosity of paste is observed as the temperature elevates which is due to the deterioration of microstructure [19].

With respect to mechanical properties, Mansour et al. [20] studied the influence of metakaolin on compressive strength of mortar at ambient temperatures. Specimens were prepared with 10%, 20% and 30% MK as partial replacements of OPC. Results showed that among three replacement levels, 10% MK was the highest compressive strength at all ages. Dinakar et al. [5] studied the effect of incorporating MK on the mechanical properties of high strength concrete with w/b ratio of 0.3. they used cement replacement of 5, 10 and 15%. Concluding that 10% replacement was the optimum dosage. Khatib [21] studied the incorporation of MK up to 20% replacement in concrete with 0.3 w/b ratio, MK with 15% replacement shows the optimum replacement as far as compressive strength concerned. Hamdy et al. reported that pozzolanic cement paste having 5% MK gives higher compressive strength values than those of OPC or the other pozzolanic cement pastes. In addition to that 5 % MK acts as nucleating agent which accelerates the hydration of OPC [22].

From other hand, Morsy et al. [23] evaluate the performance of mortars with and without MK exposed to elevated temperatures up to 800 °C. OPC was replaced with MK replacements 0%, 5%, 10% 20% and 30%.Test results indicated that MK improves the compressive strength before and after exposure to elevated temperature indicating that the 20% cement replacement of MK is the optimum percentage. However, Poon et al. investigated the performance of MK at elevated temperatures [24]. They found that concrete with high replacement of MK (20%) suffered higher loss in strength at all temperatures and suggesting that severe durability loss occur at elevated temperatures.

2 EXPERIMENTAL DETAILS

An experimental program was designed to investigate the residual properties of MK hardened cement paste subjected to temperatures up to 900 °C. Major parameters of our study were the different dosages of MK of the binder (as replacement of cement) and the value of maximum temperatures. In the experiments, specimens were exposed to target maximum temperatures and then air cooled down to room temperature at 20°C before testing.

Table 2. Experimental matrix with detailed varied parameters

Water to binder ratio	
0.3	0.35
MK-0 **%**	MK-0 **%**
MK-3 **%**	MK-3 **%**
MK-6 **%**	MK-6 **%**
MK-9 **%**	MK-9 **%**
MK-12 **%**	MK-12 **%**
MK-15 **%**	MK-15 **%**

2.1 Materials

Two Ratios of water to binder (w/b) are used. In addition to 2 g/kg of liquid superplasticizer (GLENIUM® C 300 (AT)) was applied also for each mixture. Cubic form cement paste specimens were used with dimensions of 30 mm sides for compressive strength test.

Portland cement (CEM I 52, 5 N) was used. Metakaolin (Metaver N) was used as supplementary material.

312

2.2 Curing and heating regimes

The way of mixing was to mix dry binder (Cement + Metakaolin) during 30 seconds to ensure homogenous mixing. All amount of Water with superplasticiser were added and mixed with ¾ of binders. In addition, the remaining amount was gently added. After that the fresh paste was poured into 30 mm cube (24 cubes per mixture) and vibrated for 1 min to remove air bubbles. The specimens were demolded 24 h after the casting and placed in a water tank. After 7days of water curing, they were transferred to an environmental chamber maintained at 20 °C and 65±5 % relative humidity. It was then naturally cooled down in laboratory conditions. The parameter combinations resulted 12 mixtures are shown in Table 2. All 288 specimens from each mixture comprised eight groups according to different temperatures. all groups were tested at the age of 90 days. In which the first group was tested directly in ambient temperature to determine the strength after curing. The second, third, fourth, fifth, sixth, seventh, and eight groups were tested after three hours exposure at temperatures, 50 °C, 150 °C, 300 °C, 400 °C, 500 °C, 800 °C and 900 °C respectively, During the heat load a program controlled electric furnace was used. The heating rate was set at 4°C per minute to simulate both natural fire and oil/gas industry temperatures. Heating curve was similar to standard fire ISO 834 curve for buildings up to 800 °. Residual compressive strengths were measured for specimens with an ALPHA 3-3000S test machine, and then the average values of the measurements were chosen and analysed.

3 RESULTS AND DISCUSSIONS

3.1 At ambient temperature

The compressive strength values of OPC–MK Pozzolanic cement pastes are graphically represented as a function of MK replacements in *Fig. 1*. It shows that all the specimens made in this study are high strength.

For pastes with 0.3 w/b ratio, the mixture contains 3% of MK had exhibited lower strength with 77.54 MPa comparatively than the other MK percentages. On the other hand, it can be seen that the compressive strength was the highest for the mixture with 9% of MK achieving strength of 119.68 MPa. This clearly shows that the replacement level of 9 % was the optimum as far as the compressive strength is concerned. This is slightly less than the replacement levels of 15% and 10% reported in a previous study for the same w/b ratio of 0.30 [21, 5]. However, at this study the reduction in compressive strength for previous compared to MK 9% is explained as the result of a clinker dilution effect. The dilution effect is a result of replacing a part of cement by the equivalent quantity of MK.
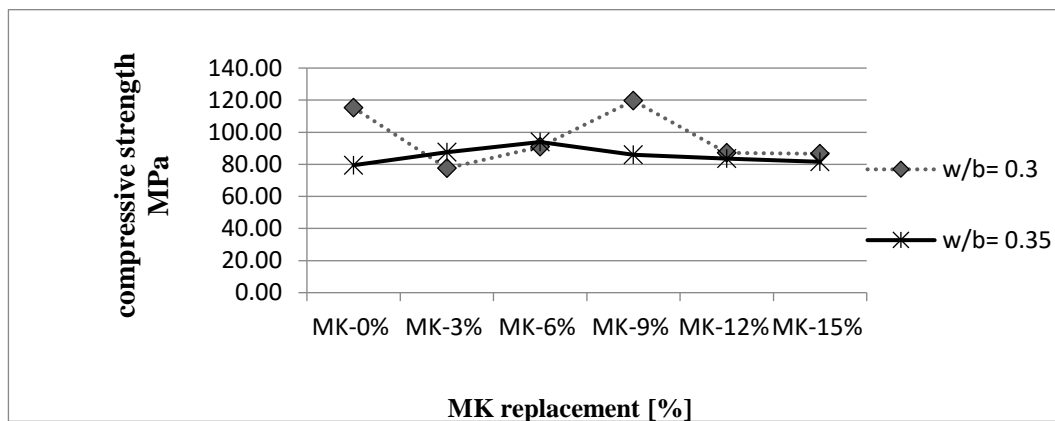

Fig. 1: compressive strength of different MK replacements with respect to w/b ratio

With time, the compressive strength differences between the MK mixtures and OPC concrete becomes smaller. This might be due to the fact that all cementitious materials reactions were close to completion, or had stopped; mainly because the reactions between MK and OPC mixtures were slowed down with time (Wild and Khatib 1997) [9].

At this study, short incremental replacement was used in order to increase the accuracy of the optimum dosages. In which, the higher compressive strength was achieved by 9% replacement which is slightly lower than that were had been gotten by the previous researchers. Nevertheless mixtures with 0.35 w/b ratio, Results showed Clear tendency of the optimal amount toward 6%. This is slightly higher than found by Hamdy [22]. MK acts as nucleating agent which accelerates the hydration, it is clear that the compressive strength of all cement pastes increases with increasing time of hydration up to 90 days. This is mainly due to the increase of the amount of hydration products such as CSH, CAH and CASH and their later accumulation within the available pores giving high strength [26].

3.2　At high temperature

The specimens showed different performance on surface cracking and residual compressive strength after exposing to high temperatures. It is presented and discussed herein.

3.2.1　Surface cracking

Evolution of surface cracks as a result of the elevated temperatures is presented in *Fig. 2.*

Hardened cement paste specimens during temperature loading undergo to chemical and physical changes leading to surface cracks. There were no macroscopic observable changes on the cubes surface up to maximum temperature 500 °C neither for OPC. However, the number and size of cracks strongly grew at thermal loads of up to 900 °C for mixtures with 0% MK content, and in less degree for mixes contain amount of MK.
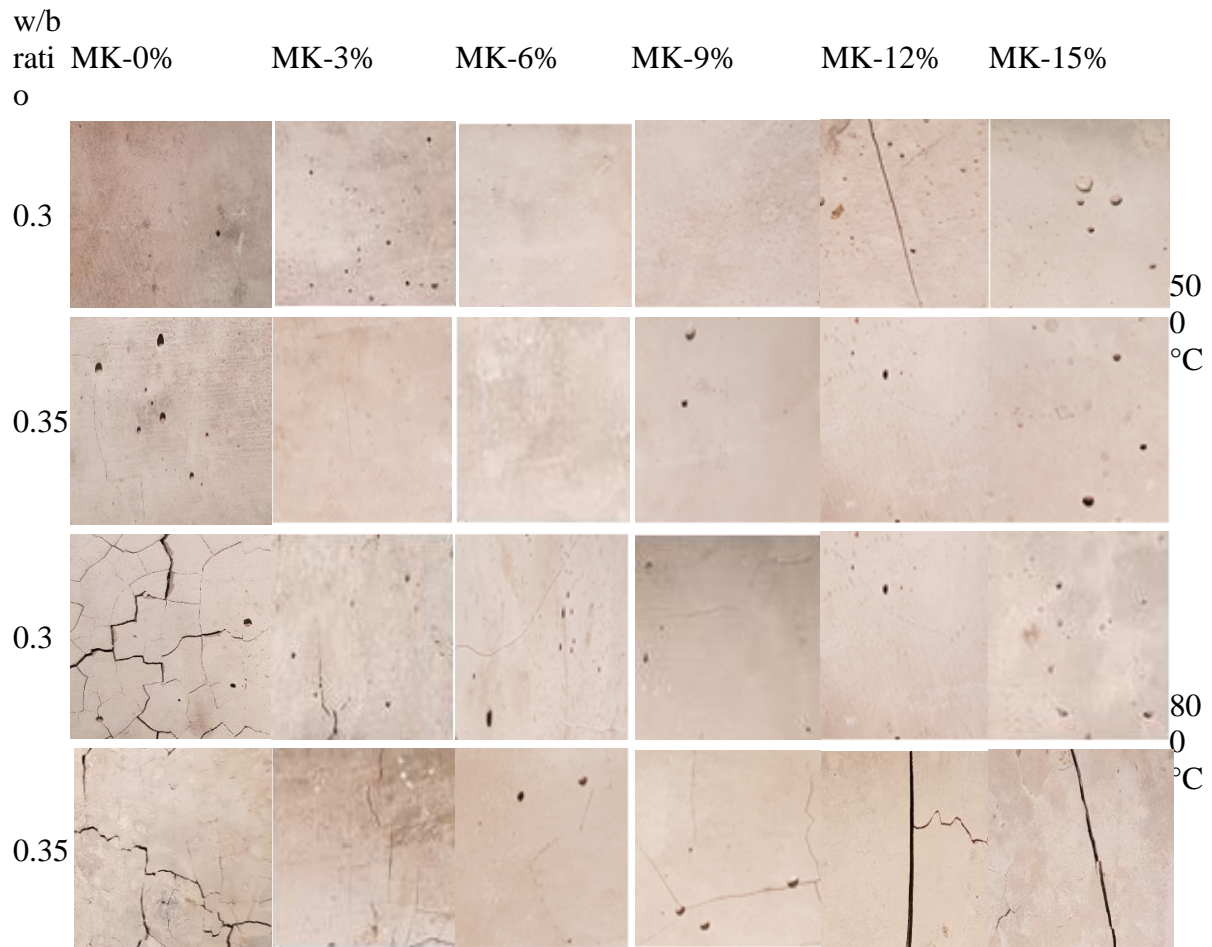
w/b ratio	MK-0%	MK-3%	MK-6%	MK-9%	MK-12%	MK-15%	
0.3							500 °C
0.35							
0.3							800 °C
0.35							

Fig. 2. Effect of different MK dosages on the Surface cracking with both w/b ratios at high temperatures

This can be attributed to the following for OPC, cracks largely caused by chemical processes occurring in the cement stone. It is well known that decomposition of portlandite which is most rapid at about 500 °C, as well as part of the C–S–H phases could decompose at different steps up to 800 °C [27]. Moreover, after cooling rehydration of CaO could considerably increase the extent of the crack development with further changes in volume. Humidity can cause 44 % of volume increasing due to rehydration of CaO [28]. Number of cracks increased as a function of time after cooling down. In addition to that, the number of cracks can also be explained with the different amounts of MK in the cement. Increasing MK or pozzolana content results in decreasing portlandite content of the cements). However, more portlandite is consumed by the higher amount of MK in the pozzolanic reaction (During the hydration process they consume part of the portlandite forming calcium-silicate-hydrates).

3.2.2 Relative Residual Compressive strength

The compressive strengths of the hardened cement paste specimens are presented related to the compressive strength measured at 20 °C called relative residual compressive strength (RRCS) as functions of the maximum temperature and the different MK content. The compressive strength values at 20 °C were in *Table 3*.

Table 3. Compressive strength of 20 °C

w/b ratio	MK-0%	MK-3%	MK-6%	MK-9%	12%	15%	
0.3	115.19	77.54	90.96	119.68	87.18	89.84	
0.35	81.80	87.50	93.90	86.02	83.57	81.57	

1. Samples prepared without MK:

The mixtures with 0 % MK exhibited the lowest relative residual compressive strength up to 400 °C of specimens prepared with 0.3 w/b after a thermal load of 500 °C is 76%. For 0.35 is 69%, of the values measured at a temperature of 20 °C. By increasing the thermal load up to 900 °C, the specimens still coherent and compressive strength tests could not be carried out especially for specimens prepared with 0.3 w/b ratios.
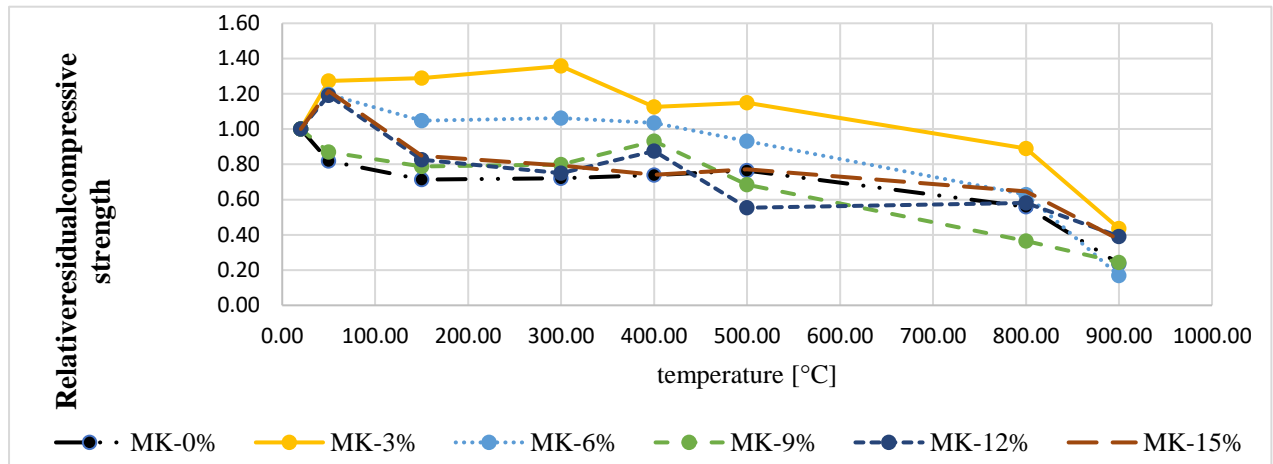

Fig. 3. Effect of the amount of MK on relative residual compressive strength of concrete at elevated temperatures with w/b= 0.3

2. Samples prepared with MK (w/b= 0.3):

The RRCS generals decrease gradually up to 500 °C heat loading. However it decreases as MK content increases. This was mainly due to ability of this material to densify the microstructure and eliminate the large pores; which led to the formation of internal stresses induced by build-up of vapour. For all mixtures the tendency of RRCS is almost similar, as can be seen in Fig. 3 In which by increasing temperatures the RRCS is decreased. However, by comparing the various types of the studied mixes it can be clearly observed that the matrix containing 3 % MK exhibited the highest RRCS (115%) among the six types of mixes at 500 °C. A slight reduction in the RRCS was observed at 800 °C, yet it is still close to that value at 20 °C (89 %).

Other researchers poon et al (2003), (2001) observed HSC with higher replacement of MK exhibited higher loss in strength at higher temperatures [10], they concluded relatively large pore area fraction available in high MK mixes at high temperature, which are suffered more than silica fume, pure OPC and fly ash concretes [6]. Furthermore dissociation of the CH crystals, incremental increase of pore pressure and the crystal transformation of quartz. Mercury intrusion porosimetry (MIP) test data showed an increase in porosity and average pore diameter with the rise in exposure temperature all of these reasons lead to internal cracking. The micro structural coarsening was found to adversely affect the impermeability of concrete at elevated temperatures and subsequently the durability. Moreover, the dense microstructure as reference to the high surface area in a function of replacement amount also lead to spalling in presence of vapour [10].

3. Samples prepared with MK (w/b= 0.35):

Mixtures prepared with w/b ratio 0.35 showed similar behaviour. *Figure 4* showed the relative residual compressive strength of the various mixes. MK with 9 %, showed less losses

of RRCS (76 %) than other mixes at 500%. By increasing the intensity up to 800 °C RRCS remains only 51 % of the value measured at a temperature of 20 °C.
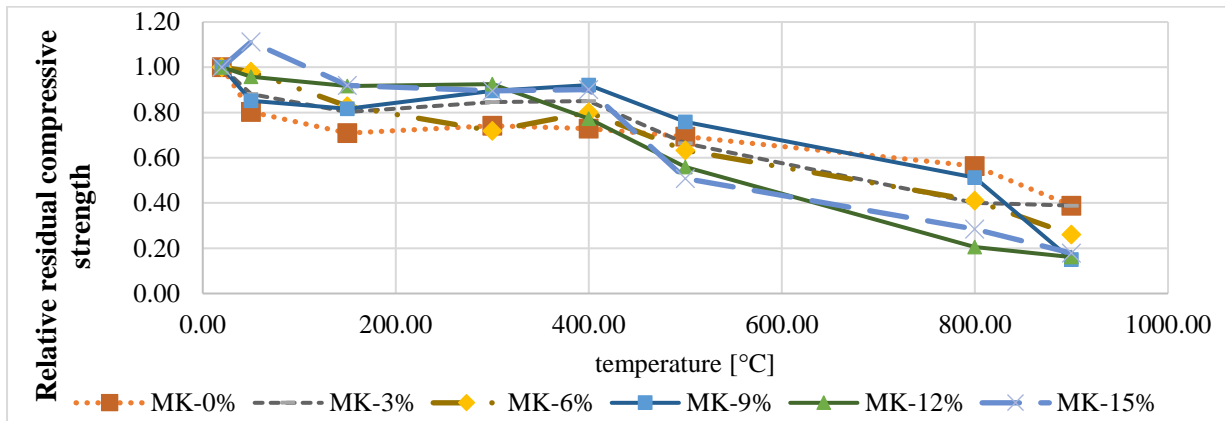

Fig. 4 Effect of the amount of MK on relative residual compressive strength of concrete at elevated temperatures with w/b= 0.35

Water makes differences in the results, as the w/c ratio increases; pore size is enlarged in addition to the pore volume and porosity increase [29]. The presence of MK, however, causes refinement in pore structure, in that pastes containing MK the packing effect decrease the threshold diameter and increase the percentage of small pores [30, 31]. The likelihood of spalling has been seen to increase with concrete that has a lower water to cement ratio and a lower permeability [32], thus the optimum amount shifted with increase the water content. That explains why MK 9 % was higher than the value related to 0.3 w/b ratio. The other mixtures (12 and 15 %) will more prone to spalling beyond 400 °C because with increasing MK content the porosity decreases as well *Fig. 2*. (Alaa el all.,[33] were obtained with the inclusion of 10% MK. the semi-crystalline CSH (CaO. $SiO_2.nH_2O$) overlapping with calcite ($CaCO_3$) was formed as hydration product. For CSH and calcium aluminosilicate (CASH), more importantly, This hydrothemal phase is known of its refractoriness during high temperature, This result is expected because the MK pozzolan contains a relatively large quantity of Al_2O_3, about 37% and low amount of CaO. However CASH increased with the inclusion of MK.

The results of compressive strength tests have correlated patterns of cracks. In which the highest number of cracks can be seen on the specimens prepared from pure Portland cement.

4   CONCLUSIONS

The main goal of the present study was to define the optimum dosage of MK. Different MK replacements were used i.e., 0, 3, 6, 9, 12 and 15% of the cement mass. The study also provided analysis of post-heating characteristics of hardened cement paste.

From the results, the following conclusions can be drawn:

− *Optimum dosages of MK, at ambient temperature, were 9 % and 6% in cement paste with w/b ratio of 0.3 and 0.35 respectively.*
− *According to the relative residual compressive strength, 3 % of MK content has the highest value among other ratio at high temperatures for w/b ratio of 0.3*
− *According to the relative residual compressive strength, 9 % of MK content has the highest value among other ratio at high temperatures for w/b ratio of 0.35*
− *MK has significant influence on surface cracks due to elevated temperatures. In which the more the paste contains MK the less the cracks occur*

− *Excessively increasing the amount of MK leads to increase the probability of spalling*
− *Different amounts of w/b ratio have significant effect on optimum MK dosage at both ambient and elevated temperatures*

ACKNOWLEDGMENT

REFERENCES

[1] Kimball S. M. (2016). *Menial commodity summaries 2016*. Department of the Interior, U.S. Geological Survey, 11202, < http://minerals.usgs.gov/minerals/pubs/mcs/2016/mcs2016.pd >.

[2] Rashad, A.M., (2015). *An investigation of high-volume fly ash concrete blended with slag subjected to elevated temperatures*. J. Cleaner Prod. 93, 47–55.

[3] Rashad, A.M., (2016). *A brief on blast-furnace slag and copper slag as fine aggregate in mortar and concrete based on Portland cement*. Rev. Adv. Mater. Sci. 44, 221–237.

[4] Phan L.T., (1996). Fire *Performance of High Strength Concrete: A Report of the State-of-the-Art.* Building and Fire Research Laboratory, National Institute of Standards and Technology, Maryland, 1996, pp. 5–25.

[5] Dinakar P., Pradosh K. Sahoo, and Sriram G. (2013). *Effect of Metakaolin Content on the Properties of High Strength Concrete.* International Journal of Concrete Structures and Materials Vol.7, No.3, pp.215–223, September 2013.

[6] Poon CS, Lam L, Kou SC, Wong YL, Wong R. (2001). *Rate of pozzolanic reaction of metakaolin in high performance cement pastes.* Cem Concr Res 2001; 31(9):1301–6.

[7] Caldarone M.K., Gruber K.A., and Burg R.G. (1994). *High-Reactivity Metakaolin: A New Generation Mineral Admixture.* Conc. Int., Vol. 16, no. 11, 1994, pp. 37–40.

[8] Wild, J.M. Khatib, and A. Jones, "Relative Strength Pozzolanic Activity and Cement Hydration in Superplasticised Metakaolin Concrete," Cem. Conc. Res., Vol. 26, no. 10, 1996, pp. 1537–1544.

[9] Wild S., Khatib, J. M. (1997). *Portlandite consumption of metakaolin cement Pastes and mortars. Cement and Concrete Research*. 27(1), 137–146.

[10] Poon CS. (2003). *Deterioration and Recovery of Metakaolin Blended Concrete Subjected to High Temperature.* Fire Technology, 39, 35–45, 2003 Kluwer Academic Publishers. Manufactured in The United States

[11] Bastami M., Chaboki-Khiabani A., Baghbadrani M., Kordi M. (2011). *Performance of high strength concretes at elevated temperatures*. Scientia Iranica A (2011) 18 (5), 1028–1036

[12] Harry F.W. Taylor. (1997). **Cement Chemistry** T. Telford (1997)

[13] Peng G.-F., Huang Z.-S. (2008). **Change in microstructure of hardened cement paste subjectedtoelevatedtemperatures**.Construction.Building.Material., 22 (2008),pp. 593599, 10.016/J.CONBUILDMAT.2006. 1.002

[14] Nadeem A., Memon S.A., Lo T.Y. (2013). **Qualitative and quantitative analysis and identification of flaws in the microstructure of fly ash and metakaolin blended high performance concrete after exposure to elevated temperatures.** Constr. Build. Mater., 38 (2013), pp. 731741, 10.1016/j.con build mat. 2012.09.062

[15] Kodur V.K.R., Sultan M.A. (2003). **Effect of temperature on thermal properties of high strength concrete.** J. Mater. Civ. Eng., 15 (2003), pp. 101-107, 10.1039/B910216G

[16] Demirel B., Keleştemur O. (2010). **Effect of elevated temperature on the mechanical properties of concrete produced with finely ground pumice and silica fume.** Fire Saf. J., 45 (2010), pp. 385-391, 10.1016/j.firesaf.2010.08.002

[17] Aydın S., Baradan B. (2007). ***Effect of pumice and fly ash incorporation on high temperature resistance of cement based mortars***. Cem. Concr. Res., 37 (2007), pp. 988-995, 10.1016/j.cemconres.2007.02.005

[18] Lea F.C. (1922). ***The resistance to fire of concrete and reinforced concrete***. J. Soc. Chem. Ind., 41 (1922), pp. 395R-396R, 10.1002/jctb.5000411814

[19] Ghosh S., Sarkar S., Harsh S. (1993). *Mineral Admixtures in Cement and Concrete*, 1993.

[20] Said-Mansour M., Kadri E.-H., Kenai S., Ghrici M., Bennaceur R. (2011). *Influence of calcined kaolin on mortar properties.* Constr. Build. Mater. 25(5) (2011) 2275–2282. doi:10.1016/j.conbuildmat.2010.11.017.

[21] Khatib, J. M. (2008). *Metakaolin concrete at a low water to binder ratio.* Construction and Building Materials, 22(8), 1691–1700.

[22] Hamdy El-Diadamony A, Ahmed A. Amer A, Tarek M., Sokkary b , Samir El-Hoseny. (2015). *Hydration and characteristics of metakaolin pozzolanic cement pastes.* Faculty of Science, Zagazig University, Zagazig, Egypt b Housing and Building National Research Center, Cairo, May 2015

[23] Morsy M. S., Rashad A. M., and El-Nouhy H. A. (2009). *Effect of elevated temperature on physico-mechanical properties of metakaolin blended cement mortar*. Structural Engineering and Mechanics, vol. 31, no. 1, pp. 1–10, Jan. 2009.

[24] Poon, C.S., Azhar S., Anson M., and Wong Y.L., (2003). *Performance of metakaolin concrete at elevated temperatures.* Cem. Concr. Compos., 25: 83-91.

[25] Nadeem A., Ali S., Memon b., Tommy Y. L. (2014). *The performance of Fly ash and Metakaolin concrete at elevated temperatures.* Construction and Building Materials 62 (2014) 67–76.

[26] Echart A., Ludwig H.M., Stark J. (1995). *Hydration of the four main Portland cement clinker phases*. Zem-Kalk-Gip 28 (8) (1995) 443–452.

[27] Guo X, Meng F, Shi H. (2017). *Microstructure and characterization of hydrothermal synthesis of Al-substituted tobermorite.* Constr Build Mater. 2017;133:253–60.

[28] Eurocode 2. Design of concrete structures. (2002). *Part 1 General rules structural fire design*. EN 1992-1-2:2002, February 25.

[29] Cook RA, Hover KC. (1999). *Mercury porosimetry of hardened cement pastes.* Cem. Concr. Res. 1999; 29: 933-943.

[30] Khatib J. M., Wild S. (1996). *Pore size distribution of metakaolin paste*. Cem. Concr. Res. 26 (1996) 1545 – 1553.

[31] Bredy P., Chabannet M., Pera J. (1989). *Microstructural and porosity of metakaolin blended cements*. Mater. Res. Soc. Symp. Proc. 137 (1989) 431 – 436.

[32] Chowdhury S. H. (2014). *Effect of elevated temperature on mechanical properties of high strength concrete.* in ST Smith (ed.), 23rd Australasian Conference on the Mechanics of Structures and Materials (ACMSM23), vol. II, Byron Bay, NSW, 9-12 December, Southern Cross University, Lismore, NSW, pp. 1077-1082. ISBN: 9780994152008

[33] Alaa M. Rashad , Dina M. Sadek. (2017). *An investigation on Portland cement replaced by high-volume GGBS pastes modified with micro-sized metakaolin subjected to elevated temperatures.* International Journal of Sustainable Built Environment (2017) 6, 91–101

REINFORCED-CONCRETE SLABS AT THE ULTIMATE LIMIT STATE AND IN FIRE

Pietro G. Gambarova[1] and Sara Morazzini[2]
[1]Politecnico di Milano, Milan, Italy
[2]MS Structural Engineer, Milan, Italy

ABSTRACT

An almost square heavy-duty reinforced-concrete slab is investigated before and after the addition of a stiffening beam along the only unsupported side. (The other three sides are fully or partially supported by underneath walls). The risk of fire and the limited thickness face to increasing loads (thickness = 35 cm and side = 8 m) required the free edge to be stiffened. Previous in-situ tests and finite-element analyses have confirmed the efficacy of slab strengthening under service loads. Here, the Yield-Line Method is adopted to quantify the extra-capacity provided by the stiffening beam, both at the ultimate limit state (ULS) and in fire. Three are the most interesting issues with design implications: (a) simple versus complex but more realistic mechanisms (at the ULS and in fire); (b) mixed slab-beam mechanisms versus slab-localized mechanisms under increasing temperature; and (c) fire-sensitivity ensuing from curtailment of the top reinforcement.

1   INTRODUCTION

Limited thickness, architectural adaptability and reduction of underneath obstructions (like columns and walls) make reinforced- and prestressed-concrete two-way slabs an ideal structural choice for the floors of multi-storey buildings, bridge decks and foundation mats *(slabs-on-grade)*, see – for instance – the classic books by Szilard (1974) [1], Hughes (1976) [2], Park and Gamble (2000) [3] and Ventsel and Krauthammer (2001) [4].

Two-way slabs, however, rouse suspicion in many structural designers for some unquestionable reasons: (a) shear and punching close to point-like and linear supports or to point-like loads; (b) corner hogging in simply-supported slabs and corner curling in slabs on grade; (c) discontinuities in the geometry (as in *stepped slabs*); (d) bar arrangement (which should be *aligned with the planes of the principal moments*); and (e) the complexity of mathematical analysis.

Though these critical issues can be overcome today thanks to increasingly-powerful numerical tools, designers always long for simple, dependable and intuitive design methods, which have the added benefit of yielding *reference results* helping the designer to check the numerical output. Such is the case of the Yield-Line Method (ACI 318M-14, 2015; *fib*, 2013; UNI EN 1992-1-2/EC2, 2005), which is among the methods based on materials rigid-plastic behavior and Limit Analysis (Jones and Wood, 1967 [5]; Kennedy, 2004 [6]; Nielsen and Hoang, 2010 [7]).

Combining the Yield-Line Method with other limit-analysis methods (such as the *strip method* for reinforcement design, see Hillerborg, 1996 [8], and Favre et al., 1996) [9]), and with elastic FE analysis is a very effective way to refine the design (Bamonte and Gambarova, 2009 [10]).

Within this context, after a concise presentation of the structural case including its elastic behavior (prior to and after upgrading), a heavy-duty RC slab is investigated according to the following steps: (a) possible yield-line patterns and failure mechanisms; (b,c) yield-line analysis at the ultimate limit state and in fire; and (d) role of bar curtailment in fire. For the loads reference is made to the Italian Highway Code (2012) [11], which is close to ASSHTO (2010) [12].

## 2   THE STRUCTURAL CASE: A HEAVY-DUTY RC SLAB

A heavy-duty slab belonging to a waste-water treatment plant close to Milan (Italy) was designed and built sixteen years ago to bear heavy trucks and dumpers (Figure 1a). The clear in-plan dimensions are 7.64 m in the north-south direction and 8.20 m in the west-east direction; the thickness is constant and equal to 35 cm. As shown in Figure 1b, the west and south sides rest on 30 cm-thick RC walls. The north side is (a) partially supported along the first and fourth quarter of its length, and (b) partially unsupported in the central half, but along the entire side there is a continuity with the extension of the slab in the north direction. The east side was originally free, but recently a stiffening beam has been added at the extrados (L section, Figure 1c). In this way, the safety level during the simultaneous passage of three axles of 12 t each in one direction, and two axles of 9 t each in the opposite direction has been increased. The variable load (54 t) is assumed to be uniformly distributed in the analysis, since the vehicles transmit their loads in ten points. Studs embedded in the slab guarantee the composite action between the beam and the slab. The horizontal part of the beam acts as a 2 m-wide sidewalk; a second sidewalk has been added along the west side (Figure 1b) to limit the traffic to the passage of a single vehicle at a time.
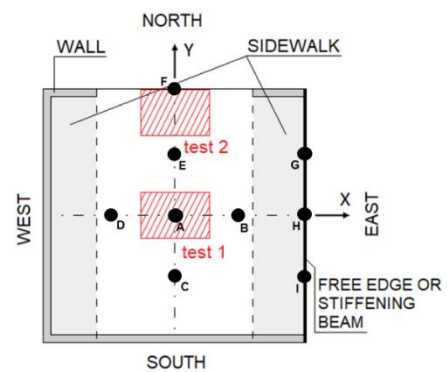
(a)   (b)
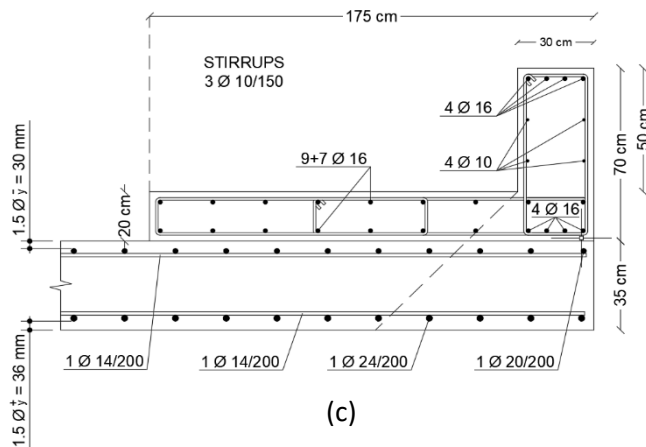
The section of the stiffening beam and the reinforcement are set out in Figure 1c, where the dashed line indicates the part of the slab, that works with the web of the beam.

Fig. 1. (a) Lateral view of the slab, with the unsupported side in the forefront (east side); (b) in-plane section with the positions of the test loads and of the LVDTs to measure the vertical displacement; and

(c) section and reinforcement (beam and slab).

Slab: f_{ck} = 25 MPa ; E_c = 31 GPa

Stiffening beam: f_{ck}* = 60 MPa ; E_c* = 39 GPa

Reinforcement: f_{yk} = 450 MPa; E_s = 200 GPa

3 PREVIOUS TESTS AND NUMERICAL ANALYSES

To check the efficacy of slab repairing and strengthening under the service loads, a heavy 4-axle truck (mass = 35600 kg) was moved onto the slab in order to have the two back axles (mass = 22163 kg) close to the centroid of the slab (Test 1) or close to the partially-supported north side (Test 2), see Figure 1b. The loaded area was 2.5 wide and 1.60 m long. Nine 10 mm-stroke LVDTs were placed under the slab.

The behavior of the slab was mostly elastic, since no spurious displacements affected the readings, thanks also to the very uniform ambient temperature during the tests (8°C).

In Test 1, the maximum displacement w_A (in the centroid of the slab) was 1.14 mm.

In the finite-element analysis (SAP 2000) the slab was discretized by means of 1600 shell-type elements, 40 in the x direction and 40 in the y direction; the thickness of the elements was t = 35 cm for most of the slab. (The east sidewalk was introduced by locally increasing the thickness of the slab; the west sidewalk was neglected, because of its minor contribution to slab bending).

The results of the numerical analysis (not reported in this paper) show that the best fitting of the experimental results is obtained with the west and south sides simply supported, and the north side partially clamped (close to the extremities) and partially free (in the central part).

4 SIMPLE VERSUS COMPLEX FAILURE MECHANISMS

The Yield Line Method is used to investigate slab behavior under an evenly-distributed load. Concrete resistance is taken for granted, while the plastic behavior of the sections is guaranteed by the plastic behavior of steel reinforcement. As usually assumed in traditional Limit Analysis based on plastic hinges and yield lines, the steel is introduced as a perfect rigid-plastic material.

Being a method based on the kinematic theorem of Limit Analysis, yield lines provide upper-bound values for the ultimate load by investigating the most consistent mechanisms and by minimizing – for each of them - the ultimate load in respect of the free parameters characterizing the yield-line pattern. The most probable mechanism is, therefore, the one

providing the minimum bearing capacity. Five mechanisms are considered (Figure 2), based on the following assumptions:

- the slab is assumed to be square ($a = b = 8$ m); its thickness $t = 35$ cm is increased to $t^* = 45$ cm in the evaluation of the own weight in the upgraded slab, to take care of the sidewalks and of the stiffening beam; the length of the central unsupported part of the north side is equal to $a/2$;

- the corner effects – with yield-line *bifurcation* or *fanning* - are neglected;

- the west/south sides are simply-supported or clamped (negative limit moment $m_L^- = 0$ or $\neq 0$);

- the simply-supported stiffening beam along the east side is introduced through its positive limit moment M_y^+; this side becomes *free* (free edge = FE) by putting $M_y^+ = 0$;

- the partially-supported north side characterized by flexural continuity is treated as simply-supported or clamped in Mechanisms I, II and III (Figures 2a,b,c), while partial support is assumed in Mechanisms IV and V (Figures 2d,e,f) with the central part free;

- in Mechanisms IV and V, the west-side constraint plays no role; in Mechanism IV, the east-side constraint likewise plays no role. (No rotations around the axis y in both cases).

- Contrary to Mechanisms I, II, III and IV, Mechanism V depends on three free parameters.

The expressions of the ultimate loads and the values of the free parameters minimizing the ultimate load can be found in Gambarova et al. (2018) [14] for Mechanisms I, II, III and IV. In Mechanisms I, II and V the ratio $k = M_y^+/(m_y^+a)$ between the positive limit moment of the stiffening beam M_y^+ and the total positive limit moment of the slab in the y-direction (m_y^+a) has the value 0.56 at 20°C. As for the sub-cases Va and Vb, their long and complex expressions for the ultimate load are reported in Morazzini (2018) [13] and will be the subject of a subsequent paper.

The limit moments per unit length developed by the reinforcement was evaluated according to the following relationships: $m_i^+ = 0.9\,f_yA_id_i^+$ and $m_i^- = 0.9\,f_yA_i{}'d_i^-$, where $i = x,y$; d_i^+, $d_i^- =$ effective depths of bottom/top reinforcement; A_i, $A_i{}' =$ sections per unit length of bottom/top reinforcement.

5   FAILURE MECHANISM WITH THREE FREE PARAMETERS

Mechanism V is a fairly obvious development of Mechanism IV in the event of a rather weak or nonexistent stiffening beam along the east side. Mechanism V, however, is characterized by three free (unknown) parameters (Figures 2e,f): α and β define the position of the central node where yield lines 1, 2 and 3 converge, and γ defines the origin of yield line 3. As indicated in Figures 2e,f, two subcases can be easily recognized: Va for *$0.5 \leq \alpha \leq 0.75$*, and Vb for *$0.75 < \alpha \leq 1$*.

I (a)   II (b)   III (c)

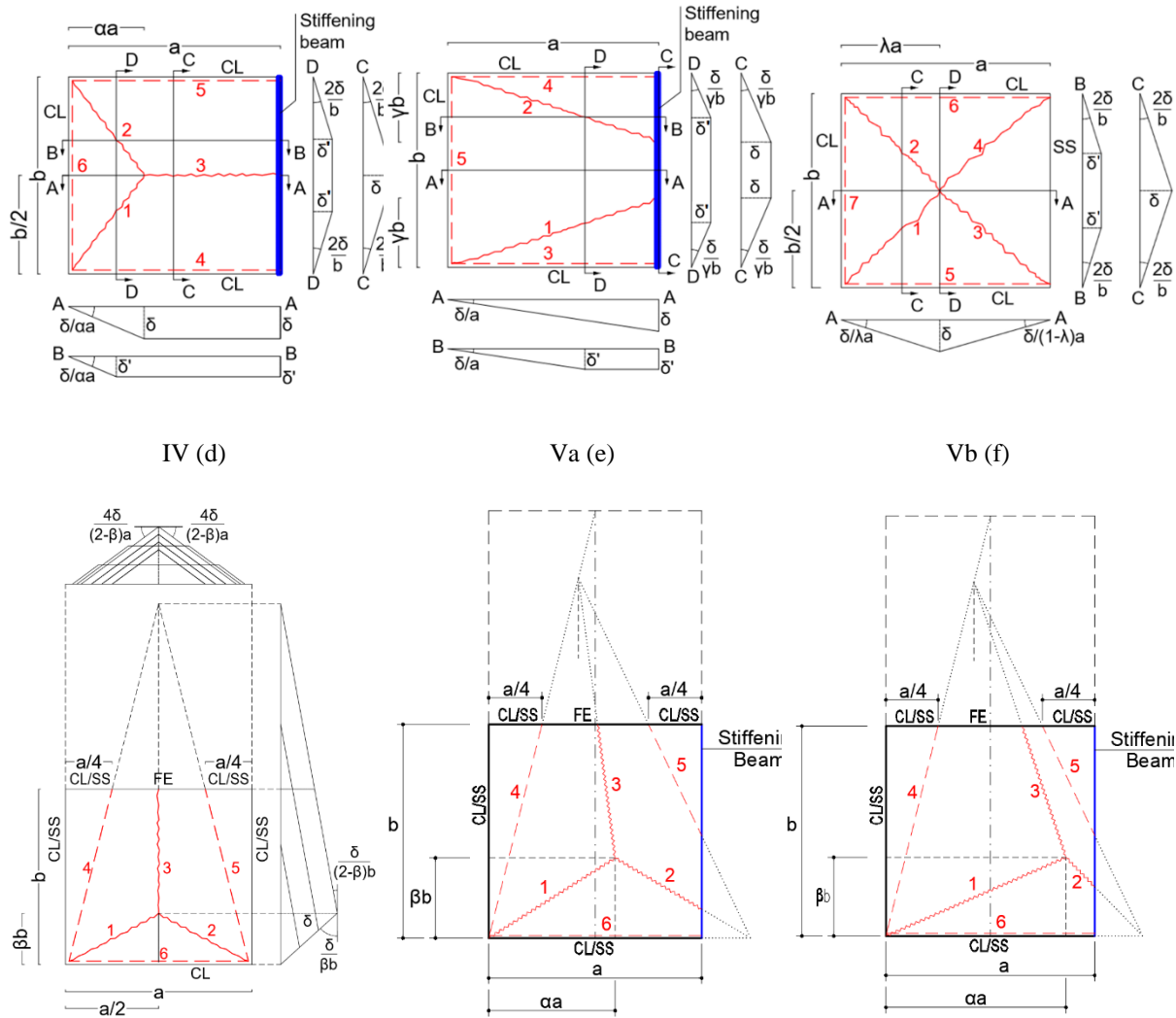IV (d)   Va (e)   Vb (f)

Fig. 2. Failure mechanisms and controlling key factors: (a) I: bending in the y-direction, with weak beam or no beam; (b) II: bidirectional bending, with weak beam or no beam; (c) III: bidirectional bending, with strong beam; (d) IV: bending in the x-direction, with strong beam; and (e,f) V: bidirectional bending, with weak beam or no beam; α,

β, γ = free parameters; note that in Va, $\alpha < 0.5$ has no practical interest; CL/SS = clamped/simply-supported side.
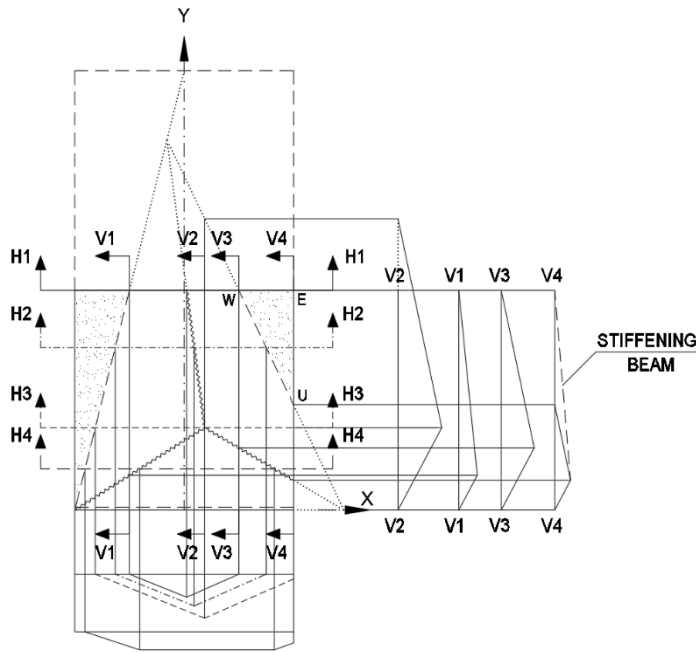
Fig. 3. Mechanism Va: virtual displacements.

With reference to Mechanism Va in Figure 2e, the first step was to carry out the kinematic analysis, with (a) the identification of the centroids of the sectors and the evaluation of their displacements; (b) the formulation of the external work L_e performed by a uniformly-distributed load; (c) the evaluation of the rotations astride each yield line (*x*- and *y*-components); and (d) the formulation of the internal work L_i performed by the limit moments (*x*- and *y*-components) developed by the plasticized reinforcement astride each yield line. All the details are given in Morazzini (2018) [13], since the three unknown parameters α, β and γ make the expressions of the kinematic and static quantities quite complex.

The second step was the formulation of the ultimate load $p_u(α, β, γ)$, and the third step the minimization of p_u to determine the set of values of α, β and γ, which define the most probable mechanism and the ultimate bearing capacity p_u^* of the slab.

The minimization was performed numerically by varying the values of α, β and γ within the ranges: *0.5 ≤ α ≤ 0.75* or *0.75 < α ≤ 1; 0 < β ≤ 1*, and *0 < γ ≤ 1*; the increments were 0.05 for α, 0.025 for β and 0.0325 for γ. In the square slabs (Figure 3), as well as in the rectangular slabs with *a/b = 0.5* (not presented in this paper), the load p_u^* exhibited two minimums associated with Mechanisms Va and Vb, respectively, but the former minimum was always (slightly) smaller than the latter. Whether this observation may be generalized is still open to investigation.

As indicated in the third point of the previous section, the clamping effect along a side is represented by the negative limit moment developed by the top reinforcement along the same side. Hence, if along a side the top reinforcement is absent or there is no continuity or overlapping of the top reinforcement with the reinforcement of the structural member underneath (for instance, a wall), the limit moment along the side is zero and the side is *simply-supported*.

Finally, in order to simplify the expressions of the kinematic and static parameters involved in the external and internal works, a number of dimensionless parameters was introduced:

$ω = m_y^-/m$; $μ = m_x^+/m$; $η = m_x^-/m$; $k = M_y^+/(m\,a)$, where $m = m_y^+$ (reference moment)

In drawing up this paper, Mechanism V has been checked in the limit cases α = 0.5 (where Mechanism Va coincides with Mechanism IV, and must yield the same results in terms of bearing capacity p_u^*) and α = 0.75 (where Mechanisms Va and Vb coincide).

Note that in all the analyses performed on Mechanism V, the contribution of the top reinforcement along the yield line W-U (Figure 3) was neglected because the *rigid cantilever*

WEU - while providing a supporting action - can hardly provide a resisting moment. Note also that the kinematics of the stiffening beam was introduced in a simplified way (dashed line in Figure 3).

6   ULTIMATE LIMIT STATE

The ultimate bearing capacity p_u* was evaluated in accordance with the five failure mechanisms, and comparisons were made with the design ultimate load p_{ud}:

$p_{ud} = p_p \, \psi_p + p_v \, \psi_v = 23.6/26.8$ kN/m^2 (before/after strengthening, dashed/full lines in Figure 4)

where p_p (perm. load) = 8.6/11.0 kN/m^2 ; p_v (variable load) = 8.3 kN/m^2 ; $\psi_p = 1.3$; $\psi_v = 1.5$.

The values of the reference limit moment and of the parameters adopted in the analysis are:

$m = m_y^+ = 241$ kN m/m, where the design strength at yielding has been introduced for the reinforcement ($f_{yd} = f_{yk}/\gamma_s$ with $\gamma_s = 1.15$); net cover of the bottom bars $c = 36$ mm.

$\omega = 0.713$; $\mu = 0.319$; $\eta = 0.330$; $k = 0.56$

In Figure 4, the bearing capacities provided by the five mechanisms are reported, in the event of absent or totally ineffective top reinforcement. Note that q_u stands for both p_{ud} and p_u*.

The bottom segmental curve refers to those situations in which the stiffening beam is absent (Mechanisms I , II and V). By contrast, the top segmental curve refers to those situations in which the stiffening beam is in place (Mechanisms I, II and V). In Mechanisms III and IV the stiffening beam plays no role, as the east side is assumed to remain straight and undergoes no virtual displacements.

Note that (a) adding the stiffening beam is always beneficial (except in Mechanisms III and IV); and (b) Mechanism V is always the strongest among the stiffened/unstiffened mechanisms (apart from Mechanism IV), something that was unexpected, since Mechanism V is definitely the most realistic one (at least by intuition) and as such should involve the minimum of internal work.
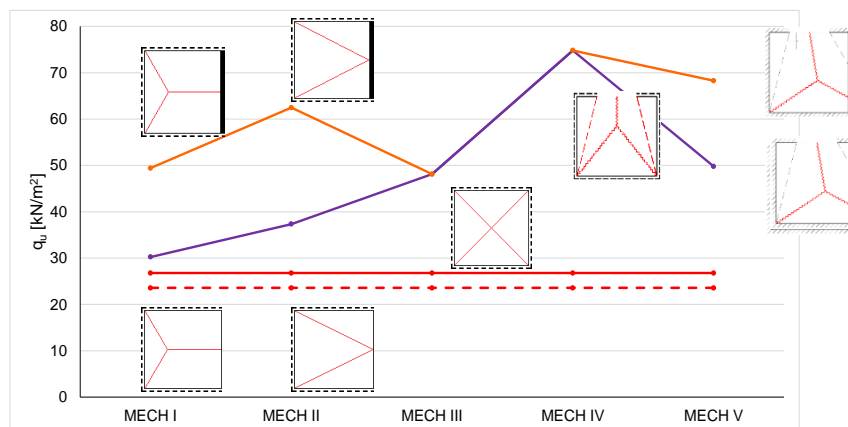

Fig. 4. Ultimate bearing capacities (p_u*) and ultimate design loads (p_{ud}, dashed and full horizontal lines) before and after the addition of the stiffening beam along the east side, respectively.

7 SLAB IN FIRE

The bearing capacity $p*^{fire}$ under the standard fire ISO 834 (Buchanan and Abu, 2017 [15]) was evaluated for the five mechanisms and comparisons were made with the design load in fire p_d^{fire}:

$p_d^{fire} = p_p + p_v^{fire} = 16.9/19.3$ kN/m^2 (before/after strengthening)

where p_p (permanent load) = 8.6/11.0 kN/m^2 ; p_v^{fire} (variable load in fire) = 8.3 kN/m^2 ;

The values of the reference limit moment and of the parameters adopted in the analysis are:
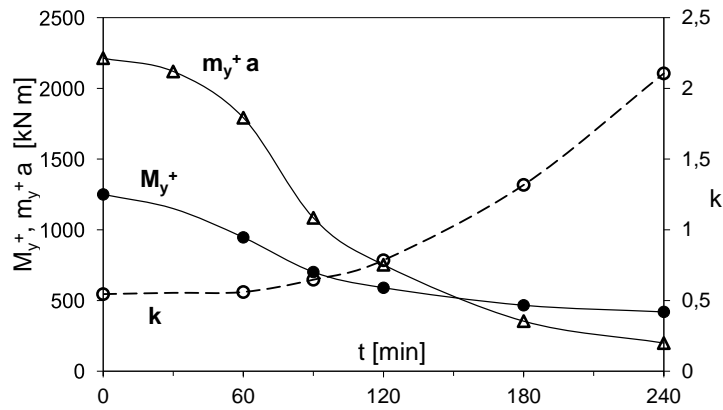
$m = m_y^{+fire} = 277$ kN m/m, where the characteristic strength at yielding has been introduced for the reinforcement ($f_{yk}^{fire} = f_{yk}/\gamma_s^{fire}$ with $\gamma_s^{fire} = 1$); net cover of the bottom bars reduced to $c* = 10$ mm (to take care of possible infringements of construction tolerances and to enhance fire effect);

$\omega = 0.713$; $\mu = 0.319$; $\eta = 0.330$; $k = 0.56$ at 20°C (beginning of the fire; $t = 0$).

For the limit moments per unit length: $m^{+fire}(t) = 0.9 \, A_s^{fire} \, f_{yk}(20°C) \, d^{fire}$ and $m^{-fire}(t) = 0.9 \, A_s' \, f_{yk}(20°C) \, d'^{fire}$, where A_s^{fire} is the total steel section resulting from the reduction of the section of each bar A_j based on the ratio $f_{yk}(T_j)/f_{yk}(20°C)$; d^{fire} = effective sectional depth (positive bending, from the top fibers to the centroid of the reduced steel section); d'^{fire} = effective sectional depth (negative bending, from the centroid of the cold top reinforcement to the centroid of the reduced concrete section in compression). The top bars were assumed to be *cold* throughout the fire and the value 20 mm/h (see EuroCode 2 "Fire Design") was introduced for the penetration rate v_h of the 500°C isothermal line into the concrete, starting from the exposed surface (= intrados of the slab). For $f_{yk}(T)$ reference was made to the curve 1 of EuroCode EC2 (hot-rolled tension reinforcement with $\varepsilon_{s,fire} \geq 2\%$, given that in limit analysis there is no limit to steel elongation).

To obtain the response curves of the slab after adding the stiffening beam, the parameter $k = M_y^+(t)/[m_y^+(t) \, a]$ has to be introduced. In Figure 5, the parameter k is plotted as a function of fire duration t, as well as the resisting/limit moments developed by the y-oriented bars of the slab and by the beam, in agreement with the composite section of Figure 1c. Note that k more than quadruples at a fire duration of 4 hours, because the beam is definitely less sensitive to high temperature than the slab, thanks to the solid section of the beam, which efficiently protects the reinforcement.

In Figure 6 (where $p*^{fire}$ and p_d^{fire} are indicated with q_u), the bearing capacity corresponding to each of the five mechanisms is plotted as a function of fire duration, without (a) and with (b) the stiffening beam. In the former case, the weakest mechanism is Mechanism I (fire resistance = 95 minutes), while in the latter case Mechanisms I and III are equally probable (fire resistance = 133 minutes = +40%), which indicates that in fire adding the stiffening beam tends to move the failure mechanism from composite mechanisms (like Mechanism I) to slab-centered mechanisms (like Mechanism III), something justified by the increasing role of the stiffening beam in fire.

Fig. 5. Limit moments ($m_y^+ a$ for the slab, and M_y^+ for the beam) and their ratio (k), as a function of fire duration (ISO 834 standard fire).

Finally, curtailing the top bars by limiting their length can have a sizable effect on the bearing capacity (Figure 7, where p^{*fire} is indicated with p_u); for instance, curtailing the top bars as in Figure 7e can decrease the bearing capacity by more than 20% at a fire duration of 120 minutes (Case ▲ compared with Case △). Note that, in Figure 7, the reduction of d'^{fire} because of concrete deterioration in compression has not been introduced.
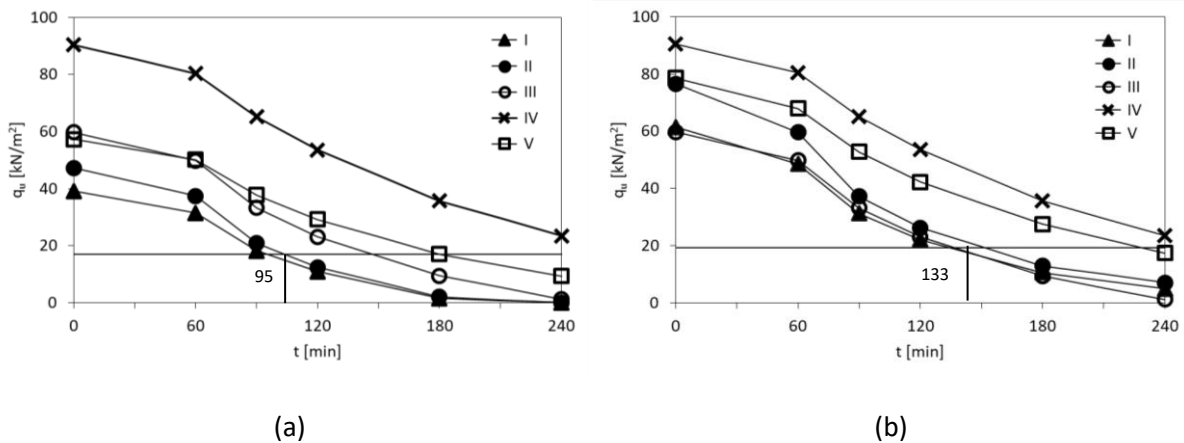

(a)

(b)

Fig. 6. Bearing capacity as a function of fire duration for the simply-supported slab (no or ineffective top reinforcement): east side (a) free; and (b) stiffened.
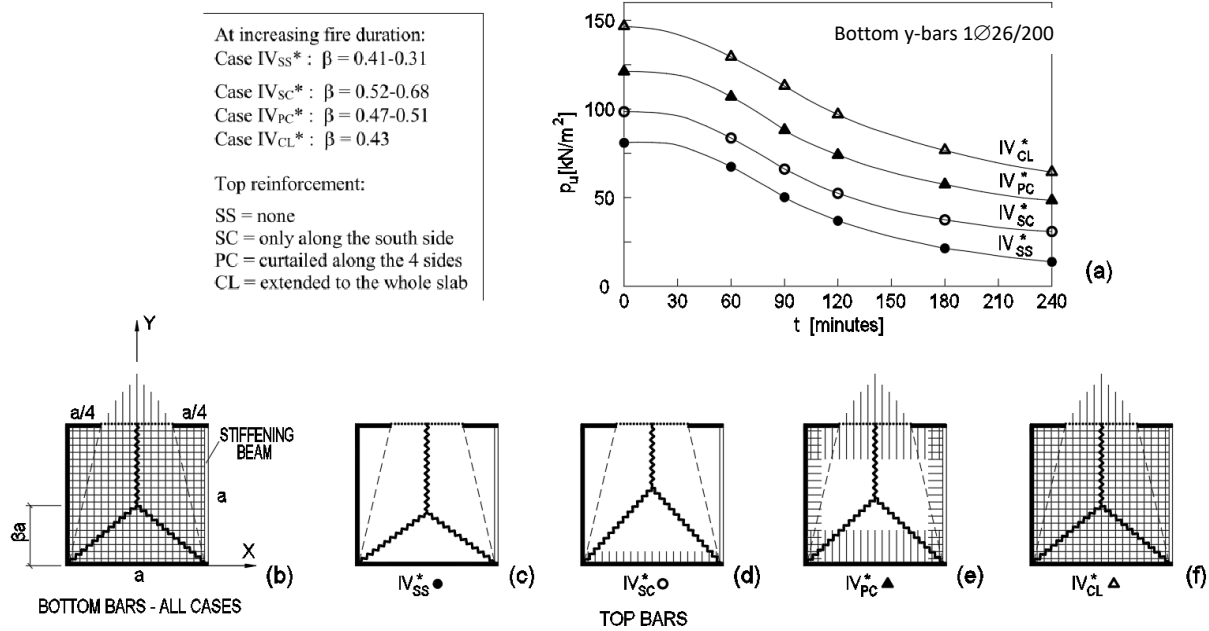
328

Fig. 7. Bearing capacity of a square slab in fire (a), with uniformly-distributed bottom bars (b) and curtailed top bars

(c-f): no top bars ● (c); top bars effective only along the south side ○ (d); top bars extended to ¼ of each supported side ▲ (e); and top bars extended to the entire slab △ (f); t = fire duration (standard ISO 834 fire).

8 CONCLUDING REMARKS

The heavy R/C slab investigated in this paper shows once more the benefits offered by Limit Analysis (in the form of the Yield-Line Method), especially in the case of 2D structures with mixed boundary constraints, where each single constraint often plays a hardly-quantifiable role.

Simple and apparently less realistic mechanisms are shown to be more probable than complex and more realistic mechanisms, a welcomed aspect, as in the latter case the increasing number of free parameters makes it very time-consuming to evaluate the bearing capacity.

Extending the Yield-Line Method to fire conditions shows that adding stiffening beams along free sides tends to increase the probability of *slab-related mechanisms* compared with *coupled slab-beam mechanisms*, because thin slabs are more heat sensitive than solid beams, where the bottom reinforcement is offered extra protection by the generally larger concrete covers.

In fire, top bars play a crucial role, thanks to the protection offered by the thickness of the slab. Curtailing these bars, however, should be performed with care, especially when negative inclined yield lines diverge from the corners of the clamped sides and insufficiently-anchored top bars beyond these yield lines might be unable to fully develop their limit/plastic moment.

Last but not least, elastic analysis and/or in-situ tests are always welcome as a tool to provide preliminary information on the most realistic failure mechanism and on constraints effectiveness.

REFERENCES

[1] Szilard R. (1974). Theory and Analysis of Plates: Classical and Numerical Methods. Prentice Hall, N.J.

[2] Hughes P. (1976). Limit State Theory for Reinforced Concrete Design. Pitman Publishing Co.

[3] Park R. and Gamble W.L. (2000). Reinforced Concrete Slabs. John Wiley & Sons, Inc., New York.

[4] Ventsel E. and Krauthammer T. (2001). Thin Plates and Shells: Theory, Analysis, and Applications. Marcel Dekker Inc., New York.

[5] Jones L.L. and Wood R.H. (1967). Yield-Line Analysis of Slabs. V. 5. Elsevier Publishing Co.

[6] Kennedy G. and Goodchild C.H. (2004). Practical Yield Line Design. The Concrete Centre, Blackwater – Camberley (Surrey, U.K.).

[7] Nielsen M.P. and Hoang L.C. (2010). Limit Analysis and Concrete Plasticity. CRC Press.

[8] Hillerborg A. (1996). Strip Method Design Handbook. E & FN SPON.

[9] Favre R., Jaccoud J.P., Koprna M. and Radojicic A. (1996). Dimensionnement des Structures en Béton – Dalles, Murs, Colonnes et Fondations. Traité de Génie Civil, V.8, PPUetR, Lausanne (Switzerland).

[10] Bamonte P. and Gambarova P.G. (2009). Analysis at the Ultimate Limit State of a R/C Slab Supporting Desiccated-Sludge Silos. European J. of Environmental and Civil Engineering, V.13, No.6, 685-706.

[11] Italian Code for Highways (2012). Limit Mass – Clause 62. Ministerial Decree, January 24, 2012, No.1.

[12] AASHTO (2010). Bridge Design Specifications – Clause 3.6.1.2, 5th Edition.

[13] Morazzini S. (2018). RC Slabs with Mixed Constraints: Ultimate Limit State and Fire (in Italian). MS Dissertation defended on July 25, 2018, at the Politecnico di Milano, 162 p.

[14] Gambarova P.G., Lo Monte F., Mousavi S.M.S., Torregiani P.L. and Zecchillo M. (2018). Repairing and Upgrading of a Heavy-Duty RC Slab. ACI SP 326 on "Durability and Sustainability of Concrete Structures".

[15] Buchanan A.H. e Abu A.K. (2017). Structural Fire Design for Fire Safety/Edition 2. Wiley Pub.

STEEL FIBERS ON SHEAR STRENGTH OF CONCRETE AT AMBIENT AND ELEVATED TEMPERATURES

Naser S. Alimrani and György L. Balázs
Corresponding author email: alimrani.naser@epito.bme.hu
Budapest University of Technology and Economics (BME), Budapest, Hungary.

ABSTRACT

This paper experimentally investigated the behaviour of concrete at elevated temperatures in terms of shear deterioration using steel fibres. Forty five specimens of push-off model were used in which three samples for each category of maximum temperatures. Five maximum temperatures have been investigated i.e. 20, 150, 300, 500 and 700 °C.

The main objective of this research is to investigate the effect of steel fibres on the behaviour of concrete at different maximum temperatures in terms of shear failure. Using steel fibres has demonstrated significant effects to enhance the ductility of the shear deterioration at ambient temperature. Thus three main categories have been used at this paper plain concrete, 40 kg/m³ and 80 kg/m³. It is worth to mention that, due to the fact that this test is still currently being implemented, not all of the abovementioned results are addressed at this paper.

1 INTRODUCTION

Most structural fire investigations have been focused on the flexural behaviour of beams and slabs or on the axial performance of columns. Only little attention has been directed at studying the shear performance of concrete in fire [1]. However, many experimental results showed shear-failure tendencies especially when the elevated temperatures is provided [1-5]. Walraven introduced the so called "missing link" in the mechanism of transmission of forces across cracks. He evaluated the direct transfer of forces between the rough concrete crack faces, generally denoted by the term "aggregate interlock" [4,10]. Over time, it has been modified and has given rise to the new models, which emerge when incorporating new parameters, such as adhesion, aggregate interlock, dowel action, or axial restraint, as stated in some state-of-the-art reports, for example, the ASCE-ACI Committee 426 (1973) and 445 (1998) [5] and [6].

The push-off test is a non-standard, but widely recognized, test used to study the mechanisms of shear transfer. This test has the advantages of being relatively small, inexpensive, easy to perform, and not needing any highly specialized pieces of testing equipment [6]. Anderson [7] was one of the first to experimentally test push-off specimens. He used two different concrete mixes. With a compressive strength of 20.68 MPa and 51.71 MPa to obtain the mechanical properties with respect to shear. Using some results from Anderson, Hanson [8] developed, based on push-off tests, previous expressions involving parameters of rough interfaces and properties of the reinforcements. Birkeland and Birkeland [9] were the first to propose a linear expression to evaluate the ultimate longitudinal shear stress of the concrete surface. From another hand, Mattock worked on push-off specimen's tests and developed shear stress expressions. Some of his remarkable works, both individually and collectively were published in the years between (1969) and (2001) [5,11].

Furthermore, many of other papers were concerned about *the influence of elevated temperatures*. Al-Owaisy [12] studied the influence of elevated temperatures on residual shear transfer strength. The conclusions indicate that shear transfer strength is affected significantly when exposed to elevated temperatures. The results also showed that shear

transfer strength of higher amount shear reinforcement specimens was higher than those of lower shear reinforcement ones, both before heating and after exposure to each particular temperature. Xiao et. al., [13] studied the influence of compressive strength of concrete in transferring shear across a crack. Results showed that a higher compressive strength HSC results in more brittle shear failure, irrespective of the elevated temperature. Nevertheless, the elevated temperature can reduce the shear brittleness. Results of Naus et al. (1976) illustrated that the shear strength was inversely proportional to the exposure temperature showing that shear transfer strength of concrete during fire can drop to 48% of its ambient strength showing also that light weight aggregate (LWA) concrete has better shear transfer performance during fire [1].

One of the most promising structural applications of steel fibres-reinforced concrete (SFRC) is the use of fibres as shear reinforcement or part of the shear reinforcement, due to the brittle nature of shear failure. This is of further importance when dealing with high-strength concrete (HSC), which is inherently more brittle than conventional concrete [14-15]. On the other hand, the failure mode changed from shear to simultaneous (shear and bending) failure for the beam containing steel fibres and no stirrup based on different compressive strength of concrete and the type of steel fibres [16].

2 EXPERIMENTAL PROGRAM

Forty five push-off specimens were cast and prepared to be tested. The specimens were cast in three different categories based on the amount of fibres. Category A contains no fibres, category B contains 40 kg/m^3 which is almost equivalent of 0.5% of the volume and category C contains 80 kg/m^3 which is the equivalent of 1% of the volume (*Table 1.*). Each category or category has a total number of fifteen specimens of push-off model. They are distributed over five limits of maximum temperatures i.e. 20, 150, 300, 500 and 700 °C in which each maximum temperature has 3 specimens. In addition to that, forty five corresponding prisms 7 x 7 x 25 cm^3 were cast and tested under each different maximum temperatures. Testing these prisms provided the results with the flexural strength of the mixtures as well as the residual compressive strength after exposed to elevated temperatures. Finally, three cubes of 150 mm sides for each category were tested at 20 ℃ for evaluating the compressive strength of the mix.

Table 1. General details of the specimens

Name	Fibres amount (kg/m³)	Elevated temperatures (°C)	Specimen`s ID (based on category`s name and temperature)
Category A	0	20, 150, 300, 500 and 700	A-20, A-150, A-300, A-500 and A-700
Category B	40	20, 150, 300, 500 and 700	B-20, B-150, B-300, B-500 and B-700
Category C	80	20, 150, 300, 500 and 700	C-20, C-150, C-300, C-500 and C-700

2.1 Materials and mix proportions

Table 2 summarizes the mix proportions of the concrete. Ordinary Portland cement was used (CEM I 52.5 N). Danube quartz gravel was used as coarse aggregate with size range 4 to 8 mm. Natural sand was used as fine aggregate with maximum size 4 mm. Dramix 5D was used as steel fibres with length 60 mm, diameter 0.9 mm and nominal tensile strength 2.300

N/mm^2. MasterGlenium 300, a second generation of polycarboxylic ether polymers was used as superplasticizer.

Table 2. mix proportions

Series	Fine aggregate (kg/m^3)	Coarse aggregate (kg/m^3)	Cement (kg/m^3)	Water (kg/m^3)	Superplasticizer (kg/m^3)	Fibres amount (kg/m^3)
Category A	829	1013	400	152	3.33	-
Category B	832	1006	400	152	3.33	40
Category C	817	999	400	152	3.33	80

2.2 Specimens preparations

Push-off specimens were cast in a 60 liter mixer then were formed in a rectangular metal molds (*Fig*. 1.b) with dimensions as in *Fig*. 1.a. Compaction phase followed the casting using electricalal table vibrator. Twenty four hours after casting, specimens were cured in natural water for seven days. Two notches, 4 mm width by 75 mm length, were cut using saw cut-off machine.
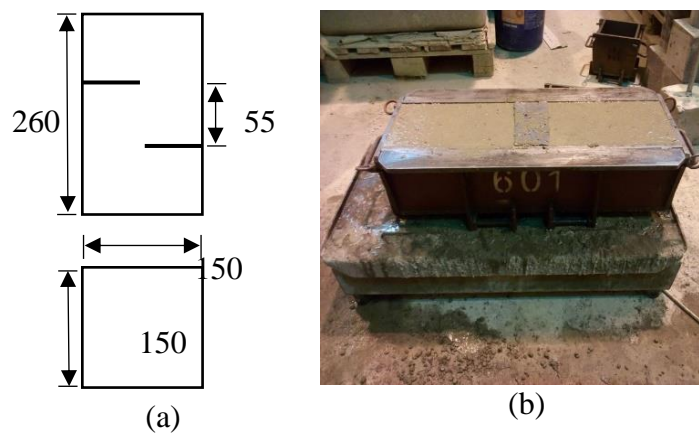

Figure 1: Different phases (a) push-off used dimensions and (b) metal mold of concrete and vibration

2.3 Elevated temperatures program

Following seven days of water curing, specimens were stored at laboratory conditions until 28 days. Groups A-20, B-20 and C-20 were tested at 20 °C, whereas the others were heated in an electrical furnace until the sample reached the target temperature. Then this temperature was kept for two hours. Afterward specimen was taken out to be air cooled for 24 hours before testing in the laboratory conditions. The specimens were heated slowly with a heating rate of 5 ºC/min to avoid steep thermal gradient. Two thermocouples were installed in the specimen surface and 50 mm deep. For temperatures of 500 and 700 °C, specimens were kept in a steel cage during heating to protect the oven from explosive spalling (*Fig*. 2).

Figure 2: Electrical oven used in heating the specimens, showing the specimen covered by steel cage and two thermocouples from inside the oven to outside

2.4 Push-off loading test

After 24 hours finishing the heating test, the push-off test was carried out using INSTRON testing machine with a capacity of 600 kN. The specimens were loaded in their vertical axis (*Fig.* 3) in displacement control with a rate of 0.06 mm/min. The load is applied through steel plates of 60 mm width and 40 mm thick at both sides (*Fig*. 3.a). Teflon sheets were placed between the loaded surfeces to compensate for nonparallel loading surfaces. Displacement values were measured by means of linear variable differential transformers (LVDTs), fixed horizontally for crack width (Fig 3.b) and vertically slip (*Fig* 3.a) on both faces of the specimen. All measurements were recorded continuously each half a second using software.
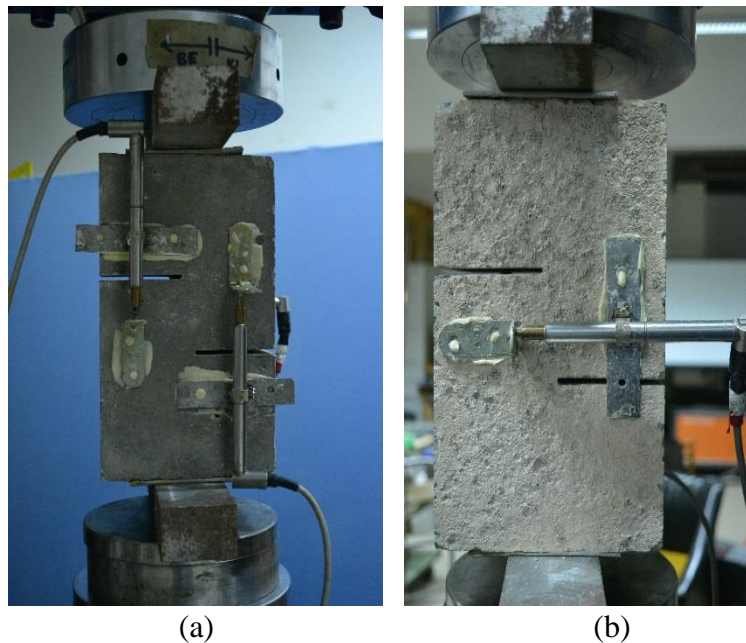

(a)   (b)

Figure 3: push-off loading test, (a) typical push-off loading test showing vertical LVDTs and (b) push-off loading test showing horizontal LVDTs

3 EXPERIMENTAL RESULTS

3.1 Thermal response

Thermocouples were used to measure temperature during heating on two locations: at the surface of the specimen and at 50 mm depth form the surface, respectively. *Figure* 4 shows the temperature measurements vs. time of two categories i.e. categorys A_700 and C_700, respectively. The oven temperatures was recoded paralelly. The figure shows a slight increase in temperatures in category C compared to category A. That can be attributed to the fact that category C conntains steel fibres, that has high properties of conductivity, unlike category A which has not. It should be noted here that the figure shows the increasing temperatures only until the temperature of the oven reaches 700 °C.
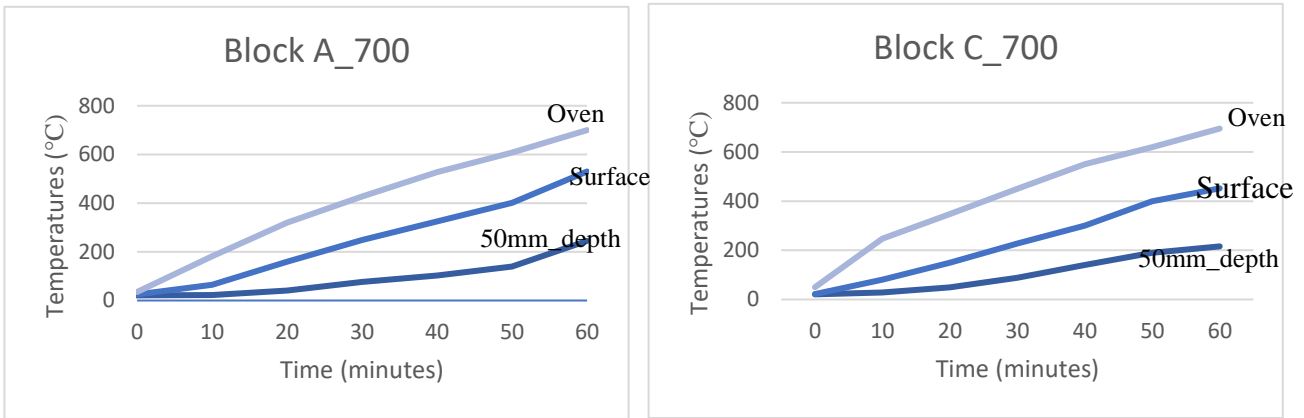

Figure 4: Temperatures of two categories of the push-off specimens in three different places i.e. oven, surface of the specimen and in 50 mm depth

Mass of the specimen was measured before heating and after. The mass loss is mainly due to two reasons. The first reason is the evaporation of free water during heating, the second reason is spalling by losing parts or the entire of the concrete surface. Since water to cement ratio was the same for all mixes, i.e., 38%, there was no significant differences between the three categorys as far as spalling is not concerened. *Figure* 5 shows the percentages of loses in mass of the push-off specimens due to elevated temperatures.
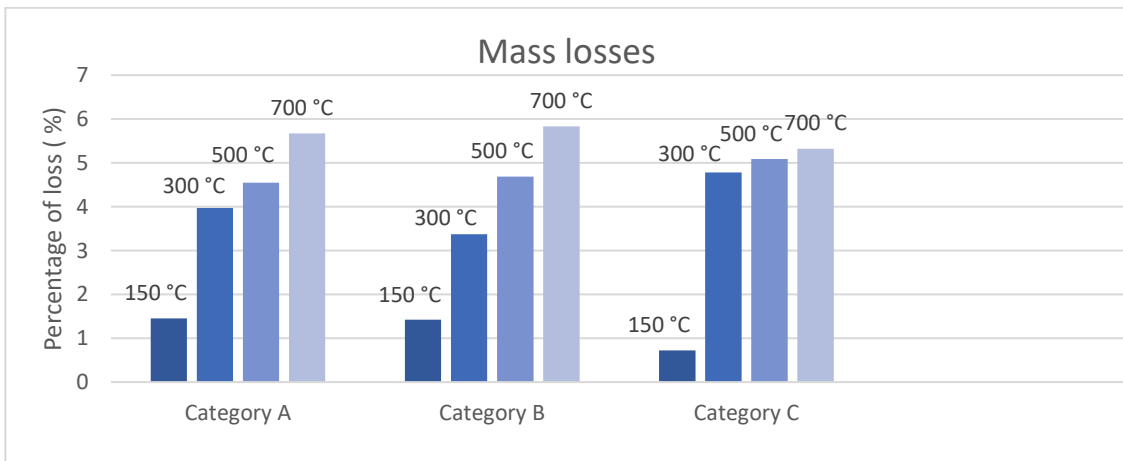

Figure 5: Percentages of losses in mass of the push-off specimensn (measuered before and after fire)

3.2 Mechanical properties

The nominal shear stress has been calculated from the following expression:

$$\tau_{u\,=}\,P_u\,/\,A_c$$

where Pu is the peak load and Ac is the shear plane area (B×Hs) which equals (150×5.5) mm². See *Fig.* 1 (a). Compressive strength is calculated by taking the average of the remained parts of the prisms after bending test. Tensile strength is measured by a derivation of the beam equation $f = Mc/I$. In the case of third-point loading, which is the loading usually employed

$$f_{ct,fl} = \frac{PL}{bd^2}$$

where $f_{ct,fl}$ = computed felxural-tensile stress at failure (modulus of rupture) in MPa. *P* is load at failure (in N). *L* is span length (mm). *b* is width of beam (mm). *d* is depth of beam (mm). On the other hand, for peak loads values, the average of maximum values for the three samples was calculated and reported in *Table* 3. The results show clear increase in mechanical properties including compressive strength, tensile strength and shear stress of concrete due to increasing the amount of fibres. The influence of temperature is not included at the table.

Table 3. Summary of varied experimental results

Specimen ID	Peak load P_u (KN)	Shear strengt τ_u (MPa)	Crack width (mm)	Crack slip (mm)	Compressive strength f_c (MPa)	Flexural-tensile strength $f_{ct,fl}$ (MPa)
A - 20	28.99	3.51	0.006	0.092	78.83	0.54
B - 20	114.89	13.93	0.018	0.059	90.62	0.74
C - 20	113.69	13.78	0.436	0.146	94.41	0.96

3.3 Shear stress–crack deformation curves

Shear stress, as mentioned before, is defined as $\tau_{u\,=}\,P_u\,/A_c$. For all push-off specimens, A_c is the same in which equals 5.5×150 mm². Crack slip and width are relative movement the shear faces in both directions vertically and horizontally, respectively. *Fig*. 6 shows force-crack slip and force-crack width for the three plain concrete categories. Generally, crack width and crack slip have similar results. This behavior was also reported by previous studies (Barragan, 2006). As far as steel fibres is concerned, ultimate shear stress (expressed in force) is increased by increasing the amount of steel fibres. Fig. 6 shows the influence of that by comparing the results between the corresponding reslults of A, B and C categories. The figure shows also the influence of the steel fibres in increasing the ductility of the mixures. the ductile behaviour of the mix is illustrated in the second part of the curves, after cracks occure. The degree of decline for the curves determine the ductile behaviour of the specimen. Generally, the degree of decline is less for the speciemens that have higher amount of steel fibres.
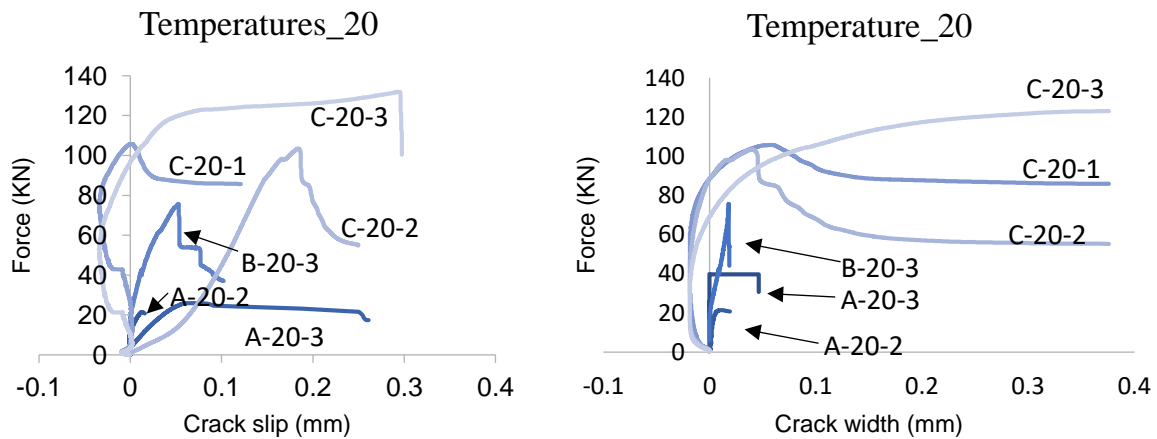
Figure 6: Shear stress-crack width and crack slip curves at 20 ºC

It is worth to mention that several results of crack slip and crack width showed minus deformation slightly before positive one (*Fig*. 6). The possible interpretation for that is the technical way of testing specimens. In which the specimen is set vertically headed on both sides with steel plates without any type of restrictions in horizontal direction. In such setting, the possibility of the specimen to rotate slightly at the beginning is likely to occur. To overcome such behaviour, many researchers (Echegaray-Oviedo, 2014) used an external restraint steel frame to confine the specimen.

3.4 Failure modes

The typical mode of failure in tested push-off categories can be seen in *Fig*. 7. For category A, the crack initiates at one of the notch faces, thus can be called as shear crack. Once the crack initiates, major propagation follows splitting the specimen from the shear plane into two parts completely. In some cases, the first crack occurs near the shear plane (called in literature as "secondary tensile crack"). However, the first crack does not control the failure to the end. Another crack follows at the shear plane to control the failure of the specimen spalling it to a completely two parts. The latter note has been recorded by previous researchers [14]. Mode of failure in plain concrete is significantly different from that of steel fibred. It shows also that the existence of the fibres controls the crack opening, at category C and less at category B. However, developing of the crack through the shear plane does not split the specimen. Some surface spalling occurs in the region around shear plane. *Fig*. 7 (C - 20).
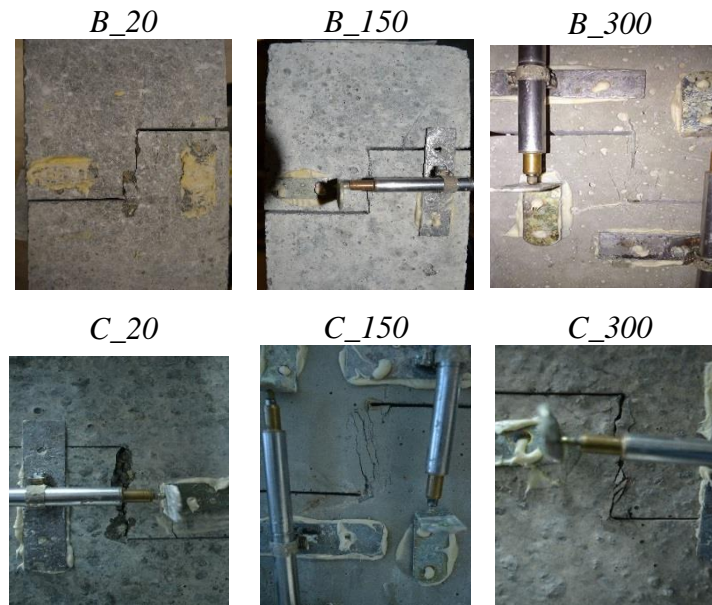
B_20 *B_150* *B_300*

C_20 *C_150* *C_300*
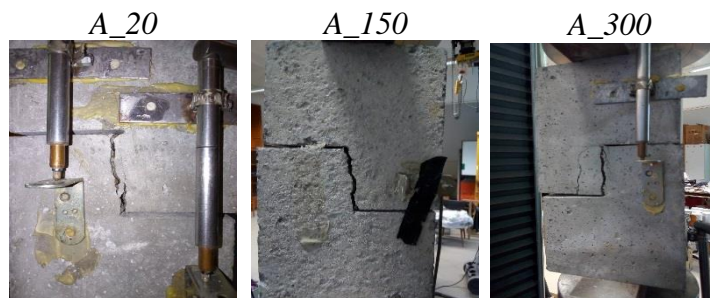
Figure 7: Different modes of failure due to different categories at 20, 150 and 300 ºC

4 CONCLUSIONS

The authors presented some of the test results for push-off direct shear strength tests of fibre-reinforced concrete under 5 temperature effects. The specimens were categorized into plain specimens, with 0.5% and with 1% volume of steel fibres. The compressive strength of the specimens was between 80 to
95 MPa. The results of 9 out of 45 specimens are presented in this paper. The following are the main conclusions of the study:

- *Thermal conductivity of concrete is slightly affected by using steel fibres*
- *Increasing temperatures causes loss in mass of concrete. However, it has no significant influence on difference of mass losses between fibre and plain concrete.*
- *Increasing the amount of steel fibres let to increase the mechanical properties of the concrete i.e. compressive strength, tensile strength and ultimate shear strength*
- *The amount of steel fibres affects the ductility of concrete*
- *Increasing amount of steel fibres control the failure mode and the crack opening*
- *Experimental technique requires development in which horizontally control is provided.*

ACKNOWLEDGEMENTS

REFERENCES

[1] Sarhat, S., and Green, M. (2017). *Effect of elevated temperatures on the shear transfer strength of concrete: a review*. Proceedings of 2nd International Fire Safety Symposium IfireSS 2017. Italy, pp 581-588
[2] Regan, P. E. (1993). *Research on shear: a benefit to humanity or a waste of time?*. The Structural Engineer. Vol. 71, No 19/5 October

[3] Kani, G. N. J. (1964). *The Riddle of Shear Failure and Its Solution.* ACI Journal. Vol. 61 (28), pp 441-467

[4] Walraven, J. (1980). *Aggregate Interlock: A theoretical and experimental analysis.* PhD Dissertation, Delft University of Technology

[5] Santos, P. M. D, Júlio, E. N. B. S. (2012). *A state-of-the-art review on shear-friction. Engineering Structure*. Vol. 45, pp 435-448

[6] Echegaray-Oviedo, J. (2014). *Upgrading the push-off test to analyze the contribution of steel fibres on shear transfer mechanisms.* PhD Thesis. Institute of Concrete Science and Technology (ICITECH), Universitat Politècnica de València. Spain

[7] Anderson A. R. (1960). *Composite designs in precast and cast-in-place concrete*. Progressive Architecture. Vol. 41(9), pp 172–179

[8] Hanson N. W. (1960). *Precast-prestressed concrete bridges. 2. Horizontal shear connections*. Development Department Bulletin D35. Portland Cement Assoc. Vol. 2(2), pp 38–58

[9] Birkeland P. W., Birkeland H., W. (1966). *Connections in precast concrete construction.* Journal of the American Concrete Institute. Vol. 63(3), pp 345–468

[10] Walraven, J. C. (1981). *Fundamental analysis of aggregate interlock*. Journal of Structural Division. Vol. 107, No. 11, pp. 2245–2270

[11] Hofbeck J. A., Ibrahim I. O., Mattock A., H. (1969). *Shear transfer in reinforced concrete*. Journal of the American Concrete Institute. Vol. 66(2), pp 119–128

[12] Al-Owaisy, S. (2007). *Effect of High Temperatures on Shear Transfer Strength of Concrete*. Journal of Engineering and Development. Vol. 11, No. 1, pp 92-103

[13] Xiao, J, Li, Z., and Li J. (2014). *Shear transfer across a crack in high-strength concrete after elevated temperatures.* Construction and Building Materials, Vol. 71, pp 472–483

[14] Barragan B., Gettu R., Agullo L., Zerbino R. (2006). *Shear failure of steel fibres-reinforced concrete based on push-off tests*. ACI Materials Journal. Vol. 103, No. 4, pp 251-257

[15] *fib*. (2010). *Shear and punching shear in RC and FRC elements*. Bulletin 57, 2010

[16] Cuenca, E., and Serna, P. (2010). *Shear behaviour of self-compacting Concrete and Fibres Reinforced concrete Push-Off Specimens: Design, Production and Placement of self-compacting Concrete.* RILEM Book-S Vol. 1, pp. 429-438

FIRE SAFETY OF TIMBER STRUCTURES

EXPERIMENTAL FIRE RESISTANCE PERFORMANCE OF TIMBER LIGHTWEIGHT FLOOR AND WALL ASSEMBLIES

D. Dhima[1]*, S. Hameury[1], A. Bouchaïr[2,3], M. Audebert[4]

[1] CSTB, Centre Scientifique et Technique du Bâtiment, Marne-la-Vallée, France
[2] Université Clermont Auvergne, Institut Pascal, France.
[3] CNRS, Institut Pascal, France.
[4] Université de Lyon, Ecole Nationale d'Ingénieur de Saint-Etienne, France

ABSTRACT

This paper presents the results of an experimental study performed at CSTB to evaluate the fire resistance of timber-framed walls and floors exposed to the ISO 834-1 time-temperature curve. The timber-frames were protected by various types of layers including gypsum plasterboards or/and wood-based panels. A total of twenty-nine fire tests have been realised [1, 2 and 3]. The influence of various parameters such as cladding geometry, fasteners spacings, quality and quantity of fire protection layers and their layout, as well as the type of insulating materials in the cavity has been investigated. Temperatures in different sections of each tested specimen have been recorded and analysed. Finally, the experimental results were compared with the fire performances estimated according to FIT method [4].

1   INTRODUCTION

One of the main fire safety strategy aims to limit the spread of the hazards from the room of the fire origin by satisfying the load carrying capacity of the structure and the separating function of the boundaries (i.e., walls and floors) for a required time. This required time is normally expressed in terms of fire resistance (FR), using fire exposure of the standard temperature-time curve and is specified by building regulations. In France, the design of lightweight timber-frame assemblies is based on a series of guideline called DTU such as DTU 25.41, 31.2, 31.3, 36.2 [5, 6, 7, 8]. In a first section of this paper are briefly described the tested configurations of timber-framed wall and floor assemblies. In a second section, the FR results of the experimental campaign are given (see also [1] and [2]). In a third section a brief analysis of experimental results is presented (see also [3]). Finally, in a forth section, the experimental and calculated FR of tested walls and floors, as well as the observed and calculated charring and failure times of fire side claddings, are compared. The calculated values are defined according to "Fire safety in timber buildings" (FIT) guideline [4].

2   DESCRIPTION OF TIMBER LIGHTWEIGHT WALL AND FLOOR ASSEMBLIES

2.1   Tested configurations

The tested configurations of timber lightweight assemblies studied in the frame of this research are representative of those usually employed by the timber industry in France.

A total amount of 13 full-scale wall specimens (3 m by 3 m) and 13 full-scale floor specimens (4 m by 3 m) has been carried out. Further 8 small-scale wall specimens (1,2 m by 1,2 m) and 4 small-scale floor specimens (1,85 m by 1,3 m) have been tested. Concerning the small-scale specimens, 4 specimens of small sizes have been tested simultaneously in the same furnace.

The small-scale specimens were first tested to evaluate the influence of different type of insulating materials on the FR performance of the lightweight wall and floor assemblies. The

insulating material leading to the shortest failure time of the claddings exposed to the fire was then selected for the full-scale specimens.

The fire behaviour of five different insulating materials has been analysed: glass-wool (kraft paper on one side) - 15 kg/m^3; cellulose wadding - 48 kg/m^3; wood fibre - 50 kg/m^3; hemp - 30 kg/m^3; sheep wool - 13 kg/m^3.

The cladding exposed to the fire was composed of two layers of standard gypsum plasterboard BA13A (type A with a thickness of 12,5 mm of each layer) for 4 small-scale wall specimens and one layer of gypsum plasterboard BA15F (type F with a thickness of 15 mm) for the remaining 4 small-scale wall specimens, as well as for the 4 small-scale floors. The only difference between the small-specimens tested simultaneously was the insulation type. The shortest failure time of the fire side claddings was achieved with glass wool.

This insulating material was therefore retained to carry out the full-scale tests apart for 3 tests (two with wall and one with floor). For these three tests, glass wool and wood fibre were used simultaneously to compare their fire behaviour. Figure 1 illustrates a full-scale wall specimen composed of two different insulating materials placed in each half of tested specimen. The spacing for the studs of all wall specimens was 600 mm. For fire side cladding composed of one layer, the spacing of the fasteners was 300 mm; for the configuration with two layers (fig. 2), the fasteners spacings of first and second layer were respectively 600 and 300 mm.
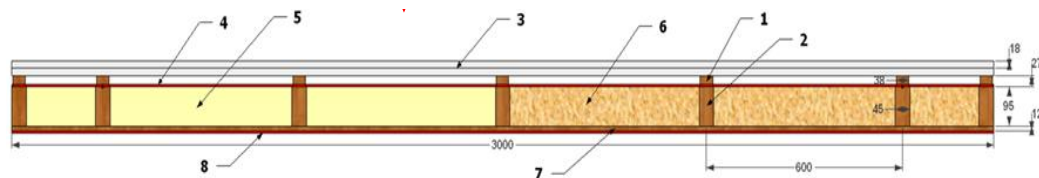

Figure 1: Horizontal cross-sections type of configurations 11, 12 and 13 (see table 3).

Where: 1) wooden battens, 2) wooden studs, 3) fire side cladding, 4) vapour barrier, 5) insulation material glass wool, 6) insulation material wood fibre, 7) rain screen, 8) opposite fire side cladding.

Figure 2 illustrates a full-scale floor specimen composed of two different insulating materials.
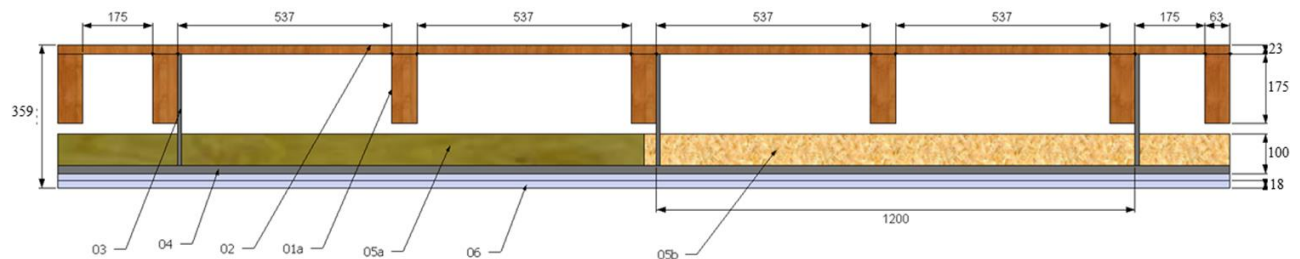

Figure 2: Vertical cross-sections of configuration 12 and 13 (see table 4).

Where: 01a) wood joist, 02) softwood panel, 03) ceiling hanger, 04) horizontal element of ceiling steel framework, 05a) wood fibre, 05b) glass wool, 06) fire side cladding (horizontal screen).

The spacings of the wooden joists and/or the "C" cross-section of horizontal steel framework, where the fire side claddings are fixed, were: 600 mm for configurations 1, 2, 4, 5 and 6, 500 mm for configurations 3, 7, 8, 9, 10 and 11 and 450 mm for configurations 12 and 13. For horizontal screens composed by one layer the fasteners spacing was 250 mm (see configurations 1, 3, 4, 5, 6 and 8). For horizontal screens of specimens composed of two layers the spacings of the fasteners of first and second layer were respectively 600 and 250

342

mm (see configurations 2, 7, 9 and 11) and, 300 and 150 mm for configurations 12 and 13. For specimens composed from three layers (config. 10) the fasteners spacings of first and second layer were 600 mm and for the third layer were 250 mm.

2.2 Test set up

Thermocouples type K were used to measure the temperatures in different points of walls and floors such as: interfaces between different layers of the claddings, back of fire side cladding (face cavity), in the void behind the insulation (or in the plenum), in both sides of claddings opposite to fire and in the wooden studs and joists. Details on thermocouple locations are given in references [1 and 2].

Three to five cross-sections of each wall tested specimen and nine sections for each floor specimen have been equipped with thermocouples. Fire tests have been carried out according to the European standards NF EN 1363-1 and NF EN 1364-1 for the walls and according to NF EN 1363-1 and NF EN 1365-2 for the floors. All tests have been conducted with ISO 834-1 time-temperature curve.

3 EXPERIMENTAL RESULTS

3.1 Experimental results of small-scale wall specimens

In table 1 are given the main results of the small-scale wall tests such as the falling time of different layers of fire side claddings, the time of charring start of wooden studs, the real FR achieved, and standard classification obtained for tested configurations.

Table 1: Fire-resistance of the small-scale wall tests.

Specim.	Cladding exposed to fire	Cladding non-exposed to fire	Insulation type	Fall of 1st layer (min)	Fall of 2nd layer (min)	Start of studs charring (min)	Real fire resistance	Standard classification
1	2 BA13A	2 OSB (2 x 9)	Glass wool	41	41	38	EI49	EI30
2			Cellulose wadding	29.5	not observed	39	EI50	EI30
3			Wood fibre	24	44	36	EI50	EI30
4			Hemp	28	45.5	37	EI50	EI30
5	1 BA15F		Glass wool	65	-	24	EI65	EI60
6			Cellulose wadding	77	-	25	EI77	EI60
7			Wood fibre	73	-	30	EI73	EI60
8			Sheep wool	72	-	27	EI78	EI60

3.2 Experimental results of small-scale floor tests

In table 2 are given the main results of the small-scale floor tests such as: the falling time of fire side claddings, the time of charring start of wooden joists, the real FR achieved, and standard classification obtained for tested configurations.

Table 2: Fire resistance of the small-scale wooden floor tested specimens.

Specim	Cladding exposed to fire	Cladding unexposed to fire	Insulation type	Fall of the cladding exposed (min)	Start of joists charring (min)	Real fire resistance	Standard classification
1			glass wool	24	24	EI28	EI15
2	1 BA15F	1 OSB (1 x 15)	wood fibre	25	24.5	EI32	EI30
2			Stone wool	27	27	EI35	EI30
4			Cellulose wadding	26	25	EI32	EI30

3.3 Experimental results of full-scale wall specimens

In table 3 are given the main results of the full-scale wall tests such as: the falling time of different layers of fire side claddings, the time of charring start of wooden studs, the real FR achieved, and standard classification obtained for tested configurations. These results are analysed in §4.

Table 3: Fire resistance of the full-scale wooden wall tested specimens.

Config.	Cladding exposed to fire	Cladding unexposed to fire	Fall of 1st layer (min)	Fall of 2nd layer (min)	Start of stud charring (min)	Real fire resistance	Standard classifica.
1	1 BA13A	2 OSB 9	18	-	14.5	EI29	EI15
2	2 BA13A	2 OSB 9	28.5	41.5	38	EI43	EI30
3	2 BA13A	2 OSB 9	30	42.5	38	EI45	EI30
4	1 BA18A	2 OSB 9	41	-	39	EI48	EI30
5	2 OSB 12	2 OSB 9	11.3	17.2	14	EI34	EI30
6	1 BA13A + 1 OSB 9	1 MDF 15	22.3	28	25	EI36	EI30
7	Douglas fir cladding (1 x 18) 1 OSB 12	2 BA13A	21	29.5	26	EI71	EI60
8	2 BA13F	1/2 surface (2 OSB9) and 1/2 surface (2 plywood 9)	59.7	65	46.5	EI68	EI60
9	1 BA13A + 1 BA18A	1 OSB 9	27.5	47.5	47.5	EI51	EI60
10	2 BA15F	1 OSB 9	81	83	64	EI84	EI60
11	2 BA18A	1 OSB 12	63	no	no	EI80	EI60
12	Stone wool (1 x 60), (31kg/m3) + 1 OSB 12	2 BA18A	26	41	32	EI90	EI90
13	2 BA18A + Stone wool (1 x 40), (118.2 kg/m3)	1 OSB 12	80	85	90	EI90	EI90

1.1 - Experimental results of full-scale floor tests

In table 4 are given the main results of the full-scale floor tests such as: the falling time of fire side claddings, the time of charring start of wooden joists, the real FR achieved, and standard classification obtained for tested configurations. These results are analysed in §4.

Table 4: Fire resistance of the full-scale wooden floor tested specimens.

Conf.	Cladding exposed to fire	Fall of the 1st layer (min)	Fall of the 2nd/3rd layer (min)	Time of start of charring in joists (min)	Time with T_{pl} =300°C	Time with $T_{back-panel}$ =300°C	Real fire resist.	Standard classifica.
1	1 BA13A	15	-	14.5-	15	15	EI15	EI15
2	2 BA13A	19	29	29	31	29	EI39	EI30
3	1 BA15F	26	-	24	28	20	EI35	EI30
4	1 BA18A	29,5	-	29.5	31	29	EI35	EI30
5	1 x 25 (1/2-plywood)	27	-	29	29	27	EI32.5	EI30
	1 x 25 (1/2-plywood fireproofed)	27	-	26	26	27	EI32.5	EI15
6	1 x 22 plywood	20	-	18	20	18	EI26	EI15
7	2 BA15F	29	53	55	55	48.5	EI58	EI30
8	1 BA25	31	-	33	32	28.5	EI37	EI30
9	1 BA13A+1 BA18A	34	44	44	46,5	46	EI50	EI30
10	3 BA15F	27	48/67	68	68	68	EI68	EI60
11	2 BA18A	32	53	52	55	51	EI59	EI30
12	2 BA18A	55	79	84	81	80	EI89	EI60
13	2 BA18A	46	77	88	81	75	EI91	EI60

4 ANALYSIS OF EXPERIMENTAL RESULTS

4.1 Experimental results of small-scale specimens – insulation effect

The test results with small-scale specimens given in the tables 1 and 2 show that fire side cladding that collapse first were those of specimens with cavities filled with glass wool insulation. Secondly, if the same fire side cladding is used for the walls and floors the FR is higher when this cladding is used for a wall (see results with fire side cladding gypsum plasterboard BA15F). As a first approach we considered that the same effect of insulation is valuable for full-scale tests. This approach has at least been verified by full-scale tests of specimen configurations. 11, 12 and 13 of table 3 and those of configurations 12 and 13 of table 4 that have been tested with two insulations.

4.2 Experimental results of full-scale wooden specimens

The results of full-scale test showed the following effects:

Effect of compositions of fire side claddings: for the same compositions of fire side claddings, FR of walls is higher that FR of floors. For example, for claddings composed with one or two layers of gypsum plasterboard BA13 the real FR of walls are respectively EI29 and EI43 and those of floors are respectively EI15 and EI39 (see config. 1 and 2 of tables 3 and 4); for claddings with one layer of BA18A (thickness 18 mm) the FR of a wall and a floor are respectively EI48 and EI35 (see config. 4 of tables 3 and 4) and for claddings with two layers BA15F (see config. 10 and 7 of tables 3 and 4), the same values are respectively EI84 and EI58. Indeed, the fire claddings collapse before in the case of floors, compared with walls, even if the spacings of studs or joists in one direction and the spacing of screws in the other direction are the same. This means that the load of cladding applied on the cladding situated between two succeeded screws play an important role in its FR. Without surprise in all cases, the increase of cladding layers increases significantly FR of the assemblies.

Effect of materials of fire claddings: the influence of material type of fire claddings is a very important parameter for FR too. For example, the gypsum plasterboards type F (reinforced with glass fibre) compared with type A increase significantly the FR of assemblies (see and compare configurations 2, 3 with 8 or 10 and 11 of table 3 and configurations 2, 3, 4 and 8 or 2, 7, 9 and 11 of table 4).

Effect of fire retardants products used for wooden claddings: fire side cladding of a full-scale floor specimen, fire test n°5 (see table 4), was composed of a plywood layer 25 mm thickness. 50% of this cladding was composed by a normal plywood, and 50% by a fireproofed plywood. The fire resistances observed were the same. Consequently, even if the number of comparisons is limited we cannot consider that fire retardants clearly improve the FR.

Effect of screw spacings: the fire side claddings of full-scale floor specimens of fire tests 11, 12 and 13 were strictly the same, but the screw spacings changed. As mentioned in §2.1, the screw spacings of first and second layer were respectively 600 and 250 mm for the configuration 11, and 300 and 150 mm for configurations 12 and 13. The real experimental fire resistances of these configurations are EI59, EI89 and EI90. It's easy to see that the decrease of screw spacing increases the FR of floor assemblies. The same results have been observed for wall assemblies for different private tests.

5   COMPARISONS OF EXPERIMENTAL AND CALCULATED RESULTS

5.1   Experimental and calculated fire resistance of wooden walls and floors assemblies

The fire resistance, in terms of insulation, of some full-scale wooden walls and floors tested assemblies have been defined according to chapter 5 "Separating timber structures" of FIT guideline [4]. The scope of application of this method is given in the same reference. Table 5 shows the insulation times (t_{ins}) calculated according to FIT method (additive component method) and defined experimentally for ten wooden wall assemblies and eleven wooden floor assemblies (for configuration numbers see tables 3 and 4). Regarding the insulation time of each configuration two values have been calculated, the first one takes into account the glass wool in the cavity and the second one without insulation in the cavity.

Table 5: Comparison of experimental and calculated fire resistance of wooden walls and floors assemblies.

Config.	Compositions of fire side claddings, insulations and oposite fire side claddings	t_{ins}-experimental fire resistance (min)	t_{ins}-calculated fire resistance with GW in the cavity (min)	t_{ins}-calculated fire resistance without insulation in the cavity (min)
	Full-scale wooden wall specimens			
1	1BA13A+GW+2OSB9	29.0	27.4	24.5
2	2BA13A+GW+2OSB 9	43.0	39.8	38.0
3	2BA13A+GW+2OSB 9	45.0	39.8	38.0
4	1BA18A+GW+2OSB 9	48.0	36.3	34.2
5	2OSB 12+GW+2OSB 9	34.0	27.6	24.7
6	1BA13A+1OSB 9+GW+1MDF 15	36.0	37.5	37.1
7	1Douglas fir 18+1OSB 12+GW+2BA13A	71.0	46.1	46.9
9	1BA13A+1BA18A+GW+1OSB 9	51.0	42.6	40.1
10	2BA15F+GW+1OSB 9	84.0	60.1	62.2
11	2BA18A+GW+1OSB 12	80.0	55.8	54.2
	Full-scale wooden floor specimens			
1	1BA13A+GW+1OSB 15	15.0	26.8	24.3
2	2BA13A+GW+1OSB 15	39.0	39.3	37.8
3	1BA15F+GW+1OSB 15	35.0	33.2	37.6
4	1BA18A+GW+1OSB 15	35.0	35.7	34.0
6	1Plywood 22+GW+1OSB 15	26.0	28.8	26.5
7	2BA15F+GW+1OSB 15	58.0	51.7	55.4
9	1BA18A +1B13A+GW+1OSB 15	50.0	51.4	50.3
10	3BA15F+GW+1OSB 15	68.0	68.7	69.1
11	2BA18A+GW+1OSB 15	51.0	56.7	55.6
12	2BA18A+GW/WF*+1OSB 15	89.0	56.7	55.6
13	2BA18A+GW/WF*+1OSB 15	91.0	56.7	55.6
	GW/WF*: Glass Wool insulation for the half of the floor and Wood Fibre for the other half			

The analysis of these results shows that:

For wall assemblies consisted of fire side claddings composed by one or two layers of gypsum plasterboard (see configurations n° 1, 2, 3, 4, 5) $t_{ins,calculated}$ are slightly lower than $t_{ins,experimental}$. For these walls we could easily conclude that the FIT method gives satisfactory results. For the configuration 6 too, we consider that the calculated value is acceptable even if the calculated value is slightly higher than experimental one. For the wall configurations n° 7, 9,10 and 11 the calculated values are significantly conservative.

For floor assemblies, four of $t_{ins,calculated}$ values are lower than the experimental ones and between them two are significantly conservative, while seven $t_{ins,calculated}$ values are slightly higher than experimental ones. It is important to compare wall configuration l and the floor configuration 1. For both of them, $t_{ins,calculated}$ values are nearly the same, but the experimental results are significantly different. According to these results the FIT method applied for calculation of $t_{ins,calculated}$ of floor composed with one layer of gypsum plasterboard BA13A leads significantly to unsafety results. It is also interesting to compare the calculated and experimental values of configurations 11, 12 and 13. The calculated values are strictly the same. This means that the calculated values are based only in the composition of different layers of the floors or the walls. As explain in §4.2, the difference between experimental values of those three configurations is related to screw spacings. Apparently, FIT method doesn't take into account the influence of this parameter. In the table 5 are also given the

insulation times of walls and floors without insulation in the cavities. The aim of these calculations was to compare for the same configurations the calculated results with and without insulation. The comparisons of calculated results show that in most of configurations (16/21) the t_{ins} with glass wool in the cavity is higher than t_{ins} without insulation. The analysis of great number of the private industrial tests and the references [9], [10] and [11], show that in general the t_{ins} of assemblies with insulation in cavities is lower than t_{ins} of those without insulation.

5.2 Comparison of charring and failure times of fire side claddings of full-scale wooden wall and floor tested specimens

In tables 6 and 7 are compared respectively the experimental charring times ($t_{ch}(exp)$) of studs or joists situated behind the fire claddings and the experimental failure times ($t_f(exp)$) of fire claddings with the calculated charring and failure times $t_{ch}(cal)$, $t_f(cal)$, of some of the full-scale wooden wall and floor tested specimens.

Wall results

For the seven configurations of considered walls $t_{ch}(cal)$ calculated values are mostly lower than the experimental ones ($t_{ch}(exp)$), except for configuration 4 when the difference is significant (17.5 minutes) and for the configuration 1 when the calculated value is slightly higher than the observed one.

Regarding the failure time, for 5 configurations $t_f(cal)$ is lower than $t_f(exp)$ and for one of them (configuration 4) the difference is significant (20.5 minutes). For configurations 9 and 10, $t_f(cal)$ is slightly higher than $t_f(exp)$. It is important to observe that for walls and floors with fire claddings composed of one or two gypsum plasterboard, type BA13A, the FIT method leads to satisfactory results, while with gypsum plasterboard type BA18 this method leads to very safety values.

Floor results

For the seven configurations of considered floors, the observed and calculated charring times are of the same order of magnitude, even if for two of them $t_{ch}(cal)$ is slightly higher than $t_{ch}(exp)$.

Regarding the failure time, for 6 configurations, the observed and calculated times are of the same order of magnitude, even if for two of them $t_f(cal)$ is higher than $t_f(exp)$. For the configurations 4 and 8 the difference is more significant, and as observed with tested walls, the calculated results obtained with gypsum plasterboard different from BA13A are more safety. The configuration 9 is out of range of the formulas given by FIT method.

As conclusion, the calculated values $t_{ch}(cal)$ and $t_f(cal)$, obtained for the claddings of walls and floors composed by gypsum plasterboard type BA13A, could be considered safe. For the other types of gypsum plasterboard, it would be interesting to check the formulas given by FIT with other full-scale fire test results and to improve it if necessary.

Table 6: Comparison of observed and calculated charring and failure times of fire side cladding of wooden wall specimens.

Configuration (see table 3)	Cladding exposed to fire	t_{ch}(cal)	t_{ch}(exp)	t_f(cal)	t_f(exp)
1	1 BA13A	15.5	15	16.8	18.0
2	2 BA13A	33.0	38	38.5	41.5
3	2 BA13A	33.0	38	38.5	42.5
4	1 BA18A	21.5	39	21.5	41.0
8	2 BA13F	45.5	46.5	60.0	65.0
9	1 B13A + 1 BA18A	41.8	47.5	49.0	47.5
10	2 BA15F	56.0	64	80.0	83.0

Table 7: Comparison of observed and calculated charring and failure times of fire side cladding of wooden floor specimens.

Configuration (see table 4)	Horizontal cladding exposed to fire	t_{ch}(cal)	t_{ch}(exp)	t_f(cal)	t_f(exp)
1	1 BA13A	15.5	14.5	15.5	15.0
2	2 BA13A	31.0	29.0	28.0	29.0
3	1 BA15F	20.0	24.0	25.0	26.0
4	1 BA18A	20.0	29.5	20.0	29.5
7	2 BA15F	46.0	48.5	57.0	53.0
8	1 BA25A	25.5	33.0	20.0	32.0
9	1 BA18A+1 BA13A	39.8	45.0	-	44.0

2 - CONCLUSIONS

In this paper the experimental results of twenty-six full-scale and three small-scale FR tests of wooden walls and floors assemblies have been presented and analysed. Based on comparison between experimental versus calculated results, the following conclusions can be drawn:

1) The compositions of fire claddings of wall and floor assemblies is one of the most important parameters for obtained FR. The integrity of fire side claddings with two or more layers is higher than for single-layer and therefore, FR is higher.
2) The fire side cladding material type is one of very important parameter for the FR of assemblies. The difference of FR for the same thickness of gypsum board type A and F is significant.
3) The screw spacings used for the claddings play a significant role in obtained experimental FR. Indeed, the decrease of screw spacings significantly increases the FR of wooden assemblies.
4) The use of fire retardants for wood claddings does not impact the FR.
5) The use of glass wool insulation conducts to the lowest FR of wooden assemblies.
6) The fire resistance times, in terms if insulation, calculated according to the FIT method, are acceptable for assemblies with fire side claddings composed of one or two gypsum layers of plasterboard type BA13A. The method needs to be improved for other types of claddings, for different screw spacings and for the configurations without insulations in the cavities.
7) The calculated charring times (see FIT method) of studs and joists protected by gypsum plasterboard claddings are essentially safety and the obtained results could be considered

satisfactory. The FIT method needs to be improved for claddings composed of gypsum plasterboard different from BA13.

8) The calculated failure times (see FIT method) of fire claddings of wooden assemblies are essentially safety and the obtained results could be considered satisfactory.

ACKNOWLEDGMENT

REFERENCES

[16] Rapports d'essais de résistance au feu de cloisons n° RS11-053/C à RS11-053/L, RS14-102/B, RS14-102/C et RS16-008, et d'maquettes de closions (RS11-053A et RS053-B), CSTB, France.

[17] Rapports d'essais de résistance au feu de planchers n°RS12-098 à RS12-108, RS14-102/A et RS16-009 et de maquettes de planchers RS12-001, CSTB, France.

[18] Dhima D., Gaillard J-M., Etude du comportement au feu de parois et planchers constitués de structures bois, CSTB Référence 26025597-260028282-v2, 05 juin 2018, CSTB, France.

[19] Fire Safety in Timber Buildings, Technical guideline for Europe, SP Report 2010:19, ISBN 978-91-86319-60-1, SP Trätek, Box 5609, SE-114 86 Stockholm, Sweden.

[20] NF DTU 25.41: Ouvrages en plaques de plâtre — Plaques à faces cartonnées, décembre 2012

[21] NF DTU 31.2: Construction de maisons et bâtiments à ossature en bois, janvier 2011

[22] NF DTU 31.3: Charpentes en bois assemblées par connecteurs métalliques ou goussets, janvier 2012

[23] NF DTU 36.2: Travaux de bâtiment — Menuiseries intérieures en bois, janvier 2011

[24] Sultan M.A., Bénichou N, Fire Resistance Performance of Lightweight Floor Assemblies, Designing Structures for Fire Conference, Baltimore, MD., Sept. 30-Oct. 1, 2003, pp. 203-214.

[25] Bénichou N.; Sultan M.A., Design considerations for fire resistance of lightweight-framed assemblies, CSCE 2003, Annual Conference, Moncton, N.B., June 4-7, 2003, pp. 567-1 - 567-10.

[26] Sultan M. A., Parameters affect the fire resistance performance of floor systems, CIB World Building Congress 2004, Toronto, Ont., May 2-7, 2004, pp. 1-10.

FIRE RESISTANCE OF NAIL-LAMINATED TIMBER ASSEMBLIES

Lindsay Ranger[1], Christian Dagenais[2], Noureddine Bénichou[3]
[1]FPInnovations, Ottawa, Canada,
[2]FPInnovations, Québec, Canada, [3]National Research Council Canada, Ottawa, Canada

ABSTRACT

The National Building Code of Canada recognizes the fire resistance of nail-laminated timber (NLT) assemblies by assigning fire-resistance ratings based on their thickness; however, there is no known test data which confirms this performance. Full-scale fire resistance testing was conducted on two wall (nominal 2x6 and 2x8) and one floor (nominal 2x6) NLT assemblies to assess their fire performance. The application of protection on the exposed and unexposed side of the assemblies was investigated. Due to gaps that can form between boards integrity failure is a concern, which highlighted the need for protection on the unexposed side of assemblies. Guidance on proper detailing to address smoke leakage and to improve fire resistance are provided.

1   INTRODUCTION

Building codes around the world are evolving to allow taller wood buildings due to an increasing awareness and desire for sustainability. The fire performance of the wood products needs to be well understood to ensure sound fire safety design of these buildings. The National Building Code of Canada (NBCC) [1] requires a fire resistance rating (FRR) of 1 h for buildings up to six stories built using combustible construction, and 2 h for tall buildings (not currently permitted to be of combustible construction following the prescriptive code provisions).

Solid timber assemblies have historically been used in Canada for large commercial and industrial buildings. The NBCC recognizes the fire resistance of solid timber assemblies by assigning conservative fire-resistance ratings based on their use (i.e., floor or wall) and depth of section; however, there few test results which verify this performance. A review of North American records yielded no data to directly confirm these ratings.

Solid timber is now commonly constructed and referred to as nail-laminated timber (NLT). NLT is used in the construction of floors, but there are also applications for its use as vertical elements for elevator or stair shafts. These assemblies are comparatively economical, sustainable, architecturally appealing, and relatively simple to construct (not requiring any specialized equipment for construction). Due to increasing popularity, NLT design guides [2][3] have recently been published in North America which provide builders with guidance on design and construction, however very limited information is provided on fire performance.

2   PROCEDURE

A testing program was initiated to address the technical knowledge gaps on the fire performance of NLT assemblies to assess fire resistance, smoke leakage, and charring rates [4]. Due to natural imperfections in lumber, gaps can form between NLT boards during construction which may present an opportunity for smoke migration, as well as localized

352

increased charring rates. This research is intended to support designers and builders of mass timber buildings and to provide scientific justification for Authorities Having Jurisdiction to approve this type of construction.

Full-scale tests were carried out to assess the fire resistance of NLT assemblies in accordance with CAN/ULC-S101 [5]. Testing was completed at the National Research Council Fire Research Laboratory in Ottawa, ON, Canada.

Three assemblies were constructed using nominal SPF No.2 lumber, and 75 mm (3") nails spaced 450 mm o.c., as recommended in the Canadian NLT guide [2]. This included:

1. *2x6 NLT wall (140 mm), 1 layer 12.7 mm (½") plywood on unexposed side*
2. *2x8 NLT wall (184 mm), 2 layers 12.7 mm (½") Type C gypsum board on both sides*
3. *2x6 NLT floor (140 mm), 1 layer 12.7 mm (½") plywood on unexposed side*

2.1 Wall Construction and Instrumentation

The NLT wall assemblies were constructed using two panels, with total dimensions of 3658 mm 12') x 3048 mm (10'). The wall assembly detail is shown in *Fig. 1a*. The panels were fastened together with pairs of 8 x 160 mm screws spaced at 305 mm (12") o.c., installed at a 45º angle. An NLT surface, as installed in the wall furnace, is shown in *Fig.1b*.

a) Dimensions in mm   b)
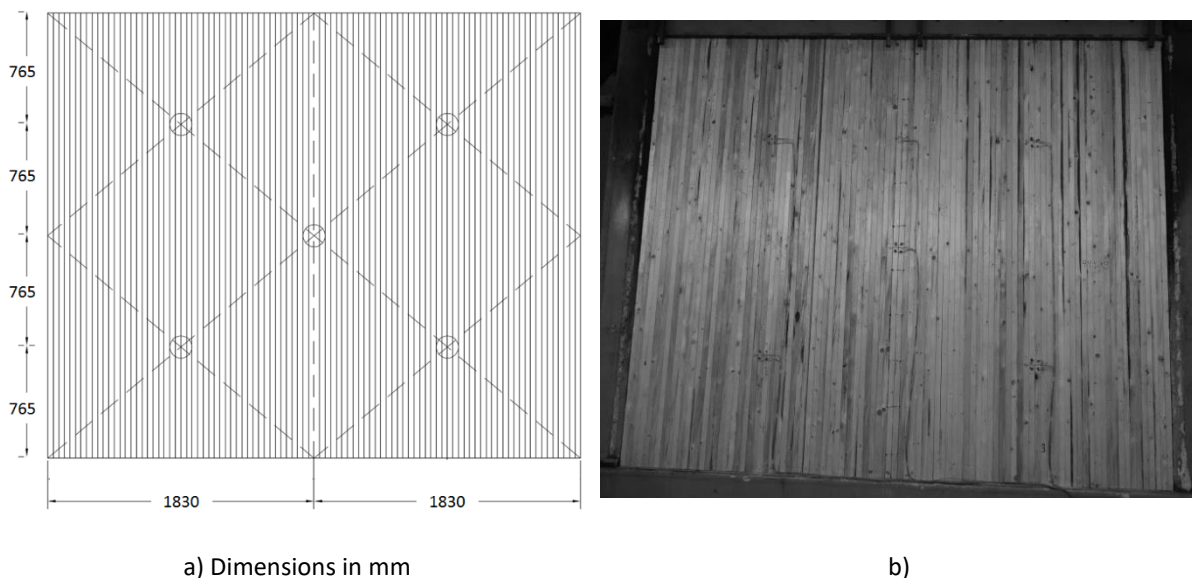
Fig. 1. a) NLT wall construction detail; b) NLT wall surface

The 2x6 wall was protected on the unexposed side by one layer of 12.7 mm (½") plywood, no protection was provided on the exposed side. A cross-section of the 2x6 wall is shown in *Fig. 2a*, which includes thermocouple installation depths. The average moisture content of the exposed face before the test was 8.6%. A 335 kN/m load was applied.

The 2x8 wall was protected with two layers of 12.7 mm (½") direct applied Type C gypsum board on both sides of the assembly. A cross-section of the 2x8 wall is shown in *Fig. 2b*. The gypsum board was adhered with 57 mm (2 ¼") Type S screws spaced at 305 mm (12") o.c. and 38 mm (1 ½") from the edges. Effort was made to ensure that the gypsum joints did not

to line up with spaces between NLT boards, when possible. The average moisture content of the exposed face before the test was 8.9%. A load of 450 kN/m was applied.

The assemblies were instrumented with thermocouples embedded within the assemblies at five location (depicted in *Fig. 1a*) to assess charring and failure of the assemblies. Nine thermocouples were placed across the unexposed surface of the assemblies, as per the CAN/ULC-S101 standard. Thermocouples were installed at five depths within the NLT, at 15, 25, 50, and 75 mm from the exposed side. For the 2x6 wall assembly thermocouples were placed at the NLT and plywood interface. For the 2x8 wall assembly thermocouples were installed at the interface between the NLT and gypsum board on the exposed and unexposed sides. For both wall tests two thermocouples were installed in the joint at depths of 15 and 75 mm from the exposed side.
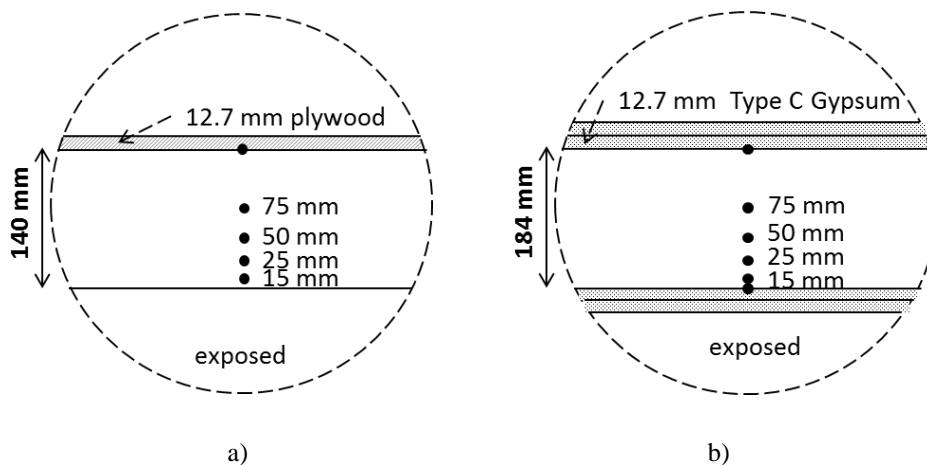
Fig. 2. a) 2x6 NLT wall and floor detail; b) 2x8 NLT wall detail

2.2 2x6 Floor Construction and Instrumentation

The NLT floor consisted of three panels with overall dimensions of 4495 mm (177") x 3937 mm (155") span. The panels were fastened together with 8 x 160 mm spaced at 305 mm (12") o.c. The floor assembly detail is shown in *Fig. 3*. Embedded thermocouples were installed at the same depths as the 2x6 wall (see *Fig. 2a*). Nine thermocouples were placed across the unexposed surface of the assemblies, as per the CAN/ULC-S101 standard. A 4.8 kPa load was applied.
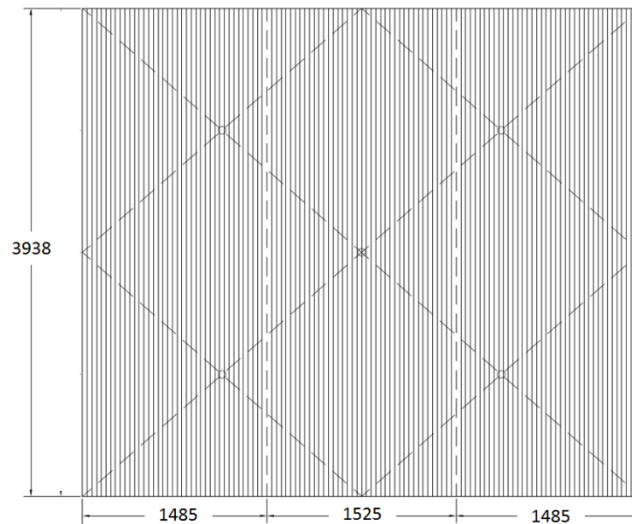
Fig. 3. 2x6 NLT floor assembly detail, dimensions in mm

3 RESULTS

3.1 2x6 Wall

For the 2x6 wall assembly, 33 min into the test integrity failure occurred, resulting in a FRR of 30 min; ignition of a cotton pad was used to confirm the failure. This initial failure occurred at a plywood joint. Once burn-through was detected a piece of plywood was used to cover the spot, allowing the test to continue. Additional burn through spots occurred at 50 min, 52 min, and 63 min, each of which was also covered with a piece of plywood. *Fig. 3* shows a plywood piece covering the initial failure, and a secondary failure that occurred close by. These secondary spots were all through the plywood layer and not a plywood joint. The test ran until structural failure at 71 min. At failure, the maximum deflection was 67 mm at mid-height.
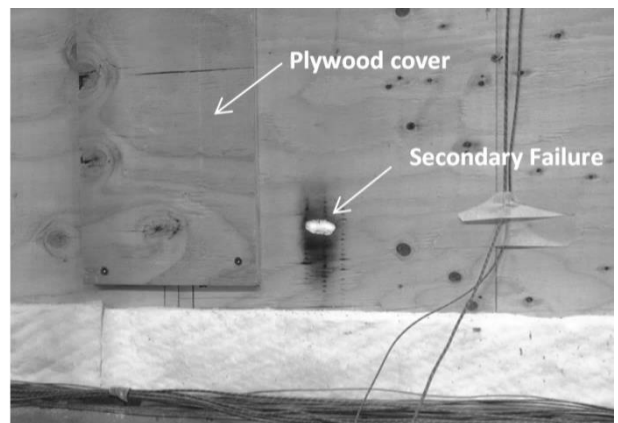
Fig. 3. 2x6 wall integrity failure

Despite several locations of integrity failure, the maximum measured temperature increase from thermocouples on the unexposed surface was 41ºC. This is within the limit according to CAN/ULC-S101, where temperatures on the unexposed side cannot rise more than an average of 140ºC or more than 180ºC at any individual point. One thermocouple between the NLT and the plywood increased 38ºC, whereas the other locations generally stayed at ambient. The average thermocouple readings are presented in *Fig. 4a*.

After the test the plywood was removed from the back of the assembly to assess areas of localized charring, which can be seen in *Fig. 4b*. The residual depth of the section was measured using a resistograph (which determines depth of sections based on resistance) and measured from a cut section. The remaining depth of the section was roughly 75 mm.
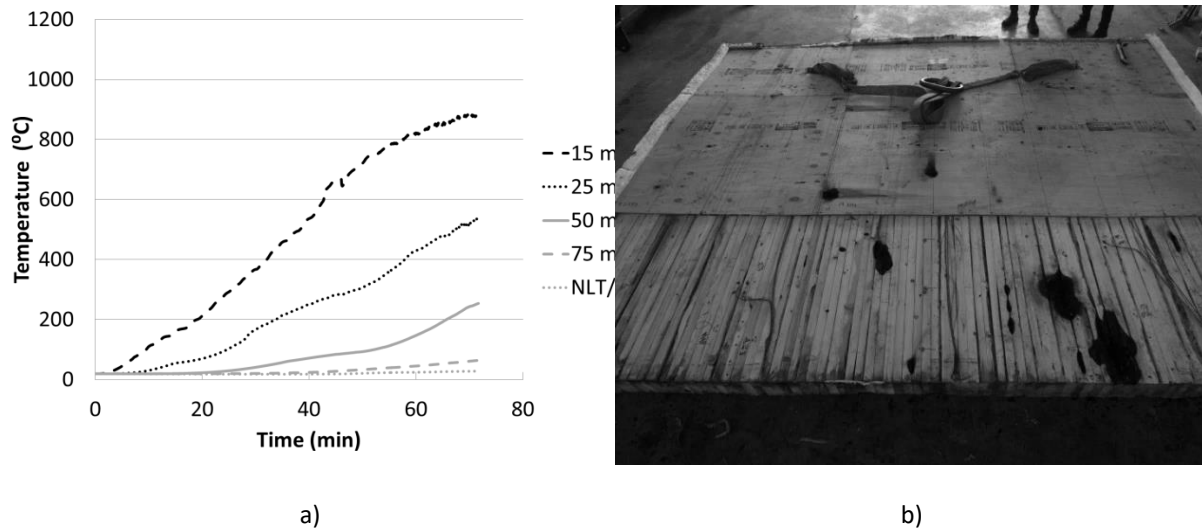
a)

b)

Fig. 4. a) Average temperatures in 2x6 wall assembly; b) Localized charring through 2x6 wall, plywood removed

3.2 2x8 Wall

In the 2x8 NLT wall test, the first layer of gypsum was observed to begin falling off after 90 min of fire exposure. The second layer began falling off after 2 h. The test ran until structural failure at 3 h 37 min, yielding a FRR of 3 h; failure of the assembly is shown in *Fig. 5a*. The maximum deflection was 120 mm at mid-height. There was no evidence of smoke leakage to the unexposed side during the test.

Average temperatures at embedded thermocouple locations in the 2x8 NLT wall are shown in *Fig. 5b*. Temperatures on the unexposed side did not increase, and the temperatures between the NLT and gypsum board on the unexposed side did not increase more than 20°C.

Following the test, gypsum board was removed from the unexposed side which revealed a three small burn-though spots. The residual cross section was determined to be approximately 100 mm.
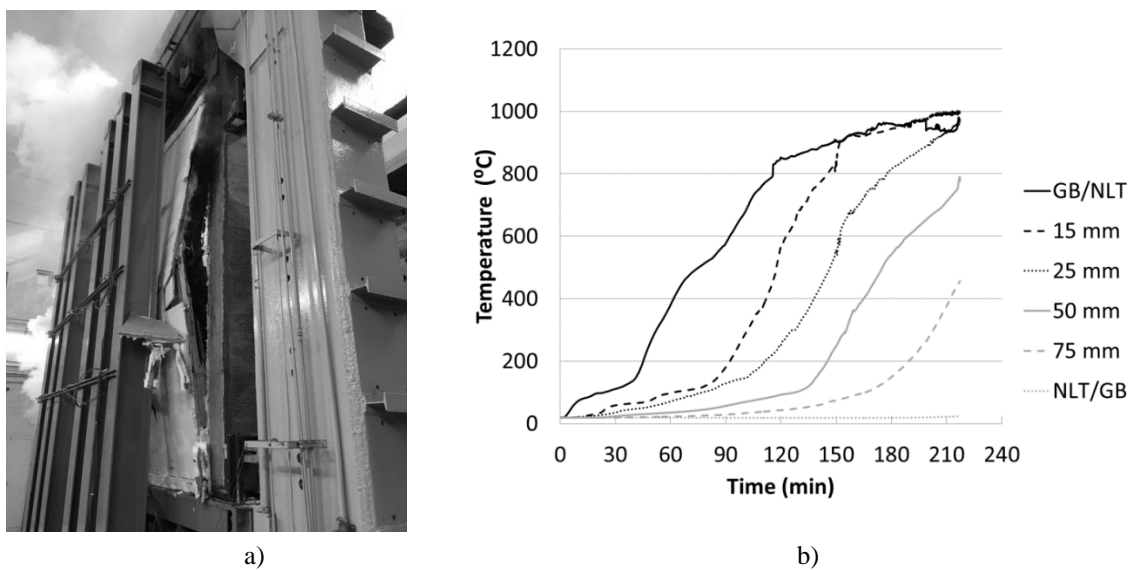

a)

b)

Fig. 5. a) Structural failure of 2x8 wall; b) Average temperatures in 2x8 wall assembly

3.3 2x6 Floor

During the 2x6 floor test there was some intermittent smoke leakage through the plywood joints. The test stopped after 101 min because the temperature in the exhaust exceeded a safety threshold, before failure was reached, however a 1.5 h rating was still achieved. Upon inspection of the assembly after the test, it was evident that structural failure was likely imminent, had the test not been stopped. There were also a few locations where integrity failures were soon to occur. At failure, the maximum deflection was 87 mm, measured at mid-span. The condition of the exposed floor surface after the test is shown in *Fig. 6a*.

Average temperatures at embedded thermocouple locations in the 2x6 NLT floor are shown in *Fig. 6b*. One thermocouple on the unexposed side increased 22°C, and two of the thermocouples between the NLT and plywood increased between 60-70°C.
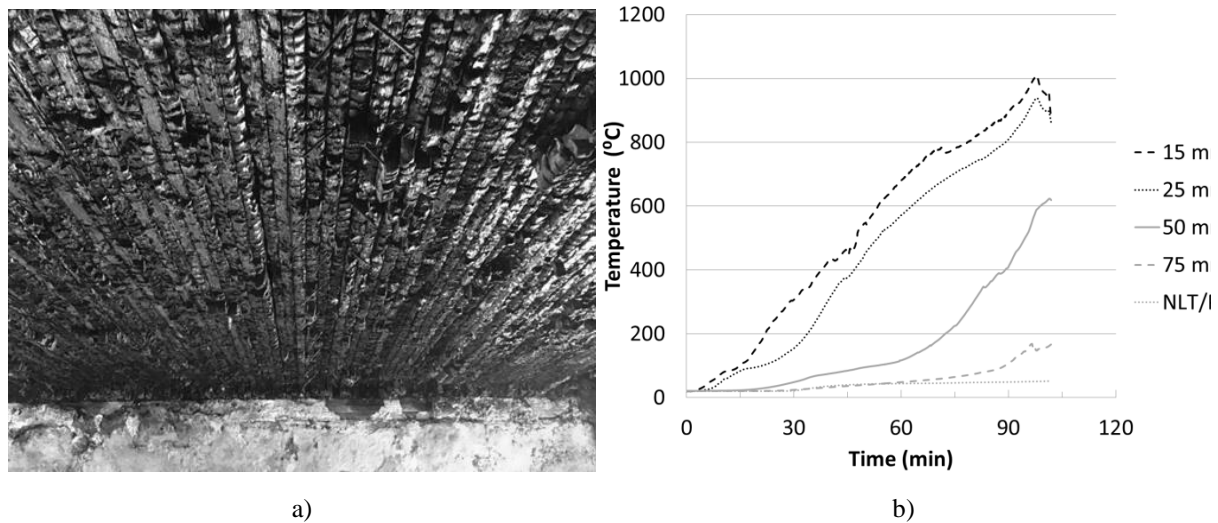

a)   b)

Fig. 6 a) Condition of floor surface after test; b) Average temperatures in 2x6 floor assembly

4   DISCUSSION

4.1 Charring Rates

Thermocouple data was analyzed to assess the time at which the wood had charred, which was determined based on a criteria of 300°C. Charring rates were then calculated by dividing the thermocouple depth by the time to reach 300°C, using *Eq. (1)*. *Table 1* presents the charring rates for each of the tests.

$$\beta_o = d/t \tag{1}$$

where β_o is the one-dimensional charring rate (mm/min)

d   is the depth of charring (mm)

t   is the time from the onset of charring until 300°C is reached (t)

When protection is provided on the exposed side of a mass timber assembly, the encapsulation time can be determined based on the average time that the surface beneath the protection increases 250°C or any one point increases 270°C, as is currently being considered for acceptance into the NBCC for encapsulated mass timber construction [6]. For this test series, the 2x8 wall was the only assembly to include encapsulation; its encapsulation time was determined to be 47.7 min, based on a single point.

Table 1. Charring rates of NLT assemblies evaluated at embedded thermocouple depths (mm/min)

	15 mm	25 mm	50 mm	75 mm
2x6 wall 12.7 mm plywood on unexposed	0.56	0.55	0.77[1]	-[2]
2x8 wall 2 x 12.7 mm Type C gypsum, both sides	0.42	0.30	0.43	0.49[3]
2x6 floor 12.7 mm plywood on unexposed	0.47	0.60	0.60	-[4]

[1] Only 2 thermocouples exceeded 300ºC; [2] Charring did not reach this depth;

[3] Only 4 thermocouples exceeded 300ºC; [4] Only 1 thermocouple exceeded 300ºC

A char rate of 0.65 mm/min is commonly used for softwoods, and can also be used for other mass timber products such as glulam and structural composite lumber [7]. The charring rates presented in Table 1 are generally in line with or less than 0.65 mm/min, only being exceeded after longer exposures (greater than 1 h) when the depth of char was 50 mm or more.

The 2x8 wall exhibited consistently slower charring rates. This can be attributed to gypsum board which stayed in place well beyond the encapsulation time. The first layer fell off around 90 min and the second layer after 2 h. The inclusion of direct applied gypsum board to mass timber not only delays the onset of charring and involvement in the fire, but also continues to insulate the wood while it stays in place, thus reducing the charring rate of the wood.

4.2 Protection on the unexposed side

The CAN/ULC-S101 standard procedure places nine thermocouples on the unexposed side to measure surface temperatures and evaluate insulation failure. Alternatively, if flame or hot gases, enough to ignite a cotton pad, pass through the assembly integrity failure is deemed to have occurred.

Because of the nature of NLT as a product, using multiple lumber boards laminated together, the natural imperfections in the lumber can impact the overall quality of the assembly. There are various defects that are typical in lumber such as twisting, cupping, bowing, wane, etc. These can result in two boards not pressed in full contact with each other, which can create gaps or pockets between the boards which can lead to localized increased charring rates. Due to the gaps that form between NLT boards, corner rounding and an increased char rate would be expected.

The thermocouple data collected during these tests did not capture all details of the overall performance of the assembly. After each test, the protection layers on the unexposed side were removed to assess the condition of the NLT itself. It was apparent in a few locations that charring had reached the unexposed side of the assembly (as was shown in *Fig. 3b*). In the 2x6 wall test, the plywood was not enough to prevent integrity failure, which indicates the need for gypsum protection on the unexposed side of the assembly. Typically, to improve fire resistance, protection is added to the exposed side of the assembly; however, in the case of NLT, gypsum (or other means of protection) is needed on the unexposed side to delay integrity failures at locations of increased charring to achieve longer FRRs. A 15.9-mm Type X gypsum board can provide 30 minutes of additional fire resistance to CLT assemblies

when used on the exposed side [7]; if this were to be used on the unexposed side of an NLT assembly above a layer of plywood, it is expected that it would provide at least the same additional protection time (provided the assembly is still capable of supporting any applied loads), if not more due to the significantly reduced localized fire exposure. The gypsum board may also limit charring at gaps if it prevents air flow through the assembly. During installation of any protection, it would be prudent to avoid joints lining up with NLT gaps. If multiple layers of protection are used care must be taken to prevent overlap of joints.

NLT uses a repetitive construction method. In terms of structural fire resistance, localized increased charring does not have a significant impact on the overall residual structural capacity of the assembly after fire exposure because the majority of the boards are charring at a slower more consistent rate. Both wall assemblies failed structurally once approximately 50% of the section depth had charred. In both tests, localized burn-though of the assemblies occurred, but the overall structural fire resistance was not greatly impacted.

5   CONCLUSIONS

Three full-scale fire resistance tests were conducted on NLT assemblies, which included a nominal 2x6 wall, 2x8 wall, and 2x6 floor. The 2x6 wall and floor had one layer of 12.7 mm plywood on the unexposed side and the 2x8 wall had two layers of 12.7 mm Type C gypsum board on both sides. All three assemblies experienced spots of localized charring which extended the entire depth of the NLT boards, but were not detected by the thermocouples throughout the assembly or on the unexposed side.

The 2x6 wall assembly experienced integrity failures at several locations early on, but the test was able to continue until structural failure. This highlighted the need for additional protection on the unexposed side of the assembly. Had additional protection been provided on the unexposed side it is likely a 1 h FRR could have been reached. The assigned fire resistance ratings for the assemblies are given in *Table 2*.

The 2x8 wall assembly achieved a 3 h FRR. The gypsum board on the exposed side provided 45.9 min of encapsulation; the base layer stayed in place for 2 hours which likely reduced the charring rate in the assembly. The 2x6 floor did not reach failure, but achieved a FRR of 1.5 h.

Table 2. Assigned fire resistance ratings for NLT assemblies

Assembly	Load	Failure	FRR	Type of failure
2x6 wall	335 kN/m	33 min	30 min	Integrity
		1 h 11 min	1 h	Structural
2x8 wall	450 kN/m	3 h 37 min	3 h	Structural
2x6 floor	4.8 kPa	[1]	1.5 h	[1]

[1] Test stopped before failure reached

These test results demonstrate that NLT can be used in the construction of mass timber buildings and can be designed to meet various FRRs. The use of protection on the unexposed side of an NLT assembly can delay integrity failures by reducing localized increased charring at gaps by limiting air flow through the assembly.

ACKNOWLEDGMENT

REFERENCES

[1]   The National Building Code of Canada (2015). Commission on Building and Fire Codes. National Research Council Canada. Ottawa, Canada.

[2]   *Nail-Laminated Timber. Canadian Design and Construction Guide v1.0.* (2017). Binational Softwood Lumber Council. Forestry Innovation Investment Ltd. Canada.

[3]   *Nail-Laminated Timber. U.S. Design and Construction Guide v1.0.* (2017). Binational Softwood Lumber Council. United States.

[4]   Ranger, L., Dagenais, C., Bénichou, N. (2019) *Evaluating Fire Performance of Nail-Laminated Timber*. FPInnovations. Ottawa, Canada.

[5]   CAN/ULC-S101 (2014). *Fire Endurance Tests of Building Construction and Materials.* Underwriters Laboratory of Canada (ULC). Toronto, Canada.

[6]   National Building Code of Canada Proposed Change 1027. NBC15 Div.B 3.1. Encapsulated Mass Timber Construction (2017). Canadian Commission on Building and Fire Codes.

[7]   Dagenais, C. *Fire Performance of Cross-Laminated Timber Assemblies.* Revised Ch 8. CLT Handbook. (2014) FPInnovations. Québec, Canada.

FIRE PERFORMANCE OF TIMBER-CONCRETE COMPOSITE FLOORS

Erica C. Fischer, Annabel Shephard, Andre R. Barbosa, and Arijit Sinha
Oregon State University, Corvallis, United States

ABSTRACT

Timber-concrete composite floors provide enhance diaphragm rigidity and strength for seismic design, and therefore are becoming more commonly used in high seismic regions. However, the fire resistance is typically solely based on the strength of the timber portion. These tests examined the structural behaviour of two timber-concrete composite systems during a standard fire exposure. Both cross-laminated timber and nail laminated timber were tested and constructed with self-tapping screws and MiTek truss plates, respectively, to transfer forces between the timber and concrete. The results indicate that the systems have significant fire resistive behaviour when subjected to a standard fire exposure.

1 INTRODUCTION

North America is rapidly adopting the use of mass timber products in mid- and high-rise building construction. These mass timber products lend themselves to offsite prefabrication, more precision in production, decreased construction time, lighter foundation systems, and reduced seismic demands. In many buildings, mass timber floors are designed with a concrete topping due to acoustic, vibration, or fire barrier design constraints (Pei et al. 2016). Mass timber high-rise building construction in the United States is currently hindered by the confines of the building codes (IBC 2018).

The current version of the International Building Code (IBC 2018) categorizes building construction in four Types. Type I construction is non-combustible construction materials (i.e. steel and concrete) used in high-rise buildings. Mass timber is Type IV-HT, heavy timber Type IV construction, which has a height limitation of 26 m). *Tall mass timber* is a term that refers to mass timber buildings that exceed this height limitation. Due to the structural performance and fire resistance of mass timber walls and floors, the International Code Council (ICC) voted to split the Type IV construction category into three parts for the next version of the IBC (IBC 2021). These three types of Type IV construction, Type IV-A, IV-B, and IV-C allow for mass timber buildings of heights 82 m, 55 m, and 26 m respectively.

The current building code does not currently recognize composite systems for strength and fire performance of a building. For fire performance, designers are forced to demonstrate life safety performance of exposed timber systems through the char-rate calculations (CEN 2004, NDS 2017).

Concrete toppings are utilized on mass timber floors for vibration, acoustics, and fire barriers. Engineers are taking advantage of these concrete toppings by developing composite connectors to transfer forces between the timber panels and concrete. These composite systems have enhanced structural performance and can span longer distances (Higgins et al. 2017). There is limited research on the fire performance of timber-concrete composite floors. The majority of the research occurred outside of the US and does not consider cross-laminated timber (CLT) (O'Neill 2009, Frangi et al. 2010), timber-concrete composite systems (Fragiacomo et al. 2012, Lineham et al. 2016, Wiesner et al. 2017), and joints within the system. Dagenais et al. (2016) tested three timber-concrete composite floors. One CLT-concrete, one screw laminated timber (SLT)-concrete, and one LVL-concrete composite floor

assembly to understand how shear connectors impact heat transfer in the assemblies. CLT-concrete composite systems were tested using self-tapping screws to transfer forces between the timber and concrete, and the SLT-concrete composite floor assembly used truss plates. Results indicated that the type of shear connector had little to no impact on the heat transfer in the assembly and that the floor assemblies reached a fire-resistance of over three hours. In addition, the presence of a shear connector and a concrete topping did not change the char rate of the timber. In the US, Type I construction requires two to three hours of fire resistance rating (IBC 2018). These tests indicate that composite CLT-concrete floors would meet this fire resistance requirement. These assemblies, however, did not include the joint between the CLT inter-panel connections.

The structural efficiency and fire resistance of a floor system depends upon the integrity of the fastening system and connection details used to connect the CLT panels together. O'Neill (2009) tested LVL-concrete composite systems with screw connections and concluded that the thermal expansion of the concrete slab is resisted by the composite action with the timber members. The restraint to thermal expansion induces an axial force in the timber members, which improves the system's resistance to gravity loads. O'Neill (2009) did not include cooling portions of the fire into experiments leaving a gap in knowledge of how the system will perform during the cooling phase of the fire. Frangi et al. (2010) also used screw connections to test similar timber-concrete composite floors as O'Neill (2009). The conclusion of this research was that the performance of the shear connectors governs the fire-performance. While these two experimental programs did not use CLT, the results indicate that the timber-concrete composite floors can have significant fire resistance. Fragiacomo et al. (2012) tested the fire-performance of CLT floors in fire conditions. However, the specimens tested in this program did not use a concrete topping used insulating cladding on the exposed surface of the CLT panels. Most recently, researchers at the University of Edinburgh (Lineham et al. 2016, Wiesner et al. 2017) tested a series of CLT beams under four-point bending and fire loading conditions. This testing program used an innovative testing approach consisting of radiant panels applying a constant heat flux on the bottom surface of the beams. These specimens did not include a composite concrete topping.

Composite action between timber panels and concrete toppings are achieved through connectors that are embedded both in the timber and concrete to transfer mechanical forces between the two materials. Previous tests have used a variety of different connectors. O'Neill (2009), Frangi et al. (2010), and Dagenais et al. (2016) used fully threaded screws to transfer mechanical loads between the CLT panels and the concrete topping. Dagenais et al. (2016) used truss plates between every third lamination of SLT panels to obtain composite action between the SLT panel and the concrete. These composite floors are anticipated to have higher load carrying capacity, and therefore better fire resistance than the timber alone.

2   OBJECTIVES

This paper provides an overview of the testing results from a furnace test of two floor systems: (1) CLT-concrete composite floors using fully-threaded screws to transfer mechanical forces between the timber and concrete and (2) NLT-concrete composite floors using truss plates to transfer forces between the timber and concrete. These tests aim to validate the char rates when using composite assemblies and generate data to investigate the fundamental mechanics of timber-concrete composite floors in fire scenarios.

3   MATERIALS AND METHODS

Two full-scale timber-concrete composite floors were tested in the furnace at the National Research Council of Canada. One specimen was CLT-concrete composite and one was NLT-concrete composite. The specimens were supported on the edges of the furnace using rollers to simulate a simply supported boundary condition. The floors were exposed to the ASTM E119 (ASTM 2016) fire curve. A distributed load of 3.8 kPa was applied to each specimen and sustained throughout the entirety of the test. This represents a typical design load for an office building in the US. The following sections detail the specimens and instrumentation.

3.1   CLT-concrete composite floor

The CLT-concrete composite floor consisted of a 5-ply, 175 mm thick, V2 stress grade Spruce-Pine-Fir (SPF) CLT conforming to ANSI/APA PRG-320 (2017). Fully-threaded 9.5 mm diameter self-tapping screws 200 mm in length were drilled into the unexposed surface of the CLT panel at an angle of 45 degrees. The screws were embedded 133 mm into the CLT, with the remainder length embedded in the 57 mm concrete topping. The concrete had a 28-day compressive strength of 34.4 MPa. W152 x 152 (W6 x 6) gauge 9/9 welded wire mesh was embedded in the concrete slab for shrinkage reinforcement. No additional tensile reinforcement was provided.

Along the centre of the specimen was a spline connection. This connection represented a typical panel-to-panel connection. Timber screws that were 152 mm in length were used for the connection and spaced at 102 mm along the length of the specimen. The width of the spline was 152 mm and plywood was used for the spline connection.

The tested specimen was 1219 mm wide by 4800 mm long. The screws were spaced at approximately 305 mm spacing in each direction with a 533 mm spacing at the midspan. The first screws were spaced 76 mm from the end of the floor along the length of the beam and 152 mm from each end along the width of the beam. The CLT was fully exposed to the fire. Figure 1a shows the construction of the CLT specimen.
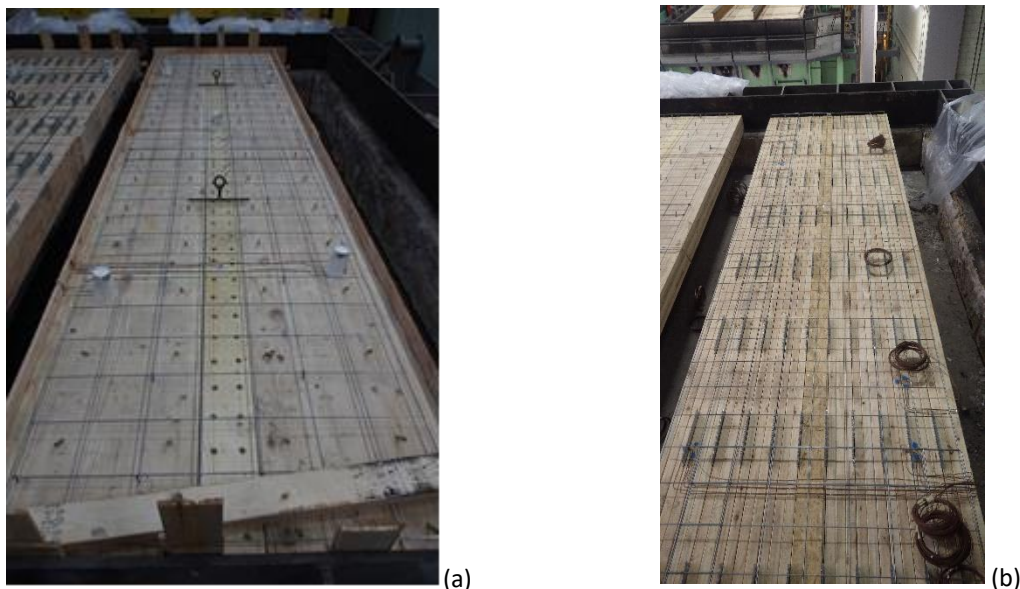

(a)   (b)

Fig. 1. Construction of timber-concrete composite floors: (a) CLT-concrete composite floor, and (b) NLT-concrete composite floor

3.2 NLT-concrete composite floor

The NLT-concrete composite floor consisted of 38 x 140 mm (nominal 2x6) lumber boards of SPF No. 2 species that were joined together in "beams" of 3 boards. Each beam used 3 x 0.12 nails to attach the boards together. Two rows of nails each at 25 mm from the top and bottom edge of the board, and 51 mm from each end of the board. The nails were staggered in spacing every 127 mm. The same pattern was used on the opposite side, but staggered by 127 mm.

A shrinkage gap was incorporated into the specimen by removing a lamination at the midpoint of the panel. A piece of 6 mm thick plywood was placed above the shrinkage gap to support the concrete during construction. A small cut down timber piece was lightly nailed in place beneath the gap in the panel. This piece was not the full height of the NLT boards.

The tested specimen was 1257 mm wide by 4800 mm long. The composite connectors used for the NLT-concrete composite floor were Mitek MT-20 truss plates spaced at 610 mm on centre along the length of the floor specimen and placed every third lamination along the width. The edge of the first plate was located 140 mm from the edge of the floor specimen on both ends. Each truss plate was 254 mm in length and 127 mm in height with 89 mm of the plate pressed between the laminations of the timber and the remainder of the truss plate embedded in the 76 mm thick concrete topping. The concrete deck used the same mix design as the CLT-concrete composite floor specimen and the same welded wire mesh reinforcement. Figure 1b shows the truss plates installed in the NLT-concrete composite floor and an overall view of the specimen while under construction.

3.3 Instrumentation

Both floor assemblies were instrumented with Type K thermocouples to measure the temperature distribution through the composite floor cross-section. Thermocouples were embedded within the timber panels, attached to the shear connectors, and embedded within the concrete. The depths of the thermocouples were chosen such that one thermocouple was located within each lamination of the CLT-concrete composite specimen. The same depths were used for the NLT-concrete composite specimen.

3.4 Fire testing

The two specimens were installed side-by-side with insulation between the two specimens and on either side to prevent flame through. The two specimens were allowed to deflect independently of one another. Figure 2a shows the fire exposed side of the two specimens from inside of the furnace. This figure also shows the thermocouples inside of the furnace that measured the gas temperature throughout the test. The loading apparatus used at the NRC has the capability of applying distributed loading to the specimens as shown in Figure 2b. With the load imposed, the two specimens were exposed to a standard fire (ASTM 2016).

Fig. 2. Fire testing setup at the NRC: (a) view of exposed timber surface from inside furnace, and (b) distributed loading apparatus

4 RESULTS

4.1 Observations

Pieces of the CLT specimen began to fall off at around 53 minutes and continued throughout the test. One of the disadvantages of testing side-by-side specimens is that when one specimen loses load-carrying capacity and collapses into the furnace, the test needs to stop. The goals of these tests were to collect temperature and displacement data to inform the fundamental behaviour of timber-concrete composite floors in a fire, verify the char rate of timber within a timber-concrete composite floor assembly, and collect data that can be used to benchmark numerical modelling capabilities. Therefore, to not stop the test prematurely and to test both specimens to failure, the slope of the deflection curves was tracked throughout the test. At about 90 minutes of standard fire exposure, the CLT-concrete composite floor deflection began to increase rapidly. At about 105 minutes, the load was removed from the specimen, while maintaining the load on the NLT-concrete composite floor. The test continued until 185 min (3 hr 5 min) when structural failure of the CLT-concrete composite floor occurred.

4.2 Displacement data results

After the initial loading the deflection of the CLT and NLT specimens was about 2 mm. For the first 103 minutes, the midspan displacement of the NLT specimen was greater than the CLT specimen. However, at about 103 minutes, when the CLT specimen began to increase in deflection rate, the CLT specimen mid-span displacement began to be larger than the NLT specimen midspan displacement. This is about the time when the load on the CLT specimen was removed.

Fig. 3 shows the midspan displacement histories for both of the specimens with the time of load removal on the CLT-concrete specimen indicated at 105 minutes. Both specimens had achieved runaway deflection at the point of structural failure of the CLT specimen.
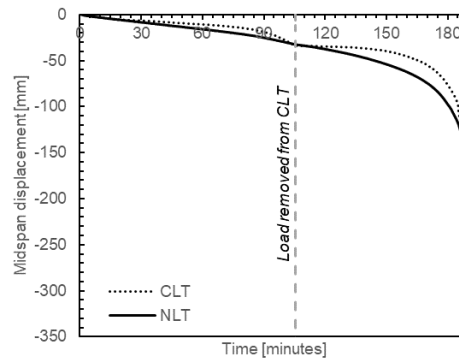
Fig. 3. Midspan displacement history during tests

4.3 Temperature data and char rate results

After the test, both specimens were removed from the furnace and measurements of char depth were taken along the length of each specimen. About 25.4 mm and 38 mm of CLT and NLT remained uncharred respectively. Throughout the specimen four laminations were charred. The layout of the thermocouples allowed for the authors to measure the temperature distribution through the cross section of each specimen. Char rates were inferred from the thermocouple data by assuming the char front reached the depth of the thermocouple when the temperature exceeded 300°C. This is a commonly used method of determining char rate from experimental tests (Dagenais et al. 2016).

The resulting charring rates for the CLT as determined from the thermocouple data were 0.66 mm/minute for the first lamination, 0.80 mm/minute for the second lamination, and 0.60 mm/minute for the third lamination. These char rates are assumed to be specific to each lamination of the CLT. The char rates are shown in Table 1 and plotted in Fig. 4 for different sections where temperature distribution through the full cross-section was measured. CLT-1 and CLT-2 are located at the approximate quarter points along the length of the floor and are offset from the centreline of the panel. The NDS char rate for CLT considering delamination is 0.76 mm/min, which is a reasonable approximation for what was measured during the test.

Because the CLT almost completely charred, the temperature at the CLT-concrete interface increased to a maximum average temperature of 474°C by the end of the test. At the point the load was removed from the specimen, the temperature at the interface was an average of 24°C. The temperature of the shear connector at the time of load removal was an average of 23°C and 65°C at the time of structural failure. These thermocouples were attached to the top of the shear connector.

Figure 4 shows the char depth versus time for both specimens. This plot shows that the char depth was not influenced by the removal of load from the CLT specimen. The load was removed at 105 minutes, and the slope of the char depth is constant at that time. The CLT specimen did, however, exhibit delamination throughout the test. This was evidenced through video cameras placed at the viewing holes of the furnace and inside of the furnace. The panel used in the test adhered to PRG-320 (2017), and therefore the adhesives did not meet the strict requirements for delamination in fire of PGR-320 (2018). The char rate of the specimen was therefore higher than it would have been if delamination was limited.

The resulting char rate calculated using the data from the thermocouples for the NLT-concrete composite floor was more consistent than the CLT-concrete composite floor specimen. The char rates were 0.68, 0.57, and 0.63 mm/minute for depths 35 mm, 70 mm, and 150 mm from the bottom of the 2x6 boards respectively. The NDS char rate is 0.64

mm/min and the Eurocode char rate is 0.7 mm/min. The measured char rates for the NLT specimen demonstrate the char rates in the NDS and Eurocode are a reasonable approximation. The char rates are shown in Table 1 and plotted in Fig. 4 are located at about the quarter points along the length of the floor specimen and offset from the centreline, which had a shrinkage gap. At the interface of the NLT and the concrete, the average maximum temperature was 219°C. The average maximum temperature of the top of the shear connector embedded in the concrete was 70°C.

Table 1. Resulting char rates (average)

Location	Charring rate (mm/min)	
	CLT	NLT
35 mm	0.66	0.68
70 mm	0.80	0.57
105 mm	0.60	0.63
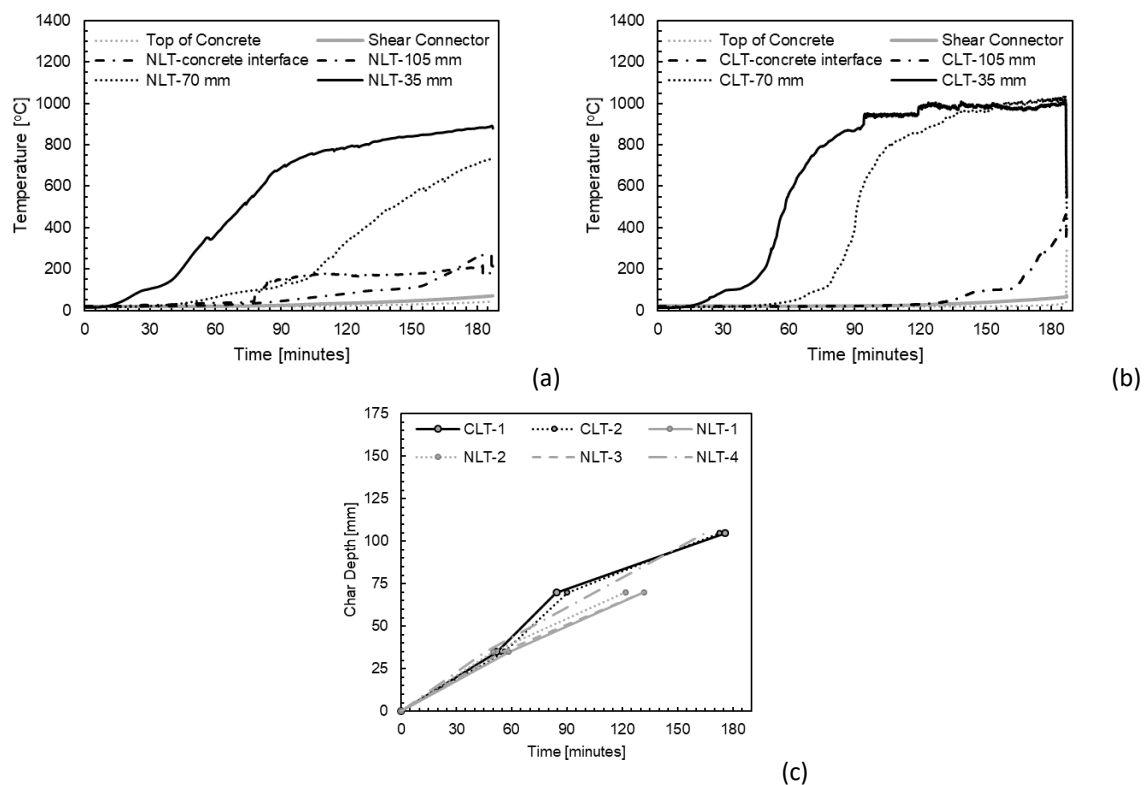
Fig. 4. Experimental temperature data (a) average temperature distribution through NLT-concrete composite specimen, (b) average temperature distribution through CLT-concrete composite specimen, and (c) char depth progression during tests at varying sections

5   CONCLUSIONS

Two timber-concrete composite floors were evaluated for fire-resistance. The objectives of these tests are to observe and investigate the performance of timber-concrete composite floors and any impact the composite system had on the fire resistance of the assemblies. These assemblies reached significant fire resistance when subjected to a 3.8 kPa distributed

load. Delamination of the CLT contributed to a significant loss of load carrying capacity and higher char rate.

Due to the delamination of the CLT during the test, additional tests should be performed using new CLT adhesive products that adhere to the PRG-320 (2018) standard. These tests will demonstrate the fire resistance for using composite CLT-concrete floors. Additional tests considering different types of shear connectors that provide more flexibility and ease of construction may also yield different results with regards to time to structural failure.

ACKNOWLEDGMENT

REFERENCES

[1] ANSI/AWC NDS (2015). National Design Specification (NDS) for Wood Construction. American Wood Council (AWC): Leesburg, VA.

[2] ANSI, «Standard for Performance-Rated Cross-Laminated Timber (ANSI/APA PRG 320-2017),» APA - The Engineered Wood Association., Tacoma (WA), 2012.

[3] ANSI, «Standard for Performance-Rated Cross-Laminated Timber (ANSI/APA PRG 320-2018),» APA - The Engineered Wood Association., Tacoma (WA), 2018.

[4] ASTM International (2016). ASTM E119-16a Standard Test Methods for Fire Tests of Building Construction and Materials. West Conshohocken, PA; ASTM International.

[5] CEN (2004). Eurocode 5: Design of timber structures – Part 1-2: General – Structural fire design. European Committee for standardization: Geneva, Switzerland.

[6] Dagenais, C., Ranger, L., Cuerrier-Auclair, S. (2016). Understanding Fire Performance of Wood-Concrete Composite Floor Systems. In: World Conference on Timber Engineering, WCTE 2016. 22-25 August 2016; Vienna, Austria.

[7] Frangi, A., Knobloch, M., and Fontana, M. (2010). Fire Design of Timber-Concrete Composite Slabs with Screwed Connections. Journal of Structural Engineering, 136(2), pp. 219-228.

[8] Fragiacomo, M., Menis, A., Clemente, I., Bochicchio, G., Tessadri, B. (2012). Experimental and Numerical Behaviour of Cross-Laminated Timber Floors in Fire Conditions. World Conference on Timber Engineering: Auckland, New Zealand.

[9] Higgins, C., Barbosa, A.R., Blank, C. (2017). Structural Tests of Concrete Composite-Cross-Laminated Timber Floors, Structural Engineering Research Laboratory, Report No. 17-01, School of Civil and Construction Engineering, Oregon State University, Corvallis, Oregon, United States of America. URL: https://cce.oregonstate.edu/sites/cce.oregonstate.edu/files/pdfs/som_report_osu_1701.pdf

[10] IBC (2018). International Building Code. International Code Council: Country Club Hills, IL.

[11] IBC (2021). International Building Code. International Code Council: Country Club Hills, IL.

[12] Lineham, S.A., Thomson, D., Bartlett, A.I., Bisby, L., Hadden, R.M. (2016). Structural response of fire-exposed cross-laminated timber beams under sustained loads. 85, pp. 23-34.

[13]   O'Neill, J.W. (2009). The Fire Performance of Timber-Concrete Composite Floors. A Thesis Accepted by the Department of Civil and Natural Resources Engineering of University of Canterbury.

[14]   Osborne, L. (2015). Fire resistance of long span composite wood-concrete floor systems (Project No. 301009649), FP Innovations.

[15]   Pei, S., Rammer, D., Popovski, M., Williamson, T., Line, P., van de Lindt, J.W. (2016). An Overview of CLT Research and Implementation in North America. In: World Conference on Timber Engineering, WCTE 2016. 22-25 August 2016; Vienna, Austria.

[16]   Wiesner, F., Randmael, F., Wan, W., Bisby, L., Hadden, R.M. (2017). Structural response of cross-laminated timber compression elements exposed to fire. Fire Safety Journal, 91, pp. 56-67.

[17]

FIRE PERFORMANCE OF PROTECTED AND UNPROTECTED CONCEALED TIMBER CONNECTIONS

Aba Owusu[1], Osama (Sam) Salem[2] and George Hadjisophocleous[1]

[1]Dept. of Civil and Environmental Engineering, Carleton University, Ottawa, Ontario, Canada
[2]Dept. of Civil Engineering, Lakehead University, Thunder Bay, Ontario, Canada

Abstract

The research presented in this paper aimed to investigate the structural performance of protected concealed wood-steel-wood (WSW) beam connections subjected to fire. In such concealed WSW connections, steel T-stub connector and bolts, which mainly cause the rapid charring of wood, were protected using wood strips and plugs, respectively. Four full-size glulam beam bolted connection test assemblies were experimentally examined: two connection assemblies, one protected and the other unprotected, were tested at ambient temperature under gradually-increased monotonic loads until failure; whereas the other two test assemblies, which were identical to those examined at ambient temperatures, one protected and the other unprotected, were subjected to CAN/ULC-S101 standard fire while being loaded to 100% of the ultimate design load capacity of the weakest connection configuration. The experimental results revealed that, although the protected connection configuration had slightly less moment-resisting capacity than that of the unprotected configuration at ambient temperature, it had an increased fire resistance time by about 70%.

Keywords: WSW connections, glulam beams, fire protection, fire resistance testing.

1   INTRODUCTION

The use of wood in building construction around the world has considerably increased in the past few decades due to its renewability and sustainability. There are mainly two types of construction associated with wood: light frame construction and heavy timber construction. In heavy timber construction, structural members are joined together using connections involving steel plates and bolts. In case of fire, beam-to-column connections are typically the weakest link, as the presence of steel components helps in transferring heat to the interior of the wooden connection, and thus increases the charring rate and consequently decreases the connection's fire resistance time.

Most fire resistance studies focussed on axially-loaded connections (Racher *et al*., 2010) under either compressive or tensile loading perpendicular to wood grain (Audebert *et al*., 2012), or parallel to wood grain (Peng. *et al*., 2010). Therefore, there is urgent need to investigate the structural fire performance of moment-resisting timber connections, to fully understand the behavior of such connections that can effectively be utilized in tall wood buildings that are susceptible to lateral loads which can develop bending moments on such connections. In a few research studies, such as those conducted by Zarnani and Quenneville (2014) and Xu *et al*. (2015), numerical models were developed to determine the moment-resisting capacities and failure modes of timber-steel hybrid connections at ambient temperature.

To better understand the behaviour of wooden connections in fire, a few researches have focused on studying large-size experiments of different connection configurations, such as exposed steel-wood-steel (SWS), concealed wood-steel-wood (WSW), and seated connections. It has been observed that the concealed type connection performs relatively poor in fire because of the reduction in member size due to wood removal because of the slotted cut required to

accommodate the steel T-stub connector plate that also transmitted more heat to the core of the wood section and consequently shortened the fire resistance time (Ali *et al*, 2016). In this study, fire resistance of glulam beams having cross-sectional dimensions of 140-mm wide x 191-mm high x 1900-mm long was investigated. All beam sections were connected at their ends to two fire-protected steel columns that were 3200-mm long using four A307 bolts. The glulam beams were subjected to two-point loads that were one-third beam span length apart. In addition to the experimental tests conducted in this study, all beams along their end connections were modelled using ABAQUS Standard software. The developed finite element (FE) models' predictions were validated using the experimental results obtained from this study. It was also observed from both, experimental and numerical outcomes that, the rate of degradation of the connection's strength during fire resistance tests was mainly dependent on the exposure of the steel components, e.g., bolts and plates, to fire. Moreover, the reduction of the cross-sectional dimensions due to wood charring initiated brittle failure in all test assemblies, such as wood splitting.

In another study conducted by Petrycki and Salem (2017), the fire performance of full-size concealed (WSW) glulam connections using two and three rows of bolts, each of two bolts, with four- and five-times the bolt diameter end distances were experimentally investigated. It was concluded that increasing the number of bolt rows from two to three rows enhanced the fire resistance time of the glulam beam-to-column connections by a greater increment than that observed by increasing the bolt's end distance from four- to five-times the bolt diameter. Also, from the failure patterns of the connections of this study, all test assemblies experienced brittle failure with minor deformations developed in the connecting steel bolts.

The research presented in this paper has focussed on studying the structural behaviour of concealed WSW glulam bolted connections at both, ambient and elevated temperatures. One connection configuration had its steel components fire exposed, whereas the other connection configuration had its steel components, e.g., T-stub connector and bolts, fire protected using wood strips and plugs, respectively.

2 TEST SPECIMENS, TEST SETUP AND PROCEDURE

2.1 Test specimens

Four 1600-mm long glulam beams of 184 x 362 mm cross-sectional dimensions were used in this experimental study. Each beam section was connected to a fire-protected steel column by steel T-stub section made of 12.7-mm (1/2") thick plate and four 19.1-mm (3/4") diameter A325M high-strength bolts. The bolt end distance, edge distance, and spacings were designed in accordance with CSA 086-14. The glulam material utilized in all four test specimens was black spruce–pine, grade 24f-EX. A slotted cut of 15-mm wide was prepared at the center of the beam cross section to accommodate the web of the steel T-stub connector, allowing slightly more than 1.0 mm clearance on each side of the steel plate, as per CSA 086-14. A 30-mm diameter spade bit was used to create circular holes in the beam front and back faces to accommodate the bolts' heads, washers, and nuts. As shown in Figs. 1(a) and (b), two connection configurations were prepared with the beam in each configuration connected to the steel plate using four bolts in two rows. Fig. 1(a) shows the unprotected connection configuration, labelled (N), in which neither the steel plate nor the bolts' heads or nuts were fire protected. Fig.1 (b) shows the other connection configuration, labelled (P), that was made using the same bolt pattern; however, the bolts' heads and nuts and the steel plate's top and bottom edges were fire protected using glued-in wood plugs and strips, respectively. The wood plugs used to cover the bolt' heads and nuts had thicknesses of 30 mm and 20 mm, respectively.
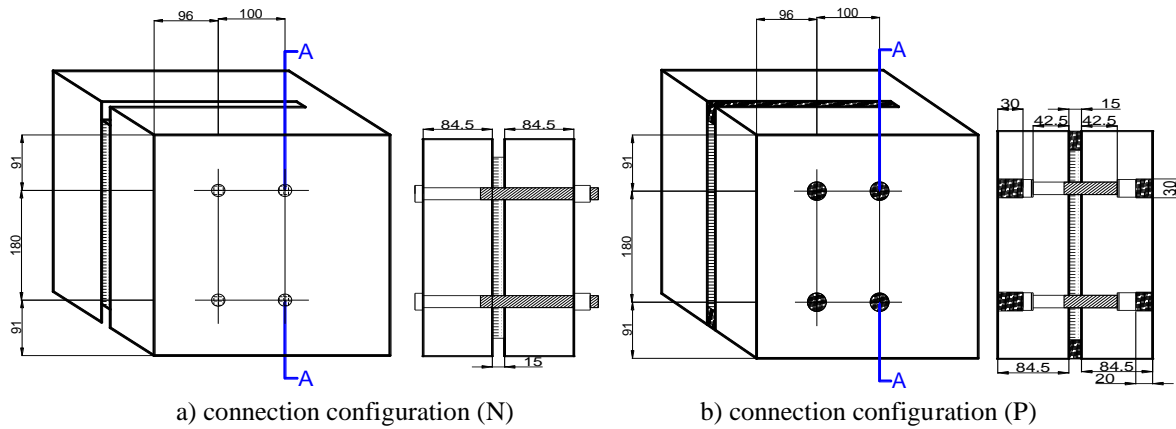
a) connection configuration (N)   b) connection configuration (P)

Fig. 1. Test connection assemblies: a) connection configuration (N) without fire protection; b) connection configuration (P) with fire protection.

For the fire resistance tests presented in this paper, the connection configuration (N) had twelve metal-shielded K-type thermocouples (TC) installed at different locations: four TC from the beam front face (TC1 through TC4); six from the beam back face; one from the beam top side (TC11); and one from the beam bottom side (TC12), as shown in Fig. 2(a).
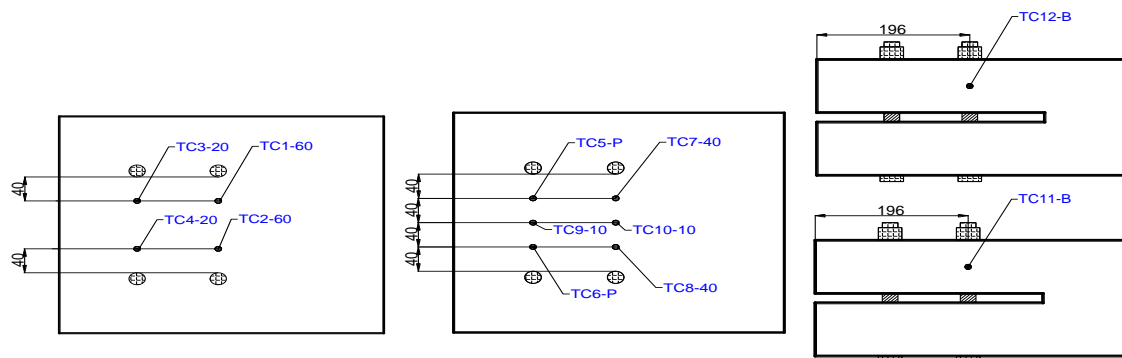
a) configuration (N) thermocouples layout; from the beam front face (left); back face (middle); and top and bottom sides (right)
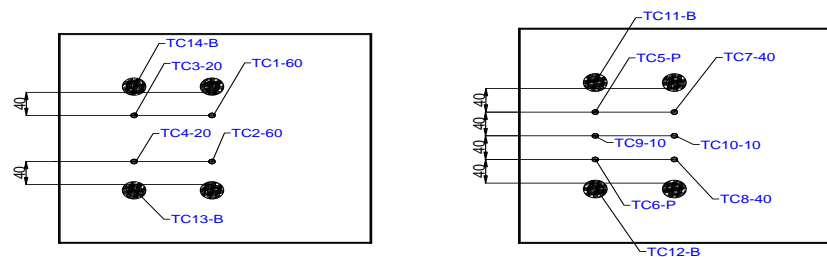
b) configuration (P) thermocouples layout; from the beam front face (left); and back face (right)

Fig. 2. Thermocouples layouts: a) configuration (N) thermocouples layout; b) configuration (P) thermocouples layout.

Fig. 2(a) also indicates the depth (in mm) at which each TC was embedded inside the wood section. For instance, TC1 and TC2 were installed at 60-mm deep from the beam front face; TC3 and TC4 at 20-mm deep from the beam front face; TC7 and TC8 at 40-mm deep; and TC9 and TC10 at 10-mm deep. TC5 and TC6 were employed to measure the steel plate temperatures, whereas TC11 and TC12 measured the temperatures of one of the top bolts and one of the bottom bolts, respectively. For the connection configuration with fire protection,

372

labelled (P), fourteen metal-shielded K-type thermocouples (TC) were used: six were installed from the beam front face and eight from the beam back face, as shown in Fig. 2(b). TC5 and TC6 measured the steel plate temperatures. TC11 and TC12 measured the temperatures of the bolt nuts underneath the 20-mm thick wood plug, whereas TC13 and TC14 measured the temperatures of the bolt heads underneath the 30-mm thick wood plug. All glulam beam sections were stored indoor before being tested; hence they experienced between 1- and 2-mm shrinkage in their cross-sectional dimensions due to the reduction in their moisture contents (MC) by the time the experiments were conducted. The moisture contents of the glulam sections were measured right before testing, and the average MC was recorded as 8%.

2.2 Test setup and procedure

Both, ambient and fire resistance experiments presented in this paper were conducted at Lakehead University's Civil Engineering Structures Laboratory and Fire Testing and Research Laboratory (LUFTRL), respectively. Each glulam beam was connected at one end using T-stub steel connector that was rigidly attached to a fire-protected supporting steel column. A point load was applied 1400 mm away from the beam support using a Universal Testing Machine (UTM), as shown in Fig. 3(a). During testing, the deflections of the beam in response to the gradually-increased loading were measured using two Linear Variable Differential Transformers (LVDTs): one was 200 mm away from the support; and the other was located at where the load was applied, near the free end of the beam. All test assemblies were loaded until the beam connection failed.

a) ambient temperature test setup   b) fire resistance test setup

Fig. 3. Test setups: a) ambient temperature test setup; b) fire resistance test setup.

The two connection configurations presented in this paper, were tested at ambient and elevated temperatures. In fire resistance tests, both connection configurations were exposed to CAN/ULC-S101 standard fire while being loaded to 100% of the ultimate design load capacity of the weakest connection configuration. The monotonic constant applied load was deliberately chosen to be equal to the ultimate design load capacity of the weakest connection configuration in order to compare the fire resistances of the two different connection configurations independently from their moment-resisting capacities. The supporting steel column and the top side of the glulam beams were completely protected using 1.0-inch thick ceramic-fibre blanket. Fig.3(b) shows a fire resistance test setup for a general glulam beam installed inside the fire testing furnace. During fire test, the beam connection failure criterion was set to a maximum beam end deflection that corresponded to a connection rotation magnitude of 0.1 radians. However, fire tests were continued beyond this point until the applied load dropped significantly, at which the beam couldn't sustain any load increase. One low-thermal elongation ceramic rod was placed vertically through a predrilled small hole in the furnace roof and was attached to a displacement transducer installed outside the furnace to allow the measurement of the beam vertical displacements at 200-mm distance from the beam supporting column. In addition to the mechanical measurements, thermal measurements were recorded during fire resistance testing. The measured temperatures were used to determine the average wood charring rate since there was total burnout of the beam section as the furnace cooled

down overnight. Knowing the actual average wood charring rate helped in determining how the bolts contributed to the heat transfer within the wood section.

3   EXPERIMENTAL RESULTS AND DISCUSSION

The experimental data measured from both ambient and elevated temperatures tests were analysed to determine the connections' failure loads, rotations, and failure modes. In addition, for the fire resistance tests, average wood charring rate and temperatures with respect to time were also analysed.

3.1   Ambient temperature tests

Table 1 lists the connections' failure loads and maximum moment-resisting capacities. It was noticed that the beam connection configuration (N), where the bolts' heads and nuts and the steel plate's top and bottom edges were exposed, exerted a maximum moment magnitude that is 7% greater than that of the connection configuration (P) with fire protection. This is due to the wood section reduction caused by embedding the bolts' heads and nuts into the glulam beam cross section in the connection configuration with fire protection applied.

Table 1. Summary of ambient temperature tests results

Connection configuration	Failure load (kN)	Maximum moment (kN.m)	Maximum rotation (Rad)	Failure mode (numerical)	Failure mode (experimental)
N	18.9	26.5	0.012	Splitting	Splitting
P	17.7	24.8	0.017	Splitting	Splitting/Internal row shear out

Fig. 4 represents the moment-rotation relationship developed for the two connection configurations experimentally examined at ambient temperature. The beam connection without fire protection failed mainly due to wood splitting occurred at the top row of bolts with a beam-column rotation of 0.012 rad. Hence, a sudden drop in the connection's moment happened, as shown in Fig. 4. However, the beam connection was still able to sustain the applied load that was gradually increased after the sudden drop at a rate of 2.0 kN per minute until another wood split developed at the bottom row of bolts, as shown in Fig. 5. For the other beam connection configuration with protection, configuration (P), the rotation increased linearly with the gradually-increased load until the connection experienced a sudden drop due to splitting of the top row of bolts under tensile stresses, Fig. 5. Afterwards and with increased loading, the top row of bolts started to exhibit row shear out. It is noteworthy that the reduction in the beam section's effective width due to the circular notches created to accommodate the bolts' heads and nuts in connection configuration (P) contributed to the reduction in the moment-resisting capacity of this connection configuration compared to the other connection configuration with no fire protection, configuration (N). However, both connection configurations exhibited brittle failures, such as splitting and row shear out, as shown in Fig. 5.
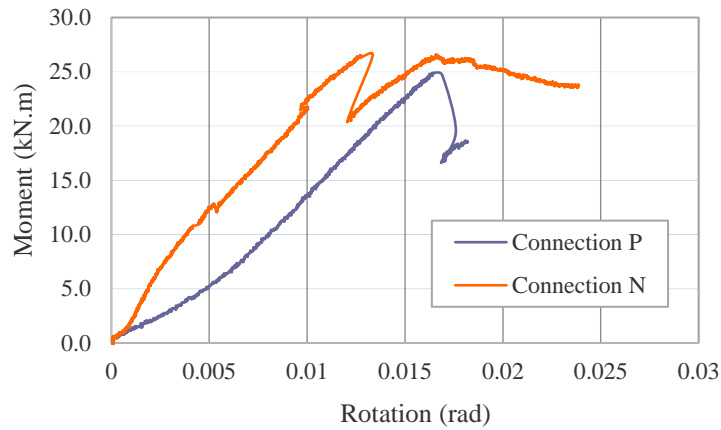
Fig. 4. Moment-rotation relationships of the beam connection configurations with protection (P) and without protection (N)

Fig. 5. Failure modes of the two beam connection configurations in ambient temperature tests; N (left) and P (right)

3.2   Fire resistance tests

3.2.1   Time to failure

The fire resistance tests' results summarised in Table 2 show that the time to failure of the connection configuration (P), with fire protection, was recorded at about 56.0 minutes, which is 23 minutes (about 70%) more than that of the other connection configuration (N). Therefore, unlike the ambient temperature tests, the connection configuration with fire protection significantly performed better than that with no protection in fire condition. This confirms that, with simple fire protection means, such as wood plugs and strips to protect the bolts' heads and nuts and the steel plate edges, respectively, a fire resistance rating of 45 minutes can be achieved for glulam beam WSW concealed connections like the ones experimentally examined and presented in this paper.

Table 2. Summary of fire resistance tests results.

Connection configuration	Applied moment (kN.m)	Time to failure (min)	Average charring rate (mm/min)	Failure Mode
N	14.8	33.0	0.67	Splitting
P	14.8	56.0	0.80	Splitting

3.2.2   Charring rate

Both beam connection configurations were completely burnout by the time the furnace was cooled down and opened the next day. Therefore, there was no residual glulam sections to be assessed to determine the actual wood charring rate. However, using *Eq. (1)* along with the thermal measurements captured during fire testing by the thermocouples installed at depths of 10 mm and 20 mm into the glulam section, the average wood charring rate was estimated.

$$C = \beta t \qquad (1)$$

where   C   is taken equal to 10 mm,

       t is the time difference for heat transferred between 10 mm and 20 mm depth at 300 °C which is the nominal wood charring temperature.

In addition, the results from Table 2 show that the beam connection configuration (P) had a higher estimated wood charring rate compared to that of the connection configuration (N).

3.2.3   Connection rotations

Fig. 6(a) shows the time-rotation relationships of the two beam connection configurations during the fire resistance tests. Both connections configurations had rotations that increased linearly during the early stages of the tests followed by an exponential rise that started in the connection configuration (P) about 25 minutes later than that of the connection configuration (N). This can be attributed to the fact that, the protected bolts' heads and nuts did not experience considerable increase in its temperatures at early stage of the fire test; hence there was no considerable charring of the wood section inner core, which resulted in much less rotations of the connection configuration (P) for longer time in fire condition. Fig. 6(b) shows a slight increase in the rotation of the protected connection configuration (P) at about 30 minutes from the start of the fire test.
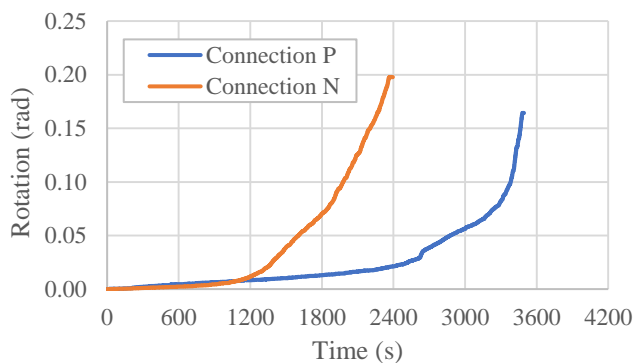
a) connections' time-rotation relationships   b) connection configuration (P) in fire

Fig. 6. Time-rotation relationships of the beam connection configurations (P), with protection, and configuration (N), with no protection, throughout fire resistance tests

3.2.4   Time-temperature curves

Fig. 7 shows the thermal measurements taken during the fire resistance test of the beam connection configuration (N), with no protection. As shown in the figure, wood temperatures at 20-mm depth from the beam front face, measured by TC3 and TC4, reached 100°C after about 5 minutes from the start of the fire test. At this stage, the moisture trapped in the wood section started to evaporate, and consequently the wood started to pyrolyze then eventually char at approximately 300°C, at about 12 to 17 minutes. From the time-temperature curves shown in Fig. 7, it can also be observed that, at the time of the structural failure of the connection, the thermocouples at 20-mm deep from the beam face (TC3 and TC4) had recorded temperatures that were extremely higher (about 800°C) than the wood charring temperature. In addition, the thermocouples embedded at 40-mm deep from the beam face (TC7 and TC8) recorded temperatures around 200°C, while the thermocouples embedded at 60-mm deep from the beam face (TC1 and TC2) recorded temperatures around only 100°C.
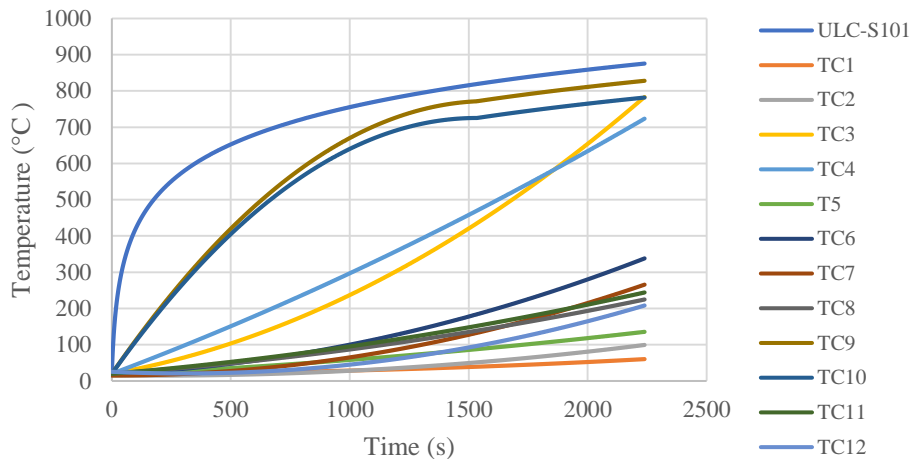
Fig. 7. Time-temperature curves developed using the thermal measurements of the connection configuration with no fire protection, configuration (N)

4. CONCLUSIONS

In the experimental study presented in this paper, the behaviour of wood-steel-wood (WSW) concealed connections, with and without fire protection, was investigated at both ambient and elevated temperatures. The study focussed on the performance of the tested connections regarding the connection's rotational behaviour, moment-carrying capacity, and failure mode. Outcomes of this study helped in drawing the following conclusions;

- The connection configuration (N) without fire protection exerted a maximum moment-resisting failure capacity that is about 7% greater than that of the connection configuration (P) with protection in ambient temperature tests;
- Both connection configurations exhibited initial failure mode of wood splitting at the top row of bolts, followed by splitting at the bottom row of bolts in connection configuration (N) and row shear out in the top row of bolts in connection configuration (P);
- The time to failure of the connection configuration (P) was about 56.0 minute in standard fire condition, which is 23.0 minutes more than that of connection configuration (N);
- The connection with fire protection, configuration (P), maintained a slightly increased linear rotation-time relationship for about 25.0 minutes more than what the connection without fire protection, configuration (N), exhibited;
- The unique experimental results developed out of this study confirm that, with simple fire protection means, such as wood plugs and strips to protect the bolts' heads and nuts and the steel plate edges, respectively, a fire resistance rating of 45 minutes can be achieved for glulam beam WSW concealed connections.

5. RECOMMENDATION

It is recommended that when considering both, the connection moment-resisting capacity and its fire resistance, the top and bottom edges of the steel T-stub connector and the bolts' heads and nuts should be protected as detailed in connection configuration (P) of this paper. Further analytical work is to be extended to derive a relationship between the thickness of the wood plug protection and the fire resistance time of the WSW concealed connections.

REFERENCES

[1] Audebert M., Dhima D., Taazount M., Bouchaïr A. (2014). Experimental and numerical analysis of timber connections in tension perpendicular to grain in fire. Fire Safety Journal 63, pp. 125-137.

[2] Buchanan A., Abu A.K. (2017). Structural design for fire safety, 2nd Edition, John Wiley & Sons Ltd.

[3] CAN/ULC-S101-14. (2014). Standard Methods of Fire Endurance Tests of Building Construction and Materials, Fifth Edition, Canada.

[4] CSA Standard 086-14. (2014). Engineering design in wood. Canadian Standards Association, Ottawa, Ontario.

[5] ISO 834-1. (1999). Fire resistance tests - Elements of building construction, Part 1: General requirements, International Organization for Standardization, Switzerland.

[6] Peng L., Hadjisophocleous G., Mehaffey J., Mohammad M. (2012). Fire performance of timber connections, Part 1: Fire resistance tests on bolted wood-steel-wood and steel-wood-steel connections. Journal of Structural Fire Engineering 3(2), pp. 107–132.

[7] Petrycki A., Salem O. (2017). *Experimental fire testing of concealed steel-glulam timber semi-rigid bolted connections*, *Proceedings of the 6th International Conference on Engineering Mechanics and Materials*, CSCE, May 31st to June 3rd, Vancouver, Canada.

[8] Racher P., Laplanche K., Dhima D., Bouchaïr A. (2010). Thermo-mechanical analysis of the fire performance of dowelled timber connection. Engineering Structures 32(4), pp. 1148-1157.

[9] Ali S., Hadjisophocleaus G., Akotuah A.O., Erochko J., Zhang X. (2016). Study of the fire performance of hybrid steel-timber connections with full-scale tests and finite element modelling, Proceedings of the International Conference on Applications of Structural Fire Engineering, 15th-16th October, Dubrovnik.

[10] Xu B.H., Bouchaïr A., Racher P. (2015). Mechanical behaviour and modelling of dowelled steel-to-timber moment-resisting connections. Journal of Structural Engineering 141(6).

[11] Zarnani P., Quenneville P. (2014). Design method for coupled-splice timber moment connections. Proceedings of the 13th World Conference on Timber Engineering, WCTE2014, Quebec, Canada.

FIRE RESISTANCE TESTING OF GLULAM BEAM END CONNECTIONS UTILIZING THREADED STEEL RODS IN A PILOT CONNECTION CONFIGURATION

Cory Hubbard and Osama (Sam) Salem
Dept. of Civil Engineering, Lakehead University, Thunder Bay, Ontario, Canada

ABSTRACT

Bolt and plate connections offer a simple yet strong connection in timber buildings; however, their fire resistance, when unprotected, is minimal. For the research presented in this paper, four full-size glulam beam connections, each utilized two concealed threaded steel rods that were inserted into the end of a glulam beam section, near the top and bottom sides, were experimentally examined. Two small holes carved into one side of the beam, where the rod ends are inserted, were employed to insert a steel washer and a nut, in each hole, to mechanically fasten the threaded rod's embedded end. The main study parameter was the rod embedment length; where 200 mm and 250 mm embedment lengths with the use of same 38.1-mm square washer were experimentally examined to investigate their effects on the beam connection strength. A design load reflecting the connection's ultimate design moment-resisting capacity was applied at the end of the cantilevered beam that was then exposed to elevated temperatures that followed CAN/ULC-S101 standard time-temperature curve. Results revealed that, the beam connection of 200-mm embedment length lasted about 58 minutes in fire, whereas the connection of 250-mm embedment length lasted about 62 minutes.

1   INTRODUCTION

Nowadays, glued-laminated timber (glulam) is one of the most commonly-used engineered-wood products, which has its potential still being researched to utilize its abilities fully. The areas most lacking in the available design guidelines of glulam are embedded-rod connections (Hunger *et al.*, 2016) and moment-resisting connections (Petrycki and Salem, 2017). Glued-in threaded steel rods have been in use and experimentally tested since the late 1980's; however, there are no consistent design procedures for their application (Barillas, 2014; Fragiacomo and Batchelar, 2012). Some design approaches and code models have been published; however, there are some discrepancies and even partial contradictions between the different available models (Steiger *et al.*, 2006). The interaction between wood, adhesive and metal, introduces several variables which need to be carefully considered, making it difficult to predict the connection's failure (Oh, 2016). A primary issue with connections composed of glued-in rods in timber sections is when the connection must be made on site. This type of application has been shown to carry a high risk of having the rods being improperly bonded since the effectiveness of the grouting process cannot be visually checked (Batchelar and McIntosh, 1998). Therefore, it is highly recommended that the gluing process is done in a controlled environment, where skilled workers can check their work and ensure a proper bond between the steel rods and the wood sections.

Timber connections utilizing embedded rods have the advantage of being superior in fire performance compared to other connection types since the steel rods are completely concealed inside the wood section. Even a connection where only a slight portion of the steel rod is exposed still has considerably high charring rate due to the fact that steel components quickly conduct heat into the connection (Barber, 2017). Also, issues with the epoxy at elevated temperatures still need to be further investigated. A study done by Di Maria *et al.*

(2017) shows that epoxy deteriorates, and thus the connection can easily fail when the temperature surrounding the rod reaches thresholds of only 50°C to 60°C.

A practical solution to the epoxy problem at elevated temperatures is to mechanically fasten the steel rods, instead. In addition, such a connection can be easily assembled in the field, eliminating the common possibility of bond failure in the glued-in rods, as well as avoiding the epoxy deterioration issues at elevated temperatures. This paper presents the results of an experimental study undertaken to investigate the behaviour of glulam beam end connections, utilizing mechanically-fastened threaded steel rods and subjected to standard fire.

2   EXPERIMENTAL PROGRAM

Four full-size test assemblies were experimentally examined in the study presented in this paper. Two configurations were used for the rod-glulam connections. The test variable for the two configurations was rod embedment length.

2.1 Materials

2.1.1   Glulam sections

The glulam beam sections (135 mm x 314 mm) used in all test assemblies were S-P-F, comprised of 90% black spruce. The beam sections were manufactured to meet the 24F-ES/NPG stress grade with architectural appearance grade. The individual lamina stocks that were used to build up the beam sections measured approximately 24 mm x 47 mm. The laminations were finger jointed at their ends and glued together in horizontal and vertical layers. Since the beam sections were manufactured to provide symmetrical alignment of the laminations along the cross sectional width and depth, the beam sections had a homogeneous layup. The main mechanical design properties of the glulam are listed in Table 1, below.

Table 1: Mechanical properties of glulam sections (Nordic Structures, 2015)

Property	Strength (MPa)
Bending moment, F_b	30.7
Longitudinal shear, F_v	2.5
Compression perpendicular to grain, F_{cp}	7.5
Compression parallel to grain, F_c	33.0
Tension parallel to grain, F_t	20.4
Tension perpendicular to grain, F_{tp}	0.51
Modulus of elasticity, E	13100

2.1.2   Threaded rods

The threaded rods used in the experiments had a diameter of 19.05 mm (3/4"), length of 910 mm and stress grade of SAE J429-Grade 2. Using a band saw, the rods were cut to two pieces: 470 mm and 520 mm for the test assemblies with 200-mm and 250-mm embedment lengths, respectively. The remaining cut off rod sections was used as tension coupons, and thus was tested on a Tinus Olsen Universal Testing Machine at Lakehead University's Civil Engineering Structures Laboratory to confirm the stress grade of the rods. The average tensile force exerted by the rods were recorded as 90.0 kN, confirming the rods stress grade.

2.1.3 Washers

The washers used for the experiments were fabricated from a 12.7-mm thick steel flat bar with a stress grade of 300W, as specified by CSA G40.20-04/G40.21-13. There were eight washers fabricated; all had dimensions of 38.1 mm x 38.1 mm (1.5" x 1.5"). A 20.6-mm (13/16") diameter hole was drilled in the centre of each washer to allow the insertion of the rods.

2.2 Test assembly details and fabrication process

The two threaded rods employed in the glulam beam pilot connection configuration had embedment lengths of either 200 mm or 250 mm. Every beam section had a line marked perpendicular to the wood grain at the required embedment length, and a line marked parallel to the grain down the centre of the 314-mm wide face. Two lines, each was offset 80 mm on either side of the centre line, were then marked parallel to the grain. Next, two little rectangles were marked directly below the embedment length line and centred on each of the offset lines. Rectangles measured 41.3-mm (1-5/8") wide and 30-mm thick to accommodate the washer and nut thicknesses. All rectangles were then carved out into a rectangular prism using a wood chisels to a depth of approximately 87 mm, as shown in *Fig. 1a*. A 20.6-mm (13/16") diameter hole was then drilled in line centred with each carved out hole on the beam's 314-mm wide face and also centred on the beam's 135-mm wide face at the end of the beam section to the required embedment length using a precise portable drilling station as shown in *Fig. 1b*.
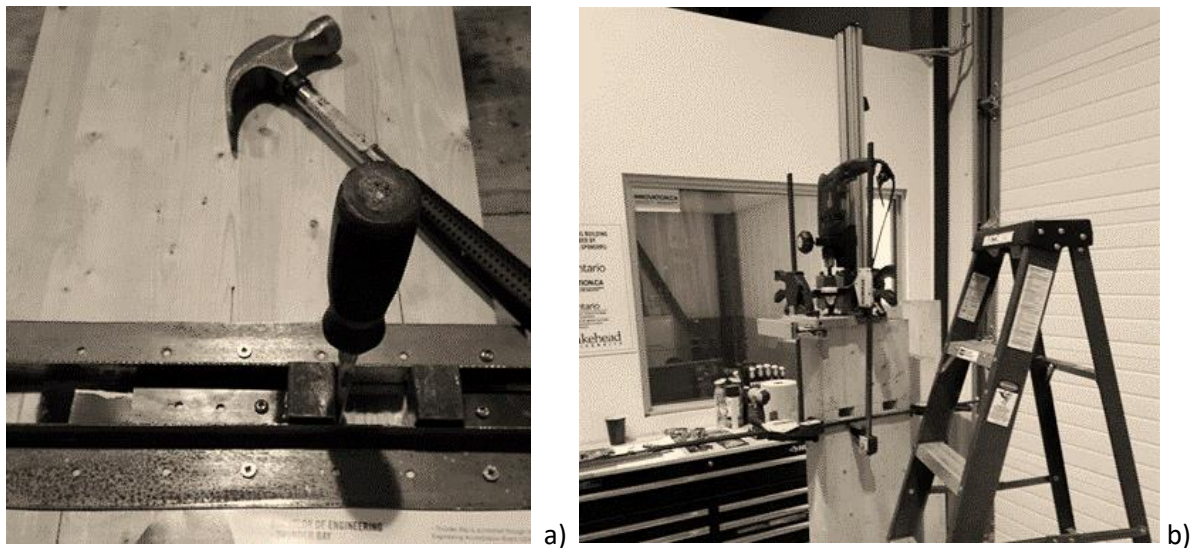
Fig. 1. a) A beam section being chiselled; b) A beam section being drilled

2.3 Test assembly design

The main purpose of this study is to confirm that a fully-concealed connection of a glulam beam sized at 135-mm wide x 314-mm high can achieve a one-hour fire resistance rating with no additional fire protection. The experimental testing of the pull-out strength of an individual steel rod mechanically fastened into a glulam section was conducted and documented (Hubbard and Salem, 2018). In the prior study conducted by the authors, the average pull-out tensile force of the threaded rod mechanically fastened into glulam beam section with 200-mm embedment length and 38.1-mm wide square washer was recorded at

69.0 kN, whereas the average tensile force was recorded at 79.0 kN for the connections with 250-mm embedment length.

The threaded steel rods in glulam beam-column connections was also tested at ambient temperatures prior to conducting the fire resistance tests presented in this paper, and the tests outcomes are being prepared to be published as a journal article. Having the top steel rod subjected to tensile force and the lower part of the wood section under compression, the connection moment-resisting capacity was calculated at 10.0 kN.m, using principles of mechanics. The ambient temperature tests performed on the connection assemblies with 200-mm and 250-mm embedment lengths revealed that both assemblies have an average ultimate failure moment of 16.0 kN.m which is about 60% greater than the calculated design value, eliminating all design safety factors described in CSA 086-14.

The nominal charring rate of the glulam sections experimentally tested in the research project presented in this paper was about 0.7 mm/min (Nordic Structures 2015). Therefore, after one-hour fire exposure, a char layer of about 42-mm thick can be formed on the bottom and the two sides of the glulam beam, as shown in *Fig. 2a*. Considering the width of the washer is 38.1 mm and is located in the centre of the beam width, the beam should still have about 6.5 mm of wood protection at the washers' sides. The tests matrix with the corresponding fire resistance predicted times to failure is presented in *Table 2*.
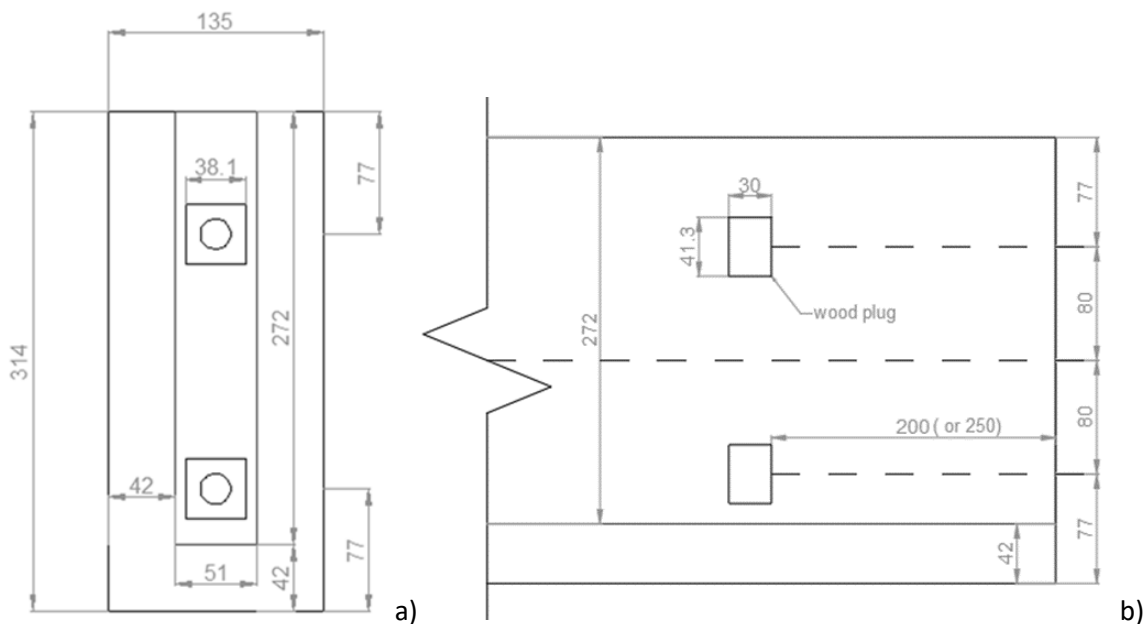
Fig. 2. a) Beam-to-column connection's cross section; b) Beam-to-column connection's side view

Table 2. Threaded rod in glulam beam-column connection tests matrix

Test configuration	Test replicates	Embedment length (mm)	Washer size (mm)	Safe design load applied (kN.m)	Predicted time to failure (min)
Test 200-1.5	2	200	38.1 (1.5 in)	10.0	60
Test 250-1.5	2	250	38.1 (1.5 in)	10.0	60

2.4 Tests setup and procedure

Each test assembly was fixed to a strong steel support using two threaded steel rods. The carved cut out holes on the beam face, which accommodated the steel rods' nuts and washers,

were then plugged with a small fitting chunk of glulam and glued in place with wood glue as shown in *Fig. 3a*. Both, the glulam beam and the fire-protected steel support were placed inside the large-size fire testing furnace accommodated at Lakehead University's Fire Testing and Research Laboratory (LUFTRL), as shown in *Fig. 3b*. The beam top side was fire protected using a 1-inch thick layer of ceramic fibre blanket insulation to simulate the existence of a slab on top of the beam. Test beams were loaded to 100% of the calculated design moment-resisting capacity of the weakest connection configuration. A hydraulic jack mounted to the strong loading steel structure that surrounded the furnace was used to apply the transverse load on the beam via an insulated steel post which was installed through an opening in the furnace roof. One draw-wire displacement transducer was installed outside the furnace and attached to a long ceramic rod that was inserted through the furnace roof at 200-mm distance away from the face of the steel support to facilitate the measurement of the beam's vertical displacements. Another draw-wire displacement transducer was installed and attached to the insulated steel loading post to measure the vertical displacements of the beam free end. The measured displacements from both transducers were used to determine the rotation of the beam-to-column connections. As for thermal measurements of the wood and steel components of the connections during fire tests, twelve metal-shielded K-type thermocouples were placed on each specimen: six thermocouples were installed in the wood section on the beam front face; and the other six mirrored on the back face of the beam, *Fig. 3b*.

a)   b)

Fig. 3. a) Beam's side holes being plugged; b) A general fire resistance test setup

As per CAN/CSA-S101, the total transverse load was applied in 25% increments, with the total applied load being applied at least 30 minutes before the commencement of the fire resistance test. Deflections of each test assembly were measured during fire testing until the test assembly could no longer hold the applied load, or the test assembly reached the maximum measurable amount of deflection, at which the test was terminated.

3   EXPERIMENTAL RESULTS AND DISCUSSION

3.1 Time-rotation relationships

The test specimens' failure criterion was determined to be a maximum beam-to-column connection rotation of 0.1 radians. It was observed that the test assemblies underwent two different trends of increased rotations with time in all four fire resistance tests. The connection rotations slightly increased in a linear trend during the first half of the test time (about 30 minutes). For the second half of the test time, the beam connection rotations increased exponentially over time until failure. Time-rotation relationships for all connection

assemblies are shown in *Fig. 4*. All linear trends of the connection rotation increase with time in all four fire tests are very similar; however, the experimental results show that the connection configurations with 250-mm rod embedment length were stiffer than those of 200-mm embedment length.
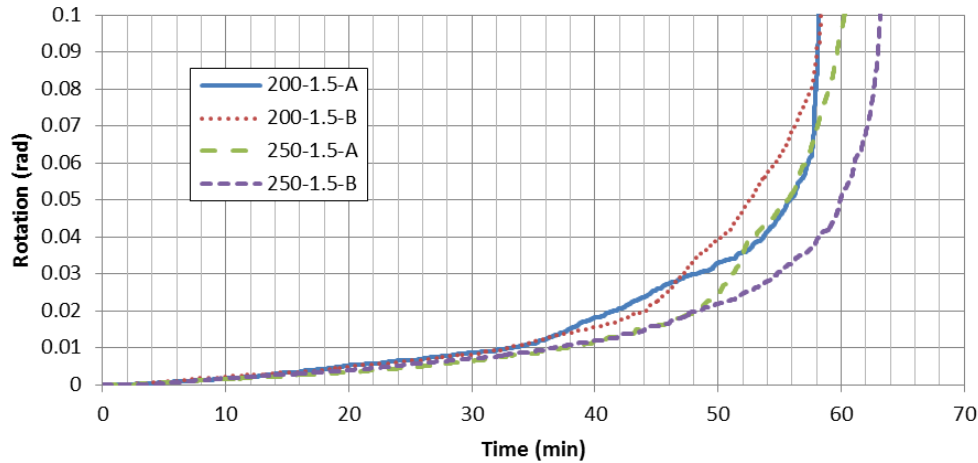

Fig. 4. Full time-rotation relationships of all four fire resistance tests

The last 10 minutes of the fire tests show a better representation of the failure modes and exact fire resistance times of the tested connections, as shown in *Fig. 5*. Fire resistance tests showed that the 200-mm embedment length connections failed just after about 58 minutes of fire exposure. The failure mode in the two 200-mm embedment length connections was mainly splitting in the wood section along the steel rod as shown by the sharp increase in the connection's rotation just before the 0.1-radian failure criterion was achieved. Also, the termination of these two fire tests was due to the fact that the split beam section could no longer hold the full applied load. The other two fire resistance tests conducted on the 250-mm embedment length connections failed a few minutes past an hour. The failure mode of these two 250-mm embedment length connections was mainly due to bending deformations in the steel rods from the very elevated temperatures, as proven by the rapid increase in the connection's rotations just before the 0.1-radian failure criterion was achieved. The termination of these two fire resistance tests was due to the beam reaching the maximum measurable amount of deflection. It was concluded that the 250-mm embedment length beam connections were able to sustain the applied design load sufficiently longer than the 200-mm embedment length beam connections at elevated temperatures to allow a one-hour fire resistance rating to be assigned for the 250-mm embedment length tested connections. The conclusion was made mainly because the longer steel rods had more contact with the wood allowing a gradual increase in the connection's rotations, as well as the rod being bended instead of having the wood snaps along the shorter steel rod.
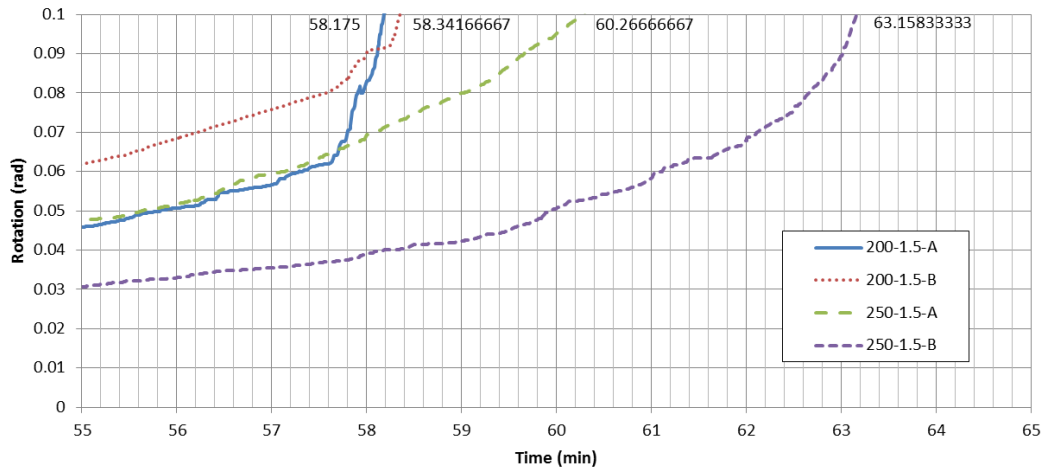
Fig. 5. Time-rotation relationships for all four fire resistance tests throughout the last 10 minutes

3.2 Failure modes

The pictures shown in *Fig. 6* are in good agreement with the graphed results presented in *Fig. 4* and *Fig. 5*; where the 200-mm embedment length connections failed in brittle failure modes due to the wood splitting as shown in *Fig. 6a*. The wood splitting caused the test to be terminated due to the connection not being able to hold the applied full design load. With the wood splitting, the top steel rod did not exhibit noticeable deformations, whereas the bottom steel rod experienced slightly more deformations compared to the top one, as shown in *Fig. 6b*.
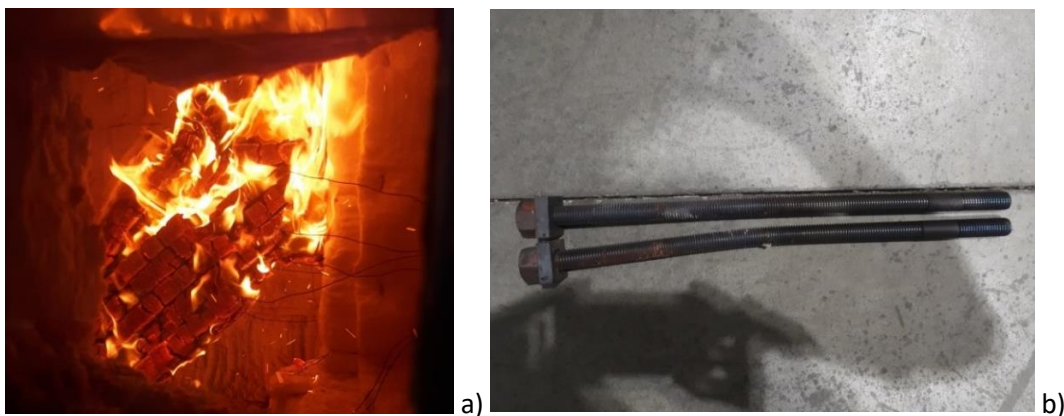
Fig. 6. a) Test 200-1.5-A connection just after failure; b) Test 200-1.5-A steel rods after failure

The pictures shown in *Fig. 7* are also in good agreement with the graphed results presented in *Fig. 4* and *Fig. 5*; where the failure of the 250-mm embedment length connections was a relatively ductile failure mode due to the steel rods deforming, *Fig. 7a*. The steel rods deforming caused the test to be terminated due to the beam reaching the maximum measurable amount of deflection. Also, with the longer rod embedment length, there was more wood to resist the shear stresses imposed by the top steel rod; therefore, this allowed the steel rods to be considerably heated causing the bottom rod to deform excessively, as shown in *Fig. 7b*.
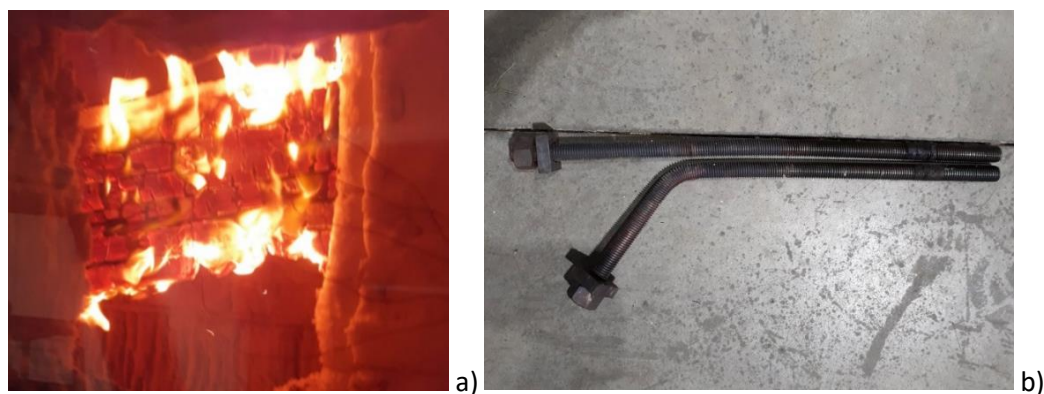
Fig. 7. a) Test 250-1.5-A connection just after failure; b) Test 250-1.5-A steel rods after failure

3.3 Summary of test results

In general, increasing the rod embedment length from 200 mm to 250 mm increased the fire resistance time of the tested beam-to-column connections from just under an hour, at an average of 58.25 minutes, to just above an hour, at an average of 61.75 minutes. *Table 3* provides a summary of the results of the four fire resistance tests.

Table 3. Summary of results of the four fire resistance tests on glulam beam-to-column connection assemblies

Test No.	Embedment length (mm)	Washer size (mm)	Fire resistance time (min)	Average fire resistance time (min)
200-1.5-A	200	38.1 (1.5 in)	58.2	58.25
200-1.5-B	200	38.1 (1.5 in)	58.3	
250-1.5-A	250	38.1 (1.5 in)	60.3	61.75
250-1.5-B	250	38.1 (1.5 in)	63.2	

4   CONCLUSIONS

Based on the experimental outcomes and the analysis of the fire resistance test results conducted afterwards, a few conclusions have been driven and are listed as follows;

- Increasing the steel rod embedment length from 200 mm to 250 mm increased the fire resistance time of the glulam beam-to-column connection from slightly under an hour to just above an hour, allowing a one-hour fire resistance rating to be assigned for the 250-mm embedment length tested connections without the need for additional fire protection;

- The 250-mm embedment length connection exhibited a relatively ductile failure compared to that of the 200-mm embedment length connection which failed mainly due to wood splitting;

- Any fire-exposed steel components would cause the beam-to-column connection to fail faster in fire; therefore, the protection provided by the wood section greatly helps in enhancing the fire resistance of the connections that utilized embedded, mechanically-fastened steel rods into the glulam beam sections compared to similar connections but with fire-exposed steel connecting components.

ACKNOWLEDGMENT

REFERENCES

[1] Barber D. (2017). Determination of fire resistance ratings for glulam connectors within US high rise timber buildings. Fire Safety Journal 91, pp 579-585.

[2] Barillas E.G. (2014). Capacity of connections in glulam with single and multiple glued in steel rods. Master's thesis. UBC, Vancouver, Canada, 20 December 2014.

[3] Batchelar M.L., McIntosh K.A. (1998). Structural joints in glulam. 5th World Conference on Timber Engineering, Montreux, Switzerland, 17-20 August 1998, pp 289-296.

[4] CSA Standard 086-14. (2014). Engineering design in wood. Canadian Standards Association, Ottawa, Ontario.

[5] Di Maria V., D'Andria L., Muciaccia G., Ianakiev, A. (2017). Influence of elevated temperature on glued-in steel rods for timber elements. Construction and Building Materials 147, pp 457-465.

[6] Fragiacomo M., Batchelar M. (2012). Timber frame moment joints with glued-in steel rods. I: Design. Journal of Structural Engineering, ASCE, 138(6), pp 789-801.

[7] Hubbard C., Salem O. (2018). Experimental determination of pull-out strength of threaded steel rods mechanically fastened into glulam beam sections. 6th International Conference on Speciality in Structural Engineering, CSCE, Fredericton, Canada, 13-16 June 2018.

[8] Hunger F., Stepinac M., Rajčić V., Kuilen J.W.G. (2016). Pull-compression tests on glued-in metric thread rods parallel to grain in glulam and laminated veneer lumber of different timber species. European Journal of Wood and Wood Products 74(3), pp 379–391.

[9] Nordic Structures. (2015). Design Properties of Nordic Lam. In Technical Note S01. Nordic Structures, Canada, 2015.

[10] Oh J. (2016). Timber moment connections using glued-in steel rods. Master's thesis. UBC, Vancouver, Canada, April 2016.

[11] Petrycki A., Salem O. (2017). Experimental fire testing of concealed steel-glulam timber semi-rigid bolted connections. 6th International Conference on Engineering Mechanics and Materials, CSCE, Vancouver, Canada, 31 May - 3 June 2017.

[12] Steiger R., Gehri E., Widmann R. (2007). Pull-out strength of axially loaded steel rods bonded in glulam parallel to the grain. Materials and Structures 40(8), pp 827-838.

FIRE SAFETY OF HERITAGE BUILDINGS

EVALUATION OF STRUCTURAL BEHAVIOUR OF A FRANCO-BYZANTINE BASILICA IN CYPRUS AFTER A FIRE ATTACK

Kyriacos A. Kyriakides[1] and George Hadjisophocleous[2]
[1]Ministry of the Interior –Paphos District Administration Office, Paphos Cyprus
[2]Carleton University, Ottawa, Ontario Canada

ABSTRACT

This paper presents experimental and simulation results of the effect of fire and high temperature on a Franco-Byzantine Basilica Church in Cyprus. Natural building limestones from a local ancient quarry were heated in the laboratory to various temperatures (150-900 ℃) and their thermal properties at these elevated temperatures were determined experimentally. The physicomechanical (density, porosity, uniaxial compressive strength, colour changes) characterisation of the test specimens showed that the properties of limestones change with heating. These changes influence the strength and durability of the stones. The thermomechanical properties of the limestones derived from the experiments were used in thermal and structural models to predict the behaviour of masonry monuments during a fire and to evaluate their residual strength after exposure to fire.

1   INTRODUCTION

Ancient and historical buildings and their protection and restoration are nowadays in the focus of interest of the scientific community around the world. Natural disasters like fire may potentially damage or even completely destroy such monuments. As performance-based techniques become increasingly accepted in the design of fire-safe buildings, the ability to predict the response of structural elements exposed to realistic fire scenarios is imminent. Hence the study of the behavior of natural building stones subjected to fire attack is important in the evaluation of the structural safety of monumental buildings.

In Cyprus, monumental masonry structures, such as churches, are widespread. In particular, Franco-Byzantine Basilica churches[1], dating back to the beginning of the 19th century, are found in both cities and rural areas. A total of 30 such monuments is found in the Bishopric of Morphou alone[2], whereas an equally significant number is reported to exist in the Kyrenia region[3]. In total, the number of Franco-Byzantine Basilica churches on the island exceeds 250[4-5].

Despite suffering from fire attacks at different periods of history, the repair and restoration of many of these churches did not take into consideration the structural evaluation of the monument after fire and did not account for the relevant loss of material. This paper presents experimental and simulation results of the effect of fire and high temperatures on a Franco-Byzantine Basilica Church in Cyprus.

2   EXPERIMENTAL AND THEORETICAL BACKGROUND

A field survey was conducted in several churches of the Franco-Byzatine type to determine the average fire load. It was found that all churches had similar interior furniture. The average fire load was estimated around 55 kg/m² of wood equivalent, which corresponds to 880 MJ/m^2 [6].

Fire in the monument was simulated using the computational fluid dynamic model FDS [7] The program solves the governing equations for a specific fire scenario and returns the adiabatic temperatures on the inner face of the walls and the arch elements and the hot gas temperatures at selected areas. An example of the temperature profile of thermocouples and adiabatic temperature devices is shown in Fig 1.
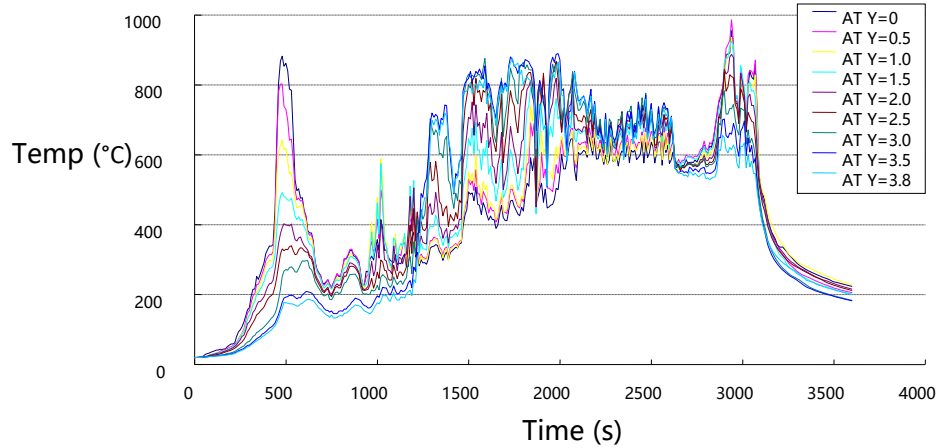

Figure 1. Adiabatic wall temperature (Y = 0~3.8)

The adiabatic temperatures from fire modeling (FDS) represent convective and radiative reference temperatures that can be used as boundary conditions to calculate conduction heat transfer in the solid material.

For this study, the general conduction equation for the two-dimensional grid derived in polar coordinates (eq. 1) is used [6]:

$$\rho c \frac{\partial T}{\partial t} = \frac{1}{r}\frac{\partial}{\partial r}(rk\frac{\partial T}{\partial r}) + \frac{1}{r}\frac{\partial}{\partial \theta}(\frac{k}{r}\frac{\partial T}{\partial \theta}) + S \qquad \textbf{(1)}$$

The z-direction of the control volume is assumed to be unity; S is the heat source and c the specific heat.

A computer program in FORTRAN was developed to give the solution of the discretization equation. The developed conduction model was used to calculate the temperatures in the limestone of the church arch located over the iconostasi (the arch that for the selected fire scenario is subjected to the most severe conditions). As boundary conditions for these calculations, the adiabatic surface temperatures obtained from FDS near this arch were used. The arch was divided into control volumes with dimensions of 1 mm in the radial direction and 10.6 degrees in the circumferential direction. Fig. 2 illustrates the arch of the church with the stone elements marked with numbers from 1 to 17. Similar points are defined on the left hand side of the arch. These points coincide with the points used by FDS to calculate the adiabatic temperatures.
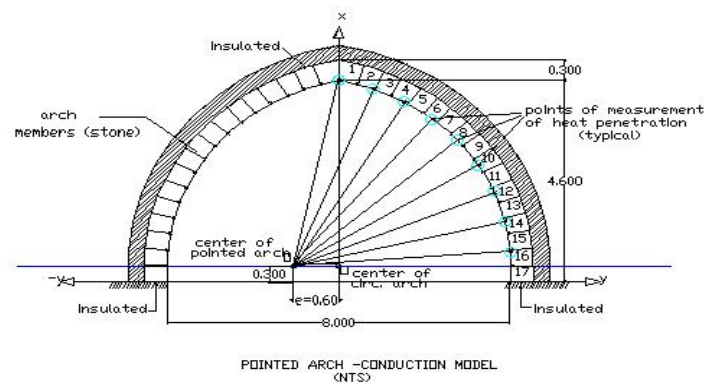
Figure 2. The arch used in the conduction model

An example of temperature predictions, which demonstrates the temperature variation with time at the right side (84.8°) of the arch is shown in Figs 3-4. The maximum temperature reached at different depths is the temperature that was used in the structural model. This maximum temperature is recorded by the model.

From the figures it can be concluded that the arch temperatures induced by the fire scenario under consideration, affect the stone elements of the arch to a significant depth. In particular, the temperature from the inner face of the elements (approx. 800 ℃) drops to 150 ℃ at a depth of 80 mm. From that depth the temperature drops gradually to ambient at the outer face of the stone elements. The mechanical properties of the limestones corresponding to the predicted maximum temperatures are used in the structural model.
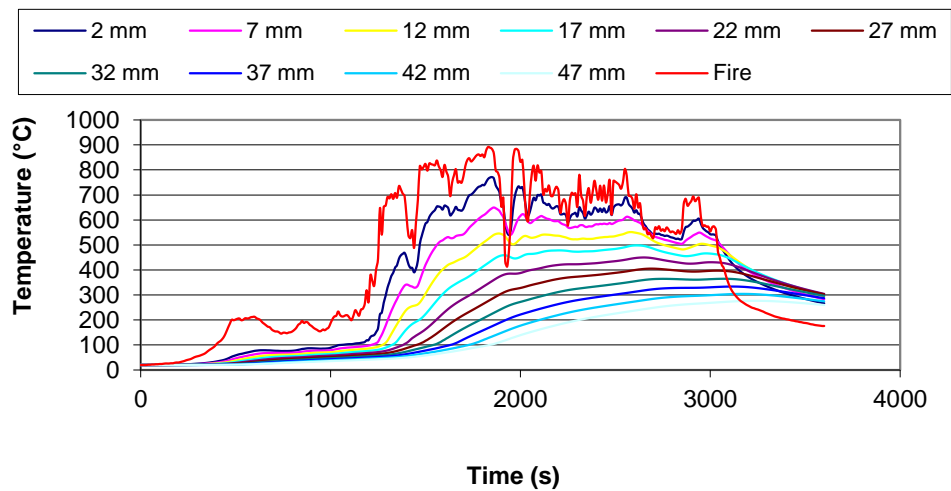
Figure 3. Temperature profile (right side of arch)
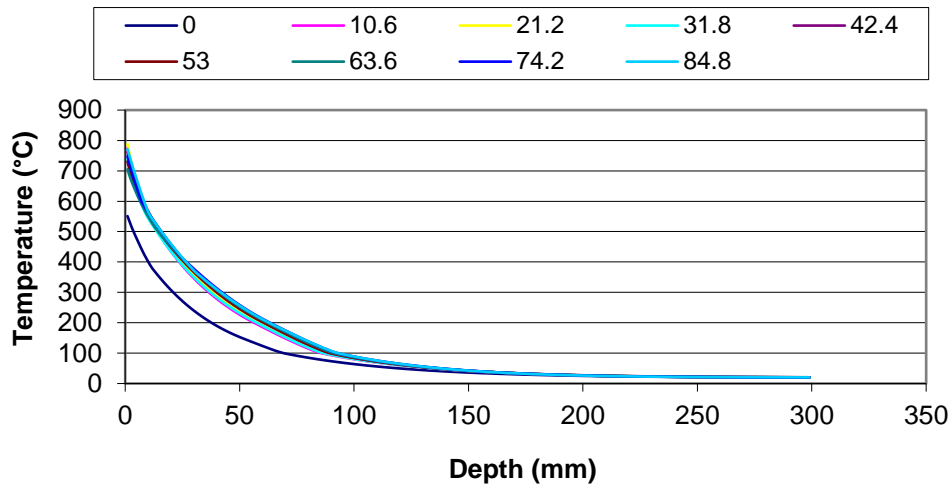
Figure 4. Maximum temperature (right side of arch, full depth (300 mm)

3   STRUCTURAL MODELING

Basilica structures usually house a façade, a hall, a presbytery and an apse; often a bell tower is present as well. More generally, churches are characterized by the presence of large wall panels without internal partition walls, slenderness of some vaulted structures (folded vaults), presence of thrusting elements of large span (arches, vaults and domes) and a lack of intermediate connections.

The church under consideration in this study is the Panagia Chryseleousa church (Fig. 5) located in the village of Ineia, Paphos. The church was built in 1883 with natural limestone from a quarry located adjacent to the village. The interior face of the stone work is covered with lime wash and is painted.

Figure 5. Exterior (left) and interior (right) photos of the monument under study

The interior dimensions of the church are 8.0 m wide by 22.0 m long by 8.50 m height (intrados of the vault). The thickness of the arches is 0.30 m wide by 0.30 m height, while the thickness of the buttresses is 1.70 m for the corner buttresses and 1.40 m for the five buttresses in-between; the thickness of the vault is 0.50 m. From the original drawings kept in the Archives of the District Administration of Paphos and from field measurements and observations, the digital architectural drawings of the church were produced (Fig. 6).
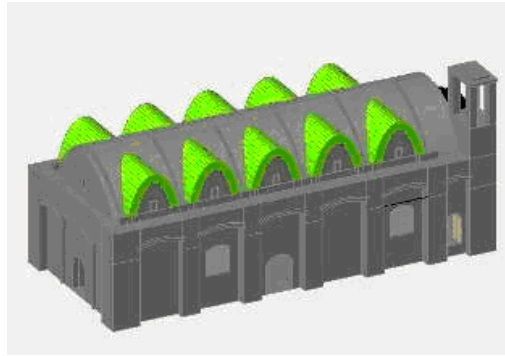
Figure 6. Architectural model of the monument under study

The mathematical modeling of masonry shows several difficulties that arise from the need to take into account the non linear behaviour and the progressive degradation of the stiffness when strains increase. In the case of old stone masonry, other irregularities also have to be considered. These are the different dimensions and locations of the stones, the non-homogeneous distribution of the mortar, the great scattering in the mechanical characteristics of the elements and the uncertainty on the structural complexity.

In this study, a structural model which works independently from the heat transfer model was developed. The finite element method was used to implement the model. The structural model was produced from the digital 3-D architectural drawings using a routine that produces nodes and elements by reading these drawings[6]. Material properties were assigned to each element by the user following the results of experiments and of the thermal model. The latter produced a thermal gradient which was used in the assignment of material properties. In particular, each solid element of the arch was sliced in smaller pieces according to the temperature gradient in the natural stone. Density and Young's Modulus of Elasticity derived from experimental work (Table 1) were assigned to each piece of the element according to the maximum temperature at that point. The number of the divisions of the original stone element relied on its geometry and the gradient of the temperature within the element itself.

Temperature (°C)	Compressive strength (N/mm²)	Open Porosity (%)	Average Apparent Density (kg/m³)	Young's Modulus (MPa)
20	24.2	23.0	1961	19
150	26.9	30.1	1936	21
300	25.4	27.2	1912	16
450	22.8	26.0	1895	7
480	19.6	nd	1892	nd
600	22	25.8	1888	3
750	14.2	29.7	nd	nd
900	nd	34.5	nd	nd

Table 1 : Properties of limestone specimens at elevated temperatures

The structural analysis computer program used was STAAD.Pro. The structural model was produced with 8-node solid elements for walls and arches and with shell elements for the vaults of the church. The individual stones of the arches were measured on site and used in the model as solid elements to capture the 3-dimensional behaviour of the units.

For the transformation of the geometrical 3-D and surface elements from AutoCAD to STAAD a computer routine was produced in Visual Basic to couple the two programs. This routine reads a block from AutoCAD and reproduces a structural (8-node, shell, etc.) element in STAAD. The element produced is placed automatically at the reciprocal coordinates of the original architectural drawing.

Fig. 7 represents the corresponding structural model produced from the CAD drawings.
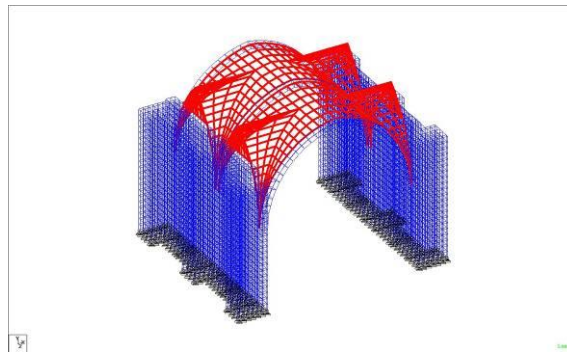
Figure 7. Structural model of walls, vaults, arches and buttresses

For the purpose of this study, the stone elements of the arches were sliced into 8 pieces so that better details could be taken from heat transfer modeling at the inner face of the arch material. The structural STAAD model of the arches with the sliced stone elements is illustrated in Fig. 8.
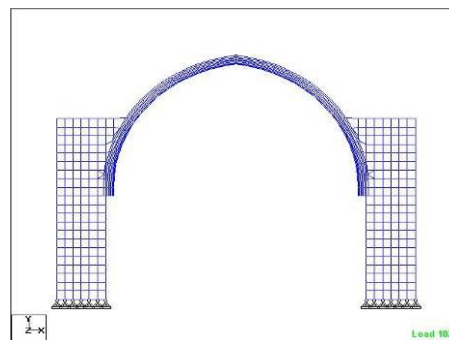

Figure 8. Structural model of arches and buttresses (Pinned supports)

The STAAD model was run for several loading occasions including thermal load (load due to temperature increase in the structural elements of the arches). Fig. 9 illustrates stresses in arches and buttresses of the church from dead loads.
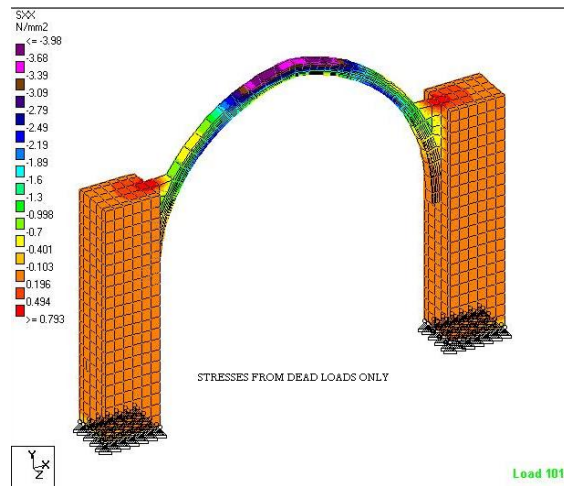
Figure 9. Solid stress contours on arches and buttresses from dead loads

It is obvious that under static loads the arches of the church are working only in compression and the thrust in the structural elements is much less than what they can sustain. Fig. 10 represents stress contours in the arches and buttresses from dead and thermally induced loads. The expansion coefficient was calculated at each temperature. Poisson ratio was taken from bibliography[8]; for damping the value used in the model is that of concrete.

Figure 10. Solid stress contours on arches and buttresses from dead and thermally induced loads

The results shown above indicate that in the bottom three parts (20 mm, 20 mm and 40 mm) the stresses exceed the allowable stress derived from the experiments. Comparing these results with the results obtained from the heat penetration model, where only the first 10-20 mm exceeded the temperature of 750 ºC where the material seems to disintegrate, it can be concluded that the thermally induced stresses prevail in the evaluation of the safety of the arch.

To account for the damage in the limestone due to both thermal stresses and elevated temperatures (over 750°C), a section 80 mm thick was removed from the bottom of the arch.

Compression stresses over this depth exceeded the compressive strength of the limestone material. The resulting section of the arch elements was now 30 mm wide by 22 mm in height. The resultant stress field in the structure was derived from a new analysis, after replacing the elements with their new dimensions. Fig. 11 illustrates the resulting stresses on the structure due to dead loads at ambient temperature, while Fig. 12 illustrates the resulting stresses on the structure with the reduced height of the arch stones (i.e. from 30 to 22 cm).
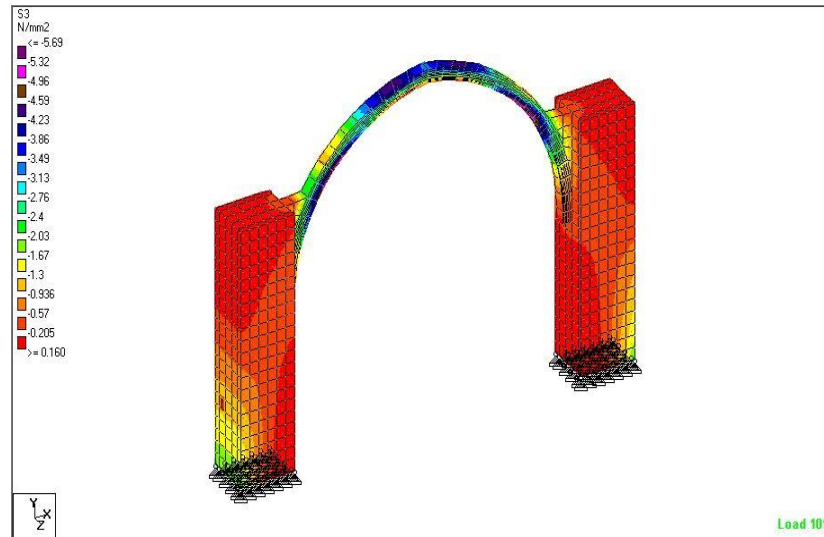
Figure 11. Solid stress contours on arches and buttresses from dead loads (arch stones 30 cm in height)
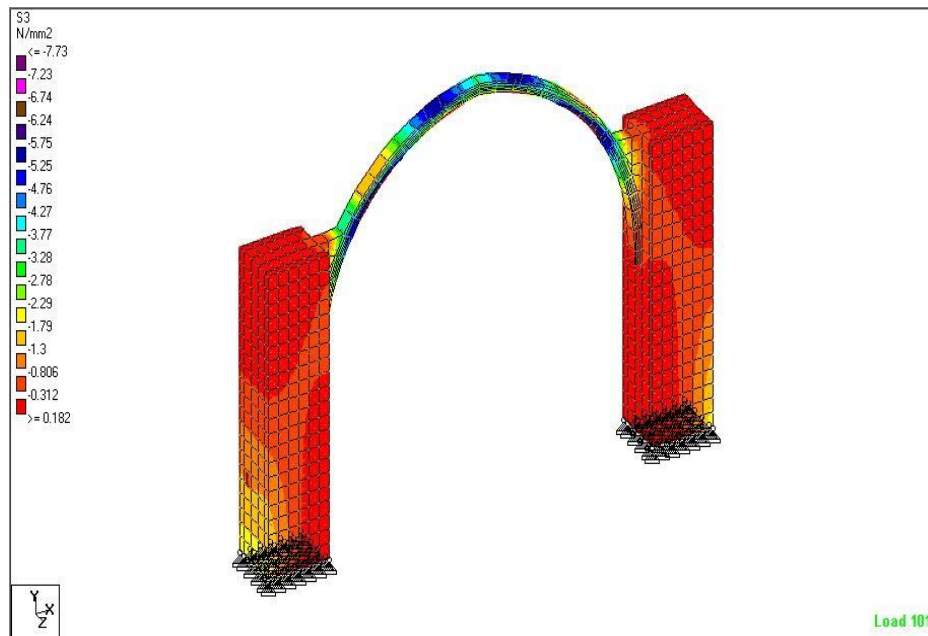

Figure 12. Solid stress contours on arches and buttresses from dead loads (arch stones reduced to 22 cm in height)

396

Comparing the results shown in Figs. 11-12, it can be concluded that by removing from the stone elements the disintegrated part and the part that fails due to thermally induced stresses, the resulting stresses are increased by 35%. The increase of the stresses is analogous to the reduction of the material section.

4   CONCLUSIONS

As far as the structural behaviour of the arch subjected to elevated temperatures is concerned, from the results it can be concluded that, at the temperatures of the fire scenario under consideration, there is up to 35% loss of material section and a consequent analogous increase of the stress field. Using the graph derived by Romano[9] for the arch of the church under consideration (Fig. 13), with a=80º and e/R=0.15, we get t/R~0.055 (Fig. 14). This leads to t=22 cm as the minimum allowable thickness of the arch. So, according to the theory of Limit Analysis, fire reduces the section of the arch to the limits of collapse.
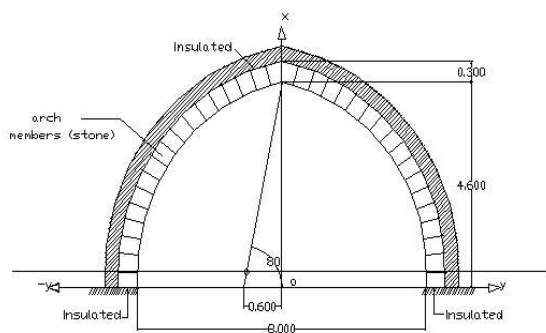

Figure 13. Geometrical characteristics of the arch under consideration
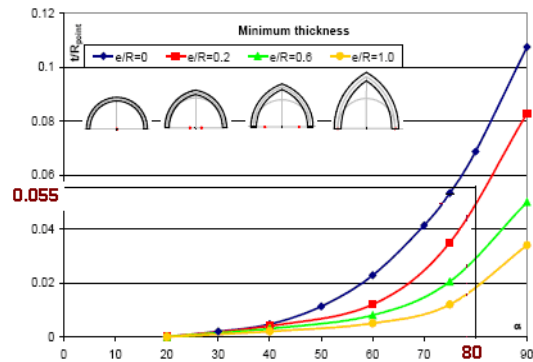

Figure 14. Minimum thickness of arch for the church under consideration

The same conclusion can be derived by comparing the resulting thrust lines from dead loads (Fig. 15) and dead and temperature loads (Fig. 16).
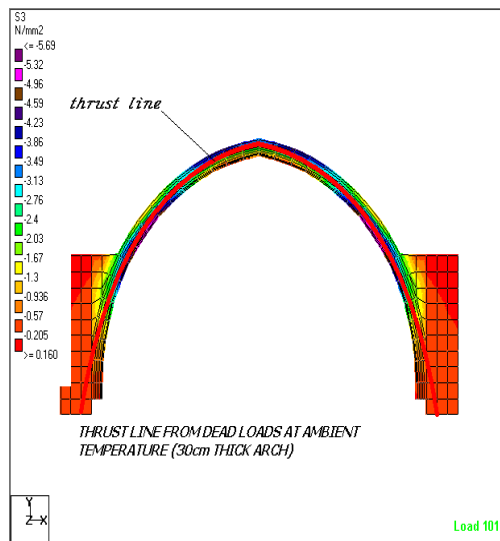
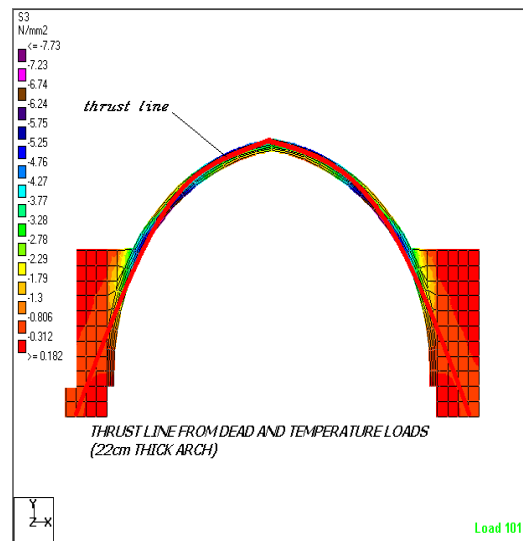Figure 15. Thrust line from dead loads at ambient temperature

Figure 16. Thrust line from dead and temperature loads

The thrust line from the STAAD elastic analysis (considering the non-linear behaviour of the stone material after being subjected to elevated temperatures) is in very good agreement with the results of the theory of Limit Analysis.

REFERENCES

[1]   Sotiriou, G. (1935), *The Byzantine monuments of Cyprus*, Athens.

[2]   Myriantheus, D. (2000), *Ecclesiastical Architecture (13th-20th Century)*, In: Holy Bishopric of Morfou, 2000 years of Art and Holiness, pp. 71-96, Nicosia

[3]   Anonymous (2006), *Travelogue of the Christian Monuments of Kyrenia region*, Holly Metropolite of Kyrenia, Nicosia.

[4]   Myriantheus, D. (2008), *Ecclesiastical architecture in Cyprus at second half of 19th and beginning of 20th Century*, International Congress …., Nicosia, Cyprus 29 Apr – 3 May.

[5]   Myriantheus, D. (2009), *Personal Communication*

[6]   Kyriakides, A.K. (2010), *Structural behavior of historical monuments after fire attack*, PhD Thesis, Carleton University, Canada.

[7]   Fire *Dynamics Simulator (Version 5). Technical Reference Guide NIST Special Publication 1018-5*

[8]   Properties of common solid materials. http://www.efunda.com/materials/common_matl/Common_Matl.cfm?MatlPhase=Solid&MatlProp=Mechanical#

[9]   Romano, A. (2005), *Modeling, analysis and testing of masonry structures*, PhD Thesis, Univesrità degli Studi di Napoli, Italy.

FIRE SAFETY EVALUATION OF HERITAGE BUILDINGS ON THE HISTORIC CENTRE OF VISEU

[1]António Correia, [1]Paulo Figueiredo, [2]Ricardo Almeida, [3]Raimundo Silva, [3]Nuno Correia
[1]Coimbra Polytechnic - ISEC, Coimbra, Portugal
[2]Politechnic Institute of Viseu, Viseu, Portugal
[3]Faculty of Sciences and Technology – University of Coimbra, Coimbra, Portugal

ABSTRACT

In recent years, the rehabilitation of old urban centers has been a priority in the main great cities in the world [1,2,3]. This rehabilitation aims to rebuild old buildings, to provide good conditions for people to live in, and visit. However, the great number of old buildings is a threat to the fire safety of the whole area. The fire safety is an issue of major importance, in these areas, due to the high fire load and also the close proximity between buildings [4]. Moreover, the occupancy of heritage buildings, is most of the times by people of older ages, which is a factor of aggravated risk for the occupants and for the entire block. This fire safety must be assessed by performance-based analyses, putting together the smoke and flame spread in the building, with the evacuation of the building.

1   INTRODUCTION

In this paper, a fire performance-based analysis will be presented, on a heritage building, in the old centre of Viseu, in Portugal [5]. This building is an Old Theater, which is now being refurbished to the use of an University for 3rd age people. This brings added problems to the fire safety of the building and its occupants, due to their difficulty in evacuating the building, with the aggravating fact that in old urban centers, the buildings are very close to each others, providing almost instant propagation of a fire.

The use of softwares Pyrosim and Pathfinder will be adopted to this study, allowing to test different fire scenarios, and evaluate the egress conditions of the occupants, in real time. The simulations of propagation, smoke spread and evacuation will be carried out simultaneously.

Results to be expected with this paper, are the real fire safety of the occupants, and the fire risk for propagation of a fire to the neighbor buildings in the block. The process of rehabilitation of heritage buildings must be adapted, to fulfill fire safety issues, which are more critical in old urban centers.

This paper aims to analyse the fire risk of an old building, more specifically, the old Chorus of the city of Viseu, located in the historic centre, in "Rua Direita" and the influence of its occurrence in the neighboring buildings located in the same street.

For this work a performance-based analysis on the fire performance of the building is made using the Pyrosim programme. This is a Fire Dynamics Simulator (FDS) software that simulates the propagation of flames, temperatures and smokes inside the building in the representative three-dimensional model of the building under study. Several simulations are carried out with and without fire-fighting measures that allow comparisons and evaluation of the influence of the implemented measures and thus to conclude the best solution for fire safety of the building. With the same three-dimensional model, a study of the paths to evacuate occupants using the Pathfinder programme is also carried out.

2 CHARACTERIZATION OF THE BUILDING "OLD CHORUS OF VISEU"

2.1 Building characterization

The building was used, from December 1955 by "Old Chorus of Viseu", to hold meetings, shows and cultural events, until the year 2006, being until the date of this work, abandoned and in ruins. The building consists of three floors: ground floor, first floor and attic. The main elements that characterize the building are (*Fig. 1*):

• On the facades, interior and exterior walls at ground level and exterior walls of the first floor, the main element is stone (granite) masonry;

a) Facade of the building;

b) View of compartment walls

c) View of an exterior wall;

d) View of the attic timber structure

Fig. 1. Views of the case study building;

The structure is made of masonry stone walls, and timber structural elements in floors and roof.

The main materials present in the building are granite, lime and plaster mortars, wood, ceramic materials such as tiles and mosaics, both inside the building and in the façade, elements such as guards and accessories, glass windows;

The building has only two exits: the main entrance, and a stairway to the back terrace.

3 NUMERICAL MODELLING OF THE FIRE

3.1 Introduction

The creation of virtual models for fire simulation, makes it possible to analyse the dynamics of development of temperatures, smoke and flames in the course of a fire from ignition to extinction, as well as the resulting effects, thus allowing to assess the influence of structural, material and environmental factors. Using computer simulations, it is possible to verify temperatures at various points, visibility and development of smoke, and to analyse the efficiency of fire-fighting measures such as sprinkler and smoke control systems (active/passive ventilation), allowing a performance-based analysis. *Fig. 2* depicts the 3D model of the building and the surrounding block.
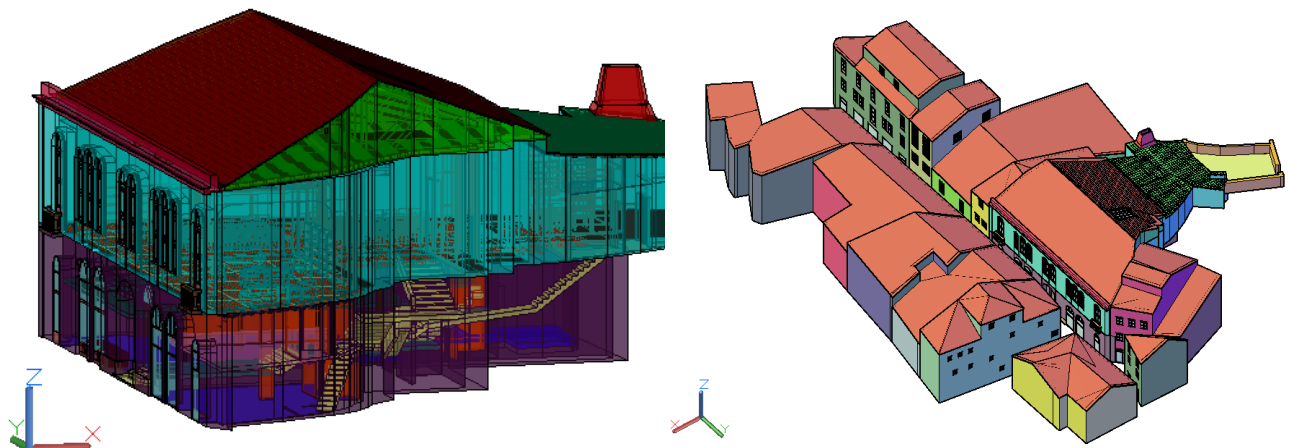

Fig. 2. a) 3D-Model of the building Old Theatre of Viseu; b) 3D-Model of the surrounding buildings

3.2 Computational modelling FDS with interface Pyrosim

Parameters such as solid or liquid state, thermal properties (density, specific heat, conductivity, emissivity and absorption coefficient) and pyrolysis are defined in the field of material editing, and the program allows to add other parameters. The materials library of Pyrosim was used to define the parameters chosen for the previously described materials, except for the wood and glass which were obtained from the CFast program library, due to the lack of parameters of these materials in the. Pyrosim library.

For the simulation of fire development it is important to define the characteristics of the surfaces of the materials present in the model using fire curves that relate the heat radiation rate (HRR) to the time from ignition to fire extinction.

Fig. 3 present some fire curves used in the present study:

401
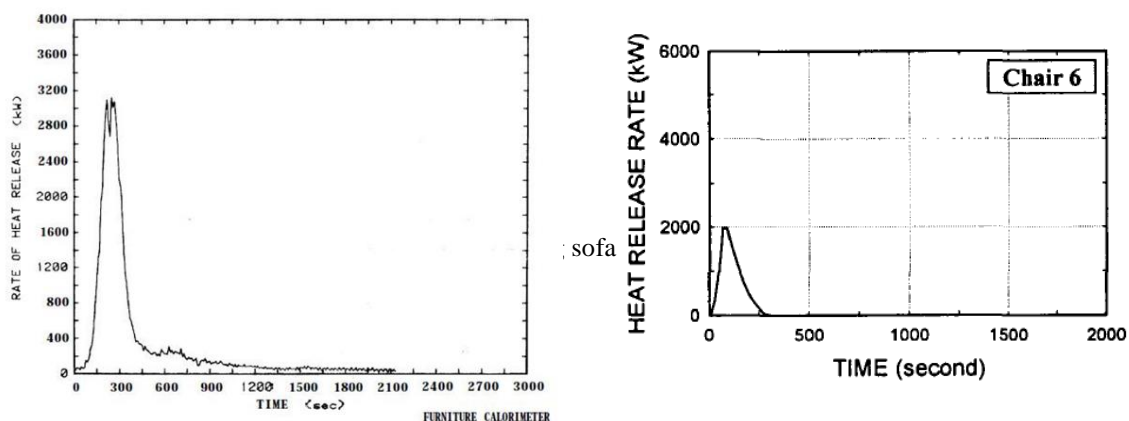
3.3 Computational modelling of the evacuation with Pathfinder interface.

The purpose of using computer models for the evacuation of occupants is to verify if the number of escape routes in the building will be sufficient for the evacuation in good time for the number of occupants inside, during the occurrence of a fire [8].

The computational modelling allows to simulate the behaviour and movement during evacuation, allowing the observation and obtaining valuable information, verifying the existence of traffic jams and also if the exits are well positioned, allowing them to be effectively used in case of emergency. It is also possible to obtain representations of the egress paths and decisions made by occupants in the evacuation. In addition, the modelling enables risk assessment, identifying the hazards resulting from evacuation and quantifying the risk.

This software, developed and marketed by Thunderhead Engineering [8], is based on the "continuous network" model, in which a two-dimensional (continuous) space is applied to the building, and allows occupants to move from one point to another through the building. The most important step in modelling the egress of buildings, is the introduction and characterization of occupants. It is possible to define the number of occupants (quantity, density or type of pre-defined profile), uniform or random arrangement in the space. The profile and behaviour of exit choice of the occupants are previously defined, being possible to change them during the simulation. *Fig. 4* depicts a view of the 3D model used to study the evacuation of the Old Theatre of Viseu.
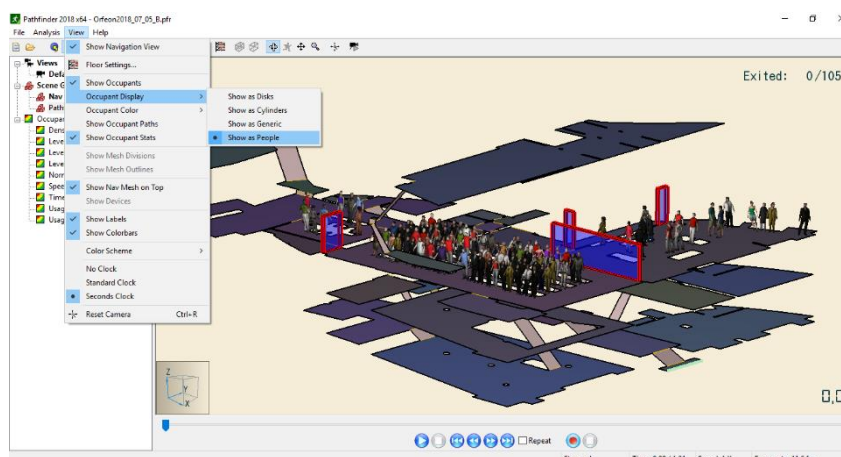

Fig. 4. 3D-Model of the evacuation of the Old Theatre of Viseu

4   FIRE SCENARIOS AND RESULTS

4.1 Definition of the fire scenarios

For the present study, four fire scenarios were considered, which are presented as follows:

Scenario A: It is a model without any fire-fighting measures, and will serve as a basis for comparison between the various models.

Scenario B: In model B an exhaust system was implemented, consisting of three exhaust fans placed in the upper windows of the rear wall of the events room, with exits through the rear annex of the building (*Fig. 5 a)*).

Scenario C: In model C, in addition to the measures implemented in model B, an automatic water extinguishing system was implemented using sprinklers of type "total flood".

Scenario D: Due to the concern with the conservation of a historic building which an automatic water extinguishing system could cause, an alternative was created to use the same system but with gas as shown in *Fig. 5 b)*. In this case argon, was adopted, with a mass flow of 1664 kg/m2.s, with a model with the same number of sprinklers as the water, with activation programmed for 60 seconds after the start of the fire, due to the asphyxiating effect of the gas on the human presence. It should be noted that in this model the measures of exhaustion and automatic opening of skylight are maintained.

Fig. 5. View of the 3D model a) Scenario B, with exaust fans   b) Scenario D, with argon sprinklers

The Pyrosim and Pathfinder software allow simultaneous visualization of fire and evacuation simulation results in the same screen, allowing to verify the development of smoke and flames and compare with the evacuation of the occupants, allowing the visualization of their exposure to the fire hazards at every moment until the exit of the building.

4.2 Results analysis for fire scenario A

Some results for the fire scenario A, are presented in *Fig. 6* and *Fig. 7*.
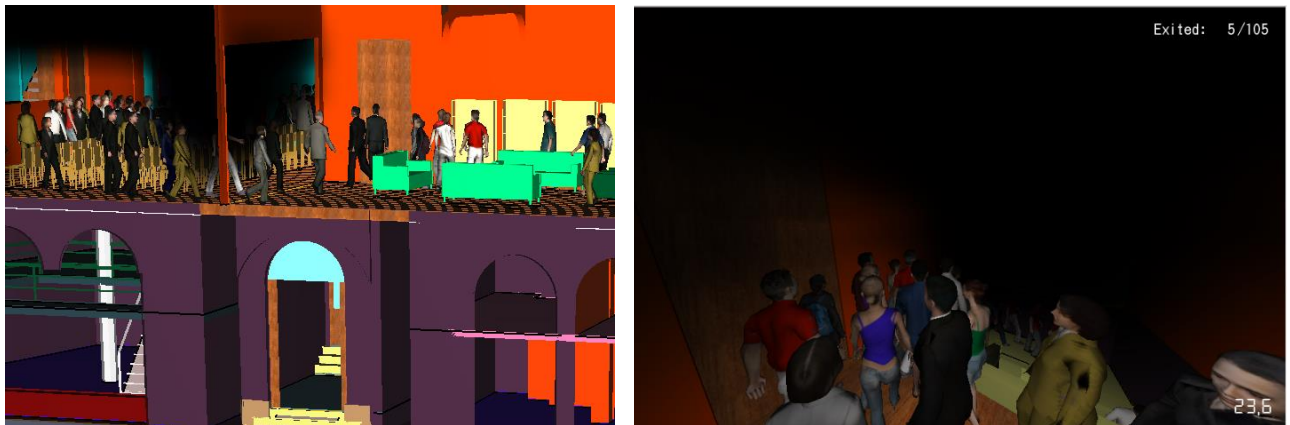
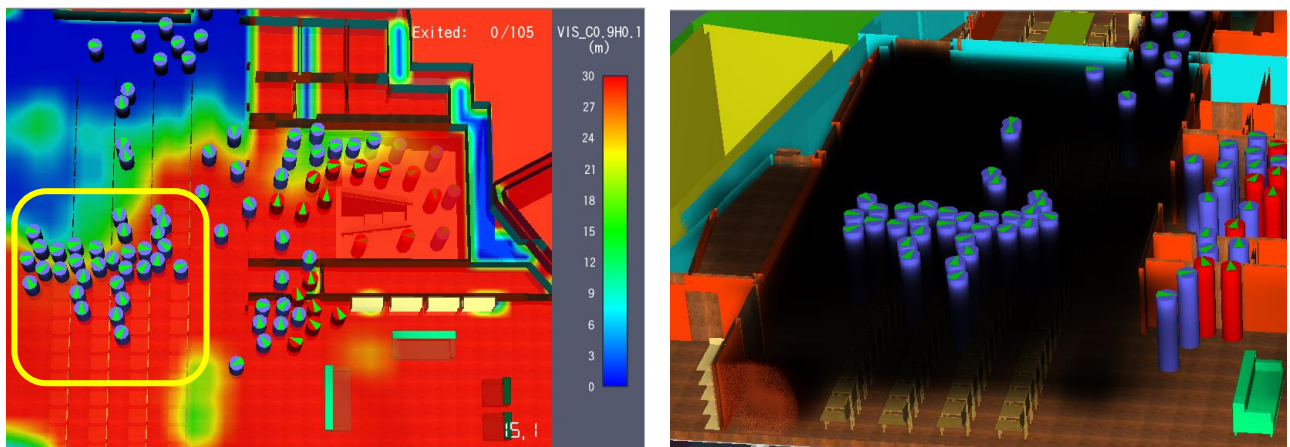*Fig. 6.* a) Scenario A after 5 seconds   b) Scenario B

Fig. 7. a) Plan view of visibility distances, after 20 seconds   b) A group of occupants trapped in the main room

It is possible to observe in *Fig. 6* that in after 5 seconds of the beginning of the fire, a great amount of smoke is already filling in the ceiling of the main room, and some part of the escape route of the occupants. In *Fig. 7*, after 20 seconds it is shown a group of people trapped in the main room, due to the great amount of smoke.

4.3 Results analysis for fire scenario B

In model B, the development of the fire is identical to model A up to 15 seconds, at which time the smoke exaust fans placed in the events room and the automatic opening of the skylight in the stairs start operation. In *Fig. 8. a)* it is possible to visualize the improvement of visibility in the stairway compared to model A. In *Fig. 8. b)*, the breaking of the windows is observed, which occurred at 133, 279 and 282 seconds, respectively.
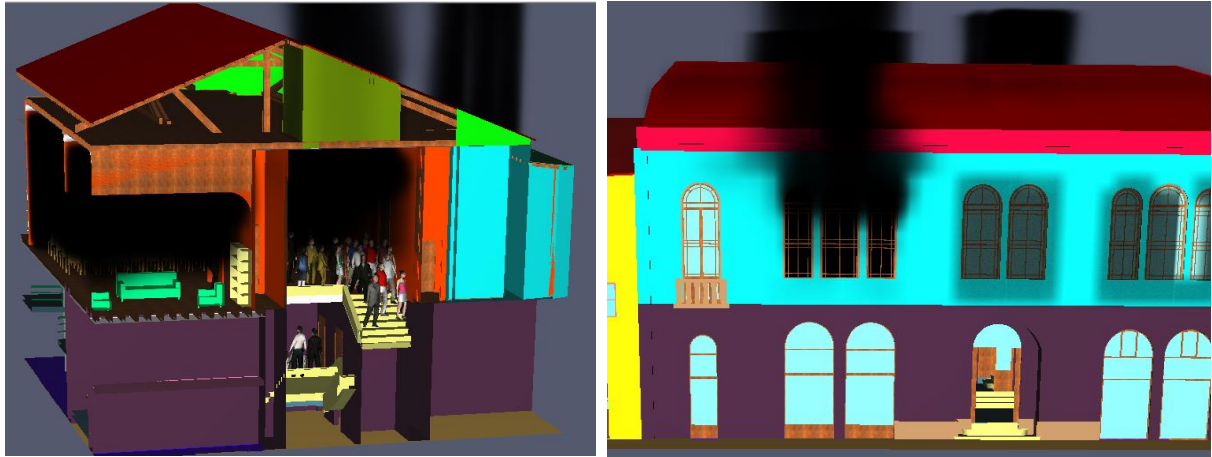
Fig. 8. a) Stairway view, after 23.6 seconds, scenario B   b) Breaking of the windows, scenario B

4.4 Results analysis for fire scenario C

In model C, as previously described, an automatic sprinkler water extinguishing system was implemented. The first sprinkler comes on at 9.80 seconds and the other sprinklers are in operation as the respective sprinkler temperatures are reached (*Fig. 9*).

Fig. 9. a) Sprinklers functioning in scenario C   b) View of the access corridor and stairway to the terrace

Despite the improvements in evacuation conditions, there is a group of 22 occupants who remain in the event room 38.50 seconds after the onsetbeginning of the fire, encased in smoke, exposed to the risk of intoxication. As this point, despite of the expected improved conditions fire safety for the occupants, it seems to be necessary to reduce the number of occupants in the event room and to create an arrangement of seats with more corridors allowing a greater fluidity in evacuation. In fact, the measures implemented in this scenario do not seem to be enough to provide full safety to all ocuupants. For sure, the fact that occupants in this building are supposed to be old people, must play an important role in these results. In fact, numerical simulations were carried out with a reduction of occupants in the main room, from 80 to 50 people, and the results were satisfactory.

4.5 Results analysis for fire scenario D

In model D, an automatic gas extinguishing system with the use of sprinklers was implemented, as shown in *Fig. 10 a)*. In this model the extinguishing system was

programmed to act 60 seconds after the beginning of the fire in order to avoid the human presence at the place of application.

The evacuation model was selected with the reduced number of people in the event room, since up to 60 seconds the scenario is identical to model B. So, the number of occupants at this instant of time, was taken from the scenario B simulation. In this model, there remains the problem of visibility reduction in the back annex corridor area, affecting at 12 seconds ten occupants as shown in *Fig. 10. b)*.
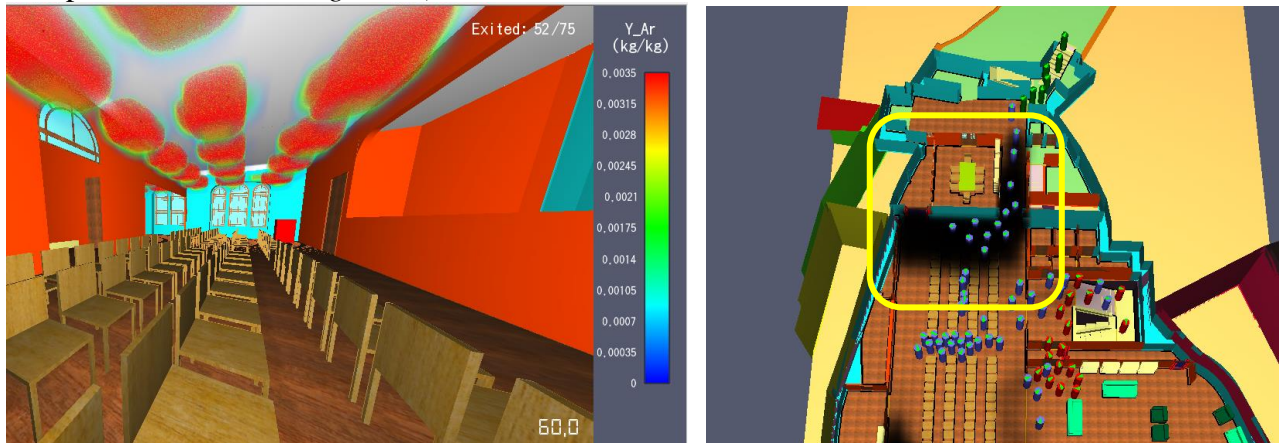

Fig. 10. a) Activation of the gas sprinkler system, after 60 seconds b) Occupants surrounded by fire, scenario D

In *Fig. 11* it is possible to observe that in scenario D, the glass breaking occurs at 141.6 seconds, 278.5 seconds and 285.8 seconds. It is verified that the automatic gas extinguishing system is not sufficient to contain the fire inside the building.
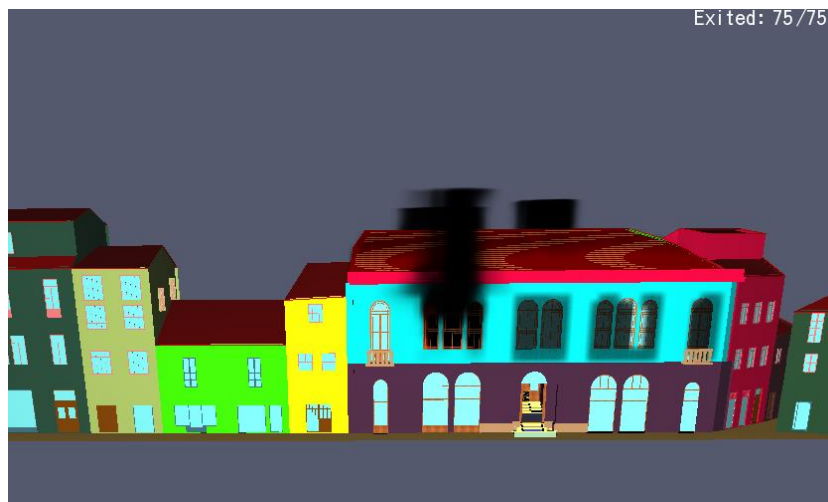
Fig. 11.   Breaking of the glass windows, in scenario D

5   CONCLUSIONS

The analysis of the results of the four models exposed in the scope of this work allows to conclude that in model C, the conjugation of the smoke exhaust system, automatic water extinguishing system, opening of the skylight in the roof of the stairway area together with the reduction of eighty to fifty occupants in the event hall has effective results in the safe evacuation of all the occupants present in the building. It should be noted that the analysis of the evacuation model allows to conclude that the existence of two emergency exits on

opposite sides of the building allows evacuation of the occupants in a timely manner and increases the level of safety of the occupants. It was concluded that the model C, together with the limitation of the number of occupants in the event room, obtained the best result in terms of safety in the evacuation of people, besides the containment of the fire inside the building making it difficult to spread to neighbouring buildings. The elaboration of the D model using an automatic gas extinguishing system which despite the high cost of the material and the feasibility of its application (only works effectively in enclosed compartments) has the main objective to demonstrate the potential of this type of software that provide an appreciable amount and variety of fire-fighting solutions to implement and verify the extent of their impact on the development of fire and smoke.

ACKNOWLEDGMENT

REFERENCES

[1] Mealha, Irene Ruiz (2009). *Medidas de Segurança Contra Incêndios em Angra do Heroísmo.* MsC Thesis, University of Coimbra.

[2] Rodrigues, João Paulo Correia; Figueira, Rui Alberto Faísca; Coelho, António Leça (2010). *Avaliação do Risco de Incêndio em Centros Urbanos Antigos. Parte I – Aplicação Informática sobre o Método de ARICA.* II Congresso Internacional – VI Encontro Nacional de Riscos

[3] Rodrigues, João Paulo Correia; Figueira, Rui Alberto Faísca; Coelho, António Leça (2012). Avaliação do Risco de Incêndio em Centros Urbanos Antigos. Parte II – Aplicação Informática sobre o Método de ARICA. II Congresso Internacional de Riscos – VI Encontro Nacional, Revista Territorium, nº19, 2012

[4] Primo, Vítor Martins. *Segurança Contra Incêndio em Edifícios.* Universidade Lusófona do Porto, Porto

[5] Figueiredo, Paulo Jorge (2019). *Segurança contra Incêndios em Edifícios de Centros Urbanos Antigos – O Antigo Orfeão e o Centro Histórico de Viseu.* MsC Thesis, Polytechnic Institute of Coimbra.

[6] Lawson, J.R., Walton, W.D. e Twilley, W.H. (1984). *NBSIR 93-2787 Fire Performance of Furnishings As Measured in the NBS Furniture Calorimeter. Part I.* Center for Fire Research, National Engineering Laboratory, National Bureau of Standards, U.S. Department of Commerce, Washington, D. C.

[7] Kim, J., Lilley, D. (2000). Heat Release Rates of Burning Items in Fires. AIAA 2000-0722. 38th Aerospace Sciences Meeting & Exhibit. Reno.

[8] Thunderhead Engineering (2014). PyroSim User Manual.

FIRE CHEMISTRY FIRE DYNAMICS AND COMBUSTION

TOWARD A STANDARDIZED UNIFORMLY DISTRIBUTED CELLULOSIC FIRE LOAD

Jean-Marc Franssen[1], Antonio Gamba[1], Marion Charlier[2]

[1]Dpt of Urban and Environmental Engineering, Liege University, Belgium

[2]ArcelorMittal Global R&D, Esch-sur-Alzette, Luxembourg

ABSTRACT

This paper describes a series of experimental tests performed on uniformly distributed fire load made of wood sticks. The aim of this campaign was to define a fuel load arrangement that would lead to a fire with the characteristics recommended for office building occupations in EN 1991-1-2. This means a fire load density of 511 MJ/m² and a medium fire propagation.

The ignition procedure that was developed is described as well as the fuel arrangement that leads to a continuous isotropic fire propagation. For the 11 tests performed, the evolution of the radius of the fire is given as a function of time as well as the constant t_α that characterises the t^2 fire. The size of the sticks is not the dominant parameter that influences the fire spread, whereas the presence or not of a ceiling has an overwhelming influence and the volumetric ratio of wood in the fire load allows controlling the fire spread. Values of the volumetric ratio are proposed that should lead to a slow, a medium or a fast fire.

1   INTRODUCTION

A huge number of so-called "natural" fire tests have been performed over the years in full scale compartments with cellulosic fire load. The objectives of these tests were diverse, either linked to the fire dynamics (temperature development, determination of the relationship between the opening factor and the rate of heat release, occurrence of flashover, occurrence of backdraft…) or to the structural behaviour (development of the tensile membrane action, behaviour of particular structural elements) [1]. The recent interest in the so-called "travelling fires" brought a renewed attention to these "natural" fire tests. It turned out yet that the lack of a standardized procedure lead to the fact that different fuel load arrangements were used in these tests. Wood cribs have been used most of the time, but with cribs of different dimensions, timber sticks with different sections and different distances between the cribs. In some tests the cribs were ignited and the fire was left to develop uncontrolled [2], whereas in other tests the cribs have been linked to each other with a steel U channel filled with paraffin to guarantee a rapid fire spread and a rapid development toward a uniform temperature in the compartment [3]. In some tests the fire did not develop as expected and the scientists in charge had to manipulate the fire, either by creating new openings [4], introducing a forced ventilation or adding some liquid fuel to the initially cellulosic fire load [5]. This diversity in procedures makes it impossible to compare the results between each other and to come to conclusive findings. Within the context of the Research Found for Coal and Steel research project "TRAFIR" (Characterization of TRAvelling FIRes in large compartments) sponsored by the E.U. Commission, the fire lab of Liège University has recently performed a series of fire tests with uniformly distributed cellulosic fire loads, with the aim of defining an arrangement of the wood sticks that would lead to a desired fire development. The objective was, using a fire load density as recommended in Eurocode 1 for office buildings, i.e. 511

MJ/m^2, to come to a fuel arrangement that would lead to a medium fire development also recommended for office buildings [6]. This paper reports the tests that have been performed and the results in term of fire spread and time constant t_α of the t-square fire.

2 FIRST SERIES OF TESTS

A first series of five tests has been performed in the fire lab of Liege University in order to, first, establish an ignition procedure that would ensure a reliable and reproducible ignition of the fire load and, second, to investigate at a reasonable cost some important parameters, thus allowing to take first important decisions before performing the more expensive tests that should lead to the final conclusions.

2.1 Ignition procedure

After several attempts based on trials and errors, the ignition procedure was based on a steel cylinder container with a diameter of 106 mm and a height of 25 mm in which 40 ml of denatured ethanol at 96% were placed. This liquid releases enough combustible vapours at ambient temperature to ensure an easy ignition, but not that fast that all liquid would have disappeared by the time the timber fuel load has been installed.

Two electrical igniters were located overhead the cylinder as shown in *Fig. 1.a* to allow ignition from a distance by connecting the igniters to the two poles of a 9 V battery (or to a 19 V transformer taken from a desktop computer, because the battery may fail to trigger the igniters if the wires from the battery to the igniter are too long).
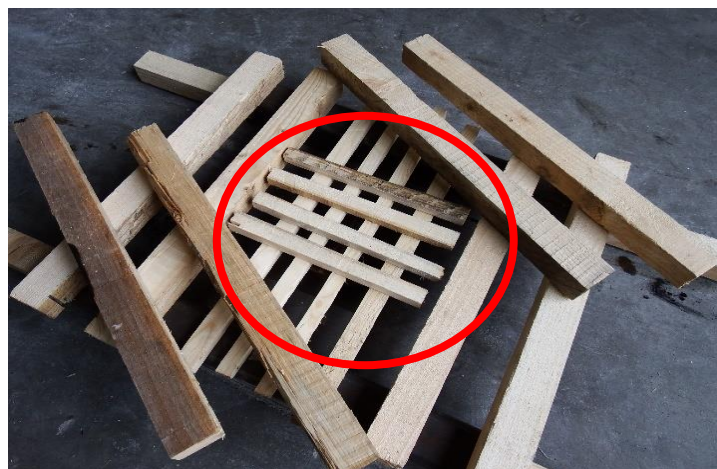
Fig. 1. a) Electrical igniters b) Two layers of lath

Four laths of 15 mm x 18 mm made of *Picea abies* (spruce) were placed on the cylinder and another layer of 4 similar laths on top and perpendicularly to the first layer as shown in the circle drawn in *Fig. 1.b*.

In the 11 tests that were performed, ethanol was ignited by a single electrical igniter in 8 tests, the first electrical igniter failed to ignite the ethanol and the second electrical igniter had to be used in 2 tests, and one test needed a third igniter to be inserted to the steel cylinder among the wood sticks already installed. For all tests, ignition of the ethanol lead to a subsequent ignition of the timber cribs.

2.2 Fuel load arrangement

A 3 mm thick steel plate was used on which 4 steel tube 50 mm x 50 mm were laid to create a clear space between the steel plate and the first layer of wood cribs (the steel cylinder of the igniter was directly laid on the steel plate).

It was decided from the beginning that the fuel load would be laid uniformly on the floor area, as opposed to an arrangement in wood cribs, in order to lead to a continuous horizontal fire propagation, as opposed to a propagation in steps from crib to crib.

It was also decided that the sticks would not be laid in only 2 perpendicular directions but in 3 directions rotated by 60 degrees from layer to layer as shown in *Fig. 2.a* for a test of the first series, in order to favour a horizontal fire propagation as isotropic as possible. *Fig. 2.b* for example, shows a nearly circular shape of the burnt area for a test of the second series where the upper layers have been removed after the test.

Fig. 2. a) Fuel arrangement before the test b) Isotropic horizontal propagation

In most tests, the sticks in any direction were located in the same position for different layers. This means that the sticks of layer $i+3$ were laid above the sticks of layer i as shown in *Fig. 2.a*. In some tests, the sticks were shifted laterally by half the distance between the sticks. This means that the sticks of layer $i+6$ were laid above the sticks of layer i whereas the sticks of layer $i+3$ and those of layer $i+9$ were shifted laterally as shown in *Fig. 2.b*.

These tests were made with a 2 meters diameter fire load. The test set up was located in the horizontal furnace of the fire lab that is 4 meters long, 3 meters wide and 1.41 meters deep. As the steel plate was located approximately 0.41 m above the floor of the furnace, the walls of the furnace extended 1 meter above the fire load (that is, approximately, 0.8 m above the upper layers of sticks).

Wood sticks were made of *Picea abies* with an average density between 443 kg/m³ and 478 kg/m³ and a moisture content, with respect to the dry mass, on the day of the test between 13.2% and 14.2%.

2.3 Measurements
The horizontal fire spread on the upper layer was measured by two different methods.

1) Visual observation of the flaming appearing on the horizontal surface of the upper layer of sticks during the test, as long as the radiation from the fire would allow.
2) Observations of pictures from a still camera that was taking shot at a 30 seconds interval.

The evolution of the mass loss was recorded continuously by 3 load cells that supported to steel plate. A grid of perpendicular timber beams spaced at 0.57 meter was installed to

support the steel plate and transfer the load to the 3 load cells. One layer of gypsum was laid on the timber beams to separate them from the steel plate. From the 5th test, an additional layer covering the whole surface was installed as combustion of some timber beams had started at the end of test L_A 4.

The evolution of the Rate of Heat Release as a function of time, *RHR(t)*, was computed by means of a backward finite difference scheme with a time step of 60 seconds, see *Eq. (1)*. An effective combustion heat of 14 MJ/kg was used for wood, from a combustion factor m of 0.8 and a net calorific value H_u of 17.5 MJ/kg as recommended in Eurocode 1 [6].

$$RHR(t) = -14 \frac{\Delta m}{\Delta t} \tag{1}$$

where   *m*   is the mass (fuel load + steel plates + gypsum layers + timber beams)

       t   is the time.

Other quantities have been measured but are not reported here due to space constrains: temperatures on the surface of some sticks of the upper layer, heat flux on vertical and horizontal surfaces in some points just above the upper layer, heat flux on a vertical surface at some points away at a distance from the fire, vertical flame length above the fire and temperature evolution in the centreline of the plume.

2.4 Results

The first parameter that was investigated was the influence of the size of the sticks. Three tests were performed with respectively 6 layers of B x H = 35 x 30 mm² sticks with a pitch (axis distance) of 80 mm for test L_A1, 6 layers of 45 x 35 mm² sticks with a pitch of 124 mm for test L_A2, and 3 layers of 45 x 60 mm² sticks with a pitch of 110 mm for test L_A3.

Although the sticks differed in dimensions of the section, with a specific surface of respectively 124 m²/m³, 102 m²/m³ and 78 m²/m³, no significant difference was observed in terms of spread rate (0.65 mm/s, 0.7 mm/s and 0.6 mm/s) with no correlation between the specific surface and the spread rate. Also the time constant t_α of the *t*-square model did not show a clear variation with values of 10.4 min, 13.2 min and 13.2 min (see *Fig. 6* that illustrates the best fit method used for calculating the values of the time constants). It appeared also that the growth rate was far above the target value of 5 minutes that was aimed at for an office building.

A second group of two tests was then performed with the same sections and same pitch as those used for tests L_A1 and L_A2, now rotated by 90 degrees (B x H = 30 x 35 mm² and 35 x 45 mm²). The major difference is that a ceiling made of insulating fibre boards was placed above the fuel load (vertical distance between the fuel load and the ceiling = 990 mm and 915 mm). A clear layer of 280 mm was left between the walls of the furnace and the ceiling. This, plus the fact that the ceiling covered only 2.66 meters of the 4 meters long furnace lead to the fact that the fire was not air controlled.

The propagation rates were significantly influenced by the presence of the ceiling. In test L_A4, the spread rate was observed at 0.9 mm/s during the first 10 minutes of the test and increased to 2.95 mm/s for the last 3 minutes. In tests L_A5, the spread rate was observed at 0.85 mm/s during the first 11 minutes of the test and increased to 7 mm/s for the last 2 minutes. The difference between the first 3 tests and the 2 tests with a ceiling can be observed on *Fig. 3* that gives the evolution of the radius of the fire as a function of time. The time constant t_α for these tests was 6.9 minutes in test L_A4 and 5.5 minutes in tests L_A5.
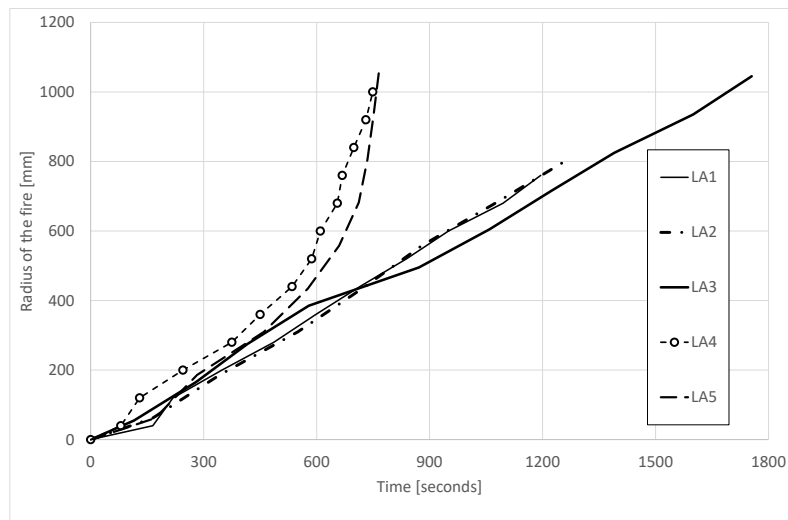
Fig. 3. Evolution of the radius of the fire in the tests L_A

3 SECOND SERIES OF TESTS

A second series of six tests was performed in larger facility where fire loads of 3 meters in diameter located on a 4,40 x 4,40 m² steel platform could be tested.

3.1 Description of the ceiling

From the results of the first test series, it was decided that all tests would be made with a ceiling located above the fire load due to the high influence of the ceiling on the fire dynamics (See *Fig. 3*). The ceiling was made of 4 timber columns suporting a grid of timber beams under which OSB board were fixed. Mats of insulating fibres were used to protect the columns and the OSB boards from the attack of the fire. The lower surface of this ceiling was 2.50 meters above the steel platform. The dimension in plan were 4.88 x 4.72 m² and a downstand of 0.35 m was running on the 4 sides of the ceiling.

Fig. 4 shows the ceiling during a test, at the beginning of the fire. Plate thermometers used to recompute the radiative flux as well as the grid supporting a thermocouple tree in the centreline of the fire are also visible. The results of these measurements are still under interpretation at the time of writing this paper and will be presented in subsequent communications.

Fig. 4. The ceiling used in the second series of tests

413

3.2 Tested configurations and results

Different tests were performed in a couple of days, capitalising from each test to define the next one, in the limits of the available material that had to be purchased beforehand. In test L_B5, some laths of 15 x 15 mm² of the species *Pinus sylvestris* were inserted to see whether this would favor a faster fire spread compared to companion test L_B1. In test L_B4, bands of PMMA have been inserted in three layers. Based on a specific mass of 1180 kg/m³ and a gross heat of combustion of 26.8 kJ.kg for PMMA [7], a value of 15.215 MJ/kg was used for the average heat of combustion to compute the rate of heat release from the mass loss, see *Eq. 1*.

The main parameters of these tests as well as the main results are summarized in *Table 1*.

Table 1. Parameters and results of the second series of tests

Test	B [mm]	H [mm]	Number of	Pitch [mm]	Density [kg/m³]	Moisture content [%]	t_α [min.]
L_B1	30	35	6	80	468	16.9	10.9
L_B2	34	45	6	135	502	16.6	9.4
L_B3	30	35	12	160	468	14.1	2.1
L_B4	34	45	5	135	502	20.2	4.2
	100	3	3	270	1180	(PMMA)	
L_B5	30	35	5	80	468	16.9	7.3
	15	15	4	80	554	13.5	
L_B7	30	35	9	120	468	16.9	7.5

The evolution of the radius of the fire is shown on *Fig.* 5.
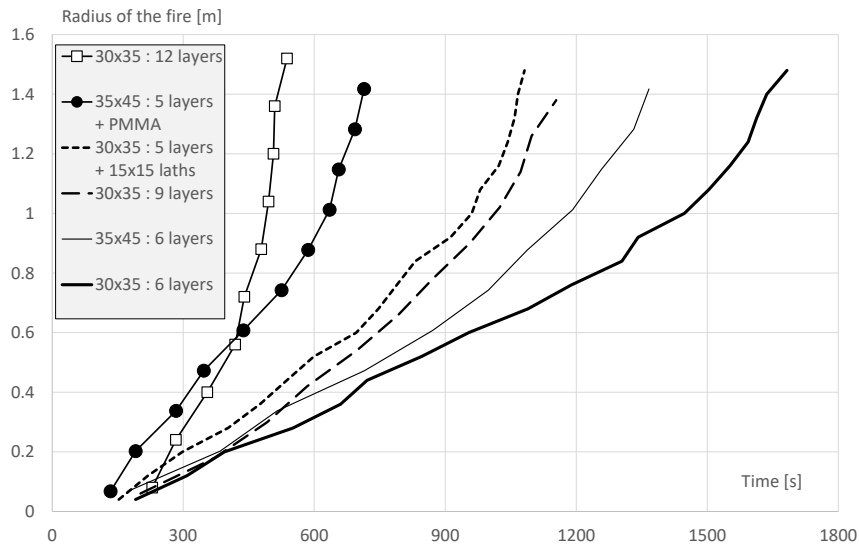

Fig. 5. Evolution of the radius of the fire for the second series of tests

The procedure to derive for each test the best fit t^2 curve from the experimental Rate of Heat Release curve involves a certain degree of human decision. The best fit curve ends at the last point that was recorded before water was applied on the fire to stop the tests. It starts with an

horizontal tangent on the time axis. A human decision has to be taken as where to fix the starting point of the curve. In fact, each test is characterised by an ignition phase when only noise is recorded that has to be eliminated. *Fig. 6*, for example, shows the best fit curve derived for test L_B7 when the starting time is set to 6 minutes.
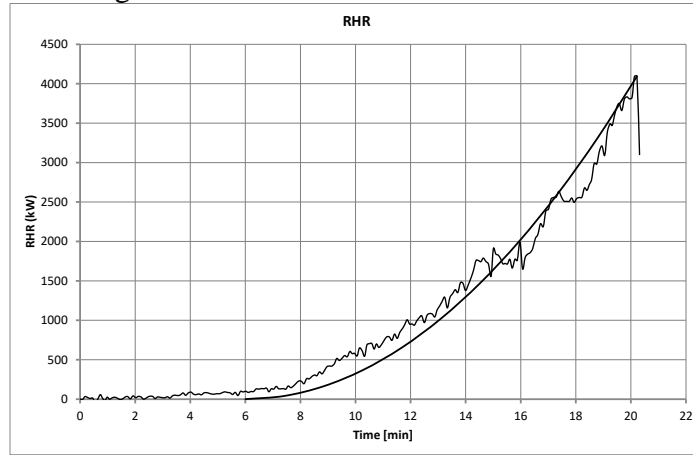

Fig. 6. Recorded RHR curve and best fit curve

The clearest interpretation of the test results is obtained when only the tests made of the section 30 x 35 mm² are considered. For the tests L_B3, L_B7 and L_B1, *Fig. 7* shows the values of the parameter t_α in minutes that was calculated as a function of the volumetric percentage of wood contained in the fuel load. Three values are presented for each test in order to reflect the degree of uncertainty linked to the choice of the starting time of the best fit curve. For each test, the lowest value of t_α (grey dots) is derived from the latest reasonable choice of the starting time, whereas the highest value (orange dots) is derived from the earliest reasonable choice and the value represented by the blue dots is the best choice if only one value has to be mentionned, from the agreed decision of the first two authors.

From the best linear regression on the three test results, it appears that a fast fire can be produced with wood content of 17 ±1%, a medium fire with a wood content of 22.5±1.5% and a slow fire with a wood content of 33.5±3%.
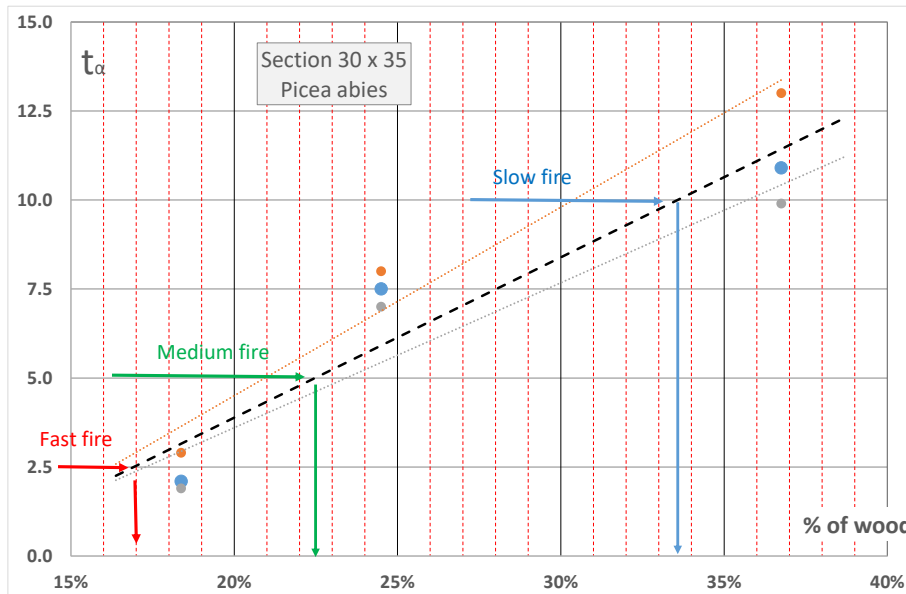

Fig. 7. Parameter t_α (in minutes) as a function of the volumetric wood content in the fire load

4 CONCLUSIONS

- 40 ml of denaturised ethanol in a 106 mm diameter cylinder on which two perpendicular layers of 15 x 18 mm² laths of *Picea abies* are located is an appropriate means for igniting a wood crib.
- A continuous layer made of several layers of wood sticks turned by 60° from layer to layer ensures a progressive and isotropic fire spread.
- Within the limits of the dimensions tested (from 30 x 35 to 45 x 60 mm²), the size of the sticks does not influence the spread rate significantly.
- The presence of a ceiling above the fire load influences significantly the fire spread. The influence of the distance between the fire load and the ceiling has not been investigated here.
- For a given configuration and dimensions of the wood sticks, the volumic wood content in the fire load has a very high influence on the spread rate.
- With sections of 30 x 35 mm² of pine tree that is commercially dry (moisture content from 14 to 17%) and with a ceiling that is approximately 2.20 meters above the fire load, a medium t^2 fire is likely to develop with a volumetric wood content around 22.5 % (17 % for a fast fire and 34% for a slow fire). The reproduceability of these results could not be investigated in this experimental campaign
- All tests results are available as open data: https://orbi.uliege.be/handle/2268/233374

REFERENCES

[1] Bisby L., Gales J., Maluk C. (2013). *A contemporary review of large-scale non-standard structural fire testing*, Fire Sci. Rev., vol. 2, no. 1, p. 1.

[2] Horová K., Jána T., Wald F. (2013). *Temperature heterogeneity during travelling fire on experimental building*, Adv. Eng. Softw., vol. 62–63, pp. 119–130.

[3] J. Chlouba, F.Wald, Z. Sokol (2012). *Temperature of connections during fire on steel frame building. International Journal of Steel Structures.* DOI: 10.1007/bf03249479.

[4] Rush D., Lange D., Maclean J. Rackauskaite E. (2015). *Effects of a travelling fire on a concrete column – Tisova Fire Test.* in Proceedings of the 4th International Conference on Applications of Structural Fire Engineering, Dubrovnik, Croatia, pp. 362–367.

[5] Pyl L., Schueremans L., Dierckx W., Georgieva I. (2012). *Fire safety analysis of a 3D frame structure based on a full-scale fire test,* Thin-Walled Structures.

[6] CEN- European Committee for Standardization, *EN 1991-1-2, Eurocode 1: Actions on structures – Part 1-2: General actions – Actions on structures exposed to fire*. 2002.

[7] Walters R., Hackett S., Lyon R (2000). *Heats of combustion of high temperature polymers*. Fire and Materials, Vol. 24, Issue 5, pp. 245-252.

A COMPARISON OF METHODS FOR THE CALCULATION OF FURNITURE HEAT RELEASE RATE

Bronwyn Forrest[1] and Elizabeth J. Weckman[1]
[1]University of Waterloo, Waterloo, Canada

ABSTRACT

Methods have been developed to calculate heat release rate (HRR) of burning materials. For materials with known heats of combustion and mass loss rates burning in controlled, well-ventilated environments, calculation of HRR is relatively simple and accurate. However, in real furniture fires, specifically ones that develop in ve87ntilation-limited environments, there is added difficulty due to the unknown values for mass burning rates and heat of combustion, irregular shapes of the furniture, and flame characteristics that are greatly impacted by the evolution of the smoke layer over time. This paper explores the application of existing calculation methods to the estimation of HRR of furniture during real fires in ventilation-limited environments. Examination and comparison of estimates obtained by the different methods demonstrate issues with their use in estimating fire characteristics in these fire environments.

1 INTRODUCTION

Heat release rate (HRR) is considered to be the most important value for a fire hazard assessment as it is essentially a measure of the power of the fire [1]. HRR is used as an important input to a variety of models, both computational and numerical, in order to determine the risk associated with fire, structural integrity of a specified building during a fire, fire growth & spread, and the possible impacts of these factors on human egress [2]. Upholstered furniture poses a difficult problem for fire safety engineers and researchers alike as the complex nature of the material and the environment the furniture is burning in can greatly impact the physics and chemistry of the combustion process [3]. In these situations, interactions and characteristics of fire behaviour are poorly understood making it difficult to determine which correlation or equation is appropriate to use, even for a defined fire scenario. The data used for the methods chosen in this paper were obtained from a series of repeatable full-scale fire tests (and therefore deemed suitable for a numerical comparison) conducted at the University of Waterloo Live Fire Research Facility [4]. These experiments were fuelled by three types of couches tested three times each for a total of nine tests. The couches were custom constructed with a standard wooden frame and different combinations of polyurethane foam and fabric, some treated with fire-retardant (FR) in adherence with certain furniture standards from around the world. Couch A was constructed with both non-FR foam (0.44 wt% chlorine) and polyester fabric (0.17 wt% chlorine). Couch Type B had both FR foam (3.0 wt% chlorine) and FR polyester fabric (5.2 wt% bromine and 3.6% wt chlorine). Couch C was constructed with non-FR foam (0.9 wt% chlorine) and non-FR fabric (0.11 wt% chlorine). The couches were ignited with a small wooden crib and isopropanol wick in adherence with BS 5852 [5]. The tests were conducted in the two-storey 'burn house' located at the UW lab. The 'burn house' was completely sealed during the duration of the tests in order to achieve a ventilation-limited environment. The 'burn house' was instrumented with thermocouples in various locations and a water-cooled heat flux gauge positioned 3m away from the couch. The couches were placed on weigh scales and security cameras were positioned at various locations to record the fires. The data from each of the

nine tests as well as some cone calorimeter results serve as the inputs into the selected models discussed in the next section.

INPUT PARAMETERS AND CALCULATION METHODS

This section describes the methods chosen to calculate HRR for each test, as well as how key input parameters, such as the heat of combustion and flame areas, were determined. The last method described has been developed for the purpose of attempting to correlate bench-scale cone calorimeter test data to results from the large-scale tests. The results from this final method should be considered preliminary, and other ways of extrapolating cone calorimeter data to large-scale HRR estimates could alternately have been explored.

1.1 Heat of Combustion

There are several documented values for the heat of combustion for polyurethane foam in the literature, however, in a complex fuel like upholstered furniture, the heat of combustion must take into consideration the fabric as well as the foam. Furthermore, the heat of combustion for treated foam can vary drastically depending on the specific chemical composition, so it was determined that finding a specific heat of combustion for the materials used in these nine tests was needed. The heat of combustion for the couches was determined from cone calorimeter tests in which representative materials in the couch combinations described above were tested. Using the Fire Testing Technology (FTT) ConeCalc5 software, [6] the total heat released (THR) in kJ/m^2, as well as the mass of the sample and the surface area of the sample ($88.4cm^2$) were used to generate values for the heat of combustion of each combination via Equation (1) below:

$$\Delta H_{c,eff}\left(\frac{kJ}{kg}\right) = \frac{THR\left(\frac{kJ}{m^2}\right)*0.00884m^2}{m_{sample}(kg)} \tag{1}$$

The resulting heats of combustion for the three couch types are compiled in Table 1 below:

Table 11: Effective Heats of Combustion for the Couches

Couch Type	Heat of Combustion (kJ/kg)
A non-FR	14450
B FR	9655
C non-FR	14263

1.2 Video Footage

It was found that security camera video footage obtained during the experiments was a crucial component in understanding the burning characteristics of the couches as well as how the smoke layer impacted fire growth and therefore, the resulting value of heat release rate. The video footage was primarily used in the area source radiation approximation method described in Section 2.4. First, the pixel dimensions for the height of the back cushion and length of the couch along the front of the sitting cushions were determined. Then, a screenshot corresponding to the time of peak measured heat flux was spliced from the video. A representative screenshot is shown in *Figure 1* below. Using an image editing tool, rectangles were drawn over two areas on the screenshot: the main flame area (left hand rectangle, black, in *Figure 1*) and any surrounding flame areas (right hand rectangle, grey, in

Figure 1). The ratio of the dimensions of the flame areas to the dimensions of the couch, in conjunction with knowing the actual dimensions of the couch, allowed for the conversion of pixels to meters for the rectangular areas. These were then used as inputs to the area source calculation method. Characteristic temperatures of the flame, T_f, in each rectangular area were based on a relative scale of colour saturation; the closer the area was to yellow, (or white in the case of the grey-scale image below) the closer the chosen value was to 1100K. In all cases, the temperature of the flaming area was assumed to be 1100K and the temperature of the secondary fire area (grey rectangle) was scaled according to relative colour. The values of temperature and dimensions are subject to change based on the person conducting the analysis, so efforts to make this process more consistent are currently being carried out.
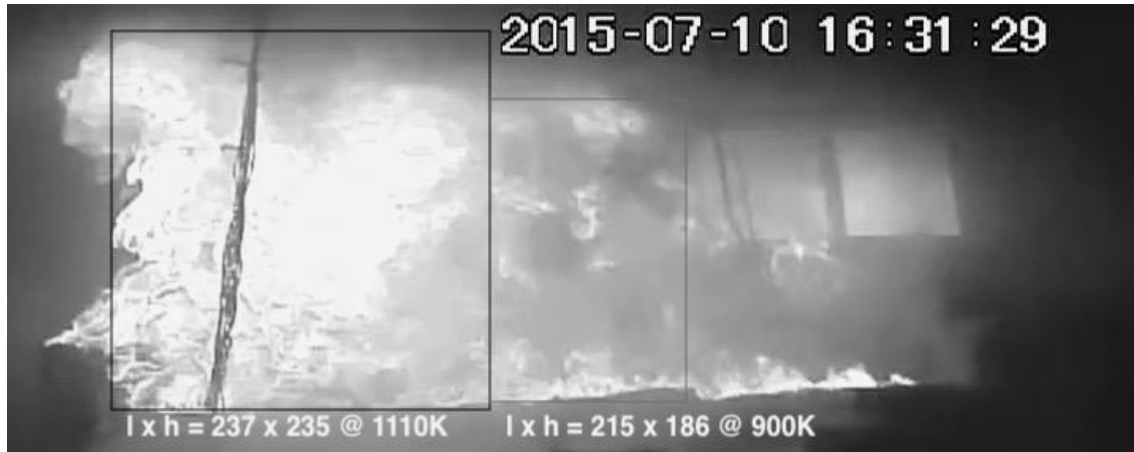

Figure 1: Example screenshot and areas of the flame area and surrounding area with pixel dimensions and temperatures used for T_f input in the area source approximation method described below.

1.3 Babrauskas Correlations

Two HRR correlation methods developed by Brabauskas for furniture were used, as given in Equations (2) and (3) below. The first uses bench scale data (cone calorimeter) with a mass and style factor, and the second uses pre-determined factors based on the characteristics of the furniture. Due to differences in the couches used in these tests and the bench scale tests compared to the furniture used in the original work, some adaptations to the original formulas were made. For the first correlation method, the bench scale tests are supposed to be conducted at 25kW/m² however, the present materials did not ignite at this level of irradiance. Instead, ignition was achieved at 35kW/m², so the co-efficient 0.63 was changed to 0.45 to account for this difference in flux [7]. Also, the frames used in these couches were wooden, however they did not burn so they are considered to not be part of the combustible mass. Therefore, the mass factor used in these calculations was determined by taking the full mass of the couch and multiplying it by the wooden frame factor of 0.3. In reality, this number is very close to the total volume of combustible foam and fabric in each couch as well. This inherently takes into consideration the frame component and so an individual frame factor was not included in the calculations. As per the literature, the style factor was 1 (rectilinear shaped furniture), the padding factor was 1 (for polyurethane foam), for couches A and B, the fabric factor was considered to be 1 (thermoplastics) and lastly, couch C fabric did not melt, so the factor of 0.4 was used [8].

$$\dot{Q} \ (kW) = \frac{0.63*25}{35} * \dot{q}_{bs} \ [mass \ factor][style \ factor]$$
$$(2)$$

$$\dot{Q} \ (kW) = 210[fabric \ factor][padding \ factor][mass \ factor][style \ factor]$$
$$(3)$$

1.4 Area Source Radiation Approximation

The first step in this method is to carry out the video analysis outlined in section 2.2. Once the values of the height, L_1, and length, L_2, of the rectangular flame areas were determined, values for S (L_1/L_2) and α (L_1*L_2/R^2, where R is the distance between the fire and the heat flux gauge) were calculated to find a corresponding configuration factor for those particular areas [9]. Using Equations (4) and (5) below [10], the $\dot{Q}$ of each area was calculated and the final, or total $\dot{Q}$ as seen in the tables below, was the sum of both areas. T_{sur} was always 273K because the heat flux gauge used in the experiments was water-cooled. The gauge was placed at R = 3m away from the couch (input for the radius variable) and finally, χ_{rad} was considered to be 0.3 [10].

$$q \ (\tfrac{kW}{m^2}) \ = \ 5.67x10^{-8}\big(T_f^4 - T_{sur}^4\big) * configuration \ factor \qquad (4)$$

$$\dot{Q} \ (kW) = \frac{4\pi R^2}{\chi_{rad}} \qquad (5)$$

1.5 Mass Loss Rate Method

Mass loss was recorded over the duration of the burn as the couches were placed on weigh scales. The mass loss was multiplied by the effective heat of combustion determined for each couch (shown in *Table 1*) as shown in Equation (6) below [10]. Two values for HRR are compared in the next section, one the average HRR over the period of steady burning and the second a peak value of HRR seen in that same time period.

$$\dot{Q}(kW) = \dot{m} * \Delta H_{c,eff} \qquad (6)$$

1.6 Cone Extrapolation Method

In this method, the mass loss rates averaged over the periods of steady burning for the cone sample and couch were divided by 0.00884m^2 (surface area of cone sample) and 0.97m^2 (surface area of couch most involved in fire) respectively to get a value of $\dot{m}''$ for each. These values were compared to see how many times greater the couch $\dot{m}''$ was compared to the cone. This factor is labelled as X in Equation (8) below. Next, $\dot{m}''$ for the cone was multiplied by the effective heat of combustion as measured in Section 2.1 to get a value of HRR for the cone sample, referred to as $\dot{Q}_c$, shown by Equation (7) below. To get a final 'extrapolated' value of HRR for the couch, referred to as $\dot{Q}_e$, the value of $\dot{Q}_c$ was multiplied by the area of couch burning (0.97m^2) and the factor X to adjust for differences between the mass burning rate in the cone calorimeter relative to the couch.

$$\dot{Q}_c \ (kW) = \ \dot{m}''_{cone} \ * \ \Delta H_{c,eff} \qquad (7)$$

$$\dot{Q}_e \ (kW) = \ \dot{Q}_c * X * A_{couch} \qquad (8)$$

2 RESULTS AND DISCUSSION

In the following section, the results are tabulated for each calculation method and organized based on couch type and corresponding test number.

2.1 Correlations of Babrauskas

Table 2: Fire Heat Release Rates for Three Couch Types Using Babrauskas Correlations

Tests (Couch Type)	Correlation 1 HRR (kW)	Correlation 2 HRR (kW)
1, 4, 7 (B: FR)	931, 962, 944	3783, 3912, 3838
2, 5, 8 (A: non-FR)	1251, 1244, 1170	3817, 3798, 3570
3, 6, 9 (C: non-FR)	571, 614, 573	1318, 1418, 1323

Values of HRR for Couch A and Couch C are consistent with the expected trends. For Couch B, values of HRR estimated using the second correlation are higher than expected. Reasons for this are discussed in the next section.

2.2 Area Source Radiation Approximation

Table 3: Fire Heat Release Rates for Three Couch Types Using Area Source Approximation

Tests (Couch Type)	HRR
1, 4, 7 (B: FR)	1091, 1183, 1184
2, 5, 8 (A: non-FR)	1341, 1464, 1246
3, 6, 9 (C: non-FR)	1191, 1192, 1198

Generally, values of HRR estimated using the area source radiation approximation are lower than expected. This is most likely due to the difficulty of establishing an accurate flame area or flame temperature, partly due to the imaging tool used, and also due to the thick, black smoke layer that descends over the flame, making it difficult to assess where the entirety of the fire is located.

2.3 Mass Loss Rate Method

Table 4: Fire Heat Release Rates for Three Couch Types Using Mass Loss Rate

Tests (Couch Type)	Averaged over Period of Steady Burning	Absolute Peak (during period of steady burning)
1, 4, 7 (B: FR)	1374, 1313, 1385	2386, 2226, 2244
2, 5, 8 (A: non-FR)	2427, 2469, 2451	3369, 3339, 3353
3, 6, 9 (C: non-FR)	1214, 1321, 1579	2511, 2721, 2462

This method demonstrates the expected trends in HRR for the three types of couch. Couch A has the highest values, followed by couch C then couch B. It should be noted however, that steady burning was achieved for couch B around 300s into the tests, however, for couch C, steady burning was established much later, about 600s into the tests. This contrast in fire growth is due to the difference in burning characteristics between the fabrics – regardless of FR additives.

2.4 Cone Extrapolation Method

Table 5: Fire Heat Release Rates for Three Couch Types Using Cone Extrapolation Method

Tests (Couch Type)	HRR
1, 4, 7 (B: FR)	1374, 1279, 1180
2, 5, 8 (A: non-FR)	2115, 3198, 2554
3, 6, 9 (C: non-FR)	1215, 1278, 2533

In general, HRR values estimated using the cone extrapolation method were consistent with expectation. The differences in predicted HRR between tests, for example test 3 and 9 are due to a large difference in the mass loss rate over the time selected as the period of steady burning in the full-scale experiments. The mass loss rate was larger for test 9 compared to test 3, resulting in a larger factor of how many times greater the couch mass burning rate was compared to the cone mass burning rate for test 9. In fact, the couch mass burning rate was estimated to be 33 times greater for test 9, and only 16 times greater for test 3. This factor of almost double accounts for the large differences in HRR between these tests. As stated previously, this method should be considered preliminary, and more investigation into making it more consistent across tests should be done.

2.5 Overall Discussion

Trends in HRR seen across all methods for the three couch types are that couch A, the non-FR couch, consistently has the highest values for HRR, followed by the other non-FR couch C, and as anticipated couch B has the lowest values of HRR predicted and calculated. The only discrepancies in this trend are found when HRR is estimated using the Babrauskas correlations. The averaged HRR in the cone is lower for couch C than couch B, which was interesting due to the small traces of FR in the couch C materials. However, it was observed that the fabric used in couch C has a different burning profile compared to polyester. Polyester melted and pooled which caused a quicker ignition to the underlying foam, which is registered in cone calorimeter test data in the averaged values of HRR per unit area over the first 180s after ignition. However, couch C fabric charred and created a barrier-like effect between the flame and the foam underneath, effectively lowering the HRR over the first 180s when the foam has not yet ignited. In the second Babrauskas correlation, due to the fact that polyester melts, the thermoplastic factor of 1 was used in the calculations for couch B. However, it was found that using a value closer to 0.5 resulted in a HRR prediction which was lower and more comparable to the HRR values calculated using the other methods. This suggests that more investigation should be done to determine a fabric factor for FR fabrics and PU foam as well.

The values for HRR between the radiative, cone extrapolation and averaged HRR from the mass loss rate data over a period of steady burning resulted in comparable numbers for couch B. Values from the cone extrapolation and averaged HRR over a period of steady burning were very comparable for couch C and had some agreement with the values from the radiative method. Couch A however, had the least consistent set of calculated values of HRR amongst these three methods. Estimates of HRR using the area source radiation method seemed extremely low as these values were around 1000kW below the averaged value of HRR over the period of steady burning. There was better agreement between the cone extrapolation method and the averaged HRR over period of steady burning, but even these two values were not as close as seen for the other couches. This is potentially due to the evolution of the smoke layer and its impact on overall fire development in these tests.

As each method requires a different set of input parameters, the calculated values of HRR were expected to be different. Methods that are based on similar inputs, like the cone

extrapolation and mass loss rate methods, were expected to lead to more comparable values of HRR due to the fact that mass loss rate and heat of combustion were key input parameters. The differences seen indicate a few points: work is still needed to develop strategies to extrapolate values of HRR from bench scale to large-scale estimates, the type of large-scale environment greatly impacts the heat release rate, and more investigation into how the material chemistry dictates burning characteristics is needed to provide valuable information to develop new HRR calculation methods. For example, understanding how the couch C fabric burned compared to polyester was key to understanding why the couch C fires took much longer to develop and reach a peak time of steady burning, and why with certain methods, the predicted values were lower than a couch with FR treated materials.

A set of correlations and equations should be developed that can take into consideration the material interactions and fire environment. It is not anticipated, however, that any one method can account for all the physics and chemistry present across the range of possible fire situations. Therefore, it is likely that a number of different HRR calculation methods using a variety of inputs will have to be applied to obtain the best possible estimate as well as to gain insight into multiple possible outcomes.

2.6 Future Work

In terms of future work, it was found that video footage was crucial in these analyses. It was needed to properly carry out the area source radiation method and was also a key component to understanding the trends and differences in values across the tests. A more precise method of measuring the flame areas using tools such as edge detection to extract information such as flame heights and diameters, as well as to track the smoke layer and determine how it interfaces with the fire plume, are being developed. The new information will also provide inputs for other methods not explored in this study. Future work should also investigate new ways to determine the heat of combustion for complex fuel loads. The values used in this study are preliminary as only one set of cone calorimeter experiments was used to determine the heats of combustion. Lastly, it should be noted that while having a peak value of HRR is useful, a time-resolved curve provides significantly more insight into the details of fire development, as well as improved input into computational models used in hazard and/or risk assessments.

3   CONCLUSIONS

Several conclusions can be drawn from this study:

> The non-FR couch consistently had higher values of peak HRR compared to the FR couch B, as well as couch C.

> Methods which had similar input parameters (mass loss rate and heat of combustion) resulted in more comparable estimates of peak HRR, compared to methods with very different input parameters (such as temperature and area).

> One method was not better than another for this set of full-scale fire scenarios, therefore it is encouraged that several different methods be tried to provide more information on HRR. Results highlight the need for new strategies based on improved understanding and correlation of parameters unique to the materials burning as well as key aspects of the fire environment.

ACKNOWLEDGMENTS

REFERENCES

[1] Babrauskas V., Peacock R. (1991). *Heat Release Rate: The Single Most Important Variable in Fire Hazard.* Fire Safety Journal. Elsevier Science Publishers, England 1991.

[2] Cai N., Chow W.K. (2012) *Numerical Studies on Heat Release Rate in Room Fires on Liquid Fuel under Different Ventilation Factors,* in: International Journal of Chemical Engineering. Volume 2012, Article ID: 910869. https://www.hindawi.com/journals/ijce/2012/910869/

[3] Fleischmann C. *Evaluating the Fire Threat From Upholstered Furniture*, in: Emerging Trends eNewsletter, Retrieved Jan 29th 2019 from the SFPE website. https://www.sfpe.org/page/FPE_ET_Issue_39

[4] Senez, P., Mulherin, P., Weckman, E. (2017) *Repeatability of Underventilated Compartment Fire Testing with Complex Fuel Packages.* Fire and Materials 2017, San Francisco, CA, pp. 342-355

[5] British Standards Institute (2006) BS 5852:2006 Methods of test for assessment of the ignitability of upholstered seating by smouldering and flaming ignition sources, London UK.

[6] Fire Testing Technology (2009) ConeCalc5 software, East Grinstead UK.

[7] Kransy J., Haber W., Parker W., Babrauskas V. (2008) *Fire Behaviour of Upholstered Furniture and Mattresses.* Cambridge University Press, UK.

[8] Ames S.A., Babrauskas V., Parker W.J. *Upholstered Furniture: Predictions by Correlations*, in: Heat Release in Fires, Elsevier Science Publishers Ltd., England 1992, p. 521.

[9] Drysdale D. (2011) *Heat Transfer: Configuration Factors,* in: An Introduction to Fire Dynamics, Wiley & Sons Publications, UK, p. 66.

[10] Gorbett G.E., Pharr J.L. (2011) *Heat Release Rate*, in: Fire Dynamics, Pearson Education Inc., New Jersey, p. 137, 159, 160.

A PRACTICAL FORMULA FOR TRAJECTORY OF FLAME EJECTED FROM AN OPENING

[1]Kazunori Harada, [1]Daisaku Nii, [2]Yi-Chul Shin, [2]Kye-Won Park, [3]Masaki Noaki, [4]Yoshifumi Ohmiya
[1]Kyoto University,Kyoto, Japan
[2]Fire Insurers Laboratory of Korea, Republic of Korea
[3]Building Research Institute, Ibaraki, 305-0802 Japan
[4]Tokyo University of Science, Noda, Japan

ABSTRACT

To design a building against ejected flames from an opening, the trajectories of flame should be studied in order to evaluate the heat impact on neighbouring elements. As a classical study, Yokoi measured a variety of trajectories depending on the aspect ratio of ejecting plane. The data were summarized by diagrams, but explicit functions are not available. Thus the engineers have to read the diagram by eye. To facilitate the design, the trajectory data were fitted with a mathematical function. The parameters in the function were estimated to fit to Yokoi's data and correlated with aspect ratio of ejecting plane. It was found that the overall agreement with the Yokoi's data is satisfactory in the range of aspect ratios between 1 and 6.4. The developed formulae were compared with other experiments published in literatures and validated. The set of formulae would be useful in performance- based design of fire resistance and fire confinement against ejected flames.

1   INTRODUCTION

In the fire safety design of buildings and built environment, consideration on the effect of ejected flame from an opening is important. For example, the temperature profile is needed to assess the possibility of fire spread to upper floors and/or adjacent buildings and to assure satisfactory fire resistance of façade and structural elements affected by an ejected flame.

As to the behaviour of ejected flame, Yokoi conducted comprehensive research on the trajectory and temperature profile [1]. The classical results are still valid and being used for performance-based design of buildings [2][3][4]. However, the use of trajectory formulae is limited only to the case of ejected flame to an open environment where there is no wall above an opening. To calculate the trajectory, engineers must read values from Yokoi's diagram by eye and calculate trajectory position by hand in order to obtain temperature values. In practice, the task is tedious and needs for closed-form formulae are obvious.

Law [5] proposed a practical method to identify the area affected by an ejected flame. However the area is evaluated with conservative assumptions. Mizuno *et al*.[6] proposed a cubic function to fit to the Yokoi's trajectory data. However the use of cubic function was limited because the function could not represent the behaviour of ejected flame adhering to wall surface. As to physical modelling, Himoto *et al*.[7] proposed a model based on entrainment characteristics. The results were compared with model-scale experiments of an ejected flame from an opening of a pressurized and non-pressurized compartment. However, there are still uncertainties in predictions.

In this study, the classical Yokoi's diagram was investigated and closed-form formulae were fitted to trajectory data. The results were compared with experiments conducted by other researchers and the formula was validated for wider range of application.

2   DERIVATION OF FORMULAE FOR EJECTED FLAME TRAJECTORY

2.1 Yokoi's trajectory data

Yokoi conducted systematic model-scale experiments on an ejected flame from an opening. The shapes of trajectories were measured and summarized in a diagram shown in *Fig.1* as relationships between non-dimensional horizontal distance $x/(H_u-z_n)$ and non-dimensional vertical distance $z/(H_u-z_n)$, where x and z are the horizontal and vertical distances from the centroid of the ejecting plane [m], (H_u-z_n) is the height of ejecting plane, H_u is the height of upper edge of opening [m], H_u is the height of upper edge of opening [m], z_n is the height of neutral plane [m]. As shown in *Fig. 1a)*, the distances x and z are measured from the centroid of ejecting surface locating on opening surface at height $z_n +(2/3)(H_u-z_n)$.
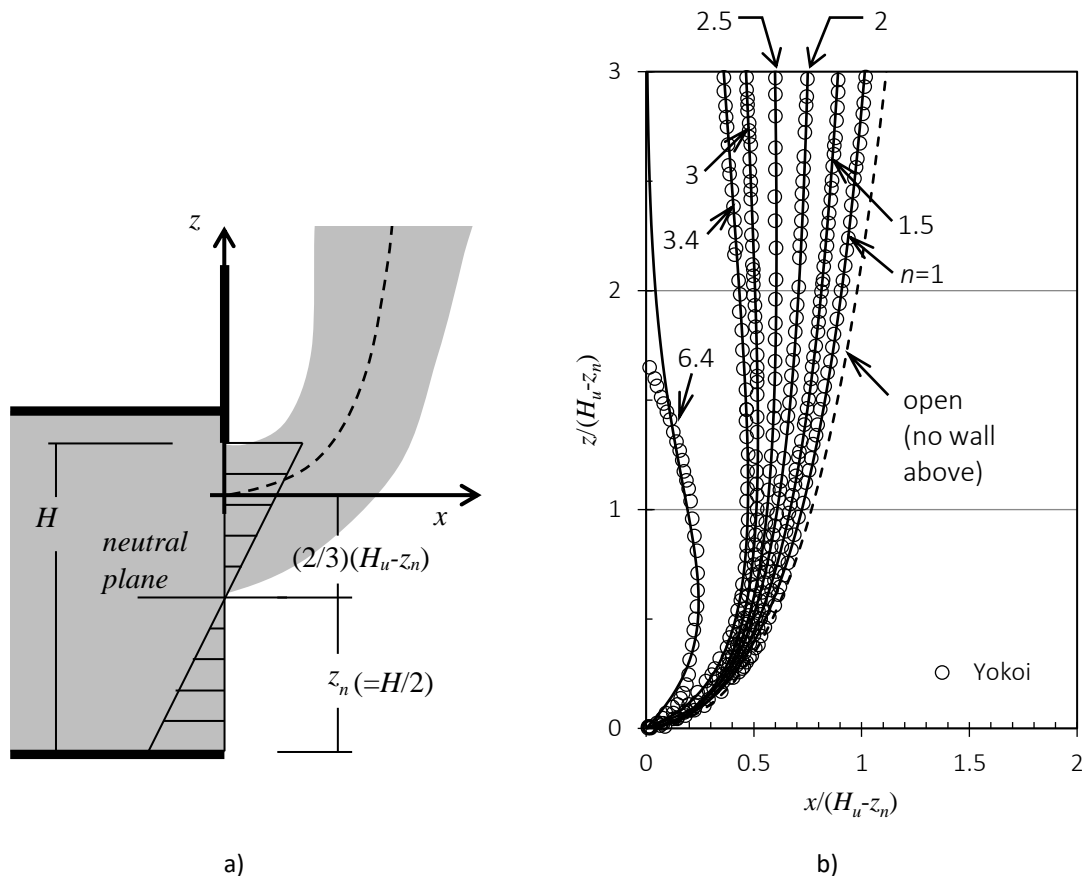

Fig. 1 Trajectories of plume axis ejected from an opening, a) notations b) trajectories of plume axis shown by symbols. Solid line denotes fitting results described in section 2.2.

The aspect ratio of ejecting surface, *n*, is defined by

$$n = B/(H_u - z_n) \tag{9}$$

where B is the width of an opening [m]

   H_u is the upper height of an opening above baseline [m],

   z_n is the height of neutral plane above baseline [m].

Yokoi assumed that the neutral plane is located at the middle of opening height, $z_n=H/2$, when he summarizes his measured data.

As shown in *Fig. 1b)*, the trajectories depends on the aspect ratio of ejecting plane. When the aspect ratio is small, the flame goes apart from wall. The trajectory is close to that in open space where no walls exist above an opening. As the aspect ratio is increased, the trajectory tends to adhere to wall surface. In case of aspect ratio 2.5, the trajectory rises up almost in parallel to wall surface. In case of larger aspect ratios, the trajectories bend toward the wall surface.

2.2 Curve fitting to Yokoi's trajectory data

In order to represent the changes of trajectory by the aspect ratio of an ejecting surface, a closed form mathematical function was selected. In case of small aspect ratio, the trajectory goes away from the wall. In case of large aspect ratio, the trajectory adheres to the wall above an opening. The mathematical function should be able to represent these characteristics. One of the possible functional forms is

$$\frac{x}{H-z_n} = C\left(\frac{z}{H-z_n}\right)\exp\left\{-a\left(\frac{z}{H-z_n}\right)^m\right\} \tag{10}$$

where the coefficients C[-], a [-] and power m[-] should be determined by fitting the function to Yokoi's trajectory data. The value of x is maximized at $z=(H-z_n)/am^{1/m}$ and converges to zero as z tend to infinite. These features are convenient to express the shape of trajectories.

Using Yokoi's data, the best-fit coefficients were searched for every aspect ratio. Conventional least square method was applied to get the sets of best fit results of (C, a, m). The results are shown in *Fig. 1b)* by solid lines. The overall agreement is satisfactory.

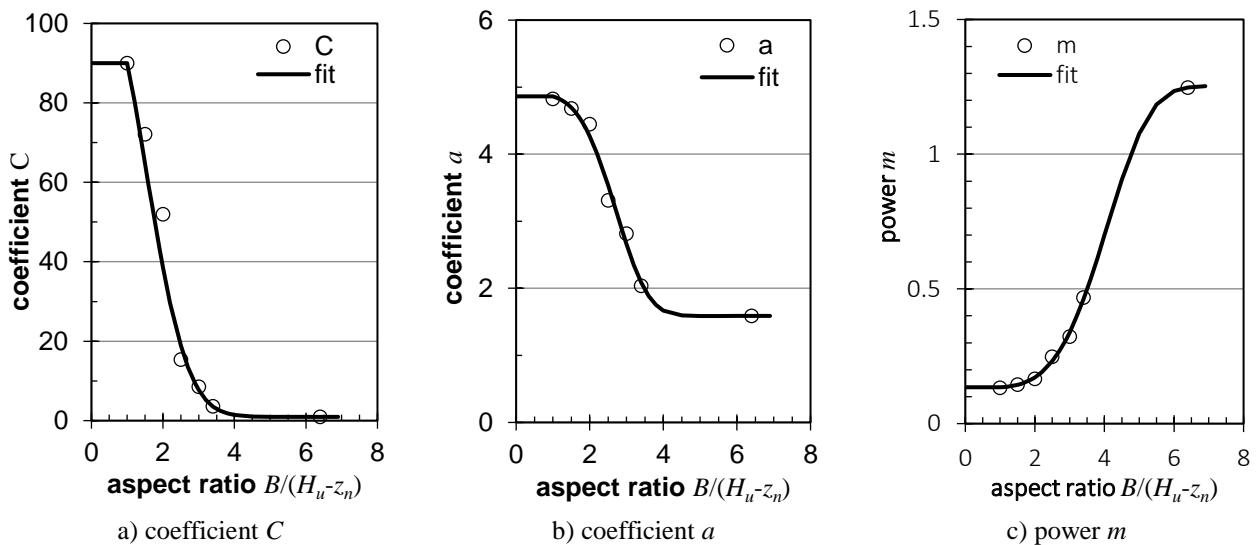a) coefficient C b) coefficient a c) power m

Fig. 2 Coefficients C, a and power m as fitted to Yokoi's trajectory data

The resulting values of the coefficients and the power are shown in *Fig. 2*. The values are fairly dependent on the aspect ratio. The relationships were approximated by the following functions

$$C = 110\exp(-0.209n^{2.36}) + 0.945 \qquad (1 \le n \le 6.4) \tag{11}$$

$$a = 3.31\exp(-0.0121n^{4.13}) + 1.59 \qquad (1 \le n \le 6.4) \tag{12}$$

$$m = -1.12\exp(-0.00175n^{4.32}) + 1.25 \qquad (1 \le n \le 6.4) \qquad (13)$$

The equations were developed to fit to the data for $1 \le n \le 6.4$. However it is possible to apply the values for $n=1$ to smaller aspect ratios because the changes of the trajectory are small for the aspect ratios smaller than 1. Even if the aspect ratio tends to zero, the trajectory should converge to the one for open space as shown by dotted line in Fig. *1b)*. In case of large aspect ratios, $n>6.4$, the equations are out of range. However it is possible to apply the equations because the ejected plume only adheres to the wall surface above the opening.

2.3 Consideration on pressurized fire room

If the fire compartment has more than one opening, or if the compartment is pressurized by mechanical system, the neutral plane does not necessarily locates between upper and lower edge of an opening. If $z_n < H_l$, the compartment is pressurized and the fire gas is pushed strongly out from the opening. In that case, the equivalent height of ejection could be used to account for the effect of pressure rise.

As shown in *Fig. 3a)*, the neutral plane is located below an opening. The mass flow rate of fire gas ejected from the opening is

$$m_{ex} = \frac{2}{3}\alpha B\sqrt{2\rho_s(\rho_0 - \rho_s)g}\{(H_u - z_n)^{3/2} - (H_l - z_n)^{3/2}\} \qquad (14)$$

where m_{ex} is the mass flow rate of gas ejected from the opening [kg/s],

α is the flow coefficient of the opening [-],

B is the width of opening [m],

ρ_s is the density of room gas [kg/m^3],

ρ_0 is the density of outside air [kg/m^3],

g is the gravitational acceleration [m/s^2],

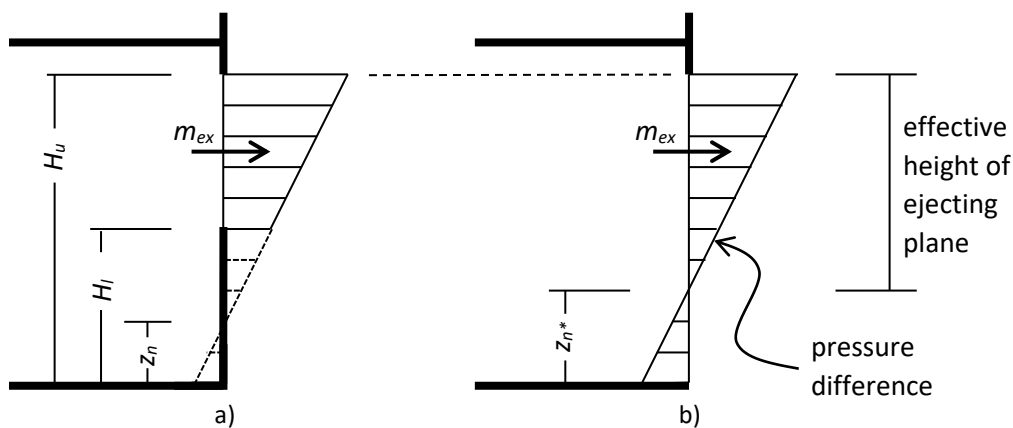H_l is the lower height of the opening [m].

Fig. 3. a) Ejected mass flow from overall height, b) equivalent mass flow from an opening with a neutral plane inside

As shown in *Fig. 3b)*, assume an opening large enough to include the neutral plane inside, $H_l < z_n^* < H_u$, the mass flow rate of fire gas ejected from a window is

$$m_{ex} = \frac{2}{3}\alpha B\sqrt{2\rho_s(\rho_0 - \rho_s)g}\,(H_u - z_n^*)^{3/2} \tag{15}$$

where z_n^* is the effective height of neutral plane that gives equivalent mass flow rate [m].

By equating *Eq. (14)* and *Eq.(15)*, the effective height of ejecting plane, H_u-z_n^*, would be

$$H_u - z_n^* = \{(H_u - z_n)^{3/2} - (H_l - z_n)^{3/2}\}^{2/3}. \tag{16}$$

By replacing the term *H-z* with H_u-z_n^* in *Eq. (10)*, trajectory can be calculated for any locations of neutral plane.

2.4 Distance along trajectory

Distance along axis of ejected flame is important to calculate the temperature distribution. Using Yokoi's data shown by symbols in *Fig. 1b)*, the distances along axes were calculated numerically. The non-dimensional additional distance was defined by $(z'-z)/(H_u/z_n)$ where z' is the distance along flame axis [m].

The calculated results are shown in *Fig. 4*. Non-dimensional additional distances increase sharply right after ejection. Then the distances converge to constant value as the trajectories rises up in parallel to wall surface. When the aspect ratio is small, the additional distance is large. As the aspect ratio is increased, additional distances are reduced.
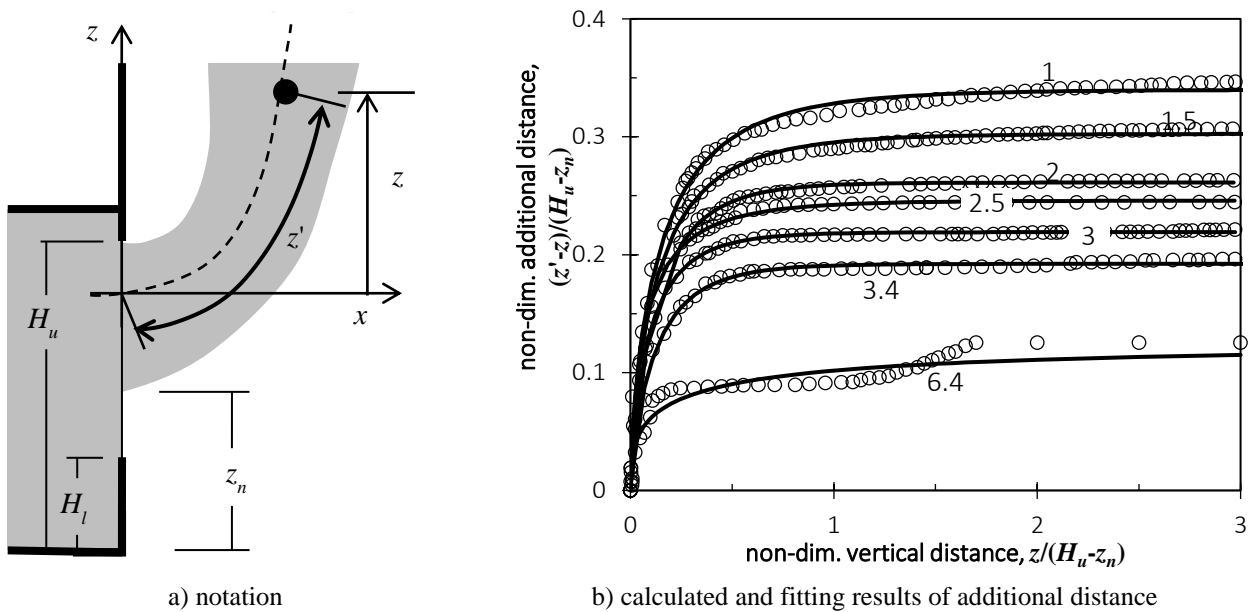

a) notation   b) calculated and fitting results of additional distance

Fig. 4. Distance along axes of elected flame

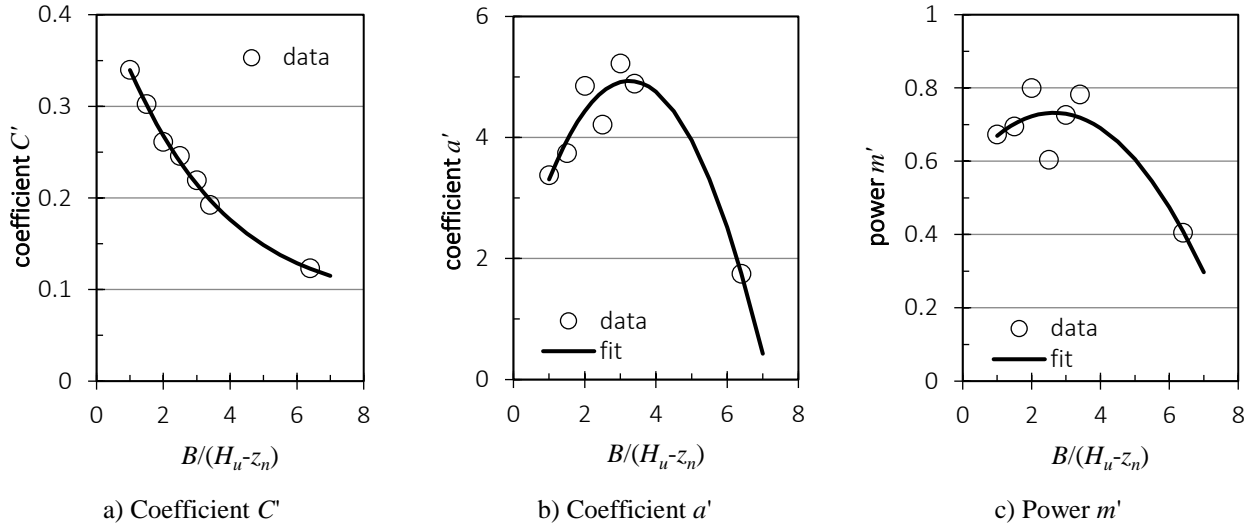a) Coefficient C' b) Coefficient a' c) Power m'

Fig. 5. Estimated parameters for additional distance

The calculated values of additional distances were fitted with the following equation

$$\frac{z'-z}{H_u - z_n} = C'[1 - \exp\{-a'(\frac{z}{H_u - z_n})^{m'}\}]$$ (17)

where the coefficients C', a' and the power m' were estimated by fitting *Eq.(17)* to calculated data. As shown in *Fig. 5*, the results were correlated with aspect ratio as

$$C' = 0.345\exp(-0.297n^{1.07}) + 0.0833,$$ (18)

$$a' = -0.321n^2 + 2.09n + 1.54,$$ (19)

$$m' = -0.0230n^2 + 0.122n + 0.571.$$ (20)

3   COMPARISON WITH OTHER EXPERIMENTS

In order to validate the developed formulae, comparisons were made with other experiments conducted independently.

3.1 Model scale experiments with an opening of various aspect ratios

Ohmiya *et al.*[8] conducted a series of model scale experiments for various aspect ratios of ejecting plane. The sizes of model-scale compartments were 0.5m cube or 1.5m cube. Among the experiments, trajectory data for aspect ratios 1 and 4 are available. Asimakopoulou *et al.* [9] conducted a series of experiments using a model box sized 0.6 x 0.6 x 0.9 m. Trajectory data are available in case of aspect ratios 0.8 and 1.0. These trajectory data are compared with the proposed equations, *Eq. (10)* to *Eq. (13)*.

The calculated trajectories are in fair agreement with those in literatures. As a general tendency, trajectory tends to adhere to wall as the aspect ratio is increased. The tendency was well reproduced. In case of aspect ratio 0.8, the condition is out of the range of original Yokoi's data. Even though the trajectory is slightly away from wall surface, the shape of trajectory was reproduced well.
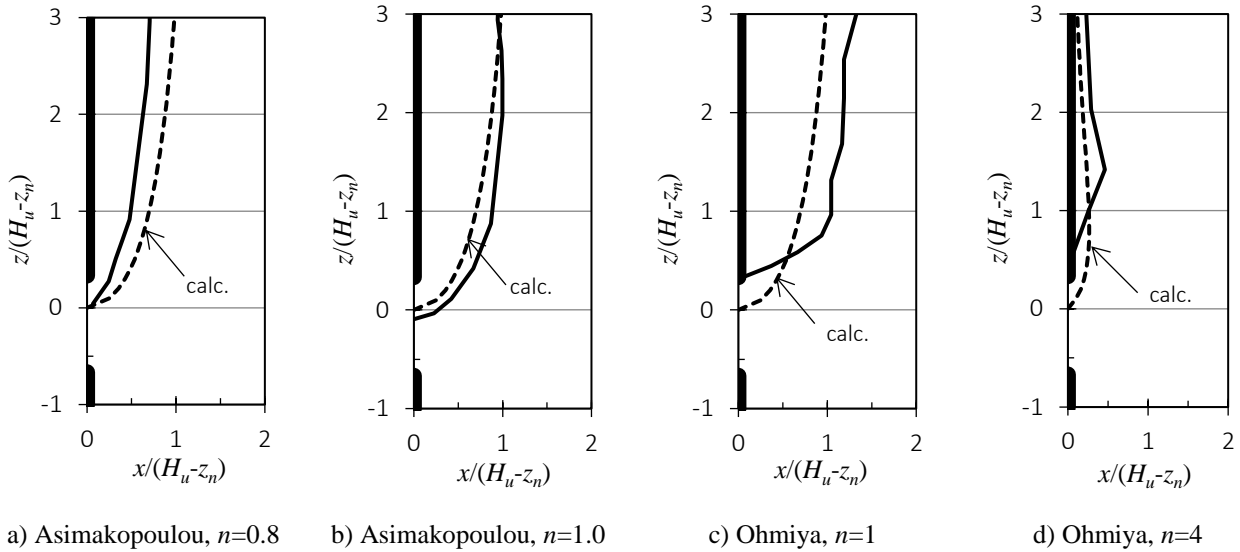
a) Asimakopoulou, $n=0.8$ b) Asimakopoulou, $n=1.0$ c) Ohmiya, $n=1$ d) Ohmiya, $n=4$

Fig. 6. Comparison of calculated trajectories with experiments by Ohmiya *et al.* [8] and by Asimakopoulou *et al.* [9]. (Solid lines: literature data, dashed lines: calculations)

3.2 Ejected flame from a pressurized compartment

Himoto *et al.*[10] carried out a series of experiments using 0.9m cubic model-scale box. In some of the experiments, the room was pressurized with supplied air. As a result, the neutral plane was located at lower positions. By considering the location of neutral plane, the agreement is satisfactory.
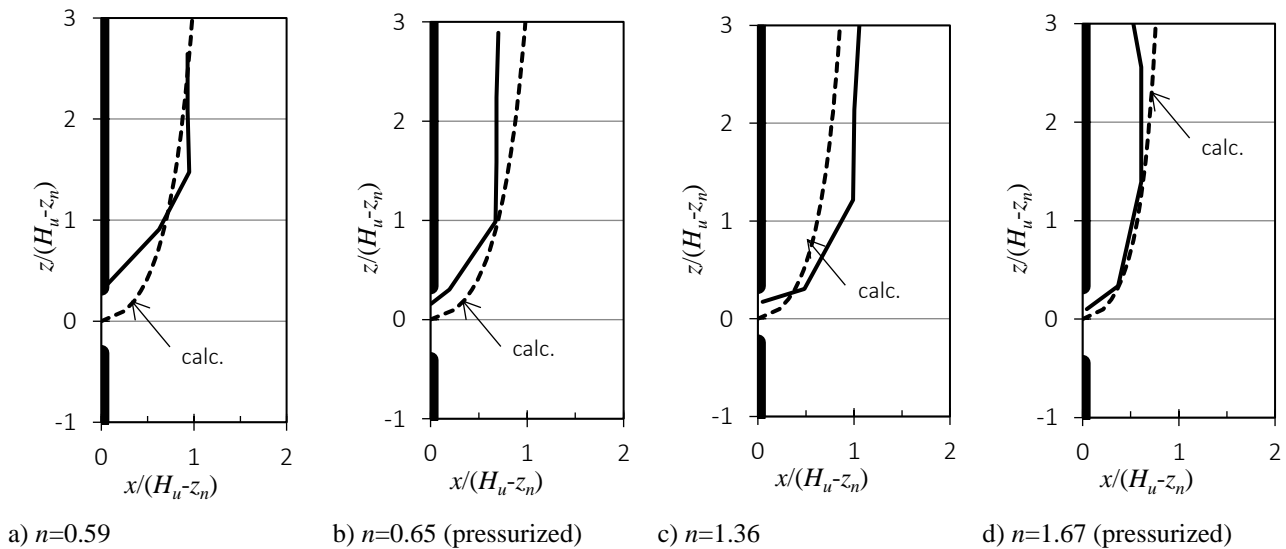

a) $n=0.59$ b) $n=0.65$ (pressurized)   c) $n=1.36$ d) $n=1.67$ (pressurized)

Fig. 7. Comparison of calculated trajectories with experiments by Himoto *et al.*[10]. (Solid lines: literature data, dashed lines: calculations)

3.3 Ejected flame from an upper opening

Li *et al.*[11] investigated the behaviour of elected flame out from upper opening of a model box. The box was equipped with two openings at different heights. One opening was located at the bottom of one wall. Another opening was located at the top of opposite wall. As a

result, the neutral plane was located below the lower edge of an opening ejecting a flame. To account for the location of neutral plane, *Eq. (16)* was applied to calculate the effective height of ejecting plane. As shown in *Fig. 8*, the agreement is satisfactory.
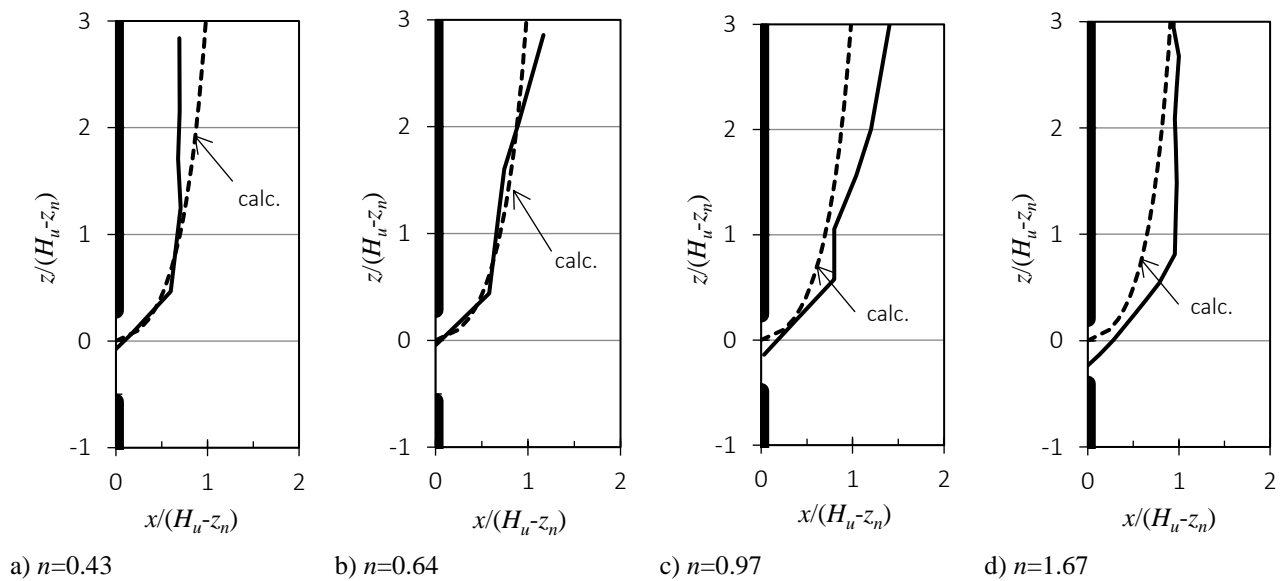

a) n=0.43   b) n=0.64   c) n=0.97   d) n=1.67

Fig. 8. Comparison of calculated trajectory with experiments by Li *et al.*[10]. (Solid lines: literature data, dashed lines: calculation)

4   CONCLUSIONS

To develop a practical method to calculate the trajectory of ejected flame from an opening, Yokoi's data was analysed and mathematically reformulated. The main developments are as follows:

- The classical Yokoi's trajectory data were fitted with mathematical formulae describing the shape of trajectory. The parameters were estimated by least square method to fit to Yokoi's data.

- The formula was extended so as to include the cases when neutral plane is located below the lower edge of an opening.

- The developed mathematical formulae were verified and validated against other trajectory data published in literatures.

REFERENCES

[1]   Yokoi S. (1960), Study on the prevention of fire-spread caused by hoy upward current, BRI Report No.34, Building Research Institute, Ministry of Construction, Japan

[2]   Architectural Institute of Japan (2013), Recommendations for design fire loads and fire actions in buildings (in Japanese)

[3]   Architectural Institute of Japan (2017), Recommendation for fire resistant design of steel structures (in Japanese)

[4]   Architectural Institute of Japan (2018), Handbook on design calculation methods of fire behaviour (in Japanese)

[5]   Law M (1978) Fire safety of external building elements—the design approach, AISC Eng J., Second Quarter, American Institute of Steel Construction

[6] Mizuno K., Wakamatsu T., Tanaka T. (2006), A three-dimensional heat flow analysis model of steel structural members upon fire exposure – prediction of temperature of exterior steel structural members exposed to fire -, J. Environmental Engineering, No. 607, pp. 7-14, Architectural Institute of Japan (in Japanese)

[7] Himoto K., Tsuchihashi T., Tanaka Y., Tanaka T. (2009) Modelling the trajectory of window flames with regard to flow attachment to the adjacent wall, Fire Safety Journal, 44, pp. 250–258

[8] Ohmiya Y., Yusa S., Matsuyama K., Harada K. (2001), Prediction method of opening jet plume behaviour in the presence of an opening soffit, Proceedings of the 5th Asia-Oceania Symposium on Fire Science and Technology, pp. 171-185, Newcastle, Australia

[9] Asimakopoulou E. K., Kolaitis D. I., Founti M. A., Chotzoglou K. (2016), Characteristics of externally venting flames and their effect on the facade: a detailed experimental study, Fire Technology, vol. 52, pp. 2043–2069

[10] Himoto K., Tsuchihashi T., Tanaka Y., Tanaka T. (2009), Modeling thermal behaviors of window flame ejected from a fire compartment, Fire Safety Journal, 44 pp. 230–240

[11] Li J. J., Lin S. H., Yao B., Ji J., Gao Z. H., Sun J. H. (2017), Experimental Study on Thermal Buoyancy Influence on the Spill Flame Plume in Dual-Openings Compartment Fires, Fire Technology, 53, 947–966

COMPARING SMOKE DENSITY CHAMBER AND FULL-SCALE TEST RESULTS

Jennifer Ellingham[1], Hannah Carton[2], Elizabeth J. Weckman[1]
[1]University of Waterloo, Waterloo, Canada, [2]Carleton University, Ottawa, Canada

ABSTRACT

The University of Waterloo Fire Research Group conducted a series of full-scale fire tests involving couches with different combinations of polyurethane foam and fabric in 2015. Videos were analyzed to rank the amount and relative optical density of smoke produced by each couch during the full-scale fires. Representative foam and fabric samples were then tested to the ISO 5659-2 standard in the smoke density chamber. Optical density estimates from the full-scale and smoke density chamber tests were compared to assess the potential use of small-scale results to estimate smoke production in these full-scale, ventilation-limited fire scenarios. Results suggest that the values of specific optical density from the smoke density chamber may not be appropriate for direct use in assessing smoke production in the larger-scale fires since smoke density chamber results were not a good indicator of pattern, rank, or value of smoke produced in the 2015 fire scenarios.

1   INTRODUCTION

A series of nine well-instrumented, full-scale test burns involving couches made from three different polyurethane foams and fabrics with varying levels of fire retardant [1] were conducted at the University of Waterloo Live Fire Research Facility. Each type of couch was tested three times in a ventilation-limited environment intended to mimic energy-efficient homes [1]. The repeatability of the tests has previously been reported [2]. Video recordings were analyzed to rank the amount and optical density of smoke produced during the fires. Subsequently, the smoke density chamber was used to test the three different couch foams and foam/fabric combinations to rank the optical density at small-scale for comparison to the apparent behaviour in the full-scale test burns. Together, the foam and fabric made up the majority of the material that burned during the tests with only a small portion of the frame and other materials involved in the fire. Similarly, the foam (without fabric) comprised more than 50% of the fuel loading for the portion of the full-scale tests considered in the smoke production from the fire. Therefore, in this paper the smoke density chamber results for the foam alone and the foam/fabric combinations are used to rank the optical density at small-scale for comparison to the observed smoke evolution in the full-scale test burns.

The smoke density chamber is a small-scale test used to measure specific optical density of smoke from a sample of material. A 75 mm by 75 mm sample of the material is subjected to a constant surface radiant heat flux of up to 50 kW/m^2 [3]. The test can be completed with or without a piloted ignition. The quantity of smoke produced is measured via attenuation of a light beam within the sealed test chamber. The smoke density chamber can be used to test samples in accordance with several standards including ISO 5659-2, ASTM E662, NFPA 258, and BS 6401 [4]. With the addition of Fourier transform infrared spectroscopy (FTIR) data, results are sometimes used via the ISO 19703 standard to characterize fire effluents for risk and hazard assessments [5]. This paper focuses on use of the ISO 5659-2 standard, which first came into effect in 1994 [3], for testing smoke production from a series of different combinations of polyurethane foam and fabric used in the furnishings which were burned in full-scale fire tests. The ISO standard was chosen over the other standards listed above

because the sample is oriented horizontally (rather than vertically) and can be exposed to a heat flux up to 50 kW/m^2 (rather than only 25 kW/m^2) [3,6]. The change in sample orientation allowed the specimen mass to be measured throughout the test via a load cell mounted beneath the burning sample [3,6].

The repeatability (within lab) and reproducibility (between labs) of results with the smoke density chamber depend on the material being tested and the orientation of the sample [3,6,7]. Uncertainty increases when the material changes shape or the surface of the material changes its position relative to the heater during the test (for example with a melting sample) [7] or if the material does not readily ignite at 25 kW/m^2 [3]. The polyurethane foams and some of the fabrics used in the present testing melted when exposed to heat so they could not be tested in the vertical orientation used in ASTM, NFPA, and BS standard test methods [6,7]. In addition, they did not readily ignite at 25 kW/m^2 even in well-ventilated conditions. Due to the factors above, however, it is expected that the uncertainty in the smoke density results will be well above stated repeatability and reliability values (±25%) for the smoke density chamber [3,7,8]. In contrast, the ISO standard indicates values of repeatability and reproducibility for flexible polyurethane foam of ±36% and ±70% respectively [3] so the intent here is only to rank the materials for their relative smoke density. Even when used for this purpose, previous round robin studies have shown that if smoke density values of different materials are within 12% of each other, there can be disagreement on their relative ranking from lab to lab in terms of their propensity to produce smoke [7]. Some research appears to advocate the use of maximum optical density measured to estimate visibility in fire situations [9], while other findings appear to contradict this [3,6-8]. This paper compares optical density estimates obtained from video recordings in full-scale furnishing fire experiments and smoke density chamber tests of the same furnishing materials to assess the potential use of small-scale results to estimate smoke production in these full-scale, ventilation-limited fire situations.

2   EXPERIMENTAL APPARATUS AND PROCEDURE

2.1 Smoke Density Chamber

A smoke density chamber with an enhanced photomultiplier control unit was used for the small-scale tests [10]. The data was recorded using the SmokeBox software package version 3.7 [11]. The ISO 5659 conical radiant furnace modification was used to comply with the ISO 5659-2 standard for testing [3,4]. Calibration and testing procedures used were based on the ISO 5659-2 standard and the user's manuals for the smoke density chamber and SmokeBox software package [3,10,11].

All samples were conditioned to constant mass before testing, cut to size within the requirements of the standard and wrapped in aluminium foil [3]. All foam and fabric samples were cut from scraps of the material originally used to build the couches in 2015. Foam samples were cut to 25 mm in depth, so the ratio of foam to fabric in the test specimens are not the same as those in the actual couch. The assembly, with fabric on top of the foam, was consistent to that in each couch. First, three samples of each foam type were tested in mode three (50 kW/m^2, no pilot ignition source) [3]. Three samples of each foam and fabric combination were then tested in mode three as well. Mode three was selected because experience within the University of Waterloo Fire Research Group has indicated that the foams did not ignite at 25 kW/m^2 even in well-ventilated conditions. Piloted ignition was not used to more closely match the radiant ignition that occurred in the full-scale furnishing fire tests. After each test, the chamber was wiped down thoroughly with a damp cloth; it was wiped with a cleaning agent between tests of different materials. The optical windows were

cleaned using a micro-fibre cloth and isopropyl alcohol until no residue remained between every test as well.

Results obtained in the smoke density chamber test include, among others, the maximum specific optical density, corrected maximum specific optical density, time to maximum specific optical density, and the time to reach 90% of the maximum specific optical density. The optical density of smoke is a measure of the degree of opacity of smoke, taken as the negative common logarithm of the relative transmission of light [3]. The maximum specific optical density is the highest value recorded during the test and was selected here as an indicator of the overall smoke production capability of the sample. A higher rank was assigned for a higher specific optical density because it indicated that the smoke from a sample was more dense. The clear beam specific optical density was not used in this analysis because this correction accounts for smoke residue that is deposited on the optical windows during the test and there was no equivalent measure for residue deposited on the video lens in the full-scale tests. To compare the speed of smoke production, the time to 90% of maximum specific optical density was selected for this analysis instead of using the time to maximum specific optical density. By using this parameter, a shorter time indicated faster smoke production and thus that material was assigned a higher rank in terms of how quickly it might have generated smoke in the real fire situation.

2.2 Full-Scale Burn House

The University of Waterloo steel 'burn house' is a two-story, fire hardened structure with 120 m^2 of floor space. The 2015 tests in the structure had a standard layout with a couch, chair, coffee table, and side table situated in the "living room". Three different foam and fabric combinations were used to produce the three different sets of couches and chairs on a common frame design [1]. Details of the tests have previously been reported [2]. In this paper, the foam and fabric combinations will be referred to as Type A, B, and C for simplicity.

Before each test, the house was sealed to mimic an energy-efficient home with low ventilation to the exterior. After ignition of the couch using a BS 5852 crib [1], the fire progressed unimpeded and a ventilation-limited environment developed. This low ventilation environment should be similar to that developed in the sealed smoke density chamber although it is clear that they are not direct analogues of one another.

In the full-scale tests, smoke and fire growth were monitored using thermocouples, weigh scales, gas sensors, a heat flux meter, smoke detectors, and video cameras located throughout the house. There was no specific instrumentation to directly measure the optical density during the tests. Instead, in this study video recordings from the camera facing the couch, with a view of the East window on the first floor as shown in *Fig.1*, were analyzed to estimate the amount and density of smoke in the burn house.

Once the smoke layer descended below the top of the window, the density of the smoke in front of the window could be observed. Therefore, an image from when the smoke layer was part way down the window was selected for analysis. An image in which the smoke layer had increased to the bottom of the window could have been used, but in some cases by this time the fire was in front of the window or the camera had changed to infrared due to low lighting conditions. This is a very rudimentary method for determining visual density of the smoke (an estimate of opacity), given the potential impacts of fire proximity, overall light levels and exterior back lighting. As it is also subjective, three different individuals completed independent analyses to assign a rank to the smoke density from 1 (most dense) to 9 (least dense) for each test based on the same set of nine images.

Fig. 13. Sample Video Image

The rate of smoke production for a fire from each couch type was estimated based on how long it took, after ignition of the crib, for the smoke layer to descend to the top of the window as judged from the video recordings. Three different individuals again completed independent analyses of this indicator and reported the corresponding test times. Shorter times indicate faster smoke production and are assigned a higher rank.

3 RESULTS

3.1 Smoke Density Chamber

The average and standard deviation of the three repeat smoke density chamber tests and subsequent ranking for each material combination are reported in *Table 1* [3]. Both the mean and standard deviation are provided here so differences between each rank can be better understood.

Table 12. Smoke Density Chamber Results

Type	Foam	Fabric	Max. Specific Optical Density			Time to 90% of Max. Specific Optical Density (s)		
			Mean	Std.Dev.	Rank	Mean	Std.Dev.	Rank
Foam Only								
A	1	N/A	114.0	0.3	2	58.7	2.9	2
B	2	N/A	110.5	8.2	3	69.0	8.5	3
C	3	N/A	116.3	0.1	1	53.0	4.4	1
Foam and Fabric								
A	1	1	119.9	0.9	1	108.0	9.5	3

B	2	3	94.3	24.9	3	60.7	5.7	2
C	3	2	119.3	0.5	2	46.3	6.1	1

3.2 Full-Scale Burn House

The estimated mean, standard deviation and consequent ranking for the visual density of the smoke and rate of smoke production observed during the three full-scale tests of each couch type and each operator (i.e. N=9) are shown in *Table 2*.

Table 13. **Burn House Results**

Type	Ranked Visual Density			Time to Top of Window (s)		
	Mean	Std.Dev.	Rank	Mean	Std.Dev.	Rank
A	6.1	1.1	2	283	26	2
B	6.6	2.1	3	582	31	3
C	2.0	0.9	1	253	44	1

4   DISCUSSION

The smoke density chamber test results shown in *Table 1* indicate that type A and type C materials had low standard deviations in values of optical density compared to type B materials. During the small-scale tests, unlike the other materials, individual samples of type B materials ignited at significantly different times after the start of the test (having both the longest and shortest times to ignition). This led to large differences in the amount and density of the smoke produced. However, on average, type B materials had the least dense smoke. These observations were reflected in the visual density results from the full-scale tests as well; mean values reported in *Table 2* for this material are comprised of a wider range of values than either of the other materials as reflected by the higher standard deviation. In contrast, type C materials very clearly have the most dense smoke in the full-scale tests; however, results of optical density obtained in smoke density chamber tests do not clearly indicate whether type A or type C materials have more dense smoke. This is not unexpected because the differences in measured data for type A and type C materials are well below the previously established limit of 12% that would be required to ascertain a clear ranking [7].

From smoke density chamber data, type C materials appear to have slightly faster smoke development than the other materials (10% and 24% faster for the foam only and foam/fabric tests respectively). This general pattern is reflected in the full-scale test results where the type C materials showed approximately 10% faster smoke development. The smoke development estimates for type A and type B materials in the smoke density chamber based on foam only and foam/fabric results suggest contradictory rankings for rate of smoke production between the two. In contrast, type B materials very clearly have the slowest smoke development in the full-scale tests. Type B fires took almost twice the amount of time as type A or type C to produce enough smoke to reach the top of the window.

Generally speaking, the small-scale smoke density chamber results were inconsistent in capturing the patterns of behaviour and magnitude of smoke evolution observed at full-scale in the burn house. Even within results from the smoke density chamber, foam and fabric combination data (which arguably better represents the full-scale furniture) did not agree with data from foam only tests with respect to value or ranking from highest to lowest smoke

production. Thus, for this series of tests and these materials, the smoke density chamber results were not a good indicator of smoke production at full-scale in terms of overall behaviour, ranking, and especially magnitude of smoke produced. Further tests are required to see if similar inconsistencies would be found for other materials at small and full-scale. Nonetheless, based on this small series of tests, it is evident that caution should be exercised in applying optical density values from the smoke density chamber to life safety and risk assessments.

5   CONCLUSIONS

Based on this test series the following conclusions can be drawn:

−   *The smoke density chamber results and rankings based on foam samples differed from those when both foam and fabric were tested.*

−   *The smoke density chamber results inconsistently matched estimated patterns and magnitudes of smoke evolution that were observed at full-scale.*

−   *The smoke density chamber results were not a good indicator of patterns, ranking, or values for smoke production at full-scale. Caution should be exercised in interpreting and using these values.*

−   *Further tests are required to determine whether similar trends amongst results hold true for other materials in other scenarios.*

ACKNOWLEDGEMENTS

REFERENCES

[1]   Forrest, B., Weckman, E. J., Ellingham, J., White, C. (2018). *A Comparison of Methods for the Calculation of Heat Release Rate*. Combustion Institute – Canadian Section: Spring Technical Meeting (CI/CS 2018), Toronto, Canada, 14-17 May 2018.

[2]   Senez, P., Mulherin, P., Weckman, E. (2017) *Repeatability of Underventilated Compartment Fire Testing with Complex Fuel Packages.* Fire and Materials 2017, San Francisco, United States, pp. 342-355.

[3]   ISO 5659-2 (2006). *Plastics - Smoke Generation - Part 2: Determination of Optical Density by a Single-Chamber Test*, International Organization for Standardization, Geneva, Switzerland.

[4]   Fire Testing Technology. *NBS Smoke Density Chamber*. Available: http://www.fire-testing.com/sdc. [Accessed 1 May 2018].

[5]   ISO 19703 (2018). *Generation and Analysis of Toxic Gases in Fire - Calculation of Species Yields, Equivalence Ratios and Combustion Efficiency in Experimental Fires*, International Organization for Standardization, Geneva, Switzerland.

[6]   Flisi, U. (1990). *Testing the Smoke and Fire Hazard*. Polymer Degradation and Stability 30, 153-168 pp.

[7]   Lee, T. G. (1971). *NBS Technical Note 708: Interlaboratory Evaluation of Smoke Density Chamber*, National Bureau of Standards, Washington, United States.

[8]   Drysdale, D. (2011). *An Introduction to Fire Dynamics, Third Edition*, Chichester, United Kingdom, John Wiley & Sons Ltd.

[9]   Lee, T. G. (1973). *NBS Technical Note 757: The Smoke Density Chamber Method for Evaluating the Potential Smoke Generation of Building Materials*, National Bureau of Standards, Washington, United States.

[10] Fire Testing Technology. (2008) *Users' Guide for the Smoke Density Chamber: For Instruments with the FTT Enhanced PM Unit*, East Grinstead, United Kingdom.

[11] Fire Testing Technology. (2008). *Users' Guide for the SmokeBox Software Package Version 3.7: For Use With The FTT Smoke Density Chamber*, East Grinstead, United Kingdom.

CORRECTION FACTORS AND APPLICABILITY OF VENTILATION RATES FOR USE OF FLAMMABLE AND COMBUSTIBLE LIQUIDS

Xia Zhang
WSP in Canada, Ottawa, Canada

ABSTRACT

For the use of flammable and combustible liquids, the National Fire Code of Canada (NFCC) requires that ventilation shall be sufficient to ensure that flammable vapour concentrations outside the zone identified as Class I, Zone 0 or 1 do not exceed 25% of the lower explosive limit of the flammable vapour. At the same time, it states that a mechanical ventilation system is deemed to comply with the requirement if it is capable of exhausting at least 18 $m^3/h/m^2$ of room area, but not less than 250 m^3/h, and notes that the ventilation rate is normally adequate for rooms with low floor to ceiling height or small enclosed spaces. However, it does not provide a prescriptive minimum ventilation rate for rooms with high floor to ceiling height or large enclosed spaces, and the applicability of the ventilation rate. The paper proposes correction factors for ventilation rates for these cases and discusses the applicability of the ventilation rates.

1   INTRODUCTION

The use of flammable and combustible liquids often produces flammable vapors. When flammable vapors mix with air and form mixtures with the concentration in the range of flammable limits, the mixtures can produce flash fires or explosion. To prevent flash fires or explosions, preventive measures are required. One of the measures is ventilation, through which flammable mixtures are limited to smaller areas.

The National Fire Code of Canada (NFCC) requirement for ventilation rates for the use of flammable and combustible liquids is performance-based, i.e., ventilation … shall be sufficient to ensure that flammable vapour concentrations outside the zone identified as Class I, Zone 0 or 1, do not exceed 25% of the lower explosive limit of the flammable vapour [1]. Similar performance requirement can be found elsewhere, such as NFPA (National Fire Protection Association) 30 and 69 [2, 3].

The NFCC also states that a mechanical ventilation system is deemed to comply with the requirement if it is capable of exhausting at least 18 $m^3/h/m^2$ of room area, but not less than 250 m^3/h [1]. Similar prescriptive requirements can be found elsewhere, such as NFPA 33 [4]. However, the NFCC does not provide application conditions of the ventilation rate, while the note to the NFCC provision states that "a mechanical ventilation rate of at least 18 m^3/h per square metre of floor area, but not less than 250 m^3/h, is normally adequate for rooms with low floor to ceiling height or small enclosed spaces where Class I liquids are dispensed" [1], and indicates that the ventilation rate applies to rooms with low floor to ceiling height or small enclosed spaces.

Other assumptions frequently found in codes and standards include the lower limit of the explosive range of vapors of flammable and combustible liquids of 1% in air [4] and perfect mixing [3, 4]. Flammability limits and explosive limits are used interchangeably in different references and the paper will use the explosive limits for uniformity.

NFCC does not provide a prescriptive minimum ventilation rate for rooms with high floor to ceiling height or large enclosed spaces, and the applicability of the ventilation rate. The paper will propose correction factors for ventilation rates for these cases and discusses the applicability of the ventilation rates.

2 CORRECTION FACTORS FOR VENTILATION RATES FOR LONG DURATION OF VAPOUR AND GAS RELEASE

For cases with long duration of vapour and gas release, rearranging Equation D.15 of NFPA 69 [3],

$$C = \frac{G}{Q}\left(1 - e^{-KN}\right) \tag{1}$$

where   C is the concentration

G is the release rate [m^3/min]

Q is the airflow rate [m^3/min]

K is the mixing efficiency factor

N is the required number of air changes

with the assumption that the effective air changes, i.e., the product of the mixing efficiency factor and the required number of air changes, is sufficiently large, produces

$$Q = \frac{G}{C} \tag{2}$$

Based on the equation, the minimum ventilation rate of 18 m^3/h/m^2 required for small spaces in the NFCC [1] produces a steady-state concentration of 0.25%, 25% of LEL (Lower Explosive Limit) of 1%, for a release rate of 0.045 m^3/h/m^2 or 0.015 m^3/h/m^3 space within a height of 3 m. The ventilation rate is for small spaces as provided in NFCC and for liquids with an LEL not less than 1%.

For the cases with significant differences from the basic application conditions or assumptions, to keep the effective ventilation rate or effective air changes for each small space the same as those for the basic application conditions or assumptions, the minimum ventilation rate need be increased with the following coefficients

- The coefficient for the mixing efficiency: this coefficient is unnecessary for small rooms as mixing closes to perfect. However, for rooms with high height or large area, mixing is far from perfect and this coefficient becomes necessary. It is recommended that the coefficient be taken as the reciprocal of the mixing efficiency based on specific ventilation design, and given in NFPA 69 or by other good engineering practice.
- The coefficient for the high room height: this coefficient is unnecessary for low room heights because the ventilation rate is provided for the case. For high room heights, additional ventilation is necessary for space above 3 m height in a similar way to that for the space within 3 m height. It is recommended that the coefficient for the high room height be taken as the ratio of the height in meter to 3, the assumed low room height in meter.
- The coefficient for the lower LEL: this coefficient is unnecessary for liquids with an LEL not less than 1%. For those with LEL less than 1%, the ventilation rate need be increased

to sufficiently ventilate the space so that the concentration of the mixture is below 25% of the LEL, instead of 25% of LEL of 1% typically assumed.

The overall coefficients are a product of the above coefficients because each coefficient addresses a separate factor that affects the concentration of vapour in air. The ventilation rate equation with these coefficients can be written in the form

$$Q = \frac{G_0'' A}{0.25\%} \left(\frac{K_0}{K} \frac{H}{H_0} \frac{0.25\%}{C} \right)$$
(3)

where   G" is the release rate per area [$m^3/min/m^2$]

A is the area [m^2]

K is the mixing efficiency

H is the height [m]

C is the 25% of LEL

0 is the base scenario

For the cases with $K_0 = 1$, $G_0'' = 0.045$ $m^3/h/m^2$ (or 0.015 $m^3/h/m^3$ space and $H_0 = 3$ m), Equation (3) reduces to

$$Q = 18A \left(\frac{1}{K} \frac{H}{3} \frac{0.25\%}{C} \right)$$
(4)

The factor 18 in Equation (4) is the 18 $m^3/h/m^2$ provided in the NFCC as the minimum ventilation rate. If it is used as the base ventilation rate to calculate a required ventilation rate, coefficient for mixing efficiency (1/K), coefficient for ceiling height (H/3), and coefficient for LEL (0.25%/C) need be incorporated.

3 CORRECTION FACTORS FOR VENTILATION RATES FOR SHORT DURATION OF VAPOUR AND GAS RELEASE

For cases with short duration of vapour and gas release, Equation D.11 of NFPA 69 [3] gives

$$\frac{C}{C_0} = e^{-KN}$$
(5)

$$N = \frac{Qt}{V}$$
(6)

where   C is the concentration

C_0 is the initial concentration

K is the mixing efficiency factor

N is the required number of air changes

t is the time duration [h]

V is the volume [m^3]

The ventilation rate of 18 $m^3/h/m^2$ provided in the NFCC produces 6 air changes per hour for a space with a height of 3 m and reduces the initial concentration from 100% to 0.248% within 1 h. The concentration of 0.248%, less than 25% of 1%, complies with the requirement of NFCC for liquids with an LEL of 1%.

For liquids with a lower LEL, the effective air changes per hour required to reduce the concentration from 100% (C_0) to 25% of the lower LEL within 1 h can be calculated by rearranging Equation (5) into

$$KN = -\ln \frac{C}{C_0} \tag{7}$$

and the ventilation rate can be calculated by rearranging Equation (6)

$$Q = \frac{NV}{t} \tag{8}$$

For cases with large spaces or high floor to ceiling heights, to keep the effective ventilation rate or effective air changes for each small space the same as those for the basic application conditions or assumptions, coefficients for mixing efficiency and for high floor to ceiling height also need be applied in similar way to those for the ventilation rates for the long duration of vapor and gas release.

The overall coefficients are a product of the above coefficients because each coefficient addresses a separate factor that affects the concentration of vapour in air. The ventilation rate equation with these coefficients can be written in the form

$$Q = \frac{NHA}{t} = \frac{N_0 H_0 A}{t} \left(\frac{1}{K} \frac{H}{H_0} \frac{KN}{N_0} \right) \tag{8}$$

Based on the implicit conditions indicated by the NFCC [1], $N_0 = 6$ with a mixing coefficient of 1, and $H_0 = 3$ m. Therefore, Equation (8) reduces to

$$Q = \frac{18A}{t} \frac{1}{K} \frac{H}{3} \frac{1}{6} \ln \frac{C_0}{C} \tag{9}$$

The factor $18/t$ in Equation (9) is the 18 $m^3/h/m^2$ provided in the NFCC as the minimum ventilation rate. If it is used as the base ventilation rate to calculate a required ventilation rate, the coefficient for the mixing efficiency ($1/K$), the coefficient for the ceiling height ($H/3$), and the coefficient for the lower LEL ($1/6 \ln(C_0/C)$) need be incorporated.

4   APPLICABILITY OF VENTILATION RATES

NFCC does not provide clear limitations for which certain ventilation rates can be applied. Instead, the limitations need be derived from good engineering practice. For applications with long duration of vapour and gas release, the limitations can be derived from the following provisions:

−   The area within 915 mm (3 ft) in all directions from any open containers, supply containers, waste containers, spray gun cleaners, and solvent distillation units or such equipment and extending to the floor or grade level shall be classified as Class I, Division 1 or Class I, Zone 1 [4].

- Ventilation shall be sufficient to ensure that flammable vapour concentrations outside the zone identified as Class I, Zone 0 or 1, do not exceed 25% of the lower explosive limit of the flammable vapour [1]
- For processes similar to spray, ventilation is required at a rate of 75 m^3/L liquid evaporation for solvent with a lower flammability limit of 1% [4].
- For processes similar to open liquid surface, ventilation is required at 0.50 to 0.75 m^3/sec/m^2 (30 – 45 m^3/min/m^2, 100 to 150 cfm/ft^2) liquid surface for liquid with an LEL of 1% [5].

To comply with these provisions, ventilation need be provided for 915 mm of the vapour and gas source to ventilate vapour and gas releases to 25% of the LEL of the flammable vapour. Over a floor area with a 3 ft radius, for the effective air changes of 6.0/h (18 m^3/h/m^2 space with a height of 3 m) or 0.1/min and liquids with LEL of 1.0%,

- The volume of a semi-sphere with a radius of 915 mm is 1.52 m^3.
- Effective ventilation in a volume of 1.52 m^3 is 1.52 x 0.1 = 0.15 m^3/min, which complies with the requirement for
    o Liquid evaporation of 0.15 m^3/min / 75 m^3/L = 0.002 L/min.
    o Liquid surface of 0.15 m^3/min / 45 m^3/min/m^2 = 0.0033 m^2.

Clearly, the specific values produced above for the applicability of ventilation rates are based on the electrical area classification. As a result, these values could change when the electrical area classification changes. However, the methodology used to produce the specific values remains valid for the general use of flammable and combustible liquids.

5   DISCUSSION

The proposed correction factors for ventilation rates for the use of flammable and combustible liquids are to address the performance requirement that flammable vapour concentrations do not exceed 25% of the lower explosive limit of the flammable vapour. While the actual ventilation rates will be higher than 18m^3/h/m^2, the increased ventilation rates are considered to comply with only the minimum code requirements because the increase is to address the conditions that are significantly different from those for which the minimum requirements in codes and standards are developed, specifically, high floor to ceiling heights, large enclosed spaces, and lower LELs. No safety margin above the minimum code requirements is included in these coefficients.

The proposed correction factors for large enclosed spaces and high floor to ceiling heights are the same for long and short durations of vapor and gas releases, and those for lower LEL are different for long and short durations of vapor and gas releases.

6   CONCLUSIONS

- Correction factors for ventilation rates for the use of flammable and combustible liquids are proposed to consider the effects of large enclosed spaces, high floor to ceiling heights, and lower LELs.
- The proposed correction factors for large enclosed spaces and high floor to ceiling heights are the same for long and short durations of vapor and gas releases, and those for lower LEL is different for long and short durations of vapor and gas releases.
- Applicability of ventilation rates for the use of flammable and combustible liquids is given in the form of liquid evaporation and liquid surface. The results depend on the electrical

area classification but the methodology used to produce the results remains valid for the general use of flammable and combustible liquids.

ACKNOWLEDGMENT

REFERENCES

[1] National Research Council of Canada, Canadian Commission on Building and Fire Codes. (2015). National Fire Code of Canada 2015. National Research Council of Canada.

[2] National Fire Protection Association. (2018). NFPA 30-18 Flammable and Combustible Liquids Code, 2018 Edition.

[3] National Fire Protection Association. (2014). NFPA 69-14 Explosion Prevention Systems, 2014 Edition.

[4] National Fire Protection Association. (2018). NFPA 33-18 Standard for Spray Application Using Flammable or Combustible Materials, 2018 Edition.

[5] National Fire Protection Association. (2018). NFPA 34-18 Dipping and Coating Processes Using Flammable or Combustible Liquids, 2018 Edition.

EMPTYING AND FILLING PROCESS OF A ROOM SUBJECT TO FIRE: EFFECT OF THE INLET AND OUTLET SURFACE AREA RATIO

El Mehdi KOUTAIBA[1], Gabriel GIOVANNELLI[1], Olivier VAUQUELIN[2] and Paul LARDET[1]

[1]CSTB, France

[2]Université d'Aix-Marseille, IUSTI, France

ABSTRACT

The present research work examines theoretically and numerically the emptying-filling box problem in a room subject to fire. The fire plume fills the room gradually which is simultaneously emptied thanks to its connections with the outside. The process is studied as a displacement ventilation flow once the steady state is reached. A theoretical description to predict the interface position is presented in this paper. The theoretical solutions are based on the recent works of Vauquelin [1] and Koutaïba [4] in the general non-Boussinesq case. In particular, it is shown that those relations depend on two geometrical parameters.

Mainly, we investigate to what extent a difference between the inlet and outlet areas and the associated discharge coefficients can have a significant impact on the smoke layer characteristics.

The problem is also studied numerically by performing simulations using the code Fire Dynamics Simulator (FDS, NIST)[15]. Numerical results are compared to the analytical relations.

Keywords: Emptying-filling box model; layer interface height; stratification.

1   INTRODUCTION

In fire safety engineering, design methods for smoke management systems are more and more oriented towards complex and precise approaches to deal with fluid and fire dynamics using CFD models such as FDS. If these tools allow a more realistic modeling of physical phenomena and thus the finding of the most appropriate optimized solution to fulfill the fire safety goals, they do not, conversely, allow their users to catch and understand the dependencies between the different physical or geometrical parameters involved in the simultaneous emptying filling process. The relatively simple fire models, often referred to as two-zone models are more suitable when parametric studies or simple rough estimations are needed. This kind of approach was first studied by Thomas [17] for fire safety engineering and later by Linden *et al.* [7] for thermal comfort purposes. Many more recent research investigated this process ([9], [18] and [19]) to study the different existing transient modes of the simultaneous filling and emptying process. However, very few tries to highlight some important dependencies and mainly one of the most important ones when the question is about designing smoke management systems. Thus, the present work investigates to what extent a difference between the inlet and outlet areas and the associated discharge coefficients can have an impact on the smoke layer characteristics.

447

2   THEORETICAL MODEL

As shown in figure 1, we consider the simultaneous filling and emptying of a cuboid box. The studied room height is denoted H and its surface is denoted S. the room communicates with the outside through an opening at the bottom part of the room (doors or openings on the floor) of surface $\Box_2$ and an exhaust vent in the ceiling of surface $\Box_1$. This surface areas are characterized by the discharge coefficients Cd_1 and Cd_2 parameterizing the effect of the *vena contracta* at the outlet and inlet of the room. We consider that the fire is set at ground level and creates a continuous source of buoyancy in the form of a plume of buoyancy flux denoted B which rises, entraining fresh air in its ascent. The buoyancy flux generated by the fire can be related to the convective heat $\dot{Q}_c$ using ideal gas law such as $B = g\dot{Q}_c/\rho_a T_a c_p$, ρ_a being the ambient air density, c_p the specific heat of air at constant pressure and T_a the ambient temperature.

The fire plume reaches the ceiling and creates instantaneously a thin smoke layer. The plume continuously supplies the smoke layer, but simultaneously, a part of the smoke is evacuated naturally through the ceiling exhaust vent due to the hydrostatic pressure difference between the inside and outside of the box caused by the higher temperature of the smoke layer.
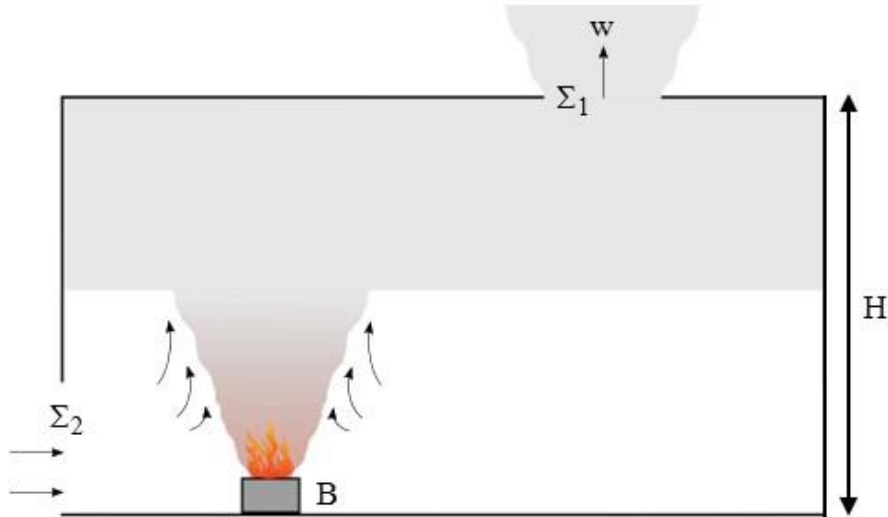

Fig. 1. Schematic of the studied configuration.

A situation of ideal displacement flow is assumed, which supposes a box aspect ratio $H/S^{1/2}$ sufficiently small that the effect of plumes 'overturning' is negligible (Kaye & Hunt [8]) and a base opening (for the incoming ambient air) large enough to overcome bidirectional flows at the vent or an inlet jet strongly mixing the interface (Coffey & Hunt [9]; Hunt & Coffey[10]).

The work of Koutaïba [4] presents a theoretical model to predict the position of the dimensionless smoke-free height denoted ζ at steady state based on the buoyancy and mass flow rate balance equations on the control volume defined by the upper layer. The turbulent plume was modeled based on the similarity solutions developed by Morton *et al.*[11]. Most of the empirical correlations used in fire safety engineering ([12],[13] and [14]) are based on this model which represents of turbulence by introducing a simple entrainment coefficient α. The steady state equation formulation by Koutaïba [4] is:

$$\frac{\zeta^{5/3}\left(\zeta^{5/3} + \kappa_2\Theta\right)^2}{1-\zeta}\left(\frac{\kappa_2\Theta}{\zeta^{5/3}}\Lambda' + 1\right) = \frac{2\kappa_2}{\kappa_1^2}\Lambda^2 \qquad (21)$$

$$\eta = \frac{\kappa_1 \Theta}{\zeta^{5/3}} \qquad and \qquad \omega = \sqrt{2\eta(1-\zeta)}$$

With
$$\Theta = \frac{B^{2/3}}{gH^{5/3}}, \qquad \Lambda = \frac{\Sigma_1 \Sigma_2}{H^2 \sqrt{\Sigma_1^2 + \Sigma_2^2}} \qquad \Lambda' = \Sigma_1 \Big/ \sqrt{\Sigma_1^2 + \Sigma_2^2}$$

$$\kappa_1 = 2.48\alpha^{4/3}, \qquad \kappa_2 = 0.4\alpha^{-4/3}$$

Where $\zeta = z/H$ is the dimensionless smoke-free height, $\eta = (\rho_a - \rho)/\rho$ the density deficit in the smoke layer (ρ being the smoke layer density and ρ_a the ambient air density), $\omega = w/\sqrt{gh}$ the dimensionless outflow mean velocity (w being the outflow mean velocity), Θ can be interpreted as an indicator of the source strength relative to the local height, Λ and Λ' are two geometrical parameters, κ_1 and κ_2 are two constants depending on the entrainment coefficient α. g is the gravitational acceleration.

The unique real root of the equation (1) gives the value to ζ at the steady state. Assuming that the entrainment coefficient is constant, it can be seen that the smoke layer height depends on four main physical quantities. The first one is the local height then the opening areas Σ_1 and Σ_2 defined by the geometrical variables Λ' and Λ. This latter has been already defined by Linden *et al*. [7]. However, the model presented here is defined in the general non-Boussinesq case contrary to the one developed by the latter. This approach shows a fourth dependence on the power of the fire contained in the variable Θ but also on the second geometrical variable Λ'.

3   EFFECT OF THE INLET AND OUTLET SURFACE AREAS

It can be noted from equation 1 that two cases seem more interesting regarding the geometrical variables Λ and Λ'. The first one corresponds to the case where the two surface areas Σ_1 and Σ_2 are equal. The geometrical variables become $\Lambda = \Sigma / \sqrt{2} H^2$ and $\Lambda' = 1/\sqrt{2}$. Equation 1 can be written:

$$\frac{\zeta^{5/3}\left(\zeta^{5/3} + \kappa_2 \Theta\right)^2}{1-\zeta}\left(\frac{\kappa_2 \Theta}{\sqrt{2}\zeta^{5/3}} + 1\right) = 2\kappa_2 \Big/ \kappa_1^2 \Lambda^2 \qquad (22)$$

The problem then depends on the two parameters Λ and Θ. From this formulation, one can find the two-dimensional evolution (on both variables Λ and Θ) of the dimensionless smoke-free height ζ. Figure 2 shows, in the case where the openings have the same surface area, the evolution of ζ as a function of the geometrical parameter Λ, and the parameter Θ (source strength relative to the local height). We can notice that Θ has a greater influence for small values of the geometric variable Λ.

In the second case, we investigate the situation where the opening surface area Σ_2 is largely greater than the exhaust vent Σ_1. Considering this assumption, one can assume that the opening surface area tends towards infinity, the two geometrical parameters become $\Lambda' = 0$ and $\Lambda = \Sigma_1 / H$. Equation 1 takes the form already presented by Vauquelin [1]:

$$\frac{\zeta^{5/3}\left(\zeta^{5/3} + \kappa_2 \Theta\right)^2}{1-\zeta} = 2\kappa_2 \Big/ \kappa_1^2 \Lambda^2 \qquad (23)$$
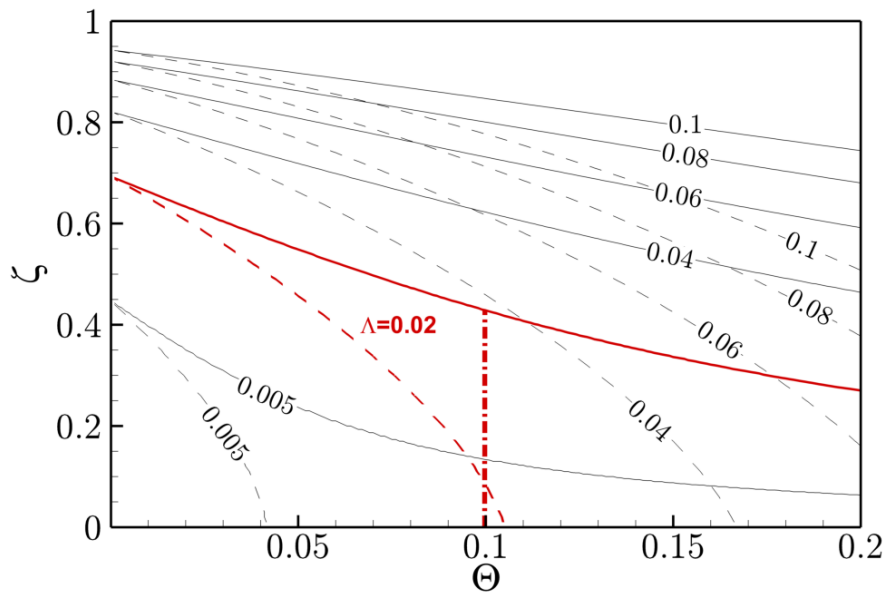
Fig. 4 The geometrical parameter Λ curves as a function of the dimensionless smoke-free height ζ and Θ. The case of equal surfaces is presented in dashed line and the case when the inlet surface area tends towards infinity is presented in continuous line

Figure 4 shows a comparison between the two cases where the inlet surface area tends towards infinity and the one where it is supposed to be equal to the exhaust vent surface. We can note, for example, that for the same $\Theta = 0.1$ value, a huge difference can be seen between the two cases for $\Lambda=0.02$.

Indeed, the theoretical model expects that with equal surfaces the room is almost fully filled ($\zeta \approx 0$). Whereas, with an inlet surface area much bigger than the exhaust vent it is expected that the room is almost half-filled ($\zeta \approx 0.45$).
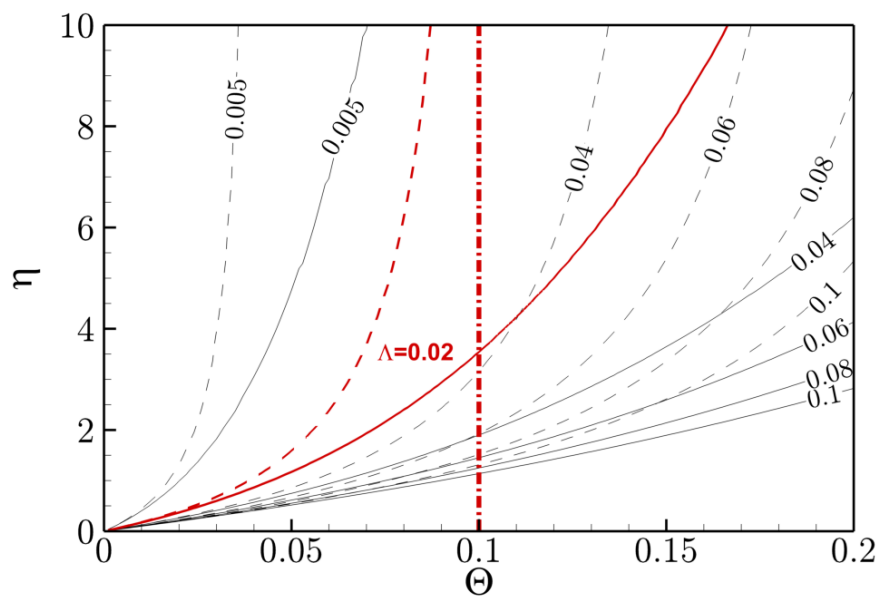
Figure 5 presents another comparison concerning the density deficit in the smoke layer. For the same $\Theta = 0.1$ value, the case with an inlet surface area that tends towards infinity gives a density deficit of about $\eta=0.39$, which corresponds, for an ambient density of *1.2 kg/m³*, to a smoke layer density of *0.24 kg/m³*. When the surfaces are equal the density deficit will tend towards the fire source density deficit.
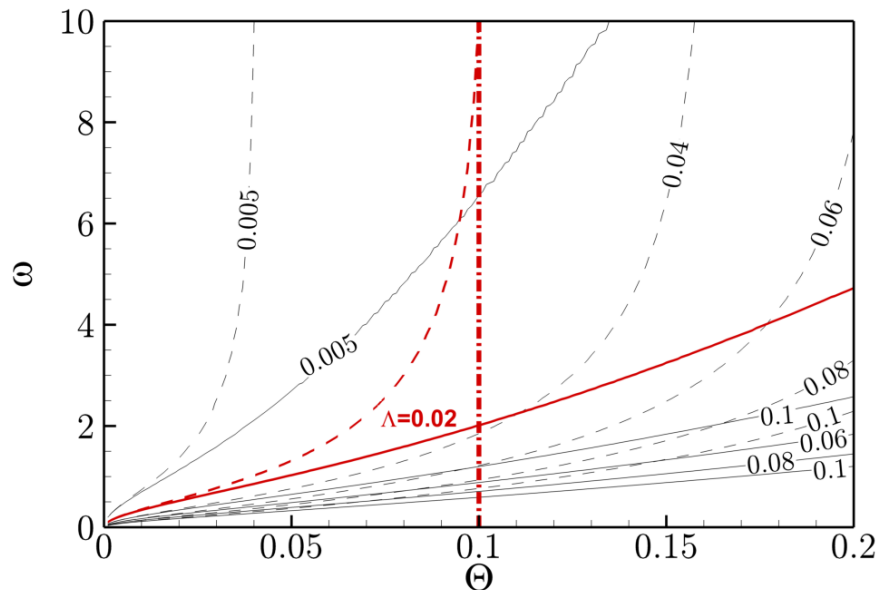

Fig. 6 The geometrical parameter Λ curves as a function of the dimensionless outflow mean velocity ω and Θ. The case of equal surfaces is presented in dashed line and the case when the inlet surface area tends towards infinity is presented in continuous line

Figure 6 presents the last comparison concerning the dimensionless outflow mean velocity. The same observations can be made regarding this quantity. Indeed, the two cases show a huge difference for the same value of the parameter *Θ = 0.1*. This difference is normal since the smoke layer height is bigger when the surfaces are equal which increases the hydrostatic pressure difference and thus the flow velocity at the exhaust vent.

Application

This application consists of confronting the theoretical model to numerical simulations performed using the CFD model FDS (Fire Dynamics Simulator v6). Comparisons with small scale experimental results from Koutaïba [4] and Haouari Harrak *et al.*[3] are also demonstrated in this section. The comparisons are made qualitatively in order to ascertain the results found earlier and emphasise the dependencies observed. This latter will concern only the smoke layer height once the steady state is reached.

A simple cuboid box, of dimensions 10 m $\times$ 10 m $\times$ 10 m, is modeled with a centrally located fire. The mesh is uniform. The grid cell size is fixed to $\delta=10$ cm i.e. $9.65 \leq D^* / \delta \leq 18.3$ where D^* is the characteristic diameter of the plume such as:

$$D^* = \left(\dot{Q} \left(\rho_0 c_p T_0 \sqrt{g} \right)^{-1} \right)^{2/5}$$

The walls are assumed adiabatic and radiation is disabled in FDS. This assumption is made since the theoretical model does not take into account the radiation transfer. This hypothesis implies mainly that the lower layer temperature will remain equal to the initial temperature. The fuel considered is heptane (C_7H_{16}).

In FDS, the location of the interface between the smoke upper layer and the cool lower layer is estimated using Janssens and Tran [16] method which evaluates the layer height and the average temperature from a continuous vertical profile of temperature.

In the theoretical model, the use of the similarity solution model assumes that the plume is released from a source point of buoyancy. For fire plumes released from a source of finite area, to consider the real source characteristics, a correction on the origin position is introduced. Multiple studies are found in the literature concerning the position of the virtual origin of a fire plume. The best known being the one presented by Heskestad [13] based on the flame height. A more recent work by Haouari Harrak *et al*. [3] has been conducted based on small-scale tests and on the theoretical work of McCaffrey [14]. This recent work on the virtual origin correction of Haouari Harrak *et al*. [3] is used in this comparison.

Also, the discharge coefficient used to consider the effect of the *vena contracta* at the outlet is based on the work done by Vauquelin et al. [6] which defines it as a function of the smoke characteristics and the outlet geometry.
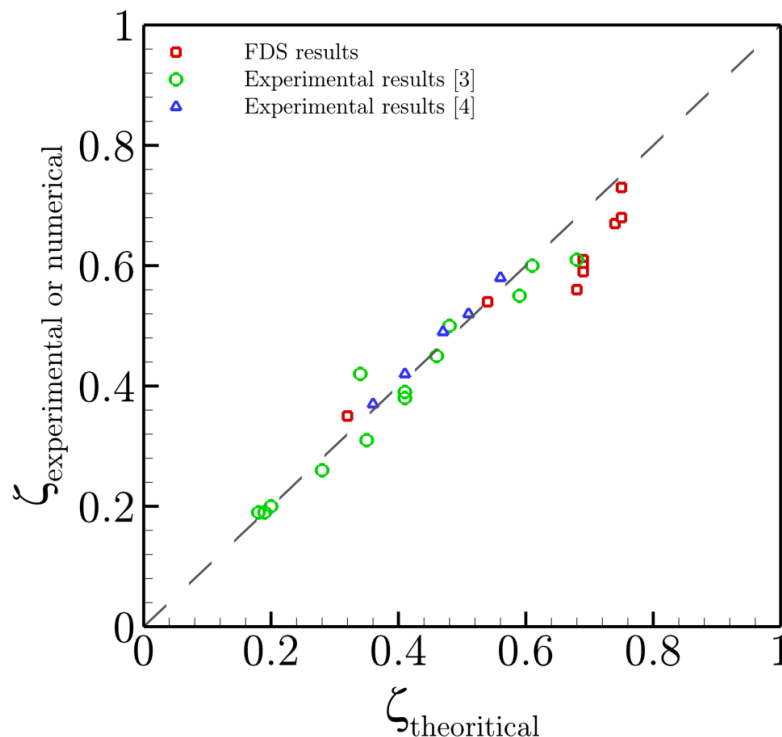

Figure 7. Predictions of interface height

Figure 7 compares numerical and experimental results to the theoretical predictions. In the numerical simulations six values Σ_I are considered: 1, 4, 9, 16, 25 and 36 m^2. A constant prescribed HRR varying from 1 MW to 5 MW is used. A good agreement is observed

between the two approaches with a maximum difference of about 22 %. The theoretical model correctly predicts the experimental results found in [3] and [4].

4   CONCLUSION

We have examined the theoretical model presented by Koutaiba [4] concerning the emptying filling problem in naturally ventilated compartment in case of fire. In particular, it is shown that the emptying filling box model in the general non-boussinesq case depends on the fire power and two geometrical parameters (that depend themselves on the inlet and outlet areas).

We investigated to what extent these two geometrical parameters can have a significant impact on the smoke layer characteristics. In fact, we highlighted how the hydrostatic pressure difference can drastically prevent the smoke layer from flowing out freely. It is shown that this effect depends on the fire power inside the compartment, and for some values the difference can go from fully filling the room with equal inlet and outlet surfaces to a half-filled room if the inlet opening is much bigger than the exhaust vent.

The model is confronted by 3D simulations using the CFD code FDS and small-scale experiments, a good agreement is found between the approaches. These results highlight the dependencies on the emptying filling problem. It also describes the physics and entrainment models used in two zone codes. The comparison between the theoretical and the CFD approaches shows that the two are viable and can be both used to help the engineer to find the best possible smoke control solution.

5   REFERENCES

[1] Vauquelin, O., "Oscillatory behaviour in an emptying-filling box", J. Fluid Mech., 2015, pp. 712-726, vol. 781.

[2] Vauquelin, O., Koutaiba, E., Blanchard, E., & Fromy, P., "The discharge plume parameter Γd and its implications for an emptying-filling box", J. Fluid Mech., 2017, pp. 171-182, vol. 817.

[3] Haouari Harrak, S., Mehaddi, R., Boulet P., Koutaïba, E.M., Giovannelli G., Beker S., "Virtual origin correction for a fire plume in a room under displacement ventilation regime", *Int. J. Thermal Sc.*, 2019, pp. 243-253, vol. 136.

[4] Koutaïba, E.M., "Contributions théoriques et expérimentales sur la ventilation naturelle hors cadre Boussinesq : application au désenfumage des bâtiments", PhD thesis, Université d'Aix-Marseille, 2016.

[5] Vauquelin, O., "Oscillatory behaviour in an emptying-filling box", J. Fluid Mech., 2015, pp. 712-726, vol. 781.

[6] Vauquelin, O., Koutaiba, E., Blanchard, E., & Fromy, P., "The discharge plume parameter Γd and its implications for an emptying-filling box", J. Fluid Mech., 2017, pp. 171-182, vol. 817.

[7] Linden P. F., Lane-Serff G. F. & Smeed D. A., "Emptying filling boxes, the fluid mechanics of natural ventilation", *J. Fluid Mech.* , 1990, pp. 309–335, vol. 212.

[8] Kaye, N. B. and Hunt, G. R. (2007) Overturning in a filling box. Journal of Fluid Mechanics 576, 297.

[9] Coffey, C. J. & Hunt, G. R. 2010 The unidirectional emptying box. J. Fluid Mech. 660, 456–474.

[10]   Hunt, G.R. & Coffey, C.J. 2010 Emptying boxes – classifying transient natural ventilation flows. J. Fluid Mech. 646, 137–168.

[11]   Morton, B. R., Taylor, G. I. & Turner, J. S., Turbulent gravitational convection from maintained and instantaneous sources. Proc. Roy. Soc., A234 (1956) 1-23.

[12]   Cetegen, B. M., Zukoski, E. E. & Kubota, T., Entrainment in the near and far field of fire plumes. Combust. Sci. Techno. 39(1984) 305-31.

[13]   Heskestad, G. 1984 Engineering relations for fire plumes. Fire Safety J. 7, 25-32.

[14]   B. J. McCaffrey. Momentum implications for buoyant diffusion flames. Combustion and Flame, 52:149–167, 1983

[15]   McGrattan, K., Hostikka, S. McDermott, R., Floyd, J., Weinschenk, C. and Overholt ,K.. Fire Dynamics Simulator, User's Guide. NIST.

[16]   Janssens, M.L. and Tran, H.C. Data Reduction of Room Tests for Zone Model Validation. Journal of Fire Science, 10:528–555, 1992. 213

[17]   Thomas, P.H., Hinkley, P.L., Theobald, C.R. & Simms, D.L., Investigations into the flow of hot gases in roof venting. Fire Research technical Paper No. 7, Fire Research Station, Watford, UK, 1963.

[18]   Q. Tan, Y. Jaluria, Mass flow through a horizontal vent in an enclosure due to pressure and density differences, Int. J. Heat Mass Tran. 44 (8) (2001) 1543–1553,

[19]   R. Harish, K. Venkatasubbaiah, Numerical simulation of turbulent plume spread in ceiling vented enclosure, Eur. J. Mech. B Fluid 42 (2013) 142–158

THE EFFECTS OF A VENTILATION-LIMITED FIRE ENVIRONMENT ON FURNITURE BURNING CHARACTERISTICS

Bronwyn E Forrest[1], Elizabeth J Weckman[1], Noah Ryder[2] & Peter Senez[1]
[1]University of Waterloo, Waterloo, Canada
[2]Fire & Risk Alliance, Maryland, United States of America

ABSTRACT

Modern homes are being constructed for energy efficiency which brings many societal benefits; however, many associated changes have been made to building codes without characterizing potential fire safety implications. This paper strives to build a stronger foundation for scientific understanding of ventilation-limited of fires by investigating the effects of a ventilation-limited environment on the burning characteristics of three different furniture types. Oxygen and carbon monoxide concentrations are measured at various locations in a two-storey burn structure and correlated to the heat release rate and mass loss of the fuel. To complement the data, video footage is analyzed to enhance understanding of the evolution of the smoke layer and its interconnections with the above parameters. It was found that oxygen levels in both storeys decreased below 10% which was found to have an impact on the mass loss and heat release rate.

1   BACKGROUND

Modern homes are being constructed for energy efficiency which brings many societal benefits; however, many associated changes have been made to building codes without characterizing potential fire safety implications. For example, when fires start in energy efficient homes the fire environment can become ventilation-limited, which substantially alters the associated fire risk to occupants and firefighters when compared to the better-understood ventilated fire development. This paper reports research intended to build a better foundational understanding in two key areas: 1) how ventilation-limited burning affects the physics and development of compartment fires, and 2) how this mode of burning affects the quantities and time evolution of fuel pyrolysis and incomplete combustion products (such as CO). Better understanding in the above areas will provide key insight into the impacts of ventilation-limited fire environments on human safety and egress as well as potential implications in terms of firefighter safety and response.

As a starting point, it is important to review the overall physics of well-ventilated (fuel-controlled) and ventilation-limited fires. Well-ventilated fires occur in situations where there is sufficient oxygen available for combustion [1]. Fire growth and heat release are entirely dependent on the rate at which the fuel is pyrolyzed, mixed with oxygen and burned. On the contrary, ventilation-limited fires can occur when overall oxygen levels decrease, so there is no longer sufficient oxygen available to combust all of the pyrolyzing fuel [1]. The heat released from the fire then depends on the quantity of oxygen available. Due to reduced levels of oxygen, combustion is less efficient and more soot, fuel pyrolysis products and products of incomplete combustion are released [1].

As modern homes shift towards being more energy-efficient, building envelopes are becoming better insulated, and buildings are increasingly designed to limit energy and mass transfer from the controlled interior to the ambient and variable conditions of the exterior environment. Thus, the interior environment is effectively mechanically controlled thereby limiting the ventilation in the event of a fire. In the few experimental studies where low

ventilation fire environments have been investigated, oxygen levels as low as 6% in the hot layer have been measured [4] with overall levels of oxygen in the compartment observed to range from under 10% to 18% depending on the fuel source and details of the ventilation pathways [5,6,7]. At these levels of oxygen, combustion is not very efficient and consistent with this, yields of incomplete combustion products increased and a dense smoke layer filled the compartment space. When sufficient fuel was available, as the fire grew and the smoke layer descended, the oxygen concentrations continued to decrease until the fires self-extinguished [5,6,7]. The impacts of ventilation pathways, oxygen deprivation and smoke layer development on mass loss rate of the fuel, heat release rate, and gaseous transport between compartments and levels of a structure are not well understood from a scientific perspective. Yet, these fire situations pose several major fire safety concerns. Development of ventilation-limited fire environments inside a structure can lead to increased yields of soot, carbon monoxide and material-specific products such as hydrogen cyanide (HCN) or other toxic gases, potentially exposing occupants to increased risk of life-threatening health effects. Secondly, it is important to understanding the impact of the different fire environment on traditional firefighting tactics [2]. Traditional firefighting ventilation tactics may include opening windows and doors, potentially increasing the rate of fire growth risking onset of flashover [1], thereby exposing firefighters to increased hazard [2, 3].

This investigation explores key elements of the behaviour of ventilation-limited furniture fires in a two-storey structure. Fire development is examined by evaluating gaseous transport and the smoke layer/fire interface to determine the resultant effects on the mass loss and heat release rate. The impacts on occupant tenability and firefighter safety are examined in the context of measured levels of oxygen and time to oxygen depletion, as well as increased carbon monoxide and smoke production. Results form a first step towards identifying and addressing potential fire safety concerns associated with modern home construction in hopes to benefit occupants and firefighters.

2   METHODS

A series of nine furniture tests were conducted in the two-storey burn structure at the University of Waterloo's Live Fire Burn Facility. The burn structure has a steel outer frame and is outfitted with interior steel stud walls covered in gypsum wall board throughout the lower floor. An additional layer of concrete board is installed on the areas of the walls and ceiling directly exposed to fire. Non-combustible fiber insulation is installed in the burn room to provide additional fire resistance at the ceiling where the couch fires were conducted. The structure has an open stair and was largely airtight with the exception of leakage associated with functional window and door openings.

Fuel for the nine furniture fires consisted of three different furniture types, with each tested three times. Fires were initiated with a small wooden crib and isopropanol wick consistent with BS 5852 [8]. Each couch combination was specially built to have the same wooden-frame and similar amounts of foam and fabric, some of which was fire-retardant (FR). Couch A was constructed with non-FR (0.44% wt chlorine) polyurethane foam and non-FR (0.17% wt chlorine) polyester fabric. Couch B was constructed with FR (3.0% wt chlorine) polyurethane foam and FR (5.2% wt bromine; 3.6% wt chlorine) polyester fabric. Lastly, Couch C was constructed with lightly-FR (0.9% wt chlorine) polyurethane foam and non-FR (0.11% wt chlorine) fabric.

For these tests, the structure was instrumented with thermocouples, a heat flux gauge and video cameras to monitor overall fire development. The couches were placed on load cells to

record mass loss with time. Electrochemical sensors, placed in three different locations (the burn room, the other main floor compartment and a second level compartment), were used to measure carbon monoxide (CO) and oxygen with time. The sensors were placed at a height of approximately 24 inches from the floor in each location. During post-processing, the heat release rate was calculated as the product of the mass loss rate of the couch and an effective heat of combustion [9]. For this, the current output from the weigh scale was smoothed using a 10-point moving average before the mass loss rate, used in the heat release rate calculation, was determined. There are many documented heats of combustion for polyurethane foam. Because the couches each contained different combinations of foams and fabrics, however, a specific value for the heat of combustion was determined for each couch type via a cone calorimeter test of each material combination. The effective heat of combustion was calculated using Equation (1), based on the measured value of total heat released (THR), the surface area and the mass of the sample [10].

$$\Delta H_{c,eff} = \frac{THR \left(\frac{kJ}{m^2}\right)*0.00884 m^2}{m_{sample}\,(kg)} \tag{1}$$

The calculated heats of combustion for couches A, B and C respectively are: 14,450 kJ/kg, 9,655 kJ/kg and 14,263 kJ/kg. Output voltages from the electrochemical sensors were converted into percent volume and parts per million (ppm) for O_2 and CO, respectively, using linear calibration curves.

3 RESULTS

Based on preliminary analysis of video recordings of the overall progression of the fire, a number of times have been noted that correspond to key events in each test. These times correspond to the following events: ignition of the BS 5852 crib, ignition of the couch, smoke layer descent to window level, and measured peak heat release rate (PHRR). The series of images below (page 5) provides qualitative information from the security camera video footage during the tests at each of the key event times. While the importance of the other event times is routine and understood, in this test series, the time of smoke layer descent to top of the window is also important as it is reflective of the time at which the smoke layer has descended sufficiently to significantly interact with the top of the visible fire plume. It alsoroughly corresponds to when the smoke layer descends below the stairway threshold allowing flow of the smoke up the stair to the second floor. The time of this event corresponds to the time in the video at which the top frame around the window cannot be seen and smoke can be seen coming down over the window itself. Table 1 provides results for key measurements obtained during the testing, including PHRR, O_2, and CO concentrations. As can be observed, O_2 concentration drops to 10% or below in all locations for all tests indicating that ventilation-limited conditions are observed through the entirety of the structure. Peak CO values exceeded 1700 ppm in most locations, thereby surpassing the Acute Exposure Guideline Levels (AEGL) value associated with life-threatening health effects or death over a 10-min duration [11]. Even in the second-floor compartment peak CO concentrations exceeded the AEGL limit of 420 ppm associated with irreversible or other serious long-term adverse health effects [11].

Table 14 Summary of Important Measurements from Each Test

Test, Couch	Peak HRR (kW)	Lowest Oxygen %vol (BR/1F/2F)*	Peak CO ppm+ (BR/1F/2F)

Test 2, Couch A non-FR	2300	8 / 7 / 7	2200/ 1800 / 1500
Test 4, Couch B FR	1300	8 / 9 / 10	2500 / 2100 / 1900
Test 3, Couch C lightly-FR foam; heavy fabric	1400	9 / 6 / 8	2300 / 2000 / 1600

*BR stands for burn room, 1F stands for first floor and 2F stands for second floor; + actual magnitudes of CO peaks may be capped by saturation of the detectors used in the BR.

4   DISCUSSION

As seen in the series of images and Figures 1-6 below, there are several qualitative differences in the burning characteristics of the three couches. The HRR at the time that the smoke layer reaches the top of the window frame varies for each couch type. Couch B (Fig 3), the FR couch, has the smallest fire size when the smoke layer reaches the top of the window. This supports the notion that due to the FR additives the combustion process is less efficient, resulting in a slower increase to the PHRR and higher yield of products of incomplete combustion. This is also intuitively consistent with the image taken at the point of PHRR as there appears to be more smoke in the compartment at that time in comparison to what is observed for the other couches. For couches A and C (Fig 2 and Fig 4), the fire size is visually similar at the point where the smoke descends to the top of the window, though couch A is likely slightly larger. At the time of PHRR, more smoke had been produced by the fire on couch A, enough that the far arm rest was obscured from view, compared to couch C. As expected, the fire on non-FR couch A takes the least amount of time to reach its peak heat release rate (346 s). Smoke also descended to the top of the window in the least amount of time for this test (322 s). The second fastest times for smoke to fill to window level (377 s) and the fire to reach peak heat release rates (433 s) are found for the FR couch B, both significantly slower than values seen for couch A. The lightly-FR couch C with fabric cover took the longest time for both smoke descent (629 s) and peak heat release rate (686 s). This may be attributed to properties of the fabric cover, since the fabric on couch C chars and effectively creates a barrier between the flame and surface of the foam underneath. While these results may seem counter-intuitive, it is postulated that the FR properties of couch B enhance smoke production and simultaneously lead to a lower PHRR, though that peak is reached earlier in the fire which can, in part, be attributed to the difference in fabric performance resulting in earlier exposure of the polyurethane foam.

As seen in Figures 1-6, the evolution of heat release rate, mass loss, oxygen concentration and carbon monoxide concentration with time all follow the expected trends. As the heat release rate starts to increase, the mass loss decreases while the CO levels increase and O_2 levels decrease. The O_2 levels in the burn room are lowest very near the time of peak heat

	Couch A	Couch B	Couch C
Crib Ignition	0 s	0 s	0 s
Couch Ignition	49 s	20 s	23 s
Smoke at Window	322 s	377 s	629 s

PHRR	 346 s	 433 s	 686 s

Fig 1. Mass loss and Gaseous Trends from non-FR Couch A.

Fig 2. Heat Release Rate, Event Markers, Oxygen and Carbon Monoxide Trends from non-FR Couch A

Fig 3. Mass loss and Gaseous Trends from FR Couch B

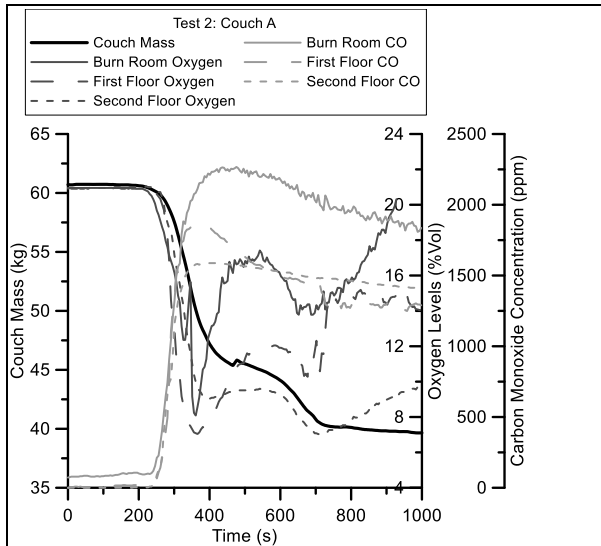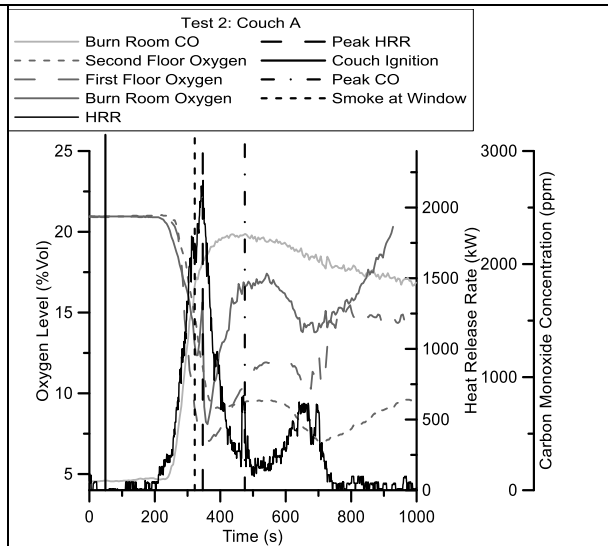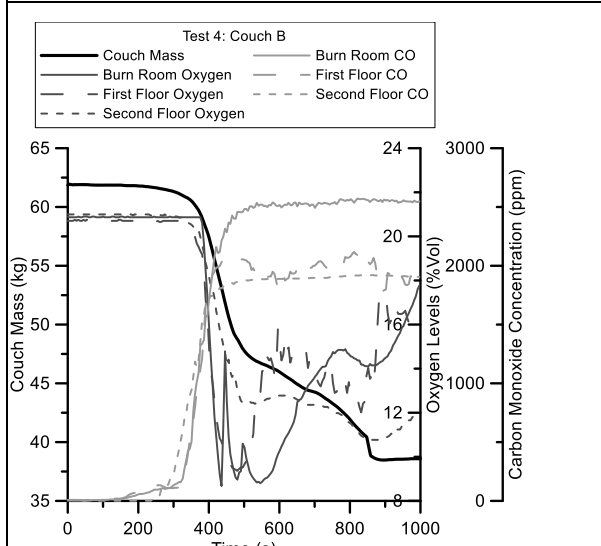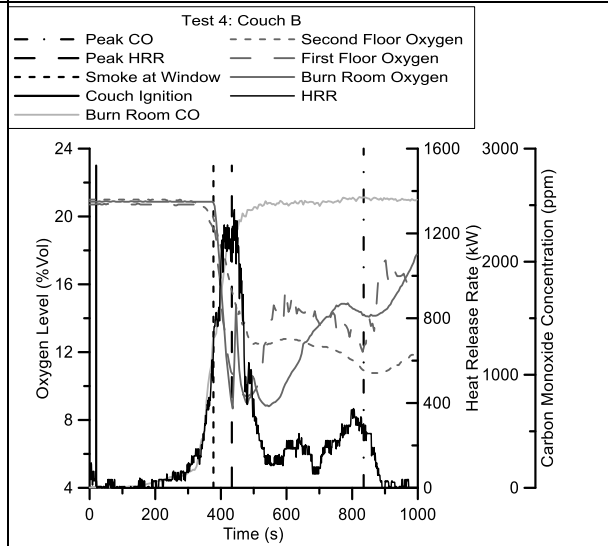*Fig 4*. Heat Release Rate, Event Markers, Oxygen and Carbon Monoxide Trends from FR Couch B.
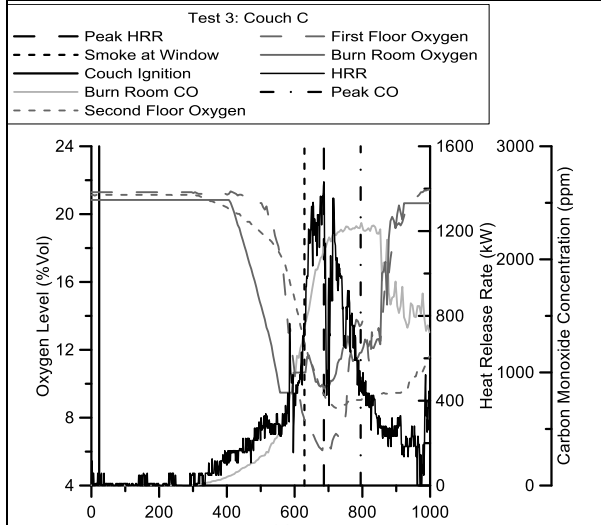

Fig 5. Mass loss and Gaseous Trends from non-FR Couch C.
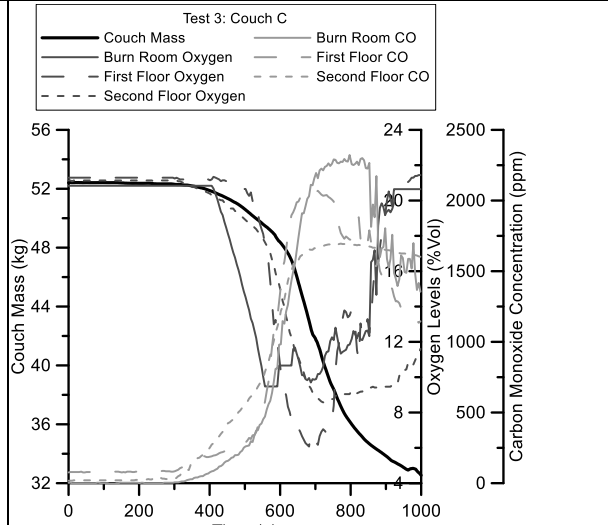

Fig 6. Heat Release Rate, Event Markers, Oxygen and Carbon Monoxide Trends from non-FR Couch C

release rate. Measured peak concentrations of CO and lowest concentrations of O_2 occur in the burn room first, followed by the other first floor compartment and finally the second-floor compartment. It is interesting to observe that when the smoke descends to the top of the window, the slope of the time resolved plot of second floor CO concentration increases, supporting that when the smoke layer descends to top window height, there is significant flow of smoke up the stairs to the second-floor compartments. Oxygen levels decrease to under 10% in each compartment and in both levels of the structure, which is consistent with values previously reported in the literature for compartments with minimal to no openings or ventilation [4,5,6,7]. As oxygen levels decrease on the main floor, the fire pulls oxygen from other areas of the house to support burning which is clearly seen in the figures above. In fact, the lowest concentrations of oxygen measured at each location are all reached near the period of peak mass loss and steady burning of the fires.

It is clear from the present results that oxygen depletion in the environment and descent of the smoke layer impact overall fire growth and development in several different ways. It is reported in the literature that pool fires self-extinguish when oxygen levels between 15%-18% are reached or when the compartment space completely fills with smoke and no additional oxygen is introduced [4,5,7]. In the three furniture fires considered here, the foam and fabric in the couches nearly completely burned. Thus, it did not appear that the upholstery materials self-extinguished even though recorded O_2 levels decreased well below 15%-18% levels in the burn room (8%), the other main floor compartment (6-10%) and the upper level (7-10%). This indicates that, even as O_2 levels in the burn room decreased, there was sufficient combined heat feedback to the fuel surface from the hot smoke layer and flaming fire plume that fuel was still vaporized and a portion of that fuel mixed with sufficient air to remain involved in the combustion process. Measurements point to a potential staging of ventilation in these fires. As O_2 became limited in the burn room, additional O_2 to support burning was drawn first from the adjacent main floor compartment and then from the second level continually providing the fire with new O_2 to support combustion. Heat flux from the flame and smoke layer, in conjunction with the available O_2, facilitated continuing pyrolysis and combustion of the foam and fabric. Despite the values of PHRR reached, the wooden frames did not significantly participate in the fire. In this respect, it can likely be considered that the fires self-extinguished as the foam and fabric was consumed; past that point, combined levels of oxygen availability and heat feedback to the fuel could no longer support combustion.

5   CONCLUSIONS

As can be observed through the present results, the different types of fuel across the three couches had an impact on the specifics of the fire growth as well as generation of smoke and products of combustion. It is also evident that independent of the type of fuel, the fires became ventilation-limited in all cases with production of large quantities of smoke. While prior literature indicated that fires may self-extinguish for O_2 concentrations in the range of 15-18%, mass loss and burning continued for O_2 concentrations significantly below these levels in the present fires. This indicates that when heat flux to the fuel, from both the flame and smoke layer, is sufficient, pyrolysis of the fuel and combustion can continue as long as O_2 can be locally supplied to the fire. The quantity of CO produced in the test fires, combined with evidence that fires can be sustained at vastly reduced O_2 levels, are sufficient to raise concerns with regards to occupant safety and potentially merit reassessment of current firefighting best-practices for

ventilation-limited fires in new energy efficient building environments. These results show that it is important to understand how the modification and building of homes to fit into any energy–efficient model affects fire growth and development. Further attempts to more completely characterize both physical and chemical aspects of fire environments should be made, particularly with the emergence of many new green and sustainable construction practices.

ACKNOWLEDGMENT

REFERENCES

[1] Karlsson B & Quintiere J.G. (2000*) Chapter 2: A Qualitative Description of Enclosure Fires* in: Enclosure Fire Dynamics. CRC Press LLC, pp. 24-36.

[2] Roman J. (2014). New Fires, New Tactics. NFPA Journal. Retrieved February 26, 2019 from: https://www.nfpa.org/News-and-Research/Publications/NFPA-Journal/2015/January-February-2015/Features/Fire-Tactics

[3] Norwood P.J. & Ricci F. (2014). Ventilation Limited Fire: Keeping it Rich and Other Tactics Based off Science. Fire Engineering Magazine. Retrieved February 26, 2019 from: https://www.fireengineering.com/articles/2014/01/ventilation-limited-fire-keeping-it-rich-and-other-tactics-based-off-science.html

[4] Utiskul Y., Quintiere J.G., Rangwala A.S., Ringwelski B.A., Wakatsuki K., Naruse T. (2005) *Compartment Fire Phenomena Under Limited Ventilation.* Fire Safety Journal, Vol 40, pp. 367-390

[5] Andrews G.E., Ledger J., Plylaktou H.N. *Enclosed Pool Fires in Low Ventilation Enclosures: Flame Temperatures and Global Heat Loss Using Gas Analysis.* Fire Safety Science-Proceedings of the Sixth International Symposium, pp. 591-602.

[6] Peatross M.J., Beyler C. *Ventilation Effects on Compartment Fire Characterization.* Proceedings of the Fifth International Symposium of Fire Safety Science, pp.403-414.

[7] Pretrel H., Such J.M. (2005) *Effect of ventilation procedures on the behaviour of a fire compartment scenario.* Nuclear Engineering and Design, Vol 235, pp. 2155-2169.

[8] British Standards Institute (2006) BS 5852:2006 Methods of test for assessment of the ignitability of upholstered seating by smouldering and flaming ignition sources, London UK.

[9] Gorbett G.E., Pharr J.L. (2011) *Heat Release Rate* in: Fire Dynamics, Pearson Education Inc., New Jersey, p. 137.

[10] Fire Testing Technology (2009) ConeCalc5 Software, East Grinstead UK.

[11] Committee on Toxicology, National Research Council. (2010) *Acute Exposure Guideline Levels for Selected Airborne Chemicals.* The National Academics Press, Washington DC, Vol 8, p. 52.

[12] Hamins A., Fischer S.J., Kashiwagi T., Klassen M.E., Gore J.P (1994). *Heat Feedback to the Fuel Surface in Pool Fires.* Combustion Science and Technology , Vol 97, pp. 37-62.

FORMATION MECHANISM OF CARBON MONOXIDE IN WOOD COMBUSTION: AN ATOMISTIC STUDYING USING REACTIVE FORCEFIELD

Huali Hao [1], Cheuk Lun Chow [1], Denvid Lau*, [1]

1 Department of Architecture and Civil Engineering, City University of Hong Kong, Hong Kong, China

* Corresponding author: denvid@mit.edu

ABSTRACT

An accurate prediction of the carbon monoxide which is the main cause of the life death in a fire is critical for reducing the fire casualties. In this work, the chemical reaction pathway for the oxidation of cellulose is analyzed by using the molecular dynamics simulation with the reactive forcefield, and the carbon monoxide release mechanism is revealed. It is found that even in the situation where the oxygen is sufficient of complete combustion, carbon monoxide is mainly released from the thermal decomposition of the carboxyl group formed during the combustion, and then it is oxidized to form carbon dioxide. Our works enable us to accurately predict the formation of carbon monoxide in wood combustion. The fundamental knowledge of chemistry in the combustion can help to improve the fire safety codes and lay a foundation for a safer design of timber building with a reduction of fire risk.

1   INTRODUCTION

Wood has long been a conventional construction material in human history before the wide use of concrete and has regained its popularity in modern society as the concept of the green building becomes the mainstream [1]. Since wood is a combustible material, the fire safety issue of timber buildings becomes very critical. The ability to predict wood combustion behavior has become increasingly important as fire safety engineering moves toward a performance-based approach to building design. As the majority of fire deaths within buildings are a direct result of exposure to carbon monoxide (CO) generated in a fire [2], reducing the CO release is an efficient way to minimize the fire losses. However, the mechanism of formation CO in wood combustion remain ambiguous resulting in the difficulty in CO control.

Although the experimental and numerical approaches can asses the CO generation in wood combustion, they are challenging to disentangle the CO release mechanism [3-4]. As an approach that can clearly characterize the atom configuration and rearrangement, molecular dynamics (MD) simulation is a powerful means to disentangle the fundamental mechanisms which are difficult to be revealed by the experiment [5]. The reactive forcefield (ReaxFF) developed in MD simulation enables the breakage and formation of bonds with the associated charge rearranged [6]. MD simulation with ReaxFF has been the only technique capable of providing the spatial and temporal resolution necessary to characterize a variety of fundamental issues of chemical reactions such as the initial chemical steps of decomposition, detailed chemical reaction pathways and the molecular structure of products [7]. Recently, MD with ReaxFF has successfully utilized in the analysis of hydrocarbon oxidation, the decomposition and reaction of energetic materials, and the thermal decomposition of epoxy resin etc [8, 9]

Wood mainly contains cellulose, hemicellulose, and lignin [10]. During the wood combustion, one important product char can significantly affect the reactivity because it can act as a thermal

barrier between fire and virgin wood [11]. This char is mainly formed as a result of cellulose decomposition. Moreover, for the structure application of wood, the mechanical properties of wood highly depend on the cellulose. Understanding the combustion behavior of cellulose not only enables us to figure out the reactivity of wood combustion but also provides an insight into the wood performance in a fire.

The objective of this work is to develop an approach that can accurately predict the chemical reaction of cellulose in the combustion and figure out the CO release mechanism. The combustion system where cellulose molecules are mixed with oxygen molecules is first constructed. The combustion process is simulated by equilibrating the system at a specific temperature with ReaxFF. The reaction pathway can be figured out by characterizing the products generated during combustion. As the temperature can significantly affect the reaction pathway and products generated [12], the combustion under different temperatures is simulated. The formation of CO is detailedly analyzed. This understanding of CO release mechanisms in wood combustion can help us to reduce the deadly injury caused in a fire attack.

2   SIMULATION METHODS

2.1 Simulation details

Fig. 1 shows the structure of cellulose fibril at different scales. The cellulose fibril has a crystalline structure revealed by experiments [13]. The crystalline cellulose I_β has been found to be predominant in wood and accordingly is chosen as the representative cellulose model [14]. The cellulose has a monoclinic unit cell with dimensions of a = 7.8 Å, b = 8.2 Å, c = 10.4 Å and an angle γ = 96.5° at the ab plane. There are two parallel chains in the unit cell where one chain (the origin chain) is positioned at the corner of the unit cell parallel to the *c* axis direction, and the second chain (the center chain) passes through the center of the *ab* plane. Each chain in the unit cell is made up of two glucose residues linked by the β (1-4) glycosidic linkage [15]. To simulate the combustion of cellulose, a periodic system containing a chain with glucose residues bonded and 100 oxygen molecules is created in Materials Studio software from Accelrys [16]. The MD simulations are performed in LAMMPS [17] with a constant number of atoms in a constant volume where we control the temperature using a thermostat. The geometry optimization and energy minimization by conjugate gradient method are performed to the modeled structure. The structure is equilibrated for 1 ns in the isothermal and isochoric ensemble at different temperatures namely 2000 K, 2500 K and 3000 K. The total simulation time for the system is determined by the extent of oxidation for the bonded glucose residues and simulations are terminated when no further oxidation is observed.

2.2 Reactive forcefield

In the ReaxFF, all connectivity-dependent interactions (bond energy, valence angle energy, torsion angle energy, conjugation energy, the energies of van der Waals interaction and Coulomb interaction) are bond order dependent ensuring that the energy contribution disappears upon bond breaking. The bond order (BO`) in the ReaxFF is calculated directly from the instantaneous interatomic distance r_{ij} as expressed by [7]:

$$BO_{ij}' = \exp[p_{bo,1}(\frac{r_{ij}}{r_0^\sigma})^{p_{bo,2}}] + \exp[p_{bo,3}(\frac{r_{ij}}{r_0^\pi})^{p_{bo,4}}] + \exp[p_{bo,5}(\frac{r_{ij}}{r_0^{\pi\pi}})^{p_{bo,6}}] \tag{1}$$

where r_0 is the equilibrated distance between atom i and atom j; the $p_{bo,1}$ and $p_{bo,2}$ are the coefficient of the σ bond; $p_{bo,3}$ and $p_{bo,4}$ are the coefficient of the first π bond; and $p_{bo,5}$ and $p_{bo,6}$ are the coefficient of the second π bond. Since the bond orders and partial charges of atoms are updated in each MD time-step iteration, the connectivity of the system continuously changes over time [9]. ReaxFF can provide a good description of the structure and reactivity of the chemical systems with the CO traced formation and the CO variation quantified. The parameters of ReaxFF for hydrocarbons have been developed [18, 9] and used as the initial parameters. MD simulation with ReaxFF can be served as an effective approach to predict the chemical reactions involved in the combustion of various hydrocarbons.
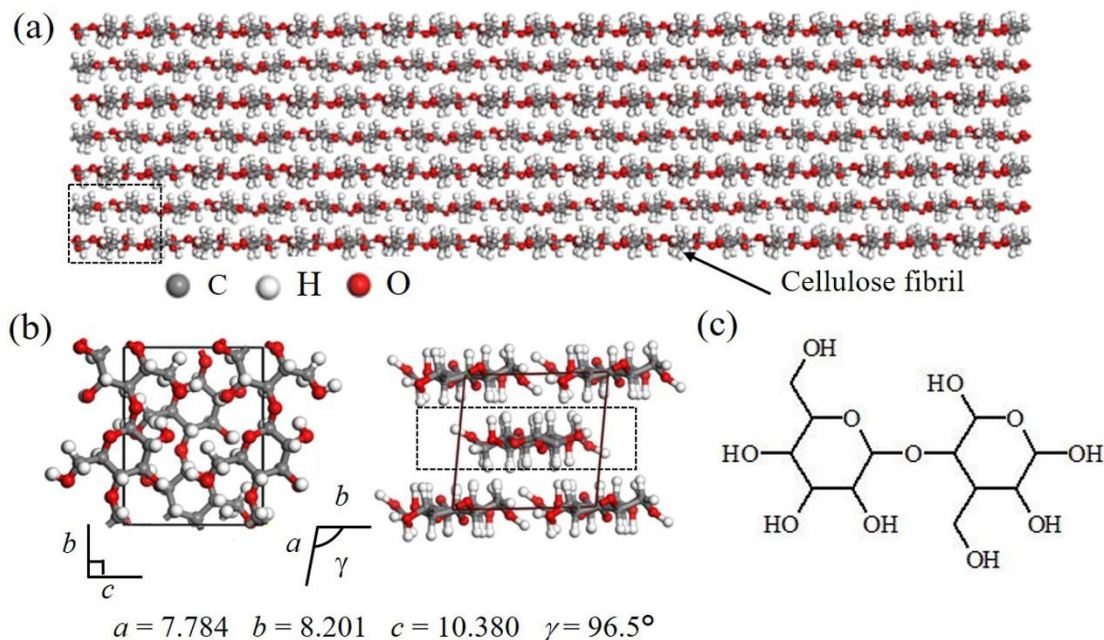

Fig. 1. (a) Structure of cellulose fibril where the linear chain is made up of glucose molecules. (b) the structure of a unit cell for the crystalline cellulose consisting of two parallel chains. (c) the molecular structure of each chain in the unit cell where two glucose residues are linked by the β (1-4) glycosidic linkage.

3   RESULTS AND DISCUSSIONS

Fig. 2 shows the examples of bond breaking and formation involved in the combustion simulation by using ReaxFF. The covalent bond between two glucose residues is firstly broken with the formation of the levoglucosan and the glucose at 2000 K and 2500 K as shown in Fig. 2(a). Then these molecules decompose into small molecules with low carbon content associated with dehydration as shown in Fig. 2(b). More energy can be provided at 3000 K leading to the bonded glucose residues directly break into molecules with low carbon content. Through analysis the reaction occurs MD simulation with ReaxFF the decomposition process, CO mainly comes from the decomposition of carboxyl group independent of the temperature as shown in Fig. 3. To validate the results predicted by MD with ReaxFF, the decomposition of the bonded glucose residues is also performed by quantum mechanical with density functional theory (DFT) calculation. The covalent energy terms including bond energy term, angle energy term and torsion angle energy term varied during the decomposition process predicted by ReaxFF is similar to that obtained by DFT. For a more robust validation, the experiment such as

thermogravimetric analysis coupling Fourier-Transform-Infrared spectroscopy will also be conducted to reveal the reaction mechanism in the combustion of cellulose.
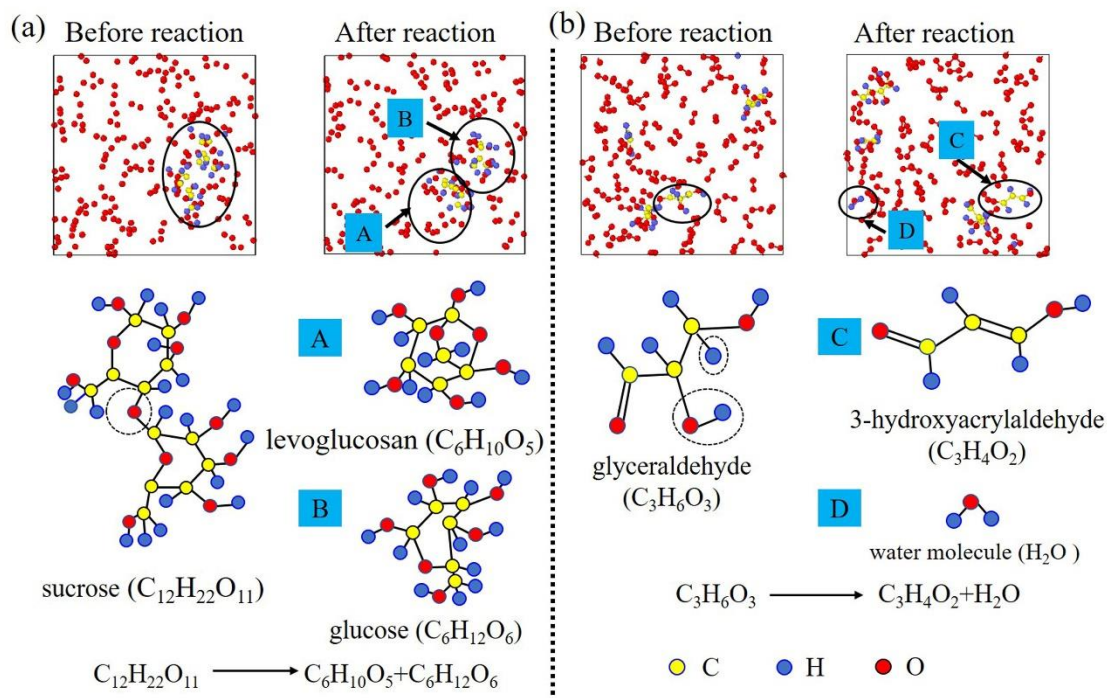
Fig. 2. Details of bond breakage and formation in the combustion of bonded glucose residues by MD with ReaxFF. The initially bonded glucose residues suffer from the thermal decomposition to form the levoglucosan and the glucose. During the decomposition, the intermediate product glyceraldehyde generated is decomposed to the 3-hydroxyacrylaldehyde by dehydration.
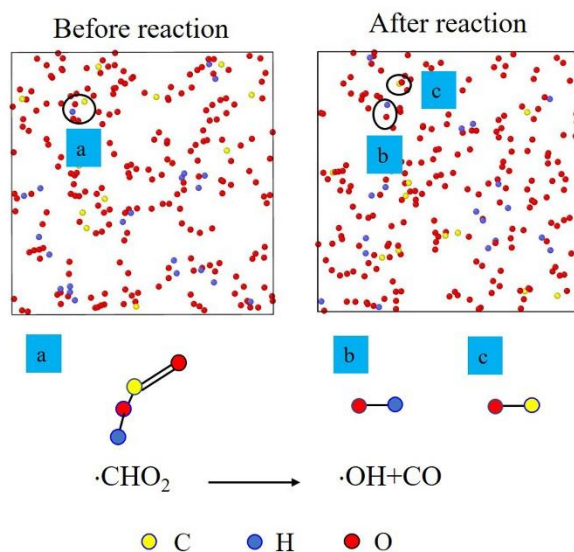

Fig. 3. Details of the decomposition for the carboxylic group with CO released.

After thermal decomposition, CO formed reacts with oxygen to form carbon dioxide (CO_2). *Fig .4* shows the probability of CO and CO_2 formation during the combustion process. It is clear that the CO is firstly released during the decomposition of the intermediate molecules. The number of formed CO is increased with the combustion time elongated. During the decomposition stage, CO_2 is also released. When the bonded glucose residues are totally decomposed into CO and CO_2, the content of CO is maximum. After that, the number of CO is reduced because of the oxidation of CO. Meanwhile, the peak value of CO formed rises with the temperature increased. This is because with the increment of temperature, small molecules with low carbon content are prone to form. The probability to form CO in increased temperature is improved. Comparing with the CO formed during the decomposition process, more time is required for the oxidation of CO into CO_2. Furthermore, with the increment of temperature, the time needed for complete oxidation is shorter. This is due to a higher temperature promotes the decomposition and improve the collision probability among atoms.
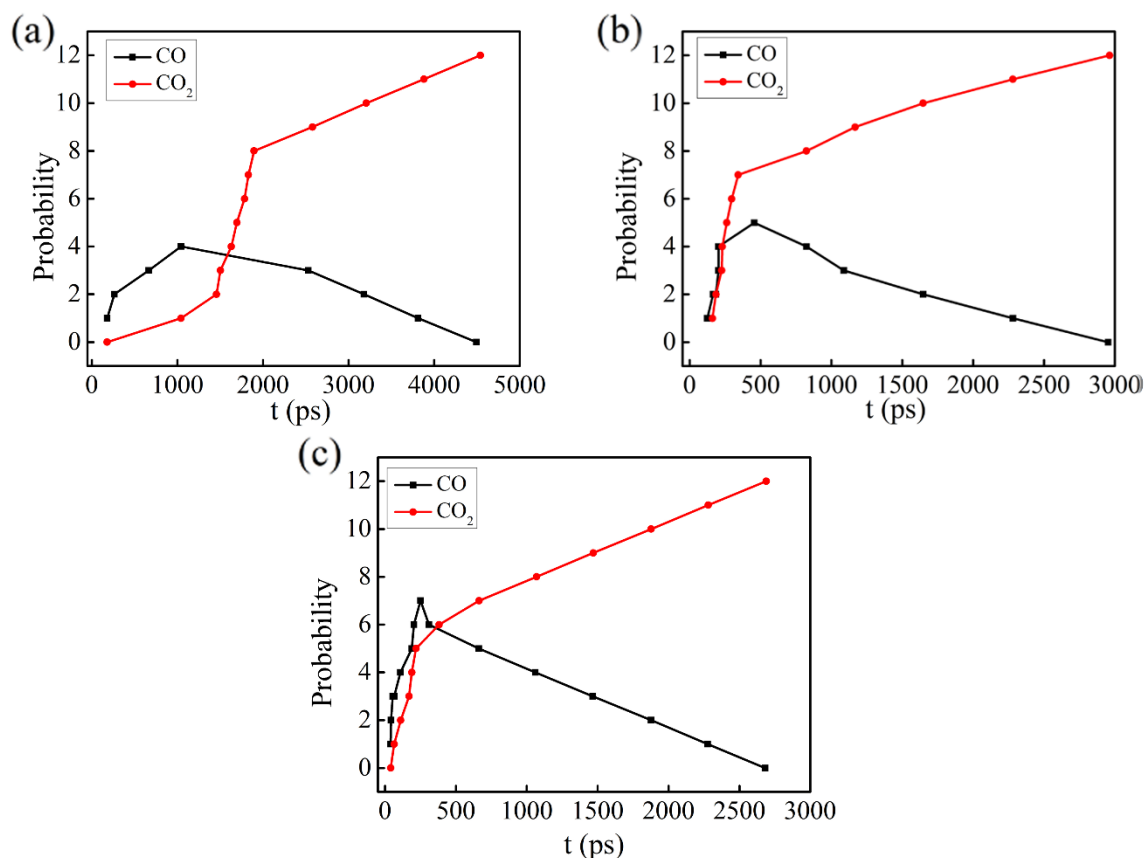
Fig. 4. The probability of CO and CO_2 formation at different temperatures (a) 2000 K; (b) 2500K; (c) 3000K. The CO is firstly formed following by CO_2 released during the decomposition process. The formed CO becomes to be oxidized with the formation of CO_2 when the number of CO reaches the peak.

In summary, although the oxidation is sufficient for complete combustion, CO is also formed during the combustion process. An adequate time of combustion can ensure that all the formed CO is oxidized to form CO_2. Generally, the combustion of bonded glucose residues can be divided into two stages. The first stage is related to the thermal decomposition of the bonded glucose residues with the formation of CO, CO_2, H_2O and intermediate molecules. Here, CO is mainly from the decomposition of the formed carboxyl group. The second stage is the oxidation

of CO to form CO_2. By comparing the time consumption for the two stages, the time for the oxidation process is several times longer than that for the thermal decomposition process.

4 CONCLUSIONS

As CO released in a fire of timber building severely threatens the life of human beings, an accurate understanding on the formation mechanism of CO is critical for its control. In this work, the chemical reaction pathway for the oxidation of cellulose is analyzed, and the CO release mechanism is revealed by using the MD with ReaxFF. The results of this work can be summarized as follows:

(1) The bonded glucose residues are firstly decomposed into molecules with low carbon content with the release of CO and CO_2.
(2) CO mainly comes from the carboxyl group formed which are independent of the temperature.
(3) When the bonded glucose residues are totally decomposed into CO and CO_2, the content of CO reaches the peak. The peak value is increased with temperature.
(4) CO is oxidized to form CO_2 after thermal decomposition. The time to complete oxidation is significantly longer than that for the completion of decomposition.

Our work provides an approach to establish the reaction mechanisms in the combustion because the details of the chain reaction for the combustion, including the intermediates, free radicals, the combustion products, and the energy change can be obtained. The ability to predict the combustion behavior lays a foundation for safe timber building design by controlling the CO generation.

ACKNOWLEDGMENT

REFERENCES

[1] Lowden L.A., Hull T.R. (2013). Flammability behavior of wood and a review of the methods for its reduction, Fire Science Reviews 2 (2013). doi:10.1186/2193-0414-2-4. 2013.09.12, 1–19 pp.

[2] Pitts W.M., Johnsson E.L., Bryner S.P. (1994). *Carbon monoxide formation in fires by high-temperature anaerobic wood pyrolysis*, Symposium (International) on Combustion, 25 (1994). doi.org/10.1016/S0082-0784(06)80789-7. 1994.04. 1455–1462 pp.

[3] Ragland K.W., Aerts D.J. (1991), *Properties of wood for combustion analysis*, Bioresource Technology, 37 (1991). doi.org/10.1016/0960-8524(91)90205-X. 1991.02, 161–168 pp.

[4] Hu Z.X., Utiskul Y.Y., Quintiere J.G., Trouve A. (2007). *Towards large eddy simulations of flame extinction and carbon monoxide emission in compartment fires*, Proceedings of the Combustion Institute 31 (2007). doi.org/10.1016/j.proci.2006.08.053. 2537–2545 pp.

[5] Leroch, S., Wendland M. (2012). *Simulation of Forces between Humid Amorphous Silica Surfaces: A Comparison of Empirical Atomistic Force Fields,* Journal of Physical Chemistry C 116 (2012). doi:10.1021/jp302428b. 2012.11.50, 26247–26261 pp.

[6] Duin A.C.T., Strachan A. Stewman S., Zhang Q.S., Xu X., Goddard W.A. (2003). *ReaxFFSiO Reactive Force Field for Silicon and Silicon Oxide Systems*. Journal of Physical Chemistry A, 107 (2003). doi:10.1021/jp0276303. 2003.04.19, 3803–3811 pp.

[7]   Zheng, M., Li X.X., Liu J., Guo L. (2013). Initial Chemical Reaction S*imulation of Coal Pyrolysis via ReaxFF Molecular Dynamics*, Energy & Fuels 27 (2013). doi:10.1021/ef400143z. 2013.05.06, 2942–2951 pp.

[8]   Diao, Z., Zhao Y.M., Chen B., Duan C.L., Song S. (2013). *Reactive force field for molecular dynamics simulations of epoxy resin thermal decomposition with model compound*, Journal of Analytical and Applied Pyrolysis, 104 (2013). doi.org/10.1016/j.jaap.2013.05.005. 2013.11.14, 618–624 pp.

[9]   Chenoweth K., Duin A.C.T., Goddard W.A. (2008). *ReaxFF Reactive Force Field for Molecular Dynamics Simulations of Hydrocarbon Oxidation*, Journal of Physical Chemistry 112 (2008). doi:10.1021/jp709896w. 2008.01.16, 1040–1053 pp.

[10]   Shafizaheh F. (1982). *Chemistry of pyrolysis and combustion of wood*, Progess in Biomass Conversion 3 (1982). doi.org/10.1016/B978-0-12-535903-0.50006-4. 1982.01.23, 51–76.

[11]   Babrauskas, V. (2005). *Charring rate of wood as a tool for fire investigations*, Fire Safety Journal 40 (2005). doi.org/10.1016/j.firesaf.2005.05.006. 2005.09.06, 528–554 pp.

[12]   Tam L.H., Zhou A., Yu Z.C., Qiu Q.W., Lau D. (2017). *Understanding the effect of temperature on the interfacial behavior of CFRP-wood composite via molecular dynamics simulations*, Composite Part B 109 (2017). doi.org/10.1016/j.compositesb.2016.10.030. 2017.01.10, 227-237 pp.

[13]   Nishiyama Y., Langan P., Chanzy H. (2002). *Crystal structure and hydrogen-bonding system in cellulose Iß from synchrotron X-ray and neutron fiber diffraction,* Journal of The American Chemical Society 124 (2002). doi:10.1021/ja0257319. 2002.07.10, 9074–9082 pp.

[14]   Hao H.L, Tam L.H., Lu Y., Lau D. (2018). *An atomistic study on the mechanical behavior of bamboo cell wall Constituents*, Composites Part B 153 (2018). doi.org/10.1016/j.compositesb.2018.05.046. 2018.10.15, 222–231 pp.

[15]   Gomes T.C., Skaf M.S. (2012). *Cellulose-builder: a toolkit for building crystalline structures of cellulose*, Journal of Computational Chemistry 33 (2012). doi: 10.1002/jcc.22959. 2012.03.15, 1338–1346 pp.

[16]   BIOVIA (2007), Accelrys Software Inc. Materials Studio.

[17]   Plimpton S. (1995). *Fast parallel algorithms for short-range molecular dynamics*, Journal of Computational Physics 117(1995). doi.org/10.1006/jcph.1995.1039. 1995.03.01, 1–19 pp.

[18]   [18] Duin A.C.T., Dasgupta S., Lorant F., Goddard III W.A. (2001) *ReaxFF: A reactive force field*

[19]   *for hydrocarbons*, Journal of Physical and Chemistry A 105 (2001). doi: 10.1021/jp004368u. 2001.09.22, 9396-9409 pp

EFFECT OF CHAR BURNING MECHANISM ON WOOD COMBUSTION

Islam Gomaa and Nour Elsagan

National Research Council of Canada, Ottawa, Canada

ABSTRACT

This work discusses the effect of char burning mechanism on overall wood heat release rate (HRR). Five different kinetic models for char combustion were used in numerical simulation of a cone calorimeter experiment. Results of heat release rate per unit area (HRRPUA) from the simulations were compared against the experimental results. The investigated models were variations of oxidation and gasification mechanisms. Oxidation mechanisms overestimated the char consumption and the overall HRR. The gasification mechanism underestimated the char consumption and the overall HRR from the wood sample. The best performance was obtained from a combined oxidation-gasification model. The model assumes parallel partial oxidation by oxygen and gasification by carbon dioxide forming carbon monoxide in the gas phase.

1   INTRODUCTION

Wood is a common fuel in compartment fires and is the primary fuel in wood based constructions. A validated wood combustion model would be valuable in simulating fire incidents involving wood as a fuel. Under fire conditions, wood undergoes pyrolysis then char combustion. This work investigates different char combustion models and their effect on overall HRR of wood. The evaluation was based on comparing the HRRPUA from a cone calorimeter experiment with a simulated cone calorimeter test. In the simulations, the wood pyrolysis model was kept the same while changing the char combustion model only. The software used for the simulations is the Fire Dynamic Simulator (FDS) [1]. FDS is a computational fluid dynamics (CFD) model of fire-driven fluid flow. The software uses Large eddy Simulations (LES) for modelling turbulent flow. FDS is developed by the National Institute of Standards and Technology (NIST) and VTT Technical Research Center of Finland [2].

The following subsections show the operating conditions for the cone calorimeter experiment and the numerical simulations parameters.

1.1. Experimental conditions for the cone calorimeter

- Heater temperature: ~760°C (incident heat flux ~ 50 kw/m^2)
- Sample surface dimensions: 10×10 cm
- Wood type: SPF #2
- Approximate density: 430 kg/m^3
- Moisture content: ~ 10%
- Backing: ~20 mm insulation and 3 mm steel plate

1.2. Numerical simulations parameters

- Domain dimensions: 0.4 m $\times$ 0.4 m $\times$ 0.4 m
- Cell size: 0.01 m $\times$ 0.01 m $\times$ 0.01 m
- Number of meshes: 16

- Heater temperature: 760°C
- Density: 430 kg/m^3
- Auto ignition temperature: 250°C [3]
- Moisture content: 10%

Figures 1- a, b and c show photos of the cone experimental setup, the numerical model and a snapshot of the temperature profile from the simulations; respectively.
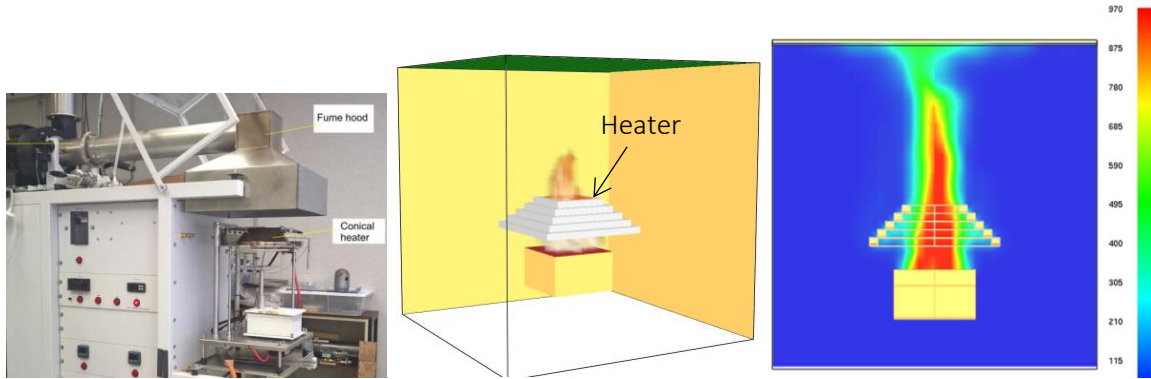
Fig. 2. Cone calorimeter a) experimental set and b) numerical modeling domain c) temperature distribution

1.3. HRR from the cone calorimeter experiment

The experimental HRR is presented together with the simulation results in the results and discussion section. The material used was an SPF wood sample. Experimental results show two distinct peaks of HRR; one peak at the beginning of the test and another peak around 2500~2800 seconds. There is a semi flat behaviour of HRR between these peaks followed by another semi flat section after the second peak. The second flat portion might be attributed to drift behaviour emanating from the gas analyzer in the cone. Ideally a gradual decay to zero HRR was expected when combustion has ceased.

2   GLOBAL WOOD REACTION MECHANISM

Figure 2 shows the global wood reaction mechanism that is used in the numerical simulations. The model was adopted from TGA experiments conducted by Bilbao et al. [4], [5]. In this model, wood consists of cellulose, hemicellulose and lignin. Each component undergoes thermal decomposition to generate volatile matter and char according to different kinetics. Then volatiles burn via a mixing controlled step to form combustion products. Char undergoes subsequent conversion to combustible gases or combustion products depending on the char burning mechanism. The effect of moisture was considered by including a mass percentage of moisture in the wood that evaporates at 100°C.
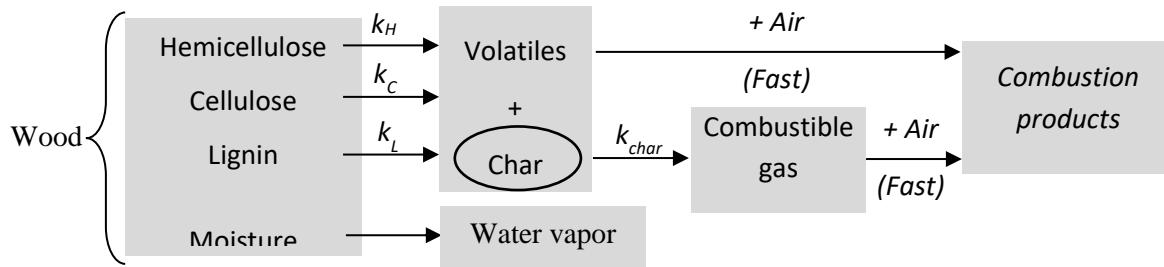
Fig. 3. Wood combustion model

Shown below are the stoichiometric coefficients and heat of reaction for each reaction step. Tables 1 and 2 present the kinetic parameters for each reaction and thermodynamic properties for each material; respectively.

Hemicellulose ➜ 0.8 Volatiles + 0.2 Char, ΔH = 450 kJ/kg, $k_H = A_H$ EXP$[-E_H/RT]$ (1)

Cellulose ➜ 0.8 Volatiles + 0.2 Char, ΔH = 450 kJ/kg, $k_C = A_C$ EXP$[-E_C/RT]$ (2)

Lignin ➜ 0.8 Volatiles + 0.2 Char, ΔH = 450 kJ/kg, $k_L = A_L$ EXP$[-E_L/RT]$ (3)

Moisture ➜ Water vapor, Reference temperature = 100°C   (4)

Volatiles + 6.37(Air) ➜ 7.37(Combustion Products), ΔH = -19313 kJ/kg   (5)

Char ➜ Combustible gases, ΔH & k_{char} are mechanism dependant   (6)

Combustible gas + (Air) ➜ Combustion Products, ΔH = mechanism dependant   (7)

Table 15. Kinetic parameters table

Material	Reaction rate	A (1/s)	E (kJ/kmole)	Ns (-)	Notes
Hemicellulose	k_H	9.83	4.27E4	1	[5]
Cellulose	k_C	3.02E7	1.13E5	1	[4]
Lignin	k_L	6.28E5	1.12E5	1	[4]
Char	k_{char}	Model dependant	Model dependant	Model dependant	
Moisture	NA	NA	NA	NA	evaporate @ 100°C
Volatiles	NA	Infinity	NA	NA	Mixing controlled
Combustible gas	NA	Infinity	NA	NA	Mixing controlled

Table 16. Thermodynamic properties [6]

Material	Conductivity (W/m.K)	Specific heat (kJ/kg.K)	Absorption Coefficient (1/m)	Emissivity (-)	Density (kg/m³)
Wood (all three components)	$0.182(T/293)^{0.679}$	$1.68(T/293)^{0.649}$	1000	0.76	380
Char	$0.089(T/293)^{0.304} + (2.9E-3)\sigma(T)^3$	$1.445(T/293)^{0.266}$	7000	0.973	76

where T is temperature in Kelvins and σ is Stefan–Boltzmann constant (5.67E-8 W/m²·K⁴)

3   CHAR REACTION MECHNAISMS

Five reaction mechanisms for char combustion have been considered to model char consumption. The simulated HRRPUA from each mechanism was compared against the HRRPUA from a cone calorimeter experiment. The five mechanisms are:

- No char combustion
- Single step char combustion
- Two-step char combustion
- Char gasification
- Combined oxidation-gasification model

The following subsections discuss each mechanism tested in the simulations and the results are further shown in section 4.

3.1. No char combustion

First, char combustion was neglected in the simulations. The reaction rate of char combustion is relatively slow compared to pyrolysis reactions of wood components (i.e lignin, cellulose and hemicellulose). Accordingly, in a fire incident, the contribution of char combustion to the HRR was expected to be much less than that of wood components. In this simulation char layer keeps growing and never gets consumed.

3.2. Single-step char combustion

The first and simplest model to be considered as a char combustion mechanism is a single-step oxidation by oxygen producing carbon dioxide (*Eq. (8)*).

$$\textbf{Char (\~Carbon) + O}_2 \rightarrow \textbf{ char combustion products (\~CO}_2\textbf{)} \qquad \textbf{(8)}$$

Ideally, if char is purely made out of elemental carbon and CO_2 is the only product, the heat of reaction should be ΔH=-393.5 kJ/mole or ~32.8 MJ/kg_{carbon}. However, char produced from wood pyrolysis has some ash content and its chemical composition might contain trace amounts of hydrogen, oxygen and nitrogen. Also, char combustion, in a fire scenario, might not be 100% complete (i.e. trace amount of carbon monoxide might exist in the combustion products). So, a value of *25 MJ/kg_{char}* was used as a total heat of combustion of char in this study.

In this model, the total heat of combustion is generated within the char (i.e. within the solid phase). This results in exponential acceleration of the reaction rate of char combustion. This is because reaction rates in the Arrhenius expression are exponential function in temperature.

Several values of kinetic parameters were selected from the literature to be used in the numerical simulations. In all cases, the kinetic parameters were obtained using TGA experiments of char reacting with air or oxygen. The kinetic parameters from each reference are shown in Table 17.

Table 17. Kinetic parameters from each reference

rate #	A	E	n_s	n_{O2}	Reference
1	2.38E8	1.25E5	0.49	0.53	[7]
2	9.02E13	1.926E5	1.51	1.91	[6]
3	5.67E9	1.6E5	1	0.78	[8]
4	1.4E11	1.826E5	0.9	-	[9]
5	4.85E14	2.286E5	1.16	-	[9]

3.3. Two-steps char combustion

A possible mechanism for char combustion is the two-steps char oxidation mechanism; the first step is partial oxidation of char/carbon to form carbon monoxide (CO) that diffuses outside the char layer and into the gas phase. The second step is CO combustion to CO_2.

The mechanism for the two-step model can be expressed using the following reactions:

Char (~C) + ½ O_2 ➔ partial combustion products (~CO)   (9)

Partial combustion products (~CO) + ½ O_2 ➔ complete combustion products (~CO_2) (10)

Ideally, if char is purely made out of carbon and CO_2 is the only end product, heat of reactions for *Eq. 9 and 10* should be ΔH= -110.5 kJ/mole or ~-9.21 MJ/kg$_{carbon}$ and ΔH= -283 kJ/mole or ~ 23.58 MJ/kg$_{carbon}$; respectively. Realistically, the ideal heat of reactions for *Eq. 9* and *10* were scaled down by the realistic total heat of combustion of char (i.e. multiplied by *25/32.8*) to account for ash content and incomplete combustion of char to CO.

The kinetic parameters of this mechanism are the same as the single step mechanism. However, the major difference is the portion of the overall char heat of combustion that occurs within the solid phase versus the portion that occurs in the gas phase. Although, the total heat of combustion form both mechanisms are equal and the kinetic parameters for the solid phase pyrolysis are the same, the rate of char consumption and overall rate of wood combustion are slower (see subsections 4.2 and 4.3). In this mechanism only 28% of the total heat of combustion occurs in the solid phase. To put this into perspective, the following governing equations are considered [2];

$$\rho_s c_s \frac{\partial T_s}{\partial t} = \frac{\partial}{\partial x}\left(k_s \frac{\partial T_s}{\partial x}\right) + \dot{q}_s''' \quad \text{(11), where} \quad \dot{q}_s''' = \dot{q}_{s,c}''' + \dot{q}_{s,r}''' \quad \text{(12)}$$

Equation *11* is the solid phase conduction heat transfer equation. Where T_s is the solid phase temperature, x is the depth, k_s is the thermal conductivity, c_s is specific heat and $\dot{q}_s'''$ is a heat source term in the solid phase consisting of heat from chemical reactions and radiation heat transfer.

Where, $\dot{q}_{s,c}'''$ is the heat production/loss rate per unit volume as a result of the solid phase reactions

The chemical source term $\dot{q}_{s,c}'''$ is expressed as follows:

$$\dot{q}_{s,c}'''(x) = -\rho_s(0) \sum_{\alpha=1}^{N_m} \sum_{\beta=1}^{N_{r,\alpha}} r_{\alpha\beta}(x) H_{r,\alpha\beta} \quad \text{(13)}$$

where $H_{r,\alpha\beta}$ is the heat of reaction and "$r_{\alpha\beta}$" is the reaction rate. α is an index for material components. β is an index for the number of reaction. The reaction rate expression within the solid phase would be:

$$r_{\alpha\beta} = \left(\frac{\rho_{s,\alpha}}{\rho_s(0)}\right)^{n_{s,\alpha\beta}} A_{\alpha\beta} exp\left(-\frac{E_{\alpha\beta}}{RT_s}\right) \left[X_{O_2}(x)\right]^{n_{O_2,\alpha\beta}} \quad \text{(14)}$$

Where, $n_{s,\alpha\beta}$ is the solid phase reaction order, *A and E* are Arrhenius kinetic parameters, $X_{O_2}(x)$ is the oxygen volume fraction at depth *(x)* and $n_{O_2,\alpha\beta}$ is the reaction order with respect to oxygen volume fraction within the solid phase.

Looking at the governing equations *11 to 14*, one can see that the reaction rate "*r*" depends on the solid phase temperature "T_s" which depends on $\dot{q}_{s,c}'''$ which depends on "H_r" and "*r*": Higher "H_r" results in higher $\dot{q}_{s,c}'''$, which results in higher $\frac{\partial T_s}{\partial t}$ (i.e. faster heating rate of the solid phase) which

results in faster reaction rate "*r*". This explains the theoretical difference between the two mechanisms.

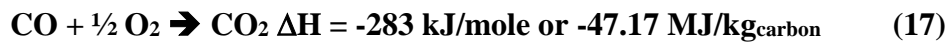### 3.3.1. Effect of diffusion depth

Oxidation of char is a heterogeneous reaction which involves the diffusion of oxygen into the solid phase (i.e char). The concentration of oxygen within the solid phase is calculated in FDS based on the assumption of simultaneous diffusion and consumption of oxygen so that the concentration profile within the solid phase is in equilibrium. The volume fraction of oxygen (X_{O_2})at any depth (x) within the solid phase is calculated in FDS using the following equation [2]:

$$X_{O_2}(x) = X_{O_2,g} \, exp(\frac{-x}{l_g}) \qquad (15)$$

Where $X_{O_2,g}$ is the gas phase oxygen volume fraction and l_g is the diffusion depth. The diffusion depth is an input to the model. A higher value assigned for l_g means higher $X_{O_2}(x)$, which consequently increases the rate of char oxidation (See Eq. 14). In this study, four different diffusion depths were investigated; 1, 0.1, 0.01 and zero mm.

3.4. Char gasification

Another mechanism for char consumption is gasification. In this mechanism, char is gasified by its combustion product, carbon dioxide (CO_2), to form CO. CO then reacts with oxygen in the gas phase, to form CO_2. This model is usually called the two film model [10]. The first/outer film is the CO_2 film. The second/inner film is the CO film. This mechanism is well known in the field of coal combustion. The conditions for this mechanism are fast reaction rates that results in a short chemical time scale in comparison to the diffusion time scale. Under these conditions, oxygen doesn't reach the surface of char. Oxygen is consumed by carbon monoxide (CO) to form a high concentration of carbon dioxide (CO_2) film. In this model, the rate of char consumption is limited by the rate of CO_2 gasification reaction. Ideally, if char is purely made out of elemental carbon, the mechanism would be as follows:

$$C(s) + CO_2 \rightarrow 2CO \; \Delta H = +172.51 \text{ kJ/mole or } 14.37 \text{ MJ/kg}_{carbon} \quad (16)$$

$$CO + \tfrac{1}{2} O_2 \rightarrow CO_2 \; \Delta H = -283 \text{ kJ/mole or } -47.17 \text{ MJ/kg}_{carbon} \qquad (17)$$

The ideal heat of reactions from *Eq. 16* and *17* have been scaled down by the realistic total heat of combustion of char (i.e. multiplied by *25/32.8*).

There are two main differences in this mechanism compared to the previous combustion mechanisms. The first difference is that the solid phase reaction is endothermic. The second difference is that the reaction rate is much slower than the combustion rate even at the same temperatures. Given the governing equations *11 to 14*, this mechanism should result in slower char consumption and a lower HRR curve in general.

3.5. Combined oxidation-gasification model

The last model is a combined oxidation-gasification mechanism. Based on the results from the previous models (section 4), it became clear that a better mechanism to model char combustion is

to consider the combustion route as well as the gasification route. If the temperature of char was low (i.e. 300 ~ 500C), the two-step oxidation mechanism would be a suitable model since reaction rate would be slow allowing for oxygen to diffuse into the char. However, if the char temperature was very high, gasification by CO_2 would be the most probable scenario. For intermediate temperature range both mechanisms would contribute to the char consumption. In the proposed model, char is being consumed partially by O_2 and partially by CO_2. It is important to note that the O_2 reaction is exothermic and CO_2 reaction is endothermic. The reactions of this model should be as follows:

$$Char(\sim C) + CO_2 \rightarrow 2CO \quad (18)$$

$$Char(\sim C) + \tfrac{1}{2} O_2 \rightarrow CO \quad (19)$$

$$CO + \tfrac{1}{2} O_2 \rightarrow CO_2 \quad (20)$$
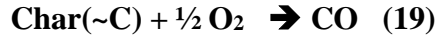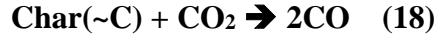
Ideally, the governing equations of species transport (the convection-diffusion equation) and species diffusion inside the solid phase should determine the contribution of each reaction in the overall char consumption. However, in FDS, the profile of O_2 concentration within the solid phase is imposed by defining a gas diffusion depth parameter in the input file. Also, the resolution of the gas phase mesh is not fine enough to resolve the gradient of O_2 and CO_2 near the char surface which is important to determine the diffusion rate of O_2 and CO_2 through the gas phase towards the char surface. Because of that, *Eq. 18 and 19* were combined. The combined reaction is given in *Eq. 21*. The complementary gas phase reaction would be *Eq.22*.

$$Char (\sim C) + xO_2 + yCO_2 \rightarrow zCO \quad (21)$$

$$zCO + lO_2 \rightarrow mCO_2 \quad (22)$$
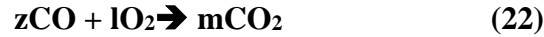
The kinetic parameters and heat of reaction for *Eq. 21* were obtained by finding values that provides the best possible fit for the experimental HRR curve. Kinetic parameters and the heat of reaction were limited within the range of kinetic parameters and heat of reactions corresponding to partial oxidation and gasification. The final kinetic parameters and heat of reactions are given in Table 18.

Table 18. Combined oxidation-gasification kinetic parameters (Best cone calorimeter HRR fit)

Reaction #	A(1/s)	E(kJ/Kmol)	n_s	n_{O2}	ΔH
R. 16	2E4	1.2E5	1	-	+1000 kJ/kg$_{char}$
R. 17	Mixing controlled	Mixing controlled	NA	NA	-26000 kJ/kg$_{char}$

4   RESULTS AND DISCUSSION

4.1. No char combustion

Figure 3 shows the experimental HRRPUA compared to the simulation result. As discussed in section 3.1, it was assumed in this simulation that char is formed and gets accumulated with no further reaction. Generally, the figure shows lower heat release from the simulation relative to the experiment. Moreover, the simulation was not able to capture the second heat release peak from the experiment. This model overestimates the protective effect of char since char forms a non-reactive layer on the wood surface. However, this is not the real behaviour observed from the

experimental results. Consequently, char oxidation models were explored in the following simulations.

4.2. Single step char combustion

First, oxidation of char to carbon dioxide in one step was conducted using the 5 rates stated in table 3. The results are presented in Fig. 4a.The figure shows that, assuming one step oxidation of char resulted in very high heat release in a very short period. This is attributed to the fact that all the exothermic heat of char oxidation was released within the wood sample in this model.
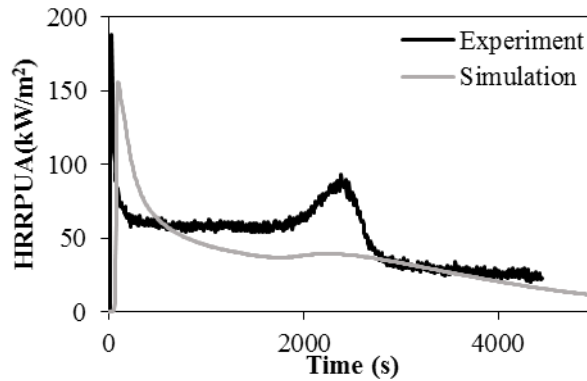
Fig. 4. Experimental and simulations results for HRRPUA. Simulations are assuming no further char reactions
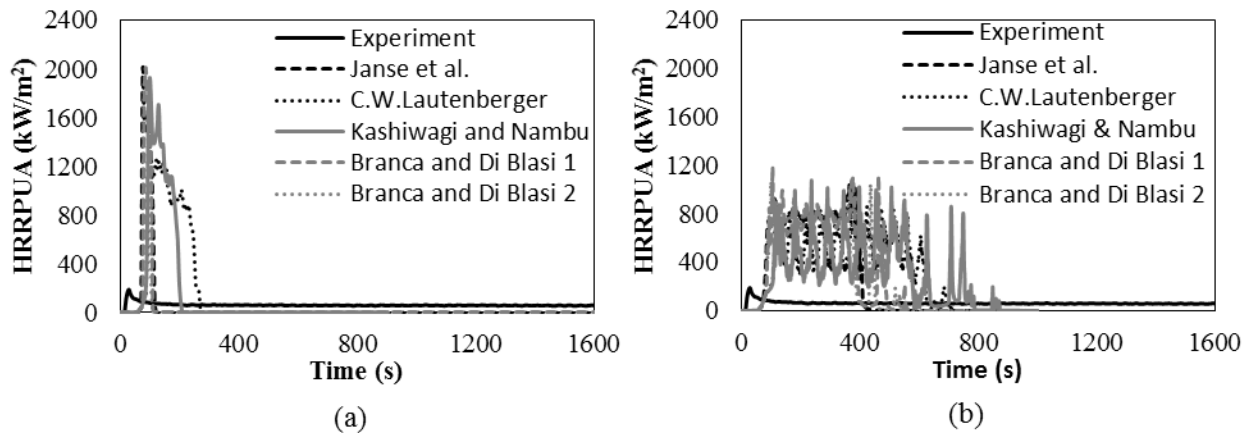
Fig. 5. Experimental and simulations results for HRRPUA. Simulations are assuming (a) single step char oxidation, (b) two-step char oxidation; both using 5 rates

4.3. Two-step char combustion

Simulations were then performed using the same 5 rates in table 3 using the two-step char oxidation model. Details of this model are given in section 3.3. The simulation results are compared to the experimental HRRPUA in Fig. 4b. The HRRPUA from the simulations using the different reaction rates are still much higher than the experimental one and the wood is completely consumed in shorter time in the simulations. On the other hand, the results showed lower heat release and longer duration compared to the results of one-step oxidation mechanism presented in Fig.4a. This is due

478

to the release of all the heat of char combustion within the solid phase in the one-step mechanism, while only ~28% of the heat of combustion is released in the solid phase in the two-step mechanism. This resulted in different rates of consumption of wood components as demonstrated by Fig. 5a.

Figure 5a shows the profiles of the density of cellulose; as a representative of wood components versus time. Those profiles are from the simulations using 4 different mechanisms; one-step oxidation, two-step oxidation, gasification and the combined model. It can be clearly seen that, the rate of consumption of cellulose in case of the one-step mechanism is higher than that in case of the two-step mechanism.

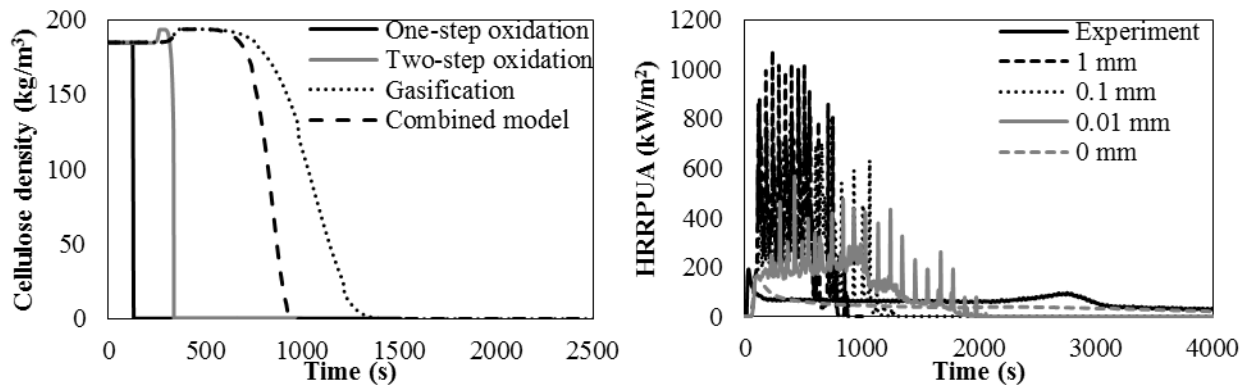Fig. 6. (a) Cellulose density profiles from simulations using four different mechanisms; one-step oxidation, two-step oxidation, gasification and the combined model, (b) Experimental and simulations results for HRRPUA. Simulations are assuming two-step oxidation of char and using the rate parameters from Takashi and Numba [8]. Four diffusion depths are used; 1, 0.1, 0.01 and 0 mm.

4.3.1. Effect of diffusion depth

In all the simulations presented earlier; the diffusion depth applied in the model was 1 mm. However, diffusion depth of O_2 into the solid material (i.e char) might be another factor affecting the rate of char consumption. Four different diffusion depths; 1, 0.1, 0.01 and zero mm were investigated. In the four simulations, the rate from Takashi and Numba [8] was used and two-step char oxidation was assumed. The results are shown in Fig. 5b. Decreasing the diffusion depth decreases the rate of char consumption where less char mass is allowed to react with O_2. Smaller diffusion depth resulted in lower heat release over a longer duration. It is worth mentioning that the results from 0 mm diffusion depth simulation (surface reaction assumption) are similar to those neglecting the char reaction (Fig. 4).

4.4. Char gasification

Gasification of char by CO_2 was also tested in our simulations. The results are shown in Fig. 7a. As expected, the HRRPUA from the simulation is lower than the experimental one. This is attributed to the fact that, the reaction is highly endothermic compared to the oxidation reactions which lowers the pyrolysis rates of the wood components. This can be seen when comparing the density profile of cellulose (as a representative of wood components) in case of gasification and two-step oxidation in Fig. 5a.
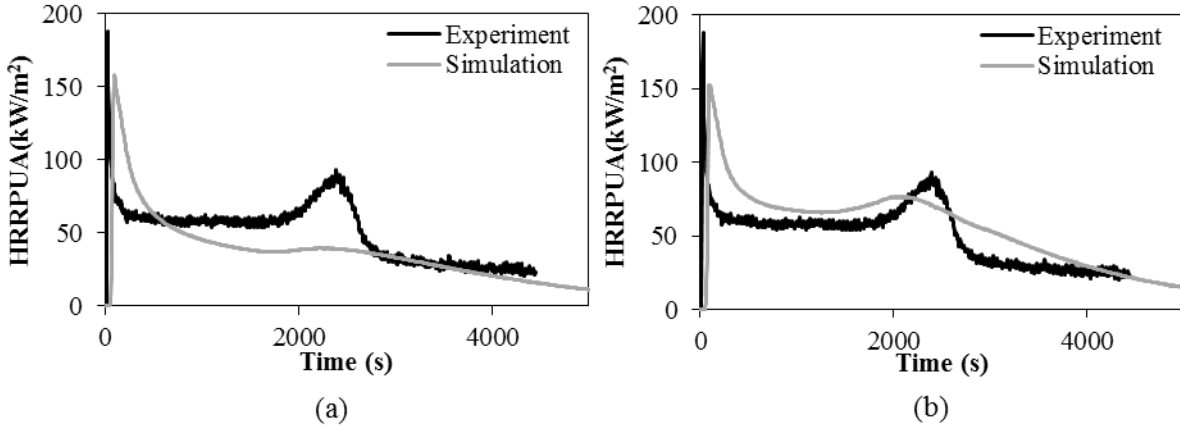
Fig. 7. Experimental and simulations results for HRRPUA. Simulations are (a) assuming char gasification mechanism, (b) using the combined model

4.5. Combined combustion-gasification model

The rates presented in table 4, for the combined combustion-gasification model, were applied in the simulation and resulted in a good fit with the experimental data as seen in Fig. 6b. The model predicted the magnitudes of the initial HRR peak and the second peak around the 2200 ~ 2500 seconds mark. This confirms the hypothesis that char consumption in fire scenarios is best modeled by considering gasification as well as partial oxidation routes. Oxidation models seem to overestimate char consumption. While gasification model seems to underestimate the char consumption. It is worth noting that the heat of reaction for the combined model is endothermic, indicating that the combined model leans slightly towards the gasification route.

On the other hand, in this model, the rate of cellulose consumption is higher than that using the gasification and less than that using the two-step oxidation model (see Fig.5)

5   CONCLUSIONS

- The effect of different mechanisms for char consumption on wood combustion was investigated
- It was concluded that different mechanisms, diffusion depth and distribution of heat release between solid and gas phases affect the HRR profile.
- A best fit model that represents a combination of char oxidation and gasification was developed
- Results from the combined combustion-gasification model was compared against experimental HRR data from a cone calorimeter experiment and predicted the trend of the HRR curve with good accuracy.

REFERENCES

[1]   K. McGrattan, S. Hostikka, R. McDermott, J. Floyd, C. Weinschenk, and K. Overholt, "Fire Dynamics Simulator User's Guide," NIST, 1019, Jan. 2017.
[2]   K. McGrattan, S. Hostikka, R. McDermott, J. Floyd, C. Weinschenk, and K. Overholt, "Fire Dynamics Simulator Technical Reference Guide Volume 1: Mathematical Model," NIST, 1018-1, Jan. 2017.

[3]   V. Babrauskas, "Ignition of Wood: A Review of The State of The Art," presented at the Interflam, London, 2001, pp. 71–88.

[4]   R. Bilbao, A. Millera, and J. Arauzo, "Thermal Decomposition of Lignocellulosic Material: Influence of The Chemical Composition," *Elsevier Sci. Publ.*, vol. 143, pp. 149–159, 1989.

[5]   R. Bilbao, A. Millera, and J. Arauzo, "Kinetics of Weight Loss by Thermal Decomposition of Xylan and Lignin. Influence of Experimental Conditions," *Elsevier Sci. Publ.*, vol. 143, pp. 137–148, 1989.

[6]   C. Lautenberger, "A Generalized Pyrolysis Model for Combustible Solids," PhD Thesis, University of California, Berkeley, 2007.

[7]   A. M. C. Janse, H. G. de Jonge, W. Prins, and W. P. M. van Swaaij, "Combustion Kinetics of Char Obtained by Flash Pyrolysis of Pine Wood," *Ind. Eng. Chem. Res.*, vol. 37, no. 10, pp. 3909–3918, Oct. 1998.

[8]   T. Kashiwagi and H. Nambu, "Global kinetic constants for thermal oxidative degradation of a cellulosic paper," *Combust. Flame*, vol. 88, no. 3, pp. 345–368, Mar. 1992.

[9]   C. Branca and C. Di Blasi, "Global Kinetics of Wood Char Devolatilization and Combustion," *Energy Fuels*, vol. 17, no. 6, pp. 1609–1615, Nov. 2003.

[10]   S. R. Turns, *An Introduction to Combustion: Concepts and Applications*, 3 edition. New York: McGraw-Hill Education, 2011.

REINFORCED CONCRETE TUNNELS EXPOSED TO FIRE: EFFECTS OF GEOMETRY AND FIRE CURVE

Francesco LO MONTE1, Patrick BAMONTE1 and Carlo BELTRAMI2
1Department of Civil and Environmental Engineering, Politecnico di Milano, Milan (Italy).
2Lombardi Ingegneria S.r.l., Milan (Italy).

ABSTRACT

Fire represents a severe condition for tunnels due to (a) the geometric features of the compartment which favours the achievement of very high temperatures and makes the intervention by fire brigades difficult, (b) the structural redundancy leading to significant indirect actions, and (c) the sizable sensitivity to fire spalling due to the relevant compression generally characterizing the lining. Repair time and cost past the fire are also critical issues, since the revenue loss connected to traffic disruption must also be considered. Within this context, this paper addresses the effect of structural choices in tunnel fire resistance, by comparing the performance of two different solutions: (1) cast-in-situ and (2) pre-cast segmental tunnel linings. To this aim, finite element analyses have been performed, proving that (I) increasing thickness and redundancy does not necessarily lead to a higher safety factor and (II) fire cooling phase (if any) must be properly taken into account.

1   INTRODUCTION

Fire represents a very stressing condition for tunnels, due to several features. On the one hand, the geometry of the compartment and the type of combustible materials (such as fuel) can lead to very high temperatures (even higher than 1000°C [1]). On the other hand, the structural layout and the mostly compressive stress state foster the introduction of significant indirect actions, which can lead to a marked increase of the initial state of stress. The aforementioned reasons strongly push for the proper evaluation of fire performance in the design phase of tunnels.

Generally speaking, concrete proves to have a satisfactory mechanical behaviour in fire owing to its incombustibility and thermal insulation capability. Fire spalling, however, due the violent expulsion of debris from the exposed layers, can jeopardize the thermal protection of the rebars, dramatically increasing the overall decay of the bearing capacity. Furthermore, time and cost of the repair phase after the fire should be properly taken into account, since the revenue loss connected to traffic disruption can be very high. Hence, avoiding spalling (for instance by introducing polypropylene fibres in the concrete mix) is of primary importance for this kind of structures.

When addressing the structural performance in natural/parametric fires, namely fires with both heating and cooling phases, another critical aspect is represented by the material properties variation. EN 1992-1-2 [2], in fact, provides all the main materials' properties as functions of temperature for concrete and steel in hot conditions, while just a few (and not so comprehensive) indications are given for the residual (after the fire) conditions. However, the structural behaviour in the cooling phase must be verified, so to guarantee the safety for the fire brigades. In this regard it is worth noting as the irreversible chemo-physical changes taking place in heated concrete make material properties dependant on the maximum temperature reached at a given

482

point rather than on the actual one [3], thus making it necessary to adopt approaches based on thermal envelopes.

In the following, the comparison in terms of fire resistance between two different technological solutions for a tunnel lining is presented, namely (1) cast-in-situ and (2) pre-cast segmental tunnel linings. Finite element analyses have been performed in order to study the effect of lining thickness and to highlight possible critical points regarding the cooling phase of the fire.

2 STRUCTURAL CASE

2.1 Geometry and construction technology

The study focuses on the comparison in terms of fire performance between two different solutions considered as alternatives for a concrete tunnel lining: (1) cast-in-situ lining (Fig.1a) and (2) pre-cast segments (Fig.1b). The first solution is characterized by the typical shape for this kind of structures, with a lining thickness of 0.9 m, consisting of ordinary concrete (f_{ck} = 28 MPa). On the other hand, the segmental tunnel lining consists of 7 segments with a thickness of 0.32 m, made of polypropylene fibre concrete (f_{ck} = 50 MPa). The cast-in-situ solution is consistent with traditional boring methods, while the pre-cast segmental tunnel lining is compatible with the use of Tunnel Boring Machine (TBM).

(a)   (b)
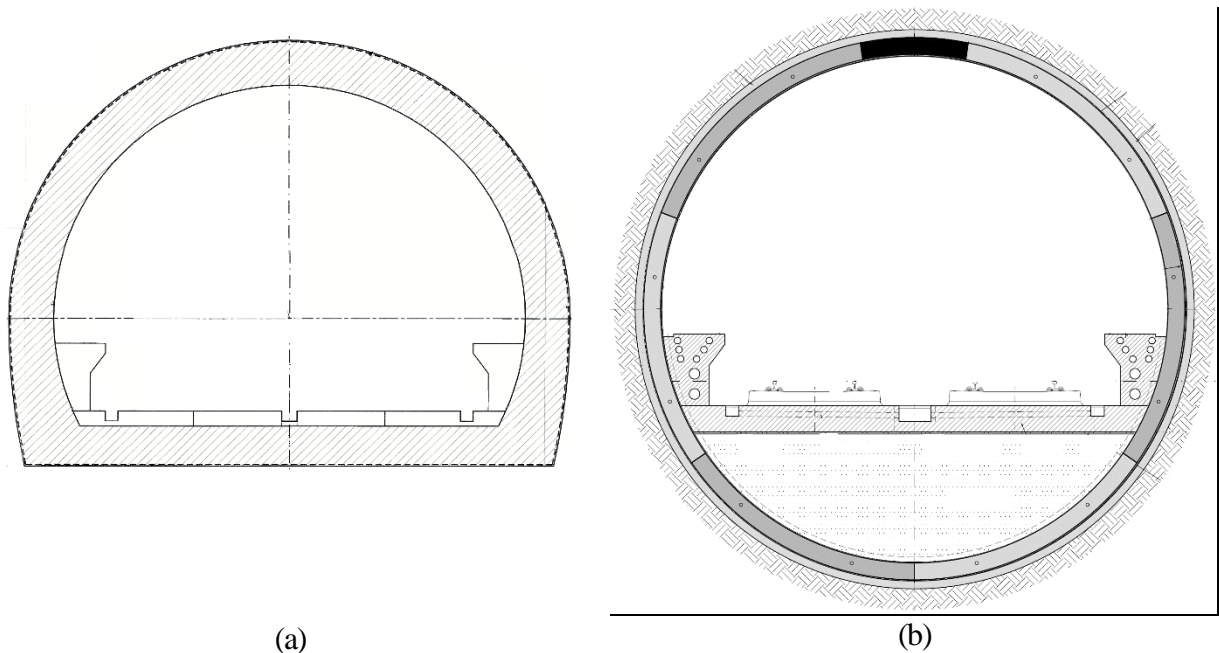
Figure 1. Cast-in-situ (a) and pre-cast segmental (b) tunnel lining.

2.2 Fire scenario

In order to assess the fire performance of the two tunnel linings, Standard Fire has been adopted (Fig.2) as requested by the designers in accordance to the Italian codes, with a heating duration of 180 minutes (chosen as common reference in the practice). In addition to the heating phase, the subsequent cooling phase has been also considered, by adopting the temperature decay curve suggested in EN 1991-1-2 (Fig.2). Accounting for the cooling phase is instrumental for

monitoring the structural safety factor during the whole fire duration, and to verify the compatibility of the intervention by fire brigades.

Figure 2. Standard Fire curve according to EN 1991-1-2 [2].

3   FINITE ELEMENT MODELLING

3.1 Material properties of concrete and steel under heating

Thermo-physical properties of concrete, such as thermal deformation, density, thermal conductivity and specific heat, have been defined according to EN 1992-1-2, neglecting the presence of moisture in concrete when cal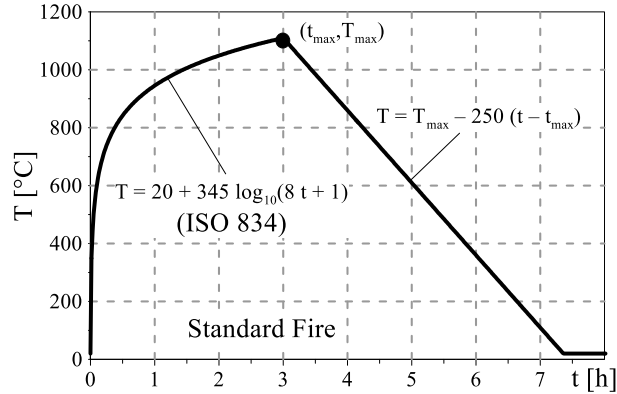culating the specific heat (this being the most severe condition). The density at room temperature is assumed as 2350 kg/m^3 (typical value for concrete), while the proposed lower limit of EN 1992-1-2 is considered for the variation of thermal conductivity.

The overall deformative behaviour can be expressed as the sum of 4 different contributions:

$$\varepsilon_{tot}(\sigma,T,t) = \varepsilon_{th}(T) + \varepsilon_{\sigma}(\sigma,T) + \varepsilon_{tr}(\sigma,T) + \varepsilon_{cr}(\sigma,T,t) \tag{1}$$

where ε_{th} is the free thermal dilation, and the other terms depend on the load and are the instantaneous load-induced strain, the thermal-transient strain and the thermal creep, respectively.

The implicit approach of EN 1992-1-2 is based on lumping the load-related contributions as follows:

$$\varepsilon_{tot}(\sigma,T,t) = \varepsilon_{th}(T) + \varepsilon_{\sigma,tr,cr}(\sigma,T) \tag{2}$$

As a consequence, the total load-induced strain in compression $\varepsilon_{\sigma,tr,cr}$ can be defined as:

$$\sigma(T) = 3 \cdot (\varepsilon_{\sigma,tr,cr} / \varepsilon_{c1}{}^T) \cdot f_c{}^T / [2 + (\varepsilon_{\sigma,tr,cr} / \varepsilon_{c1}{}^T)^3] \tag{3}$$

Such stress-strain low is known once the values of hot compression strength $f_c{}^T$ and related peak strain $\varepsilon_{c1}{}^T$ are defined. Such values are given by EN 1992-1-2 as functions of temperature, for siliceous or calcareous aggregates. To be conservative, in the following, siliceous concrete is considered. Although not explicitly reported in EN 1992-1-2, the decay of the elastic modulus with the temperature can be defined by evaluating the elastic modulus (tangent to the origin or

secant) of the constitutive law of Eq. (3). In this document the secant elastic modulus at 50% of the compressive strength is used, for all temperatures.

As regards the steel reinforcement, the behaviour is fully described in EN 1992-1-2, differentiating between ordinary and pre-stressing steel, and between hot-rolled or cold-worked steel. In this paper, the decay curve for hot-rolled steel is implemented.

3.2 Material properties in the cooling phase

As regards concrete, the decrease in density and thermal conductivity, as well as the increase in specific heat, are linked to the evaporation of free and chemically-bound water in the pores and to the increase in porosity. Since these processes are mostly irreversible, density, conductivity and specific heat during cooling are defined at any point of the model referring to the maximum temperature reached up to the given instant of analysis, and not as a function of the actual one.

The same approach has been used for elastic modulus and strength, since their decay is linked to irreversible processes such as (1) micro- and macro-cracking that takes place in the cement paste during heating due to shrinkage, thermal incompatibility between cement paste and aggregates, and self-stresses, and to (2) intrinsic degradation of the concrete constituents.

With regard to thermal expansion, the experimental tests indicate a partial recovery in the cooling phase. Therefore, total reversibility is conservatively assumed in the analyses.

3.3 Geometry and boundary conditions

Thermo-mechanical numerical analyses have been performed via the commercial finite element code Abaqus.

The two different solutions have been modelled via 3D 8-nodes finite elements in order to duly take into account the thermal gradients along the thickness and the subsequent thermal stresses. The geometrical models are reported in Fig.3, where the exposed surfaces are highlighted in red colour.
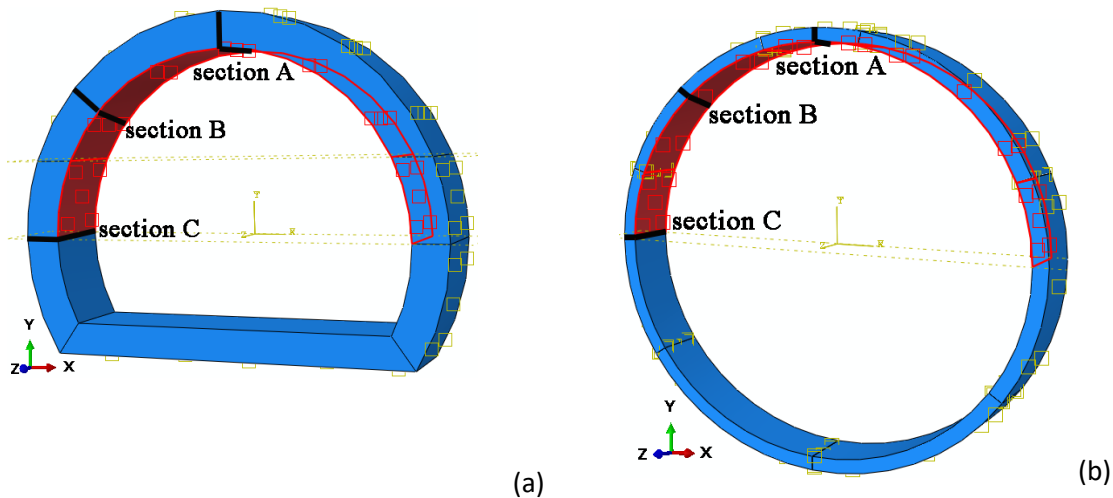

Figure 3. Finite element models for (a) cast-in-situ and (b) pre-cast segmental tunnel linings.

Fire load is applied by inputting the temperature of the hot gases (through the Standard Fire curve) and imposing the heat exchange with the exposed concrete via convection and radiation

following the provisions of EN 1992-1-2 (thermal convection coefficient of 25 W/m^2 K and thermal emissivity of concrete equal to 0.7). All the other surfaces are considered adiabatic, so to simulate the condition of several lining rings exposed to fire. In a conservative way, the heat dispersion through the soil is neglected.

For the pre-cast solution, one ring only with the average width of 1.5 m is modelled. In order to achieve comparable results (in terms of axial force and bending moment), the same reference width is adopted for the reference ring of the cast-in-situ solution.
Great attention has been devoted to the definition of internal and external constraints, being of primary importance in the evaluation of the indirect actions because of the constrained thermal dilation. For the cast-in-situ solution, perfect continuity has been restored both radially and longitudinally, since the structure is monolithic. The lateral faces of the lining ring (with normal in z-direction in Fig.3a) have been rigidly restrained in z-direction only.
In the case of the pre-cast solution, the load transmission between adjacent segments of the same ring, or between adjacent rings, is based on the contact between rigid bodies. Thus the constraint "hard contact" has been imposed at such interfaces allowing the transmission of compression only. On the other hand, the separation of the surfaces is allowed in the presence of tensile stresses. This aspect plays a key role, because such constraints are closer to a hinge rather than to flexural continuity (as in the case of the cast-in-situ solution).

Finally, it should be noted that reinforcement is expected to play a minor role in the structural behaviour, the lining being mostly subjected to compression. For this reason, rebars have not been included in the model, also because the main goal is to evaluate the internal actions in the lining. Hence, in the finite element models just concrete is modelled with a linear-elastic behaviour taking into account the variation of the elastic modulus with temperature (as previously mentioned). The reinforcement will be considered in the resistance checks.

3.4 Soil-structure interaction

Soil-structure interaction has been introduced by imposing the static pressure of the soil and constraining the external surface of the lining via linear-elastic springs, according to a simplified elastic approach (as in [4]).

Once the effective vertical pressure $\sigma_{v,eff}$ (ideally evaluated at the centre of the tunnel) and the effective water pressure σ_w are defined, the lateral pressure acting in radial direction (namely, orthogonal to the lining) can be calculated as follows:

$$\sigma_r(\theta) = \sigma_{v,eff} \cdot [\cos^2(\theta) + k_0 \cdot sen^2(\theta)] + \sigma_w(\theta) \tag{4}$$

where k_0 is the coefficient for soil static pressure (assumed to be 0.4).

The stiffness per unit area of the radial elastic springs, k_{soil}, is defined according to the following expression [4]:

$$k_{soil} = 0.5 \, E_{soil} / R_{ext} \tag{5}$$

being E_{soil} the soil elastic modulus and R_{ext} the external radius of the lining.

If the centre of the tunnel is 25 m deep, and if the specific weight of the soil is $\gamma_{soil} = 20$ kN/m^3, $\sigma_{v,eff} = \gamma_{soil} \cdot h = 500$ kN/m$^2 = 0.5$ N/mm^2. The water pressure can be disregarded in the case at issue.

With a soil elastic modulus E_{soil} = 5000 MPa and an external radius of the lining equal to 5.58 m for the cast-in-situ solution and 5.12 m for the pre-cast solution, it results k_{soil} = 448029 and 488281 kN/m^3 for cast-in-situ and pre-cast solution, respectively (average value k_{soil} = 468155 kN/m^3). Hence, the value k_{soil} = 500000 kN/m^3 has been used.

3.5 Concrete spalling

In the analysis, concrete explosive spalling should be considered for a more reliable estimation of the fire performance [5,6]. Spalling is the more or less violent detachment of concrete debris from the exposed face due to the combined action of thermal stresses and vapour pressure in the pores (due to water vaporization). Concrete spalling leads to the reduction of the cross-section bearing capacity and, eventually, to the direct exposure of the reinforcing rebars to the flames, this dramatically speeding up the decay of the structural fire resistance.

Many experimental tests from the literature demonstrated that the introduction of polypropylene fibre in the concrete mix allows to dramatically reduce the propensity to spalling, thanks to the reduction of pore vapour pressure allowed by cement past micro-cracking (induced by fibre melting at 160-170°C).

Since in the pre-cast solution polypropylene fibre can be easily introduced in the mix, spalling is neglected in this case. On the other hand, the introduction of polypropylene fibre in the cast-in-situ solution is less affordable due to the lower level of quality control in in-situ casting and to the larger volume of concrete involved. Thus, in this latter case, spalling is more likely and in the numerical modelling a limited spalling scenario is considered by assuming a detachment of the concrete cover (50 mm). This assumption has been made based on the idea that rebars represent a preferential plane for cracking.

In the following section, the results of the numerical analyses are presented together with the strength checks performed via two different methods.

4   RESULTS

4.1 Thermal profiles

Thermal profiles in the 0.25 m next to the exposed face are reported in Fig.4a at different fire durations for both solutions. As expected, thermal profiles are very similar.

In Fig.4b, the temperature at the EPDM (Ethylene-Propylene Diene Monomer) sheath is reported as a function of time. This temperature is very important, since too high values could jeopardize the effectiveness of the joints between segments. In the case at hand the temperature remained rather limited. It is worth noting that the maximum temperature is reached much later than the peak of the fire curve, due to the high thermal inertia of the concrete lining.

4.2 Internal actions

For both solutions, 3 reference sections are studied (sections A, B and C in Fig.3), by evaluating the evolution of the applied axial force and bending moment during the fire (Fig.5). Thermal dilation of concrete, in fact, induces an elongation of the lining which is partially constrained by the surrounding soil (simulated via the Winkler approach), thus increasing the compression in the lining. A curvature is also induced by the thermal gradient, since the hotter layers dilate, while the inner (and colder) core maintains its initial dimension.
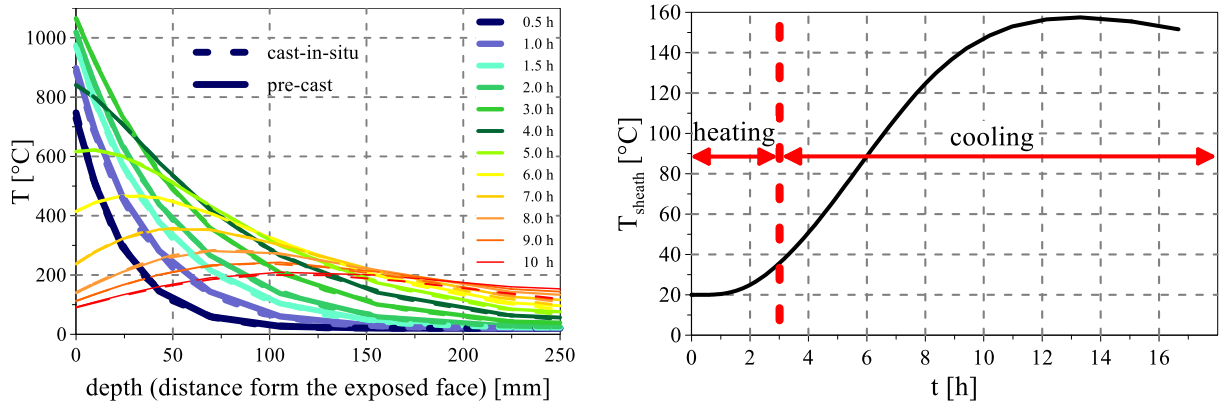
Figure 4. (a) Thermal profiles along the 0.25 m next to the exposed face of the lining at different fire durations, and (b) temperature of the EFDM sheath in the pre-cast lining.
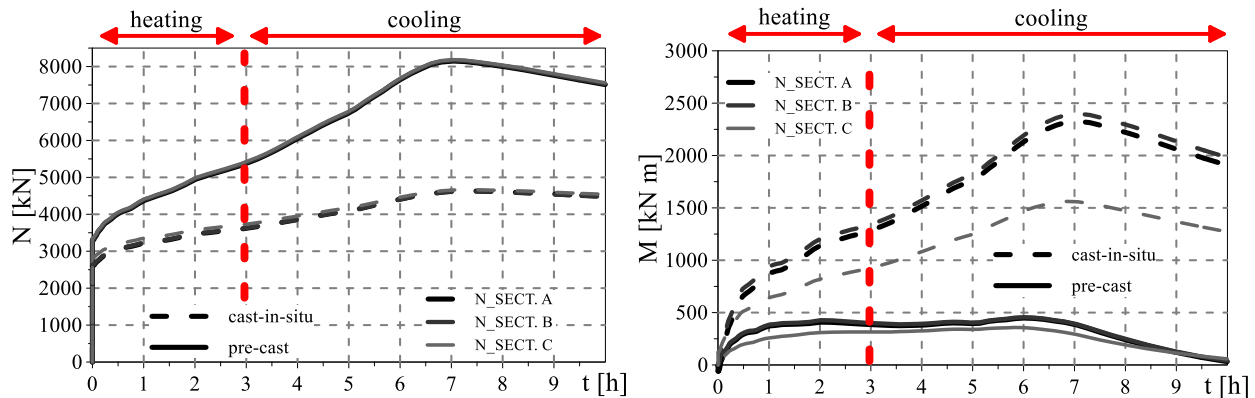

Figure 5. (a) axial force and (b) bending moments in the reference sections for cast-in-situ and pre-cast solutions as functions of fire duration.

This thermal curvature is restrained by the flexural stiffness of the lining, thus fostering the increase of the flexural bending moment. In Fig.5, axial force (positive if compression) and bending moment (positive if the internal fibres of the lining are in tension) are reported for the reference sections as a function of time.

It is worth noting that:

- the axial force increases more in the pre-cast solution than in the cast-in-situ solution, because of the higher average temperature in the former case due to its lower thickness, thus leading to a higher average dilation;
- the bending moment, on the contrary, increases much more in the case of the cast-in-situ solution due to its high flexural stiffness. The pre-cast solution in addition to its lower thickness (hence, lower flexural stiffness) results to be partially released at the segment-to-segment joints, this once more leading to smoothing down of the bending moments.

Both aspects are detrimental for the cast-in-situ solution, since the condition characterized by lower compression and higher bending moment is generally more severe for reinforced concrete. In both solutions, however, bending moment and axial force increase even in the cooling phase,

488

due to the high thermal inertia of concrete that leads to a progressive release of the heat stored during the heating phase in the hotter layers to the inner (and stiffer) part.

4.3 Strength checks

Since linear-elastic analyses have been carried out, the collapse of the structure cannot be evaluated numerically. Hence, strength checks must be performed in the most stressed sections (continuity sections and/or segment joints). In this context, a critical issue is represented by the lack of a clear procedure for performing simplified sectional strength checks during cooling.

For this reason, two possible methods have been adopted in the following for evaluating the resistant bending moment as a function of the axial force:

- classic *limit analysis*, in which the design compressive strength of concrete at any point of the section is considered according to the maximum temperature reached up to the time of verification (Fig.6);
- *500°C isotherm method*, in which, however, the envelope of the maximum temperature up to the time of verification is used. (If the actual temperature was used instead of the envelope, during the cooling phase a complete – and unrealistic – recovery of compressive strength would take place).

Evaluating the resistant bending moment, steel temperature is assumed to be the same of the adjacent concrete fibre (as suggested in EN 1992-1-2). As abovementioned, no recovery of compressive strength and elastic modulus during cooling takes place for concrete.

As regards the yield strength of steel, complete recovery is implemented for maximum temperatures lower than 500°C, and negligible recovery for higher temperatures.

In Table 1, the main parameters implemented in the strength checks are reported, assuming $\gamma_M = 1$ according to EN 1992-1-2 provisions.

In Fig.7, the comparison between resistant bending moment M_{Rd} and the external bending moment M_{Ed} is shown for both solutions in section B, which is the most stressed one (Fig.5).

On the basis of the above-discussed assumptions, the fire resistance is higher than the demand for the whole fire duration for the pre-cast solution only, while in the cast-in-situ solution sectional failure is reached after almost 7 hours (hence in the cooling phase!). In Table 2, safety factors are reported for both solutions.

The difference between *limit analysis* and *500°C isotherm method* depends on the different way concrete decay is addressed. In the former case, each concrete fibre is considered able to attain the compressive strength related to the maximum temperature reached, while in the latter method, concrete which has never reached 500°C is considered as in virgin conditions and otherwise it is considered completely damaged ($f_{cd} = 0$ MPa).

The higher compression in the pre-cast solution makes the contribution to the bending resistant moment of concrete more important, thus making the difference between *limit analysis* and *500°C isotherm method* more evident. In the case at issue, in fact, a negative bending moment occurs, yielding to a decrease of the resistant bending moment during fire driven by the decrease of the internal lever arm (due to the degradation of hot concrete). This decrease is limited in the case of the cast-in-situ solution (because of the larger thickness), this explaining why the difference between *limit analysis* and *500°C isotherm method* is negligible. On the opposite, in

pre-cast solution the much lower thickness emphasizes such process. The difference between *limit analysis* and *500°C isotherm method* is however always lower than 10%.

Table 1. Parameters adopted in the sectional strength checks.

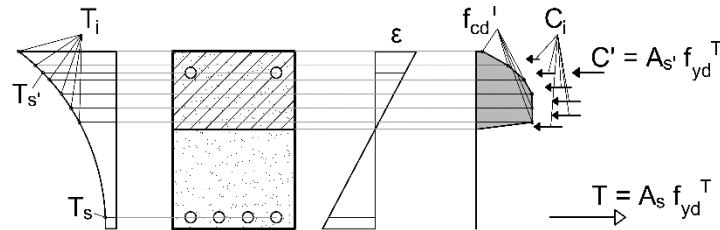| solutions	$f_{cd} = f_{ck}$ [MPa]	$f_{yd} = f_{yk}$ [MPa]	A's	As	c_{total} [mm]
cast-in-situ	28	450	7 Ø24	7 Ø24	62
pre-cast	50	450	6 Ø10	6 Ø10	55

Figure 6. Limit sectional analysis at high temperature.
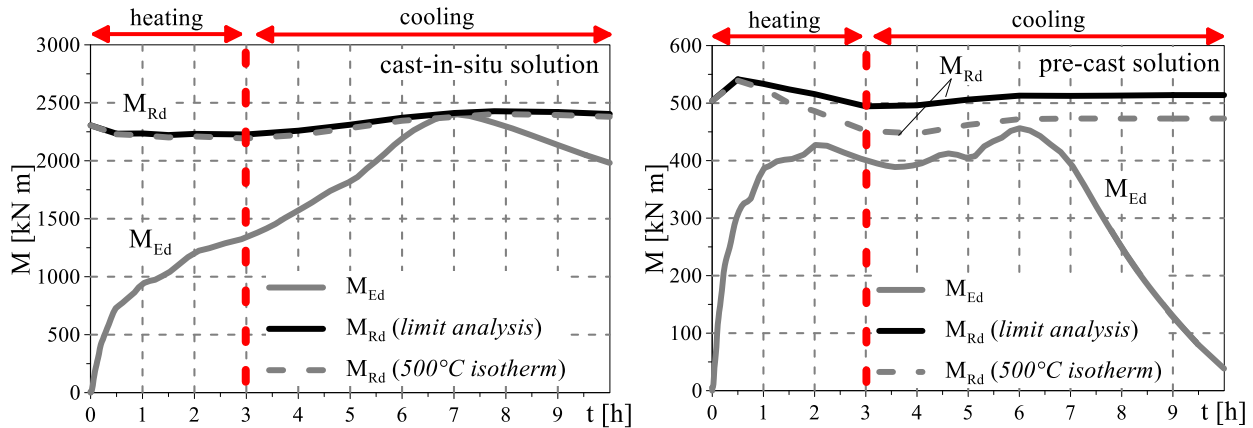
Figure 7. Comparison between resistant moment M_{Rd} and applied moment M_{Ed}, as a function of the fire duration, for the (a) cast-in-situ and (b) pre-cast solutions (reference section B).

Table 2. Safety factor ($F_s = M_{Rd} / M_{Ed}$).

	limit sectional analysis	*500°C isotherm method*
	minimum F_s	minimum F_s
cast-in-situ solution	1.00 (7 h)	0.99 (7 h)
pre-cast solution	1.12 (6 h)	1.03 (6 h)

5 CONCLUSIONS

In the present paper the fire performance of tunnel linings is discussed by comparing two possible solutions, namely cast-in-situ and pre-cast segmental linings. In particular, it is shown the strong effect of indirect actions induced by restrained thermal dilation, which lead to an evident increase of compression (up to 2.5 and 1.7 times in pre-cast and cast-in-situ solutions, respectively) and – especially – of the bending moment. This is more evident in the cast-in-situ solution (characterized by higher thickness), where the maximum acting moment is up to 5 times higher than in the pre-cast solution, while the axial force is 1.8 lower. Such behaviour entails a

490

high damage to the lining, since the static regime is characterized by a predominantly bending action, and therefore a high level of cracking. On the other hand, the adoption of pre-cast segmental lining showed some advantages in term of overall fire performance, since it allows to significantly reduces the bending moment (meaning that segments mainly work in compression), thanks to the lower flexural stiffness and to the quasi-hinges at the segment-to-segment joints. Furthermore, in this latter case, spalling is expected to be more easily avoided via a proper design of the concrete mix, in particular by adding polypropylene fibre. Finally, it is worth noting that the most severe conditions (namely, lowest safety factors) were observed to occur in the cooling phase for both solutions.

REFERENCES

[1] FIT. (2005). *Technical Report – Part 1: Design Fire Scenarios*. European Thematic Network FIT – Fire in Tunnels, Rapporteur A. Haack, supported by the European Community under the 5th Framework Programme 'Competitive and Sustainable Growth' Contract n° G1RT-CT-2001-05017.

[2] EN 1992-1-2:2004. (2004). *Eurocode 2 - Design of concrete structures - Part 1-2: General rules - Structural fire design*. European Committee for Standardization (CEN), Brussels (Belgium).

[3] Bamonte P., Kalaba N., Felicetti R. (2018). *Computational study on prestressed concrete members exposed to natural fires*. Fire Safety Journal (2018) 97, pp. 54-65.

[4] Colombo M., Martinelli P., di Prisco M. (2015). *A design approach for tunnels exposed to blast and fire*. Structural Concrete 2015 (2). DOI: 10.1002/suco.201400052.

[5] Lilliu G., Meda A. (2013). *Nonlinear Phased Analysis of Reinforced Concrete Tunnels Under Fire Exposure*. Journal of Structural Fire Engineering 4 (3).

[6] Lo Monte F., Felicetti R., Meda A., Bortolussi A. *Explosive spalling in reinforced concrete tunnels exposed to fire: experimental assessment and numerical modelling*. Proc. World Tunnel Congress 2019, 3-9 May 2019, Naples (Italy).

MINIMUM HEAT FLUX REQUIRED FOR PILOTED FLAMING IGNITION OF WOOD PRODUCTS

[1]Christian Bernier, [1]Hugo Messier, [2]Elizabeth Weckman
[1]Technorm inc., Montreal, Canada
[2]University of Waterloo, Waterloo, Canada

ABSTRACT

When considering origin and cause fire investigations, it is postulated that certain building materials can be exposed to low level heat flux for prolonged periods before ignition. The systematic application of the scientific method and the basic methodology proposed by the NFPA 921 requires that a hypothesis be tested before selecting a final probable fire scenario. Common methods for testing the time to ignition and minimum heat flux required for flaming ignition are the Cone Calorimeter and Lateral Ignition and Flame Test (LIFT). However, these methods both use relatively high heat flux levels and evaluate the behaviour of a material under exposure for a period of less than 30 minutes. This paper, based on a series of experiments, examines the minimum heat flux required for piloted flaming ignition of four common wood products used as construction materials. Different orientations were tested for each material. Wood, plywood, oriented strand board and low-density fiberboard samples were exposed to heat fluxes ranging from 4 kW/m^2 to 14 kW/m^2 for durations up to 4 hours. The heat flux was generated by common construction lamps equipped with 500 watt halogen bulbs. Distance between the bulb and samples was varied in order to increase or decrease the magnitude of heat flux applied to the surface of the specimens. A total of 115 samples were tested and their response to heating documented. The lowest recorded heat fluxes leading to piloted flaming ignition were: (1) wood: 9.9 kW/m^2, (2) plywood: 10.7 kW/m^2, (3) oriented strand board: 7.3 kW/m^2, (4) low-density fiberboard: 4.6 kW/m^2.

1   INTRODUCTION

The most common methods for testing the time to ignition and minimal heat flux required for piloted flaming ignition are the Cone Calorimeter[1] and Lateral Ignition and Flame Test[2] (LIFT). Both these methods evaluate this parameter on a time period of less than 30 minutes. When considering fire dynamics, ignition of secondary fuel packages and flame spread within a compartment that has already reached ignition, these values are adequate. However, when considering origin and cause investigations, the initial materials ignited and the heat source at which they are exposed become the predominant parameters of interest. In such cases, certain materials can be exposed to low heat flux levels for much longer periods than 30 minutes. This experimental study examines the minimum heat flux required for piloted flaming ignition of four common construction materials. For this, wood, plywood, Oriented Strand Board and low-density fiberboard samples were exposed to heat fluxes ranging from 4 kW/m^2 to 14 kW/m^2 for durations up to 4 hours.

2 BACKGROUND

Literature review shows that much work regarding the ignition of wood and cellulosic materials has been done. The SFPE handbook[3] gives a very detailed description of how the heating of solid fuels leads to flaming ignition. The pyrolysis process, production of gaseous fuel, heat transfer mechanism as well as piloted ignition is well explained by Torero[3]. Early studies by Lawson and Simms[4] established that the critical heat flux for ignition of wood was 12 kW/m^2. This value is widely used in literature[5] and the scientific community as the minimum heat flux required for ignition; however, it is based on radiant exposures of duration below 30 minutes.

The Ignition Handbook[6] gives a very detailed review of ignition for many solid fuels. For wood, different modes of ignition are proposed by Babrauskas[6]: glowing, glowing to flaming and flaming. At low heat flux levels, it is shown that glowing may be visible and is considered as a localized ignition that may also serve as a pilot for later flaming ignition. Babrauskas[7] published a state-of-the-art review which showed that the surface temperature of wood is approximately 250°C at the minimum heat flux for ignition, in the glowing mode. As the heat flux rises, the surface ignition temperature also rises. Most studies reviewed were done at heat fluxes ranging from 15 to 40 kW/m^2 and showed piloted ignition of wood at surface temperatures ranging from 300 – 365°C.

Janssens[8] established an interesting difference between ignition of hardwoods and softwoods. He showed that oven-dried specimens of hardwood ignited at surface temperatures ranging between 300-311°C as opposed to softwoods between 349-364°C. Early work by Buchanan[9] supports these results revealing that hemicellulose ignites at lower temperatures than cellulose and lignin ignites at even higher temperatures. As hardwoods are generally known to have higher fractions of hemicellulose than softwoods, this supports their lower ignition temperatures.

When considering ignition scenarios leading to how a fire began (i.e. Origin and Cause Investigations), materials may be exposed to lower heat fluxes for much longer periods. In most cases, the lower the heat flux imposed on the specific combustible, the longer the time to ignition. Few experiments and results have been published on ignition for heat fluxes below 15 kW/m^2. Spearpoint and Quintiere[10] did some very interesting research in which they examined the minimum heat flux for piloted ignition of 50 mm thick samples of several wood species in the cone calorimeter. Four types of wood were tested under heat fluxes ranging from 8 to 40 kW/m^2 in 2 different orientations: across grain and along the grain. The lowest incident heat flux for piloted ignition of hardwood was 10 kW/m^2. Across grain samples showed lower critical heat fluxes for ignition than along grain specimens with some experimentally obtained values of critical heat flux as low as 8 kW/m^2. It was also noted that the ignition mechanism under low heat flux appeared to be different than for high heat flux exposures.

A study performed by Babrauskas[11] on low temperature, long-term ignition of wood revealed stunning results. Even though an average surface temperature of 250°C is accepted for the ignition of externally heated wood samples, his study reveals that samples exposed to 77°C for long periods of time can self-heat and ignite. In low temperature long-term heat exposures, self-heating becomes the dominant phenomenon leading to ignition. This phenomenon was investigated more in depth by Gratkowski et al[12] who investigated the role of self-heating in the smouldering ignition of ¾ inch maple plywood exposed to radiant heat fluxes ranging between 6 and 15 kW/m^2. These experiments were done in the cone calorimeter for durations up to 8 hours. In order to evaluate the role of self-heating in smouldering ignition, the plywood samples were

monitored with multiple thermocouples installed at different depths in the specimen. The study revealed that higher internal (subsurface) temperatures in the sample profile indicated that self-heating was an important factor in the ignition of the specimen. Experimental data showed that the lowest, non-piloted heat flux leading to smouldering ignition was 7.5 kW/m^2. One of four criteria had to be present for ignition to be achieved: (1) observable glowing, (2) recorded temperatures above 400°C, (3) evidence of smoulder propagation wave or (4) evidence of decomposition or residual white ash. Although much research has already been done on the ignition of wood, very few studies were found for exposure at low heat flux and longer exposure times.

Ignition characteristics for plywood are often grouped with those for whole wood in the literature, for example Babrauskas[6]. As noted above, Gratkowski et al[12] determined that the lowest heat flux for smouldering ignition of maple plywood was 7.5 kW/m^2. In 1961, Shoub and Bender[13] tested ½ inch thick plywood and achieved ignition at heat fluxes of 4.3 kW/m^2 after 5.2 hours of exposure. This value is much lower than any other study examined, but it should be noted that during these experiments, no direct heat flux measurements were taken, so the uncertainty in level of heat flux is high and the value will not be used as a benchmark here. Dillon[14] proposed a critical heat flux of 8 kW/m^2 from data obtained in the cone calorimeter; however, this value was an estimate only and no ignitions were achieved when testing samples at this level of heat flux. Considering the similarity between plywood and whole wood then, the lowest piloted flaming ignition heat flux will be considered as 10 kW/m^2 [10].

Very few studies are reported on ignition of Oriented Strand Board (OSB). Hirle and Balog[15] examined the influence of heat flux on the self-ignition of OSB. Heat fluxes ranging from 31 to 55 kW/m^2 were applied to 8mm, 14 mm and 25 mm samples. These tests were conducted without a pilot and no lower heat fluxes than 31 kW/m^2 were studied. The lowest heat flux leading to ignition reported in the Ignition Handbook[6] is 14.8 kW/m^2 for ½ inch OSB so this value is adopted here.

Similarly, there is little information in the literature related to ignition characteristics of fibreboard. This material is commonly used in the construction industry for sheathing board, for flat roof insulation and also as ceiling tiles (suspended ceilings) so it comes with different coatings and density. Zichermand and Allard[16] tested the ignition of fiberboard in a Setchkin furnace. They achieved glowing ignition at surface temperatures of 250°C similar to those observed for ignition of wood[7]. NBS tested high density fibreboard (900 kg/m^3) in the LIFT and found that the minimum heat flux for piloted radiant ignition was 9.7 kW/m^2. Cone calorimeter tests by Babrauskas[6] for low-density fiberboard (270 kg/m^3) found ignition to occur under incident heat fluxes of 8 kW/m^2. No details regarding the time to ignition or the specific coating, thickness or type of fiberboard were given. Shoub and Bender[13] found that low-density fiberboard (290 kg/m^3) auto-ignited in 0.92h when exposed to heat flux of 4.3 kW/m^2; however, considering that no direct heat flux measurements were taken in the study, the uncertainty related to reported levels of heat flux is high. Therefore, these values will be considered later, but will not be used as a benchmark for this material. The lowest heat flux leading to ignition reported in this literature review is 8 kW/m^2 [6].

Table 1 summarizes the lowest heat fluxes found in the literature leading to piloted flaming ignition for the materials in this study:

Table 1. Lowest reported incident heat flux leading to flaming ignition [kW/m^2]

Wood	Plywood	OSB	Fiberboard
10	10	14.8	8

3   EXPERIMENTAL SETUP AND PROCEDURE

Experiments were conducted in a 4'x8' open face mechanically ventilated enclosure. Standard construction lamps with 500 watt halogen (Globe T3 J-Type 00458) bulbs were used as a heat source. In order to vary the heat flux imposed on the samples, the distance between the heat source and the samples was varied. To allow accurate positioning of the heat source, a steel holding mechanism composed of threaded rods, plates and bolts was fabricated.

The heat flux emitted by the heat sources was measured during every test run with copper calorimeter heat flux gauges fabricated as per ASTM F2701-153[8]. Two different methods of piloted ignition, spark and flame, were manually applied. The spark ignition system was composed of a modified electronic barbecue ignition system. The two probes were positioned in the most thermally damaged area of the sample and a spark was produced. In some instances, the flame from a butane long nose lighter was directed for a very short period in the most thermally damaged area.

Wood, plywood, oriented strand board and low-density fiberboard were tested under exposure to heat flux from the halogen bulbs. Wood samples with dimensions of 5 inch x 5 inch x 1½ inch were cut from 2 inch x 6 inch by 8 foot long boards of typical construction lumber (spruce). The grain orientation was alternated vertical and horizontal. Plywood samples (5 inch x 5 inch x ¾ inch) were cut from a 4' x 8' sheet of standard ¾ inch plywood (spruce). The grain orientation was alternated vertical and horizontal. OSB samples (5 inch x 5 inch x 7/16 inch) were cut from a 4' x 8' sheet of standard 11mm (7/16 inch) OSB sheeting from LP Building Products. Considering the finishes on the front and back sides of the OSB are different (smooth and rough), the sides were alternated. Finally, fibreboard samples (5 inch x 5 inch x ½ inch) were cut from a 4' x 9' sheet of standard BP rigid sheathing ½ inch tar-coated low-density fibreboard (wood fiber sheathing, or Tentest). Only one side was tested since the finish on both sides and directions were the same. Before testing, all samples were conditioned for a minimum of 3 days in a 20 ºC ±2ºC and 30 % relative humidity environment.

4   RESULTS

Results of the testing are contained in Figures 1 through 4. Figure 1 summarizes data for time to ignition obtained through exposure of 25 wood samples to different heat flux levels while Figure 2 illustrates similar data obtained from the exposure of 24 plywood samples to the same range of heat flux levels. In Figure 3, results of time to ignition for varying levels of heat flux are shown for exposure of 34 OSB samples, while Figure 4 summarizes data obtained for 32 samples of low-density fibreboard. Finally, a summary of the minimum measured values of heat flux leading to flaming ignition for the 4 materials is in Table 2.

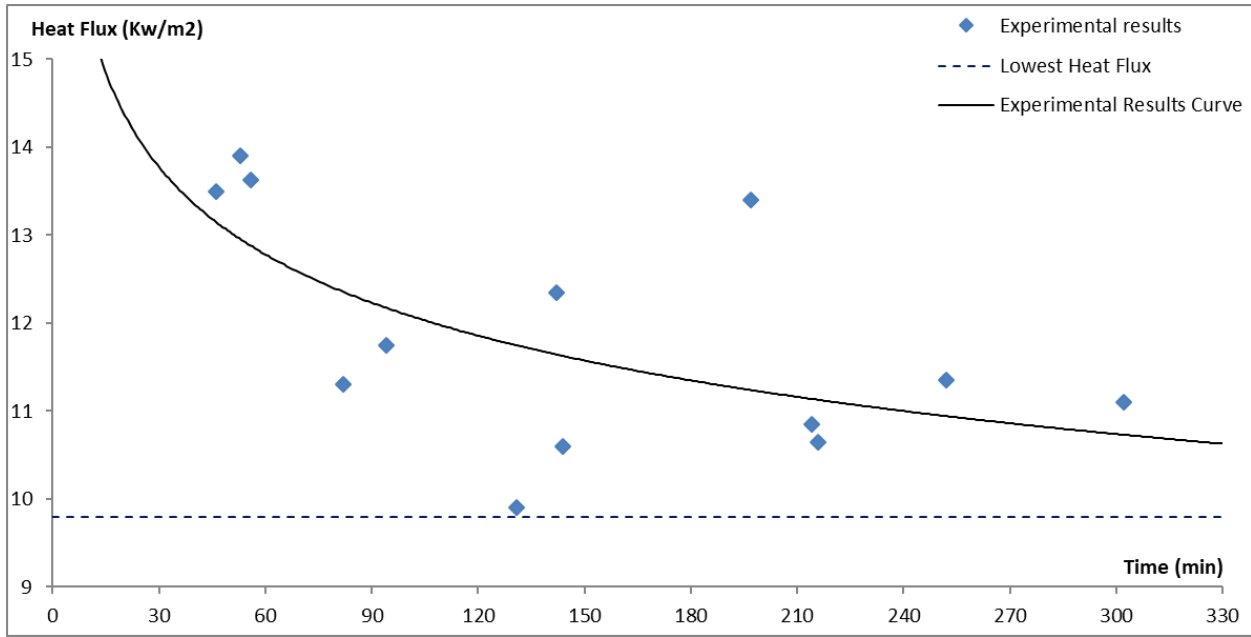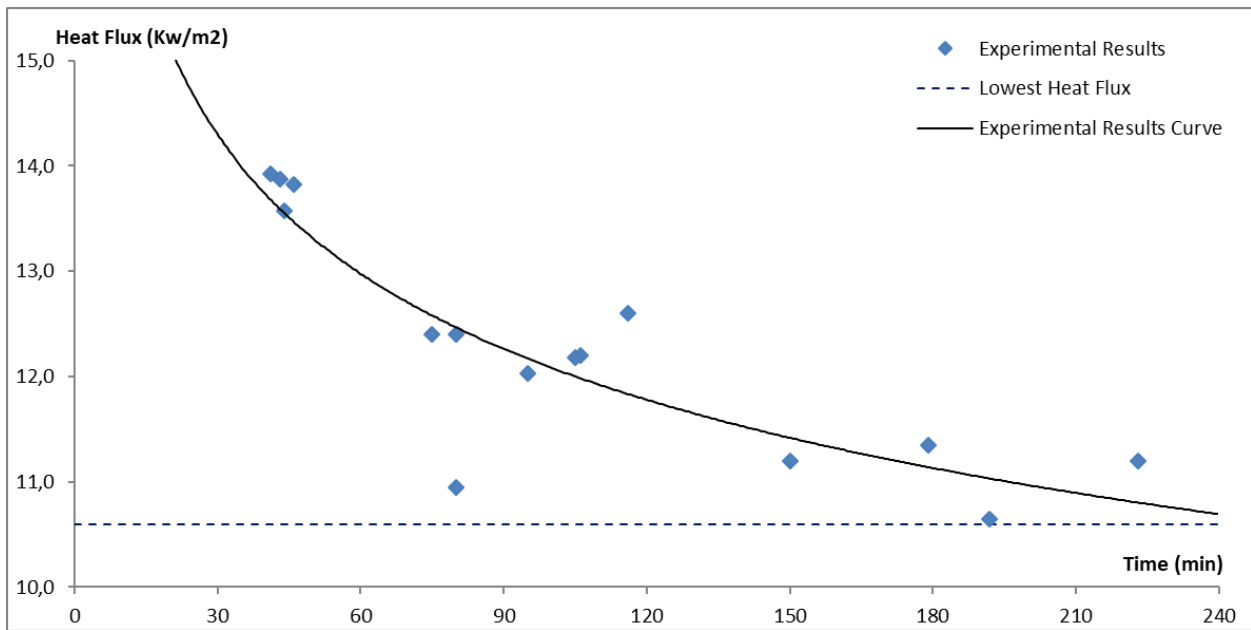Figure 1: Time to Ignition vs Heat Flux - Wood

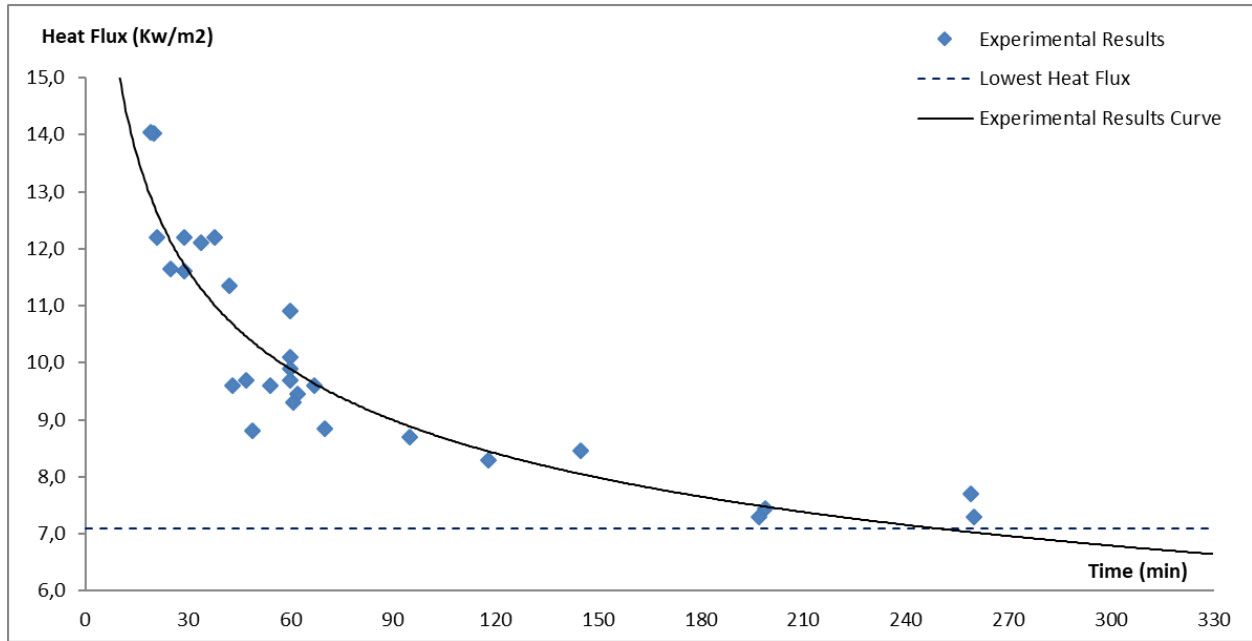Figure 2: Time to Ignition vs Heat Flux - Plywood

Figure 3: Time to Ignition vs Heat Flux - OSB

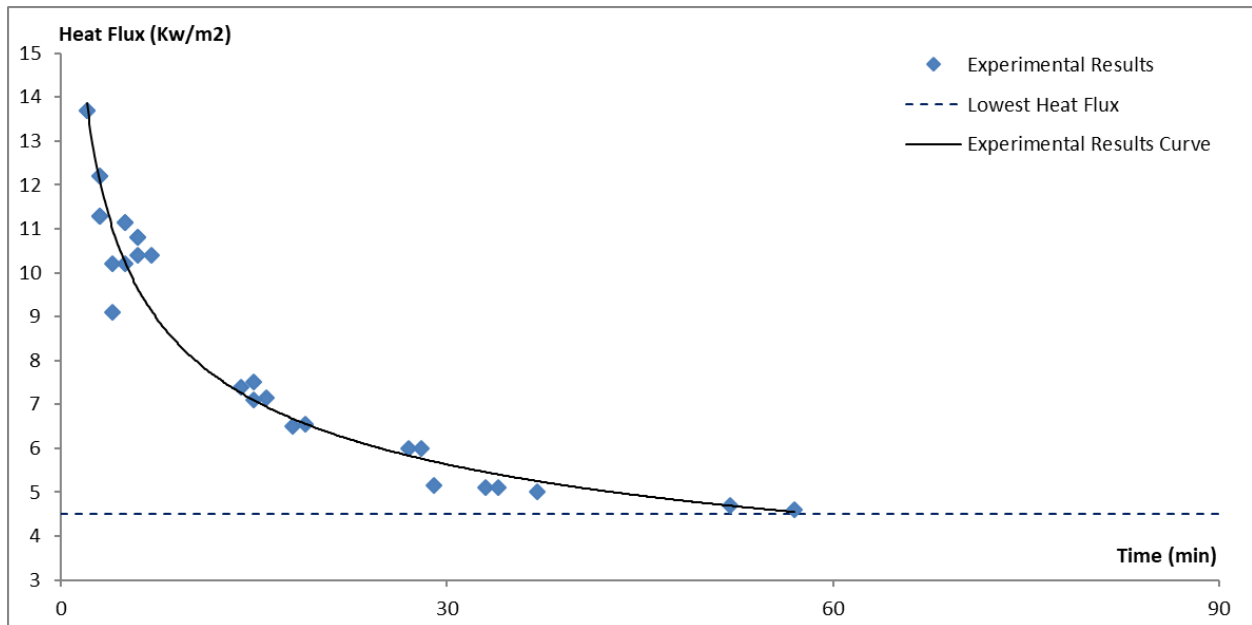Figure 4: Time to Ignition vs Heat Flux – Fiberboard

Table 2. Lowest measured incident heat flux leading to flaming ignition [kW/m^2]

Wood	Plywood	OSB	Fiberboard
9.9	10.7	7.3	4.6

497

5   ANALYSIS AND DISCUSSION

5.1 Wood and Plywood

A total of 49 samples of wood and plywood were tested under exposure to heat fluxes ranging from 9.5 kW/m^2 to 14 kW/m^2. 21 of the samples showed no sign of imminent ignition after 4 hours of exposure. In cases where samples did ignite, the measured values of time to ignition were very similar for wood and plywood and fell within the ranges expected based on previous studies. The lowest incident heat flux leading to piloted flaming ignition was 9.9 kW/m^2 which appears very comparable to the value of 10 kW/m^2 reported in the literature[10]. However, in contrast to the present study using softwoods exposed along the grain, the literature value is based on ignition of hardwoods in the across grain orientation. This is an interesting result since studies by Janssens[8] and by Buchanan[9] showed that hardwoods, due to their higher hemicellulosic composition, have lower ignition temperatures so it might be expected that hardwoods exposed in the across grain orientation would require lower minimum heat flux for piloted flaming ignition than the 9.9 kW/m^2 measured here.

During this experimental study, very minor differences were noted in times to ignition for samples exposed in both vertical and horizontal orientations along the grain. Any differences observed could not necessarily be linked to the orientation. When considering wood, many other factors impact the behaviour and time to ignition. It was noted that knots, cracks and imperfections in wood and plywood played significant roles in ignition of the samples. In particular, specimens that had knots in the exposed region decomposed more rapidly and ignited at lower heat fluxes and shorter time periods than samples without such imperfections.

5.2 Oriented Strand Board (OSB)

The results for OSB showed much less variability than wood and plywood. This was expected because it is an engineered product. The fabrication of these types of panels is very controlled and the inherent defects of wood are not present. The lowest heat flux that led to piloted ignition was 7.3 kW/m^2. This value is less than half the value of 14.8 kW/m^2 that was found in the literature[6] possibly because most of the work reviewed had been done at much higher heat flux levels, with no pilot.

Since OSB has a different finish on its backside than its front, the orientation of the samples was alternated. When comparing the results, only very minor differences were observed. The overall behaviour of OSB was markedly different than that observed for wood and plywood. Initially, not much pyrolysis from the OSB samples was observed but eventually, thermal degradation began and very rapidly conditions favourable for ignition were met and ignition occurred. Certain specimens exhibited signs that suggested a form of self-heating or smouldering ignition was ongoing before the flaming ignition as well. These specimens showed considerable thermal decomposition on the backside of the sample, although no ignition had occurred. It was also observed that areas of the OSB that had ink markings showed more rapid thermal decomposition than adjacent areas.

5.3 Fiberboard (low-density)

The results gathered for low-density fiberboard were very interesting. The minimum recorded heat flux for piloted flaming ignition was 4.6 kW/m^2. Samples tested at 4.6 kW/m^2 and 4.7 kW/m^2 ignited in 57 and 52 minutes, but the samples tested at 4.1 kW/m^2 and 4.3 kW/m^2 did not show any visible smoke or sign of imminent ignition after 4 hours of exposure to the heat source.

The value observed here is almost half the value of 8 kW/m^2 that was reported in the literature[6]; however, there was no mention as to the type of fiberboard tested, the duration of the test, nor the coatings. In fact, very little data was found regarding the minimum heat flux required for ignition of fibreboard in general and there was none specifically related to tar coated fiberboard panels.

The results for fiberboard showed much less variability than wood and plywood most likely because the fabrication of these panels, as for OSB, is very controlled and the inherent defects of wood are not present. The tar coating applied on the fiberboard proved to have a considerable effect on the ignition of the samples. The overall behaviour of the fiberboard specimens was much different that wood, plywood and OSB. Within the first minute of exposure to the heat source, thermal decomposition had begun. Volatiles were clearly visible in most instances within 30 seconds. When testing at heat fluxes in the range of 4 to 5 kW/m^2, pyrolysis and visible smoke production either occurred rapidly, or did not occur at all. When observing the sample surface prior to the moment when ignition conditions were favourable, very minimal thermal damage was visible. Even though much visible smoke was produced, the surface of the specimen seemed barely decomposed. Even after ignition had occurred and extinguishment was done, very little thermal damage was visible. The extinguished samples continued to smoulder even after being well soaked to put out the flames; two samples left aside (intentionally) were completely consumed overnight.

6   CONCLUSIONS

Table 3 summarizes the experimental results for minimum heat flux for flaming ignition from this study compared to the values found in the background literature.

Table 3. Lowest incident heat flux leading to flaming ignition [kW/m^2]

	Wood	Plywood	OSB	Fiberboard
Literature	10	10	14.8	8
Measured	9.9	10.7	7.3	4.6

The main observations from this experimental study were:

− Measured minimum heat flux values for ignition of wood and plywood results were very similar to the values found in the literature

− Measured minimum heat flux values for ignition of OSB and Fiberboard were half the values found in the literature

− Grain orientations had minor impact on time to ignition, while knots, cracks, imperfections and ink markings accentuated thermal decomposition and thus tended to shorten times for ignition

Certain samples exhibited signs of self-heating and smouldering combustion under exposure to these very low levels of incident heat flux

REFERENCES

[1]   ASTM E 1354-04 (2004): *Standard Test Method for Heat and Visible Smoke Release Rates for Materials and Products Using an Oxygen Consumption Calorimeter*, ASTM International, West Conshohocken, PA, 2004.

[2]   ASTM E 1321-97 (1997): *Standard Test Method for Determining Material Ignition and Flame Spread Properties*, ASTM International, West Conshohocken, PA, 1997.

[3]   Torero, J. (2016), *Flaming Ignition of Solid Fuels*, SFPE handbook of fire protection engineering, 5th ed., New York, Springer, Society of Fire Protection Engineers, 2016, pp.633-661.

[4]   Lawson, D.I., Simms, D.L. (1952), *The ignition of wood by radiation*, British J. Applied physics, 1952, 3, pp. 288-292.

[5]   Drysdale, D. (1998), *An Introduction to Fire Dynamics*, 2nd edition, Wiley, 1998, pp. 211-227

[6]   Babrauskas, V. (2003), *Ignition handbook*. Issaquah, WA: Fire Science Publishers, 2003

[7]   Babrauskas, V. (2001), *Ignition of Wood: A Review of the State of the Art*, Interflam 2001, Interscience Communications Ltd, London, 2001, pp. 71-88

[8]   Janssens, M. L. (1991), *Fundamental Thermophysical Characteristics of Wood and Their Role in Enclosure Fire Growth* (Ph. D. dissertation), University of Gent, Belgium (1991)

[9]   Buchanan, M. A. (1952), *The Ignition Temperature of Certain Pulps and Other Wood Components*, TAPPI, 1952, 35, pp. 209-211

[10] Spearpoint M.J., Quintiere J.G. (2001), *Predicting the piloted ignition of wood in the cone calorimeter using an integral model – effect of species, grain orientation and heat flux*, Fire Safety Journal 36, 2001, pp. 391-404.

[11] Babrauskas, V. (2001), *Pyrophoric Carbon and Long-term, Low-temperature Ignition of Wood*, Fire and Arson Investigator, 51:2, 2001, pp. 12-14.

[12] Gratkowski M.T., Dembsey N.A., Beyler C.L. (2006), *Radiant smouldering ignition of plywood*, Fire Safety Journal, 41, 2006, pp 427-443.

[13] Shoub H., Bender E. W. (1961), *Radiant ignition of wall finish materials in a small home*, NBS 8172, National Bureau of Standards, Washington, DC, 1961

[14] Dillon S. E. (1998), *Analysis of the ISO 9705 Room/Corner test: Simulations, Correlations and Heat Flux Measurements*, NIST-GCR-98-756, University of Maryland, 1998

[15] Hirle S., Balog K. (2017), *The Effect of the Heat Flux on the Self-Ignition of Oriented Strand Board*, Slovak University of Technology in Bratislava, vol 25, Number 40, 2017

[16] Zicherman, J.B., Allard D.L. (1992), *Fire Performance of Fire-retardant Wood Fiberboard Ceiling Tile*, Fire and Materials 16, 1992, pp 187-196.

[17] Braun E., Allen P.J (1984)., *Flame Spread on Combustible Solar Collector Glazing Materials*, NBSIR 84-2887, NBS, 1984

[18] ASTM F2702-15 (2015), *Standard Test Method for Radiant Heat Performance of Flame Resistant Clothing Materials with Burn Injury Prediction*, ASTM International, West Conshohocken, PA, 2015

EFFECTS OF THICKNESS ON THE SELF-EXTINCTION OF TIMBER

David Morrisset[1], Angus Law[2], Richard Emberley[1]

[1] California Polytechnic State University – San Luis Obispo, United States of America
[2] The University of Edinburgh – United Kingdom

ABSTRACT

A series of experiments was conducted using Redwood to explore the critical thickness at which self-extinction (auto-extinction) of timber does not occur for a constant heated area. Timber samples with uniform area (95x95mm) were exposed to a constant external heat flux from a vertical mass loss cone heater. Each sample varied in thickness (45-95mm) and the occurrence of self-extinction of flaming combustion was recorded. The critical mass loss rate of 2.98 ± 0.4 g/s-m^2 was determined at the point of extinction and was compared to other critical mass loss values recorded in literature. It was found that the average critical mass loss rate observed for 45mm and 95mm samples were within 0.11 g/s-m^2 of one another, indicating that sample thickness does not affect the phenomenon of extinction for the thicknesses and conditions of the methodology used.

1   INTRODUCTION

Timber has ironically served both as one of the earliest construction materials for mankind as well as our most common fuel source. It is no surprise that timber burns - however it is commonly misunderstood that in many cases, timber cannot sustain flaming combustion on its own. Without an external heat flux, flaming timber will often experience self-extinction due to an insufficient mass loss rate to maintain the flame and overcome heat losses. Self-extinction is an occurrence that is well documented [1-4], but further investigation into the phenomenon is required as many questions remain about the factors that may affect this.

The use of timber in the built environment has gained popularity on a global scale as building designers pursue more sustainable practices. To ensure safety, timber construction must survive burnout of the contents in the compartment and maintain structural integrity [5]. Achieving and maintaining self-extinction is fundamental to survive burnout. While the self-extinction of timber has been studied, there remains little understanding of the effect that sample thickness has on the phenomenon. Self-extinction has not been observed for thin specimens (e.g. match sticks) but has been observed in relatively thick specimens (100-150mm). This demonstrates a critical dimension exists at which timber can sustain combustion without an external heat flux.

Structural timber varies greatly in size and thickness; conventional light-frame timber is generally used to describe timber on the order of 2 in x 4 in (50mm x 100mm) through 2 in x 12 in (50mm x 300mm), while heavy timber describes structural members having a minimum dimension of no less than 4 in (100mm) [6]. Due to this variation in construction timber, the effect of sample thickness on self-extinction must be characterized. This paper serves to explore the bounds of which a sample can be treated as a semi-infinite solid as well as the self-extinction threshold of sample thickness.

2   SELF-EXTINCTION THEORY

The phenomenon of self-extinction has been observed in both solid timber and engineered timbers in a variety of species [2-4]. Parameters for self-extinction can be quantified through an energy balance of the char and pyrolysis layers within the timber, as seen in *Figure 1*.

For a given section of timber exposed to a sufficiently large incident heat flux, a heated layer undergoes pyrolysis, producing flammable gases and a carbonaceous char layer. The released gasses eventually exist within the flammable limits and then ignite either through piloted ignition, or through auto-ignition upon the gas reaching a critical ignition temperature. Sustained ignition can only occur when the net energy into the heated surface is enough to overcome heat losses due to in-depth conduction, convection, and re-radiation while still providing enough energy to create sufficient pyrolysis gasses.
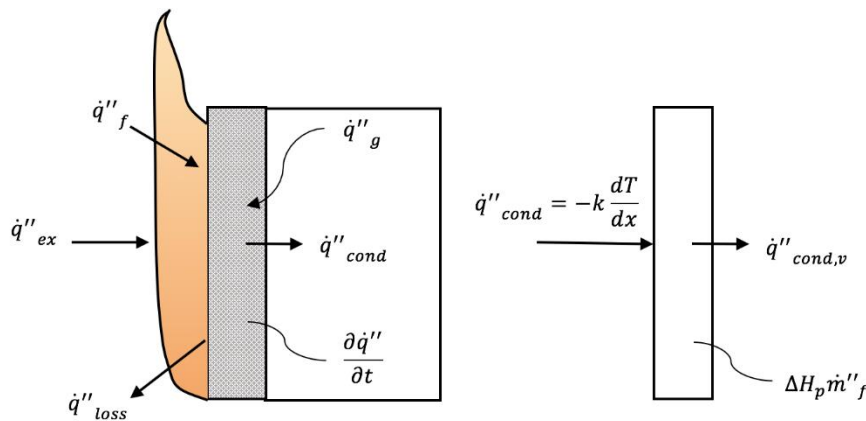

Figure 1. A depiction of the energy balance over the char layer (Left) and the layer of timber further in depth undergoing pyrolysis (Right). It should be noted that this figure assumes that the sample has been burnt for a sufficient time to develop a char layer.

The external heat flux acting on the front of the sample represents the incident heat from the radiant source, while a separate term represents the radiation feedback from the fire once a flame sheet is established on the ignition face. Losses from the char layer are attributed to re-radiation and convection. Oxidization in the char layer serves to generate heat as the char experiences further combustion [4]. Other energy that is not stored in the char layer, effectively raising the local temperature of the char, is then conducted into the pyrolysis layer.

Of the energy entering the pyrolysis front, $\Delta H_p \dot{m}''_f$ is used to gasify the timber into volatiles. The remaining energy is conducted further in-depth into the sample. As long as a sufficient amount of energy is put into degrading the timber, a mass loss rate will continue to be produced and sustain flaming combustion. Based on the observation of self-extinction alone, there must exist a critical mass loss rate at which flaming combustion can no longer be sustained. Values of such critical mass loss rates are well documented in literature [2-4]. Energy balances over both the char layer and the pyrolysis zone in *Figure 1* can be combined to yield an equation similar to that presented by Emberley, et al. [2] .

$$\dot{m}''_f = \frac{1}{\Delta H_p}\left[\dot{q}''_{ex} + \dot{q}''_f + \dot{q}''_g - \dot{q}''_{loss} - \left[-k\frac{dT}{dx}\Big|_{x=x_{char}}\right] - \frac{\partial q''}{\partial t}\right]$$ (1)

Many terms presented in *Eq. (1)*, such as generation in the char layer and the radiant feedback from the flame sheet, can be difficult to quantify and require additional testing. Determining the point at which self-extinction occurs within a timber sample has been previously described with two parameters; a critical mass loss rate, and a critical external heat flux at the point of self-extinction [2,4].

As a timber sample burns, there is an initial transient period of mass loss, which is characterized by rapid mass loss. This transient phase often features spikes in mass loss due to accelerated and uneven burning or flare-ups on the surface (see *Figure 2*). Based upon previous testing, self-extinction is generally observed within the steady state portion of the test.
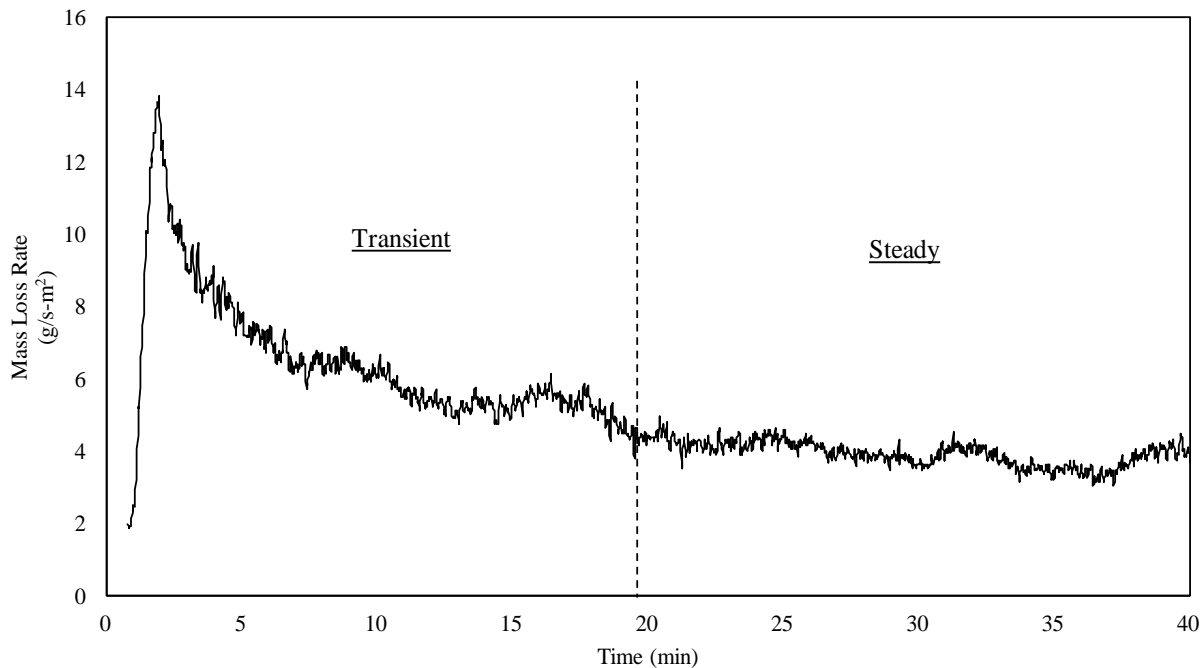

Figure 2. Mass loss data for a test of a 45mm Redwood sample. The vertical dashed line indicates an approximate transition from the transient burning phase to a steady state.

If there exists a portion of the sample sufficiently far from the exposed face such that heat does not transfer through the entire thickness of the sample, the sample can be treated as a semi-infinite solid. This assumption renders the sample thickness irrelevant so long as there always exists a portion that does not see thermal penetration from the heat source [7].

Due to the surface regression of the char, a specimen will inevitably stop representing a semi-infinite solid at some point if it is allowed to continue burning indefinitely. The semi-infinite solid assumption has been built into self-extinction testing thus far in literature. However, the nature of investigating the effect of sample thickness will inherently cause a breakdown in the semi-infinite assumption. By reducing the thickness (i.e. the characteristic length scale) of the

sample, the heat being conducted through the sample takes less time to penetrate the back-boundary condition. Once the timber no longer behaves as a semi-infinite solid, the heat conducted into the remaining timber will be stored in the virgin timber (or lost through the rear boundary conditions) as opposed to being further conducted into the sample. The increased energy storage could serve to raise the temperature within the timber and increases the rate of pyrolysis within the portion of unburnt timber. A higher rate of pyrolysis could then create a scenario that prevents, or at least delays, self-extinction.

The criteria for semi-infinite conditions are set by a specified increase in the back-face temperature. If a value of 0.5% of the difference between the back-face temperature and the ambient temperature is used as this criterion, then the time at which a material ceases to behave as semi-infinite can be described as $t \approx L^2/(16\alpha)$ – where L represents the thickness of the material and α represents the thermal diffusivity [1]. When considering light-timber (45mm thickness for nominal 50mm timber) and heavy-timber (95mm thickness for nominal 100mm timber), each would cease to be a semi-infinite solid in approximately 25 minutes and 113 minutes, respectively (assuming thermal properties for Yellow Pine as a generalization) [1].

The distinction of whether a timber member is thermally thick or thermally thin speaks to the thermal gradients within the sample. These two conditions are defined by the Biot number such that, $Bi = hl_{ch}/k$, where a sample can be considered thermally thin if its Biot number is significantly less than one [1]. The Biot number serves as a ratio between the rate heat will conduct through a material, compared to the heat lost to convection. Therefore, a thermally thin material will have little to no temperature gradients in-depth for any one-dimensional heat transfer. It is important to clarify that self-extinction in timber is consistently observed with thermally thick materials, but it has been supposed that thermally thin samples of timber could sustain flaming combustion without an external heat flux due to this geometry [1]. Previous work has characterized the effect that a thin cylindrical geometry on burning due to flaming on a larger surface area [8]. However, varying the thickness of a timber samples with a uniform surface area has not been tested, particularly in the context of self-extinction.

3 TEST METHODOLOGY

In order to observe the effects of sample thickness on the phenomenon of self-extinction, samples of various thickness were allowed to burn unimpeded until the sample receded to the point at which self-extinction was observed. For the sake of these tests, both the surface area exposed to the heat source and the incident heat flux remained constant between trials.

As seen in *Figure 3*, an ISO Mass Loss Cone Calorimeter at the University of Edinburgh was used in the vertical orientation to supply the external heat flux to the sample and remained on for the duration of the test. The scale associated with the cone was also used to record the mass loss of each sample. Each sample was exposed to 35 kW/m^2 and ignited with the pilot of the Mass Loss Calorimeter. Based on preliminary testing, 35 kW/m^2 was chosen to produce a more uniform char surface compared to higher heat fluxes. Trials were conducted for sample thickness of 95mm and 45mm, which correspond to the nominal dimensions for light-timber and heavy-timber as defined previously. All samples were Redwood with a moisture content of 9.7% (determined in accordance with ASTM D4442) [9].
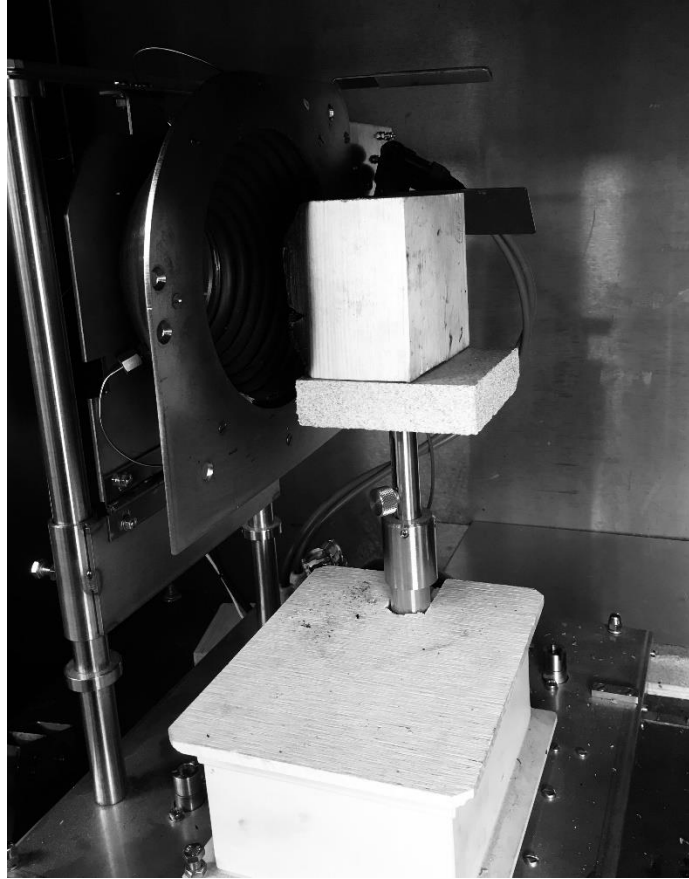
Figure 3. The Mass Loss Cone Calorimeter used for testing. Samples were tested in the vertical orientation with all sample sides uninsulated, as seen in testing conducted by Emberley, et al [2].

Each test was conducted until self-extinction occurred and all flaming visibly extinguished. When observed, the time to self-extinction was recorded. For each sample that extinguished, both the depth of unburnt timber and the thickness of the remaining char layer were measured. The critical mass loss rate for self-extinction was determined from the data recorded for each test. These values were compared to existing values in literature, and also served to signify any variation in self-extinction conditions for differing thicknesses. Additionally, the critical external heat flux at the point of extinction was measured by placing a Schmidt-Boelter heat flux gauge at the given distance from the cone at which the sample extinguished (i.e. the location of the regressed char surface).

4   RESULTS & DISCUSSION

Results from experiments so far have shown a consistent critical mass loss rate for self-extinction across different thicknesses. A value of 2.98 ± 0.4 g/s-m^2 was recorded at the point of extinction across the experiments; an example of which can be seen in *Figure 4*.

While there is no existing literature that defines the critical mass loss rate for Redwood specifically, the value determined from experimentation is within the realm of results seen in previous studies on self-extinction; Radiata Pine for example, has been recorded to have a critical mass loss rate of 3.65 ± 0.2 g/s-m^2 at the point of self-extinction [2]. Samples of both

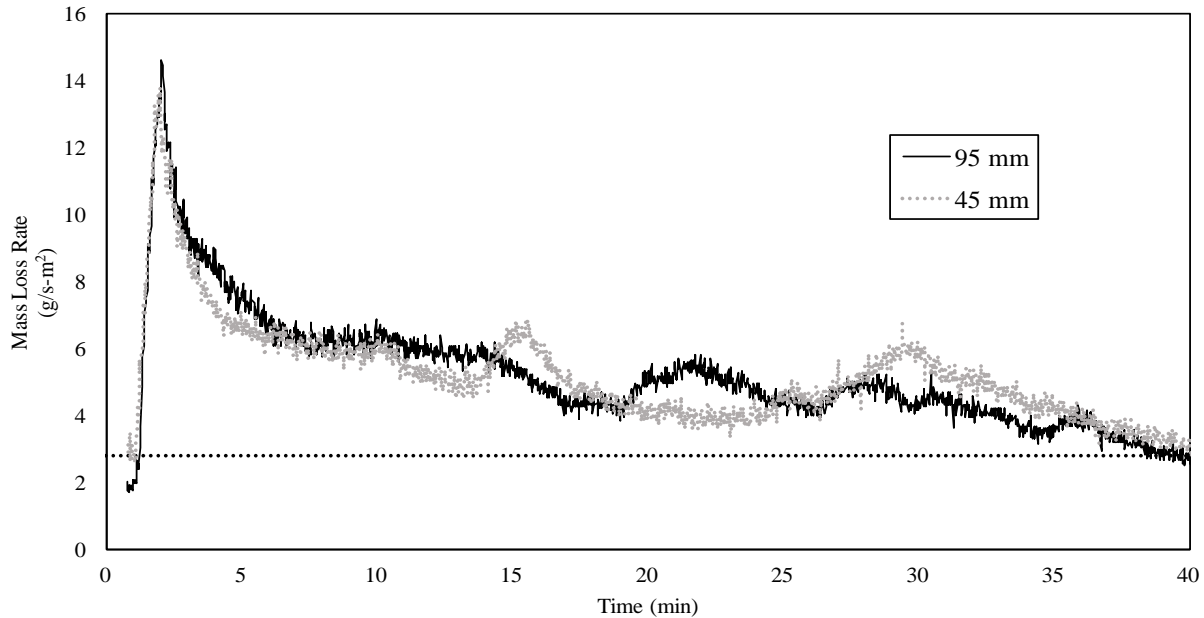95mm and 45mm consistently demonstrated self-extinction (n=4 for both 95mm and 45mm samples).

Figure 4. Mass loss data recorded for a single 95mm sample and a single 45mm sample exposed to 35 kW/m². The sample was visibly observed to self-extinguish at approximately 40 minutes. The mass loss rate at the point of extinction is indicated by the horizontal dashed line.

As seen in *Table 1*, both the 95mm and 45mm samples experienced self-extinction within similar time scales. The 45mm samples extinguished on average 6 minutes sooner than the 95mm samples, and receded 2mm less than the 95mm samples. Based upon the semi-infinite solid theory described previously, the 95mm samples extinguished before ever losing the semi-infinite condition. The 45mm samples however would not be expected to remain as a semi-infinite solid for the duration of the test. According to theory, the thermal wave will reach the back-face of the 45mm samples in approximately 25 minutes. The resulting extinction of the 45mm samples suggests that a semi-infinite solid condition is not required for the phenomenon of self-extinction.

These results however can only be used to describe one-sided heating at 35 kW/m²; further testing is required to gain insight into self-extinction behaviour if the sample was to be heated from multiple sides. The reduction in receded distance and time to extinction observed in the 45mm samples could be attributed to the thermal wave breaching the back face and allowing for higher convective losses at the back face, which then expedites the process of extinction.

Table 1. A summary of the averaged results across the 95mm and 45mm trials. The total receded distance describes the distance the char front regressed from the plane at which the sample face was placed at the beginning of the test – the same location where the 35 kW/m² was calibrated.

Initial Thickness	Burn Time	Total Receded Distance	Critical Mass Loss Rate
[mm]	[min:sec]	[mm]	[g/s-m²]
95	44:50 ± 6:42	13.71 ± 1.7	3.03 ± 0.1
45	38:47 ± 2:43	11.67 ± 1.3	2.92 ± 0.4

The range of receded distances between trials varied from 10.5mm to 15.5mm, considering both 95mm and 45mm samples. After testing, the heat flux was recorded at both 10.5mm and 15.5mm from the plane at which the 35 kW/m² was originally determined. The resulting critical external heat flux ranged from 30.8 kW/m² to 29.5 kW/m², at 10.5mm and 15.5mm, respectively. Additional trials of 25mm samples were attempted, however vertical samples warped over the course of the experiment and flame spread along the sides and top of the samples instead of maintaining the flame sheet on the front face. Therefore, those results were not considered in this analysis.

5   SUMMARY & FURTHER WORK

The established methodology of this experimental series was aimed at illustrating the effect sample thickness has on the self-extinction of timber. A consistent value was established for the critical mass loss rate, and a fairly consistent regression distance was used to determine a range for the critical heat flux at extinction. This work is ongoing, and the authors intend to continue expand on the results presented here. Preliminary results indicate that sample thickness does not affect the critical mass loss rate at extinction or the distance the sample will recede prior to extinction. These results are applicable to the methodology used, however this testing should be further expanded to other species, heat intensities, orientations, and sample sizes.

Additional experiments must also be conducted to see the effect of samples smaller than 45mm, in an effort to characterize a critical thickness at which extinction may not occur. Testing using 25mm samples resulted in a condition in which the sample was no longer burning on only the front face. An investigation into sizes between 45mm and 25mm could require a change in methodology to prevent such warping. Further research should also work to relate the critical external heat flux at extinction, as measured in this experimentation, to the energy balance described in *Eq. (1)*. While additional testing will be required, these results lay the groundwork for further investigation into the interaction of self-extinction and geometric aspects of timber samples.

Department for technical support. Additionally, the individual work of Alex Schnorr, Charles Damico, Adin Gilman-Cohen, and Michal Krajcovic was greatly beneficial to the results of this testing.

REFERENCES

[1] D. Drysdale, An Introduction to Fire Dynamics, 3rd ed, John Wiley & Sons, Ltd, West Sussex, England, 2011.

[2] R. Emberley, T. Do, J Yim, J.L. Torero, "Critical heat flux and mass loss rate for extinction of flaming combustion of timber." Fire Safety Journal 91, 252-258, 2017.

[3] R. Emberley, A. Inghelbrecht, Z. Yu, J.L. Torero, "Self-extinction of timber." Proceedings of the 36th Combustion Institute, Elsevier, 2016.

[4] A. Bartlett, "Auto-Extinction of Engineered Timber," Doctor of Philosophy, The University of Edinburgh, 2018.

[5] S.H. Ingberg, Tests of the Severity of Building Fires, presented at in: Proceedings of the Thirty-Second Annual Meeting of the National Fire Protection Association, Atlantic City, 1928.

[6] California Building Code (CBC) Ch. 23 – Wood, §2303 & Ch. 7A – Materials and Construction Methods for Exterior Wildlife Exposure, §702A, 2016

[7] J. Torero, "Flaming Ignition of Solid Fuels." SFPE Handbook of Fire Protection Engineering, Springer, 2016, pp. 633–661.

[8] Thomas, P.H. (1974). 'Effects of fuel geometry in fires'. Building Research Establishment

CP 29/74.

[9] Standard Test Method for Determining Direct Moisture Content Measurement of Wood and Wood-base Materials, (ASTM D 4442-16), Amer. Soc. for Testing and Materials, Philadelphia.

EVACUATION

USE OF STATISTICAL APPROACH ON STOCHASTIC EGRESS BUILDINGS SIMULATIONS

Quentin Jullien[1], Rémi Coutant[1], Paul Lardet[1], Nicolas Pinoteau[1]

1 : Centre Scientifique et Technique du Bâtiment, Champs-sur-Marne, France

ABSTRACT

Safe evacuation is becoming a major concern due to the increase of population density and disabilities associated to obesity or aging of some populations [1].

The goal of evacuation engineering is to demonstrate the safe egress of all occupants of a building before the sustainability conditions become death threatening.

The RSET (Required Safe Egress Time) is often used as a safety criterion. Many recent modelling tools present input data linked to behavioral parameters (associated to each occupant) expressed as statistical distributions. Thus, the output of the model is expressed as a distribution. The main challenge today is to construct the framework for evacuation safety engineering based on a statistical approach. This paper is one of the first steps to build it.

1   INTRODUCTION

The evacuation safety engineering relies on evacuation modeling tools. During the last years, several evacuation modeling tools have been proposed on the market (BuildingEXODUS, Pathfinder, Pedestrian Dynamics, …). A broad review of the existing models has been established by the National Institute of Standards and Technology [2]. Fueled by the increase of numerical capability, many of these software rely on microscopic models. The amount of required entry data for these models has boomed in the attempt to describe in detail physical (reaction time, walking speed) and behavioral characteristics (leadership, patience) of each pedestrian individually. Many of these parameters are proposed with default values in the different software facilitating the preparation of the simulation. As a consequence, the influence of some parameters cannot be clearly identified by users without in depth knowledge of the models.

To use the existing simulation tools in a performance-based engineering of evacuation, two issues must be addressed.

- *First, as any engineering analysis, it is required to choose the adequate entry data associated to the hazard and scenario. Given the number of input parameters proposed by some evacuation tools on the market, it is not feasible to declare representative distributions for all variables. It is therefore necessary to identify the key parameters that condition the RSET. A sensitivity analysis methodology is proposed to do it.*
- *Secondly, it is necessary to define a RSET safety criterion. Since the input of the stochastic models are partially expressed as statistical distributions, the definition of the safety RSET should be expressed statistically (associated to a failure probability).*

The goal of this paper is to address these two issues using a statistical analysis run on case studies using the software BuildingEXODUS to illustrate a method potentially applicable to other tools and building geometries.

2   BUILDINGEXODUS OVERVIEW AND GEOMETRIES

The numerical tool used in this study is BuildingExodus. It is based on a discretization of space by interconnected nodes of 50 cm x 50 cm using Moore's connection model. Each occupant has his own characteristics. Two occupants cannot be on the same node.

Several input geometries were used for the statistical analysis to quantify the architectural impact on the output. This impact can be observed through similarities or differences in outputs. The output of the simulations is the RSET defined as the exit time of the last occupant of the building. The geometries may yield second order phenomena such as congestion phenomena induced by reduction of the path sections (doors, corridors). These phenomena modify the RSET output. Furthermore, the geometry also modifies the weight of the different parameters on the RSET. For example, long escape distances will provide substantial importance to pedestrian walking speed while short exit distances might favor reaction time in conditioning the escape time.

To include the effect of geometry on the statistical analysis, 6 different geometries [A, B, C, D, E, F] were selected: 2 with very different evacuation distances and 4 with different numbers of bottleneck (called congestion levels thereafter). The two different evacuation distance geometries are composed of a 5 m x 5 m room where the occupants are initially. This room is considered connected to a 10 and 85 meters long corridor leading to the exit (respectively *Fig. 1* and *Fig. 2*).
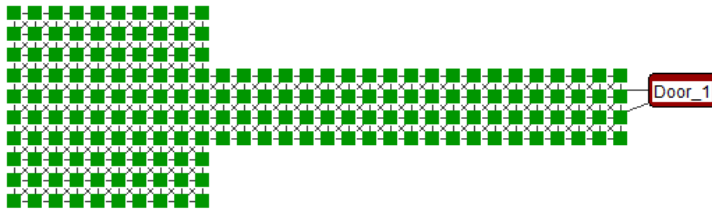

Fig. 1. Geometry 'A' with a 10 meters evacuation corridor

Fig. 2. Geometry 'B' with a 85 meters evacuation corridor

The geometry without congestion level is represented by a 35 meters long corridor where the occupants are initialized on the leftmost nodes (*Fig. 3*).
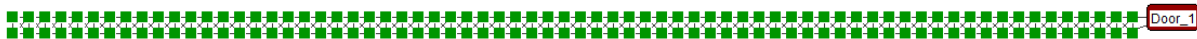

Fig. 3. Geometry 'C' without level of congestion

The other three geometries with different levels of congestion are composed of a 5 m x 5 m room where the occupants are initially. The rooms are connected to 1, 2 or 3 levels of congestion, then to a 10 meters long evacuation corridor (*Fig. 4 a) and b)* and *Fig. 5*).
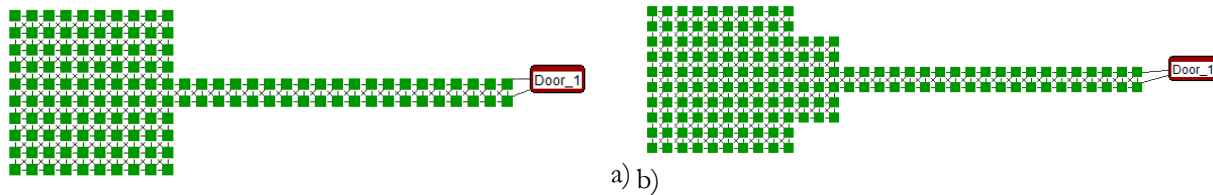

a) b)

Fig. 4. a) Geometry 'D' with 1 level of congestion; b) Geometry 'E' with 2 levels of congestion
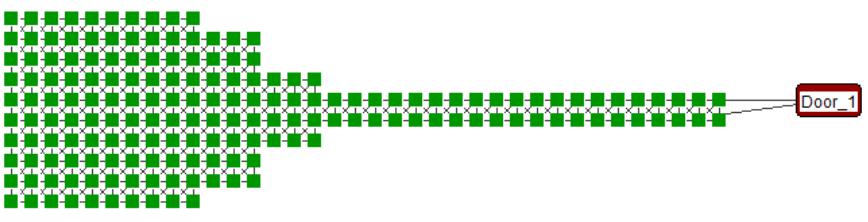

Fig. 5. Geometry 'F' with 3 levels of congestion

3   SENSITIVITY

The sensitivity analysis proposed here uses three steps:

− *the Latin Hypercube Sampling (LHS) method,*
− *the Sobol indices,*
− *the Bootstrap confidence interval.*

It allows to sort out the input data in regard to their influence on the RSET. This sensitivity analysis method is independent from the software to perform the egress simulations.

3.1 Sampling

A sensitivity analysis requires to explore the entire definition domain of each input variable. However, this is not suitable to an engineering approach due to high computational time. Thus, since most of the input variables are quantitative in nature (speed, leadership, reaction time), these variables need to be sampled to work on a subset of values representative of their theoretical density. Sampling is performed using an iterative algorithm, with one sample selected for each iteration. With enough iterations, the sampled values become distributed in a way that approximates the theoretical distribution of the population. There are several sampling methods, the main ones being the Monte Carlo method and the LHS method. The LHS method [4] is selected due to its ability to sample uniformly each definition interval of each variable. The process of the LHS can be summarized as follows:

− *Divide the theoretical distribution into N intervals of equal width;*
− *Randomly select a cumulative probability from each interval;*
− *Transform each cumulative probability into a random value from the specified theoretical distribution using the inverse function of the cumulative probability (here a walking speed).*

– Randomly match the values of each variable with all other variables

Table 1 represents modifiable input parameters available on BuildingEXODUS with the probability laws they follow or with their possible discrete values set (from BuildingExodus manuals and the literature). The geometry of the building studied, the number of occupants and their spatial position are defined as constants. Indeed, the geometry is represented by a fixed graph. The number of occupants and their initial positions are set constant from one simulation to another to only study the influence of the other parameters. The fixed initial positions allow to keep a coherence on the exit times of the occupants according to their own parameters.

Table 1. Modifiable parameters used in BuildingEXODUS

Input	Nature	Type [unit]	Law followed/Fluct. set
Exit target	Qualitative	Digit of door	{Nearest;1;2,…}
Gene (use to create a social group)	Qualitative	Integer	{0;1;2,…}
Group leader	Qualitative	Binary	{0;1}
Building geometry	Set of nodes and edges	-	Constant
Number of persons	Quantitative	Integer	Constant
Spatial positions	Vector of positions	-	Constant
Leadership Man : Drive M.	Quantitative	Real	Uniform([5;15])
Leadership Woman : Drive W	Quantitative	Real	Uniform([1;10])
Mobility coefficient	Quantitative	Real	{1;0,95;0,94;0,89;0,81;0,69;0,57}
Patience	Quantitative	Integer [sec]	Uniform({1;…;1000})
Pre-evacuation time	Quantitative	Integer [sec]	Uniform([0;30])
Walking speed Man	Quantitative	Real [m/sec]	Normal(1,30;0,13)
Walking speed Woman	Quantitative	Real [m/sec]	Normal(1,24;0,14)

Within each simulation, the panels of persons are composed of 50 men and 50 women with identical characteristics (except leaderships and travel speeds which are gender-specific). Each simulation is therefore characterized by 7 input parameters. In order to limit the number of separated parameters and reduce the computational time, these 100 persons have similar characteristics. This way, only 7 parameters must be studied rather than 500. To further reduce the number of factors, it is interesting to consider a new factor "walking speed". Its probability density is the concatenation of the densities of walking speed for men and walking speed for

women, weighted by mobility coefficients. In this way, the number of factors decreases from 7 to 5.

3.2 Sobol indices

This part describes briefly the Sobol indices principle and its asset to the sensitivity study. Mathematical details are available in [5], [6] and [7]. In this section, a theoretical set of factors $X = (X_1, X_2, \ldots , X_n)$ represents a set of physical parameters like $X = (age, weight, height, \ldots)$. $U_i = (X_{i1}, X_{i2}, \ldots , X_{ik})$ represents a ith subset of these parameters.

Each sensitivity index related to the set of factors U_i is theoretically between 0 and 1 because according to the variance decomposition formula, $V(U_i)$ is less than or equal to $V(Y)$ where Y represents the output, in this study the RSET. The Y analytic formula is unknown and obtained using egress simulations. The factors or sets of factors with the highest sensitivity indices most influence the response of the model. They are therefore the most important factors or sets of factors within the model.

There are several kinds of indices:

- *First-order indices, S_i: S_i are associated with the main effect of the X_i factor alone. It corresponds to the percentage of the variance of Y induced by X_i alone. For example, $S_1 = S_{age}$ represents the part of variability of the considered output inducted by the age factor.*
- *Higher-order indices, $S_{i,j}, S_{i,j,k}, \ldots$: $S_{Ui} = S_{i1,i2, \ldots ,ik}$ are associated with the effect of the interaction between the set of factors $U_i = (X_{i1}, X_{i2}, \ldots , X_{ik})$. For example, $S_{1,3} = S_{age,height}$ represents the part of variability of the considered output inducted by the interaction between the factors age and height.*
- *Total indices, S^T_{Ui}: They are associated with all effects associated to the set of factors $U_i = (X_{i1}, X_{i2}, \ldots , X_{ik})$. It's the sum of indices associated with $X_{i1}, X_{i2}, \ldots , X_{ik}$.*

Fig. 6 below illustrates the composition of each sensitivity index among each combination of 4 theoretical factors.
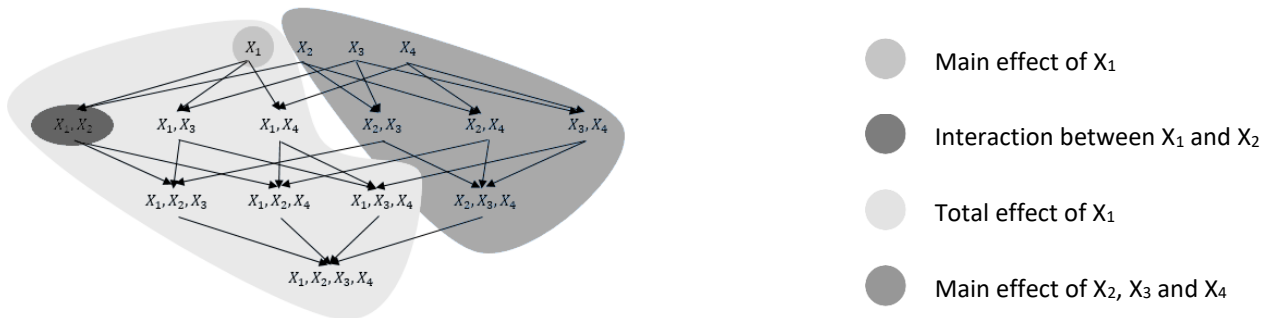

Fig. 6. Different kinds of Sobol indices

3.3 Bootstrap

Bootstrap techniques are statistical inference methods that assess the sensitivity of statistical indicators in a sample by analyzing its possible subsamples [8]. The bootstrap creates "new samples" only by drawing in the old one, with replacement from the initial sample. This is called resampling. The bootstrap technique goal is to assign a confidence interval to the sensitivity indices.

We are interested in the statistical variable X distributed according to a specific law in a population P. We do not have the global population census, but we do have the observed values of X on a sample size n: $x = (x_1, x_2, ..., x_n)$. The basic idea of the bootstrap is the following:

- *A parameter T of the population P is estimated from the sample by the statistic s(x) ;*
- *To improve the knowledge that one has of T over P, one proceeds to a resampling by drawing with B samples of size n in the sample x. These "bootstrap samples" are designated by $x_1*, x_2*, ..., x_B*$;*
- *Then $s(x_b*)$ is calculated for each bootstrap sample and statistical indicators of the distribution of $s(x_b*)$ are considered.*

In order to determine a confidence interval from the B values obtained by bootstrap, the standard error method can be used. This is based on the estimated mean $t*$, on the estimated standard deviation $s*$ of the distribution of $s(x_b*)$ and on the order quantile $1 - \alpha/2$ of a Student law at n-1 degrees of freedom, $q_{1-\alpha/2,n-1}$, where α represents the significance level. The proposed interval is *Eq. (1)*.

$$IC_\alpha = \left[t^* - q_{1-\frac{\alpha}{2},n-1} s^*; t^* + q_{1-\frac{\alpha}{2},n-1} s^* \right]$$

(1)

3.4 Results

The 90% confidence intervals obtained for the geometries A and B relative to the evacuation corridors are represented in *Fig. 7*. As one can see, the longer the evacuation corridors, the higher the walking speed is, to the detriment of reaction time. Indeed, in the 10 meters' corridor geometry, the RSET is greatly controlled by the pre-evacuation time because occupants can cross the corridor rapidly. But in a longer corridor geometry, the RSET would rather be controlled by the walking speed because the evacuation distance would be longer. Regarding leaderships (Drive) and patience, they are negligible because the geometry does not lead to substantial congestion phenomena.
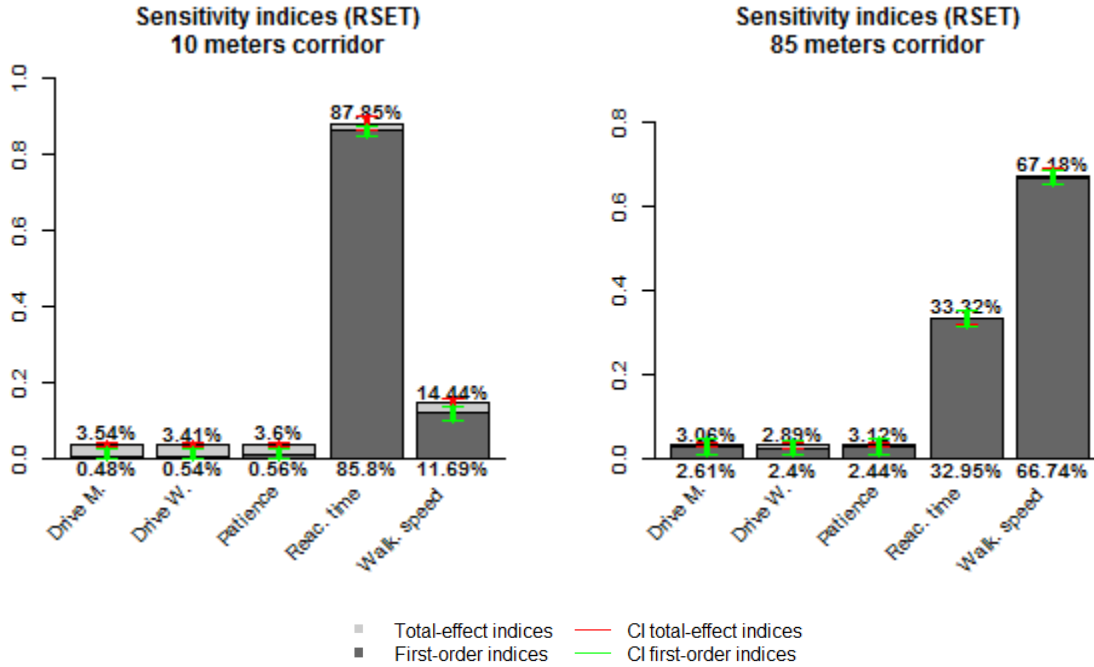
Fig. 7. Sensitivity indices obtained for the geometries relative to the evacuation corridors

The 90% confidence intervals obtained for the geometries C, D, E, F relative to the number of levels of congestion are represented in *Fig. 8*. The reaction time really impacts the RSET variations because the geometry is relatively small, however it remains very similar.
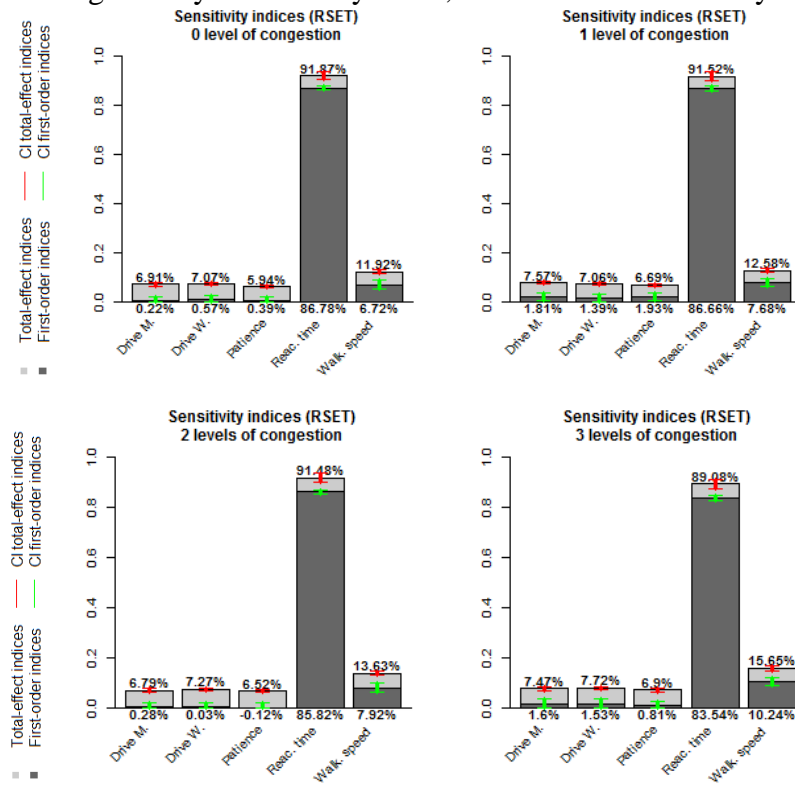

Fig. 8. Sensitivity indices obtained for the geometries relative to the levels of congestion

3.5 Synthesis

The sensitivity indices obtained for geometries A and B relative to corridors emphasize that the longer are corridors, the more speed walking influences the RSET variations. It shows that speed walking has to be known with accuracy for large-scale geometries. Because these geometries are quite large, leaderships (Drives) are less influential because there are a few number of travel conflicts. The indices estimated for geometries relative to congestion (C, D, E and F) follow the same trend. For these geometries, levels of congestion do not seem to be important into RSET variations. It can be noted that leadership may become more influential if the density of pedestrians increases. Among all sensitivity analysis, the reaction time is important. It must absolutely be known with precision, so the simulations are as close to reality as possible.

4   DETERMINATION OF AN RSET SAFETY CRITERION

The RSET is compared to the ASET (Available Safe Egress Time) to determine if a safety evacuation is possible. However, the ASET is usually deterministic whereas, by opposition, the RSET as said before is stochastic due to statistical distributions of the entry parameters. Thus, it is necessary to establish a safety criterion to compare properly ASET and RSET.

4.1 Distribution function

From a set of evacuation simulations, it is possible to draw the estimated RSET distribution function. This kind of graphs shows the probability for the RSET to take a value less or equal to a fixed x to define a safety criterion that is referred hereafter as the "safety RSET". The *Fig. 9 a) and b)* respectively represent the distribution functions associated with previous geometries. They also emphasize the bigger RSET found which can be interpreted as a safety RSET. But it is severe. In *Fig 9. a)*, it's possible to notice that the evacuation distance plays a significant role on the safety RSET as expected: the longer the evacuation distance, the longer the safety RSET is. On the contrary, in *Fig 9. b)*, the number of levels of congestion does not seem to be significantly important about the safety RSET: RSET variations are relatively slight.
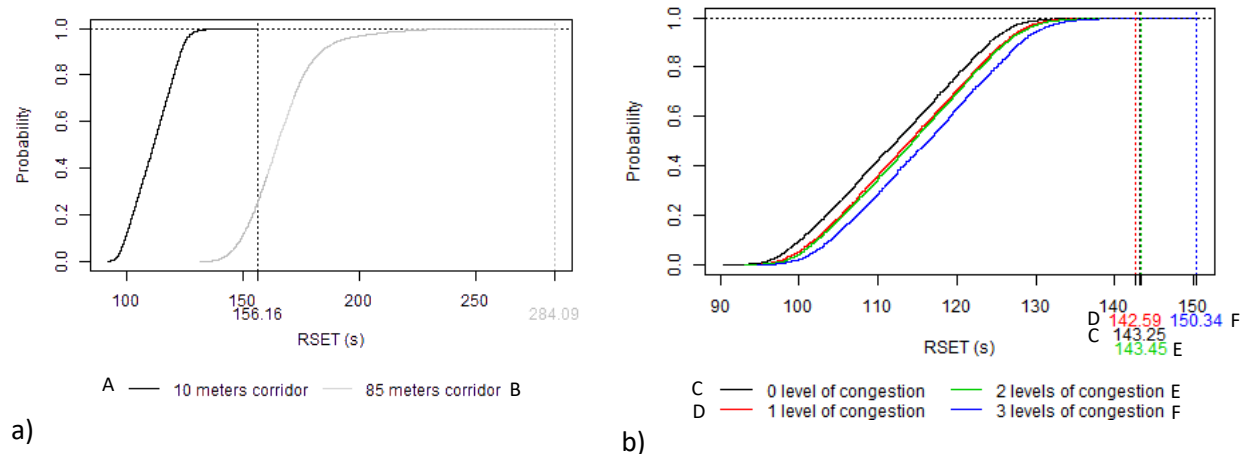

a)

b)

Fig. 9. Distribution functions obtained for the geometries characterized by their a) corridors; b) levels of congestions

4.2 Knowledge of parameters

A distribution of RSET being subject to a random part due to the stochastic part of simulators, they can be framed using confidence intervals with specific thresholds. More specifically, each quantile α of the distribution can be framed as explain in *Eq. (2)* [3]:

$$I_\alpha = \left[\tilde{F}^{-1}\left(\alpha - c_{1-\frac{p}{2}}\sqrt{\frac{\alpha(1-\alpha)}{n}}\right); \tilde{F}^{-1}\left(\alpha + c_{1-\frac{p}{2}}\sqrt{\frac{\alpha(1-\alpha)}{n}}\right)\right]$$

(2)

where $\tilde{F}^{-1}(x)$ represents the quantile of RSET of order x, α represents the quantile to frame, $c_{1-p/2}$ represents the quantile of the normal centered and reduced distribution of order $1-p/2$ (p represents the significance level, generally, $p = 0.1$ or 0.05) and n represents the length of the sample.

The interval length $L_{I\alpha}$ is given by *Eq. (3)*:

$$L_{I_\alpha} = \tilde{F}^{-1}\left(\alpha + c_{1-\frac{p}{2}}\sqrt{\frac{\alpha(1-\alpha)}{n}}\right) - \tilde{F}^{-1}\left(\alpha - c_{1-\frac{p}{2}}\sqrt{\frac{\alpha(1-\alpha)}{n}}\right)$$

(3)

which contains three constants: α, $c_{1-p/2}$ and n. Since the function $\tilde{F}^{-1}$ returns a specific quantile of a distribution, when a sample is added in this distribution, the interval can vary. So, with an iterative algorithm, it is possible to study the convergence of $L_{I\alpha}$. Likewise, when 2 parameters among α, $c_{1-p/2}$ and n are fixed, it is possible to find the third.

Sometimes, just one boundary of an interval is interesting. For example, in the case of RSET, the lower boundary is not meaningful whereas the upper boundary can provide information like safety RSET or the number of simulations which went wrong. In this way, the confidence interval can be asymmetrized: admitting significance levels p_1 and p_2 for lower and upper boundary respectively. *Eq. (4)* gives the expression for this interval. If one of the two boundaries is calculated with a 0% significance level, this boundary becomes identical to the estimated distribution function.

$$I_{\alpha_L, \alpha_U} = \left[\tilde{F}^{-1}\left(\alpha - c_{1-p_1}\sqrt{\frac{\alpha(1-\alpha)}{n}}\right); \tilde{F}^{-1}\left(\alpha + c_{1-p_2}\sqrt{\frac{\alpha(1-\alpha)}{n}}\right)\right]$$

(4)

4.3 Synthesis

The determination of a safety criterion allows to compare easily ASET and the RSET. At first sight, the calculated maximum value appears satisfying, but it is not a reliable criterion: as a stochastic approach is used extreme values can be omitted by the study even with a LHS method; on the contrary, they can also be overestimated and give extremely severe criteria. Thus, a quantile and particularly the 95th percentile associated to a confidence level of 90% (which are commonly used values in the field of statistics) can be suitable to define a safety RSET criterion. As written above, the length of the confidence interval is linked to the number of simulations. The convergence on the confidence interval length can be used to statue on simulations number.

5   LIMITATIONS

The selected geometries are simple enough to test robustness of the method. Calculated results are in good agreement with expected results on such simple configurations and demonstrate the approach relevancy. Indeed, it can be expected that reaction time and speed would be the most influent parameters. Nevertheless, generalizing of this result would require a deeper exploration of more complex geometrical configurations. Furthermore, only five parameters are studied in this paper. Thus, the scope of reachable conclusions is limited. Increasing the number of simultaneously studied parameters would require a huge number of calculations. Therefore, using this approach in an engineering context requires to improve the method to reduce this calculations number.

Finally, results also rely on input parameter ranges presently coming from the literature and default values. A study on these ranges should be done too to be able to generalize results.

6   CONCLUSION

This paper presents two methodologies to better characterize the influence of the entry parameters on the RSET and to give a RSET safety criterion. It is part of a broader work to propose a framework in France for evacuation safety engineering. As said previously, this paper is one of the first steps. Indeed, only two test case geometries and their variations have been presented. The geometries are humble but give interesting and expected results. Further test cases will be studied to continue to test methodologies robustness.

A great advantage of these methodologies is their universality. Thus, a current work with authorities is under development: assess the applicability of these methods to other evacuation modeling tools through a benchmark.

Moreover, these methodologies and particularly the one on the sensitivity analysis can be improved. Some works have already begun on the use of other methods for indices calculation. In addition, an analysis has started to treat persons with different characteristics and/or more parameters simultaneously. Then, the probabilistic nature of the safety criterion implies to share an acceptable failure probability level and further discussions must be held on that topic.

Finally, in parallel to the reliability and statistic approaches to determine safety thresholds, physical analysis is carried out to increase the representativity and robustness of the calculations of egress times. In particular, the sensitivity analysis results can allow to identify the most influential input data and get a better knowledge of them.

REFERENCES

[1]   K. Boyce. (2017). *Safe evacuation for all - Fact or Fantasy? Past experiences, current understanding and future challenges*. Fire Safety Journal, IAFSS 2017.

[2]   E. D. Kuligowski, R. D. Peacock, Bryan L. Hoskins. (2005). *A Review of Building Evacuation Models*. NIST, Technical Note 1471, July 2005.

[3]   Q. Jullien, P. Lardet. (2016). *Stochastic analysis of egress simulations. Fire and Evacuation Modelling Technical Conference* (FEMTC), Torremolinos, Spain 2016.

[4]   M. Stein. (1987). *Large Sample Properties of Simulations Using Latin Hypercube Sampling*. Technometrics vol. 29, no. 2, May 1987, pp 143–153.

[5]   I. M. Sobol. (1993). *Sensitivity estimates for non linear mathematical models*. Math. Model. Comput. Exp. 1, pp 407–414, 1993.

[6]   I. M. Sobol. (2001), *Global sensitivity indices for nonlinear mathematical models and their Monte Carlo estimates*, Mathematics and computer in Simulations 55 (2001), pp 271–280.

[7]   R. Faivre, B. Iooss, S. Mahévas, D. Makowski, H. Monod. (2013). *Analyse de sensibilité et exploration de modèles*, Editions Quae, 2013.

[8]   M. Gardner, D. Altman, D. Machin, T. Bryant. (2005). *Statistics with confidence Intervals ans Statistical Guideline*s, BMJ Books, 2005.

THE INFLUENCE OF SIGNAGE COLOUR ON EXIT CHOICE: OBSERVED BEHAVIOUR DIFFERS FROM VERBAL REPORT

Max Kinateder[1], William H Warren[2], Karen B Schloss[3]

[1] National Research Council Canada, Ottawa, Canada

[2] Department of Cognitive, Linguistic, and Psychological Sciences, Brown University, USA

[3] Department of Psychology and Wisconsin Institute for Discovery, University of Wisconsin-Madison, USA

ABSTRACT

Building occupants are typically informed about fire evacuation routes through coloured and illuminated emergency exit signs. The presence of other coloured illuminated signs may distract occupants when searching for safe exit. Such distractions could lead to confusion and even harmful outcomes if occupants misinterpret the sign colours, mistaking non-exit signs for exit signs. This contribution presents data from a virtual reality experiment that tested which coloured signs people would walk toward in an emergency. Participants were immersed in a virtual room with two doors straight ahead from the starting position. An illuminated sign with different coloured vertical bars was placed above each door (green, red, yellow, magenta, blue, and grey). On each trial, a fire alarm sounded, and participants walked toward the door that they thought was the exit. Participants were most likely to walk toward green signs. However, in a post-experiment survey most participants reported that exit signs should be red [1]. This demonstrates a dissociation between the way self-reported expected behaviour in emergency situations and actual behaviour. These results have implications for the design of exit signs. Occupants, and maybe building designers too, may not always correctly anticipate how occupants will use information that should guide them towards safety. Overall, this result emphasizes the importance of behavioural experiments of evacuation behaviour.

1   INTRODUCTION

Emergency exit signs are used to inform building occupants about safe egress routes in emergency situations. Exit signs should provide guidance when needed, but be unobtrusive otherwise. Building and safety codes typically require exit signs to either display white illuminated pictogram/text ("EXIT/SORTIE") on a coloured background, or a coloured pictogram/text on a white or clear background [e.g., 2]. Most building codes around the world prescribe green as the colour for exit signs. However, certain codes, such as the National Fire Protection Association (NFPA) 101 let users choose between red and green exit signs.

Colour is an important design feature because it can convey information under low visibility, when pictograms or text may be illegible. Low visibility conditions, for example smoke filled environments, also tend to be ones under which building occupants may require guidance about evacuation routes. However, other coloured signs near exit signs might be distracting, confusing building occupants about which routes afford safe egress. A particularly dangerous scenario could arise if occupants inferred that the colours of non-exit signs were more likely to signal 'exit' than the colours of exit signs do. Thus, it is important to understand how occupants interpret the colour of exit signs.

Here, we present data from a study investigating people's inferences about which colours are more likely to signal 'exit' in a simulated emergency, i.e. their *colour inferences*. Understanding colour inferences is important for effective exit sign designs because designs are easier to interpret when the encoded mapping between perceptual features and concepts (e.g., the colour of actual exit signs) matches people's expectations (e.g., their prediction about the colour of exit signs) [3-6].

Some previous work suggested that people associate green signs with exit signs [e.g., 7, 8, 9]. Most of these studies, however, were conducted in countries that require exit signs to be green. Consequently, it is unclear if participants were more likely to choose green because it mimicked the colour of exit signs in their immediate environment, which we refer to as the *local exposure hypothesis*, or because green was associated with concepts that signalled "safe exit,", which we refer to as the *semantic association hypothesis*. Although context shapes how people infer meaning from colour [5, 10, 11], the green-associated concepts of "go" [12] and "safety" [13] seem particularly relevant for signalling "safe exit" in emergencies. In contrast, the concepts of "stop" [12] and "danger" [14-16] which are associated with red could have the opposite effect.

We dissociated the local exposure and semantic association hypotheses by evaluating exit choice in a region where exit signs are mandated to be red. In addition, participants in our study walked by multiple red exit signs on their way to the testing laboratory. If participants still infer that green signs are exit signs, that would support the notion that colour inferences for exit signs are not based on local exposure but rather due to semantic associations.

We tested the two hypotheses in a controlled virtual reality laboratory setting. Immersive virtual reality (VR) experiments allow balancing ethical considerations with those of data validity [17, 18]. Previous VR studies found that egress behaviour improved when participants were guided by exit signs compared to no signs [19], and attention improved with dynamic exit signs compared to standard exit signs [20]. We present results from a study in which participants chose one of two exits while walking in VR. Above each door there were differently coloured signs (all pairs of red, yellow, green, blue, magenta, and white). After the walking task was completed, participants were asked which colour exit signs typically were in their environment and what colour they thought exit signs should be. We found that responses to these questions were at odds with the results from the walking task: participants reported that red would be best for exit signs, yet they were most likely to walk toward green signs [1].

2 METHODS

2.1 Sample

Twenty-four undergraduate students (twelve female, mean age 19.79 years, SD 1.28) participated in the study. All of them had normal or corrected to normal vision, gave informed consent, and were compensated for their participation. The study was approved by the Brown University Institutional Review Board.

2.2 Test setup

The virtual environment consisted of a virtual replica of the physical lab space. However, instead of facing a single door, in each trial participants saw two identical exit doors on one end of the room. A coloured backlit exit sign with four vertical bars was placed over each of the two doors.

Testing was conducted in a 14x16 m laboratory space at Brown University. The VR set-up allowed participants to physically walk in VR does not require input devices for navigation. Orientation and head position were recorded using a hybrid ultrasonic-inertial tracking system (sampling rate of 60 Hz; IS-900, Intersense, Billerica MA). The system can track position and rotation at 360° at an angular resolution of 0.10° in the trackable area. The virtual environment was presented using an untethered head-mounted display (HMD; Rift DK1 for the first 16 participants, Rift CV1 for the last eight participants; Oculus, Irvine CA; 110° diagonal field of view; set at 6.4 cm IPD (no individual adjustments). A mobile battery pack carried in a small backpack, along with the DK1 control box was used to power the HMD. The virtual environment was generated on a workstation pc (frame rate of 60 fps), using the Vizard 4 software package (WorldViz, Santa Monica CA). The displays were transmitted wirelessly to the HMD using two HDTV transmitters, and presented stereoscopically. Head position and orientation coordinates from the tracker were used to update the display with a latency of 50-67 ms (3-4 frames).

2.3 Design, Displays, and Procedure

The study used a within-subjects repeated measures design. Participants were presented with all 15 pairwise combinations of 6 exit sign colours (red, yellow, green, blue, magenta, and white). Each pair of colours appeared four times, twice with one of the colours over the left door and the other over the right, and twice with the opposite left/right assignments. This resulted in a total of 60 trials. By having each colour appear an equal number of times on the left and right, we ensured that any tendency to walk to one colour over another was not driven by a bias towards one of the two doors. The trial order was pseudo-randomized for each participant.

At the beginning of each trial participants were placed 10.87 m equidistant from two identical doors (one to the left and one to the right). Each door had a coloured backlit sign over the door frame. Two seconds after trial start, a fire alarm sounded and participants picked whichever door seemed to be appropriate to walk toward. A trial ended when participants reached one of the doors. Participants then returned to the starting position. Prior to testing, participants completed two practice trials in which the signs were both coloured white. Short breaks were interleaved every 15 trials to reduce the risk of simulator sickness.

After participants had completed the walking task, they answered a series of questions in which they rated the alarm's realism (4 point Likert scale from *very unrealistic* to *very realistic*) and answered free-response questions about exit sign colours. One question asked them to report the typical colour of an emergency exit sign in their home state, the state where the study was conducted, and inside the university building where the testing took place. They were also asked to report which colour they deemed most appropriate for emergency exit signs.

3   RESULTS

3.1 Walking task

Figure 8A illustrates the proportion of times each colour was chosen. The green exit sign was chosen most often. A binary logistic regression was used to predict which exit choice (left/right) by exit sign colour. We tested models for each of the two hypotheses (local exposure vs. semantic association) by defining the reference category (intercept) of the logistic regression model according to the hypothesis (i.e., green for the semantic association hypothesis and red for the local exposure hypothesis).
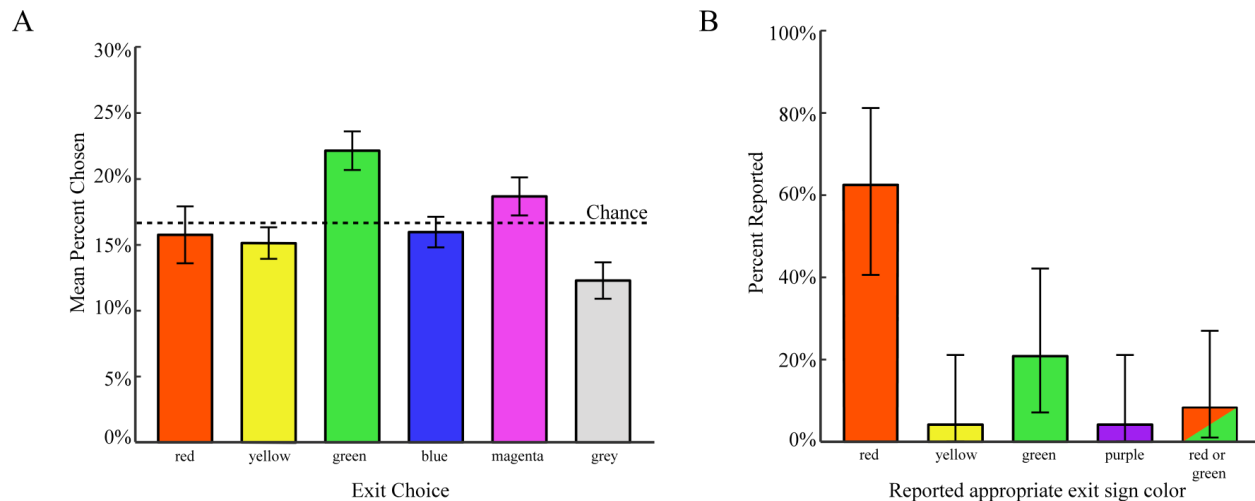
Figure 8. (A) Proportion of times participants walked toward each of the coloured signs, averaged across participants. Error bars represent standard errors of the means. (B) Reported appropriate colours for exit signs. Error bars represent multinomial confidence intervals

In the first logistic regression, participants were significantly more likely than chance to pick the door with the green exit signs (Odds = 1.64, $p < .001$), and significantly less likely to pick a door with a sign with any other colour except the magenta sign (all ps $< .001$, see [1] for more detailed results). These results support the semantic association hypothesis.

In a second logistic regression, we used red exit signs as the reference category to test the local exposure hypothesis. There were no differences between red and any other colour except for green as described above, Odds = 1.97, $p < .001$, and white, Odds = 0.61, $p < .01$, where green was chosen more often than red, and was chosen less often. These results challenge the local exposure hypothesis.

3.2 Post-experiment exit sign questionnaire

All participants stated that exit signs in their home-states and in the state where the study was conducted were typically red. Three quarters of the participants correctly reported that the colours in the university building where testing was conducted were red; three stated that these were green, and three reported that they did not know. 62.5 % responded that red would be the appropriate colour for an emergency exit sign, whereas only 20.9 % reported that green was most appropriate, $X^2(4) = 29.333$, $p < .01$ (see Figure 8B). These results directly contradict the finding that the same participants had a robust tendency to walk toward the green sign (Figure 8A). Finally, 91.7 % of participants rated the alarm as either *realistic* or *very realistic*.

4 CONCLUSIONS

The data discussed here and originally reported in [1], found that participants were most likely to walk to doors with green signs in simulated emergency. Later on, however, the same participants were most likely to report that exit signs should be red. These results lead to two conclusions:

1. The results challenge the local exposure hypothesis because participants did not walk toward the signs that had the colour of exit signs in their local environment. It was especially surprising by how infrequently participants walked toward the red sign, given

that our sample had grown up and lived in an environment with predominantly red exit signs. In addition, the results lend some support to the semantic association hypothesis; participants may have walked toward green doors because of associations between green and concepts of "*safety*" and/or "*go.*" Future research will need to determine how specific semantic associations influence interpretations of colours during fire evacuation.

2. Observed behaviour contradicted verbal report. This dissociation has implications for design and testing of evacuation signage. We argue that exit signs should be studied behaviourally in ecologically valid environments, rather than exclusively relying only on people's subjective reports. Although interviews and questionnaires can yield important insights on how occupants think about design, relying on subjective reports risks reproducing the status quo and may not correctly predict how occupants will behave during evacuations.

This study had two main limitations. First, participants were always aware that the fire alarm was part of a simulation, even though the virtual environment replicated the physical environment of the lab as closely as possible. Second, the nature of a lab study is more similar to the character of an announced fire drill than a real fire emergency.

All in all, the present study contributes to the growing body of literature demonstrating that people form inferences about the meanings of colours, which influence their interpretations of the world [1]. Understanding these inferences will enable more effective use of colour in design, which is especially critical for emergency egress when occupants make fast decisions that influence the safety of themselves and others.

ACKNOWLEDGEMENTS

REFERENCES

[1]   M. Kinateder, W. H. Warren, and K. B. Schloss, "What color are emergency exit signs? Egress behavior differs from verbal report," *Applied Ergonomics,* vol. 75, pp. 155-160, 2019/02/01/ 2019.

[2]   National Fire Protection Association, "NFPA 101 life safety code," ed. Quincy MA, USA: National Fire Protection Association, 2015.

[3]   D. A. Norman, *The design of everyday things: Revised and expanded edition*: Basic books, 2013.

[4]   B. Tversky, J. B. Morrison, and M. Betrancourt, "Animation: can it facilitate?," *International journal of human-computer studies,* vol. 57, pp. 247-262, 2002.

[5]   K. B. Schloss, L. Lessard, C. S. Walmsley, and K. Foley, "Color inference in visual communication: the meaning of colors in recycling," *Cogn Res Princ Implic,* vol. 3, p. 5, 2018.

[6]   K. B. Schloss, C. C. Gramazio, T. S. Parker, and A. S. Wangs, "Visual Semantics of Colormap Data Visualizations," *IEEE Transactions on Visualization and Computer Graphics,* in press.

[7]   J. Troncoso, D. Nilsson, and E. Ronchi, "Response to Emergency Way Finding Systems by People from Different Cultures," ed: Sweden: Department of Fire Safety Engineering, Lund University, 2014.

[8]   E. Ronchi, D. Nilsson, S. Kojić, J. Eriksson, R. Lovreglio, H. Modig, *et al.*, "A virtual reality experiment on flashing lights at emergency exit portals for road tunnel evacuation," *Fire Technology,* vol. 52, pp. 623-647, 2016.

[9]   A. W. Heskestad, "Performance in smoke of wayguidance systems," *Fire and materials,* vol. 23, pp. 375-381, 1999.

[10]   A. Elliot and M. A. Maier, "Color-in-context theory," *Advances in Experimental Social Psychology,* vol. 45, pp. 63-125, 2012.

[11]   N. Humphrey, "The colour currency of nature," in *Colour for architecture*, T. Porter and B. Mikellides, Eds., ed London: Studio-Vista, 1976, pp. 95-98.

[12]   C. K. Or and H. H. Wang, "Color–concept associations: A cross-occupational and-cultural study and comparison," *Color Research & Application,* vol. 39, pp. 630-635, 2014.

[13]   D. Nilsson, H. Frantzich, and W. Saunders, "Coloured Flashing Lights to Mark Emergency Exits-Experiences from Evacuation Experiments," *Fire Safety Science,* vol. 8, pp. 569-579, 2005.

[14]   M. F. Lesch, P.-L. P. Rau, Z. Zhao, and C. Liu, "A cross-cultural comparison of perceived hazard in response to warning components and configurations: US vs. China," *Applied Ergonomics,* vol. 40, pp. 953-961, 2009/09/01/ 2009.

[15]   D. S. Leonard, "Does color of warnings affect risk perception?," *International Journal of Industrial Ergonomics,* vol. 23, pp. 499-504, 1999/03/20/ 1999.

[16]   K. Pravossoudovitch, F. Cury, S. G. Young, and A. J. Elliot, "Is red the colour of danger? Testing an implicit red–danger association," *Ergonomics,* vol. 57, pp. 503-510, 2014.

[17]   M. Kinateder and W. H. Warren, "Social influence on evacuation behavior in real and virtual environments," *Frontiers in Robotics and AI,* vol. 3, p. 43, 2016.

[18]   M. Kinateder, D. Nilsson, M. Kobes, M. Müller, P. Pauli, and A. Mühlberger, "Virtual Reality for Fire Evacuation Research," in *Federated Conference on Computer Science and Information Systems*, Warsaw, Poland, 2014, pp. 319-327.

[19]   C. H. Tang, W. T. Wu, and C. Y. Lin, "Using virtual reality to determine how emergency signs facilitate way-finding," *Applied Ergonomics,* vol. 40, pp. 722-730, Jul 2009.

[20]   E. Duarte, F. Rebelo, J. Teles, and M. S. Wogalter, "Behavioral compliance for dynamic versus static signs in an immersive virtual environment," *Appl Ergon,* vol. 45, pp. 1367-75, Sep 2014.

COMPARISON OF EVACUATION STRATEGIES IN A HOSPITAL INFIRMARY IN CASE OF FIRE

Amarildo Benzane, João Paulo Rodrigues
Coimbra University, Portugal

ABSTRACT

This paper presents the results of a numerical modeling on the fire evacuation of a hospital infirmary. Although it is a case study, the results obtained can be extrapolated to hospitals' infirmaries in general. The modelling considered bedridden and not bedridden patients. The using of lifts was also evaluated, being the time needed for evacuation, the average number of patients evacuated and the number of lifts needed to evacuate determined. Five fire scenarios, four considering horizontal evacuation and one vertical evacuation using lifts, have been considered. The horizontal evacuation consisted on transferring the patients from a compartment in fire to another safe in the same floor and the vertical evacuation consisted on the evacuation of the patients using lifts from the compartment in fire to the ground-floor and then to outside the building. The effect of the pre-movement time, the origin of the fire, the type of occupants (bedridden and non-bedridden), among other parameters have been tested. The results showed that the horizontal evacuation was more effective than the vertical one using lifts.

Keywords: patients, fire, evacuation, numerical simulation, risk.

1   INTRODUCTION

The fire safety regulations state in general that in case of fire the occupants should not use the lifts for evacuating a building. The occupants can be trapped in the lift in case of fire and the lift's shaft can be filled of smoke being fatal for the users. The fire safety regulations state that in case of fire the lifts must stop the gear and travel to the reference floor and stop there with the doors open [1 and 2]. Only the stairs should be used for evacuation, which is not always the best way due to the different type of people that may arise there, as for example disabled, elderly, obese and in some cases bedridden.

Some authors say that in certain cases the use of lifts in evacuation of a building in case of fire, can be an appropriate mean of escape, for example in high-rise buildings or hospitals. In these case the lifts have to be provided with additional warranties, such as duplicate power supplies or protected communication systems [3]. The vertical evacuation using lifts in hospitals is practical for situations where patients cannot evacuate by their own means or need to take with life support systems. The patients with walking capabilities should use the stairs while the disabled may use the lifts.

In extreme situations, the patients without motion problems and the hospital staff can use the lifts for evacuation in order of not being subjected to hazardous conditions such as toxic gases and smoke and also high temperatures. However, this vertical evacuation in large hospitals should be to shelter areas, if possible, two floors below the fire [4 and 5].

Some studies in high-rise buildings evaluated the lifts' capacity for evacuation people in normal situations. They have concluded that in peak times the lifts can transport between 5 and 7.5% of

the occupants in residential buildings and 13 and 18 % in office buildings. This means that occupants can be transported to the upper floors in 67 to 100 min in residential buildings and 29 to 40 min in office buildings [6]. A Building Traffic Simulator (BTS) studied the influence of the modern lift call system on the number of occupants carried between the down-peak and up-peak. The BTS found that in down-peak lifts have carried between 22.5% and 27% of the occupants and in up-peak 15% the occupants. The reason for these figures is that lifts have fewer calls and can reverse the movements easier in down-peak. This reduces the round-trip time and increases the carrying capacity of the lifts.

Depending on the location of the lifts in relation to the fire origin, the effects of the fire mainly in terms of smoke may occur sooner or later. This period of time is important for the evacuation between floors using lifts [7]. In these cases, the lifts should prioritize being the evacuation of the affected floors first and only then the other floors. This strategy may ensure an efficient evacuation of the building in case of fire.

In this paper, they are presented the results of the evacuation modeling of a hospital infirmary block in case of fire and compared the horizontal with vertical evacuation using or not lifts. The impact of the pre-movement time in the evacuation, the location of the fire origin and the type of occupants (bedridden and non-bedridden) have been analyzed. The study has used the Fire Dynamics Simulator (FDS) software with the evacuation model (Evac) [8].

2   CASE STUDY

The infirmary block (IB) studied is developed in the horizontal plane, with an area of 1058 m², having 23 m length and 46 m width. A smoke control system in the horizontal evacuation routes, with four smoke extractors and two air insufflators (red rectangles are smoke extractors and green are air insufflators) (*Fig. 1a*) has been considered. Three lifts (Elev-1, Elev-2 and Elev-3) of 7.5 m² area each for evacuating bedridden patients have also been considered (*Fig. 1a*). The IB has also two emergency evacuation exits (EE-1 and EE-2) with 2 m width each. The IB has in terms of rooms, four infirmary rooms (R6, R7, R8 and R9), two isolation rooms (R4 and R5), two treatment rooms (R10 and R14), two offices (R11 and R13), one meeting room (R1) one living or dining room (R2) and one medicine preparation room (R12) (*Fig. 1b*). In addition, there were two horizontal evacuation routes (HER-1 and HER-2) with 1.80 m and 2.71 m width, respectively (*Fig. 1b*).

The study considered the influence of two type of occupants on the evacuation, bedridden or large size occupants (LSO) and not bedridden or normal size occupants (NSO). For these types of occupants, different displacement speeds have been considered. Thus, the ONS moved at 0.60 m/s and the LSO moved at 0.22 m/s. The displacement speeds adopted for each group of occupants were based on the studies of Proulx and Jiang [9, 10, 11 and 12].

Table 1. smoke control system

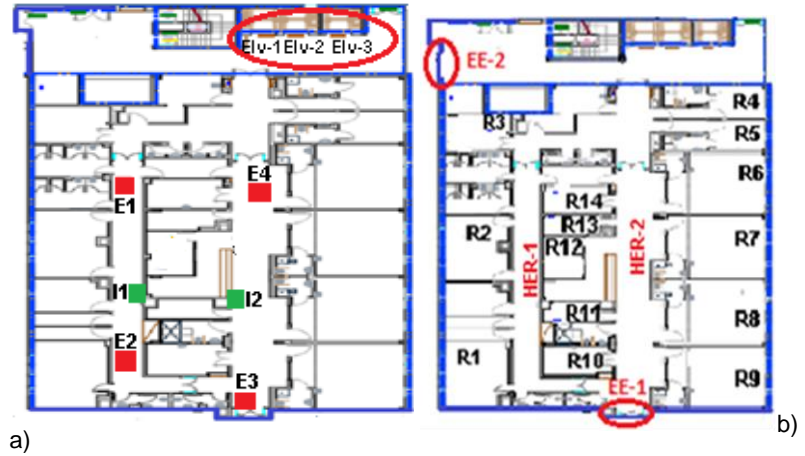| Type	Device	Flow rates (m³/s)
Extraction	E 1	1.5
Extraction	E 2	1.5
Extraction	E 3	2.5
Extraction	E 4	2.5
Insufflation	I 1	1.8
Insufflation	I2	3

Fig. 1. Fire compartment - Infirmary block (IB).

2.1 Parameters adopted in the simulation

The numerical simulations have used the FDS+Evac software. Several parameters have been considered such as the age of the occupants (elderly of both gender), occupants' location, displacement speeds, normal and disabled occupants, geometry of the building (stairs, evacuation routes, walls and dimensions, etc.), type of fire, existence and location of the smoke control system.

The general parameters and respective values adopted to guarantee the minimum evacuation conditions were:

- The devices for measuring the Fractional Effective Dose (FED), temperature and visibility were placed along the evacuation routes HER-1, HER-2 and HER-3 with a distance between them of 2.25m in horizontal and 0.25m in vertical.
- The average displacement speed adopted was between 0.1 and 1.02m/s corresponding to people moving with a walking frame [11 and 12];
- A fire load was 280 MJ/m^2 considering that the fire compartment under study is part of a hospital [13].
- Maximum temperature for evacuation of 80°C measured at a minimum height of 1.75 m above the floor [14];
- The toxic gases (FED) with a value less than 0.1 [15 and 16];
- A burner with an area of 1 m^2 and a heat release rate of 5 MW, [13];
- A visibility measured at 1.80 m height for a right foot of 3.00 m [1, 16, 17, 18 and 19], however, the present study adopted 1.75 m since it is multiple of the mesh used (0.25 m);
- The smoke extraction devices were at a height of 3 m and the air insufflation devices were at 0.5 m from the floor;
- The fire curve used is of average growth rate as recommended for hospital rooms (*Fig. 2*) [13].
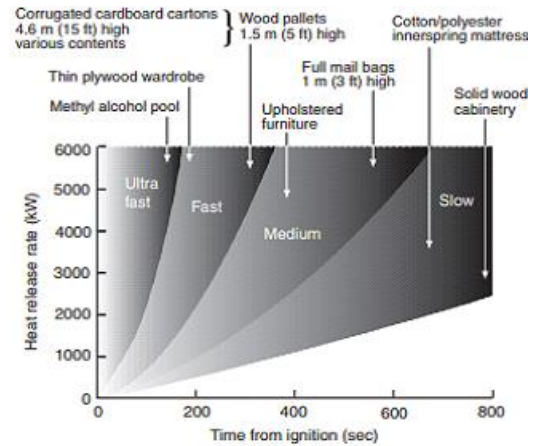

Fig. 2. T-square set of growth curves [20]

For the infirmary block (scenario_IB) they were considered a fire origin in room R3 or R12 (FFR3/R12), with or without lifts (Elev) and smoke control system (RSCS). The fire scenarios studied were of type: scenario_IB_FFR3_RSCS, scenario_IB_FFR12_RSCS, and scenario_IB_Elev_FFR6_RSCS.

2.2 Fire origins

Two fire origins were considered, one in the medicine's preparation room-R12, compartment with occupants, (*Fig. 3a*) and another in the bed disinfection room-R3, compartment without occupants (*Fig. 3b*). The medicine's preparation room-R12 was chosen because it was located almost at the center of the IB and the fire can easily spread to rooms with a lot of patients (R7 and R8) (*Fig. 3a*). In another way, the fire in the bed disinfection room-R3 was chosen because it is located far away from compartments with occupants and the fire can be known by the occupants with the fire alarm (*Fig. 3b*). The number of occupants to evacuate were 100 (*Fig. 3c*) that has already the increasing of more 30% as recommended for hospital rooms [1].
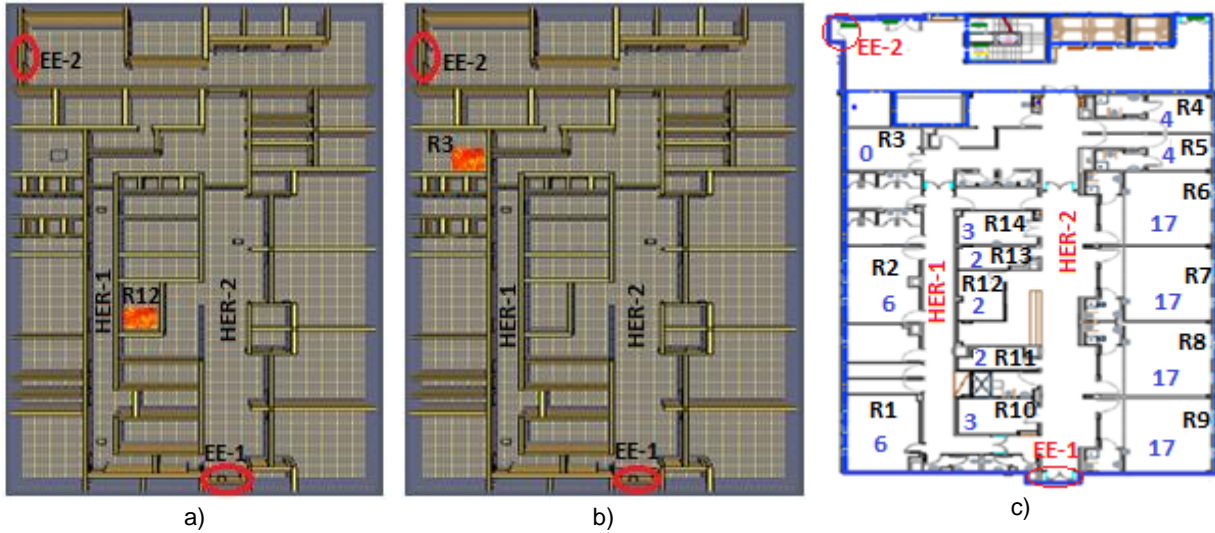
Fig. 3. Infirmary Block; a) fire origin in the preparation of medicines room, b) fire origin in the disinfection of beds room and c) distribution of the occupants by room.

For the analysis of the vertical evacuation, the fire was considered in the medicine's preparation room-R12 because if considered in the bed disinfection room it would block the access to the lifts. Thus, the pre-movement ended at 30s for the first fire origin, consisting on both horizontal and vertical evacuation, and at 180 s for the second fire origin, consisting only on horizontal evacuation.

3 RESULTS

In this section only results of two of a total of the five fire scenarios analyzed, are presented. The two fire scenarios considered the origin of the fire in room-R12 (medicine's preparation room), one with horizontal evacuation and another with vertical evacuation. The room had two type of occupants, reason for which the time of the pre-movement reduced considerably and was fixed in 30 s (Fig. 4a). The nurse-R11 ward (Fig. 4b) ended the pre-movement at 60 s, nurses' rooms R7 and R8, (Fig. 4c) ended after 90 s, nurses' rooms-R6 and R9 and the treatment rooms-R10 and R14 (Fig. 4d) ended at 120 s. The pre-movement in the remaining rooms was up to 180 s (Fig. 4e). For the rooms which the end of the pre-movement was before 180 s, their proximity to the origin of the fire was taken into account as well as the alert due to the entrance of the smoke in the rooms.
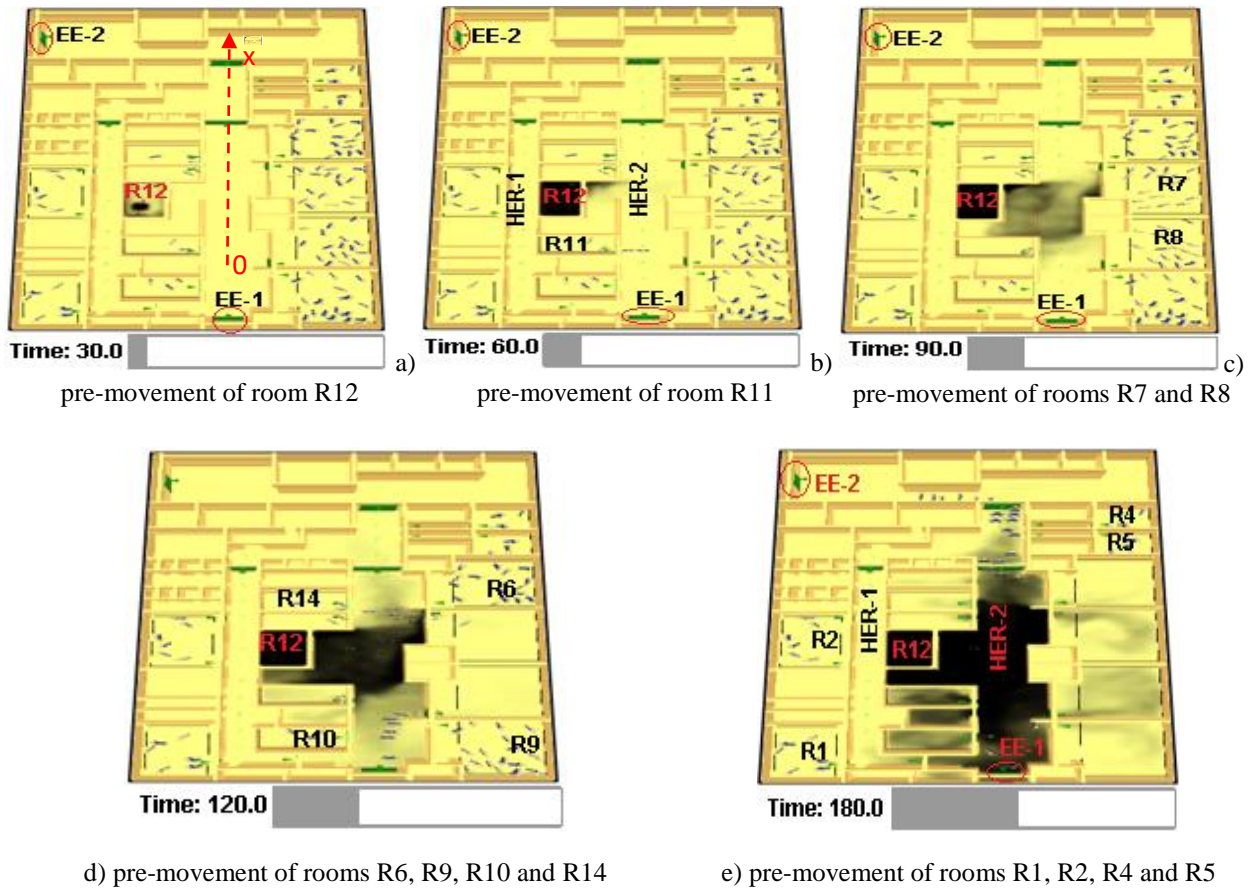
a) pre-movement of room R12

b) pre-movement of room R11

c) pre-movement of rooms R7 and R8

d) pre-movement of rooms R6, R9, R10 and R14

e) pre-movement of rooms R1, R2, R4 and R5

Fig. 4. Location of occupants and smoke spread for pre-movements times: a) 30s; b) 60s; c) 90s; d) 120s d) 180s

3.1   Scenario_IB_NSO_FFR12_RSCS

The evacuation of the fire compartment for scenario_ID_NSO_FFR12_RSCS was completed in 318 s, through the two emergency exits (EE-1 and EE-2). The end of the pre-movement time was at 30 s after starting the numerical simulation. Through the emergency exit EE-1 abandoned the fire compartment 54 occupants, being the last one at 314 s (solid lines and dashed in black) and through the emergency exit EE-2 abandoned 46 occupants, being the last one at 348 s (solid lines and red dashed lines) (*Fig. 5*).

In the horizontal evacuation route HER-1 the temperature of the gases was below 80°C at 1.75m above the floor and visibility was very high on the safety side (*Figs. 6 and 7*). In certain zones, for distances from 6.75 to 18 m, at a time instant of 348 s, the maximum temperature of 80ºC was reached slightly below the 1.75 m of height but this does not affect the evacuation.
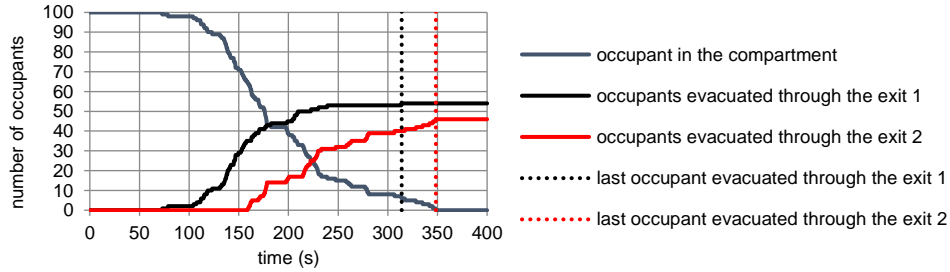
Fig. 5. Number of occupants that evacuated the fire compartment through each emergency exit
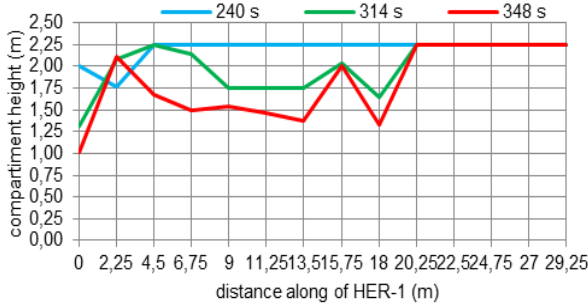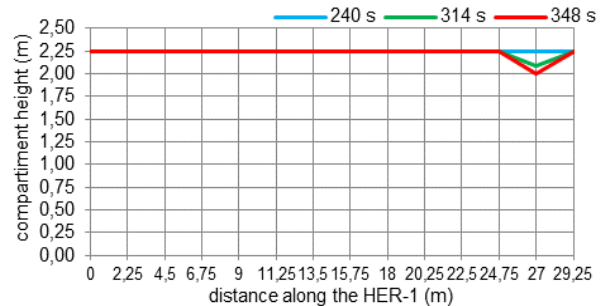

Fig. 6 Temperature of 80 °C along HER-1

Fig. 7 Visibility points along HER-1

The results in the horizontal evacuation route HER-2 for the temperature (*Fig. 8)* and visibility (*Fig. 9*) were worse than the ones for the evacuation route HER-1. This is justified by the fire origin that was in this case was near the HER-2. After 240 s of numerical simulation the maximum temperature of 80 ℃ registered oscillations all over HER-2, at some points above and in others below the 1.75 m in height. Nevertheless, 84% of the occupants had evacuated the fire compartment (*Fig.8*). From 314 to 348 s the temperature of the gases was above 80 °C, between 1 and 1.25 m above the floor, in most of the HER-2. This means that the 6 occupants that left the fire compartment on that time may have suffered serious burns.

In what concerns the visibility (*Fig. 9*) along HER-2 it was different than the temperature because after the 13.5 m it has descended from the 2.25 m to 1.25 of the floor, especially after 314s. This means that the occupants had in this case some difficulties in the evacuation. Although the temperature of the gases above 80 °C was recorded for only 0.75 m from the floor, the HER-2 was passable because the critical visibility of 1.25 m from the floor was only registered further than 13.5 m of the emergency exit.
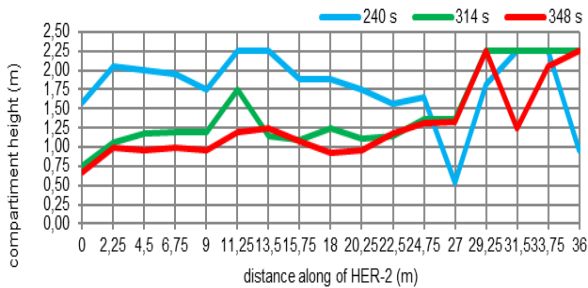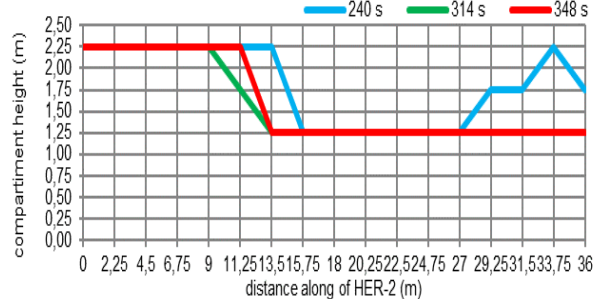

Fig. 8 Temperature of 80 °C along HER-2

Fig. 9 Visibility points along HER-2

3.2 Scenario_IB_Elev_FFR12_RSCS

The results of the evacuation using lifts (lift-1, lift-2 and lift-3) is presented in *Fig. 10*. The number of occupants as well as the time at which the last occupant evacuates the fire compartment are presented. From the 100 occupants to evacuate in 450s using lifts, all not disabled, 65% had and 35% hadn't evacuated (blue line). Lift-1 had evacuated 16 occupants (black lines), lift-2 evacuated 22 occupants (red lines) and lift-3 evacuated 26 occupants (purple lines) in approximately 400s. The occupants per lift are indicated in Table 2. The last occupant in lift-1, on its third movement, was at 392s, in lift-2 was at 398s and on lift-3 was at 401s.

Table 2. Number of occupants carried in each movement of the lifts and evacuation times

Lifts	Number of occupants carried in the three movements			Time for the last occupant leaving the lift (s)	Remarks
	1st	2nd	3rd		
Lift-1	6	8	2	392	lines in bold and black dashed (*Fig. 10*)
Lift-2	10	6	6	398	lines in bold and red dashed lines (*Fig. 10*)
Lift-3	9	11	6	401	lines in bold and dotted with purple (*Fig. 10*)
Total	25	25	14	-	35 occupants hadn't evacuated the building.
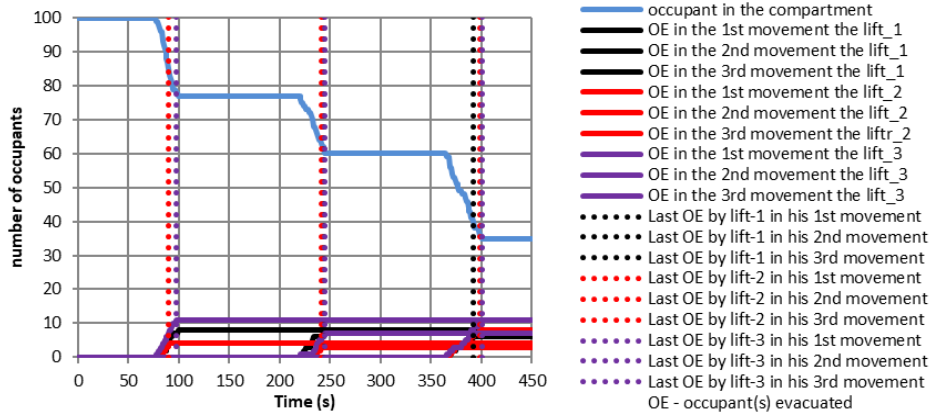
Fig. 10. Number of occupants evacuating by lift

Fig. 11 shows the development of temperature along HER-1 showing that from 0 to 18 m the temperature of 80 ºC was recorded at nearly 1.25 m above the floor, that is, below the minimum height of 1.75 m adopted in the present study for a normal and safe evacuation. After the 18 m the temperature was recorded on the safe side for a normal evacuation. The visibility only reduces after the 18m when the temperature reduces for heights below 1.75m (*Fig. 12*).

Fig. 11. Temperature of 80 °C along HER-1

Fig. 12. Visibility points along HER-1

In what concerns the HER-2 the maximum temperature for the gases of 80 °C was registered at 1 m above the floor, however near the lifts' doors (distance of 36 m) was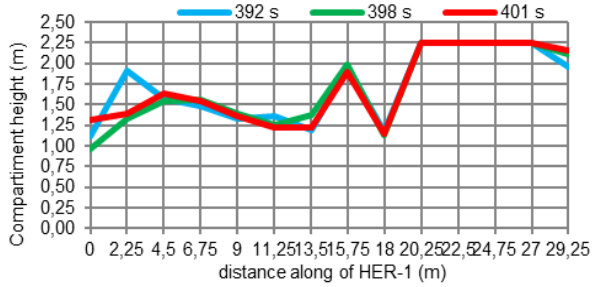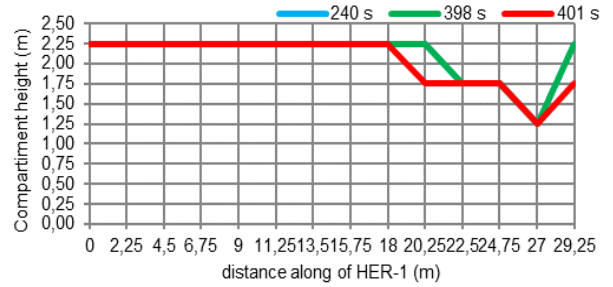 at least 1.75 m above the floor (*Fig. 13*). That is, the lifts area had temperatures on the safe side compatible with the evacuation. On the other hand, at 335.5 s, all occupants were already in the elevator shaft (safe zone). The visibility for the HER-2 was recorded on the safety side between the distances of 0 to 9 m, however from 11.25 to 36 m the same visibility was at only 1.25 m above floor (0.5 m below the minimum height of 1.75 m) (Fig. 13).

The temperature and visibility were unfavorable to evacuate in large part of HER-2, but they were good in the lift shaft. The 35 occupants which had not evacuated the fire compartment were not consequence of the maximum temperature or visibility but due to the insufficient number of lifts for evacuating the occupants in the same time as in a horizontal evacuation. The time necessary for the lifts open and close is usually a problem in the evacuation process. In this study it was observed that increasing the number of lifts from 3 to 4 could solve the problem.
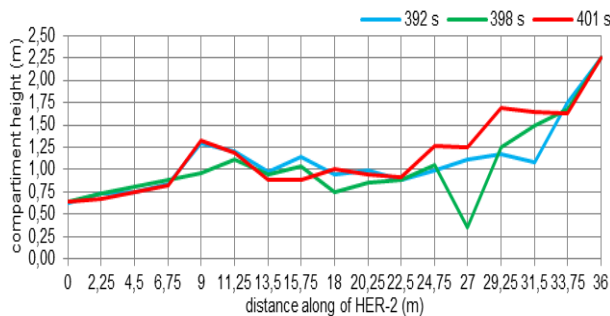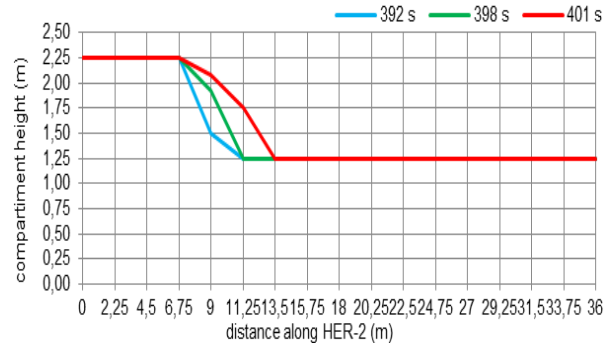

Fig.12 Temperature of 80 °C along HER-2

Fig. 13 Visibility points along HER-2

3.3. Summary of results

A total of five scenarios have been tested and the results are presented in Table 3.

Table 3. Comparison of the results between the fire scenarios

Scenarios	Number of occupants	Number of occupants leaving fire compartm.	Number of injured	Time of last occupant leaving fire compartment [s]	Evacuation time [s]
scenario_ID_NSO_FFR12_RSCS		100	2	-	318
scenario_ID_Elev _FFR12_RSCS		**65**	**-**	**401**	**-**
scenario_ID_LSO_FFR12_RSCS	100	100	6	-	317
scenario_ID_NSO_FFR3_RSCS		**100**	**-**	**-**	**262**
scenario_ID_LSO_FFR3_RSCS.		100	5		332

The scenario_ID_Elev _FFR12_RSCS (in red) was the worst of the analyzed ones because only 65% of the occupants evacuate. However, from all occupants that evacuate the fire compartment, none was injured because during the evacuation with the lifts the conditions of visibility and temperature were good. The lifts were not a good choice on the evacuation since the time taken for the tips up and down, doors to open and the occupants enter and leave them, were critical and the 3 lifts existing in this infirmary block were not enough for the evacuation. One more lift or maybe larger lifts or with higher carrying capacity could solve the problem.

The scenario_ID_NSO_FFR3_RSCS (in green) was the best since the evacuation totally occurred in 262 s. It was assumed that this scenario led to possible injuries, although the critical temperature as well as the visibility was only 1.0 m and 1.25 m above the floor, respectively. The values in reference were registered in only a few locations of the evacuation route thus not constituting an obstacle to the evacuation.

4   CONCLUSIONS

The results of this study on the evacuation of an infirmary block of a hospital, using the FDS+Evac software, showed that the fire safety system was in some extent effective. The smoke control system, the widths of the evacuation routes and emergency exits, as well as the convenient distribution of the emergency doors, helped on the safe evacuation of this fire compartment. The occupants evacuated in general with a temperature of the gases under 80°C and a visibility of at least 10 m.

The lifts were not efficient on the evacuation due to the lower carrying capacity and the necessary movements for the occupants enter and leave them. This problem is even worse if they are bedridden among the occupants. The evacuation by the normal evacuation routes was better when compared with the evacuation using lifts for the same number of occupants. This can be even improved by using a correct distribution of emergency exits with an appropriate width and using an efficient smoke control system.

The horizontal evacuation is also preferable to the evacuation by lifts because the occupants don't need to wait as in the case of the lifts. The intermittency than can occur in a horizontal evacuation is due to the displacement speed of the occupants. The intermittency in the case of evacuation by lifts is due to among other factors the displacement speed of the occupants, the

closing and open of the doors of the lifts, the time necessary to enter and leave the lifts, the carrying capacity of the lifts, as well as the time needed for the up and down trips of the lifts.

Another disadvantage of using lifts on the evacuation was the convergence of all occupants on the entrance. This could also occur in the entrance of the stairs' boxes but the process is not so worst as for the lifts because in this case the occupants need to wait for the lifts. Nevertheless, a building should never have only one stair for evacuation. The lifts could help in the evacuation of a hospital when there are disabled people as for example bedridden.

REFERENCES

[1] Law 1532 (2008). *Technical Regulation of Fire Safety in Buildings*. Decrees and Laws, Portugal.

[2] ABNT NBR 13994 (2000). *Lifts for transport of disables*. Brazilian Standards.

[3] Health Technical Memorandum 05-03 (2006). *Operational provisions. Part E: Escape lifts in healthcare premises*, Department of Health and Social Care, UK.

[4] New York Center for Terrorism Planning and Preparedness (2006). *Hospital Evacuation Protocol*, Agency for Healthcare Research and Quality, USA.

[5] Wallask, S. (2005). *Performing Emergency evacuations. A supplement to Healthcare Security and Emergency Management*, HCPro Inc., Marblehead, MA, USA.

[6] Siikonen, M. L. & Hakonen, H. (2002). *Efficient Evacuation Methods in Tall Buildings*, Proceedings of the International Congress on Vertical Transportation Technologies, Milan, Italy.

[7] Howkins, R.E. (2002). *Elevators for Emergency Evacuation and Egress,* Elevators, 50. 124-131.

[8] Korhonen, T. (2018). *Fire Dynamics Simulator with Evacuation*, FDS+Evac. Technical Reference and User's Guide,* NIST, USA.

[9] Proulx, G., & Pineau, J. (1996). *Review of evacuation strategies for occupants with disabilities*, NRC – National Research Center, Report IRC-IR-712, Canada.

[10] Jiang, Z. M., Zhang, P. H., Shang, R. X. & Tian, X. L. (2014). *Investigation and simulation on human evacuation behaviour in large hospital building in Shenyang.* Procedia Engineering, 71, 101–106.

[11] Society of Fire Protection Engineering (2002). *Handbook of Fire Protection Engineering*. 3rd ed., USA.

[12] Shi, L., Xie, Q., Cheng, X., Chen, L., Zhou, Y., & Zhang, R. (2009). *Developing a database for emergency evacuation model*. Building and Environment, 44(8), 1724-1729.

[13] EN 1991-1-2 (2002). *Eurocode 1: Actions on structures - Part 1-2: General actions - Actions on structures exposed to fire,* European Committee for Standardization, Brussels, Belgium.

[14] European Guideline nº 19 (2009). Fire Safety Engineering Concerning Evacuation from Buildings, CFPA-E Guideline No 19:2009 F, France.

[15] INSTA 950 (2012). Fire Safety Engineering - Verification of fire safety design in buildings. Standard Norge, Norway.

[16] Singapore Civil Defense Force (2015). *Singapore Fire Safety Engineering Guidelines,* Singapore.

[17] Lougheed, G.D. (2000). *Considerations in the Design of Smoke Management Systems for Atriums*. Construction Technology Update No. 48, NRC – National Research Center, Canada.

[18] Sub-Committee on Fire Protection, (2001). *Smoke Control and Ventilation: Research project on smoke control systems on passenger ships.* 46th session, USA.

[19] Yan, T., MingHeng, S., YanFeng, G., & JiaPeng, H. (2009). *Full-scale experimental study on smoke flow in natural ventilation road tunnel fires with shafts*, Tunnelling and Underground Space Technology 24(6):627-633.

[20] Bukowski, R. W. & Hurley, M. J. (2003). *Fire Hazard Analysis Techniques*. NFPA - Fire Protection Handbook, section 3, 121-134.

SMOKE CONTROL AND VENTILATION

ENGINEERING SMOKE MANAGEMENT IN LARGE SPACES WITH LOW CEILING USING FDS

[1]Anand Sudhi, [2]Man Pun Wan

[1]School of Mechanical and Aerospace Engineering

[2]Nanyang Technical University, Singapore

ABSTRACT

Managing smoke in spaces with low ceiling heights and large area using Smoke and Heat Exhaust Ventilation (SHEV) systems poses a challenge as the smoke reservoir depth often breaches the clear height required. In this context, this work uses CFD to (a) estimate the minimum reservoir depth (h_o) required by an axisymmetric plume in a low ceiling space (b) estimate the parameters of low ceiling – large space where h_o is below the clear height of 2.5 m (c) understand the effect of beams on the ceiling jet and h_o (d) analyze 3 smoke extraction strategies using an open office model. A ceiling height lower than 4.5 m with a ceiling jet travel distance greater than 20 m was concluded as a low ceiling –large space. The minimum smoke depth required is 45% of the ceiling height. Obstruction of beams further deepened the reservoir while decelerating the ceiling jet flow. Dividing the area into smaller zones and extracting smoke closer to the fire source was observed to be the most efficient.

1 INTRODUCTION

Buildings such as open offices and under-ground carparks usually have low ceiling heights with large open space. Managing smoke in the event of a fire in such low ceiling large spaces is a significant design challenge. The lack of safe depths for a smoke reservoir magnifies the practical problem of smoke control as the smoke layer lowers swiftly to human head height, obscuring the visibility levels of the evacuees and raising the toxicity levels. Thus, controlling the smoke reservoir depth to a clear height is the primary design challenge in such low ceiling large spaces.

As available depth for forming a smoke reservoir often breaches tenability criteria in such spaces, well designed passive and active management of smoke is necessary to maintain a tenable environment during the evacuation. Impulse jet fans have shown to be highly effective [1] [2] to control smoke for safe evacuation in underground car parks which is an example of a space with low ceiling-large space. However, in spaces with higher occupancies like open office, ducted transverse ventilation is suitable to maintain a stable smoke layer height for evacuation and avoiding smoke logged areas for available egress routes. Zhang [3] performed numerical and experimental studies on the smoke movement and its control strategy in a low ceiling-large space with flat ceiling using transverse ventilation systems. They increased the effectiveness of smoke control systems by increasing the exhaust rate and the number of openings. Wu et al [4] experimentally studied the efficiency of the smoke control system in a low ceiling-large space with barriers. They considered the influence of exhaust rate, the number of exhaust opening and area of the smoke zone on the effectiveness of the smoke control system. The results showed that the smoke exhaust effectiveness in the case with more smoke exhaust openings showed improved smoke management. Though these studies addressed strategies to control smoke in low ceiling-large spaces, critical parameters where transverse smoke control strategies fail due to the lack of adequate height for smoke reservoir formation are not clearly defined.

For smoke extraction systems to be effective, a smoke reservoir needs to be established. The minimum smoke depth defined in the design requirements of NFPA 92 [5] is at least 20% of the floor to ceiling height. This depth accounts for a ceiling jet depth of 10% that impinges on a wall and folds back below it to form an additional 10% fold back jet, which then travels back to the fire origin. Though it is a good start to use 20% as the minimum smoke depth, further engineering analysis may be necessary [5], especially with low ceiling heights. However, the definition of a large space with a low ceiling where the smoke reservoir depth is below the clear height is not well defined.

In this context, this study uses Fire Dynamics Simulator (FDS) [6] to estimate the critical ceiling height and smoke depth to define low ceiling - large spaces and explore strategies to control the smoke spread and tenability breach. Following studies are presented in this paper,

- – Estimation of the minimum depth of the smoke reservoir
- – Parametric study to understand the influence of ceiling height, smoke reservoir length and beam depth on minimum smoke reservoir depth and define a critical ceiling height and smoke depth for a low ceiling large space
- – Simulate smoke extraction strategies in an open office model with a ceiling height lower than the critical height
    - – Active control of the ceiling jet using multiple extraction points
    - – Passive control of the ceiling jet using smoke barriers and multiple smoke reservoirs
    - – Zonal activation of extraction vents to concentrate smoke extraction closer to the fire source.
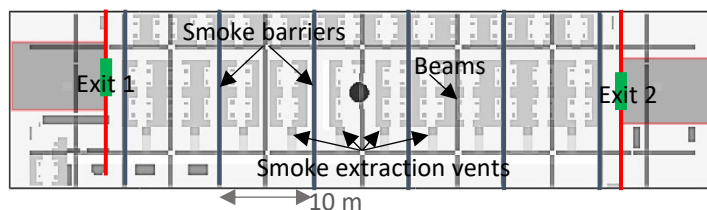
2   SET- UP OF NUMERICAL SIMULATIONS

Figure 43: CAD geometry of the computational domain (a) fire at the middle (b) Exits at each ends along the length of the office (c) smoke barriers under alternating beams (10 m apart)

The CFD simulations in this study were conducted using Fire Dynamics Simulator (FDS) v6.6 [6]. FDS is a low Mach number, thermally driven flow simulator for modeling the evolution of smoke and heat transport during fire. The software uses Large Eddy Simulation (LES) version of the Navier-Stokes Equation and is optimized to give reasonable predictions on smoke and heat transport using course mesh sizes. The chemistry solver uses a single step mixing controlled combustion model assuming infinitely fast chemistry. The goal of this study is not to examine flow phenomena like the flow around the fire source or the entrainment of air into the smoke, rather predict and visualize the smoke patterns and its transport. To that purpose, FDS is capable of obtaining predictions within reasonable computation times.
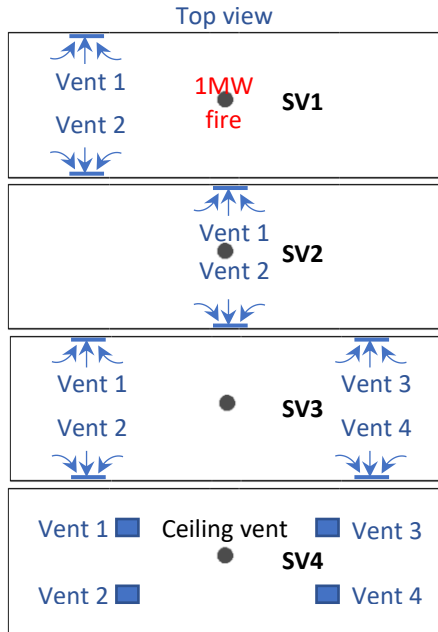
Figure 44: Smoke extraction vent positions for estimation of min. smoke reservoir depth (section 3.1)

2.1 Computational models

Figure 44 shows an open office dimensions: 20 m (width) x 60 m (length) x 4 m (height) with a 1 MW fire in the center.

-     Mesh cells size: 0.25m x 0.25 m x 0.1 m (Refinement near the fire plume: 0.125m)
-     Models:
-     Combustion: default mixture fraction model
-     Fuel: Polyurethane
-     Smoke production: soot yield of 0.1
-     Baroclinic generation of vorticity is considered
-     Turbulence: Standard Smagorinsky LES, $C_D = 0.20$.
-     Visibility factor (C): 8 (for illuminated exit signs)

2.2 Smoke extraction design

The smoke extraction rate required for maintaining the necessary smoke layer height for a design fire is calculated from the empirical results described in BR368 [7]. The fire used in this study is classified as a large fire according to the condition given below,

For large fires,

$$Y \leq 10(A_f)^{0.5}$$

Where, Y is the height of the plume (2.5 m), and A_f is the area of the fire (4 m²). As stated in BR 368 [7], Hansell [8] derived a relation between the air entrainment rate (M_f) into the smoke plume rising above the fire as a function of the perimeter of the fire (P) and the smoke plume height (Y) given as,

$$M_f = C_e P Y^{1.5} (kgs^{-1})$$

Where $C_e = 0.21$ for large open rooms like open-plan offices with a low ceiling [7] and perimeter of the fire is 14 m as per the requirements set by SCDF in the design of the smoke control system [9]. As per the empirical relations specified in BR368 [7], the total volumetric extraction of smoke required to establish a stable smoke reservoir at the clear height of 2.5 m (Y) is 12 m3/s.

An axisymmetric smoke plume is used in this study, located in the middle of the smoke reservoir. Effects of fire placed near a wall are not evaluated in this study. The office model used in section 3.2 is assumed to have a grated ceiling at 2.75 m with 75% free area, which is not however modeled in the simulation to lower computation times. Influence of the perforated ceiling will be added in future publications. Other obstructions like air-conditioning ducts are not included in the current study. Though the design heat release rate (1 MW) corresponds to a sprinkler-controlled fire, the influence of the sprinkler on smoke is not modeled in the present study.
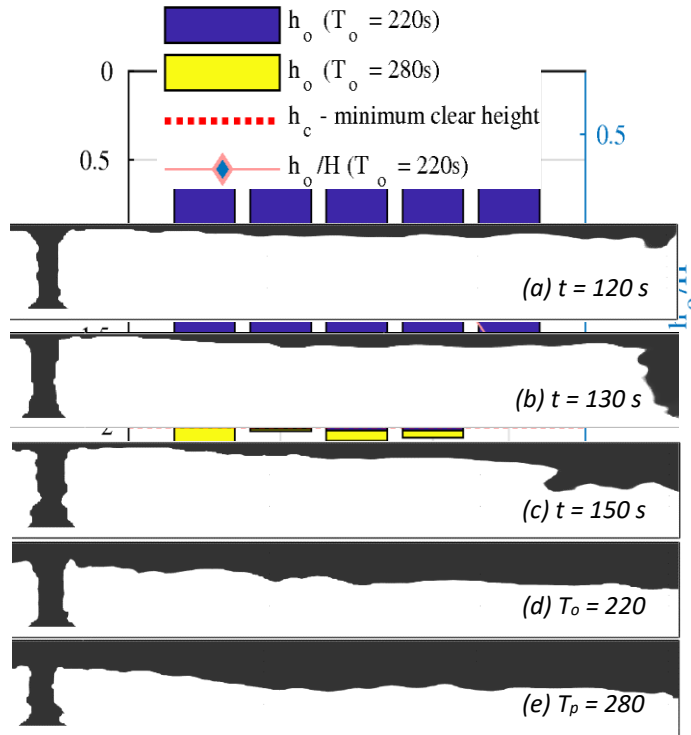
Figure 45: Formation of a smoke reservoir

3 RESULTS AND DISCUSSION

The critical obstacle in designing a smoke management system in low-ceiling spaces like open offices is to form a smoke reservoir above a minimum clear height (h_c) of 2.5 m [7]. This minimum reservoir depth (h_o) corresponds to the space needed by the ceiling jet to fold back from a wall or barrier and form a stable reservoir. The instances where this minimum reservoir depth (h_o) breaches below 2.5 m (h_c) can be used as a critical parameter to classify low ceiling spaces. In section 3.1, the minimum smoke reservoir depth (h_o) is defined and used to identify the critical case of large spaces with a low ceiling $(h_o$ is below $h_c)$ using parametric analysis. In section 3.2, strategies to manage smoke in such a large space with a low ceiling are discussed.

3.1 Minimum smoke reservoir depth (h_o)

Figure 45 shows the mechanism of smoke reservoir formation for a 60 m x 20 m x 4.5 m room which is a typical case of a low ceiling large space (defined in subsection 3.1.1). A 1 MW fire is placed in the middle of the room. At 120 s, the buoyant ceiling jet has traveled a length of 30 m, thickening along the way due to air entrainment into the jet [10]. Thereafter, the jet impinges on to the wall and travels along the wall as a wall jet (130 s). As the wall jet is hotter than the ambient air, the buoyant forces fold it back below the ceiling jet as seen at 150 s. The fold-back jet continues to travel back to the source of the reservoir and forms a stable smoke reservoir at 220 s (T_o) and corresponds to the minimum smoke reservoir depth (h_o). Thereafter the reservoir deepens with time, and at 280 s (T_p) the global deepening of the reservoir becomes uniform.

The smoke reservoir depth at T_o and T_p are shown in Figure 46 with and without smoke extraction. Four choices of extraction locations (SV1, SV2, SV3, SV4) were chosen as described in Figure 1. The blue bars in Figure 46 show the average smoke depths at T_o, and the yellow bars show the increment in smoke depth till T_p. The red dotted line represents a clear height (h_c) of 2.5 m. It is observed that the smoke depth at T_o is same when smoke extraction systems are active and inactive. T_o represents the time when the fold-back jet reaches back to the fire and forms a stable reservoir. Beyond T_o the SHEV systems are capable of maintaining the smoke near the clear height. Hence, T_o (220s) represents a good indication of the time taken for reaching a minimum stable smoke reservoir depth. Before T_o, the effect of smoke extraction vents is localized to their location as a global smoke reservoir depth has not formed making the extraction process ineffective. Further increase in smoke extraction rates yielded no reduction in smoke depth at T_o.

The minimum smoke reservoir depth *(h$_o$)* advised by NFPA 92 [5] after considering the depths of ceiling jet and the fold-back jet is 20% of the ceiling height *(H)* that is *ho/H = 0.2*. However, for a large space (60 m) with a low ceiling (4.5 m), the simulations (Figure 46) showed a minimum reservoir depth of 45% *(h$_o$/H = 0.45)*. Further analysis on the variation of *h$_o$/H* is studied in the next section where a parametric study on the effect of ceiling height and compartment length on *h$_o$* is studied to define critical parameters for a large space with a low ceiling.

3.1.1 Ceiling height

Figure 48 (a) shows the variation of minimum smoke layer depths with ceiling height for a 60 m long reservoir with fire in the middle. 60 m is also the maximum reservoir length permitted by most codes [9] [7] after which chances for smoke cooling and sinking are high. The red dotted line represents the clear height *(hc)* of 2.5 m for the respective ceiling heights *(H)*. The linear increase of *h$_o$* (blue bars) with increasing *H* is attributed to the increasing air entrainment into the plume. However, *ho/H* is inversely proportional to the ceiling height (red marker) as the increment in *h$_0$* is outweighed by increase of *H*. The linear decrease of the required smoke depth *(ho/H)* with ceiling height is however not drastic and a minimum smoke reservoir depth of 0.45 or above is required to ensure that the smoke

Figure 47: Evolution of ceiling jet bulb with travel distance of the ceiling jet (Figure shows half of the reservoir length)

removal systems can control the smoke depth. It can also be concluded that the critical ceiling height feasible to maintain the smoke layer above the clear level height is 4.5 m *(H$_{cr}$)* for a 60 m long smoke reservoir with an axisymmetric plume.

As *H* increases, for instance, in an atrium space, the fraction of minimum smoke depth can be close to the recommendations in NFPA 92 [5]. Future work will explore the height dependence. Further analysis in this paper is based on a 4.5 m high room.
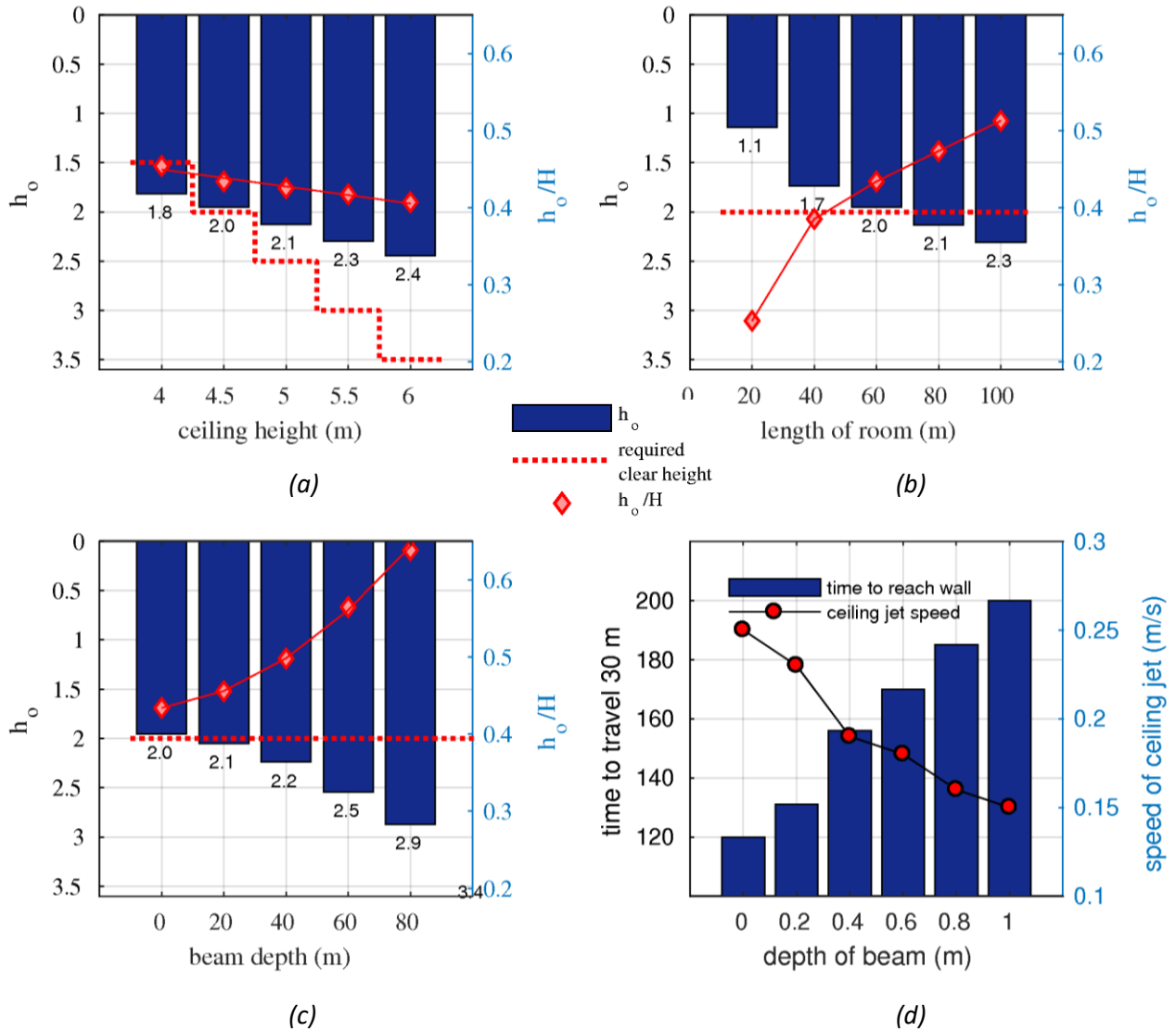
Figure 48 : Factors influencing the minimum smoke depth (a) variation with ceiling height (b) variation with compartment length (c) variation with structural beam depth (d) decelerating effect on the ceiling jet by structural beams

3.1.2 Smoke reservoir length

Figure 48 (b) shows the variation of minimum smoke layer depths with the reservoir lengths for a compartment of ceiling height 4.5 m with an axisymmetric fire plume. *ho/H* for a 20 m long reservoir is 0.25 which is closer to the recommendation in NFPA 92 [5]. However, the increase of *ho/H* from 20 m reservoir to a 60 m reservoir is steep. This increase can be accounted for from the bulging of the ceiling jet with travel distance as seen in Figure 47. The bulging is observed when the ceiling jet with higher momentum which is generated during the steeper growth stage of the t^2 fire pushes past the ambient air and slow-moving incipient jet. This interaction results in a hydraulic jump [1, p. 450] leading to increased air entrainment. This effect was observed to be pronounced between a travel distance of 20 m and 40 m and will be studied in our future works. Beyond a 40 m long reservoir, *ho/H* shows a slow linear increase between 0.40 and 0.50 as seen

in Figure 48(b). Such effects can also be observed when the location of the fire is offset from the middle along the length of the reservoir.

Considering the linear variation of minimum smoke depth (ho/H) due to change in ceiling height Figure 48 (a) and reservoir length Figure 48 (b), it can be concluded that the minimum smoke reservoir depth between 45% - 50% of the ceiling height is recommended for large spaces with a low ceiling. Also, a 4.5 m ceiling height is a reasonable estimate to define the critical height below which the minimum smoke reservoir depth is below the clear height. Thus, a low ceiling–large space can be defined with a critical ceiling height lower than 4.5 m with a ceiling jet travel distance of more than 20 m.

It is also observed that the critical ceiling height (H_{cr}) of 4.5 m is relaxed as the travel length of the ceiling jet is shorter than 20 m due to a much thinner ceiling jet from the lower entrainment. Hence it is recommended that multiple shorter smoke zones be used in large spaces with a low ceiling.

When the fire is located at the far end of a 60 m reservoir, the mass flow from the plume can drastically increase due to the wall effect resulting in a higher H_{cr} and will be investigated in future works.

3.1.3 Interaction with structural beams

When designing smoke control strategies for low ceiling spaces, it is a usual practice to use the space above the visual ceiling to form a smoke reservoir by employing grated ceilings or highly perforated ceilings. With such designs, the ceiling jet encounters obstructions such as structural beams or air ducts. Figure 49 (a) shows the thin ceiling jet of a flat ceiling which impinges on the wall and folds back at 120 s. In contrast, the presence of a 0.7 m deep beam causes the ceiling jet to become thicker and slower in its spread (Figure 49 (b)). The ceiling jet shows a snaking motion as it dips below the transverse beams and rises back up once the beam is cleared. This snaking motion results in considerable turbulent mixing which results in a thicker smoke layer behind the ceiling jet. Also, the loss of momentum of the ceiling jet while impinging on the transverse beams leads to slower smoke spread as seen in Figure 49. As seen in Figure 48 (d), the average speed of the ceiling jet in travelling 30 m decreases linearly with increasing beam depths. The deceleration of the ceiling jet can, in turn, increase the Available Safe Egress Time (ASET) for evacuation if the ceiling is high enough to maintain the initial smoke depth behind the ceiling jet. However, once the thick ceiling jet folds back from the wall and forms the smoke reservoir,

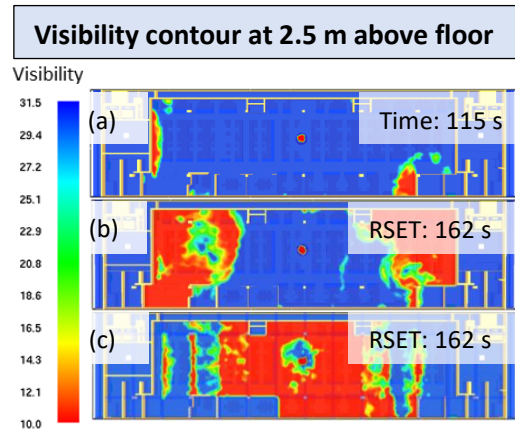Figure 49: Interaction of structural beams with the ceiling jet

Figure 51: (a) Flat ceiling at RSET (b) Flat ceiling at 2 x RSET (c) Ceiling with beams at RSET
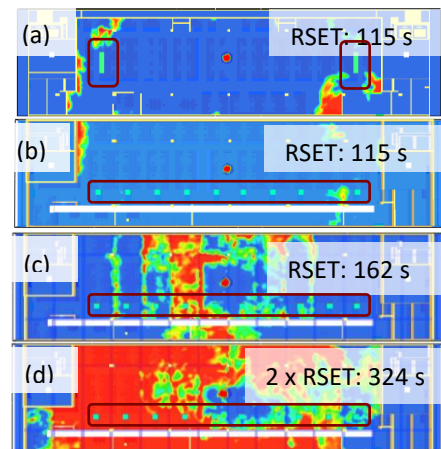

Figure 50: Active control of ceiling jet: Extraction vents are (a) extraction vents at the exits (b-d) uniformly distributed between beams

ho increases considerably with increasing beam depths, as seen in Figure 48 (c). That is, in comparison to a flat ceiling, the minimum smoke reservoir depth required dips below the required clear height as seen in Figure 48 (c). Hence, it is imperative to account for the effects of beams, if present, while designing smoke removal systems in low ceiling large spaces.

Thus, for space with $H < 4.5$ m or when an obstruction such as beams are present in the ceiling, the following section discusses alternate strategies to control and manage smoke to reduce the smoke spread and tenability breach.

3.2 Strategies to control smoke reservoir

In this section, three approaches to control the smoke layer depth and smoke spread in a low ceiling - large space is explored in an open office model (Figure 44). A 1 MW fire is placed in the middle of the office. Figure 51 (a) and (b) shows the visibility at 2.5 m above the floor for a flat ceiling space (60 m x 20 m x 4 m). Tenability conditions are breached (red regions) when the visibility drops below 10 m. Required Safe Egress Time (RSET) was calculated for 166 occupants as 162 s using FDS+EVAC. Before impinging the wall, the ceiling jet depth is maintained well above the clear height. However, the exits are made untenable when the jet fold backs below itself at the wall (Figure 51 (a)). The rest of the space is rendered untenable as the

fold back jet travels back to the location of the plume (Figure 51 (b)). In contrast, as seen in (Figure 51 (c)), the presence of beams of depth 0.7 m contribute to slowing down the ceiling jet and maintains tenable conditions at Required Safe Egress Time (RSET). However, the depth of the ceiling jet is below the clear height thus rendering the space below it untenable (visibility < 10 m).

Figure 52: Passive control of smoke spread using 1.5 m deep smoke barrier

3.2.1 Active control of the ceiling jet

As seen in Figure 46, the use of smoke extraction vents at the ceiling (SV4) contributes to a lower h_o/H by directly extracting from the ceiling jet before the reservoir forms. The black boxes in Figure 50 represent the position of the extraction vents in the open office which are activated by the spot type detectors placed on the ceiling and ramps up to full power in 60 s. In Figure 50 (a), a single extraction vent at the ceiling is positioned near the exit to reduce the strength of the ceiling jet and reduce the fold back of the jet from the wall. In Figure 50 (b), the extraction points are uniformly distributed along the length of the office. It is however observed that such active

control of the ceiling jet is not feasible as the momentum of the ceiling jet is high enough to brush past the smoke extraction vents and fold back the wall. The tenability at the exit is breached (visibility < 10 m) at the same time as Figure 51 (a) where smoke extraction is absent. Hence it can be concluded that controlling the ceiling jet is not feasible for flat ceilings.
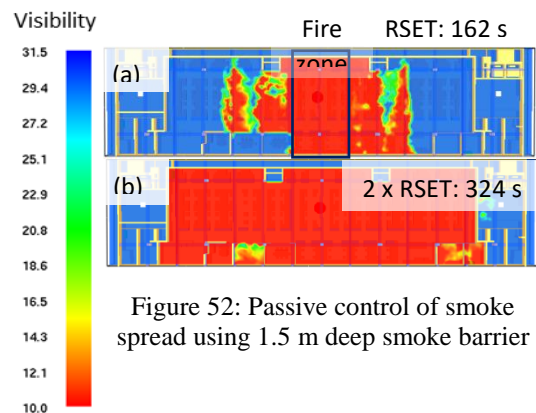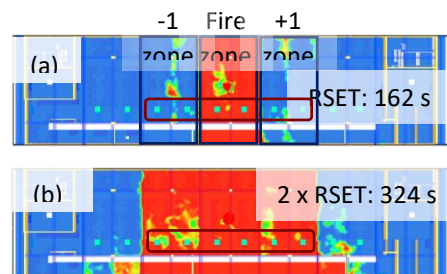

Figure 53: Activation of SHEV in 3 zones simultaneously (fire zone and two adjoining zones)

However, if the office has exposed structural beams (Figure 50 (c)), the space between the transverse and longitudinal beams trap the ceiling jet as it loses momentum when obstructed by the beam. This local reservoir improves the efficiency of the smoke extraction vents and thins out the ceiling jet and diminishes its momentum further. As seen in Figure 50 (b), the ceiling jet does not reach the exits at RSET and the local visibility breach < 10 m at 2.5 m height is controlled in comparison to Figure 51 (c). However, the visibility breach at 2 x RSET (Figure 50 (d)) over the entire space as the minimum smoke reservoir height (h_o) of a 4 m office is below the clear height of 2.5 m.

Figure 54: Activation of SHEV in 3 zones (fire zone and two adjoining zones) sequentially by respective smoke detectors

3.2.2 Passive control using smoke barriers

As controlling the ceiling jet fails for a flat ceiling, an alternative method is to limit the spread of smoke and breach of tenable conditions by step by step accumulation of smoke in multiple smoke zones. The zones are separated by smoke barriers positioned below a structural beam and dropped down till 2.5 m from the floor as shown in Figure 44. The ceiling jet forms a much shorter reservoir (10 m x 20 m) in the fire zone and once filled, spills over to the successive zones. Figure 53 shows that the smoke spread and visibility breach is limited to just 3 zones at RSET and the exits are rendered with tenable conditions. However, the smoke spreads and tenable conditions are lost in all zones at 2 x RSET.

3.2.3 Zonal activation of smoke extraction vents

Smoke extraction from the shorter reservoir established by the smoke barrier can further restrict the smoke spread and limit areas with visibility breach < 10 m. In addition, the activation of smoke extraction vents closer to the fire source can reduce wastage by increasing the ratio of smoke to ambient air extraction. Extraction vents are activated in the fire zone and the two adjoining zones simultaneously in Figure 52. It is observed that the visibility breach and smoke spread is limited to the 3 zones at 2 x RSET. The ratio of smoke to ambient air extraction can be further increased by individually activating the extraction vents in each zone by their respective detectors (Figure 54). With such a sequential activation of the extraction vents, the smoke spread can be further reduced.

4   CONCLUSIONS

In this paper, smoke reservoir formation and control for a large space with a low ceiling are studied using FDS. Following conclusions were drawn from the simulations.

− Minimum smoke reservoir depth is below the clear height of 2.5 m for ceiling heights lower than 4.5 m and ceiling jet travel distance greater than 20 m. Such spaces can be classified as low ceiling – large space. Presence of beams further exacerbates the smoke depth.
− The minimum reservoir depth for low ceiling – large space is 45% - 50% of the ceiling height
− When the minimum smoke depth is below the clear height, dividing the space into multiple smoke zones and distributing the extraction around the fire and the adjoining zones minimizes the smoke spread and increases smoke extraction efficiency.
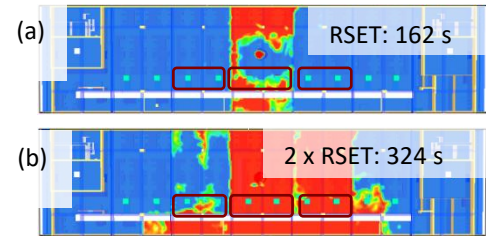
ACKNOWLEDGMENT

REFERENCES

[1] B. Alianto, N. Astari, D. Nareshwara and Y. S. Nugroho, "Modeling of Smoke Control in Underground Parking-garage Fires," *International Journal of Technology,* vol. 8, pp. 1296-1305, 2017.

[2] S. Lu, Y. Wang, R. Zhang and H. Zhang, "Numerical Study on Impulse Ventilation for Smoke Control in an Underground Car Park," *Procedia Engineering,* vol. 11, pp. 369-378, 2011.

[3] P. Zhang, "Study on the law of smoke movement and its control strategy in flat space (In Chinese)," Harbin Engineering University, Harbin, 2016.

[4] W. Wu, L. Xu, L. Tao, X. Chen and J. Yao, "Study on effectiveness of smoke exhaust in large flat space using hot smoke experiment," 2012, 31(10),1038-1040. (In Chinese).

[5] NFPA , "NFPA 92: Standard for Smoke Control Systems," National Fire Protection Association, 2009.

[6] Fire Dynamic Simulator 6.6, "https://pages.nist.gov/fds-smv/," National Institute of Standards and Technology (NIST), 2019. [Online].

[7] H. P. Morgan, B. K. Ghosh, G. Garrad and e. al, BR368: Design methodologies for smoke and heat exhaust ventilation, BRE Electronic Publications, 1999.

[8] G. O. Hansell, "Heat and mass transfer process affecting smoke," PhD Thesis, South Bank University, London, 1993.

[9] SCDF, "Code of Practice for Fire Precautions in Buildings," Singapore Civil Defence Force, Singapore, 2018.

[10] H. Morgan , G. Daniel, H. J. John, H. Kazunori, K. Erica, T. Jose, W. J. John and W. Christopher, SFPE Handbook of Fire Protection Engineering, New York: Springer-Verlag , 2016.

IMPACT OF AIR HANDLING VELOCITIES ON SMOKE BEHAVIOR AND MANAGEMENT

[1]Delaney Seeburger, [1]Katie Nute, [1]Richard Emberley, [2]José L. Torero
[1]California Polytechnic State University, San Luis Obispo, USA
[2]University College London, London, UK

ABSTRACT

Plume entrainment and smoke management theory assumes a quiescent environment with velocities driven solely by temperature differentials. The presence of other velocity sources is important in fire analysis because ambient disturbances can significantly change plume entrainment. To investigate this phenomenon and the potential consequences, a review of smoke management and Heating, Ventilation, and Air Conditioning (HVAC) standards was conducted. A fire modelling analysis on allowable velocities and subsequent effects on plume behaviour was completed using the Fire Dynamics Simulator (FDS). Standards and guidelines were examined and compared across the duration of air handling usage before and after smoke detection and management. Comparison of the impact of cross-flows, fire location, and HVAC systems was completed with a generic fire (1.0m x 1.0m).

1   INTRODUCTION

The presence of other velocity sources is important in fire analysis because ambient disturbances can significantly change plume entrainment. Entrainment rate analysis is complicated by the fact that entrainment rates are known to vary depending on the location of a fire with respect to obstructions. Furthermore, ambient velocities can create cross-flows which lead to a breakdown of axis-symmetric plume correlations. To investigate this phenomenon and the potential consequences, a review of smoke management and Heating, Ventilation, and Air Conditioning (HVAC) standards was conducted.

A fire modelling analysis on the allowable velocities and subsequent effects on plume behavior was completed in Fire Dynamics Simulator (FDS). Standards and guidelines such as the American Society of Heating, Refrigeration, and Air Conditioning Engineers (ASHRAE) Handbook, National Fire Protection Association (NFPA) Standard 92, *Standard for Smoke Control Systems*, and Approved Document F, *Building Regulation in England for the Ventilation Requirements to Maintain Indoor Air Quality* were examined and compared across the duration of air handling usage in a space before and after smoke detection and management. Even with these guidelines, HVAC design intrinsically depends on individual spaces and engineering judgement.

To assess the impact and significance of HVAC-induced flows per the various regulatory design requirements on smoke management, the requirements were then implemented in an FDS model of a generic room. Velocity profiles within the space before and after detection were compared and the duration of time to a quiescent environment was determined. Finally, a comparison of the impact of cross-flows, fire location, and HVAC systems or plume entrainment and smoke movement was completed with a generic fire (1.0 m x 1.0 m).

2   BACKGROUND

HVAC system designs vary depending on the location, geometry and functionality of a space. While the goal of HVAC systems in providing thermal comfort and fresh air circulation to building occupants is universal, several techniques may be used to achieve this. There are three types of air that can be entering or exiting a space. These are supply, return, and exhaust air. The primary focus of this study is supply air, which is the conditioned air that enters an occupied space and has the largest effect on the indoor environment. The most common HVAC systems are mixed air systems. Mixed air systems use high velocity diffusers placed overhead to deliver supply air horizontally along the ceiling. When exit velocity is high enough, a low pressure area is created between discharged air and the surface of the ceiling or surrounding walls causing the air to cling to the surface [1]. This is referred to as the "Surface Effect" and can be used to induce critical circulation in a mixed air system. Partially mixed systems and full thermal stratification systems use lower discharge velocities and the negative buoyancy of cool air to keep only the lower occupied portion of a space cool. This study will not focus on stratified systems as the compartment environment is less affected by impinging supply air velocities from these systems.

Diffuser design is another critical component effecting the indoor environment. Outlets can be located on the ceiling, walls or floor of a space. Overhead diffusers typically have the highest velocities especially in a heating mode where buoyancy forces need to be overcome in order to reach the occupied area. Sidewall outlets are typically located close to the ceiling and are angled towards the ceiling to take advantage of the surface effect. Floor mounted outlets are frequently used for large applications and discharge vertically with relatively low velocities. Diffusers can be spaced using the T50/L ratios supplied in the ASHRAE handbook after a total required CFM has been determined and diffuser type selected [2]. Because the throw distance is typically ten ft., diffusers are usually spaced within ten ft. of each other to ensure complete coverage of an area. The ratio can be multiplied by a characteristic length in order to determine the throw distance (distance from the diffuser where air reaches a specified velocity, typically 50-150 fpm) of a diffuser which corresponds to diffuser spacing.

It is also necessary to note the response of the building in a fire scenario in order to understand the indoor environment. Approximately 85% of buildings use a containment strategy where dampers shut off ductwork to limit the spread of fire and smoke throughout the building [3]. Some newer buildings use engineered smoke control to positively pressurize the space surrounding the fire and limit the spread of smoke. These systems can be categorized into dedicated smoke control systems and non-dedicated systems. Dedicated systems are installed specifically to perform a smoke control function while non-dedicated systems share components with another system such as the building HVAC system [4]. Fans and ducts used for stairwell pressurization are an example of a dedicated system while HVAC systems with added smoke control functionality are considered non-dedicated systems.

The focus of several studies on the effects of make-up air systems has been on atrium smoke control systems. Such systems have supply and exhaust rates that are orders of magnitude greater than those produced by an HVAC system. However, previous studies have shown that velocities below those mandated by codes and standards can impact plume and smoke layer behavior. The study by Kerber [5] indicated that velocities as low as 1 m/s may lead to rapid smoke-layer descent as the make-up air deflects the plume. This same study posited that asymmetrical vent location with respect to the fire lead to plume rotation which in turn dramatically increased the

turbulence of the plume. Studies performed by Pongratz [6] and Hilditch [7] confirm that additional velocities, such as those from HVAC systems may tilt the flame, disturb the plume trajectory, and even enhance entrainment of fresh air into the plume. These conclusions corroborate an earlier study by Hadjisophocleous and Zhou [8] which also determined numerically that flame deflection may occur at velocities around 1 m/s. A study by Ayala [9] combined different vent areas and configurations, heat release rates, and fire locations into 84 simulations. Adverse conditions were found to develop at values below the velocity threshold of 1 m/s prescribed by international codes.

NFPA 92, Chapter 6 covers the standards for non-dedicated systems. Stipulations include using smoke dampers to keep interconnected supply and exhaust systems distinct, sequencing of supply and exhaust fan activation, smoke control mode having the highest priority of an HVAC system, and the provision of outside air for pressurization [10]. The maximum makeup air velocity permitted is 1.02 m/s as significant plume deflection and smoke layer disruption may occur above this velocity. When the HVAC system has no smoke control functionality, it will be shutoff when fire is detected in a zone. However, residual temperature and velocity gradients may still be present in the space. Initiation of smoke control mode must take place within 10 seconds of receiving an activation command. Therefore, depending on the detection mechanism and fire characteristics, an HVAC system could be operating for several minutes after ignition takes place.

In the UK, Approved Document F requirements have similar objectives. However, the standard is adjusted for performance-based design in that performance criterion and tenability limits are outlined without specifying how such conditions are to be met. Supply rate for buildings other than dwellings is mandated to be no less than 10 L/s/person as the incidence of health effects below this rate becomes significant [11]. Exposure levels to various pollutants including carbon monoxide and nitrogen dioxide are regulated by concentration. Assumptions made in determining the values for these performance criteria are described in the appendices of the document.

3   DATA AND METHODS

In order to investigate the interaction between residual velocities and combustion products, a case study was conducted using a roughly 3,000 SF lecture hall in the Engineering IV building at California Polytechnic State University. The HVAC system was modelled as a mixed air system with angled diffusers and return air grills located on the ceiling. Pyrosim and FDS were used to model the space and simulate several scenarios. The geometry of the room was modelled in Pyrosim with dimensionally accurate obstructions for the floor slab, walls, and ceiling. All doors and windows were assumed to be closed and diffusers were modelled as two ft. by two ft. vents with a volumetric flowrate of 350 CFM. The return grills were modelled as openings that allowed air to exit the model without creating a pressure drop at the vent. The model was run first without a fire to investigate the baseline conditions inside the space. Figure 1 shows the steady state velocity slices at a time of 354 seconds. After thirty minutes of simulation time, the volumetric flowrate was set to zero in order to observe the residual velocities in the space after the HVAC was shut off. The results can be seen in the figures below. The room reached quiescent conditions approximately 16 minutes after the system was shut off and had residual velocities for 5 minutes after shutoff. Quiescent conditions were reached when the overall velocities within the compartment were reduced to such an extent as to have an insignificant impact on fire behaviour.
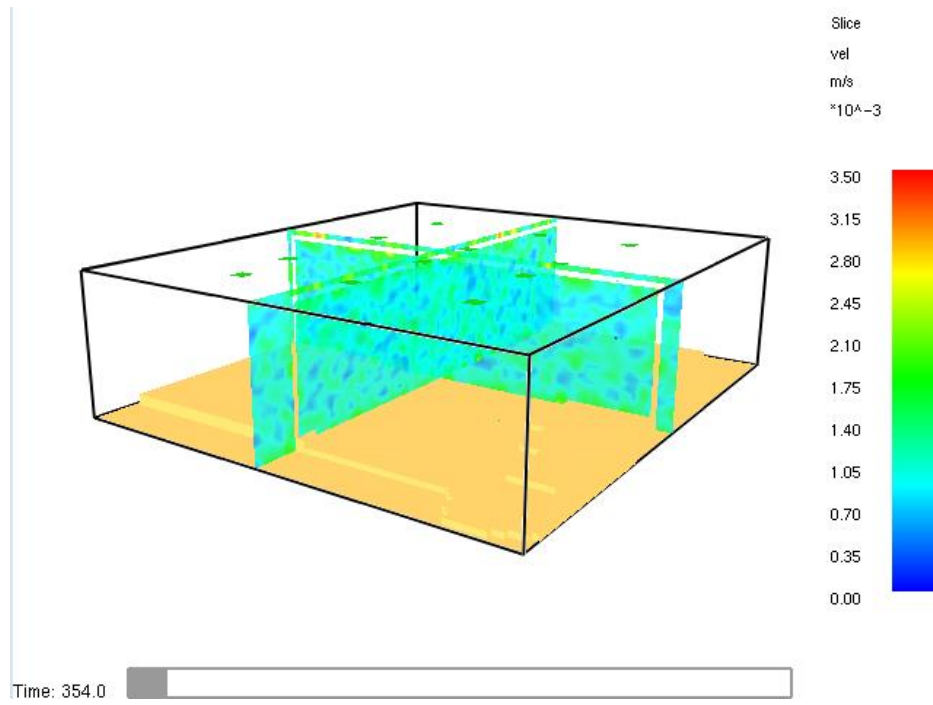
Figure 1. Steady State Velocities with HVAC on
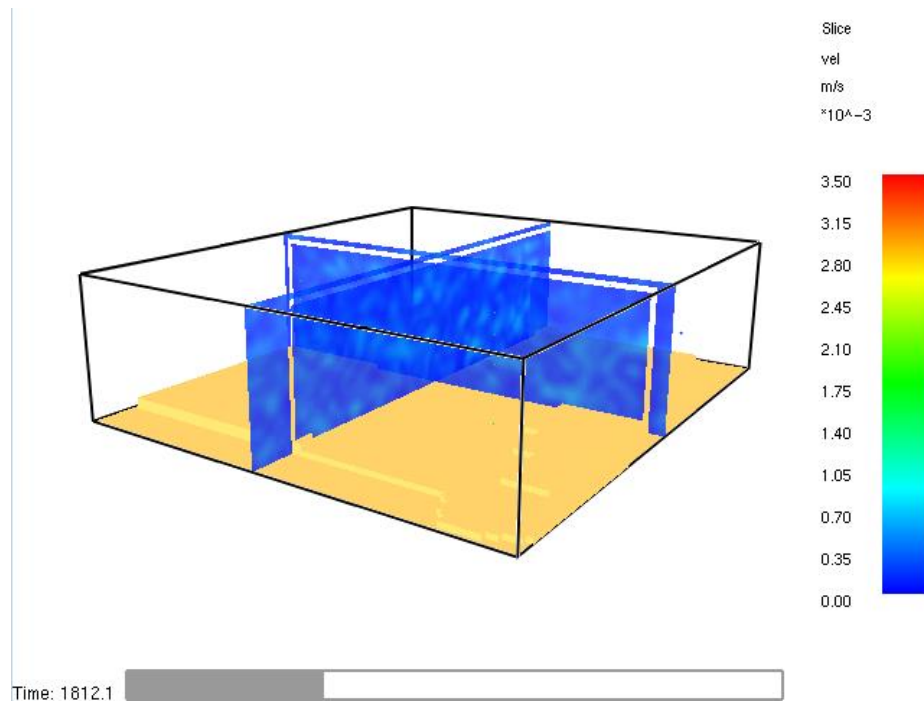
Figure 2. Velocities Immediately After HVAC Shutoff
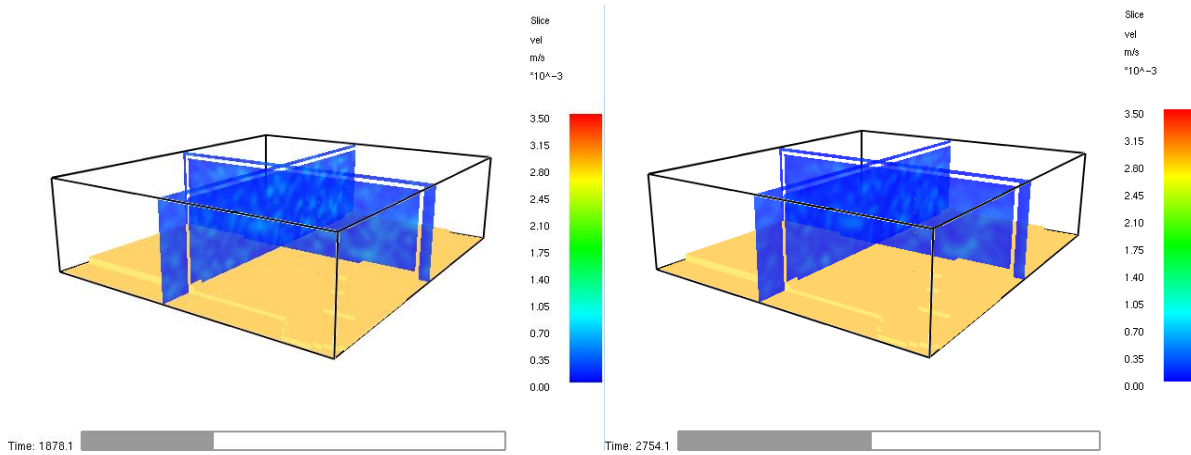
Figure 3. Velocity Slices Approximately 1 Minute and 16 Minutes after Shutoff

Velocity probe trees were placed at the approximate quarter points of the room at five different heights (Figure 4). A steady-state 500 kW fire was added at the approximate center of the space to create a fire scenario. The fire used exhibited no growth period. HVAC vents were disabled in order to obtain baseline velocities within the compartment due solely to fire effects. A third model with both a fire and active HVAC was created to analyse the contributions of both types of velocity sources. In order to allow air movement within the compartment to reach the no-fire steady state conditions, ignition was delayed until 1,800 seconds. Probe trees were placed in the same locations as the baseline simulation. Additionally, four Cleary Photoelectric smoke detectors were placed within the room. A generic spacing of 30 ft. (9.14 m) was used in accordance with the requirements of NFPA 72 (Figure 5). The HVAC vents were controlled such that upon activation of any detector a 10 second delay would occur before the vents were shutdown. This was to simulate the maximum time allowed by NFPA 92 between receipt of a detection signal and smoke control system activation. To aid in visualization, 2D soot concentration and visibility slice files were added every 0.5 m from the floor to the ceiling.

Figure 4a. Probe Tree Location

Figure 4b. Smoke Detector Location

554

4   RESULTS

Velocity probes at the same elevation showed agreement for the no-fire case. When the data is plotted, the velocities are shown to reach a maximum when the HVAC system first starts. As the air within the space becomes as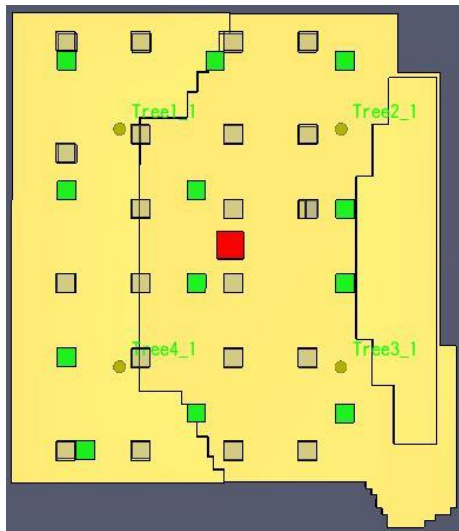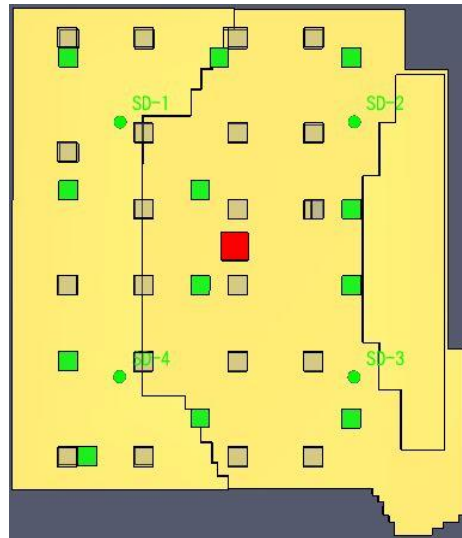similated into the motion induced by the HVAC system, the velocity decreases to a steady state value. HVAC shutoff occurred 10 seconds after smoke detector activation, between 1,810 and 1,816 seconds. Correlation between probes in the scenario with fire was also high. Similar trends are present for all the probes. Due to the way in which the model was setup, the buoyant effects of the fire plume dominate the velocities in the compartment. The velocities induced by the HVAC system are much lower than those induced by the fire. This is most evident when velocities for the three scenarios are plotted together as the fire only and fire and HVAC cases can be shown on the secondary axis while the HVAC only case must be shown on the primary axis if it is to be visible at all (Figure 5). The velocities in the scenarios with fire are at least one order of magnitude greater than those without a fire.
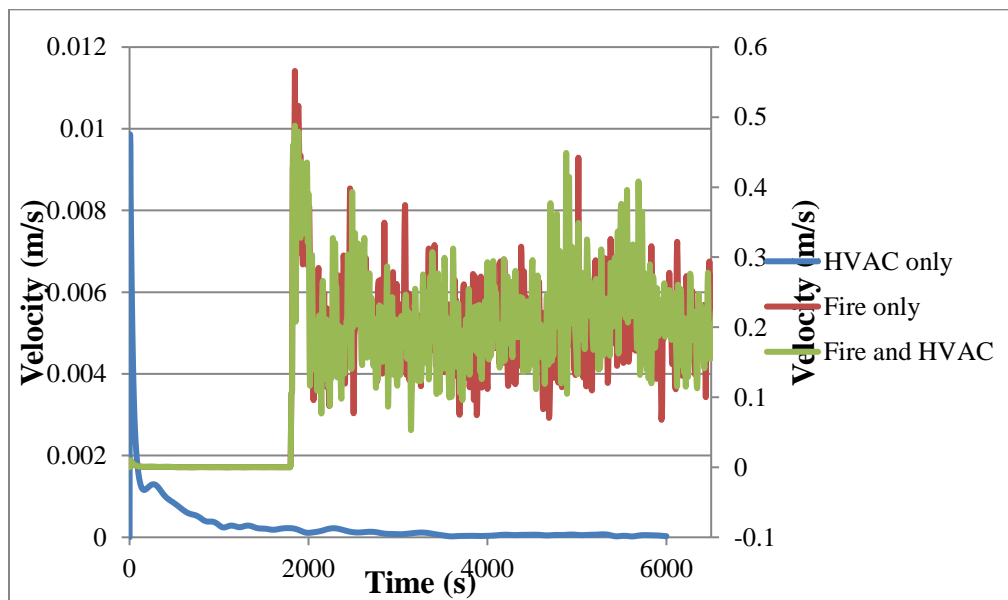
Figure 5. Comparision of Tree 2 Probe at 3.5m for all three cases

The similarity between the four probe tree results may arise from the nearly symmetric arrangement of HVAC components within the compartment. The fire location was also chosen with symmetry in mind. Another factor that contributes to these results is the relatively low diffuser velocity. Higher diffuser velocities would cause greater disturbance of the ambient conditions and potentially have a greater effect on the fire plume. A fire that showed a more standard growth rate would also impact the results in terms of detector activation and HVAC shutoff. Currently the fire is either "on" or "off". This causes the buoyant effects of the fire plume to supersede the effects of the HVAC system quickly instead of growing such that ambient velocities transition from HVAC dominated to buoyancy dominated.

This does not prevent the HVAC velocities from influencing products of combustion. Visibility slice files placed every half meter from the floor to the ceiling were used to assess the influence of HVAC in the presence of buoyancy dominant conditions. The contrast between the fire only and fire and HVAC cases was most evident at 2,192 seconds when the fire had been burning for 392 seconds and the HVAC had been shut down for 374 seconds. Slice files at two and three

555

meter elevations were viewed simultaneously to visualize the effect of elevation on smoke movement. Visibility of ten meters was used as a benchmark visibility distance in accordance with values recommended by Yamada and Akizuki [12]. In the fire only case, visibility was worse with increasing distance from the fire, a trend which persisted regardless of elevation. When HVAC effects were included the visibility range was more varied throughout the discrete planes regardless of elevation. Slice files at two and three meter elevations are shown at 2,192 seconds or roughly 6.5 minutes after the fire was started (Figure 6). Despite having been shut down for over six minutes and being smaller than the buoyant velocities, the residual velocities from the HVAC system still impact smoke movement within the compartment.
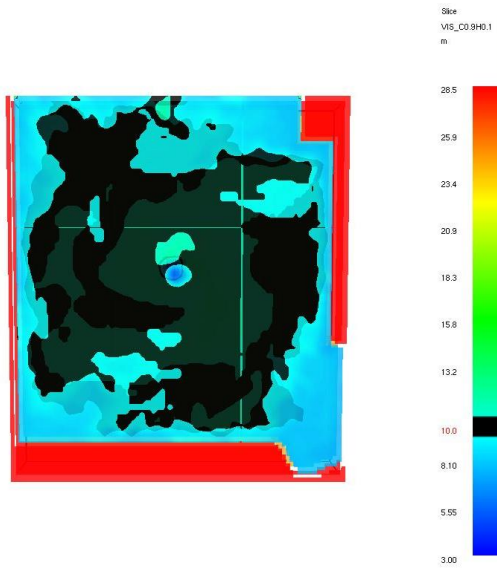
Figure 6a. Fire Only Case	Figure 6b. Fire and HVAC Case
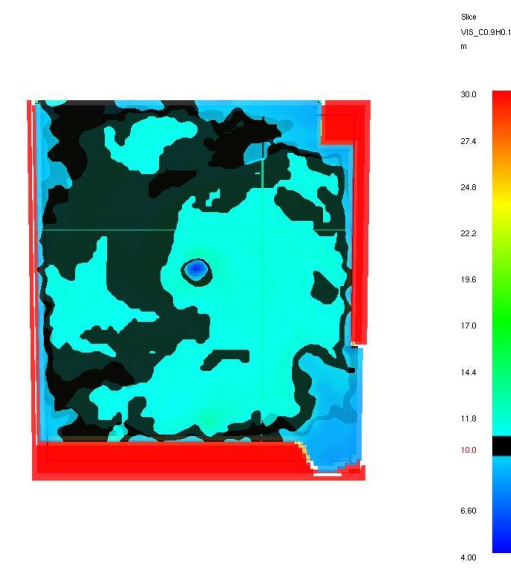
5   CONCLUSIONS

The presence of velocity sources beyond those generated by the buoyant smoke plume impacts the behaviour of the fire and smoke plume. Previous research indicates that even velocity sources less than code or standard requirements can disturb the flame, alter plume trajectory, and increase entrainment. The velocities produced as part of HVAC systems have the potential to cause the aforementioned effects on a fire. The effects generated by the HVAC system are dependent on the configuration of the system and size of the space. Both factors contribute to the velocities in ways that are not fully understood. More evidence, both qualitative and quantitative, is necessary for refining and advancing the understanding of HVAC impact on smoke behaviour and management. Specifically, the impact of compartment dimensions and non-symmetric HVAC location on fire and plume dynamics should be studied.

REFERENCES

[1]   2011 ASHRAE Handbook: Heating, Ventilating, and Air-Conditioning Applications. American Society of Heating, Refrigerating, and Air Conditioning Applications Engineers, Inc., 2011.

[2]   ASHRAE Pocket Guide for Air Conditioning, Heating, Ventilation, Refrigeration. ASHRAE, 2013.

[3]   Klote, John H. Handbook of Smoke Control Engineering. ASHRAE, 2012.

[4]   "Integration: HVAC Fans and Smoke Control." Next-Generation Control Engineer Advice, Control Engineering, www.controleng.com/single-article/integration-hvac-fans-and-smoke-control/2cc0293db41eb03327d2adbb18ff4b6a.html.

[5]   Kerber, S. And Milke, J. "Using FDS to Simulate Smoke Layer Interface Height in a Simple Atrium," Fire Technology, 43, pp. 45-75, 2007.

[6]   Pongratz, C. and Milke, J., "Methods to Increase Velocity of Makeup Air for Atrium Smoke Control – A CFD Study," University of Maryland, 2014.

[7]   Hilditch, R. and Torero, J., "Smoke Management for Modern Infrastructure," University of Edinburgh, 2016.

[8]   Hadjisophocleous, G. and Zhou, J., "Maximum Velocity fo Makeup Air for Smoke Management Systems in Atria and other Large Spaces", ASHRAE RP 1300, Carleton University, Ottawa, 2007.

[9]   Ayala, P., Cantizano, A., Rein, Guillermo, and Gutierrez-Montes, C., "Factors Affecting the Make-Up Air and Their Influence on the Dynamics of Atrium Fires," Fire Technology, 54, pp. 1067-1091, 2018.

[10] "NFPA 92." NFPA, www.nfpa.org/codes-and-standards/all-codes-and-standards/list-of-codes-and-standards/detail?code=92.

[11] Ministry of Housing, Her Majesty's Government. "Ventilation: Approved Document F." *GOV.UK*, GOV.UK, 1 Dec. 2010, www.gov.uk/government/publications/ventilation-approved-document-f.

[12] Yamada, T., Akizuki, Y., "Visibility and Human Behavior in Fire Smoke," SFPE Handbook, Springer, 2016.

SPECIAL TOPICS IN FIRE SAFETY ENGINEERING

FIRE PROTECTION DESIGN FOR AUTOMATED STORAGE AND RETRIVAL SYSTEMS (ASRS) WAREHOUSES

Paul Lhotsky[1], Carlo Mastroberardino[1] and George Hadjisophocleous[2]
[1]Civelec Consultants Inc., Montreal, Canada
[2]Carleton University Ottawa, Canada

ABSTRACT

The fire protection for most of the automated storage and retrieval system (ASRS) warehouses is not covered by the National Fire Protection Association (NFPA) standards. The design of the fire protection will depend on the ASRS configuration, type of storage containers, materials to be stored and configuration of flue spaces. The tote handling ASRS usually have open top containers that may accumulate water from sprinklers, this may increase the weight of containers and reduce the water penetration within the system. The fire protection design requires analyses of the required protection and life safety of occupants within the building. Given the value of the equipment, stored goods and cost of downtime, a reliability study should also be completed to help to determine the required redundancy of the fire protection system. The fire protection engineer plays a major part in the design team and his/hers input to all members of the design professionals is important to ensure that all systems affected by the fire protection design are properly designed.

1   INTRODUCTION

A number of new modern warehouses have automated storage and retrieval systems. These systems increase the efficiency of the warehouse and in most of the time increase the storage density. The fire protection design criteria for these systems is very limited and major changes can be expected in the event that the fire protection design is not considered during the design of the buildings and its various systems. As the conditions vary from one ASRS to another, the fire protection engineer's input is crucial for the design of a safe building and adequate fire protection of the ASRS.

2   GENERAL

2.1 Base building

Most of the buildings with ASRS are large (vary from 100,000 ft^2 to 1,000,000 ft^2) and they frequently over 75 ft high. These buildings have number of loading dock doors with a receiving dock area and a shipping dock area. Depending of the type of goods stored, the warehouse can be subdivided into multiple climate sections, for example a freezer section, a cooler section, a controlled humidity section etc. In many cases there may be a complex HVAC system as well as a refrigeration system. The base building fire protection design generally includes water supplies, fire pumps, underground water supply piping and a ceiling sprinkler system.

2.2 Automated Storage and Retrieval System

There are number of different types of ASRS. ASRS can be classified into the following categories: Pallet handling system – Crane type; Pallet handling system – Shuttle type; Tote handling system – Shuttle type; Tote handling system – Crane type; Tray handling system – Crane type; Tote handling system – Top access; and Crane systems

The crane type systems use a crane that will access pallets, trays or totes frequently two deep and will deliver the load to a conveyer system. The pallet storage is frequently over 70 ft high and would have approximately 5 ft crane aisle. The storage is similar to a double or multiple row rack system. In some installations, the pallet storage at the ground level will be used for manual picking of products. The tote or tray systems are usually divided to multiple levels with levels between 30 to 40 ft high. The storage in these systems is usually very dense with very limited flue spaces for water penetration.

The shuttle type systems have normally one shuttle per level of storage of totes. These systems usually have access aisles located at approximately every 10 ft of elevation. The shuttles in this type of systems pick up the totes and deliver the totes to an elevator system located at one extremity of the system. The other extremity is usually used for access into the system and has platforms at each walkway level. Most of these systems will have open top containers (totes) with limited drainage capabilities. The storage is very dense and, in some configurations, has very narrow transverse flue spaces and in some cases the transversal flue spaces are completely blocked.

The top access system stores totes resting on top of each other. These systems have tracks for robots that can move in 4 directions on the railing. The robots will lift the totes from the storage area (usually referred to as hive) and move the totes to another location within the hive or to an elevator usually located within the hive. This type of systems are up to 30 ft high with access to the storage only from the top.

2.3 Storage classification

Most of the ASRS trays or totes are made of plastic. The majority of the totes have open tops. The typical classification, because of the totes or trays, is class A exposed plastics. The open top totes if not provided with adequate drainage will accumulate water that is normally required to cool and wet the storage surfaces. The weight of accumulated water should be added to the weight of stored items in the totes and the structure of ASRS is to be designed for this additional load. Some ASRS systems will handle oils, aerosols or other products that may require a higher level of protection than exposed plastics.

The pallet ASRS will probably have storage of idle pallets within the system. It is important to determine where and how the idle pallets will be stored within the ASRS. The sprinkler system should be designed accordingly.

3   CODES AND APPROVALS

3.1 Building Codes

Depending on the country, the local building codes will determine the minimum level of safety required for the building and for the occupants. Most of the modern building codes have an

option to provide an alternative solution (code equivalence) to provide the required level of building safety and occupant safety.

3.2 Reference Codes

Most Building Codes will refer to other codes and standards for the design of the sprinkler systems and the fire alarm systems. In North America the building codes require that sprinkler systems and water supply meet the requirements of NFPA. Usually in case of a discrepancy between the building code and the referenced code the building code has precedence. Note that generally the building code specifies the version of the reference code (for example NFPA 13 – 2013).

3.3 Good Engineering Practice

Several times the Building Code or the referenced code by the Building Code does not have a method on how to protect the ASRS system. FM Global [1][2] has datasheets that provide a good guideline for the protection of ASRS systems. Good knowledge of fire protection and the ASRS system is essential to determine adequate fire protection for ASRS. The fire protection engineer should be careful when using multiple codes. If the engineer selects the least demanding from each code the overall protection may be less than when a single code is used in its entirety.

3.4 Authorities Having Jurisdiction

In order to obtain a building permit most of the municipalities will review compliance with the Building Code. As most of these installations will require alternative solutions to provide the code required level of safety, the review will take longer, and the fire protection engineers should be prepared to explain and defend the alternative solutions.

3.5 Owners

Some of the owners will impose operational conditions and budget limitations. The fire protection engineer should be prepared to provide reasonable cost estimates of the fire protection systems and to take into consideration the operational requirements. Note that the level of safety required by the codes cannot be reduced.

3.6 Insurance Representatives

Some insurance brokers and insurance representatives are very knowledgeable, and some have never encountered projects with ASRS. Insurance requirements may exceed the code requirements or may recommend and accept a lower level of protection. The design engineer is responsible to design the fire protection system to meet the level of safety required by codes, even if the insurance company would accept a lower level of protection.

3.7 Design Team

The design of fire protection and life safety for the building and the ASRS system is generally under the direction of the fire protection engineer. It is essential that the fire protection engineer works closely with the architect and all the members of the engineering team. This should include the design team of the ASRS. In some occasions the ASRS design team will advise how to design the fire protection for the ASRS. If this is the case the fire protection engineer should carefully evaluate the recommendations. The ASRS design team may not have a good fire protection knowledge but base the design recommendation on previous projects or other non-applicable codes.

The fire protection engineer will be required to provide information and instructions to the entire design team. For example, the architect will require the location of sprinkler rooms, pump rooms etc. The structural engineer will require loads for the water mains. It is not unusual to have differential movement between the building columns and the ASRS columns near the roof of over 2 ft. This creates a challenge in feeding sprinklers within the ASRS system from the roof.

The following are some areas that need special attention:

The fire protection engineer should assure that the underground piping is designed to resist high pressures if fire pumps will feed the underground piping.

Seismic movements are dependent on soil conditions and the seismic zone. Most of the building codes will require seismic design to meet the building code rather than the NFPA 13. [3]

The electrical and mechanical engineers will require information as to the coordination with the fire protection design.

Any special conditions generated by the alternative solutions should be discussed with the design team.

Due to the building height, the ventilation systems may force air with high velocity that should be shut in case of fire.

Any conveyers, shuttles and cranes should be shut down in case of fire.

4   FIRE PROTECTION DESIGN

4.1 Water supplies

The fire protection engineer should determine the water flow demand of the fire protection system. If municipal water supplies are available, a water test should be made to determine the available flows and pressures. Note that the actual flow should be in the same range as the actual fire protection water flow demand.

When required the fire protection engineer should determine if a water reservoir is required, if fire pumps are required and to determine the size of the underground piping and the location of hydrants, control valves and water entrances into the building. The fire protection engineer should specify the hydrostatic testing procedure and flushing rates of the piping.

4.2 Reliability

Due to the high cost of the ASRS system, the size of the building, the cost of products that will be stored in high density and high business interruption costs, the evaluation of the reliability of the fire protection system is essential.

To increase system reliability the system should be designed with some redundancies. For example, two independent water supplies and two fire pumps may be considered. Consideration should also be given to loop the underground main, location of control valves and the number of sprinkler entrances. In some cases, an emergency generator may be required, which brings additional requirements.

The design of the fire protection systems should take into consideration that the access to storage is limited and the fire-fighters may not be able to reach high elevations within the ASRS system.

Because of this a fire protection system that will extinguish the fire rather than just control it should be considered. Additional redundancy may be required by the fire department.

4.3 Required space - Building

The fire protection system may require numerous sprinkler systems and will have large manifolds for sprinkler risers. The required space for the manifolds must be coordinated with the architect. For tall buildings, there will be requirement to brace the sprinkler risers to the wall. The structural engineer must design the structure so that it can support the load from the sprinkler risers. These loads will be quite large in areas with expected seismic movements. In case of a freezer or cooler, the sprinkler room should be insulated and heated.

Most of the sprinkler systems protecting the ASRS will require a fire pump. Two pumps may be required for reliability. The architect should be advised on the size of the pump rooms. The engineer should advise if the pump will be electric driven or diesel. The size of the room should be able to accommodate the mechanical equipment. The ability to service the equipment should be taken into consideration when sizing the rooms.

4.4 ASRS protection

The fire protection engineer should obtain information as to the longitudinal and transversal flue spaces. Frequently these flue spaces are completely blocked with tote support and guidance structures. The fire protection engineer should be able to evaluate the water flow obstructions within the flue spaces.

If the system uses totes, boxes or trays as storage carriers, the combustibility of the carrier may increase the classification of combustibles. The fire protection design will change if the totes are to be considered as "open top containers".

The NFPA has little or no guidance for the protection of ASRS. FM Global has a data sheet 8-34 [1] that provides guidance for the protection of ASRS system as well as guidance when standard rack protection can be used. Note that FM standards are usually accepted by the insurance companies but require an alternative solution to be used, which has to be permitted by the authority having jurisdiction.

The location of sprinklers and piping should be coordinated with the ASRS manufacturer to make sure that the sprinkler system will not interfere with the operation of the ASRS. Special attention should be given to allow access in case of required repairs to the sprinkler system.

Most of the ASRS have multiple levels of platforms and conveyer systems. Most of the time sprinkler protection will be required under the platforms and under some conveyers.

4.5 Conventional storage

These warehouses will have areas to deal with goods that are not compatible with the ASRS and will be stored separately. The fire protection engineers may have to do fire modelling to determine the effect of building height on sprinkler activation. Studies have shown that the fire will be much larger due to the delay in sprinkler activation and sprinkler densities based on NFPA 13 for low storage may not provide adequate protection [2].

4.6 Roof sprinkler system

Depending on the design of the fire protection within the ASRS the roof sprinkler system must be designed to be compatible with the ASRS fire protection and to protect the conventional storage.

5 LIFE SAFETY

5.1 Exiting

In many occasions the ASRS manufacturers have a designs that limit access into the ASRS and sometimes the ASRS design will have very long dead end aisles that may trap maintenance staff in the case that a fire starts near the egress from the ASRS. The fire protection engineer should identify these problems and demand that the ASRS be modified to eliminate dead end aisles to meet the Building Code level of safety.

In most cases an alternative solution will be required with the demonstration that all personnel can safely evacuate the building. The Ontario Building Code has an equation that can be used to calculate time to exit. The sprinkler design should provide adequate structural protection to minimize the potential collapse of ASRS or the building.

5.2 Fire Alarm Systems

In some instances, a very early smoke detection system may have to be used to reduce the delay until the sprinkler system will activate the fire alarm system and initiate the evacuation signal. In some cases, additional fire or smoke detection may be required to activate the fire alarm system and to stop ventilation, conveyers, cranes shuttles etc.

The fire alarm system design should take into consideration access for inspection and maintenance as some areas will have no or very limited access due to the ASRS.

6 CONCLUSIONS

The design of fire protection system is very complex and requires a fire protection engineer who has experience and good knowledge of the ASRS, fire modelling, codes and insurance requirements, costs and design of sprinkler systems. The fire protection engineer will be called upon to assure fire safety of the building and life safety.

REFERENCES

[1]   FM Global. Storage of Class 1, 2, 3, 4 and Plastic Commodities – Property Loss Prevention Data Sheets 8-9. West Gloucester (RI): FM Global Research; 2018

[2]   FM Global. Protection for Automatic Storage and Retrieval Systems – Property Loss Prevention Data Sheets 8-34. West Gloucester (RI): FM Global Research; 2017

[3]   National Fire Protection Association. NFPA 13, Standards for the Installation of Sprinkler Systems. Quincy (MA): NFPA; 2013.

FIRE SAFETY/SECURITY OF TRANSPORTATION INFRASTRUCTURES BRIDGES VS TUNNELS

Stefan Zmigrodzki
CIMA+, Montréal, Canada

ABSTRACT

Following tunnel fires in Europe at the turn of the centuries, fire safety/security has become an issue for transportation infrastructures. There are however, significant differences between tunnels and bridges regarding both aspects; safety of people and security of structures. Safety of people, an important aspect for tunnels, is practically not an issue for bridges; security of structures however, poses serious problems. While tunnels are simple "bored holes" or reinforced concrete frames, bridges can present a variety of structural systems more or less fire resistant. Fire scenarios for tunnels are quite easily predictable; in the case of bridges, they depend on many parameters. Gasoline tankers and other dangerous goods are normally prohibited in tunnels but they are allowed on roads; cargo trains and ships represent even a bigger hazard for bridges. The differences between bridges and tunnels result therefore in a different approach in dealing with fire hazards.

1   INTRODUCTION

Fire as risk for transportation infrastructures has become increasingly an issue as cases of fire and subsequent losses of tunnels and bridges have become a reality in the recent years. The series of tragic events in tunnels, which have occurred in Europe in 1996-2001 and have caused the loss of lives (over 200 persons perished) and an important economic impact, have led to changes in codes and standards. An upgrading of many tunnels has followed. Bridge fires, which have occurred over the years, with some exceptions, did not have the same impact. There was no loss of lives and the economic impact was less important; the status quo has basically prevailed in dealing with fire hazards. The aim of this paper is to shed some light on the differences between tunnels and bridges from the perspective of fire hazards and related issues.

2   FIRE HAZARDS FOR TRANSPORTATION INFRASTRUTURES

Fire hazards for transportation infrastructures are related to combustible loads of road vehicles, trains, ships, public utilities and storage. Main hazards on roads come from gasoline tankers and other dangerous goods; the combustible load of tankers is about 300 MW compared to 100 MW for heavy goods vehicles ([1] to [3]); an example of a gasoline tanker on fire is shown in Fig 1.

Fig. 1. Fire of a gasoline tanker under The Paramount Blvd. Bridge (Montebello, CA 2011)

Hazards on railways are related to combustible loads of transported cargos, these loads are much bigger than those on roads. As example of fire of a cargo train Fig 2 shows the fire of the seventy-four cars freight train carrying crude oil; the fire has occurred in Lac Megantic in Quebec in 2013 causing the death of 47 people and a complete destruction of the downtown.

Fig. 2. Fire of the cargo train in Lac Megantic (Québec, 2013) and the consequences.

Combustible loads of subway or intercity cars are relatively small when compared to cargo trains but the full scale tests conducted recently ([4] and [5]) have shown that such fires can reach more than 50 MW at the peak. Fig 3 gives examples of two passenger train fires.

Fig. 3. Fires of passenger trains: a) The Samleshwari Express (India, 2011), b) The Chester Train (Australia, 2010)

Hazards on waterways are related to combustible loads of cargo ships; the highest category of fire hazards. There are few reported cases of ship fires but the one in New York in 1973 shown in Fig 4, can serve as example; two ships collided near the harbor and have caught fire; one of

them loaded with light crude oil. The ships were interlocked when passing under the Verrazano-Narrows Bridge and the flames have reached the bottom of the bridge.

Fig. 4. Ship fire near the Verrazano-Narrows Bridge in New York in 1973

Material stored or vehicles parked below bridges and public utilities carried by bridges can represent also fire hazards and examples are given in Fig 5. On the left, fire of dismounted wooden service decks stored under The Łazienkowski Bridge over the Vistula River in Warsaw (Poland) [6]; the propagation of an intense heat through the superstructure causing fire of public utilities, has led to the loss of all spans. On the right, fire of trucks parked under The Mathilde Bridge over The Seine River in Rouen (France) [7]; following the overturning of a tanker which caught fire on the bridge, the fuel has spilled over and reached the trucks below.
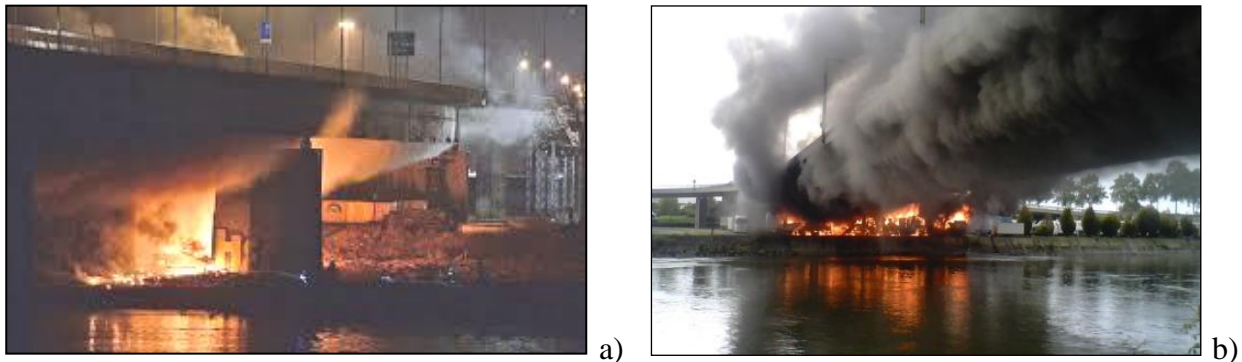
Fig. 5. Fires of material/vehicles below bridges: a) The Łazienkowski Bridge (Poland), b) The Mathilde Bridge (France)

3   SAFETY-SECURITY ISSUES

The difference between bridges and tunnels with regards to the exposure of users and infrastructures to fire hazards can be summarized as follows:

- Fire scenarios can be quite easily defined for tunnels while for bridges they depend on combustible loads on and below bridges, both hazards are independent from each other;
- Safety of users in tunnels is the most important aspect while in the case of bridges it is almost not an issue;
- Security of tunnel structures is easy to control while the security of bridges depends on the type of the structural system and the specific fire hazards.

3.1 Tunnels

Safe evacuation of users requires ventilation of tunnels to ensure a smoke free environment in the early phase of the fire, this phase is reflected in fire curves and it is one of the basic parameters for the design of ventilation systems and egress routes.

As far as the security of structures is concerned, there are two categories of tunnels; tunnels bored in rocks and tunnels built as structural frames. The consequences of fire in both cases are very different and The Mont Blanc Tunnel after the fire of a trailer loaded with butter and flour in 1999 shown in Fig 6, explains the difference. After 52 hours of burning the bored hole in the mountain remained while in the case of a structural frame a complete collapse of the sector would have to be expected. Fortunately, the cases of big fires in structural tunnels have not been reported until now.

Fig. 6. The Mont Blanc Tunnel after the fire in 1999

The preservation of structural tunnels faces the problem of very high temperatures (over 1000°C) in a confined environment, reached within minutes. Such temperatures are beyond the limit of the resistance of concrete; the loss of resistance begins at ± 300°C (spalling at ± 250°C) and 600°C is viewed as the practical limit for concrete as material ([8] to [11]). Concrete structures require therefore protection to reduce the temperature on the surface of the elements; passive and active protections are in use for this purpose.

- **Road Tunnels**

Fires are caused mainly by the collision of vehicles and the seize of fire depends on the characteristics of the traffic and the number of heavy goods vehicles (HGV) in the tunnel. HGV are considered for the combustible load as the dangerous goods (gasoline tankers) are generally prohibited in tunnels. The fire scenario for a specific tunnel and the corresponding fire curve are established from the engineering analysis. In tunnels where an occasional passage of dangerous goods must be allowed, such operation is usually under escort and when the tunnel is closed for the traffic, otherwise, a higher design fire has to be considered.

- **Railway Tunnels**

There are no standards for hazards related to cargo trains; such hazards are however different from those in road tunnels as the problem of safety of people is limited to train operators. Furthermore, the risks of derailment in railway tunnels and subsequent fires are rather small. In addition, a moving cargo train on fire can be easily evacuated outside a tunnel reducing hazards.

3.2 Bridges

Bridges are open-air structures, well exposed to the natural ventilation and they normally provide users with enough time and space for a safe evacuation; the safety of people is therefore not an issue. Security of structures however, poses serious problems and should be investigated for each and every bridge with respect to its specific hazards. There are two categories of hazards:

- Combustible loads and their location on bridges (gasoline tankers, cargo trains, public utilities) and below bridges (gasoline tankers, cargo trains, cargo vessels, storage);
- Hazards related to the performance of bridge structures exposed to fire; simple or continuous slabs, beams or girders, frames, trusses, arches, suspended bridges, cable stayed bridges, etc…; the list of structural systems is quite large.

- **Hazards related to combustible loads**

As hazards from combustible loads below bridges are the most important and independent from the use and the type of bridges; no distinction should be made between road and railway bridges. Considering combustible loads on roads, railways, waterways and in free spaces; there are many possible fire scenarios for bridges and they represent important hazards when compared to tunnels.

- **Hazards related to the performance of structures**

The structural performance of bridges depends not only on their systems but also on the material (steel or concrete) the superstructure is built of. The response to fire of concrete and steel and their use for construction of bridges, can be briefly summarized as follows:

- Concrete is a "bad" heat conductor with the performance limit reached after a longer period of time; concrete is in use for many short and medium span bridges;
- Steel is a "good" heat conductor with the performance limit reached after a shorter period of time; steel is in use for almost all medium and long span bridges, plus many short span bridges built as composite (steel girders with concrete slab).

Based on these characteristics, it could be expected that the response to fire of concrete bridges is better than of steel bridges; to some extend it is true and for small combustible loads, concrete bridges are a logical solution when dealing with fire hazards. For larger fires however, it is not the case and as demonstrated in many publications ([12] to [20]) on bridge fires, the consequences are quite similar as shown in examples in Fig.7:

- Collapse of the McArthur Maze Bridge in Oakland (2007) after a gasoline tank fire; bridge built as composite (steel girders with concrete slab).
- Loss of concrete and exposure of the rebar of the I-270/I-70 Bridge in Ohio (2015) after an ethanol tank fire; bridge built as thick concrete slab.

The extend of damages was different but the consequences were the same; both bridges had to be demolished and rebuilt.
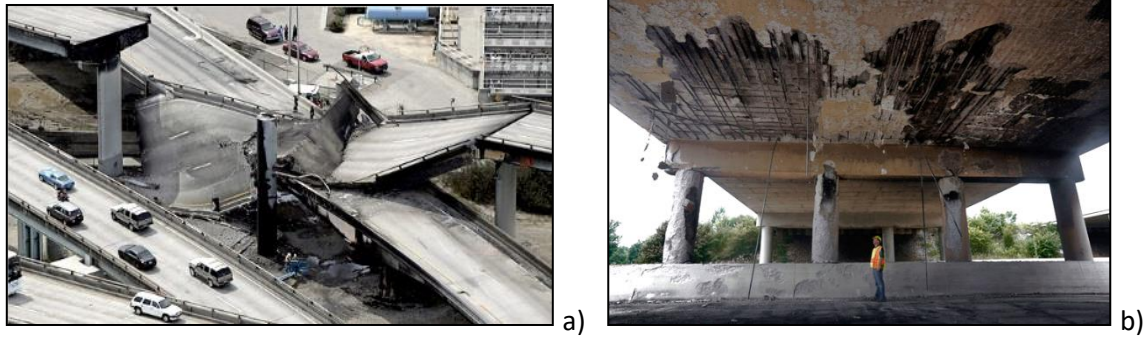
Fig. 7. Example of losses: a) The McArthur Maze Bridge, Oakland (2007), b) The I-270/I-70 Bridge, (Ohio) (2015)

3.3 Safety/security issues of tunnels and brides - Summary

Safety/security issues of bridges vs road tunnels is summarized in the table below.

Table 1. Safety/Security Issues - Bridges versus Tunnels

	Tunnels	Bridges		
Structures	Bored Tunnels or Structural Concrete Frames (Buried Structures)	Abutments - Monolithic concrete		
		Spans	Concrete	Thick Slabs (simple/cont.)
				Beams/Girders (simple/cont.)
				Monolithic Frames,
			Steel	I Girders/Beams (simple/cont.)
				Box Girders (simple/cont.)
				Trusses (simple/cont.)
				Arches
				Cables (cable-stayed bridges)
				Hangers (suspension bridges)
Fire Seize & Scenario	HGV : ±100 MW (curve RWS) Note : Tankers (±300 MW) are prohibited	Fire below Bridges	Tankers : ±300 MW Note : Inlc. Parking, Storage, etc..	Public Utilities
			Cargo Trains >> 1 000 MW	
			Cargo Ships >> 1 000 MW	
		Fire on Bridges : Scenario depends on Structure / Exposure		
Impact of Fire	Safety of People : Egress Route Ventilation	Practically No Issue		
	Security of Structures : Passive Protection Active Protection	Damages up to The Loss		

4 DEALING WITH FIRE HAZARDS

Safety/security issues are reflected in two North American standards:

-   NFPA 502 "Standard for Road Tunnels, Bridges, and Other limited Access Highways" [21];
-   NFPA 130 "Standard for Fixed Guideway Transit Passenger Rail Systems" [22].

In both standards an engineering analysis is an essential part of the design/evaluation procedure to address safety/security issues in both, tunnels and bridges. An assessment of risks and appropriate measures aiming the reduction of risks are the key elements in this procedure.

4.1 Tunnels

To reduce fire hazards, continuous detection and monitoring of heat and gazes, traffic control with cameras in real time, barriers, traffic signs, etc.…, are the tools in use in modern tunnels.

In case of fire, ventilation systems provide a smoke free environment for the evacuation of users; security of structures is assured by passive or active protection. Passive protections consist of boards or sprayed coatings and their thickness is function of the ability of the structure to resist the temperature loads [23]. For fire of a HGV they are usually about 30 mm thick and cover completely the inner face of a tunnel; boards are attached to structures with stainless steel bolts resistant to high temperature. Active protections or fixed fire fighting systems (FFFS), are also in use to damp the heat and control the temperature on the inner face of a tunnel; they act like sprinklers in buildings using water of mists to cool the air in the tunnel. The impact of water/mists on ventilation should however be considered in the design. Dealing with fire hazards in tunnels is covered by many publications and examples are given in references ([24] to [27]); as said, an engineering analysis is a key element in the procedure and an adequate selection of the design fire for the concept of ventilation and protection of structures, is an important element in such analysis.

4.2 Bridges

-   **Protection**

As mentioned earlier, safety of users is not an issue but protecting/preserving bridge structures is a problem. Using for protection boards or thick sprayed coatings like in tunnels, would be a very complicated and costly approach. Such protections would have to correspond to the fire seize of a gasoline tanker and its thickness would result in an additional weight plus related wind and earthquake loads acting on a structure. For existing bridges to be upgraded for fire hazards and affected by years of service (corrosion), this could present a real problem; in addition, such protection would hide structural elements making them inaccessible for inspection. Cargo trains and vessels with much bigger combustible loads represent another type of hazards and assuring protection would enter in a different category. Such solution is good for buildings but for bridges exposed to environmental attacks [28], other means are necessary to assure the structural security. Contrarily to tunnels where passive or active protections solve the problem, the dealing with fire hazards in the case of bridges should be focused on a general concept and measures aiming the reduction of fire hazards.

-   **Concept**

One solution which could be used for the concept of new bridges and provide an adequate level of protection is a sacrificial cover of the rebar; the resistance of concrete girders or slabs to temperature loads would be part of the concept [29] thus preventing a bridge from collapse, repairs however, would be unavoidable after fire.

Limiting the exposure of a structure by increasing the height of a bridge, would help reducing temperature in structural elements; however, the case of The Wiehtal Bridge (Germany) fire [30], proves a rather relative character of such measure. After a collision with a car, a gasoline tanker has fallen from the bridge and caught fire; part of the span had to be replaced.

- **Reduction of risks of fire**

The reduction of risk of fire would be the only way of addressing effectively fire issues; such risks would be part of parameters considered in an overall design of new bridges and the evaluation of existing bridges ([31] to [34]). The probability of fire is already very low and it can be further decreased, by controlling the elements of risks.

The control of the fire hazards should however be always put in the perspectives of other design parameters, which determine life-cycle performance of bridges; this aspect does not necessary apply to tunnels where the introduction of passive or active protections does not affect such parameters.

5 LIFE-CYCLE PERFORMANCE

5.1 Tunnels

From the perspective of the life-cycle, the "good" long-term structural performance of most tunnels reflects their character, tunnels are built as buried concrete structures with limited exposure to environmental attacks and this aspect makes an important difference when compared to bridges.

5.2 Bridges

The life-cycle performance of bridges resulting from an exposure to environmental attacks such as sunrays, temperature changes, de-icing salts used on roads in norther countries, etc.…, should not be affected by dealing with fire hazards.

Based on the probability of occurrence it is doubtful the risk related to fire would prevail in many cases. As example, the deterioration of concrete bridges affected by de-icing salts in Quebec and the actual leaning towards steel structures, is not necessary "in line" with the philosophy of the design of bridges against fire hazards.

The risk related to fire hazards will always remain one of the parameters in the design or the evaluation bridges. There are many examples of "poor performance" of bridges due to a "poor design" of standard projects, and in some cases, such performance has resulted in failure. Introducing the dealing with fire hazards, as new parameter in conceptual design should not be done to the detriment of the existing parameters, many engineers have still the difficulty to deal properly in spite of decades of experiences ([35] and [36]).

6 CONCLUSIONS

Higher combustible loads below bridges on one side and different types of bridge structures on the other, result in a variety of fire scenarios when compared to tunnels, making the dealing with fire hazards for bridges much more complex. The dealing becomes a new aspect for bridges and measures aiming to assure the control fire hazards new design parameters; a very different context than in the case of tunnels.

5

The "extended family" of parameters requires an integrated, holistic approach in design of bridges to take care of all parameters at the same time; the life-cycle performance being a paramount criterion. High-level skills will always be required from structural engineers to guarantee that the design of a bridge for fire does not have a negative impact on the overall performance of the infrastructure. This situation seems to be behind some reluctance to tackle the issues related to fire safety/security of bridges at a larger scale.

REFERENCES

[1] Inagson H. et al. (2014). *Tunnel Fire Dynamics.* Springer.

[2] Maevski I. (2011). *Design Fires in Road Tunnels, a Synthesis of Highway Practice.* National Cooperative Highway Research Program (NCHRP) Synthesis 404.

[3] Staffansson J. (2010). *Selecting design fires.* Department of Fire Safety Engineering and Systems Safety, Lund University, Sweden, Report 7032 Lund.

[4] Hadjisophocleous G. (2012). *Full-scale Experimentations for Heat Release Measurements of Railcar Fires.* 5th Intern. Symposium on Tunnel Safety & Security, New York, 2012.

[5] Zhen Y. & Ingason H. (2014). *A new Methodology of Design Fires for Train Carriages.* 6th Intern. Symposium on Tunnel Safety & Security, Marseille, France, 2014.

[6] Zobel H. et al. (2016). *Łazienkowski Bridge in Warsaw – Structural Damage and Restoration Method.* de Gruyter, Archives of Civil Engineering, Vol. LXII, Issue 4, Part 1, 2016.

[7] Godart B. et al. (2015). *Diagnosis, assessment and repair of the Mathilde bridge close to collapse during a fire.* Structural Engineering International 3/2015.

[8] Klingsch E.W.H. (2014). *Explosive Spalling of Concrete in Fire.* ETH Zurich.

[9] Deeny S. (2008). *Spalling of Concrete: Implications for Structural Performance in Fire.* Australasian Conference on the Mechanics of Structures and Materials (ACMSM20), 2008.

[10] Choi J. (2008). *Concurrent Fire Dynamics Models and Thermomechanical Analysis of Steel and Concrete Structures.* Georgia Institute of Technology.

[11] Khoury G. (2000). *Concrete Spalling Review.* Swedish National Road Administration.

[12] Peris-Sayol G. et al. (2016) *Detailed Analysis of the Causes of Bridge Fires and Their Associated Damage Levels.* ASCE, Journal of Performance of Constructed Facilities.

[13] Schumacher J. (2016). *Assessment of Bridge-Structures Under Fired Impact: A Case Study Approach,* University of Rhode Island.

[14] Cook W. (2014). *Bridge Failure Rates, Consequences, and Predictive Trends.* Utah State University.

[15] Lee G.C. et al. (2013). *A Study of U.S. Bridge Failures (1980-2012).* Technical Paper MCEER-13-0008, 2013.

[16] Yongjun Liu et al. (2013). *Bridges in Fire: State-of-the-Art and Research Needs.* Applied Mechanics and Materials, Trans Tech Publications, Switzerland, 2013.

[17] Giuliani et al. (2012). *Vulnerability of bridges to fire.* Technical University of Denmark.

[18] Garlock M. (2012). *Fire hazard in bridges: Review, assessment and repair strategies.* Engineering Structures 35, 89–98, 2012.

[19] Pennsylvania Department of Transportation. (2011). *Effects of Fire Damage on the Structural Properties of Steel Bridge Elements.* University of Pittsburgh.

[20]   Wendy LeAnn Moore W.L-A. (2008). *Performance of fire-damaged pre-stressed concrete bridges*. Missouri University of Science and Technology.

[21]   NFPA 502 Standard for Road Tunnels, Bridges, and Other Limited Access Highways.

[22]   NFPA 130 Standard for Fixed Guideway Transit Passenger Rail Systems.

[23]   Zmigrodzki S. (2012). *Temperature Loads and Passive Protection in Structural Tunnels*.   5th Intern. Symposium on Tunnel Safety & Security. New York, 2012.

[24]   Hiscock C. et al. (2010). *A Risk Analysis Methodology for Tunnel Fire Safety.* Fire Life Safety Conference, Graz 2010.

[25]   Almand K. (2008). *Safety & Security in Roadway Tunnels*. American Association of State Highway and Transportation Officials (AASHTO) - Standing Committee on Highways.

[26]   PIARC Techn. Committee C3.3 Road tunnel operation. *Risk Analysis for Road Tunnels.* 2008.

[27]   PIARC Techn. Committee C3.3 Road tunnel operation. *Integrated Approach to Road Tunnel Safety*". 2007.

[28]   Mostafaei H. et al. (2014). *Technologies for Protection and Resistance Enhancement of Critical Infrastructures against Extreme Fire*. National Research Council of Canada, 2014.

[29]   McIntyre J. (2007). *Fire Protection of NU Girders on the Herb Gray Parkway*. 9th International Conference on Short and Medium Span Bridges, Calgary July 2014.

[30]   Wikpedia *Wiehltalbrücke* https://de.wikipedia.org/wiki/Wiehltalbr%C3%BCcke

[31]   Wright W. (2013). *Highway Bridge Fire Hazard Assessment - Draft Final Report*. Virginia Polytechnic Institute and State University.

[32]   Wright W. (2013). *Highway Bridge Fire Hazard Assessment Draft - Guide Specification for Fire Damage Evaluation in Steel Bridges*. Virginia Polytechnic Institute and State University.

[33]   Kodur V. et al. (2013). *Evaluating Fire Resistance of Steel Girders in Bridges.* Journal of Bridge Engineering, ASCE, July 2013, 633-643.

[34]   Naser M.Z., Kodur V.K.R. (2015). *A probabilistic assessment for classification of bridges against fire hazard*. Fire Safety Journal 76, 2015.

[35]   Zmigrodzki S. (2014). *Sustainability of Infrastructures vs Climate Changes*. 37th IABSE Symposium; Madrid, September 2014.

[36]   Zmigrodzki S. (2016). *Life-cycle performance as results of basic design considerations*. 5th Intern. Symposium on Life-Cycle Civil Engineering; Delft, Netherlands, October 2016.

AN EXPERIMENTAL STUDY ON POSSIBLE THERMAL HAZARDS OF CELLULAR PHONES

Jessie H.Y. Kwok[1], C.H. Cheng[1], W.K. Chow[1] and C.L. Chow[2]

[1]Research Centre for Fire Engineering, Department of Building Services Engineering, The Hong Kong Polytechnic University, Hong Kong, China

[2]Department of Architecture and Civil Engineering, City University of Hong Kong, Hong Kong, China

ABSTRACT

Fire and explosion hazards of cellular phones crowded enclosure such as in train cars should be carefully watched as many passengers are using phones or even charging phones while travelling for long distance trips. The thermal behavior of two cellular phone models (labelled as Phone A and Phone B) which were complained to be too hot were studied experimentally and reported in this paper. Three sets of experiments were carried out on the phones. Both phones A and B appeared to be safe under proper working conditions, though for phone A the battery was swollen with sparks observed in accelerated tests in which thermal insulation was imposed.

1   INTRODUCTION

The frequency of fires caused by electronic devices is increasing, with many such fires arising from cellular phones [1]. Sparkling flames were reported [2] while charging the cellular phone on the bed. Cellular phones might catch fires accidentally [3-5]. Such a fire incident was reported to burn down a house a few years ago in Hong Kong [3]. A cellular phone even exploded by itself in a train car [4]. This could be very hazardous as almost every passenger has a cellular phone and improper uses of cellular phones are likely to trigger electrical fire. Cellular phones themselves might not catch fire easily. However, they can become overheated if left in the charging mode for a long time. In most cellular phone fire accidents, the cause of fire or explosion was ascribed to the batteries.

Lithium-ion batteries are widely used in cellular phones since they offer better performance than many other types of battery. The advantages of lithium-ion batteries include high energy and power density, longer life time and higher charging rate, making them much more attractive for consumer products [6]. However, lithium-ion batteries contain reactive and flammable materials, and billions of lithium-ion cells are used in cellular phones. Thus, there are concerns on thermal hazards [7,8] as several serious lithium-ion battery related fire incidents have been reported [9].

Thermal hazards of lithium-ion battery-pack is a function of the cells, pack, system design and manufacture in IEEE 1625 and 1725 standards [10,11]. The hazard of lithium-ion batteries should be addressed by a system-level approach combining cells, battery pack, host device, power supply or adapter end user/environment. Each of these components has a role to play in ensuring pack safety. Besides, the operating temperature range for lithium-ion cell specified by IEEE is between 10°C and 45°C with a charging cutoff voltage 4.25 V and a maximum specified charging rate [10]. Battery cells with higher state of charge are more thermally reactive [6]. An internal circuit is used to monitor the state of the battery including temperature, charge level of the battery core section and the charging/discharging rate. The circuit controls the battery cell

including charging of the battery [12]. Lithium-ion batteries have potential safety issues and thermal runaway [13] is the most important phenomenon to consider. Under overcharging conditions, cells with Circuit Interrupt Device will be activated. The chance for cell temperature becoming close to that triggering separator shutdown is very low. When cell temperature reaches the melting point of the separator material, a faulty cell safety device will be activated to avoid overheating. When the separator shuts down, internal resistance of the battery increases and the current decreases. Once the pores of the separator close up due to softening, charging or discharging of the battery is discontinued to prevent thermal runaway [6]. If lithium-ion batteries are overheated, exothermal reactions will take place and will lead to thermal runaway with excessive amount of heat generated to give fire or even explosion [14,15].

In the present study, the thermal hazards of two cellular phone models, phone samples A and B, were investigated by measuring the temperature rise under different conditions. The goal is to study phone overheating under different scenarios.

2 EXPERIMENT 1

Two phone samples were selected in the present study: Phone A is the same brand of the exploded phone reported in a house fire [3], and Phone B is another brand which users frequently complain to be very hot.

There are two parts in Experiment 1 on thermal hazards of the two phone samples (Fig. 1):

− Part I:

The cellular phone was checked to ensure that it was operating properly and it was not being charged. The back cover was removed from the cellular phone. Key components of the cellular phone including back cover, battery, antenna, speaker, LCD screen and circuit board were connected to the thermocouple by using silver paste. The temperatures of all the components of the cellular phone were recorded by connecting them to the data logger. The test was carried out under various cellular phone activities including running applications in the background, playing games, watching movies, listening to music and searching websites. Temperatures were measured at one-minute intervals up to about 100 minutes. This test was intended to study the thermal behavior in different activities.

− Part II:

The measurements in Part I were repeated with the cellular phone in the charging mode.

The variations of temperature of different components of the phone operated without charging in Part I are shown in Fig. 2(a). The ambient temperature was kept between 22 and 23 °C. The temperature of the back cover was close to that of ambient temperature. Temperatures of all other components were higher than the ambient temperature. Temperature of the circuit board was the highest and about 20 °C above the ambient. During the first 20 minutes, temperature of the circuit board sharply increased since the load of the phone was increasing. The temperature of the circuit board was then fluctuated between 38 to 43 °C. Since the highest temperature of the cellular phone was 43 °C, ignition of cellular phone itself is impossible.
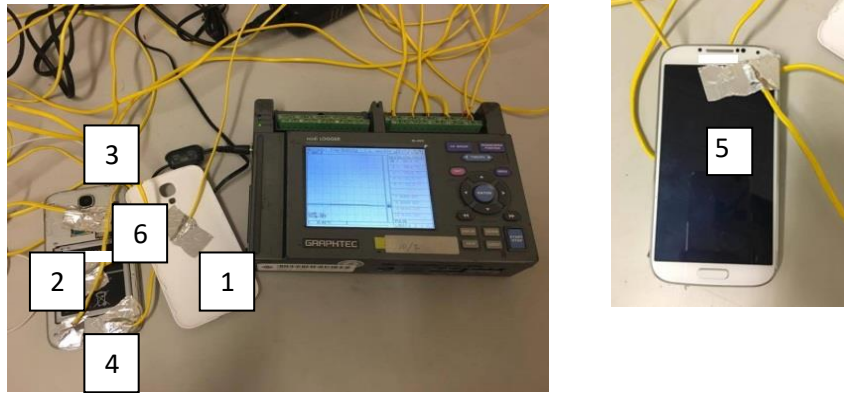
Fig. 1. Different components of phone: 1 back cover, 2 battery, 3 antenna, 4 speaker, 5 LCD screen, 6 circuit board, for Phone A in Experiment 1
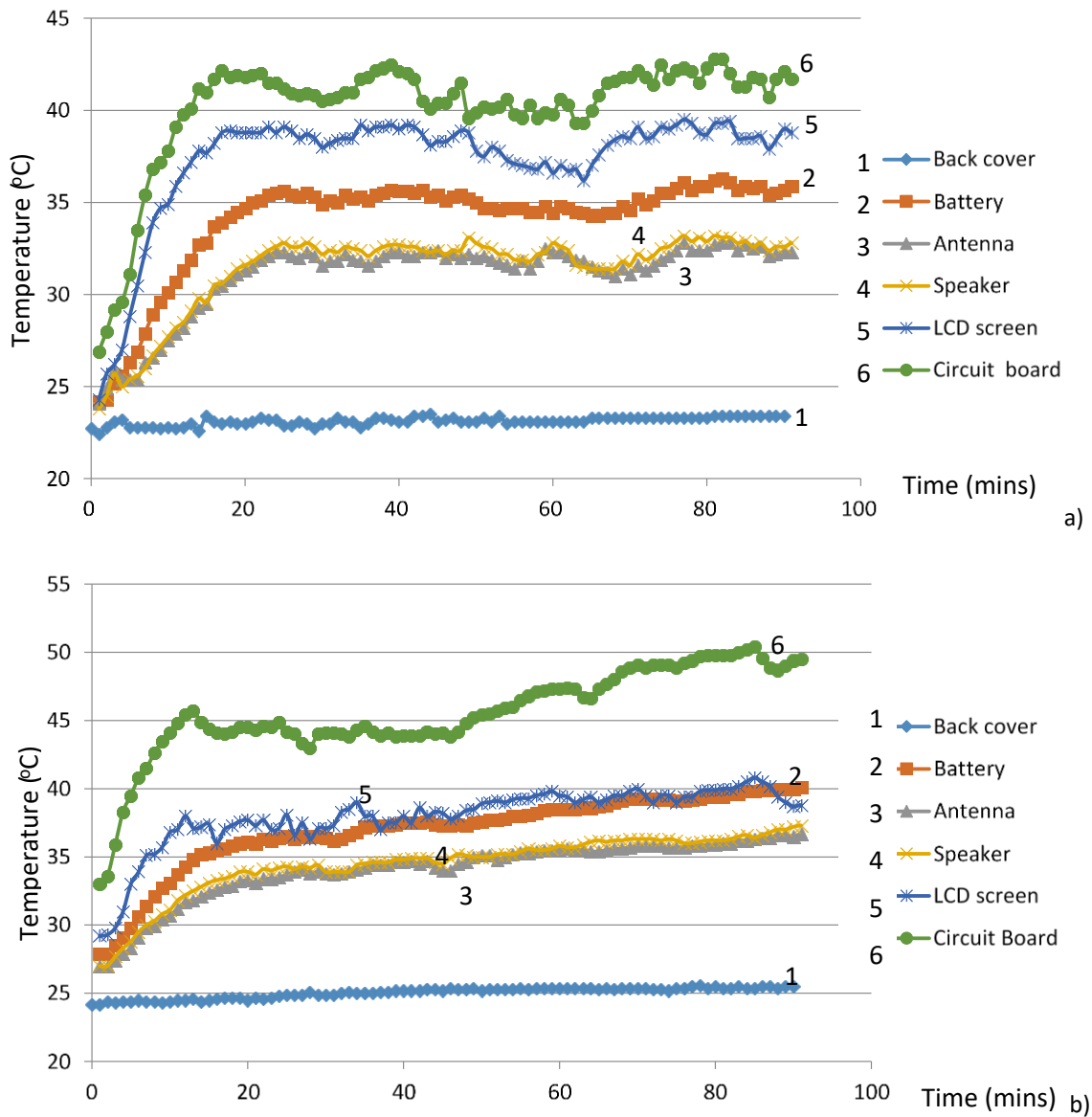

Fig. 2. Transient temperatures of different components for Phone A in Experiment 1. a) Part I; b) Part II

For Part II, Phone A was being operated and charged at the same time and the temperature variations are shown in Fig. 2(b). The back cover (or ambient) temperature was around 25 °C and the temperatures of all other components of the cellular phone were higher than the ambient temperature. During the first 10 minutes, the temperature of circuit board increased rapidly from 33 °C to 46 °C, and remained almost constant at around 45 °C from 10 to 50 minutes. After that it started increasing again to reach the highest temperature of 50 °C and dropped slightly afterwards. The possibility of ignition of cellular phone with charging is negligible.

From the experimental results, playing games would consume the battery faster and then heat up the cellular phone faster. Besides, online browsing is another process that consumes more power in discharging the battery. While browsing a web, the cellular phone would operate many functions including Wi-Fi connections to display online content, support the wireless data transfer, and display the video information. The discharge current can be very high, up to 4A, and is likely to cause overheating and a temperature well above 50 °C. Therefore, the cellular phone may be overheated after some time. The circuit board was heated up to the highest temperature among other components in all activities. Phone A is operated with a powerful CPU generating more heat without a cooling device. The more powerful the CPU used, the hotter it became and the easier to be overheated.

Comparing the results on the temperatures of different components in Part I and II, it is observed that the cellular phone was heated up more quickly when simultaneously in use and charging than without charging. This is natural as both operations generate heat. Given the small size of a cellular phone, it is more difficult to have the heat dissipated efficiently. As a consequence, the battery can be overheated. Higher complexity in circuit design with higher power consumption coupled with higher compactness of cellular phone will be difficult to keep cool, leading to thermal hazards.

From Experiment 1 on Phone A, it is observed that using the phone while it is being charged can give high temperatures.

Phone B was tested by repeating Part II, that is, in the charging mode. Transient temperatures of different components of the cellular phone are shown in Fig. 3. The temperature of the back cover reached up to 43 °C. The corresponding temperature for Phone A was only about 25 °C (ambient temperature). This indicates the large difference in thermal behavior of different brands of cellular phones, possibly due to difference in battery quality.

3 EXPERIMENT 2 ON LIMITING HEAT DISSIPATION BY THERMAL INSULATION

An additional thermal hazard scenario was carried out to study battery fire for Phone A. The phone was put between thermal insulation materials to limit thermal dissipation as shown in Fig. 4. Application software was activated while charging the batteries. The objective was to observe the effect of thermal insulation materials on the temperature of the phone battery. This testing condition is intended to simulate charging from a power bank while the phone was put inside a bag.

Variations of the temperatures of the battery and circuit board are shown in Fig. 5. When the temperature of the battery rose to 53.9 °C, charging was terminated. The phone was then allowed to cool down for about 20 minutes to 43.8 °C and phone operation and charging were re-started again. When the temperature of the circuit board increased to 74.8 °C, all the applications

stopped running automatically. However, the temperature of the battery kept rising. At 63.5 °C, the battery had no response and a small spark was observed. The battery was swollen but it was neither ignited nor did it explode.

As expected, the cellular phone reached a higher temperature when lagged with thermal insulation. Lithium-ion battery used in the phone should have internal protection devices to cut off the charging status, or to stop running applications when the temperature of the device was too high. This provision would protect the phone, and would also prevent thermal ignition and explosion. When the temperature of the battery increased to 53.9 °C, the phone stopped charging until cooling down to an acceptably low temperature. As the phone was a second-hand product, the functions of the internal protection device might have been damaged and failed to operate the second time. The use of second-hand phone is intended to simulate phones encountered in general.

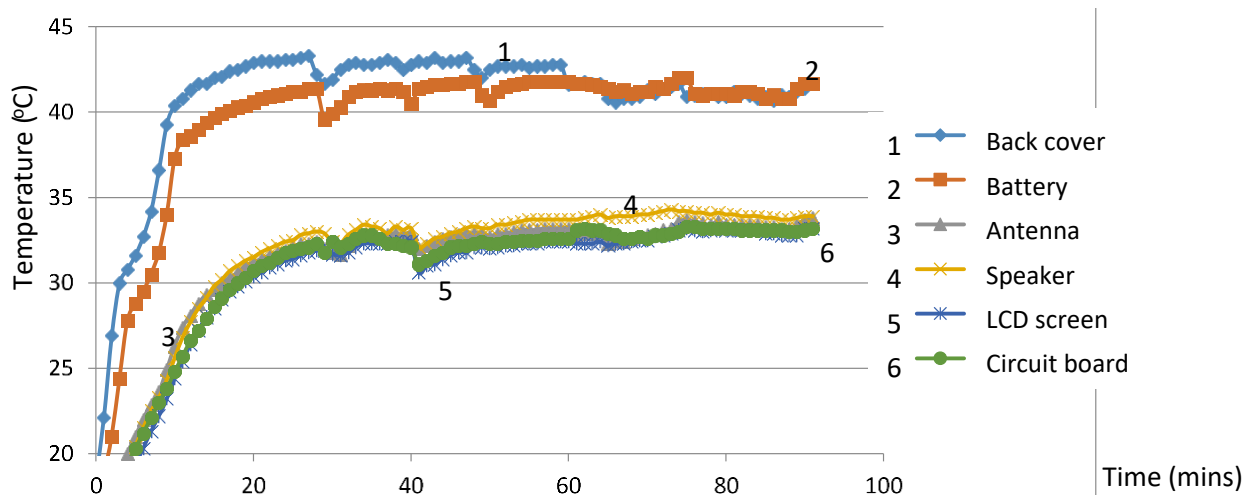*Fig. 3.* Transient temperatures of different components for Phone B in Part II of Experiment 1

Back cover
Battery
Antenna
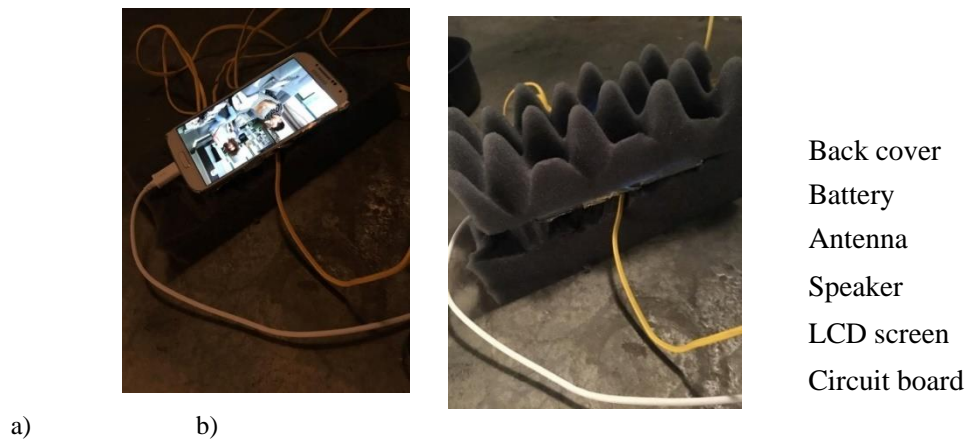Speaker
LCD screen
Circuit board

Fig. 4. Experiment 2 for Phone A. a) Experimental setup; b) Thermal insulation materials
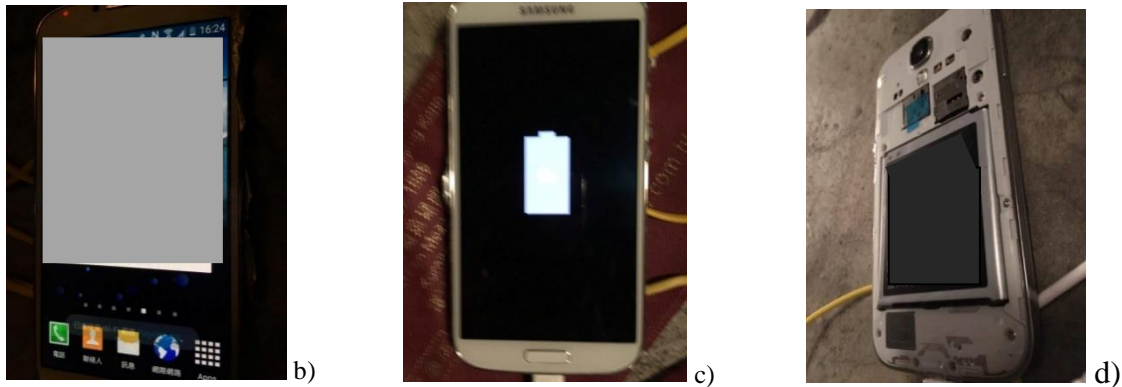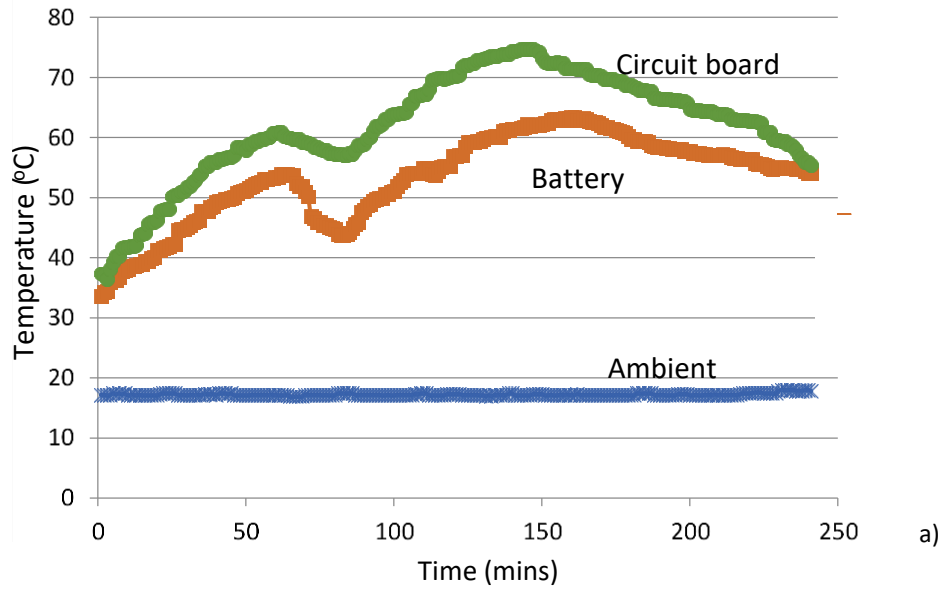
Fig. 5. Results for Phone A in Experiment 2. a) Transient temperatures measured; b) Warning signal 1; c) Warning signal 2; d) Back of phone, with brand blinded

4   EXPERIMENT 3 ON USING NON-GENUINE BATTERY

Many users would replace an old battery by a battery not manufactured by the same company because of lower cost. Another scenario was carried out with a non-genuine battery with procedures following Experiment 1 for Phone A (Fig. 1). Except for the battery, other components of the phone remained unchanged.

The temperatures of the non-genuine battery and the circuit board were observed to increase at a faster rate (Fig. 6) than when using the original battery (Fig. 3). When the temperature of the battery reached 55 °C, the phone stopped charging until it cooled down to 45 °C. The phone was then recharged until the temperature reached 56.2 °C, and then charging stopped.

The built-in internal protection device of Phone A was activated to protect the phone even when using a non-genuine battery. However, the efficiency of the internal protection device was lower in the second time. Cooling rate of the phone was much slower.

A non-genuine battery may not meet the safety standards and would result in hazardous consequences.
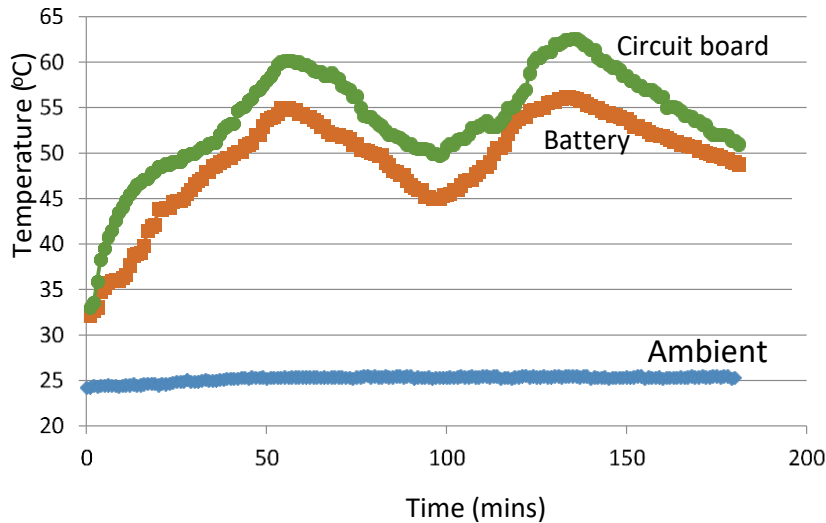

Fig. 6. Transient temperatures on Phone A for Experiment 3

In order to avoid battery fire or explosion, fire safety management [16] should be implemented in high-speed railway system:

− Passengers should not use the phone while charging, particularly in a crowded moving train inside a tunnel in a high-speed railway system.
− Adequate ventilation should be provided in train cars [17] to have better cooling effect. Note that battery in notebook computer also caught fire recently [18].
− Avoid using low quality non-genuine batteries in the train car. The high-speed railway system security guard should check this before boarding the train.

5   CONCLUSIONS

The thermal hazards of cellular phones leading to fire and explosion should be watched carefully. The consequences could be very hazardous if explosion occurs in a crowded space like the train car. The passenger loading could be very high and each person might carry more than one cellular phone while travelling in high-speed railway system across cities. Having phone explosion accident as experienced in 2013 [3] in an empty train would give very different consequences.

The above experiment shows that using cellular phone while charging it, the phone can be heated up to high temperatures. When the temperature of the battery exceeds the limit, the internal protection device would be activated to provide safety precautions. The tested cellular phones should be safe if one is not using non-genuine batteries, or the battery protection can cut off the current when heated up to a high temperature. Nevertheless, the use of non-genuine batteries is

quite common, and thermal hazards, even when not involving explosion, could be dangerous when it occurs in a crowded enclosure like the train. This could trigger panic among the passengers, and over-reactions could be much more dangerous than the thermal hazard itself.

ACKNOWLEDGMENT

REFERENCES

[1] Mckeever J. (2015). *Fire department warns people about charging cellphones on your bed.* 27 May 2015. http://fox61.com/2015/05/27/hamden-fire-caused-by-charging-cellphone/ (accessed 8 February 2017).

[2] Scheinblum J. (2015). *Cell phone causes fire in Hamden*. 28 May 2015. http://wtnh.com/2015/05/28/cell-phone-causes-fire-in-hamden/ (accessed 8 February 2017).

[3] Oriental Daily (2013). *Phone explodes and burns down a house*. 27 July 2013 – In Chinese. http://orientaldaily.on.cc/cnt/news/20130727/00174_001.html (accessed 2 January 2017).

[4] Apple Daily (2015). *Cell phone exploded inside MTR train car*. 30 March 2015 – In Chinese. http://hk.apple.nextmedia.com/news/art/20150330/19095166 (accessed 2 January 2017).

[5] Mexico News Daily (2018). *Sonora man suffers severe burns when cell phone explodes in his pocket.* 4 May 2018. https://mexiconewsdaily.com/news/sonora-man-gets-a-surprise-when-cell-phone-explodes/ (accessed 19 September 2018).

[6] Larsson F., Andersson P., Blomqvist P., Lorén A., Mellander BE. (2014). *Characteristics of lithium-ion batteries during fire tests*. Journal of Power Sources 271 (2014) 414-420 pp.

[7] Tullo A. (2006). *Dell recalls lithium batteries*. Chemical and Engineering News 84 (2006) 11 p.

[8] Castalone A. (2007). *N91 cell phone explode.* 27 July 2007. https://www.mukamo.com/nokia-n91-cell-phone-explodes/ (accessed 5 February 2017).

[9] Zhang Z.J., Ramadass P., Fang W., Pistoia G. (Eds.) (2014). *Lithium-ion batteries advances and applications*. Amsterdam: Elsevier, 409-435 pp.

[10]   IEEE 1625:2008. IEEE Standard for rechargeable batteries for multi-cell mobile computing devices.

[11]   IEEE 1725:2011. IEEE Standard for rechargeable batteries for cellular telephones.

[12]   Young J.S. (1998). *Battery cell having an internal circuit for controlling its operation.* Journal of Power Sources 70 (1998) 309 p.

[13]   Jhu C., Wang Y., Wen C., Shu C. (2012). *Thermal runaway potential of $LiCoO_2$ and $Li(Ni_{1/3}Co_{1/3}Mn_{1/3})O_2$ batteries determined with adiabatic calorimetry methodology*. Applied Energy 100 (2012) 127-131 pp.

[14]   Larsson F., Andersson P., Mellander B.E., Sandén B., Wallgren P. (Eds.). (2014). *Systems perspectives on electromobility.* Göteborg: Chalmers University of Technology, 33-44 pp.

[15]   Jacoby M. (2007). *Burning batteries.* Chemical and Engineering News 85 (2007) 26-28 pp.

[16]   Chow W.K. (2000). *Fire safety management using modeling technique.* Journal of System Safety 36 (2000) 17-24 pp.

[17]   Chow W.K., Yu P.C.H. (2000). *Simulation on energy use for mechanical ventilation and air-conditioning (MVAC) systems in train compartments*. Energy - The International Journal 25 (2000): 1-13.

[18]   news.com.au (2018). *Laptop explodes on Madrid commuter train*. 18 September 2018.

[19]   https://www.news.com.au/world/breaking-news/laptop-explodes-on-madrid-commuter-train/news-story/2072b1d067398754f01cacd8de639e7f (accessed 1 October 2018).

[20]

IFireSS2019-Paper111b

REACTION OF IN-WALL PIPES TO REAL FIRE ENVIRONMENTS

Jennifer Ellingham[1], Bronwyn Forrest[1], Elizabeth J. Weckman[1] & Haemi Pollett[2]
[1]University of Waterloo, Waterloo, Canada, [2]Uponor North America, Mississauga, Canada

ABSTRACT

A large-scale wall fire test unit was developed at University of Waterloo to study response of materials, assemblies, and in-wall systems to thermal gradients similar to real fires. A 1.8m x 1.8m wall section, with depth to 0.3m, is exposed to a symmetric, repeatable fire exposure. This paper reports results from tests on in-wall crosslinked polyethylene (peroxide crosslinking method) PEX-a pipe systems. Sections of 0.013m and 0.051m diameter pipe, with and without fittings, insulation or water-fill, are installed horizontally and vertically in wood and steel stud walls exposed to fire. Fire room, wall, and in-wall pipe temperatures are measured. Thermal gradients on the wall result in higher temperatures and larger horizontal deflections in pipes at the top of the wall. Fittings, insulation and water-fill decreased temperatures. Further tests are needed to better understand the full response of in-wall pipes to real fire exposure.

1   INTRODUCTION

This paper details results from a preliminary series of experiments aimed toward investigating the response of a wall and in-wall crosslinked polyethylene (PEX-a) pipes to a thermal gradient similar to that developed in a real fire environment. Tests were conducted in the new University of Waterloo (UW) Live Fire Research Facility large-scale wall fire test apparatus [1]. Previous work has shown that the test apparatus has a repeatable and symmetric thermal gradient for a given fuel load [2]. In contrast to certification tests, these large-scale tests are designed to study response of materials, assemblies, and in-wall systems under thermal gradients similar to those in a real fire. The data is important to improve our understanding and modelling of the impact of real fires on built assemblies. This information is necessary to predict how a change in one aspect of a design may impact the fire performance of a system as well as for next generation product development. A product must still be certified to meet all recognized North American Building or Mechanical Codes [3], including fire testing such as ASTM E84 [4], ULC S102 [5] or UL 723 [6], but these tests are often not useful for research as they are single repeat, expensive tests and only include instrumentation necessary to determine if the test is passed. Full-scale wall fire performance tests, such ASTM E119 [7], ULC S101 [8] or UL 263 [9], are even more expensive and are usually instrumented only to determine pass-fail for a product and employ a standard temperature-time curve to apply only a uniform temperature exposure to the wall. Some small and intermediate-scale tests have been conducted for research but most studies have focused on performance of specific structural components [10] or have used small samples and uniform temperature exposures [11-14]. There have been few, if any, previous studies which have employed large-scale wall fire tests to expose well-instrumented walls containing in-wall systems to repeatable thermal gradients in order to investigate their response in a real fire environment [1,2,15,16]. Such information is of interest when designing systems where it is

critical to maintain water supply well into a fire event, or for systems with specific routing or features, such as through wall penetrations.

2 EXPERIMENTAL DESIGN AND INSTRUMENTATION

2.1 Test Apparatus

The design and initial characterization of the large-scale wall fire test apparatus used for this test series were based on previous large-scale experiments and fuel characterizations in the furniture calorimeter at the UW Live Fire Research Facility [17,18]. The apparatus is housed in a modified 6.1m sea container with custom insert designed to hold 1.8m x 1.8m wall sections with a depth of up to 0.3m as shown in *Fig. 21*. Further details can be found in [1,15,16]. The unit can be used to test individual materials, wall assemblies, and in-wall systems. The fuel load, shown in *Fig. 22*, and ventilation configuration were selected based on the desired temperature-time profile from previous results [1]. Three softwood cribs centred on the wall and ignited sequentially were used to create a repeatable and symmetric thermal environment in the fire compartment [2]. Four tests were conducted with up to 40 thermocouples (32 permanent and 8 test specific) recording the fire compartment environment and 16 permanent thermocouples recording the back room and wall frame conditions [2]. Unless otherwise noted, permanent apparatus thermocouples are 24 AWG, Type K with ceramic insulation and Inconel over braid with a welded bead while test specific thermocouples are 24 AWG, Type K glass fibre insulated wires with a twisted bead.
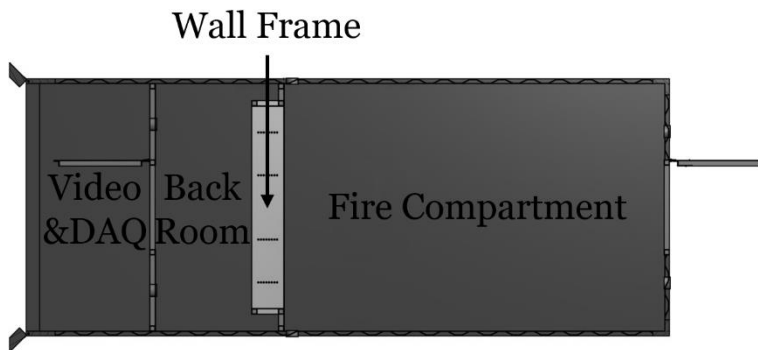

Fig. 21: Test Apparatus Layout [2]

Fig. 22: Fuel Layout [2]

2.2 Wall Assemblies

The wall assemblies for all four tests were stud walls clad on each side with one layer of 0.016m Type 'X' drywall and no insulation in the wall cavities. Detailed information on the materials used can be found in a previously published paper documenting thermal symmetry and repeatability for the tests [2]. Walls for each test had four cavities with studs spaced 0.4m apart and one cavity with studs 0.2m apart although the location of this latter cavity changed depending on the test. When the in-wall pipes were in vertical orientation, the smaller cavity was at the centre of the wall so that the two large test cavities housing pipes were equal distance from the fire but did not directly contact one another (*Fig. 3*). Conversely, when the in-wall pipes were in the horizontal orientation, the smaller cavity was at one side to facilitate installation of the pipes (*Fig. 4*). For the tests, the exposed wall drywall seam was also changed from horizontal,

per good construction practice, to vertical to prevent hot gases from entering the instrumented cavities. Wall type and pipe mounting for each test in the series are summarized in *It was* found that security camera video footage obtained during the experiments was a crucial component in understanding the burning characteristics of the couches as well as how the smoke layer impacted fire growth and therefore, the resulting value of heat release rate. The video footage was primarily used in the area source radiation approximation method described in Section 2.4. First, the pixel dimensions for the height of the back cushion and length of the couch along the front of the sitting cushions were determined. Then, a screenshot corresponding to the time of peak measured heat flux was spliced from the video. A representative screenshot is shown in *Figure 1* below. Using an image editing tool, rectangles were drawn over two areas on the screenshot: the main flame area (left hand rectangle, black, in *Figure 1*) and any surrounding flame areas (right hand rectangle, grey, in *Figure 1*). The ratio of the dimensions of the flame areas to the dimensions of the couch, in conjunction with knowing the actual dimensions of the couch, allowed for the conversion of pixels to meters for the rectangular areas. These were then used as inputs to the area source calculation method. Characteristic temperatures of the flame, Tf, in each rectangular area were based on a relative scale of colour saturation; the closer the area was to yellow, (or white in the case of the grey-scale image below) the closer the chosen value was to 1100K. In all cases, the temperature of the flaming area was assumed to be 1100K and the temperature of the secondary fire area (grey rectangle) was scaled according to relative colour. The values of temperature and dimensions are subject to change based on the person conducting the analysis, so efforts to make this process more consistent are currently being carried out.
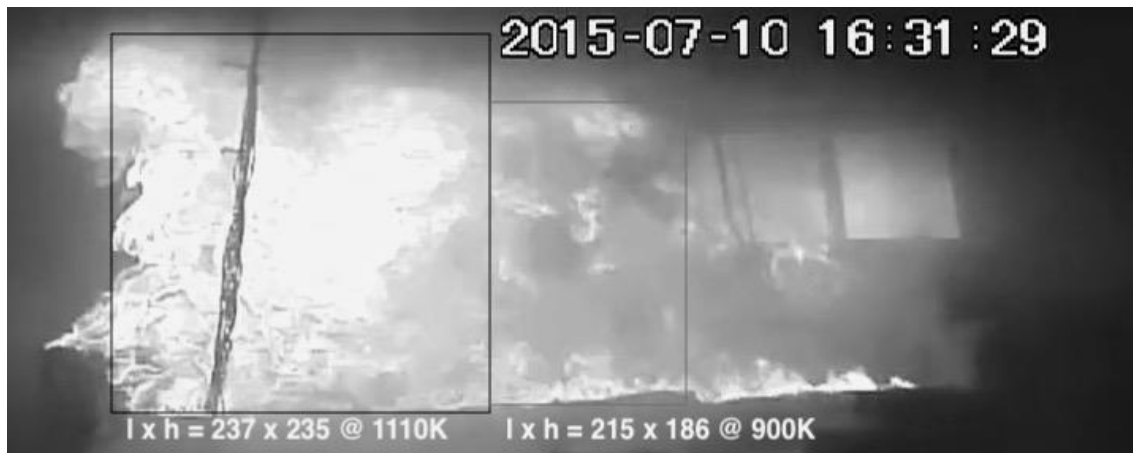

Figure 1: Example screenshot and areas of the flame area and surrounding area with pixel dimensions and temperatures used for T_f input in the area source approximation method described below.

In all four tests, 18 test specific thermocouples were used to measure the temperature progression at three wall depths. Thermocouples were hung on chains 0.23m away from the wall in the fire compartment to estimate the fire side gas temperature (visible in *Fig. 22*). On the non-fire side, thermocouples were installed on the exposed drywall (visible in *Fig. 23*) and unexposed drywall with a small insulation pad to better contact the wall and shield the sensor from the adjacent air. At each of the three wall depths, thermocouples were installed at the "top", "middle", and "bottom" of the wall in two horizontal positions. The "bottom" thermocouples were located 0.31m from the top of the lower stud. The "middle" thermocouples were located 0.89m from the top of the lower stud. The "top" thermocouples were located 1.47m from the top of the lower

stud, which corresponded to 0.33m from the bottom of the upper stud. For the vertical pipe tests, the thermocouples were centred on the stud cavities containing the pipes. For the horizontal pipe tests, one thermocouple was centred on the stud cavity as in the vertical tests, and the other was at the centre of the wall. A video camera recorded the exposed wall (fire side) and two cameras recorded the top and bottom of the unexposed wall (non-fire side).

Table 19: Test Wall Differences

	Stud Type	# of Pipes	Pipe Orientation	Seam Orientation
Test 1	Wood	8	Vertical	Horizontal
Test 2	Steel	8	Vertical	Horizontal
Test 3	Steel	4	Horizontal	Vertical
Test 4	Wood	4	Horizontal	Vertical

2.3 In-Wall Pipes

The first two tests were conducted with crosslinked polyethylene (PEX-a) pipes in a vertical configuration as shown in *Fig. 23*. PEX-a pipes of 0.013m and 0.051m nominal diameter, with and without fittings, insulation or water-fill, were installed in the walls. Test pipes were each cut to 1.78m in length. Pipes with fittings had the fittings installed at approximately 1.47m from the bottom of the pipe. The insulated pipe was wrapped with R2.0, 0.051m wide, 0.003m thick pipe wrap insulation after the thermocouples were installed. An end cap was installed at the bottom end of the water-filled pipe and the pipe was filled with water to above the top thermocouple position and left open at the top so that any water evaporating during the test would not be confined. Each pipe was held in place within the cavity with wire and the ends were stuffed with insulation to prevent hot gases from entering the inside of the pipe. Depending on the pipe, test specific thermocouples were installed at top, middle, and bottom locations on the exposed exterior side of the pipe, inside the pipe, and on the unexposed exterior side of the pipe to observe heat transfer through the pipe and fitting as applicable. Sealed, metal sheathed thermocouples were used to measure the top and bottom inner temperatures of the water-filled pipe.

The third and fourth tests were conducted with PEX-a pipes in a horizontal configuration as shown in *Fig. 63*. Pipes of 0.013m and 0.051m nominal diameter were installed at the top and bottom of the walls. Test pipes were each cut to 1.42m in length. The pipes ran through all wall cavities and were held in place by holes drilled in the studs. Both ends of each pipe were stuffed with insulation to prevent hot gases from entering the inside of the pipe. Thermocouples were installed on the outside surfaces of the pipe on both the exposed and unexposed sides, as well as in the interior of the pipe to observe the heat transfer through the pipe in locations where the wall temperatures were also monitored. Straight lines were drawn on the pipes from end to end and the straight edge of each pipe was traced onto the exposed wall so any deflection of the pipe could be determined after the test was complete.

Fig. 23: Vertical Pipe Configuration

Fig. 58: Horizontal Pipe Configuration [2]

3   RESULTS AND DISCUSSION

Previous work established that the fuel load and ventilation configuration selected for this test series provided a repeatable temperature-time profile in the fire compartment at the test wall. After an average 19.3 minute growth period, temperatures plateaued for 8.4 minutes at 708°C before beginning to decay [2]. Although, temperatures in the fire compartment cooled down within approximately an hour, each test was continued for at least four hours as temperatures in the wall and in-wall pipes continued to change over that period. Also of note is the fact that no pipes melted during tests in which the integrity of the cladding remained intact. In one instance, localized melting did occur where flames were able to penetrate the wall cavity and directly impinge on the top of a pipe. The remainder of this section presents and discusses the wall and pipe results.

3.1 Wall Assembly

Wall thermal penetration results from Test 1 are shown in *Fig. 25*. As expected, there is a clear temperature gradient from floor to ceiling in the fire compartment, with hot gases accumulating at the top. This is clearly reflected in temperatures on the back sides of the gypsum cladding of the exposed and unexposed walls. Temperatures on the back side of the exposed wall remain well below those in the fire compartment at the same height. It took 17-22 minutes for the top of the exposed wall to heat to 100°C, and about 45 minutes to reach peak temperatures of 278°C. Temperatures on the exterior surface of the unexposed wall increase due to through wall heat transfer via radiation from the exposed wall, convection from the air movement within the stud cavities, and conduction through the studs and cladding but did not rise to 100°C in any of the tests.

3.2 In-Wall Pipes

Results from the series of vertical and horizontal piping system exposure tests are contained in *Fig. 5* through *Fig. 8* and discussed in two sections below. In each test, empty lengths of control pipe of both diameters, as applicable, were inserted into each cavity to provide a comparative reference for other pipe configurations within that cavity (pipes with fitting, water-filled, insulated pipe). Results in each figure are plotted with those from the control for that experiment. It should be noted at this point that these tests were intended to cover a wide range of pipe configurations to provide direction toward further research. As a result, tests have not been repeated and while trends are in all cases consistent with expectation, quantitative results serve as only preliminary estimates which should be refined through additional testing.

3.2.1 Vertical Pipes

As expected, given the thermal gradient in the fire compartment and wall, temperatures measured at the top of all vertically mounted pipes were significantly higher than at the bottom. The thermal gradient is clearly evident in the temperature-time curves for the control and water-filled pipe shown in *Fig. 26*. Also seen is the clear gradient that develops across each pipe, indicative of the rate of heat transfer from the exposed to the unexposed side. Temperatures in the water-filled pipe followed similar patterns to those measured on the control pipe section but remained lower throughout the test as a result of heat absorption by the water within the pipe. The maximum recorded water temperature was 88°C; however, the water level dropped by 0.008m and 0.011m in Test 1 and Test 2 respectively, suggesting that water at the very top of the pipe must have heated sufficiently to evaporate.

Not plotted here, peak temperatures at both collar and fitting locations on pipes installed with typical as-built fittings are lower than seen on control pipes of the same size at the same height. Fitting temperatures are lower and lag slightly behind the collar temperatures as well. Differences can be explained by a combination of the larger thermal mass and differences in thermal conductivity of the fitting and pipe materials. There may also be less overall heating of the fittings since the collars stick out past the top of the fitting at the connection point.
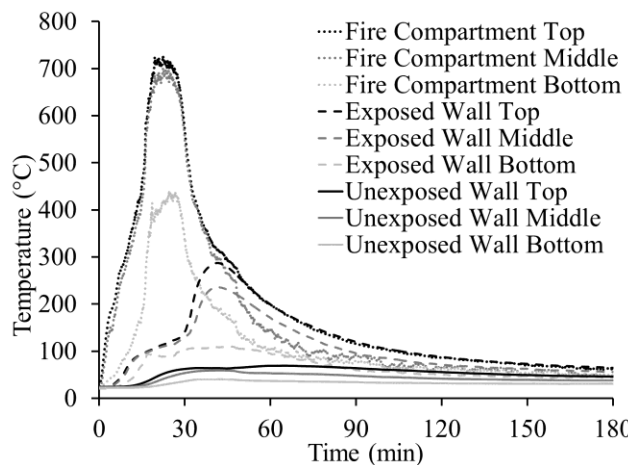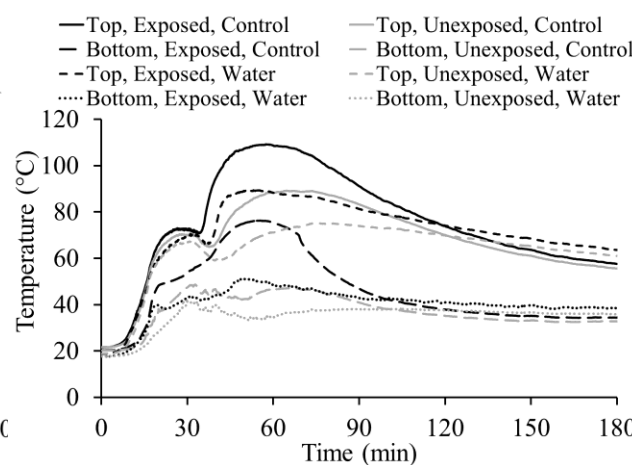

Fig. 25: Test 1 Wall Thermal Penetration

Fig. 26: Test 1 Water-Filled Pipe Results

As anticipated, measured temperatures for all pipe configurations with higher overall thermal mass than control sections, including pipes with fittings, insulation wrapped pipes, and water-filled pipes (see *Fig. 26*), changed more slowly than those for the control pipes and reached lower peak temperatures. Conversely, these pipes retained heat for longer than the control pipes as well.

3.2.2 Horizontal Pipes

The significant temperature difference between the horizontal pipes installed at the top and bottom of the wall is illustrated in *Fig. 27*. The heating of the top pipes resulted in deflections that were larger than those observed for the bottom pipes as demonstrated in *Fig. 28*. Due to their thinner walls and lower rigidity at room temperature, the 0.013m pipes deflected more than the 0.051m pipes.

On average, temperatures measured during thermal exposure of the horizontal pipes are 26°C warmer than those at equivalent positions on the vertical pipes. This may be due to the large length of pipe exposed to a relatively constant temperature in a horizontal piping run, in contrast to only a very small exposure area on the surface of each pipe in the vertical test configuration.

Although preliminary, it is clear from the above results that overall response times and specific temperatures reached varied significantly depending on details of the piping configuration under test, suggesting that more tests are required to better understand the thermal response of different pipe configurations across a range of heating scenarios.
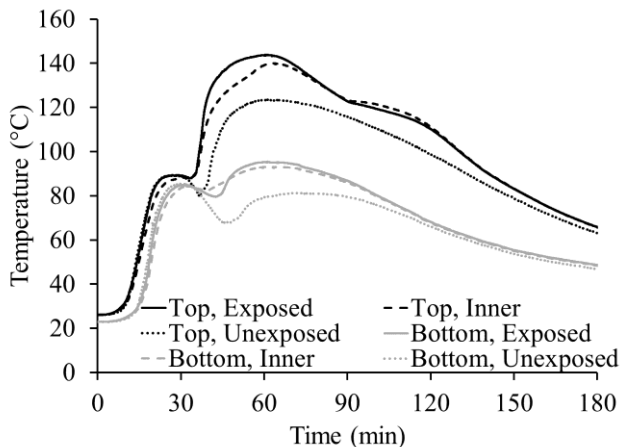
Fig. 27: Test 3 Horizontal Pipe Results
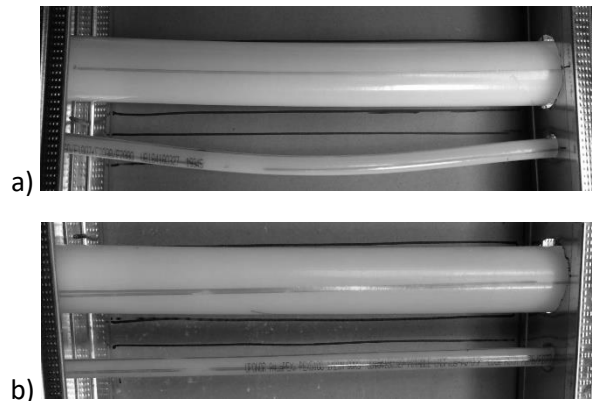
Fig. 28: Test 3 Horizontal Pipe Deflections at the a) Top and b) Bottom of the Wall [2]

4   CONCLUSIONS

Several conclusions can be drawn from this study:

–   *There is a clear temperature gradient from the exposed to the unexposed side of the wall cavities which results in significantly higher pipe temperatures at the top of the pipes than at the bottom for both vertical and horizontal piping configurations. This, in turn, leads to larger horizontal pipe deflections at the top of the wall compared to the bottom of the wall.*

- *The thermal response of vertical pipes with fittings, insulation wrapped pipes and water-filled pipes was slower than for the control pipe resulting in lower peak temperatures and longer heat retention for these configurations.*
- *Measured temperatures of water in the pipe did not reach the boiling point but small amounts of water did evaporate.*
- *No pipes melted without direct flame impingement.*
- *A minimum of four hours was required to fully capture the thermal response of the wall system.*
- *The small number of tests allows preliminary conclusions to be drawn but further tests are required to improve understanding of the thermal response of in-wall PEX-a pipes to this or other real fire exposures.*

ACKNOWLEDGMENT

REFERENCES

[1]   DiDomizio M. (2017). *Experimental Study of Thermal Degradation of Fire Resisting Compartment Partitions in Fires*. University of Waterloo [PhD].

[2]   Ellingham J., Forrest B., Weckman E. J., Pollett H. (2018). *A New Method for Testing In-Wall Systems Exposed to Real Fire Environments*. ASTM Workshop on Advancements in Evaluating the Fire Resistance of Structures, Washington, United States, 6-7 December 2018.

[3]   National Research Council Canada. (2010). *National Building Code of Canada, Canadian Commission on Building and Fire Codes*. Ottawa, Canada.

[4]   ASTM International. (2013). *ASTM E84: Standard Test Method for Surface Burning Characteristics of Building Materials*. West Conshohocken, United States.

[5]   Underwriters Laboratories of Canada. (2010). *CAN/ULC S102: Standard Method of Test for Surface Burning Characteristics of Building Materials and Assemblies*. Toronto, Canada.

[6]   Underwriters Laboratories. (2018). *UL 723: Standard for Test for Surface Burning Characteristics of Building Materials*. Northbrook, United States.

[7]   ASTM International. (2014). *ASTM E119: Standard Test Method for Fire Tests of Building Construction and Materials*. West Conshohocken, United States.

[8]   Underwriters Laboratories of Canada. (2014). *CAN/ULC S101: Standard Methods of Fire Endurance Tests of Building Construction and Materials*. Toronto, Canada.

[9]   Underwriters Laboratories. (2018). *UL 263: Standard for Fire Tests of Building Construction and Materials*. Northbrook, United States.

[10]   Bisby L., Gales J., and Maluk C. (2013). *A contemporary review of large-scale non-standard structural fire testing*. Fire Science Reviews 2(1). doi: 10.1186/2193-0414-2-1

[11]   Frangi A., Schleifer V., Hugi E. (2012). *A New Fire Resistant Light Mineral Wool*. Fire Technology 48, pp. 733–752.

[12]   Rahmanian I. (2011). *Thermal and Mechanical Properties of Gypsum Boards and Their Influences on Fire Resistance of Gypsum Board Based Systems*. University of Manchester [PhD].

[13]   Takeda H. (2003). *A model to predict fire resistance of non-load bearing wood-stud walls*. Fire and Materials 27(1), http://doi.wiley.com/10.1002/fam.816, pp. 19–39.

[14]   Takeda H., Mehaffey J. R. (1998). *WALL2D: A model for predicting heat transfer through wood-stud walls exposed to fire*. Fire and Materials 22(4), pp. 133–140.

[15]   DiDomizio M., Daun K., Weckman E. J. (2017). *Characterization of the heat exposure on a compartment wall in a large-scale fire*. 9th International Conference on Inverse Problems in Engineering, Waterloo, Canada.

[16]   DiDomizio M., Weckman E. J., Roos R. (2017). *Decomposition of Large-Scale Multicomponent Construction Assemblies Exposed to Real Fires*. 15th International Fire and Materials Conference, San Francisco, United States.

[17]   DiDomizio M., Weckman E. J., Roos R. (2015). *Experimental Evaluation of Damage and Thermal Penetration in Residential Walls under Realistic Fire Loads*. Combustion Institute – Canadian Section: Spring Technical Meeting (CICS 2015), Saskatoon, Canada, pp. 24–29.

[18]   Obach M. (2011). *Effects of Initial Fire Attack Suppression Tactics on the Firefighter and Compartment Environment*. University of Waterloo [MASc].

DRAINAGE CHARACTERISTICS OF COMPRESSED AIR FOAM SUBJECTED TO THERMAL RADIATION

Oluwadamilola OKUNROUNMU[1], Paul LHOTSKY[2] and George HADJISOPHOCLEOUS[1]
[1]Department of Civil and Environmental Engineering, Carleton University, Canada
[2]CIVELEC Consultants, Canada

ABSTRACT

This paper investigates the drainage characteristics of aqueous foams at ambient temperature and when exposed to thermal radiation. The response of foam to heat, mass loss of foam and time to half mass loss of foams at different expansion ratios and imposed thermal radiation were studied. Aqueous foam was subjected to constant heat fluxes in the range of 0-60 kW/m^2. The foams were generated from a compressed air foam system.

The results showed that all the foams exhibited similar drainage patterns, in terms of foam mass loss and temperature profile, but at different drainage rates. At ambient temperature, foams with lower expansion ratios drained faster than foams with higher expansion ratios because of their higher solution content. On the contrary, when foams were subjected to thermal radiation, the results showed that a higher drainage rate was observed in foams with high expansion ratios exposed to the same or higher irradiance levels than foams with low expansion ratios.

KEYWORDS: drainage rate; expansion ratio; foam mass loss; thermal radiation.

1   INTRODUCTION

Fire-fighting foams are effective fire suppression agents used to prevent, control or completely extinguish fires. Fire suppression is attained when fuel vaporization is reduced such that a flammable mixture cannot be formed, or the fuel oxidation rate is decreased below a rate to generate enough heat to sustain a flammable mixture. This is achieved by cooling the burning fuel, eliminating oxygen from the flammable vapors and separating the flames from the fuel surface.

Fire-fighting foams are generated either by air-aspirated nozzles or compressed air foam systems (CAFs). The air-aspirated system creates foam at the nozzle through agitated mixing of air and a foam solution at the point of application, whereas foam is generated inside the hose for compressed air foam system. Research had shown that CAF systems could generate foams with superior fire extinguishing performance than air-aspirated system because the CAF foams have a better stability and rheology [1]. Furthermore, CAF systems are used for the protection of buildings from being ignited by radiation emitted from a fire in an adjacent building or exterior flames due to their radiation-absorption characteristics. The aqueous foams are also applicable to wild fires as the foams can adhere to sloped, vertical, horizontal and slippery surfaces. In addition, CAF systems can be used to protect equipment of various sizes as the foam expansion ratio could be regulated to combat specific fire types and sizes.

Many studies had been conducted to investigate the drainage characteristics of fire-fighting foams at ambient temperature and when exposed to thermal radiation. The foam mass losses and thermal absorption properties of fire-fighting foams were studied by several researchers and reported in different papers [2-6]. Persson [2] investigated the resistance of air-aspirated foams to thermal radiation and ignition inhibition of fuel when covered with a foam layer. The technique

used for the tests could only measure foam mass losses with only foam in the pan. Foams with expansion ratios of 6.5 - 11.5 were subjected to heat fluxes up to 35 kW/m^2. Isaksson and Persson [3] modified the experimental set-up to investigate the ignition time of fuel placed underneath the foam and foam mass losses when subjected to heat fluxes up to 43 kW/m^2.

Magrabi et al. [4] investigated the drainage characteristics of compressed air foam in terms of drainage rate, evaporation rate and foam collapse when exposed to heat fluxes between 0-40 kW/m^2. Foams with expansion ratio of 5-30 were used for the tests. The effect of aging on the thermal absorption properties of foam in relation to the expansion ratio was later investigated by the same authors in another study [5]. The experimental set-up was similar to the study by Persson [2] so they could only measure foam collapse with only foam in the test pan.

Lattimer [6] investigated the drainage characteristics of aqueous foam at low expansion ratios in the ranges of 3 -10 when subjected to radiant heating in the ranges of 0-50 kW/m^2. It was reported that foams with lower expansion ratios drained faster than the foams with higher expansion ratios. Foam mass losses at high irradiance level was by foam evaporation and solution drainage while foam disintegration at ambient temperature was only by solution drainage. As the irradiance level increased, the duration for complete foam disintegration decreased.

The aim of this study is to investigate the drainage characteristics of compressed air foams at ambient temperature and elevated temperatures. The response of foam to heat, mass loss of foam and foam mass loss rate at different expansion ratios and imposed thermal radiation were studied. The compressed air foam was subjected to constant heat fluxes of 20 kW/m^2, 40 kW/m^2 and 60 kW/m^2 respectively. The paper concludes with a summary of major findings from the study.

2   EXPERIMENTAL SET-UP

A small-scale test apparatus was developed to perform tests that expose compressed air foam to a constant thermal radiation and to collect relevant data as shown in *Fig 1.0*. The apparatus comprised of a test pan, a drain collection container, thermocouples, a heat flux gauge, a radiant heater, measuring scale and a data acquisition system. A cone calorimeter was used to generate a constant heat flux of thermal radiation on a 60 mm thick aqueous foam layer. The foam sample was placed at 25 mm below the radiator cone. The test pan was made of stainless steel with dimensions of 100 mm x 100 mm x 60 mm. The bottom of the pan had an opening of 5 mm in diameter, connected to a tube for drainage collection.
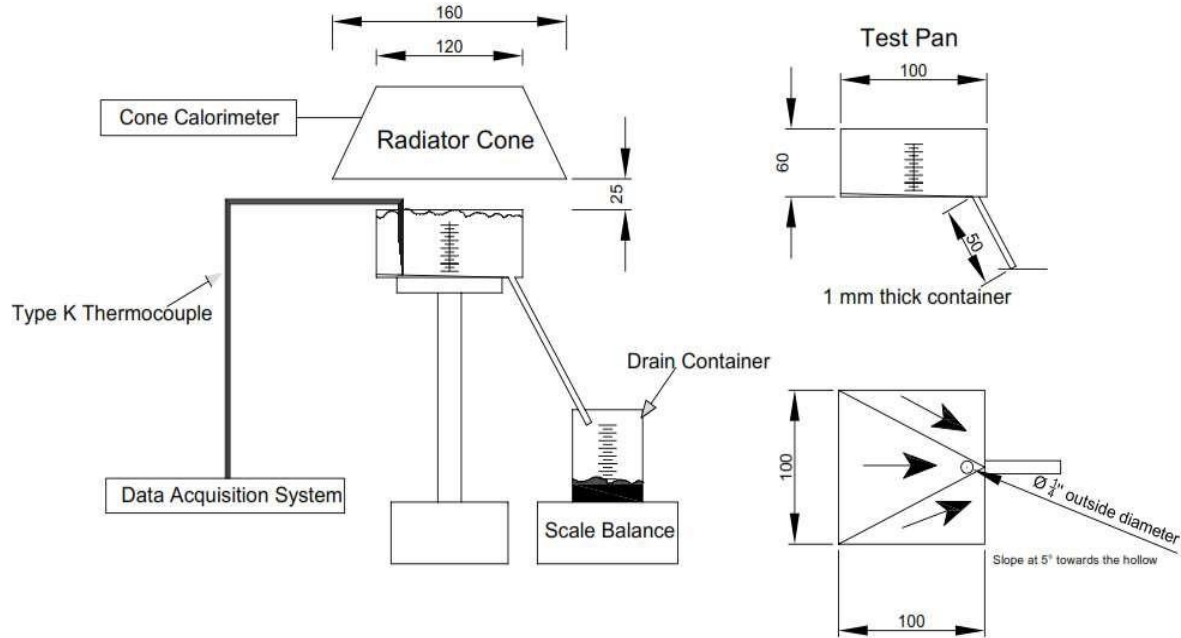
Fig 1.0 - Drainage Test Set Up

3 RESULTS AND DISCUSSION

3.1 General behaviour of foam when exposed to heat

Fire-fighting foam undergoes several stages of disintegration when exposed to heat. The first stage involves thermal expansion of air bubbles at the upper foam layer. As the heat penetrates further, the foam begins to collapse due to evaporation of the foam from the exposed surface and loss of liquid through the discharge outlet. During this period, the drainage rate increases, and the underlying foam layers are exposed to intense heat leading to their thermal expansion. The subsequent foam layers begin to collapse as more foam solution drains off and evaporates. As the test progresses, the loss of liquid is reduced, and foam mass loss is dominated by evaporation.

3.2 Response of foam to heat

The response of the foam when subjected to constant radiant heating was studied by placing Type K thermocouples at a height of 0 mm (TC 1), 10 mm (TC 2), 20 mm (TC 3) and 30 mm (TC 4) respectively from the bottom of the test pan to obtain temperature readings during the test. The thermocouples were connected to a National Instrument multiplexer and interfaced with a data acquisition system, Labview, to record data at every second interval. Foams with expansion ratio ranging from 9.7 to 15.8 were subjected to thermal radiation of 20 kW/m^2, 40 kW/m^2 and 60 kW/m^2. The results are presented in this section. Note that the foam expansion ratio is represented by the letter "E".

    i.   Effect of 20 kW/m^2 heat flux on the foam with an expansion ratio of 10.5

Fig 2 shows the temperature profiles of the foam with E = 10.5 at an irradiated constant heat flux of 20 kW/m^2. Thermal expansion of the upper 30 mm thick foam layer was observed during the first 150 s of the test leading to increase in the temperatures of the underlying foam layers.

The foam height was reduced to 20 mm at 212 s due to intensive foam evaporation and solution drainage. It took 108 s before the next 10 mm of foam depleted due to decreasing incident heat flux as a result of increased distance between the cone heater and surface of the remaining foam layers . During this period, the mass loss rate of the foam decreased from an average of 0.02 kg/s.m^2 to 0.005 kg/s.m^2. At this stage, most of the solution drainage had ceased as the mass loss of the foam was dominated by evaporation. The drainage rate remained steady until the foam layers had completely depleted. The test was truncated at 8 min 20 s after complete disintegration of the foam.
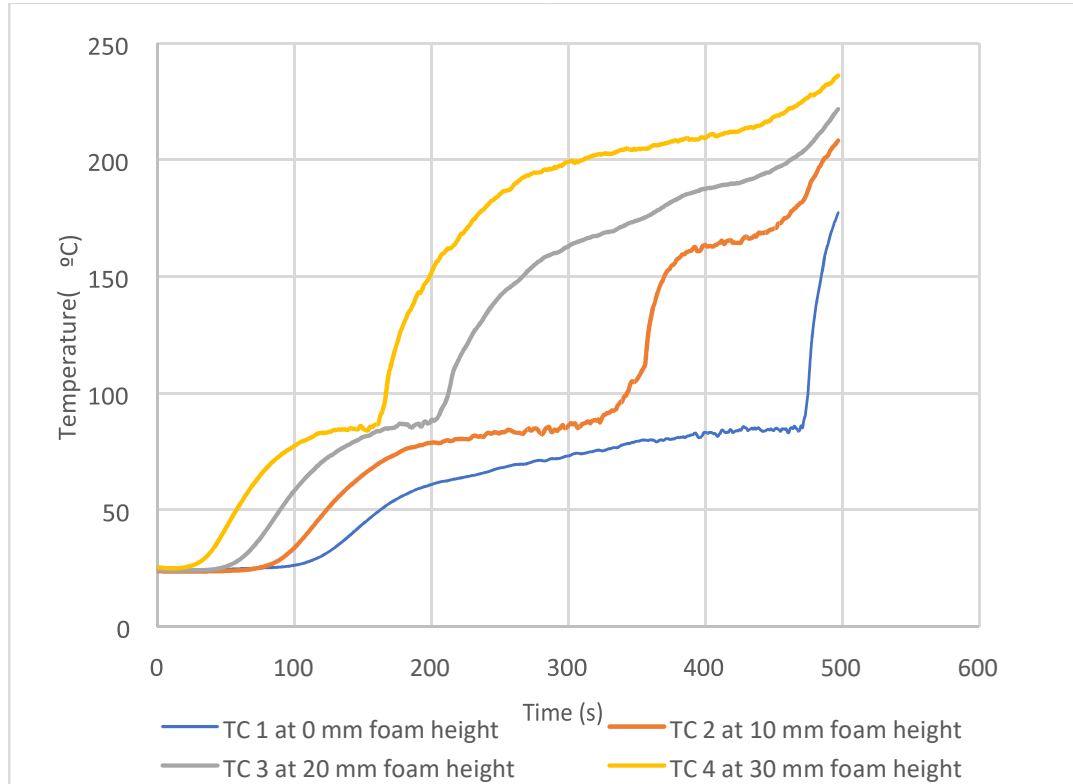

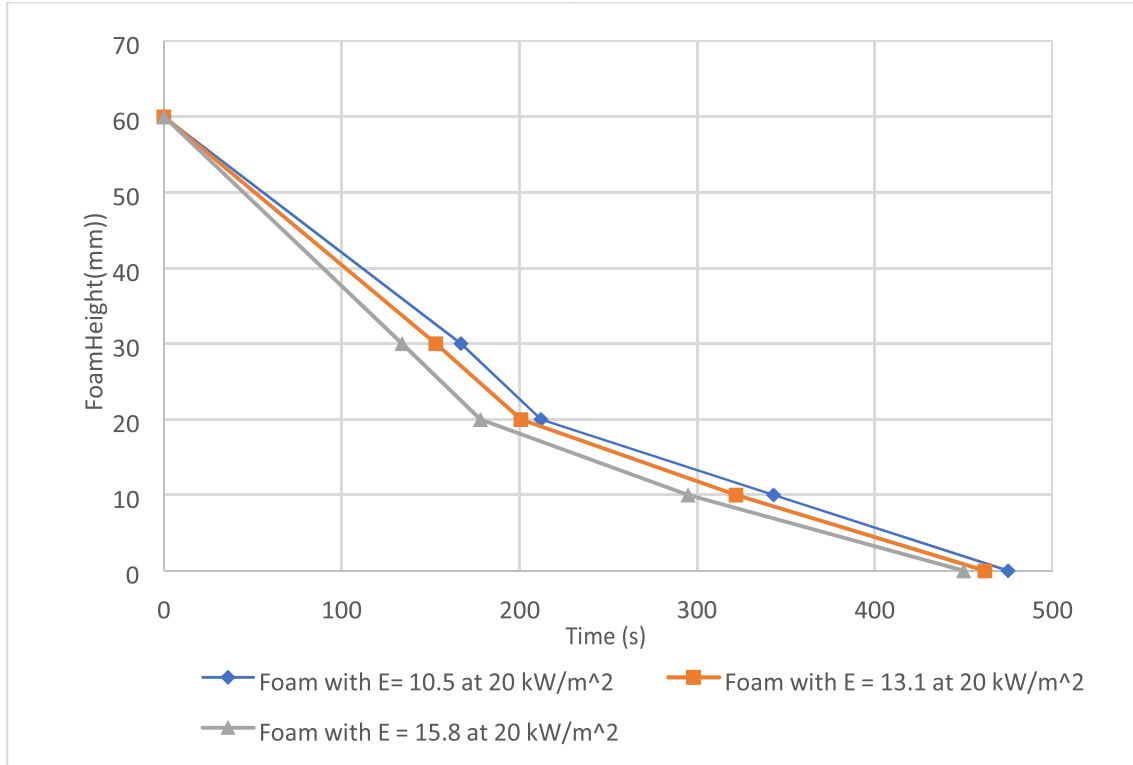*Fig 2* - Temperature profile of foam with E = 10.5 at an irradiated heat flux of 20 kW/m^2

Fig 3.0 - Foam height with time for foams at an irradiated heat flux of 20 kW/m^2

Foams with higher expansion ratios (E= 13.1 and E = 15.8) exhibited similar trend of temperature profiles like the foam with E= 10.5 but they had higher drainage rates resulting in shorter test duration for foams with higher expansion ratio when subjected to the same heat flux as shown in Figure 3. The mass loss rate of foams increased with increasing irradiance level. The average mass loss rates of foams when exposed to 20 kW/m^2, 40 kW/m^2 and 60 kW/m^2 were 0.02 kg/s.m^2, 0.035 kg/s.m^2 and 0.05 kg/s.m^2 respectively.

3.3 Foam mass loss at ambient temperature

Free drainage test of foams was conducted to investigate the mass loss of foams at ambient temperature. Since no heat was imposed during the test, mass loss of foam was by drainage of the foam solution from the foam bed. Three tests were conducted using foams with E = 8, 9 and 11 as shown in *Fig 4*. The test results on free drainage of foams showed higher drainage rate in foams with low expansion ratio due to higher solution content in them.

Overall, all the tested foams exhibited similar drainage patterns, in terms of foam mass loss, but at different drainage rates. As the foam expansion ratio increased, the time required for the foam to lose half its mass and the percentage of dry foam increased.
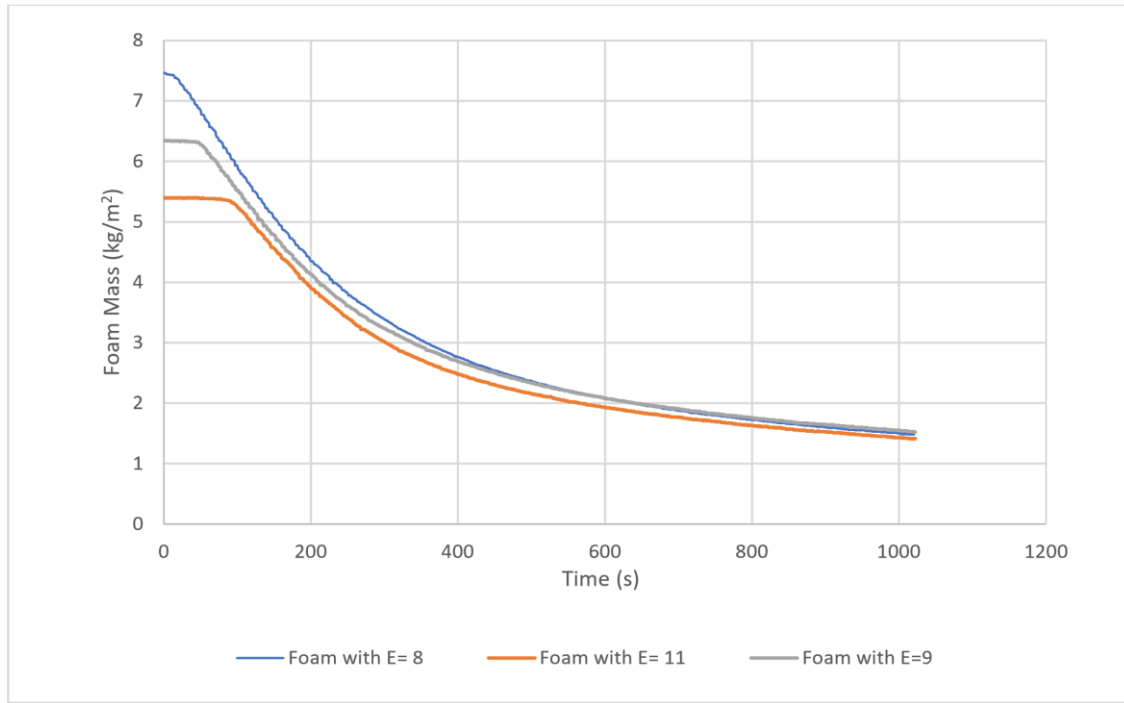
Fig 4 - Free drainage of foams with E = 8, 9 and 11 at ambient temperature
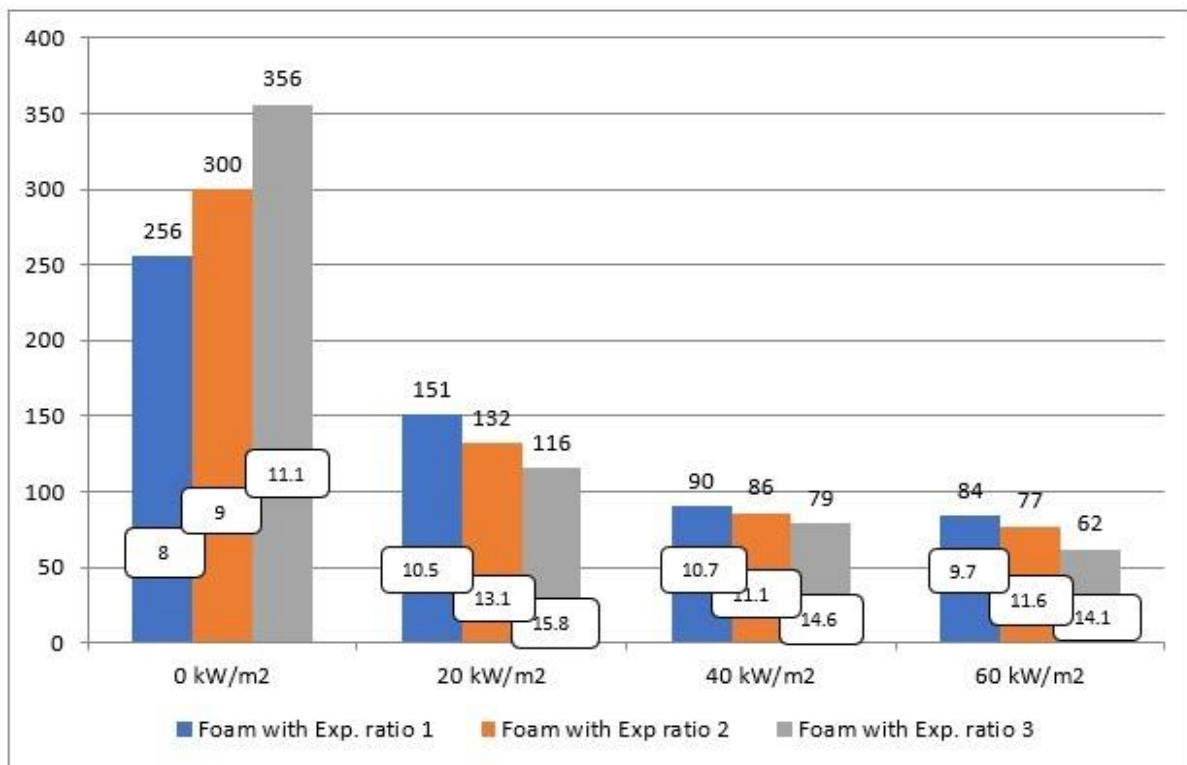
3.4 Time to half mass loss of foams

Fig 5 - Time to half mass loss of foams in seconds at different heat fluxes.

Fig 5 shows the time to half mass loss of foams in seconds at ambient temperature and imposed heat fluxes. The values in the boxes represent the values of the expansion ratios. At ambient temperature, the time for foams to reduce to half their initial masses increased as the foam expansion ratios increases. The results show that free drainage took place at a faster rate in foams with low expansion ratios than foams with higher expansion ratio.

On the other hand, the time to half mass loss of foams when subjected to radiant heating decreased as the foam expansion ratio increases. Generally, the time to half mass loss of foams decreased at higher irradiance level, resulting in faster drainage rate.

4   CONCLUSIONS

This study investigated the drainage characteristics of aqueous foams at ambient temperature and when exposed to thermal radiation by considering the response of foam to heat, mass loss of foam and time to half mass loss of foams with different expansion ratios.

The results showed that all the foams exhibited similar drainage pattern, in terms of foam mass loss and temperature profile, but at different drainage rates.

At ambient temperature, foams with lower expansion ratios drained faster than foams with higher expansion ratios because of their higher solution content. On the contrary, high drainage rate was observed in foams with higher expansion ratios at the same or higher irradiance level.

REFERENCES

[1]   Kim, A. K., & Crampton, G. P. (2009). Evaluation of the Fire Suppression Effectiveness of Manually Applied Compressed-Air-Foam (CAF) System. Fire Technology,48(3), 549-564. doi:10.1007/s10694- 009-0119-3.

[2]   Persson H. (1992) Fire extinguishing foams-resistance against heat radiation. SP Report 1992:54, Swedish National Testing and Research Institute, Boras, Sweden.

[3]   Isaksson S & Persson H. (1997) Fire extinguishing foam—Test method or heat exposure characterisation. SP Report 1997:09, Swedish National Testing and Research Institute, Boras, Sweden.

[4]   Magrabi S.A., Dlugogorski B.Z., & Jameson G.J. (1997). Attenuation of thermal radiation by aqueous foam. Proceedings of the 24th Australia and New Zealand Chemical Engineering Conference, Rororua, New Zealand, September 29–October 1, SF2a:319.

[5]   Magrabi, S. A., Dlugogorski, B. Z., & Jameson, G. J. (2008). The Performance of Aged Aqueous Foams for Mitigation of Thermal Radiation. Developments in Chemical Engineering and Mineral Processing,8(1-2), 93-112. doi:10.1002/apj.5500080107.

[6]   Lattimer B.Y., Hanauska C.P., Scheffey J.L. & Williams F.W. (2003). The use of small-scale test data to characterize some aspects of firefighting foam for suppression modeling. Fire Safety Journal 38; 2003; p. 117-146.

CANNABIS FACILITIES – LOOKING BEYOND THE HAZE

Dominic Esposito and Ivan Bolliger
JENSEN HUGHES, Ottawa, Canada

ABSTRACT

Cannabis, pot, weed, marijuana? The legalization of cannabis occurred in Canada on October 17, 2018. This was a grand undertaking by the government which has the potential to cause logistical and societal challenges. From a building perspective, new cannabis storage, processing and retail facilities are expected but do the current prescriptive requirements of the building code adequately address the fire and life safety risks in these buildings? Also, it is not evident how to treat these facilities based on the requirements of the building code and fire code. This paper will provide a summary of the hazards in cannabis facilities relative to the requirements of the National Building Code of Canada (NBC) and National Fire Code of Canada (NFC) and discuss if there should be additional considerations for these facilities from a fire and life safety perspective. Designers and building officials will have to navigate perceived challenges with these facilities including but not limited to classification of these facilities, fire loading, explosive atmospheres, security measures, interior finish requirements, all of which may have an impact on fire and life safety. These facilities could be considered farm buildings or industrial buildings with different hazards and a better understanding of these facilities will provide designers and building officials a more transparent path when designing/evaluating these facilities so that there is not an undue fire and life safety risk.

1 INTRODUCTION

On October 17, 2018, the legalization of cannabis occurred in Canada. This was grand undertaking by the government which has the potential to cause logistical and societal challenges. From a building perspective, new cannabis storage, processing and retail facilities are expected, and this paper explores if the prescriptive requirements of the building code and fire code adequately address the fire and life safety risks in these buildings.

Designers and building officials will have to navigate perceived challenges with these facilities including but not limited to classification of these facilities, fire loading, explosive atmospheres, security measures, interior finish requirements, all of which may have an impact on fire and life safety.

This paper explores the requirements of the National Building Code of Canada (NBC) [1] and National Fire Code of Canada (NFC) [2]. The NBC and NFC are model codes that are maintained and updated by the Canadian Commission on Building and Fire Codes (CCBFC) with the support of the National Research Council Canada (NRC). As model codes, they are not applicable unless adopted by policy or legislation. However, the provinces and territories look to the NBC/NFC when updating their Codes, which in several jurisdictions, are largely based, if not entirely based on the NBC and NFC.

2   BACKGROUND

Cannabis, pot, weed, marijuana? There are several names used which may be due to the fact that cannabis has been illegal for many years and there was an underground industry that made use of coded language to communicate regarding cannabis activities [3], [4].

The term cannabis is now common place in Canada but what exactly is cannabis? There is much discussion on the taxonomical treatment and the specie(s) belonging to the genus Cannabis and are represented by many varieties with unstable taxonomic foundations [5].

Cannabis is derived from the cannabis plant (e.g., Cannabis sativa, Cannabis indica). Cannabis can be grown in a variety of climates, but it is increasing being cultivated indoors using hydroponic technology as growing cannabis indoors leads to predictable growing results.

The main active ingredients in cannabis is delta-9 tetrahydro-cannabinol, commonly known as THC [3] and Cannabidiol (CBD) is another. The different cannabinoids in the Cannabis sativa plant are still being researched [6]. The THC ingredient gives a person psychoactive effects (i.e., mind altering effects) called a "high." Different cannabis products will have different levels of THC potency. Unlike THC, CBD does not produce a high or intoxication. CBD is also being studied for its possible therapeutic uses [7].

Some examples of forms of cannabis include the following:

- Marijuana: Made of dried flowers and leaves of the cannabis plant that is typically smoked or made into edible products like cookies or brownies.
- Hashish: Made from the resin of the cannabis plant and can be smoked or added to food.
- Hash oil: Thick oil obtained from hashish that can be smoked and is the most potent cannabis product [6].

There are different types of facilities that are related to cannabis facilities that can have an impact on building and fire codes which include the following:

- Retail facilities: These types of facilities would be where the final product is sold to consumers and are similar to typical retail facilities were people buy goods or services.
- Growing facilities: These types of facilities are where the cannabis is grown. An outdoor facility would not be subject to building code requirements and the subject of this paper is related to indoor facilities.
- Processing facilities: These types of facilities are where the cannabis is transformed to the final product that can be consumed.
- Storage facilities: Facilities were the final product is stored for distribution.

A building could potentially include growing facilities, processing facilities, and storage facilities under the same roof.

3   APPLICATION OF THE NBC AND NFC

With the legalization of cannabis, there have been concerns with respect to buildings where there is the growing and processing of cannabis relative to the application of building codes and fire codes.

Cannabis facilities come in different forms and the occupancy of these facilities could vary. Cannabis processing has different hazards than cannabis storage or growing.

The codes are written to address a wide variety of buildings and contain a minimum set of requirements to provide a level of fire and life safety that is acceptable to Canadian society. There may be other features to consider for these facilities as good practice which would be above the minimum requirements of the codes.

4   SUMMARY OF HAZARDS

There has been concerns over the location of cannabis retail stores and their location in the community (e.g., near schools). However, the location of these stores is not a building code issue, rather, a zoning issue which would not be considered in the development of the NBC.

There are hazards in cannabis facilities which have been identified in jurisdictions such as Colorado or where there were illegal operations [8]. Also, NFPA 1, 2018 edition includes a new Chapter, Chapter 38 "Marijuana Growing, Processing or Extraction Facilities" [9] and outlines concerns which are addressed by provisions in the Chapter. There are non-fire safety related issues such as the potential for mould, potential for poor indoor air quality, etc., however, this paper is limited to fire and life safety only.

Some hazards include the following:

- With respect to the production process, the process could involve liquid butane or propane as a solved to extract the THC. This could be an explosion hazard.
- Ignition sources such as hot lights hanging close to plastic room dividers and overloaded electrical services are common.
- Special equipment is used to extract the THC and CBD and there are inherent hazards with equipment that is not specifically designed for extraction but is used for this purpose. If there is a leak in the equipment there is the potential for the release of flammable gases.
- There could be increased hazards from unique and uncertified/tested experimental techniques and processes.
- There are security issues with these facilities and as result, egress for the occupants is to be considered as well as Fire Department access.
- Fumigants may be toxic or flammable. If an ignition source is present during fumigation, this could result in a fire or explosion. Additionally, it may not be safe to enter the facility until fumigants have been ventilated from the facility.
- Some extraction process involve carbon dioxide (CO_2). CO_2 exposure can cause different symptoms that range from headaches to extreme cases of unconsciousness and death if the concentration of CO_2 is high.
- Due to the conditions in these facilities, interior finishes that are moisture resist are desired but may have a higher flame-spread rating than other conventional materials.

The NBC/NFC, electrical code, and occupational health and safety regulations, to a certain extent, have requirements relating to reducing the impact of the hazards (risk) within buildings. As indicated previously, the NBC/NFC contain minimum requirements only and as with any facility, a heightened level of fire and life safety should be explored.

5   CONSIDERATION AS A FARM BUILDING

If a building is permitted to be considered a farm building, the Code offers relaxations over other conventional buildings. Similar to the NBC/NFC, the National Farm Building Code of Canada

(NFBC) 1995 [10] is a model code that is not applicable unless adopted via legislation or policy. As per NBC Sentence 1.1.1.1.(3) of Division B, farm buildings are to conform to the requirements of the NFBC.

It is acknowledged that the NFBC is an older document that requires updating and is not consistently used in jurisdictions across Canada. The farming industry has evolved since the last update to the NFBC and farming operations have become more complex and the provisions of the NFBC no longer reflect modern farming operations [11]. The provisions of the NBFC are currently being updated with the goal to publish changes and introduce a Section for farm buildings in the NBC 2020. Based on the discussions of technical committees, the requirements for farm buildings will be enhanced but the fundamental rationale of having relaxations to the conventional requirements for farm buildings will remain which is based on the preface to the NFBC:

> "The rationale of having special requirements for farm buildings, as distinct from other buildings, is based on the low human occupancy load, the remote location of typical farm structures or the special nature of the occupancies involved."

If growing is being undertaken only in a facility, it would be considered no different than growing any other crop but processing involves different elements/hazards.

New definitions have been proposed for the NBC 2020 that include the definition of agricultural occupancy. If a building in which cannabis is grown meets the definition of agricultural occupancy then the building could be considered an agricultural building (i.e., a farm building). A farm building would be required to be located on land used for the purposes of farming such that a cannabis facility that is not on farm land would not be considered a farm building. The determination on whether the building is permitted to be on farm land is considered a zoning issue that is not addressed by the NBC.

With any farm buildings, there are some storage areas and some processing may occur. Processing is specifically referenced to in the new definition. However, if the processing adds value to the product, then the building would no longer be considered a farm building. A proposed change to the NBC 2020 has been suggested to clarify the amount of processing permitted in a farm building via the introduction of an explanatory Note to the Code.

"The term "processing" refers to activities carried out for the purpose of maintaining the quality of agricultural products or making them saleable with a minimum amount of processing [12]."

For example, if carrots are being stored in the building, then the building is a farm building but if the carrots are being canned in the building (i.e., adding value) then the building would not be considered a farm building, rather it would be considered an industrial building. Another condition for the use of the relaxation of requirements for farm buildings is the occupant load. If the occupant load is greater than 1 person per 40 m², the building would not be considered a farm building to which the relaxations for farm buildings would apply.

As such, a cannabis facility where there is growing only could potentially be considered a farm building which would be subject to less onerous requirements than an industrial building. The fire and life safety requirements for farm buildings are minimal and related to the safety of persons only.

6   CONSIDERATION AS AN INDUSTRIAL BUILDING

If the facility is not considered a farm building with low human occupancy, then by application of the NBC, the facility is required to be classified as per one of the major occupancies prescribed by the Code. A facility where cannabis is sold (e.g., a store), is considered to contain a Group E major occupancy (mercantile occupancy). The classification of retail cannabis spaces is unlikely to cause controversy, however, for a facility where cannabis is grown and/or processed, it is not obvious which major occupancy classification applies.

The NBC has specific definitions for occupancy and a cannabis growing or processing facility is considered to contain an industrial major occupancy as per Sentence 1.4.1.2.(1) of Division A:

- *Industrial occupancy means the occupancy or use of a building or part thereof for the assembling, fabricating, manufacturing, processing, repairing or storing of goods and materials.*

For industrial occupancies, there are three different types that are defined in Sentence 1.4.1.2.(1) of Division A:

- *High-hazard industrial occupancy (Group F, Division 1) means an industrial occupancy containing sufficient quantities of highly combustible and flammable or explosive materials which, because of their inherent characteristics, constitute a special fire hazard.*
- *Medium-hazard industrial occupancy (Group F, Division 2) means an industrial occupancy in which the combustible content is more than 50 kg/m² or 1 200 MJ/m² of floor area and not classified as a high-hazard industrial occupancy.*
- *Low-hazard industrial occupancy (Group F, Division 3) means an industrial occupancy in which the combustible content is not more than 50 kg/m² or 1 200 MJ/m² of floor area.*

The concern regarding processing is that the processing of cannabis could involve the use of butane, propane, or other hazardous materials to extract the THC and CBD. The extraction materials could be an explosion hazard such that a processing facility may be considered to contain a high-hazard industrial occupancy. Consideration of the occupancy as subsidiary to the major occupancy (principal use) would require evaluation. With respect to a growing facility, the definitions of Group F, Division 2 and Group F, Division 3 occupancies refer to combustible content. Contents include elements which are not part of the building structure. Combustible contents would include furniture, storage, etc. but would not include elements such as interior finishes, combustible elements in wall construction, etc.

In order for contents to not be considered combustible contents, these contents would be required to be classified as noncombustible which is a defined term as per NBC Sentence 1.4.1.2.(1) of Division A.

- *Noncombustible means that a material meets the acceptance criteria of CAN/ULC-S114, "Test for Determination of Non-Combustibility in Building Materials."*

The test referenced has mass loss, flaming, and temperature rise criteria. Although live plants have a high amount of water content, plants would not pass the specified test and are considered combustible contents. Consideration of subtracting the water content from the fire load is not

readily addressed by the NBC, however, this approach may be considered by a designer but would be subject to approval by the Authority Having Jurisdiction (AHJ).

Cannabis requires a certain area to grow and produce the maximum yield for consumer consumption. It is not desired to provide as many plants as possible per area, rather, plant density is related to optimal growing conditions as the crowding of plants will adversely impact the maximum amount of light that the lower branches will receive.

The size and shapes of plants will also vary based on the variety and strain of the plant. Some variety/strains are short with small diameters while others are tall and broad. With indoor growing conditions there is more control over the shape and size of the plant compared to outdoor growing. Indoor growing conditions are managed to regulate the time it takes the plant to flower for maximum production. In addition, the height of the plant is also managed as the artificial lights used for growing can only penetrate a certain distance into the plant so that growing taller plants could yield negative production results.

A conservative approach could be taken to determine the fire load in kg/m^2 and MJ/m^2 and the following could be considered:

- Number of plants per m²: The number of plants per m² varies and plants are spaced to maximize their output which is typically in the range of 4-9 plants per m² [13]. A facility is expected to have several different rooms in a growing operation which would involve growing rooms, mother rooms, vegetation rooms, storage rooms, etc. The density of plants in mother rooms and vegetation rooms will be less than in growing rooms. Consideration should also be given to plants on racks (i.e., additional plants will be provided on racked tiered systems such that the number of plants per m^2 will be increased).
- Mass of a single plant: A plant contains roots, stems, branches, leaves, buds and seeds. The output per plant varies and is in the range of 500 g/m² (dry) and is considered to be the buds and some branches/stems. Cannabis will lose between 25% and 77% of its original weight when dried [14]. The waste material, which compromises the remainder of the plant is also to be estimated and although the majority of the mass of the plant consists of water, this can be conservatively counted as part of the fuel load.
- Heat of Combustion: The heat of combustion for cannabis is not readily available and although different, using the heat of combustion of tobacco could be considered which can be found in the SFPE Handbook of Fire Protection [15].

Based on the above, the fuel load of the plants can be estimated. There would be expected to be other incidental combustibles in support of the growing operations such as combustible components of equipment, cultivation tools, etc., and these combustibles are to be estimated but are not expected to significantly impact the fuel load when averaged across the entire floor area as permitted by the NBC.

The calculations for Group F, Division 2 and Group F, Division 3 occupancies would permit the corridors and other similar spaces to be included in calculation and these areas would be expected to have limited combustibles which would further reduce the combustible content calculated as per m² of the industrial occupancy.

Based on the above approach, a growing facility would be expected to contain a Group F, Division 3 occupancy. This would address occupancy classification, but, as indicated previously, the Code prescribes fuel load ranges based on kg/m^2 or MJ/m^2 but would permit the fuel load to be averaged throughout the floor area of the facility such that spaces that would not be expected to contain combustibles or where there will be limited combustibles (e.g., corridors) to be included which would reduce the average fuel load. Theoretically, in any industrial facility, there can be a concentrated fuel load in one location but when averaged out, it could be demonstrated that the facility contains a Group F, Division 3 occupancy rather than a Group F, Division 2 occupancy. Currently, there is no upper limit to the fire load in Group F, Division 2 occupancies.

A concentrated fuel load in one area of the building could result in a severe fire with a lesser duration than if combustibles were stored evenly across the entire floor area. Is there enough redundancy in the Code to address both these scenarios? These scenarios are not specific to industrial occupancies and are also found in other occupancies.

Calculation of the fuel load may be challenging to a designer and may require the engagement of a fire protection professional to determine the occupancy of the building, or a designer may make conservative assumptions that would lead to overdesign of a building.

The observations on concentrated fuel load and challenges to determine the fuel load is not specific to cannabis facilities and would require further study to assess.

7   GUIDANCE IN CANADIAN JURISDICTIONS

As legalization of cannabis occurred in Canada on October 17, 2018, there is a limited guidance that is available in Canadian jurisdictions.

The City of Edmonton Fire Rescue has published a cannabis guideline [16] to inform people of their obligations related to operating cannabis retail stores, cannabis cultivation facilities, and cannabis processing facilities within the City of Edmonton. For the most part, the guidelines refer to the conventional building code and fire code requirements with added commentary. For example, the City of Edmonton guidelines refer to Health Canada requirements for employee tracking in and out of grow rooms or product vaults. The tracking and access is typically done through swipe card stations. The guideline explains that this is permitted if there is free access from these rooms as required by the building/fire code.

There are also changes proposed to the Ontario Fire Code (OFC) [17], which is the fire code that is applicable in the province of Ontario and includes the following:

- Farm buildings that contain cannabis extraction facilities involving the use of hazardous material (e.g., flammable liquids or combustible liquids) would be subject to certain portions of the OFC.
- Extraction operations involving the use of hazardous material (e.g., flammable liquids or combustible liquids) would not be permitted below grade and in buildings containing a residential occupancy.
- Specific requirements for egress aisles and door hardware.

- Specific ventilation requirements if the process involves a flammable gas including requirements for interlocks and gas detection.

A draft standard has also been published (public review of the standard will be completed at the end of February 2018) and the content of the standard at the writing of this paper has not been finalized. The standard "CAN/ULC-S4400, Standard for Safety of Premises, Buildings and Equipment Utilized for the Cultivation, Processing and Production of Cannabis" [18] has been developed to set a baseline in ensuring the safety (including fire safety) and security of cannabis facilities. Ideally the standard will be eventually referenced by the model codes but that process is not automatic and may take significant time.

8   CONCLUSION

The design of cannabis facilities requires consideration of the use of the building (production, storage, processing, etc.) and an understanding associated with the different types of use.

A better understanding of these facilities will provide designers and building officials a more transparent path when designing/evaluating these facilities so that there is not an undue fire and life safety risk as well as ensuring that overly conservative designs are not enforced where there are no real additional hazards.

REFERENCES

[1]   Canadian Commission on Building and Fire Codes (2015). *National Building Code of Canada*. Ottawa: National Research Council of Canada.

[2]   Canadian Commission on Building and Fire Codes (2015). *National Fire Code of Canada*. Ottawa: National Research Council of Canada.

[3]   University of Washington (2013, June). *Learn About Marijuana – Science-based Information for the Public*. Retrieved from http://learnaboutmarijuanawa.org/

[4]   Wright, J. (2017, November 17). *Weed, cannabis, pot or marijuana: what's the difference?* Retrieved from https://www.cbc.ca/news/canada/new-brunswick/weed-pot-cannabis-marijuana-whats-the-difference-1.4405440

[5]   Pollio, A. (2016). The name of Cannabis: a short guide for nonbotanists, *Cannabis and Cannabinoid Research*, 1:1, 234–238, DOI: 10.1089/can.2016.0027.

[6]   Alcohol and Drug Foundation. (2018). *Drug Facts – Cannabis.* Retrieved from https://adf.org.au/drug-facts/cannabis/

[7]   Government of Canada. (2018, December 27). About Cannabis. Retrieved from https://www.canada.ca/en/health-canada/services/drugs-medication/cannabis/about.html

[8]   Roman, J. (2016). Welcome to the Jungle. *NFPA Journal*, September/October 2016. Retrieved from https://www.nfpa.org/News-and-Research/Publications/NFPA-Journal/2016/September-October-2016/Features/Growing-Pains

[9]   National Fire Protection Association. (2017). *NFPA 1 Fire Code (2018 ed.).* Quincy, MA: Author.

[10]   Canadian Commission on Building and Fire Codes (1995). *National Farm Building Code of Canada*. Ottawa: National Research Council of Canada.

[11]   Esposito, D. (2017). *Farm Buildings Consultation Document*. Ottawa: National Research Council of Canada.

[12]   Canadian Commission on Building and Fire Codes (2018). *Proposed Change 1015*. Ottawa: National Research Council of Canada.

[13] Caulkins, J., Cohen, M., & Zamarra, M. (Accessed 2019). *Estimating Adequate Licensed Square Footage for Production.* Retrieved from https://lcb.wa.gov/publications/Marijuana/BOTEC%20reports/5a_Cannabis_Yields-Final.pdf

[14] Warner, M. L., Alford, I., Lawrence, D. M., Kohl, A. C., Williams, S. J., & Yeatman, D.T. Comparative analysis of freshly harvested cannabis plant weight and dried cannabis plant weight, *Forensic Chemistry, Volume 3, 2017*, 52-57.

[15] Hurley, M.J. (2016). *SFPE Handbook of Fire Protection Engineering* (5th ed.). New York, NY: Springer.

[16] City of Edmonton Fire Rescue. (2018). *Edmonton Fire Rescue - Cannabis Guidelines.* Edmonton, AB: City of Edmonton Fire Rescue.

[17] Ministry of Community Safety and Correctional Services. (2018, October 22). *Public Consultation on Proposed Changes to the Fire Code Relating to Hazardous Extraction Operations in All Buildings and to Hazardous Cannabis Extraction Operations in Farm Buildings.* Retrieved from https://www.ontariocanada.com/registry/view.do?postingId=26746&language=en

[18] Underwriters Laboratories of Canada. (2018). *First public review draft proposed first edition CAN/ULC-S4400 Standard for safety of premises, buildings and equipment utilized for the cultivation, processing and of Cannabis.* Toronto, ON: Author.

FIRE SAFETY CHALLENGES IN CORRECTIONAL FACILITIES – TRANSFORMING REAL-WORLD CHALLENGES INTO RESEARCH-BACKED SOLUTIONS

Michael Kruszelnicki[1], Yoon Ko[2]
[1]Correction Service Canada, Canada;
[2]National Research Council, Canada

ABSTRACT

Fire safety poses a number of unique challenges within Correctional facilities. In the last 5 years, Correctional Service Canada (CSC) has worked with the National Research Council (NRC) to review and validate various assumptions and technologies within Correctional Facilities.

This paper intends to provide an appreciation for the challenges encountered and how these challenges were addressed in an operational correctional setting. Full details of each research effort are not provided in this paper but rather those results that affect the correctional environment and the policies that resulted therefrom.

1 INTRODUCTION

Correctional Facilities face a number of unique challenges when it comes to fire safety. Some of these challenges include non-cooperative populations, populations having limited control over their movement, a population with behavioural challenges, security concerns, as well as competing values (i.e. security and incarceration versus rehabilitation and responsibility).

Over the last six years, the author has worked within the Correctional system in an effort to ensure the fire safety of institutions, correctional staff, offenders and visitors.

Over this period, a number of specific fire safety challenges were encountered in which a partnership was formed with the National Research Council (NRC) to review and validate various assumptions and technologies for Correctional Facilities.

Four such efforts stand out as being of potential interest to the wider community:

1. Kitchen hood suppression using water in residential-style correctional facilities. A mock-kitchen was constructed and a series of grease fires were ignited in an attempt to validate an existing fire suppression practice in residential-style correctional facilities.
2. In a response to concerns raised by Correctional Officers, CSC and NRC studied the effects of smoke of specific concentration and content typical to that which could be expected as a result of a cell-fire. This allowed CSC to establish guidelines and limitations for front-line responders in the event of a cell-fire in a correctional facility.
3. Smudging (a first nations practice) is permitted within CSC facilities as a human right. CSC and NRC studied various materials subject to smouldering to determine whether or not it was possible for a sophisticated smoke detection system to differentiate between smudging products and other sources.

609

4. Trying to minimize suspension points (suicide prevention) is a reality facing CSC. Included in that is an effort to minimize suspension points caused by fire and life safety devices. In October 2018, CSC and NRC set out to validate whether it is possible to provide an Aspirating Smoke Detection system (ASD) in such a way that its presence would not be detected and which would not create a suspension hazard. A secondary goal was also to have this device minimize nuisances and tamper alarms.

The intent of this paper is not to go into great scientific detail on these challenges but rather to go over the challenges that each of these posed in an operational correctional environment. Accordingly, this paper discusses the methodology and considerations that were taken into account in order to provide an appreciation for how these challenges were responded to in an operational correctional environment operating on a 24-7 basis.

2 KITCHEN HOOD SUPPRESSION

2.1 Background

In 2006, CSC made a decision, in consultation with the AHJ at the time, to provide additional fire protection to *residential ranges* in order to provide an increased level of fire safety and property protection.

The decision made was to use a misting sprinkler within residential-style living units. The sprinkler selected was the EA-1 Protectospray Nozzle. The nozzle was located within or below the residential-style exhaust hood located directly above the stove.

2.2 Specific correctional challenges

The Correctional Service Canada has the mandate to rehabilitate offenders. This mandate includes a model consisting of providing living units at varying degrees of security and at varying degrees of offender responsibility and independence.

The responsibility model consists of an 8-person apartment-style unit that includes a common area consisting of a living room and a kitchen. The offenders living in these units are responsible for cooking their own meals on a daily basis in this kitchen.

Similar apartment-style kitchens are also provided in minimum-security free-egress living units.

A number of cooking fires have occurred in these units despite efforts to promote proper cooking habits and to limit the use of deep-frying and other fire-prone cooking methods.

2.3 Objections

In 2013, a consultant who had been commissioned to install these heads raised objections based on the fact that these sprinklers introduced water into a cooking environment (where the fire may be oil-based). These objections halted the project in question and challenged CSC to provide support to this practice that had been underway for the past seven years.

Additional objections included the fact that there were inconsistencies in how this nozzles were being installed. There was no consistent approach with where the heads were being located in relation to the range/range-hoods. In most installations, the heads were off-centred so as to not conflict with the location of the range-hood exhaust fan and/or lighting. Additionally, in some

locations, the heads were installed at a 90-degree angle (sidewall orientation) rather than pendant-style.

2.4 Code considerations

The locations where the EA-1 Protectospray Nozzle were installed consisted of residential style kitchens located within a B-1 (Detention) occupancy. These kitchens are not industrial kitchens as they are used for small group feeding (typically less than 10 people) and offenders are given the responsibility of preparing their own meals within their small group. This is a concept known within CSC as the "responsibility model" or "small group feeding".

As these systems fall outside of industrial kitchen applications, only the requirements of NFPA-13 (Standard for the installation of sprinkler systems) applied which called for traditional ceiling sprinklers. There was no requirement for range-top fire suppression system as would be provided for NFPA-96 (Standard for ventilation control and fire protection of commercial cooking operations).

Since NFPA-13 does not restrict sprinklers within a specific distance of residential stoves, the installation of these nozzles was deemed acceptable by the AHJ.

2.5 Selection and installation

The EA-1 was selected due having been originally listed for use in protecting commercial cooking deep- fryer equipment. It was deemed that such a sprinkler, although not required by code, would add an additional degree of safety to CSC residential-style installations in order to better control the risk posed by inmate meal preparation. A "medium" heat-rating of 165-C was selected so as to avoid accidental operation due to cooking heat.

CSC had considered the following facts:

1. The EA-1 water-based system creates a mist rather than the droplets that would otherwise be produced by a typical sprinkler head.
2. Such an installation is in excess to that which is required. The minimum requirement under the hood is to provide nothing so this was literally a "better than nothing" approach.
3. The risk posed from grease fires mixing with water was already present: water-based droplet-producing sprinklers that were mounted at the ceiling were already permitted by NFPA-13. The earlier activation of a mist system prior to the activation of the ceiling-mounted droplet-style sprinklers was theoretically better than a delayed ceiling sprinkler activation dropping water directly on the fire in the event of a grease fire.
4. The risk posed by grease fires was already mitigated by internal policies prohibiting deep-frying.
5. The water-based mist system was to be interconnected with a switch designed to turn off power to the cooking surface. This again exceeds minimum requirements.

The EA-1 Protectospray was installed within the range hood (Figure 1). The EA-1 was interconnected with a flow meter connected to the electrical source for the stove such that operation of the sprinkler shuts the stove off. Other sprinklers in the room (provided for NFPA-13 conformance) are not interconnected with the range shut-off.

Figure 63 - Protectospray nozzle in hood

2.6 NRC Partnership and Research

CSC needed demonstrable evidence of the effectiveness of the EA-1 Protectospray nozzle that was being used in CSC establishments in order to determine the optimal design for the use of these nozzles based on several parameters such as nozzle location and temperature rating.

In response to the need of CSC to address the residential kitchen fire safety issue, NRC carried out a study to evaluate the effectiveness of the hood EA-1 nozzle in suppressing cooking oil fires, and to optimize its use. The following content is from the NRC Client Report "Residential Oven Range Fire Protection" dated March 31, 2015 authored by Dr. Andrew Kim and Sasa Muradori.

2.6.1 Test Facility And Procedures

In the study, full-scale fire tests were conducted in a compartment simulating a kitchen area with oven range and ventilation hood.

2.6.2 Test Room And Test Methodology

The test compartment was a 4 m by 4 m room with a 2.4 m high ceiling. One side of the test compartment was fully open (i.e. room with only three side walls) to simulate a typical kitchen/living room arrangement of the CSC residential facility.

The compartment was equipped with a kitchen counter as well as a simulated oven range with a ventilation hood above. A water mist EA-1 nozzle was installed within the ventilation hood. The EA-1 nozzles used were TYCO Type EA-1 PROTECTOSPRAY water mist nozzles produced by Tyco Fire Protection Products. They are automatic (frangible bulb) directional spray nozzles, designed for use in fixed water spray systems. They are external deflector-type nozzles and discharge a uniformly filled cone of medium velocity water droplets. The EA-1 nozzles had temperature ratings of either 162°C (325°F) or 121°C (250°F) with K-factor of 1.4.

A residential-style (NFPA 13 compliant TY3231) sprinkler head was provided by Tyco Fire Protection Products and was installed on the ceiling of the test compartment. It was a pendant type quick response, standard coverage, decorative, 3 mm glass bulb-type spray sprinkler designed for use in light or ordinary hazard, commercial occupancies. It had temperature ratings of 79°C (175°F) with K factor of 5.6 l/min bar$^{0.5}$.

2 L of cooking oil in a pot was put on a stove top burner, and was continuously heated until the cooking oil auto ignited. This simulated the worst possible fire scenario in the CSC residential facility as identified at the site visit.

A thermocouple tree was installed on top of the kitchen counter on the right side of the oven range. The thermocouple tree had five thermocouples in 25.5 cm intervals, with the first one at 25.5 cm above the counter top. One heat flux meter was installed on the right side wall directly facing the oven range. A thermocouple was attached to the EA-1 nozzle and sprinkler to monitor the temperature at the nozzle. Also, a thermocouple was inserted into the oil in the pot on top of the simulated oven range to monitor the oil temperature. A video camera was set up to record the tests, which was used to obtain data regarding fire ignition and extinguishment.
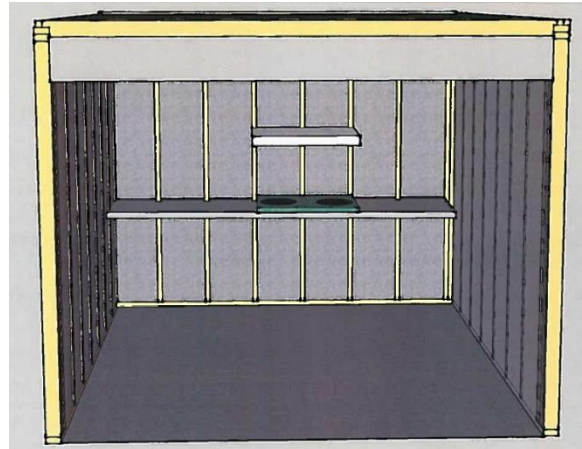
Figure 2 shows a drawing of the test compartment.

A total of 11 tests were conducted in order to test a number of parameters. These parameters included a) temperature rating of two types of EA-1 sprinklers (162°C vs. 121°C), b) suppression achieved by EA-1 versus suppression achieved by ceiling sprinklers only, c) impact on the placement of the EA-1 with respect to the location of the fire on the range top, d) proximity of ceiling sprinklers, e) impact of providing a baffle to assist with heat build-up, and e) impact of having the fan running.

Figure 64-Test compartment

The test proceeded with background data collection, heating of the cooking oil until it auto-ignited, activation of water spray either from the ceiling sprinkler or the hood EA-1 nozzle, and fire suppression. Each test was videotaped. The test procedure was as follows:

    1. At t = 0 s, the data acquisition system and video camera started.

    2. The heating element was turned on to heat the cooking oil in the pan.

    3. When the cooking oil reached approximately 350— 370°C, it auto ignited. This time was noted in the video camera to coordinate with the data acquisition system.

    4. When the sprinkler head or the EA-1 nozzle reached its activation condition, water was sprayed from these nozzles. This time was recorded.

    5. Water spray continued until the cooking oil fire either suppressed or went out of control. When the cooking oil fire was extinguished, this time was noted.

    6. lf the cooking oil fire went out of control, manual extinguishment of the fire was attempted.

2.6.3 Observations

The test results showed that both the ceiling sprinkler and the hood EA-1 nozzle extinguished the cooking oil fire once they are activated. The EA-1 nozzle, installed under the kitchen hood, was much more effective in extinguishing the cooking oil fire. In most cases, cooking oil fire was extinguished within 20 s from nozzle activation by the EA-1 nozzle, regardless of its location

with respect to the cooking oil fire. Comparing with the hood nozzle, the ceiling sprinkler was slow in extinguishing the cooking oil fire, taking more than 1 min to extinguish the fire.

When the EA-1 nozzle activated, there was a big flare-up, then the fire was quickly extinguished. When the sprinkler activated, there was smaller flare-up and the sprinkler spray controlled the fire, but it took a longer time to suppress and extinguish the cooking oil fire.

However, both the sprinkler and EA-1 nozzle had the problem of slow activation. Both activated almost 2 min after the ignition of the cooking oil fire. By the time the sprinkler and the EA-1 nozzles activated, the cooking oil fire had grown into a much bigger fire involving other combustibles in the kitchen area. All combustibles, including the kitchen hood and cabinets, were consumed by the fire by the time of their activation.

The lower temperature rated EA-1 nozzle (250°F/121°C) was a little quicker to activate than the higher temperature rated EA-1 nozzle (325°F/162°C), but both were too slow to contain the cooking oil fire within the oil pan before they activated to extinguish the fire.

When both the sprinkler and the EA-1 nozzles were used in the test, they activated within a few seconds of each other. However, in two tests, the sprinkler installed on the ceiling activated, but the EA-1 nozzle did not activate and the ceiling sprinkler extinguished the fire.

The operation of the exhaust fan was found to be of no impact to the time of suppression.

2.7   Conclusions

The results from the testing confirmed that the practice to install under-hood suppression within CSC residential cooking exhaust hoods was at least as safe as simply installing ceiling sprinklers to code and in fact provided an additional level of safety to that which was otherwise being provided by minimum standards.

Based on these results, CSC implemented a few additional changes to further improve this design. Namely, the installation of nozzles with a lower heat rating per the NRC recommendation. Additionally, CSC implemented a change in their Technical Criteria Document to require that new residential kitchens be installed with shunt relays for the electrical system for these stoves to be tied directly to the fire alarm system rather than the aforementioned flow meter. Thereby, any fire alarm condition turns off *all* cooking ranges in the building further minimizing the risk of fire.

3   SMOKE TOXICITY AS IT RELATES TO SKIN EXPOSURE

3.1 Background
A typical offender cell contains furniture and personal items, including electronics and gadgets, approved for possession. In the event of an evacuation or fire response, Correctional Officers are provided with Self Contained Breathing Apparatus (SCBA) to protect Officers from air-borne contaminants.

3.2 Specific Correctional Challenges

Until 2016, Correctional Officers were being trained on conducting Search and Rescue in the event of a fire. This effort consisted of entering into smoke-filled environments and conducting sweeps of offender cells in order to potentially remove an incapacitated offender.

In 2016, the department concluded that this practice could potentially expose Correctional Officers to risk of injury since only SCBA was being provided rather than full bunker gear. The departmental position was updated to confirm that Search and Rescue was to be conducted by the responding fire departments and that Correctional Officers were only to respond in a) assisting with the evacuations, and b) initial fire suppression efforts for manageable fires.

CSC's 2016 Fire Safety Manual defined a limit of 10 feet (3 m) visibility for Correctional Officers to respond to fires. When visibility drops below this level, Correctional Officers are not permitted to respond and must defer to the response of the municipal fire department.

3.3 3.3 Objections

The Correctional Officers responded with the concern that responding in this type of environment without full skin protection placed them at risk of exposure to toxicants through skin absorption

3.4 NRC Partnership And Research

CSC needed demonstrable evidence of whether the response that Officers were being directed towards posed a threat. The officers are already provided with respiratory protection. Therefore, tenability and toxicological conditions at the 10' (3 m) threshold of a typical cell fire had to be determined.

The following content is from the NRC Client Report "A Study of an Inmate Cell Fire with a Special Focus on Smoke Toxicity on Skin" authored by Dr. Yoon Ko, Dr. Steve Gwynne and Dr. Jamie McAlister.

3.4.1 *Literature Review*

The project consisted of two steps. The first was a literature review in order to determine what would be the expected properties of a typical cell fire. To do so, a medium-security cell setup was selected as this was deemed to be the highest security level (greatest risk) while also having the highest fire load with respect to permitted content (cell effects, combustible furnishings).

It was determined that polycyclic aromatic hydrocarbons (PAHs), monocyclic aromatic hydrocarbons (MAHs), polychlorinated biphenyls (PCBs), polychlorophenols (PCPs), dioxins, and furans are of most concern with regards to their ability to penetrate through the skin and enter the systemic circulation.

These elements were those that were used as the basis for the full scale test.

3.4.2 *Test And Procedures*

Further to the literature review, a full scale test was conducted using a mock-up of an inmate cell and included an adjacent corridor.

To simulate one of the worst-case scenarios, the sprinkler system activation was delayed in the test. This allowed the conditions to deteriorate, resulting in a low visibility of 3 m in the corridor at 21 minutes. Beyond this time, officers are expected to retreat to a place of safety and await the assistance of the responding Fire Department, as per Section 5.3 of the Fire Safety Manual. Thus, the toxicant concentrations measured in the corridor until visibility reached the 3 m criterion were analysed to assess toxicant skin exposures.

The measured data were analysed to determine the likelihood that attending correctional officers would be exposed to toxicants through dermal absorption, given that breathing apparatus was being worn during emergency response.
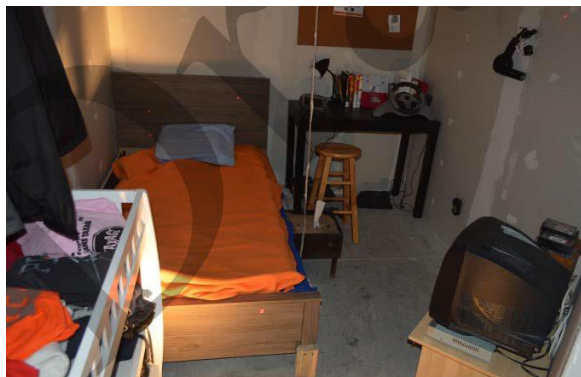
Figure 65-Furnished Test Cell

3.4.3   Observations

The test results show that the fire developed relatively slowly in the inmate cell because the fire retardant mattresses and bedding (which were ignited first), delayed flaming combustion and fire spread. Nonetheless, the temperature and smoke density in the cell increased quickly to the level that could have activated the sprinkler system and smoke detection system in a very early stage of the fire.

Detectable concentrations of dioxins, furans, toluene diisocyanate, PAHs, PCBs, and PCPs were not found in the full-scale testing. Hydrogen chloride and hydrogen cyanide, which are gases that are irritating to the skin, were found in full-scale testing; however, the concentrations measured for the first 21 minutes were insufficient to cause skin irritation. Benzene and formaldehyde, which are known carcinogens, were measured in the air samples. Factoring the dermal absorption rates into the analysis, it is concluded that there is no apparent carcinogenic risk associated with benzene or formaldehyde exposure to skin for the duration of the first 21 minutes, while the visibility was tenable and staff exposure might still be possible. It was therefore found during the test that if attending officers were dressed as expected and followed the attending protocol as expected, then there was no apparent carcinogenic risk through dermal absorption.

3.5   Conclusions

It was demonstrated that even in the worse case (when the fire was permitted to build up), the level of toxicants that could present issues via skin absorption was not present or not present in sufficient quantity to pose a health risk during the first 20 minutes at the limit which officers .

The testing resulted in minor changes to CSC protocols such that officers that respond to fires according to the stated limits are now directed to shower and wash their clothing following each SCBA response in a smoke contaminated environment so as to minimize and eliminate irritant material from the skin.

4   METHOD TO DIFFERENTIATE BETWEEN NUISANCE SMOKE AND FIRE

4.1 Background

Smudging is a First Nations practice that involves the use of smoke for traditional purification ceremonies. CSC supports this practice as an accommodation that is granted to offenders under religious practices. Despite the desire to permit this practice, smudging can have an impact on the smoke detection systems and can initiate a fire alarm system.

4.2 Specific Correctional Challenges

CSC has been moving towards the increased use of Aspirating Smoke Detection (ASD). Due to the prevalence of false alarms due to smudging, CSC tried to find a solution that would a) identify the optimal sensitivity setting for these types of units, and b) be capable of establishing a threshold sensitivity such that smudging products would not initiate a fire alarm condition but other products of combustion (ex: toilet paper, waste basket, smoldering bedding, cigarette/contraband) would.

4.3 NRC Partnership And Research

CSC needed an analytical comparison between the smoke produced in fire and the smoke produced by smudging.

The following content is from the NRC Client Report "A Study of an Inmate Cell Fire with a Special Focus on Smoke Toxicity on Skin" authored by Dr. Yoon Ko and Mark Weinfurter.

4.3.1   Test And Procedures

The test consisted of a comparison between photoelectric smoke detection, ionization sensing detection, and ASD using air sampling tubes and a laser analysis chamber.

Two types of testing were conducted: cone calorimeter test and a room scale testing of various sources.

Material that was tested included toilet paper, plastic waste, bedding sheet strips, cigarettes, a mattress, and newspapers. These were compared with the nuisance (non fire) sources from smudging materials consisting of sage, mugwort, juniper and white pine.

The sources were placed at varying locations for each test and each test looked at each material separately.

Three sensitivity settings were considered (standard, enhanced and high).

4.3.2   Observations

The level of smoke obscuration measured from the smudging source tests was significantly higher than that which resulted from the same amount of the smouldering sources tested in the room.

4.4 Conclusions

The current detection technologies do not have abilities to distinguish nuisance indications between fire and non-fire sources. To filter the nuisance signatures, multiple detection technologies would need to be used concurrently for sensing chemical, thermal and optical

characteristics of smoke sources. Accordingly, this testing did not yield the solution that was desired for CSC.

However, it was suggested that limiting the quantity of materials used in the smudging activities might be able to reduce nuisance alarms; however, each smudging material burns differently, and when several smudging materials are mixed, the mixture would burn differently.

It was also suggested that with a sensitivity setting set low enough (a higher threshold), and with a very small quantity of smudging materials, i.e. less than 1 g of materials like Juniper.

CSC's new installations are now using "standard sensitivity settings" to minimize the number of nuisance alarms while continuing to detect all other sources of fire. To date, CSC has not modified any internal policies on smudging.

5   REDUCTION OF SUSPENSION POINTS IN SMOKE DETECTION SYSTEMS

5.1   Background

The National Building Code of Canada requires that all sleeping rooms (ie. Offender cells) be provided with smoke detection connected to a fire alarm system. Over the years, these systems have been the source of many issues.

5.2   Specific Correctional Challenges

Originally prone to being vandalized or modified to conceal contraband, smoke detectors were eventually provided with protective cages (Figure 4) to make these devices inaccessible to offenders. Regrettably, these cages came to be used as suspension points – areas within a cell from which an offender can affix a ligature for the purpose of self-harm.

Figure 66-Protective Cages for Smoke Detectors

As a result, various solutions were implemented over the years. The use of Aspirating Smoke Detection (ASD) is increasing in popularity due to the fact that it removes the detection device from the offender space. Until recently ASD sample points were being located within the air return vent for offender cells. However, there has been some concern regarding the optimal placement therein. Additionally, many offenders block their air grilles (despite not being permitted to do so) such that air cannot travel into the vent which impacts the ability of the smoke detection to detect smoke.

A solution was presented to install the ASD sample points behind the light fixtures. This solution is based on a similar installation implemented by the California Prisons.

5.3   NRC Partnership And Research

CSC needed an analytical validation that ASD sample points, hidden behind light fixtures, can effectively detect smoke within an offender cell.

The following content is from the NRC Client Report "CSC On-Site Detection Tests" authored by Dr. Yoon Ko, Mark Weinfurter, Eric Gibbs, and Dr. Max Kinateder.

5.3.1 Test And Procedures

The tests were conducted in general conformance with CAN/ULC S529 "Standard For Smoke Detectors For Fire Alarm Systems", Section 41.2, "paper fire test" and Section 42, "smouldering smoke test" (CAN/ULC, 2015). The paper fire scenario was of particular interest to CSC since the scenario is presumed to be representative to potential fires in inmate cells.

CAN/ULC-S529 requires that the response time of a detector shall be not more than 240 seconds (4 minutes) for the paper fire scenario. Thus, the responses of the ASD systems were evaluated following that criterion and were used as the benchmark to represent the successful test criteria for detection.

The smouldering smoke test was conducted for the purpose of information gathering, but the performance criterion of CAN/ULC-S529 for smouldering fires was not used a benchmark for success as it was deemed by CSC that such fires did not reflect typical cell fires in that sustaining smouldering without leading to combustion would be difficult to achieve.

The smoke detection tests were conducted at an inmate cell (Figure 5) in Donnacona Institution in Donnacona QC. The room has built-in furniture, a toilet and a sink, and the room had a door and a window. The ceiling was smooth, but a light fixture was installed on ceiling and wall corner.

A smoke source was placed at the center of the room on the floor. The smoke obscuration level inside the test room was measured using an NRC smoke meter.

Figure 67-Test room for ASD

5.3.2 Test Results And Recommendations

The pass/fail criteria was set at 4 minutes detection time as this is the minimum requirement for detection devices under CAN/ULC-S529.

The best installation point found from the on-site tests was on the side of the light fixture through a drilled hole (mock rivet). With these sampling points, the ASD system read the obscuration comparable to the actual obscuration in the room both for the paper and smouldering fire.

The performance of the ASD tube hidden on the side of the light fixture close to the ventilation duct was similar to that of the sampling tube installed within return ventilation duct.

Faster response times were generally observed for the sampling point located on the side of the light fixture that was closer to the ventilation duct opening (the right hand side in the tests) than for the sample point located on the far side. The far sample point could not be consistently observed to comply with the required benchmark.

Additionally, faster response times were noted for the paper fire than for a smouldering fire.

5.4 Conclusions

The results from the testing were sufficient that CSC has begun to implement a number of pilot projects to further validate the hidden-ASD approach. Each installation must be subject to the test methodology of CAN/ULC-S529 as was conducted by the NRC prior to acceptance.

A few key features to note include the fact that such installations will only be permitted on cells with solid doors. Additionally, weatherproofing gaskets will be removed from all light fixtures in order to allow for the drawing of air into the light fixture. Special care is also being taken to ensure that the light fixtures are not inadvertently provided with a positive air pressure (for example from a service space or conduit) which would otherwise overpower the air sampling. This last challenge is being met by tightly sealing the backs of the light fixtures so that the only open penetration into the fixture is the air sample tube for the ASD.

6   OVERALL CONCLUSION

Operating in a correctional environment poses numerous challenges that are otherwise not encountered in other occupancies. Each of those challenges must be met with real solutions that can be implemented in a timely manner and that can function as required. In each of the above cases, numerical and scientific evidence was sought in order to provide a sound footing and to deal in an open and transparent manner with all those involved. The Correctional Service of Canada is committed to providing sound thought and reason in all of its applications dealing with fire and life safety. The ongoing collaboration that has been established with the National Research Council is a testament that the requirements for security and life safety can be balanced.

EVALUATION OF THE IGNITION RESISTANCE OF BUILDING COMPONENTS IN WILD-LAND URBAN INTERFACE: REVIEW OF TEST METHODS

Masoud Adelzadeh [1], Noureddine Benichou [1], Islam Gomaa [1], Steven Gwynne [2], Alex Bwalya [1], Mohamed Sultan [1]

[1] National Research Council Canada, Ottawa, Canada
[2] Movement Strategies, London, UK

ID: 187

ABSTRACT

In recent years, significant Wildland Urban Interface (WUI) fire losses have occurred in Canada and around the world. With increasing occurrence of large fire losses in WUI areas, there is more need to improve the resiliency of building and infrastructure at WUI areas. Improving structural ignition resistance against WUI fires are crucial, since the extent of damages in these incidents is closely related to the number of buildings that ignite. This study presents a critical review of test standards designed to evaluate the ignition resistance of building elements. The test standards from various countries and jurisdictions have been reviewed. The results of the review show that the existing standards do not sufficiently address WUI hazards, primarily because they do not completely address all aspects of a realistic WUI exposure. The effects of radiant heat and direct flame impingement are better addressed compared to embers/firebrands. For most existing standards the link between the test exposure conditions and realistic WUI exposure are not clearly established. Developing test methods for better evaluation of firebrands and the effect of wind is necessary.

1 BACKGROUND

1.1 Wildfires

Wildland urban interface areas (WUI) are areas where the built environment is in the vicinity of the wildlands. Wildfires pose a distinct hazard to the built environment. Although the annual number of wildfires has been decreasing since 1990 [1], the losses due to wildfires has been increasing in recent years. In 2016 Fort McMurray wildfire, the most expensive natural disaster in the history of Canada, 90,000 people were evacuated and the direct insured loss was approximately 4 billion dollars [2]. About 2,400 structures burned and resulted in 0.4 % reduction in the national GDP [3]. The second most costly wildfire in Canadian history is 2011 Slave lake wildfire, during which 12000 people were evacuated and the estimated total cost of damages was 550 million dollars [2].

Approximately 97% of the area burned is caused by 3% of the wildfires [4]. Aggressive wildfire suppression policies during the past decades has contributed to the accumulation of fuels and denser and continuous forest cover. The result of this policy (and the subsequent presence of more vegetation) has been the occurrence of larger and more intense wildfires [5]. In addition, land use policies, expansion of low-density residential development, and population growth has increased the number of people and structures at risk – as more are located in WUI areas. In United States, the WUI has expanded by 52% from 1970 to 2000, and it is expected to grow by another 10% by 2030 [6]. In terms of life safety and loss of life there has not been large fatalities

in Canada's recent wildfires; however, in the Great Matheson Fire of Black River-Matheson, ON, 223 people lost their lives [2]. More recently, Camp Fire in California claimed the life of 86 peoples and destroyed 18,804 structures [7].

According to latest report from the Intergovernmental Panel on Climate Change (IPCC), global warming is estimated to be 1.0°C [8]. This will likely reach 1.5°C within 30 years. The report also predicts a severe and widespread impact on extreme weather events, including wildfires as temperatures increase by more than 1.5°C. It is expected that as a result of climate change more Canadian forest area will be burned. This increase will be geographically variable but in general the environmental factors described will produce more (and potentially more severe) fires. [9]

1.2 Wildland Urban Interface

In context of threats posed by wildfires to structures, WUI could be defined as a set of conditions which causes ignition of structures produced directly from the fire flames, radiant heat or airborne embers as a result of a fire burning in wildland. FireSmart [10] defined WUI as areas where residential, industrial, or agricultural developments are located within or near wildland. NFPA 1144 [11] defines WUI interface as a location in which "topographical features, vegetation fuel types, local weather conditions, and prevailing winds result in the potential for ignition of the structures within the area from flames and firebrands of a wildland fire". International wildland urban interface code defines WUI as geographical area where structures and other human development meets or intermingles with wildland or vegetative fuels [12]. It is clear from these definitions that the current state of practice prioritizes ignitions as the primary concern. Yet it is important to realise that similar to any other natural hazard, WUI events are complex phenomena that has social, environmental, economic, and political dimensions. It is also important not to limit the WUI concept to a narrow interface area between the urban development and the forested area, but to instead consider WUI as an incident that effects the community, structures, firefighting resources and infrastructure even if they are not physically located at the interface area. Certain exposure types, such as embers (firebrands), from a wildfire could reach far beyond the location of the wildfire. Spotting distances in the range of 10 kilometres are reported in the literature [13]. Therefore, being located outside of the WUI does not ensure safety from the fire itself.

In reaction to wildfire losses several codes and guidelines have been developed around the world. The most notable codes are California Building Code (CBC), International Wildland Urban Interface Code (IWUIC) published by ICC, and the Australian Construction of buildings in bushfire-prone areas. There are also a few standards and guidelines have been developed, among them NFPA standards and Fire Smart handbooks.

1.3 WUI Disaster Sequence

Wildfires are either caused by human activity or through a natural event such as lighting. Irrespective of the ignition source, large wildfires will develop in the presence of severe weather conditions, and low humidity in the fuels. Wind also plays a significant role in severity, direction and speed of progress, and exposure conditions at the interface. These fire conducive elements make controlling the fire difficult for firefighters. Once a large fire reaches an urban development multiple simultaneous structural fires may grow beyond the capacity of the firefighting resources. In some case even access to water will be limited since the water distribution infrastructure is compromised and is not functional.

Therefore, when aiming to reduce the consequences of a WUI fire it is crucial to reduce or eliminate the likelihood of structural ignitions – both from the fire and from transition of the fire between buildings. Once a building is ignited in the absence of adequate firefighting response, the fire may engulf the structure and subsequently be the source of ignition for neighbouring buildings. Evidence of structure to structure fire spread [14], demonstrates that spatial separation requirements in the building codes are not sufficient to mitigate the spread of fire from one building to another.

2 STANDARD TEST METHODS

Building regulations try to be unbiased with regard to the type of construction or materials used, therefore it is important to have a set of standard test methods that provide a measure of performance irrespective of type of materials used. Most exiting fire tests in the building codes are intended to prevent the spread of fire originating from inside the building. While WUI fire exposure is external. While some of these test methods are still beneficial they need to be adapted to provide a better measure of performance in WUI context.

2.1 Exterior walls

CAN/ULC S101 in Canada and ASTM E119/UL 263/NFPA 251 in USA and ISO 834 in Europe describe the standard method of determining the fire resistance of building components. During fire resistance tests, the assembly is exposed to heat from a furnace whose temperature follows a specific time temperature curve. The assembly fails if the fire passes through the assembly, or the temperature of the unexposed side rises by a certain amount (usually 140°C on average or 180°C locally), or if the assembly collapses. Since these tests are developed to represent the fire severity of a compartment fire, they impose a very high temperature (1100°C) that is not representative of an external transient fire source. Nonetheless these tests could still be considered as conservative scenario for comparison. In Canada, the National Building Code of Canada (NBCC) imposes requirements for fire resistance ratings of walls. These requirements are only for interior fire exposure. This is clearly not true for wildfire exposure since the fire exposure is primarily external.

Another consideration regarding the fire resistance is to impose a realistic rating that is analogous to the WUI fire exposure. WUI exposure from wildfire itself is much shorter (in the order of couple of minutes) compared to compartment fire exposure. Depending on the scenario the fire exposure may not directly originate from a wildfire but through a secondary ignition, in which case the exposure could be longer, but still at a much lower temperature. To account for this lower temperature the standard fire curve could be replaced with an external fire time temperature curve similar to what Eurocode suggests (Euro Code1 part 1-2 clause 3.2.2). The maximum temperature of the Euro code's exterior fire exposure curve is approximately 700°C. While imposing a temperature curve seems to be a reliable and repeatable way of simulating exposures in standard tests, a more realistic approach would be to simulate the effects of an external fire is by simulating the incident heat flux rather than temperature.

SFM 12-7A-1[15]/ASTM E2707 [16] utilizes a diffusion burner to expose the wall to a short 10min exposure to a 150kW fire. The test attempts to simulate a scenario where an indirect exposure of flame impingement happens as a result of ignition of plants, trash, a deck or other combustible materials beside the wall. Unless fire resistance of a longer period is also prescribed

in addition to this test, the test does not apply to a scenario where the building is exposed a large radiation source for a long duration of time, such a burning adjacent building.

AS 1530.8.2 [17] is the Australian test standard for WUI exposure. AS 1530.8.2 is intended for severe fire exposure or direct flame impingement (BAL FZ); for lower exposure levels another standard AS 1530.8.1 [18] is used, which exposes the specimen to a radiant heat, burning embers and burning debris. During AS1530.8.2 a representative element of construction or combination of elements is exposed to the standard fire curve. The test duration is 90 min which includes a 30 min exposure to standard fire and a 60 min monitoring period. AS 1530.8.1 provides standard test methods to determine the performance when a specimen is exposed to radiant heat, burning embers and burning debris. Exposure to burning embers is simulated by application of a small gas flame and exposure to burning debris is simulated by wood cribs. Initially, the radiant heat rapidly rises until it reaches a specified maximum radiant heat of either 12.5, 19, 29, or 40 kW/m^2 depending on the severity of exposure. The maximum radiation is maintained for two minutes followed by a gradual decay period. The total radiant heat exposure period is 10 minutes. Overall, the Australian approach is more representative of the WUI exposure. It still has shortcomings - the main one being the lack of wind during the tests. Radiation exposure are more representative of the approaching wildfire.

2.2 Roofs

Roofs are probably the most vulnerable part a building to ignition hazard from wildfire. There are a few existing test methods that measure the ability of a roof assembly to resist the passage of fire into the attic and spread of fire on the roof surface. Most of these tests consider the production of embers by the roof assembly that could ignite other combustible materials on or around the building. In Canada, CAN/ULC-S107 is used to measure the roof performance, which follows a similar procedure as ASTM E-108, UL 790 and NFPA 276. During the test the assembly is exposed to either flames from a calibrated burner, or burning standard brands. The roof assemblies are classified based on their effectiveness against fire exposure, flammability/combustibility, and degree of fire protection provided to the roof deck, structural integrity and propensity to produce flying brands. They provide three classes, Class A, Class B, and Class C. Class A is the most resistant and Class C the least resistant.

2.3 Vents

While protecting the roofs by ignition resistant materials could protect the combustible materials in the attic, the entry of embers through vents or other openings could compromise the effectiveness of the fire protection system. Most existing codes and standards, have recognized this fact and recommend using a metal mesh to prevent the entry of embers into the attic. Recent full-scale studies at IBHS has shown that protecting opening with wire mesh may not be completely effective.

A recently developed ASTM E2886 [19] attempts to measure the performance of vents to resist the entry of embers and direct flames. During the test, a fan pulls a flow of generated embers through the vent. The ember generator consists of a rotating steel mesh tumbler. Standard burning wood cribs (Class C, refer to ASTM E108) are placed inside the rotating tumbler and the embers generated by the agitation of the brands and steel nuts that passes the perimeter steel mesh is transported by the flow of air through the vent. The test is continued until no ember is left in the tumbler. If the vent prevents the ignition of cotton pads located at after the vent, it passes the test.

2.4 Decks

Combustible decking material during a WUI event could be a vulnerable section of a building. And because decks are attached to the building, ignition of decking could result in the spread of fire to the building itself. Firebrands from the wildfire could accumulate under or within the crevices of the deck and result in the ignition of the deck. There are a few standard test methods for decks. California building code has adopted SFM 12-7A-4 for this purpose. The test exposes a 24 inch by 24 inch sample of the deck to a either a flame (SFM 12-7A-4A) or a burning brand (SFM 12-7A-4B). Two scenarios are considered. In the first, it is assumed that the accumulation of brands under the deck has resulted in a fire that effects the deck. The second scenario assumes the firebrands are accumulated over the deck and the heat from the accumulated embers igniting the deck. During the deck flame test the deck is exposed to a flame of 80 kW for 3 minutes, equivalent to 1 kg of paper. The sample fails if there is runaway combustion, structural collapse, or flaming dripping materials. The test procedure requires the sample to be observed for 40 minutes after the flame exposure.

ASTM E2632 [20] test method is almost identical to SFM 12-7A-4A. In SFM-7A-4B /ASTM 2726 [21], a standard burning brand (Standard brand of ASTM E108) is placed over the deck while a fan blows an air flow of approximately 5.4 m/s (12mph) over the specimen and the sample is observed for 40 minutes for signs of sustained flaming or falling brands. In all tests, the samples need to be exposed to conditions of accelerated aging or weathering to create a more realistic representation of the actual deck in the test.

2.5 Eaves

Eaves or similar projections are vulnerable to ignition especially because the wall and the eave provide partial confinement which prevents the heat from escaping freely. The materials used for the construction of eaves may not be as fire resistant at the roofing and exterior walls. Open eaves are especially a weak point for entry of flames or embers. SFM 12-7A-3 or ASTM E2957 [22] both expose a 609 mm projection to a flame of 300 kW for 10 minutes. The sample is observed for another 30 minutes to monitor the existence of glowing or flaming on the unexposed side of the specimen.

2.6 Windows

In order to assess the performance of windows exposed to direct flames SFM 12-7A-2 uses a 150 kW, 100 mm by 1000 mm diffusion burner under the target window. The specimen is exposed to a flame for 8 minutes. This test simulates a scenario where a flame is burning a combustible material around the building and under a window. This test is not representative of a radiation exposure form a wildfire and assesses a secondary flame exposure. For radiation exposure AS 1530.8.2 or AS 1530.8.1 could be considered.

3   CONCLUSIONS

Recent efforts have resulted in the development of a few WUI specific standard test methods that could be used to evaluate the performance of building components or construction materials. These tests attempt to simulate the exposure conditions during a WUI fire event. While most scenarios targeted by these tests are reasonable and beneficial for comparison purposes, they lack sufficient scientific reasoning and data with regard to severity, type and duration of exposure expected during a WUI incident. Some exposure types such as ember exposure is less addressed

while in reality most ignitions in a wildfire are caused by embers. Wind speed used for the test are not representative of worst-case WUI fire scenarios and there is no rational on the magnitude of wind speeds selected. It is important in the future developments to invest more efforts in stablishing a risk informed link between the realistic WUI fire events and the standard test methods. Particularly regarding ember exposure, there is not enough data on what test ember exposures are representative of a realistic WUI exposure. Despite noteworthy efforts to standardize the ember generation in testing of vents, there is still no reliable and repeatable way of ember generation to be used in standard testing of the materials/assemblies.

REFERENCES

[1] Natural Resources Canada. Canadian National Fire Database. 2018; Available from: http://cwfis.cfs.nrcan.gc.ca/ha/nfdb.

[2] Public Safety Canada. Canadian disaster database. 2013, September 12; Available from: https://www.publicsafety.gc.ca/cnt/rsrcs/cndn-dsstr-dtbs/index-en.aspx.

[3] Statistics Canada, Fort McMurray 2016 Wildfire – Economic Impact. 2017 2017-03-16; Available from: https://www150.statcan.gc.ca/n1/pub/11-627-m/11-627-m2017007-eng.htm.

[4] Flannigan, M., et al., Future wildfire in circumboreal forests in relation to global warming. Journal of Vegetation Science, 1998. 9(4): p. 469-476.

[5] Busenberg, G., Wildfire management in the United States: the evolution of a policy failure. Review of policy research, 2004. 21(2): p. 145-156.

[6] Theobald, D.M. and W.H. Romme, Expansion of the US wildland–urban interface. Landscape and Urban Planning, 2007. 83(4): p. 340-354.

[7] Cal Fire, Top 20 Largest California Wildfires 2019; Available from: http://www.fire.ca.gov/communications/downloads/fact_sheets/Top20_Acres.pdf.

[8] IPCC, Summary for Policymakers. In: Global warming of 1.5°C. An IPCC Special Report on the impacts of global warming of 1.5°C above pre-industrial levels and related global greenhouse gas emission pathways, in the context of strengthening the global response to the threat of climate change, sustainable development, and efforts to eradicate poverty [V. Masson-Delmotte, P. Zhai, H. O. Pörtner, D. Roberts, J. Skea, P.R. Shukla, A. Pirani, W. Moufouma-Okia, C. Péan, R. Pidcock, S. Connors, J. B. R. Matthews, Y. Chen, X. Zhou, M. I. Gomis, E. Lonnoy, T. Maycock, M. Tignor, T. Waterfield (eds.)]. 2018: World Meteorological Organization, Geneva, Switzerland,. p. 32.

[9] Flannigan, M., et al., Future fire in Canada's boreal forest: paleoecology results and general circulation model-regional climate model simulations. Canadian journal of forest research, 2001. 31(5): p. 854-864.

[10] Partners in Protection, FireSmart: Protecting Your Community from Wildfire. 2003: Partners in Protection.

[11] NFPA 1144 Standard for reducing structure ignition hazards from wildland fire. NFPA, 2013.

[12] International Wildland-Urban Interface Code 2015. 2015, International Code Council, Illinois.

[13] Koo, E., et al., Firebrands and spotting ignition in large-scale fires. International Journal of Wildland Fire, 2010. 19(7): p. 818-843.

[14] Maranghides, A., et al., A Case Study of a Community Affected by the Waldo Fire Event Timeline and Defensive Actions. 2015.

[15] California Building Code, Chapter 7A [SFM], Materials and Construction Methods for Exterior Wildfire Exposure, Exterior Wall Siding and Sheathing, SFM Standard 12-7A-1.

[16] ASTM E2707-15 Standard Test Method for Determining Fire Penetration of Exterior Wall Assemblies Using a Direct Flame Impingement Exposure, ASTM International, West Conshohocken, PA, 2015, https://doi.org/10.1520/E2707-15.

[17] AS 1530.8.2, Methods for fire tests on building materials, components and structures Part 8.2: Tests on elements of construction for buildings exposed to simulated bushfire attack—large flaming sources, Standards Australia, Standards Australia GPO Box 476, Sydney, NSW 2001, Australia, 2007.

[18] AS 1530.8.1, Methods for fire tests on building materials, components and structures Part 8.1: Tests on elements of construction for buildings exposed to simulated bushfire attack—Radiant heat and small flaming sources, Standards Australia, Standards Australia GPO Box 476, Sydney, NSW 2001, Australia, 2007.

[19] ASTM E2886/E2886M-14 Standard Test Method for Evaluating the Ability of Exterior Vents to Resist the Entry of Embers and Direct Flame Impingement, ASTM International, West Conshohocken, PA, 2014, https://doi.org/10.1520/E2886_E2886M-14.

[20] ASTM E2632/E2632M-13e1 Standard Test Method for Evaluating the Under-Deck Fire Test Response of Deck Materials, ASTM International, West Conshohocken, PA, 2013, https://doi.org/10.1520/E2632_E2632M-13E01.

[21] ASTM E2726/E2726M-12a(2017) Standard Test Method for Evaluating the Fire-Test-Response of Deck Structures to Burning Brands, ASTM International, West Conshohocken, PA, 2017, https://doi.org/10.1520/E2726_E2726M-12AR17. 2017.

[22] ASTM E2957-17 Standard Test Method for Resistance to Wildfire Penetration of Eaves, Soffits and Other Projections, ASTM International, West Conshohocken, PA, 2017, https://doi.org/10.1520/E2957-17. 2017

A STUDY OF THE EFFECT OF SMOKE TOXICITY FROM AN INMATE CELL FIRE

Yoon Ko[1], Jamie McAllister[2], Steve Gwynne[3], Michael Kruszelnicki[4]

[1]NRC, Canada; [2]FireTox, US; [3]Movement Strategies, UK; [4]Correction Service Canada, Canada

ABSTRACT

A full-scale inmate cell fire test was conducted to obtain measurements of toxic effluent from smoke. The measured data were analysed to determine the likelihood that correctional officers would be exposed to toxicants through dermal absorption, given that breathing apparatus was being worn during emergency response. The test set-up includes various instrumentation to measure HRR, temperature, visibility and concentrations of toxic effluents. For the measurements of toxicants, air samples were continuously acquired from the test set-up to monitor carbon monoxide, carbon dioxide, hydrogen chloride, hydrogen cyanide and formaldehyde. Single-point air samples and wipe samples were also taken for dioxins, furans, benzene, toluene diisocyanate, PAHs, PCBs and PCPs, which are carcinogens with potential dermal exposure risks.

1 INTRODUCTION

Correctional Facilities face a number of unique challenges. In the last five years, Correctional Service Canada (CSC) has worked with the National Research Council (NRC) to review and validate various assumptions and technologies made within Correctional Facilities.

One such effort was in response to concerns raised by Correctional Officers, CSC and NRC studied the effects of smoke of specific concentration and content typical to that which could be expected as a result of a cell-fire. This allowed CSC to establish guidelines and limitations for front-line responders in the event of a cell-fire in a correctional facility.

This paper presents the smoke toxicity study that experimentally investigated smoke production and toxicity generated from a typical inmate cell fire. Common furnishing and items allowed and found in inmate cells are made from synthetic plastics, foams and polymers. These materials can pose a serious danger to the health of those affected as during smouldering and flaming combustion these materials can produce a large amount of smoke containing asphyxiant gases, irritant gases and carcinogens. This study focused on toxicants that are capable of penetrating the skin and entering the blood stream and then producing harmful effects.

2 LITERATURE REVIEW

To design a representative test set-up, a literature review was first conducted on smoke toxicants that might be produced during a typical inmate cell fire. The literature review identified a list of toxicants of interest, absorption routes and exposure limits.

2.1 Burning materials

In a review of 590 correctional facility fires which occurred in the US between 2003 and 2007, Flynn [1] reported that when fires were not confined to cooking equipment or contained to trash

or rubbish, the leading items for first ignition were mattresses and bedding materials. This agrees with the findings from the study of Canadian correctional facilities fires which occurred between 1995 and 2000 [2]. Su et al. [2] reported that approximately 40% of these fires involved mattresses or bedding materials as the first item ignited, followed by 10% involving trash, 6% involving paper, and 6% involving clothing.

Only fire retardant mattresses that meet the requirements of the Correctional Service Canada, Fire Safety Manual [3] or that conform to the California Bureau of Home Furnishings, Technical Bulletin 121 can be used in the correctional facilities. Pillows must be "inherently flame-retardant", and blankets and sheets must conform to "CAN/CGSB-4. 162-M, Hospital Textiles-Flammability Performance Requirements". The flame-retardant fabrics and materials may delay ignition and flaming combustion or require a longer period of time for smouldering. However, once ignited, the effluents from combustion of these materials, whether in flaming or smouldering, can be more toxic than non-retardant products due to the halogenated compounds often used as flame retardants.

In addition, many typical household items are allowed in an inmate cell, such as a television, gaming system, stereo system, and fan. These materials are made of plastics, foams, and composites and are a large source of asphyxiant gases, irritant gases, and carcinogens. Additional items of concern are desks, stands, and dressers made of luan wood, pressboard, fibreboard or other composite materials made with glues and adhesives. These items also contribute to the overall toxicity of effluents produced during a fire.

2.2 Emergency responses

According to the Correctional Service Canada Fire Safety Manual [3], correctional officers serving as the Fire Emergency Officer (FEO) will execute fire emergency procedures in accordance with the fire safety plan. If it is a manageable fire, FEOs extinguish the fire. If it is beyond staff control and requires fire department intervention, FEOs are instructed to assist in offender evacuation for impeded egress buildings. During these evacuations, FEOs must use self contained breathing apparatus (SCBA) and evacuate inmates to a place of safety. If visibility is reduced to approximately 3 m (10 ft) or the area becomes too hot, "officers shall not proceed but shall immediately begin to release all cell doors, giving verbal orders to offenders and retreat and await the assistance of the responding Fire Department" [3]

2.3 Anticipated fire effluents and exposure routes

Assuming that SCBAs are fitted and employed appropriately, inhalation of fire toxicants would be prevented; however, dermal absorption of fire toxicant could be possible. Therefore, anticipated fire effluents from an inmate cell fire were first reviewed for potential to be deposited on and absorbed through theskin of correctional officers.

Asphyxiant and irritant gases, which are readily generated from the combustion of wood and cellulosic materials, include carbon monoxide, carbon dioxide, hydrogen cyanide, nitrogen oxides, sulfur dioxides, and hydrogen chloride. Inhalation of some of these gases may cause injuries and death; however, none of these gases effectively penetrate through the skin into the systemic circulation.

According to the World Health Organization [4], carcinogenic compounds are also found in by-products from fire. These include polycyclic aromatic hydrocarbons (PAHs), dioxins, polychlorinated biphenyls (PCBs), nitrosamines, and heavy metals, which may be produced in

the types of fires that commonly occur in correctional facilities involving plastics and beddings treated with retardants. Many of these compounds are bound to soot and could deposit on surfaces including human skin. The toxicant inspections conducted for firefighter gear identified the presence of lead, mercury, phthalates, and PAHs on firefighter hoods and gloves [5]. Some of the carcinogens may lead to skin irritation, but acute exposures do not present any long-term health effects. Notably, not all carcinogens deposited on the skin could be absorbed into the skin.

Thus, a list of toxicants likely to be produced based upon the inmate cell fire scenarios were refined to identify those carcinogens likely to penetrate through the dermis and enter into the bloodstream. To accomplish this task, various literary resources were utilized including the Agency for Toxic Substances and Disease Registry (ATSDR), the Canadian Workplace Exposure Database (CWED) referencing values from the Canada Labor Code (CLC), and the International Agency for Research on Cancer (IARC) Firefighting Monographs [4].

It was determined that polycyclic aromatic hydrocarbons (PAHs), monocyclic aromatic hydrocarbons (MAHs), polychlorinated biphenyls (PCBs), polychlorophenols (PCPs), dioxins, and furans are of most concern with regards to their ability to penetrate through the skin and enter the systemic circulation. The main component of mattresses and bedding materials, polyurethane foam, is known to produce MAHs, such as benzene and toluene. The pyrolysis of chlorinated plastics, such as polyvinylchloride found in appliances and electronics, can lead to the production of polychlorinated biphenyls (PCBs), polychlorophenols (PCPs), dioxins, and furans. Lastly, polycyclic aromatic hydrocarbons (PAHs) are produced from the incomplete combustion of organic materials, and hence, are common in all types of fires. As such, air samples taken during fire testing were monitored for these products of combustion.

3 FULL-SCALE FIRE TEST

3.1 Test set-up

A full-scale mock-up inmate cell was constructed with dimensions of 2.3 m (W) X 3.4 m (L) X 2.4 m (H), under a large hood. Adjacent to the inmate cell, a corridor (2 m wide and 3 m long) was constructed, as shown in *Fig. 1*-a). One side of the corridor was closed, but the other was open so that smoke could mitigate and be collected by the hood. The walls, ceiling, and floor of the corridor and the cell were lined with Type X gypsum boards.

3.2 Burning materials and ignition source

As per the lists of personal items allowed for inmates (provided by CSC as per Directive 566-12 [6]), the test cell was furnished with a bed, desk and other items (see *Fig. 1*-b). The total mass of the fuel was 124 kg.

To ignite the mattress and beddings, a standard sand burner having 0.31 x 0.31 m square surface as required by the CAN-ULC 9705 [7] was placed at the centre of the floor next to the bed. A burner output of 50 kW was first used, then the output was increased to 100 kW after about 10 minutes.

3.3 Sprinkler system

CSC inmate cells are protected with smoke detection system and automatic sprinkler systems. To simulate one of the worst case scenarios that could occur due to a concealed fire or malicious

destruction, it was decided to activate the sprinkler system manually *after* flashover during the test; i.e. significantly beyond the time when it would normally be expected to activate. A wall type sprinkler head was installed below the ceiling on the diagonal wall of the test cell.

3.4 Instrumentations

The hood system over the cell and the corridor was used to collect the smoke from the fire. The hood system was instrumented to measure the heat release rate (HRR) of fire. Inside the test rooms, a thermocouple tree was installed at the centre of the room and in the corridor. In each tree, 16 thermocouples were evenly distributed along the height of the room. A smoke meter was installed in the room and in the corridor.

3.5 Toxicant sampling

A gas sampling system was built around the test room and corridor. A gas sampling probe was installed in both the room and the corridor at a height of 1.5 m, and the sampling tube was connected to a FTIR (Fourier-transform infrared spectroscopy) gas analyzer for continuous measurements of carbon monoxide, carbon dioxide, hydrogen chloride, hydrogen cyanide and formaldehyde throughout the test.

Through the gas sampling line in the corridor, single-point air samples were also acquired to measure for carcinogens; Dioxins, Formaldehyde, Furans, Benzene, Toluene Diisocyanate, PAHs, PCBs, and PCPs. The single-point air samples were collected twice in the corridor during the test: [Air sample #1] during the development of fire and [Air sample #2] during the fire suppression.

To collect data on surface deposits in addition to the toxicants carried by the smoke effluent in transit, post-test wipe samples were also acquired. The post-test wipe samples were collected from a sooty wall in the corridor because the corridor was the location where correctional officers would most likely be positioned when assisting with evacuation of inmates. The wipe samples were taken to determine the concentration of carcinogens (or their solid form constituents) likely to condense and adhere on the walls of the corridor with the assumption that similar concentrations would also be likely to condense and adhere on the skin's surface of attendant officers.

4   TEST RESULTS

4.1 Fire development

For approximately 15 minutes from the start of the test, the mattress and beddings only smouldered because of their fire retardancy. After18.5 min from the start of the test, flaming combustion started and resulted in the first peak HRR of 660 kW at 26.5 minutes (see *Fig. 2.* a). However, the fire developed slowly to the size that would be considered "manageable' as per the CSC Fire Safety Manual [3] at about 20 minutes. The fire spread accelerated affecting the entire room (i.e.flashover) at 40 minutes, with the maximum HRR of about 2.2 MW. The sprinkler system was activated in 1.5 minutes from the point of flashover. The sprinkler system was so effective that the measured HRR dropped very quickly to 60 kW.

4.2 Smoke and visibility

Within about 5 minutes, ceiling temperatures in the room increased to the level that could trigger the sprinkler system installed in the cell (the temperature rating of the sprinkler head is 74°C).

Since the automatic activation of the sprinkler was disabled during the test to allow the fire to develop to a worst case condition, the fire slowly developed as the hot smoke filled up the cell and corridor. The temperature in the corridor became untenable at 42 minutes reaching the temperature criterion of 120°C (see *Fig. 3)* for thermal tolerance to convective heat for unprotected skin.

The smoke density measured in the room reached a level of 0.03 OD/m within 1 minute, which would normally be expected to trigger a smoke detector having the standard detection sensitivity of 2.5%/ft (0.03 OD/m). The visibility in the corridor became untenable at 21 minutes reaching the limit of 3 m.

a)   b)
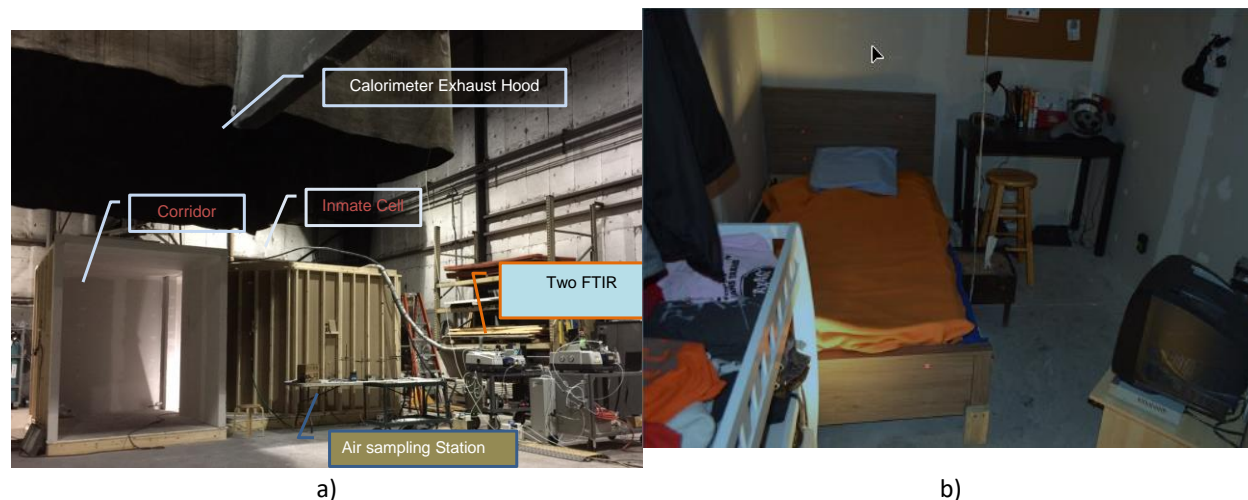
Fig. 1. a) Test setups; b) Furnished test inmate cell

4.3 Toxicant measurements

Continuous air samples were obtained from the cell and the corridor to monitor concentrations of carbon monoxide, carbon dioxide, hydrogen chloride, hydrogen cyanide and formaldehyde over the entire duration of the fire testing. . *Fig. 2.* b) shows FTIR gas analyser results from the corridor. The measured carbon monoxide and carbon dioxide reached the Occupational Exposure Limit (OEL) at 24 minutes and 40 minutes respectively. It should be noted that these gases are not absorbed through the skin in meaningful concentrations, and with use of SCBA, there would be minimal concern that officers will inhale these fire toxicants. Therefore, the focus was on dermally absorptive toxicants measured in the corridor up until the visibility was reduced to 3 m, after which correctional officers are instructed to evacuate the hazardous area [3].

Hydrogen chloride

As per the International Agency for Research on Cancer (IARC) classification, HCL does not have carcinogenic effect on humans but is a skin irritant. For the first 21 minutes, while visibility remained tenable in the corridor, the measured concentration of hydrogen chloride in the corridor was 1600-1800 ppm. This value is much lower than the concentrations of 40,000 - 100,000 ppm found to be "irritating to the skin" in humans [8] [9], during tests where HCl solutions were applied directly to the skin rather than through exposure to smoke effluent.

Hydrogen Cyanide

Hydrogen cyanide causes toxic asphyxia when inhaled and also causes skin irritation. Hydrogen cyanide is not listed by IARC as to its potential carcinogenicity in humans [10] [11]. For the first 21 minutes, while visibility remained tenable, the measured maximum concentration of hydrogen cyanide was 20-30 ppm. A concentration of hydrogen cyanide reported to cause adverse effects through skin absorption [12] was 20,000 ppm for 8-10 minutes of exposure; the measured concentration in this study is much lower than the reported value.

Formaldehyde

Formaldehyde is a Group 1 carcinogen with dermal absorption potential. For the first 21 minutes, the measured value marginally exceeded the OELs based on air samples, yet was an insignificant quantity of the carcinogen to be effective on skin. This is because the rate of skin absorption of formaldehyde through the skin is known to be less than 10% of the air concentration [13]. Given this, there is no apparent carcinogenic risk associated with formaldehyde exposure to the skin of correctional officers based upon the concentrations present when applying the 10-ft visibility criteria.

Single air samples for carcinogenic compounds

The single air samples taken in the corridor during the development of fire (at 36 minutes) and during the fire suppression (at approximately 42 minutes) were analysed for the carcinogens with potential skin effects. Detectable concentrations of dioxins, furans, toluene diisocyanate, PCBs and PCPs were not found in both air samples. Most of PAHs were not found except naphthalene, which showed concentrations that were still lower than OEL. However, benzene was found with concentrations of 0.580 ppm and 3.0 ppm at 36 minutes and 42 minutes (after the activation of the sprinkler system), respectively.

Benzene

Benzene is an IARC Group 1 carcinogen with dermal absorption potential. Canada Labour Codes (CLC) indicates that the short-term OEL is 2.5 ppm, and a concentration of 0.5 ppm is the level "easily absorbed through skin". Research suggested that approximately 68% of benzene in air is absorbed through skin. Hence, the concentration of 0.58 ppm, which was measured at the first air sampling (collected at 36 minutes), does not pose apparent carcinogenic risk associated with benzene exposure to skin; i.e. equates to approximately 0.40 ppm dermal absorption.

Wipe sample measurements

The post-test wipe samples were analysed for dioxins, furans, PAHs, PCBs and PCPs. No detectable levels of these carcinogens were found in the samples.
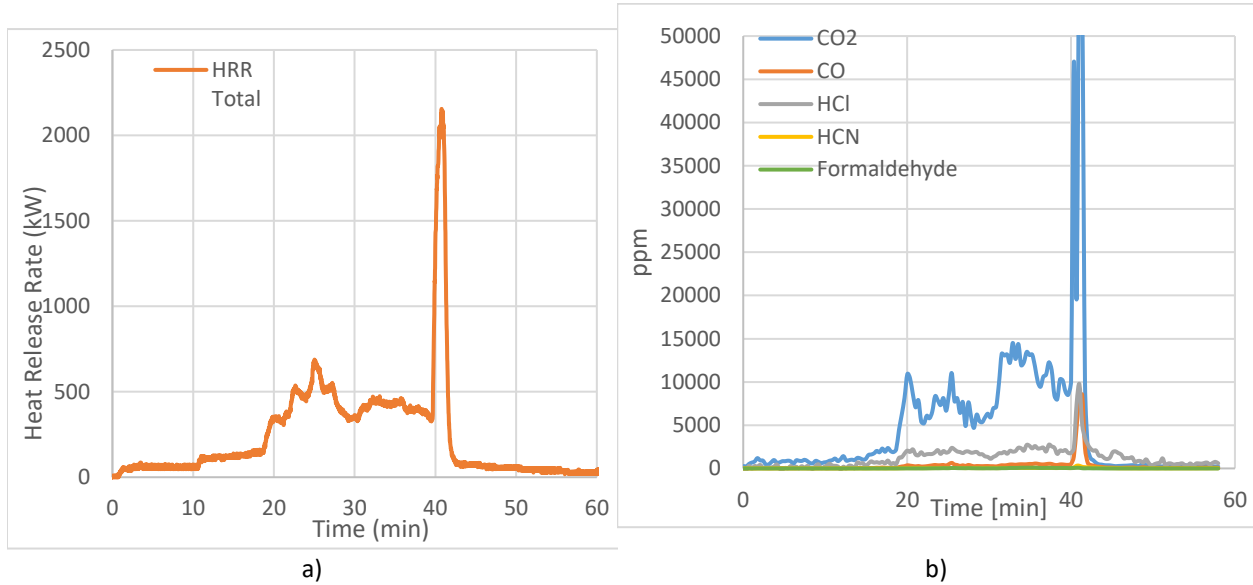
Fig. 2. a) HRR; b) FTIR results from the corridor
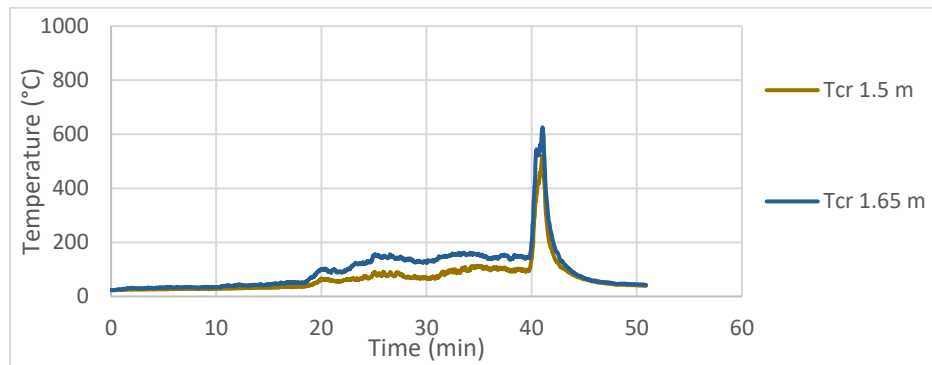
Fig. 3. Corridor temperature at 1.5 m and 1.65 m heights

5   CONCLUSIONS

A full-scale inmate cell fire test was conducted to obtain measurements of toxic effluent from smoke. The measured data were analysed to determine the likelihood that attending correctional officers would be exposed to toxicants through dermal absorption, given that breathing apparatus was being worn during emergency response.

The test results show that the fire developed relatively slowly in the inmate cell because the fire retardant mattresses and bedding (which were ignited first), delayed flaming combustion and fire spread. Nonetheless, the temperature and smoke density in the cell increased quickly to the level that could have activated the sprinkler system and smoke detection system in a very early stage of the fire.

To simulate one of the worst-case scenarios, the sprinkler system activation was delayed in the test. This allowed the conditions to deteriorate, resulting in a low visibility of 3 m in the corridor at 21 minutes. Beyond this time, officers are expected to retreat to a place of safety and await the assistance of the responding Fire Department, as per Section 5.3 of the Fire Safety Manual

634

[3]. Thus, the toxicant concentrations measured in the corridor until visibility reached the 3 m criterion were analysed to access toxicant skin exposures.

Detectable concentrations of dioxins, furans, toluene diisocyanate, PAHs, PCBs, and PCPs were not found in the full-scale testing. Hydrogen chloride and hydrogen cyanide, which are gases that are irritating to the skin, were found in full-scale testing; however, the concentrations measured for the first 21 minutes were insufficient to cause skin irritation. Benzene and formaldehyde, which are known carcinogens, were measured in the air samples. Factoring the dermal absorption rates into the analysis, it is concluded that there is no apparent carcinogenic risk associated with benzene or formaldehyde exposure to skin for the duration of the first 21 minutes, while the visibility was tenable and staff exposure might still be possible. It was therefore found during the test that if attending officers were dressed as expected and followed the attending protocol as expected, then there was no apparent carcinogenic risk through dermal absorption.

The results produced during this experiment will be of use in determining the viability of responder intervention to particular fire scenarios and their need of dedicated protective equipment.

ACKNOWLEDGMENT

REFERENCES

[21] [1] [22]   J. D. Flynn, Prisons and Fires, Quincy, MA: National Fire Protection Association , 2010.

[23] [2] [24]   J. Su, R. Gaw, K. Richardson, B. Taber and D. Carpenter, "Smoke detectors in prison cells, NRCC-47651," Institute for Research in Construction, National Research Council of Canada, 2006.

[25] [3] [26]   Correctional Service Canada, "Fire Safety Manual," 2016.

[27] [4] [28]   World Health Organization, "IARC Monographs on the Evaluation of Carcinogenic Risks to Humans: Painting, Firefighting, and Shiftwork, Volume 98.," 2010.

[29] [5] [30]   J. McAllister, " Health Effects in Groups Exposed to Wildland and Urban Fires. In Health Effects from Combustion Products," Royal Society of Chemistry, Abingdon, Oxfordshire, 2014.

[31] [6] [32]   Correctional Service Canada, "Commissioner's Directive 566-12, Personal Property of Offenders, October 19, 2015 (effective date).," 2015.

[33] [7] [34]   ULC, "CAN/ULC-9705 Fire Tests - Full-scale Room Test for Surface Products," Ottawa, 2013.

[35] [8] [36]   TOXNET, "Hazard Substance Database: Hydrogen Chloride, https://toxnet.nlm.nih.gov," 2015.

[37] [9] [38] National Academy of Science, "National Research Council (US), Acute Exposure Guideline Levels for Selected Airborne Chemicals, Volume 4," National Academies Press, Washington, D.C., 2004.

[39] [10] [40] TOXNET, "Hazard Substance Database: Hydrogen Cyanide, https://toxnet.nlm.nih.gov," 2007.

[41] [11] [42] World Health Organization, "Hydrogen Cyanide and Cyanides: Human Health Aspects, Concise International Chemical Assessment Document 61.," 2004.

[43] [12] [44] P. Drinker, "Hydrocyanic acid gas poisoning by absorption through the skin.," *Journal of Industrial Hygiene,* vol. 14, no. 1-2, 1932.

[45] [13] [46] Department of Health and Human Services, "NIOSH Skin Notation Profiles-Formaldehyde/Formalin, Publication No. 2011–145.," 2011.

HIGH ENERGY ARC FAULTS (HEAF) IN CANADIAN NUCLEAR PLANTS

Hossam Shalabi and George Hadjisophocleous
Fire Safety Engineering, Carleton University, Ottawa, Onatrio, Canada

ABSTRACT

An increase in the number of High Energy Arc Fault (HEAF) events in international nuclear power plant fire event data has been identified. The international HEAF operational experience demonstrates that substantial damage can occur during a HEAF event. In many cases, HEAF events caused extra challenges to the safe shutdown of a reactor. HEAF can produce loss of essential electrical power, cause physical damage and generate products of combustion that can present significant challenges to the nuclear operator and fire response teams.

This paper discusses Canada's HEAF events and the international experience, current HEAF prediction models, issues and limitations of the models. The paper also deliberates on HEAF current research and different HEAF types and their consequences. There are two sets of recommendations presented in this paper, the first set if for Canadian Nuclear Power Plants and the second set for the international nuclear industry.

1   INTRODUCTION

In nuclear power plants, switchgear provides means to isolate and de-energize specific electrical components and buses in order to clear downstream faults, perform routine maintenance, and replace necessary electrical equipment. These protective devices may be categorized by the insulating medium, such as air or oil, and are typically specified by voltage classes, i.e. low, medium, and high voltage [1]. Switchgears, load centers and bus bars/ducts can encounter catastrophic failure that manifests as rapid release of energy in the form of heat, light and severe damages to metals. The failure may eventually lead to initiation of fire involving the electrical device itself or any flammable material that is exposed to it, such as cable trays or nearby panels. This event is known as a High Energy Arc Fault (HEAF). The event is also referred to as high energy, energetic or explosive electrical equipment [2]. The high-energy events most commonly take place in two phases. The first phase is mostly distinguished by rapid release of electrical energy. Consequently, a fatal failure occurs in electrical enclosures along with ejection of hot projectiles from damaged electrical components. Also, phase one of HEAF can result in fire involving electrical devices. Phase two, is characterized by a follow up fire initiated in phase one which normally results in severe damage of inflammable material in Zone of Influence (ZOI) of HEAF. HEAF in electrical equipment is initiated in one of three ways: poor physical connection between the switchgear and the holding rack, environmental conditions, or the introduction of a conductive foreign object.

Figure 1 shows how a HEAF progresses in less than a few seconds. The degree of damage includes pressure rise effects (i.e. severe equipment deformation, thrown doors, degraded fire barriers) which potentially can affect equipment in other fire zone(s). Pressure effects are mainly dependent on room configuration and electrical characteristics of the event.

The operating experience from nuclear power plants (NPP) as well as from other nuclear installations worldwide has recognized a non-negligible number of HEAF events and resulting fires. These incidents characteristically occur within high voltage components such as

switchgears and circuit breakers, or at high voltage cables. In addition, the operating experience appears to show that the numbers of HEAF incidents are increasing. One reason for this increase of incidents can be a result of the aging infrastructure. Fire Events" published June 25, 2013 [3], demonstrates that HEAF events have the potential to be major risk contributors with substantial safety consequences and considerable economic loss.
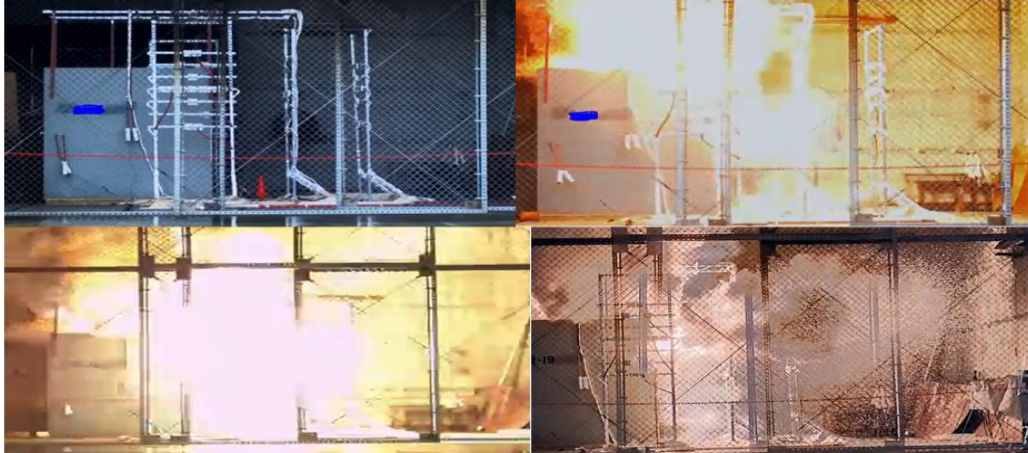

Fig. 1. HEAF progression

Due to the high safety significance and importance to nuclear regulators, the Organisation for Economic Co-operation and Development (OECD) has initiated in 2009 an international activity on HEAF to investigate these phenomena in nuclear power plants in more detail to better understand fire risk at nuclear power plants. The OECD program tends to characterize the effects of HEAF by deploying various phenomena. The employed phenomena include the pressure of enclosures, temperature of enclosures, heat release rate and heat flux to target equipment. Other electrical parameters such as arc voltage, arc current and arc duration were also subjected to measurement during the experiments. It is believed that an international group that can pool international knowledge and research means better accomplishes this. The OECD FIRE Database task group [4] indicated that 48 of the in total 392 fire events are HEAF induced fire events.

2 DISCUSSION

2.1 NUREG/Cr 6850 Fire PRA Methodology For Nuclear Power Facilities

NUREG/CR 6850 [5] currently provides the sole guidance on how to assess the fire risk of HEAF events through probabilistic risk assessment using both statistical and empirical fire modeling. These methods define the zone of influence and materials ignited by HEAF events initiated in switchgear equipment and bus ducts. The main standards used for calculation purposes are NFPA 70E [6] and IEEE 1584 [7]. Computer models are available most of which are based on the calculations provided by IEEE 1584 or in Appendix D of NFPA 70E.

NUREG/CR 6850 assessment methodology is based on defining the potential zone of influence for HEAF events. The potential zone of influence is defined according to electrical features of the components. Zone of influence can be deployed to estimate the potential damage to safety related structures, systems and components (SSCs). According to NUREG/CR 6850, HEAF events are assumed to occur in electrical equipment that operate at 440V, or equipment that operate at greater voltage. Motor Control Centers (MCC) with switchgears, which are used to

directly operate equipment, should be evaluated as potential HEAF source. According to NUREG/CR 6850, switchgears that are greater than 4.16 KV, are likely to experience HEAF events that will cause impacts outside of cabinet of origin. However, for panels with lower voltage the effects are estimated to remain within the panels [8].

All vulnerable components or movable/operable structural elements located within 0.9 m horizontally of either the front or rear panels/doors, and at or below the top of the faulting cabinet section, will suffer physical damage and functional failure [5]. Exposed cables, or other exposed flammable or combustible materials or transient fuel materials located within this same region (0.9 m horizontally) will be ignited [5]. In the zone of influence of electrical cabinets and switchgears HEAF events, the initial arcing causes destruction of the faulting device. Furthermore, adjacent switchgear within the cabinet trips open and the cabinet door will be blown open due to the metal plasma and mechanical shock. The cabinet fire will burn with a fire intensity and severity documented in experiments in NUREG/CR 6850. Unprotected cables will be damaged and drop into the panel in an open-air configuration. Also, any unprotected cable in the first overhead cable tray, in case of being located within 1.5 m vertical distance from the top of the cabinet will be severely damaged. Any unprotected cable or flammable material that is located within 0.9 m from the front door of the cabinet will also be exposed to ignition [5].

There are two methods used for HEAF. The first is described in NUREG/CR-6850, Volume 2: Detailed Methodology, Appendix M for Chapter 11, High Energy Arcing Faults" [5]. This method specifies the following assumptions:

- The first unprotected cable tray within 1.5 m of the top of the cabinet will ignite.
- Vulnerable equipment within 0.9 m horizontally of the front or rear doors will be destroyed.
- The faulting device is destroyed.
- Adjacent cubicles in the same cabinet bank will trip open.
- Unprotected cables that enter the panel in an airdrop configuration are destroyed.

This method has unidentified degree of uncertainty, because it resulted from one single well-documented HEAF event that happened at the San Onofre Nuclear Generating Station [9].

The second method is in Supplement 1 of NUREG/CR-6850 and EPRI 1011989" section 7 bus duct (counting) guidance for high energy arcing faults (FAQ 07-0035) [10]. This method specifies the following assumptions for HEAFs happening in bus ducts:

- Exposed combustible material within these zones will ignite.
- An ejection of the molten material from the bottom of the bus duct and down to the right circular cone of an angle of 15 degrees from the vertical axis. An ejection of the molten material will be outwards from the fault point in the shape of a sphere with a 1.5 feet radius.
- A diameter expansion of the cone to a maximum of 20 feet and beyond will fall straight down in a cylindrical shape of 20 feet diameter.

The Core Damage Frequency (CDF) associated with a HEAF scenario involving damage only to the first target is calculated as: [5]

$$CDF_i = \lambda_g \cdot W_L \cdot W_{is} \cdot P_{ns} \cdot ccdp_i \qquad (1)$$

Where: λ_g = the generic frequency for HEAFs;

W_L = the location weighting factor;

W_{is} = the ignition source weighting factor;

$ccdp_i$ = the CCDP for a scenario including targets in the ZOI only; and

P_{ns} = the probability of no suppression. If all targets are inside the ZOI, a value of 1.0 should be assumed. If there are postulated targets outside the ZOI, the probability of no suppression can be calculated following the approach provided in Appendix P using the manual suppression curve for HEAFs.

2.2   HEAF Events In Canada

HEAF events identified in OECD FIRE database are documented. The events are identified according to definition developed by FIRE project. The OECD FIRE database project has declared that 48 out of 145 fire events that were reported from 1979 to mid-2012 are HEAF events according to the database. Two of the reported HEAF fire events were in Canada. Details on the HEAF event identified in OECD FIRE database are as follows:

On April 2005, an electrical fault and fire on the Main Output Transformer (MOT) caused a Turbine to trip. A severe failure occurred on the blue phase winding of the MOT at the same time with a failure to red phase isolated phase bus potential transformer (surge arrester) cubicle (explosion but no fire). The fire was extinguished by transformer deluge system. Subsequent to notification of the event, the reactor was manually shut down. The transformer casing was raptured and as a result of 68200 Litres of transformer insulating oil was spilled over 1-2 hours. Before the catastrophic failure of the MOT, there was no sign that the MOT was indicating any problems with the transformer. Semi-annual oil analysis indicates normal results. Moreover, no significant gas increase was noticed until the failure occurred. However, root-cause analysis indicated that according to evidences in hand, the incident was caused by material failure in the MOT. In order to determine the failure mode, forensic disassembly was arranged. As the transformer was unable to dissipate generated heat, a failure occurred. The pressure of the undissipated heat removed the doors of from the transformer cubicle, deformed the cubicle and opened fused links.

The second HEAF event reported in Canada took place on October 2005. A 600 V AC 1600 A class 4 breaker was racked into its cubical and lead to an electrical arc/fireball. As the breaker was moved to the connect position, an electrical fault occurred. Consequently, a catastrophic failure happened in the breakers. The failure led to an electrical arc and fireball, which erupted, from the switchgear with burns sustained to the employee. The emergency response team instantly terminated the fire. The employee was moved and diagnosed with 1st and 2nd degree burns on the thighs. After the breaker was repaired, it was tested three times in the test position before receiving a permission to be connected again. At the time of the breaker failure, the door of the breaker compartment was in the place and the screws were engaged. However, hot gas and flames vented through louvers to and burned the employee.

In order to prevent similar failures in the future, corrective actions were taken. Significant improvements were applied to protocol and equipment designs. Moreover, a verification process has been implemented. Since shutters prevent inadvertent contact between components and the buses during the maintenance, they play a significant role in the process. Therefore, shutter design improvement opportunities were vastly investigated by manufacturers and engineered

material manager supply chain. Broken shutters were removed from the breaker cabinet and staff received training on technical advice verification. A team of electrical experts were chosen to address the shortfalls of the protective clothes in such events. Lastly, the emergency communication protocol was improved [11].

2.3 ARC Flash Versus ARC Blast

The arc flash and arc blast phenomena differ vastly from one and other.

Arc Flash: damage is contained in within the general confines of the component of origin. These events are associated with minor damage and minimal bus bar degradation from melting/vaporization [6].

Arc Blast: damage is contained in within the general confines of the component of origin. However, arc blast effects have the potential to damage surrounding equipment through pressure rise effects (i.e. severe equipment deformation, thrown doors, degraded fire barriers).

During an arc flash, the voltage is likely to drop to approximately 10% of the original voltage, and the current remains unaffected. In arc blast, however, both the current and voltage need to remain unchanged for approximately 1 to 2 seconds. Consequently, the power load of arc blast is much larger. Therefore, arc blast is very difficult to obtain under a testing environment without causing power problems. The intensity of an arc flash is thus, less than arc blast.

Figure 2 demonstrates the differences in damage caused by Arc Flash and Arc Blast.
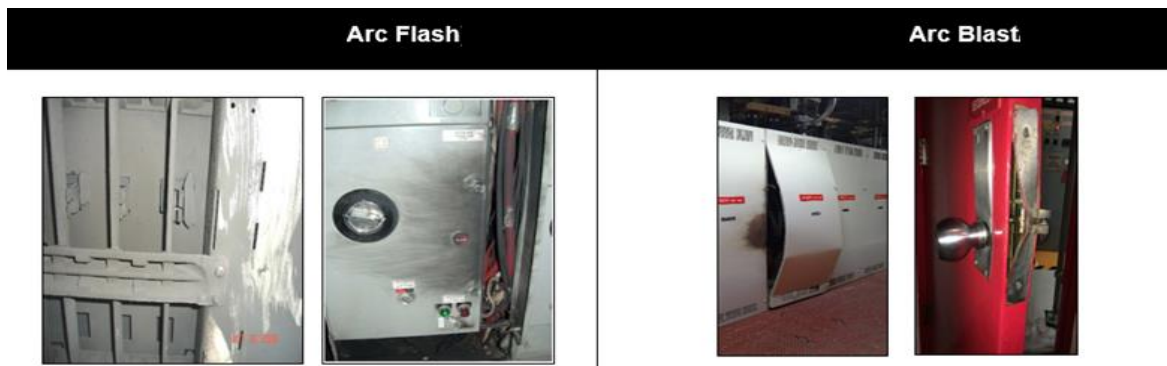
Fig. 2. Arc Flash versus Arc Blast

2.4 Copper Verus Aluminum

It has been shown that HEAF tests involving aluminum lead to significantly larger energy release than HEAF tests involving copper. The aluminum is involved in the shape of components, subcomponents or parts of the normal current carrying pathway or components, subcomponents or parts that could become involved in the fault current pathway as result of a ground fault.

Aside from the larger release of energy during the HEAF events, when aluminum is involved, dispersal of electrically conductive aluminum by-products throughout the area was observed. These by-products were not only conductive but also caused short circuiting and grounding of equipment in the area. Through the testing program when aluminum is involved, the HEAF events caused an extensive damage to test measurement and recording equipment and electrical supplies. The damage done by HEAF with aluminum involvement was vastly larger than the damage limit estimated by NUREG/CR 6850 [12]. Several tests were performed mostly on

electrical equipment containing copper and results were approximately as estimated in NUREG/CR 6850 methodology. However, the tests performed on electrical equipment that contained aluminum resulted in a damage state extensively larger than NUREG/CR 6850 estimations.

A detailed description of the test of HEAF in experimental series is as follows. The test involved a 4.16V bus duct section. The bus duct section was removed from a decommissioned United States nuclear plant and consisted of non-segregated copper bus bars, which were enclosed with an aluminum duct. The bus duct section was secured to the floor of the enclosure using wooden structural members and the open ends were secured with a sheet of electrically insulating fiber. The fiber was utilized to create a pressure boundary inside the bus duct so that it will limit the free energy release once the fault is initiated. Directly after the HEAF event was initiated, the hot gas mixture pushed the fiberboard away, which inevitably allows the arc and associated hot gas and plasma mixture to jet out of the bus duct. Consequently, hot gas and molten metal were linearly blowing from the bus duct opening as shown in figure 3. The hot gas and plasma extended nearly 9m in a horizontal direction. The damage was extended to nearly 0.9 m from the bus duct and any instrument located in that zone was affected by the temperature and heat flux. The facility was covered with an electrically conductive aluminum and number of electrical components needed to be replaced [13].
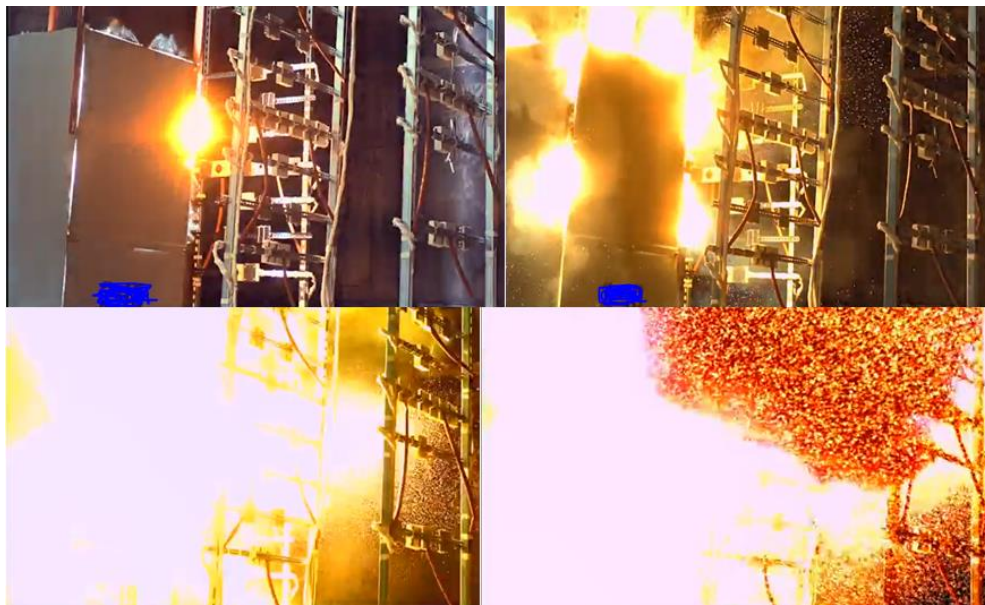
Fig. 3. Aluminium HEAF test

2.5 HEAF Prediction Models

In order to predict the damage done to SSCs due to HEAF events, simple prediction models were developed based on incident energy models such as the heat release model. However, due to the fact that HEAF events have very short duration and cause very rapid increase of temperature and pressure and, due to the release of rapidly expanding superheated vapour, and intense radiations are out of the range of current empirical fire models development of an empirical correlation for incident energy and SSC damage is a challenge. Another challenge faced in the development of

empirical correlation for incident energy and SSC damage is the variable affecting the fire hazard and equipment involved.

Due to the contribution of energetic electric arc, traditional plume fire models cannot be applied directly to the HEAF energetic phase to measure the heat release rate. HEAF might become fully developed fire involving multiple components depending on the exposed materials and equipment involved while fire plume models can only be applied when the fire is fully established. Based on arc flash calculations, assuming that the incident energy or the energy release rate can be applied using the IEEE 1584 [7] and NFPA 70E [6] calculation methods, two approaches have been proposed.

The first approach assesses the potential for ignition of nearby SSC or equipment using the point source radiation model. This approach tends to measure the potential for ignition of nearby SSC using the Critical Heat Flux (CHF) and then using Thermal Response Parameters (TRP), calculate estimated time to ignition using the incident heat flux. In order to determine whether the ignition is likely to happen, the estimated time is compared to the arc fault duration time. The applicability of this approach is however, limited to only situations where the arc fault is limited in duration due to upstream protective equipment and ignition through conduction. After ~~the~~ sufficient data was collected, a range of expected arc heat flux intensities generated by the potential flat current is established conducting an arc flash hazard analysis. Incident heat flux is then calculated at various distances using the same point source radiation model as detailed in NUREG/CR 1805 [14]. The fire subsequent to the event can then be treated using the multiple burning objects HRR.

The second approach suggests that closed switchgears cabinets, MCC panels will develop into fully developed fire either when the energy dissipated by fault reaches 10 Kw/m^2, or, when the energy dissipated by the fault current is in excess of 20 Kw/m^2 transformers, and bus ducts will develop into fully developed fires. In both cases, the inflammable materials will be affected by the subsequent fire and typical plume fire model and point source ignition models are then employed to measure the impact on nearby objects.

In order to better understand the objective of the task and provide a better characterization of HEAF events, a series of experiments are recommended. The experiments will obtain comprehensive scientific fire data on the HEAF phenomenon that are known to occur in nuclear power plants. These designed experiments will help develop a more realistic model to account for failure modes and consequences of HEAF events in addition to the development of correlation based on ignition time using variations of incident fear flux. The experiments can also be employed to validate current models, which are used to measure SSC damage potential. Moreover, the mentioned experiments will advance the sated of knowledge and provide better characterization of HEAF in the fire Probabilistic Risk Assessment (Fire PRA) and help the prediction of potential damage from HEAF events. In addition, some key questions are answered by the recommended questions such as how HEAF events can be minimized or prevented. How signs of HEAF events can be detected. [8]

3 RECOMMENDATIONS

3.1 Canadian Nuclear Power Plants
- Review and update maintenance practices designed to eliminate the underlying causes of faults (loose connections, degraded insulation, foreign materials, etc.)

- Limit the duration and magnitude of HEAF so that little damage can occur to nearby equipment and does not endanger the functionality of redundant equipment by design and location of plant SSCs. Identify potential weaknesses in the overall plant design for defense in depth, and to evaluate the benefits of plant modifications for improving safety.
- Industry survey on extent of Aluminum in all nuclear stations.
- Revise CSA N293 "Fire Protection for Nuclear Power Plants" so that contents can be modified in a risk informed manner providing a level of safety commensurate to the risk and probability indicated through the database.
- Avoid using the limited guidance provided in NUREG/CR 6850 on the ZOI for HEAF, as research has proven its inaccuracy.

3.2 International Nuclear Industry

- Need for clear definitions of Arc Flash, Arc Blast and HEAF.
- Quantify the ZOI for HEAF that contain Aluminum.
- Update and revise current HEAF guidance in NUREG/CR-6850.
- Support Fire PSA by expanding on the "rule of thumb" currently provided in NUREG 6850 by assessing the adequacy of existing HEAF ZOIs in NUREG/CR-6850 for electrical cabinets with aluminum bus bars and for bus ducts containing aluminum.
- Assess the design, effectiveness, and robustness of a suppression system for the HEAF application. Additional research is required to be dedicated on characterization of the enduring fire aspects of such events.

4   CONCLUSION

In conclusion, this paper discussed Canada's HEAF events, the international experience, current HEAF predication models issues and limitations. The paper also deliberated on HEAF current research and different HEAF types and their consequences. There were two sets of recommendations presented in this paper, the first set for Canadian Nuclear Power Plants and the second set for international nuclear industry.

REFERENCES

[1]   High Energy Arcing Fault Fires in Switchgear Equipment, A Literature Review, Jason W. Brown, Steven P. Nowlen, and Francis J. Wyant 2009.

[2]   Putorti, A., Melly, N. B., Bareham, S., & Praydis Jr, J. (2015). Characterizing the thermal effects of High Energy Arc Faults. Paper presented at the 23th International Conference on Structural Mechanics in Reactor Technology (SMiRT 23)-14th International Post Conference Seminar on FIRE SAFETY IN NUCLEAR POWER PLANTS AND INSTALLATIONS.

[3]   Organisation for Economic Co-operation and Development (OECD) Nuclear Energy Agency (NEA), Committee on the Safety of Nuclear Installations (CSNI), OECD FIRE Project - Topical Report No. 1, Analysis of High Energy Arcing Fault (HEAF) Fire Events, NEA/CSNI/R(2013)6, Paris, France, June 2013.

[4]   Organisation for Economic Co-operation and Development (OECD) Nuclear Energy Agency (NEA), Committee on the Safety of Nuclear Installations (CSNI), OECD FIRE Project - TOPICAL REPORT No. 1, Analysis of High Energy Arcing Faults, HEAF, Paris, draft, to be published 2012.

[5]   EPRI/NRC-RES Fire PRA Methodology for Nuclear Power Facilities, Final Report, (NUREG/CR-6850, EPRI 1011989), 2016.

[6]   National Fire Protection Association (NFPA), NFPA 70E "Standard for Electrical Safety in the Workplace", 2018.

[7]   IEEE 1584, "IEEE Guide for Performing Arc-Flash Hazard Calculations", IEEE, September 2018.

[8]   A Review of Current Calculation Methods Used to Predict Damage from High Energy Arcing Fault (HEAF) Events. (2015). NUCLEAR ENERGY AGENCY.

[9]   San Onofre Nuclear Generating Station, LER 362/2001-001, "Fire and RPS/ESF Actuations Caused By The Failure of a Non-Safety Related 4.16 kV Circuit Breaker," February 2, 2001.

[10] Fire Probabilistic Risk Assessment Methods Enhancements Supplement 1 to NUREG/ CR-6850 and EPRI 1011989" section 7 bus duct (counting) guidance for high-energy arcing faults (FAQ 07-0035).

[11] Analysis of high energy arcing fault (HEAF) fire events (2013). OECD Fire Project topical report NO.1. Carlos Lopez, Jason Brown, Steve Nowlen, Risk and Reliability Analysis Department. Conceptual test plan for high energy arcing fault fire experiments.

[12] Miskiewicz, D. (June 3, 2009). Bus Duct Counting Guidance for High Energy Arcing Faults.

[13] REACTORS, U. S. N. R. C. O. O. N. R. R. O. O. N. (August 21, 2017). HIGH ENERGY ARCING FAULTS IN ELECTRICAL EQUIPMENT CONTAINING ALUMINUM COMPONENTS.

[14] Fire Dynamics Tools (FDTs) Quantitative Fire Hazard Analysis Methods for the U.S. Nuclear Regulatory Commission Fire Protection Inspection Program.

AUTHOR INDEX